

GeoPlanet: Earth and Planetary Sciences

Editor-in-Chief

Paweł Rowiński

Series editors

Marek Banaszkiewicz, Warsaw, Poland

Janusz Pempkowiak, Sopot, Poland

Marek Lewandowski, Warsaw, Poland

Marek Sarna, Warsaw, Poland

For further volumes:

<http://www.springer.com/series/8821>

Subhasish Dey

Fluvial Hydrodynamics

Hydrodynamic and Sediment
Transport Phenomena

Subhasish Dey
Department of Civil Engineering
Indian Institute of Technology
Kharagpur
India

The GeoPlanet: Earth and Planetary Sciences Book Series is in part a continuation of Monographic Volumes of Publications of the Institute of Geophysics, Polish Academy of Sciences, the journal published since 1962 (<http://pub.igf.edu.pl/index.php>).

ISSN 2190-5193 ISSN 2190-5207 (electronic)
ISBN 978-3-662-50726-1 ISBN 978-3-642-19062-9 (eBook)
DOI 10.1007/978-3-642-19062-9
Springer Heidelberg New York Dordrecht London

© Springer-Verlag Berlin Heidelberg 2014

Softcover reprint of the hardcover 1st edition 2014

This work is subject to copyright. All rights are reserved by the Publisher, whether the whole or part of the material is concerned, specifically the rights of translation, reprinting, reuse of illustrations, recitation, broadcasting, reproduction on microfilms or in any other physical way, and transmission or information storage and retrieval, electronic adaptation, computer software, or by similar or dissimilar methodology now known or hereafter developed. Exempted from this legal reservation are brief excerpts in connection with reviews or scholarly analysis or material supplied specifically for the purpose of being entered and executed on a computer system, for exclusive use by the purchaser of the work. Duplication of this publication or parts thereof is permitted only under the provisions of the Copyright Law of the Publisher's location, in its current version, and permission for use must always be obtained from Springer. Permissions for use may be obtained through RightsLink at the Copyright Clearance Center. Violations are liable to prosecution under the respective Copyright Law. The use of general descriptive names, registered names, trademarks, service marks, etc. in this publication does not imply, even in the absence of a specific statement, that such names are exempt from the relevant protective laws and regulations and therefore free for general use.

While the advice and information in this book are believed to be true and accurate at the date of publication, neither the authors nor the editors nor the publisher can accept any legal responsibility for any errors or omissions that may be made. The publisher makes no warranty, express or implied, with respect to the material contained herein.

Printed on acid-free paper

Springer is part of Springer Science+Business Media (www.springer.com)

Series Editors

Geophysics	Paweł Rowiński <i>Editor-in-Chief</i> Institute of Geophysics Polish Academy of Sciences ul. Ks. Janusza 64 01-452 Warszawa, Poland p.rowinski@igf.edu.pl
Space Sciences	Marek Banaszkiewicz Space Research Centre Polish Academy of Sciences ul. Bartycka 18A 00-716 Warszawa, Poland
Oceanology	Janusz Pempkowiak Institute of Oceanology Polish Academy of Sciences Powstańców Warszawy 55 81-712 Sopot, Poland
Geology	Marek Lewandowski Institute of Geological Sciences Polish Academy of Sciences ul. Twarda 51/55 00-818 Warszawa, Poland
Astronomy	Marek Sarna Nicolaus Copernicus Astronomical Centre Polish Academy of Sciences ul. Bartycka 18 00-716 Warszawa, Poland sarna@camk.edu.pl

Managing Editor

Anna Dziembowska

Institute of Geophysics, Polish Academy of Sciences

Advisory Board

Robert Anczkiewicz

Research Centre in Kraków
Institute of Geological Sciences
Kraków, Poland

Aleksander Brzeziński

Space Research Centre
Polish Academy of Sciences
Warszawa, Poland

Javier Cuadros

Department of Mineralogy
Natural History Museum
London, UK

Jerzy Dera

Institute of Oceanology
Polish Academy of Sciences
Sopot, Poland

Evgeni Fedorovich

School of Meteorology
University of Oklahoma
Norman, USA

Wolfgang Franke

Geologisch-Paläontologisches Institut
Johann Wolfgang Goethe-Universität
Frankfurt/Main, Germany

Bertrand Fritz

Ecole et Observatoire des
Sciences de la Terre,
Laboratoire d'Hydrologie
et de Géochimie de Strasbourg
Université de Strasbourg et CNRS
Strasbourg, France

Truls Johannessen

Geophysical Institute
University of Bergen
Bergen, Norway

Michael A. Kaminski

Department of Earth Sciences
University College London
London, UK

Andrzej Kijko

Aon Benfield
Natural Hazards Research Centre
University of Pretoria
Pretoria, South Africa

Francois Leblanc

Laboratoire Atmospheres, Milieux
Observations Spatiales, CNRS/IPSL
Paris, France

Kon-Kee Liu

Institute of Hydrological
and Oceanic Sciences
National Central University Jhongli
Jhongli, Taiwan

Teresa Madeyska

Research Centre in Warsaw
Institute of Geological Sciences
Warszawa, Poland

Stanisław Massel

Institute of Oceanology
Polish Academy of Sciences
Sopot, Polska

Antonio Meloni

Istituto Nazionale di Geofisica
Rome, Italy

Evangelos Papathanassiou

Hellenic Centre for Marine Research
Anavissos, Greece

Kaja Pietsch

AGH University of Science and
Technology
Kraków, Poland

Dušan Plašienka

Prírodovedecká fakulta, UK
Univerzita Komenského
Bratislava, Slovakia

Barbara Popielawska

Space Research Centre
Polish Academy of Sciences
Warszawa, Poland

Tilman Spohn

Deutsches Zentrum für Luftund
Raumfahrt in der Helmholtz
Gemeinschaft
Institut für Planetenforschung
Berlin, Germany

Krzysztof Stasiewicz

Swedish Institute of Space Physics
Uppsala, Sweden

Roman Teisseyre

Earth's Interior Dynamics Lab
Institute of Geophysics
Polish Academy of Sciences
Warszawa, Poland

Jacek Tronczynski

Laboratory of Biogeochemistry
of Organic Contaminants
IFREMER DCN_BE
Nantes, France

Steve Wallis

School of the Built Environment
Heriot-Watt University
Riccarton, Edinburgh
Scotland, UK

Wacław M. Zuberek

Department of Applied Geology
University of Silesia
Sosnowiec, Poland

*To my wife, Swastika, and children, Sibasish
and Sagarika, for their unconditional love,
patience and continued support*

Foreword I

Various problems from the broad field of research on sediment transport, such as local scouring, sedimentation in reservoirs, erosion due to floods, dam breaching flows, aggradations, and degradations of riverbed are of fundamental importance for river engineers, geophysicists, decision makers, and environmentalists. At the same time, these problems are still far from being solved and constitute the basic issue for scientists dealing with environmental hydraulics. Even at microscale level, we realize that sediment particles respond to hydraulic forces such as shear and lift, whose effects are in turn related to basic hydrodynamic flow properties, particle size, shape, and density. Sediment transport can, in principle, be thought of as moving water exerting both lift and drag on sediment particles at rest and/or in motion. Although this concept is relatively simple numerous other, very often nonlinear, processes occur and quantitative modeling of sediment transport turns out to be extremely difficult. This is the result of the complexity of the physical processes that govern the particle transport in water bodies, manifold of important scales, meaningful uncertainties related to input data, knowledge gaps, and numerical difficulties.

This book brings together emerging perspectives from fluid mechanics, sediment transport theory, civil engineering, and mathematical modeling. Reflecting on the book's theoretical and empirical focus, the audience is two-fold: students and scholars working within the university tradition, and environmental scholars and engineers interested in solving real life problems. Together, this mix forms a creative synthesis for both sets of readers.

Although the problems of sediment transport have been studied for more than two centuries, there are not many up-to date reference books presenting the actual state of the art in the field. In view of this lack of readily available, clearly presented information, this volume fills an important void. Its analyses and discussions of also individual aspects provide the kind of basis that any student and specialist in the field would like to have in approaching this subject. It is thus a most welcome contribution to the growing body of literature on hydraulics, focusing exclusively on what is clearly the key area of concern.

Subhasish Dey has been a pioneer in the field of applied hydrodynamics, turbulence, and sediment transport. His journey in the world of science and engineering took him from the University of North Bengal through a number of stops at the Universität Stuttgart, Technische Universität Darmstadt, University of Iowa,

Technical University of Denmark, Adelaide University, University of Bradford, Chinese Academy of Science, Tsinghua University, University of Hong Kong, Università di Pisa, Università della Calabria, Politecnico di Milano, University of Florence, University of Oulu, Instituto Superior Tecnico Lisbon, National Taiwan University, National Chung Hsing University, National Cheng Kung University, Nanyang Technological University, Laboratoire Central des Ponts et Chaussées, and other academia, where he offered a course on sediment transport and/or stayed as a visiting professor, to his present home at the Indian Institute of Technology Kharagpur where he is the professor and head of the Department of Civil Engineering. This journey has given him a unique perspective on the thrilling field of sediment transport. I could personally experience his extraordinary passion and devotion to science having *Sub* (as I call him in short) as invited speaker during two international schools of hydraulics (2010 and 2012) that I had the privilege to chair. The contacts and the friendship struck up that time have brought fruit at enormous speed and we can now enjoy this fantastic tome.

Scientists and engineers working in the field of hydrodynamics, sediment transport, and related areas owe *Subhasish Dey* a debt of gratitude for producing this excellent volume. It will help young people entering the field and will serve as a valuable reference work for more experienced scientists. I believe that the field of sediment research will progress more quickly and vigorously as a result of the publication of this excellent book. This volume will also enormously enrich the Springer book series: *GeoPlanet: Earth and Planetary Sciences*.

Warsaw, March 2014

Pawel M. Rowinski

Foreword II

The traditional Fluvial Hydraulics has significantly transformed over recent decades moving from a largely empirical discipline towards a qualitatively new level of mathematically and physically rigorous methodologies of modern fluid mechanics. This step change has become possible due to the progress in modeling and experimental capabilities that led to significant advances in the understanding of the key processes involved in fluvial dynamics. The turbulence structure among them is particularly important as it is a fundamental driver of the interactions between turbulent flow and its erodible boundaries. As a reflection of these changes, the title of the discipline has changed from Fluvial Hydraulics to *Fluvial Hydrodynamics* and this book is an excellent highlight of this important transition.

Over the years, the author of this book has been among key players in the modernization of fluvial hydraulics by contributing on many fronts, from fundamental issues of open-channel flow turbulence to particle entrainment and transport. This personal involvement in the subject makes this book particularly interesting and stimulating.

The book joins a great family of recent texts on this topic, such as W. Graf and M. Altinakar (1998), A. Raudkivi (1998), G. Parker (2004), M. H. Garcia (1996, 2008), J. C. Winterwerp and W. G. M. van Kesteren (2004), A. Gyr and K. Hoyer (2007), E. Partheniades (2009), and A. J. Mehta (2013). Each of these books is unique and provides their own specific perspective on the subject. *Subhasish Dey's* book continues this tradition and the author should be highly commended for his outstanding effort. I have no doubt that this book will help in training a new generation of civil and hydraulic engineers and will inspire new discoveries in hydraulic research.

Aberdeen, March 2014

Vladimir Nikora

Foreword III

This book, *Fluvial Hydrodynamics*, by *Subhasish Dey* is based on his teaching, laboratory research, and extensive field experience for more than 30 years. His practical knowledge along with a strong scientific background has enabled him to come up at this stage. This spirit impregnates to write this excellent book that contains a wealth of theoretical as well as applied material justifying a comprehensive treatise on hydrodynamics of sediment transport. I strongly believe that the book would be a standard textbook all over the world not only for postgraduate and research level students, but also for field engineers as a practical guide and supplementary engineering handbook.

Knoxville, March 2014

Thanos Papanicolaou

Foreword IV

The book *Fluvial Hydrodynamics* that comprehensibly addresses the issues of sediment transport by turbulent flow differs from most texts in this field. It deals with every aspect of hydrodynamics related to sediment transport and is important in the context of sediment research and practice.

The author *Subhasish Dey* is not only an excellent researcher and at the forefront of current understanding of sediment transport, but also reviewed a broad spectrum of scientific literature to bring to the audience of this text an excellent volume that is up-to-date in all respects.

Beijing, March 2014

Zhao-Yin Wang

Foreword V

...I thought and still so believe that a book of this title will be of great value to the upcoming generations. As is evident from the most detailed list of contents, the book covers all possible problems, which future engineers will be confronted in their professional career, but equally in research. The exercises, a special feature in the text, presented in the book will be very useful.

Lausanne, November 2013

Walter H. Graf

Preface

*I come from haunts of coot and hern,
I make a sudden sally
And sparkle out among the fern,
To bicker down a valley.*

*By thirty hills I hurry down,
Or slip between the ridges,
By twenty thorpes, a little town,
And half a hundred bridges.*

*Till last by Philip's farm I flow
To join the brimming river,
For men may come and men may go,
But I go on forever.*

...

The Brook, Alfred Lord Tennyson (1809–1892)

Flow in a river that goes on forever is one of the most evident manifestations of gravity. The river and its characteristics must be studied, must be understood. The book, *Fluvial Hydrodynamics*, goes in this direction written by an *unknown hydraulician*.

The state of the art in fluvial hydrodynamics can be examined only through a careful exploration of the theoretical development and applied engineering technology. This book is primarily focused, since most up-to-date primary research findings in this field are presented, on the research aspects that involve a comprehensive understanding of the mechanics and physics of sediment transport by turbulent flow. It begins with the fundamentals of hydrodynamic principles applicable to open-channel flow followed by turbulence characteristics related to sediment motion. Then, the sediment dynamics are described from a classical perspective by applying the mean bed shear approach, and additionally, incorporating a statistical description of the role of turbulence. The book also describes the local scour problems at hydraulic structures and scale models. It is thus intended primarily as a course textbook at the graduate/research level and also as a guide for field engineers, keeping up with modern scientific developments. Therefore, as a simple prerequisite, the readers should have a basic background knowledge in

hydraulics/fluid mechanics and an understanding of fundamentals of calculus, probability, statistics and physics.

In the field of civil engineering, where engineers typically learn about rivers in courses called open channel hydraulics and sediment transport, sound knowledge of fluvial hydrodynamics is important because it determines the aggradations and degradations of the river systems, life span of hydraulic structures and river protection works, etc. Thus, it is not surprising that this subject is of interest to a wide circle of professions that include hydraulicians, hydrologists, geologists, sedimentologists, geographers, civil engineers, environmental engineers, and so on.

I understand from the discussions with and comments from colleagues and students over the years during delivering lectures on an international short course on *turbulent flows, sediment transport and scour* offered to different universities around the world and on the regular graduate courses on *hydraulics of sediment transport* and *turbulent fluid flows* at my Institute (Indian Institute of Technology, Kharagpur) that the phenomena concerning the dynamics of sediment particles under a turbulent flow invite many open questions. My primary attempt is therefore to address the fundamental aspects of fluvial hydrodynamics from the viewpoint of micro-mechanical interaction of sediment particles with turbulent flow.

I am of the opinion that it could be possible to build a sound understanding of fluvial hydrodynamics on the typical foundation of fluid mechanics, basic calculus, probability, statistics and physics. Introducing new aspects found in the research of turbulent flow, this book updates the theories of sediment transport. It is therefore my hope that this book would close the gap between the micro-mechanics of sediment transport and the stochastic characteristics of turbulent flow. It differs from the traditional treatments of open channel hydraulics and sediment transport in its greater emphasis on the basic physics of turbulent flow in terms of quantitative analytical information.

A course based on this book would be appropriate for graduate and research students in hydraulic engineering and earth sciences curricula and would expected to be taught by a teacher with an active interest in this field. Under these circumstances, instructors would assign students in exploring questions that arise and in discussing papers from the journals, and to involve them in laboratory experiments and/or field studies. Therefore, I have also included exercises that can be used to explore the problems of practical importance involving complex hydrodynamic phenomena in the context of sediment dynamics. I would be greatly rewarded if this book proves to be of any assistance in improving existing scarcity of textbooks on sediment transport by turbulent flow.

I express my deep sense of indebtedness to *Pawel Rowinski*, Institute of Geophysics, Polish Academy of Sciences, Warsaw, Poland, who proposed and inspired me to write this book in his capacity as the Editor-in-Chief of the Springer book series: *Geoplanet: Earth and Planetary Sciences*. He was an endless source of help and encouragement. I heartily thank *Oscar Castro-Orgaz*, University of Cordoba, Spain for reviewing the manuscript at various stages in its development. I also thank *Walter Hans Graf*, Laboratoire de Recherches Hydrauliques, École Polytechnique Fédérale, Lausanne, Switzerland for his suggestions at the final stage of

the preparation of manuscript. Comments from *Pawel*, *Oscar* and *Walter* are extremely helpful to bring the manuscript to its final stage. Further, I am thankful to my graduate student *Sk Zeeshan Ali* for checking the manuscript thoroughly. However, I of course am solely responsible if there remain any errors and lack of clarity. Readers are however invited to communicate with me by giving suggestions on how the book can be improved in forthcoming editions. E-mails can be sent to me at *sdey@iitkgp.ac.in*

This work would not have been possible without the constant encouragement and support of my parents, *Kana Dey* (mother) and *Bimalendu Dey* (father), while pursuing my school level, undergraduate, and graduate education; and of my advisors of doctoral research, *Sujit K. Bose*, (former Professor) S. N. Bose National Centre for Basic Sciences, Kolkata, India, and *Ghandikota L. N. Sastry*, (former Professor) Indian Institute of Technology, Kharagpur, India, who most inspired and educated me.

The love, support, and encouragement of my wife *Swastika*, son *Sibasish*, and daughter *Sagarika* have sustained me in this work, as in every part of my life. Every human being owes a great deal to their friends and I am no exception. I treasure my close association with all my friends for their support, cooperation, and sincere help in various ways.

March 2014, Kharagpur

Subhasish Dey

Contents

1	Introduction	1
1.1	General	1
1.2	Scope of this Book	3
1.3	Coverage of this Book	3
1.4	Physical Properties of Fluid and Sediment	4
1.4.1	Mass Densities of Fluid and Sediment	4
1.4.2	Specific Weights of Fluid and Sediment	5
1.4.3	Relative Densities of Fluid and Sediment	5
1.4.4	Viscosity of Fluid	6
1.4.5	Size of a Sediment Particle	7
1.4.6	Shape of a Sediment Particle	9
1.5	Properties of Sediment Mixture	10
1.5.1	Size Distribution	10
1.5.2	Porosity, Void Ratio, Dry Mass Density, and Dry Specific Weight	12
1.5.3	Angle of Repose	13
1.6	Properties of Fluid and Suspended Sediment Mixture	14
1.7	Terminal Fall Velocity of Sediment in Fluid	16
1.7.1	Terminal Fall Velocity of a Spherical Particle	16
1.7.2	Terminal Fall Velocity of Sediment Particles	18
1.8	Examples	21
	References	26
2	Hydrodynamic Principles	29
2.1	General	29
2.2	Rates of Deformation	32
2.3	Conservation of Mass	35
2.3.1	Continuity Equation in Three Dimensions	37
2.3.2	Continuity Equation for Open-Channel Flow	39
2.4	Conservation of Momentum	41
2.4.1	Momentum Equation in Three Dimensions	43
2.4.2	Momentum Equation for Open-Channel Flow	48

2.5	Conservation of Energy	54
2.5.1	Energy Equation for Open-Channel Flow	56
2.6	The Boundary Layer	65
2.6.1	Characteristics of Boundary Layer	66
2.6.2	von Kármán Momentum Integral Equation	69
2.7	Flow in Curved Channels	74
2.7.1	Superelevation in Curved Channels	77
2.7.2	Velocity Distributions in Curved Channels	77
2.7.3	Bed Shear Stress Distribution in Curved Channels	80
2.8	Hydrodynamic Drag and Lift on a Particle	81
2.8.1	The Drag	81
2.8.2	The Lift	84
2.9	Appendix	85
2.9.1	Navier–Stokes and Continuity Equations in a Cylindrical Polar Coordinate System	85
2.9.2	Navier–Stokes and Continuity Equations in a Spherical Polar Coordinate System	86
2.10	Examples	87
	References	93
3	Turbulence in Open-Channel Flows	95
3.1	General	95
3.2	Decomposition and Averaging Procedure	96
3.3	Continuity Equation	98
3.4	Equation of Motion (Reynolds Equations)	99
3.4.1	Shear Stress in Steady-Uniform Flow in an Open Channel	101
3.5	Classical Turbulence Theories	103
3.5.1	Prandtl’s Mixing Length Theory	103
3.5.2	Similarity Hypothesis of von Kármán	106
3.6	Classification of Flow Field in Open Channels	106
3.7	Velocity Distribution	108
3.7.1	The Linear Law in Viscous Sublayer	109
3.7.2	The Logarithmic Law in Turbulent Wall Shear Layer	109
3.7.3	Law in Buffer Layer	115
3.7.4	Log-Wake Law and Velocity Defect Law	116
3.8	Turbulence Intensity	118
3.9	Bed Shear Stress	119
3.9.1	Bed Shear Stress from Bed Slope	120
3.9.2	Bed Shear Stress from Velocity Distribution	120
3.9.3	Bed Shear Stress from Average Velocity	121
3.9.4	Bed Shear Stress from Reynolds Shear Stress Distribution	122

3.9.5	Bed Shear Stress from Turbulent Kinetic Energy Distribution	123
3.9.6	Bed Shear Stress from Spectral Density Function.	124
3.9.7	Bed Shear Stress from Vertical Reynolds Normal Stress Distribution	124
3.9.8	Bed Shear Stress and Reynolds Shear Stress for Unsteady-Nonuniform Flow: Dey–Lambert’s Approach.	125
3.10	Secondary Currents and Dip Phenomenon	131
3.10.1	Secondary Currents	131
3.10.2	Dip Phenomenon	133
3.11	Isotropic Turbulence Theory	137
3.11.1	Energy Cascade Process	137
3.11.2	Integral Scale	137
3.11.3	Kolmogorov Hypotheses	139
3.11.4	Taylor Micro-Scale	142
3.11.5	Transformation of Length Scale to Wave Number	143
3.11.6	Spectrum Function	143
3.12	Anisotropy in Turbulence	146
3.13	Higher-Order Correlations	148
3.14	Turbulent Kinetic Energy Flux	150
3.15	Turbulent Kinetic Energy Budget	151
3.16	Concept of Burst	155
3.16.1	Coherent Structures and Burst	156
3.16.2	Quadrant Analysis	158
3.17	Probability Distributions of Turbulence	162
3.17.1	Bose–Dey Universal Probability Theory	162
3.18	Double-Averaging Concept	172
3.19	Example	180
	References	183
4	Sediment Threshold	189
4.1	General	189
4.2	Definition of Sediment Threshold	190
4.3	Threshold Velocity Concept	191
4.3.1	Yang’s Threshold Velocity Model	194
4.4	Lift Force Concept	196
4.5	Threshold Bed Shear Stress Concept	198
4.5.1	Empirical Equations	198
4.5.2	Semitheoretical Analyses	199
4.5.3	Threshold Bed Shear Stress on Sloping Beds	224
4.6	Probabilistic Concept of Entrainment	230
4.6.1	Gessler’s Approach	231
4.6.2	Grass’s Approach	232

4.6.3	Wu and Chou's Approach	233
4.6.4	Other Investigations	238
4.7	Turbulence-Induced Entrainment Concept	239
4.8	Threshold of Nonuniform Sediment Motion	243
4.9	Stable Channel Design	245
4.9.1	Straight Trapezoidal Channels	245
4.9.2	Stable-Ideal Section of a Threshold Channel	246
4.10	Examples.	251
	References	254
5	Bed-Load Transport	261
5.1	General	261
5.2	Definition of Bed-Load Transport.	263
5.3	Bed Shear Stress Concept for Bed-Load Transport	264
5.3.1	du Boys' Approach.	264
5.3.2	du Boys Type Equations	266
5.3.3	Other Empirical Relationships Involving Bed Shear Stress	270
5.4	Discharge Concept for Bed-Load Transport	272
5.5	Velocity Concept for Bed-Load Transport	272
5.6	Bedform Concept for Bed-Load Transport.	273
5.7	Probabilistic Concept for Bed-Load Transport	274
5.7.1	Einstein's Approach	274
5.7.2	Empirical Refinement of Einstein Formula	280
5.7.3	Modified Einstein's Approach	281
5.7.4	Engelund and Fredsøe's Approach	283
5.8	Deterministic Concept for Bed-Load Transport	285
5.8.1	Bagnold's Approach	285
5.8.2	Yalin's Approach	289
5.9	Equal Mobility Concept for Bed-Load Transport	292
5.10	Sediment Pickup Function	292
5.11	Saltation	294
5.11.1	Characteristics of Saltation	294
5.11.2	Particle Trajectory and Characteristic Parameters (van Rijn's Approach).	295
5.12	Fractional Bed Load of Nonuniform Sediments	299
5.13	Sediment Sorting and Streambed Armoring	303
5.14	Sediment Entrainment Probability to Bed Load	305
5.15	Effects of Bed Load on Velocity Distribution	309
5.16	Effects of Bed Load on Length Scales of Turbulence	312
5.17	Effects of Bed Load on von Kármán Constant κ	315
5.18	Examples.	317
	References	322

6	Suspended-Load Transport	327
6.1	General	327
6.2	Diffusion Concept	328
6.2.1	Background	328
6.2.2	Generalized Advection–Diffusion Equation of Suspended Sediment Motion	329
6.2.3	Governing Equation of Vertical Distribution of Sediment Concentration.	333
6.2.4	Distribution of Sediment Concentration.	336
6.2.5	Stratification Effects on Concentration Distribution	352
6.2.6	Nonequilibrium Sediment Concentration Distribution	354
6.2.7	Vertical Distribution of Sediment Concentration Due to Nonuniform Streamwise Variation of Concentration.	356
6.2.8	Reference Level and Reference Concentration	359
6.2.9	Suspended Load by Diffusion Approach	362
6.3	Energy Concept	373
6.3.1	Velikanov’s Approach.	373
6.3.2	Bagnold’s Approach	377
6.3.3	Wu et al.’s Approach	379
6.4	Threshold Condition for Sediment Suspension	380
6.4.1	Cheng and Chiew’s Probabilistic Approach	381
6.4.2	Bose and Dey’s Probabilistic Approach.	382
6.5	Effects of Suspended Load on Bed-Load Transport	386
6.6	Effects of Suspended Load on Velocity Distribution.	387
6.6.1	Einstein and Chien’s Contribution	388
6.6.2	Umeyama and Gerritsen’s Contribution.	389
6.6.3	Castro-Organ et al.’s Contribution	389
6.7	Effects of Suspended Load on von Kármán Constant κ	394
6.8	Effects of Sediment Suspension on Turbulence Characteristics	397
6.8.1	Effects on Turbulent Stresses.	397
6.8.2	Response of Turbulent Bursting to Sediment Suspension.	399
6.9	Wash Load	402
6.10	Examples.	404
	References	410
7	Total-Load Transport	417
7.1	General	417
7.2	Indirect Approach.	418
7.2.1	Einstein’s Approach	418

7.2.2	Modified Einstein Procedure	419
7.2.3	Bagnold's Approach	424
7.2.4	Chang et al.'s Approach	425
7.3	Direct Approach	425
7.3.1	Laursen's Approach	425
7.3.2	Bishop et al.'s Approach	426
7.3.3	Engelund and Hansen's Approach	427
7.3.4	Graf and Acaroglu's Approach	429
7.3.5	Ackers and White's Approach	430
7.3.6	Yang's Approach	431
7.3.7	Brownlie's Approach	432
7.3.8	Karim and Kennedy's Approach	433
7.3.9	Molinas and Wu's Approach	435
7.3.10	Yang and Lim's Approach	435
7.3.11	Sinnakaudan et al.'s Approach	436
7.4	Total-Load Transport of Nonuniform Sediments	436
7.5	Examples	437
	References	451
8	Bedforms	453
8.1	General	453
8.2	Bedforms	454
8.2.1	Ripples	454
8.2.2	Dunes	458
8.2.3	Transition and Plane Bed	465
8.2.4	Antidunes	465
8.2.5	Chutes and Pools	466
8.3	Bars	467
8.4	Prediction of Bedforms	468
8.5	Mathematical Developments	474
8.5.1	Exner's Model	474
8.5.2	Kinematic Model	476
8.5.3	Potential Flow Model	480
8.5.4	Bose–Dey Instability Theory	491
8.6	Bed Features in Gravel-Bed Streams	505
8.7	Resistance to Flow Due to Bedforms	508
8.7.1	Einstein and Barbarossa's Method	511
8.7.2	Engelund's Method	512
8.7.3	Karim and Kennedy's Method	514
8.7.4	van Rijn's Method	515
8.7.5	Nelson and Smith's Method	516
8.7.6	Wright and Parker's Method	517
8.8	Examples	519
	References	525

9	Fluvial Processes: Meandering and Braiding	529
9.1	General	529
9.2	Meandering Rivers	534
9.2.1	Meander Planform Characteristics	539
9.2.2	Concepts of Meandering	539
9.3	Mathematical Modeling of Meandering Rivers	542
9.3.1	Ikeda and Nishimura's Model	542
9.3.2	Odgaard's Model	549
9.4	Braided Rivers	555
9.4.1	Mechanism of Braid Formation	556
	References	560
10	Scour	563
10.1	General	563
10.2	Scour Within Channel Contractions	564
10.2.1	Laursen's Model	565
10.2.2	Dey and Raikar's Model	567
10.2.3	Maximum Scour Depth Prediction	569
10.2.4	Other Scour Depth Predictors	571
10.3	Scour Downstream of Structures	573
10.3.1	Scour Below Drop Structures	573
10.3.2	Scour Downstream of Grade-Control Structures	576
10.3.3	Scour Downstream of Bed Sills	576
10.3.4	Scour Due to Horizontal Jets Issuing from a Gate Opening	579
10.4	Scour Below Horizontal Pipelines	581
10.4.1	Estimation of Gap Discharge	584
10.4.2	Scour Depth Estimation	586
10.5	Scour at Bridge Piers	589
10.5.1	Kinematic Model of Horseshoe Vortex	592
10.5.2	Scour Depth Prediction	594
10.6	Scour at Bridge Abutments	602
10.6.1	Scour Depth Prediction	605
10.7	Scour Countermeasures	608
10.8	Appendix	612
10.8.1	Submerged Wall Jets	612
10.8.2	Computation of Scour Due to Submerged Wall Jets	617
10.9	Examples	619
	References	635

11 Dimensional Analysis and Similitude	641
11.1 General	641
11.2 Dimensional Analysis	643
11.2.1 Synthesis of Experimental Data	643
11.2.2 Dimensional System	645
11.2.3 Buckingham Π Theorem	646
11.2.4 Steps Involved in Analysis by Π Theorem	648
11.3 Similitude	651
11.3.1 Concept of Dynamic Similitude for Model Studies. . .	651
11.3.2 Immobile Bed Model Studies.	656
11.3.3 Mobile Bed Model Studies	658
11.4 Examples.	661
References	667
About the Author	669
Author Index	671
Subject Index	681

Chapter 1

Introduction

1.1 General

The term *fluvial* is commonly used in geophysics and earth sciences to refer to the processes associated with rivers or streams, and the erosions or deposits and morphology created by them. The subject *hydrodynamics* under the curriculum of civil engineering and environmental engineering becomes more diverse including the mechanism of the processes associated with fluvial systems. Fluvial processes comprise the sediment transport and aggradations or degradations of the riverbeds. The flow over a bed formed by the loose sediment exerts a shear stress on the bed. If the stabilizing resistance to the sediment particles is lower than the bed shear stress exerted, the sediment can be mobilized. For each particle size, there is a specific velocity or bed shear stress at which the particles on the bed surface start to move, called the *threshold velocity* or *threshold shear stress*, respectively. Sediment transport by the stream flows can occur in different modes. Sediment in rivers is transported as *bed load* (coarser fractions which move close to the bed) and/or *suspended load* (finer fractions carried by the flow). There is also a component carried as *wash load* that remains near the free surface of flow. Little is known specifically about the wash load where it comes from or where it goes. Further, during the sediment transport, the riverbed takes different undular features, called the *bedforms*. All these related to sediment transport make the flow in a river rather intricate, as compared to that in a rigid-bed channel. Further, the flow in rivers is locally modified by the embedded obstacles, such as bridge piers, abutments, and pipelines and the hydraulic structures, such as barrages, drops, and sills. The modified flow has enormous erosive potential causing a *local scour* near the obstacles and the hydraulic structures.

A natural river continually picks up sediment from and drops sediment on its bed throughout its course. Where the river flows with high velocity, more sediment is picked up than dropped. In contrast, where the flow is tranquil, more sediment is dropped than picked up. These processes including the formations of bedforms, such as ripples, dunes, and antidunes, determine the complex morphology of a river. In a typical river, the largest carried sediment is of sand and gravel size, but a

larger flood can carry cobbles and even boulders. The amount of sediment carried by a large river is enormous. For instance, the Mississippi in USA annually carries 406×10^6 tons of sediment to the sea, the Hwang Ho in China 796×10^6 tons and the Po in Italy 67×10^6 tons.

The origin of the development of *fluvial hydrodynamics* dates back to the distant past, as people faced the problems due to erosion, sedimentation, and floods. The ancient civilizations particularly in the valleys of Indus, Tigris, Euphrates, Nile, and Hwang Ho rivers used the unlined canals for irrigation. Historical records suggest that about six thousand years ago, marginal embankments were built along the Hwang Ho in China; irrigation canals and flood control structures constructed in Mesopotamia; and one thousand years afterward a masonry dam built across the Nile in Egypt. In India, more than five thousand years ago, the mechanics of sediment transport by stream flows was explained by *sage Vashistha*. During the Renaissance era, famous Italian painter and scientist-cum-engineer *Leonardo da Vinci* made the first empirical studies of streams and their velocity distributions. His notebooks are full of observations that he made on rivers; and they reveal that he understood the principles of sedimentation and erosion. Since then, scientists and engineers have performed a large number of studies on rivers.

The subject *fluvial hydrodynamics*, being important in the fields of civil engineering, environmental engineering, sedimentary geology, and earth sciences, is most often used to know whether erosion or deposition of sediment or even transport of sediment can occur. If so, what are the magnitude of erosion or deposition and the duration or transport rate? Even though enormous efforts have been made by scientists and engineers to resolve various problems related to sediment transport, due to inherent complexities involved in sediment transport processes and difficulties in taking accurate measurements, inadequate landmark breakthroughs have so far been achieved on a sizable number of key problems. As such, the knowledge on such complex problems is still limited to the perceptual state. Therefore, the research on sediment transport should be directed in solving problems, that often arise in practice involving inherent complex phenomena.

Knowledge of sediment transport can be applied extensively in civil engineering such as to plan the extended life of a dam forming a reservoir. Sediment carried by a river deposits into a reservoir formed by a dam developing a reservoir delta. The delta grows with time filling the reservoir to reduce its capacity, and eventually, either the reservoir needs to be dredged or the dam needs to be abandoned. Also an adequate knowledge of the mechanics of sediment transport in a built environment is important for civil and hydraulic engineers. Flow in culverts, over spillways, below pipelines, and around bridge piers/abutments creates scour, which can damage the environment and expose the foundations of the structures being detrimental to them.

Sediment transport, being applied in solving various environmental engineering problems, is important in providing habitat for fish in rivers and other instream organisms, sustaining a hygienic stream ecosystem. On the other hand, when suspended load of sediment is substantial due to human activities, it can cause environmental hazards including the filling up of the channels by siltation.

Geologists, on the other hand, seek inverse solutions for sediment transport relationships to get an idea on the flow depth, velocity, and direction, from the characteristics of the sedimentary rocks and new deposits of sediment particles.

1.2 Scope of this Book

The aim of the science of fluvial hydrodynamics is to understand the behavior of sediment transport in natural streams and to provide a basis for predicting its responses to natural or man-made disturbances. However, in general, the basic problem of flow over a sediment bed can be stated in a rather deceptively simple way: Given the sediment characteristics, flow rate and bed slope; what are the probable flow depth and the sediment transport rate? Even for the simplest case of a two-dimensional flow over a flat bed formed by a uniform sediment size, a general solution can only be presented with estimates involving high degree of uncertainty, as much of the intricacy lies on velocity or turbulent stress distribution over a sediment bed. Advances in measurement technology and progress in understanding of the turbulence phenomena in shear flow within near-bed flow region inspire recent research trend that may append to a more satisfactory response to the basic questions. Moreover, this topic has attracted the attention not only of engineers but also of earth scientists, with potentially constructive results and contributions being published in leading journals, reports, and monographs not essentially familiar to the hydraulic engineering communities.

The objective of this book is therefore to develop a sound qualitative and quantitative basis of knowledge of the subject. This book is rather different from a typical engineering treatment of open-channel flow in its larger emphasis on fluvial streams and their interactions with structures, such as, bridge piers and abutments, bed sills. It also differs from a general earth science-oriented treatment in its extended emphasis on the analyses based on the physics of turbulent flow and its customary applications developed for engineering practices. To be useful, a special attempt is made in this book to include the new important research results on sediment transport achieved over the past years. It seems to be a demand, as over decades, there have been inadequate efforts in incorporating of new developments that help to predict sediment transport processes more accurately and are also helpful in field situations not so far included in the traditional textbooks.

1.3 Coverage of this Book

The topics of this book include hydrodynamic principles and turbulence characteristics related to open-channel flow, mechanics of sediment transport, and local scour phenomena including application examples in fluvial hydrodynamics. It is organized into eleven chapters. They are as follows:

This chapter provides an introduction to the fluvial hydrodynamics, scope and outline of this book, and the properties of fluid and sediment. Chapter 2 introduces the fundamental theories of hydrodynamics in the context of open-channel flow. Chapter 3 presents the turbulence characteristics in flow over a sediment bed. It includes most of the modern development of turbulent flow, such as bursting phenomenon, double averaging of heterogeneous flow over gravel-beds. Chapter 4 is devoted to the theories of the initiation of sediment motion. It encompasses different concepts of sediment threshold and their theoretical and empirical developments. Chapter 5 describes the concepts, theories, and empirical formulations of bed load transport and saltation, while Chaps. 6 and 7 illustrate those of suspended and total load transports, respectively. Chapter 8 demonstrates different types of bedforms and their mechanism of formation and resistant to flow. Chapter 9 describes the natural fluvial processes toward meanderings and braiding. Chapter 10 outlines comprehensive information on local scour within channel contractions, downstream of structures, below horizontal pipelines, at bridge piers and abutments, and scour countermeasures. Chapter 11 is designed to deal with the issue to describe dimensional analysis, modeling, and similitude of sediment transport and scour problems.

The general feature of all the chapters is shaped by the fundamentals, such as the definitions of the phenomena and the involved parameters as well as a series of methodologies, starting from the earlier developments and ending to the latest ones.

In the end of each chapter, bibliographical references are given.

1.4 Physical Properties of Fluid and Sediment

Following properties of fluid and sediment are of general importance to study the fluvial hydrodynamics. For the convenience, typical values, SI units, and dimensions in MLT system (also see Chap. 11) are given.

1.4.1 Mass Densities of Fluid and Sediment

The *mass density* ρ of a fluid is defined as its mass per unit volume. The mass density at a point is determined by considering the mass dm of a small volume dV surrounding the point. As dV becomes a magnitude ε^3 , where ε is the small linear distance but larger than the mean distance between molecules, the mass density at a point is given by

$$\rho = \lim_{dV \rightarrow \varepsilon^3} \frac{dm}{dV} \quad (1.1)$$

Similarly, the *mass density* ρ_s of a sediment sample is defined as its mass per unit solid volume (without void). In case of a single particle, the mass and the volume refer to those of that particle. However, the *submerged density* of a sediment sample denoted by $\Delta\rho$ is $\rho_s - \rho$.

Its unit is kg m^{-3} and dimension ML^{-3} . Typical value of ρ for water is 10^3 kg m^{-3} at standard atmospheric pressure of $1.013 \times 10^5 \text{ Pa}$ (or 0.76 m height of mercury in a barometer) and temperature of 4°C , while typical value of ρ_s for a quartz sand sample is $2.65 \times 10^3 \text{ kg m}^{-3}$. Mass density of water varies with temperature. The dependency of the mass density of water on temperature is given by $\rho = 10^3 - 6.5 \times 10^{-3}(t - 4) \text{ kg m}^{-3}$, where t is the temperature in $^\circ\text{C}$.

1.4.2 Specific Weights of Fluid and Sediment

The *specific weight* γ of a fluid is defined as its weight per unit volume. Since weight is dependent on acceleration due to gravity g , the specific weight of a fluid varies from place to place. It is therefore related to the mass density as

$$\gamma = \rho g \quad (1.2)$$

Similarly, the *specific weight* γ_s of a sediment sample is defined as its weight per unit solid volume. In case of a single particle, the weight and the volume refer to those of that particle. However, the *submerged specific weight* of a sediment sample denoted by $\Delta\gamma$ is $\gamma_s - \gamma$.

Its unit is N m^{-3} and dimension $\text{ML}^{-2} \text{T}^{-2}$. Typical value of γ for water is $9.81 \times 10^3 \text{ N m}^{-3}$ at a place where g is 9.81 m s^{-2} , while typical value of γ_s for a quartz sand sample is $2.65 \times 9.81 \times 10^3 \text{ N m}^{-3}$.

1.4.3 Relative Densities of Fluid and Sediment

The *relative density* s_f of a fluid is defined as the ratio of the mass density of fluid to the mass density of water at 4°C .

Similarly, the *relative density* s of a sediment sample is defined as the ratio of the mass density of sediment to the mass density of water at 4°C . However, the *submerged relative density* of a sediment sample denoted by Δ is $s - s_f$.

The relative density has no unit being represented by a number. Its dimension is $\text{M}^0 \text{L}^0 \text{T}^0 (=1)$. Typical values of s_f for water and s for a quartz sand sample are 1 and 2.65, respectively.

1.4.4 Viscosity of Fluid

By definition, *fluid* is a substance that deforms continuously under the action of shear force, however, small it may be. Shear force within successive layers of fluid parallel to the boundary is the consequence of the fluid flow having differential velocities of the layers. The velocities of the layers increase away from the boundary, while the fluid particles in contact with the boundary have the same velocity as the boundary, called the *no-slip condition*. For the fluids obeying the *Newton's law of viscosity*, the shear stress τ being proportional to the velocity gradient therefore is given by

$$\tau = \mu \frac{du}{dz} \quad (1.3)$$

where μ is the *coefficient of dynamic viscosity* and u is the velocity in x -direction (that is the streamwise direction) at a normal distance z from the boundary.

Rearranging Eq. (1.3), the *coefficient of dynamic viscosity* (in short, also called *dynamic viscosity*) μ is defined as the shear stress (that is the shear force per unit area) required to drag one layer of fluid with a unit velocity past another layer at a unit distance apart. Its unit is Pa s and dimension $ML^{-1}T^{-1}$. Note that the dynamic viscosity is often measured in poise (P), which equals 0.1 Pa s. Typical value of μ for water is approximately 10^{-3} Pa s at 20 °C.

Note that the *laminar flow* (also called *viscous flow*) is represented by a series of parallel layers sliding over another without any exchange of mass between the layers. In turbulent flow, however, the mixing between the layers takes place, and the shear stress τ is given by

$$\tau = (\mu + \varepsilon_t \rho) \frac{d\bar{u}}{dz} \quad (1.4)$$

where ε_t is the *coefficient of eddy viscosity* or *turbulent diffusivity* and \bar{u} is the time-averaged velocity in x -direction at a normal distance z from the boundary. Details of turbulent diffusivity and its role are given in Chaps. 3 and 6.

Removing the mass term from the dynamic viscosity expression by dividing it by the mass density ρ of fluid, the *coefficient of kinematic viscosity* (in short, also called *kinematic viscosity*) ν is obtained. Hence, it is defined as the ratio of dynamic viscosity to mass density:

$$\nu = \frac{\mu}{\rho} \quad (1.5)$$

Its unit is $m^2 s^{-1}$ and dimension $L^2 T^{-1}$. Note that the kinematic viscosity is often measured in stokes (St), which equals $10^{-4} m^2 s^{-1}$. Typical value of ν for water is approximately $10^{-6} m^2 s^{-1}$ at 20 °C.

Viscosity is dependent on temperature, but independent of pressure. The dependency of kinematic viscosity on temperature of river water is given by $\nu = [1.14 - 3.1 \times 10^{-2}(t - 15) + 6.8 \times 10^{-4}(t - 15)^2] \times 10^{-6} \text{ m}^2 \text{ s}^{-1}$, where t is in $^{\circ}\text{C}$ (Julien 1998).

1.4.5 Size of a Sediment Particle

Particle size is the most important parameter to deal with sediment transport processes. The mode of sediment transport and the corresponding mechanism are partially dependent on the particle size to be transported. The size of a sediment particle can be represented by a number of ways: *Nominal diameter*, *area diameter*, *sieve diameter*, *fall diameter*, and *sedimentation diameter*. The SI units are used to represent the sediment size in m. However, the sediment size is also expressed in mm, micron ($1 \mu\text{m} = 10^{-3} \text{ mm}$) and logarithmic units Φ .

Nominal diameter, d_n : It is the diameter of a sphere having the same volume as that of a given sediment particle:

$$d_n = \left(\frac{6V}{\pi} \right)^{1/3} \quad (1.6)$$

where V is the volume of sediment particle. The approximate volume can be estimated considering a sediment particle as an ellipsoid as $V \approx \pi a_1 a_2 a_3 / 6$, where a_1 , a_2 , and a_3 are the longest, intermediate, and shortest lengths along mutually perpendicular axes of a Cartesian coordinate system.

Area diameter, d_a : It is the diameter of a sphere having the same surface area as that of a given sediment particle:

$$d_a = \left(\frac{S}{\pi} \right)^{0.5} \quad (1.7)$$

where S is the total surface area of sediment particle. The area diameter is usually used to characterize the flat-shaped particles (Mehta et al. 1980; Dey 2003).

Sieve diameter, d : It is the diameter of a sphere equaling the side length of a square sieve opening through which a given sediment particle can just pass. For sediment sizes (0.2–20 mm) of natural streambeds, sieve diameter is approximately equaling $0.9d_n$ (US Interagency Committee 1957).

Fall diameter, d_f : It is the diameter of a sphere having a relative density of 2.65 and a same terminal fall velocity as that of a given sediment particle in quiescent, pure water at 4°C .

Sedimentation diameter, d_w : It is the diameter of a sphere having equal terminal fall velocity and relative density as those of a given sediment particle in the same sedimentation fluid under the same atmospheric pressure and temperature.

Table 1.1 Grade scale of sediment size

Class	Size range	
	mm	Φ units
Very large boulder	$4,000 \geq d > 2,000$	
Large boulder	$2,000 \geq d > 1,000$	
Medium boulder	$1,000 \geq d > 500$	
Small boulder	$500 \geq d > 250$	$-9 \leq \Phi < -8$
Large cobble	$250 \geq d > 130$	$-8 \leq \Phi < -7$
Small cobble	$130 \geq d > 64$	$-7 \leq \Phi < -6$
Very coarse gravel	$64 \geq d > 32$	$-6 \leq \Phi < -5$
Coarse gravel	$32 \geq d > 16$	$-5 \leq \Phi < -4$
Medium gravel	$16 \geq d > 8$	$-4 \leq \Phi < -3$
Fine gravel	$8 \geq d > 4$	$-3 \leq \Phi < -2$
Very fine gravel	$4 \geq d > 2$	$-2 \leq \Phi < -1$
Very coarse sand	$2 \geq d > 1$	$-1 \leq \Phi < 0$
Coarse sand	$1 \geq d > 0.5$	$0 \leq \Phi < 1$
Medium sand	$0.5 \geq d > 0.25$	$1 \leq \Phi < 2$
Fine sand	$0.25 \geq d > 0.125$	$2 \leq \Phi < 3$
Very fine sand	$0.125 \geq d > 0.062$	$3 \leq \Phi < 4$
Coarse silt	$0.062 \geq d > 0.031$	$4 \leq \Phi < 5$
Medium silt	$0.031 \geq d > 0.016$	$5 \leq \Phi < 6$
Fine silt	$0.016 \geq d > 8 \times 10^{-3}$	$6 \leq \Phi < 7$
Very fine silt	$8 \times 10^{-3} \geq d > 4 \times 10^{-3}$	$7 \leq \Phi < 8$
Coarse clay	$4 \times 10^{-3} \geq d > 2 \times 10^{-3}$	$8 \leq \Phi < 9$
Medium clay	$2 \times 10^{-3} \geq d > 10^{-3}$	
Fine clay	$10^{-3} \geq d > 5 \times 10^{-4}$	
Very fine clay	$5 \times 10^{-4} \geq d > 2.4 \times 10^{-4}$	

Φ units: In order to facilitate the sediment size representation by a nondimensional number, another standard way to specify particle sizes is the Φ scale, in which $d = 2^{-\Phi}$ (Krumbein and Sloss 1963). Taking the logarithmic of both sides, Φ units for given sediment sizes are determined as

$$\Phi = -\log_2 d = -\frac{\log_{10} d}{\log_{10} 2} \quad (1.8)$$

where d is in mm. For example, $\Phi(d = 4 \text{ mm}) = -2$. From Eq. (1.8), it implies that $\Phi(d = 1 \text{ mm}) = 0$.

Table 1.1 furnishes the sediment size classification based on grade scale, as recommended by the subcommittee on sediment terminology of the AGU (Lane 1947), which is widely used by the hydraulicians and geologists.

1.4.6 Shape of a Sediment Particle

The shape of a given sediment particle refers to the general geometric form apart from its size and material composition. In sediment analysis, one of the most relevant shape parameters is *sphericity*, S_c . According to Wadell (1932), the sphericity is defined as the ratio of the surface area of a sphere of the same volume as that of a given sediment particle to the actual surface area of the particle. The sphericity basically characterizes the motion of a settling particle relative to the fluid. As the actual surface area of a small particle is rather difficult to obtain, Wadell redefined the sphericity as

$$S_c = \left(\frac{V}{V_c} \right)^{1/3} \quad (1.9)$$

where V_c is the volume of circumscribing sphere. However, the sphericity can also be approximated as $S_c \approx d_n/a_1$. Also, Krumbein (1941) expressed the sphericity as

$$S_c = \left(\frac{a_2 a_3}{a_1^2} \right)^{1/3} \quad (1.10)$$

On the other hand, *roundness* is defined as the average radius of curvature of several edges of a given sediment particle to the radius of a circle inscribed in the maximum projected area of the particle. Unlike sphericity, roundness has been found to be a trivial parameter in the hydrodynamics of sediment transport.

Importantly, the irregular-shaped particles are usually defined by the *Corey shape factor* S_p (Vanoni 1977) as

$$S_p = \frac{a_3}{(a_1 a_2)^{0.5}} \quad (1.11)$$

The Corey shape factor which is always less than unity is typically 0.7 for naturally worn particles. The main drawback of using Corey shape factor is that it does not take into account the distribution of the surface area and the volume of the particle. For example, a cube and a sphere have the same shape factor S_p being unity. Nevertheless, the hydrodynamic characteristics, such as drag and lift forces, induced on a cubical particle and a spherical particle are different. To overcome this difficulty, Alger and Simons (1968) proposed a *shape parameter* S_{sp} that is given by

$$S_{sp} = S_p \frac{d_a}{d_n} \quad (1.12)$$

According to Heywood (1938), another shape description can be given as *volume coefficient* k_v , which is the ratio of the volume of a given sediment particle to the

cube of the diameter D of circle containing the projected area of the particle onto the plane parallel to a_1a_2 -plane. Hence, $k_v = V/D^3$. For natural sediments, k_v is approximately 0.3. He also defined *surface coefficient* k_c as $k_c = S/D^2$

1.5 Properties of Sediment Mixture

1.5.1 Size Distribution

The fluvial sediment is usually composed of mixture of particles of various sizes. The size distribution of a sediment mixture can be measured by the sieve analysis. Typical results of the sieve analysis of adequate quantity of representative sediment sample are presented in the form of a *frequency histogram* (or a *frequency curve*) (Fig. 1.1a) and a *cumulative frequency curve* (Fig. 1.1b). The cumulative frequency curve is also commonly known as *particle size distribution curve*. In the frequency curve (Fig. 1.1a), the abscissa represents the particle size d class intervals in logarithmic scale and the ordinate the percentage concentration (by weight) of the total sample contained in the corresponding intervals of the particle size class. On the other hand, the particle size distribution curve represents the variation of the percentage (by weight) of sediment finer (in the ordinate) than a given sediment size d (in the abscissa using logarithmic scale) in the total sample, as shown in (Fig. 1.1b).

Very often, the size distribution of natural well-graded sediments follows the lognormal probability curve when plotted. The probability distribution $f(d)$ and the cumulative distribution $F(d)$ can be approximated by the lognormal and the error function distributions, respectively, as given by the following expressions [see Fredsøe and Deigaard (1992)]:

$$\begin{aligned} f(d) &= \frac{1}{d\sqrt{2\pi} \ln \sigma_g} \exp \left\{ -\frac{1}{2} \left[\frac{\ln (d/d_{50})}{\ln \sigma_g} \right]^2 \right\}, \\ F(d) &= \frac{1}{2} \left\{ 1 + \operatorname{erf} \left[\frac{1}{\sqrt{2}} \cdot \frac{\ln (d/d_{50})}{\ln \sigma_g} \right] \right\} \end{aligned} \quad (1.13)$$

where σ_g is the geometric standard deviation of particle size distribution and d_{50} is the median particle diameter or 50 % finer particle size, which can be obtained from the particle size distribution curve (Fig. 1.1b). Besides the lognormal distribution, natural sediments may also have a bimodal distribution that displays two distinct peaks in a frequency distribution curve characterizing each peak as the mode of the distribution. Nonuniform sediments with a distinctive finer and coarser size of sediment mixture can have bimodal distribution.

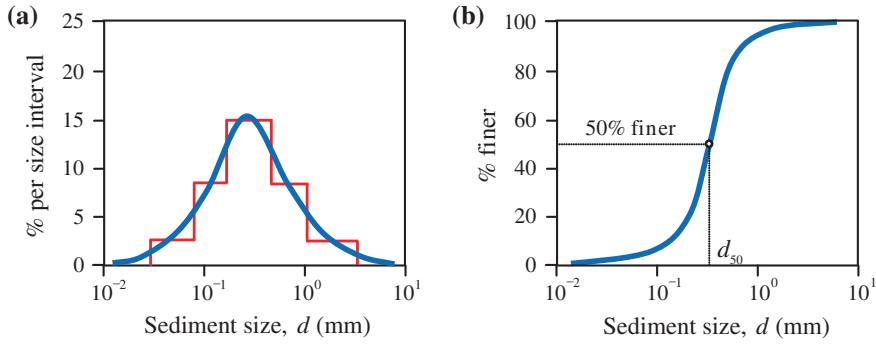


Fig. 1.1 **a** Typical frequency histogram and frequency distribution curve and **b** typical cumulative frequency distribution or particle size distribution curve

The *geometric standard deviation* σ_g is an important parameter used to determine the nonuniformity of a sediment mixture. It is expressed as

$$\sigma_g = \frac{d_{84.1}}{d_{50}} = \frac{d_{50}}{d_{15.9}} = \left(\frac{d_{84.1}}{d_{15.9}} \right)^{0.5} \quad (1.14)$$

where $d_{84.1}$ and $d_{15.9}$ are 84.1 and 15.9 % finer diameters, respectively. For a given particle size distribution, if $\sigma_g \leq 1.4$, then the sediment is considered to be uniform; otherwise, the sediment is nonuniform (Dey and Sarkar 2006). The *geometric mean size* d_g is the square root of the product of $d_{84.1}$ and $d_{15.9}$.

$$d_g = (d_{84.1}d_{15.9})^{0.5} \quad (1.15)$$

Apart from the geometric standard deviation, the *gradation coefficient* G is in use. It is given by

$$G = \frac{1}{2} \left(\frac{d_{84.1}}{d_{50}} + \frac{d_{50}}{d_{15.9}} \right) \quad (1.16)$$

In addition, Kramer (1935) proposed a *uniformity parameter* M that is defined as the ratio of the median sizes of the two portions in the particle size distribution curve separated by the median particle size d_{50} :

$$M = \frac{\sum_{i=0}^{i=50} p_i d_i}{\sum_{i=50}^{i=100} p_i d_i} \quad (1.17)$$

where i is the cumulative percentage of sediment finer than d_i and p_i is the fraction of each size class in percentage. Kramer's uniformity parameter $M = 1$ for uniform sediment and $M < 1$ for nonuniform sediment.

The relationship between d_i and Φ_i is therefore expressed as

$$\Phi_i = -\frac{\log_{10} d_i}{\log_{10} 2} \quad (1.18)$$

1.5.2 Porosity, Void Ratio, Dry Mass Density, and Dry Specific Weight

The *porosity* ρ_0 of a sediment mixture is defined as the volume of void per unit total volume. If the volume of void is V_v and the volume of solid is V_s , then the porosity is given by

$$\rho_0 = \frac{V_v}{V_v + V_s} \quad (1.19)$$

Komura (1963) gave an empirical relationship for the porosity of unconsolidated saturated sediment as

$$\rho_0 = 0.245 + \frac{0.14}{d_{50}^{0.21}} \quad (1.20)$$

where d_{50} is in mm. Using the laboratory experimental and field data, Wu and Wang (2006) modified Komura's relationship as

$$\rho_0 = 0.13 + \frac{0.21}{(0.002 + d_{50})^{0.21}} \quad (1.21)$$

The *void ratio* e of a sediment mixture is defined as the volume of void per unit volume of solid; and hence, it can be related with the porosity as

$$e = \frac{V_v}{V_s} = \frac{\rho_0}{1 - \rho_0} \quad (1.22)$$

The *dry mass density* ρ_d and the *dry specific weight* γ_d of a sediment mixture are defined as the mass and the weight of solid per unit total volume, respectively. They are expressed in terms of porosity as

$$\rho_d = \rho_s(1 - \rho_0), \quad \gamma_d = \gamma_s(1 - \rho_0) \quad (1.23)$$

1.5.3 Angle of Repose

The *angle of repose* ϕ (or more precisely, the *critical angle of repose*) is the steepest angle of descent of the slope with respect to the horizontal plane when the sediment particles submerged in water are on the verge of sliding on the sloping surface of a sediment heap. The angle of repose therefore corresponds to a so-called sediment avalanche. The angle of repose is approximately equal to the angle of internal friction at the contacts of the sediment particles. Hence, ϕ approximately equals $\arctan \mu_d$, where μ_d is the static Coulomb friction coefficient. Note that the force, in addition to inertia, opposing the motion of noncohesive sediments at contacts is friction. The friction coefficient μ_d is therefore described as the ability of a particle to resist motion (sliding) relative to its submerged gravity component normal to the sliding; it therefore represents the ratio of the tangential resistive force to the downward normal force.

In mechanics of sediment transport, the angle of repose is assumed to be equivalent to the pivoting angle ϕ of the superimposed particle resting over the bed particles at the point of contact P over which it can move (Fig. 1.2). It is evident that the superimposed particle can roll over either the points of contact of the valley formed by the two bed particles or the single point of contact of a bed particle, depending on the arrangement or the orientation of bed particles and according to the direction of superimposed particle tending to move. Importantly, the angle of repose varies significantly with the nonuniformity of sediments, while for uniform sediments, the values of ϕ lie in between 28 and 32°.

Zhang et al. (1989) proposed an empirical relationship for the angle of repose of noncohesive sediment with sediment size as

$$\phi = 32.5 + 1.27d_{50} \quad (1.24)$$

where ϕ is in deg and d_{50} in mm. Equation (1.24) is applicable for the sediment size range $0.2 \leq d_{50} \leq 4.4$ mm.

For a simple case of spherical particles, Fig. 1.2 clearly depicts that the angle of repose varies with the ratio of the size of superimposed spherical particle to that of bed particles over which it rests. Ippen and Eagleson (1955) gave an equation of angle of repose for spherical particles as

$$\tan \phi = 0.866 \left[\left(\frac{d}{k_s} \right)^2 + 2 \left(\frac{d}{k_s} \right) - \frac{1}{3} \right]^{-0.5} \quad (1.25)$$

where d is the sediment particle diameter and k_s is the bed particle size or bed roughness height. Li and Komar (1986) showed that the angle of repose decreases with an increase in d/k_s . The relationship, which is applicable for $0.3 < d/k_s < 3$, is

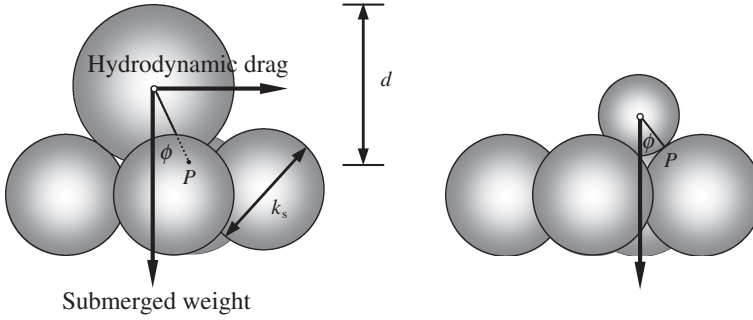


Fig. 1.2 Schematic of pivoting angles of superimposed sediment particles relative to bed particles

Table 1.2 Values α and β as proposed by Li and Komar (1986)

Shape	α	β
Sphere	51.3	0.33
Ellipsoidal gravels	31.9	0.36
Angular gravels	36.3	0.72 for $dk_s > 1$
	36.3	0.55 for $dk_s < 1$

$$\phi = \alpha \left(\frac{d}{k_s} \right)^{-\beta} \quad (1.26)$$

where α and β are coefficient and exponent dependent on the shape of the particles, respectively. Li and Komar (1986) determined the values of α and β for spheres, ellipsoidal, and angular gravels, as given in Table 1.2.

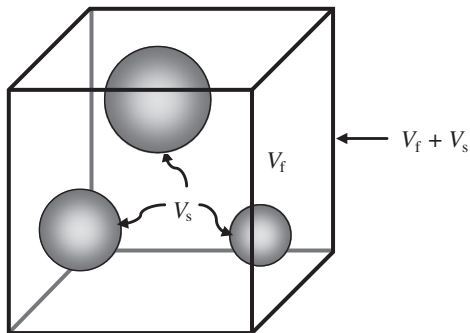
It is pertinent to mention that in natural conditions, the values of angle of repose vary to a wide range that it is not easy to determine in field situations.

1.6 Properties of Fluid and Suspended Sediment Mixture

Figure 1.3 shows a schematic of sediment suspension in fluid, called *fluid–sediment mixture*, consisting of a volume of sediment V_s and a volume of fluid V_f . Note that the volume of fluid here equals the volume of void, that is $V_f = V_v$. The *sediment concentration* C by volume is defined as

$$C = \frac{V_s}{V_f + V_s} \quad (1.27)$$

Fig. 1.3 Schematic of sediment suspension in fluid



On the other hand, the *sediment concentration* c by mass is defined as

$$c = \frac{\rho_s V_s}{\rho V_f + \rho_s V_s} = \frac{(\rho_s/\rho)C}{1 + [(\rho_s/\rho) - 1]C} \quad (1.28)$$

Equation (1.28) remains same for the sediment concentration by weight, since the equation is transformed to weight of the quantities by multiplying the numerator and the denominator with the same value of g . In case of water as a fluid, Eq. (1.28) becomes $c = sV_s/(V_f + sV_s) = sC/(1 + \Delta C)$, where $\Delta = s - 1$. Sediment concentration is usually expressed in parts per million (ppm) by mass or weight, that is $10^6 c$. However, sediment concentration is also expressed in mass per unit volume of concentration, $\rho_s C$, or in weight per unit volume of concentration, $\gamma_s C$. The *mass density of fluid-sediment mixture* ρ_m is expressed as

$$\rho_m = \rho + (\rho_s - \rho)C \quad (1.29)$$

The *specific weight of fluid-sediment mixture* γ_m is

$$\gamma_m = \gamma + (\gamma_s - \gamma)C = \rho_m g \quad (1.30)$$

The *kinematic viscosity of fluid-sediment mixture* v_m is

$$v_m = \frac{\mu_m}{\rho_m} \quad (1.31)$$

where μ_m is the dynamic viscosity of fluid-sediment mixture. Based on the experimental results for $0.2 \leq C \leq 0.6$, Bagnold (1954) formulated the dynamic viscosity of water-sediment mixture as

$$\mu_m = \mu \left[1 + \frac{1}{(0.74/C)^{1/3} - 1} \right] \left[1 + \frac{0.5}{(0.74/C)^{1/3} - 1} \right] \quad (1.32)$$

Here, μ is the dynamic viscosity of a clear water. Also, an empirical relationship for μ_m was given by Lee (1969) as

$$\mu_m = \mu(1 - C)^{-(2.5+1.9C+7.7C^2)} \quad (1.33)$$

1.7 Terminal Fall Velocity of Sediment in Fluid

1.7.1 Terminal Fall Velocity of a Spherical Particle

The gravitational fall velocity of sediment is one of the key parameters in sediment transport, especially when sediment suspension is the dominant process. It acts as a restoring force against turbulent entraining force acting on the particle. Knowledge on fall velocity of a particle is thus important. In sediment transport, although natural sediment is seldom spherical, the fall velocity of a rigid sphere is usually used as an approximation in predicting fall velocity of a sediment particle in natural streams.

In hydrodynamics, a particle falls at its terminal velocity if its velocity is constant due to the drag exerted by the fluid through which it falls. As a falling particle accelerates under the gravity, the drag force acting on the particle increases with an increase in velocity, causing the acceleration of the particle or in turn, the inertia force acting on the particle to reduce. At the point, the particle ceases to accelerate and continues falling at a constant velocity, called the *terminal fall velocity* or *settling velocity*. A free-falling particle therefore attains its terminal fall velocity w_s when the submerged gravity force F_G of the particle equals the upward drag force F_D , as shown in Fig. 1.4.

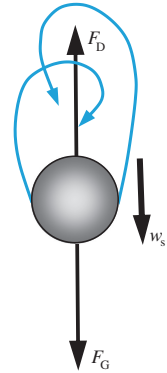
For a spherical particle falling with a terminal fall velocity w_s in a column of water, the following equation is thus obtained:

$$\underbrace{\Delta \rho g \frac{\pi}{6} d^3}_{F_G} = \underbrace{C_D \frac{\rho}{2} w_s^2 \frac{\pi}{4} d^2}_{F_D} \Rightarrow w_s = \left(\frac{4}{3} \cdot \frac{\Delta g d}{C_D} \right)^{0.5} \quad (1.34)$$

where Δ is $s - 1$, ρ is the mass density of water, d is the diameter of falling particle, and C_D is the drag coefficient.

Neglecting all inertia terms, Stokes (1851) analyzed the Navier–Stokes equations for laminar flow range of particle Reynolds number $R_e (= w_s d / \nu) < 1$ aided by

Fig. 1.4 Schematic of a sphere falling in a static fluid with a terminal fall velocity w_s



a stream function to derive a solution for the drag as $F_D = 3\pi\mu dw_s$ (see Sect. 2.8) that yields

$$C_D = \frac{24}{R_e} \quad (1.35)$$

Oseen (1927) included some inertia terms in solving the Navier–Stokes equations to obtain the drag coefficient as

$$C_D = \frac{24}{R_e} \left(1 + \frac{3}{16} R_e \right) \quad (1.36)$$

Afterward Goldstein (1929), who gave an extended solution of Oseen's approximation, determined the drag coefficient as

$$C_D = \frac{24}{R_e} \left(1 + \frac{3}{16} R_e - \frac{19}{1280} R_e^2 + \frac{71}{20480} R_e^3 + \dots \right) \quad (1.37)$$

Equation (1.37) is applicable for $R_e \leq 2$. For $R_e > 2$, the drag coefficient that could not be found theoretically had to be determined empirically. Schiller and Naumann (1933) used experimental data for $R_e < 800$ to fit a curve with the following relationship:

$$C_D = \frac{24}{R_e} (1 + 0.15 R_e^{0.687}) \quad (1.38)$$

Rouse (1938) used the available experimental data to prepare a $C_D(R_e)$ curve for the estimation of terminal fall velocity of a sphere, as shown in Fig. 1.5. Figure 1.5 also provides a good comparison of the variation of C_D with R_e obtained from the formulas given by different investigators. Importantly, in turbulent settling region

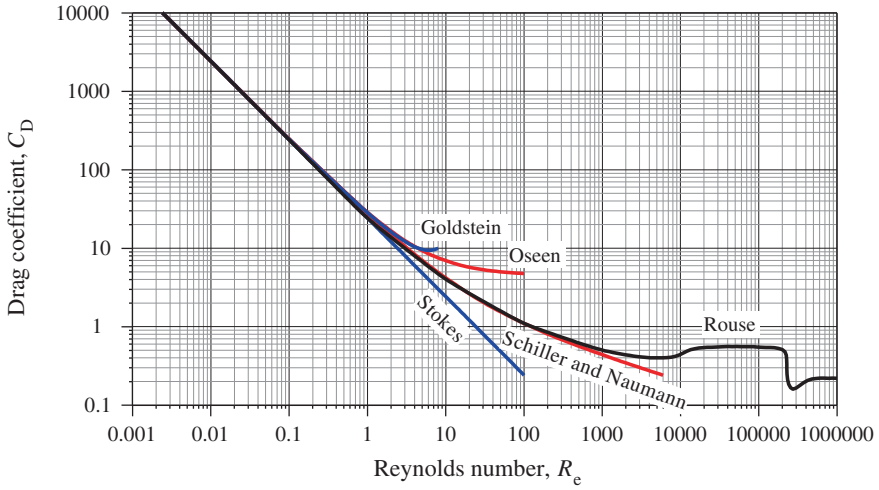


Fig. 1.5 Drag coefficient as a function of particle Reynolds number for sphere

of particle Reynolds number, $R_e > 10^3$, the drag coefficient is not only poorly correlated with the particle Reynolds number R_e but also invariant of it for certain ranges of R_e .

1.7.2 Terminal Fall Velocity of Sediment Particles

Rubey (1933) was the first to introduce a formula for the determination of terminal fall velocities of gravel, sand, and silt particles. Since then, many investigators put forward number of semitheoretical and empirical relationships for the terminal fall velocity of sediment particles. Generally, the drag coefficient, according to Cheng (1997), can be generalized as

$$C_D = \left[\left(\frac{P}{R_e} \right)^{1/m} + Q^{1/m} \right]^m \quad (1.39)$$

where P and Q are the coefficients and m is an exponent. The particle Reynolds number R_e is estimated by using nominal diameter d_n of sediment particles, as $R_e = w_s d_n / \nu$. The nominal diameter is approximated as $d_n = d/0.9$, where d is the median sieve diameter of sediment. Using Eq. (1.39), the expression for terminal fall velocity is obtained from Eq. (1.34) (Wu and Wang 2006):

Table 1.3 Values P , Q , and m

References	P	Q	m
Rubey (1933)	24 (for $d_n \leq 1$ mm) and 0 (for $d_n > 1$ mm)	2.1	1
Zhang (1961)	34	1.2	1
Zanke (1977)	24 (for $d_n \leq 1$ mm) and 0 (for $d_n > 1$ mm)	1.1	1
Raudkivi (1990)	32	1.2	1
Fredsøe and Deigaard (1992)	36	1.4	1
Julien (1998)	24	1.5	1
Cheng (1997)	32	1	1.5
Soulsby (1997)	26.4	1.27	1
She et al. (2005)	35	1.56	1
Wu and Wang (2006)	$53.5 \exp(-0.65S_p)$	$5.65 \exp(-2.5S_p)$	$0.7 + 0.9S_p$
Camenen (2007)	24.6	0.96	1.53

Table 1.4 Formulas given by Hallermeier (1981), Chang and Liou (2001) and Guo (2002)

References	Formula	Range of D_*
Hallermeier (1981)	$w_{sc} = \frac{v}{d_n} \cdot \frac{D_*^3}{18}$	$D_* \leq 3.42$
	$w_{sc} = \frac{v}{d_n} \cdot \frac{D_*^{2.1}}{6}$	$3.42 < D_* \leq 21.54$
	$w_{sc} = 1.05 \frac{v}{d_n} D_*^{1.5}$	$D_* > 21.54$
Chang and Liou (2001)	$w_{sc} = 1.68 \frac{v}{d_n} \cdot \frac{D_*^{1.389}}{1 + 30.22D_*^{-1.611}}$	—
Guo (2002)	$w_{sc} = \frac{v}{d_n} \cdot \frac{D_*^3}{24 + 0.866D_*^{1.5}}$	—

$$w_s = \frac{P}{Q} \cdot \frac{v}{d_n} \left[\sqrt{\frac{1}{4} + \left(\frac{4Q}{3P^2} D_*^3 \right)^{1/m}} - \frac{1}{2} \right]^m \quad \wedge \quad D_* = d_n \left(\frac{\Delta g}{v^2} \right)^{1/3} \quad (1.40)$$

where D_* is the nondimensional particle parameter.

Table 1.3 furnishes the values of P , Q , and m obtained from the formulas given by different investigators for naturally worn sediment particles with shape factor $S_p \approx 0.7$.

In addition, Hallermeier (1981), Chang and Liou (2001), and Guo (2002) put forward the expressions for $w_s(D_*)$, which could not be arranged in the form given by Eqs. (1.39) and (1.40). For natural sediment particles, the formulas are given in Table 1.4.

A number of relationships for terminal fall velocity for the case of natural sediment particles are found in the literature. Dietrich (1982) analyzed the experimental data and obtained a formula as

$$w_s = \frac{v}{d_n} 10^{-c_1 + c_2 \log D_* - c_3 (\log D_*)^2 - c_4 (\log D_*)^3 + c_5 (\log D_*)^4} \quad (1.41)$$

where $c_1 = 1.25572$, $c_2 = 2.92944$, $c_3 = 0.29445$, $c_4 = 0.05175$, and $c_5 = 0.01512$.

Another formula proposed by Ahrens (2000) can be given in terms of aforementioned variables as

$$w_s = \frac{v}{d_n} \left\{ 0.055 D_*^3 \tanh \left[\frac{12}{D_*^{1.77}} \exp(-4 \times 10^{-4} D_*^3) \right] + 1.06 D_*^{1.5} \tanh \left[0.016 D_*^{1.5} \exp \left(-\frac{120}{D_*^3} \right) \right] \right\} \quad (1.42)$$

In an attempt to obtain a more realistic relationship, Jiménez and Madsen (2003) developed a formula by fitting the relatively long expression given by Dietrich (1982). It is

$$W_* = \left(0.954 + \frac{20.48}{S_*} \right)^{-1} \quad \wedge \quad W_* = \frac{w_s}{(\Delta g d_n)^{0.5}} \quad \vee \quad S_* = d_n \frac{(\Delta g d_n)^{0.5}}{v} \quad (1.43)$$

where W_* is the nondimensional terminal fall velocity and S_* is another nondimensional particle parameter.

Experiments evidenced that in water with dense sediment suspension, the flow around adjacent settling particles induces a greater drag, as compared to that in a clear water. It is known as *hindered settling effect* that results in a terminal fall velocity w_{sc} in a suspended sediment water (sediment-laden water) to reduce from that in a clear water. According to Richardson and Zaki (1954), the terminal fall velocity (or hindered fall velocity) w_{sc} in water with suspended sediment concentration C can be determined by

$$w_{sc} = w_s (1 - C)^n \quad (1.44)$$

where w_s is the terminal fall velocity in a clear water and n is an empirical exponent varying from 4.9 to 2.3 for R_e increasing from 0.1 to 10^3 . However, the exponent n is approximately 4 for the particle sizes ranging from 0.05 to 0.5 mm.

Oliver (1961) conducted experiments on terminal fall velocity in water with suspended sediment. He used the data of his experiments and those of McNown and Lin (1952) to propose a formula:

$$w_{sc} = w_s (1 - 2.15C)(1 - 0.75C^{0.33}) \quad (1.45)$$

Sha (1965) proposed a formula applicable for fine sediment $d_{50} \leq 0.01$ mm:

$$w_{sc} = w_s \left(1 - \frac{C}{2d_{50}^{0.5}} \right)^3 \quad (1.46)$$

Soulsby (1997) proposed a formula for the hindered fall velocity in a dense sediment suspension. In his formula (see Table 1.3), a simple change in the values of P and Q due to C is required for the estimation of w_{sc} as given below:

$$P = \frac{26}{(1 - C)^{4.7}}, \quad Q = \frac{1.3}{(1 - C)^{4.7}} \quad (1.47)$$

Although the empirical formulas summarized here would be adequate for the approximate estimations required by engineers, an accurate estimation of the terminal fall velocity for sediment particles is rather far from being resolved. Nevertheless, the formula that includes a shape factor given by Wu and Wang (2006) seems to be more complete.

1.8 Examples

Example 1.1 A sieve analysis of the riverbed sediment weighing 31.4 N is done. The relative density of sediment is measured as 2.65. The particle size distribution is given in the following table:

Size fraction (mm)	Weight retained (N)	Size fraction (mm)	Weight retained (N)
$d < 0.15$	0	$1.18 < d < 1.25$	6.712
$0.15 < d < 0.25$	0.864	$1.25 < d < 1.4$	4.092
$0.25 < d < 0.425$	1.392	$1.4 < d < 1.7$	0.988
$0.425 < d < 0.6$	1.824	$1.7 < d < 2$	0.332
$0.6 < d < 1$	7.724	$2 < d$	0.284
$1 < d < 1.18$	7.188		

- (i) Plot the particle size distribution and % finer versus Φ curves;
- (ii) determine d_i and Φ_i for $i = 15.9, 50, 84.1$, and 90 % finer;
- (iii) calculate σ_g , d_g , and G ; and
- (iv) calculate ρ_0 , e , ρ_d , and ϕ .

Solution

The particle size distribution curve that is plotted in a semilogarithmic graph representing percentage finer versus sieve size is prepared through following steps. On the graph, the sieve size scale is logarithmic. To find the percentage finer (that is the percentage of sediment passing through each sieve), the percentage retained in each sieve is first obtained as

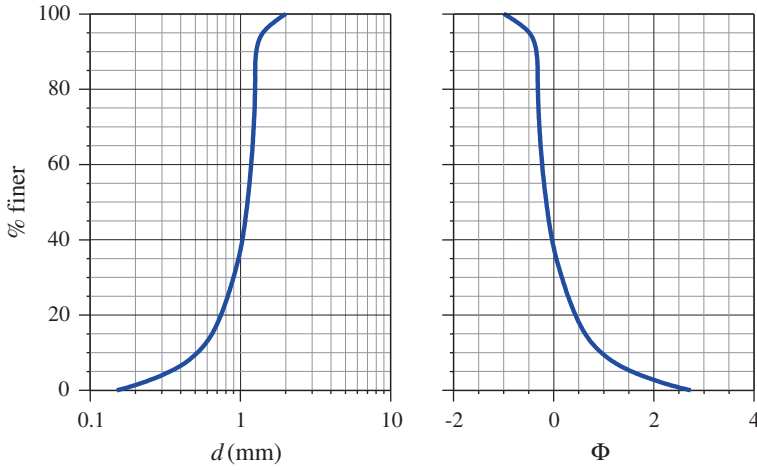


Fig. E1.1 Particle size distribution and % finer versus Φ curves

$$\% \text{ retained} = (\text{weight of sediment retained in the sieve} \div \text{total weight}) \times 100 \%$$

The next step is to determine the cumulative percentage of the sediment retained in each sieve. Thus, the total amount of sediment that is retained in each sieve and the amount in the previous sieves are added. The percentage finer (or the cumulative percentage passing) of the sediment is estimated by subtracting the percentage retained from 100 % as

$$\% \text{ finer} = 100 \% - \% \text{ cumulative retained}$$

Then, Φ is determined from Eq. (1.18).

- (i) The particle size distribution and % finer versus Φ curves obtained from the given sieve analysis are shown in Fig. E1.1.
- (ii) From the particle size distribution curve (Fig. E1.1), the following particle sizes d_i and Φ_i corresponding to the given % finer (denoted as fraction i in the form of subscript of d and Φ) are obtained:

$$d_{15.9} = 0.65 \text{ mm}, d_{50} = 1.12 \text{ mm}, d_{84.1} = 1.27 \text{ mm and } d_{90} = 1.36 \text{ mm}$$

$$\Phi_{15.9} = 0.62, \Phi_{50} = -0.16, \Phi_{84.1} = -0.34 \text{ and } \Phi_{90} = -0.44$$

(iii) Using the particle sizes determined in (ii), one can obtain

$$\sigma_g = \left(\frac{1.27}{0.65} \right)^{0.5} = 1.398 \Leftarrow \text{Eq. (1.14)}$$

$$d_g = (1.27 \times 0.65)^{0.5} = 0.909 \text{ mm} \Leftarrow \text{Eq. (1.15)}$$

$$G = \frac{1}{2} \left(\frac{1.27}{1.12} + \frac{1.12}{0.65} \right) = 1.429 \Leftarrow \text{Eq. (1.16)}$$

(iv) Using $d_{50} = 1.12$ mm, one can calculate from Wu and Wang's equation:

$$\rho_0 = 0.13 + \frac{0.21}{(0.002 + 1.12)^{0.21}} = 0.335 \Leftarrow \text{Eq. (1.21)}$$

$$e = \frac{0.335}{1 - 0.335} = 0.504 \Leftarrow \text{Eq. (1.22)}$$

$$\rho_d = 2.65 \times 10^3 (1 - 0.335) = 1,762.25 \text{ kg m}^{-3} \Leftarrow \text{Eq. (1.23)}$$

To calculate ϕ , the equation given by Zhang et al. is used:

$$\phi = 32.5 + 1.27 \times 1.12 = 33.92^\circ \Leftarrow \text{Eq. (1.24)}$$

Example 1.2 A sample of $2 \times 10^{-3} \text{ m}^3$ of river water is evaporated to collect suspended sediment of 5.2 N (dry weight), having $d_{50} = 0.1$ mm and $s = 2.65$. Determine C , c , ρ_m , γ_m , and μ_m . Consider μ for a clear water as 10^{-3} Pa s .

Solution

Weight of sediment = 5.2 N; and total volume of water including sediment = $2 \times 10^{-3} \text{ m}^3$

Therefore, one can calculate

$$V_s = \frac{5.2}{\gamma_s} = \frac{5.2}{2.65 \times 9.81 \times 10^3} = 2 \times 10^{-4} \text{ m}^3 \Leftarrow \text{Definition of specific weight}$$

$$V_f + V_s = 2 \times 10^{-3} \text{ m}^3$$

$$C = \frac{2 \times 10^{-4}}{2 \times 10^{-3}} = 0.1 \Leftarrow \text{Eq. (1.27)}$$

$$c = \frac{2.65 \times 0.1}{1 + (2.65 - 1)0.1} = 0.227 \Leftarrow \text{Eq. (1.28)}$$

$$\rho_m = 10^3 + (2.65 \times 10^3 - 10^3)0.1 = 1,165 \text{ kg m}^{-3} \Leftarrow \text{Eq. (1.29)}$$

$$\gamma_m = 1165 \times 9.81 = 11,428.65 \text{ N m}^{-3} \Leftarrow \text{Eq. (1.30)}$$

To calculate μ_m , the equation given by Lee is used:

$$\mu_m = 10^{-3}(1 - 0.1)^{-(2.5+1.9 \times 0.1+7.7 \times 0.1^2)} = 1.34 \times 10^{-3} \text{ Pa s} \Leftarrow \text{Eq. (1.33)}$$

Example 1.3 Determine the terminal fall velocity w_s in water for a spherical particle with diameter of 5 mm. The relative density of sediment is measured as 2.65. Consider $g = 9.81 \text{ m s}^{-2}$ and ν for a clear water $= 10^{-6} \text{ m}^2 \text{ s}^{-1}$.

Solution

For the nominal diameter $d = 5 \text{ mm}$, assume a value of $C_D = 0.4$. Calculation of w_s is as follows:

$$w_s = \left[\frac{4}{3} \cdot \frac{(2.65 - 1)9.81 \times 5 \times 10^{-3}}{0.4} \right]^{0.5} = 0.519 \text{ m s}^{-1} \Leftarrow \text{Eq. (1.34)}$$

Check: For $R_e (= w_s d / \nu = 0.519 \times 5 \times 10^{-3} / 10^{-6}) = 2,595$, $C_D = 0.43$ is obtained from Fig. 1.5.

For the next trial, consider $C_D = 0.43$ and estimate w_s again as above. The estimated w_s is as 0.5 m s^{-1} .

Check: For $R_e (= w_s d / \nu = 0.5 \times 5 \times 10^{-3} / 10^{-6}) = 2,500$, $C_D = 0.43$ is obtained from Fig. 1.5. Thus, the assumed and the calculated values of C_D are equal.

Therefore, the terminal fall velocity, $w_s = 0.5 \text{ m s}^{-1}$

Example 1.4 A sample of riverbed sand has a nominal diameter of 0.5 mm. The relative density of sediment is measured as 2.65. Find the terminal fall velocity w_s using different formulas. Consider $S_p = 0.7$, $g = 9.81 \text{ m s}^{-2}$, and ν for a clear water $= 10^{-6} \text{ m}^2 \text{ s}^{-1}$.

Solution

For the nominal diameter $d_n = 0.5 \text{ mm}$, $D_* [= d_n (\Delta g / \nu^2)^{1/3}]$ is calculated as $D_* = 0.5 \times 10^{-3} \{[(2.65 - 1)9.81] / (10^{-6})^2\}^{1/3} = 12.65$.

Use Eq. (1.40) to determine w_s for the values of P , Q , and m given in Table 1.3. The estimated values of w_s are furnished in Table 1.5.

From formulas given in Table 1.4 and Eqs. (1.41)–(1.43), following estimations are made:

Table 1.5 Results of w_s

References	P	Q	m	w_s (m s ⁻¹)
Rubey (1933)	24 (for $d_n \leq 1$ mm)	2.1	1	0.0612
Zhang (1961)	34	1.2	1	0.0707
Zanke (1977)	24 (for $d_n \leq 1$ mm)	1.1	1	0.0796
Raudkivi (1990)	32	1.2	1	0.0719
Fredsøe and Deigaard (1992)	36	1.4	1	0.0658
Julien (1998)	24	1.5	1	0.0703
Cheng (1997)	32	1	1.5	0.0611
Soulsby (1997)	26.4	1.27	1	0.0737
She et al. (2005)	35	1.56	1	0.0637
Wu and Wang (2006)	$53.5 \exp(-0.65S_p)$	$5.65 \exp(-2.5S_p)$	$0.7 + 0.9S_p$	0.0651
Camenen (2007)	24.6	0.96	1.53	0.0664

Hallermeier formula:

$$w_{sc}(3.42 < D_* \leq 21.54) = \frac{10^{-6}}{0.5 \times 10^{-3}} \cdot \frac{12.65^{2.1}}{6} = 0.069 \text{ m s}^{-1}$$

Chang and Liou formula:

$$w_{sc} = 1.68 \frac{10^{-6}}{0.5 \times 10^{-3}} \cdot \frac{12.65^{1.389}}{1 + 30.22 \times 12.65^{-1.611}} = 0.076 \text{ m s}^{-1}$$

Guo formula:

$$w_{sc} = \frac{10^{-6}}{0.5 \times 10^{-3}} \cdot \frac{12.65^3}{24 + 0.866 \times 12.65^{1.5}} = 0.064 \text{ m s}^{-1}$$

Dietrich formula:

$$\begin{aligned} w_s &= \frac{10^{-6}}{0.5 \times 10^{-3}} 10^{-1.25572 + 2.92944 \log 12.65 - 0.29445(\log 12.65)^2 - 0.05175(\log 12.65)^3 + 0.01512(\log 12.65)^4} \\ &= 0.074 \text{ m s}^{-1} \Leftarrow \text{Eq. (1.41)} \end{aligned}$$

Ahrens formula:

$$\begin{aligned} w_s &= \frac{10^{-6}}{0.5 \times 10^{-3}} \left\{ 0.055 \times 12.65^3 \tanh \left[\frac{12}{12.65^{1.77}} \exp(-4 \times 10^{-4} \times 12.65^3) \right] \right. \\ &\quad \left. + 1.06 \times 12.65^{1.5} \tanh \left[0.016 \times 12.65^{1.5} \exp \left(-\frac{120}{12.65^3} \right) \right] \right\} = 0.07 \text{ m s}^{-1} \Leftarrow \text{Eq. (1.42)} \end{aligned}$$

Jiménez and Madsen formula:

For the nominal diameter $d_n = 0.5$ mm, $S_* [= d_n(\Delta g d_n)^{0.5}/v]$ is calculated as $S_* = 0.5 \times 10^{-3}[(2.65 - 1)9.81 \times 0.5 \times 10^{-3}]^{0.5}/10^{-6} = 44.98$

$$w_s = [(2.65 - 1)9.81 \times 0.5 \times 10^{-3}]^{0.5} \left(0.954 + \frac{20.48}{44.98} \right)^{-1} = 0.064 \text{ m s}^{-1}$$

\Leftarrow Eq. (1.43)

Example 1.4 therefore produces a somewhat varying estimation of terminal fall velocity for a given sediment size, when formulas proposed by different investigators are used.

References

- Ahrens JP (2000) The fall-velocity equation. *J Waterw Port Coast Ocean Eng* 126(2):99–102
- Alger GR, Simons DB (1968) Fall velocity of irregular shaped particles. *J Hydraul Div* 94(3):721–737
- Bagnold RA (1954) Experiments on a gravity-free dispersion of large solid spheres in a Newtonian fluid under shear. *Proc R Soc London A* 255(1160):49–63
- Camenen B (2007) Simple and general formula for the settling velocity of particles. *J Hydraul Eng* 133(2):229–233
- Chang H-K, Liou J-C (2001) Discussion of ‘The free-velocity equation’. *J Waterw Port Coastal Ocean Eng* 127(4):250–251
- Cheng N-S (1997) Simplified settling velocity formula for sediment particle. *J Hydraul Eng* 123(2):149–152
- Dey S (2003) Incipient motion of bivalve shells on sand beds under flowing water. *J Eng Mech* 129(2):232–240
- Dey S, Sarkar A (2006) Scour downstream of an apron due to submerged horizontal jets. *J Hydraul Eng* 132(3):246–257
- Dietrich WE (1982) Settling velocity of natural particles. *Water Resour Res* 18(6):1615–1626
- Fredsøe J, Deigaard R (1992) *Mechanics of coastal sediment transport*. World Scientific, Singapore
- Goldstein S (1929) The steady flow of viscous fluid past a fixed spherical obstacle at small Reynolds numbers. *Proc R Soc London A* 123(791):225–235
- Guo J (2002) Logarithmic matching and its applications in computational hydraulics and sediment transport. *J Hydraul Res* 40(5):555–565
- Hallermeier RJ (1981) Terminal settling velocity of commonly occurring sand grains. *Sedimentology* 28(6):859–865
- Heywood H (1938) Measurement of the fineness of powdered material. *Proc Inst Mech Eng* 140(1):257–347
- Ippen AT, Eagleson PS (1955) A study of sediment sorting by waves shoaling on a plane beach. Technical Memorandum 63, Beach Erosion Board, United States Army Corps Engineers
- Jiménez JA, Madsen OS (2003) A simple formula to estimate settling velocity of natural sediments. *J Waterw Port Coast Ocean Eng* 129(2):70–78
- Julien PY (1998) *Erosion and sedimentation*, 1st edn. Cambridge University Press, Cambridge
- Komura S (1963) Discussion of ‘Sediment transportation mechanics: introduction and properties of sediment’. *J Hydraul Div* 89(1):263–266
- Kramer H (1935) Sand mixtures and sand movement in fluvial model. *Trans Am Soc Civ Eng* 100:798–838
- Krumbein WC (1941) Measurement and geological significance of shape and roundness of sedimentary particles. *J Sediment Petrol* 11(2):64–72
- Krumbein WC, Sloss LL (1963) *Stratigraphy and sedimentation*. Freeman, San Francisco

- Lane EW (1947) Report of the subcommittee on sediment terminology. *Trans Am Geophys Union* 28(6):936–938
- Lee DI (1969) The viscosity of concentrated suspensions. *Trans Soc Rheol* 13(2):273–288
- Li Z, Komar PD (1986) Laboratory measurements of pivoting angles for applications to selective entrainment of gravel in current. *Sedimentology* 33(3):413–423
- McNown JS, Lin PN (1952) Sediment concentration and fall velocity. In: *Proceedings of the second midwestern conference on fluid mechanics*, Ohio State University, Ohio, pp 402–411
- Mehta AJ, Lee J, Christensen BA (1980) Fall velocity of shells as coastal sediment. *J Hydraul Div* 106(11):1727–1744
- Oliver DR (1961) The sedimentation of suspensions of closely-sized spherical particles. *Chem Eng Sci* 15(3–4):230–242
- Oseen C (1927) *Hydrodynamik*. Akademische Verlagsgesellschaft, Leipzig
- Raudkivi AJ (1990) *Loose boundary hydraulics*. Pergamon, New York
- Richardson JF, Zaki WN (1954) Sedimentation and fluidisation, part I. *Trans Inst Chem Eng* 32(1):35–53
- Rouse H (1938) *Fluid mechanics for hydraulic engineers*. Dover, New York
- Rubey W (1933) Settling velocities of gravel, sand and silt particles. *Am J Sci* 225(148):325–338
- Schiller L, Naumann A (1933) Über die grundlegenden berechnungen bei der schwerkraftaufbereitung. *Zeitschrift des Vereines Deutscher Ingenieure* 77(12):318–320
- Sha YQ (1965) Introduction to sediment dynamics. Industry Press, Beijing
- She K, Trim L, Pope D (2005) Fall velocities of natural sediment particles: a simple mathematical presentation of the fall velocity law. *J Hydraul Res* 43(2):189–195
- Soulsby RL (1997) *Dynamics of marine sands*. Thomas Telford, London
- Stokes GG (1851) On the effect of the internal friction of fluids on the motion of pendulums. *Trans Cambridge Philos Soc* 9:80–85
- US Interagency Committee (1957) Some fundamentals of particle size analysis: a study of methods used in measurement and analysis of sediment loads in streams. Report number 12, Subcommittee on Sedimentation, Interagency Committee on Water Resources, St. Anthony Falls Hydraulic Laboratory, Minneapolis, Minnesota
- Vanoni VA (1977) *Sedimentation engineering*. ASCE Manual number 54, American Society of Civil Engineers, New York
- Wadell H (1932) Volume, shape and roundness of rock particles. *J Geol* 40(5):443–451
- Wu W, Wang SSY (2006) Formulas for sediment porosity and settling velocity. *J Hydraul Eng* 132(8):858–862
- Zanke U (1977) Berechnung der sinkgeschwindigkeiten von sedimenten. *Mitteilungen des Franzius-Instituts für Wasserbau*, Technical University, Hannover, Heft 46:230–245
- Zhang RJ (1961) *River dynamics*. Industry Press, Beijing (in Chinese)
- Zhang RJ, Xie JH, Wang MF, Huang JT (1989) *Dynamics of river sedimentation*. Water Power Press, Beijing

Chapter 2

Hydrodynamic Principles

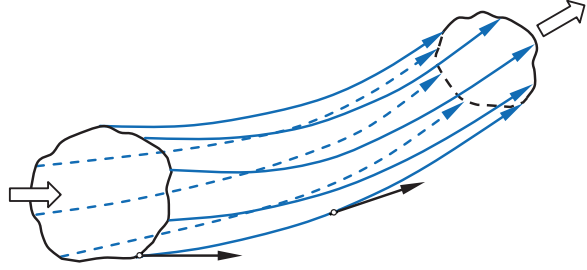
2.1 General

The hydrostatic phenomenon is simplified by the absence of shear stress within the fluid and in contact with the solid boundary. In contrast, the hydrodynamic phenomenon becomes rather complex. As the fluid flows over a solid boundary, whether stationary or moving, the fluid velocity in contact with the boundary must be the same as that of the boundary, termed *no-slip*. Thus, a velocity gradient is created over the boundary, as the fluid velocity increases with the normal distance from the boundary. The resulting differential velocity normal to the boundary gives rise to the shear stress within the fluid and on the boundary, as already discussed in Newton's law of viscosity, Eq. (1.3). Fluid flows as a result of the action of forces set up by the pressure difference or the gravity. Fluid motion is controlled by the inertia of fluid and the effect of the shear stress exerted by the surrounding fluid. Therefore, the resulting fluid motion cannot be easily analyzed theoretically; and the theories are often essentially supplemented by the experiments. The fluid motion can be defined in the following ways:

The path traced by an individual fluid particle over a period of time is known as *pathline*, which describes the trajectory (position at successive intervals of time) of a particle that started from a given position. On the other hand, *streakline* provides an instantaneous picture of the positions of all the particles which have passed through a particular point at a given time. Streakline is therefore the locus of points of all the fluid particles that have passed continuously through a particular spatial point in the past. Since the flow characteristics may vary from instant to instant, a streakline is not necessarily the same as a pathline.

In analyzing a fluid flow, one often makes use of the idea of a *streamline*, which is an imaginary line whose tangents at every point along the imaginary line represent velocity vectors at that moment. It implies that at a given instant, there is no flow across the streamline. Since there can be no flow through a solid boundary, the streamline in contact with or nearest to the solid boundary is known as *limiting streamline*. Let us consider a particle moves in the direction of the streamline at any instant; it has a displacement ds having components dx , dy , and dz and the

Fig. 2.1 Streamtube, where curved lines with arrows represent streamlines. The two arrows tangential to the lowest streamline show the velocity vectors at those points



velocity vector \mathbf{v} having components u , v , and w in the x -, y -, and z -direction, respectively. Then, the equation of streamline is

$$\frac{dx}{u} = \frac{dy}{v} = \frac{dz}{w} \quad (2.1)$$

For a continuous stream of fluid, streamlines are continuous lines extending to infinity upstream and downstream or forming closed curves, but they cannot intersect. When flow conditions are steady and laminar, then the pathlines and the streamlines are identical; however, if the flow is fluctuating or turbulent, this is not the case. A family of streamlines through every point on the perimeter of a small area of the fluid flow cross section forms a *streamtube* (Fig. 2.1). Since there is no flow across a streamline, no fluid can enter or leave a streamtube except through its ends. It thus behaves as if it were a solid tube.

The *Lagrangian approach* of the fluid flow is the method of looking at fluid motion, where the observer follows an individual fluid particle as it moves through space and time. To illustrate its use, let $(x_A(x_0, y_0, z_0, t), y_A(x_0, y_0, z_0, t), z_A(x_0, y_0, z_0, t))$ be the position at an instant t of a fluid particle that had an initial position (x_0, y_0, z_0) at time t_0 . Hence, by definition, $x_A(x_0, y_0, z_0, t = t_0) = x_0(x_0, y_0, z_0)$. The velocity components are given by

$$\left. \begin{aligned} u(x_0, y_0, z_0, t) &\equiv \lim_{\Delta t \rightarrow 0} \frac{x_A(x_0, y_0, z_0, t_0 + \Delta t) - x_A(x_0, y_0, z_0, t_0)}{\Delta t} \\ &= \lim_{\Delta t \rightarrow 0} \frac{x_A - x_0}{\Delta t} = \frac{\partial x_A(x_0, y_0, z_0, t)}{\partial t} \\ v(x_0, y_0, z_0, t) &= \frac{\partial y_A(x_0, y_0, z_0, t)}{\partial t} \\ w(x_0, y_0, z_0, t) &= \frac{\partial z_A(x_0, y_0, z_0, t)}{\partial t} \end{aligned} \right\} \quad (2.2)$$

In the above, $\Delta t = t - t_0$. The partial derivatives signify that the differentiation is performed keeping initial position (x_0, y_0, z_0) fixed. Then, the acceleration components are given by

$$\left. \begin{aligned} a_x(x_0, y_0, z_0, t) &= \frac{\partial u(x_0, y_0, z_0, t)}{\partial t} = \frac{\partial^2 x_A(x_0, y_0, z_0, t)}{\partial t^2} \\ a_y(x_0, y_0, z_0, t) &= \frac{\partial v(x_0, y_0, z_0, t)}{\partial t} = \frac{\partial^2 y_A(x_0, y_0, z_0, t)}{\partial t^2} \\ a_z(x_0, y_0, z_0, t) &= \frac{\partial w(x_0, y_0, z_0, t)}{\partial t} = \frac{\partial^2 z_A(x_0, y_0, z_0, t)}{\partial t^2} \end{aligned} \right\} \quad (2.3)$$

On the other hand, the *Eulerian approach* of the fluid flow is the method of looking at fluid motion that focuses on specific locations in the space through which the fluid flows, as over the time. To describe velocity components, it is written as

$$\left. \begin{aligned} u &= u(x, y, z, t) \\ v &= v(x, y, z, t) \\ w &= w(x, y, z, t) \end{aligned} \right\} \quad (2.4)$$

Then, to determine the acceleration, having known that as the acceleration means the rate of change of velocity of a fluid particle at a position while noting that the particle moves from that position at the time it is being studied, the acceleration component in x -direction is

$$\left. \begin{aligned} a_x &= \lim_{\Delta t \rightarrow 0} \frac{\Delta u(x + u\Delta t, y + v\Delta t, z + w\Delta t, t + \Delta t)}{\Delta t} \\ &= u \frac{\partial u}{\partial x} + v \frac{\partial u}{\partial y} + w \frac{\partial u}{\partial z} + \frac{\partial u}{\partial t} \\ a_y &= u \frac{\partial v}{\partial x} + v \frac{\partial v}{\partial y} + w \frac{\partial v}{\partial z} + \frac{\partial v}{\partial t} \\ a_z &= u \frac{\partial w}{\partial x} + v \frac{\partial w}{\partial y} + w \frac{\partial w}{\partial z} + \frac{\partial w}{\partial t} \end{aligned} \right\} \quad (2.5)$$

Note that the first three terms in the right-hand side of Eq. (2.5) are referred to as *convective acceleration* (also occasionally called *advective acceleration*) and the last terms in the right-hand side of Eq. (2.5) are the *local acceleration* (also occasionally called *temporal acceleration*).¹ The convective terms are quadratic in the velocity components and hence they are nonlinear. This introduces the major complexity in having the solution of the equations of fluid motion. On the other hand, as the Lagrangian approach does not have nonlinearity, one might thought that it could be relatively convenient to use. This is, however, not the case, as the

¹ *Convective acceleration* is the acceleration of fluid due to space at a given time, while the *local acceleration* is the acceleration of fluid due to time at a given spatial location.

internal force terms due to viscosity introduced by the Newton's laws become nonlinear in the Lagrangian approach. Further, the physical laws, such as the Newton's laws and the laws of conservation of mass and energy, apply directly to each particle in the Lagrangian approach. However, the fluid flow is a continuum phenomenon, at least down to the molecular level. It is not possible to track each particle in a complex flow field. Thus, the Lagrangian approach is rarely used in hydrodynamics.

In the Eulerian approach, individual fluid particles are not tracked; instead, a control volume is defined. The flow parameters are described as fields within the control volume, expressing them as a function of space and time. Hence, one is not concerned about the location or velocity of a particular fluid particle, but rather about the velocity, acceleration, etc. of whatever particle happens to be at a particular location and at a given time. Since the fluid flow is a continuum phenomenon, the Eulerian approach is usually preferred in hydrodynamics. Notwithstanding that the physical laws, such as the Newton's laws and the laws of conservation of mass and energy, apply directly to particles in a Lagrangian approach, some transformations or reformulations of these laws are required for the use with the Eulerian approach.

2.2 Rates of Deformation

In a fluid flow, if the fluid elements do not undergo rotation as it flows, then the flow is called *irrotational*. In consideration of a frictionless or ideal fluid flow, no shear stresses act on the surface of the elements. Only normal stresses or pressures act following the Pascal's law. Then, the resultant of all surface forces acting on the element should pass through the centroid of the element irrespective of its shape. As a result, there can be no turning moment on the element and it remains in the same orientation at all its locations provided the element remains undisturbed initially. On the other hand, rotation of elements is inevitable, where viscous forces come into play. In a real fluid flow, a fluid element gets distorted as it moves. Note that distortion is not always rotation which is identified by the change in orientation of the diagonal or the axis of the element. An element may, however, get distorted without undergoing rotation or vice versa. A fluid element can undergo four types of motion or deformation: (1) translation, (2) rotation, (3) extensional strain, and (4) shear strain. These types of motion are time dependent.

Consider a rectangular fluid element $ABCD$ at time t and then after elapsing a small interval of time dt , the element undergoes four types of motion to become $A'B'C'D'$ at time $t + dt$, as shown in Fig. 2.2. The translation is defined by the displacement $u dt$ and $v dt$ of the corner B . The rotation of the diagonal BD is expressed as $\omega_z dt = \theta + d\alpha - 45^\circ$, where ω_z denotes the angular velocity or rate of rotation about an axis parallel to z -axis.

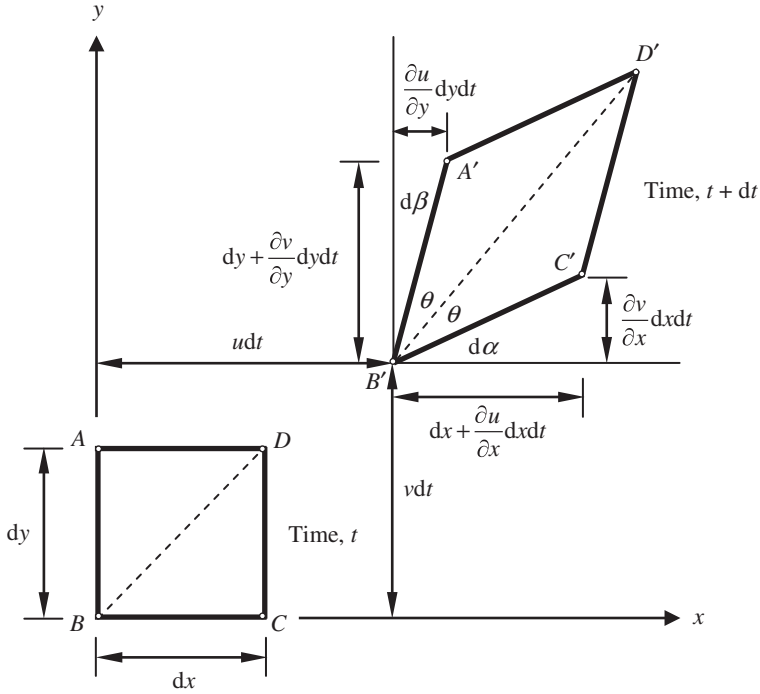


Fig. 2.2 Deformation of a moving fluid element

Using the summation of angles $2\theta + d\alpha + d\beta = 90^\circ$ yields

$$\omega_z dt = \frac{1}{2}(d\alpha - d\beta) \quad (2.6)$$

Referring to Fig. 2.2, $d\alpha$ and $d\beta$ are expressed as

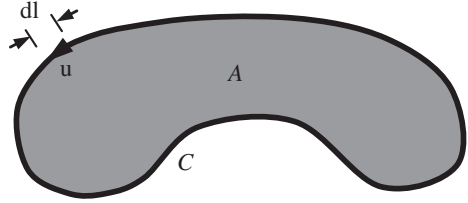
$$d\alpha = \lim_{dt \rightarrow 0} \arctan \left(\frac{\frac{\partial v}{\partial x} dx dt}{dx + \frac{\partial u}{\partial x} dx dt} \right) \approx \frac{\partial v}{\partial x} dt \quad (2.7a)$$

$$d\beta = \lim_{dt \rightarrow 0} \arctan \left(\frac{\frac{\partial u}{\partial y} dy dt}{dy + \frac{\partial v}{\partial y} dy dt} \right) \approx \frac{\partial u}{\partial y} dt \quad (2.7b)$$

Substituting Eqs. (2.7a, b) into Eq. (2.6), the rate of rotation or angular velocity about z -axis is obtained as

$$\omega_z = \frac{1}{2} \left(\frac{\partial v}{\partial x} - \frac{\partial u}{\partial y} \right) \quad (2.8)$$

Fig. 2.3 Definition sketch for fluid circulation



Similarly, the rates of rotation about x - and y -axis are

$$\omega_x = \frac{1}{2} \left(\frac{\partial w}{\partial y} - \frac{\partial v}{\partial z} \right), \omega_y = \frac{1}{2} \left(\frac{\partial u}{\partial z} - \frac{\partial w}{\partial x} \right) \quad (2.9)$$

Note that if the rates of rotational components vanish, then the flow is irrotational, for which the conditions are

$$\omega_x = \omega_y = \omega_z = 0 \Rightarrow \frac{\partial w}{\partial y} = \frac{\partial v}{\partial z}, \frac{\partial u}{\partial z} = \frac{\partial w}{\partial x}, \frac{\partial v}{\partial x} = \frac{\partial u}{\partial y} \quad (2.10)$$

The *vorticity* is the tendency of a fluid element to spin. The components of vorticity in three dimensions are expressed as follows:

$$\Omega_x = 2\omega_x = \left(\frac{\partial w}{\partial y} - \frac{\partial v}{\partial z} \right), \Omega_y = 2\omega_y = \left(\frac{\partial u}{\partial z} - \frac{\partial w}{\partial x} \right), \Omega_z = 2\omega_z = \left(\frac{\partial v}{\partial x} - \frac{\partial u}{\partial y} \right) \quad (2.11)$$

The *circulation* is the line integral around a closed curve of the fluid velocity (Fig. 2.3). It can be considered as the amount of push along a closed boundary or path. Thus, it provides an estimation of the strength of the rotational flow. Circulation can be related to the vorticity by the *Stokes theorem* as

$$\Gamma = \oint_C \mathbf{u} \cdot d\mathbf{l} = \int \int_A \Omega dA \quad (2.12)$$

where $d\mathbf{l}$ is the linear increment along the contour C and A is the area within the contour.

The components of circulation in three dimensions are expressed as follows:

$$\begin{aligned} \Gamma_x &= \int \int_y \left(\frac{\partial w}{\partial y} - \frac{\partial v}{\partial z} \right) dy dz, \quad \Gamma_y = \int \int_z \left(\frac{\partial u}{\partial z} - \frac{\partial w}{\partial x} \right) dz dx, \\ \Gamma_z &= \int \int_x \left(\frac{\partial v}{\partial x} - \frac{\partial u}{\partial y} \right) dx dy \end{aligned} \quad (2.13)$$

The two-dimensional shear strain rate is generally defined as the average decrease in angle between two lines which are initially perpendicular to each other before the strained state. Taking AB and BC as initial lines (Fig. 2.2), the *shear strain rate* is

$$\epsilon_{xy} = \frac{1}{2} \left(\frac{d\alpha}{dt} + \frac{d\beta}{dt} \right) = \frac{1}{2} \left(\frac{\partial v}{\partial x} + \frac{\partial u}{\partial y} \right) \quad (2.14)$$

Similarly, other components of shear strain rate are

$$\epsilon_{yz} = \frac{1}{2} \left(\frac{\partial w}{\partial y} + \frac{\partial v}{\partial z} \right), \quad \epsilon_{zx} = \frac{1}{2} \left(\frac{\partial u}{\partial z} + \frac{\partial w}{\partial x} \right) \quad (2.15)$$

The extensional strain in x -direction is defined as the fractional increase in length of horizontal side of the element. The *normal strain rate* in x -direction is

$$\epsilon_{xx} dt = \frac{1}{dx} \left[\left(dx + \frac{\partial u}{\partial x} dx dt \right) - dx \right] = \frac{\partial u}{\partial x} dt \Rightarrow \epsilon_{xx} = \frac{\partial u}{\partial x} \quad (2.16)$$

Similarly, other components of normal strain rate are

$$\epsilon_{yy} = \frac{\partial v}{\partial y}, \quad \epsilon_{zz} = \frac{\partial w}{\partial z} \quad (2.17)$$

2.3 Conservation of Mass

Except in the relativistic processes ($E = mc^2$, where E is the energy, m is the mass of the matter, and c is the speed of the light) after Albert Einstein in 1905, matter is neither created nor destroyed. This principle of *conservation of mass* can be applied to the fluid flow.

Considering an enclosed region in the flow constituting a control volume (CV) (Fig. 2.4), the equation of conservation of mass can be written in terms of mass flux as

$$\begin{aligned} \text{Mass flux entering} &= \text{Mass flux leaving} \\ &+ \text{Change of mass in the CV per unit time} \end{aligned}$$

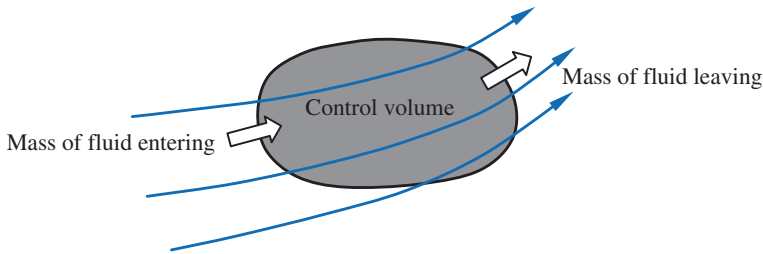
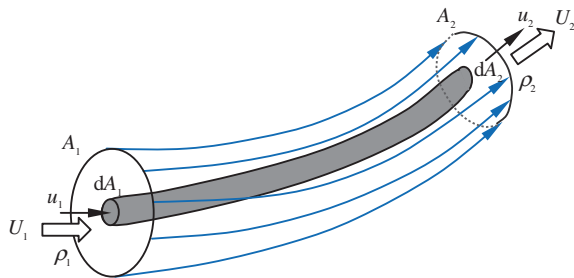


Fig. 2.4 Control volume in a fluid flow

Fig. 2.5 Definition sketch for the fluid flow through a streamtube showing an elementary streamtube



For the steady flow, there is no change of mass of fluid in the *CV* and the relation reduces to

$$\text{Mass flux entering} = \text{Mass flux leaving}$$

Applying this principle to a steady flow in a streamtube (Fig. 2.5) having an elementary cross-sectional area, through which the velocity to be considered as constant across the cross section, since there can be no flow across the wall of a streamtube, the conservation of mass for the region between sections 1 and 2 is

$$\rho_1 u_1 dA_1 = \rho_2 u_2 dA_2 = d\dot{m} = \text{constant} \quad (2.18)$$

The mass influx or mass entering per unit time at section 1 equals the mass efflux or mass leaving per unit time at section 2. In Fig. 2.5, u is the velocity through the elementary cross-sectional area dA , ρ is the mass density of fluid and the subscripts denote sections. Therefore, for a steady flow, it implies that the mass flow rate, termed *mass flux* $d\dot{m}$, across any cross section of the elementary streamtube is constant. This is known as the *continuity equation* for the compressible fluid flow through an elementary streamtube. Therefore, the continuity equation of the fluid flow for the entire cross section of the streamtube can be obtained integrating Eq. (2.18) as

$$\rho_1 U_1 A_1 = \rho_2 U_2 A_2 = \dot{m} = \text{constant} \quad \wedge \quad U = \frac{1}{A} \int_A u dA \quad (2.19)$$

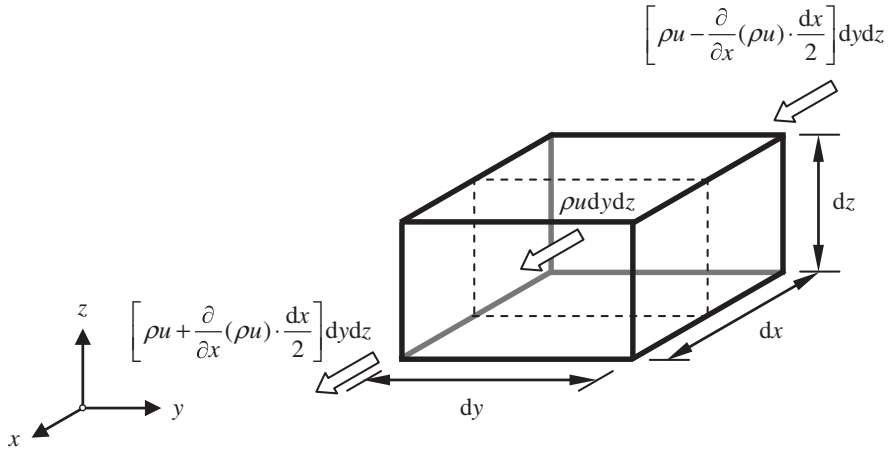


Fig. 2.6 Definition sketch for the derivation of three-dimensional continuity equation of fluid flow in a control volume element

where U is the average velocity through the cross-sectional area A .

If the fluid is incompressible, then $\rho_1 = \rho_2 = \rho$; and Eq. (2.19) reduces to

$$U_1 A_1 = U_2 A_2 = Q = \text{constant} \quad (2.20)$$

where Q is the discharge or volume rate of flow.

2.3.1 Continuity Equation in Three Dimensions

Differential mode of continuity equation is used to analyze two- and three-dimensional flows. To derive three-dimensional continuity equation of fluid flow, a control volume element of fluid $dx dy dz$, having a mass density ρ , with a center at (x, y, z) in a Cartesian coordinate system is considered (Fig. 2.6). The velocity components in x -, y - and z -direction are u , v , and w , respectively. The mass influx of fluid flow through the back face of the control volume by advection in the x -direction is given by

$$\left[\rho u - \frac{\partial}{\partial x}(\rho u) \cdot \frac{dx}{2} \right] dy dz$$

In the above expression, the first term, $\rho u dy dz$, is the mass influx through the central plane normal to the x -axis, as shown by the broken line in Fig. 2.6. The second term, $[\partial(\rho u)/\partial x](dx/2) dy dz$, is the change of mass flux with respect to distance in x -direction multiplied by the distance $dx/2$ to the back face.

Similarly, the mass efflux through the front face of the control volume in x -direction is given by

$$\left[\rho u + \frac{\partial}{\partial x}(\rho u) \cdot \frac{dx}{2} \right] dydz$$

Therefore, the net mass flux out in x -direction through these two faces is obtained as

$$\frac{\partial}{\partial x}(\rho u) dx dy dz$$

The other two directions yield similar expressions; and hence, the net mass flux out of the control volume is

$$\left[\frac{\partial}{\partial x}(\rho u) + \frac{\partial}{\partial y}(\rho v) + \frac{\partial}{\partial z}(\rho w) \right] dx dy dz$$

From the concept of conservation of mass, the net mass flux out of the control volume plus the rate of change of mass in the control volume, given by $(\partial \rho / \partial t) dx dy dz$, equals the rate of production of mass in the control volume, which is zero, by definition of the conservation of mass. Thus, the three-dimensional continuity equation of fluid flow is given by

$$\frac{\partial}{\partial x}(\rho u) + \frac{\partial}{\partial y}(\rho v) + \frac{\partial}{\partial z}(\rho w) = -\frac{\partial \rho}{\partial t} \quad (2.21)$$

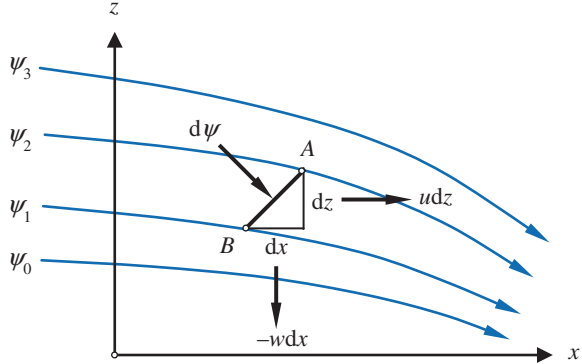
which must hold for every point in the flow of a compressible fluid. For incompressible fluid flow ($\rho = \text{constant}$), Eq. (2.21) simplifies to

$$\frac{\partial u}{\partial x} + \frac{\partial v}{\partial y} + \frac{\partial w}{\partial z} = 0 \quad (2.22)$$

The kinematic relation in terms of the components of normal strain rate can be obtained using Eqs. (2.16) and (2.17) into Eq. (2.22). It is

$$\varepsilon_{xx} + \varepsilon_{yy} + \varepsilon_{zz} = 0 \quad (2.23)$$

Thus, the sum of the components of normal strain rate vanishes to satisfy the continuity. If Eq. (2.22) reduces to only two terms, regardless of the coordinate system, a useful device is to introduce the so-called *stream function* ψ , defined so as to satisfy the continuity identically. For example, for two-dimensional incompressible flow in xz plane, the continuity equation (Eq. 2.22) reduces to

Fig. 2.7 The stream function

$$\frac{\partial u}{\partial x} + \frac{\partial w}{\partial z} = 0 \quad (2.24)$$

If the stream function is defined as ψ such that

$$u = \frac{\partial \psi}{\partial z}, \quad w = -\frac{\partial \psi}{\partial x} \quad (2.25)$$

By direct substitution of Eq. (2.25), Eq. (2.24) is satisfied identically, assuming that the ψ is continuous to the second-order derivatives. The stream function has a useful physical significance:

$$d\psi = \frac{\partial \psi}{\partial x} dx + \frac{\partial \psi}{\partial z} dz = -w dx + u dz \Rightarrow \psi = - \int w dx + \int u dz \quad (2.26)$$

Equation (2.26) implies that the line of constant ψ ($d\psi = 0$) is the line across which no flow takes place; that means it is a streamline. However, the difference between the values of stream functions ψ_1 and ψ_2 of two neighboring streamlines is numerically equal to the flow rate per unit width (denoted by Δq) between those two streamlines.

$$\psi_2 - \psi_1 = \Delta q \quad (2.27)$$

It is illustrated in Fig. 2.7, where the flow rate across section AB is $d\psi$ explaining now the flow across the two streamlines $d\psi = \Delta q = -w dx + u dz$.

2.3.2 Continuity Equation for Open-Channel Flow

The continuity equation of unsteady flow in open channel states that the difference of mass influx into and mass efflux out of the control volume must be equal to the

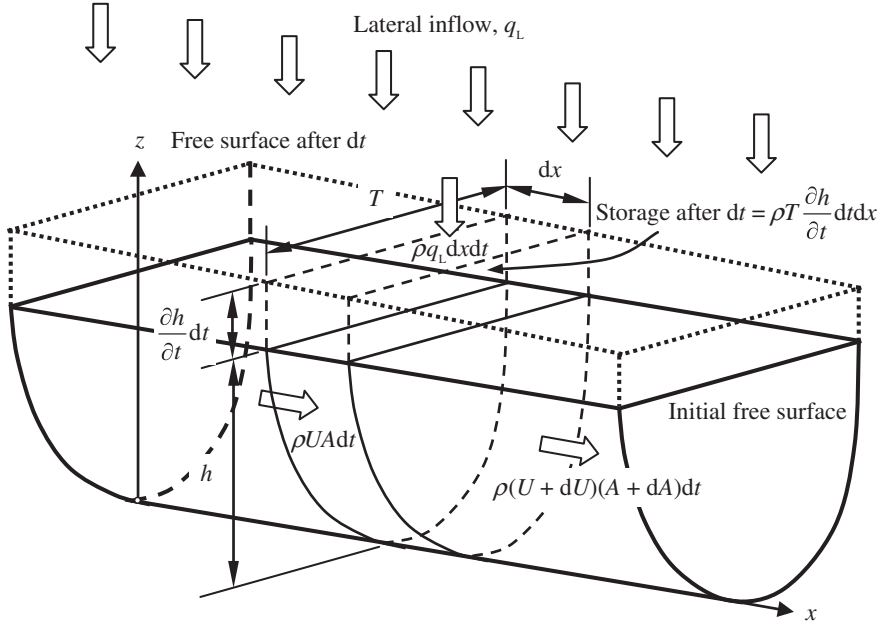


Fig. 2.8 Continuity of an unsteady flow in an open channel

rate of increase in fluid mass within the control volume. In Fig. 2.8, the initial free surface is shown by the solid lines, while the final free surface after a small interval of time dt is shown by the dotted lines. The flow is analyzed through a space between two sections having an elementary distance dx apart to form a control volume. The flow in the channel is fed laterally with a uniform flow rate q_L . Note that q_L may also arise in the form of seepage flow (injection) normal to the wetted perimeter of the channel. The mass influx in time dt into the control volume is

$$\underbrace{\rho U A dt}_{\text{Main flow}} + \underbrace{\rho q_L dx dt}_{\text{Lateral flow}}$$

where U is the area-averaged flow velocity through left section and A is the flow area of the left section.

The mass efflux in time dt out of the control volume is

$$\rho(U + dU)(A + dA)dt \Rightarrow \rho \left(U + \frac{\partial U}{\partial x} dx \right) \left(A + \frac{\partial A}{\partial x} dx \right) dt$$

where $U + dU$ is the area-averaged flow velocity through right section and $A + dA$ is the flow area of the right section. Note that $dU = (\partial U / \partial x) dx$ and $dA = (\partial A / \partial x) dx$.

The rate of increase in fluid mass in time dt within the control volume is

$$\rho T \frac{\partial h}{\partial t} dt dx$$

where T is the top width of the flow and h is the initial flow depth.

The continuity of flow in an open channel is therefore given by

$$\rho U A dt + \rho q_L dx dt - \rho \left(U + \frac{\partial U}{\partial x} dx \right) \left(A + \frac{\partial A}{\partial x} dx \right) dt = \rho T \frac{\partial h}{\partial t} dt dx \quad (2.28)$$

Simplifying,

$$U \frac{\partial A}{\partial x} + A \frac{\partial U}{\partial x} + T \frac{\partial h}{\partial t} = q_L \quad (2.29)$$

Using $Q = UA$ and $\partial A = T \partial h$ at a given section, Eq. (2.29) becomes

$$\frac{\partial Q}{\partial x} + \frac{\partial A}{\partial t} = q_L \quad (2.30)$$

Further, using hydraulic depth $h_d = A/T$ and $\partial A = T \partial h$ at a given section, Eq. (2.29) can be given as

$$U \frac{\partial h}{\partial x} + h_d \frac{\partial U}{\partial x} + \frac{\partial h}{\partial t} = \frac{q_L}{T} \quad (2.31)$$

Equations (2.30) and (2.31) are the two different forms of the *continuity equation for an unsteady flow in open channels*. For a rectangular channel with no lateral flow ($q_L = 0$), Eq. (2.30) reduces to

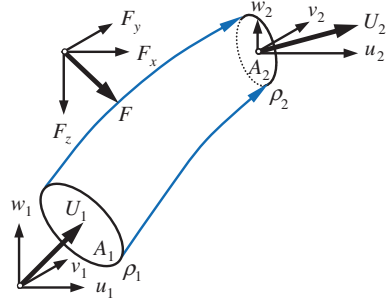
$$\frac{\partial q}{\partial x} + \frac{\partial h}{\partial t} = 0 \quad (2.32)$$

where q is the discharge per unit width ($=Uh$). This equation was first introduced by de Saint-Venant (1871).

2.4 Conservation of Momentum

The momentum equation is a statement of Newton's second law of motion and relates the sum of the forces acting on a fluid element to its acceleration or the rate of change of momentum in the direction of the resultant force. The change of momentum flux in the control volume is obtained from the difference between the momentum efflux and the momentum influx in the control volume. Let us consider

Fig. 2.9 Control volume as a streamtube with influx and efflux normal to the control sections



a simple case of flow through a streamtube, as shown in Fig. 2.9, denoting the flow parameters with subscripts 1 and 2 at the entrance and the exit, respectively. The rate of change of momentum in the horizontal direction according to Newton's second law of motion is caused a horizontal force component F_x , such that

$$F_x = \rho_2 A_2 U_2 u_2 - \rho_1 A_1 U_1 u_1 = \dot{m}(u_2 - u_1) \quad \wedge \quad \rho_1 A_1 U_1 = \rho_2 A_2 U_2 = \dot{m} \quad (2.33)$$

The value of F_x is positive in the direction in which u is assumed to be positive. Similarly, in three dimensions, F_y and F_z can be given as follows:

$$F_y = \dot{m}(v_2 - v_1), \quad F_z = \dot{m}(w_2 - w_1) \quad (2.34)$$

To summarize the position, the total force exerted on the fluid in a control volume in a given direction equals the rate of change of momentum in the given direction of the fluid passing through the control volume. Therefore,

$$F = \dot{m}(U_{\text{out}} - U_{\text{in}}) \quad (2.35)$$

The nonuniform distribution (variation with the vertical distance) of velocity affects the computation of momentum in the flow based on the area-averaged velocity $U (=Q/A)$. The actual and the area-averaged velocity distributions are illustrated in Fig. 2.10. Based on the area-averaged velocity, the momentum flux of the fluid passing through a section is expressed as $\beta \dot{m}U$, where β is known as the *momentum coefficient* or *Boussinesq coefficient*. The equation balancing the momentum flux calculated from the actual velocity distribution and that obtained from the area-averaged velocity corrected by β is used to determine momentum coefficient β as

$$\int_A (\rho u dA \cdot u) = \beta \dot{m}U \Rightarrow \int_A \rho u^2 dA = \beta \rho U^2 A \quad (2.36)$$

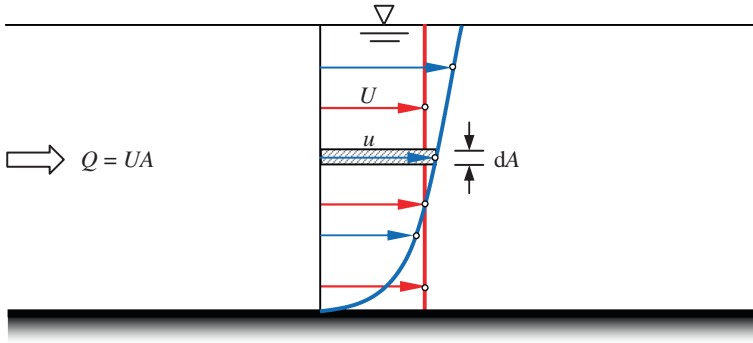


Fig. 2.10 Velocity distribution and area-averaged velocity in an open-channel flow

where u is the velocity through an elementary area dA . Solving for β yields

$$\beta = \frac{1}{A} \int_A \frac{u^2}{U^2} dA \quad (2.37)$$

In straight prismatic channels, β roughly varies from 1.01 to 1.12 (Chow 1959).

2.4.1 Momentum Equation in Three Dimensions

2.4.1.1 Equations of Motion for Inviscid Flow (Euler Equations)

In Euler equations of motion, the resultant force on a fluid element equals the product of the fluid mass and its acceleration, acting in the direction of the resultant. A control volume element of fluid $dx dy dz$, having a mass density ρ , with a center at (x, y, z) in a Cartesian coordinate system is considered (Fig. 2.11). Assuming that the fluid is inviscid (frictionless), the contact forces are pressure forces acting normally on the faces of the element. The pressure intensity at the center of the element is p . Let the component of the body force per unit mass in the x -direction be g_x . The extraneous force in the x -direction acting on the element is $g_x \rho dx dy dz$. The net force in the x -direction is then

$$\begin{aligned} F_x &= \left(p - \frac{\partial p}{\partial x} \cdot \frac{dx}{2} \right) dy dz - \left(p + \frac{\partial p}{\partial x} \cdot \frac{dx}{2} \right) dy dz + g_x \rho dx dy dz \\ &= \left(-\frac{\partial p}{\partial x} + g_x \rho \right) dx dy dz \end{aligned} \quad (2.38)$$

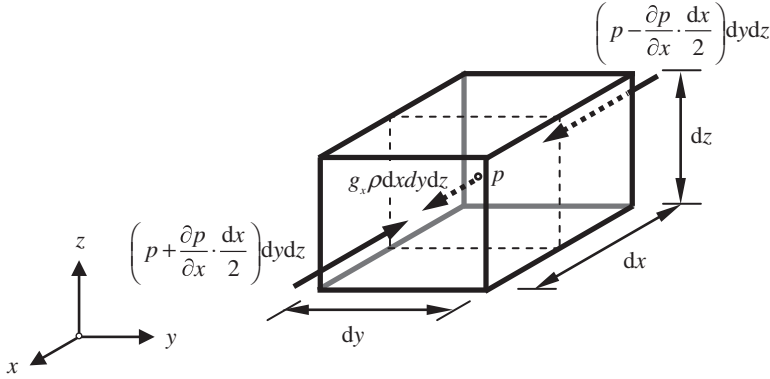


Fig. 2.11 Forces acting on a fluid element in x -direction

According to Newton's second law of motion, the net force F_x in x -direction equals the product of the mass and acceleration, that is, $(\rho dx dy dz) a_x$. Hence, using Eq. (2.5) into Eq. (2.38) yields

$$u \frac{\partial u}{\partial x} + v \frac{\partial u}{\partial y} + w \frac{\partial u}{\partial z} + \frac{\partial u}{\partial t} = -\frac{1}{\rho} \cdot \frac{\partial p}{\partial x} + g_x \quad (2.39)$$

Similarly,

$$u \frac{\partial v}{\partial x} + v \frac{\partial v}{\partial y} + w \frac{\partial v}{\partial z} + \frac{\partial v}{\partial t} = -\frac{1}{\rho} \cdot \frac{\partial p}{\partial y} + g_y \quad (2.40)$$

$$u \frac{\partial w}{\partial x} + v \frac{\partial w}{\partial y} + w \frac{\partial w}{\partial z} + \frac{\partial w}{\partial t} = -\frac{1}{\rho} \cdot \frac{\partial p}{\partial z} + g_z \quad (2.41)$$

where g_y and g_z are the body forces per unit mass in y - and z -direction, respectively. Equations (2.39)–(2.41) are known as the *Euler equations of motion*.

2.4.1.2 Equations of Motion for Viscous Flow (Navier–Stokes Equations)

Stress Components in Cartesian Coordinates: Nine stress components, as shown in Fig. 2.12, are acting on the faces of the three-dimensional fluid element, whose each face is normal to the coordinate axis of a Cartesian coordinate system. The normal stresses are denoted by σ , considering positive in the outwards and having a subscript to indicate its direction according to the axis. The effects of viscosity are to cause shear or tangential stresses in the fluid. The shear stresses are denoted by τ , having first subscript to indicate the direction of the normal to the plane over which the stress acts and the second subscript to indicate the direction.

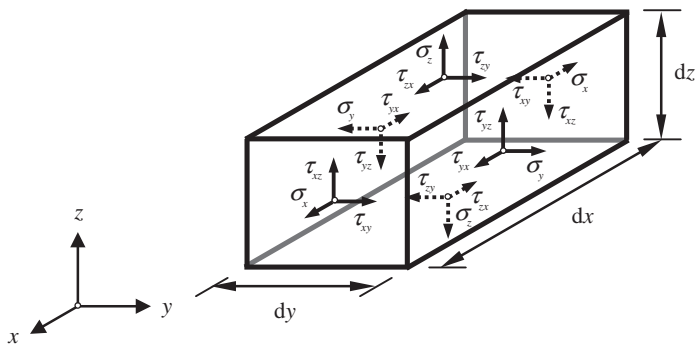


Fig. 2.12 Stress components on a fluid element in Cartesian coordinates

Let the moment be taken about an axis through the center of the element parallel to the z -axis to show that

$$\underbrace{\tau_{xy} dy dz}_{\text{Shear force}} dx - \underbrace{\tau_{yx} dx dz}_{\text{Shear force}} dy = 0 \Rightarrow \tau_{xy} = \tau_{yx} \quad (2.42)$$

Similarly,

$$\tau_{yz} = \tau_{zy}, \quad \tau_{zx} = \tau_{xz} \quad (2.43)$$

Hence, the stress components that define the state of stress at a point can be conveniently written in a matrix format as

$$\begin{matrix} \sigma_x & \tau_{xy} & \tau_{xz} \\ \tau_{yx} & \sigma_y & \tau_{yz} \\ \tau_{zx} & \tau_{zy} & \sigma_z \end{matrix}$$

Equations of Motion in Terms of Stress Components: Referring to Fig. 2.13, the shear stresses are included in the equations of motion. Let the stress components at the center (x, y, z) of the fluid element be τ_{xy} , τ_{yz} , τ_{zx} , σ_x , σ_y , and σ_z that follow above matrix. Accordingly, the stresses are obtained on six faces of the fluid element shifting the positions by a distance of one half of the length of the element.

According to Newton's second law of motion, the product of the mass and acceleration of the element, that is, $(\rho dx dy dz) a_x$, equals the summation of the forces (net force) acting on the element in the x -direction. Thus,

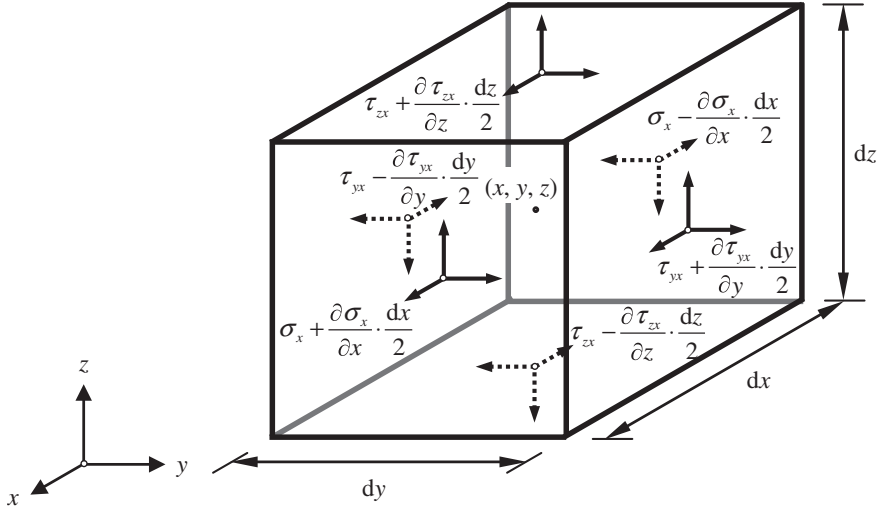


Fig. 2.13 Stress components on a fluid element in x-direction

$$\begin{aligned}
 (\rho dx dy dz) a_x = & \left(\sigma_x + \frac{\partial \sigma_x}{\partial x} \cdot \frac{dx}{2} \right) dy dz - \left(\sigma_x - \frac{\partial \sigma_x}{\partial x} \cdot \frac{dx}{2} \right) dy dz \\
 & + \left(\tau_{yx} + \frac{\partial \tau_{yx}}{\partial y} \cdot \frac{dy}{2} \right) dx dz - \left(\tau_{yx} - \frac{\partial \tau_{yx}}{\partial y} \cdot \frac{dy}{2} \right) dx dz \\
 & + \left(\tau_{zx} + \frac{\partial \tau_{zx}}{\partial z} \cdot \frac{dz}{2} \right) dx dy - \left(\tau_{zx} - \frac{\partial \tau_{zx}}{\partial z} \cdot \frac{dz}{2} \right) dx dy \\
 & + g_x \rho dx dy dz
 \end{aligned} \quad (2.44)$$

Dividing both sides of Eq. (2.44) by the element mass, $\rho dx dy dz$, and taking the limit as the element reduces to a point, that is, $dx dy dz \rightarrow 0$, the general form of equations of motion in three dimensions can be written using Eqs. (2.5) and (2.44) as

$$u \frac{\partial u}{\partial x} + v \frac{\partial u}{\partial y} + w \frac{\partial u}{\partial z} + \frac{\partial u}{\partial t} = g_x + \frac{1}{\rho} \left(\frac{\partial \sigma_x}{\partial x} + \frac{\partial \tau_{yx}}{\partial y} + \frac{\partial \tau_{zx}}{\partial z} \right) \quad (2.45a)$$

$$u \frac{\partial v}{\partial x} + v \frac{\partial v}{\partial y} + w \frac{\partial v}{\partial z} + \frac{\partial v}{\partial t} = g_y + \frac{1}{\rho} \left(\frac{\partial \tau_{xy}}{\partial x} + \frac{\partial \sigma_y}{\partial y} + \frac{\partial \tau_{zy}}{\partial z} \right) \quad (2.45b)$$

$$u \frac{\partial w}{\partial x} + v \frac{\partial w}{\partial y} + w \frac{\partial w}{\partial z} + \frac{\partial w}{\partial t} = g_z + \frac{1}{\rho} \left(\frac{\partial \tau_{xz}}{\partial x} + \frac{\partial \tau_{yz}}{\partial y} + \frac{\partial \sigma_z}{\partial z} \right) \quad (2.45c)$$

In Newtonian fluid, both the normal and the shear stress components are related to the velocity gradients so that the viscous stresses are proportional to the shear strain rates. The normal stresses can be defined in terms of a linear deformation by

the dynamic viscosity μ ($=v\rho$, where v is the coefficient of kinematic viscosity) and a second viscosity μ_s to account for the volumetric deformation, defined as the sum of the velocity gradients or the components of normal strain rate along each of the three coordinate axes (Streeter 1948). The normal stresses are as follows:

$$\sigma_x = -p + 2\mu \frac{\partial u}{\partial x} + \mu_s \left(\frac{\partial u}{\partial x} + \frac{\partial v}{\partial y} + \frac{\partial w}{\partial z} \right) \quad (2.46a)$$

$$\sigma_y = -p + 2\mu \frac{\partial v}{\partial y} + \mu_s \left(\frac{\partial u}{\partial x} + \frac{\partial v}{\partial y} + \frac{\partial w}{\partial z} \right) \quad (2.46b)$$

$$\sigma_z = -p + 2\mu \frac{\partial w}{\partial z} + \mu_s \left(\frac{\partial u}{\partial x} + \frac{\partial v}{\partial y} + \frac{\partial w}{\partial z} \right) \quad (2.46c)$$

In a three-dimensional case, extending the Newton's law of viscosity, the components of shear stress are

$$\tau_{xy} = \tau_{yx} = \mu \left(\frac{\partial v}{\partial x} + \frac{\partial u}{\partial y} \right), \quad \tau_{yz} = \tau_{zy} = \mu \left(\frac{\partial w}{\partial y} + \frac{\partial v}{\partial z} \right), \quad \tau_{zx} = \tau_{xz} = \mu \left(\frac{\partial u}{\partial z} + \frac{\partial w}{\partial x} \right) \quad (2.47)$$

The effect of the second viscosity μ_s is of secondary importance being small in practice. A good approximation is to set

$$\mu_s = -2\mu/3$$

that is, the *Stokes hypothesis*; and the pressure may be seen to be the average from Eqs. (2.46a–c) as

$$p = -\frac{1}{3}(\sigma_x + \sigma_y + \sigma_z) \quad (2.48)$$

As an exemplar, using Eqs. (2.46a), (2.47) and (2.48) into Eq. (2.45a) and applying the Stokes hypothesis, the equation of motion in x -direction is

$$u \frac{\partial u}{\partial x} + v \frac{\partial u}{\partial y} + w \frac{\partial u}{\partial z} + \frac{\partial u}{\partial t} = g_x - \frac{1}{\rho} \cdot \frac{\partial p}{\partial x} + \nu \nabla^2 u + \frac{\nu}{3} \cdot \frac{\partial}{\partial x} \left(\frac{\partial u}{\partial x} + \frac{\partial v}{\partial y} + \frac{\partial w}{\partial z} \right) \quad (2.49)$$

where

$$\nabla^2 = \frac{\partial^2}{\partial x^2} + \frac{\partial^2}{\partial y^2} + \frac{\partial^2}{\partial z^2}$$

Similarly,

$$u \frac{\partial v}{\partial x} + v \frac{\partial v}{\partial y} + w \frac{\partial v}{\partial z} + \frac{\partial v}{\partial t} = g_y - \frac{1}{\rho} \cdot \frac{\partial p}{\partial y} + \nu \nabla^2 v + \frac{\nu}{3} \cdot \frac{\partial}{\partial y} \left(\frac{\partial u}{\partial x} + \frac{\partial v}{\partial y} + \frac{\partial w}{\partial z} \right) \quad (2.50a)$$

$$u \frac{\partial w}{\partial x} + v \frac{\partial w}{\partial y} + w \frac{\partial w}{\partial z} + \frac{\partial w}{\partial t} = g_z - \frac{1}{\rho} \cdot \frac{\partial p}{\partial z} + \nu \nabla^2 w + \frac{\nu}{3} \cdot \frac{\partial}{\partial z} \left(\frac{\partial u}{\partial x} + \frac{\partial v}{\partial y} + \frac{\partial w}{\partial z} \right) \quad (2.50b)$$

For unsteady and incompressible flow, by reference to the continuity equation (Eq. 2.22), Eqs. (2.49) and (2.50a, b) reduce to

$$u \frac{\partial u}{\partial x} + v \frac{\partial u}{\partial y} + w \frac{\partial u}{\partial z} + \frac{\partial u}{\partial t} = g_x - \frac{1}{\rho} \cdot \frac{\partial p}{\partial x} + \nu \nabla^2 u \quad (2.51a)$$

$$u \frac{\partial v}{\partial x} + v \frac{\partial v}{\partial y} + w \frac{\partial v}{\partial z} + \frac{\partial v}{\partial t} = g_y - \frac{1}{\rho} \cdot \frac{\partial p}{\partial y} + \nu \nabla^2 v \quad (2.51b)$$

$$u \frac{\partial w}{\partial x} + v \frac{\partial w}{\partial y} + w \frac{\partial w}{\partial z} + \frac{\partial w}{\partial t} = g_z - \frac{1}{\rho} \cdot \frac{\partial p}{\partial z} + \nu \nabla^2 w \quad (2.51c)$$

The above equations are known as the *equations of motion for viscous fluid flow* or the *Navier-Stokes equations*. These equations in other coordinate systems are given in Appendix (Sect. 2.9).

2.4.2 Momentum Equation for Open-Channel Flow

2.4.2.1 Momentum Equation for Gradually Varied Steady Flow

A gradually varied steady flow through an open channel, whose bed is inclined at an angle θ with the horizontal, is considered. Figure 2.14 shows the forces acting on the flow within the control volume between sections 1 and 2. The application of Newton's second law of motion, in a one-dimensional flow case, to this control volume along the streamwise direction is made equating the resultant of all the external forces acting on the fluid body with the rate of change of momentum in the flowing fluid body. Thus,

$$F_1 - F_2 + F_w \sin \theta - F_f = \rho Q (\beta_2 U_2 - \beta_1 U_1) \quad (2.52)$$

where F_1 and F_2 are the resultants of the hydrostatic pressure forces in the direction of flow acting at sections 1 and 2, respectively, F_w is the weight of the

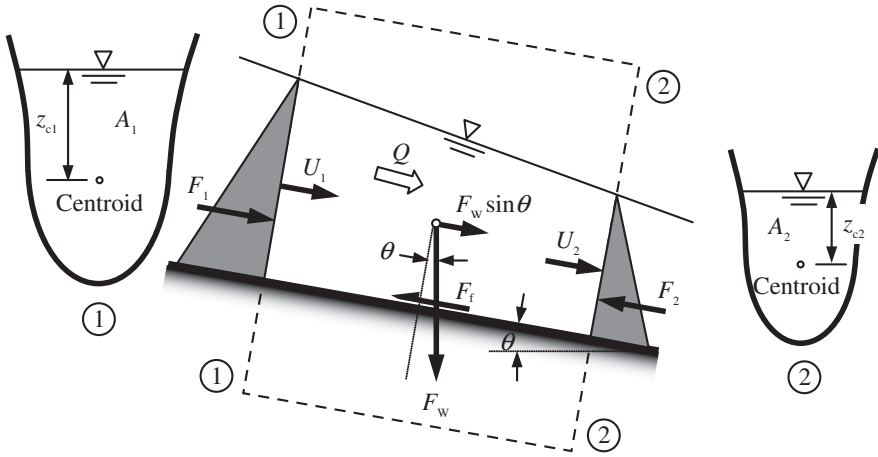


Fig. 2.14 Momentum principle applied to a gradually varied steady flow in an open channel. Forces acting on a control volume are shown

fluid within the control volume, F_f is the total external force due to frictional resistance acting along the contact surface between the fluid and the channel boundary, Q is the total flow discharge, U_1 and U_2 are the area-averaged flow velocities at sections 1 and 2, respectively, and β_1 and β_2 are the momentum coefficients at sections 1 and 2, respectively.

Assuming θ to be small or a horizontal bed ($\theta \approx 0$), F_f to be negligible for a short reach of a prismatic channel and also $\beta_1 = \beta_2 = 1$, Eq. (2.52) reduces to

$$F_1 - F_2 = \rho Q(U_2 - U_1) \quad (2.53)$$

The resultants of the hydrostatic pressure forces in the streamwise direction (that is, the horizontal direction for $\theta \approx 0$) acting on the plane flow areas A_1 and A_2 are expressed as

$$F_1 = \rho g z_{c1} A_1, \quad F_2 = \rho g z_{c2} A_2 \quad (2.54)$$

where g is the acceleration due to gravity, and z_{c1} and z_{c2} are the distances to the centroid of respective flow areas A_1 and A_2 from the free surface. Substituting $U_1 = Q/A_1$, $U_2 = Q/A_2$, and Eq. (2.54) into Eq. (2.53) yields

$$\frac{Q^2}{gA_1} + z_{c1}A_1 = \frac{Q^2}{gA_2} + z_{c2}A_2 \quad (2.55)$$

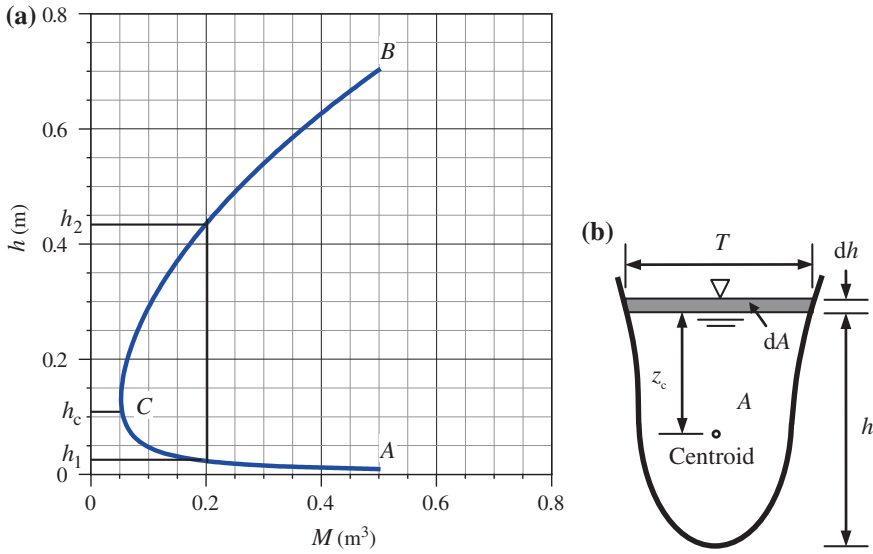


Fig. 2.15 **a** The specific force diagram and **b** a channel section

The left-hand and right-hand sides of Eq. (2.55) are analogous and therefore may be expressed by a general momentum or force function for any flow cross section as

$$M = \frac{Q^2}{gA} + z_c A \quad (2.56)$$

The first term of the right-hand side of Eq. (2.56) represents the momentum flux passing through the channel section per unit weight of fluid, and the second term is the force per unit weight of fluid. The sum of these two terms is called *specific force* and is denoted by M .

To illustrate the variation of specific force M with flow depth h given by Eq. (2.56), the *specific force diagram* [that is, $M(h)$ curve] for a given rectangular channel having width of 2 m carrying a flow discharge of $0.3 \text{ m}^3 \text{ s}^{-1}$ is drawn as shown in Fig. 2.15a. The $M(h)$ curve has two limbs, AC and BC. The lower limb AC asymptotically approaches the abscissa, while the upper limb BC rises upwards and extends indefinitely to the right. Thus, for a given value of specific force M (say $M = 0.2 \text{ m}^3$ of water as shown in Fig. 2.15), the $M(h)$ curve predicts two possible flow depths, a low stage $h_1 (=0.023 \text{ m})$ and a high stage $h_2 (=0.436 \text{ m})$. These depths are termed *sequent depths*. For instance, h_1 is the sequent depth of h_2 and vice versa. However, at point C on the $M(h)$ curve, the two depths merge and the specific force becomes a minimum [$M_{\min}(h_c = 0.132 \text{ m}) = 0.052 \text{ m}^3$, where h_c is the *critical depth*], termed *critical flow condition*. Mathematically, the minimum value of the specific force can be obtained from Eq. (2.56) by taking the first derivative of M with respect to h and setting the resulting expression equal to zero. Thus,

$$\frac{dM}{dh} = 0 \Rightarrow -\frac{Q^2}{gA^2} \cdot \frac{dA}{dh} + \frac{d}{dh}(z_c A) = 0 \quad (2.57)$$

Referring to Fig. 2.15b, note that for a change in flow depth dh , the corresponding change of the moment of the flow area, $d(z_c A)$, can be obtained as

$$d(z_c A) = \left[(z_c + dh)A + \frac{T(dh)^2}{2} \right] - z_c A \approx Adh \Rightarrow \frac{d}{dh}(z_c A) = A \quad (2.58a)$$

or

$$\frac{d}{dh}(z_c A) = \frac{d}{dh} \int_A h dA = \int_A \frac{dh}{dh} dA = A \quad (2.58b)$$

Using Eq. (2.58a) or Eq. (2.58b), $T = dA/dh$, $U = Q/A$, and $h_d = A/T$ into Eq. (2.57) yields

$$\frac{U_c^2}{2g} = \frac{h_d}{2} \Rightarrow Fr_c \left(= \frac{U_c}{\sqrt{gh_d}} \right) = 1 \quad (2.59)$$

where Fr is the flow Froude number and subscript “c” refers to the quantity for the critical condition. The above equation provides the criterion for the *critical flow*, which states that at the critical flow condition, the velocity head is equal to half the hydraulic depth or the flow Froude number is unity. In conclusion, at the critical flow condition, the specific force is a minimum for a given discharge, and the corresponding flow depth is termed *critical depth*, h_c . More discussion on critical flow is available in Sect. 2.5.1.

2.4.2.2 Momentum Equation for Gradually Varied Unsteady Flow

One can proceed to obtain equations describing an unsteady open-channel flow considering a control volume with a short reach of dx (Fig. 2.16). The bed is inclined at an angle θ with the horizontal. Applying Newton’s second law of motion in the streamwise direction (x -direction), one gets

$$pA - \left[pA + \frac{\partial(pA)}{\partial x} dx \right] + F_W \sin \theta - F_f = ma_x \quad \wedge \quad a_x = U \frac{\partial U}{\partial x} + \frac{\partial U}{\partial t} \quad (2.60)$$

where m is the mass of the fluid element ($=\rho A dx$). Using the expressions for the weight of fluid in the control volume $F_W = \rho g A dx$, the bed frictional resistance $F_f = \tau_0 P dx$, m , and a_x into Eq. (2.60) yields

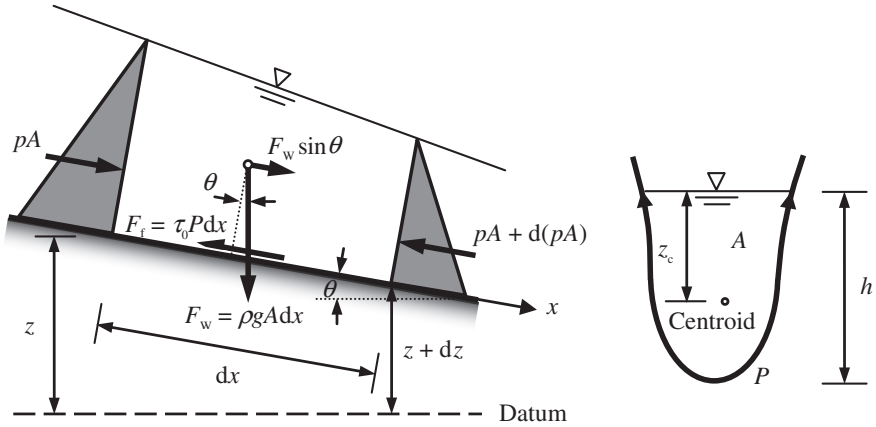


Fig. 2.16 Definition sketch for the derivation of momentum equation of a gradually varied unsteady flow in open channel

$$-\frac{\partial(pA)}{\partial x} dx + \rho g A dx \sin \theta - \tau_0 P dx = \rho A dx \left(U \frac{\partial U}{\partial x} + \frac{\partial U}{\partial t} \right) \quad (2.61)$$

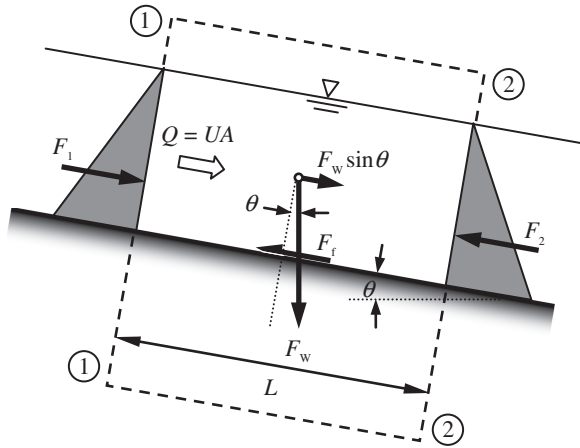
where τ_0 is the bed shear stress and P is the wetted perimeter of the channel. For a small bed slope ($\theta = \text{small}$), one can assume $\sin \theta \approx \tan \theta = -\partial z / \partial x = S_0$ (say). Dividing both sides of Eq. (2.61) by the weight of fluid, $\rho g A dx$, in the control volume and rearranging, one gets

$$-\frac{1}{\rho g A} \cdot \frac{\partial(pA)}{\partial x} + S_0 - S_f = \underbrace{\frac{U}{g} \cdot \frac{\partial U}{\partial x}}_{\text{Dynamic pressure slope}} + \underbrace{\frac{1}{g} \cdot \frac{\partial U}{\partial t}}_{\text{Acceleration slope}} \quad \wedge \quad \frac{\tau_0}{\rho g R_b} = S_f \quad (2.62)$$

where S_f is the friction slope and R_b is the hydraulic radius ($=A/P$). The first term of the left-hand side of Eq. (2.62) can be expressed in a more general way as

$$\frac{1}{\rho g A} \cdot \frac{\partial(pA)}{\partial x} = \frac{1}{\rho g A} \cdot \frac{\partial}{\partial x} (\rho g z_c A) = \frac{1}{A} \cdot \frac{\partial}{\partial x} (z_c A) = \frac{1}{A} \cdot \frac{\partial}{\partial x} \int_A h dA = \frac{1}{A} \int_A \frac{\partial h}{\partial x} dA = \frac{\partial h}{\partial x} \quad (2.63)$$

Fig. 2.17 Definition sketch for a steady uniform flow



Then, Eq. (2.62) becomes

$$\underbrace{S_f = S_0}_{\substack{\text{Kinematic} \\ \text{Uniform flow}}} - \underbrace{\frac{U}{g} \cdot \frac{\partial U}{\partial x}}_{\substack{\text{Diffusive} \\ \text{Quasi-steady} \\ \text{Steady-nonuniform flow}}} - \underbrace{\frac{1}{g} \cdot \frac{\partial U}{\partial t}}_{\substack{\text{Dynamic} \\ \text{Unsteady-nonuniform flow}}} \quad (2.64)$$

This equation is called the *general dynamic equation for gradually varied unsteady flow*. It is applicable as indicated in Eq. (2.64). It shows how nonuniformity and unsteadiness contribute to the equation of motion. Equation (2.64), also called *de Saint-Venant equation*, was first introduced by de Saint-Venant (1871).

2.4.2.3 Momentum Equation for Steady Uniform Flow

Referring to Fig. 2.17, for a steady uniform flow, $F_1 = F_2$ and $U_1 = U_2 = U$. Then, Eq. (2.52) reduces to

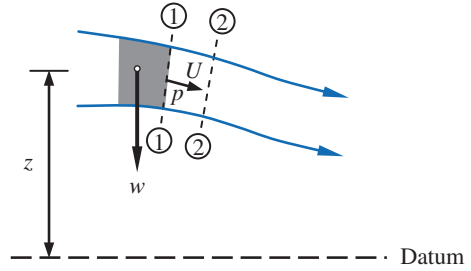
$$F_w \sin \theta - F_f = 0 \quad (2.65)$$

Using $F_w = \rho g A L$, $F_f = \tau_0 P L$, and $\sin \theta = S_0$ yields

$$\rho g A L S_0 - \tau_0 P L = 0 \quad (2.66)$$

Experiments revealed that the bed shear stress τ_0 is a function of dynamic pressure, $\lambda_f \rho U^2 / 2$, where λ_f is a friction parameter. Hence, rearranging Eq. (2.66) yields

Fig. 2.18 Definition sketch for the derivation of energy equation of fluid flow



$$U = C_R (R_b S_0)^{0.5} \quad \wedge \quad C_R = \left(\frac{2g}{\lambda_f} \right)^{0.5} \quad (2.67)$$

where C_R is the Chézy coefficient. The above equation, that defines the flow resistance, is called the *Chézy equation*, which is applicable for uniform flow in open channels. The flow depth in uniform flow is called *normal flow depth* and is denoted by h_0 .

However, the most widely used flow resistance equation for steady uniform flow is the *Manning equation*. It is

$$U = \frac{1}{n} R_b^{2/3} S_0^{0.5} \quad (2.68)$$

where n is Manning roughness coefficient. Note that the Manning equation is an empirical equation.

2.5 Conservation of Energy

An element of fluid, as shown in Fig. 2.18, acquires the potential energy due to its elevation z above the datum and the kinetic energy due to its velocity U .

If weight of the element is w , then the potential energy is wz . Thus,

$$\text{potential energy per unit weight} = z \quad (2.69)$$

Then, the kinetic energy is $wU^2/(2g)$. Thus,

$$\text{kinetic energy per unit weight} = \frac{U^2}{2g} \quad (2.70)$$

A steady fluid flow also does work due to hydrostatic pressure force acting on the cross section of fluid, as the fluid flows. If the hydrostatic pressure p acting at the section 1–1 having a cross-sectional area A , then the pressure force exerted on

1–1 is pA . The section 1–1 moves to 2–2 after a weight of fluid w transported along the streamtube. Then, the volume of fluid passing through the section 1–1 is $w/(\rho g)$. The distance between 1–1 and 2–2 is $w/(\rho g A)$. The pressure energy or the work done by the pressure is $pA \times w/(\rho g A) = pw/(\rho g)$. Therefore,

$$\text{pressure energy per unit weight} = \frac{p}{\rho g} \quad (2.71)$$

Equations (2.69)–(2.71) together represent the total energy per unit weight H in the fluid flow.

Each of the equations has the dimension of a length, called the *head*; and they are often referred to as the *hydrostatic or piezometric pressure head*, $p/(\rho g)$; the *velocity head*, $U^2/(2g)$; the *potential head*, z ; and the *total head*, H . Therefore, for a steady flow of an inviscid fluid along a streamline, the energy equation is as follows:

$$\frac{p}{\rho g} + \frac{U^2}{2g} + z = H \quad (2.72)$$

This equation is also commonly called *Bernoulli's equation*. Interestingly, Bernoulli derived it from the integration of the Euler equation along a streamline containing same terms as in Eq. (2.72).

The nonuniform distribution (variation with the vertical distance) of velocity affects the computation of kinetic energy in the flow based on the area-averaged velocity U ($=Q/A$). Figure 2.10 illustrates the nonuniform and area-averaged velocity distributions and was already used in the context of momentum calculation. Based on the area-averaged velocity, the kinetic energy flux of the fluid passing through a section is expressed as $\alpha \dot{m} U^2/2$, where α is known as the *energy coefficient* or *Coriolis coefficient*. The equation balancing the kinetic energy flux calculated from the actual velocity distribution and that obtained from the area-averaged velocity corrected by α is used to determine energy coefficient α as

$$\int_A \left(\rho u dA \frac{u^2}{2} \right) = \alpha \dot{m} \frac{U^2}{2} \Rightarrow \int_A \rho \frac{u^3}{2} dA = \alpha \rho \frac{U^3}{2} A \quad (2.73)$$

Solving for α yields

$$\alpha = \frac{1}{A} \int_A \frac{u^3}{U^3} dA \quad (2.74)$$

In straight prismatic channels, α varies approximately from 1.03 to 1.36 (Chow 1959).

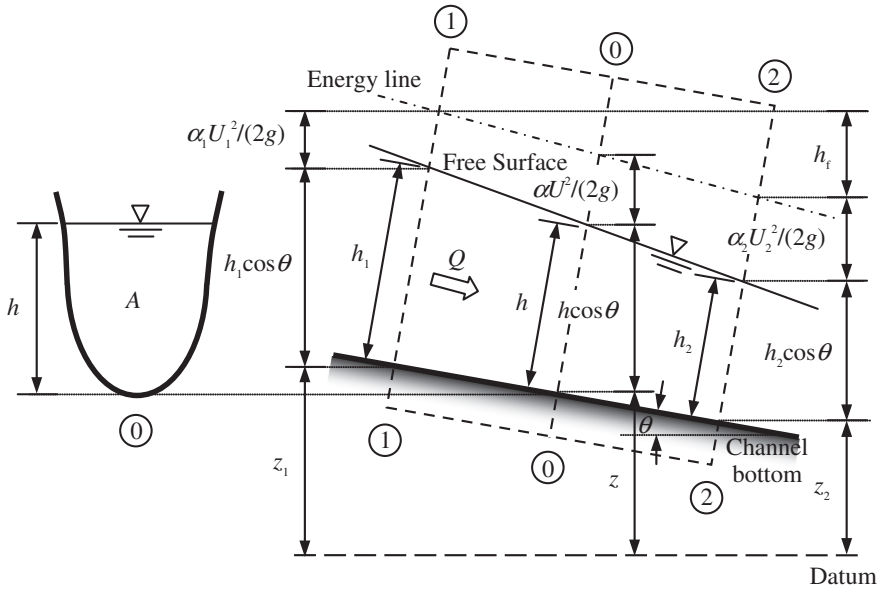


Fig. 2.19 Definition sketch for the derivation of energy equation of a gradually varied steady flow in an open channel

2.5.1 Energy Equation for Open-Channel Flow

Figure 2.19 illustrates the energy heads in a gradually varied steady flow in an open channel, whose bed is inclined at an angle θ with the horizontal. In an open-channel flow, the free surface represents the hydrostatic pressure head, provided there is no curvilinearity in the streamlines in the flow. It implies that $p/(\rho g) = h \cos \theta$, where h is the flow depth. Considering a suitable datum, the Bernoulli's equation is applied to the flow section 0-0, and the total energy head H is given by

$$z + h \cos \theta + \alpha \frac{U^2}{2g} = H \quad (2.75)$$

where α is the energy coefficient, U is the area-averaged velocity, and z is the elevation of the channel bottom above the datum. It is pertinent to mention that as the velocity distribution along the vertical distance varies, the velocity head, which is based on the constant velocity distribution U , that is truly identical for all points across the flow section, is corrected by α .

According to Bernoulli's equation, the total energy head at the upstream section 1 should be equal to the total energy head at the downstream section 2 plus the loss of energy head h_f between the two sections (Fig. 2.19). Thus,

$$z_1 + h_1 \cos \theta + \alpha_1 \frac{U_1^2}{2g} = z_2 + h_2 \cos \theta + \alpha_2 \frac{U_2^2}{2g} + h_f \quad (2.76)$$

This is the *energy equation for gradually varied flow* in an open channel. Assuming θ to be small or a horizontal bed ($\cos \theta \approx 1$) and h_f to be negligible for a short reach of a prismatic channel and also $\alpha_1 = \alpha_2 = 1$, Eq. (2.76) becomes

$$z_1 + h_1 + \frac{U_1^2}{2g} = z_2 + h_2 + \frac{U_2^2}{2g} = \text{constant } (=H) \quad (2.77)$$

Either of the above equations is known as the *energy equation for open-channel flow*.

2.5.1.1 The Specific Energy

Specific energy at a channel section is defined as the total energy head or the total energy per unit weight of the flow at the section with respect to the channel bottom. It means $z = 0$ in Eq. (2.75). Therefore, for a given channel section, the specific energy, denoted by E , is

$$E = h \cos \theta + \alpha \frac{U^2}{2g} \quad (2.78)$$

For θ to be small and $\alpha \approx 1$ (for simplicity), Eq. (2.78) becomes

$$E = h + \frac{U^2}{2g} \quad (2.79)$$

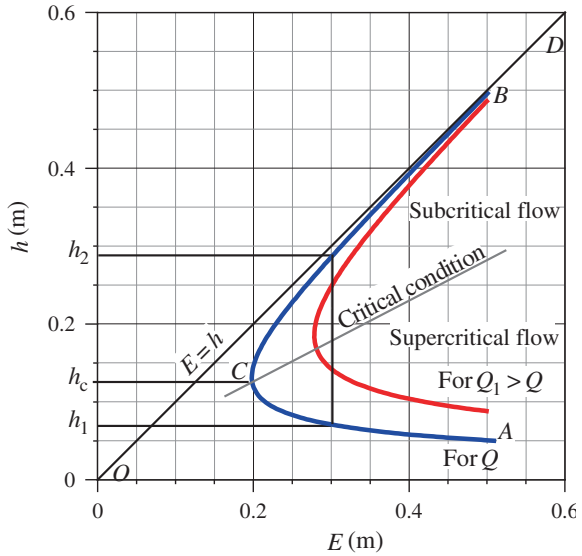
The specific energy, as indicated by Eq. (2.79), is the sum of the flow depth and the velocity head. Substituting $U = Q/A$, Eq. (2.79) becomes

$$E = h + \frac{Q^2}{2gA^2} \quad (2.80)$$

Since for a given channel section, $Q = Q(h)$ and $A = A(h)$, the specific energy E is a function of flow depth h only.

To illustrate the variation of specific energy E with flow depth h given by Eq. (2.80), the *specific energy diagram* [that is, $E(h)$ curve] for a given rectangular channel having a width of 2 m carrying a flow discharge of $Q = 0.3 \text{ m}^3 \text{ s}^{-1}$ is drawn, as shown in Fig. 2.20. The $E(h)$ curve has two limbs, AC and BC . The lower limb AC asymptotically approaches the abscissa toward the right, while the upper limb BC rises upwards and approaches the line OD as it extends to the right. The line OD that passes through the origin and is inclined at an angle 45° represents the hydrostatic pressure head or the flow depth h . Thus, for a given value of

Fig. 2.20 The specific energy diagram

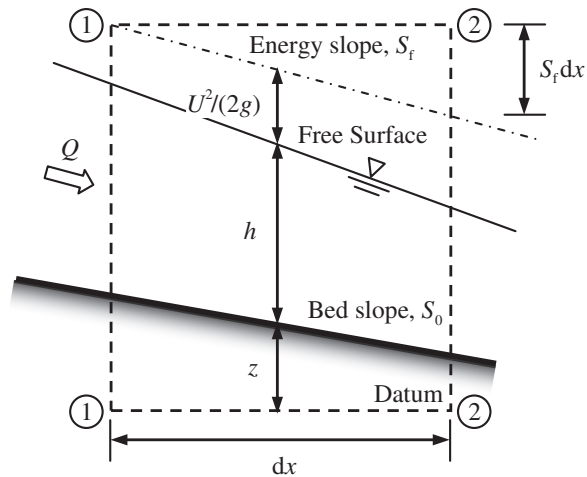


specific energy E (say $E = 0.3$ m of water as shown in Fig. 2.20), the $E(h)$ curve predicts two possible flow depths, a low stage h_1 ($=0.071$ m) and a high stage h_2 ($=0.286$ m). These depths are termed *alternate depths*. For instance, h_1 is the alternate depth of h_2 , and vice versa. However, at point C on the curve, the alternate depths merge and the specific energy becomes a minimum. The flow corresponding to a minimum specific energy is known as *critical flow* and the resulting flow depth is termed *critical depth*, h_c . In Fig. 2.20, the minimum specific energy $E_{\min} = 0.198$ m corresponds to a critical depth $h_c = 0.132$ m. When the flow depth is greater than the critical depth, the flow velocity is less than the critical velocity for a given discharge, and hence, the flow is called *subcritical*. On the other hand, when flow depth is less than the critical depth, the flow is *supercritical*. Hence, h_1 is the supercritical flow depth and h_2 is the subcritical flow depth. With the change in discharge, the $E(h)$ curve changes its position. Figure 2.20 also shows another $E(h)$ curve for a discharge $Q_1 = 0.5 \text{ m}^3 \text{ s}^{-1}$, which is greater than the previous discharge $Q = 0.3 \text{ m}^3 \text{ s}^{-1}$. The $E(h)$ curve of Q_1 lies on the right side of $E(h)$ curve of Q . Similarly, the $E(h)$ curve of a discharge less than Q will lie on the left side of $E(h)$ curve of Q .

Mathematically, the minimum value of the specific energy can be obtained from Eq. (2.80) by taking the first derivative of E with respect to h and setting the resulting expression equal to zero. Thus,

$$\frac{dE}{dh} = 0 \Rightarrow 1 - \frac{Q^2}{gA^3} \cdot \frac{dA}{dh} = 0 \quad (2.81)$$

Fig. 2.21 Schematic of a gradually varied flow in an open channel



Using $T = dA/dh$ and $h_d = A/T$ into Eq. (2.81) yields

$$\frac{Q^2 T}{g A^3} = 1 \Rightarrow \frac{U_c^2}{2g} = \frac{h_d}{2} \Rightarrow Fr_c \left(= \frac{U_c}{\sqrt{gh_d}} \right) = 1 \quad (2.82)$$

Equation (2.82) provides the criterion for the *critical flow*, which is similar to that discussed in Sect. 2.4.2. In summary, at the critical flow condition, the specific energy is minimum for a given discharge. Hence, for critical condition, $h = h_c$, $U = U_c$, and $Fr = Fr_c = 1$; for subcritical condition, $h > h_c$, $U < U_c$, and $Fr < 1$; and for supercritical condition, $h < h_c$, $U > U_c$, and $Fr > 1$.

2.5.1.2 The Gradually Varied Flow

Figure 2.21 shows a schematic of a *gradually varied flow* (GVF) in a prismatic open channel. The definition of a GVF indicates two conditions: (1) steady flow and (2) practically parallel streamline flow, that is, a hydrostatic pressure distribution prevailing along the depth. The derivation of a GVF profile is based on the following assumptions:

- The channel is prismatic.
- The flow depth is indifferent whether it is measured in the vertical or normal (to the channel bed) direction. It means the bed slope is small; and hence, $h \approx h \cos \theta$ such that $\cos \theta \approx 1$.
- The head loss at a channel section is identical as for a uniform flow having the same velocity and hydraulic radius of the section. Thus, the resistance equation, such as the Manning equation, for the uniform flow can be used to determine the energy slope of a GVF.

- (d) The friction coefficient is independent of the flow depth and unchanged throughout the channel reach, that is under consideration.

Considering $\cos \theta \approx 1$ and $\alpha \approx 1$ and differentiating Eq. (2.75) with respect to x , one gets

$$\frac{dH}{dx} = \frac{dz}{dx} + \frac{dh}{dx} + \frac{d}{dx} \left(\frac{U^2}{2g} \right) \quad (2.83)$$

Using $U = Q/A$ and $T = dA/dh$, the last term of the right-hand side of Eq. (2.83) is developed as

$$\frac{d}{dx} \left(\frac{U^2}{2g} \right) = \frac{d}{dh} \left(\frac{Q^2}{2gA^2} \right) \frac{dh}{dx} = -\frac{Q^2}{gA^3} \cdot \frac{dA}{dh} \cdot \frac{dh}{dx} = -\frac{Q^2 T}{gA^3} \cdot \frac{dh}{dx} \quad (2.84)$$

Substituting Eq. (2.84) into Eq. (2.83) and rearranging yield

$$\frac{dh}{dx} = \frac{S_0 - S_f}{1 - \frac{Q^2 T}{gA^3}} \quad \wedge \quad \frac{dH}{dx} = -S_f \quad \vee \quad \frac{dz}{dx} = -S_0 \quad (2.85)$$

where S_f is the energy or friction slope and S_0 is the bed slope. Further, using $h_d = A/T$ and $Q = UA$ into Eq. (2.85), it produces

$$\frac{dh}{dx} = \frac{S_0 - S_f}{1 - Fr^2} \quad \wedge \quad Fr = \frac{U}{\sqrt{gh_d}} \quad (2.86)$$

This is the general differential equation of a *GVF* and predicts the free surface profiles. Flow with a positive value of dh/dx refers to an increase in flow depth along the streamwise direction and is called *backwater curve*. On the other hand, flow with a negative value of dh/dx refers to a decrease in flow depth along the streamwise direction and is called *drawdown curve*. However, for a uniform flow, $dh/dx = 0$ or $S_0 = S_f$.

Classification of Bed Slope: A downward bed slope (positive value of S_0) is classified as *steep* if the normal depth is less than the critical depth (that is, the normal flow is supercritical) and *mild* if the normal depth is greater than the critical depth (that is, the normal flow is subcritical).² Other types of slopes are *critical* ($S_0 = S_c > 0$ and $h_0 = h_c$), *horizontal* ($S_0 = 0$ and $h_0 \rightarrow \infty$), and *adverse* ($S_0 < 0$ and $h_0 = \text{imaginary}$). The slopes are designated using the first characters as *S*, *M*, *C*, *H*, and *A* for steep, mild, critical, horizontal, and adverse slopes, respectively. Further, to designate the flow profiles (that is, free surface profiles) corresponding to a given slope, the second characters 1, 2, and 3 are used as the subscript of the

² Alternatively, a downward slope is *steep* if it exceeds the critical slope S_c (that is the slope at which the normal depth of flow is critical depth). Hence, $S_0 > S_c$. Similarly, *mild slope* can be explained.

Fig. 2.22 Steep slope profiles (*S*-profiles)

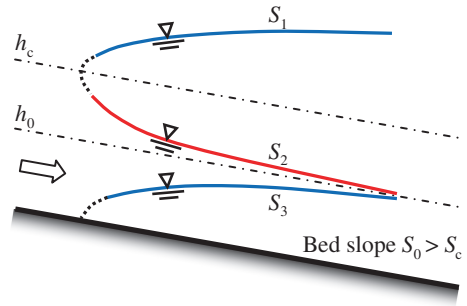


Fig. 2.23 Mild slope profiles (*M*-profiles)

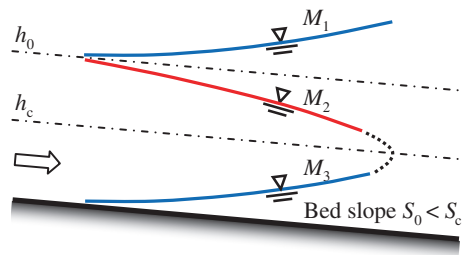


Fig. 2.24 Critical slope profiles (*C*-profiles)

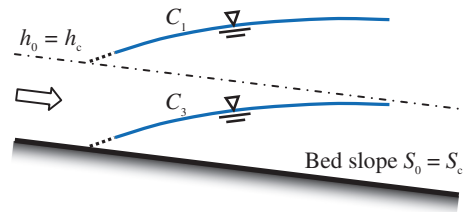
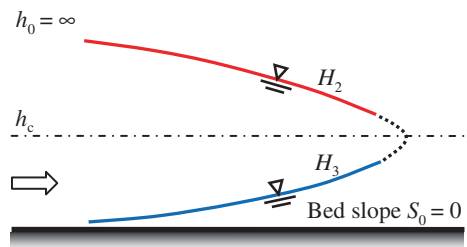
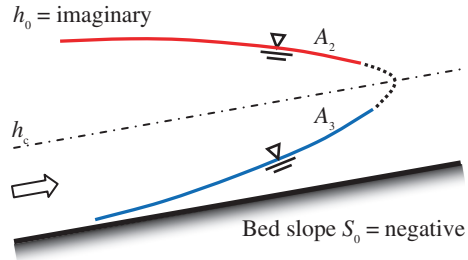


Fig. 2.25 Horizontal slope profiles (*H*-profiles)



first characters referring to the zone, where the actual depth h lies with respect to the flow depth lines for h_c and h_0 and the channel bed. By convention, zone 1 refers to the zone above the upper line, whichever (either h_c or h_0) it may be; zone 2 is the zone between the two lines; and zone 3 is the zone between the bed and the lower line. Figures 2.22, 2.23, 2.24, 2.25 and 2.26 show various flow profiles.

Fig. 2.26 Adverse slope profiles (A-profiles)



A number of methods to compute steady GVF from Eq. (2.86) are furnished in Chow (1959). The direct and standard step methods solve the energy equation between two consecutive channel sections. Dey (2000) presented a generalized numerical solution in the *Chebyshev form* for the standard step method. Then, a number of numerical methods are also available to integrate the differential equation, Eq. (2.86). These methods do not allow a direct solution, and therefore, trial-and-error method of solution is to be used (Chaudhry 2008).

2.5.1.3 Pressure Distribution in Curvilinear Flow

In the preceding cases, the streamlines were straight and parallel to the channel bottom. For instance, streamlines in a uniform flow are practically parallel and those in GVF may also be regarded as parallel, since the variation of flow depth is gradual that the streamlines have neither considerable curvature nor steep divergence/convergence. However, in real-life cases, the streamlines in several flow situations have pronounced curvature and/or divergence/convergence that the effects of acceleration components on the flow section are significant.

When the streamlines in a fluid flow have substantial curvature, the flow is called *curvilinear flow*. The curvature of streamlines is to induce considerable acceleration component normal to the direction of flow, called *centrifugal acceleration*. Thus, the pressure distribution in a curvilinear flow over the flow depth departs from the hydrostatic law, that is, $p = \rho gh$. Such curvilinear flows may be either convex or concave as shown in Figs. 2.27a, b. In a convex flow situation guided by a convex boundary, the centrifugal acceleration acts upward against the gravity and the resulting pressure is less than the hydrostatic pressure. On the other hand, in a concave flow situation guided by a concave boundary, the centrifugal acceleration acts downward to add to the gravity and the resulting pressure is greater than the hydrostatic pressure. Likewise, when streamlines have considerable divergence/convergence to develop appreciable acceleration normal to the flow direction, the pressure distribution again departs from the hydrostatic law. The distribution of pressure can be obtained by the Euler equations (Eqs. 2.39–2.41). In normal or radial direction of flow, it is

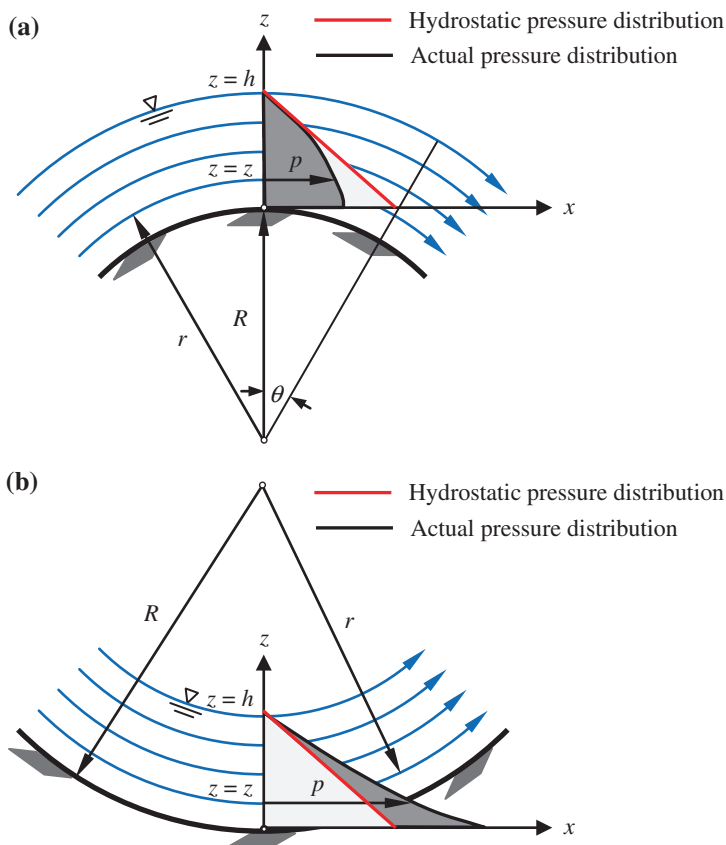


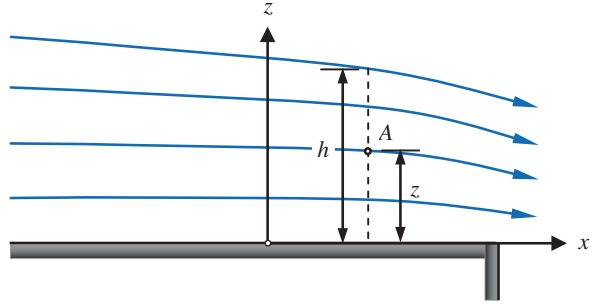
Fig. 2.27 Pressure distributions in curvilinear flows: **a** convex flow and **b** concave flow

$$\frac{\partial}{\partial z} \left(\frac{p}{\rho g} + z \cos \theta \right) = \pm \frac{a_r}{g} \quad (2.87)$$

where a_r is the centrifugal acceleration at the radius of curvature r of the streamline and θ is the angle between the section of interest and the vertical line. The centrifugal acceleration at any point in a curvilinear flow is $a_r = u^2/r$, where u is the tangential velocity at r . It is positive for the concave flow and negative for the convex flow. Integrating Eq. (2.87) within limits $z = z$ and $z = h$ yields

$$\frac{p}{\rho g} = (h - z) \cos \theta \pm \frac{1}{g} \int_h^z \frac{u^2}{r} dz \quad (2.88)$$

Fig. 2.28 Schematic of flow with a small free surface curvature



The above expression can be evaluated if $u = u(r)$ is known using $r = R \pm z$, where positive z is for convex flow and negative z for concave flow. Here, R is the radius of curvature of the channel boundary. For instance, (1) u can be invariant of r , as an average velocity; (2) u is proportional to r for forced vortex type of flow; and (3) u is proportional to r^{-1} for free vortex type of flow.

2.5.1.4 Pressure Distribution in Flow with Small Free Surface Curvature

Figure 2.28 shows a schematic of a free overfall whose free surface curvature is relatively small varying from a finite value at the free surface to zero at the channel bottom. According to Boussinesq approximation (Jaeger 1957), a linear variation of the streamline curvature at any point A at a vertical distance z is assumed. Hence, the radius of curvature r of a streamline at A is expressed as

$$\frac{1}{r} = \frac{z}{h} \cdot \frac{1}{r_s} \quad (2.89)$$

where r_s is the radius of curvature of the free surface. For small free surface curvature, it can be approximated as

$$\frac{1}{r_s} = \frac{d^2h}{dx^2} \quad (2.90)$$

where x is the streamwise distance. The normal acceleration a_z based on the aforementioned assumption is given by

$$a_z = Kz \quad \wedge \quad K = \frac{U^2}{h} \cdot \frac{d^2h}{dx^2} \quad (2.91)$$

where U is the average flow velocity over depth h ; hence, it is constant along the vertical distance. Considering the bottom as a datum and then integrating Eq. (2.87), the hydrostatic pressure head h_p at point A is obtained as

$$h_p = \left(\frac{p}{\rho g} + z \right) = -\frac{1}{g} \int Kz dz + C = -\frac{K}{g} \cdot \frac{z^2}{2} + C \quad (2.92)$$

Using the boundary condition, at $z = h$, $p = 0$, and $h_p = h$, it leads to

$$C = h + \frac{K}{g} \cdot \frac{h^2}{2} \quad (2.93)$$

Hence, from Eq. (2.92), the hydrostatic pressure head h_p is obtained as

$$h_p = h + \frac{K(h^2 - z^2)}{2g}, \quad \therefore \quad h_p = h + \Delta h \quad (2.94)$$

It indicates that the variation of hydrostatic pressure head is given by Δh . Therefore, the depth-averaged value of Δh can be determined as

$$\overline{\Delta h} = \frac{1}{h} \int_0^h \Delta h dz = \frac{1}{h} \cdot \frac{K}{2g} \int_0^h (h^2 - z^2) dz = \frac{Kh^2}{3g} \quad (2.95)$$

The effective hydrostatic pressure head h_{ep} is therefore

$$h_{ep} = h + \frac{Kh^2}{3g} = h + \frac{U^2 h}{3g} \cdot \frac{d^2 h}{dx^2} \quad (2.96)$$

Note that $d^2 h/dx^2$ is negative for convex flow and positive for concave flow.

2.6 The Boundary Layer

According to the concept of the ideal fluid flow (that is, the potential flow), a streamline follows the solid boundary, termed *limiting streamline*, involving a finite fluid velocity at the boundary. It, in fact, implies that the fluid particles slip at the boundary, as a result of which, the no-slip condition is not preserved in the ideal fluid flow. However, in real fluid flow, the viscosity causes the fluid particles to have no motion at the boundary preserving a no-slip condition. In reality, the velocity, that is zero at the boundary, keeps increasing with the perpendicular distances away from the boundary. The change in velocity is discernible only within a layer adjacent to the boundary. The layer close to the solid boundary affected by the boundary shear is called *boundary layer*, where the viscous effects

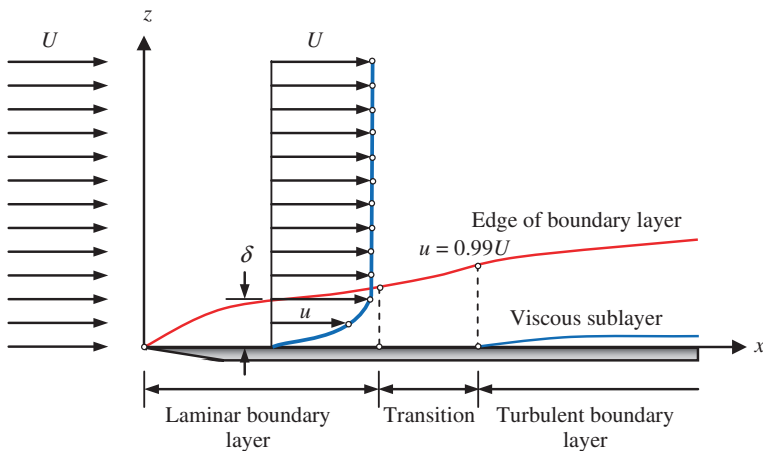


Fig. 2.29 Details of a boundary layer developed over a flat plate

are prominent. This phenomenon was discovered by Prandtl (1904). He, however, arbitrarily suggested the boundary layer to extend up to 99 % of the free stream velocity U . Hence, it is possible to define the *boundary layer thickness* δ as that the distance from the boundary where the local velocity u equals $0.99U$:

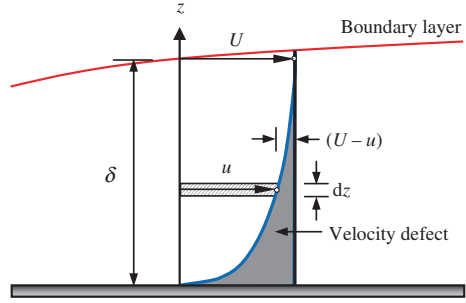
$$\delta = z|_{u=0.99U}$$

In fluid flow outside the boundary layer, the effects of viscosity may be vanishingly small that the theory of ideal fluid flow is applicable. Importantly, *boundary layer is not a streamline*. It is worth mentioning that the concept of boundary layer is the most significant contribution to the development of hydrodynamics.

2.6.1 Characteristics of Boundary Layer

Consider a fluid flow over a flat plate aligned parallel to the approaching free stream, as shown in Fig. 2.29. The approaching free stream that has a velocity U suffers retardation in the vicinity of the plate due to the viscous resistance offered by the solid boundary. The boundary layer starts growing from the leading edge of the plate. Its thickness increases with distance from the leading edge as more and more fluid is to decelerate by the viscous resistance near the solid boundary. Near the leading edge, the flow in the boundary layer is entirely laminar. With an increase in distance, the laminar boundary layer thickness grows becoming progressively unstable and eventually changes to a turbulent boundary layer over a *transition region*. The transition occurs in the range $R_x = 3 \times 10^5$ to 10^6 ,

Fig. 2.30 The velocity defect



where $R_x = Ux/\nu$. Even in the region of the turbulent boundary layer, the turbulence becomes suppressed to such a degree that the viscous effects predominate and a very thin layer adjacent to the solid boundary remains laminar, which is called the *viscous sublayer*.

The boundary layer thickness is the distance from the boundary to a point where the velocity is $0.99U$, which has already been discussed. It is based on the fact that beyond this arbitrary limit of vertical distance $z|_{u=0.99U}$, the viscous stresses are practically absent. Other definitions of thickness, such as *displacement thickness* and *momentum thickness*, are also useful in boundary layer theory.

The presence of a boundary introduces a retardation to the free stream velocity in the vicinity of the boundary. The difference $(U - u)$, called the *velocity defect*, causes a decrease in the mass flux as compared to the mass flux of the free stream that would pass through the same section in the absence of the boundary layer (see Fig. 2.30). To compensate for this defect, the actual boundary may be imagined to have been displaced by a *displacement thickness* δ^* such that the mass flux would be the same as that of an ideal fluid flowing over the displaced boundary. The equivalence of the two mass fluxes yields the displacement thickness in incompressible flow ($\rho = \text{constant}$) as

$$\int_0^\delta \rho u dz = \int_{\delta^*}^\delta \rho U dz \Rightarrow \int_0^\delta u dz = \int_0^\delta U dz - U\delta^*, \quad \therefore \quad \delta^* = \int_0^\delta \left(1 - \frac{u}{U}\right) dz \quad (2.97)$$

Further, the retardation of flow within the boundary layer causes a reduction in the momentum flux as well. The *momentum thickness* θ is defined as the thickness of an imaginary layer in free stream flow which has a momentum flux equals the deficiency of momentum flux over the entire section caused to the actual mass flux within the boundary layer. Mathematically, for an incompressible flow ($\rho = \text{constant}$), it can be developed as

$$\rho U^2 \theta = \int_0^\delta \rho u (U - u) dz, \quad \therefore \quad \theta = \int_0^\delta \frac{u}{U} \left(1 - \frac{u}{U}\right) dz \quad (2.98)$$

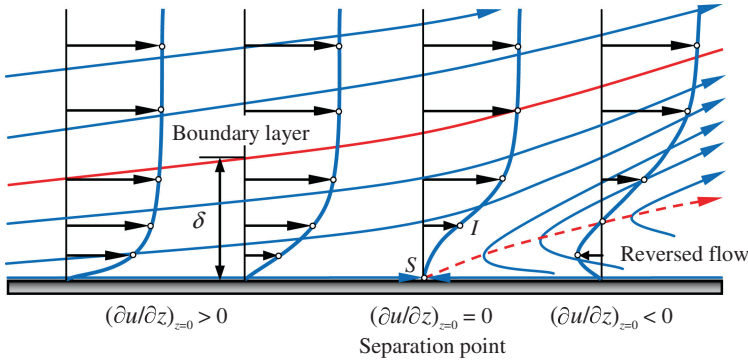


Fig. 2.31 Boundary layer separation

The *shape factor* H_s , that is defined as the ratio of the displacement thickness to the momentum thickness is used to determine the nature of the flow.

$$H_s = \frac{\delta^*}{\theta} \quad (2.99)$$

For a higher value of shape factor H_s , a stronger adverse pressure gradient ($\partial p / \partial x > 0$) is indicated. Conventionally, $H_s = 2.59$ is typical for laminar flow, while $H_s = 1.3 - 1.4$ is typical for turbulent flow.

2.6.1.1 Boundary Layer Separation

In a favorable streamwise pressure gradient ($\partial p / \partial x < 0$), the flow is accelerated by the pressure force and thereby the boundary layer thickness keeps thin. In contrast, when the flow encounters an adverse streamwise pressure gradient ($\partial p / \partial x > 0$) along the solid boundary, the flow is decelerated by the pressure force, thereby causing the boundary layer to thicken. Then, the flow cannot advance too far in the region of adverse pressure gradient due to the insufficient kinetic energy that the fluid flow possesses. As a result, the boundary layer is deflected from the wall, known to be the *separated boundary layer*, which progresses into the main flow, as shown in Fig. 2.31. In general, the flow downstream the *separation point* (point S) experiences the adverse pressure gradient and turns to the reverse direction of the main flow that exists in the upper region of the separation line. As a result of the flow reversal, the boundary layer is thickened rapidly. The separation point is defined as the limit between the main and the reverse flow in the immediate vicinity of the wall. Further, in explaining the separation phenomenon by the

potential flow theory, the streamlines within the boundary layer in the vicinity of the boundary layer separation are shown in Fig. 2.31. At the separation point, a streamline originates from the wall at a certain angle due to the merger of two limiting streamlines moving in the opposite direction. The separation point can be determined by the condition that the velocity gradient normal to the wall becomes zero on the wall, that is, $\partial u / \partial z|_{z=0}^S = 0$.

The integral equation of the boundary layer to be discussed in the Sect. 2.6.2 is only applicable to the extent where the separation point occurs. At a short distance downstream the separation point, the boundary layer becomes so thick that the assumptions that are made in deriving the boundary layer equation no longer apply. In a steady flow, the event of separation that occurs only in a decelerated flow can be obtained from the relation between the pressure gradient $\partial p / \partial x$ and the velocity distribution $u(z)$ with the aid of the Navier–Stokes equations. From Eq. (2.51a) with the boundary condition $u = w = 0$ (no-slip at the wall, $z = 0$) in a two-dimensional flow, one can have at $z = 0$

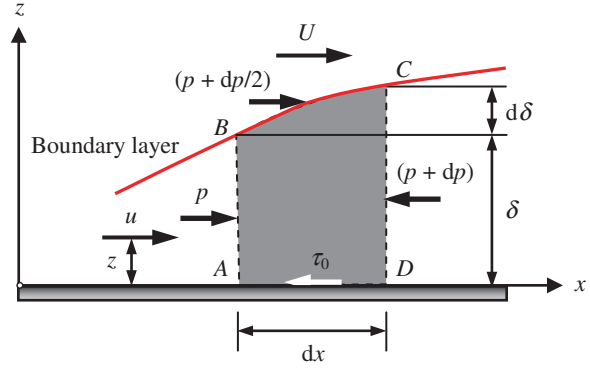
$$\mu \frac{\partial^2 u}{\partial z^2} \Big|_{z=0}^S = \frac{\partial p}{\partial x} \Rightarrow \frac{\partial^3 u}{\partial z^3} \Big|_{z=0} = 0$$

In the vicinity of the wall, the curvature of the velocity distribution $\partial^2 u / \partial z^2$ depends only on the pressure gradient $\partial p / \partial x$. The curvature $\partial^2 u / \partial z^2|_{z=0}$ at the wall does changeover its sign with $\partial p / \partial x$. In flow with a decreasing pressure (accelerated flow, $\partial p / \partial x < 0$), the prevailing condition is $\partial^2 u / \partial z^2|_{z=0} < 0$; and therefore, $\partial^2 u / \partial z^2$ is negative over the entire boundary layer thickness (Fig. 2.31). On the other hand, in flow within the near-wall layer of increasing pressure (decelerated flow, $\partial p / \partial x > 0$), the prevailing condition is $\partial^2 u / \partial z^2 > 0$. In flow with $\partial^2 u / \partial z^2 < 0$ at some distance above the wall, there must exist a point (point *I*) for which $\partial^2 u / \partial z^2 = 0$, which is an *inflexion point* of the velocity distribution within the boundary layer (Fig. 2.31). It suggests that in the region of decelerating potential flow, the velocity distribution within the boundary layer always displays an inflexion point. Since there exists $\partial^2 u / \partial z^2 < 0$ at the edge of the boundary layer, the velocity distribution that has a separation point with $\partial u / \partial z|_{z=0} = 0$ must have an inflexion point.

2.6.2 von Kármán Momentum Integral Equation

Consider a control volume *ABCD* of elementary length dx having a boundary layer thickness δ , as shown in Fig. 2.32. For a steady flow, the forces on the control surface are caused by the pressure and the wall or boundary shear stress. As the flow is almost parallel, a uniform pressure at a section can be assumed, neglecting the hydrostatic pressure. The components of force (per unit area and width) in x -direction are shown in Fig. 2.32. Since the boundary layer is thin, the pressure within the boundary layer at a section equals the pressure in the free stream portion at that section outside the boundary layer. The summation of forces in x -direction is

Fig. 2.32 Control volume in the boundary layer



$$\sum F_x = p\delta - (p + dp)(\delta + d\delta) + \left(p + \frac{dp}{2}\right)d\delta - \tau_0 dx \quad \wedge \quad dp = \frac{\partial p}{\partial x} dx \quad (2.100)$$

Simplifying and neglecting second-order terms, Eq. (2.100) becomes

$$\sum F_x = -\left(\delta \frac{\partial p}{\partial x} + \tau_0\right) dx \quad (2.101)$$

Change of momentum flux in the control volume is

$$\begin{aligned} & \underbrace{\int_0^\delta \rho u^2 dz + \frac{\partial}{\partial x} \left(\int_0^\delta \rho u^2 dz \right) dx}_{\text{Through } CD} - \underbrace{\int_0^\delta \rho u^2 dz}_{\text{Through } AB} + \underbrace{\rho U(w dx - u d\delta)}_{\text{Through } BC} \\ &= \frac{\partial}{\partial x} \left(\int_0^\delta \rho u^2 dz \right) dx + \rho U(w dx - u d\delta) \end{aligned}$$

By Newton's second law of motion, one can write

$$-\left(\delta \frac{\partial p}{\partial x} + \tau_0\right) dx = \frac{\partial}{\partial x} \left(\int_0^\delta \rho u^2 dz \right) dx + \rho U(w dx - u d\delta) \quad (2.102)$$

The continuity of flow for the control volume that constitutes the equation is³

³ The mass flux through BC can be obtained as $\rho(\hat{u}\hat{i} + \hat{w}\hat{k}) \cdot (-d\delta\hat{i} + dx\hat{k}) = \rho(-u d\delta + w dx)$.

$$\underbrace{- \int_0^\delta \rho u dz}_{\text{Through } AB} + \underbrace{\int_0^\delta \rho u dz + \frac{\partial}{\partial x} \left(\int_0^\delta \rho u dz \right) dx}_{\text{Through } CD} + \underbrace{\rho(w dx - u d\delta)}_{\text{Through } BC} = 0, \quad (2.103)$$

$$\therefore \rho(w dx - u d\delta) = - \frac{\partial}{\partial x} \left(\int_0^\delta \rho u dz \right) dx$$

Using Eq. (2.103) into Eq. (2.102) and replacing partial differential by total differential yield

$$-\delta \frac{dp}{dx} - \tau_0 = \frac{d}{dx} \int_0^\delta \rho u^2 dz - U \frac{d}{dx} \int_0^\delta \rho u dz \quad (2.104)$$

Further, the pressure gradient dp/dx can be determined from the Bernoulli's equation (Eq. 2.72), considering the potential head $z = 0$. Hence,

$$\frac{p}{\rho g} + \frac{U^2}{2g} = H \Rightarrow p + \frac{\rho}{2} U^2 = \text{constant} \quad (2.105)$$

Differentiating with respect to x and rearranging, Eq. (2.105) becomes

$$\frac{dp}{dx} = -\rho U \frac{dU}{dx} \quad (2.106)$$

Substituting the expression of dp/dx into Eq. (2.104), the wall shear stress τ_0 for incompressible flow ($\rho = \text{constant}$) is obtained as

$$\tau_0 = -\rho \frac{d}{dx} \int_0^\delta u^2 dz + \rho U \frac{d}{dx} \int_0^\delta u dz + \rho U \delta \frac{dU}{dx}, \quad (2.107)$$

$$\therefore \tau_0 = \rho \frac{d}{dx} (U^2 \theta) + \rho U \delta \frac{dU}{dx}$$

Equation (2.107) is the generalized *von Kármán momentum integral equation*, which can be applicable for both laminar and turbulent boundary layer flows.

If the flow has a zero-pressure gradient $dp/dx = 0$, then $dU/dx = 0$; and Eq. (2.107) reduces to

$$\tau_0 = \rho U^2 \frac{d\theta}{dx} \quad (2.108)$$

2.6.2.1 Laminar Boundary Layer Over a Flat Plate in a Zero-Pressure Gradient Flow

The *laminar boundary layer* is formed as a result of flow over a short reach of the leading edge of a flat plate. In practice, it always prevails, even in flows that are evidently turbulent. To apply von Kármán momentum integral equation for such a flow situation, the assumption on the velocity u distribution, which is reasonably a function of η ($=z/\delta$) and invariant of x , is an essential prerequisite. For an approximate analysis of a laminar boundary layer, a third-order polynomial law ($u/U = A + B\eta + C\eta^2 + D\eta^3 = f$, where A , B , C , and D are the coefficients) of velocity distribution that satisfies the boundary conditions (1) $u(z = 0) = 0$, (2) $\partial^2 u / \partial z^2 (z = 0) = 0$, (3) $u(z = \delta) = U$, and (4) $\partial u / \partial z (z = \delta) = 0$ was assumed by Prandtl within the boundary layer ($0 \leq z \leq \delta$). The coefficients are obtained as $A = C = 0$, $B = 3/2$ and $D = -1/2$. Therefore, the velocity distribution is

$$\frac{u}{U} = f(\eta) \quad \wedge \quad f(0 \leq \eta < 1) = \frac{3}{2}\eta - \frac{1}{2}\eta^3, \quad f(\eta \geq 1) = 1 \quad (2.109)$$

Inserting Eq. (2.109) into Eq. (2.108), one can obtain

$$\begin{aligned} \tau_0 &= \rho U^2 \frac{d\theta}{dx} = \rho U^2 \frac{d\delta}{dx} \int_0^1 f(1-f) d\eta = \rho U^2 \frac{d\delta}{dx} \int_0^1 \left(\frac{3}{2}\eta - \frac{1}{2}\eta^3 \right) \left(1 - \frac{3}{2}\eta + \frac{1}{2}\eta^3 \right) d\eta \\ &= 0.139 \rho U^2 \frac{d\delta}{dx} \quad \wedge \quad \theta = \delta \int_0^1 f(1-f) d\eta \end{aligned} \quad (2.110)$$

Further, applying Newton's law of viscosity at the boundary, one gets

$$\tau_0 = \mu \left. \frac{du}{dz} \right|_{z=0} = \mu \frac{U}{\delta} \cdot \left. \frac{df}{d\eta} \right|_{\eta=0} = \mu \frac{U}{\delta} \cdot \frac{d}{d\eta} \left(\frac{3}{2}\eta - \frac{1}{2}\eta^3 \right) \Big|_{\eta=0} = \frac{3}{2} \mu \frac{U}{\delta} \quad (2.111)$$

Equating Eqs. (2.110) and (2.111) and rearranging yield

$$\delta d\delta = 10.79 \frac{\nu}{U} dx \quad (2.112)$$

The above equation is integrated as follows:

$$\int_0^\delta \delta d\delta = 10.79 \frac{\nu}{U} \int_0^x dx \quad \wedge \quad \frac{\delta^2}{2} = 10.79 \frac{\nu}{U} x, \quad \therefore \quad \delta = 4.643 x R_x^{-0.5} \quad (2.113)$$

Equation (2.113) can be used to determine the boundary layer thickness $\delta(x)$, which varies directly as a square root of distance x . Substituting the expression for δ into Eq. (2.111), the wall shear stress expression $\tau_0(x)$ is obtained. It is

$$\tau_0 = 0.323\rho U \left(v \frac{U}{x} \right)^{0.5} = 0.323\mu \frac{U}{x} R_x^{0.5} \quad (2.114)$$

It indicates that the wall shear stress varies inversely as a square root of distance x . Equation (2.114) can be used to determine the wall shear resistance per unit width F_τ on the surface of the plate for a given length $x = 0$ to L as

$$F_\tau = \int_0^L \tau_0 dx = 0.646\rho U (vUL)^{0.5} = 0.646\rho U v R_L^{0.5} \quad \wedge \quad R_L = \frac{UL}{v} \quad (2.115)$$

2.6.2.2 Turbulent Boundary Layer Over a Flat Plate in a Zero-Pressure Gradient Flow

For the approximation of a turbulent boundary layer, a 1/7-th power law of velocity distribution, which is a good replacement of the logarithmic law (Sect. 3.7.2), as proposed by Prandtl, can be assumed within the boundary layer ($0 \leq z \leq \delta$). Thus,

$$\frac{u}{U} = f(\eta) \quad \wedge \quad f(0 \leq \eta < 1) = \eta^{1/7}, \quad f(\eta \geq 1) = 1 \quad (2.116)$$

Inserting Eq. (2.116) into Eq. (2.108), one can obtain

$$\tau_0 = \rho U^2 \frac{d\delta}{dx} \int_0^1 f(1-f) d\eta = \rho U^2 \frac{d\delta}{dx} \int_0^1 \eta^{1/7} (1 - \eta^{1/7}) d\eta = \frac{7}{72} \rho U^2 \frac{d\delta}{dx} \quad (2.117)$$

Blasius (1912, 1913) obtained the wall shear stress for hydraulically smooth flow as

$$\tau_0 = 2.28 \times 10^{-2} \rho U^2 \left(\frac{v}{U\delta} \right)^{0.25} \quad (2.118)$$

Equating Eqs. (2.117) and (2.118) and rearranging yield

$$\delta^{0.25} d\delta = 0.235 \left(\frac{v}{U} \right)^{0.25} dx \quad (2.119)$$

The above equation is integrated as follows:

$$\int_0^{\delta} \delta^{0.25} d\delta = 0.235 \left(\frac{v}{U} \right)^{0.25} \int_0^x dx \quad \wedge \quad \delta^{1.25} = 0.294 \left(\frac{v}{U} \right)^{0.25} x, \quad (2.120)$$

$$\therefore \delta = 0.376 x R_x^{-0.2}$$

Hence, the turbulent boundary layer thickness increases with distance as $x^{0.8}$, as compared to the laminar boundary layer thickness that varies as $x^{0.5}$. It indicates that the turbulent boundary layer thickness grows faster. Substituting the expression for δ into Eq. (2.118) yields

$$\tau_0 = 2.91 \times 10^{-2} \rho U^2 \left(\frac{v}{U_x} \right)^{0.2} = 2.91 \times 10^{-2} \rho U^2 R_x^{-0.2} \quad (2.121)$$

The wall shear resistance per unit width F_τ on the surface of the plate for a given length $x = 0$ to L is

$$F_\tau = \int_0^L \tau_0 dx = 3.638 \times 10^{-2} \rho U^2 L \left(\frac{v}{UL} \right)^{0.2} = 3.638 \times 10^{-2} \rho U^2 L R_L^{-0.2} \quad (2.122)$$

2.7 Flow in Curved Channels

Flow in a curved channel is influenced by the centrifugal acceleration, which induces a three dimensionality in the flow characterized by a helical (spiral) motion with a superelevated free surface. The helical motion can be viewed across a cross section as a transverse circulation. The differential centrifugal acceleration u^2/r along a vertical line due to vertical variation of streamwise velocity u in open channel is the cause of the transverse circulation. As a result, a helical motion is initiated when the flow enters the curved (bend) portion of the channel. The helicoidal flow is gradually fully developed becoming in an equilibrium state, where the flow structure remains unchanged from cross section to cross section. Such a flow situation eventually prevails, if a prismatic channel has an adequately long curved reach. The streamlines near the free surface are deflected toward the outer bank, whereas those near the bed are inclined toward the inner bank (Fig. 2.33). Hence, the near-bed velocity and the bed shear stress are generally directed toward the inner bank.

The flow in a curved channel is analyzed in cylindrical polar coordinates restricting to a subcritical flow having a hydrostatic pressure distribution (Fig. 2.34). In natural channels, the flow depth is in general much smaller than the

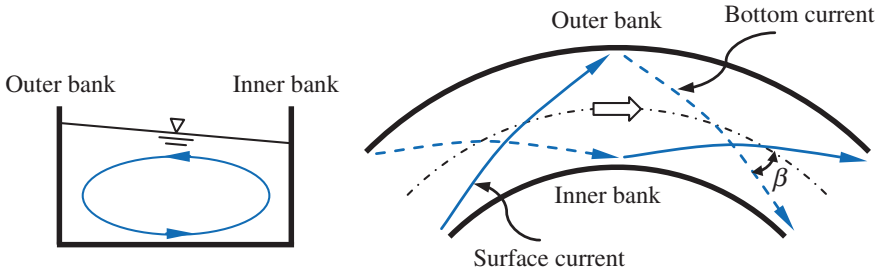


Fig. 2.33 Flow in a curved channel

width and the radius of curvature. In cylindrical polar coordinates, the velocity components (u_r , u_θ , u_z) are in r -, θ -, and z -direction, respectively. Note that $\partial s = r\partial\theta$. Referring to Fig. 2.34, the forces in the tangential direction, that is, θ -direction, is given by

$$[(\tau_\theta + d\tau_\theta) - \tau_\theta + \rho g S_\theta dz] dr ds = \left(\frac{\partial \tau_\theta}{\partial z} + \rho g S_\theta \right) dr ds dz \quad \wedge \quad d\tau_\theta = \frac{\partial \tau_\theta}{\partial z} dz$$

where τ_θ and S_θ are the shear stress and the slope of the channel in θ -direction, respectively. Applying Newton's second law of motion in θ -direction yields

$$\begin{aligned} a_\theta \rho dr ds dz &= \left(\frac{\partial \tau_\theta}{\partial z} + \rho g S_\theta \right) dr ds dz \Rightarrow a_\theta = \frac{1}{\rho} \cdot \frac{\partial \tau_\theta}{\partial z} + g S_\theta \\ a_\theta &= u_\theta \frac{\partial u_\theta}{\partial s} + \frac{u_\theta u_r}{r} + u_r \frac{\partial u_\theta}{\partial r} + u_z \frac{\partial u_\theta}{\partial z} + \frac{\partial u_\theta}{\partial t}, \\ \therefore u_\theta \frac{\partial u_\theta}{\partial s} + u_r \frac{\partial u_\theta}{\partial r} + u_z \frac{\partial u_\theta}{\partial z} + \frac{\partial u_\theta}{\partial t} &= \frac{1}{\rho} \cdot \frac{\partial \tau_\theta}{\partial z} + g S_\theta - \frac{u_\theta u_r}{r} \end{aligned} \quad (2.123)$$

where a_θ is the total acceleration in θ -direction. On the other hand, the forces in the radial direction, that is, r -direction, is given by

$$\begin{aligned} [(\tau_r + d\tau_r) - \tau_r] dr ds + [p - (p + dp)] ds dz \\ = \left(\frac{\partial \tau_r}{\partial z} - \rho g S_r \right) dr ds dz \quad \wedge \quad d\tau_r = \frac{\partial \tau_r}{\partial z} dz \quad \vee \quad dp = \frac{\partial p}{\partial r} dr = \rho g S_r dr \end{aligned}$$

where τ_r and S_r are the shear stress and the slope of the free surface in r -direction, respectively. Applying Newton's second law of motion in r -direction yields

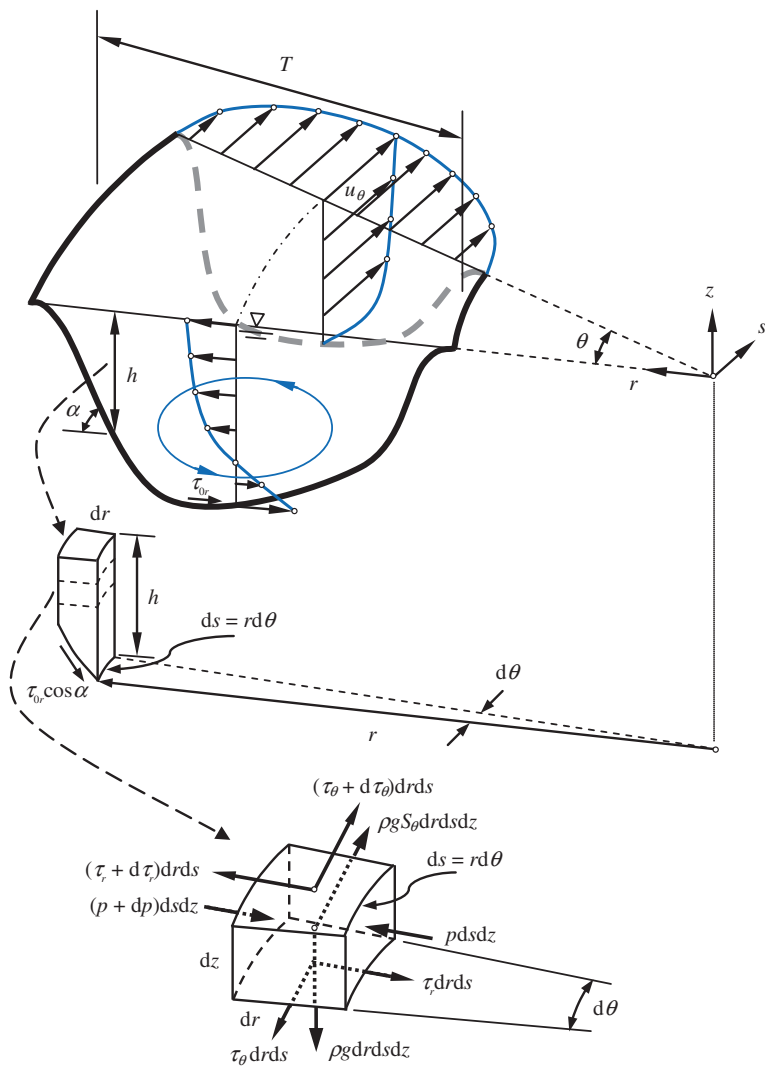


Fig. 2.34 Velocity and force distributions in flow through a curved channel

$$\begin{aligned}
 a_r \rho dr ds dz &= \left(\frac{\partial \tau_r}{\partial z} - \rho g S_r \right) dr ds dz \Rightarrow a_r = \frac{1}{\rho} \cdot \frac{\partial \tau_r}{\partial z} - g S_r \\
 a_r &= u_\theta \frac{\partial u_r}{\partial s} + u_r \frac{\partial u_r}{\partial r} - \frac{u_\theta^2}{r} + u_z \frac{\partial u_r}{\partial z} + \frac{\partial u_r}{\partial t}, \\
 \therefore u_\theta \frac{\partial u_r}{\partial s} + u_r \frac{\partial u_r}{\partial r} + u_z \frac{\partial u_r}{\partial z} + \frac{\partial u_r}{\partial t} &= \frac{1}{\rho} \cdot \frac{\partial \tau_r}{\partial z} - g S_r + \frac{u_\theta^2}{r}
 \end{aligned} \tag{2.124}$$

where a_r is the total acceleration in r -direction. The continuity equation is

$$\frac{\partial u_r}{\partial r} + \frac{u_r}{r} + \frac{\partial u_\theta}{\partial s} + \frac{\partial u_z}{\partial z} = 0 \quad (2.125)$$

2.7.1 Superelevation in Curved Channels

The *superelevation* Δz of the free surface is the difference between the free surface level at the outer and the inner banks. It can be approximated as

$$\Delta z = \int_{r_i}^{r_o} S_r dr \quad (2.126)$$

where r_o and r_i are the radii of curvature of outer and inner banks, respectively. The slope of the free surface in radial direction can be obtained by balancing the radial force components acting on the column of fluid with depth h . Neglecting the bed resistance, the net pressure force due to the free surface slope in r -direction is balanced by the centripetal force. It yields

$$\int_0^h \frac{u_\theta^2}{r} \rho dr ds dz = \rho g h S_r dr ds \Rightarrow S_r = \frac{1}{gh} \int_0^h \frac{u_\theta^2}{r} dz = \beta_r \frac{U^2}{gr} \quad \wedge \quad \beta_r U^2 h = \int_0^h u_\theta^2 dz \quad (2.127)$$

where β_r is the correction factor and U is the depth-averaged tangential velocity. Then, using Eq. (2.127) into Eq. (2.126), the superelevation Δz is obtained as

$$\Delta z = \int_{r_i}^{r_o} \beta_r \frac{U^2}{gr} dr \approx \beta_r \frac{U_a^2 T}{gr_c} \quad (2.128)$$

where U_a is the cross-sectional averaged tangential velocity, T is the width of the free surface, and r_c is the radius of curvature of the centerline of the channel. In Eq. (2.128), β_r can be assumed as unity.

2.7.2 Velocity Distributions in Curved Channels

In a steady fully developed flow, $\partial u_\theta / \partial t = \partial u_r / \partial t = 0$ and $\partial u_\theta / \partial s = \partial u_r / \partial s = 0$. Further, the radial and the vertical velocity components are negligible as compared

to the tangential velocity components. Hence, $u_\theta = u_\theta(z)$ and $u_r = u_z = 0$. From Eqs. (2.123) and (2.124), one can obtain

$$\frac{1}{\rho} \cdot \frac{\partial \tau_\theta}{\partial z} + gS_\theta = 0 \quad (2.129a)$$

$$\frac{1}{\rho} \cdot \frac{\partial \tau_r}{\partial z} - gS_r + \frac{u_\theta^2}{r} = 0 \quad (2.129b)$$

Integration of Eq. (2.129a) produces a linear distribution of tangential shear stress as

$$\tau_\theta = \rho ghS_\theta \left(1 - \frac{z}{h}\right) \quad (2.130)$$

Following the concept of the mixing length (see Sect. 3.5), it can be written as

$$\tau_\theta = \rho l^2 \left| \frac{du_\theta}{dz} \right| \frac{du_\theta}{dz} = \rho \varepsilon_t \frac{du_\theta}{dz} \quad (2.131)$$

where l is the mixing length and ε_t is the eddy viscosity or turbulent diffusivity. Equating Eqs. (2.130) and (2.131), ε_t can be determined from

$$\varepsilon_t = ghS_\theta \left(1 - \frac{z}{h}\right) \left(\frac{du_\theta}{dz} \right)^{-1} \quad (2.132)$$

if a suitable velocity distribution, $u_\theta = u_\theta(z)$, is assumed. Note that by the concept of the isotropic turbulence

$$\tau_r = \rho \varepsilon_t \frac{du_r}{dz} \quad (2.133)$$

Using Eqs. (2.132) and (2.133) yields

$$\tau_r = \rho ghS_\theta \left(1 - \frac{z}{h}\right) \left(\frac{du_\theta}{dz} \right)^{-1} \frac{du_r}{dz} \quad (2.134)$$

Equation (2.134) can be used in Eq. (2.129b) to determine the radial velocity distribution, as $u_\theta = u_\theta(z)$.

For tangential velocity distribution, Rozovskii (1957) assumed

$$\frac{u_\theta}{U} = 1 + \frac{g^{0.5}}{\kappa C_R} (1 + \ln \tilde{z}) \quad (2.135)$$

where κ is the von Kármán constant, C_R is the Chézy coefficient, and $\tilde{z} = z/h$. Using Eq. (2.135), Rozovskii (1957) derived the radial velocity distribution in case of a hydraulically smooth flow as

$$\frac{u_r}{U} = \frac{h}{r} \cdot \frac{1}{\kappa^2} \left(\phi_1 - \frac{g^{0.5}}{\kappa C_R} \phi_2 \right) \quad \wedge \quad \phi_1 = \int \frac{2 \ln \tilde{z}}{\tilde{z} - 1} d\tilde{z} \quad \vee \quad \phi_2 = \int \frac{\ln^2 \tilde{z}}{\tilde{z} - 1} d\tilde{z} \quad (2.136)$$

On the other hand, in case of a hydraulically rough flow, Rozovskii (1957) derived the radial velocity distribution as

$$\frac{u_r}{U} = \frac{h}{r} \cdot \frac{1}{\kappa^2} \left\{ \phi_1 - \frac{g^{0.5}}{\kappa C_R} [\phi_2 + 0.8(1 + \ln \tilde{z})] \right\} \quad (2.137)$$

The angle β of the velocity vector at any depth with the tangential direction, as shown in Fig. 2.33, can be obtained from $\beta = \arctan(u_r/u_\theta)$.

Kikkawa et al. (1976) also derived the velocity distributions from the equation of motion, where the eddy viscosity was assumed to be same as that of a two-dimensional flow in a straight channel. They suggested the equation of motion that governs by the secondary flow as

$$\frac{\partial^4 \psi}{\partial z^4} = u_\theta \frac{\partial u_\theta}{\partial z} \quad (2.138)$$

where ψ is the stream function. Neglecting the nonlinear interaction between the secondary flow and the main flow, the tangential velocity distribution could be shown as

$$\frac{u_\theta - u_s}{u_*} = -\frac{1}{\kappa} \ln \tilde{z} \quad (2.139)$$

where u_s is the tangential velocity at the free surface and u_* is the shear velocity. Kikkawa et al. (1976) derived the radial velocity distribution in a fully developed flow by integrating Eq. (2.138) as

$$\frac{u_r}{U_a} = \frac{U^2}{U_a^2} \cdot \frac{h}{r} \cdot \frac{1}{\kappa} \left(\phi_A - \frac{1}{\kappa} \cdot \frac{u_*}{U_a} \phi_B \right) \quad (2.140)$$

where U is the depth-averaged tangential velocity, which is a function of r , and ϕ_A and ϕ_B are as follows:

$$\phi_A = -15 \left(\tilde{z}^2 \ln \tilde{z} - \frac{\tilde{z}^2}{2} + \frac{15}{54} \right) \quad (2.141a)$$

$$\phi_B = \frac{15}{2} \left(\tilde{z}^2 \ln^2 \tilde{z} - \tilde{z}^2 \ln \tilde{z} + \frac{\tilde{z}^2}{2} - \frac{19}{54} \right) \quad (2.141b)$$

Equation (2.140) indicates that the radial velocity distribution $u_r(z)$ is proportional to U^2 and h/r .

Odgaard (1989) assumed the tangential and the radial velocity distributions as

$$\frac{u_\theta}{U} = \frac{m+1}{m} \tilde{z}^{1/m} \quad \wedge \quad m = \kappa \frac{U}{u_*} = \kappa \left(\frac{8}{\lambda_D} \right)^{0.5} = \kappa \frac{C_R}{g^{0.5}} \quad (2.142a)$$

$$u_r = \frac{1}{h} \int_0^h u_r dz + 2u_r|_{ca} \left(\tilde{z} - \frac{1}{2} \right) \quad (2.142b)$$

where m is the reciprocal of exponent, λ_D is the Darcy-Weisbach friction factor, and $u_r|_{ca}$ is the centrifugally induced component. For a fully developed flow, Odgaard (1989) gave

$$U = \frac{m}{\kappa} (ghS)^{0.5} \quad (2.143a)$$

$$\frac{u_r|_{ca}}{U} = \frac{1}{\kappa^2} \cdot \frac{(m+1)(2m+1)}{1+m+2m^2} \cdot \frac{h}{r} \quad (2.143b)$$

Odgaard argued that the ratio h/r is nearly a constant varying between 7.2 and 8, while m can vary between 3 and 6 in a curved channel.

2.7.3 Bed Shear Stress Distribution in Curved Channels

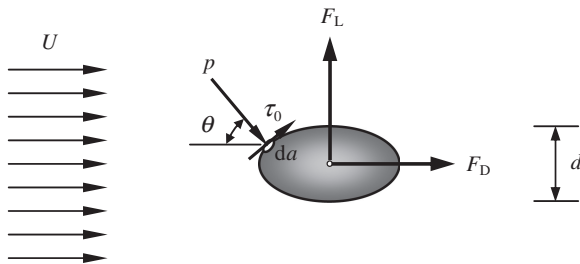
The bed shear stress in a curved channel is decomposed into tangential $\tau_{0\theta}$ and radial τ_{0r} components. The tangential component of the bed shear stress can be given by

$$\tau_{0\theta} = \rho g \frac{U^2}{C_R^2} \quad (2.144)$$

From a radial velocity distribution similar to that of Rozovskii (1957) (Eq. 2.137), Jansen et al. (1979) derived the radial component of bed shear stress as

$$\tau_{0r} = -\frac{2\rho gh}{r\kappa^2} \cdot \frac{U^2}{C_R^2} \left(1 - \frac{g^{0.5}}{\kappa C_R} \right) \quad (2.145)$$

Fig. 2.35 Hydrodynamic drag and lift due to flow past a particle



2.8 Hydrodynamic Drag and Lift on a Particle

When a real fluid flows past a solid particle, the hydrodynamic force of resistance contributes in two ways. Firstly, resistance due to viscosity is developed at the wall of the particle in the form of shear stresses. Secondly, differential pressure intensities act normal to the wall. The integration of both the forces over the entire surface of the particle composes the total hydrodynamic force. The component of the hydrodynamic force in the flow direction is called *drag*, which is the force by which the fluid tends to drag the particle. On the other hand, the component normal to the flow direction is called *lift*, which is the force by which the fluid tends to lift the particle (Fig. 2.35).

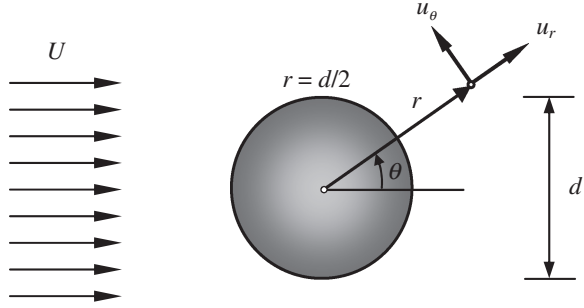
2.8.1 The Drag

The drag on the body of the particle is made up of two contributions, namely *skin friction drag* and *form or pressure drag*. Thus, drag is the sum of the components of the wall shear stress τ_0 and the pressure p in the flow direction, respectively. Thus, referring to Fig. 2.35, τ_0 and p act on an elementary area da tangentially and normally, respectively; and the drag is given by

$$F_D = \underbrace{\int_a \tau_0 \sin \theta da}_{\text{Skin friction drag}} + \underbrace{\int_a p \cos \theta da}_{\text{Form drag}} \quad (2.146)$$

where a is the total surface area. The above equation suggests that both the contributions to the drag can therefore be theoretically calculated. It, however, requires knowledge of the wall shear stress distribution on the surface of the particle and the pressure distribution around the particle. Nevertheless, the integrals of Eq. (2.146) cannot be evaluated easily, as the description of τ_0 and p becomes uncertain due to the boundary layer separation phenomenon, as described in the preceding section. It is therefore simpler to measure the drag

Fig. 2.36 Creeping flow past a spherical particle



experimentally and express it as a function of dynamic pressure force $(\rho U^2/2)A$, where A is the projected area of the particle on a plane, that is normal to the flow direction. Thus,

$$F_D = \frac{1}{2} C_D \rho U^2 A \quad (2.147)$$

where C_D is the drag coefficient being determined experimentally (see Sect. 1.7).

2.8.1.1 Creeping Flow About a Spherical Particle (Stokes' Law)

The basic assumption for a *creeping flow* is that the inertia terms are negligible in the momentum equation if the particle Reynolds number R_e is very small ($R_e \ll 1$, where $R_e = Ud/\nu$ and d is the size or diameter of the particle). This is the special case of creeping viscous flow, where viscous effects predominate.

Let a creeping flow of free stream velocity U about a solid spherical particle of diameter d be considered (Fig. 2.36). Using a spherical polar coordinates (r, θ) , the radial and tangential velocity components u_r and u_θ are related to the Stokes stream function ψ by the relations

$$u_r = \frac{1}{r^2 \sin \theta} \cdot \frac{\partial \psi}{\partial \theta}, \quad u_\theta = -\frac{1}{r \sin \theta} \cdot \frac{\partial \psi}{\partial r} \quad (2.148)$$

For a creeping flow, the Navier–Stokes equations in two-dimensional spherical coordinates reduce to

$$\frac{1}{\rho} \cdot \frac{\partial p}{\partial r} = \nu \nabla^2 u_r, \quad \frac{1}{\rho} \cdot \frac{1}{r} \cdot \frac{\partial p}{\partial \theta} = \nu \nabla^2 u_\theta \quad \wedge \quad \nabla^2 = \frac{\partial^2}{\partial r^2} + \frac{\sin \theta}{r^2} \cdot \frac{\partial}{\partial \theta} \left(\frac{1}{\sin \theta} \cdot \frac{\partial}{\partial \theta} \right) \quad (2.149)$$

Using Eq. (2.148) into Eq. (2.149) yields

$$\frac{\partial p}{\partial r} = \frac{\mu}{r^2 \sin \theta} \cdot \frac{\partial}{\partial \theta} (\nabla^2 \psi), \quad \frac{\partial p}{\partial \theta} = -\frac{\mu}{\sin \theta} \cdot \frac{\partial}{\partial r} (\nabla^2 \psi) \quad (2.150)$$

Eliminating p , one finds

$$\nabla^4 \psi = 0 \text{ or } \left[\frac{\partial^2}{\partial r^2} + \frac{\sin \theta}{r^2} \cdot \frac{\partial}{\partial \theta} \left(\frac{1}{\sin \theta} \cdot \frac{\partial}{\partial \theta} \right) \right]^2 \psi = 0 \quad (2.151)$$

Making substitution $\psi = f(r) \sin^2 \theta$, it allows to reduce Eq. (2.151) to a fourth-order ordinary differential equation

$$\left(\frac{d^2}{dr^2} - \frac{2}{r^2} \right) \left(\frac{d^2 f}{dr^2} - \frac{2f}{r^2} \right) = 0 \quad (2.152)$$

A substitution of $f = r^k$ leads to fourth-order polynomial, whose roots are $k = -1, 1, 2$, and 4 . Thus, the general solution for f becomes

$$f(r) = Ar^{-1} + Br + Cr^2 + Dr^4 \quad (2.153)$$

where A, B, C , and D are the constants of integration. The boundary conditions are the following: (1) at $r = d/2$ (at surface), $\psi = 0$ ($u_r = 0$ at surface), and $\partial \psi / \partial r = 0$ ($u_\theta = 0$ at surface) and (2) at $r \rightarrow \infty$, $\psi \rightarrow (Ur^2/2) \sin^2 \theta$. It leads to $A = Ud^3/32$, $B = -3Ud/8$, $C = U/2$, and $D = 0$. Then, the desired stream function for a creeping flow is obtained as

$$\psi(r, \theta) = \frac{1}{16} Ud^2 \sin^2 \theta \left(\frac{d}{2r} - \frac{6r}{d} + \frac{8r^2}{d^2} \right) \quad (2.154)$$

Then, the velocity components are obtained from Eq. (2.148) as

$$u_r = U \cos \theta \left(1 + \frac{d^3}{16r^3} - \frac{3d}{4r} \right), \quad u_\theta = U \sin \theta \left(-1 + \frac{d^3}{32r^3} + \frac{3d}{8r} \right) \quad (2.155)$$

With known u_r and u_θ , the pressure is determined by integrating Eq. (2.150). The result is

$$p = p_\infty - \frac{3\mu d U}{4r^2} \cos \theta \quad (2.156)$$

where p_∞ is the uniform free stream pressure. This exerts a pressure drag on the spherical particle. In addition, a wall shear stress exerts a drag. The shear stress distribution is given by

$$\tau_{r\theta} = \mu \left(\frac{1}{r} \cdot \frac{\partial u_r}{\partial \theta} + \frac{\partial u_\theta}{\partial r} - \frac{u_\theta}{r} \right) = -\mu U \frac{\sin \theta}{r} \cdot \frac{3d^3}{16r^3} \quad (2.157)$$

Then, the total drag can be obtained from Eq. (2.146) as

$$F_D = - \int_0^\pi \tau_{r\theta}|_{r=d/2} \sin \theta da - \int_0^\pi p|_{r=d/2} \cos \theta da \quad \wedge \quad da = \pi d \frac{d}{2} \sin \theta d\theta, \\ \therefore F_D = 2\pi\mu dU + \pi\mu dU = 3\pi\mu dU \quad (2.158)$$

This is known as the *Stokes' law* (Stokes 1851). Note that viscous shear force contributes two-third and pressure force one-third. Equation (2.158) is strictly valid only for $Re \ll 1$, but satisfactorily agrees with the experimental data up to $Re \approx 1$.

2.8.2 The Lift

As already discussed, fluid flowing past a particle exerts hydrodynamic force on the surface of the particle. Lift is the component of this force. It acts normal to the flow direction. The total lift force is the integral of the pressure forces normal to the flow direction. Thus,

$$F_L = \int_a p \sin \theta da \quad (2.159)$$

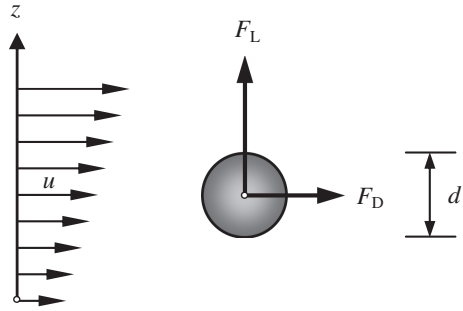
Analogous to Eq. (2.147), lift can also be expressed as a function of dynamic pressure force ($\rho U^2/2$)A, where A is the planform area. Thus,

$$F_L = \frac{1}{2} C_L \rho U^2 A \quad (2.160)$$

where C_L is the lift coefficient being determined experimentally.

Further, when a small spherical particle spinning with an angular velocity ω is placed in a uniform free stream, in addition to drag a lift due to *Magnus effect* acts on the particle. Rubinow and Keller (1961) formulated it as

$$F_L = \frac{\pi}{8} \rho d^3 U \omega \quad (2.161)$$

Fig. 2.37 Shear flow past a spherical particle

It is pertinent to mention that the lift due to *Magnus effect* on a rotating cylinder in an ideal (inviscid) fluid flow is given by $F_L = \rho U \Gamma$, where Γ is the circulation of the cylinder.

2.8.2.1 Lift in a Shear Flow

Particle in a shear flow, that has a spatially nonuniform velocity distribution, experiences a transverse force on the particle, even when the particle is prevented from a spinning motion (Fig. 2.37). The shear lift is originated from the inertia effects in the viscous flow around the particle and is fundamentally different from the hydrodynamic lift. The expression for the inertia *shear lift* was first obtained by Saffman (1965, 1968). It is

$$F_L = \alpha_L \rho d^2 u \left(v \frac{\partial u}{\partial z} \right)^{0.5} \quad (2.162)$$

where α_L is the Saffman lift coefficient, being equal to 1.615.

2.9 Appendix

2.9.1 Navier–Stokes and Continuity Equations in a Cylindrical Polar Coordinate System

Navier–Stokes equations in cylindrical polar coordinates (r, θ, z) with corresponding velocity components (u, v, w) for an incompressible fluid flow are given as follows:

$$\begin{aligned}
u \frac{\partial u}{\partial r} + \frac{v}{r} \cdot \frac{\partial u}{\partial \theta} - \frac{v^2}{r} + w \frac{\partial u}{\partial z} + \frac{\partial u}{\partial t} &= g_r - \frac{1}{\rho} \cdot \frac{\partial p}{\partial r} \\
+ v \left\{ \frac{\partial}{\partial r} \left[\frac{1}{r} \cdot \frac{\partial}{\partial r} (ru) \right] + \frac{1}{r^2} \cdot \frac{\partial^2 u}{\partial \theta^2} - \frac{2}{r^2} \cdot \frac{\partial v}{\partial \theta} + \frac{\partial^2 u}{\partial z^2} \right\}
\end{aligned} \tag{2.163a}$$

$$\begin{aligned}
u \frac{\partial v}{\partial r} + \frac{v}{r} \cdot \frac{\partial v}{\partial \theta} + \frac{uv}{r} + w \frac{\partial v}{\partial z} + \frac{\partial v}{\partial t} &= g_\theta - \frac{1}{\rho} \cdot \frac{1}{r} \cdot \frac{\partial p}{\partial \theta} \\
+ v \left\{ \frac{\partial}{\partial r} \left[\frac{1}{r} \cdot \frac{\partial}{\partial r} (rv) \right] + \frac{1}{r^2} \cdot \frac{\partial^2 v}{\partial \theta^2} + \frac{2}{r^2} \cdot \frac{\partial u}{\partial \theta} + \frac{\partial^2 v}{\partial z^2} \right\}
\end{aligned} \tag{2.163b}$$

$$\begin{aligned}
u \frac{\partial w}{\partial r} + \frac{v}{r} \cdot \frac{\partial w}{\partial \theta} + w \frac{\partial u}{\partial z} + \frac{\partial w}{\partial t} &= g_z - \frac{1}{\rho} \cdot \frac{\partial p}{\partial z} \\
+ v \left[\frac{1}{r} \cdot \frac{\partial}{\partial r} \left(r \frac{\partial w}{\partial r} \right) + \frac{1}{r^2} \cdot \frac{\partial^2 w}{\partial \theta^2} + \frac{\partial^2 w}{\partial z^2} \right]
\end{aligned} \tag{2.163c}$$

The continuity equation for an incompressible flow is

$$\frac{\partial u}{\partial r} + \frac{u}{r} + \frac{1}{r} \cdot \frac{\partial v}{\partial \theta} + \frac{\partial w}{\partial z} = 0 \tag{2.164}$$

2.9.2 Navier–Stokes and Continuity Equations in a Spherical Polar Coordinate System

Navier–Stokes equations in spherical polar coordinates (r, θ, φ) with corresponding velocity components (u, v, w) are as follows:

$$\begin{aligned}
u \frac{\partial u}{\partial r} + \frac{v}{r} \cdot \frac{\partial u}{\partial \theta} + \frac{w}{r \sin \theta} \cdot \frac{\partial u}{\partial \varphi} - \frac{v^2 + w^2}{r} + \frac{\partial u}{\partial t} &= g_r - \frac{1}{\rho} \cdot \frac{\partial p}{\partial r} \\
+ v \left(\nabla^2 u - \frac{2u}{r^2} - \frac{2}{r^2} \cdot \frac{\partial^2 v}{\partial \theta^2} - \frac{2v}{r^2} \cot \theta - \frac{2}{r^2 \sin \theta} \cdot \frac{\partial w}{\partial \varphi} \right)
\end{aligned} \tag{2.165a}$$

$$\begin{aligned}
u \frac{\partial v}{\partial r} + \frac{v}{r} \cdot \frac{\partial v}{\partial \theta} + \frac{w}{r \sin \theta} \cdot \frac{\partial v}{\partial \varphi} + \frac{uv}{r} - \frac{w^2}{r} \cot \theta + \frac{\partial v}{\partial t} &= g_\theta - \frac{1}{\rho} \cdot \frac{1}{r} \cdot \frac{\partial p}{\partial \theta} \\
+ v \left(\nabla^2 v + \frac{2}{r^2} \cdot \frac{\partial u}{\partial \theta} - \frac{v}{r^2 \sin^2 \theta} - \frac{2 \cos \theta}{r^2 \sin^2 \theta} \cdot \frac{\partial w}{\partial \varphi} \right)
\end{aligned} \tag{2.165b}$$

$$\begin{aligned}
u \frac{\partial w}{\partial r} + \frac{v}{r} \cdot \frac{\partial w}{\partial \theta} + \frac{w}{r \sin \theta} \cdot \frac{\partial w}{\partial \varphi} + \frac{wu}{r} + \frac{vw}{r} \cot \theta + \frac{\partial w}{\partial t} &= g_\varphi - \frac{1}{\rho} \cdot \frac{1}{r \sin \theta} \cdot \frac{\partial p}{\partial \varphi} \\
+ v \left(\nabla^2 w - \frac{w}{r^2 \sin^2 \theta} + \frac{2}{r^2 \sin \theta} \cdot \frac{\partial u}{\partial \varphi} + \frac{2 \cos \theta}{r^2 \sin \theta} \cdot \frac{\partial v}{\partial \varphi} \right)
\end{aligned} \tag{2.164c}$$

where

$$\nabla^2 = \frac{1}{r^2} \cdot \frac{\partial}{\partial r} \left(r^2 \frac{\partial}{\partial r} \right) + \frac{1}{r^2 \sin \theta} \cdot \frac{\partial}{\partial \theta} \left(\sin \theta \frac{\partial}{\partial \theta} \right) - \frac{1}{r^2 \sin^2 \theta} \cdot \left(\frac{\partial^2}{\partial \varphi^2} \right)$$

The continuity equation for an incompressible flow is

$$\frac{1}{r^2} \cdot \frac{\partial}{\partial r} (r^2 u) + \frac{1}{r \sin \theta} \cdot \frac{\partial}{\partial \theta} (v \sin \theta) + \frac{1}{r \sin \theta} \cdot \frac{\partial w}{\partial \varphi} = 0 \quad (2.166)$$

2.10 Examples

Example 2.1 The velocity distribution in a wide channel is given by $u/u_{\max} = (z/h)^{1/n}$, where u_{\max} is the maximum velocity at a flow depth h . Find the depth-averaged velocity, momentum coefficient β and energy coefficient α .

Solution

The depth-averaged velocity U is obtained as

$$U = \frac{1}{h} \int_0^h u dz = \frac{1}{h} \int_0^h u_{\max} \left(\frac{z}{h} \right)^{1/n} dz = \frac{n}{1+n} u_{\max}$$

Therefore, the velocity distribution can be expressed in terms of depth-averaged velocity as

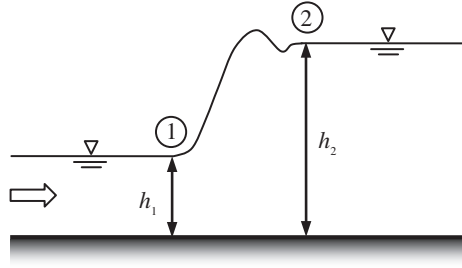
$$u = u_{\max} \left(\frac{z}{h} \right)^{1/n} = \frac{1+n}{n} U \left(\frac{z}{h} \right)^{1/n}$$

For a wide channel, the momentum coefficient β given by Eq. (2.37) can be expressed as

$$\beta = \frac{1}{h} \int_0^h \frac{u^2}{U^2} dz = \frac{1}{h} \int_0^h \frac{1}{U^2} \left(\frac{1+n}{n} \right)^2 U^2 \left(\frac{z}{h} \right)^{2/n} dz = \frac{(1+n)^2}{(2+n)n}$$

Again, for a wide channel, the energy coefficient α given by Eq. (2.74) can be expressed as

$$\alpha = \frac{1}{h} \int_0^h \frac{u^3}{U^3} dz = \frac{1}{h} \int_0^h \frac{1}{U^3} \left(\frac{1+n}{n} \right)^3 U^3 \left(\frac{z}{h} \right)^{3/n} dz = \frac{(1+n)^3}{(3+n)n^2}$$

Fig. E2.1 Hydraulic jump

Example 2.2 Determine the critical depth for a water discharge of $8 \text{ m}^3 \text{ s}^{-1}$ flowing in a trapezoidal channel with a base width of 3 m and a side slope of 1 horizontal to 2 vertical.

Solution

For base width, $b = 3 \text{ m}$ and side slope, $z = 1/2 = 0.5$, the area A and the top width T are

$$A = (b + zh)h = 3h + 0.5h^2, \quad T = b + 2zh = 3 + h$$

The condition of a critical flow is

$$f(h) = \frac{Q^2 T}{g A^3} = 1 \Leftarrow \text{Eq. (2.82)}$$

$$\therefore f(h) = \frac{Q^2 T}{g A^3} = \frac{8^2(3 + h)}{9.81(3h + 0.5h^2)^3} = \frac{6.524(3 + h)}{(3h + 0.5h^2)^3}$$

Adopting the trial-and-error method, the solution of the above equation is $f(h = 0.854) \approx 1$. Therefore, the critical depth is 0.854 m.

Example 2.3 Derive the relationship for the sequent depth ratio of a *hydraulic jump*⁴ on a horizontal floor of a rectangular channel, as shown in Fig. E2.1. Also determine the energy loss.

Solution

The specific force equation between sections 1 and 2 for a prismatic rectangular channel having a width b can be given by

$$\frac{Q^2}{g A_1} + z_{c1} A_1 = \frac{Q^2}{g A_2} + z_{c2} A_2 \Leftarrow \text{Eq. (2.55)}$$

⁴ *Hydraulic jump* occurs when there is a rapid change in flow depth resulting from a low stage (supercritical) to a high stage (subcritical) with an abrupt rise in free surface elevation. It is therefore a local phenomenon due to a transition from a supercritical flow to a subcritical flow.

Substituting $Q = U_1 A_1 = U_2 A_2$, $A_1 = bh_1$, $A_2 = bh_2$, $z_{c1} = h_1/2$, $z_{c2} = h_2/2$, and $F_1 = U_1/(gh_1)^{0.5}$, the above equation becomes

$$\left(\frac{h_2}{h_1}\right)^2 + \frac{h_2}{h_1} - 2F_1^2 = 0$$

where h_1 and h_2 are the sequent depths and F_1 is the Froude number in low stage. The feasible solution for the sequent depth ratio of the quadratic equation is

$$\frac{h_2}{h_1} = \frac{1}{2} \left[(1 + 8F_1^2)^{0.5} - 1 \right]$$

Béanger (1828) was the first to apply the momentum equation across a hydraulic jump to obtain the above equation, which is often called the *Béanger equation*. Applying the specific energy concept, the energy loss ΔE in a hydraulic jump can be expressed as

$$\Delta E = E_1 - E_2 = \left(h_1 + \frac{U_1^2}{2g} \right) - \left(h_2 + \frac{U_2^2}{2g} \right)$$

where E_1 and E_2 are the specific energies at sections 1 and 2, respectively. In the above, the energy coefficients are assumed to be unity, that is, $\alpha_1 = \alpha_2 = 1$. Applying the continuity equation, the discharge per unit width q is given by $q = U_1 h_1 = U_2 h_2$, and then, the above equation becomes

$$\Delta E = -(h_2 - h_1) + \frac{q^2}{2g} \left(\frac{1}{h_1^2} - \frac{1}{h_2^2} \right)$$

Further, applying $q = U_1 h_1$ and $F_1 = U_1/(gh_1)^{0.5}$, the equation of sequent depth ratio or the Béanger equation is expressed as

$$\frac{q^2}{g} = \frac{h_1 h_2}{2} (h_1 + h_2)$$

Therefore, the energy loss ΔE in a hydraulic jump is formulated as

$$\Delta E = \frac{(h_2 - h_1)^3}{4h_1 h_2}$$

Example 2.4 Derive the relationship of the critical depth in terms of alternate depths in the flow through a rectangular channel.

Solution

Since the specific energy is same at two sections (low and high stages), assuming $\alpha_1 = \alpha_2 = 1$, it gives

$$h_1 + \frac{U_1^2}{2g} = h_2 + \frac{U_2^2}{2g}$$

Then, applying $q = U_1 h_1$ yields

$$h_2 - h_1 = \frac{q^2}{2g} \left(\frac{1}{h_1^2} - \frac{1}{h_2^2} \right)$$

Again, the condition of a critical flow in a rectangular channel can be obtained from Eq. (2.82) as

$$h_c^3 = \frac{q^2}{g}$$

Thus, the relationship of the critical depth in terms of alternate depths is obtained as follows:

$$h_c = \left(\frac{2h_1^2 h_2^2}{h_1 + h_2} \right)^{1/3}$$

Example 2.5 Oil with a free stream velocity of 1 m s^{-1} flows over a thin plate of 1.5 m wide and 2.5 m long. Determine the boundary layer thickness and the wall shear stress at a distance of 1.5 m from the leading edge of the plate and also calculate the total resistance on one side of the plate. Consider coefficient of kinematic viscosity of oil $\nu = 10^{-5} \text{ m}^2 \text{ s}^{-1}$ and relative density of oil $s = 0.8$.

Solution

Given data are as follows:

Free stream velocity, $U = 1 \text{ m s}^{-1}$; plate width, $b = 1.5 \text{ m}$; plate length, $L = 2.5 \text{ m}$; coefficient of kinematic viscosity of oil, $\nu = 10^{-5} \text{ m}^2 \text{ s}^{-1}$; and relative density of oil, $s = 0.8$.

The mass density of oil, $\rho = 0.8 \times 10^3 \text{ kg m}^{-3}$

The Reynolds number R_x at $x = 1.5 \text{ m}$ is

$$R_x = \frac{Ux}{\nu} = \frac{1 \times 1.5}{10^{-5}} = 1.5 \times 10^5 < 3 \times 10^5$$

It is low enough to allow a laminar boundary layer

The boundary layer thickness δ at $x = 1.5$ m is

$$\delta = 4.643xR_x^{-0.5} = 4.643 \times 1.5(1.5 \times 10^5)^{-0.5} = 0.018 \text{ m} \Leftarrow \text{Eq. (2.113)}$$

The wall shear stress τ_0 at $x = 1.5$ m is

$$\tau_0 = 0.323\mu \frac{U}{x} R_x^{0.5} = 0.323(10^{-5} \times 0.8 \times 10^3) \frac{1}{1.5} (1.5 \times 10^5)^{0.5} = 0.667 \text{ Pa} \\ \Leftarrow \text{Eq. (2.114)}$$

The Reynolds number R_L at the end of the plate having a length $L = 2.5$ m is

$$R_L = \frac{UL}{\nu} = \frac{1 \times 2.5}{10^{-5}} = 2.5 \times 10^5 < 3 \times 10^5$$

The R_L is to allow a laminar boundary layer.

The wall shear resistance per unit width F_τ on one side of the plate of length $L = 2.5$ m can be obtained from

$$F_\tau = 0.646\rho U\nu R_L^{0.5} = 0.646 \times 0.8 \times 10^3 \times 1 \times 10^{-5} (2.5 \times 10^5)^{0.5} \\ = 2.584 \text{ N m}^{-1} \Leftarrow \text{Eq. (2.115)}$$

Therefore, the total resistance is $F_R = F_\tau b = 2.584 \times 1.5 = 3.876 \text{ N}$

Example 2.6 Water that has a free stream velocity of 1.5 m s^{-1} at the entrance flows through a 2.5 m wide rectangular channel. Determine the length of the channel required to obtain a fully developed turbulent flow for the flow depth of 0.5 m and also calculate the wall shear stress at the location of the fully developed flow and the total resistance on the channel base up to that location. Consider coefficient of kinematic viscosity of water $\nu = 10^{-6} \text{ m}^2 \text{ s}^{-1}$. Assume the length of the channel over which the laminar boundary layer exists is negligibly small as compared to that over which the turbulent boundary layer exists.

Solution

Given data are as follows:

Free stream velocity, $U = 1.5 \text{ m s}^{-1}$; channel width, $b = 2.5$ m; and coefficient of kinematic viscosity of water, $\nu = 10^{-6} \text{ m}^2 \text{ s}^{-1}$.

Fully developed flow depth, $h = \delta = 0.5$ m.

Considering a turbulent boundary layer, the equation of boundary layer is used as

$$\delta = 0.376xR_x^{-0.2} = 0.376x \left(\frac{Ux}{\nu} \right)^{-0.2} \Leftarrow \text{Eq. (2.120)} \\ \therefore x = 3.396\delta^{1.25} \left(\frac{U}{\nu} \right)^{0.25} = 3.396 \times 0.5^{1.25} \left(\frac{1.5}{10^{-6}} \right)^{0.25} = 49.97 \text{ m}$$

The Reynolds number R_x at $x = 49.97$ m is

$$R_x = \frac{Ux}{\nu} = \frac{1.5 \times 49.97}{10^{-6}} = 7.496 \times 10^7 > 10^6$$

Noting that the transition occurs in the range $R_x = 3 \times 10^5$ to 10^6 , the $R_x = 7.496 \times 10^7$ is therefore large enough to allow a turbulent boundary layer. However, the length up to the transition is $x = R_x(\nu/U) = 10^6(10^{-6}/1.5) = 0.667$ m, which is negligibly small in comparison to the length required to form the fully developed turbulent flow, that is, $x = 49.97$ m.

The wall shear stress τ_0 at $x = 49.97$ m is

$$\begin{aligned}\tau_0 &= 2.91 \times 10^{-2} \rho U^2 R_x^{-0.2} = 2.91 \times 10^{-2} \times 10^3 \times 1.5^2 (7.496 \times 10^7)^{-0.2} \\ &= 1.742 \text{ Pa} \Leftarrow \text{Eq. (2.121)}\end{aligned}$$

The wall shear resistance per unit width F_τ for $L = x = 49.97$ m and $R_L = R_x = 7.496 \times 10^7$ is

$$\begin{aligned}F_\tau &= 3.638 \times 10^{-2} \rho U^2 L R_L^{-0.2} \\ &= 3.638 \times 10^{-2} \times 10^3 \times 1.5^2 \times 49.97 (7.496 \times 10^7)^{-0.2} = 108.84 \text{ N m}^{-1} \\ &\Leftarrow \text{Eq. (2.122)}\end{aligned}$$

Therefore, the total resistance is $F_R = F_\tau b = 108.84 \times 2.5 = 272.1$ N

Example 2.7 A spherical particle having a diameter $d = 4$ mm is placed in a free stream of water with a velocity $U = 1.2$ m s⁻¹. Determine the drag and the lift acting on the particle. The drag and lift coefficients are given by $C_D = 24R_e^{-1}(1 + 0.15R_e^{0.687})$ and $C_L = 0.85C_D$, where $R_e = Ud/\nu$. Consider coefficient of kinematic viscosity of water $\nu = 10^{-6}$ m² s⁻¹.

Solution

Given data are as follows:

Particle diameter, $d = 4$ mm; free stream velocity, $U = 1.2$ m s⁻¹ and coefficient of kinematic viscosity of water, $\nu = 10^{-6}$ m² s⁻¹.

The particle Reynolds number R_e is

$$R_e = \frac{Ud}{\nu} = \frac{1.2 \times 4 \times 10^{-3}}{10^{-6}} = 4.8 \times 10^3$$

The drag and lift coefficients are

$$\begin{aligned}C_D &= \frac{24}{R_e} (1 + 0.15R_e^{0.687}) = \frac{24}{4.8 \times 10^3} [1 + 0.15(4.8 \times 10^3)^{0.687}] = 0.259 \\ C_L &= 0.85C_D = 0.85 \times 0.259 = 0.22\end{aligned}$$

The drag is

$$\begin{aligned} F_D &= \frac{1}{2} C_D \rho U^2 A = \frac{1}{2} \times 0.259 \times 10^3 \times 1.2^2 \times \frac{\pi}{4} (4 \times 10^{-3})^2 \\ &= 2.343 \times 10^{-3} \text{ N} \Leftarrow \text{Eq. (2.147)} \end{aligned}$$

The lift is

$$\begin{aligned} F_L &= \frac{1}{2} C_L \rho U^2 A = \frac{1}{2} \times 0.22 \times 10^3 \times 1.2^2 \times \frac{\pi}{4} (4 \times 10^{-3})^2 \\ &= 1.991 \times 10^{-3} \text{ N} \Leftarrow \text{Eq. (2.160)} \end{aligned}$$

References

- Bélanger JB (1828) Essai sur la solution numérique de quelques problèmes relatifs au mouvement permanent des eaux courantes. Carilian-Goeury, Paris
- Blasius H (1912) Das aehnlichkeitsgesetz bei reibungsvorgangen. Zeitschrift des Vereines Deutscher Ingenieure 56:639–643
- Blasius H (1913) Das aehnlichkeitsgesetz bei reibungsvorgängen in flüssigkeiten. Mitteilungen über Forschungsarbeiten auf dem Gebiete des Ingenieurwesens 131:1–41
- Chaudhry MH (2008) Open-channel flow. Springer, New York
- Chow VT (1959) Open channel hydraulics. McGraw-Hill Book Company, New York
- de Saint-Venant B (1871) Theorie du mouvement non permanent des eaux, avec application aux crues de rivières et à l'introduction des marées dans leur lit. Comptes Rendus de l'Académie des Sciences, vol 73, Paris, pp 147–154, 237–240
- Dey S (2000) Chebyshev solution as aid in computing GVF by standard step method. J Irrig Drainage Eng 126(4):271–274
- Jaeger C (1957) Engineering fluid mechanics. Saint Martin's Press, New York
- Jansen P, van Bendegom L, van den Berg J, de Vries M, Zanen A (1979) Principles of river engineering. Pitman, London
- Kikkawa H, Ikeda S, Kitagawa A (1976) Flow and bed topography in curved open channels. J Hydraul Div 102(9):1327–1342
- Odgaard AJ (1989) River-meander model. I: development. J Hydraul Eng 115(11):1433–1450
- Prandtl L (1904) Über flüssigkeitsbewegung bei sehr kleiner reibung. Verhandlungen des III. Internationalen Mathematiker Kongress, Heidelberg, pp 484–491
- Rozovskii IL (1957) Flow of water in bends in open channels. Academy of Sciences of the Ukrainian Soviet Socialist Republic, Kiev
- Rubinow SI, Keller JB (1961) The transverse force on a spinning sphere moving in a viscous fluid. J Fluid Mech 11:447–459
- Saffman PG (1965) The lift on a small sphere in a slow shear flow. J Fluid Mech 22:385–400
- Saffman PG (1968) Corrigendum, the lift on a small sphere in a slow shear flow. J Fluid Mech 31:624
- Stokes GG (1851) On the effect of the internal friction of fluids on the motion of pendulums. Trans Cambridge Philos Soc 9:80–85
- Streeter VL (1948) Fluid dynamics. McGraw-Hill Book Company, New York

Chapter 3

Turbulence in Open-Channel Flows

3.1 General

Fluid flows are broadly classified into two categories: *laminar flow* and *turbulent flow*. The difference between them can still be best illustrated by the well-known experiment of Osborne Reynolds (Reynolds 1883). Laminar flow occurs at relatively low flow velocity and is envisaged as a layered flow in which fluid layers smoothly slide over each other, thus maintaining a differential flow velocity in fluid layers (normal to the flow direction), without any exchange of fluid mass in between the layers. As the flow velocity exceeds a certain limiting value,¹ the laminar flow becomes unstable, resulting in the formation of *eddies*² which spread throughout the fluid medium. Such highly irregular, random, and fluctuating flow is termed *turbulent flow*.

More specifically, in hydrodynamics, *turbulence* in a fluid flow is characterized by irregular and chaotic motion of fluid particles, whose velocities change rapidly in space and time. In other way around, at a fixed point in the fluid medium, the velocity and the pressure do not remain invariant of time but fluctuate very irregularly with a high frequency. This essentially includes low momentum diffusion (that is, the mixing of mass without bulk motion), high momentum advection (that is, the mixing of mass with bulk motion), and rapid variation of velocity and pressure in space and time, as already stated. Further, the turbulent diffusivity, which causes a rapid mixing and an increased rate of momentum transfer, is another important feature. As most of the fluvial hydrodynamic-related phenomena are turbulent, an understanding of turbulence characteristics in open-channel flow is highly essential. In fact, the turbulence is an intricate phenomenon by nature and is not easy to define. However, one can indicate its characteristic

¹ Laminar flow changes over to turbulent flow, if the Reynolds number $Re [=UD/\nu]$ for pipe flow and $U(4R_b)/\nu$ for open-channel flow] is greater than 2000. Here, U is the average flow velocity, D is the pipe diameter, ν is the coefficient of kinematic viscosity, and R_b is the hydraulic radius.

² Eddies can be defined as swirls of fluid parcels with highly irregular shapes and wide range of sizes that are in a continual state of generation, evolution, and decay, as a cyclic process (Middleton and Southard 1984).

features from the measurement of instantaneous velocity data. The most significant characteristic of turbulence is its randomness and intermittency, which make a deterministic approach potentially infeasible. Thus, one has to rely on statistical analysis of temporal velocity data.

It is pertinent to mention that the time-averaged flow may be two- or three-dimensional, but the turbulence is always three-dimensional and rotational and occurs at high flow velocities or, in turn, at large Reynolds numbers. Eddies play a major role in turbulence; thus, the random velocity fluctuations that characterize the turbulent flow are maintained by the mechanism of eddy diffusion which is not present in laminar flow. Turbulent flow is highly dissipative, and viscous shear stresses perform deformation work at the expense of the turbulent kinetic energy (TKE). Thus, without continuous supply of energy provided by the time-averaged flow, turbulence cannot be sustained. Therefore, *turbulence properties* are primarily characterized by the following features:

1. *Fluctuations*: The disorderly motion of fluid particles causes three-dimensional velocity fluctuations that are superimposed on a mean value of each velocity component.
2. *Randomness*: The randomness of a fluctuating velocity component has a specific continuous energy spectrum which drops off to zero at high wave numbers (small eddy size).
3. *Mixing process*: The readily available supply of energy in flow is to enhance the mixing and to increase the fluxes of mass, momentum, and energy in a fluid flow called *diffusivity*.
4. *Self-perpetuating motion*: Once initiated, turbulence in a fluid flow can maintain itself by producing new eddies to replenish those annihilated by viscous diffusion.

Significant progress since early 1960s provided considerable evidence that a turbulent shear layer exhibits a quasi-deterministic structure of irregular, but repetitive spatially temporal flow structures known as *coherent structures* (Robinson 1991; Smith 1996). Further, such structures are self-perpetual and thus can be assumed to be cyclic phenomena. Importantly, they are the cause of most of the TKE production in a fluid flow (Grass et al. 1991).

Finally, turbulence is the property of the flow, but not the property of the fluid. Thus, the characteristics of turbulent flow are highly dependent on the boundary conditions. However, sediment motion is closely related to the turbulence phenomenon, because sediment movement is maintained by the flow against the bed resistance and the gravity.

3.2 Decomposition and Averaging Procedure

In turbulent flow, hydrodynamic quantities, such as velocity and pressure at a given point in space, do not remain constant in time, but perform highly irregular fluctuations. Visualization of turbulent flow revealed that the eddies, which

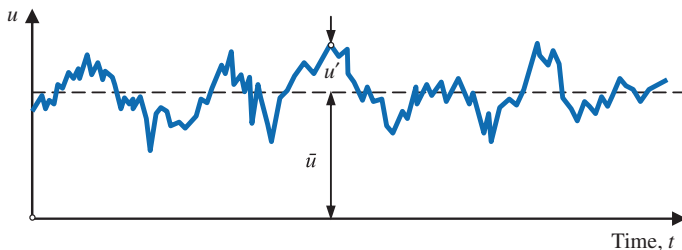


Fig. 3.1 Time variation of u' and its decomposition

continually appear and then degenerate, are the cause of the said fluctuations. It is therefore convenient to describe a hydrodynamic quantity by separating the time-averaged value from its fluctuations. Such a decomposition of an instantaneous value of a hydrodynamic quantity is called the *Reynolds decomposition* (Reynolds 1895). Figure 3.1 schematically illustrates the time variation and the decomposition of velocity component in x -direction, denoted by u .

According to the Reynolds decomposition, the instantaneous velocity components (u , v , w) in the Cartesian coordinate system (x , y , z) and the instantaneous pressure intensity p are expressed as

$$u = \bar{u} + u', \quad v = \bar{v} + v', \quad w = \bar{w} + w' \quad (3.1a)$$

$$p = \bar{p} + p' \quad (3.1b)$$

where \bar{u} , \bar{v} , and \bar{w} are the time-averaged velocity components in (x , y , z), u' , v' , and w' are the fluctuations of u , v , and w , respectively, \bar{p} is the time-averaged pressure intensity, and p' is the fluctuations of p .

The time-averaged value of a hydrodynamic quantity, say u , is given by

$$\bar{u} = \frac{1}{t_\infty} \int_{t_0}^{t_0+t_\infty} u dt \quad (3.2)$$

where t_0 is any arbitrary time and t_∞ is the time over which the averaging is performed. The time t_∞ should be sufficiently long time in order to obtain the time-independent time-averaged value of the quantity. Thus, the time-averaged values of all the fluctuations are equal to zero. Similarly, the time-averaged values of the derivatives of all the fluctuations also vanish.

$$\overline{u'} = \overline{v'} = \overline{w'} = \overline{p'} = 0 \quad (3.3a)$$

$$\frac{\partial \overline{u'}}{\partial x} = \frac{\partial^2 \overline{u'}}{\partial x^2} = \frac{\partial \overline{uu'}}{\partial x^2} = \dots = 0 \quad (3.3b)$$

However, the quadratic terms resulting from the products of cross-velocity fluctuations, such as $\overline{u'u'}$, $\overline{u'v'}$, and $\overline{\partial u'v'}/\partial x$, do not reduce to zero. Bar denotes the time-averaging.

It is pertinent to mention that in turbulent flow, the velocity fluctuations (u' , v' , w') influence the progress of the time-averaged velocity components (\bar{u} , \bar{v} , \bar{w}), so that (\bar{u} , \bar{v} , \bar{w}) exhibit an apparent increase in resistance to deformation. This results in an apparent increase in viscosity, giving rise to *apparent stresses*, which are termed *turbulent stresses* or *Reynolds stresses*.

The following relationships that arise from the time-averaging procedure are known as the *Reynolds conditions*, written with two quantities, say e and f :

$$\begin{aligned} \overline{e+f} &= \bar{e} + \bar{f}, \quad \overline{ce} = c\bar{e}, \quad \bar{c} = c, \quad \frac{\partial \bar{e}}{\partial s} = \frac{\partial \bar{e}}{\partial s}, \quad \bar{e} = \bar{e}, \quad \overline{ef} = \bar{e}\bar{f}, \\ \overline{e'} &= 0, \quad \overline{e'f'} = 0, \quad \overline{ef} = \bar{e}\bar{f} + \overline{e'f'}, \quad \int f ds = \int \bar{f} ds \end{aligned} \quad (3.4)$$

where c is the constant and s is the space and time coordinates, that is, (x, y, z, t).

3.3 Continuity Equation

For incompressible fluid flow, the conservation of mass given by Eq. (2.22) in the Cartesian coordinate system can be expressed in terms of instantaneous velocity components (symbols remain same) as

$$\frac{\partial u}{\partial x} + \frac{\partial v}{\partial y} + \frac{\partial w}{\partial z} = 0 \Rightarrow \frac{\partial u_i}{\partial x_i} = 0 \quad (3.5)$$

In the above equation, for convenience, Einstein's summation convention is used in tensor form, where u_i is the velocity component in i -direction.

The Reynolds decomposition is applied to Eq. (3.5), and then, averaging is performed by taking into account the Reynolds conditions. Since $\overline{\partial u'/\partial x} = \overline{\partial v'/\partial y} = \overline{\partial w'/\partial z} = 0$, it yields the continuity equation for time-averaged part as

$$\frac{\partial \bar{u}}{\partial x} + \frac{\partial \bar{v}}{\partial y} + \frac{\partial \bar{w}}{\partial z} = 0 \Rightarrow \frac{\partial \bar{u}_i}{\partial x_i} = 0 \quad (3.6)$$

Applying the Reynolds decomposition to Eq. (3.5) and then using Eq. (3.6) yield the continuity equation for fluctuating part as

$$\frac{\partial u'}{\partial x} + \frac{\partial v'}{\partial y} + \frac{\partial w'}{\partial z} = 0 \Rightarrow \frac{\partial u'_i}{\partial x_i} = 0 \quad (3.7)$$

Thus, the time-averaged velocity components and their fluctuations satisfy the continuity equation.

3.4 Equation of Motion (Reynolds Equations)

The Navier–Stokes equations (Eqs. 2.51a–c) for an incompressible fluid flow in the Cartesian coordinate system can be expressed in terms of instantaneous velocity components (symbols remain same) as

$$u \frac{\partial u}{\partial x} + v \frac{\partial u}{\partial y} + w \frac{\partial u}{\partial z} + \frac{\partial u}{\partial t} = g_x - \frac{1}{\rho} \cdot \frac{\partial p}{\partial x} + \nu \nabla^2 u \quad (3.8a)$$

$$u \frac{\partial v}{\partial x} + v \frac{\partial v}{\partial y} + w \frac{\partial v}{\partial z} + \frac{\partial v}{\partial t} = g_y - \frac{1}{\rho} \cdot \frac{\partial p}{\partial y} + \nu \nabla^2 v \quad (3.8b)$$

$$u \frac{\partial w}{\partial x} + v \frac{\partial w}{\partial y} + w \frac{\partial w}{\partial z} + \frac{\partial w}{\partial t} = g_z - \frac{1}{\rho} \cdot \frac{\partial p}{\partial z} + \nu \nabla^2 w \quad (3.8c)$$

where

$$\nabla^2 = \frac{\partial^2}{\partial x^2} + \frac{\partial^2}{\partial y^2} + \frac{\partial^2}{\partial z^2}$$

where g_x , g_y , and g_z are the body forces per unit mass or gravity components in (x , y , z) and ρ is the mass density of fluid. Equations (3.8a–c) can then be reorganized as

$$\frac{\partial(u^2)}{\partial x} + \frac{\partial(uv)}{\partial y} + \frac{\partial(uw)}{\partial z} + \frac{\partial u}{\partial t} = g_x - \frac{1}{\rho} \cdot \frac{\partial p}{\partial x} + \nu \nabla^2 u \quad (3.9a)$$

$$\frac{\partial(vu)}{\partial x} + \frac{\partial(v^2)}{\partial y} + \frac{\partial(vw)}{\partial z} + \frac{\partial v}{\partial t} = g_y - \frac{1}{\rho} \cdot \frac{\partial p}{\partial y} + \nu \nabla^2 v \quad (3.9b)$$

$$\frac{\partial(wu)}{\partial x} + \frac{\partial(wv)}{\partial y} + \frac{\partial(w^2)}{\partial z} + \frac{\partial w}{\partial t} = g_z - \frac{1}{\rho} \cdot \frac{\partial p}{\partial z} + \nu \nabla^2 w \quad (3.9c)$$

Applying the Reynolds decomposition to Eqs. (3.9a–c) and then averaging by taking into account the Reynolds conditions yield

$$\bar{u} \frac{\partial \bar{u}}{\partial x} + \bar{v} \frac{\partial \bar{u}}{\partial y} + \bar{w} \frac{\partial \bar{u}}{\partial z} + \frac{\partial \bar{u}}{\partial t} = g_x - \frac{1}{\rho} \cdot \frac{\partial \bar{p}}{\partial x} + \nu \nabla^2 \bar{u} - \left(\frac{\partial \overline{u'u'}}{\partial x} + \frac{\partial \overline{u'v'}}{\partial y} + \frac{\partial \overline{u'w'}}{\partial z} \right) \quad (3.10a)$$

$$\bar{u} \frac{\partial \bar{v}}{\partial x} + \bar{v} \frac{\partial \bar{v}}{\partial y} + \bar{w} \frac{\partial \bar{v}}{\partial z} + \frac{\partial \bar{v}}{\partial t} = g_y - \frac{1}{\rho} \cdot \frac{\partial \bar{p}}{\partial y} + \nu \nabla^2 \bar{v} - \left(\frac{\partial \overline{v'u'}}{\partial x} + \frac{\partial \overline{v'v'}}{\partial y} + \frac{\partial \overline{v'w'}}{\partial z} \right) \quad (3.10b)$$

$$\bar{u} \frac{\partial \bar{w}}{\partial x} + \bar{v} \frac{\partial \bar{w}}{\partial y} + \bar{w} \frac{\partial \bar{w}}{\partial z} + \frac{\partial \bar{w}}{\partial t} = g_z - \frac{1}{\rho} \cdot \frac{\partial \bar{p}}{\partial z} + \nu \nabla^2 \bar{w} - \left(\frac{\partial \overline{w'u'}}{\partial x} + \frac{\partial \overline{w'v'}}{\partial y} + \frac{\partial \overline{w'w'}}{\partial z} \right) \quad (3.10c)$$

These equations are known as the *Reynolds equations* or more explicitly *Reynolds-averaged Navier–Stokes (RANS) equations*. The set of equations can be expressed in tensor form

$$\bar{u}_j \frac{\partial \bar{u}_i}{\partial x_j} + \frac{\partial \bar{u}_i}{\partial t} = g_{x_i} - \frac{1}{\rho} \cdot \frac{\partial \bar{p}}{\partial x_i} + \nu \frac{\partial^2 \bar{u}_i}{\partial x_j^2} - \frac{\partial \overline{u'_i u'_j}}{\partial x_j} \quad (3.11)$$

Note that the RANS equations (Eqs. 3.10a–c) are identical to the Navier–Stokes equations (Eqs. 2.51a–c) if $(\bar{u}, \bar{v}, \bar{w})$ are replaced by (u, v, w) , except the last terms within parentheses. These last terms are obtained from three cross products of velocity fluctuations and provide additional stresses developed due to turbulence. Hence, they are called the *turbulent stresses* or *Reynolds stresses*. Since both sides of the RANS equations have dimension of acceleration, the equations are multiplied all throughout by mass density of fluid ρ to convert the dimension into stress. Hence, the stresses can be expressed as a stress tensor called *Reynolds stress tensor*. They are

$$\begin{matrix} \sigma_x & \tau_{xy} & \tau_{xz} \\ \tau_{yx} & \sigma_y & \tau_{yz} \\ \tau_{zx} & \tau_{zy} & \sigma_z \end{matrix} = -\rho \left(\begin{matrix} \overline{u'u'} & \overline{u'v'} & \overline{u'w'} \\ \overline{v'u'} & \overline{v'v'} & \overline{v'w'} \\ \overline{w'u'} & \overline{w'v'} & \overline{w'w'} \end{matrix} \right) \Rightarrow \sigma_i \delta_{ij} + \tau_{ij}(1 - \delta_{ij}) = -\rho \overline{u'_i u'_j} \quad (3.12)$$

where σ_x , σ_y , and σ_z are the *Reynolds normal stresses* in (x, y, z) , τ_{xy} , τ_{xz} , τ_{yx} , τ_{yz} , τ_{zx} , and τ_{zy} are the *Reynolds shear stresses*, and δ_{ij} is the *Kronecker delta*, defined as $\delta_{ij} (i = j) = 1$ and $\delta_{ij} (i \neq j) = 0$. These Reynolds stresses are developed due to turbulent fluctuations and are given by time-averaged values of the quadratic terms of the velocity fluctuations. As these terms are added to the ordinary viscous stresses and have a similar influence on the flow, the viscosity that arises in turbulent flow is often called *eddy viscosity*. In general, these Reynolds stresses far outweigh the viscous stresses in turbulent flow.

The terms $\overline{u'_i u'_j}$ are called *second moments* or *second-order correlations*, while the *first moments* are always zero ($\overline{u'_i} = 0$). However, the second moments are never zero unless the velocity fluctuations are zero. Let us discuss more about the second moments $\overline{u'_i u'_j}$ for $i = j$. The *root mean square (RMS)* of a second moment provides us with an idea about the magnitude of fluctuations and hence is often called *turbulence intensity*. It is defined by

$$\text{RMS of } u_i = (\overline{u'_i u'_i})^{0.5} = \left(\frac{1}{t_\infty} \int_{t_0}^{t_0+t_\infty} u'_i u'_i dt \right)^{0.5} \quad (3.13)$$

This second moment is therefore a correlation of u'_i with itself and is thus called an *autocorrelation*.

On the other hand, the case of second moment $\overline{u'_i u'_j}$ for $i \neq j$ can be discussed further. Considering a two-dimensional shear flow along x -axis with vertical direction in z -axis (that is, on xz plane), it can be written as

$$u = \bar{u} + u', \quad \bar{u} = \bar{u}(z), \quad \frac{d\bar{u}}{dz} > 0, \quad \bar{w} = 0, \quad w = w'$$

The upward vertical motion of fluid parcels is caused by the eddies ($w' > 0$) to arrive a level z_2 from a lower level z_1 that is immediately below the level z_2 . Note that \bar{u} at z_2 is greater than \bar{u} at z_1 . In order to retain the original time-averaged velocity \bar{u} in the vertical motion of the fluid parcel, a $-u'$ at layer z_2 is induced by the eddies. On the other hand, a downward vertical motion of fluid parcels caused by the eddies ($w' < 0$) arriving from a higher level induces a $+u'$ in the lower layer. Therefore, in a shear flow, a $+w'$ is accompanied by a $-u'$ and a $-w'$ by a $+u'$. Thus, their product $u'w'$ is in general nonzero and indeed negative. It means that the Reynolds shear stress, $\tau_{xz} = -\rho \overline{u'w'}$, is positive, as $\overline{u'w'} < 0$.

3.4.1 Shear Stress in Steady-Uniform Flow in an Open Channel

For a steady-uniform flow (that is, a zero-pressure gradient in the streamwise direction), the basic equations are the two-dimensional continuity equation and Reynolds-averaged Navier–Stokes (RANS) equations. It is assumed that the channel bed that makes an angle θ (down streamwise) with the horizontal is aligned along the x -direction. The flow depth h remains unchanged all throughout the channel reach wherein the flow is steady-uniform. The continuity equation is automatically satisfied. For two-dimensional steady flow, the RANS equations reduce to x -component (along the channel bed) and z -component (normal to the channel bed)

$$\bar{u} \frac{\partial \bar{u}}{\partial x} + \bar{w} \frac{\partial \bar{u}}{\partial z} = g_x - \frac{1}{\rho} \cdot \frac{\partial \bar{p}}{\partial x} + \nu \left(\frac{\partial^2 \bar{u}}{\partial x^2} + \frac{\partial^2 \bar{u}}{\partial z^2} \right) - \left(\frac{\partial \overline{u'u'}}{\partial x} + \frac{\partial \overline{u'w'}}{\partial z} \right) \quad (3.14a)$$

$$\bar{u} \frac{\partial \bar{w}}{\partial x} + \bar{w} \frac{\partial \bar{w}}{\partial z} = g_z - \frac{1}{\rho} \cdot \frac{\partial \bar{p}}{\partial z} + \nu \left(\frac{\partial^2 \bar{w}}{\partial x^2} + \frac{\partial^2 \bar{w}}{\partial z^2} \right) - \left(\frac{\partial \overline{w'u'}}{\partial x} + \frac{\partial \overline{w'w'}}{\partial z} \right) \quad (3.14b)$$

Further, with $\bar{w} = 0$, $g_z = -g \cos \theta$, and the flow parameters to be invariant of distance in x -direction, the z -component of RANS equation (Eq. 3.14b) gives an equation of pressure by integrating within limits z and h

$$\frac{\partial \bar{p}}{\partial z} = -\rho g \cos \theta - \rho \frac{\partial \overline{w'w'}}{\partial z} \Rightarrow \bar{p} = \rho g(h - z) \cos \theta + \rho \overline{w'w'} \Big|_{z=z}^{z=h} \quad (3.15)$$

where g is the acceleration due to gravity. Note that $\bar{p}(z = h) = 0$ (gauge pressure) and $\bar{p}(z = z) = \bar{p}$, and $\overline{w'w'}$ at the free surface ($z = h$) is zero. Hence, Eq. (3.15) becomes

$$\bar{p} = \rho g(h - z) \cos \theta - \rho \overline{w'w'} \Big|_{z=z} \quad (3.16)$$

On the other hand, with $\bar{u} = \bar{u}(z)$, $\bar{w} = 0$, $g_x = g \sin \theta$, and the flow parameters to be invariant of distance in x -direction, the x -component of RANS equation (Eq. 3.14a) reduces to

$$\begin{aligned} -\mu \frac{d^2 \bar{u}}{dz^2} - \frac{d(-\rho \overline{u'w'})}{dz} &= \rho g \sin \theta \quad \wedge \quad \sin \theta \approx S_0 \\ -\frac{d}{dz} \left[\mu \frac{d\bar{u}}{dz} + (-\rho \overline{u'w'}) \right] &= \frac{\tau_0}{h} \quad \wedge \quad \tau_0 = \rho g h S_0 \end{aligned} \quad (3.17)$$

where μ is the coefficient of dynamic viscosity of fluid ($=\nu\rho$), S_0 is the bed slope, which is approximately equal to $\sin \theta$, and τ_0 is the bed shear stress. In the above equation, partial differentials are replaced by the total differentials.

The terms inside the square bracket in the left-hand side of Eq. (3.17) are expressed as

$$\mu \frac{d\bar{u}}{dz} + (-\rho \overline{u'w'}) = \tau_v + \tau_{xz} = \tau \quad (3.18)$$

where τ_v is the shear stress due to viscosity [$=\mu(d\bar{u}/dz)$], τ_{xz} is the shear stress due to turbulence or Reynolds shear stress [$=-\rho \overline{u'w'}$], and τ is the total shear stress at z . Therefore, Eq. (3.17) becomes

$$-\frac{d\tau}{dz} = \frac{\tau_0}{h} \quad (3.19)$$

Integrating Eq. (3.19) within limits z and h yields

$$\tau = \left(1 - \frac{z}{h}\right) \tau_0 \quad (3.20)$$

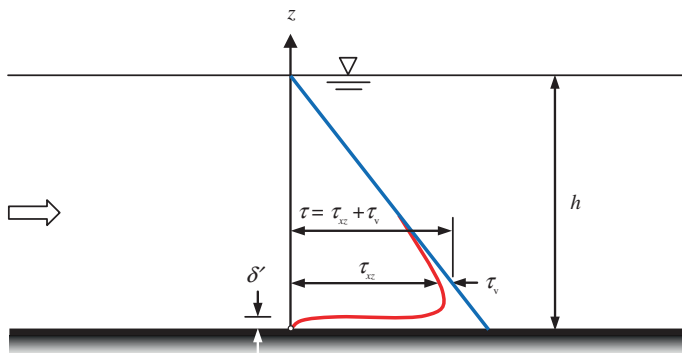


Fig. 3.2 Shear stress distribution in a steady-uniform flow in an open channel

Figure 3.2 schematically shows the distributions of total shear stress τ , viscous shear stress τ_v , and Reynolds shear stress τ_{xz} . The total shear stress τ linearly decreases with an increase in vertical distance z , as given by Eq. (3.20), being zero at the free surface ($z = h$) and maximum ($\tau = \tau_0$) at the bed ($z = 0$). At the bed, there is no turbulence ($u' = w' = 0$); thus, the Reynolds shear stress $\tau_{xz} (= -\rho \overline{u'w'})$ is zero. The damping of Reynolds shear stress τ_{xz} in the buffer layer and the viscous sublayer is discussed in Sect. 3.7.3. Therefore, the viscous shear stress is dominant in a very thin layer near the bed, where the flow is laminar. This thin layer having a thickness δ' is called *viscous sublayer* (see Sect. 2.6.1). In contrast, above the viscous sublayer, that is, in the main flow region, the Reynolds shear stress dominates (Fig. 3.2). The measurements showed that the viscous shear stress in the viscous sublayer is almost constant and is equal to the bed shear stress.

3.5 Classical Turbulence Theories

As the turbulence phenomena are extremely complex, no full-proof theory is available to describe the phenomena completely. The existing theories are primarily based on the semiempirical hypotheses, which establish a relationship between the Reynolds shear stresses caused by the exchange of momentum and the time-averaged velocities. The basic theories proposed by Ludwig Prandtl and Theodore von Kármán are described here.

3.5.1 Prandtl's Mixing Length Theory

Prandtl (1925) introduced the mixing length concept in order to determine the Reynolds shear stress in a turbulent shear flow. He simulated the momentum

exchange on a macro-scale being analogous to that of the molecular motion of a gas to explain the mixing phenomenon induced by the turbulence in a fluid flow and thus established the *mixing length theory*.

In a turbulent shear flow, the eddies forming the fluid parcels generate and then degenerate after traveling an average distance l , termed *mixing length*, to change their momentum by a new environment in the fluid. These fluid parcels travel both in streamwise (that is horizontal) and in vertical directions and are presumed to retain their original time-averaged velocity at the arrival position. Figure 3.3a schematically shows such a fluid parcel located at level 1 (higher level) to move a distance l at level 2 (lower level) due to eddy motion. The velocity of the fluid parcel at level 1 is still retained when it just arrives at level 2 and then decreases to the velocity at level 2 soon after by exchanging the momentum with the fluid in the neighborhood of level 2. This action accelerates up the fluid at level 2, which causes a development of Reynolds shear stress τ_{xz} acting at level 2 while accelerating at level 2. The streamwise instantaneous velocity fluctuations of the fluid parcel at level 2 is given by³

$$u' = \left(\bar{u} + l \frac{d\bar{u}}{dz} \right) - \bar{u} = l \frac{d\bar{u}}{dz} \quad (3.21)$$

where l is the mixing length. Following Prandtl's hypothesis, the vertical velocity fluctuations w' are of the same order of magnitude of u' , that is, $lu'/l = lw'/l$. Thus,

$$-w' = l \frac{d\bar{u}}{dz} \quad (3.22)$$

Here, the negative sign is due to the downward movement of fluid parcel. However, the other case, that is the upward motion of a fluid parcel arriving from a lower level, is clearly illustrated in Fig. 3.3b. In this case, a $-w'$ is accompanied by a $+u'$ and a $+w'$ by a $-u'$, making the product $u'w'$ always a negative. Thus, the Reynolds shear stress τ_{xz} becomes

$$\tau_{xz} = -\rho \overline{u'w'} = \rho l^2 \left(\frac{d\bar{u}}{dz} \right)^2 \quad (3.23)$$

This yields the turbulent flow model of the mixing length. Equation (3.23) is rearranged introducing a modulus sign to have an absolute value of the velocity gradient in order to retain the sign and then expressed analogous to the Newton's law of viscosity (Eq. 1.3). Therefore,

³ The velocity at level 1 is expressed as $\bar{u}(z+l) = \bar{u}(z) + d\bar{u}$. If $\bar{u}(z+l)$ is expanded in a Taylor series up to the linear term only, then $d\bar{u} = \bar{u}(z+l) - \bar{u}(z) = l d\bar{u}/dz$. Hence, the velocity at level 1 is given by $\bar{u} + l d\bar{u}/dz$. However, velocity at level 2 is \bar{u} .

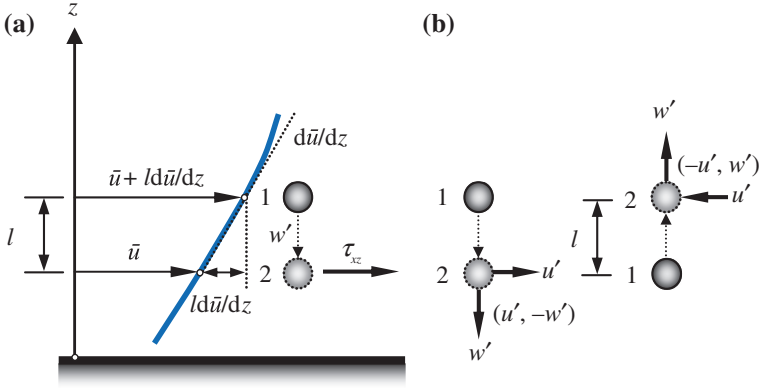


Fig. 3.3 **a** Sketch illustrating the mixing length concept in turbulent flow showing a fluid parcel moving downward and **b** sketch explaining the fluid parcels moving downward (*in the left*) and upward (*in the right*) to result in velocity fluctuations at the arrival position (level 2) as $(u', -w')$ and $(-u', w')$, respectively

$$\tau_{xz} = \rho l^2 \left| \frac{d\bar{u}}{dz} \right| \frac{d\bar{u}}{dz} \Rightarrow \tau_{xz} = \rho \varepsilon_t \frac{d\bar{u}}{dz} \quad \wedge \quad \varepsilon_t = l^2 \left| \frac{d\bar{u}}{dz} \right| \quad (3.24)$$

where ε_t is the coefficient of eddy viscosity or turbulent diffusivity. In Eq. (3.24), the eddy viscosity assumption is also known as *Boussinesq hypothesis*. Using Eq. (3.24) into Eq. (3.18) yields

$$\tau = (\mu + \rho \varepsilon_t) \frac{d\bar{u}}{dz} = \rho(\nu + \varepsilon_t) \frac{d\bar{u}}{dz} \quad (3.25)$$

According to Prandtl, the mixing length l is proportional to the vertical distance z from the boundary. For a laminar flow, l must vanish, as the transverse motion of fluid is inhibited. The l varies linearly with z within the wall shear layer

$$l = \kappa z \quad (3.26)$$

where κ is the von Kármán constant, determined experimentally as 0.41. It is considered to be a universal constant in flow over solid boundaries. Near the solid boundary, viscous effects become substantial and thus have a damping effect on the mixing length.⁴

⁴ The modified mixing length model of van Driest (1956) that incorporates the viscous effect is as follows:

$$l = \kappa z \Gamma(\bar{z}^+) \quad \wedge \quad \Gamma(\bar{z}^+) = 1 - \exp\left(-\frac{\bar{z}^+}{B_d}\right) \quad \vee \quad \bar{z}^+ = \frac{z u_*}{\nu}$$

where $\Gamma(\bar{z}^+)$ is the van Driest damping function and B_d is the damping factor.

3.5.2 Similarity Hypothesis of von Kármán

In the flow region outside of the viscous sublayer, von Kármán (1930) developed an important relationship for the mixing length l based on the similarity hypothesis. He assumed the following: (1) Except in the vicinity of the solid boundary, turbulence phenomena are not influenced by the viscosity and (2) the basic features of turbulence at different positions are similar, that is, they differ only in time and length scales. Alternatively, the mixing length l is a function of the distribution of time-averaged velocity in turbulent flow, while it is indirectly related to the distance z from the boundary. He originally derived two alternative expressions relating the Reynolds shear stress and the velocity distribution: one in terms of the Reynolds shear stress itself and the other in terms of the Reynolds shear stress gradient. They are given as

$$\tau_{xz} = \rho l^2 \left(\frac{d\bar{u}}{dz} \right)^2, \quad \frac{d\tau_{xz}}{dz} \sim \rho l^2 \frac{d\bar{u}}{dz} \cdot \frac{d^2\bar{u}}{dz^2}$$

Applying the similarity hypothesis, von Kármán proposed the mixing length l as

$$l = \kappa \frac{|d\bar{u}/dz|}{|d^2\bar{u}/dz^2|} \quad (3.27)$$

Equation (3.27) indicates that the mixing length l is a function of local velocity distribution in the neighborhood of a point.

3.6 Classification of Flow Field in Open Channels

Traditionally, the flow field in open channels can be classified into different flow layers, depending on the flow characteristics (Fig. 3.4). Interestingly, specific characteristics are exhibited in various flow layers, whose thicknesses are divided according to certain values of nondimensional vertical distances from the solid boundary. They are expressed as $\tilde{z}^+ = zu_*/\nu$ and/or $\tilde{z} = z/h$.

1. *Viscous sublayer* ($\tilde{z}^+ \leq 5$): It is the thin layer, where the flow is purely laminar without any turbulence (no velocity fluctuations), being developed adjacent to a smooth solid boundary; however, the flow outside this layer is essentially turbulent. It is already discussed in Sect. 2.6. According to the measurements, the viscous shear stress that is prevalent within this layer is constant and equals the bed shear stress.
2. *Transition or buffer layer* ($5 < \tilde{z}^+ < 30$): In this layer, the changeover from a laminar flow to a turbulent flow takes place. Hence, the flow in this layer is

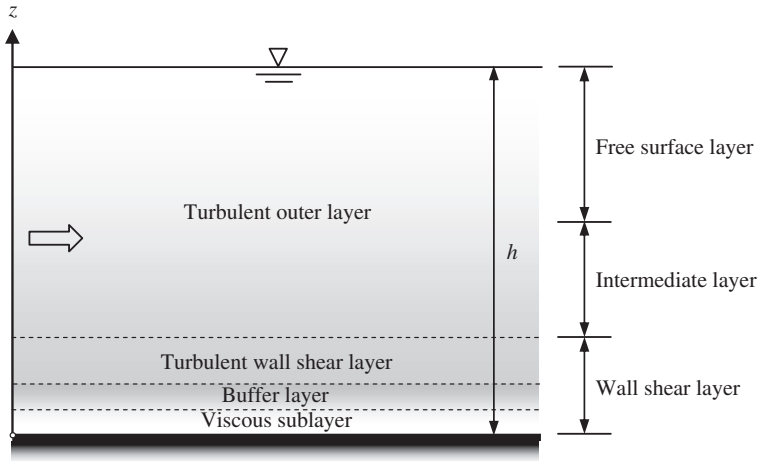


Fig. 3.4 Classification of flow field in different layers (layer thickness not according to scale)

influenced by both viscosity and turbulence. The thickness of this layer is about five times thicker than that of viscous sublayer.

3. *Turbulent wall shear layer* ($\tilde{z}^+ \geq 30, \tilde{z} < 0.2$): It is the layer (immediately above the buffer layer) wherein the Reynolds shear stress is predominant and the viscous shear stress is effectively negligible. Measurements showed that the Reynolds shear stress is constant within the layer and equals the bed shear stress. Note that in this layer, Prandtl introduced the mixing length concept and found that the logarithmic law of velocity distribution (*the law of the wall*) is preserved. Hence, this layer is also known as *logarithmic layer*.
4. *Turbulent outer layer* ($0.2 \leq \tilde{z} \leq 1$): In this layer, velocity is almost invariant of vertical distance due to the presence of large eddies, which produce a strong mixing of fluid in flow.

Note that up to the turbulent wall shear layer from the boundary is called *inner layer*.

On the other hand, Nezu and Nakagawa (1993) differentiated the flow layers from the viewpoint of TKE budget. There are three spectral subranges of velocity fluctuations: (1) *Turbulent energy containing range*, where the TKE comes from the time-averaged velocity, (2) *inertial subrange*, where the TKE is transmitted to smaller-scale eddies, and (3) *viscous dissipation range*, where the TKE is dissipated into heat. It is discussed in Sect. 3.11 in details. Nezu and Nakagawa argued that the TKE transfer in open-channel flow is analogous to this cascade process through the spectral subranges. From this analogy, the turbulent flow field in open channel can be divided into three flow layers. These flow layers are also shown in Fig. 3.4 and discussed as follows:

1. *Wall shear layer* ($\tilde{z} < 0.2$): This is the inner layer of a fully developed turbulent flow, whose length scale is defined by ν/u_* (for smooth flow) and velocity scale by the shear velocity u_* . In fact, the layer is regarded as a turbulent bursting (that is the processes of ejections and sweeps, discussed in Sect. 3.16) prone near-boundary flow region, having a range $\tilde{z}^+ \leq 50$, where the TKE production rate exceeds the TKE dissipation rate. In this layer, the law of the wall is preserved.
2. *Free surface layer* ($0.6 < \tilde{z} \leq 1$): In this layer, the flow field is governed by the outer variables. The length scale is defined by the flow depth h or the boundary layer thickness δ and the velocity scale by maximum streamwise velocity U_{\max} . The TKE dissipation rate exceeds the TKE production rate within this layer. As a result of this, the TKE is transmitted from the wall shear layer to this layer by a TKE diffusion process.
3. *Intermediate layer* ($0.2 \leq \tilde{z} \leq 0.6$): This layer is influenced by the composite characteristics of the wall shear layer and the free surface layer; however, the viscous effects are practically negligible. In this layer (having a range $\tilde{z}^+ > 50$), a near-equilibrium TKE budget is maintained, where the TKE production rate equals the TKE dissipation rate.

3.7 Velocity Distribution

Regarding the velocity distribution over a solid boundary, we are indebted to the physical insight of Ludwig Prandtl and Theodore von Kármán. They deduced the velocity distributions in the wall shear layer and the outer layer plus intermediate overlapping between these two in the intermediate layer. For the wall shear layer, Prandtl (1933) argued that the velocity distribution depends on the bed shear stress τ_0 , mass density of fluid ρ , viscosity of fluid ν , and vertical distance z from the boundary, but not on the maximum or the free stream velocity U_{\max} . Hence, the law of the wall can be given in functional form as

$$\bar{u} = f_1(\tau_0, \rho, \nu, z)$$

Conversely, for the outer layer, von Kármán (1930) deduced that the boundary acts as a source of deceleration to decrease the local flow velocity $\bar{u}(z)$ below the maximum or the free stream velocity U_{\max} in the way of independent of viscosity of fluid ν , but dependent on bed shear stress τ_0 , mass density of fluid ρ , vertical distance z , and boundary layer thickness δ . Hence, the law of the outer layer is

$$U_{\max} - \bar{u} = f_2(\tau_0, \rho, z, \delta)$$

In the above equation, the $(U_{\max} - \bar{u})$ is called *velocity defect*.

For the intermediate layer, a simplified overlapping law shows that the velocity distributions of wall shear layer and outer layer merge smoothly. Hence,

$$\bar{u}(\text{wall shear layer}) = \bar{u}(\text{outer layer}).$$

3.7.1 The Linear Law in Viscous Sublayer

In viscous sublayer ($\tilde{z}^+ \leq 5$), the viscous shear stress τ_v is constant and equals the bed shear stress τ_0 . That is,

$$\tau_v = \rho v \frac{d\bar{u}}{dz} = \tau_0 \Rightarrow d\bar{u} = \frac{u_*^2}{v} dz \quad \wedge \quad \tau_0 = \rho u_*^2 \quad (3.28)$$

Integrating and applying the no-slip condition at the boundary, that is $\bar{u}(z = 0) = 0$, yield

$$u^+ = \tilde{z}^+ \quad \wedge \quad u^+ = \frac{\bar{u}}{u_*} \quad \vee \quad \tilde{z}^+ = \frac{z u_*}{v} \quad (3.29)$$

Thus, the *linear law* of velocity distribution exists in the viscous sublayer. Equation (3.29) holds good for the range $0 < \tilde{z}^+ \leq 5$.

3.7.2 The Logarithmic Law in Turbulent Wall Shear Layer

It is appropriate to discuss the turbulent wall shear layer before the buffer layer, which is characterized by both viscous and turbulence properties. In turbulent wall shear layer ($\tilde{z}^+ \geq 30$, $\tilde{z} < 0.2$), the total shear stress τ contains only the turbulent shear stress τ_{xz} and practically $\tau_v \approx 0$. According to Prandtl's mixing length theory,

$$\tau_{xz} = \rho l^2 \left(\frac{d\bar{u}}{dz} \right)^2 = \tau_0 \quad (3.30)$$

Substituting $l = \kappa z$ yields

$$d\bar{u} = \frac{u_*}{\kappa z} dz \quad (3.31)$$

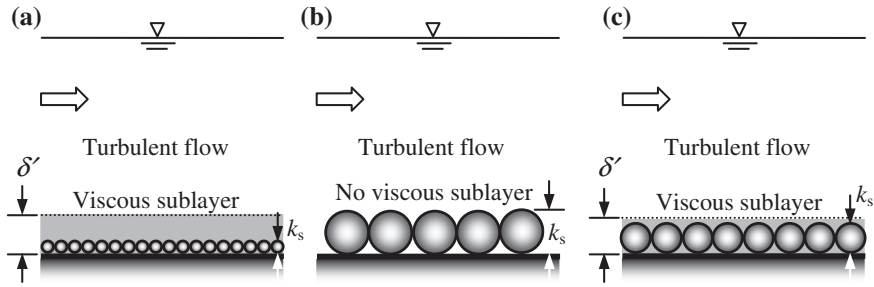


Fig. 3.5 Different flow regimes: **a** smooth, **b** rough, and **c** transition

Integrating Eq. (3.31), one gets

$$u^+ = \frac{1}{\kappa} \ln z + C \quad (3.32)$$

where C is the integration constant. Using the boundary condition $\bar{u}(z = z_0) = 0$, where z_0 is the zero-velocity level, produces

$$u^+ = \frac{1}{\kappa} \ln \left(\frac{z}{z_0} \right) \quad (3.33)$$

By the modification of the mixing length theory introduced by Prandtl, the logarithmic velocity distribution is applicable to both the buffer layer and the turbulent outer layer. On the other hand, in the viscous sublayer, the boundary roughness plays an important role in defining the velocity distribution, which was first observed by Johann Nikuradse in pipe flows (Nikuradse 1933). He introduced the concept of equivalent roughness k_s , called *Nikuradse's equivalent roughness* or *equivalent sand roughness* (Schlichting and Gersten 2000). Based on the experimental findings on roughness, the flow regimes are classified as hydraulically smooth, rough, and transitional flows⁵ (Figs. 3.5a–c). In this context, the shear Reynolds number $R_* (=u_* k_s / \nu)$ plays a decisive role in defining the *flow regimes*.

1. *Hydraulically smooth flow* ($R_* \leq 5$): In this flow, the boundary roughness height k_s is much smaller than the viscous sublayer thickness δ' . Thus, the roughness elements are submerged by the viscous sublayer (Fig. 3.5a). The main flow outside the viscous sublayer cannot therefore sense the roughness. Hence, the velocity distributions in turbulent wall shear and outer layers are not affected by the boundary roughness, but affected by the fluid viscosity.

⁵ More explicitly, the *flow regimes* are called (1) *hydraulically smooth flow regime*, (2) *hydraulically rough flow regime*, and (3) *hydraulically transitional flow regime* of turbulent flow.

2. *Hydraulically rough flow* ($R_* \geq 70$): In this flow, the boundary roughness height is much larger than the viscous sublayer thickness (Fig. 3.5b). Near the boundary, the roughness produces eddies annihilating the viscous sublayer. The roughness elements are therefore exposed to the main flow region. The velocity distributions in turbulent wall shear and outer layers are affected by the boundary roughness, but not by the fluid viscosity.
3. *Hydraulically transitional flow* ($5 < R_* < 70$): In this flow, the boundary roughness height is typically in the order of viscous sublayer thickness (Fig. 3.5c). The velocity distributions are affected by both the boundary roughness and the fluid viscosity.

According to Nikuradse's study on pipe flows, the expressions for zero-velocity level z_0 for different flow regimes are

$$\text{Smooth flow: } z_0(R_* \leq 5) = 0.11 \frac{v}{u_*} \quad \wedge \quad R_* = \frac{u_* k_s}{v} \quad (3.34a)$$

$$\text{Rough flow: } z_0(R_* \geq 70) = \frac{k_s}{30} \quad (3.34b)$$

$$\text{Transition: } z_0(5 < R_* < 70) = 0.11 \frac{v}{u_*} + \frac{k_s}{30} \quad (3.34c)$$

It is important to note that the zero-velocity level z_0 in smooth flow is a function of viscosity v and shear velocity u_* , but not a function of roughness k_s . However, z_0 in rough flow is a function of k_s , but not a function of v and u_* . On the other hand, the transitional case has a composite effect of smooth and rough flows. The ASCE Task Force (1963) on friction factor in open channels reported that for open-channel roughness similar to that encountered in pipes, the resistance equations similar to those of pipe flows are adequate. Here, boundary roughness is discussed with reference to the roughness types that are often encountered in engineering practice. In reality, the solid boundaries including sediment beds exhibit some roughness. Since there can be an unlimited number of possible surface states, a standard roughness is essentially introduced to describe the roughness effect on a fluid flow. Here, it is assumed that a solid boundary is covered with a layer of spheres packed together as closely as possible, as is obtained in case of sandpaper. Thus, the standard roughness is called *sand roughness*. The diameter of the sphere is called the *sand roughness height* and is a measure of the boundary roughness. Therefore, it is adequate to consider the effects of sand roughness on the law of the wall. However, technically rough boundary or sediment bed can be generally assigned to so-called *equivalent sand roughness* or simply *equivalent roughness*. The equivalent roughness formulas for sediment beds given by various investigators are summarized in Table 3.1.

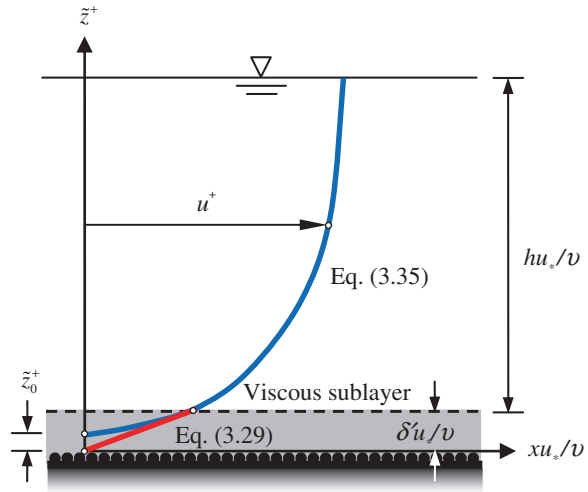
In the above discussion, the roughness limits are given in terms of sand roughness or its equivalent value. These types of rough boundaries are categorized by *k-type*, where the roughness affects the flow scale with roughness height k_s .

Table 3.1 Equivalent roughness formulas for sediment beds

References	Formula
Wilson (1987)	$k_s = 5d_{50}\Theta \quad \wedge \quad \Theta = u_*^2/(\Delta g d_{50}) \quad \vee \quad \Delta = s - 1 \quad \wedge \quad s = \rho_s/\rho$
Yalin (1992)	$k_s = d_{50}[5\Theta + (\Theta - 4)^2(0.043\Theta^3 - 0.289\Theta^2 - 0.203\Theta + 0.125)]$
van Rijn (1993)	$k_s = 3d_{90}\Theta$
Sumer et al. (1996)	$k_s(w_s > 0.9u_*) = d_{50}(2 + 0.6\Theta^{2.5})$ $k_s(w_s \leq 0.9u_*) = d_{50}[4.5 + 0.25\exp(0.6W_*^4)\Theta^{2.5}]$ $\wedge \quad W_* = w_s/(\Delta g d_{50})^{0.5}$
Camenen et al. (2006)	$k_s = d_{50}(0.6 + 1.8 W_{*s}^{1.2}\Theta^{1.7}Fr^{-2.4}) \quad \wedge \quad W_{*s} = w_s\Delta^{2/3}/(gv)^{1/3}$ $\vee \quad Fr = U/(gh)^{0.5}$

Note Θ is the Shields parameter, Δ is the submerged relative density of sediment, s is the relative density of sediment, ρ_s is the mass density of sediment, w_s is the terminal fall velocity of sediment, and Fr is the flow Froude number

Fig. 3.6 Velocity distribution in a smooth flow regime. All dimensions are nondimensional



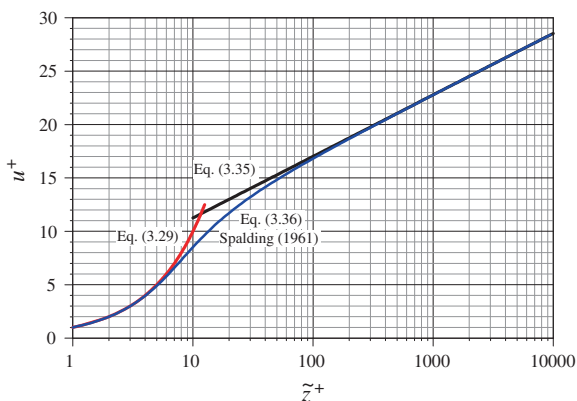
The other category of rough boundaries is known as *d-type*, where the roughness elements are large enough and closely spaced, so that the flow passes over the top of the elements with stagnant fluid in between the elements (Jiménez 2004). Further, in sediment bed with bedforms, the total roughness can be obtained by adding the two values: $k_{s|total} = k_{s|sand} + k_{s|bedforms}$.

Reverting to the velocity distribution, for smooth flow, such as a plane sediment bed formed by median particle size less than 0.25 mm, it is customary to express Eq. (3.33) in another form as

$$u^+ = \frac{1}{\kappa} \ln \tilde{z}^+ + B|_{smooth} \quad \wedge \quad B|_{smooth} = -\frac{1}{\kappa} \ln \tilde{z}_0^+ \quad \vee \quad \tilde{z}_0^+ = \frac{z_0 u_*}{v} \quad (3.35)$$

where $B|_{smooth}$ is the integration constant for a smooth flow. Nikuradse suggested that $\kappa \approx 0.4$ and $B|_{smooth} \approx 5.5$ using Eq. (3.34a), but afterward, more accurate data analysis produced $\kappa \approx 0.41$ and $B|_{smooth} \approx 5$. Figure 3.6 shows a schematic

Fig. 3.7 Velocity distribution in the inner layer and a portion of the outer layer



nondimensional velocity distribution in a smooth flow regime, where rough elements are small enough to be covered by the viscous sublayer. The merger of the linear distribution (Eq. 3.29) with the logarithmic distribution (Eq. 3.35) at the edge of the viscous sublayer is noticeable (Fig. 3.7).

Between $5 < R_* < 70$, called the *buffer layer*, the velocity distribution is neither linear nor logarithmic, but is instead a smooth merge between the two. Spalding (1961) deduced a single composite equation covering the entire wall shear layer. It is as follows:

$$\tilde{z}^+ = u^+ + \left[\exp(\kappa u^+) - 1 - \kappa u^+ - \frac{(\kappa u^+)^2}{2} - \frac{(\kappa u^+)^3}{6} \right] \exp(-\kappa B|_{\text{smooth}}) \quad (3.36)$$

Equation (3.36) holds good not only in the viscous sublayer and the logarithmic wall shear layer, but also in the outer layer for the range $\tilde{z}^+ > 100$, as shown in Fig. 3.7.

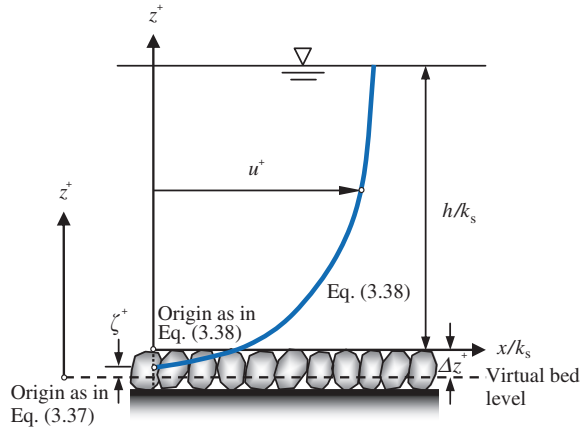
For rough flow, such as a sediment bed formed by gravels, Eq. (3.33) can be expressed in another form as

$$u^+ = \frac{1}{\kappa} \ln z^+ + B|_{\text{rough}} \quad \wedge \quad z^+ = \frac{z}{k_s} \quad \vee \quad B|_{\text{rough}} = \frac{1}{\kappa} \ln \left(\frac{1}{\zeta^+} \right) \quad \wedge \quad \zeta^+ = \frac{z_0}{k_s} \quad (3.37)$$

where $B|_{\text{rough}}$ is the integration constant for a rough flow, which is 8.5 for $\kappa \approx 0.4$ using Eq. (3.34b). Figure 3.8 shows a schematic nondimensional velocity distribution in a rough flow regime, where roughness elements are large enough, such that the viscous sublayer could not be formed.

It is important to note that the origin of z -axis is considered at a convenient depth at the top or below the top of the roughness elements. The *virtual reference level* (also called *virtual bed level* of a sand- or a gravel-bed) of a rough boundary is considered passing through the origin of z -axis and lying on the x -axis.

Fig. 3.8 Velocity distribution in a rough flow regime. All dimensions are nondimensional



For instance, van Rijn (1984) assumed that the origin of z -axis is at $0.25k_s$ below the top of the roughness elements. It is, however, advisable to use the following form of Eq. (3.37), setting the origin of z -axis at the top of the roughness elements (Fig. 3.8). The logarithmic law then becomes

$$u^+ = \frac{1}{\kappa} \ln \left(\frac{z^+ + \Delta z^+}{\zeta^+} \right) \quad (3.38)$$

where $\Delta z^+ = \Delta z/k_s$ and Δz is the depth of the origin of z -axis or the virtual bed level from the top of the roughness elements. Δz is also known as *zero-plane displacement*, which can be determined by fitting the measured velocity data (see Sect. 5.15) (Dey and Das 2012; Dey et al. 2012).

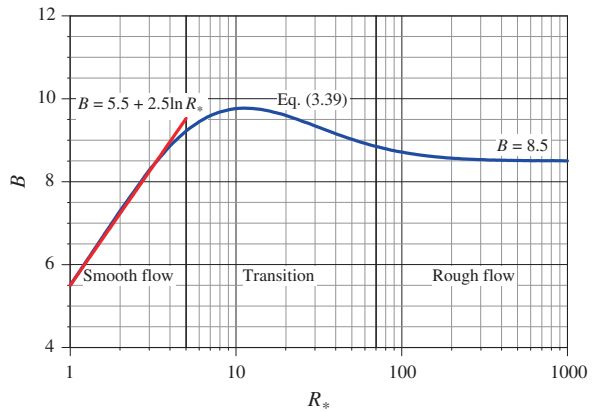
For immobile rough boundary streams or technical rough boundaries, the average values of $B|_{\text{rough}}$ (and their standard deviation) obtained by different investigators are $8.5 (\pm 0.15)$ of Reynolds (1974), $8.47 (\pm 0.9)$ of Kironoto and Graf (1994), and $8.42 (\pm 0.22)$ of Song et al. (1994). However, Dey and Raikar (2007) obtained it as $7.8 (\pm 0.37)$ for gravel-beds under the near-threshold condition (weakly mobile). It is less than those reported in the literature for immobile rough boundary streams. Importantly, in flow with unrest surface particles at the near-threshold condition, there prevails a decreasing tendency of the value of $B|_{\text{rough}}$.

The expression of B in composite form for both smooth and rough flows, as well as transitional range between them, was given by García (2008) as

$$B = 8.5 + (2.5 \ln R_* - 3) \exp[-0.121(\ln^{2.42} R_*)] \quad (3.39)$$

Figure 3.9 shows the variation of B with R_* obtained from Eq. (3.39). For smooth flow, B is a function of R_* as $B = 5.5 + 2.5 \ln R_*$, while for rough flow, $B = 8.5$.

Fig. 3.9 Integration constant B as a function of shear Reynolds number R_* obtained from Eq. (3.39)



3.7.3 Law in Buffer Layer

In buffer layer ($5 < \tilde{z}^+ < 30$), the flow is characterized by both viscosity and turbulence. Hence, it somewhat possesses a composite property of both the viscous sublayer and the turbulent wall shear layer. Although an analytical solution for the buffer layer is not available, it can no longer be neglected in turbulence research, because it plays a critical role in the bursting phenomena. However, a theoretical curve for the velocity distribution in this layer can be obtained numerically from the differential equation given by Nezu and Azuma (2004) using the van Driest's model. It is as follows:

$$\frac{du^+}{d\tilde{z}^+} = \frac{2\left(1 - \frac{\tilde{z}^+}{R_*}\right)}{1 + \left[1 + 4I^{+2}\left(1 - \frac{\tilde{z}^+}{R_*}\right)\right]^{0.5}} \quad \wedge \quad I^+ = \frac{lu_*}{v} \quad (3.40)$$

The modified mixing length model of van Driest (1956) that incorporates the viscous effects is

$$I^+ = \kappa \tilde{z}^+ \Gamma(\tilde{z}^+) \quad \wedge \quad \Gamma(\tilde{z}^+) = 1 - \exp\left(-\frac{\tilde{z}^+}{B_d}\right) \quad (3.41)$$

where $\Gamma(\tilde{z}^+)$ is the van Driest damping function and B_d is the damping factor, which can be assumed as 26.

Further, the modified mixing length model of van Driest can also be used to describe the damping of Reynolds shear stress distribution in the buffer layer and the viscous sublayer. In two-dimensional open-channel flow, according to Nezu

and Azuma (2004) [also see Nezu and Nakagawa (1993)], the Reynolds shear stress distribution with viscous effects is given by

$$-\frac{\overline{u'w'}}{u_*^2} = 1 - \tilde{z} - \frac{du^+}{d\tilde{z}^+} \quad (3.42)$$

3.7.4 Log-Wake Law and Velocity Defect Law

In the outer layer ($0.2 < \tilde{z} \leq 1$), the velocity distribution that has an excess velocity deviates from the logarithmic law, as the distance increases from the boundary, especially for $\tilde{z}^+ > 1,000$. The reason for the departure is attributed to the assumption of constant shear stress and linearly varying mixing length throughout the fluid. Coles (1956) gave the complete description of the velocity distribution, including the wake law, called the *log-wake law*. It is as follows:

$$u^+ = \frac{1}{\kappa} \ln\left(\frac{z}{z_0}\right) + \underbrace{\frac{2\Pi}{\kappa} \sin^2\left(\frac{\pi}{2}\tilde{z}\right)}_{\text{Wake function}} \quad \wedge \quad \tilde{z} = \frac{z}{h} \quad (3.43)$$

where Π is *Coles' wake parameter*. Note that the sine function in the last term of the right-hand side of Eq. (3.43) can be approximated by

$$\sin^2\left(\frac{\pi}{2}\tilde{z}\right) \approx 3\tilde{z}^2 - 2\tilde{z}^3$$

The last term in fact describes the velocity enhancement in the turbulent outer layer and is called the *wake function*. The wake function is zero at the boundary ($z = 0$) and increases gradually toward the free surface and reaches a maximum value of $2\Pi/\kappa$ at the free surface ($z = h$).⁶ The advantage of Eq. (3.43) is that it is a complete and reasonably accurate expression covering entire range of a two-dimensional boundary layer flow, whether fully developed or not.

The usual form of Coles' wake law is in terms of the velocity defect that would require information on the maximum velocity $u = U_{\max}$ of a vertical distribution of velocity that usually occurs at the free surface $z = h$, unless there is a dip (discussed in Sect. 3.10). Equation (3.33) is used to obtain the velocity defect law

⁶ The forms of the log-wake law for smooth and rough flows are as follows:

$$\begin{aligned} \text{Smooth flow: } u^+ &= \left(\frac{1}{\kappa} \ln \tilde{z}^+ + B|_{\text{smooth}} \right) + \frac{2\Pi}{\kappa} \sin^2\left(\frac{\pi}{2}\tilde{z}\right) \\ \text{Rough flow: } u^+ &= \left(\frac{1}{\kappa} \ln \tilde{z}^+ + B|_{\text{rough}} \right) + \frac{2\Pi}{\kappa} \sin^2\left(\frac{\pi}{2}\tilde{z}\right). \end{aligned}$$

that provides the outer form of the law of the wall (Schlichting 1979). It is as follows:

$$\Delta U_{\max}^+ = -\frac{1}{\kappa} \ln \tilde{z} \quad \wedge \quad \Delta U_{\max}^+ = \frac{\Delta U_{\max}}{u_*} \quad \vee \quad \Delta U_{\max} = U_{\max} - \bar{u} \quad (3.44)$$

In relation to the log-wake law (Eq. 3.43), the *velocity defect law* can be given as follows (Coleman 1981; Coleman and Alonso 1983):

$$\Delta U_{\max}^+ = -\frac{1}{\kappa} \ln \tilde{z} + \frac{2\Pi}{\kappa} \cos^2\left(\frac{\pi}{2} \tilde{z}\right) \quad (3.45)$$

The time-averaged velocity distribution for smooth flow was expressed by Dean (1976) as a combination of logarithmic and wake terms. According to him, the log-wake law and the velocity defect law are as follows:

$$u^+ = \left(\frac{1}{\kappa} \ln \tilde{z}^+ + B|_{\text{smooth}} \right) + \frac{1}{\kappa} [(1 + 6\Pi)\tilde{z}^2 - (1 + 4\Pi)\tilde{z}^3] \quad (3.46a)$$

$$\Delta U_{\max}^+ = -\frac{1}{\kappa} \ln \tilde{z} + \frac{1}{\kappa} [2\Pi - (1 + 6\Pi)\tilde{z}^2 + (1 + 4\Pi)\tilde{z}^3] \quad (3.46b)$$

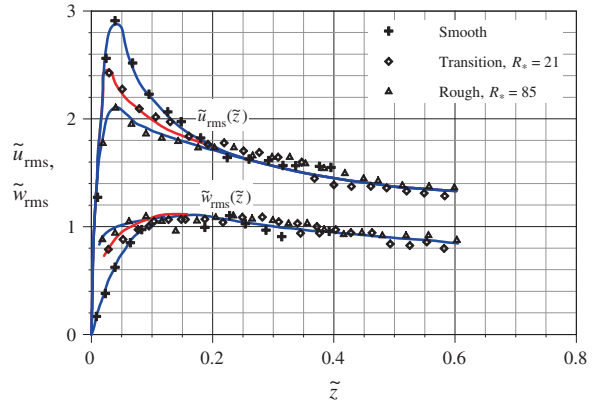
Guo et al. (2005) introduced a cubic correction term to satisfy the requirement of a zero-velocity gradient at the edge of the boundary layer. Combining the logarithmic law, the wake law and the cubic correction produced a modified log-wake law. The log-wake law and the velocity defect law are as follows:

$$u^+ = \left(\frac{1}{\kappa} \ln \tilde{z}^+ + B|_{\text{smooth}} \right) + \frac{2\Pi}{\kappa} \sin^2\left(\frac{\pi}{2} \tilde{z}\right) - \frac{\tilde{z}^3}{3\kappa} \quad (3.47a)$$

$$\Delta U_{\max}^+ = -\frac{1}{\kappa} \ln \tilde{z} + \frac{2\Pi}{\kappa} \cos^2\left(\frac{\pi}{2} \tilde{z}\right) - \frac{1 - \tilde{z}^3}{3\kappa} \quad (3.47b)$$

Dey and Raikar (2007) used the experimental velocity distributions to estimate the wake parameter Π for gravel-beds under the near-threshold condition. The average value of Π (and its standard deviation) was 0.11 (± 0.026). Due to the feeble movement of surface particles at the near-threshold condition, the value of Π is slightly greater than that of immobile rough boundaries, for example, 0.09 of Kironoto and Graf (1994) and 0.08 of Song et al. (1994). The lone case of negative value of Π ($= -0.03$) for a gravel-bed of $k_s = 23$ mm was reported by Kironoto and Graf (1994). In contrast, for smooth boundary streams, the values of Π are relatively high. Coleman (1981) obtained an average value of Π as 0.19, Nezu and Rodi (1986) as 0.2, Steffler et al. (1985) as 0.08–0.15, and Kirkgöz (1989) as 0.1. Coleman (1981) and Nezu and Rodi (1986) studied the flow with reasonably large Reynolds numbers. However, for low flow Reynolds numbers, the value of Π increases as high as 0.23 (Dong et al. 1991; Nezu and Nakagawa 1993; Nikora and Goring 2000).

Fig. 3.10 Components of turbulence intensity in smooth, transition, and rough flows (Grass 1971)



3.8 Turbulence Intensity

The degree of velocity fluctuations is one of the most important characteristics of turbulence; hence, its measurement has received top priority in studying turbulence. Earlier, hot-film anemometer (HFA) was used, and in recent years, acoustic Doppler velocimeter (ADV) and laser Doppler anemometer (LDA) are being used to measure the turbulent characteristics in fluid flow.

The velocity fluctuations are represented in the form of root mean square (RMS), termed *turbulence intensity* [also see Eq. (3.13)]. The root-mean-square values of velocity fluctuations in streamwise $u_{\text{rms}} [= (\overline{u'u'})^{0.5}]$, lateral $v_{\text{rms}} [= (\overline{v'v'})^{0.5}]$, and vertical $w_{\text{rms}} [= (\overline{w'w'})^{0.5}]$ directions are written in nondimensional form, dividing them by either the shear velocity u_* or the depth-averaged flow velocity U . Note that the turbulence intensity is the square root of Reynolds normal stress (divided by ρ) [see Eq. (3.12)]. The experimental results of Grass (1971) are shown in Fig. 3.10. The conclusions of the results are as follows:

1. The turbulence intensity is zero at the boundary and increases rapidly to reach its peak value within a short distance ($z = 0.04\text{--}0.12 h$) from the boundary. Away from the boundary, in the main flow region, the turbulence intensity is rather less and nearly a constant.
2. In the main flow region, the vertical component of turbulence intensity approaches the shear velocity, $w_{\text{rms}}/u_* \approx 1$, while the streamwise component of turbulence intensity is slightly greater than the shear velocity.
3. Near the boundary, the turbulence intensity is influenced by the boundary roughness. As the boundary roughness increases, lesser is the streamwise turbulence intensity and greater is the vertical turbulence intensity. However, the influence of boundary roughness disappears in the main flow region.
4. The distribution of turbulence intensity across the depth is more uniform in case of the rough boundary than in case of the smooth boundary.

Nezu (1977) gave the following exponential law of streamwise and vertical components of turbulence intensity:

$$\tilde{u}_{\text{rms}} = B_u \exp(-C_u \tilde{z}), \quad \tilde{v}_{\text{rms}} = B_v \exp(-C_v \tilde{z}), \quad \tilde{w}_{\text{rms}} = B_w \exp(-C_w \tilde{z}) \quad (3.48)$$

where $\tilde{u}_{\text{rms}} = u_{\text{rms}}/u_*$, $\tilde{v}_{\text{rms}} = v_{\text{rms}}/u_*$, $\tilde{w}_{\text{rms}} = w_{\text{rms}}/u_*$, and B_u , B_v , B_w , C_u , C_v and C_w are the constants.

Nezu (1977) used HFA to obtain $B_u = 2.3$, $B_v = 1.63$, $B_w = 1.27$, and $C_u = C_v = C_w = 1$ for smooth and rough flows. From LDA measurements, Nezu and Rodi (1986) obtained values of $B_u = 2.26$, $B_w = 1.23$, $C_u = 0.88$, and $C_w = 0.67$ for smooth and rough flows. Cardoso et al. (1989) reported $B_u = 2.28$ and $C_u = 1.08$ for smooth flow; Kironoto and Graf (1994) reported $B_u = 2.04$, $B_w = 0.97$, $C_u = 1.14$, and $C_w = 0.76$ for rough flow; and Dey and Raikar (2007) obtained $B_u = 2.07$, $B_w = 0.95$, $C_u = 1.17$, and $C_w = 0.69$ for rough and feebly mobile streams. Note that Eq. (3.48) cannot be applied to the near-boundary flow region where viscous effects are significant. Motivated by the modified mixing length model of van Driest (1956), Nezu (1977) put forward a combined model between the viscous sublayer and the outer layer as

$$\tilde{u}_{\text{rms}} = 2.3 \exp\left(-\frac{\tilde{z}}{R_*}\right) \Gamma(\tilde{z}^+) + 0.3 \tilde{z}^+ [1 - \Gamma(\tilde{z}^+)] \quad \wedge \quad \Gamma(\tilde{z}^+) = 1 - \exp\left(-\frac{\tilde{z}^+}{B_d}\right) \quad (3.49)$$

where $\Gamma(\tilde{z}^+)$ is the van Driest damping function and B_d is the damping factor. The value of B_d for this case is approximately 10. The viscous effects on \tilde{u}_{rms} appear to be dominant for $\tilde{z}^+ \leq 10$.

On the other hand, Nikora and Goring (1998) proposed the logarithmic law of turbulence intensity components for mobile gravel-bed streams as

$$\tilde{u}_{\text{rms}}^2 = 1.9 + 1.32 \ln \tilde{z}, \quad \tilde{v}_{\text{rms}}^2 = 0.59 + 0.22 \ln \tilde{z}. \quad (3.50)$$

3.9 Bed Shear Stress

It is always a challenging task to determine bed shear stress $\tau_0 (= \rho u_*^2)$ and hence shear velocity u_* in laboratory experimental flumes or field channels. However, the bed shear stress can be determined by using the following methods.

3.9.1 Bed Shear Stress from Bed Slope

For steady-uniform flow in a wide open channel, the bed shear stress τ_0 can be calculated traditionally from the bed slope S_0 as

$$\tau_0 = \rho g h S_0 \quad (3.51)$$

Note that in the above equation, S_0 actually represents an energy slope, which equals the bed slope for a uniform flow. However, this method is not appropriate for local and small-scale estimates of the variation in bed shear stress.

3.9.2 Bed Shear Stress from Velocity Distribution

In fully developed turbulent flow in open channels, the expression in the inner layer, as well as outer layer, is assumed to be in the form of log-wake law as given by Eq. (3.43). Then, it can be reorganized as follows:

$$\bar{u} = \frac{u_*}{\kappa} \ln \tilde{z} + \frac{u_*}{\kappa} \ln \left(\frac{h}{z_0} \right) + \frac{2\Pi}{\kappa} u_* \sin^2 \left(\frac{\pi}{2} \tilde{z} \right) = K_1 \ln \tilde{z} + K_2 + K_3 \sin^2 \left(\frac{\pi}{2} \tilde{z} \right) \quad (3.52)$$

The velocity data, $\bar{u}(\tilde{z})$, can be fitted to Eq. (3.52) by the least-squares method, and the coefficients K_1 , K_2 , and K_3 can then be calculated. In this way, the shear velocity u_* can be determined from the value of K_1 , assuming the von Kármán constant $\kappa = 0.41$. However, it is always advisable to use the velocity data within the logarithmic wall shear layer ($\tilde{z} < 0.2$) to determine u_* . Then, Eq. (3.33) can be reorganized as follows:

$$\bar{u} = \frac{u_*}{\kappa} \ln z + \left(-\frac{u_*}{\kappa} \right) \ln z_0 = C_1 \ln z + C_2 \quad (3.53)$$

The velocity data, $\bar{u}(\tilde{z} < 0.2)$, can be fitted to Eq. (3.53) by the least-squares method to calculate the coefficients C_1 and C_2 , and then, u_* can be determined from the value of C_1 , assuming $\kappa = 0.41$. The method of least-squares fitting of Eq. (3.53) for the velocity data in the inner layer is known as *Clauser method* (Clauser 1954). Once u_* is obtained, the bed shear stress $\tau_0 (= \rho u_*^2)$ can be estimated. This method is widely used to evaluate the local bed shear stress. Although the method is rather easy, the velocity measurement errors influence the estimation of bed shear stress. Further, this method is useful in field studies, provided the velocity distributions in the inner layer are quite logarithmic.

3.9.3 Bed Shear Stress from Average Velocity

The bed shear stress τ_0 can be expressed as a function of dynamic pressure due to an average velocity U of flow as

$$\tau_0 = \frac{\lambda_D}{8} \rho U^2 \quad (3.54)$$

where λ_D is the Darcy–Weisbach friction factor. The Colebrook–White equation⁷ can be used to evaluate λ_D (Colebrook and White 1937). It is as follows:

$$\frac{1}{\lambda_D^{0.5}} = -0.86 \ln \left(\frac{k_s P}{14.8A} + \frac{2.51}{Re \lambda_D^{0.5}} \right) \quad (3.55)$$

where A is the flow area, P is the wetted perimeter, and Re is the flow Reynolds number. In a channel or an experimental flume, the bed is rough consisting of sediment particles and the sidewalls are usually smooth. It suggests that the friction factor $\lambda_{D|w}$ associated with smooth wall is different from the friction factor $\lambda_{D|b}$ associated with rough bed. Consequently, the shear stress $\tau_{0|w}$ associated with wall is significantly different from the shear stress $\tau_{0|b}$ associated with bed. Hence, Vanoni's (1975) method of *sidewall correction* can be applied to such a composite roughness due to smooth wall and rough bed for a given cross section of a channel. Using the continuity equation, the discharge Q is as follows:

$$Q = AU = A|_w U|_w + A|_b U|_b \quad (3.56)$$

The average velocity U , considered to be same as $U|_w$ and $U|_b$, can be computed once Q is known. The equation of force in the streamwise direction (x -direction) is given by

$$-A \frac{dp}{dx} = \rho \frac{\lambda_D}{8} U^2 P = \rho \frac{\lambda_{D|w}}{8} U|_w^2 P|_w + \rho \frac{\lambda_{D|b}}{8} U|_b^2 P|_b \quad (3.57)$$

where dp/dx is the streamwise pressure gradient. Using $U = U|_w = U|_b$ into Eq. (3.57), one gets

$$P \lambda_D = P|_w \lambda_{D|w} + P|_b \lambda_{D|b} \quad (3.58)$$

⁷ The Colebrook–White equation is an implicit equation. An explicit form of the Colebrook–White equation was given by Haaland (1983). It is as follows:

$$\frac{1}{\lambda_D^{0.5}} = -0.782 \ln \left[\left(\frac{k_s P}{14.8A} \right)^{1.1} + \frac{6.9}{Re} \right].$$

As the hydraulic grade line is same for the smooth wall and the rough-bed regions, equating forces to the wall and the bed regions, one can obtain

$$\frac{P\lambda_D}{A} = \frac{P|_w\lambda_D|_w}{A|_w} = \frac{P|_b\lambda_D|_b}{A|_b} \quad (3.59)$$

The Reynolds numbers of flow for different regions are as follows:

$$Re = \frac{4UA}{vP}, \quad Re|_w = \frac{4UA|_w}{vP|_w}, \quad Re|_b = \frac{4UA|_b}{vP|_b} \quad (3.60)$$

Using Eq. (3.60) into Eq. (3.59), one gets

$$\frac{Re}{\lambda_D} = \frac{Re|_w}{\lambda_D|_w} = \frac{Re|_b}{\lambda_D|_b} \quad (3.61)$$

As the wall is smooth, Blasius equation can be used to evaluate $\lambda_D|_w$. It is as follows:

$$\lambda_D|_w = \frac{0.316}{Re|_w^{0.25}} \quad (3.62)$$

Using Eqs. (3.56)–(3.62), the following equation is obtained:

$$\lambda_D|_b = 0.316 Re|_b \left(\frac{4UA}{vP|_w} - \frac{Re|_b P|_b}{P|_w} \right)^{-1.25} \quad (3.63)$$

Again, using Eq. (3.61) into Eq. (3.55), the Colebrook–White equation becomes

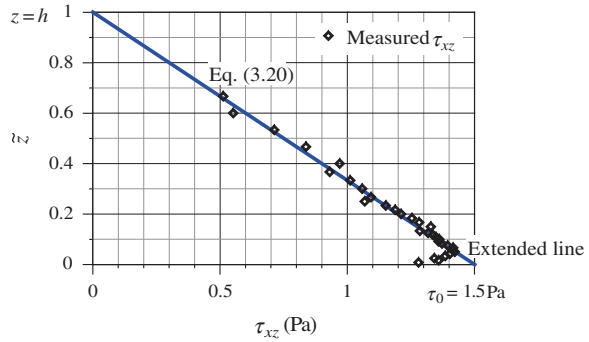
$$\frac{1}{\lambda_D|_b^{0.5}} = -0.86 \ln \left(\frac{k_s U}{3.7v Re|_b} + \frac{2.51}{Re|_b \lambda_D|_b^{0.5}} \right) \quad (3.64)$$

For the given data of A , U , P , $P|_w$, $P|_b$, v , ρ , and k_s , the unknowns $Re|_b$ and $\lambda_D|_b$ can be determined numerically solving Eqs. (3.63) and (3.64). Then, Eq. (3.54) can be used to estimate the bed shear stress $\tau_0|_b [= (\lambda_D|_b/8)\rho U^2]$. For uniform flow, this method was effectively used by Dey (2003).

3.9.4 Bed Shear Stress from Reynolds Shear Stress Distribution

For uniform flow, the bed shear stress τ_0 can be obtained from the measured data plots of the Reynolds shear stress distribution ($\tau_{xz} = -\rho \overline{u'w'}$) extending the linear

Fig. 3.11 Determination of bed shear stress τ_0 from Reynolds shear stress τ_{xz} distribution (Dey et al. 2012)



portion of the distribution on to the boundary, as shown in Fig. 3.11. Then, the bed shear stress τ_0 can be obtained as

$$\tau_0 = \tau_{xz}|_{\text{bed}} = -\rho \overline{u'w'}|_{\text{bed}} \quad (3.65)$$

Note that the Reynolds shear stress distribution has a near-bed damping (see Fig. 3.11) and becomes zero at the bed. Hence, one should not misunderstand, because Eq. (3.65) indicates an extrapolated value of the linear portion of the Reynolds shear stress distribution above the bed, although τ_{xz} on the bed is zero. The linear variation (shown by the inclined straight line) therefore simulates the total shear stress distribution, as represented by Eq. (3.20). However, this method somewhat provides a direct estimation and is useful for the fully developed turbulent flow with large Reynolds numbers (Dyer 1986). Nevertheless, due to inherent uncertainty involved in near-bed measurements of fluctuating velocity, the extrapolated values of Reynolds shear stress could be erroneous as a result of data scattering in Reynolds shear stress distributions.

3.9.5 Bed Shear Stress from Turbulent Kinetic Energy Distribution

Simple relationships between the TKE and the shear stress were proposed in turbulence models (Galperin et al. 1988), while further studies by Soulsby and Dyer (1981) and Stapleton and Huntley (1995) showed that the TKE is proportional to the bed shear stress. It is as follows:

$$\tau_0 = C_k \rho k \quad \wedge \quad k = \frac{1}{2} (\overline{u'u'} + \overline{v'v'} + \overline{w'w'}) \quad (3.66)$$

where k is the TKE and C_k is a proportionality constant, being approximately 0.19 (Kim et al. 2000).

3.9.6 Bed Shear Stress from Spectral Density Function

López and García (1999) [also see Gross and Nowell (1985)] put forward the spectral method for the estimation of bed shear stress. They used the estimated values of TKE dissipation rate ε in the inertial subrange of the spectral domain.

$$\tau_0 = \rho(\varepsilon \kappa z)^{2/3} \quad (3.67)$$

The estimation of ε can be done by using Kolmogorov second hypothesis that predicts the following equality describing the true inertial subrange (Pope 2001):

$$\varepsilon = \left(\frac{k_w^{5/3} S_{uu}}{C} \right)^{3/2}$$

where k_w is the wave number, S_{uu} is the spectral density function for u' , and C is the constant approximately equaling 0.51 for the inner layer and 0.55 for the outer layer of wall shear flow (Bradshaw 1967). The $S_{uu} [= (0.5u/\pi)F_{uu}(f)]$, where F_{uu} is the spectral density function for $u'(f)$ is a function of $k_w [= (2\pi/u)f]$. The ε is usually estimated by a best fit to the measured S_{uu} in the inertial subrange, as explained in Sect. 5.16.

3.9.7 Bed Shear Stress from Vertical Reynolds Normal Stress Distribution

Kim et al. (2000) suggested a modification of the determination of bed shear stress from TKE. They used only the vertical component of Reynolds normal stress (variance of vertical velocity component) distribution, since instrumental noise errors associated with the vertical velocity fluctuations are smaller than those for horizontal velocity fluctuations (Voulgaris and Trowbridge 1998). The bed shear stress is then

$$\tau_0 = C_z \rho \overline{w'w'} \quad (3.68)$$

where C_z is a proportionality constant, being approximately 0.9 (Kim et al. 2000).

3.9.8 Bed Shear Stress and Reynolds Shear Stress for Unsteady-Nonuniform Flow: Dey-Lambert's Approach

In nature, most of the stream flows are often unsteady and nonuniform, and hence, it is important to determine the bed shear stress in such situations. Dey and Lambert (2005) obtained the expressions for the bed shear stress and the Reynolds shear stress for an unsteady-nonuniform flow in open channels, assuming the logarithmic law of the wall and using the two-dimensional RANS and continuity equations. The derivation is as follows:

The RANS equation for two-dimensional unsteady-nonuniform flow in open channels is given by

$$\bar{u} \frac{\partial \bar{u}}{\partial x} + \bar{w} \frac{\partial \bar{u}}{\partial z} + \frac{\partial \bar{u}}{\partial t} = \frac{1}{\rho} \left(-\frac{\partial \bar{p}}{\partial x} + \frac{\partial \tau_{xz}}{\partial z} \right) \quad (3.69)$$

where \bar{p} is the time-averaged piezometric (hydrostatic) pressure at a vertical distance z from the bed and τ_{xz} is the Reynolds shear stress at a vertical distance $z (= -\rho \overline{u'w'})$.

The time-averaged velocity components and the Reynolds shear stress are expressed in the following functional forms:

$$\bar{u} = U\psi(\tilde{z}, t) \quad (3.70a)$$

$$\bar{w} = U\varphi(\tilde{z}, t) \quad (3.70b)$$

$$\tau_{xz} = -\rho \overline{u'w'} = \tau_0 \xi(\tilde{z}, t) \quad (3.70c)$$

where U is the depth-averaged velocity, τ_0 is the bed shear stress, that is $\tau_{xz}|_{z=z_0}$, z_0 is the zero-velocity level, that is $z|_{\bar{u}=0}$, being equal to $0.033k_s$, k_s is the equivalent roughness assumed to be median size of bed sediment d , and $\tilde{z} = z/h$. The logarithmic law of the wall is

$$\bar{u} = \frac{1}{\kappa} \left(\frac{\tau_0}{\rho} \right)^{0.5} \ln \left(\frac{z}{z_0} \right) \quad (3.71)$$

The depth-averaged velocity U can be given by

$$U = \frac{1}{h - z_0} \int_{z_0}^h \bar{u} dz = \frac{\beta}{\kappa} \left(\frac{\tau_0}{\rho} \right)^{0.5} \quad (3.72)$$

where $\beta = -\ln \tilde{z}_0^{1/(1-\tilde{z}_0)} - 1$ and $\tilde{z}_0 = z_0/h$. Partially differentiating Eqs. (3.70a) and (3.70c), one can obtain

$$\begin{aligned} \frac{\partial \bar{u}}{\partial x} &= \psi \frac{\partial U}{\partial x} - \frac{U}{h} \tilde{z} \frac{\partial \psi}{\partial \tilde{z}} \cdot \frac{\partial h}{\partial x}, \quad \frac{\partial \bar{u}}{\partial z} = \frac{U}{h} \cdot \frac{\partial \psi}{\partial \tilde{z}}, \quad \frac{\partial \tau_{xz}}{\partial z} = \frac{\tau_0}{h} \cdot \frac{\partial \xi}{\partial \tilde{z}}, \\ \frac{\partial \bar{u}}{\partial t} &= \psi \frac{\partial U}{\partial t} - \frac{U}{h} \tilde{z} \frac{\partial \psi}{\partial \tilde{z}} \cdot \frac{\partial h}{\partial t} + U \frac{\partial \psi}{\partial t} \end{aligned} \quad (3.73)$$

Partially differentiating Eq. (3.70b) yields

$$\frac{\partial \bar{w}}{\partial z} = \frac{U}{h} \cdot \frac{\partial \varphi}{\partial \tilde{z}} \quad (3.74)$$

Using the continuity equation of two-dimensional time-averaged velocity components, that is $\partial \bar{u}/\partial x + \partial \bar{w}/\partial z = 0$, and using Eq. (3.73) (first equation), one gets

$$\frac{\partial \varphi}{\partial \tilde{z}} = \tilde{z} \frac{\partial \psi}{\partial \tilde{z}} \cdot \frac{\partial h}{\partial x} - \frac{h}{U} \psi \frac{\partial U}{\partial x} \quad (3.75)$$

Integrating Eq. (3.75), the following equation is obtained:

$$\varphi = \frac{\partial h}{\partial x} \int_{\tilde{z}_0}^{\tilde{z}} \tilde{z} \frac{\partial \psi}{\partial \tilde{z}} d\tilde{z} - \frac{h}{U} \cdot \frac{\partial U}{\partial x} \int_{\tilde{z}_0}^{\tilde{z}} \psi d\tilde{z} = \psi \tilde{z} \frac{\partial h}{\partial x} - \frac{1}{U} \left(h \frac{\partial U}{\partial x} + U \frac{\partial h}{\partial x} \right) \int_{\tilde{z}_0}^{\tilde{z}} \psi d\tilde{z} \quad (3.76)$$

The continuity equation (Eq. 2.32) for depth-averaged unsteady-nonuniform flow in open channels is

$$h \frac{\partial U}{\partial x} + U \frac{\partial h}{\partial x} + \frac{\partial h}{\partial t} = 0 \quad (3.77)$$

Using Eq. (3.77) into Eq. (3.76), the expression of φ becomes

$$\varphi = \psi \tilde{z} \frac{\partial h}{\partial x} + \frac{1}{U} \cdot \frac{\partial h}{\partial t} \int_{\tilde{z}_0}^{\tilde{z}} \psi d\tilde{z} \quad (3.78)$$

Inserting Eq. (3.78) into Eq. (3.70b), equation of \bar{w} is obtained as

$$\bar{w} = \bar{u} \tilde{z} \frac{\partial h}{\partial x} + \frac{\partial h}{\partial t} \int_{\tilde{z}_0}^{\tilde{z}} \psi d\tilde{z} \quad (3.79)$$

Substituting Eqs. (3.70a, b), (3.73) and (3.79) into Eq. (3.69) yields

$$U\psi^2 \frac{\partial U}{\partial x} + \psi \frac{\partial U}{\partial t} - \frac{U}{h} \left(\bar{z} - \int_{\bar{z}_0}^{\bar{z}} \psi d\bar{z} \right) \frac{\partial \psi}{\partial \bar{z}} \cdot \frac{\partial h}{\partial t} + U \frac{\partial \psi}{\partial t} = \frac{1}{\rho} \left(-\frac{\partial \bar{p}}{\partial x} + \frac{\tau_0}{h} \cdot \frac{\partial \xi}{\partial \bar{z}} \right) \quad (3.80)$$

The piezometric pressure gradient is given by

$$\frac{\partial \bar{p}}{\partial x} = -\rho g \left(S_0 - \frac{\partial h}{\partial x} \right) \quad (3.81)$$

The de Saint-Venant equation of motion (Eq. 2.64) for unsteady-nonuniform flow in open channels is

$$\frac{U}{g} \cdot \frac{\partial U}{\partial x} + \frac{\partial h}{\partial x} - S_0 + \frac{\tau_0}{\rho g h} + \frac{1}{g} \cdot \frac{\partial U}{\partial t} = 0 \quad (3.82)$$

For simplicity, the momentum coefficient is assumed to be unity in Eq. (3.82), as the momentum coefficient varies from 1.01 to 1.1 in straight open channels. Rearranging Eq. (3.82), it gives

$$\frac{\rho h U}{\tau_0} \cdot \frac{\partial U}{\partial x} = -\frac{\rho g h}{\tau_0} \left(\frac{\partial h}{\partial x} - S_0 + \frac{1}{g} \cdot \frac{\partial U}{\partial t} \right) - 1 = -\lambda - 1 \quad (3.83)$$

where λ is the streamwise pressure gradient parameter, which is given by

$$\lambda = \frac{\rho g h}{\tau_0} \left(\frac{\partial h}{\partial x} - S_0 + \frac{1}{g} \cdot \frac{\partial U}{\partial t} \right) \quad (3.84)$$

In Eq. (3.84), for steady flow, $\partial U / \partial t = 0$, and for uniform flow, $\partial h / \partial x = 0$. In accelerating and decelerating flows, $\lambda < -1$ and $\lambda > -1$, respectively.

Using Eqs. (3.83) and (3.84) into Eq. (3.80) yields

$$\begin{aligned} & -(\lambda + 1)\psi^2 + (\psi - 1) \frac{\rho h}{\tau_0} \cdot \frac{\partial U}{\partial t} - \left(\bar{z} - \int_{\bar{z}_0}^{\bar{z}} \psi d\bar{z} \right) \frac{\rho U}{\tau_0} \cdot \frac{\partial \psi}{\partial \bar{z}} \cdot \frac{\partial h}{\partial t} + \frac{\rho h}{\tau_0} U \frac{\partial \psi}{\partial t} \\ & = -\lambda + \frac{\partial \xi}{\partial \bar{z}} \end{aligned} \quad (3.85)$$

Dividing Eq. (3.71) by Eq. (3.72) and equating with Eq. (3.70a) give

$$\frac{\bar{u}}{U} = \frac{1}{\beta} \ln \left(\frac{\bar{z}}{\bar{z}_0} \right) = \psi \quad (3.86)$$

Equation (3.86) represents the self-similar velocity distribution that remains independent of time ($\partial\psi/\partial t = 0$) and streamwise distance x . Substituting Eq. (3.86) into Eq. (3.85) and making $\partial\psi/\partial t = 0$ result in

$$\begin{aligned} \frac{\partial \xi}{\partial \tilde{z}} = & \lambda - (\lambda + 1) \frac{1}{\beta^2} \ln^2 \left(\frac{\tilde{z}}{\tilde{z}_0} \right) + \left[\frac{1}{\beta} \ln \left(\frac{\tilde{z}}{\tilde{z}_0} \right) - 1 \right] \frac{\rho h}{\tau_0} \cdot \frac{\partial U}{\partial t} \\ & - \frac{1}{\beta} \left\{ 1 - \frac{1}{\beta} \left[\ln \left(\frac{\tilde{z}}{\tilde{z}_0} \right) + \frac{\tilde{z}}{\tilde{z}_0} - 1 \right] \right\} \frac{\rho U}{\tau_0} \cdot \frac{\partial h}{\partial t} \end{aligned} \quad (3.87)$$

At the zero-velocity level ($\tilde{z} = \tilde{z}_0$), the above equation becomes

$$\left. \frac{\partial \xi}{\partial \tilde{z}} \right|_{\tilde{z}=\tilde{z}_0} = \lambda - \frac{\rho h}{\tau_0} \cdot \frac{\partial U}{\partial t} - \frac{1}{\beta} \cdot \frac{\rho U}{\tau_0} \cdot \frac{\partial h}{\partial t} \quad (3.88)$$

Integrating Eq. (3.87) and using the boundary condition $\xi|_{\tilde{z}=\tilde{z}_0} = 1$ yield

$$\begin{aligned} \xi = & 1 + \lambda(\tilde{z} - \tilde{z}_0) - (\lambda + 1) \frac{1}{\beta^2} \left\{ \tilde{z} \ln^2 \left(\frac{\tilde{z}}{\tilde{z}_0} \right) - 2 \left[\tilde{z} \ln \left(\frac{\tilde{z}}{\tilde{z}_0} \right) - \tilde{z} + \tilde{z}_0 \right] \right\} \\ & + \left[\frac{\tilde{z}}{\beta} \ln \left(\frac{\tilde{z}}{\tilde{z}_0} \right) - \left(1 + \frac{1}{\beta} \right) (\tilde{z} - \tilde{z}_0) \right] \frac{\rho h}{\tau_0} \cdot \frac{\partial U}{\partial t} \\ & + \frac{1}{\beta} \left[\frac{\tilde{z} + \tilde{z}_0}{\beta} \ln \left(\frac{\tilde{z}}{\tilde{z}_0} \right) - \left(1 + \frac{2}{\beta} \right) (\tilde{z} - \tilde{z}_0) \right] \frac{\rho U}{\tau_0} \cdot \frac{\partial h}{\partial t} \end{aligned} \quad (3.89)$$

Substituting λ from Eq. (3.84) and $\partial U/\partial x$ from Eq. (3.77) into Eq. (3.89), the equation of nondimensional Reynolds shear stress for unsteady-nonuniform flow in open channels is obtained as

$$\begin{aligned} \xi = & 1 + (\tilde{z} - \tilde{z}_0) \frac{\rho g h}{\tau_0} \left(\frac{\partial h}{\partial x} - S_0 \right) - \frac{1}{\beta^2} \left\{ \tilde{z} \ln^2 \left(\frac{\tilde{z}}{\tilde{z}_0} \right) - 2 \left[\tilde{z} \ln \left(\frac{\tilde{z}}{\tilde{z}_0} \right) - \tilde{z} + \tilde{z}_0 \right] \right\} \\ & \times \frac{\rho U}{\tau_0} \left(U \frac{\partial h}{\partial x} + \frac{\partial h}{\partial t} \right) + \frac{1}{\beta} \left[\tilde{z} \ln \left(\frac{\tilde{z}}{\tilde{z}_0} \right) - \tilde{z} + \tilde{z}_0 \right] \frac{\rho h}{\tau_0} \cdot \frac{\partial U}{\partial t} \\ & + \frac{1}{\beta} \left[\frac{\tilde{z} + \tilde{z}_0}{\beta} \ln \left(\frac{\tilde{z}}{\tilde{z}_0} \right) - \left(1 + \frac{2}{\beta} \right) (\tilde{z} - \tilde{z}_0) \right] \frac{\rho U}{\tau_0} \cdot \frac{\partial h}{\partial t} \end{aligned} \quad (3.90)$$

The bed shear stress τ_0 can be obtained from Eq. (3.90) using the boundary condition $\tau_{xz}|_{z=h} = 0$ as

$$\begin{aligned}\tau_0 = & -(1 - \tilde{z}_0)\rho gh \left(\frac{\partial h}{\partial x} - S_0 \right) + \frac{1}{\beta^2} [\ln^2 \tilde{z}_0 + 2(\ln \tilde{z}_0 + 1 - \tilde{z}_0)] \rho U \left(U \frac{\partial h}{\partial x} + \frac{\partial h}{\partial t} \right) \\ & + \frac{1}{\beta} (\ln \tilde{z}_0 + 1 - \tilde{z}_0) \rho h \frac{\partial U}{\partial t} + \frac{1}{\beta} \left[\frac{1 + \tilde{z}_0}{\beta} \ln \tilde{z}_0 + \left(1 + \frac{2}{\beta} \right) (1 - \tilde{z}_0) \right] \rho U \frac{\partial h}{\partial t}\end{aligned}\quad (3.91)$$

Using Eqs. (3.90) and (3.91), the equation of Reynolds shear stress τ_{xz} can be obtained as

$$\begin{aligned}\tau_{xz} = & -(1 - \tilde{z})\rho gh \left(\frac{\partial h}{\partial x} - S_0 \right) \\ & - \frac{1}{\beta^2} \left\{ \tilde{z} \ln^2 \left(\frac{\tilde{z}}{\tilde{z}_0} \right) - \ln^2 \tilde{z}_0 - 2 \left[\tilde{z} \ln \left(\frac{\tilde{z}}{\tilde{z}_0} \right) + \ln \tilde{z}_0 + 1 - \tilde{z} \right] \right\} \rho U \left(U \frac{\partial h}{\partial x} + \frac{\partial h}{\partial t} \right) \\ & + \frac{1}{\beta} \left[\tilde{z} \ln \left(\frac{\tilde{z}}{\tilde{z}_0} \right) + \ln \tilde{z}_0 + 1 - \tilde{z} \right] \rho h \frac{\partial U}{\partial t} \\ & + \frac{1}{\beta} \left\{ \frac{1}{\beta} \left[(\tilde{z} + \tilde{z}_0) \ln \left(\frac{\tilde{z}}{\tilde{z}_0} \right) + (1 + \tilde{z}_0) \ln \tilde{z}_0 \right] + \left(1 + \frac{2}{\beta} \right) (1 - \tilde{z}) \right\} \rho U \frac{\partial h}{\partial t}\end{aligned}\quad (3.92)$$

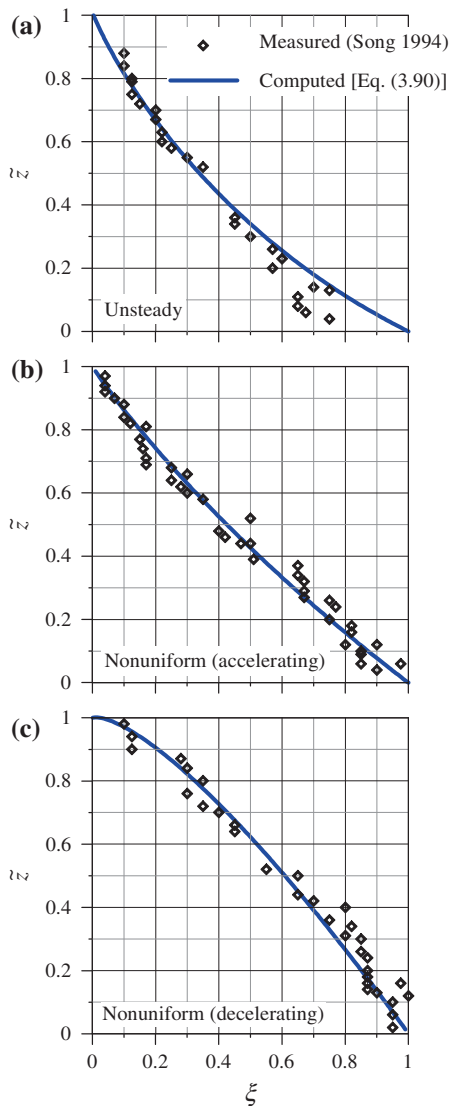
The distribution of Reynolds shear stress in nondimensional and dimensional forms can be computed by using Eqs. (3.90) and (3.92), respectively, if h , U , S_0 , $\partial h/\partial x$, $\partial h/\partial t$, $\partial U/\partial t$, k_s , and τ_0 are known. As a priori, Eq. (3.91) can be used to estimate the bed shear stress τ_0 for unsteady-nonuniform flow. Figures 3.12a–c present $\tilde{z}(\xi)$ curves computed using Eq. (3.90), where the values of τ_0 were calculated from Eq. (3.91). Three cases are considered in Figs. 3.12a–c: (a) Unsteady, (b) nonuniform accelerating, and (c) nonuniform decelerating flows. Interestingly, the Reynolds shear stress distributions are no longer linear. The computed curves are in agreement with the experimental data of Song (1994) for unsteady and nonuniform flows in open channels.

It is also important to recognize that the Reynolds shear stress in unsteady-nonuniform flow modifies the flow field due to change in turbulence structure. Therefore, Eq. (3.92) can be utilized to determine the influence of the Reynolds shear stress on the mixing length. The Reynolds shear stress τ_{xz} is related to the mixing length l as follows:

$$\tau_{xz} = \rho l^2 \left(\frac{\partial \bar{u}}{\partial z} \right)^2 \quad (3.93)$$

Using Eq. (3.73) (second equation) into Eq. (3.93), the mixing length is expressed as

Fig. 3.12 Nondimensional Reynolds shear stress distributions $\xi(\bar{z})$ and comparison with the data of Song (1994): **a** unsteady, **b** nonuniform accelerating flow, and **c** nonuniform decelerating flow



$$l = \left(\frac{\tau_{xz}}{\rho U^2} \right)^{0.5} \frac{h}{\partial \psi / \partial \bar{z}} \quad (3.94)$$

In the above equation, τ_{xz} from Eq. (3.92) can be substituted to obtain the modification in mixing length due to unsteady-nonuniform flow.

3.10 Secondary Currents and Dip Phenomenon

3.10.1 Secondary Currents

In case where there is a three-dimensional flow field, the flow is often regarded as comprising of two flow components, such as *primary flow* and *secondary flow*. The primary flow is parallel to the main direction of fluid motion, and the secondary flow is transverse to it. In most of the cases, the secondary flow is a relatively minor flow superimposed on the primary flow and is commonly termed *secondary currents*.

Prandtl (1952) divided the secondary currents into two categories. Secondary currents which are the consequence of the mean flow skewing due to curvilinearity of streamlines are called the *secondary currents of Prandtl's first kind*, and those currents which are caused by the flow nonuniformities near the walls induced by the anisotropic turbulence ($\overline{u'u'} \neq \overline{w'w'}$) are called the *secondary currents of Prandtl's second kind*. The latter category is the main focus here as that is induced by the turbulence. The maximum velocity of the second kind is of the order of 5 % of the mean streamwise velocity (Nezu and Nakagawa 1993).

In a Cartesian coordinate system, the equation of motion of time-averaged vorticity Ω_x about x -axis is given as follows (Perkins 1970):

$$\begin{aligned}
 \underbrace{\frac{\partial \Omega_x}{\partial t}}_{\text{Unsteady}} + \underbrace{\bar{u} \frac{\partial \Omega_x}{\partial x} + \bar{v} \frac{\partial \Omega_x}{\partial y} + \bar{w} \frac{\partial \Omega_x}{\partial z}}_I &= \underbrace{v \nabla^2 \Omega_x}_{II} + \underbrace{\Omega_x \frac{\partial \bar{u}}{\partial x}}_{III} + \underbrace{\Omega_y \frac{\partial \bar{u}}{\partial y} + \Omega_z \frac{\partial \bar{u}}{\partial z}}_{IV} \\
 + \underbrace{\frac{\partial^2}{\partial y \partial z} (\bar{v}'v' - \bar{w}'w')}_V &+ \underbrace{\left(\frac{\partial^2}{\partial y^2} - \frac{\partial^2}{\partial z^2} \right) (-\bar{v}'w')}_VI + \underbrace{\frac{\partial}{\partial x} \left[\frac{\partial}{\partial y} (-\bar{u}'w') - \frac{\partial}{\partial z} (-\bar{u}'v') \right]}_{VII}
 \end{aligned} \tag{3.95}$$

where Ω_y and Ω_z are the vorticities about y -axis and z -axis, respectively. Here, x -axis is in the streamwise direction, y -axis is transverse to the streamwise direction, and z -axis is in the vertical direction. The vorticities are expressed as

$$\Omega_x = \left(\frac{\partial \bar{w}}{\partial y} - \frac{\partial \bar{v}}{\partial z} \right), \quad \Omega_y = \left(\frac{\partial \bar{u}}{\partial z} - \frac{\partial \bar{w}}{\partial x} \right), \quad \Omega_z = \left(\frac{\partial \bar{v}}{\partial x} - \frac{\partial \bar{u}}{\partial y} \right) \tag{3.96}$$

Equation (3.95), which is applicable for both first and second kinds, is most readily derived by eliminating the pressure term between the RANS equations in y -direction and z -direction in addition to continuity equation. Various terms involved in Eq. (3.95) are discussed as follows:

The first term unsteady signifies the time dependence of streamwise vorticity Ω_x and vanishes in case of steady flow. The term I represents the total advection of Ω_x by the primary flow and the secondary currents. The term II accounts for the

viscous diffusion of Ω_x . The term *III* indicates the streamwise stretching of Ω_x . The term *IV* describes the vorticity production through the skewing of the mean shear by a transverse gradient of streamwise velocity. The secondary flows can be produced in a curved channel due to centrifugal action on the basis of terms *III* and *IV*. Such flows correspond to Prandtl's first kind, and the terms *III* and *IV* vanish for uniform flow in straight channels, as $\partial\bar{u}/\partial x = 0$ and $\Omega_y\partial\bar{u}/\partial y + \Omega_z\partial\bar{u}/\partial z = 0$. The term *V* represents the production of a rotational acceleration of a fluid element about the streamwise axis due to turbulence anisotropy, while the term *VI* is to suppress it. The term *VII* signifies the vorticity production due to Reynolds shear stress gradient in nonuniform flow. For uniform flow, the terms $\bar{u}\partial\Omega_x/\partial x$, *III*, and *VII* vanish.

Since it is difficult to solve Eq. (3.95) in its full form, a suitable turbulence assumption is required to do so. In a steady-uniform flow, for the secondary current of Prandtl's second kind, which is primarily turbulence induced, the term $\partial\Omega_x/\partial t = 0$ and the terms *I-IV* are negligible in comparison to the terms *V* and *VI* (Nezu and Nakagawa 1993; Ikeda 1981). Hence, Eq. (3.95) reduces to

$$\frac{\partial^2}{\partial y \partial z} (\overline{v'v'} - \overline{w'w'}) = \left(\frac{\partial^2}{\partial y^2} - \frac{\partial^2}{\partial z^2} \right) \overline{v'w'} \quad (3.97)$$

In the above equation, the production of vorticity due to turbulence anisotropy (left-hand side) is balanced by the suppression of vorticity due to Reynolds shear stress (right-hand side). Using an eddy viscosity model, the higher-order terms of the Reynolds shear stress can be approximated as

$$-\overline{v'w'} = \varepsilon_t \left(\frac{\partial \bar{w}}{\partial y} + \frac{\partial \bar{v}}{\partial z} \right) \quad (3.98)$$

where ε_t is the eddy viscosity. Ikeda (1981) obtained an approximate formulation for the depth-averaged eddy viscosity from the logarithmic law as

$$\varepsilon_t = \frac{\kappa}{6} \bar{u}_* h \quad (3.99)$$

where \bar{u}_* is the spatially averaged shear velocity in the transverse direction. It varies sinusoidally in the transverse direction in a wide channel due to the formation of a cellular structure of secondary currents.

Nakagawa et al. (1981) attempted to establish the vorticity production term $(\overline{v'v'} - \overline{w'w'})/u_*^2$ a universal. Then,

$$\frac{\overline{v'v'} - \overline{w'w'}}{u_*^2} \approx \alpha_0 \frac{-\overline{u'w'}}{u_*^2} \quad (3.100)$$

where α_0 is a proportionality constant being approximated as unity.

Ikeda (1981) assumed a linear distribution of the difference in the Reynolds normal stresses as

$$\frac{\overline{v'v'} - \overline{w'w'}}{\bar{u}_*^2} = \frac{\tau_0}{\rho \bar{u}_*^2} (1 - \tilde{z}) \quad \wedge \quad \tilde{z} = \frac{z}{h} \quad (3.101)$$

The bed shear stress $\tau_0 = \rho u_*^2$ that varies sinusoidally in the transverse direction (y-direction) can be simulated as

$$\frac{\tau_0}{\rho \bar{u}_*^2} = 1 + a_b \cos(k_w \tilde{y}) \quad \wedge \quad \tilde{y} = \frac{y}{h} \quad (3.102)$$

where a_b is the amplitude of the sinusoidal distribution of τ_0 in the transverse direction and k_w is the wave number.

From the solution of Eq. (3.97), using Eqs. (3.98)–(3.102), Ikeda (1981) obtained a transverse series of secondary current cells for which $k_w = \pi n$, where n is an integer. According to Townsend (1976), the dominant cell, for which $k_w = \pi$, mainly contributes to the production of secondary currents. Ikeda (1981) obtained a cellular secondary circulation by setting $k_w = \pi$ as follows:

$$v^+ = \frac{6a_b}{\kappa\pi^2} \left[\frac{2}{\pi} \cos \pi \tilde{z} - (2\tilde{z} - 1) \sin \pi \tilde{z} \right] \sin \pi \tilde{y} \quad \wedge \quad v^+ = \frac{\bar{v}}{\bar{u}_*} \quad (3.103a)$$

$$w^+ = \frac{6a_b}{\kappa\pi^2} [(2\tilde{z} - 1) \cos \pi \tilde{z} + 1] \cos \pi \tilde{y} \quad \wedge \quad w^+ = \frac{\bar{w}}{\bar{u}_*} \quad (3.103b)$$

The above equations can simulate the circular counter-rotating cells of diameter h . Rodríguez and García (2008) experimentally captured the cellular structure in a rectangular flume, confirming the above derivation.

Figures 3.13a, b schematically show that the secondary currents in a wide channel are characterized by a well-defined cellular structure, while those in a narrow channel are characterized by a strong free surface vortex paired with a comparatively weaker bottom vortex. In a wide channel, the corner-induced secondary currents are observed near the sidewalls and are characterized by the flow moving into the apex of the corner with a return flow moving away from the corner (Perkins 1970; Gessner 1973; Galletti and Bottaro 2004). The corner vortices are damped within a short distance in the transverse direction from the sidewalls.

3.10.2 Dip Phenomenon

In open-channel flow, sidewall effects are more important in narrow channels, while the bed effects are important in the central portion of wide channels (see Figs. 3.13a, b). Based on the ratio of channel width B to flow depth h , termed

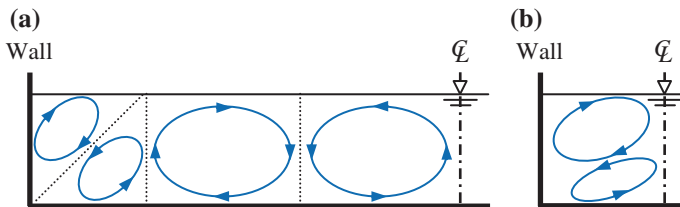


Fig. 3.13 Secondary currents in **a** a wide channel and **b** a narrow channel

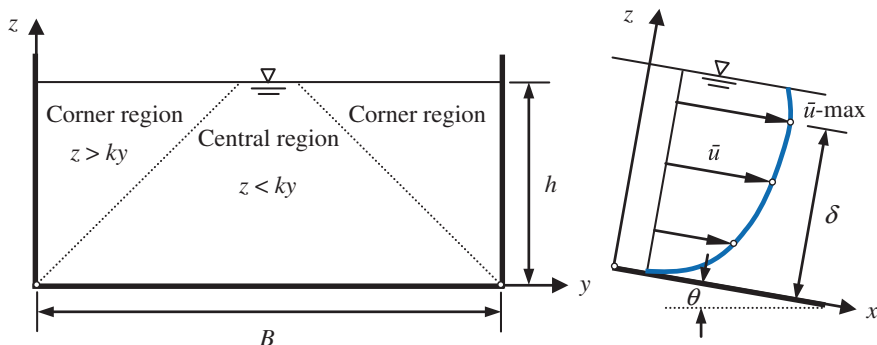


Fig. 3.14 Division of flow region and velocity dip

aspect ratio, the wide and narrow channels are defined. For instance, aspect ratio $B/h < 5$ applies to narrow channels and $B/h > 10$ to wide channels. Narrow channels present strong secondary currents, and as a result, the maximum velocity appears below the free surface, which is called the *dip phenomenon* (Chow 1959).

Tracy and Lester (1961) argued that the open-channel flow may be divided into two regions: the *central region* flow and the *corner region* flow that exists in the vicinity of the wall. Besides, Keulegan (1938) proposed that a flow region can be divided using a straight division line as shown in Fig. 3.14; one region is associated with the bed and the other two regions with the sidewalls. Yang and Lim (1997) obtained the expression for the central portion as $kh < y < (B - kh)$, where k is the slope of the division line and y is the distance from the sidewall. From the experimental results, it was found that the logarithmic law can be applicable to express the velocity distribution near the bed, but failed in the outer region.

Yang et al. (2004) derived the *modified logarithmic law* including the dip phenomenon. The derivation is as follows:

For a steady-uniform turbulent flow in an open channel (Fig. 3.14), the RANS equation in x -direction using the continuity equation yields

$$\begin{aligned} \frac{\partial}{\partial y} \left(\bar{u}\bar{v} - \frac{\tau_{xy}}{\rho} \right) + \frac{\partial}{\partial z} \left(\bar{u}\bar{w} - \frac{\tau_{xz}}{\rho} \right) &= gS_0 \quad \wedge \quad \frac{\tau_{xy}}{\rho} = \nu \frac{\partial \bar{u}}{\partial y} - \overline{u'v'} \\ \vee \quad \frac{\tau_{xz}}{\rho} &= \nu \frac{\partial \bar{u}}{\partial z} - \overline{u'w'} \end{aligned} \quad (3.104)$$

where S_0 is the streamwise bed slope ($\approx \sin\theta$). In the central region (Fig. 3.14), it can be assumed that the vertical gradient $\partial(\cdot)/\partial z$ dominates, allowing to neglect the transverse gradient $\partial(\cdot)/\partial y$ (on the horizontal plane). Since the viscous shear stress is negligible as compared to the Reynolds shear stress, that is, $-\overline{u'w'} \gg \nu \partial \bar{u}/\partial z$, Eq. (3.104) reduces to

$$\frac{\partial}{\partial z} (\bar{u}\bar{w} + \overline{u'w'}) = gS_0 \quad (3.105)$$

Integrating Eq. (3.105) and introducing a global shear velocity u_* yield

$$-\frac{\overline{u'w'}}{u_*^2} = 1 - \tilde{z} - \alpha_1 \tilde{z} + \frac{\bar{u}\bar{w}}{u_*^2} \quad \wedge \quad \alpha_1 = \frac{ghS_0 - u_*^2}{u_*^2} \quad (3.106)$$

Assuming an empirical model, Yang et al. (2004) gave

$$\frac{\bar{u}\bar{w}}{u_*^2} = -\alpha_2 \tilde{z} \quad (3.107)$$

where α_2 is a positive coefficient. Using Eq. (3.107) into Eq. (3.106) yields

$$-\frac{\overline{u'w'}}{u_*^2} = 1 - \tilde{z} - \alpha \tilde{z} \quad \wedge \quad \alpha = \alpha_1 + \alpha_2 \quad (3.108)$$

According to Boussinesq hypothesis, one can approximate

$$-\overline{u'w'} = \varepsilon_t \frac{d\bar{u}}{dz} \quad (3.109)$$

Thus, Eq. (3.108) becomes

$$\frac{d\bar{u}}{dz} = \frac{u_*^2}{\varepsilon_t} (1 - \tilde{z} - \alpha \tilde{z}) \quad (3.110)$$

A parabolic distribution of eddy viscosity $\varepsilon_t(z)$ is obtained by using Eqs. (3.20) (that is, the linear law of fluid shear stress), (3.31) (that is, the logarithmic law of streamwise velocity) and (3.109). It is

$$\varepsilon_t = \kappa u_* z (1 - \tilde{z}) \quad (3.111)$$

Inserting Eq. (3.111) into Eq. (3.110) and then integrating with a boundary condition $[\bar{u}(z = z_0) = 0]$ yield

$$\bar{u}^+ = \frac{1}{\kappa} \left[\ln \frac{\tilde{z}}{\tilde{z}_0} + \alpha \ln(1 - \tilde{z}) - \alpha \ln(1 - \tilde{z}_0) \right] \quad \wedge \quad \bar{u}^+ = \frac{\bar{u}}{u_*} \quad \vee \quad \tilde{z}_0 = \frac{z_0}{h} \quad (3.112)$$

where z_0 is the zero-velocity level. Since $\tilde{z}_0 \ll 1$, then $\ln(1 - \tilde{z}_0) \rightarrow 0$ and

$$\bar{u}^+ = \frac{1}{\kappa} \left[\ln \frac{\tilde{z}}{\tilde{z}_0} + \alpha \ln(1 - \tilde{z}) \right] \quad (3.113)$$

This is the *modified logarithmic law* including the dip phenomenon, deduced by Yang et al. (2004). It is evident from Eq. (3.113) that the dip phenomenon is governed by the term $\alpha \ln(1 - \tilde{z})$ with α as a dip correction factor.

The location of the maximum velocity (\bar{u} maximum) can be obtained by differentiating Eq. (3.113) with respect to z and setting $d\bar{u}/dz = 0$. It is as follows:

$$\delta = \frac{h}{1 + \alpha} \quad (3.114)$$

Yang et al. (2004) proposed an empirical formula for the dip correction factor as $\alpha = 1.3 \exp(-\tilde{y})$. At the centerline of the channel, it is $\alpha = 1.3 \exp(-0.5B/h)$. However, according to Wang et al. (2001), the maximum velocity is located at

$$\delta = h \left[0.44 + 0.212\tilde{y} + 0.05 \sin \left(2 \frac{\pi}{2.6} \tilde{y} \right) \right]$$

On the other hand, Absi (2011) derived the *modified log-wake law* including the dip phenomenon. Instead of a parabolic distribution as given by Eq. (3.111), he approximated the eddy viscosity $\varepsilon_t(z)$ in accordance with the log-wake law given by Nezu and Rodi (1986) as follows:

$$\varepsilon_t = \kappa u_* h (1 - \tilde{z}) \left[\frac{1}{\tilde{z}} + \pi \Pi \sin(\pi \tilde{z}) \right]^{-1} \quad (3.115)$$

where Π is the Coles' wake parameter. Using Eq. (3.115) into Eq. (3.110), the nondimensional differential equation is obtained as

$$\frac{d\bar{u}^+}{d\tilde{z}} = \frac{1}{\kappa} \left(1 - \alpha \frac{\tilde{z}}{1 - \tilde{z}} \right) \left[\frac{1}{\tilde{z}} + \pi \Pi \sin(\pi \tilde{z}) \right] \quad (3.116)$$

Integration of Eq. (3.116) for $\tilde{z}_0 \ll 1$ yields the modified log-wake law. It is as follows:

$$\bar{u}^+ = \frac{1}{\kappa} \ln \frac{\tilde{z}}{\tilde{z}_0} + \frac{2\Pi}{\kappa} \sin^2\left(\frac{\pi}{2} \tilde{z}\right) + \frac{\alpha}{\kappa} \ln(1 - \tilde{z}) - \frac{\alpha\Pi}{\kappa} \int_{\tilde{z}_0}^{\tilde{z}} \frac{\tilde{z}}{1 - \tilde{z}} \sin(\pi\tilde{z}) d\tilde{z} \quad (3.117)$$

3.11 Isotropic Turbulence Theory

3.11.1 Energy Cascade Process

Richardson's (1922) concept of turbulence is a *turbulent flow to be composed of variable sizes of eddies*. The sizes of the eddies define the characteristic length scale ℓ of the eddies, which are also characterized by the *velocity scale* $u(\ell)$ and the *time scale* $\tau(\ell)$ [= $\ell/u(\ell)$] being a function of the *length scale* ℓ . The large sizes of eddies are unstable and eventually disintegrated into smaller eddies. The TKE that an initial large eddy possesses is distributed into the smaller eddies, which also undergo the similar process of disintegration, giving rise to even smaller eddies that take over the TKE from their predecessor eddies and so on. In this process, the TKE is transferred from the large-scale motions to smaller-scale motions until attaining an adequately small length scale so that the fluid molecular viscosity can effectively dissipate the TKE into heat. Therefore, the large eddies as a continuous process are transformed successively into smaller and smaller eddies in a cascade process with the TKE being transferred from large to small scale (Fig. 3.15).

Richardson notably summarized the turbulence processes in a nice rhyming verse (Richardson 1922):

*Big whorls have little whorls;
Which feed on their velocity;
And little whorls have lesser whorls,
And so on to viscosity
(in the molecular sense).*

3.11.2 Integral Scale

Eddies of the largest size, termed *macro-turbulence*, are characterized by the length scale ℓ_T , which is comparable with the flow length scale L , for example the flow depth in an open-channel flow, and the velocity scale $u_T(\ell_T)$ having an order of magnitude of turbulence intensity given by $(2k/3)^{1/2}$, which is comparable with the mean flow velocity U , where k is the TKE. It is assumed that the TKE of eddies

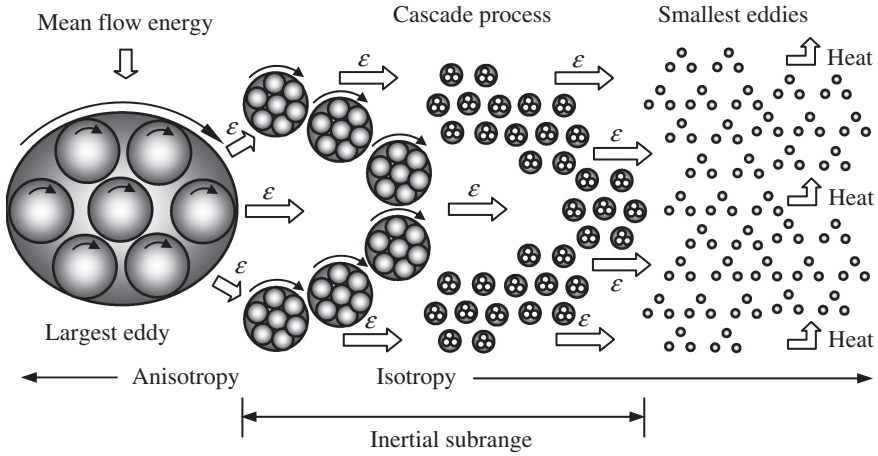


Fig. 3.15 Energy cascade process

of velocity scale u_T is dissipated in time scale τ_T . The length scale ℓ_T is referred to as the *integral scale* of turbulence and is given by

$$\ell_T \sim \frac{k^{3/2}}{\varepsilon}$$

where ε is the TKE dissipation rate. In the above, the proportionality constant is in the order of unity. The velocity scale u_T is

$$u_T = k^{1/2}$$

The Reynolds number corresponding to the large eddies is termed *turbulence Reynolds number* R_T , which is given by

$$R_T = \frac{u_T \ell_T}{\nu} = \frac{k^2}{\varepsilon \nu}$$

The large eddies contain TKE of the order of u_T^2 to be dissipated in time scale $\tau_T = \ell_T/u_T$, such that the rate of TKE transfer, known as *TKE dissipation rate* ε , from the large eddies, is assumed to a scale as $u_T^2/\tau_T = u_T^3/\ell_T$ being independent of viscosity ν . Note that the R_T corresponds to a sufficiently large Reynolds number.

Besides the integral scale, note that the large-scale eddies, which are *macro-turbulent eddies*, in an open-channel flow, can be regarded as of the order of Prandtl's mixing length l , which is a function of the distance from the bed, corresponding to the location z (Yalin 1977).

3.11.3 Kolmogorov Hypotheses

Kolmogorov (1941) postulated that for sufficiently large Reynolds numbers, eddies of small size are statistically isotropic, that is, they could not be discriminated by a specific spatial direction. The isotropic simply implies that $\overline{u'u'} = \overline{v'v'} = \overline{w'w'}$. Therefore, Kolmogorov hypothesis of *local isotropy* states:

At sufficiently large Reynolds numbers, but not infinite, the small-scale turbulent motions ($\ell_T \gg \ell$) are statistically isotropic.

The terminology *local isotropy* indicates the isotropy at small-scale motions, while the large-scale motions can still remain anisotropic. Let the length scale ℓ_E be the threshold length scale to changeover the large-scale anisotropic eddies ($\ell_T > \ell_E$) to the small-scale isotropic eddies ($\ell_E > \ell$). Then, for the large Reynolds numbers, ℓ_E is related to the integral scale ℓ_T (that is, the large-scale eddies) as

$$\ell_E \approx \frac{\ell_T}{6}$$

In general, eddies of large size are anisotropic, since they are determined by the specific geometrical characteristics of the boundaries. Kolmogorov argued that in the Richardson's energy cascade process, this geometrical and directional information of the large-scale eddies is vanished in the chaotic scale reduction process as the TKE is transferred to successively smaller eddies. The statistics of the small-scale motions is characterized by a universal feature, as they are identical for all turbulent flows when the Reynolds numbers are sufficiently large. Therefore, the small-scale motions at large Reynolds numbers are invariant of the mean flow and the boundary conditions.

The small-scale eddies are dependent on the rate of transfer of TKE, t_{KE} , to them from the larger-scale eddies and the viscous diffusion, which is related to the kinematic viscosity ν . This rate of transfer of TKE is approximately equal to the TKE dissipation rate, that is, $t_{KE} \approx \varepsilon$. Therefore, Kolmogorov first similarity hypothesis states:

In all turbulent flows at sufficiently large Reynolds numbers, the statistical properties of the small-scale motions ($\ell < \ell_E$) have a universal form that is entirely determined by the average kinetic energy dissipation rate ε and the kinematic viscosity ν .

Therefore, the *universal equilibrium range* refers to the length scale range $\ell < \ell_E$. A shorter time scale τ , in this range, is required as compared to the time scale τ_T corresponding to large eddies, that is, $\tau (= \ell/\nu) < \tau_T (= \ell_T/\nu)$. Thus, a dynamic equilibrium of small eddies is quickly attained with the rate of transfer of TKE, t_{KE} , to them from the larger-scale eddies. Since the small-scale motions are determined by simply two parameters, such as TKE dissipation rate and viscosity, there are unique in length, velocity, and time scales that can be deduced by using dimensional analysis as follows:

$$\eta \equiv \left(\frac{v^3}{\varepsilon}\right)^{1/4}, \quad u_\eta \equiv (\varepsilon v)^{1/4}, \quad \tau_\eta \equiv \left(\frac{v}{\varepsilon}\right)^{1/2} \quad (3.118)$$

This set of equations provides the *Kolmogorov micro-scales*. The η , u_η , and τ_η are known as Kolmogorov length, velocity, and time scales. There are two distinctive characteristics stemming from the definition of Kolmogorov micro-scales. They are as follows:

1. The Reynolds number corresponding to the small eddies is

$$R_\eta = \frac{u_\eta \eta}{v} = \frac{(\varepsilon v)^{1/4} (v^3/\varepsilon)^{1/4}}{v} = 1$$

Thus, the energy cascade continues to be smaller and smaller scales until the Kolmogorov micro-scales are small enough for the dissipation of TKE to be effective.

2. The TKE dissipation rate corresponding to the small eddies is

$$\varepsilon = v \left(\frac{u_\eta}{\eta}\right)^2 = v \left[\frac{(\varepsilon v)^{1/4}}{(v^3/\varepsilon)^{1/4}}\right]^2 = \frac{v}{\tau_\eta^2} \Rightarrow \frac{u_\eta}{\eta} = \frac{1}{\tau_\eta}$$

It provides a consistent description of the velocity gradient of dissipative eddies.

The ratios of small-scale to large-scale eddies are readily determined by using integral scale $\ell_T \sim k^{3/2}/\varepsilon$ in Eq. (3.118). They are

$$\frac{\eta}{\ell_T} \sim R_T^{-3/4}, \quad \frac{u_\eta}{u_T} \sim R_T^{-1/4}, \quad \frac{\tau_\eta}{\tau_T} \sim R_T^{-1/2} \quad (3.119)$$

It is evident that at large Reynolds numbers, the velocity and time scales of small-scale eddies are smaller than those of large eddies. At sufficiently large Reynolds numbers, the ratio η/ℓ_T is so small that there is a range of length scale ℓ that is very small as compared to ℓ_T and however very large as compared to η , that is, $\ell_T \gg \ell \gg \eta$. Since the eddies in this range are much larger than the dissipative eddies, it may be imagined that their Reynolds numbers are large. As a result of this, their motion is little influenced by the viscosity. This leads to Kolmogorov second similarity hypothesis that states:

In all turbulent flows at sufficiently large Reynolds numbers, the statistical properties of the motions of scale ℓ in the range $\ell_T \gg \ell \gg \eta$ have a universal form that is entirely determined by the average kinetic energy dissipation rate, but independent of kinematic viscosity.

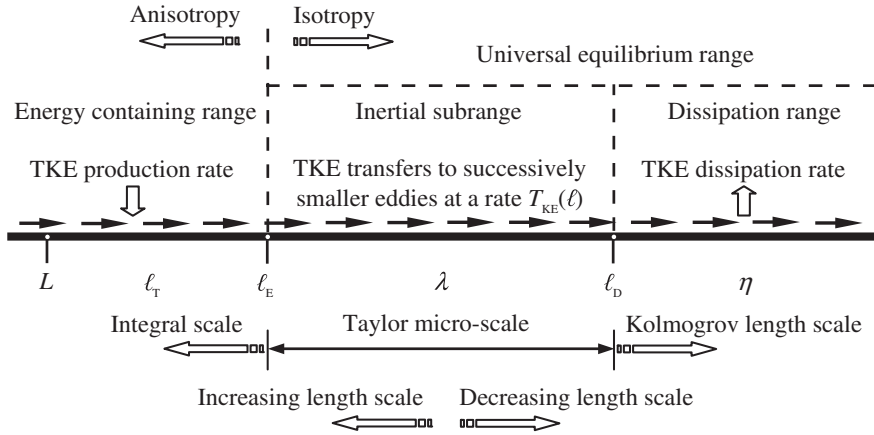


Fig. 3.16 Sketch illustrating length scales and their ranges including TKE transfer process

It is therefore suitable to introduce a new length scale ℓ_D ($\approx 60\eta$ for large Reynolds numbers), such that the range can be given by $\ell_E > \ell > \ell_D$. The length scale ℓ_D divides the *universal equilibrium range* ($\ell < \ell_E$) into two subranges:

1. The *inertial subrange* ($\ell_E > \ell > \ell_D$) where the motions are governed by the inertial effects, but the viscous effects remain negligible.
2. The *dissipation range* ($\ell < \ell_D$) where the motions undergo the viscous effects.

The length scales and their ranges are illustrated by a simple sketch, as shown in Fig. 3.16. It shows that the *energy containing range*, which has a size range ℓ_E ($=\ell_T/6$) $< \ell < 6\ell_T$, possesses bulk of the TKE.

The TKE dissipation rate ε corresponding to the eddies in the inertial subrange of size ℓ is

$$\varepsilon = \frac{u_\eta^3}{\eta} = \frac{u_\eta^2}{\tau_\eta} = \frac{\eta^2}{\tau_\eta^3}$$

Given the eddy size ℓ and TKE dissipation rate ε , the characteristic velocity and time scales are

$$u(\ell) = (\varepsilon \ell)^{1/4} = u_\eta \left(\frac{\ell}{\eta} \right)^{1/3} \sim u_T \left(\frac{\ell}{\ell_T} \right)^{1/3}$$

$$\tau(\ell) = \left(\frac{\ell^2}{\varepsilon} \right)^{1/3} = \tau_\eta \left(\frac{\ell}{\eta} \right)^{2/3} \sim \tau_T \left(\frac{\ell}{\ell_T} \right)^{2/3}$$

It is the corollary of the Kolmogorov second similarity hypothesis that in the inertial range, the velocity scale and the time scale decrease with a decrease in length scale ℓ .

3.11.4 Taylor Micro-Scale

In a turbulent shear flow, all time-averaged quantities except \bar{u}_i are spatially independent. In such a situation, the TKE production rate equals the TKE dissipation rate of the same quantity (Hinze 1987). It suggests a TKE budget equation

$$\underbrace{-\overline{u'_i u'_j s'_{ij}}}_{\text{Production Rate}} = \underbrace{2\nu \overline{s'_{ij} s'_{ij}}}_{\text{Dissipation Rate}} \quad \wedge \quad s_{ij} = \frac{1}{2} \left(\frac{\partial \bar{u}_i}{\partial x_j} + \frac{\partial \bar{u}_j}{\partial x_i} \right) \quad \vee \quad s'_{ij} = \frac{1}{2} \left(\frac{\partial u'_i}{\partial x_j} + \frac{\partial u'_j}{\partial x_i} \right)$$

where s_{ij} is the shear strain rate, which is discussed in Sect. 2.2 with different symbols [see Eqs. (2.14) and (2.15)], and s'_{ij} is the fluctuating shear strain rate. Let the equation of TKE dissipation rate for the isotropic turbulence be written (remembering that the small-scale motions tend to be isotropic) as

$$\varepsilon = 2\nu \overline{s'_{ij} s'_{ij}} = 15\nu \overline{\left(\frac{\partial u'}{\partial x} \right)^2} \quad (3.120)$$

A new length scale λ , called *Taylor micro-scale*, is introduced (Taylor 1935), and it can be defined as

$$\overline{\left(\frac{\partial u'}{\partial x} \right)^2} \equiv \frac{\overline{u' u'}}{\lambda^2} \quad (3.121)$$

The scaling of u'^2 follows the condition of isotropic turbulence, that is, $\overline{u' u'} = \overline{v' v'} = \overline{w' w'}$, so that $\overline{u' u'} = \overline{u'_i u'_i}/3$. Then, using Eqs. (3.120) and (3.121), the TKE dissipation rate is related to the Taylor micro-scale as

$$\varepsilon = \varepsilon|_x + \varepsilon|_y + \varepsilon|_z \Rightarrow \varepsilon = 15\nu \frac{\overline{u' u'}}{\lambda^2} \quad \wedge \quad \varepsilon|_x = \varepsilon|_y = \varepsilon|_z \quad (3.122)$$

From TKE $k = (\overline{u' u'} + \overline{v' v'} + \overline{w' w'})/2$, it can be derived $\overline{u' u'} = (2/3)k$ for isotropic turbulence. Thus, using Eq. (3.122), the Taylor micro-scale is given by

$$\lambda = \left(10 \frac{\nu k}{\varepsilon} \right)^{1/2} \quad (3.123)$$

The relationship between the Taylor micro-scale and the Kolmogorov micro-scale can be determined from the ratios of λ to ℓ_T , η to ℓ_T , and λ to η expressing them in terms of turbulence Reynolds number $R_T [= k^2/(\varepsilon\nu)]$ as follows:

$$\frac{\lambda}{\ell_T} = 10^{1/2} R_T^{-1/2}, \quad \frac{\eta}{\ell_T} = R_T^{-3/4}, \quad \frac{\lambda}{\eta} = 10^{1/2} R_T^{1/4} \quad \Rightarrow \quad \lambda = 10^{1/2} \eta^{2/3} \ell_T^{1/3}$$

Thus, at large Reynolds numbers, the Taylor micro-scale falls in between the large-scale and the small-scale eddies, that is, $\ell_T > \lambda > \eta$ (Fig. 3.16). Taylor time scale of the eddies of length scale λ is related to the Kolmogorov time scale as

$$\tau_\lambda = \frac{\lambda}{(\overline{u'u'})^{0.5}} = \left(15 \frac{v}{\varepsilon}\right)^{1/2} = 15^{1/2} \tau_\eta$$

In the characterization of turbulence, the Reynolds number $R_\lambda [= (\overline{u'u'})^{0.5} \lambda / v]$ corresponding to the Taylor micro-scale can be related to the turbulence Reynolds number R_T as

$$R_\lambda = \left(\frac{20}{3} R_T\right)^{1/2}$$

3.11.5 Transformation of Length Scale to Wave Number

The wave number k_w is defined as $k_w = 2\pi/\ell$. The length scales and their ranges can be expressed in terms of wave number. They are as follows:

$$(k_{w\eta}, k_{wD}, k_{wE}, k_{wT}) = 2\pi \cdot (\ell_\eta, \ell_D, \ell_E, \ell_T)^{-1}$$

In this way, the universal equilibrium range ($\ell_E > \ell$) is given by $k_w > k_{wE} \equiv 2\pi/\ell_E$. Similarly, the inertial subrange ($\ell_E > \ell > \ell_D$) is expressed as $k_{wD} > k_w > k_{wE}$. In nondimensional form, the wave numbers are expressed multiplying them by the Kolmogorov length scale η as

$$(\eta k_{w\eta}, \eta k_{wD}, \eta k_{wE}, \eta k_{wT}) = 2\pi\eta \cdot (\ell_\eta, \ell_D, \ell_E, \ell_T)^{-1}$$

Note that in the dissipation range, the nondimensional wave number is $\eta k_{w\eta} = 2\pi$. Figure 3.17 shows the length scales and their ranges in terms of wave number.

3.11.6 Spectrum Function

It is an important question: How is TKE distributed among the eddies of different sizes? This can be determined by the spectral analysis, which is capable of

transforming a time-domain signal to the frequency-domain signal in terms of a *spectral density function* as a function of frequency f itself or wave number k_w . In the turbulence analysis, the spectral density functions that are commonly used are energy spectrum function E and spectrum function S_{ii} of velocity fluctuations.

A nondimensional correlation function $C_u(\xi)$ between two streamwise velocity fluctuations $u'(x)$ and $u'(x + \xi)$ having a streamwise lag distance ξ can be defined as follows (Nezu and Nakagawa 1993):

$$C_u(\xi) = \frac{\overline{u'(x) \cdot u'(x + \xi)}}{\overline{u'u'}} = \int_0^\infty S_{uu}(k_w) \cos(k_w \cdot \xi) dk_w \quad (3.124)$$

where $S_{uu}(k_w)$ is a nondimensional spectrum function of u' and is given by

$$S_{uu}(k_w) = \frac{2}{\pi} \int_0^\infty C_u(\xi) \cos(k_w \cdot \xi) dk_w$$

For the case of no lag ($\xi = 0$), Eq. (3.124) becomes

$$\int_0^\infty S_{uu}(k_w) dk_w = 1 \quad (3.125)$$

The way in which the TKE is distributed over the range of scales is the fundamental characterization of turbulence. For isotropic turbulence, this can be performed by means of the *energy spectrum function* $E(k_w)$ that represents the TKE k to contain eddies of size ℓ having wave number $k_w (=2\pi/\ell)$. By definition, k is the integral of $E(k_w)$ over the full range of wave number k_w . Thus,

$$k = \frac{1}{2} \overline{u'_i u'_i} = \int_0^\infty E(k_w) dk_w$$

In developing $E(k_w)$ within the inertial subrange, $E(k_w)$ is solely dependent on wave number k_w and TKE dissipation rate ε (by Kolmogorov second similarity hypothesis). From an analogy between spatial turbulence field and spectral wave number space, the TKE dissipation rate ε is regarded as a fundamental quantity. Therefore, by dimensional analysis, the possible form for the energy spectrum function can be obtained as

$$E(k_w) = C\varepsilon^{2/3} k_w^{-5/3} \quad (3.126)$$

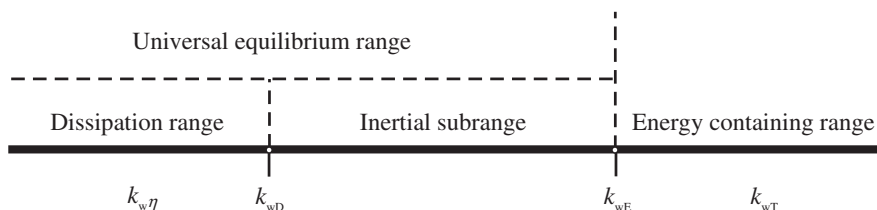
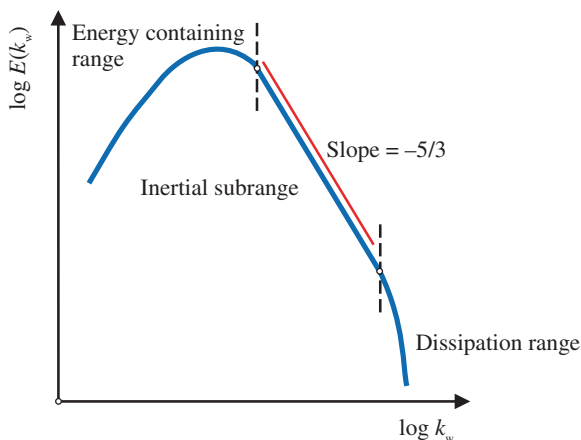


Fig. 3.17 Sketch illustrating length scales and their ranges in terms of wave number

Fig. 3.18 Illustrative sketch of energy spectrum function $E(k_w)$ curve in a log-log plot



where C is the universal Kolmogorov constant, which was experimentally determined as 1.5 (Zhou 1993). Equation (3.126) leads to the Kolmogorov hypothesis of energy spectrum function that states:

In the inertial subrange, the energy spectrum function is proportional to $-5/3$ -th power of the wave number which is a universal.

It is commonly known as Kolmogorov's $-5/3$ -th power law. The $-5/3$ -th power law can be verified only by using experimentally obtained velocity data over a sufficiently long period of time in a turbulent flow (see Fig. 5.19a). A larger Reynolds number associated with the large eddies gives rise to a larger inertial subrange. In laboratory experiments, it is, however, very difficult to reach sufficiently large Reynolds numbers to produce an adequately broad inertial subrange. Figure 3.18 schematically illustrates the energy spectrum function $E(k_w)$ curve in a log-log plot. The $-5/3$ slope of the curve in the inertial subrange corresponds to the Kolmogorov $-5/3$ -th power law. On the other hand, the energy containing range corresponds to small range of wave numbers k_w and the dissipation range to large range of k_w .

Equation (3.126) can also be expressed in terms of spectral density function S_{uu} of velocity fluctuations u' (Nezu and Nakagawa 1993):

$$S_{uu}(k_w) \sim \frac{\varepsilon^{2/3}}{u'u'} k_w^{-5/3} \quad (3.127)$$

The best possibility is that the spectrum function $F(f)$ can be readily obtained from the velocity fluctuations u' by using the fast Fourier transform (FFT) method (Bose 2009).⁸

Nezu (1977) obtained the following equations of the length scale ratios from the combined spectrum functions between the inertial subrange and the dissipation range:

$$\begin{aligned} \frac{\ell_T}{\lambda} &= \left(\frac{K}{15} R_{T\lambda} \right)^{1/2} \cong 0.21 R_{T\lambda}^{1/2}, \quad \frac{\ell_T}{\eta} = (K R_{T\lambda}^3)^{1/4} \cong 0.91 R_{T\lambda}^{3/4} \\ \wedge \quad R_{T\lambda} &= \frac{(\overline{u'u'})^{0.5} \ell_T}{\nu} \end{aligned}$$

where K is a weak function that can be given by

$$K(R_{T\lambda} > 200) \approx 0.691 + \frac{3.98}{R_{T\lambda}^{1/2}}$$

The ℓ_T/λ increases, and the inertial subrange becomes wider with an increase in $R_{T\lambda}$. So at large $R_{T\lambda}$, the $-5/3$ -th power law applies over a wide spectral range.

3.12 Anisotropy in Turbulence

The characterization of turbulent flow requires knowledge of the departure from isotropy. *Reynolds stress anisotropy tensor* b_{ik} is defined as the difference between the ratio of Reynolds stress tensor terms to the turbulent kinetic energy (TKE) and its isotropic equivalent quantity (Lumley and Newman 1977). Thus, b_{ik} is as follows:

$$b_{ik} = \frac{\overline{u'_i u'_k}}{2k} - \frac{\delta_{ik}}{3} \quad (3.128)$$

where k is the average TKE, that is $\overline{u'_i u'_i}/2$, and δ_{ik} is the Kronecker delta function, that is $\delta_{ik}(i \neq k) = 0$ and $\delta_{ik}(i = k) = 1$. Importantly, b_{ik} is a symmetric and traceless tensor bounded by $-1/3 \leq b_{ik} \leq 2/3$ and $b_{ik} = 0$ for isotropic turbulence.

⁸ The following transformation then applies:

$$S_{uu}(k_w) = \frac{\bar{u}}{2\pi} F(f) \quad \wedge \quad k_w = 2\pi \frac{f}{\bar{u}}.$$

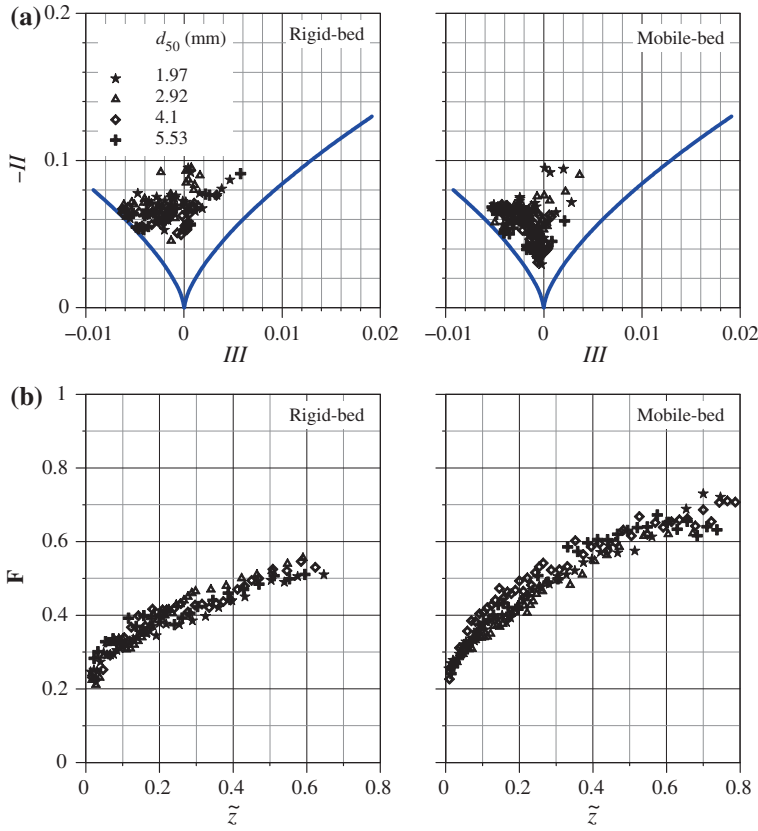


Fig. 3.19 **a** Anisotropic invariant maps (AIM) and **b** vertical distributions of anisotropic invariant function F (Sarkar 2010)

The sign of each diagonal component in b_{ik} refers to the relative contribution of the Reynolds stress relative to the TKE. However, a more convenient method for comparing the overall anisotropy is to use two principal independent invariants II ($=-b_{ik}b_{ik}/2$) and III ($=b_{ij}b_{jk}b_{ki}/3$), while the first invariant is zero ($I = b_{ii} = 0$). A cross plot of $-II$ against III is termed *anisotropic invariant map* (AIM). In an AIM, $-II$ (positive or zero) represents the degree of anisotropy and III corresponds to the nature of anisotropy. An AIM that is constructed plotting $-II$ against III with the AIM boundaries is shown in Fig. 3.19a for the data of rigid- and mobile-bed flows, obtained by Sarkar (2010). The possible states of turbulence prevail within the left- and right-curved boundaries, given by $III = \pm 6(II/6)^{3/2}$, originating from the bottom cusp (defined by $-II = III = 0$). These boundaries indicate two types of axisymmetric turbulence. The left boundary as identified by Choi and Lumley (2001) represents a *pancake-shaped* turbulence, where one component of TKE is smaller than other two that are equal. On the other hand, the right boundary represents a *cigar-shaped* turbulence, where one component of TKE is larger than

other two. The limits of one- and two-dimensional turbulence are given by the upper linear boundary, that is, $II = III + (8/9)$. Thus, for one-dimensional turbulence, $II = 8/3$ and $III = 16/9$; for two-dimensional, $II = 2/3$ and $III = -2/9$; and for three-dimensional, $-II = III = 0$. In Fig. 3.19a, the data plots adjacent to the beds start from the limit of two-dimensional turbulence, as they are close to the left curved boundary. With increasing distance from the bed, they shift slightly downward and toward left. In case of mobile-bed flow, the plots have an affinity to shift toward the bottom cusp, becoming a better isotropy.

Another method to estimate the overall anisotropy in the Reynolds stress tensor is given by the anisotropic invariant function \mathbf{F} (Lumley 1978):

$$\mathbf{F} = I + 9II + 27III \quad (3.129)$$

It is a measure of the approach to either two-dimensional turbulence ($\mathbf{F} = 0$) or a three-dimensional isotropic state ($\mathbf{F} = 1$). In other words, it is therefore convenient to ascertain the state of turbulence, that is either two- or three-dimensional. Figure 3.19b shows that the data plots collapse on a band across the flow layer, where the values of \mathbf{F} approach closer to unity in mobile-bed flow than in rigid-bed flow. It suggests that the turbulence in mobile-bed flow satisfies isotropy better than that in rigid-bed flow. While all the data for both the cases conclusively support an overall reduction in anisotropy near the bed, there is also an evidence to suggest that each case has its own AIM signature, as the rates of reduction in anisotropy are different, albeit marginally. Hence, they have their own level of anisotropy for the Reynolds shear stresses.

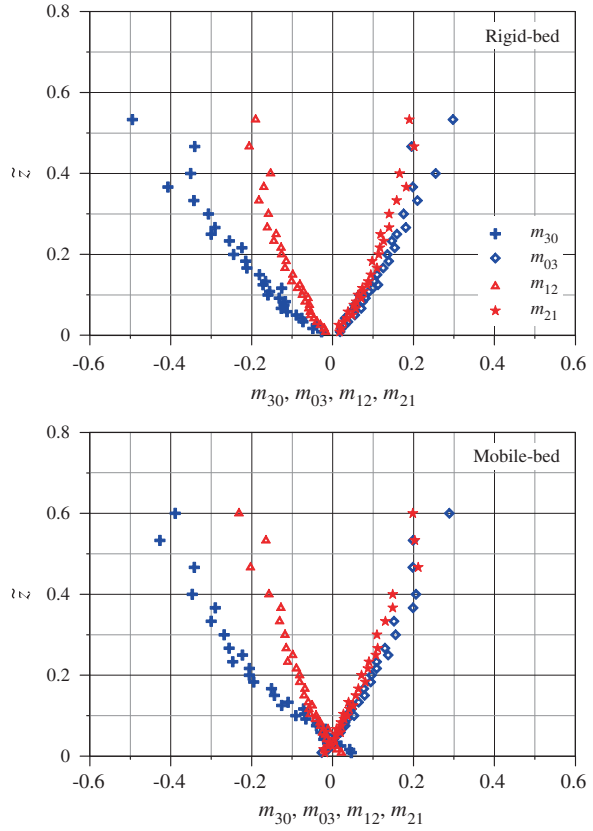
3.13 Higher-Order Correlations

Higher-order correlations that contain important stochastic information relating to the flux and diffusion of the stresses developed due to turbulence are directly attributable to the turbulent coherent structures (Simpson et al. 1981; Gad-el-Hak and Bandyopadhyay 1994). To be more explicit, third-order correlations preserve their signs positive or negative, providing useful stochastic information on the temporal distribution of velocity fluctuations with respect to the time-averaged velocity. For instance, the third-order correlation $\overline{u'_1 u'_2 u'_2}$ defines the flux of the Reynolds normal stress (RNS) $\overline{u'_2 u'_2}$ (in fact, it is RNS divided by ρ) driven by u'_1 . The set of *third-order correlations* m_{jk} are specified as follows (Rauapach 1981):

$$m_{jk}(j+k=3) = \overline{\hat{u}^j \hat{w}^k} \quad \wedge \quad \hat{u} = \frac{u'}{(\overline{u'u'})^{0.5}} \quad \vee \quad \hat{w} = \frac{w'}{(\overline{w'w'})^{0.5}} \quad (3.130)$$

With $j+k=3$ in Eq. (3.130), the M_{30} and M_{03} are *skewness* of u' and w' , respectively. The stochastic interpretation of the skewness lies on the asymmetry in the Gaussian distribution of the probability density function of velocity

Fig. 3.20 Vertical distributions of third-order correlations m_{jk} (Dey and Das 2012)



fluctuations (u' or w'). From the viewpoint of hydrodynamics, the skewness of u' is $M_{30}(=\overline{\hat{u}^3})$, defining the streamwise flux of the streamwise RNS $\overline{u'u'}$. A similar expression can be written for $M_{03}(=\overline{\hat{w}^3})$, defining the vertical flux of the vertical RNS $\overline{w'w'}$. On the other hand, the diffusion factors are $M_{21}(=\overline{\hat{u}^2\hat{w}})$ and $M_{12}(=\overline{\hat{u}\hat{w}^2})$, characterizing the diffusions of $\overline{u'u'}$ in z -direction and $\overline{w'w'}$ in x -direction, respectively. The characteristics of m_{jk} are demonstrated through experimental results of Dey and Das (2012) as follows:

Figure 3.20 presents the distributions of $m_{jk}(\tilde{z})$ for the cases of rigid-bed and mobile-bed flows. In rigid-bed flow, m_{30} and m_{12} start with small negative values near the bed and decrease (increase in negative magnitudes) with \tilde{z} . On the other hand, in mobile-bed flow, m_{30} and m_{12} start with small positive values near the bed, changing over to negative values with a slight increase in \tilde{z} . It suggests that the bed mobility influences m_{30} and m_{12} by changing the $\overline{u'u'}$ flux and the $\overline{w'w'}$ diffusion to the streamwise direction, while they propagate against the streamwise direction in rigid-bed flow. Away from the bed ($\tilde{z} > 0.06$), the $\overline{u'u'}$ flux and the $\overline{w'w'}$ diffusion occur against the streamwise direction and become pronounced with

an increase in \tilde{z} for both rigid-bed and mobile-bed flows. The trends of $m_{03}(\tilde{z})$ and $m_{21}(\tilde{z})$ in the rigid-bed flow are positive over the entire flow depth, while those in the mobile-bed flow are negative near the bed ($\tilde{z} \leq 0.06$) and positive for $\tilde{z} > 0.06$. It suggests that the $\overline{w'w'}$ flux and the $\overline{u'u'}$ diffusion are in upward direction over the entire flow depth for rigid-bed flow, while those are in downward direction in the near-bed flow region for mobile-bed flow.

Further, the fourth-order correlation termed *coefficient of kurtosis* of u' (say), $K_u (= \hat{u}^4)$, illustrates the intermittency of turbulence. The kurtosis for a standard Gaussian distribution is three. For this reason, the *excess kurtosis* is defined as $(K_u - 3)$. Therefore, $K_u > 3$ refers to a distribution with a peaky signal characteristic (leptokurtic distribution or too tall) of intermittent turbulent events, while $K_u < 3$ refers to a flat characteristic (platykurtic distribution or too flat). For instance, Andreopoulos et al. (1984) observed very high values of K_u near the wall and in the outer layer as well, specifying that the turbulence is highly intermittent in both locations. It is in conformity with the observations of Grass (1971) that ejections and sweeps provide strong intermittent contributions to turbulence production.

3.14 Turbulent Kinetic Energy Flux

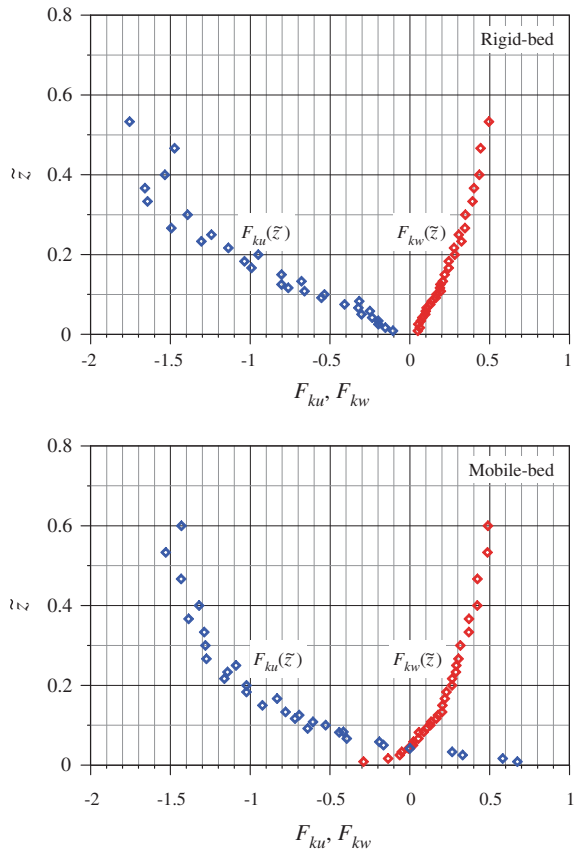
The components of TKE flux in x -, y - and z -direction are expressed as follows:

$$f_{ku} = \overline{ku'}, \quad f_{kv} = \overline{kv'}, \quad f_{kw} = \overline{kw'} \quad \wedge \quad k = \frac{1}{2}(\overline{u'u'} + \overline{v'v'} + \overline{w'w'}) \quad (3.131)$$

In two-dimensional flow, the streamwise and vertical flux of the TKE can be approximated as $f_{ku} = 0.75(\overline{u'u'u'} + \overline{u'w'w'})$ and $f_{kw} = 0.75(\overline{w'w'w'} + \overline{u'u'w'})$, respectively (Krogstad and Antonia 1999). The nondimensional form of the TKE fluxes is given by $F_{ku}, F_{kv}, F_{kw} = (f_{ku}, f_{kv}, f_{kw}) \times u_*^{-3}$.

To demonstrate the characteristics of F_{ku} and F_{kw} in rigid-bed and mobile-bed flows, the experimental results of Dey and Das (2012) are considered (Fig. 3.21). In rigid-bed flow, the F_{ku} starts with a small negative value and decreases (increase in negative value) with \tilde{z} . It implies that the F_{ku} transports against the streamwise direction over the entire flow depth. The inertia of flowing fluid layer induces a retarding effect being attributed to the negative value of F_{ku} . On the other hand, the positive F_{kw} over the entire flow depth suggests an upward transport of F_{kw} . Therefore, the negative F_{ku} and the positive F_{kw} compose a retardation process with the arrival of slowly moving fluid parcel. The influence of bed mobility is prominent in the F_{ku} and F_{kw} distributions. In mobile-bed flow, the positive F_{ku} and the negative F_{kw} in the near-bed flow region ($\tilde{z} \leq 0.06$) imply the streamwise and downward transport of TKE flux components, respectively. However, in the away-bed flow region ($\tilde{z} > 0.06$), the behavioral characteristics of F_{ku} and F_{kw} in the mobile-bed flow are similar to those in the rigid-bed flow. Therefore, the most

Fig. 3.21 Vertical distributions of TKE flux components F_{ku} and F_{kw} (Dey and Das 2012)



significant characteristic of the mobile-bed flow lies on the near-bed flow region, in which the positive F_{ku} and the negative F_{kw} compose an accelerating effect as an inrush of fluid parcel.

3.15 Turbulent Kinetic Energy Budget

To understand the physical processes in turbulence (that is, velocity fluctuations in flow), it is essential to balance the rate of conversion of kinetic energy of velocity fluctuations. The balance of the quantity under consideration is TKE, as given by Eq. (3.131) (see equation of k). For three-dimensional steady flow, the TKE budget reads

$$\begin{aligned}
\underbrace{\bar{u} \frac{\partial k}{\partial x} + \bar{v} \frac{\partial k}{\partial y} + \bar{w} \frac{\partial k}{\partial z}}_{\text{TKE advection rate}} &= - \underbrace{\frac{1}{\rho} \left[\frac{\partial(\overline{p'u'})}{\partial x} + \frac{\partial(\overline{p'v'})}{\partial y} + \frac{\partial(\overline{p'w'})}{\partial z} \right]}_{\text{Pressure energy diffusion rate, } p_D} \\
&\quad - \underbrace{\left[\frac{\partial f_{ku}}{\partial x} + \frac{\partial f_{kv}}{\partial y} + \frac{\partial f_{kw}}{\partial z} \right]}_{\text{TKE diffusion rate, } t_D} \\
&\quad + \underbrace{v \left(\frac{\partial^2 k}{\partial x^2} + \frac{\partial^2 k}{\partial y^2} + \frac{\partial^2 k}{\partial z^2} \right)}_{\text{Viscous diffusion rate, } v_D} \\
&\quad - v \left[\frac{\partial \overline{u'}}{\partial x} \cdot \frac{\partial \overline{u'}}{\partial x} + \frac{\partial \overline{v'}}{\partial x} \cdot \frac{\partial \overline{v'}}{\partial x} + \frac{\partial \overline{w'}}{\partial x} \cdot \frac{\partial \overline{w'}}{\partial x} \right. \\
&\quad + \frac{\partial \overline{u'}}{\partial y} \cdot \frac{\partial \overline{u'}}{\partial y} + \frac{\partial \overline{v'}}{\partial y} \cdot \frac{\partial \overline{v'}}{\partial y} + \frac{\partial \overline{w'}}{\partial y} \cdot \frac{\partial \overline{w'}}{\partial y} \\
&\quad \left. + \frac{\partial \overline{u'}}{\partial z} \cdot \frac{\partial \overline{u'}}{\partial z} + \frac{\partial \overline{v'}}{\partial z} \cdot \frac{\partial \overline{v'}}{\partial z} + \frac{\partial \overline{w'}}{\partial z} \cdot \frac{\partial \overline{w'}}{\partial z} \right] \\
&\quad \underbrace{\hspace{10em}}_{\text{TKE dissipation rate, } \varepsilon} \\
&\quad + \left[-\overline{u'u'} \frac{\partial \bar{u}}{\partial x} - \overline{u'v'} \frac{\partial \bar{v}}{\partial x} - \overline{u'w'} \frac{\partial \bar{w}}{\partial x} \right. \\
&\quad - \overline{v'u'} \frac{\partial \bar{u}}{\partial y} - \overline{v'v'} \frac{\partial \bar{v}}{\partial y} - \overline{v'w'} \frac{\partial \bar{w}}{\partial y} \\
&\quad \left. - \overline{w'u'} \frac{\partial \bar{u}}{\partial z} - \overline{w'v'} \frac{\partial \bar{v}}{\partial z} - \overline{w'w'} \frac{\partial \bar{w}}{\partial z} \right] \\
&\quad \underbrace{\hspace{10em}}_{\text{TKE production rate, } t_P}
\end{aligned} \tag{3.132}$$

where p' is the pressure fluctuations. In most of the literature, Eq. (3.132) is given in tensor form.⁹

The TKE budget equation describes the rate of conservation of TKE through four components of TKE budget: advection, diffusion, dissipation, and production. The diffusion rate is constituted by the pressure energy, TKE, and viscous diffusion rates. These terms are all gradients whose contribution therefore disappears by integration over the flow cross section when an overall balance is taken.

⁹ The TKE budget equation in tensor form is as follows:

$$\underbrace{\bar{u}_j \frac{\partial k}{\partial x_j}}_{\text{Advection}} = - \underbrace{\frac{1}{\rho} \cdot \frac{\partial(\overline{p'u'_i})}{\partial x_i}}_{p_D} - \underbrace{\frac{\partial(\overline{k u'_i})}{\partial x_j}}_{t_D} + \underbrace{v \frac{\partial^2 k}{\partial x_j^2}}_{v_D} - \underbrace{v \frac{\partial \overline{u'_i}}{\partial x_j} \cdot \frac{\partial \overline{u'_i}}{\partial x_j}}_{\varepsilon} + \underbrace{\left(-\overline{u'_i u'_j} \frac{\partial \bar{u}_i}{\partial x_j} \right)}_{t_P}$$

Importantly, the TKE dissipation rate ε that means a rate of conversion of TKE to internal energy is always positive, and thus, the term $-\varepsilon$ is an *energy sink*. On the other hand, the TKE production rate t_P is in general positive, being an *energy source*. In case of a negative t_P , the energy flows from the velocity fluctuations to the time-averaged flow velocity. The flow region, where t_P and ε are approximately equal and much greater than the remaining terms of the TKE budget, is called *energy equilibrium region*.

The TKE budget for a uniform open-channel flow in two-dimensional is given as follows (Nezu and Nakagawa 1993):

$$\underbrace{-\overline{u'w'}}_{t_P} \frac{\partial \bar{u}}{\partial z} = \underbrace{\frac{1}{\rho} \cdot \frac{\partial}{\partial z} (\overline{p'w'})}_{p_D} + \underbrace{\frac{\partial f_{kw}}{\partial z}}_{t_D} - \underbrace{v \frac{\partial^2 k}{\partial z^2}}_{v_D} + \varepsilon \quad (3.133)$$

As the flow is uniform, the advection term disappears in Eq. (3.133). Near-bed flow region is called *energy excess region*, where $t_P > \varepsilon$; while near the free surface, it is called *energy deficiency region*, where $\varepsilon > t_P \approx 0$. On the other hand, in the intermediate region, the TKE is transported from the near-bed region to the near-free surface region maintaining a dynamic equilibrium, in which $t_P \approx \varepsilon$. In particular, p_D and t_D in the near-bed region are controlled by the flow roughness.

In fully developed turbulent flow, the viscous diffusion rate v_D in the main flow is negligible due to large flow Reynolds numbers, but it is substantial within the viscous sublayer. However, accurate estimation of TKE dissipation rate ε is always challenging. There are several methods of estimation of ε . Among them, ε is believed to be best estimated from the Kolmogorov second hypothesis applicable to the inertial subrange:

$$\varepsilon = \left(\frac{k_w^{5/3} S_{uu}}{C} \right)^{3/2} \quad (3.134)$$

where k_w is the wave number, S_{uu} is the spectral density function for u' , and C is the constant approximately equaling 0.51 for the inner layer and 0.55 for the outer layer of wall shear flow. The estimate of ε is explained in Sect. 5.16.

The ε can also be determined from the following equation (Irwin 1973; Krogstad and Antonia 1999):

$$\varepsilon = \frac{15\nu}{\bar{u}^2} \overline{\left(\frac{\partial u'}{\partial t} \right)^2} \quad (3.135)$$

The above equation usually has a tendency to overestimate ε to some extent.

The pressure energy diffusion rate p_D can be calculated as a residual parameter from Eq. (3.133) as

$$p_D = t_P - t_D - \varepsilon \quad (3.136)$$

The nondimensional parameters of TKE budget are $T_P, P_D, T_D, E_D = (t_P, p_D, t_D, \varepsilon) \times (h/u_*^3)$. For open-channel flow, Nezu and Nakagawa (1993) gave formulations for the TKE production rate T_P and dissipation rate E_D as

$$T_P = \frac{1}{\kappa} \left(\frac{1 - \tilde{z}}{\tilde{z}} \right) \quad (3.137a)$$

$$E_D = \frac{9.8}{\tilde{z}^{0.5}} \exp(-3\tilde{z}) \quad (3.137b)$$

To illustrate the terms of TKE budget in rigid-bed and mobile-bed flows, the experimental results of Dey and Das (2012) are considered, as shown in Figs. 3.22a, b. The TKE production rate $T_P(\tilde{z})$ curves show the conversion rate of energy from the time-averaged flow to the turbulence. It has a near-bed amplification and decreases monotonically with an increase in \tilde{z} , becoming nearly constant (with a small magnitude) for $\tilde{z} > 0.3$. The E_D also decreases with \tilde{z} in the similar way, as T_P does. The distributions of E_D have a distinct lag from those of T_P . However, the $T_P(\tilde{z})$ and $E_D(\tilde{z})$ curves obtained from Eqs. (3.137a) and (3.137b), respectively, proposed by Nezu and Nakagawa (1993), overestimate the experimental data plots of T_P and E_D to some extent. The influence of bed mobility is apparent in the near-bed distributions of T_P and E_D , where the lag is reduced considerably in case of mobile-bed flow. To be explicit, the effects of bed mobility are to reduce T_P significantly and E_D feebly. The reduction of T_P in the near-bed flow region in presence of bed mobility is an effect of the damping in local Reynolds shear stress. Importantly, the difference in T_P and E_D at any depth \tilde{z} is balanced by the summation of T_D and P_D . The T_D decreases monotonically with an increase in \tilde{z} within the wall shear layer and then becomes almost invariant of \tilde{z} attaining a small magnitude. The bed mobility influences T_D by increasing its magnitude in comparison to T_D in rigid-bed flow. In rigid-bed flow, P_D is almost equaling E_D , but it decreases drastically with \tilde{z} , becoming almost invariant (with a small magnitude) of \tilde{z} for $\tilde{z} > 0.06$. The most interesting feature lies on the near-bed characteristics of P_D in mobile-bed flow. It is evident that the bed mobility is associated with a drastic changeover of P_D to a negative value, indicating a gain in turbulence production. It can be therefore concluded that in the near-bed flow region for mobile bed, the lag between TKE production and dissipation rates is narrowed down and the pressure energy diffusion rate becomes negative. Detert et al. (2010) also reported the bed mobility to be associated with a low-pressure flow mode.

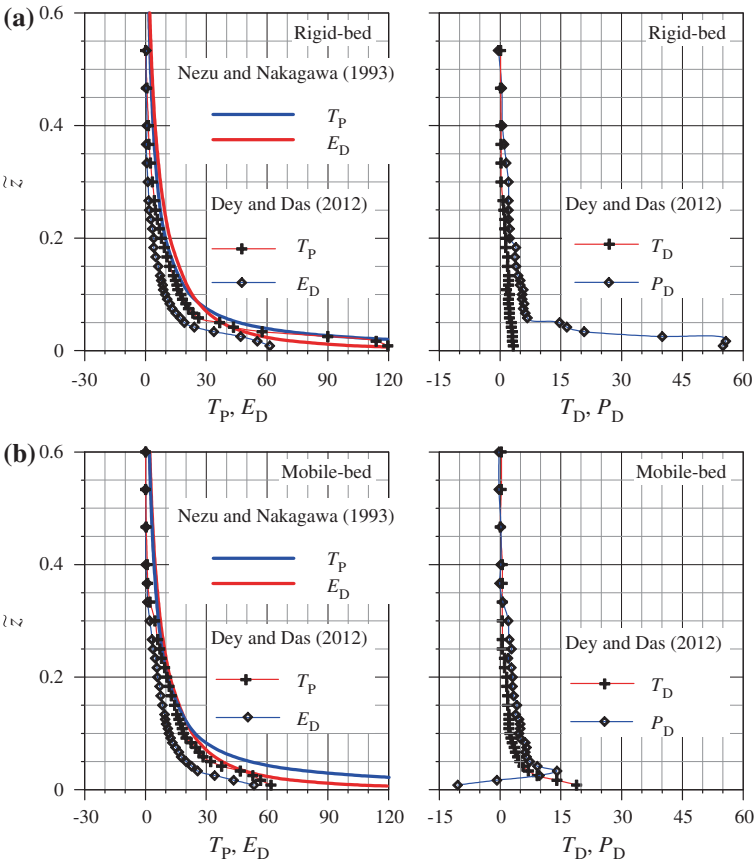


Fig. 3.22 TKE budget: **a** rigid-bed and **b** mobile-bed flows (Dey and Das 2012)

3.16 Concept of Burst

Experimental studies in 1960s and 1970s showed that the near-boundary flow has an extremely complex structure and most of the turbulence is produced there. Investigations on the viscous sublayer by Kline et al. (1967), Corino and Brodkey (1969), Grass (1971), Offen and Kline (1973, 1975) and others revealed a near-boundary flow structure dominated by the viscosity being repetitive in nature and consisting of alternate zones of three-dimensional high- and low-speed streaks with roughly regular spanwise spacing. They are known to be persistent features of the near-boundary flow in a turbulent boundary layer (Smith and Metzler 1983). The concept of *turbulent burst* is constituted by the entrainment of the near-boundary low-speed streaks into main turbulent flow. The entrained fluid streaks subsequently become unstable and collapse to cause an inrush of high-speed fluid from the outer flow region toward the boundary. The whole process is a *quasi-cyclic*

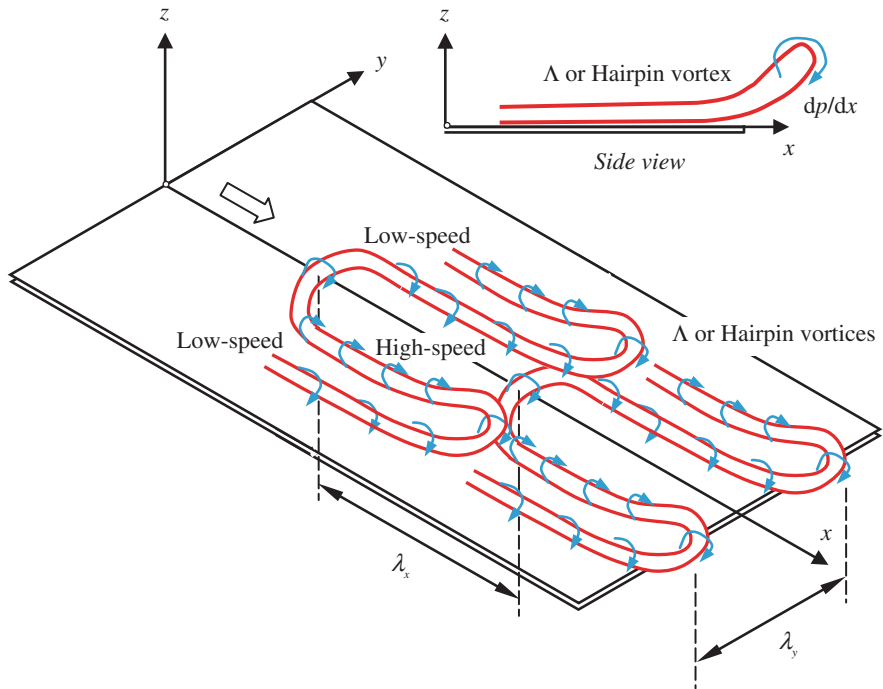


Fig. 3.23 The Λ or hairpin vortices

process. (Note: It means an approximately periodic process.) It therefore indicates that the turbulence is not as random as it was initially viewed. The concept of simply introducing a randomly fluctuating velocity to the time-averaged velocity is therefore potentially inadequate one. Spatially temporal, but orderly motions, as already mentioned as quasi-cyclic process, exist in a turbulent flow.

3.16.1 Coherent Structures and Burst

In boundary layer flow, the underlying concept of burst lies on the viscous sublayer that enlarges with time leading to an unstable process, which ends up in a burst with an emission of a fluid parcel of concentrated vortex to the outer turbulent flow in the wall shear layer. In this way, in the streamwise direction, a series of vortices (spanwise with moderately equidistant), called Λ or *hairpin vortices*, organized in turbulent spots is produced, as shown in Fig. 3.23 (Head and Bandyopadhyay 1981). These hairpin vortices, which have average length and breadth of $\tilde{x}^+ = 20-40$ and $\tilde{y}^+ = 15-20$, respectively, are streamwise vortices with slightly raised front portion having two limbs of weak transverse vortices. Here, $\tilde{x}^+ = xu_*/v$ and $\tilde{y}^+ = yu_*/v$.

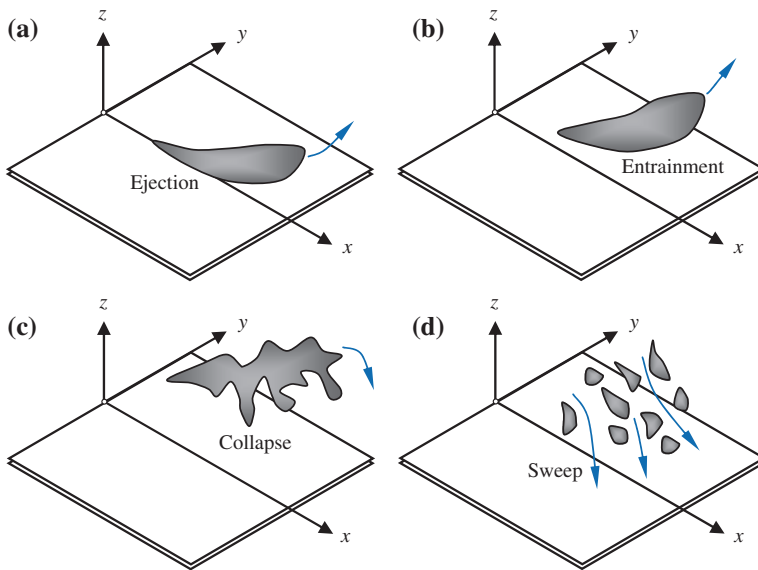


Fig. 3.24 Sequence of bursting events: **a** initiation of ejection, **b** entrainment of ejected fluid (low-speed streak) in outer flow, **c** collapse of ejected fluid (low-speed streak), and **d** inrush of fluid (high-speed streaks) or sweep

These vortices get elongated and stretched as they develop with time. The rotational motion of vortex is intensified with an increase in curvature of the stretched portion (as the front portion of hairpin is gradually lifted) reaching a maximum at the tip of the hairpin. By this mechanism, the turbulent flow is fed with the fluid vortex parcels that are produced in the near-boundary flow only. Finally, the vortex parcels collapse forming eddies of various sizes. After the burst, the viscous sublayer is recovered and the same process is continued time and again. As the destabilizing process being recursive in nature is always performed in an identical time, the bursting phenomenon becomes a quasi-cyclic process and the released vortices are very similar. In this process, the streak-like structures, called the *coherent structures*, are formed. However, away from the boundary, the structures persist for some distance, but their degree of coherence and organization diminishes with the distance from the boundary.

The sequence of bursting phenomenon is described by two significant features, such as *ejection* and *sweep* (Figs. 3.24a–d). The intermittent enlargement of viscous sublayer is in fact analogous to a boundary layer separation subject to an adverse pressure gradient, wherein a near-boundary low-speed streak (which is a hairpin vortex structure, as already mentioned) is subjected to have a separation due to a local and temporary adverse pressure gradient ($dp/dx > 0$) (Fig. 3.23). It occurs as a low-speed streak that oscillates in three dimensions to be lifted up from the boundary, resulting in a coherent low-speed fluid to entrain into the main

turbulent flow (Figs. 3.24a, b). This process is called *ejection event*. According to Nychas et al. (1973), the fluid ejection originates in the flow region $5 < \tilde{z}^+ < 50$ and the ejected fluid can reach in the flow region $80 < \tilde{z}^+ < 100$, where $\tilde{z}^+ = zu_*/v$. The fluid streak ejected into the main flow grows in size, as it is slowly advected streamwise while preserving its coherent entity. This continues over a short period of time, and eventually, the coherent structure collapses (Fig. 3.24c). Then, the ejected fluid that remains as a result of retardation is brushed away by high-speed fluid approaching the boundary as an inrush (Fig. 3.24d). This process is called *sweep event*. In other words, a portion fluid mass from the coherent structure rushes back to the near-boundary region, impinging the boundary and spreading out spanwise. During the sweep event, the downward flow generates a narrow, highly fluctuating shear layer containing multiple eddies. Two such neighboring high-speed streaks eventually unite and are to slow down the flow there, and as a result, a new near-boundary low-speed flow is reformed. Although the low-speed streaks appear at random in space and interact with neighboring streaks, the average value of the instantaneous spanwise and streamwise spacings in nondimensional form is constant, thus remaining invariant of flow Reynolds number and Froude number (Lee et al. 1974; Offen and Kline 1973). The nondimensional spanwise and streamwise spacings are as follows:

$$\lambda_y^+ = \frac{\lambda_y u_*}{v} \approx 100, \quad \lambda_x^+ = \frac{\lambda_x u_*}{v} \approx 1,300$$

where λ_y and λ_x are the spanwise and streamwise spacings, respectively.

The time period spent from the formation of the low-speed streak at time $t = 0$ to the formation of the next one at time $t = t_b$ is called the *bursting period*. After the reformation of the newly near-boundary low-speed fluid motion, the same sequence of events takes place and continues as a cyclic process. According to Smith and Metzler (1983), the average bursting time in nondimensional form is

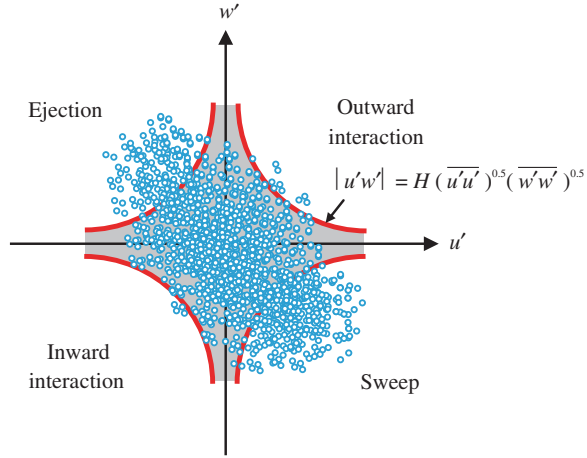
$$t_b^+ = \frac{t_b u_*^2}{v} = 480$$

However, in some cases, the maximum bursting time was found to be as high as $t_b^+ = 2,500$ (Nezu and Nakagawa 1993). The bursting events can be quantified by the quadrant analysis, which is discussed next.

3.16.2 Quadrant Analysis

The bursting events are quantified from the conditional statistics of velocity fluctuations (u' and w'). To evaluate the total Reynolds shear stress $-\rho \overline{u'w'}$ at a specific point as a sum of contributions from different bursting events, it is

Fig. 3.25 The quadrant analysis



customary to plot the fluctuations of velocity components (u' and w') according to quadrant in a $u'w'$ plane (Lu and Willmarth 1973), as shown schematically in Fig. 3.25.

The hyperbolic shaded zone bounded by the curve $|u'w'| = \text{constant}$ is called a *hole*. Introducing a parameter H called *hole size* that represents the threshold level as explained by Nezu and Nakagawa (1993), the size of the hole is decided by the curve $|u'w'| = H(\overline{u'u'})^{0.5}(\overline{w'w'})^{0.5}$. With this method, the large contributions to the Reynolds shear stress from each quadrant can be extracted leaving the smaller fluctuations of velocity components (u' and w') that belong to the hole corresponding to more quiescent periods. Therefore, the hole size H allows to differentiate between strong and weak events for small values of the hole size and only strong events for large values of the hole size. The four quadrants i ($i = 1, 2, 3$, and 4) characterize the types of bursting events. They are (1) the *outward interactions* $Q1$ ($i = 1$; $u' > 0$, $w' > 0$), (2) the *ejections* $Q2$ ($i = 2$; $u' < 0$, $w' > 0$), (3) the *inward interactions* $Q3$ ($i = 3$; $u' < 0$, $w' < 0$), and (4) the *sweeps* $Q4$ ($i = 4$; $u' > 0$, $w' < 0$). The hole size $H = 0$ means that all data of u' and corresponding w' are taken into consideration. The quadrant analysis that provides an analysis of velocity fluctuation data in quadrantwise by fixing the hole size to eliminate weak events is also known as the *analysis of conditional statistics*.

The analysis of the conditional statistics can be performed introducing a detection function $\lambda_{i,H}(t)$ defined as

$$\lambda_{i,H}(z, t) = \begin{cases} 1, & \text{if } (u', w') \text{ is in quadrant } i \text{ and if } |u'w'| \geq H(\overline{u'u'})^{0.5}(\overline{w'w'})^{0.5} \\ 0, & \text{otherwise} \end{cases} \quad (3.138)$$

where t is the time. At any point, contribution to the total Reynolds shear stress from the quadrant i outside the hyperbolic hole region of size H is given by

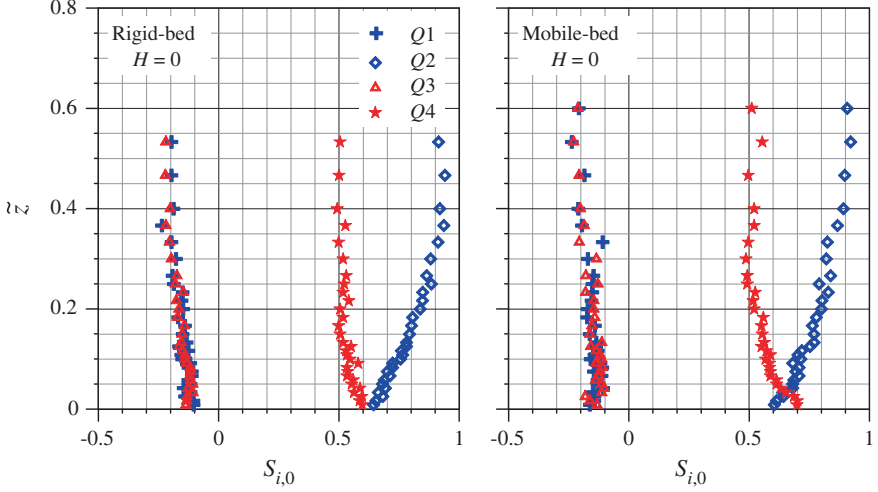


Fig. 3.26 Distributions of $S_{i,0}(\bar{z})$ in rigid-bed and mobile-bed flows (Dey and Das 2012)

$$\langle u'w' \rangle_{i,H} = \lim_{T \rightarrow \infty} \frac{1}{T} \int_0^T u'(t)w'(t)\lambda_{i,H}(z,t)dt \quad (3.139)$$

where T is the sampling duration. The Reynolds shear stress fractional contribution to each event is given by

$$S_{i,H} = \frac{\langle u'w' \rangle_{i,H}}{\overline{u'w'}} \quad (3.140)$$

It implies that $S_{i,H} > 0$ when $i = 2$ and 4 (ejections and sweeps) and $S_{i,H} < 0$ when $i = 1$ and 3 (outward and inward interactions). Therefore,

$$\sum_{i=0}^{i=4} S_{i,H} \big|_{H=0} = 1$$

Figure 3.26 shows the vertical distributions of fractional contribution $S_{i,0}(H=0)$ of the Reynolds shear stress in rigid-bed and mobile-bed flows (Dey and Das 2012). In rigid-bed flow, $Q2$ and $Q4$ events at the near-bed region contribute strongly to the total Reynolds shear stress production by approximately 64 and 60 %, respectively, while $Q1$ and $Q3$ events contribute weakly by about 10 and 14 %, respectively. It suggests that the arrival of low-speed fluid streaks from the near-bed flow region is almost revoked by that of a succession of high-speed fluid streaks from the outer flow region, as the strengths of $Q1$ and $Q3$ events are not very different. Thus, only a slowly moving process is effectively prevalent in

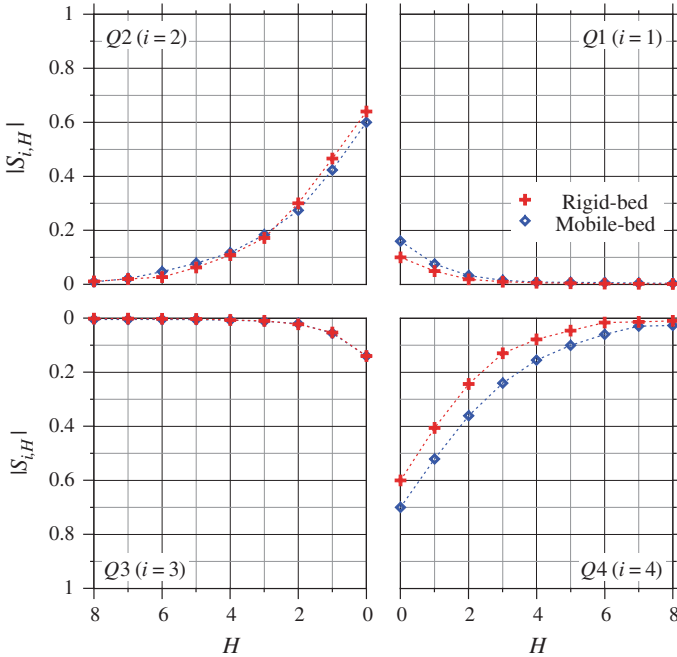


Fig. 3.27 Distributions of $|S_{i,H}|$ as a function of H at a near-bed region in rigid-bed and mobile-bed flows

the form of weak $Q2$ events. In contrast, in the mobile-bed flow, the $Q4$ events are the governing mechanism for bed mobility contributing about 70 % toward the Reynolds shear stress production, while the $Q2$ events contribute relatively less (about 60 %). The characteristic of $Q4$ events to dominate momentum transfer in the near-bed flow region is therefore strongly dependent on the bed mobility. It implies that the bed mobility is governed by the arrival of high-speed fluid streaks. However, the contributions from $Q1$ and $Q3$ events continued to be rather weak are about 16 and 14 %, respectively.

Figure 3.27 represents the distributions of the fractional contributions $|S_{i,H}|$ of the Reynolds shear stress as a function hole size H for each of the four quadrants at a near-bed region for rigid-bed and mobile-bed flows. The $|S_{i,H}|$ decreases progressively with an increase in H in all quadrants. It is obvious that when the hole size H becomes large, there remain only two contributions, ejections $Q2$ and sweeps $Q4$.

3.17 Probability Distributions of Turbulence

In open-channel flow, the random quantities are the fluctuations of streamwise and vertical velocity components (u' and w') and also their product $u'w'$, whose averaged value yields the Reynolds shear stress $-\rho\overline{u'w'}$. Due to the fact that in turbulent flow, $-\rho\overline{u'w'}$ is a nonzero quantity, it follows that u' and w' are correlated quantities. The knowledge of the probability density function (PDF) of these quantities leads to the understanding of the associated turbulent bursting phenomenon in open-channel flow (Nakagawa and Nezu 1977).

Frenkiel and Klebanoff (1967) and van Atta and Chen (1968) predicted moments of u' higher than two. They considered the correlations at two points separated in time and showed that while the even-order correlations can be predicted by assuming a Gaussian joint PDF, the odd-order correlations follow a *Gaussian based Gram-Charlier* (GC) PDF. Considering the non-Gaussian behavior of u' and w' , Antonia and Atkinson (1973) used a GC series expansion for the joint PDFs of u' and w' obtained by inverting a Gaussian-based characteristic function. To retain skewness and flatness, the series was truncated by discarding cumulants of the order higher than four. In contrast, Nakagawa and Nezu (1977) considered a joint PDF, which was Gaussian-based GC series, but of the form given by Kampé de Fériet (1966). Essentially, the prevalence of bursting in the near-bed flow provokes a non-Gaussian PDF distribution for the turbulence quantities. Bose and Dey (2010) therefore argued that the joint PDFs of u' and w' can be derived from a GC series based on the exponential distribution, which is universal being applicable for smooth- and rough-bed flows. Their theory is furnished below.

3.17.1 Bose–Dey Universal Probability Theory

3.17.1.1 Joint Probability Distribution of u' and w'

In open-channel flow, bed resistance gives rise to the production of turbulence. The instantaneous streamwise velocity u can be decomposed into a time-averaged velocity \bar{u} and its fluctuations u' , while the instantaneous vertical velocity w solely constitutes the fluctuations w' , as the time-averaged vertical velocity \bar{w} remains zero. It implies that $u = \bar{u} + u'$ and $w = w'$.

Velocity fluctuations, say u' , appear on a computer monitor (during measurement) as a traveling wave train of sharply peaked signals of random magnitude $|u'|$. For an appropriate model of the PDF $p_{u'}(u')$ of u' , let the 0th approximation be symmetric with respect to $u' = 0$, which means $p_{u'}(-u') = p_{u'}(u')$. Then, it can easily be shown that the PDF $p_{|u'|}(|u'|)$ of $|u'|$ is connected to $p_{u'}(u')$ by

$$p_{|u'|}(|u'|) = 2p_{u'}(u') \quad (3.141)$$

Now, a random signal magnitude $|u'|$ is analogous to the service or waiting time of customers arriving in a queue. Hence, if $P_0(|u'|)$ is the cumulative probability of random fluctuations exceeding magnitude $|u'|$ and if the process is stationary, then $P_0(|u'| + \Delta u')/P_0(|u'|)$ is the conditional probability of fluctuations exceeding $\Delta u'$, provided it had exceeded $|u'| = P_0(\Delta u')$, where $\Delta u'$ is an increment. This means that $P_0(|u'| + \Delta u') = P_0(|u'|) \times P_0(\Delta u')$. The solution of this functional equation is, known as *exponential distribution*, given by

$$P_0(|u'|) = \exp\left(\frac{-|u'|}{\sigma_u}\right) \quad \wedge \quad \sigma_u = (\overline{u'u'})^{0.5} \quad (3.142)$$

where standard deviation $\sigma_u > 0$, since $P_0(|u'|) \leq 1$. Hence, the cumulative probability of fluctuations up to $|u'|$, namely $P_{|u'|}(|u'|)$, is

$$P_{|u'|}(|u'|) = 1 - P_0(|u'|) = 1 - \exp\left(\frac{-|u'|}{\sigma_u}\right) \quad (3.143)$$

Therefore, by Eq. (3.141), the PDF of u' is

$$p_{u'}(u') = \frac{1}{2}p_{|u'|}(|u'|) = \frac{1}{2} \cdot \frac{d}{d|u'|} [P_{|u'|}(|u'|)] = \frac{1}{2\sigma_u} \exp\left(\frac{-|u'|}{\sigma_u}\right) \quad (3.144)$$

Equation (3.144) is a symmetric exponential distribution with standard deviation $2^{0.5}\sigma_u$. By similar arguments, the PDF of w' could be a similar distribution, with σ_u replaced by some standard deviation $\sigma_w > 0$. If u' and w' are assumed to be independent, their joint PDF is

$$p_{u',w'}(u', w') = \frac{1}{4\sigma_u\sigma_w} \exp\left(\frac{-|u'|}{\sigma_u} + \frac{-|w'|}{\sigma_w}\right) \quad \wedge \quad \sigma_w = (\overline{w'w'})^{0.5} \quad (3.145)$$

which is a two-dimensional symmetric exponential distribution. The joint PDF given by Eq. (3.145) contains arbitrary moments up to only order two. The distribution is next generalized to include higher-order moments by the well-known *Gram–Charlier (GC) series* expansion method (Cramer 1999). Consider the characteristic function χ or the Fourier integral of a PDF $p_{u',w'}(u', w')$

$$\chi(\xi, \eta) = \int_{-\infty}^{\infty} \int_{-\infty}^{\infty} \exp[i(u'\xi + w'\eta)] p_{u',w'}(u', w') du' dw' = \sum_{n=0}^{\infty} \frac{i^n}{n!} (\overline{u'\xi + w'\eta})^n \quad (3.146)$$

where the over-bar is the mean value or expectation. Expanding the quantity under the over-bar by binomial theorem, the expansion can be written as

$$\chi(\xi, \eta) = \sum_{n=0}^{\infty} \sum_{j=0}^{\infty} \frac{i^n}{j!(n-j)!} \xi^j \eta^{n-j} \overline{u^j w^{n-j}} H(n-j) = \sum_{j=0}^{\infty} \sum_{k=0}^{\infty} \frac{i^{j+k}}{j!k!} m_{jk} \xi^j \eta^k \quad (3.147)$$

where $H(n-j) = 1$, if $n \geq j$, and $H(n-j) = 0$, if $n < j$. The right most expression is obtained by interchanging the order of summation and using the definition of the function H . In Eq. (3.147), $k = n - j$ and $m_{jk} = \overline{u^j w^k}$.

For the symmetric exponential distribution given by Eq. (3.144), the integral defining the characteristic function χ_0 is evaluated as

$$\chi_0(\xi, \eta) = (1 + \sigma_u^2 \xi^2)^{-1} (1 + \sigma_w^2 \eta^2)^{-1} \quad (3.148)$$

Equation (3.148) is generalized to accommodate moments of all orders in the PDF $p_{u'w'}(u', w')$ of (u', w') as

$$\chi(\xi, \eta) = \sum_{j=0}^{\infty} \sum_{k=0}^{\infty} i^{j+k} C_{jk} \frac{(\sigma_u \xi)^j (\sigma_w \eta)^k}{(1 + \sigma_u^2 \xi^2)^{j+1} (1 + \sigma_w^2 \eta^2)^{k+1}} \quad (3.149)$$

In the above equation, the leading coefficient $C_{00} = 1$. The leading term of Eq. (3.149) for $j = k = 0$ is simply $\chi_0(\xi, \eta)$ as given by Eq. (3.148). By Fourier inversion of Eq. (3.149), one gets

$$\begin{aligned} p_{u',w'}(u', w') &= \frac{1}{4\pi^2} \int_{-\infty}^{\infty} \int_{-\infty}^{\infty} \chi(\xi, \eta) \exp[-i(u'\xi + w'\eta)] d\xi d\eta \\ &= \frac{1}{4\pi^2} \sum_{j=0}^{\infty} \sum_{k=0}^{\infty} i^{j+k} C_{jk} \int_{-\infty}^{\infty} \frac{(\sigma_u \xi)^j \exp(-iu'\xi)}{(1 + \sigma_u^2 \xi^2)^{j+1}} d\xi \int_{-\infty}^{\infty} \frac{(\sigma_w \eta)^k \exp(-iw'\eta)}{(1 + \sigma_w^2 \eta^2)^{k+1}} d\eta \\ &= \frac{1}{4\pi^2 \sigma_u \sigma_w} \sum_{j=0}^{\infty} \sum_{k=0}^{\infty} i^{j+k} C_{jk} I_j \left(\frac{u'}{\sigma_u} \right) I_k \left(\frac{w'}{\sigma_w} \right) \end{aligned} \quad (3.150)$$

where

$$I_j(x) = \int_{-\infty}^{\infty} \frac{\xi^j \exp(-ix\xi)}{(1 + \xi^2)^{j+1}} d\xi \quad (3.151)$$

In terms of nondimensional variables, $\hat{u} = u'/\sigma_u$ and $\hat{w} = w'/\sigma_w$, one can therefore write

$$p_{u',w'}(u', w') = \frac{1}{\sigma_u \sigma_w} p_{\hat{u}, \hat{w}}(\hat{u}, \hat{w}) \quad (3.152a)$$

$$p_{\hat{u}, \hat{w}}(\hat{u}, \hat{w}) = \frac{1}{4\pi^2} \sum_{j=0}^{\infty} \sum_{k=0}^{\infty} i^{j+k} C_{jk} I_j(\hat{u}) I_k(\hat{w}) \quad (3.152b)$$

The integral in Eq. (3.151) is evaluated according to Gradshteyn and Ryzhik (1980), as given in formulas 3.773 (2 and 5), yielding

$$\begin{aligned} I_0(x) &= \pi \exp(-|x|), \quad I_1(x) = -\frac{i\pi}{2} x \exp(-|x|), \\ I_2(x) &= \frac{\pi}{8} (1 + |x| - x^2) \exp(-|x|), \quad I_3(x) = -\frac{i\pi}{48} x (3 + 3|x| - x^2) \exp(-|x|) \\ I_4(x) &= \frac{\pi}{384} (9 + 9|x| - 3x^2 - 6|x|^3 + x^4) \exp(-|x|), \dots \end{aligned} \quad (3.153)$$

By direct integration and using I_{0-4} in Eq. (3.153), it can be verified that

$$\int_{-\infty}^{\infty} p_{\hat{u}, \hat{w}}(\hat{u}, \hat{w}) d\hat{u} d\hat{w} = C_{00} = 1$$

An examination of the derivation of Eq. (3.150) shows that the characteristic function of the distribution of (\hat{u}, \hat{w}) is given by Eq. (3.149) with $\sigma_u \xi$ and $\sigma_w \eta$ replaced by ξ and η , respectively. If this equation is identified with the moment generating Eq. (3.147), the coefficients C_{jk} become related to m_{jk} by

$$\begin{aligned} C_{00} &= m_{00} = 1, \quad C_{10} = m_{10}, \quad C_{20} = \frac{1}{2} m_{20} - 1, \quad C_{30} = \frac{1}{6} m_{30} - 2m_{10}, \\ C_{40} &= \frac{1}{24} m_{40} - \frac{3}{2} m_{20} + 2, \quad C_{11} = m_{11}, \quad C_{21} = \frac{1}{2} m_{21} - m_{01}, \quad C_{31} = \frac{1}{6} m_{31} - 2m_{11}, \\ C_{22} &= \frac{1}{4} m_{22} - \frac{1}{2} m_{20} - \frac{1}{2} m_{02} + 1 \end{aligned} \quad (3.154)$$

The coefficients C_{01} , C_{02} , C_{03} , C_{04} , C_{12} , and C_{13} can be found from Eq. (3.154) by commuting the subscripts. Subsequently, in Eqs. (3.157), (3.162), (3.165) and (3.167), it can be seen that moments of order greater than four contribute insignificant terms, and accordingly, the coefficients C_{jk} of order $j + k > 4$ in Eq. (3.154) are not mentioned. Estimating the moments m_{jk} using the experimental data, the coefficients C_{jk} and then the PDF $p_{\hat{u}, \hat{w}}(\hat{u}, \hat{w})$ can be obtained from Eq. (3.152b).

3.17.1.2 Marginal Distribution of \hat{u} and \hat{w}

The marginal distribution of \hat{u} is given by

$$p_{\hat{u}}(\hat{u}) = \int_{-\infty}^{\infty} p_{\hat{u},\hat{w}}(\hat{u}, \hat{w}) d\hat{w} = \frac{1}{4\pi^2} \sum_{j=0}^{\infty} \sum_{k=0}^{\infty} i^{j+k} C_{jk} I_j(\hat{u}) \int_{-\infty}^{\infty} I_k(\hat{w}) d\hat{w} \quad (3.155)$$

and by changing the order of integration, one can write

$$\begin{aligned} \int_{-\infty}^{\infty} I_k(\hat{w}) d\hat{w} &= \int_{-\infty}^{\infty} \frac{\eta^k}{(1 + \eta^2)^{k+1}} d\eta \int_{-\infty}^{\infty} \exp(-i\hat{w}\eta) d\hat{w} \\ &= \int_{-\infty}^{\infty} \frac{\eta^k}{(1 + \eta^2)^{k+1}} d\eta \cdot 2\pi\delta(\eta) = 2\pi\delta_{k0} \end{aligned} \quad (3.156)$$

where $\delta(\eta)$ is the Dirac delta function and δ_{k0} is the Kronecker symbol, that is $\delta_{k0}(k = 0) = 1$ and $\delta_{k0}(k \neq 0) = 0$. Hence, it follows from Eq. (3.156) that

$$\begin{aligned} p_{\hat{u}}(\hat{u}) &= \frac{1}{2\pi} \sum_{j=0}^{\infty} i^j C_{j0} I_j(\hat{u}) = \frac{1}{2} \exp(-|\hat{u}|) + \frac{1}{4} C_{10} \hat{u} \exp(-|\hat{u}|) \\ &\quad - \frac{1}{16} C_{20} (1 + |\hat{u}| - \hat{u}^2) \exp(-|\hat{u}|) - \frac{1}{96} C_{30} \hat{u} (3 + 3|\hat{u}| - \hat{u}^2) \exp(-|\hat{u}|) \\ &\quad + \frac{1}{768} C_{40} (9 + 9|\hat{u}| - 3\hat{u}^2 - 6|\hat{u}|^3 + \hat{u}^4) \exp(-|\hat{u}|) + \dots \end{aligned} \quad (3.157)$$

The marginal distribution of $p_{\hat{w}}(\hat{w})$ is similarly given by an expression in which \hat{u} is replaced by \hat{w} and the coefficients C_{10} , C_{20} , C_{30} , and C_{40} by C_{01} , C_{02} , C_{03} , and C_{04} , respectively. It can easily be verified that the integrals of the expressions for $p_{\hat{u}}(\hat{u})$ and $p_{\hat{w}}(\hat{w})$ between $-\infty$ and $+\infty$ equal unity. Similarly, it follows that the moments

$$m_{j0} = \int_{-\infty}^{\infty} \hat{u}^j p_{\hat{u}}(\hat{u}) d\hat{u}, \quad m_{0k} = \int_{-\infty}^{\infty} \hat{w}^k p_{\hat{w}}(\hat{w}) d\hat{w} \quad (3.158)$$

are related to C_{j0} and C_{0k} , respectively, exactly as given by Eq. (3.154).

The coefficients C_{j0} and C_{0k} appearing in the PDFs, $p_{\hat{u}}(\hat{u})$ and $p_{\hat{w}}(\hat{w})$, depend on the boundary resistance, velocity u , and distance z from the boundary. The coefficients C_{j0} and C_{0k} can therefore be estimated from the experimental data. Thus, if the relative frequency $f_{\hat{u}}(\hat{u})$ of the random variable \hat{u} is computed from the experimental data at a given z , then from Eq. (3.158), the m_{j0} are estimated by approximating $p_{\hat{u}}(\hat{u})$ by $f_{\hat{u}}(\hat{u})$ and the integrals are evaluated by a composite

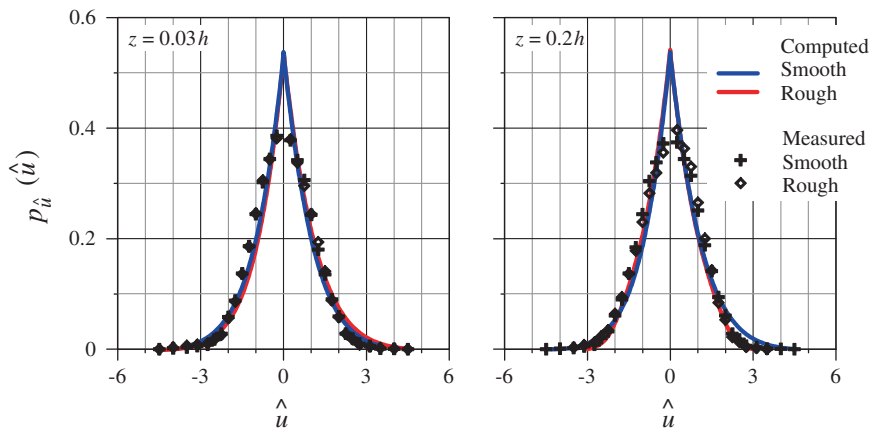


Fig. 3.28 Distributions of $p_{\hat{u}}(\hat{u})$ in smooth- and rough-bed flows at $z = 0.03h$ and $0.2h$ (Bose and Dey 2010)

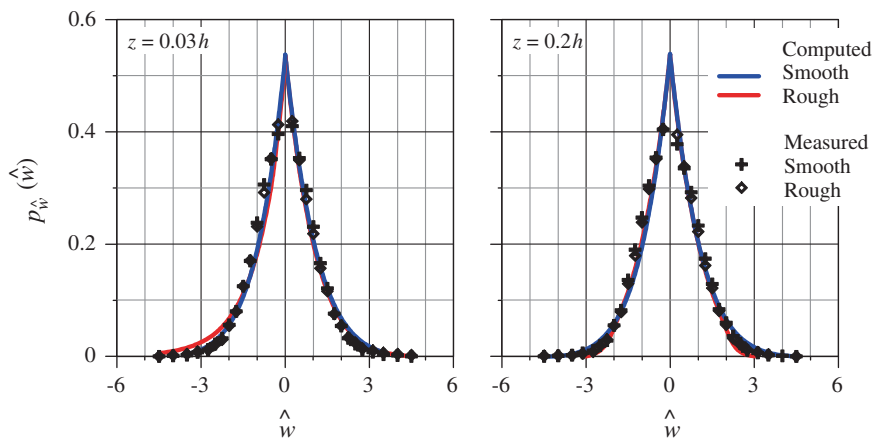


Fig. 3.29 Distributions of $p_{\hat{w}}(\hat{w})$ in smooth- and rough-bed flows at $z = 0.03h$ and $0.2h$ (Bose and Dey 2010)

Simpson's rule. Similarly, the m_{0k} are estimated from $f_{\hat{w}}(\hat{w})$ of the random variable \hat{w} . Thus, using Eq. (3.154), C_{j0} and C_{0k} are calculated and the PDFs are computed to yield the theoretical curves for $p_{\hat{u}}(\hat{u})$ and $p_{\hat{w}}(\hat{w})$. For normalizing u' and w' to obtain \hat{u} and \hat{w} , the standard deviations σ_u and σ_w are estimated from the root-mean-square values of u' and w' . Figures 3.28 and 3.29 show the $p_{\hat{u}}(\hat{u})$ and $p_{\hat{w}}(\hat{w})$ distributions for smooth- and rough-bed flows at $z = 0.03h$ and $0.2h$. In general, the computed $p_{\hat{u}}(\hat{u})$ and $p_{\hat{w}}(\hat{w})$ distributions correspond to the experimental data.

3.17.1.3 PDF of Reynolds Shear Stress

The Reynolds shear stress is defined by $\tau_{xz} = -\rho \overline{u'w'}$. Thus, $-\tau_{xz}/\rho$ is the mean value of the product of random variable $u'w'$, whose PDF depends on the joint PDF of u' and w' . Making nondimensional, one can consider the random variable $\hat{\tau} = \hat{u}\hat{w}$. Using the two-dimensional transformation $\hat{\tau} = \hat{u}\hat{w}$, $\hat{\zeta} = \hat{u}$ or \hat{w} , the marginal PDF of $\hat{\tau}$ is given in terms of the joint PDF $p_{\hat{u},\hat{w}}(\hat{u}, \hat{w})$ as

$$p_{\hat{\tau}}(\hat{\tau}) = \int_{-\infty}^{\infty} p_{\hat{u},\hat{w}}\left(\hat{u}, \frac{\hat{\tau}}{\hat{u}}\right) \frac{d\hat{u}}{|\hat{u}|} = \int_{-\infty}^{\infty} p_{\hat{u},\hat{w}}\left(\frac{\hat{\tau}}{\hat{w}}, \hat{w}\right) \frac{d\hat{w}}{|\hat{w}|} \quad (3.159)$$

Inserting Eq. (3.152b) into one of the two forms in Eq. (3.159), integrals of the following form are encountered, whose value is as follows [see Gradshteyn and Ryzhik (1980), as given in formula 3.471(9)]:

$$\int_0^{\infty} x^{\varepsilon-1} \exp\left(-\alpha x - \frac{\beta}{x}\right) dx = 2 \left(\frac{\beta}{\alpha}\right)^{\varepsilon/2} K_{\varepsilon}\left(2\sqrt{\beta\alpha}\right) \quad \text{for } \beta > 0, \quad \gamma > 0 \quad (3.160)$$

where $K_{\varepsilon}(\zeta)$ is the modified Bessel function of order ε . In this manner, Eq. (3.159) yields

$$\begin{aligned} p_{\hat{\tau}}(\hat{\tau}) = & K_0(2\tau_1) - \frac{1}{8}(C_{20} + C_{02})[K_0(2\tau_1) + \tau_1 K_1(2\tau_1) - \tau_1^2 K_2(2\tau_1)] + \frac{1}{4}C_{11}\hat{\tau}K_0(2\tau_1) \\ & + \frac{1}{64}C_{22}[(1 + \tau_1^2 + \tau_1^4)K_0(2\tau_1) + 2\tau_1(1 - \tau_1^2)K_1(2\tau_1) - 2\tau_1^2 K_2(2\tau_1)] \\ & - \frac{1}{96}(C_{31} + C_{13})\hat{\tau}[3K_0(2\tau_1) + 3\tau_1 K_1(2\tau_1) - \tau_1^2 K_2(2\tau_1)] \\ & + \frac{1}{384}(C_{40} + C_{04})[9K_0(2\tau_1) + 9\tau_1 K_1(2\tau_1) - 3\tau_1^2 K_2(2\tau_1) - 6\tau_1^3 K_3(2\tau_1) + \tau_1^4 K_4(2\tau_1)] \\ & + \dots \end{aligned} \quad (3.161)$$

where $\tau_1 = (|\hat{\tau}|)^{0.5}$. Invoking the recurrence relationship $K_{\varepsilon+1}(\zeta) - K_{\varepsilon-1}(\zeta) = (2\varepsilon/\zeta)K_{\varepsilon}(\zeta)$ of the modified Bessel function $K_{\varepsilon}(\zeta)$, the expression for $p_{\hat{\tau}}(\hat{\tau})$ simplifies to

$$\begin{aligned} p_{\hat{\tau}}(\hat{\tau}) = & K_0(2\tau_1) - \frac{1}{8}(C_{20} + C_{02})(1 - \tau_1^2)K_0(2\tau_1) + \frac{1}{4}C_{11}\hat{\tau}K_0(2\tau_1) \\ & + \frac{1}{64}C_{22}[(1 - \tau_1^2 + \tau_1^4)K_0(2\tau_1) - 2\tau_1^3 K_1(2\tau_1)] \\ & - \frac{1}{96}(C_{31} + C_{13})\hat{\tau}(3 - \tau_1^2)[K_0(2\tau_1) + \tau_1 K_1(2\tau_1)] \\ & + \frac{1}{384}(C_{40} + C_{04})[(9 - 9\tau_1^2 + \tau_1^4)K_0(2\tau_1) - 2\tau_1^3 K_1(2\tau_1)] + \dots \end{aligned} \quad (3.162)$$

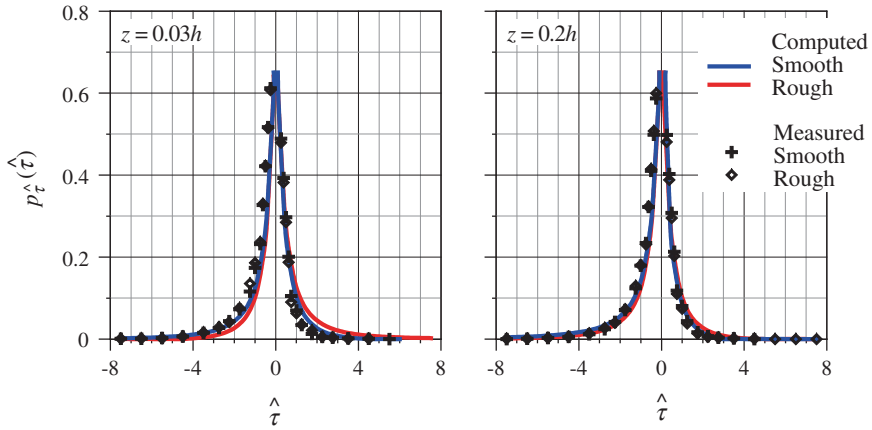


Fig. 3.30 Distributions of $p_{\hat{\tau}}(\hat{\tau})$ in smooth- and rough-bed flows at $z = 0.03h$ and $0.2h$ (Bose and Dey 2010)

It can be verified that the integral of $p_{\hat{\tau}}(\hat{\tau})$ as given by Eq. (3.162) from $-\infty$ to $+\infty$ is unity. This follows from Gradshteyn and Ryzhik (1980), as given in formula 6.561(16).

The PDF in Eq. (3.162) for $p_{\hat{\tau}}(\hat{\tau})$ contains three other coefficients C_{11} , C_{22} , and $C_{31} + C_{13}$. They are estimated from the moments as

$$\begin{aligned} \int_{-\infty}^{\infty} \hat{\tau} p_{\hat{\tau}}(\hat{\tau}) d\hat{\tau} &= C_{11} + \frac{11}{8}(C_{31} + C_{13}), \quad \int_{-\infty}^{\infty} \hat{\tau}^2 p_{\hat{\tau}}(\hat{\tau}) d\hat{\tau} = 4 + 4(C_{20} + C_{02}) + \frac{25}{4}C_{22}, \\ \int_{-\infty}^{\infty} \hat{\tau}^3 p_{\hat{\tau}}(\hat{\tau}) d\hat{\tau} &= 144C_{11} + 7407(C_{31} + C_{13}) \end{aligned}$$

Replacing $p_{\hat{\tau}}(\hat{\tau})$ by the relative frequency distribution of $\hat{\tau} = \hat{u}\hat{w}$, as observed from experiments, the required three parameters are estimated to complete the theoretical expression in Eq. (3.162). Figure 3.30 compares computed $p_{\hat{\tau}}(\hat{\tau})$ with those measured for smooth- and rough-bed flows. The experimental data collapse reasonably on the computed curves, implying that $p_{\hat{\tau}}(\hat{\tau})$ can be represented by the GC series expansion based on the exponential distribution.

3.17.1.4 Conditional Distributions of $\hat{u}\hat{w}$

The fractional contribution to the total Reynolds shear stress production from each event is given by the random variable $\hat{\tau} = \langle \hat{u}\hat{w} \rangle_{Q1}$ that corresponds to the appropriate quadrant. Following Nakagawa and Nezu (1977), the PDFs of the events $Q1$,

$Q2$, $Q3$, and $Q4$ are denoted by $p_1(\hat{\tau})$, $p_2(\hat{\tau})$, $p_3(\hat{\tau})$, and $p_4(\hat{\tau})$, respectively. It follows that

$$p_1(\hat{\tau}) + p_2(\hat{\tau}) + p_3(\hat{\tau}) + p_4(\hat{\tau}) = p_{\hat{\tau}}(\hat{\tau}) \quad (3.163)$$

The expression for $p_1(\hat{\tau})$ for outward interactions is as in the case of Eq. (3.159)

$$p_1(\hat{\tau} > 0) = \int_0^{\infty} p_{\hat{\tau}}\left(\hat{u}, \frac{\hat{\tau}}{\hat{u}}\right) \frac{d\hat{u}}{\hat{u}} = \frac{1}{4\pi^2} \sum_{j=0}^{\infty} \sum_{k=0}^{\infty} i^{j+k} C_{jk} \int_0^{\infty} I_j(\hat{u}) I_k\left(\frac{\hat{\tau}}{\hat{u}}\right) \frac{d\hat{u}}{\hat{u}} \quad (3.164)$$

Evaluating the series of integrals in the above expression for $p_1(\hat{\tau})$ by using Eq. (3.164) and simplifying by using the recurrence relation for $K_e(\zeta)$, it can be shown that

$$\begin{aligned} p_1(\hat{\tau} > 0) &= \frac{1}{2} p_{\hat{\tau}}(\hat{\tau}) + \frac{1}{4} (C_{10} - C_{01}) \tau_1 K_1(2\tau_1) \\ &\quad - \frac{1}{96} (C_{30} - C_{03}) \tau_1 [\tau_1 K_0(2\tau_1) + (4 - \tau_1) K_1(2\tau_1)] \\ &\quad + \frac{1}{32} (C_{21} - C_{12}) \tau_1 [\tau_1 K_0(2\tau_1) + (1 - \tau_1^2) K_1(2\tau_1)] + \dots \end{aligned} \quad (3.165)$$

For $\hat{\tau} > 0$, $p_1(\hat{\tau}) = 0$, the distribution of $Q1$ is one-sided, remaining on the positive side. Interestingly, the expression for $p_4(\hat{\tau})$ is the same as that given by Eq. (3.165), but for $\hat{\tau} < 0$, whereas for $\hat{\tau} > 0$, $p_4(\hat{\tau}) = 0$.

The expression for $p_2(\hat{\tau})$ for ejections is

$$p_2(\hat{\tau} < 0) = \int_{-\infty}^0 p_{\hat{\tau}}\left(\hat{u}, \frac{\hat{\tau}}{\hat{u}}\right) \frac{d\hat{u}}{\hat{u}} = \frac{1}{4\pi^2} \sum_{j=0}^{\infty} \sum_{k=0}^{\infty} i^{j+k} C_{jk} \int_0^{\infty} I_j(-\hat{\zeta}) I_k\left(-\frac{\hat{\tau}}{\hat{\zeta}}\right) \frac{d\hat{\zeta}}{\hat{\zeta}} \quad (3.166)$$

where $\hat{\zeta} = -\hat{u}$ is a substitution variable. The integrals in Eq. (3.166) can again be evaluated by using Eq. (3.160) and $K_{e+1}(\zeta) - K_{e-1}(\zeta) = (2e/\zeta) K_e(\zeta)$. Using Eq. (3.153), it is found that

$$\begin{aligned} p_2(\hat{\tau} < 0) &= \frac{1}{2} p_{\hat{\tau}}(\hat{\tau}) - \frac{1}{4} (C_{10} - C_{01}) \tau_1 K_1(2\tau_1) \\ &\quad + \frac{1}{96} (C_{30} - C_{03}) \tau_1 [\tau_1 K_0(2\tau_1) + (4 - \tau_1) K_1(2\tau_1)] \\ &\quad - \frac{1}{32} (C_{21} - C_{12}) \tau_1 [\tau_1 K_0(2\tau_1) + (1 - \tau_1^2) K_1(2\tau_1)] \end{aligned} \quad (3.167)$$

For $\hat{\tau} > 0$, $p_2(\hat{\tau}) = 0$. Moreover, the expression for $p_3(\hat{\tau})$ is identical as that given by Eq. (3.167), except that for $\hat{\tau} > 0$. For $\hat{\tau} < 0$, $p_3(\hat{\tau}) = 0$. The expressions for $p_1(\hat{\tau})$, $p_2(\hat{\tau})$, $p_3(\hat{\tau})$ and $p_4(\hat{\tau})$ evidently satisfy Eq. (3.163).

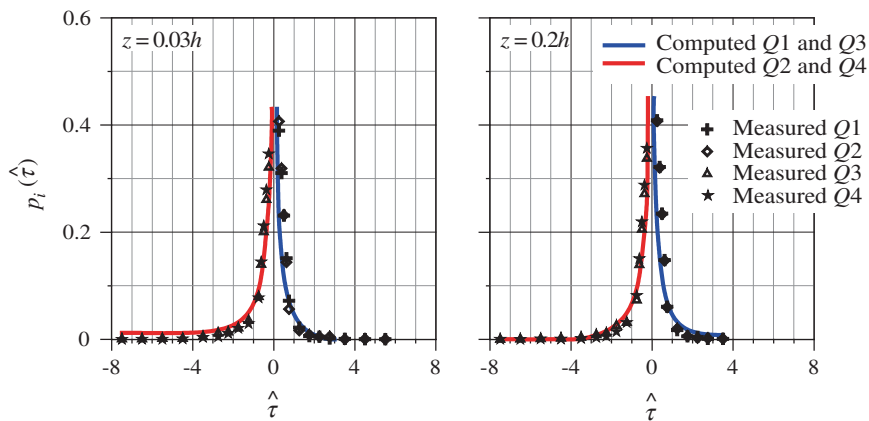


Fig. 3.31 Distributions of $p_i(\hat{\tau})$ in smooth-bed flow at $z = 0.03h$ and $0.2h$ (Bose and Dey 2010)

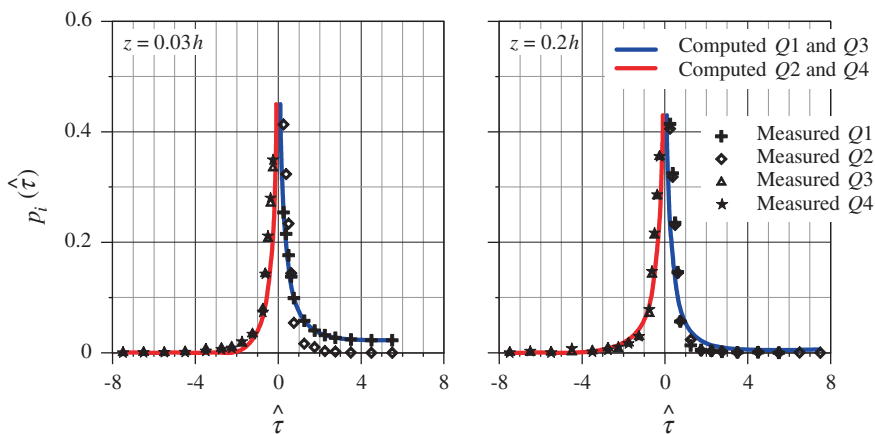


Fig. 3.32 Distributions of $p_i(\hat{\tau})$ in rough-bed flow at $z = 0.03h$ and $0.2h$ (Bose and Dey 2010)

The conditional PDFs in Eqs. (3.165) and (3.166) contain the coefficient $C_{21} - C_{12}$, which can be estimated by computing the moment as

$$\int_0^{\infty} \hat{\tau} p_1(\hat{\tau}) d\hat{\tau} = \frac{1}{2} \int_0^{\infty} \hat{\tau} p_{\hat{\tau}}(\hat{\tau}) d\hat{\tau} + \frac{1}{4} (C_{10} - C_{01}) - \frac{3}{32} (C_{21} - C_{12})$$

from the experimentally determined relative frequencies $f_1(\hat{\tau})$ and $f_{\hat{\tau}}(\hat{\tau})$ of $\hat{\tau}$.

Figures 3.31 and 3.32 compare the computed $p_i(\hat{\tau})$ with those measured for smooth- and rough-bed flows at $z = 0.03h$ and $0.2h$. It is evident that the conditional Reynolds shear stresses corresponding to ejections ($Q2$) and sweeps ($Q4$)

can be well represented by the exponential distribution, while those corresponding to outward interactions ($Q1$) and inward interactions ($Q3$) have a departure from the computed distributions. As the outward and inward interactions are the weaker events, they may not strictly follow the exponentially based distribution.

In conclusion, the universal PDF distributions of u' , w' , $u'w'$, and conditional Reynolds shear stresses in smooth- and rough-bed flows can be derived using a GC series expansion based on the exponential distribution truncating the series up to fourth order. The PDFs are easy for straightforward computation as compared to those of Nakagawa and Nezu (1977).

3.18 Double-Averaging Concept

In situations like macro-rough-bed flows (for example, boulder- or gravel-bed flow), the time-averaging assumptions are modified by the time-space-averaging to apply in the vicinity of the near-bed flow where the time-averaged flow is locally three-dimensional and significantly heterogeneous in space, as indicated in several studies particularly the recent ones (Nikora et al. 2001, 2007a, b; Rodríguez and García 2008; Franca and Lemmin 2009; Sarkar and Dey 2010; Dey et al. 2011; Dey and Das 2012).

To resolve the spatial heterogeneity, the time-averaging is conceptually supplemented by the area-averaging in the layer parallel to the mean bed surface, called the *double-averaging methodology* (DAM). The DAM produces modified momentum and continuity equations that are averaged in both time (ensemble) and space domains. In general, there are two ways to obtain the *double-averaging* (DA) equations: (1) *Time-space-averaging*, where the spatial averaging of the already time-averaged variables is performed, and (2) *space-time-averaging*, where the time-averaging of the already space-averaged variables is performed. The first option is more appropriate for describing the rough-bed flow hydrodynamics as the time-space-averaging order is consistent with the traditional turbulence research, and it seems to be physically more transparent and sound as well. The dimensions of the averaging domain in the plane parallel to the mean bed surface should be much larger than the dominant turbulence scales, but much smaller than the large-scale features in bed topography.

Since the DAM is applicable for the near-bed flow over and within the flow-roughness-element interface, it enables to have an insight into the turbulence characteristics within the flow sublayers induced by the roughness elements. These flow sublayers are the *form-induced sublayer* and *interfacial sublayer*, together called *roughness sublayer* (Fig. 3.33). The form-induced sublayer that occupies the flow region just above the roughness crests is influenced by the individual roughness elements. The interfacial sublayer is further influenced by individual roughness elements and occupies the flow region below the roughness crests.

In the DAM, the local time-averaged flow quantity is decomposed as

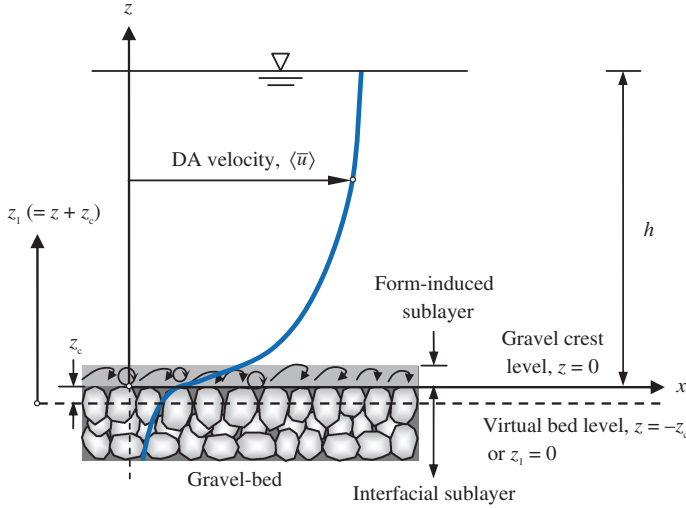


Fig. 3.33 Flow over a rough gravel-bed showing the flow sublayers (Dey and Das 2012)

$$\bar{\theta} = \langle \bar{\theta} \rangle + \tilde{\theta}$$

and the local instantaneous flow quantity follows the traditional Reynolds decomposition, that is,

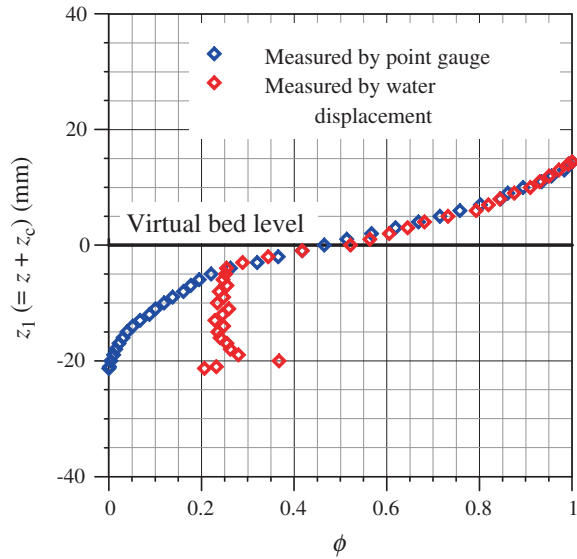
$$\theta = \bar{\theta} + \theta'$$

where $\tilde{\theta}$ is the fluctuations of the local time-averaged flow quantity $\bar{\theta}$ from the DA flow quantity $\langle \bar{\theta} \rangle$ and θ' is the fluctuations of the local instantaneous flow quantity θ from the local time-averaged flow quantity $\bar{\theta}$. Here, the intrinsic spatial averaging, that is denoted by using angle brackets $\langle \cdot \rangle$, is intended as an area integration over a surface parallel to the mean bed surface at variable elevation (Nikora et al. 2007a, b). Note that θ is a quantity defined only over the fluid phase.

Regarding the coordinate system, the bed surface is the reference of the z -axis ($z = 0$), which is positive vertically upward. The x -axis is aligned with the bed surface and positive in the streamwise direction. The origin of x -axis ($x = 0$) is located at the starting point of the DA analysis. The y -axis is directed spanwise, being positive to the right. The *virtual bed level* (also called the *mean bed level*), that is, $z_1 = 0$ or $z = -z_c$ (see Fig. 3.33), is considered aligning with the average bed surface fluctuations. The top of the interfacial sublayer, $z_1 = z_c$ or $z = 0$, is defined as the *maximum crest level* of the gravels.

The DA procedure does not differ from the standard averaging where the integration domain is totally occupied by the fluid ($z \geq z_c$, where z is the vertical distance with respect to the roughness crest level). Within the interfacial sublayer ($z \leq z_c$), the integration is, however, done only over the space not occupied by the

Fig. 3.34 Variation of roughness geometry function ϕ with $z_1 (=z + z_c)$ (Dey and Das 2012)



roughness elements. The idea of spatial averaging in open-channel flow was first introduced by Smith and McLean (1977). They averaged velocity along lines of constant distance from an undular bed. As already mentioned, the DA quantity is proposed for an area-averaging over a layer parallel to the mean bed at an elevation z . Then, the information of the quantity of voids within the integration domain is specified by the *roughness geometry function* $\phi(z)$. For $z \leq 0$ (below the roughness crest), the roughness geometry function $\phi(z)$ ($=A_f/A_0$, where A_f is the area occupied by the fluid at an elevation z within the total area A_0 for averaging) is used as a multiplier of an intrinsic DA flow quantity contributing to a superficial DA flow quantity. Within the interfacial sublayer, it is necessarily $1 \geq \phi \geq \rho_0$ (where ρ_0 is the porosity of the bed), while $\phi(z \geq z_c) \equiv 1$. In this regard, results obtained by Dey and Das (2012) are furnished, as an example.

Figure 3.34 shows the variation of $\phi(z_1)$ obtained from the measurement of the bed surface fluctuations by the point gauge. As the lower curvature of the gravels forming the inter-gravel voids could not be measured by the point gauge, the ϕ function determined by the point gauge could be only applicable for the upper portion of the interfacial sublayer. In order to obtain the actual ϕ function for the zone where the point gauge measurement was not possible, the water displacement method was adopted by placing gravels in a transparent container. Figure 3.34 also shows the actual ϕ function obtained from the water displacement method.

The generalized DA continuity and Reynolds-averaged Navier–Stokes (RANS) equations in Cartesian coordinates are given as follows (Nikora et al. 2001).

For the flow region above the roughness crest ($z \geq z_c$),

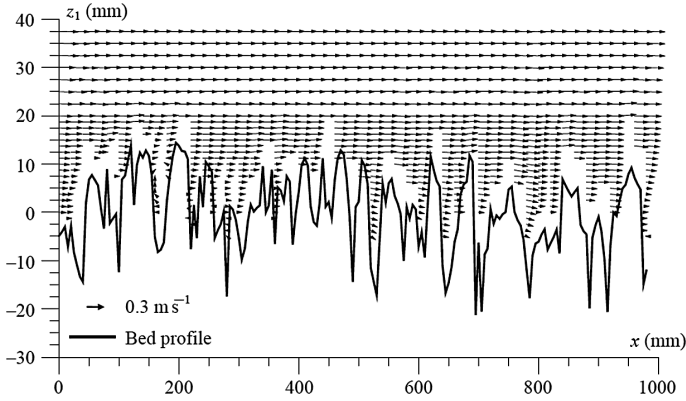


Fig. 3.35 Vector diagram for gravel-bed flow showing the local time-averaged velocities on the vertical plane of symmetry. The vector $\rightarrow 0.3 \text{ m s}^{-1}$ refers to a scale $(\bar{u}^2 + \bar{w}^2)^{0.5} = 0.3 \text{ m s}^{-1}$ (Dey and Das 2012)

$$\frac{\partial \langle \bar{u}_i \rangle}{\partial x_i} = 0 \quad (3.168a)$$

$$\frac{\partial \langle \bar{u}_i \rangle}{\partial t} + \langle \bar{u}_i \rangle \frac{\partial \langle \bar{u}_j \rangle}{\partial x_i} = g_i - \frac{1}{\rho} \cdot \frac{\partial \langle \bar{p} \rangle}{\partial x_i} - \frac{\partial \langle \bar{u}'_i \bar{u}'_j \rangle}{\partial x_j} - \frac{\partial \langle \tilde{u}_i \tilde{u}_j \rangle}{\partial x_j} + \nu \frac{\partial^2 \langle \bar{u}_i \rangle}{\partial x_j^2} \quad (3.168b)$$

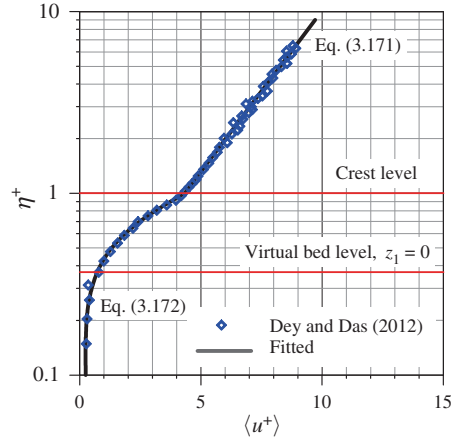
For the flow region within the interfacial sublayer ($z < z_c$),

$$\frac{\partial \phi \langle \bar{u}_i \rangle}{\partial x_i} = 0 \quad (3.169a)$$

$$\begin{aligned} \frac{\partial \langle \bar{u}_i \rangle}{\partial t} + \langle \bar{u}_i \rangle \frac{\partial \langle \bar{u}_j \rangle}{\partial x_i} = g_i - \frac{1}{\rho} \left(\frac{\partial \langle \bar{p} \rangle}{\partial x_i} + \left\langle \frac{\partial \bar{p}}{\partial x_i} \right\rangle \right) - \frac{1}{\phi} \left(\frac{\partial \phi \langle \bar{u}'_i \bar{u}'_j \rangle}{\partial x_j} + \frac{\partial \phi \langle \tilde{u}_i \tilde{u}_j \rangle}{\partial x_j} \right) \\ + \nu \left(\frac{\partial^2 \langle \bar{u}_i \rangle}{\partial x_j^2} + \left\langle \frac{\partial^2 \tilde{u}_i}{\partial x_j^2} \right\rangle \right) \end{aligned} \quad (3.169b)$$

Figure 3.35 illustrates the time-averaged velocity vectors in gravel-bed flow on the vertical plane of symmetry, obtained by Dey and Das (2012). The near-bed flow heterogeneity is evident from the magnitude, $(\bar{u}^2 + \bar{w}^2)^{0.5}$, and the direction, $\arctan(\bar{w}/\bar{u})$, of the velocity vectors. Within the flow-gravel-bed interface, the flow is slowed down due to a mixing process in presence of gravels, becoming no longer streamwise. An application of the DAM thus demands to characterize the

Fig. 3.36 Variation of normalized DA streamwise velocity $\langle u^+ \rangle$ with η^+ (Dey and Das 2012)



variable nature of time-averaged streamwise velocities representing them to DA velocities on the planes parallel to the virtual bed level.

Figure 3.36 shows the vertical distribution of normalized DA streamwise velocity $\langle u^+ \rangle$. In order to fit the data plots within the wall shear layer ($z > 0$) above the gravel crests to a logarithmic law, the $\langle \bar{u} \rangle$ and the z are scaled by u_* and Δz , respectively, such that $\langle u^+ \rangle = \langle \bar{u} \rangle / u_*$ and $\eta^+ = (z + \Delta z) / \Delta z$, where Δz is the *zero-plane displacement*. To plot the experimental data, one can consider the logarithmic law as expressed in the following form:

$$\langle u^+ \rangle = \frac{1}{\kappa} \ln \left(\frac{\eta^+}{\eta_0^+} \right) \quad (3.170)$$

where $\eta_0^+ = z_0 / \Delta z$ and z_0 is the zero-velocity level. It is clear that to plot the data $\langle u^+ (\eta^+) \rangle$ (Fig. 3.36), a prior estimation of Δz was required to arrange the data set of $\langle u^+ \rangle$ versus η^+ . Also, a subsequent determination of κ and η_0^+ was essential to fit the data to the logarithmic law given by Eq. (3.170). Note that the flow quantities within an angle bracket $\langle \cdot \rangle$ represent the superficial DA quantities (=intrinsic DA $\times \phi$).

Determination of the flow parameters was done independently, as described below:

- Step 1: Having obtained u_* from the $\langle \tau_{xz} \rangle$ distribution by projecting a straight line on the bed surface [see Eq. (3.20)], such that $u_* = (-\langle \overline{u'w'} \rangle)^{0.5} \Big|_{z=0}$, prepare the data set of $\langle u^+ \rangle (= \langle \bar{u} \rangle / u_*)$ corresponding to $\eta^+ [(z + \Delta z) / \Delta z]$ for the analysis.
- Step 2: As an initial trial, assume a very small value of Δz and then determine κ and η_0^+ from Eq. (3.170) by regression analysis. Evaluate the regression coefficient, RC .

Step 3: Increase Δz at a regular interval by a small magnitude (say 0.001) and determine κ and η_0^+ in the same way, as is done in step 2. Check RC for each value of Δz , till RC becomes maximum. Then, the corresponding values of Δz , κ , and z_0 are the determined parameters.

Dey and Das (2012) obtained the logarithmic law of $\langle u^+(\eta^+) \rangle$ within the wall shear layer above the gravel crests ($\eta^+ > 1$) as

$$\langle u^+ \rangle = 2.451 \ln \eta^+ + 4.325 \quad (3.171)$$

On the other hand, the $\langle u^+ \rangle$ distribution within the interfacial sublayer ($\eta^+ \leq 1$) can be represented by a third-degree polynomial series given by

$$\langle u^+ \rangle = 0.421 - 2.905\eta^+ + 12\eta^{+2} - 5.191\eta^{+3} \quad (3.172)$$

A close examination of the data plots for $\eta^+ \leq 1$ reveals that $\langle u^+ \rangle$ has an inflectional distribution due to an effect of the roughness geometry function, resulting from a potential mixing type of flow within the inter-gravel space. The near-invariant $\langle u^+ \rangle$ distribution toward the roughness trough ($\eta^+ \leq 0.3$) is caused by the subsurface flow beneath the gravel-bed. This is the reason why $\langle u^+ \rangle$ distribution below the gravel crests follows a polynomial law.

For a steady-uniform flow over a rough bed, the DA RANS equations provide a new definition for the total DA fluid shear stress $\langle \bar{\tau} \rangle$ in the streamwise direction:

$$\langle \bar{\tau}(z) \rangle = \underbrace{-\rho \langle \tilde{u}\tilde{w} \rangle}_{\langle \tau_f \rangle} \underbrace{-\rho \langle \overline{u'w'} \rangle}_{\langle \tau_{xz} \rangle} + \underbrace{\rho \nu \frac{d\langle \bar{u} \rangle}{dz}}_{\langle \tau_v \rangle} \quad (3.173)$$

where $\langle \tau_f \rangle$ is the DA *form-induced shear stress*, u and w are the instantaneous streamwise and vertical velocity components, respectively, $\langle \tau_{xz} \rangle$ is the spatially averaged Reynolds shear stress, and $\langle \tau_v \rangle$ is the DA viscous shear stress. Therefore, the DAM provides an additional stress term in the form of form-induced shear.

As given by Eq. (3.173), the DA total shear stress $\langle \bar{\tau} \rangle$ is the sum of the spatially averaged Reynolds shear stress $\langle \tau_{xz} \rangle$, DA form-induced shear stress (FISS) $\langle \tau_f \rangle$, and DA viscous shear stress $\langle \tau_v \rangle$. Then, the $\langle \bar{\tau} \rangle$ has to be balanced by the gravity. It has a linear distribution for $\langle \bar{\tau}(\tilde{z} \geq 1) \rangle / (\rho u_*^2) = 1 - \tilde{z}$ [see Eq. (3.20)], where $\tilde{z} = z/h$. The shear stresses are normalized as $\langle \tilde{\tau} \rangle$, $\langle \tilde{\tau}_{xz} \rangle$, $\langle \tilde{\tau}_f \rangle$, $\langle \tilde{\tau}_v \rangle = (\langle \bar{\tau} \rangle, \langle \tau_{xz} \rangle, \langle \tau_f \rangle, \langle \tau_v \rangle) \times (\rho u_*^2)^{-1}$. The variations of $\langle \tilde{\tau} \rangle$, $\langle \tilde{\tau}_{xz} \rangle$, $\langle \tilde{\tau}_f \rangle$, and $\langle \tilde{\tau}_v \rangle$ with \tilde{z} are shown in Fig. 3.37, where the horizontal line immediate below the crest level represents virtual bed level (indicated by $z_1 = 0$) and the next one is the zero-plane displacement (indicated by $z^+ = 0$). The $\langle \tilde{\tau}_{xz} \rangle$ is the governing shear stress across the flow depth. The damping in $\langle \tilde{\tau}_{xz} \rangle$ distribution within the interfacial sublayer occurs due to a reduction in turbulence level (u' and w'). In this sublayer, the decrease in $\langle \tilde{\tau}_{xz} \rangle$ is compensated partially by the appearance of FISS $\langle \tilde{\tau}_f \rangle$, as shown in Fig. 3.37, and both of them are comparable. Moreover, below the crest level,

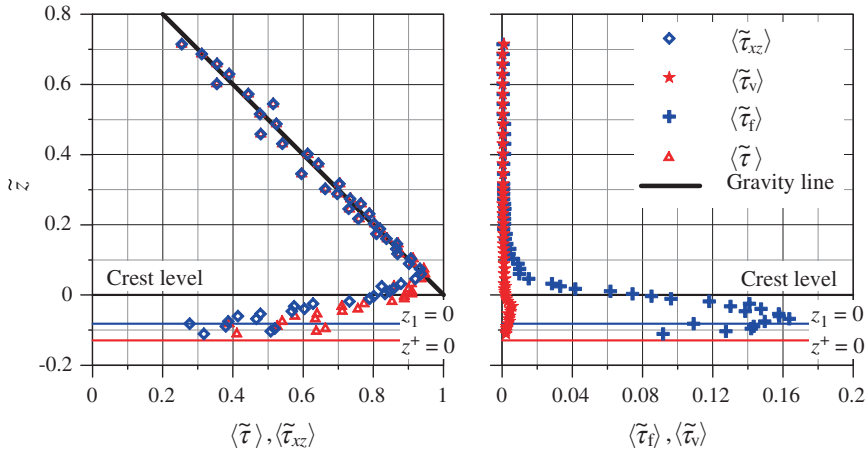


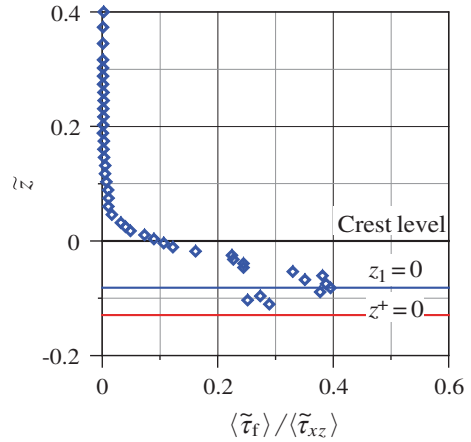
Fig. 3.37 Variations of normalized DA total shear stress $\langle \tilde{\tau} \rangle$, spatially averaged Reynolds shear stress $\langle \tilde{\tau}_{xz} \rangle$, DA form-induced shear stress $\langle \tilde{\tau}_f \rangle$, and DA viscous shear stress $\langle \tilde{\tau}_v \rangle$ with \tilde{z} (Dey and Das 2012)

in addition to the FISS, a form-drag-induced stress is also prevalent (Nikora et al. 2007b), which can be obtained from the integration of the pressure distribution across the frontal face of the gravels. Unfortunately, little progress has so far been made to evaluate the form-drag-induced stress in the flow-gravel-bed interface. However, the $\langle \tilde{\tau}_f \rangle$ remains insignificant above the roughness sublayer and so is $\langle \tilde{\tau}_v \rangle$ over the entire flow depth. Since the $\langle \tilde{\tau}_f \rangle$ and $\langle \tilde{\tau}_v \rangle$ are of negligible magnitude, the data plots of $\langle \tilde{\tau}_{xz} \rangle$ to be the dominant shear stress above the roughness sublayer collapse on the linear gravity line (Fig. 3.37). It is rather convenient to determine the thickness of the form-induced sublayer from the location where the $\langle \tilde{\tau}_f \rangle$ distribution attains a small finite value ($\langle \tilde{\tau}_f \rangle > 0$). In Dey and Das (2012), the thickness of the form-induced sublayer is $0.16h$ or $3.5k_s$. Other criterion to determine this sublayer is the location where the $\langle u^+ \rangle$ distribution departs from the logarithmic law (Nikora et al. 2004). However, it is clear that the form-induced sublayer occurs close to the gravel crests (less than a gravel size above the crest level) based on either criterion. Within the interfacial sublayer, the total shear stress $\langle \tilde{\tau} \rangle$ becomes nonlinear due to its superficial DA value obtained by the product of ϕ (Manes et al. 2007). It is

$$\langle \tilde{\tau} \rangle = \int_{\tilde{z}}^1 \phi d\tilde{z} = 1 + \int_{\tilde{z}}^0 \phi d\tilde{z} + \text{Form-drag-induced stress (nondimensional)}$$

Nikora et al. (2007b) suggested that the form drag together with viscous drag exerted by the fluid on the roughness elements (per unit fluid volume) can be

Fig. 3.38 Variation of the ratio of DA form-induced shear stress to spatially averaged Reynolds shear stress with \tilde{z} (Dey and Das 2012)



calculated as $0.5\rho C_D a_k \langle \bar{u} \rangle^2$, where $C_D(z)$ is the drag coefficient, and a_k is the local roughness density, that is the ratio of the frontal area of roughness elements to the fluid volume. The experimental data of $\langle \tilde{\tau} \rangle (= \langle \tilde{\tau}_{xz} \rangle + \langle \tilde{\tau}_f \rangle + \langle \tilde{\tau}_v \rangle)$ to show the variation with \tilde{z} are depicted in Fig. 3.37. They almost collapse on the gravity line above the gravel crest, while a reduction in $\langle \tilde{\tau} \rangle$ is apparent within the interfacial sublayer. Further if one can consider the fitting of a logarithmic law of $\langle \bar{u} \rangle$, then its applicability is legitimate above the crest level [see Eq. (3.171)]. Apparently, there is a consensus on the damping characteristic in $\langle \tilde{\tau}_{xz} \rangle$ distribution. It initiates from the flow region near the gravel crests located roughly at $\tilde{z} = 1-1.5$, becoming greater within the interfacial sublayer with a decrease in \tilde{z} . Figure 3.37 also elaborates the distribution of FISS $\langle \tilde{\tau}_f \rangle$. The FISS, as the time-averaged flow close to the gravel crests, is spatially heterogeneous, starts developing within the form-induced sublayer, and grows sharply with a decrease in \tilde{z} . Therefore, the FISS along with the form drag is to reduce the flow velocity in this sublayer. Within the interfacial sublayer ($\tilde{z} \leq 0$), the fluid momentum also gets transferred to the gravel voids having a mixing effect in the fluid. The $\langle \tilde{\tau}_f \rangle$ that is considerable for $\tilde{z} \leq 0$ attains a peak above the virtual bed level, and then, it decreases with a further decrease in \tilde{z} .

Figure 3.38 shows the variation of the ratio $\langle \tilde{\tau}_f \rangle / \langle \tilde{\tau}_{xz} \rangle$ with \tilde{z} . The $\langle \tilde{\tau}_f \rangle / \langle \tilde{\tau}_{xz} \rangle$ increases with a decrease in \tilde{z} attaining a peak at the virtual bed level. It is evident that the peak value is $(\langle \tilde{\tau}_f \rangle / \langle \tilde{\tau}_{xz} \rangle)_{\max} \approx 0.4$, as observed by Dey and Das (2012). However, below the virtual bed level, a drastic drop of $\langle \tau_f \rangle$ and $\langle \tau_{xz} \rangle$ results from a reduction in temporal (u' and w') and spatial (\tilde{u} and \tilde{w}) velocity fluctuations, respectively. More specifically, the severe reduction in $\langle \tilde{\tau}_f \rangle / \langle \tilde{\tau}_{xz} \rangle$ in this region is associated with the reduction in $\langle \tau_f \rangle$ (that is, \tilde{u} and \tilde{w}) that occurs more rapidly than that of $\langle \tau_{xz} \rangle$ (that is, u' and w').

3.19 Example

Example 3.1 Determine the depth-averaged momentum equation for the two-dimensional curvilinear turbulent flow on a flat inclined bed with a velocity distribution that follows $1/m$ -th power law.

Solution

Under consideration is a curvilinear flow over a flat rigid bed inclined at an angle θ with the horizontal (Fig. E3.1). The continuity equations in two dimensions are as follows:

$$\frac{\partial \bar{u}}{\partial x} + \frac{\partial \bar{w}}{\partial z} = 0, \quad \frac{\partial u'}{\partial x} + \frac{\partial w'}{\partial z} = 0 \quad (\text{E3.1})$$

The RANS equations in two dimensions take the form as follows:

$$\frac{\partial \bar{u}}{\partial t} + \bar{u} \frac{\partial \bar{u}}{\partial x} + \bar{w} \frac{\partial \bar{u}}{\partial z} = -\frac{1}{\rho} \cdot \frac{\partial \bar{p}}{\partial x} + \frac{1}{\rho} \cdot \frac{\partial \tau_{xz}}{\partial z} + \nu \frac{\partial^2 \bar{u}}{\partial z^2} - \frac{\partial (\overline{u'^2})}{\partial x} + g \sin \theta \quad (\text{E3.2a})$$

$$\frac{\partial \bar{w}}{\partial t} + \bar{u} \frac{\partial \bar{w}}{\partial x} + \bar{w} \frac{\partial \bar{w}}{\partial z} = -\frac{1}{\rho} \cdot \frac{\partial \bar{p}}{\partial z} + \frac{1}{\rho} \cdot \frac{\partial \tau_{xz}}{\partial x} + \nu \frac{\partial^2 \bar{w}}{\partial x^2} - \frac{\partial (\overline{w'^2})}{\partial z} - g \cos \theta \quad (\text{E3.2b})$$

The power law of velocity distribution that is a good replacement of the logarithmic law is as follows:

$$\bar{u} = U_{\max}(x, t) \left(\frac{z}{h} \right)^{1/m} \quad (\text{E3.3})$$

where m is an exponent and $U_{\max} = \bar{u}(z = h)$. Let $h(x, t)$ represent the height of the free surface at a point $(x, 0)$ on the bed. If $U(x, t)$ represents the depth-averaged velocity, then

$$U(x, t) = \frac{1}{h} \int_0^h \bar{u} dz = \frac{U_{\max}}{h^{(1+m)/m}} \int_0^h z^{1/m} dz = \frac{m}{1+m} U_{\max} \quad (\text{E3.4})$$

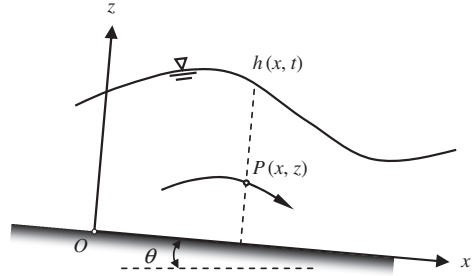
Hence, in terms of U , Eq. (E3.3) can be written as

$$\bar{u} = \frac{1+m}{m} U(x, t) \left(\frac{z}{h} \right)^{1/m} \quad (\text{E3.5})$$

Then, Eq. (E3.1) yields

$$\bar{w} = -h \frac{\partial U}{\partial x} \left(\frac{z}{h} \right)^{(1+m)/m} \quad (\text{E3.6})$$

Fig. E3.1 Definition sketch of a curvilinear flow over a flat inclined bed of an open channel



The streamwise flow is assumed to be gradual having a small curvature, where the streamwise gradient of $h(x, t)$ becomes small, that is, $|\partial h / \partial x| \approx 0$. Moreover, the total normal acceleration $d\bar{w}/dt$ along the curvilinear streamlines is assumed to be predominantly convective so that the local normal acceleration becomes zero ($\partial \bar{w} / \partial t \approx 0$). From Eq. (E3.1), the convective normal acceleration is

$$\bar{u} \frac{\partial \bar{w}}{\partial x} + \bar{w} \frac{\partial \bar{w}}{\partial z} = \bar{u} \frac{\partial \bar{w}}{\partial x} - \bar{w} \frac{\partial \bar{u}}{\partial x} = \bar{u}^2 \frac{\partial(\tan \psi)}{\partial x} = \frac{\bar{u}^2}{r} \sec^3 \psi \approx \frac{\bar{u}^2}{r} \quad (\text{E3.7})$$

where $\psi = \arctan(\bar{w}/\bar{u})$, which is the slope of the streamline through the point $P(x, z)$ being nearly zero (parallel to the free surface) (Fig. E3.1). According to Boussinesq approximation, a linear variation of the streamline curvature with depth z is obtained from Eqs. (2.89) and (2.90):

$$\frac{1}{r} \approx \frac{z}{h} \cdot \frac{\partial^2 h}{\partial x^2} \quad (\text{E3.8})$$

Thus, using Eq. (E3.5) into Eq. (E3.7), the convective normal acceleration is obtained as

$$\bar{u} \frac{\partial \bar{w}}{\partial x} + \bar{w} \frac{\partial \bar{w}}{\partial z} \approx \left(\frac{1+m}{m} \right)^2 U^2 \left(\frac{z}{h} \right)^{(2+m)/m} \frac{\partial^2 h}{\partial x^2} \quad (\text{E3.9})$$

Inserting Eq. (E3.9) into Eq. (E3.2b) and integrating with respect to z yields

$$\bar{p} = p_0 - \rho g(z - h) \cos \theta - \frac{1+m}{2m} \rho U^2 h \left[\left(\frac{z}{h} \right)^{2(1+m)/m} - 1 \right] \frac{\partial^2 h}{\partial x^2} - \rho \overline{w'^2} \quad (\text{E3.10})$$

where $p_0 = \bar{p}(z = h)$. It is assumed that the Reynolds stresses in the streamwise direction are negligible, that is, $\partial \overline{w'^2} / \partial x = 0$. Differentiating Eq. (E3.10) with respect to x produces

$$\frac{\partial \bar{p}}{\partial x} = \rho g \cos \theta \frac{\partial h}{\partial x} - \frac{1+m}{2m} \cdot \frac{\partial}{\partial x} \left\{ \rho U^2 h \left[\left(\frac{z}{h} \right)^{2(1+m)/m} - 1 \right] \frac{\partial^2 h}{\partial x^2} \right\} \quad (\text{E3.11})$$

In order to obtain the equations for h and U , one can consider the continuity equation (Eq. E3.1). At the free surface, $z = h(x, t)$, and thus,

$$\bar{w} = \frac{dh}{dt} = - \int_0^h \frac{\partial \bar{u}}{\partial x} dz = - \frac{\partial(hU)}{\partial x} + \bar{u}(h, t) \frac{\partial h}{\partial x} \quad (\text{E3.12})$$

Hence, the depth-averaged continuity equation is obtained as

$$\frac{\partial h}{\partial t} + \frac{\partial(hU)}{\partial x} = 0 \quad (\text{E3.13})$$

Neglecting the viscous stress term and using Eq. (E3.11) and the condition $\partial \bar{u}^2 / \partial x \approx 0$ into Eq. (E3.2a), the depth-averaged equation is obtained as

$$\int_0^h \left(\frac{\partial \bar{u}}{\partial t} + \bar{u} \frac{\partial \bar{u}}{\partial x} + \bar{w} \frac{\partial \bar{u}}{\partial z} \right) dz = -gh \cos \theta \frac{\partial h}{\partial x} - \gamma \frac{\partial}{\partial x} \left(h^2 U^2 \frac{\partial^2 h}{\partial x^2} \right) - \frac{\tau_0}{\rho} + gh \sin \theta \quad (\text{E3.14})$$

where $\tau_0 = \nu(\partial \bar{u} / \partial z)_{z=0}$. From the Manning equation, τ_0 is $\rho g n^2 U^2 / h^{1/3}$, where n is the Manning coefficient and $\gamma = (1 + m)^2 / [m(2 + 3m)]$. Partially integrating the third term in the left-hand side of Eq. (E3.14) and using Eq. (E3.1), the depth-averaged momentum equation is as follows

$$\frac{\partial(hU)}{\partial t} + \alpha \frac{\partial(hU^2)}{\partial x} + gh \cos \theta \frac{\partial h}{\partial x} + \gamma \frac{\partial}{\partial x} \left(h^2 U^2 \frac{\partial^2 h}{\partial x^2} \right) + \frac{g n^2 U^2}{h^{1/3}} - gh \sin \theta = 0 \quad (\text{E3.15})$$

where $\alpha = (1 + m)^2 / [m(2 + m)]$. Equation (E3.15) can be regarded as the generalized form of *de Saint-Venant equation*, where the variability of \bar{u} is in accordance with $1/m$ -th power law and the curvature of streamlines is included. Using Eq. (E3.13), Eq. (E3.15) can be rewritten as

$$\begin{aligned} \frac{\partial U}{\partial t} + (2\alpha - 1)U \frac{\partial U}{\partial x} + (\alpha - 1) \frac{U^2}{h} \cdot \frac{\partial h}{\partial x} + \gamma U \left[hU \frac{\partial^3 h}{\partial x^3} + 2U \frac{\partial(hU)}{\partial x} \cdot \frac{\partial^2 h}{\partial x^2} \right] \\ + g \cos \theta \frac{\partial h}{\partial x} + \frac{g n^2 U^2}{h^{4/3}} - g \sin \theta = 0 \end{aligned} \quad (\text{E3.16})$$

The above equation was first obtained by Bose and Dey (2007).

References

- Absi R (2011) An ordinary differential equation for velocity distribution and dip-phenomenon in open channel flows. *J Hydraul Res* 49(1):82–89
- Andreopoulos J, Durst F, Zaric Z, Javonovic J (1984) Influence of Reynolds number on characteristics of turbulent wall boundary layers. *Exp Fluids* 2(1):7–16
- Antonia RA, Atkinson JD (1973) High-order moments of Reynolds shear stress fluctuations in a turbulent boundary layer. *J Fluid Mech* 58:581–593
- ASCE Task Force (1963) Friction factor in open channels. *J Hydraul Div* 89(2):97–143
- Bose SK (2009) Numeric computing in Fortran. Narosa, New Delhi
- Bose SK, Dey S (2007) Curvilinear flow profiles based on Reynolds averaging. *J Hydraul Eng* 133(9):1074–1079
- Bose SK, Dey S (2010) Universal probability distributions of turbulence in open channel flows. *J Hydraul Res* 48(3):388–394
- Bradshaw P (1967) Conditions for the existence of an inertial subrange in turbulent flow, Aerodynamics report number 1220. National Physical Laboratory, Teddington
- Camenen B, Bayram A, Larson M (2006) Equivalent roughness height for plane bed under steady flow. *J Hydraul Eng* 132(11):1146–1158
- Cardoso AH, Graf WH, Gust G (1989) Uniform flow in smooth open-channel. *J Hydraul Res* 27(5):603–616
- Choi KS, Lumley JL (2001) The return to isotropy of homogeneous turbulence. *J Fluid Mech* 436:59–84
- Chow VT (1959) Open channel hydraulics. McGraw-Hill Book Company, New York
- Clauser FH (1954) Turbulent boundary layers in adverse pressure gradients. *J Aeronaut Sci* 21(2):91–108
- Colebrook CF, White CM (1937) Experiments with fluid friction in roughened pipes. *Proc R Soc London A* 161(906):367–381
- Coleman NL (1981) Velocity profiles with suspended sediment. *J Hydraul Res* 19(3):211–227
- Coleman NL, Alonso CV (1983) Two-dimensional channel flows over rough surfaces. *J Hydraul Eng* 109(2):175–188
- Coles D (1956) The law of the wake in a turbulent boundary layer. *J Fluid Mech* 1:191–226
- Corino ER, Brodkey RS (1969) A visual investigation of the wall region in turbulent flow. *J Fluid Mech* 37:1–30
- Cramer H (1999) Mathematical methods of statistics. Princeton University Press, Princeton
- Dean RB (1976) A single formula for the complete velocity profile in a turbulent boundary layer. *J Fluids Eng* 98(4):723–726
- Detert M, Weitbrecht V, Jinka GH (2010) Laboratory measurements on turbulent pressure fluctuations in and above gravel beds. *J Hydraul Eng* 136(10):779–789
- Dey S (2003) Incipient motion of bivalve shells on sand beds under flowing water. *J Eng Mech* 129(2):232–240
- Dey S, Das R (2012) Gravel-bed hydrodynamics: a double-averaging approach. *J Hydraul Eng* 138(8):707–725
- Dey S, Das R, Gaudio R, Bose SK (2012) Turbulence in mobile-bed streams. *Acta Geophys* 60(6):1547–1588
- Dey S, Lambert MF (2005) Reynolds stress and bed shear in nonuniform unsteady open-channel flow. *J Hydraul Eng* 131(7):610–614
- Dey S, Raikar RV (2007) Characteristics of loose rough boundary streams at near-threshold. *J Hydraul Eng* 133(3):288–304
- Dey S, Sarkar S, Ballio F (2011) Double-averaging turbulence characteristics in seeping rough-bed streams. *J Geophys Res* 116(F03020), doi:10.1029/2010JF001832
- Dong Z, Wang J, Chen C, Xia Z (1991) Turbulence characteristics of open-channel flows over rough beds. In: Proceedings of the twenty fourth meeting of International Association for Hydraulic Research, Delft, pp C33–C40

- Dyer KR (1986) Coastal and estuarine sediment dynamics. Wiley, Chichester
- Franca MJ, Lemmin U (2009) The simultaneous occurrence of logarithmic and S-shaped velocity profiles in gravel-bed river flows. *Arch Hydro-Eng Environ Mech* 56(1–2):29–41
- Frenkiel FN, Klebanoff PS (1967) Higher order correlations in a turbulent field. *Phys Fluids* 10(3):507–520
- Gad-el-Hak M, Bandyopadhyay PR (1994) Reynolds number effects in wall-bound turbulent flow. *Appl Mech Rev* 47(8):307–365
- Galletti B, Bottaro A (2004) Large-scale secondary structures in duct flow. *J Fluid Mech* 512:85–94
- Galperin B, Kantha LH, Hassid S, Rosati A (1988) A quasi-equilibrium turbulent energy-model for geophysical flows. *J Atmos Sci* 45(1):55–62
- García MH (2008) Sediment transport and morphodynamics. In: García MH (ed) *Sedimentation engineering: processes, measurements, modeling, and practice*, Manuals and reports on engineering practice number 110. American Society of Civil Engineers, Reston, pp 21–163
- Gessner FB (1973) The origin of secondary flow in turbulent flow along a corner. *J Fluid Mech* 58:1–25
- Gradshteyn IS, Ryzhik IM (1980) Table of integrals, series and products. Academic Press, New York
- Grass AJ (1971) Structural features of turbulent flow over smooth and rough boundaries. *J Fluid Mech* 50:233–255
- Grass AJ, Stuart RJ, Mansour-Tehrani M (1991) Vortical structures and coherent motion in turbulent flow over smooth and rough boundaries. *Philos Trans R Soc London A* 336(1640):35–65
- Gross TF, Nowell ARM (1985) Spectral scaling in a tidal boundary layer. *J Phys Oceanogr* 15(5):496–508
- Guo J, Julien PY, Meroney RN (2005) Modified log-wake law for zero-pressure-gradient turbulent boundary layers. *J Hydraul Res* 43(4):421–430
- Haaland SE (1983) Simple and explicit formulas for the friction factor in turbulent flow. *J Fluids Eng* 105(5):89–90
- Head MR, Bandyopadhyay P (1981) New aspects of turbulent boundary-layer structure. *J Fluid Mech* 107:297–338
- Hinze JO (1987) *Turbulence*. McGraw-Hill, New York
- Ikeda S (1981) Self forced straight channels in sandy beds. *J Hydraul Div* 107(4):389–406
- Irwin HPAH (1973) Measurements in a self-preserving plane wall jet in a positive pressure gradient. *J Fluid Mech* 61:33–63
- Jiménez J (2004) Turbulent flows over rough walls. *Ann Rev Fluid Mech* 36:173–196
- Kampé de Fériet J (1966) The Gram-Charlier approximation of the normal law and the statistical description of homogenous turbulent flow near statistical equilibrium, David Taylor model basin report 2013, Naval Ship Research and Development Center, Washington DC
- Keulegan GH (1938) Laws of turbulent flow in open channels. *J Res National Bur Stand* 21(6):707–741
- Kim S-C, Friedrichs CT, Maa JP-Y, Wright LD (2000) Estimating bottom stress in tidal boundary layer from acoustic Doppler velocimeter data. *J Hydraul Eng* 126(6):399–406
- Kirkgöz MS (1989) Turbulence velocity profiles for smooth and rough open-channel flow. *J Hydraul Eng* 115(11):1543–1561
- Kironoto BA, Graf WH (1994) Turbulence characteristics in rough uniform open-channel flow. *Water Marit Energy Proc Inst Civ Eng (London)* 106(4):333–344
- Kline SJ, Reynolds WC, Straub FA, Runstadler PW (1967) The structure of turbulent boundary layers. *J Fluid Mech* 30:741–773
- Kolmogorov AN (1941) The local structure of turbulence in incompressible viscous fluids at very large Reynolds numbers. *Dokl Akad Nauk SSSR* 30:299–303
- Krogstad PÅ, Antonia RA (1999) Surface roughness effects in turbulent boundary layers. *Exp Fluids* 27:450–460

- Lee MK, Eckelman LD, Hanratty TJ (1974) Identification of turbulent wall eddies through the phase relation of the components of the fluctuating velocity gradient. *J Fluid Mech* 66:17–33
- López F, García MH (1999) Wall similarity in turbulent open-channel flow. *J Hydraul Eng* 125(7):789–796
- Lu SS, Willmarth WW (1973) Measurements of the structures of the Reynolds stress in a turbulent boundary layer. *J Fluid Mech* 60:481–511
- Lumley JL (1978) Computational modeling of turbulent flows. *Adv Appl Mech* 18(4):123–176
- Lumley JL, Newman GR (1977) The return to isotropy of homogeneous turbulence. *J Fluid Mech* 82:161–178
- Manes C, Pokrajac D, McEwan I (2007) Double-averaged open-channel flows with small relative submergence. *J Hydraul Eng* 133(8):896–904
- Middleton GV, Southard JB (1984) Mechanics of sediment movement, Short course number 3, 2nd edn, Society of Economic Paleontologists and Mineralogists, Tulsa
- Nakagawa H, Nezu I (1977) Prediction of the contributions to the Reynolds stress from bursting events in open-channel flows. *J Fluid Mech* 80:99–128
- Nakagawa H, Nezu I, Tsujimoto T (1981) Turbulence structure with and without cellular secondary currents over various bed configurations. *Ann, Disaster Prev Res Inst Kyoto Univ* 24B:313–338 (in Japanese)
- Nezu I (1977) Turbulent structure in open channel flow. PhD thesis, Kyoto University, Kyoto
- Nezu I, Azuma R (2004) Turbulence characteristics and interaction between particles and fluid in particle-laden open channel flows. *J Hydraul Eng* 130(10):988–1001
- Nezu I, Nakagawa H (1993) Turbulence in open-channel flows. Balkema, Rotterdam
- Nezu I, Rodi W (1986) Open-channel flow measurements with a laser Doppler anemometer. *J Hydraul Eng* 112(5):335–355
- Nikora V, Goring D (1998) Spectral scaling for gravel-bed open-channel flows. In: Proceedings of the NATO advanced research workshop on stochastic models of hydrological processes and their applications to problems of environmental preservation. Water Problems Institute, Moscow, pp 239–245
- Nikora V, Goring D (2000) Flow turbulence over fixed and weakly mobile gravel beds. *J Hydraul Eng* 126(9):679–690
- Nikora V, Goring D, McEwan I, Griffiths G (2001) Spatially averaged open-channel flow over rough bed. *J Hydraul Eng* 127(2):123–133
- Nikora V, Koll K, McEwan I, McLean S, Dittrich A (2004) Velocity distribution in the roughness layer of rough-bed flows. *J Hydraul Eng* 130(10):1036–1042
- Nikora V, McEwan I, McLean S, Coleman S, Pokrajac D, Walters R (2007a) Double-averaging concept for rough-bed open-channel and overland flows: theoretical background. *J Hydraul Eng* 133(8):873–883
- Nikora V, McLean S, Coleman S, Pokrajac D, McEwan I, Campbell L, Aberle J, Clunie D, Koll K (2007b) Double-averaging concept for rough-bed open-channel and overland flows: applications. *J Hydraul Eng* 133(8):884–895
- Nikuradse J (1933) Strömungsgesetze in rauhen rohren. Verein Deutscher Ingenieure, Forschungsheft 361:1–22
- Nychas SG, Hershey HC, Brodkey RS (1973) A visual study of turbulent shear flow. *J Fluid Mech* 61:513–540
- Offen GR, Kline SJ (1973) Experiments on the velocity characteristics of ‘bursts’ and on the interactions between the inner and outer regions of a turbulent boundary layer. Report MD-31, Department of Mechanical Engineering, Stanford University, Stanford
- Offen GR, Kline SJ (1975) A proposed model of the bursting process in turbulent boundary layers. *J Fluid Mech* 70:209–228
- Perkins HJ (1970) The formation of streamwise vorticity in turbulent flow. *J Fluid Mech* 44:721–740
- Pope SB (2001) Turbulent flows. Cambridge University Press, Cambridge
- Prandtl L (1925) Bericht über untersuchungen zur ausgebildeten turbulenz. *Zeitschrift für Angewandte Mathematik und Mechanik* 5(2):136–139

- Prandtl L (1933) Neuere ergebnisse der turbulenzforschung. *Zeitschrift des Vereines Deutscher Ingenieure* 77(5):105–114
- Prandtl L (1952) *Essentials of fluid dynamics*. Blackie and Son, London
- Raupach MR (1981) Conditional statistics of Reynolds stress in rough-wall and smooth-wall turbulent boundary layers. *J Fluid Mech* 108:363–382
- Reynolds AJ (1974) *Turbulent flows in engineering*. Wiley, London
- Reynolds O (1883) An experimental investigation of the circumstances which determine whether the motion of water shall be direct or sinuous, and the law of resistance in parallel channels. *Philos Trans R Soc London A* 174:935–982
- Reynolds O (1895) On the dynamical theory of incompressible viscous fluids and the deformation of the criterion. *Philos Trans R Soc London A* 186:123–164
- Richardson LF (1922) *Weather prediction by numerical process*. Cambridge University Press, Cambridge
- Robinson SK (1991) Coherent motions in the turbulent boundary layers. *Ann Rev Fluid Mech* 23:601–639
- Rodríguez JF, García MH (2008) Laboratory measurements of 3-D flow patterns and turbulence in straight open channel with rough bed. *J Hydraul Res* 46(4):454–465
- Sarkar S (2010) *Turbulence in loose boundary streams*. PhD thesis, Department of Civil Engineering, Indian Institute of Technology, Kharagpur
- Sarkar S, Dey S (2010) Double-averaging turbulence characteristics in flows over a gravel-bed. *J Hydraul Res* 48(6):801–809
- Schlichting H (1979) *Boundary layer theory*. McGraw-Hill Book Company, New York
- Schlichting H, Gersten K (2000) *Boundary layer theory*. Springer, Berlin
- Simpson RL, Chew YT, Shivaprasad BG (1981) The structure of a separating turbulent boundary layer, part 2: higher-order turbulence results. *J Fluid Mech* 113:53–73
- Smith CR (1996) Coherent flow structures in smooth-wall turbulent boundary layers: facts, mechanisms and speculation. In: Ashworth P, Bennett S, Best JL, McLelland S (eds) *Coherent flow structures in open channels*. Wiley, Chichester, pp 804–813
- Smith CR, Metzler SP (1983) The characteristics of low-speed streaks in the near-wall region of a turbulent boundary layer. *J Fluid Mech* 129:27–54
- Smith JD, McLean SR (1977) Spatially averaged flow over a wavy surface. *J Geophys Res* 82(12):1735–1746
- Song T (1994) *Velocity and turbulence distribution in nonuniform and unsteady open-channel flow*. Doctoral dissertation, Ecole Polytechnique Federale de Lausanne, Lausanne
- Song T, Graf WH, Lemmin U (1994) Uniform flow in open channels with movable gravel bed. *J Hydraul Res* 32(6):861–876
- Soulsby RL, Dyer KR (1981) The form of the near-bed velocity profile in a tidally accelerating flow. *J Geophys Res Oceans Atmos* 86(NC9):8067–8074
- Spalding DB (1961) A single formula for the law of the wall. *J Appl Mech* 28(3):455–458
- Stapleton KR, Huntley DA (1995) Seabed stress determinations using the inertial dissipation method and the turbulent kinetic energy method. *Earth Surf Proc Land* 20(9):807–815
- Steffler PM, Rajaratnam N, Peterson AW (1985) LDA measurements in open channel. *J Hydraul Eng* 111(1):119–130
- Sumer BM, Kozakiewicz A, Fredsøe J, Deigaard R (1996) Velocity and concentration profiles in sheet-flow layer of movable bed. *J Hydraul Eng* 122(10):549–558
- Taylor GI (1935) Statistical theory of turbulence: part I–III. *Proc R Soc London A* 151(873):421–464
- Townsend AA (1976) *The structure of turbulent shear flow*. Cambridge University Press, Cambridge
- Tracy HJ, Lester CM (1961) Resistance coefficients and velocity distribution, smooth rectangular channel, Survey water-supply paper 1592-A. United States Geological, Washington, DC
- van Atta CW, Chen WY (1968) Correlation measurements in grid turbulence using digital harmonic analysis. *J Fluid Mech* 34:497–515
- van Driest ER (1956) On turbulent flow near a wall. *J Aeronaut Sci* 23(10):1007–1011

- van Rijn LC (1984) Sediment transport, part I: bed load transport. *J Hydraul Eng* 110(10):1431–1456
- van Rijn LC (1993) Principles of sediment transport in rivers, estuaries and coastal seas. Aqua Publications, The Netherlands
- Vanoni VA (1975) Sedimentation engineering, ASCE manual number 54. American Society of Civil Engineers, New York
- von Kármán T (1930) Mechanische ähnlichkeit und turbulenz. *Nachrichten von der Gesellschaft der Wissenschaften Göttingen, Mathematisch-Physikalische Klasse* 1:58–76
- Voulgaris B, Trowbridge JH (1998) Evaluation of the acoustic Doppler velocimeter (ADV) for turbulence measurements. *J Atmos Oceanic Technol* 15(1):272–289
- Wang X, Wang ZY, Yu M, Li D (2001) Velocity profile of sediment suspensions and comparison of log-law and wake-law. *J Hydraul Res* 39(2):211–217
- Wilson KC (1987) Analysis of bed-load motion at high shear stress. *J Hydraul Eng* 113(1):97–103
- Yalin MS (1977) *Mechanics of sediment transport*. Pergamon, Oxford
- Yalin MS (1992) *River mechanics*. Pergamon, Oxford
- Yang S-Q, Lim S-Y (1997) Mechanism of energy transportation and turbulent flow in a 3D channel. *J Hydraul Eng* 123(8):684–692
- Yang S-Q, Tan SK, Lim S-Y (2004) Velocity distribution and dip-phenomenon in smooth uniform open channel flows. *J Hydraul Eng* 130(12):1179–1186
- Zhou Y (1993) Interacting scales and energy transfer in isotropic turbulence. *Phys Fluids A* 5(10):2511–2524

Chapter 4

Sediment Threshold

4.1 General

When a stream flow interacts with a loose boundary composed of sediment particles, hydrodynamic force is exerted on the sediment particles forming the boundary (henceforth bed). With an increase in flow velocity, the sediment particles on the bed surface are intermittently entrained at a random rate if the magnitude of the induced hydrodynamic force (drag and lift) acting on the particles exceeds a certain threshold value to overcome the stabilizing force (that is, submerged weight of particles). The condition that is just adequate to initiate sediment motion is termed *threshold condition* or *critical condition* of sediment entrainment. Importantly, the induced bed shear stress of the stream flow in excess of that of the stream flow at threshold condition governs the sediment entrainment mechanism. The threshold of sediment movement at the bed is an important component in studying the management of rivers and channel systems, such as sediment transport, design of stable channels, and preventive measures against erosion.

In 1753, Brahms proposed that the flow velocity required to begin the particle motion is proportional to the particle's weight raised to the power one-sixth. Later, in 1914, Forchheimer explained the influence of sediment gradation, sorting, and armoring on the sediment threshold. The doctoral research study by Shields (1936) on sediment movement carried out at the Technischen Hochschule Berlin, Germany, was a phenomenal contribution (Kennedy 1995). His important finding was his diagram, well known as *Shields diagram*, that represents the variation of nondimensional threshold bed shear stress (or threshold Shields parameter) with shear Reynolds number corresponding to the threshold of sediment entrainment. It is considered to be the reference of any sediment transport research. His pioneering work which is widely applied to the fields has inspired numerous investigators conducting further studies. However, not many attempts were made before Shields (1936), but they were mostly empirical with limited applicability. Despite the fact that the Shields diagram is widely used, even as of today, researchers have identified some limitations (Miller et al. 1977; Mantz 1977; Yalin and Karahan

1979; Buffington 1999), since the diagram less complies with the experimental data plots in the smooth and the rough flow regimes (Yalin and Karahan 1979). Thus, further attempts have so far been made to modify the Shields diagram, conducting additional experiments and analyzing the problem theoretically based on deterministic and probabilistic approaches. Miller et al. (1977), Buffington and Montgomery (1997), Paphitis (2001), and Dey and Papanicolaou (2008) presented a comprehensive survey on this topic. However, after the discovery of the bursting phenomenon in turbulent flow (Kline et al. 1967), it has created a new look to further explore the sediment entrainment problem. The turbulence has so far been introduced as an average like Reynolds shear stress. The conditional statistics toward the bursting events can be the obvious treatment of the sediment entrainment problem, as the most important turbulent events remain implicit with the averaging process. It leads to an open question that to what extent the micro-mechanical processes can be studied in a deterministic framework and when the results can be determined by a probabilistic approach. Therefore, a merger of latest knowledge of turbulence with sediment entrainment theories demands its way to link between a deterministic and a probabilistic approach.

It is worthwhile to mention that the present state of knowledge has been attained progressively, as in all fields of science and technology also in sediment transport. There is no doubt a logical exercise in the development of the subject having governed by the complex phenomena. In fact, a proper understanding of the complex laws of sediment transport requires considerable period of time. In many cases, previous results and theories have been completed and/or modified by later researchers. In some cases, earlier results and theories have become outdated or replaced by now by the new ones, while others with some modifications and refinements remain still applicable.

4.2 Definition of Sediment Threshold

It is always difficult to set a clear definition of the sediment threshold. First type of definition corresponds to the sediment flux. Shields (1936) suggested that the bed shear stress has a value for which the extrapolated *sediment flux* vanishes. On the other hand, USWES (1936) put forward that the tractive force should be such that produces a *general motion* of bed particles. For the median size of sediment less than 0.6 mm, this concept was found to be inadequate. Thus, the general motion was redefined as the sediment in motion should reasonably be represented by all sizes of bed particles, such that the sediment flux should exceed $4.1 \times 10^{-4} \text{ kg s}^{-1} \text{ m}^{-1}$. From the stochastic viewpoint, Paintal (1971) suggested that due to the fluctuating mode of instantaneous velocity, there is no mean bed shear stress below which there is no flux, thus questioning the use of mean bed shear stress to define sediment threshold. However, the threshold condition is defined as the mean bed shear stress that produces a certain minimal amount of sediment flux.

Second type of definition corresponds to the bed particle motion. Kramer (1935) defined four types of bed shear stress conditions for which: (1) No particles are in motion, termed *no transport*, (2) a small number of smallest particles are in motion at isolated zones, termed *weak transport*, (3) many particles of mean size are in motion, termed *medium transport*, and (4) particles of all sizes are in motion at all points and at all times, termed *general transport*. However, Kramer (1935) expressed the difficulties in setting a clear demarcation between these regimes, but defined threshold bed shear stress to be the shear stress that initiates a *general transport*. Vanoni (1964) proposed that the sediment threshold is the condition of the particle motion in every two seconds at any location of the bed. Different threshold definitions that are in use in various studies leading to discrepancies in the data sets and introducing difficulties in making comparisons (Paintal 1971; Buffington and Montgomery 1997).

4.3 Threshold Velocity Concept

A *threshold velocity* or *critical velocity* is a near-bed velocity u_{cr} at the particle level or the average velocity U_{cr} , which is just adequate to start the sediment particle motion for a given size on the bed surface (Fig. 4.1). In principle, use of near-bed velocity for determining the threshold condition is rather uncertain. On the other hand, the idea of using average velocity for describing the threshold condition is apparently logical one, since the average velocity is easy to determine for the given discharge Q and cross-sectional area A of flow. Nevertheless, it does not provide precise results at all, since the average velocity yields an ad hoc estimation toward the threshold condition, while a near-bed velocity or a bed shear stress plays a key role toward the particle movement. For the determination of near-bed and average velocities, it would be required to introduce assumptions concerning the distribution of time-averaged streamwise velocity across the flow depth. Since it is a difficult task to measure the near-bed velocity exactly at the particle level, the magnitudes determined indirectly from the velocity distributions are in no way unambiguous. In this circumstances, defining the near-bed velocity, arbitrary assumptions are essentially introduced. For instance, an extrapolation of the velocity distribution up to the particle level could be one of the potential methods to determine a near-bed velocity, as illustrated in Fig. 4.1.

Numerous papers and reports have been published on the studies using a near-bed velocity u_{cr} at the particle level or an average velocity U_{cr} as a sediment threshold criterion. Here, only some of them are discussed. Goncharov (1964) used the threshold velocity as detachment velocity U_{cr} . It was defined as the lowest average velocity at which individual particles detach from the bed. He gave an equation of U_{cr} as

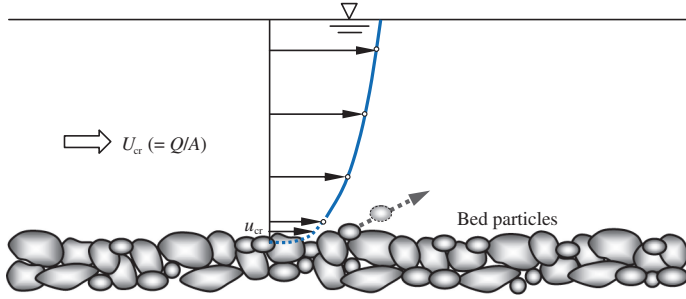


Fig. 4.1 Definition sketch of threshold velocity

$$U_{cr} = 1.07(\Delta g d)^{0.5} \log \left(8.8 \frac{h}{d_{95}} \right) \quad (4.1)$$

where h is the flow depth, d is the representative sediment size, that is the median diameter, g is the acceleration due to gravity, Δ is the submerged relative density ($=s - 1$), s is the relative density of sediment ($=\rho_s/\rho$), ρ_s is the mass density of sediment, and ρ is the mass density of water. Subscript “95” denotes the percentage finer. Similar type of equations having logarithmic term was also put forward by Lavy (1956) as

$$U_{cr} \left(\frac{h}{d_{90}} > 60 \right) = 1.4(gd)^{0.5} \log \left(12 \frac{h}{d_{90}} \right) \quad (4.2a)$$

$$U_{cr} \left(10 < \frac{h}{d_{90}} < 60 \right) = 1.4(gd)^{0.5} \log \left(156.8 \frac{h}{d_{90}} \right) \quad (4.2b)$$

Carstens (1966) proposed an equation of threshold velocity u_{cr} at the particle level by analyzing a large number of experimental data. It is

$$u_{cr} \approx 1.9(\Delta g d)^{0.5} (\tan \phi \cos \theta - \sin \theta)^{0.5} \quad (4.3)$$

where ϕ is the angle of repose of sediment and θ is the angle made by the streamwise bed slope with the horizontal.

Neill (1968) developed a design curve for the initiation of motion of coarse gravels in terms of average velocity U_{cr} as a threshold velocity and expressed as

$$U_{cr} = 1.41(\Delta g d)^{0.5} \left(\frac{h}{d} \right)^{1/6} \quad (4.4)$$

Analyzing large number of data on threshold condition, Garde (1970) proposed equations for hydraulically rough flow as

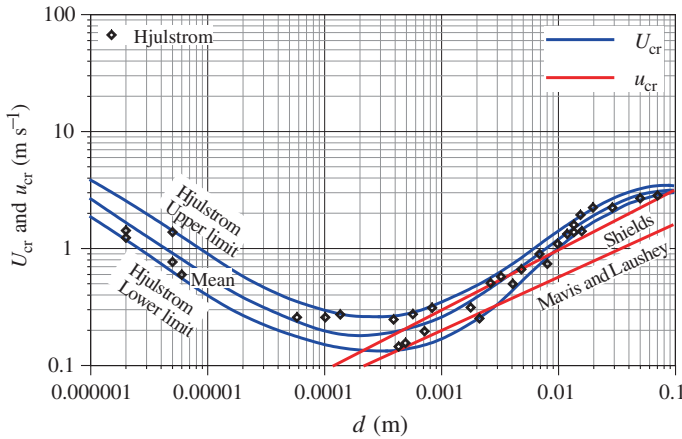


Fig. 4.2 Variations of threshold velocities, U_{cr} and u_{cr} , with median particle size d for quartz sediments (Vanoni 1977)

$$u_{cr} = 1.51(\Delta g d)^{0.5} \quad (4.5a)$$

$$U_{cr} = (\Delta g d)^{0.5} \left(0.5 \log \frac{h}{d} + 1.63 \right) \quad (4.5b)$$

Figure 4.2 shows the plots of threshold velocities (U_{cr} and u_{cr}) as a function of median sediment size d for quartz sediments ($s = 2.65$) obtained from the studies of Hjulström (1935), Shields (1936), and Mavis and Laushey (1966), as demonstrated by the ASCE Sedimentation Task Committee (Vanoni 1977). The data plots $U_{cr}(d)$ and the set of curves having upper, mean, and lower limits are obtained from Hjulström (1935).

The curve of Mavis and Laushey (1966) yields an equation of near-bed threshold velocity u_{cr} as

$$u_{cr} = 3.3\Delta^{0.5}d^{4/9} \quad (4.6)$$

It is obvious that the data of Mavis and Laushey (1966) provides an estimation that is very similar to that obtained from the data of Shields (1936) with a small sift.

Zanke (1977) recommended the following equation:

$$U_{cr} = 2.8(\Delta g d)^{0.5} + 14.7c_1 \left(\frac{v}{d} \right) \quad (4.7)$$

where c_1 is the coefficient varying from 1 for noncohesive to 0.1 for cohesive sediments and v is the coefficient of kinematic viscosity of water. Equations (4.1)–(4.7) are expressed in SI units. Though most of the earlier authors provided valuable

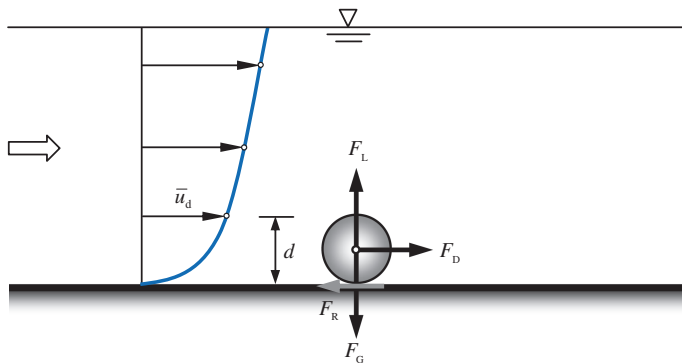


Fig. 4.3 Forces acting on a spherical sediment particle on the bed of an open channel

information regarding threshold velocity, many of them had not clearly reported the exact particle size and the location of the near-bed velocity to be taken. As such, it invites an open question as to what is meant by the threshold velocity at particle level u_{cr} or the threshold average velocity U_{cr} . Thus, the threshold velocity concept has not been categorically welcomed by the community working with sediment transport. This confusion has insisted the researchers to seek a more acceptable standard quantity like the threshold bed shear stress. Nevertheless, Yang's (1973) analytical model for the estimation of U_{cr} seems to be reasonable.

4.3.1 Yang's Threshold Velocity Model

Yang (1973) analyzed the force system on a spherical sediment particle in a stream flow on the bed of an open channel, as shown in Fig. 4.3. The particle is subjected to the hydrodynamic force (drag and lift) induced by the flow. The hydrodynamic drag force F_D is expressed as

$$F_D = C_D \frac{\rho}{2} \bar{u}_d^2 \frac{\pi}{4} d^2 \quad (4.8)$$

where C_D is the drag coefficient and \bar{u}_d is the flow velocity, considered acting at the top (that is at an elevation d from the bed) of the particle, by which the particle is dragged.

The submerged weight F_G of the particle is balanced by the drag force F_D of a falling particle, when the terminal fall velocity w_s of the particle is reached. It was already discussed in Sect. 1.7. Thus, one can write

$$F_G = \frac{\pi}{6} d^3 \Delta \rho g = \underbrace{C_{D1} \frac{\rho}{2} w_s^2 \frac{\pi}{4} d^2}_{F_D} \quad (4.9)$$

where C_{D1} is the drag coefficient at w_s , being assumed as $\psi_1 C_D$. Eliminating C_D from Eqs. (4.8) and (4.9), the drag force is

$$F_D = \frac{\pi}{6 \psi_1 w_s^2} d^3 \Delta \rho g \bar{u}_d^2 \quad (4.10)$$

Considering the law of the wall (logarithmic law) for the velocity distribution, the near-bed velocity \bar{u}_d at the particle level and the depth-averaged velocity U are obtained as:

$$\bar{u}_d = B u_* \quad (4.11a)$$

$$U = u_* \left[5.75 \left(\log \frac{h}{d} - 1 \right) + B \right] \quad (4.11b)$$

where B is the roughness function and u_* is the shear velocity. Using Eqs. (4.11a, b) into Eq. (4.10) yields

$$F_D = \frac{\pi}{6 \psi_1} d^3 \Delta \rho g \left(\frac{U}{w_s} \right)^2 B^2 \left[5.75 \left(\log \frac{h}{d} - 1 \right) + B \right]^{-2} \quad (4.12)$$

The hydrodynamic lift force F_L acting on the particle is given by

$$F_L = C_L \frac{\rho}{2} \bar{u}_d^2 \frac{\pi}{4} d^2 \quad (4.13)$$

where C_L is the lift coefficient, which is related to the drag coefficient as C_D/ψ_2 . Thus, using Eqs. (4.11a, b) into Eq. (4.13) yields

$$F_L = \frac{\pi}{6 \psi_1 \psi_2} d^3 \Delta \rho g \left(\frac{U}{w_s} \right)^2 B^2 \left[5.75 \left(\log \frac{h}{d} - 1 \right) + B \right]^{-2} \quad (4.14)$$

At sediment threshold (when the particle is about to move), the drag force F_D is balanced by the resistance force F_R . Thus, the force balance equation is

$$F_D = F_R = \psi_3 (F_G - F_L) \quad (4.15)$$

where ψ_3 is the friction coefficient. The average velocity U corresponding to threshold condition is denoted by U_{cr} .

Inserting Eqs. (4.9), (4.12) and (4.14) into Eq. (4.15), the equation of threshold average velocity U_{cr} is obtained as

$$\frac{U_{cr}}{w_s} = \left(\frac{\psi_1 \psi_2 \psi_3}{\psi_2 + \psi_3} \right)^{0.5} \left[\frac{5.75}{B} \left(\log \frac{h}{d} - 1 \right) + 1 \right] \quad (4.16)$$

Equation (4.16) is the governing equation defining the threshold condition for sediment motion for a given flow regime. For hydraulically smooth flow regime, $B(0 < R_* < 5) = 5.75 \log R_* + 5.5$ implies that U_{cr}/w_s varies significantly with R_* ; while the relative roughness d/h has little influence. Here, R_* is the shear Reynolds number, that is $u_* k_s / \nu$, u_* is the shear velocity, and k_s is the bed roughness. In contrast, for hydraulically rough flow regime, $B(R_* > 70) = 8.5$ suggests that U_{cr}/w_s is a function of relative roughness d/h only. For the transition regime ($5 \leq R_* \leq 70$), the dependency of B on R_* decreases and d/h increases with an increase in R_* ($R_* > 5$). However, the values of the coefficients (ψ_1 , ψ_2 , and ψ_3) had to be determined experimentally. The laboratory experimental data collected by various investigators were used by Yang (1973) to evaluate the coefficients. He gave the equations for the determination of threshold average velocities for both smooth and rough flows as follows:

$$U_{cr}(0 < R_* < 70) = w_s \left(\frac{2.5}{\log R_* - 0.06} + 0.66 \right) \quad (4.17a)$$

$$U_{cr}(R_* \geq 70) = 2.05 w_s \quad (4.17b)$$

4.4 Lift Force Concept

Einstein (1950), Velikanov (1955), Yalin (1963), Gessler (1966), and Ling (1995) thought that the sediment is entrained solely by the lift force. The lift force can primarily be induced for the following reasons: (1) Sediment particles on the bed surface experience maximum velocity gradient; thus, a lift acts on the particles due to considerable pressure difference, (2) sediment particles may experience lift due to the instantaneous vertical velocity fluctuations in the vicinity of the bed, and (3) the slip-spinning motion of sediment particles may result in lift due to Magnus effect (Dey 1999). Note that if the lift force equals the submerged weight of the particle, then a smallest drag force is adequate to entrain the bed particles. The lift force on a spherical particle is given by Eq. (4.13).

Jeffreys (1929) analyzed a potential flow over a circular cylinder having its axis horizontal and perpendicular to the flow. He argued that the lift to carry the cylinder is prevalent if

$$(3 + \pi^2) U^2 > 9 \Delta g r \quad (4.18)$$

where r is the radius of the cylinder. The drawback of the analysis was that the drag force was ignored. However, to apply the results in analyzing sediment entrainment, modification factors should be accounted for, as a two-dimensional model behaves in a different way from that of a three-dimensional spherical particle in a fluid flow.

Reitz (1936) discussed a similar idea to express the sediment entrainment with a lift criterion, where the circulation and the viscosity were important parameters for his analysis.

Lane and Kalinske (1939) emphasized on the turbulence for quantification of lift. They assumed that (a) the particles experience lift when the instantaneous vertical velocity fluctuations in the vicinity of the bed exceed their terminal fall velocity, (b) the variation of velocity fluctuations follows a normal-error law, and (c) a correlation exists between the velocity fluctuations and the shear velocities.

Experimental study by White (1940) and theoretical analysis by Iwagaki (1956) revealed that the inclusion of lift on the particle does not change its threshold tractive force appreciably and thereby concluded that the lift is of secondary importance.

Einstein and El-Samni (1949) measured the lift force directly as a static pressure difference between the top and the bottom points of hemispheres. They proposed the lift force per unit area f_L as

$$f_L = 0.5C_L\rho\bar{u}_{0.35d}^2 \quad (4.19)$$

where C_L is the lift coefficient assumed as 0.178 and $\bar{u}_{0.35d}$ is the flow velocity at an elevation $0.35d$ from the theoretical bed. They also studied the effects of turbulent fluctuations on lift. The experiments revealed a constant average lift force with superimposed random fluctuations that follow the normal-error law. Their results were used by the Task Committee (1966) of the Journal of Hydraulics Division estimating $f_L/\tau_{0c} \approx 2.5$, where τ_{0c} is the threshold bed shear stress. It suggests that the lift force is an important mechanism toward the threshold of sediment entrainment. However, Chepil (1961) pointed out that once the particle moves, the lift tends to diminish, while the drag increases. Using the experimental results of Emmerling (1973) and Dinkelacker et al. (1977) that the maximum near-bed pressure fluctuations equal 18 times the bed shear stress, Gyr and Hoyer (2006) used the relationship $(\pi d^2/4)18\tau_{0c} = \Delta\rho g(\pi d^3/6)$ to obtain $\tau_{0c} = 0.037\Delta\rho g d$.

Chepil (1961) measured that the lift to drag ratio is about 0.85 for $47 < UD/v < 5 \times 10^3$ in a wind stream on hemispherical roughness having diameter D , while Brayshaw et al. (1983) measured the ratio as 1.8 for the same type of roughness at $R_* = 5.2 \times 10^4$. Aksoy (1973) and Bagnold (1974) found the lift to drag ratio on a sphere of about 0.1 and 0.5 at $R_* = 300$ and 800, respectively. Apperley (1968) studied a sphere laid on gravels and found the lift to drag ratio as 0.5 at $R_* = 70$.

Watters and Rao (1971) observed the negative (downward) lift force on a sphere for $20 < R_* < 100$. Davies and Samad (1978) also reported that the lift force on a sphere adjacent to the bed becomes negative if significant underflow takes place beneath the sphere and the flow condition is $R_* < 5$, while the lift is

positive for $R_* \geq 5$. However, they could not clearly explain the cause of the negative lift force.

While the lift forces obviously contribute to the sediment entrainment, the exact magnitude of lift on a sediment particle is still unclear. Insufficient experimental results are available to determine reliable quantitative relationship for lift; as such, a threshold lift criterion has so far not been obtained which could have been a ready reference for the determination of sediment entrainment. The occurrence of negative lift at low shear Reynolds numbers has been well established, but its cause and magnitude remain uncertain. It was understood that besides the lift, the drag is always prevalent to contribute toward the sediment entrainment. For higher shear Reynolds numbers, the correlation between lift and drag is another uncertain issue, although the lift is certainly positive.

4.5 Threshold Bed Shear Stress Concept

The concept of threshold bed shear stress has been widely applied for the determination of inception of particle motion and seems to provide reasonable results. The origin of this concept lies on the experimental (laboratory and field) or theoretical determination of so-called tractive force per unit area, that is the bed shear stress, given by $\rho g h \tan \theta$. In developing a sediment threshold theory, this concept is based on the analysis of the hydrodynamic force caused by the flowing fluid and the stabilizing force due to submerged weight to formulate the threshold bed shear stress in nondimensional form, termed *threshold Shields parameter*. In doing so, the constants or the coefficients are to be determined experimentally. Therefore, all the analytical models belong to the concept of threshold bed shear stress and are semitheoretical. Besides, there are empirical equations proposed by various investigators. Due to its practical importance, the concept of threshold bed shear stress is discussed here in details.

4.5.1 Empirical Equations

Attempts have been made to correlate the threshold bed shear stress τ_{0c} with sediment properties obtained from the experimental and field measurements. Using the laboratory experimental data, Schoklitsch (1914) recommended an equation as

$$\tau_{0c} = 0.448 \rho g (\Delta S_p d^3)^{0.5} \quad (4.20)$$

where τ_{0c} is in kg m^{-2} , S_p is the Corey shape factor varying from 1 for spherical to 4.4 for flat particles, and d is in m. He worked extensively on sediment transport related issues for 40 years. Later, he refined the estimation of τ_{0c} and

recommended the equation suggested by Krey (1925) for $d \geq 6 \times 10^{-3}$ m and that by him for $10^{-4} \leq d \leq 3 \times 10^{-3}$ m. They are

$$\tau_{0c}(d \geq 6 \times 10^{-3} \text{ m}) = 7.6 \times 10^{-2} \Delta \rho g d \quad (4.21a)$$

$$\tau_{0c}(10^{-4} \leq d \leq 3 \times 10^{-3} \text{ m}) = 2.85 \times 10^{-4} \Delta \rho g d^{1/3} \quad (4.21b)$$

However, the estimation of $\tau_{0c}(3 \times 10^{-3} < d < 6 \times 10^{-3} \text{ m})$ was recommended as a transitional value in between the values obtained from Eqs. (4.21a, b).

Kramer (1935) proposed

$$\tau_{0c} = 29 \left(\frac{\Delta \rho g d}{M} \right)^{0.5} \quad (4.22)$$

where τ_{0c} is in g m^{-2} , M is the Kramer's uniformity parameter, and d is in m. Equation (4.22) is applicable for $0.24 \leq d \leq 6.52 \text{ mm}$ and $0.265 \leq M \leq 1$.

USWES (1936) recommended the following formula:

$$\tau_{0c} = 0.285 \left(\frac{\Delta d}{M} \right)^{0.5} \quad (4.23)$$

where τ_{0c} is in Pa and d is in mm. Equation (4.23) is valid for $0.205 \leq d \leq 4.077 \text{ mm}$ and $0.28 \leq M \leq 0.643$.

A simple equation of τ_{0c} was given by Leliavsky (1966) as

$$\tau_{0c} = 166d \quad (4.24)$$

where τ_{0c} is in g m^{-2} and d is in mm. None of the equations take into account the effects of fluid viscosity. Further, each of these equations produces results that differ from each other. However, these empirical equations estimate the approximate value of τ_{0c} and their use cannot be recommended for the precise estimations.

4.5.2 Semitheoretical Analyses

4.5.2.1 Shields' Approach

Shields (1936) was the pioneer in proposing a semitheoretical method for the entrainment threshold of sediments. He considered that the particles do not move at very low velocity. As the flow velocity increases to a certain value, the driving force on the sediment particles exceeds the stabilizing force, and the sediment particles start to move. The threshold of particle motion is governed by balancing the driving force (that is, drag force, in this case) and the stabilizing resistance.

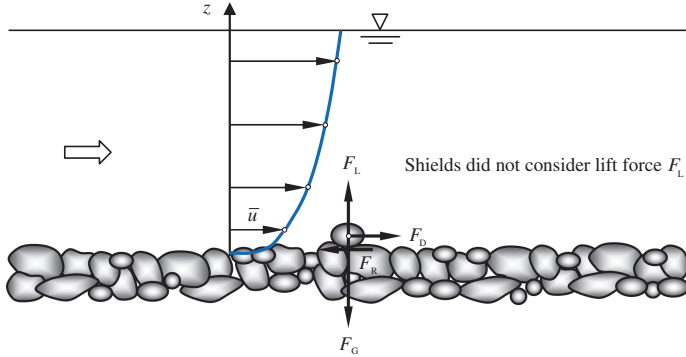


Fig. 4.4 Schematic of a particle subjected to instantaneous hydrodynamic force

Note that Shields neglected the lift force. Figure 4.4 shows a schematic of the force system when a sediment particle is about to move.

The driving force is the drag force F_D due to flow exerted on the sediment particles and is given by

$$F_D = C_D \frac{1}{2} \rho \bar{u}^2 \alpha_1 d^2 \quad (4.25)$$

where \bar{u} is the time-averaged flow velocity at an elevation $z = \alpha_2 d$ and α_1 is the particle shape factor.

The drag coefficient C_D is given by a function of particle shape factor and particle Reynolds number as

$$C_D = f_1 \left(\alpha_1, \frac{\bar{u} d}{\nu} \right) \quad (4.26)$$

Considering the bed roughness height k_s being proportional to d , the logarithmic law of wall for the velocity distribution yields

$$\bar{u} = \frac{u_*}{\kappa} \ln \left(\frac{z}{z_0} \right) = u_* f_2 \left(\alpha_2, \frac{u_* k_s}{\nu} \right) \quad (4.27)$$

where κ is the von Kármán constant (≈ 0.41) and z_0 is the zero-velocity level, that is $0.11(\nu/u_*) + 0.03k_s$.

Using Eqs. (4.26) and (4.27) into Eq. (4.25), the F_D is

$$F_D = \rho u_*^2 d^2 f_3(\alpha_1, \alpha_2, R_*) \quad \wedge \quad R_* = \frac{u_* k_s}{\nu} \quad (4.28)$$

The frictional resistance F_R to particle motion was assumed to be dependent only on the bed roughness and the submerged weight F_G of the particle. That is

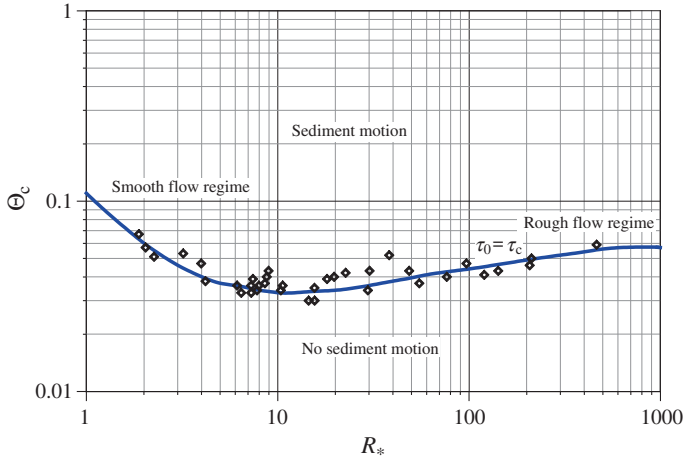


Fig. 4.5 Shields diagram representing threshold Shields parameter Θ_c as a function of shear Reynolds number R_* (Shields 1936)

$$F_R = \alpha_3 \Delta \rho g d^3 \quad (4.29)$$

where α_3 is the frictional coefficient dependent on roughness produced by the bed particles. At the threshold condition, when the sediment particles are about to move, $u_* \rightarrow u_{*c}$ (where u_{*c} is the threshold shear velocity); then, the drag is balanced by the frictional resistance, that is, $F_D = F_R$ (Fig. 4.4). Therefore, rearranging the terms

$$\frac{u_{*c}^2}{\Delta g d} = \frac{\tau_{0c}}{\Delta \rho g d} = f(R_*) \quad \wedge \quad \tau_{0c} = \rho u_{*c}^2 \quad (4.30)$$

The Shields parameter Θ is defined as

$$\Theta = \frac{u_*^2}{\Delta g d} = \frac{\tau_0}{\Delta \rho g d} \quad \wedge \quad \tau_0 = \rho u_*^2 \quad (4.31)$$

where τ_0 is the bed shear stress. Therefore, Eq. (4.30) is expressed as a threshold Shields parameter Θ_c that is

$$\Theta_c = f(R_*) \quad (4.32)$$

The relationship between Θ_c and R_* was determined experimentally.

Figure 4.5, which shows Shields' and others experimental results at incipient motion of different types of bed particles (amber, lignite, granite, barite, and sand) to correlate Θ_c to R_* , is known as *Shields diagram*. The $\Theta_c(R_*)$ curve represents the criterion for the threshold of sediment motion. For a given sediment size, the

flow condition corresponding to the region above the curve represents *sediment motion*, while the region below the curve refers to *no sediment motion*.

The $\Theta_c(R_*)$ curve in Fig. 4.5 depicts three distinct flow regions: (1) hydraulically smooth flow for $R_* \leq 2$: In this region, d is much smaller than the viscous sublayer thickness. The flow is a smooth-viscous. The curve is linearly varying, that is, $\Theta_c = 0.1/R_*$; (2) hydraulically rough flow for $R_* \geq 500$: In this region, the viscous sublayer does not exist. The flow is a rough-turbulent. The threshold Shields parameter Θ_c is invariant of fluid viscosity and is a constant as $\Theta_c = 0.056$; and (3) hydraulically transitional flow for $2 < R_* < 500$: In this region, the sediment particles are of the order of viscous sublayer thickness. There is a minimum value of Θ_c as $\Theta_c(R_* = 12) = 0.032$. Note that Shields did not have data for smooth flow regime ($R_* \leq 2$). The linear variation of the $\Theta_c(R_*)$ curve was an extrapolation.

The shortcomings of the Shields diagram are discussed here. The viscous parameter does not have any effect for $R_* \geq 70$, but Θ_c still varies with R_* in Shields diagram when the latter is greater than seventy. In addition, Shields used the bed shear stress τ_{0c} and the shear velocity u_{*c} in his diagram as dependent and independent variables, which is not appropriate as they are interchangeable. Consequently, τ_{0c} or u_{*c} remains implicit and must be determined by trial and error method.¹ Thus, attempts are made to derive the explicit equations for the Shields diagram, as furnished in Table 4.1. It is already mentioned that Shields neglected lift force in his analysis. Although it was not appropriate, its effect was accounted for implicitly by the process of calibrating the $\Theta_c(R_*)$ curve with the experimental data. Furthermore, the extrapolated portion of $\Theta_c(R_*)$ curve in smooth flow regime does not provide realistic results. Therefore, in later period, Mantz (1977) refined the Shields diagram and gave a relationship $\Theta_c(0.056 < S_* < 3.16) = 0.135S_*^{-0.261}$.

4.5.2.2 White's Approach

White (1940) assumed that the lift force has negligible influence on threshold of particle motion compared to other forces, and hence, it was neglected in his analysis. At limiting equilibrium, the drag force (shear drag) is balanced by the frictional resistance.

White (1940) classified hydraulically transitional and rough flow regimes ($R_* \geq 3.5$), and smooth flow regime ($R_* < 3.5$) in analyzing threshold of particle motion.

¹ Procedure for the determination of threshold shear velocity u_{*c} (or threshold bed shear stress τ_{0c}) by using Shields diagram (Fig. 4.5) for the given d , s , v , and g is as follows:

Step 1: Assume a suitable trial value for u_{*c} (say $u_{*c|trial}$) and then calculate R_{*c} .

Step 2: For R_{*c} , find Θ_c from the Shields diagram (Fig. 4.5) and obtain the new value of $u_{*c|new}$.

Step 3: If $u_{*c|new} \neq u_{*c|trial}$, then retry Step 1 to Step 3 with $u_{*c|new}$, until $u_{*c|new} = u_{*c|trial}$ is obtained.

Table 4.1 Explicit empirical equations for the Shields diagram

References	Equation
Brownlie (1981)	$\Theta_c = 0.22S_*^{-0.6} + 0.06 \exp(-17.77S_*^{-0.6})$, where $S_* = d(\Delta g d)^{0.5}/v$
van Rijn (1984)	$\Theta_c(1 < D_* \leq 4) = 0.24D_*^{-1}$ $\Theta_c(4 < D_* \leq 10) = 0.14D_*^{-0.64}$ $\Theta_c(10 < D_* \leq 20) = 0.04D_*^{-0.1}$ $\Theta_c(20 < D_* \leq 150) = 0.013D_*^{0.29}$ $\Theta_c(D_* > 150) = 0.055$ where D_* is the particle parameter, that is $d(\Delta g/v^2)^{1/3}$
Soulsby and Whitehouse (1997)	$\Theta_c = \frac{0.3}{1 + 1.2D_*} + 0.055[1 - \exp(-0.02D_*)]$
Wu and Wang (1999)	$\Theta_c(D_* < 1.5) = 0.126D_*^{-0.44}$ $\Theta_c(1.5 \leq D_* < 10) = 0.131D_*^{-0.55}$ $\Theta_c(10 \leq D_* < 20) = 0.0685D_*^{-0.27}$ $\Theta_c(20 \leq D_* < 40) = 0.0173D_*^{0.19}$ $\Theta_c(40 \leq D_* < 150) = 0.0115D_*^{0.3}$ $\Theta_c(D_* \geq 150) = 0.052$
Paphitis (2001)	$\Theta_c(0.1 < R_* < 10^4) = \frac{0.273}{1 + 1.2D_*} + 0.046[1 - 0.576 \exp(-0.02D_*)]$ It is the formula for the mean curve of Paphitis (2001)

In hydraulically transitional and rough flow regimes ($R_* \geq 3.5$), high flow velocity is required to move larger sediment particles, where the drag acting on the particle due to skin friction is negligible as compared to that due to pressure difference. The resultant force solely due to pressure difference pierces through the center of gravity of the particle and is directed to the flow direction, as shown in Fig. 4.6. When the particle is about to move, the pivot point is M . If p_f is the packing coefficient defined by Nd^2 , where N is the number of particles per unit area, the shear drag per particle (that is τ_{0c}/N) is given by $\tau_{0c}d^2/p_f$. At limiting equilibrium of a particle resting on the horizontal bed formed by the sediment particles, the shear drag is balanced by the product of the submerged weight F_G of the particle, as given by Eq. (4.9), and the frictional coefficient $\tan\phi$. Therefore, it yields

$$\Theta_c(R_* \geq 3.5) = \frac{\pi}{6} p_f \tan \phi \quad (4.33)$$

White introduced a factor termed *turbulence factor* T_r , which is the ratio of the instantaneous bed shear stress to the mean bed shear stress. Hence, Eq. (4.33) is modified as

Fig. 4.6 Equilibrium of an individual sediment particle in hydraulically transitional and rough flow regimes for shear Reynolds numbers $R_* \geq 3.5$

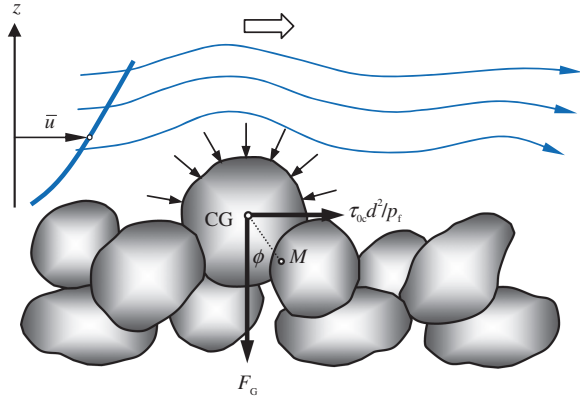
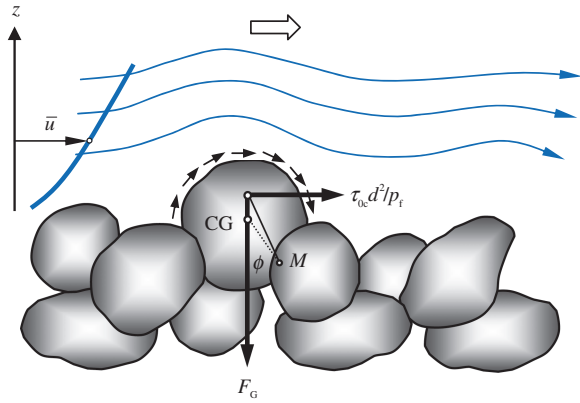


Fig. 4.7 Equilibrium of an individual sediment particle in hydraulically smooth flow regime for shear Reynolds numbers $R_* < 3.5$



$$\Theta_c(R_* \geq 3.5) = \frac{\pi}{6} \cdot \frac{p_f}{T_f} \tan \phi \quad (4.34)$$

He experimentally obtained $p_f = 0.4$ and $T_f = 4$ for fully developed turbulent flow in transitional and rough flow regimes ($33 \leq R_* \leq 1280$) yielding $\Theta_c = 0.044$ with $\phi = 40^\circ$.

In hydraulically smooth flow regime ($R_* < 3.5$), low flow velocity is required to move smaller sediment particles, where the drag due to pressure difference acting on the particle is very small as compared to the viscous force that acts tangentially on the surface of the particle (Fig. 4.7). However, the upper portion of the particle is exposed to the viscous shear drag that acts above the center of gravity of the particle in the streamwise direction, as shown in Fig. 4.7. This effect is taken into account by introducing a coefficient α_f . Therefore, the equation of sediment threshold is

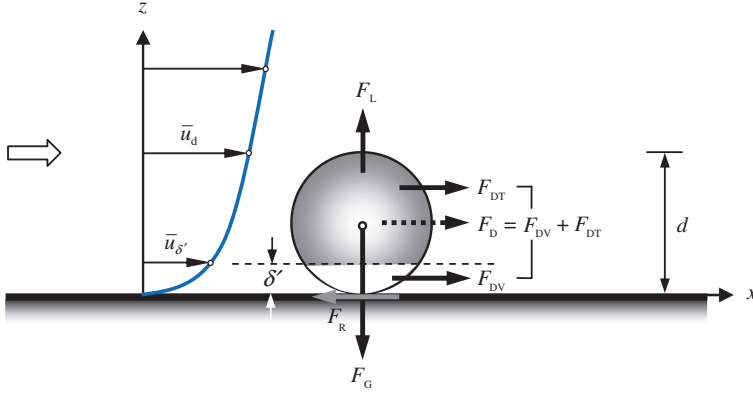


Fig. 4.8 Forces acting on an individual spherical particle resting on a horizontal bed, as considered by Iwagaki (1956)

$$\Theta_c (R_* < 3.5) = \frac{\pi}{6} p_f \alpha_f \tan \phi \quad (4.35)$$

White experimentally obtained $p_f \alpha_f = 0.34$ as an average value. Therefore, Eq. (4.35) yields $\Theta_c = 0.095$ with $\phi = 28^\circ$.

4.5.2.3 Iwagaki's Approach

Iwagaki (1956) analyzed the equilibrium of an isolated spherical particle having diameter d placed on a rough horizontal bed, as shown in Fig. 4.8. He considered the force balance within the flow region dividing into viscous sublayer and turbulent flow regions and obtained the conditions required for the beginning of sediment motion under a unidirectional stream flow.

Considering the viscous sublayer thickness of δ' , the hydrodynamic drag force in the zone of turbulent flow is F_{DT} and that in the viscous sublayer is F_{DV} (Fig. 4.8). Thus, the total drag force is

$$F_D = F_{DV} + F_{DT} \quad (4.36)$$

Introducing a fractional area β_T (projected area) exposed to the turbulent flow, F_{DV} and F_{DT} are given by

$$F_{DV} = C_{DV} \frac{\rho}{2} \bar{u}_{\delta'}^2 \frac{\pi}{4} d^2 (1 - \beta_T) \quad (4.37a)$$

$$F_{DT} = C_{DT} \frac{\rho}{2} \bar{u}_d^2 \frac{\pi}{4} d^2 \beta_T - \frac{\pi}{4} d^2 \beta_T d \left(\frac{\partial p}{\partial x} \right)_d \quad (4.37b)$$

where $\bar{u}_{\delta'}$ and \bar{u}_d are the velocity components in x -direction (streamwise) at $z = \delta'$ and d , respectively, C_{DV} and C_{DT} are the drag coefficients corresponding to $\bar{u}_{\delta'}$ and \bar{u}_d , respectively, and $\partial p / \partial x$ is the piezometric pressure gradient in streamwise direction.

Neglecting the effect of viscosity, Euler equations yield

$$-\left(\frac{\partial p}{\partial x}\right)_d = \rho \left(\frac{du}{dt}\right)_d \quad (4.38)$$

where du/dt is the total acceleration in streamwise direction, u is the instantaneous streamwise velocity component, and t is the time.

Using Eq. (4.38) into Eq. (4.37b), the equation of F_{DT} becomes

$$F_{DT} = C_{DT} \frac{\rho}{2} \bar{u}_d^2 \frac{\pi}{4} d^2 \beta_T + \rho \frac{\pi}{4} d^3 \beta_T \left(\frac{du}{dt}\right)_d \quad (4.39)$$

The hydrodynamic lift force F_L due to piezometric pressure gradient in vertical direction is

$$F_L(\delta' \leq 0.5d) = \frac{\pi}{4} d^2 (d - \delta') \left(\frac{\partial p}{\partial z}\right)_d = -\rho \frac{\pi}{4} d^2 (d - \delta') \left(\frac{dw}{dt}\right)_d \quad (4.40a)$$

$$F_L(\delta' > 0.5d) = \pi \delta' (d - \delta') (d - \delta') \left(\frac{\partial p}{\partial z}\right)_d = -\rho \pi \delta' (d - \delta')^2 \left(\frac{dw}{dt}\right)_d \quad (4.40b)$$

where w is the instantaneous velocity component in z -direction (vertical).

Iwagaki considered the two-dimensional flow on the vertical xz -plane. Neglecting the local acceleration terms and using the Reynolds decomposition for the local instantaneous velocity components as $u = \bar{u} + u'$ and $w = w'$, he expressed du/dt and dw/dt after statistical averaging as

$$\frac{du}{dt} = \bar{u} \sqrt{\left(\frac{\partial u'}{\partial x}\right)^2} + \sqrt{\bar{u}'^2} \sqrt{\left(\frac{\partial u'}{\partial x}\right)^2} + \sqrt{\bar{w}'^2} \frac{d\bar{u}}{dz} + \sqrt{\bar{w}'^2} \sqrt{\left(\frac{\partial u'}{\partial z}\right)^2} \quad (4.41a)$$

$$\frac{dw}{dt} = \bar{u} \sqrt{\left(\frac{\partial w'}{\partial x}\right)^2} + \sqrt{\bar{u}'^2} \sqrt{\left(\frac{\partial w'}{\partial x}\right)^2} + \frac{1}{2} \cdot \frac{d\bar{w}'^2}{dz} \quad (4.41b)$$

where \bar{u} is the time-averaged streamwise velocity component, and u' and w' are the fluctuations of streamwise and vertical velocity components, respectively. The overbar denotes the time-averaged of the velocity fluctuations.

Reverting to the force system, the drag force F_D is balanced by the resistance force F_R at the sediment threshold or limiting equilibrium condition (see Fig. 4.8). Thus, the force balance equation is

$$F_D = F_R = (F_G - F_L) \tan \phi \quad (4.42)$$

For a spherical sediment particle, the F_G is given by Eq. (4.9).

Iwagaki divided three flow regimes depending on the values of shear Reynolds number R_* .

Case 1 ($R_* \leq 6.83$): In this case, the bed particles are submerged in the viscous sublayer. It therefore corresponds to the smooth flow regime; the viscous flow is therefore prevalent in the bed particle vicinity. It implies that $F_{DV} = 0$, $F_L = 0$, and $\beta_T = 0$.

From the velocity distribution for smooth flow regime, it gives

$$\bar{u}_d = u_* \frac{u_* d}{\nu} = u_* R_* \quad \wedge \quad k_s = d \quad (4.43)$$

The drag coefficient C_{DV} is a function of particle Reynolds number $R_d (= \bar{u}_d d / \nu)$:

$$C_{DV} = C_{DV}(R_d) \quad \wedge \quad R_d = R_*^2 \quad (4.44)$$

Therefore, using Eqs. (4.9), (4.37a), (4.43) and (4.44) into Eq. (4.42) for the threshold condition ($u_* \rightarrow u_{*c}$), the threshold Shields parameter Θ_c is expressed as a function of R_* :

$$\Theta_c(R_* \leq 6.83) = \vartheta \tan \phi \cdot f_1(R_*) \quad (4.45)$$

where ϑ is the empirical coefficient. Iwagaki developed the theory for the equilibrium of a single particle on a flat sand-bed. In practice, this situation seldom occurs in the presence of other bed particles. Therefore, the sheltering effect for the target particle is inevitable. This is the reason why the empirical coefficient ϑ was introduced having a value of 2.5 for the range of R_* covered by all three cases.

Case 2 ($R_* \geq 51.1$): In this case, the bed particles are exposed to the main flow, and the viscous sublayer does not exist. It therefore corresponds to the rough flow regime, and the turbulent flow is prevalent in the bed particle vicinity. It implies that $F_{DV} = 0$, $\delta' = 0$, and $\beta_T = 1$. The velocity distribution for rough flow regime is defined by the logarithmic law, given by Eq. (4.27), with a zero-velocity level $z_0 = 0.03d$.

By using transverse correlations and introducing microscales, the expressions for du/dt and dw/dt , in Eqs. (4.41a, b), respectively, are given by

$$\frac{du}{dt} = \frac{\sqrt{2u'^2}}{\lambda_s} \left(\bar{u} + \sqrt{u'^2} \right) + \sqrt{\frac{w'^2}{u'^2}} \frac{d\bar{u}}{dz} + \sqrt{\frac{w'^2}{u'^2}} \sqrt{2 \left(\frac{u'^2}{\lambda_1} \right)^2 + \frac{1}{4} \left(\frac{\partial u'^2}{\partial z} \right)^2} \quad (4.46a)$$

$$\frac{dw}{dt} = \frac{\sqrt{2w'^2}}{\lambda_2} \left(\bar{u} + \sqrt{u'^2} \right) + \frac{1}{2} \cdot \frac{\partial w'^2}{\partial z} \quad (4.46b)$$

Iwagaki hypothesized that the size of the smallest eddies λ_s are responsible for turbulent kinetic energy dissipation. Considering the homogeneous isotropic turbulence, that is, λ ($=\lambda_1 = \lambda_2$), in the flow of wall region, the λ_s is correlated with Taylor microscale λ as

$$\lambda_s = \sqrt{2}\lambda \quad \wedge \quad \lambda = \lambda_0 + 5z \quad (4.47)$$

where λ_0 is the amount of increase in size of the smallest eddies depending on the wall roughness.

Using Prandtl's mixing length theory, the root-mean-square (rms) expressions for the components of velocity fluctuations are given by

$$\sqrt{\overline{u'^2}} = 2l \frac{d\bar{u}}{dz} = 2u_* \quad (4.48a)$$

$$\sqrt{\overline{w'^2}} = l \frac{d\bar{u}}{dz} = u_* \quad (4.48b)$$

where l is the mixing length defining the traversing distance of eddies. Using the logarithmic law given by Eqs. (4.27) and (4.41a) with $z = d$, the \bar{u}_d is

$$\bar{u}_d = \left(\bar{u} + \sqrt{\overline{u'^2}} \right)_{z=d} = 10.5u_* \quad (4.49)$$

Therefore, using above-developed expressions into Eq. (4.42) for the threshold condition ($u_* \rightarrow u_{*c}$), the threshold Shields parameter Θ_c is expressed as a function of R_* :

$$\Theta_c(R_* \geq 51.1) = \vartheta \tan \phi \cdot f_2(R_*) \quad (4.50)$$

The value of $\Theta_c = 0.05$ corresponding to large values of R_* for which Θ_c is independent of R_* .

Case 3 ($6.83 < R_* < 51.1$): In this case, the size of bed particles are in the order of the viscous sublayer thickness. The flow therefore corresponds to the transitional regime, and the effects of both viscous and turbulence are prevalent in the bed particle vicinity. It implies that F_{DV} , F_{DT} , F_L , δ' , and β_T exist. The velocity distribution for transitional regime is obtained from the total shear stress τ equation as follows:

$$\tau = \rho \left(v + l^2 \left| \frac{d\bar{u}}{dz} \right| \right) \frac{d\bar{u}}{dz} \quad (4.51)$$

Iwagaki put $\tau = \tau_0 (= \rho u_*^2)$ on the wall and obtained the differential equation

$$\frac{d\bar{u}}{dz} \left(\frac{d\bar{u}}{dz} > 0 \right) = \frac{1}{2l^2} \left[-v + (v^2 + 4l^2 u_*^2)^{0.5} \right] \quad (4.52)$$

Inserting $l = \kappa z$ and integrating over the limits from δ' to z , Eq. (4.52) yields

$$\bar{u} = \frac{u_*}{\kappa} \left[\frac{1}{R_l} \left(\frac{1}{2} - \sqrt{R_l^2 + \frac{1}{4}} \right) + \ln \left(2R_l + 2\sqrt{R_l^2 + \frac{1}{4}} \right) + R_{\delta'} \right] \quad (4.53)$$

where $R_l = u_* l / v = 0.4(R_z - R_{\delta'})$, $R_z = u_* z / v$, and $R_{\delta'} = u_* \delta' / v$. Therefore, for the threshold condition ($u_* \rightarrow u_{*c}$), the threshold Shields parameter Θ_c is expressed as a function of R_* :

$$\Theta_c(6.83 < R_* < 51.1) = \vartheta \tan \phi \cdot f_3(R_*) \quad (4.54)$$

Equations (4.45), (4.50) and (4.54), when they are expressed in explicit form, are of complicated types and not so convenient to use. So Iwagaki expressed them by empirical curves fitting as

$$\begin{aligned} \Theta_c(S_* \leq 2.14) &= 0.14 \\ \Theta_c(2.14 < S_* \leq 54.2) &= 0.195 S_*^{-7/16} \\ \Theta_c(54.2 < S_* \leq 162.7) &= 0.034 \\ \Theta_c(162.7 < S_* \leq 671) &= 0.195 S_*^{3/11} \\ \Theta_c(S_* > 671) &= 0.05 \end{aligned} \quad (4.55)$$

4.5.2.4 Wiberg and Smith's Approach

Wiberg and Smith (1987) analyzed the force system acting on a sediment particle for the limiting equilibrium of the particle resting over the bed formed by the sediment particles. They obtained the force balance as given by Eq. (4.42).

They expressed the submerged weight of particle F_G , drag force F_D , and lift force F_L as follows:

$$F_G = \Delta \rho g V_d \quad (4.56)$$

$$F_D = C_D \frac{1}{2} \rho \bar{u}^2 A_x = C_D \frac{1}{2} \tau_0 [f^2(z/z_0)] A_x \quad (4.57)$$

$$F_L = C_L \frac{1}{2} \rho (\bar{u}_T^2 - \bar{u}_B^2) A_x = C_L \frac{1}{2} \tau_0 [f^2(z_T/z_0) - f^2(z_B/z_0)] A_x \quad (4.58)$$

where V_d is the volume of the particle, A_x is the frontal area of the particle, \bar{u} is the velocity at an elevation z , \bar{u}_T is the velocity at the top of the particle, \bar{u}_B is the

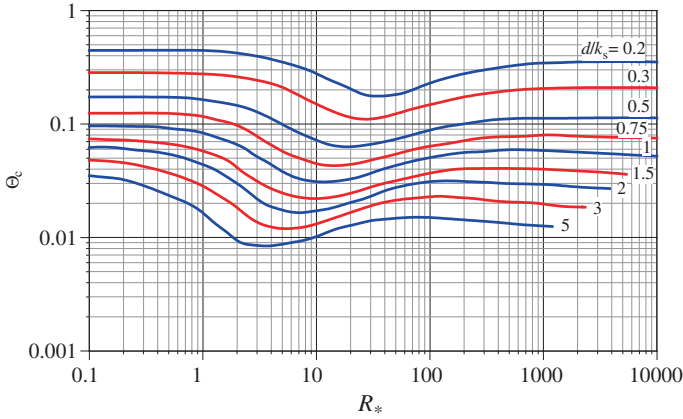


Fig. 4.9 Threshold Shields parameter Θ_c as a function of shear Reynolds number R_* for different ratios of particle size to bed roughness d/k_s (Wiberg and Smith 1987)

velocity at the bottom of the particle, z_T is the height of the top of the particle from the bed, and z_B is the height of the bottom of the particle from the bed. They assumed the bed level passing through the mid-points (the contact points) of the bed particles.

Using Eqs. (4.56)–(4.58) into Eq. (4.42), the expression for Θ_c is obtained as

$$\Theta_c = \frac{2}{C_D \alpha_0} \cdot \frac{1}{f^2(z/z_0)} \cdot \frac{\tan \phi}{1 + (F_L/F_D)_c \tan \phi} \quad (4.59)$$

where $\alpha_0 = A_x d/V_d$. Wiberg and Smith used C_D as a function of particle Reynolds number (Schlichting 1979), and $C_L = 0.2$.

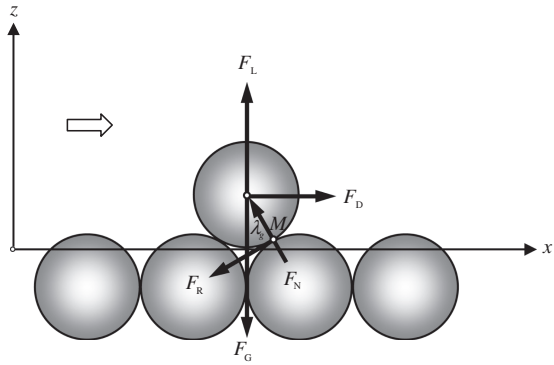
The relation of angle of repose of bed sediment was determined as a function of d/k_s by fitting the experimental data of Miller and Byrne (1966) as $\cos \phi = [(d/k_s) + z_*]/[(d/k_s) + 1]$ for the ratio of particle size to bed roughness $d/k_s > 0.5$. For natural sands, $z_* = -0.02$.

Specific information on velocity distributions for different ranges of R_* is required to solve Eq. (4.59). For smooth flow ($R_* \leq 3$) and transitional flow ($3 < R_* < 100$), Reichardt's (1951) equation of velocity distribution was used, while for rough flow ($R_* \geq 100$), the logarithmic law of velocity distribution [see Eq. (4.27)] was taken into consideration. Reichardt's (1951) equation is given by

$$\bar{u} = \frac{u_*}{\kappa} \left\{ \ln \left(1 + \kappa \frac{z R_*}{k_s} \right) - \left[1 - \exp \left(-\frac{z R_*}{11.6 k_s} \right) - \frac{z R_*}{11.6 k_s} \exp \left(-\frac{z R_*}{11.6 k_s} \right) \right] \ln \left(\kappa \frac{z_0 R_*}{k_s} \right) \right\} \quad (4.60)$$

Solving Eq. (4.59), they prepared $\Theta_c(R_*)$ curves for different ratios of particle size to bed roughness d/k_s , as shown in Fig. 4.9.

Fig. 4.10 Forces acting on a solitary spherical particle resting on bed particles, as considered by Ling (1995)



4.5.2.5 Ling's Approach

Ling (1995) studied the threshold condition of a solitary sediment particle situated on the top of the spherical particles forming the bed. Figure 4.10 shows the schematic of the force system.

On the basis of mechanical and hydrodynamic considerations, two separate criteria for the threshold of sediment motion were derived. They are *rolling threshold criterion* and *lifting threshold criterion*. Regarding the force consideration, the hydrodynamic drag F_D and lift F_L are the destabilizing forces, while the submerged weight F_G of the sediment particle is the stabilizing force. At the point of contact M for rolling, the normal reaction is F_N and the frictional resistance F_R .

Coleman's (1967) analysis of closely packed three-dimensional arrangements of spheres showed that the equation of moment about point M under rolling threshold criterion is as follows:

$$F_D l_z + F_L l_x \geq F_G l_x \quad \wedge \quad l_x = \frac{d}{4\sqrt{3}} \quad \vee \quad l_z = \frac{d}{\sqrt{6}} \quad (4.61)$$

where l_x and l_z are the lever arms. On the other hand, the lifting threshold criterion is prevalent when the lift force just exceeds the submerged weight of the particle to lift the particle off the bed. The equation is therefore

$$F_L \geq F_G \quad (4.62)$$

The hydrodynamic drag force F_D is given by

$$F_D = C_D \frac{\rho}{2} u_r^2 \frac{\pi}{4} d^2 \quad (4.63)$$

where u_r is the relative velocity between the fluid and the solitary particle.

The total lift force F_L is expressed as the sum of the shear lift F_{Ls} (Saffman 1965, 1968), the Magnus lift F_{Lm} (Rubinow and Keller 1961), and the centrifugal lift F_{Lc} . Thus,

$$F_L = F_{Ls} + F_{Lm} + F_{Lc} \quad (4.64)$$

The rolling motion of the solitary particle over the curvature of the bed particle ahead of it induces Magnus lift (due to rolling motion) and centrifugal lift (due to curvilinear motion). The components of the lift force in the right-hand side of Eq. (4.64) are given by

$$F_{Ls} = C_L \rho u_r \left(v \frac{\partial \bar{u}}{\partial z} \right)^{0.5} d^2 \quad (4.65a)$$

$$F_{Lm} = \rho \omega u_r \frac{\pi}{8} d^3 \quad \wedge \quad \omega|_{\max} = \frac{1}{2} \cdot \frac{\partial \bar{u}}{\partial z} \quad (4.65b)$$

$$F_{Lc} = s \rho \frac{\pi}{6} d^3 \cdot \frac{(d\omega)^2}{4d} \cos \lambda_g \quad (4.65c)$$

where \bar{u} is the time-averaged flow velocity in x -direction, ω is the angular velocity, and λ_g is the angle between the normal at the point of contact and the gravity force. The lift coefficient C_L was assumed to be 1.615. Saffman (1965) showed that the maximum angular velocity ω_{\max} achieved by a freely rotating particle driven by the flow is $0.5\partial\bar{u}/\partial z$. The u_r was defined as $u_r = u_f - u_x = \beta u_f$, where u_f is the average fluid velocity across the sphere and u_x is the particle velocity in x -direction. Ling assumed that the solitary particle accelerates from $\omega = 0$ to $0.5\partial\bar{u}/\partial z$. By using $\omega = 2u_x/(d\cos\lambda_g)$. He expressed F_{Ls} , F_{Lm} , and F_{Lc} as

$$F_{Ls} = \beta C_L u_f^+ (\varphi R_*)^{0.5} \tau_0 d^2 \quad (4.66a)$$

$$F_{Lm} = \beta(1 - \beta) \frac{\pi}{4 \cos \lambda_g} u_f^{+2} \tau_0 d^2 \quad (4.66b)$$

$$F_{Lc} = (1 - \beta)^2 \frac{\pi}{6 \cos \lambda_g} u_f^{+2} \tau_0 d^2 \quad (4.66c)$$

where $u_f^+ = u_f/u_*$ and $\varphi = (d/u_*)(\partial\bar{u}/\partial z)$. To maximize β , Eq. (4.64), having inserted expressions for F_{Ls} , F_{Lm} , and F_{Lc} , is differentiated with respect to β . Then,

$$\frac{\partial F_L}{\partial \beta} = 0 \Rightarrow \beta_{\max} = \frac{1}{2} \left(1 + \frac{E_1 - E_3}{E_2 - E_3} \right) \quad (4.67)$$

where $E_1 = C_L u_f^+ (\varphi R_{*d})^{0.5}$, R_{*d} is the shear Reynolds number characterized by $d(=u_*d/\nu)$, $E_2 = (\pi/4)(u_f^{+2}/\cos\lambda_g)$, and $E_3 = (\pi/6)(u_f^{+2}/\cos\lambda_g)$. He considered

$k_s = 3d$, as was done by van Rijn (1984). It implies that $R_* = 3R_{*d}$. Therefore, Eq. (4.64) is written as

$$F_L = [\beta E_1 + \beta(1 - \beta)E_2 + (1 - \beta)^2 E_3] \tau_0 d^2 \quad (4.68)$$

Case 1 ($R_{*d} \leq 1$): In this case, the linear distribution of \bar{u} can be used as given by Eq. (4.43). When the solitary particle rolls over the bed particle ahead of it, its center is raised by an amount $\delta = d(\cos\lambda_g - \cos\lambda_0)$, where $\cos\lambda_0 = 0.8164$, that is, the lowest point of the sphere (solitary particle) resting over three closely packed spheres in a three-dimensional configuration. Then, u_f^+ and φ are

$$u_f^+ = \frac{u_f}{u_*} = \frac{1}{u_*} (u_f|_{z=\delta} + u_f|_{z=d+\delta}) = \frac{R_{*d}}{2} \left(1 + 2\frac{\delta}{d} \right) \quad (4.69a)$$

$$\varphi = \frac{d}{u_*} \cdot \frac{\partial \bar{u}}{\partial z} = R_{*d} \quad \wedge \quad \frac{\partial \bar{u}}{\partial z} = \frac{u_*^2}{v} \quad (4.69b)$$

For $R_{*d} \leq 1$, C_D is

$$C_D(R_{*d} \leq 1) = \frac{24}{R_d} \quad \wedge \quad R_d = \frac{\bar{u}d}{v} \quad (4.70)$$

At the point where the solitary particle begins to roll, $\delta = 0$, $\omega = 0$, and $\beta = 1$. Then,

$$F_D = \frac{3\pi}{2} \tau_0 d^2 \quad (4.71a)$$

$$F_{Ls} = \frac{C_L}{2} R_{*d} \tau_0 d^2 \quad (4.71b)$$

$$F_{Lm} = F_{Lc} = 0 \quad (4.71c)$$

Substituting F_L given by Eq. (4.64), F_G by Eq. (4.7) and Eqs. (4.71a–c) into Eq. (4.61), the rolling threshold criterion is obtained as

$$\Theta_c(R_{*d} \leq 1) = \frac{\pi}{3(C_L R_{*d} + 6\sqrt{2}\pi)} \quad (4.72)$$

For lifting threshold criterion, once the stress reaches the rolling threshold, the solitary particle starts to roll first and then accelerates to its maximum angular velocity ω_{\max} . Finally, the particle lifts up by the shear stress corresponding to lifting threshold by rotating at the ω_{\max} . Setting $\omega = \omega_{\max}$ yields

$$\beta = 1 - \left(\frac{\varphi}{4u_f^+} \right) \cos \lambda_g \quad (4.73)$$

The lifting threshold criterion obtained from Eq. (4.62) with Eq. (4.64) is

$$\Theta_c(R_{*d} \leq 1) = \frac{\pi/6}{\beta E_1 + \beta(1 - \beta)E_2 + (1 - \beta)^2 E_3} \quad (4.74)$$

For estimation of E_1 , E_2 , and E_3 , u_f^+ and φ are obtained from Eqs. (4.69a, b), and $\delta = d(\cos \lambda_g - \cos \lambda_0)$. The estimation revealed that the maximum lift occurs at $\cos \lambda_g = 1$.

Case 2 ($R_{*d} \geq 30$): In this case, the logarithmic law distribution of \bar{u} can be used as given by Eq. (4.27). Thus, the average fluid velocity u_f , being considered equaling u_r due to $u_x \approx 0$, is

$$u_f \approx u_r = \frac{1}{d} \int_{\delta}^{d+\delta} \bar{u} dz = \frac{u_*}{\kappa} \left\{ \left(1 + \frac{\delta}{d} \right) \left[\ln \left(\frac{d+\delta}{z_0} \right) - 1 \right] - \frac{\varepsilon}{d} \left[\ln \left(\frac{\varepsilon}{z_0} \right) - 1 \right] \right\} \quad (4.75)$$

where $\varepsilon = \delta$ or z_0 whichever is larger, and $z_0 = 0.033k_s$. The velocity gradient

$$\frac{\partial \bar{u}}{\partial z} = \frac{1}{d} \int_{\delta}^{d+\delta} \frac{\partial \bar{u}}{\partial z} dz = \frac{\bar{u}_{d+\delta} - \bar{u}_{\varepsilon}}{d} = \frac{u_{*c}}{\kappa d} \left[\ln \left(\frac{d+\delta}{z_0} \right) - \ln \left(\frac{\varepsilon}{z_0} \right) \right] \quad (4.76)$$

Then, u_f^+ and φ are

$$u_f^+ = \frac{u_f}{u_*} = \frac{1}{\kappa} \left\{ \left(1 + \frac{\delta}{d} \right) \left[\ln \left(\frac{d+\delta}{z_0} \right) - 1 \right] - \frac{\varepsilon}{d} \left[\ln \left(\frac{\varepsilon}{z_0} \right) - 1 \right] \right\} \quad (4.77a)$$

$$\varphi = \frac{d}{u_*} \cdot \frac{\partial \bar{u}}{\partial z} = \frac{1}{\kappa} \left[\ln \left(\frac{d+\delta}{z_0} \right) - \ln \left(\frac{\varepsilon}{z_0} \right) \right] \quad (4.77b)$$

The rolling threshold criterion at large shear Reynolds numbers can be obtained by setting $\delta = 0$, $F_{Lm} = F_{Lc} = 0$, and $\beta = 0$ in Eqs. (4.63), (4.64), (4.66a), (4.77a, b) and substituting into Eq. (4.61). Thus,

$$\Theta_c(R_{*d} \geq 30) = \frac{\pi/6}{C_L u_f^+ \left(\frac{\varphi}{R_{*d}} \right)^{0.5} + \frac{\pi}{2\sqrt{2}} C_D u_f^{+2}} \quad (4.78)$$

Ling used the formula of Schiller and Naumann (1933) for obtaining C_D . It is

$$C_D(30 < R_{*d} < 500) = \frac{24}{R_{fd}} (1 + 0.15 R_{fd}^{0.687}) \quad \wedge \quad R_{fd} = \frac{u_f d}{\nu} \quad (4.79)$$

where R_{fd} is the particle Reynolds number characterized by u_f . He used $C_L = 1.48$.

For large shear Reynolds numbers, lifting threshold criterion is given by

$$\Theta_c(R_{*d} \geq 30) = \frac{\pi/6}{\beta E_1 + \beta(1 - \beta)E_2 + (1 - \beta)^2 E_3} \quad (4.80)$$

For estimation of E_1 , E_2 , and E_3 , the expressions for β , u_f^+ , and φ are obtained from Eqs. (4.73), (4.77a, b), respectively. The maximum lift occurs at $\cos \lambda_g = 0.92$.

Case 3 ($1 < R_{*d} < 30$): In this case, Reichardt's (1951) equation for the distribution of \bar{u} is used as given by Eq. (4.60). Therefore, u_f^+ and φ are

$$u_f^+ = \frac{u_f}{u_*} = \frac{1}{d} \int_{\delta}^{d+\delta} \bar{u} dz \quad (4.81a)$$

$$\varphi = \frac{d}{u_*} \cdot \frac{\partial \bar{u}}{\partial z} = \frac{1}{d} \int_{\delta}^{d+\delta} \frac{\partial \bar{u}}{\partial z} dz \quad (4.81b)$$

Therefore, rolling and lifting threshold criteria can be obtained from Eqs. (4.78) and (4.80) for $1 < R_{*d} < 30$. The values of $\cos \lambda_g$ were 1 and 0.92 for $R_{*d} \leq 3$ and $R_{*d} > 3$, respectively.

Figure 4.11 shows two threshold criteria (rolling and lifting) obtained from solving Eqs. (4.72), (4.74), (4.78) and (4.80), and the equations derived from Case 3. The rolling threshold produces the minimum threshold Shields parameter Θ_c required to begin the particle motion, and the lifting threshold provides the minimum stress for the sediments to come in suspension. The comparison of the curves with the experimental data of different investigators makes clear that the main feature of sediment threshold lies in between the curves defining the rolling and lifting threshold criteria. Ling argued that since the experimental definition of a threshold is rather subjective, it might be appropriate to use two threshold criteria rather than one.

4.5.2.6 Dey's Approach

Dey (1999) considered a unidirectional steady-uniform flow over a sedimentary bed. The most stable three-dimensional configuration of a spherical solitary sediment particle of diameter D resting over three closely packed spherical particles of identical diameter d forming the sediment bed is shown in Fig. 4.12.

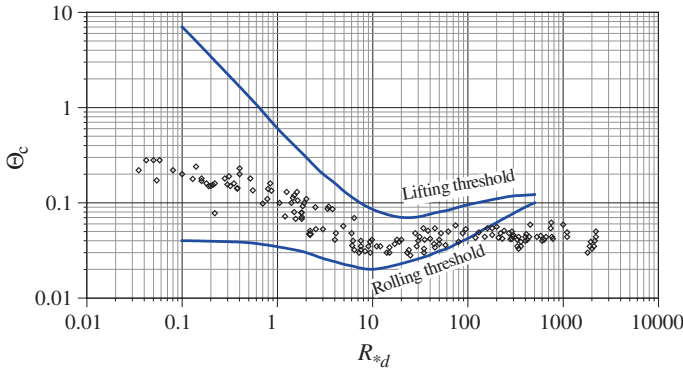


Fig. 4.11 Threshold Shields parameter Θ_c as a function of shear Reynolds number R_{*d} for rolling and lifting threshold criteria (Ling 1995). Experimental data from Gilbert (1914), Casey (1935), Kramer (1935), Shields (1936), USWES (1936), White (1940), Vanoni (1946), Meyer-Peter and Müller (1948), Neill (1967), Grass (1970), White (1970), Karahan (1975), Mantz (1977), and Yalin and Karahan (1979) are plotted for comparison

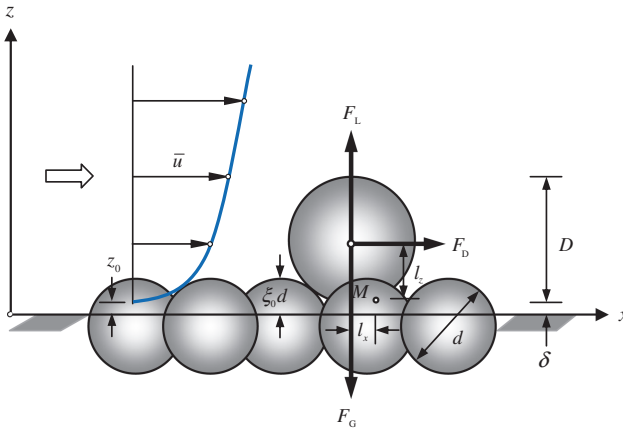


Fig. 4.12 Diagrammatic presentation of forces acting on a spherical solitary particle, as considered by Dey (1999)

Depending on the orientation of the bed particles, the solitary particle has a tendency to either roll over the valley formed by the two particles or roll over the summit of a single particle due to the hydrodynamic force. When the solitary particle is about to dislodge downstream from its original position, the equation of moment about the point of contact M downstream of the solitary particle is

$$(F_L - F_G)l_x + F_D l_z = 0 \quad (4.82)$$

The expressions for the lever arms l_x and l_z given by Dey (1999) [also see Dey et al. (1999)] are

$$l_x = \frac{\sqrt{3}}{4} \cdot \frac{Dd}{D+d} \quad (4.83a)$$

$$l_z = \frac{1}{2\sqrt{3}} \cdot \frac{D}{D+d} (3D^2 + 6Dd - d^2)^{0.5} \quad (4.83b)$$

The submerged weight F_G of the solitary particle is

$$F_G = \frac{\pi}{6} D^3 \Delta \rho g \quad (4.84)$$

The drag force F_D developed due to pressure and viscous skin frictional forces is given by

$$F_D = C_D \frac{\pi}{8} D^2 \rho u_m^2 \quad (4.85)$$

where u_m is the mean flow velocity received by the frontal area (that is, the projected area of the particle to be right angles to the direction of flow) of the solitary particle. The empirical equation of drag coefficient C_D given by Morsi and Alexander (1972) can be expressed as follows:

$$C_D = a + \frac{b}{R} + \frac{c}{R^2} \quad \wedge \quad R = \frac{u_m D}{\nu} \quad (4.86)$$

where R is the flow Reynolds number at the particle level, and a , b , and c are the coefficients dependent on R [see Morsi and Alexander (1972)].

The lift force caused by the velocity gradient in a shear flow is termed *lift due to shear effect* (F_{Ls}). For a sphere in a viscous flow, Saffman (1968) proposed the following equation:

$$F_{Ls} = C_L \rho D^2 u_m \left(\nu \frac{\partial \bar{u}}{\partial z} \right)^{0.5} \quad (4.87)$$

where \bar{u} is the time-averaged flow velocity at z .

For low shear Reynolds numbers R_* , Eq. (4.87) is applicable. However, for large shear Reynolds numbers ($R_* > 3$), the solitary particle spins into the groove, formed by three closely packed bed particles, just before dislodging from its original position due to large velocity gradient (that is, the differential velocity in the vertical direction owing to the considerable velocity difference between the bottom and the top points of the solitary particle) at the particle level (Dey et al. 1999). To

be more explicit, the hydrodynamic force acting on the upper portion of the particle is significantly greater than that acting on the lower portion of the particle, resulting in a turning moment to the particle. Therefore, the inclusion of *slip-spinning mode* is significant in the analysis of the threshold of sediment motion. The lift force caused by the spinning mode of particle is termed *lift due to Magnus effect* (F_{Lm}). Rubinow and Keller (1961) formulated it as

$$F_{Lm} = C_{L1} \rho \omega u_m D^3 \quad \wedge \quad \omega|_{\max} = \frac{1}{2} \cdot \frac{\partial \bar{u}}{\partial z} \quad (4.88)$$

The above formula of Rubinow and Keller was modified by Dey introducing a free parameter (to be experimentally calibrated) as C_{L1} . He argued that the use of a free parameter could give more realistic results; finally, he assumed $C_{L1} = C_L$.

The total lift force F_L , a combination of F_{Ls} and F_{Lm} , is expressed as

$$F_L = C_L \rho D^2 u_m \left(\frac{\partial \bar{u}}{\partial z} \right)^{0.5} \left[v^{0.5} + 0.5 D f(R_*) \left(\frac{\partial \bar{u}}{\partial z} \right)^{0.5} \right] \quad \wedge \quad R_* = \frac{u_* c k_s}{v} \quad (4.89)$$

where $f(R_* \geq 3) = 1$, $f(R_* < 3) = 0$, and R_* is the shear Reynolds number. He assumed $k_s = d$. For low values of R_* ($R_* < 3$), solitary particle does not spin.

Using Eqs. (4.83a)–(4.85) and (4.89) into Eq. (4.82), the equation of the threshold of sediment motion ($u_* \rightarrow u_{*c}$) is obtained as

$$\Theta_c = \frac{2\pi \hat{d}}{\pi C_D u_m^{+2} (3 + 6\hat{d} - \hat{d}^2)^{0.5} + 6C_L \hat{d} u_m^+ \frac{\partial u^+}{\partial \hat{z}} \left[2 \left(\frac{R_*}{\hat{d}} \cdot \frac{\partial u^+}{\partial \hat{z}} \right)^{-0.5} + f(R_*) \right]} \quad (4.90)$$

where $u_m^+ = u_m / u_{*c}$, $\hat{d} = d/D$, $u^+ = \bar{u} / u_{*c}$, and $\hat{z} = z/D$.

The \hat{d} can be determined from the information on angle of repose ϕ of bed sediments by using the expression given by Ippen and Eagleson (1955) for the spherical sediments as

$$\hat{d} = \frac{2 \tan \phi \left[6 \tan \phi + (48 \tan^2 \phi + 27)^{0.5} \right]}{4 \tan^2 \phi + 9} \quad (4.91)$$

The threshold of sediment motion over a sedimentary bed is controlled by the applied instantaneous shear stress at the bed due to turbulent bursting phenomenon. The most important events for the threshold of sediment motion are the sweep events, which have a dominant role in entraining the sediment particles at bed (Dey et al. 2011). The sweep events apply shear to the direction of flow by intruding the faster moving fluid parcels toward the bed and provides additional shear stress to the viscous shear stress. Keshavarzy and Ball (1996) reported that

the magnitude of instantaneous bed shear stress during the sweep events is much larger than the time-averaged bed shear stress. Thus, they proposed the following equation of total shear velocity for rough-turbulent regime:

$$u_{*T} = \left(1 + p_s \sqrt{\alpha_s - 1} \cos \psi\right) u_{*c} = \eta_t u_{*c} \quad (4.92)$$

where u_{*T} is the total shear velocity ($=u_{*c} + u_{*t}$), u_{*t} is the instantaneous shear velocity [$=u_{*c} p_s (\alpha_s - 1)^{0.5} \cos \psi = (\tau_{0t}/\rho)^{0.5}$], τ_{0t} is the instantaneous bed shear stress, p_s is the probability of occurring sweep events, $\alpha_s = \tau_{0t}/\tau_{0c}$, and ψ is the angle of sweeping fluid.

Therefore, the Θ_c calculated from Eq. (4.90) is modified as

$$\Theta_c = \frac{\Theta_c \text{ from Eq. (4.90)}}{\eta_t^2} \quad (4.93)$$

Keshavarzy and Ball (1996) experimentally observed that in the vicinity of the bed, the frequency of sweep events p_s and the sweep angle ψ are 30 % and 22° , respectively. In smooth flow regime, η_t is considered as unity. To solve Eq. (4.93), one needs additional information as discussed below.

The particle parameter S_* is given by $d(\Delta g d)^{0.5}/v$. The following equation is used to compute S_* being related with Θ_c and R_* :

$$S_* = R_* \left(\frac{\hat{d}}{\Theta_c} \right)^{0.5} \quad (4.94)$$

The virtual bed level was considered to be at a depth of $\xi_0 d$ below the top of the bed particles (Fig. 4.12). Thus, the normal distance δ between the virtual bed level and the bottom point of the solitary sediment particle is given by

$$\delta = \frac{1}{2\sqrt{3}} (3D^2 + 6Dd - d^2)^{0.5} - \frac{1}{2} (D + d) + \xi_0 d \quad (4.95)$$

According to van Rijn (1984), $\xi_0 = 0.25$.

The mean flow velocity received by the frontal area of the solitary particle is given by

$$u_m = \frac{2\zeta_d}{A_x} \int_{\varepsilon}^{D+\delta} \bar{u}[(z - \delta)(D + \delta - z)]^{0.5} dz \quad (4.96)$$

where A_x is the frontal area of the solitary particle exposed to the flow, that is $(D^2/4)\{\pi - \arccos(1-2Y) + 2(1-2Y)[Y(1-Y)]^{0.5}\}$, $Y = (\varepsilon - \delta)/D$, ζ_d is the coefficient being less than unity, and ε is the normal distance between the bottom point of the solitary particle or zero-velocity level and the virtual bed level,

whichever is larger. The introduction of ζ_d is pertinent here because the summits of the bed particles upstream of the solitary particle obstruct the flow velocity to a certain degree. It was found that the value of ζ_d being 0.5 produced satisfactory results.

The normalized mean velocity u_m^+ is therefore obtained as

$$u_m^+ = \frac{2\zeta_d}{\hat{A}_x} \int_{\hat{\varepsilon}}^{1+\hat{\delta}} u^+ [(\hat{z} - \hat{\delta})(1 + \hat{\delta} - \hat{z})]^{0.5} d\hat{z} \quad (4.97)$$

where $\hat{A}_x = A_x/D^2$, $\hat{\delta} = \delta/D$, and $\hat{\varepsilon} = \varepsilon/D$.

The velocity gradient $\partial\bar{u}/\partial z$ can be obtained as follows:

$$\frac{\partial\bar{u}}{\partial z} = \frac{1}{D + \delta - \varepsilon} \int_{\varepsilon}^{D+\delta} \frac{\partial\bar{u}}{\partial z} dz = \frac{\bar{u}_{D+\delta} - \bar{u}_{\varepsilon}}{D + \delta - \varepsilon} \quad (4.98)$$

Thus, the normalized velocity gradient $\partial u^+/\partial\hat{z}$ is given by

$$\frac{\partial u^+}{\partial\hat{z}} = \frac{u_{1+\hat{\delta}}^+ - u_{\hat{\varepsilon}}^+}{1 + \hat{\delta} - \hat{\varepsilon}} \quad (4.99)$$

Case 1 ($R_* \leq 3$): When the flow is hydraulically smooth, it can be assumed that the velocity distribution of the near-bed flow is solely linear, as given by Eq. (4.43). Thus, the mean flow velocity u_m^+ obtained using Eq. (4.97) is

$$u_m^+ = \frac{2\zeta_d R_*}{\hat{A}_x \hat{d}} \int_{\hat{\varepsilon}}^{1+\hat{\delta}} [(\hat{z} - \hat{\delta})(1 + \hat{\delta} - \hat{z})]^{0.5} \hat{z} d\hat{z} \quad (4.100)$$

where $\hat{\varepsilon} = 0$ if $\hat{\delta} \leq 0$, and $\hat{\varepsilon} = \hat{\delta}$ if $\hat{\delta} > 0$.

The velocity gradient determined using Eq. (4.99) is

$$\frac{\partial u^+}{\partial\hat{z}} = \frac{R_*}{\hat{d}} \quad (4.101)$$

Case 2 ($R_* \geq 70$): When the flow over a sedimentary bed is completely rough, the logarithmic velocity distribution in rough flow regime can be used as given by Eq. (4.27). The mean flow velocity u_m^+ derived using Eq. (4.97) is

$$u_m^+ = \frac{2\zeta_d}{\kappa \hat{A}_x} \int_{\hat{\varepsilon}}^{1+\hat{\delta}} [(\hat{z} - \hat{\delta})(1 + \hat{\delta} - \hat{z})]^{0.5} \ln\left(\frac{\hat{z}}{\hat{z}_0}\right) d\hat{z} \quad (4.102)$$

The velocity gradient can be determined using Eq. (4.99) as

$$\frac{\partial u^+}{\partial \hat{z}} = \frac{1}{\kappa(1 + \hat{\delta} - \hat{\varepsilon})} \ln \left(\frac{1 + \hat{\delta}}{\hat{\varepsilon}} \right) \quad (4.103)$$

Case 3 ($3 < R_* < 70$): The range of shear Reynolds number $3 \leq R_* \leq 70$ refers to transitional regime. The equation of the velocity distribution for transitional regime proposed by Reichardt (1951) can be used. It is given by Eq. (4.60). The mean flow velocity u_m^+ is determined using Eq. (4.97) as

$$u_m^+ = \frac{2\zeta_d}{\kappa \hat{A}_x} \int_{\hat{\varepsilon}}^{1+\hat{\delta}} [(\hat{z} - \hat{\delta})(1 + \hat{\delta} - \hat{z})]^{0.5} \left\{ \ln \left(1 + \frac{\kappa \hat{z} R_*}{\hat{d}} \right) - \left[1 - \exp \left(-\frac{\hat{z} R_*}{11.6 \hat{d}} \right) - \frac{\hat{z} R_*}{11.6 \hat{d}} \exp \left(-\frac{\hat{z} R_*}{3 \hat{d}} \right) \right] \ln \left(\frac{\kappa \hat{z}_0 R_*}{\hat{d}} \right) \right\} d\hat{z} \quad (4.104)$$

where $\hat{\varepsilon} = \hat{z}_0$ if $(\hat{z}_0 - \hat{\delta}) \geq 0$, and $\hat{\varepsilon} = \hat{\delta}$ if $(\hat{z}_0 - \hat{\delta}) < 0$.

The velocity gradient obtained using Eq. (4.99) is

$$\begin{aligned} \frac{\partial u^+}{\partial \hat{z}} = & \frac{1}{\kappa(1 + \hat{\delta} - \hat{\varepsilon})} \left\{ \ln \left[1 + \frac{\kappa(1 + \hat{\delta}) R_*}{\hat{d}} \right] - \ln \left(1 + \frac{\kappa \hat{\varepsilon} R_*}{\hat{d}} \right) \right\} \\ & + \frac{1}{\kappa(1 + \hat{\delta} - \hat{\varepsilon})} \left\{ \exp \left[-\frac{(1 + \hat{\delta}) R_*}{11.6 \hat{d}} \right] - \exp \left(-\frac{\hat{\varepsilon} R_*}{11.6 \hat{d}} \right) \right. \\ & \left. + \frac{(1 + \hat{\delta}) R_*}{11.6 \hat{d}} \exp \left[-\frac{(1 + \hat{\delta}) R_*}{3 \hat{d}} \right] - \left(\frac{\hat{\varepsilon} R_*}{11.6 \hat{d}} \right) \exp \left(-\frac{\hat{\varepsilon} R_*}{3 \hat{d}} \right) \right\} \ln \left(\frac{\kappa \hat{z}_0 R_*}{\hat{d}} \right) \end{aligned} \quad (4.105)$$

Simpson rule can be applied to solve Eqs. (4.100), (4.102) and (4.104).

As the exact expression for the lift coefficient C_L was not available, Eq. (4.93) was required to be calibrated extensively. The experimental data (Θ_c and R_*) on sediment threshold reported by Gilbert (1914), Casey (1935), Kramer (1935), Shields (1936), USWES (1936), White (1940), Vanoni (1946), Meyer-Peter and Müller (1948), Iwagaki (1956), Neill (1967), Grass (1970), White (1970), Karahan (1975), Mantz (1977), and Yalin and Karahan (1979) were used to calibrate Eq. (4.93), using C_L as a free parameter. The negative values of C_L for low range of R_* (≤ 3) were obtained, as reported by Watters and Rao (1971) and Davies and Samad (1978) [see Dey et al. (1999)]. The dependency of Θ_c on particle parameter S_* for different values of ϕ is presented in Fig. 4.13, which enables a direct estimation of u_{*c} . The curve for $\phi = 28^\circ$ refers to the uniform sediment size.

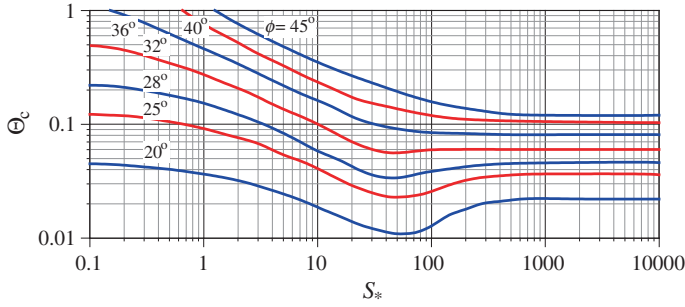


Fig. 4.13 Threshold Shields parameter Θ_c as a function of particle parameter S_* for different angles of repose ϕ

4.5.2.7 Other Investigations

Kurihara (1948) extended the work of White (1940) to obtain an expression for turbulence factor T_f in terms of R_* , turbulence intensity, and probability of bed shear stress increment. The theoretical equations were quite complex. So he proposed simpler empirical equations of Shields parameter as

$$\begin{aligned}\Theta_c(\chi_2 \leq 0.1) &= (0.047 \log \chi_2 - 0.023)\beta_2 \\ \Theta_c(0.1 < \chi_2 \leq 0.25) &= (0.01 \log \chi_2 + 0.034)\beta_2 \\ \Theta_c(\chi_2 > 0.25) &= (0.0517 \log \chi_2 + 0.057)\beta_2\end{aligned}\quad (4.106)$$

where $\chi_2 \approx 4.67 \times 10^{-3}[\Delta g/(v^2 \beta_2)]^{1/3}d$ and $\beta_2(0.265 \leq M \leq 1) = (M + 2)/(1 + 2M)$.

Egiazaroff (1965) gave yet another derivation for $\Theta_c(R_*)$. He assumed that the velocity at an elevation of $0.63d$ (above the bottom of particle) equals the fall velocity w_s of the particle. He derived an equation as

$$\Theta_c = \frac{1.33}{C_D[B_r + 5.75 \log(0.63)]^2} \quad (4.107)$$

where $B_r = 8.5$ and $C_D = 0.4$ for large R_* . Both B_r and C_D increase for low R_* . His results did not correspond to the Shields diagram.

Mantz (1977) proposed the *extended Shields diagram* to obtain the condition of maximum stability of sediment particles (Fig. 4.14). Yalin and Karahan (1979) presented a $\Theta_c(R_*)$ curve, using a large number of data collected from literature (Fig. 4.14). The $\Theta_c(R_*)$ curve provides $\Theta_c(R_* > 70) = 0.045$. Their curve is regarded as a superior curve to the Shields diagram.

Cao et al. (2006) derived a set of explicit equations for the curve of Yalin and Karahan (1979). It is

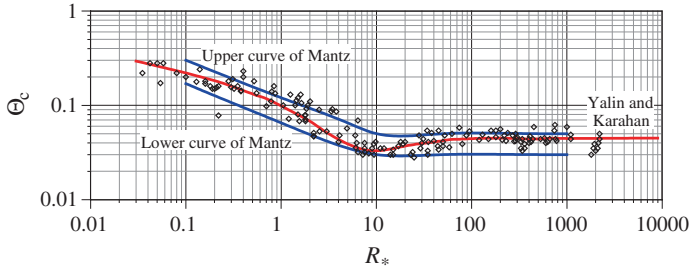


Fig. 4.14 The $\Theta_c(R_*)$ curves of Mantz (1977) and Yalin and Karahan (1979). Experimental data from Gilbert (1914), Casey (1935), Kramer (1935), Shields (1936), USWES (1936), White (1940), Vanoni (1946), Meyer-Peter and Müller (1948), Neill (1967), Grass (1970), White (1970), Karahan (1975), Mantz (1977), and Yalin and Karahan (1979) are plotted for comparison

$$\begin{aligned}\Theta_c(S_* \leq 6.61) &= 0.1414S_*^{-0.23} \\ \Theta_c(6.61 < S_* < 282.84) &= \frac{[1 + (0.0223S_*)^{2.84}]^{0.35}}{3.09S_*^{0.68}} \\ \Theta_c(S_* \geq 282.84) &= 0.045\end{aligned}\quad (4.108)$$

The analysis of Ikeda (1982) that was based on Iwagaki (1956) and Coleman (1967) could approximately derive the Shields diagram. He considered the forces acting on a solitary particle placed on a sediment bed and obtained an equation as follows:

$$\Theta_c = \frac{4}{3} \cdot \frac{\tan \phi}{(C_D + C_L \tan \phi)} \cdot \left\{ \frac{10.08}{R_*^{10/3}} + \left[\frac{1}{\kappa} \ln \left(1 + \frac{4.5R_*}{1 + 0.3R_*} \right) \right]^{-10/3} \right\}^{0.6} \quad (4.109)$$

Zanke (2003) developed a theory for the sediment threshold. He assumed that the threshold bed shear stress τ_{0c} for the initial motion in viscous flow is solely defined by the angle of internal friction ϕ or the angle of repose ϕ_1 of single particles. In turbulent flow, the fluctuations τ'_0 in the bed shear stress as well as the lift forces are induced by the velocity fluctuations. Hence, the actual (effective) threshold bed shear stress $\tau_0 + \tau'_0$ acting on a particle is greater than the average bed shear stress τ_0 . On the other hand, the effective weight of the particles is reduced. On the basis of Zanke's analytical formulation, the threshold of sediment motion can be described solely by the angle of repose of particles and the turbulence parameters. He derived the equation for sediment threshold as

$$\Theta_c = \frac{0.7 \tan(0.67\phi)}{\left[1 + 1.8 \frac{(\overline{u'^2})^{0.5} \Big|_{z=k_s}}{u_{*c}} \cdot \frac{u_{*c}}{u_{cr}} \right]^2 \left\{ 1 + 0.4 \tan(0.67\phi) \left[1.8 \frac{(\overline{u'^2})^{0.5} \Big|_{z=k_s}}{u_{*c}} \right]^2 \right\}} \quad (4.110)$$

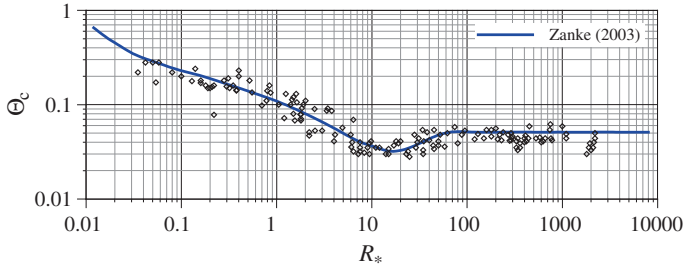


Fig. 4.15 Threshold Shields parameter Θ_c as a function of shear Reynolds number R_* (Zanke 2003). Experimental data from Gilbert (1914), Casey (1935), Kramer (1935), Shields (1936), USWES (1936), White (1940), Vanoni (1946), Meyer-Peter and Müller (1948), Neill (1967), Grass (1970), White (1970), Karahan (1975), Mantz (1977), and Yalin and Karahan (1979) are plotted for comparison

where $(\overline{u^2})^{0.5} \Big|_{z=k_s}$ is the turbulence intensity or the root mean square of streamwise velocity fluctuations at bed level and u_{cr} is the streamwise velocity at the bed level. They can be obtained from the following equations:

$$\frac{(\overline{u^2})^{0.5} \Big|_{z=k_s}}{u_{*c}} = 0.31R_* \exp(-0.1R_*) + 1.8 \exp\left(-0.88 \frac{d}{h}\right) [1 - \exp(-0.1R_*)] \quad (4.111a)$$

$$\frac{u_{cr}}{u_{*c}} = 0.8 + 0.9 \frac{u \Big|_{z=k_s}}{u_{*c}} \quad (4.111b)$$

Figure 4.15 shows the dependency of threshold Shields parameter Θ_c on shear Reynolds number R_* obtained solving Eq. (4.110) by using Eqs. (4.111a, b). The comparison of the $\Theta_c(R_*)$ curve with the experimental data of different investigators shows a good agreement.

4.5.3 Threshold Bed Shear Stress on Sloping Beds

Most of the natural riverbeds have slopes. To quantify scour and deposition of sediments along a river and its banks or to design a stable channel section, knowledge of the threshold bed shear stress on streamwise and side slopes is indispensable. Unlike the case of sediment threshold on a horizontal bed, the gravity component of the sediment particles is involved in the force analysis of sediment threshold on a sloping bed.

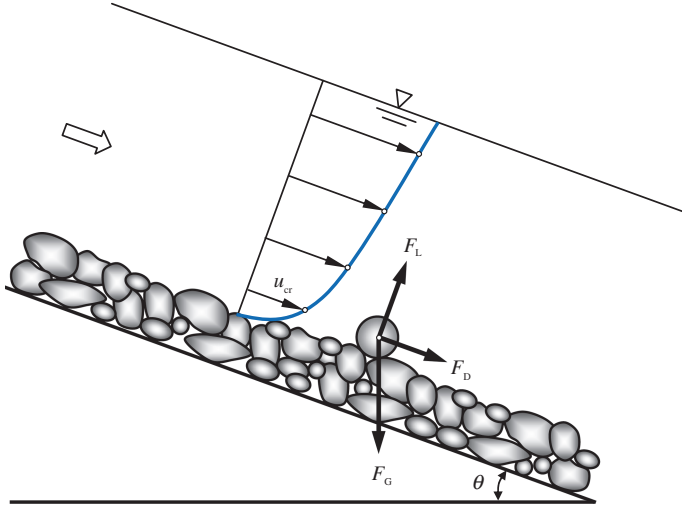


Fig. 4.16 Forces acting on a sediment particle lying on a streamwise bed slope

4.5.3.1 Threshold Bed Shear Stress on a Streamwise Sloping Bed

Considering flow over a streamwise sloping sediment bed that is inclined at an angle θ with the horizontal, Fig. 4.16 illustrates the forces acting on a sediment particle lying on the bed slope. At sediment threshold, the force balance in the streamwise direction yields

$$\tan \phi = \frac{F_G \sin \theta + F_D}{F_G \cos \theta - F_L} \quad (4.112)$$

In the above, $F_G = \Delta \rho g k_1 d^3$, $F_D = C_D \rho k_2 d^2 u_{cr}^2$, $F_L = C_L \rho k_2 d^2 u_{cr}^2$, u_{cr} is the threshold velocity at the particle level being approximated as $u_{*c\theta} / \lambda_f^{0.5}$, $u_{*c\theta}$ is the threshold shear velocity on streamwise sloping bed, and λ_f is the friction parameter.

Substituting them into Eq. (4.112), the equation of threshold Shields parameter $\Theta_{c\theta} [= u_{*c\theta}^2 / (\Delta g d)]$ on streamwise sloping bed is obtained as

$$\Theta_{c\theta} = K (\tan \phi \cos \theta - \sin \theta) \quad \wedge \quad K = \frac{k_1 \lambda_f}{k_2} \cdot \frac{1}{C_D + C_L \tan \phi} \quad (4.113)$$

For the horizontal bed ($\theta = 0$), the equation of the threshold Shields parameter $\Theta_c [= u_{*c}^2 / (\Delta g d)]$ obtained from Eq. (4.113) is

$$\Theta_c = K \tan \phi \quad (4.114)$$

Dividing Eq. (4.113) by Eq. (4.114), the ratio of threshold bed shear stress on any streamwise sloping bed to that on horizontal bed is obtained. It is

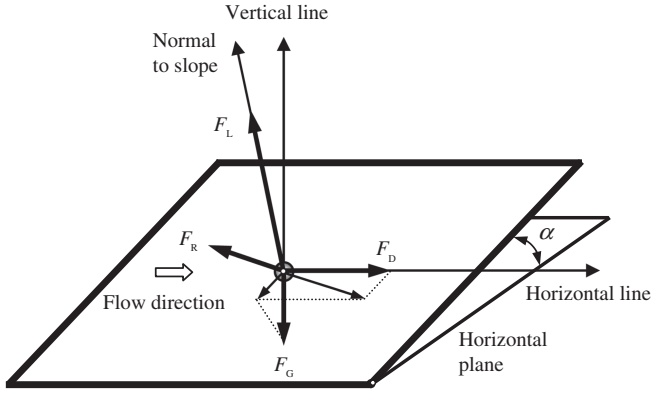


Fig. 4.17 Forces acting on a sediment particle lying on a side slope

$$\tilde{\Theta}_{c\theta} = \frac{\Theta_{c\theta}}{\Theta_c} = \frac{\tau_{0c\theta}}{\tau_{0c}} = \frac{u_{*c\theta}^2}{u_{*c}^2} = \cos \theta \left(1 - \frac{\tan \theta}{\tan \phi} \right) \quad (4.115)$$

where $\tau_{0c\theta}$ is the threshold bed shear stress on streamwise sloping bed.

For the threshold bed shear stress on a streamwise sloping bed, Eq. (4.115) was obtained by various investigators (Stevens et al. 1976; Fernandez Luque and van Beek 1976; Allen 1982; Whitehouse and Hardisty 1988; Chiew and Parker 1994; Iversen and Rasmussen 1994; Dey et al. 1999; Dey and Debnath 2000).

4.5.3.2 Threshold Bed Shear Stress on a Side Slope

Ikeda (1982) considered the flow in a channel having a side sloping bed that is inclined at an angle α with the horizontal. Figure 4.17 illustrates the forces acting on a sediment particle lying on the side slope. At sediment threshold, the force balance relationship is given by

$$F_R^2 = F_D^2 + (F_G \sin \alpha)^2 \quad (4.116)$$

where F_R is the resultant force on the plane of the bed equaling the frictional resistance between the particle and the bed at threshold.

The frictional resistance is balanced by the effective normal force component to the sloping bed multiplied by the bed friction coefficient, $\tan \phi$. Then,

$$F_R = (F_G \cos \alpha - F_L) \tan \phi \quad (4.117)$$

Using Eq. (4.9) of F_G , a quadratic equation of threshold Shields parameter $\Theta_{c\alpha}$ [= $u_{*c\alpha}^2/(\Delta g d)$, where $u_{*c\alpha}$ is the threshold shear velocity on side slope] on a side slope is obtained as

$$\hat{F}_D^2(1 - \eta^2 \tan^2 \phi) \Theta_{c\alpha}^2 + 2\hat{F}_D \eta \tan^2 \phi \cos \alpha \Theta_{c\alpha} + \sin^2 \alpha - \tan^2 \phi \cos^2 \alpha = 0 \quad (4.118)$$

where $\eta = F_L/F_D$ and $\hat{F}_D = 6F_D/(\pi \rho d^2 u_{*c\alpha}^2)$.

The positive solution of $\Theta_{c\alpha}$ obtained from Eq. (4.118) is

$$\Theta_{c\alpha} = \frac{1}{\hat{F}_D} \cdot \frac{-\eta \tan^2 \phi \cos \alpha + (\tan^2 \phi \cos^2 \alpha + \eta^2 \tan^2 \phi \sin^2 \alpha - \sin^2 \alpha)^{0.5}}{1 - \eta^2 \tan^2 \phi} \quad (4.119)$$

For horizontal bed ($\alpha = 0$), the equation of Shields parameter Θ_c [= $u_{*c}^2/(\Delta g d)$] obtained from Eq. (4.119) is

$$\Theta_c = \frac{1}{\hat{F}_D} \cdot \frac{\tan \phi}{1 + \eta \tan \phi} \quad (4.120)$$

Dividing Eq. (4.119) by Eq. (4.120), the ratio of threshold bed shear stress on any side slope to that on horizontal bed is obtained. It is denoted by $\tilde{\Theta}_{c\alpha}$ [= $\Theta_{c\alpha}/\Theta_c = \tau_{0c\alpha}/\tau_{0c} = u_{*c\alpha}^2/u_{*c}^2$, where $\tau_{0c\alpha}$ is the threshold bed shear stress on side slope].

Hence, $\tilde{\Theta}_{c\alpha}$ is expressed as

$$\tilde{\Theta}_{c\alpha} = \frac{-\eta \tan^2 \phi \cos \alpha + (\tan^2 \phi \cos^2 \alpha + \eta^2 \tan^2 \phi \sin^2 \alpha - \sin^2 \alpha)^{0.5}}{(1 - \eta \tan \phi) \tan \phi} \quad (4.121)$$

Assuming a negligible F_L ($\eta = 0$) at the threshold condition, Eq. (4.121) becomes

$$\tilde{\Theta}_{c\alpha}(\eta = 0) = \cos \alpha \left(1 - \frac{\tan^2 \alpha}{\tan^2 \phi} \right)^{0.5} = \left(1 - \frac{\sin^2 \alpha}{\sin^2 \phi} \right)^{0.5} \quad (4.122)$$

The above equation is exactly the same as that derived by Lane (1955) and Chow (1959).

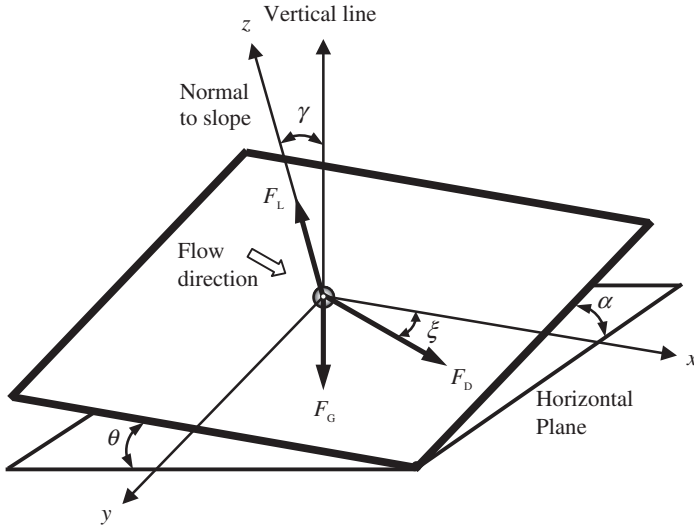


Fig. 4.18 Forces acting on a sediment particle lying on an arbitrary bed slope. The xy -plane lies on the sloping bed, and z -axis is normal to the sloping bed

4.5.3.3 Threshold Bed Shear Stress on an Arbitrary Bed Slope

Figure 4.18 represents definition sketch of forces acting on a spherical sediment particle placed on a bed having an arbitrary bed slope. When the particle is about to move downstream from its original position, the equation of force balance is

$$F_R^2 = (F_D \cos \xi + F_G \sin \theta)^2 + (F_D \sin \xi + F_G \sin \alpha)^2 \quad (4.123)$$

where F_R is the resultant force on the plane of the bed equaling frictional resistance between the particle and the bed at threshold, θ is the streamwise bed angle with the horizontal, α is the transverse bed (side sloping bed) angle with the horizontal, and ξ is the angle of inclination of flow with respect to the longitudinal axis of the channel (positive downstream).

The static frictional resistance F_R between the particle and the bed is

$$F_R = (F_G \cos \gamma - F_L) \tan \phi \quad \wedge \quad \cos \gamma = \frac{1}{(1 + \tan^2 \theta + \tan^2 \alpha)^{0.5}} \quad (4.124)$$

where γ is the angle between the line normal to the bed slope and the vertical line. Equating Eqs. (4.123) and (4.124) and expressing in nondimensional form, one gets a quadratic equation as

$$(1 - \eta^2 \tan^2 \phi) \Theta_{cs}^2 + \frac{2}{\hat{F}_D} (\zeta_1 + \eta \cos \gamma \tan^2 \phi) \Theta_{cs} + \frac{1}{\hat{F}_D^2} (\zeta_2 - \cos^2 \gamma \tan^2 \phi) = 0 \quad (4.125)$$

where $\eta = F_L/F_D$, Θ_{cs} is the threshold Shields parameter on an arbitrary sloping bed, that is $u_{*cs}^2/(\Delta g d)$ or $\tau_{0cs}/(\Delta \rho g d)$, u_{*cs} is the threshold shear velocity on an arbitrary sloping bed, that is $(\tau_{0cs}/\rho)^{0.5}$, τ_{0cs} is the threshold bed shear stress on an arbitrary sloping bed, $\hat{F}_D = 6F_D/(\pi \rho d^2 u_{*cs}^2)$, $\zeta_1 = \cos \xi \sin \theta + \sin \xi \sin \alpha$, and $\zeta_2 = \sin^2 \theta + \sin^2 \alpha$. The value of η proposed by Chepil (1958) was 0.85.

The positive solution of Eq. (4.125) is

$$\Theta_{cs} = \frac{1}{(1 - \eta^2 \tan^2 \phi) \hat{F}_D} \left\{ -(\zeta_1 + \eta \cos \gamma \tan^2 \phi) + \left[(\zeta_1 + \eta \cos \gamma \tan^2 \phi)^2 - (1 - \eta^2 \tan^2 \phi)(\zeta_2 - \cos^2 \gamma \tan^2 \phi) \right]^{0.5} \right\} \quad (4.126)$$

For horizontal bed, θ and α become zero and Eq. (4.126) reduces to Eq. (4.120).

Dividing Eq. (4.126) by Eq. (4.120), the ratio of threshold bed shear stress on any arbitrary bed slope to that on horizontal bed is obtained as

$$\tilde{\Theta}_{cs} = \frac{\Theta_{cs}}{\Theta_c} = \frac{\tau_{0cs}}{\tau_{0c}} = \frac{u_{*cs}^2}{u_{*c}^2} = \frac{1}{(1 - \eta \tan \phi) \tan \phi} \left\{ -(\zeta_1 + \eta \cos \gamma \tan^2 \phi) + \left[(\zeta_1 + \eta \cos \gamma \tan^2 \phi)^2 - (1 - \eta^2 \tan^2 \phi)(\zeta_2 - \cos^2 \gamma \tan^2 \phi) \right]^{0.5} \right\} \quad (4.127)$$

However, in general, the flow through a river or a channel is in the longitudinal direction (x -direction). Therefore, the equation of $\tilde{\Theta}_{cs}$ for this type of flow can be obtained by putting $\xi = 0$ in Eq. (4.127) as

$$\tilde{\Theta}_{cs}(\xi = 0) = \frac{1}{(1 - \eta \tan \phi) \tan \phi} \left\{ -\left(\sin \theta + \frac{\eta \tan^2 \phi}{\sqrt{\sec^2 \theta + \tan^2 \alpha}} \right) + \sqrt{\left(\sin \theta + \frac{\eta \tan^2 \phi}{\sqrt{\sec^2 \theta + \tan^2 \alpha}} \right)^2 - (1 - \eta^2 \tan^2 \phi) \left(\sin^2 \theta + \sin^2 \alpha - \frac{\tan^2 \phi}{\sec^2 \theta + \tan^2 \alpha} \right)} \right\} \quad (4.128)$$

For longitudinal bed slope, using $\alpha = 0$, Eq. (4.128) reduces to Eq. (4.115). On the other hand, for transverse bed slope, using $\theta = 0$ and $\eta = 0$, Eq. (4.128) reduces to Eq. (4.122).

Again, van Rijn (1993) and Dey (2004) proposed that the threshold bed shear stress on an arbitrary sloping bed can be obtained from the following equation:

$$\tilde{\Theta}_{cs} = \tilde{\Theta}_{c\theta} \tilde{\Theta}_{c\alpha} = \cos \theta \left(1 - \frac{\tan \theta}{\tan \phi} \right) \left(1 - \frac{\sin^2 \alpha}{\sin^2 \phi} \right)^{0.5} \quad (4.129)$$

Further, Kovacs and Parker (1994) developed a vectorial equation of sediment threshold on an arbitrary sloping bed. Including lift force, its analytical form as a quadratic equation was given by Seminara et al. (2002). It is

$$\begin{aligned} \tan^2 \phi (1 - \vartheta_L) \Theta_{cs}^2 + 2 \tan \phi (\sin \theta + \vartheta_L \cos \gamma \tan^2 \phi) \Theta_{cs} \\ + (1 + \vartheta_L)(1 - \cos^2 \gamma - \tan^2 \phi) = 0 \end{aligned} \quad (4.130)$$

where ϑ_L is the parameter quantifying the effect of lift force being approximately equal to $\eta \tan \phi$.

Besides, Calantoni and Drake (1999) used the following equation to develop a discrete particle model with an arbitrary sloping bed:

$$\tilde{\Theta}_{cs} = \cos \theta \left[\left(1 - \frac{\sin^2 \alpha}{\sin^2 \phi} \right)^{0.5} - \frac{\tan \theta}{\tan \phi} \right] \quad (4.131)$$

On the other hand, Duan et al. (2001) and Duan and Julien (2005) used the following equation:

$$\tilde{\Theta}_{cs} = \frac{\sin(\phi - \theta)}{\tan \phi} \left(1 - \frac{\sin^2 \alpha}{\sin^2 \phi} \right)^{0.5} \quad (4.132)$$

Both Eqs. (4.131) and (4.132) are expressed after additional simplification. In addition, Dey (2003) proposed an approximate estimation for $\tilde{\Theta}_{cs}$, while Zhang et al. (2005) and Chen et al. (2010) formulated $\tilde{\Theta}_{cs}$ without considering the effect of lift force.

4.6 Probabilistic Concept of Entrainment

The sediment entrainment is probabilistic in nature. It depends primarily on the turbulence characteristics in conjunction with the location of a specific particle relative to the surrounding particles of various sizes and their orientations. In addition, the compactness of the bed particles plays a role. The entrainment mechanism is also governed by the instantaneous strength of turbulence induced by the near-bed velocity fluctuations. The concept therefore gives rise to the time-averaged condition that there is a fifty percent probability for a given particle to move under the specific flow and sediment conditions.

4.6.1 Gessler's Approach

Gessler (1970) estimated the probability for the particles of a specific size to remain stationary. It was revealed that the probability of a given particle to remain stationary depends strongly on the Shields parameter Θ and feebly on the shear Reynolds number R_* . Assuming the Reynolds decomposition for the bed shear stress ($\tau_{0t} = \tau_0 + \tau'_0$), he considered if $\tau_{0t} < \tau_{0c}$ or $\tau_0^{'+} < \tau_{0c}^+ - 1$, then the sediment cannot move. Here, τ_{0t} is the instantaneous bed shear stress, τ_0 is the time-averaged bed shear stress, τ'_0 is the fluctuations of τ_{0t} with respect to τ_0 , $\tau_0^{'+} = \tau'_0/\tau_0$ and $\tau_{0c}^+ = \tau_{0c}/\tau_0$. From the experimental evidences, the $\tau_0^{'+}$ can be directly related to the probability that a sediment particle stays and therefore used to determine the particle size distribution of the retained sediment particles. The probability p_{st} of sediment particles to stay is

$$p_{st} = \frac{1}{\sigma_{\tau_0^{'+}} \sqrt{2\pi}} \int_{-\infty}^{\tau_{0c}^+ - 1} \exp\left(\frac{\tau_0^{'+2}}{-2\sigma_{\tau_0^{'+}}^2}\right) d\tau_0^{'+} \quad (4.133)$$

where $\sigma_{\tau_0^{'+}}$ is the standard deviation of $\tau_0^{'+}$. For coarse sediments, $\sigma_{\tau_0^{'+}}$ is approximately 0.57. Note that the p_{st} varies with the particle size d . For known maximum and minimum sizes of sediment particles of a bed sediment sample being d_{\max} and d_{\min} , respectively, the retained fraction of the sediment having a size less than d is given by

$$P_0(d) = \int_{d_{\min}}^d p_0(d) dd \quad (4.134)$$

where $p_0(d)$ is the frequency function of the original distribution. The particle size frequency of the retained sediment particles is

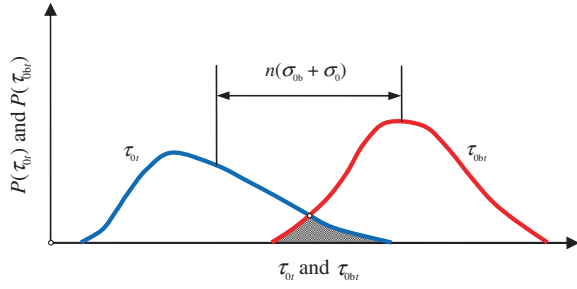
$$p_R(d) = k_0 p_{st} p_0(d) \quad (4.135)$$

where k_0 is the constant that can be determined by

$$\int_{d_{\min}}^{d_{\max}} p_R(d) dd = 1 \quad (4.136)$$

The expression for the particle size distribution of the retained sediment particles is

Fig. 4.19 Probabilities of bed shear stress τ_{0i} due to flow and threshold bed shear stress τ_{0br} corresponding to the motion of individual particles



$$P_R(d) = \frac{\int_{d_{\min}}^d p_{st} p_0(d) dd}{\int_{d_{\min}}^{d_{\max}} p_{st} p_0(d) dd} \quad (4.137)$$

The expression for particle size distribution of the transported sediment particles is

$$P_R(d) = \frac{\int_{d_{\min}}^d (1 - p_{st}) p_0(d) dd}{\int_{d_{\min}}^{d_{\max}} (1 - p_{st}) p_0(d) dd} \quad (4.138)$$

The sediments of finer size given by Eq. (4.138) cease to transport, once the armor layer is formed by sorting the sediment particles.

4.6.2 Grass's Approach

The most detailed experimental investigation on the bed shear stress fluctuations carried out so far is due to Grass (1970). He proposed to use a probabilistic description of the stresses acting on a single particle to achieve motion. He identified two probability distributions: $P(\tau_{0i})$ and $P(\tau_{0br})$ (see Fig. 4.19).

The probability distributions $P(\tau_{0i})$ and $P(\tau_{0br})$ are for the instantaneous bed shear stress τ_{0i} induced by the flow and the instantaneous bed shear stress τ_{0br} required to put the particle in motion, respectively. When these two distributions start overlapping (Fig. 4.19), the particles that have the lowest threshold bed shear stress start to move. The representative magnitudes of the probability distributions are their standard deviations being used to describe the distance of the two time-averaged bed shear stresses as $\tau_{0b} - \tau_0 = n(\sigma_{0b} + \sigma_0)$, where σ_{0b} and σ_0 are the standard deviations of τ_{0br} and τ_{0i} , respectively. Grass obtained the relationships as $\sigma_0 = 0.4\tau_0$ and $\sigma_{0b} = 0.3\tau_{0b}$, which led to $\tau_0 = \tau_{0b}[(1 - 0.3n)/(1 + 0.4n)]$. For $n = 0.625$, the result collapses with that of Shields.

where u_m is the area-averaged instantaneous velocity received by the solitary particle and A_x is the frontal area of the particle exposed to the flow. The submerged weight of the particle is given by Eq. (4.9). For the estimation of C_D , Wu and Chou (2003) used the formula of Schiller and Naumann (1933). It is

$$C_D = \frac{24}{R}(1 + 0.15R^{0.687}) \quad \wedge \quad R = \frac{\bar{u}_m(0.75d + \delta)}{v} \quad (4.140)$$

where \bar{u}_m is the area-time-averaged velocity received by the solitary particle. In this study, the ratio of drag to lift coefficients was considered to be unity (that is, $C_L = C_D$). Determination of \bar{u}_m was done considering the universal logarithmic velocity distribution in rough flow regime, given by Eq. (4.27), and assuming $z_0 = k_s/30$ with $k_s = 2d$. Thus, the \bar{u}_m is

$$\bar{u}_m = \frac{u_*}{\kappa} \cdot \frac{\int_{0.25d}^{d+\delta} [(z - \delta)(d - z + \delta)]^{0.5} \ln(15z/d) dz}{\int_{0.25d}^{d+\delta} [(z - \delta)(d - z + \delta)]^{0.5} dz} = u_* \eta_\delta \quad (4.141)$$

where η_δ is the nondimensional function of δ .

The point of action of \bar{u}_m (resultant of the distributed velocity system over the exposed area of the solitary particle) can be obtained from Eq. (4.27) by replacing $\bar{u} = \bar{u}_m$ and $z = z_m$ as $z_m = (d/15)\exp(\kappa\bar{u}_m/u_*)$. According to Wu and Lin (2002), the area-averaged instantaneous velocity u_m of the area-time-averaged velocity \bar{u}_m follows the log-normal distribution. Denoting v_m in place of logarithm of u_m , that is, $v_m (0 < u_m < \infty) = \ln(u_m)$, the probability density function p_v of v_m can be given by a Gaussian distribution as

$$p_v(v_m) = \frac{1}{\sqrt{2\pi}\sigma_v} \cdot \exp\left[-\frac{(v_m - \bar{v}_m)^2}{2\sigma_v^2}\right] \quad (4.142)$$

where \bar{v}_m is the mean of v_m and σ_v is the standard deviation of v_m .

In case of rolling threshold, the overturning moment about the pivot (M) exceeds the stabilizing moment to keep the particle in rest (see Fig. 4.20). Such a condition can be obtained to initiate the rolling motion of the solitary particle if

$$F_D l_z + F_L l_x > F_G l_x \quad (4.143)$$

where l_x and l_z are the horizontal and vertical lever arms, respectively. Using Eqs. (4.9) (for F_G), (4.139a, b), Eq. (4.143) yields

$$\bar{u}_m > E_R = \left(\frac{2l_x}{C_D l_z + C_L l_x} \cdot \frac{\Delta g \pi d^3}{6A_x} \right)^{0.5} \quad \wedge \quad \left[\begin{array}{l} l_x = 0.5 [d^2 - (0.75d + \delta)^2]^{0.5} \\ l_z = z_m - h_c = z_m - 0.125d - 0.5\delta \end{array} \right] \quad (4.144)$$

where E_R is the rolling threshold.

In case of lifting threshold, the lift force exceeds the submerged weight. To initiate the particle motion in lifting mode, the condition can be given by

$$F_L > F_G \quad (4.145)$$

Using Eqs. (4.9) and (4.139b), Eq. (4.145) yields

$$\bar{u}_m > E_L = \left(\frac{2}{C_L} \cdot \frac{\Delta g \pi d^3}{6A_x} \right)^{0.5} \quad (4.146)$$

where E_L is the lifting threshold.

The ratio of rolling to lifting threshold can therefore be obtained as

$$\frac{E_R}{E_L} = \sqrt{\frac{l_x}{l_z + l_x}} < 1 \quad \wedge \quad \frac{C_L}{C_D} = 1 \quad (4.147)$$

It indicates that the entrainment threshold in lifting is greater than that in rolling. Hence, if $E_R < \bar{u}_m < E_L$, the particle is entrained in a pure rolling mode keeping in contact with the bed particles. In contrast, if $\bar{u}_m > E_L$, the entrainment occurs in a simultaneous rolling and lifting mode. To be explicit, the particle is lifted off the bed while it starts to roll. Thus, $\bar{u}_m > E_L$ corresponds to the lifting mode.

Probability P_R of entrainment threshold in rolling mode is given by

$$\begin{aligned} P_R &= P(E_R < u_m < E_L) = P(\ln E_R < v_m < \ln E_L) \\ &= P(v_m < \ln E_L) - P(v_m < \ln E_R) \end{aligned} \quad (4.148)$$

Using the approximation of Cheng and Chiew (1998), Eq. (4.148) becomes

$$\begin{aligned} P_R &= \int_{-\infty}^{\ln E_L} p_v(v_m) dv_m - \int_{-\infty}^{\ln E_R} p_v(v_m) dv_m = \left[\int_{-\infty}^{\bar{v}_m} p_v(v_m) dv_m + \int_{\bar{v}_m}^{\ln E_L} p_v(v_m) dv_m \right] \\ &\quad - \left[\int_{-\infty}^{\bar{v}_m} p_v(v_m) dv_m + \int_{\bar{v}_m}^{\ln E_R} p_v(v_m) dv_m \right] = \frac{1}{2} \left\{ \frac{\ln E_L - \bar{v}_m}{|\ln E_L - \bar{v}_m|} \sqrt{1 - \exp \left[-\frac{2(\ln E_L - \bar{v}_m)^2}{\pi \sigma_v^2} \right]} \right. \\ &\quad \left. - \frac{\ln E_R - \bar{v}_m}{|\ln E_R - \bar{v}_m|} \sqrt{1 - \exp \left[-\frac{2(\ln E_R - \bar{v}_m)^2}{\pi \sigma_v^2} \right]} \right\} \end{aligned} \quad (4.149)$$

Using formulas for \bar{v}_m and σ_v given by Wu and Lin (2002) and a linear relationship between σ_u (=standard deviation of \bar{u}_m) and \bar{u}_m by Cheng and Chiew (1998), the \bar{v}_m and σ_v are determined as

$$\bar{v}_m = \ln \left[\frac{\bar{u}_m}{\sqrt{1 + (\sigma_u/\bar{u}_m)^2}} \right] = \ln \left(\frac{\bar{u}_m}{1.006} \right) \quad \wedge \quad \sigma_u = 0.37\bar{u}_m \quad (4.150a)$$

$$\sigma_v^2 = \ln \left[1 + \left(\frac{\sigma_u}{\bar{u}_m} \right)^2 \right] = 0.128 \quad (4.150b)$$

Substituting Eqs. (4.141), (4.144), (4.146) and (4.150a, b) into Eq. (4.149), the threshold of entrainment ($u_* \rightarrow u_{*c}$) for the rolling probability for a given δ is obtained as

$$P_R(\delta) = \frac{1}{2} \cdot \frac{\ln \left(\frac{1.137 G_L a_r}{\eta_\delta^2 \Theta_c} \right)}{\left| \ln \left(\frac{1.137 G_L a_r}{\eta_\delta^2 \Theta_c} \right) \right|} \sqrt{1 - \exp \left\{ -\frac{2}{\pi} \left[\frac{1}{0.358} \ln \left(\frac{1.137 G_L a_r}{\eta_\delta^2 \Theta_c} \right) \right]^2 \right\}} \\ - \frac{1}{2} \cdot \frac{\ln \left(\frac{1.137 G_R a_r}{\eta_\delta^2 \Theta_c} \right)}{\left| \ln \left(\frac{1.137 G_R a_r}{\eta_\delta^2 \Theta_c} \right) \right|} \sqrt{1 - \exp \left\{ -\frac{2}{\pi} \left[\frac{1}{0.358} \ln \left(\frac{1.137 G_R a_r}{\eta_\delta^2 \Theta_c} \right) \right]^2 \right\}} \quad (4.151)$$

where $G_R = 2 l_x / (C_D l_z + C_L l_x)$, $G_L = 2/C_L$, and $a_r = \pi d^2 / (6A_x)$.

As $-0.75d \leq \delta \leq 0.116d$, the mean rolling probability P_{RM} of entrainment threshold is given by

$$P_{RM} = \int_{-0.75d}^{0.116d} P_R(\delta) p_\delta(\delta) d\delta = \frac{1}{0.866} \int_{-0.75}^{0.116} P_R(\delta^*) d\delta^* \quad (4.152)$$

where $\delta^* = \delta/d$.

Further, probability P_L of entrainment threshold in lifting mode is

$$P_L = P(u_m > E_L) = P(v_m > \ln E_L) = 1 - P(-\infty < v_m < \ln E_L) \quad (4.153)$$

As was done in Eq. (4.149), Eq. (4.153) can be restructured as

$$P_L = 1 - \left[\int_{-\infty}^{\bar{v}_m} p_v(v_m) dv_m + \int_{\bar{v}_m}^{\ln E_L} p_v(v_m) dv_m \right] \\ = \frac{1}{2} \left\{ 1 - \frac{\ln E_L - \bar{v}_m}{|\ln E_L - \bar{v}_m|} \sqrt{1 - \exp \left[-\frac{2(\ln E_L - \bar{v}_m)^2}{\pi \sigma_v^2} \right]} \right\} \quad (4.154)$$

Substituting Eqs. (4.141), (4.146) and (4.150a, b) into Eq. (4.154), the threshold of entrainment ($u_* \rightarrow u_{*c}$) for the lifting probability for a given δ is obtained as

$$P_L(\delta) = \frac{1}{2} \left\{ 1 - \frac{\ln\left(\frac{1.137G_L a_r}{\eta_\delta^2 \Theta_c}\right)}{\left| \ln\left(\frac{1.137G_L a_r}{\eta_\delta^2 \Theta_c}\right) \right|} \right\} \sqrt{1 - \exp\left\{ -\frac{2}{\pi} \left[\frac{1}{0.358} \ln\left(\frac{1.137G_L a_r}{\eta_\delta^2 \Theta_c}\right) \right]^2 \right\}} \quad (4.155)$$

The mean lifting probability P_{LM} of entrainment threshold can be given as follows:

$$P_{LM} = \int_{-0.75d}^{0.116d} P_L(\delta) p_\delta(\delta) d\delta = \frac{1}{0.866} \int_{-0.75}^{0.116} P_L(\delta^*) d\delta^* \quad (4.156)$$

As rolling and lifting are independent modes, the total probability P_T and the mean total probability P_M of entrainment threshold can be obtained as

$$P_T = P_R + P_L \quad (4.157a)$$

$$P_M = P_{RM} + P_{LM} \quad (4.157b)$$

Equations (4.152) and (4.156) are solved numerically to evaluate the rolling and lifting probabilities for a given range of Θ_c .

The variation of probabilities of entrainment threshold with threshold Shields parameter Θ_c for rolling and lifting criteria is demonstrated in Fig. 4.21. The lifting probability P_{LM} increases monotonically with an increase in Θ_c , while the rolling probability P_{RM} increases initially with Θ_c reaching its peak ($P_{RM} = 0.25$) at $\Theta_c = 0.15$ and then decreases with a further increase in Θ_c . It is evident that the P_{RM} makes up more than 90 % of the total entrainment probability P_M for a given $\Theta_c < 0.05$, while the P_{LM} occupies more than 90 % of the P_M for a given $\Theta_c > 0.6$. Hence, $P_{RM}(\Theta_c < 0.05)$ and $P_{LM}(\Theta_c > 0.6)$ can be used as the approximations to P_M . However, for $0.05 < \Theta_c < 0.6$, the contributions from both P_{RM} and P_{LM} toward P_M are equally weighted.

Figure 4.22 shows the rolling and lifting threshold criteria (Θ_c as a function of R_*) obtained by Wu and Chou (2003). The comparison of the curves with those obtained by Ling (1995) shows that there is a considerable discrepancy in the results of these two studies. The reason is attributed to the assumption of a single logarithmic law of velocity distribution for the rough flow regime over the ranges of smooth and transitional flow regimes. It is apparent from the corresponding values of R_* .

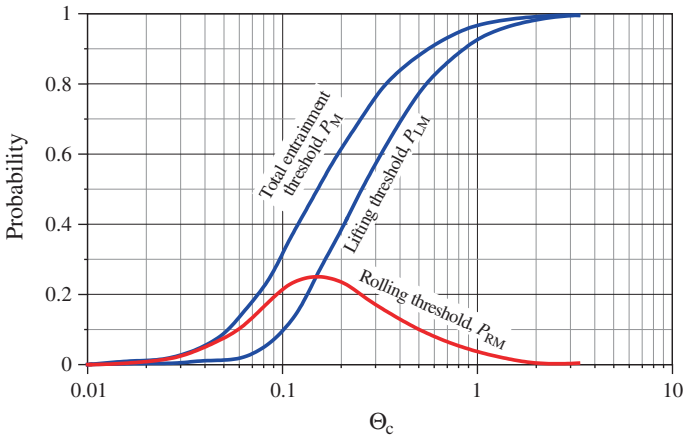


Fig. 4.21 Probabilities of entrainment threshold as a function of threshold Shields parameter Θ_c (Wu and Chou 2003)

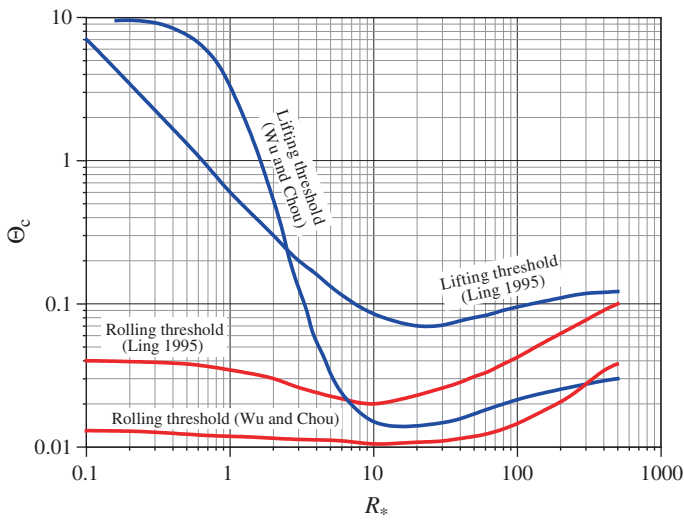


Fig. 4.22 Variation of threshold Shields parameter Θ_c with shear Reynolds number R_* for rolling and lifting threshold criteria (Wu and Chou 2003)

4.6.4 Other Investigations

Mingmin and Qiwei (1982), who developed a stochastic model, expressed the statistical parameters using the velocity of bottom flow and particle size. The probability of incipient motion, life distribution of stationary particles, number of distributions of particles in incipient motion, and intensity of incipient motion

were derived. The quadrant analysis of fluctuations of velocity components by Papanicolaou et al. (2001) showed that the ratio of Reynolds shear stress to turbulence intensity is smaller in the beds with low densely packed particles than the densely packed ones. Hence, the sediment entrainment criterion solely based on the time-averaged bed shear stress may under predict the transport, especially in low densely packed cases. Based on these, Papanicolaou et al. (2002) developed a stochastic sediment threshold model that considered the role of near-bed turbulent structures and bed micro-topography upon the initiation of unisized particle motion. The model was based on the hypothesis that the probability of occurrence of exceeding the minimum moment required to initiate rolling motion equals the probability of first displacement of a particle. The theoretical derivation was complemented by the experimental measurements of the probability and near-bed turbulence for different packing regimes. They found it reasonable to consider that on average (temporal and spatial) for a sufficient large number of data, the probability of the occurrence of intermittent turbulent events equals the sediment entrainment probability. In another attempt, Dancey et al. (2002) proposed a criterion that might be interpreted as the probability of individual particle motion considering the statistical nature of sediment motion in turbulent flow and the timescale of flow. The sediment threshold was specified by a constant value of the probability. However, a threshold criterion based on the probability of particle motion could yield relatively active sediment beds, where the mechanism is strongly dependent on the sediment packing density.

4.7 Turbulence-Induced Entrainment Concept

After the discovery of the turbulent bursting phenomena, the researchers have been encouraged to pay an increased attention in further studying the role of turbulence on sediment entrainment. The bursting events result in a high frequency and considerable pressure fluctuations on the particles lying on the bed surface and thus have a significant effect on sediment entrainment. The near-bed velocity fluctuations provoked by the bed roughness diffuse into the flow as turbulence. In the process of production of turbulence and subsequent dissipation, the size of individual eddies decreases through the diffusion process without losing energy, until eddies become small enough for viscous stresses to become dominant and dissipate the energy into heat. The sediment entrainment can be governed by the turbulence in number of ways: (1) The bed particles may be entrained by the drag exerted by a transitory eddy, (2) the low-pressure core created by an eddy or the lift created by the near-bed vertical velocity fluctuations may eject the bed particles, and (3) the high-speed inrush of the sweeping fluid may dislodge the bed particles. Importantly, the temporal mean bed shear stress maintains sediment entrainment process, while turbulent agitation (that is, velocity fluctuations) can enhance the mobility of the particles, even at the lower threshold bed shear stress at which they initiate the motion.

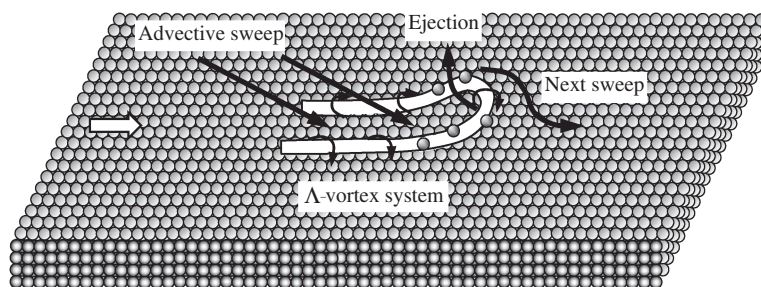


Fig. 4.23 Schematic of coherent structure during sediment entrainment

The pioneering study on the role of turbulence on sediment entrainment was due to Sutherland (1967). The observation of bed particle motion led by him to construct an entrainment concept was based on turbulent eddies disrupting the viscous sublayer and intruding the fluid on the bed. The former and the latter events have been subsequently well known as ejections and sweeps. His concept of sediment entrainment therefore remarkably corresponded with the discovery of the turbulent bursting phenomena. He concluded that the sediment entrainment is associated with a near-bed eddy impact onto the bed particles to produce a streamwise drag force that is large enough enabling to roll the particles. Heathershaw and Thorne (1985) investigated the role of the turbulent structures on the sediment entrainment in tidal channels. They argued that the entrainment is not correlated with the instantaneous Reynolds shear stress but correlated with the near-bed instantaneous streamwise velocity. Schmid (1985) reported that the sweeps are relevant mechanism for sediment entrainment, because they are the only turbulent event inducing large amount of lift on the bed particles. He visually observed the origin of the lift in combination with velocity measurements. The threshold of sediment entrainment was created by a strong deceleration of the intruding fluid by sweeps when they interacted with the bed by creating a shear layer of high vorticity. Using the concept of coherent structures, the negative pressure is produced by the apex of the developing hairpin or front vortex (Λ -vortex), which is a loop-shaped structure (see Fig. 4.23). The efficiency of the sweeps increases with a decrease in angle of attack, which is the angle between the intruding fluid and the bed surface. Field observations by Drake et al. (1988) on the mobility of gravels in alluvial streams suggested that the majority of the gravel entrainment is associated with the sweep events which give rise to the mobility of gravels. These events occur during a small fraction of time at any particular location of the bed. Thus, the entrainment process is rather episodic with short periods of high entrainment together with long periods of relatively feeble or no entrainment. Thorne et al. (1989) observed that the sweeps and the outward interactions play an important role in sediment entrainment. It is the instantaneous increase in streamwise velocity fluctuations that generate excess bed shear stresses, governing entrainment processes. In an attempt to link the characteristics of

turbulent events with the threshold of sediment entrainment, Clifford et al. (1991) and Nelson et al. (1995) suggested that the Reynolds stress component is not the most relevant parameter to the sediment entrainment. Having studied the sediment entrainment by nonuniform flow over two-dimensional dunes, Nelson et al. (1995) reported that the near-bed turbulence can change considerably and hence the sediment entrainment, while the bed shear stress remains almost unchanged. They observed that when the magnitude of the outward interactions increases relative to the other bursting events, then the sediment flux increases albeit the bed shear stress decreases. Cao (1997) gave a model for the sediment entrainment on the basis of the bursting structures. He defined that on the bed surface, a sediment particle, which may at rest, slide, or roll on the bed without detaching the bed, is entrained whenever it detaches the bed surface. If a particle comes to rest in succession to an entrainment by the turbulent bursts, a short jump or saltation occurs. As turbulent bursting is random in space and time, the entrainment rate is therefore defined as the averaged quantity over a long time period and large spatial extent compared to the temporal and spatial scales of turbulent bursts, respectively. He finally argued that the sediment entrainment is strongly dependent on the shear velocity. Sechet and Le Guennec (1999) conducted experiments to analyze the interaction between the near-bed coherent structures and the sediment entrainment. The laser Doppler velocimetry (LDV) measurements of near-bed velocity were coupled with the real-time measurements of sand particle trajectories. The period between two consecutive displacements of a sand particle is commensurable with the period between two consecutive ejections. For the displacements of small particles, the time period between two consecutive displacements has two modes. One mode is associated with the particles whose mean resting time corresponds to the mean time period of ejections, and next mode is associated with the particles whose mean resting time approximately equals the mean time period of sweeps. They concluded that the dominant mode of particle entrainment is due to ejections; the particle whose bed friction is stronger can be entrained by sweeps. Their results are therefore contradictory to the findings of the majority of other researchers.

Dey et al. (2011, 2012) studied the turbulence characteristics on immobile and sediment entrained beds. A summary of the results obtained by them is furnished below:

A reduction in Reynolds shear stress distributions over the entire flow depth in presence of sediment entrainment is prevalent. The cause of reduction is attributed to the provided momentum from the main flow to maintain particle mobility overcoming the bed frictional resistance. In addition, the near-bed Reynolds shear stress distributions undergo an excessive damping due to a diminishing level of velocity fluctuations resulting from a fall in magnitude of relative flow velocity (flow velocity minus particle velocity) of transporting sediment particles. It leads to a reduction in mobile-bed flow resistance and friction factor. The logarithmic law in the presence of sediment entrainment is characterized by a decrease in von Kármán constant and an upward shifting of the virtual bed level and the zero-velocity level. The traversing length of an eddy decreases, but the eddy size

increases in a sediment entrained flow, as compared to that in a clear-water flow. The analysis of third-order correlations reveals that during the sediment entrainment, a streamwise acceleration directing downward is established and associated with a streamwise diffusion of vertical Reynolds normal stress and a downward diffusion of streamwise Reynolds normal stress. In the near-bed flow region, the particle mobility is associated with a positive streamwise turbulent kinetic energy (TKE) flux directing toward the flow and a negative vertical TKE flux directing downward. The influence of sediment entrainment on the TKE budget is pronounced, reducing the TKE production rate and changing the pressure energy diffusion rate drastically to negative magnitude in the near-bed flow region. Conditional statistics of Reynolds shear stress showed that the sweep events are the prevailing mechanism toward the sediment entrainment.

A conceptual framework can therefore be planned to explain the physics of sediment entrainment. As a remark, the link between the findings of the near-bed turbulence characteristics and the visual observation of the sediment movement can be clarified.

An observation of sediment entrained bed revealed that the entrainment takes place as a common temporal (but continual) motion of sediment particles from the isolated regions of the bed with change in locations very frequently to cover the entire bed surface. This is well known to be governed by intermittently characterized coherent structures of turbulence. Grass (1971) and Schmid (1985) postulated that the bed particle movement is originated by the sweep events, while they interact with the bed. The sweep events during the sediment entrainment were quantified by Dey et al. (2012) contributing about 70 % toward the total Reynolds shear stress production. Figure 4.23 presents the conceptual schematic of the coherent structure during sediment entrainment. The quasiperiodic three-dimensional loop-shaped structure, called Λ -vortex, may be represented by *hairpin vortices*, characterized by a transverse vortex forming the head and two-legged vortex. Strong ejections occur upstream of the hairpin head, while sweeps are found on the downstream side. A shear layer separates ejections and sweeps. The sweeps are the part of a Λ -vortex system, as a potential physical process of particle motion. The near-bed shearing flow is highly retarded interacting with the bed roughness developing Λ -vortex that has an intense vorticity core under pressure. Inrush of faster moving fluid streaks from the outer flow is steered toward the bed in front of the head of the Λ -vortex. In the rear of the Λ -vortex, the slower moving fluid streaks are ejected toward the outer flow. In fact, Λ -vortex is capable of dislodging (lifting) the sediment particles from the bed surface through its low-pressure core and they are drifted by the near-bed flow. Therefore, the most provoking turbulence characteristic toward the sediment entrainment is a sweep producing low-pressure field, as confirmed by Dey et al. (2012) from the drastic change in pressure energy diffusion rate near the bed to a negative value. It induces a lift force transporting the bed particles collectively from the isolated regions, as was visually observed. The arrival of Λ -vortex system is rather temporal and intermittent, but it covers the whole bed surface in succession of arrivals making a continual process of sediment entrainment. This concept is in fact the basis of the

sediment entrainment by the turbulent flow. Thus, much attention is required to be given on this issue in modeling the sediment transport.

The results of this study are therefore instrumental in resolving a number of important issues that can address how to analyze the sediment entrainment phenomenon, as a future scope of research. The most important is how best to incorporate the sweep events into a theoretical model describing the sediment entrainment process. Thus, the knowledge of how the sweep events to contribute toward the near-bed Reynolds shear stress production governing the sediment motion would be an essential prerequisite. In the near-bed flow region, a gain in turbulence production due to negative pressure energy diffusion rate is another aspect that can be given adequate importance for developing a theoretical model. As the TKE production and dissipation rates are almost equal for sediment entrained flow, little is contributed from the TKE production rate toward the sediment motion. Also, a reduction in near-bed TKE dissipation rate leads to an increase in near-bed eddy size, as reflected from the increased values of the near-bed Taylor microscale in sediment entrained flow. A modified parameterization for the *Basset term* containing the temporal change of flow velocity relative to that of a particle velocity could also be prepared for inclusion in a model of sediment entrainment.

These results therefore allow to carefully elaborating a more accurate parameterization for the reduction in Reynolds shear stress in the presence of sediment entrainment. Regarding the law of the wall in sediment entrained flow, the application of traditional logarithmic law over a rough wall is highly questionable due to reduced value of von Kármán constant (leading to a reduced traversing length of eddies) and elevated levels of virtual bed and zero-velocity in sediment entrained flow. Last but not the least, as the near-bed turbulence creates the process of sediment entrainment highly probabilistic, the universal probability density functions (PDF) for the turbulence parameters developed by Bose and Dey (2010) could be employed to develop a more realistic model for sediment entrainment. It can be concluded that the state of the art of the threshold of sediment entrainment models including local turbulence properties of fluid–particle interactions is in an embryonic state. Further research is therefore required on sediment entrained flow preferably by using high-resolution flow measuring and visualizing techniques to characterize these findings in the context of sediment entrainment.

4.8 Threshold of Nonuniform Sediment Motion

The mechanism of the threshold of motion of different size fractions of a non-uniform sediment mixture is rather complex. For instance, coarse particles have greater probability to exposure to the flow, while finer ones are more likely to be shielded by the coarse particles. Essentially, the effects of hiding and exposure of the size fractions in nonuniform sediment govern the mechanism of sediment entrainment. In fact, the threshold bed shear stress of a given size fraction depends

on the particle size distribution of the sediment mixture and the surface texture. The common approach is therefore to introduce a correction factor to be appropriate for an existing formula of uniform sediment threshold or to propose a separate empirical formula for nonuniform sediment.

Egiazaroff (1965) derived a formula for the determination of threshold bed shear stress of a size fraction d_i in a sediment mixture as

$$\Theta_{ci} = \frac{0.1}{\log^2(19d_i/d_{50})} \quad (4.158)$$

where Θ_{ci} is the threshold Shields parameter for the sediment size fraction d_i , that is $\tau_{0ci}/(\Delta\rho g d_i)$, and τ_{0ci} is the threshold bed shear stress for d_i . Ashida and Michiue (1971) modified the Egiazaroff formula as

$$\Theta_{ci}(d_i/d_{50} \geq 0.4) = \Theta_c \frac{\log^2 19}{\log^2(19d_i/d_{50})} \quad (4.159a)$$

$$\Theta_{ci}(d_i/d_{50} < 0.4) = \Theta_c \frac{d_{50}}{d_i} \quad (4.159b)$$

Qin (1980) proposed the following formula for the threshold near-bed velocity u_{cri} of a size fraction d_i in a nonuniform sediment mixture:

$$u_{cri} = 0.786 \left(\frac{h}{d_{90}} \right)^{1/6} (\Delta g d_i)^{0.5} \left(1 + 2.5m \frac{d_{am}}{d_i} \right)^{0.5} \quad (4.160)$$

where $m(\eta_d < 2) = 0.6$, $m(\eta_d \geq 2) = 0.76059 - 0.68014(\eta_d + 2.2353)^{-1}$, $\eta_d = d_{60}/d_{10}$, and d_{am} is the arithmetic mean size of bed sediment.

The formula proposed by Parker et al. (1982) is

$$\Theta_{ci} = \Theta_c \left(\frac{d_{50}}{d_i} \right)^{0.982} \quad (4.161)$$

Besides the above empirical formulas, the methodology proposed by Wu et al. (2000) for the estimation of threshold bed shear stress of a given size fraction seems to be promising. He considered a mixture of spherical sediment particles with various sizes forming the streambed. The hydrodynamic force acting on a particle depends on the position of the particles lying on the bed surface. It means the particles are either sheltered by the larger ones or exposed to the flow. Wu et al. thus introduced an exposure height δ_e that is defined as the difference of the height between the top of a target particle and the particle upstream of it or the bed particle. It therefore clearly differentiates an exposed state, for which $\delta_e > 0$, from a hidden state, for which $\delta_e \leq 0$. The δ_e can therefore randomly vary within limits from $-d_j$ to d_i , where d_i is the size of the target particle and d_j is the size of the particle

upstream of it. It is assumed that δ_e follows a uniform probability distribution law, such as $p_e(-d_j \leq \delta_e \leq d_i) = (d_i + d_j)^{-1}$ and $p_e(-d_j > \delta_e \text{ or } \delta_e > d_i) = 0$.

The probability of particles d_j staying in front of particles d_i is assumed to be the fraction p_{ej} of particles d_j at the bed surface. Therefore, the total probabilities of particles d_i to be hidden and exposed due to particles d_j , P_{Hi} , and P_{Ei} , respectively, are obtained as follows:

$$P_{Hi} = \sum_{j=1}^{j=N} p_{ej} \frac{d_j}{d_i + d_j} \quad (4.162a)$$

$$P_{Ei} = \sum_{j=1}^{j=N} p_{ej} \frac{d_i}{d_i + d_j} \quad (4.162b)$$

where N is the total number of particle size fractions in the nonuniform sediment mixture. As there exists $P_{Hi} + P_{Ei} = 1$, in case of a uniform sediment mixture, it follows $P_{Hi} = P_{Ei} = 0.5$, implying an equality in hidden and exposed probabilities. However, in a nonuniform sediment mixture, P_{Ei} is greater than P_{Hi} for coarser particles and P_{Ei} is smaller than P_{Hi} for finer particles. By using the hidden and exposed probabilities, Wu et al. obtained a *hiding and exposure correction factor* denoted by η_i and then the Shields parameter Θ_{ci} for sediment size fraction d_i as

$$\Theta_{ci} = \Theta_c \eta_i \quad \wedge \quad \eta_i = \left(\frac{P_{Hi}}{P_{Ei}} \right)^{\alpha_1} \quad (4.163)$$

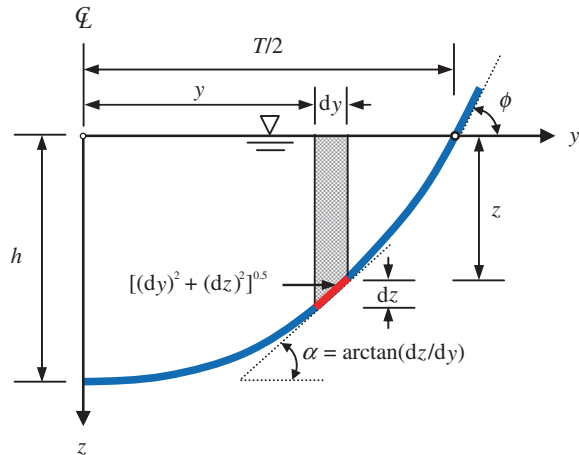
They determined $\Theta_c = 0.03$ and $\alpha_1 = 0.6$ by using laboratory experimental and field data.

4.9 Stable Channel Design

4.9.1 Straight Trapezoidal Channels

Lane (1953) developed stable channel design criterion for trapezoidal channels based on maximum allowable tractive force per unit area, that is, the bed shear stress. He showed that the maximum bed shear stress approximately equals $\rho g h \tan \theta$ on the bottom and $0.77 \rho g h \tan \theta$ on the sides of a trapezoidal channel for the range of side slope $0 < m \leq 2$, where the side slope is defined by m horizontal to 1 vertical. He also showed that there is zero bed shear stress at the corners (junction of bottom and side slope) of the channels. The threshold bed shear stress on side slope can be obtained from Eq. (4.122) as $\tau_{0c\alpha} = \tilde{\Theta}_{c\alpha} \tau_{0c}$, where τ_{0c} can be obtained from Shields or Yalin and Karahan diagram (Fig. 4.5 or Fig. 4.14).

Fig. 4.24 Schematic of stable-ideal section of a threshold channel (Glover and Florey 1951)



4.9.2 Stable-Ideal Section of a Threshold Channel

A threshold channel has a bank profile for which the sediment particles along the wetted perimeter are in a state of incipient motion. It is the essential prerequisite toward design of a stable-ideal channel section having a mobile bed at threshold of motion.

The most commonly used method for analyzing the threshold channel is the tractive force approach developed by Glover and Florey (1951). Their approach was based on following assumptions:

- Sediment particles on the channel bed are in equilibrium implying that their stability is maintained by the component of their submerged weight acting normal to the bed.
- The equilibrium of the sediment particles is assumed when the threshold bed shear stress (threshold tractive force per unit area) is balanced by the component of the submerged weight of particles per unit area opposing the motion.
- At and above the free surface of the flow, the side slope of the channel is at an angle of repose of the sediment forming the channel bed.
- At the central plane of symmetry of the channel, the side slope is zero and the bed shear stress equals its threshold value for the initiation of sediment motion.

The bed shear stress is obtained from the product of the component of the weight per unit area of the water over the elementary surface under consideration and the streamwise bed slope (Fig. 4.24).

The schematic of a stable-ideal channel section is shown in Fig. 4.24, where y -axis lies along the free surface running transverse to the flow direction and z -axis is positive vertically downward. The origin of the coordinate system (that follows a left-hand rule) lies on the free surface at the half of the top width of flow. The last assumption can be used to formulate the bed shear stress acting on the elementary

surface having a length $[(dy)^2 + (dz)^2]^{0.5}$, inclined at an angle α with the horizontal, and a unit streamwise thickness. Then,

$$\tau_{0cz} = \rho g z \tan \theta \cos \alpha \quad \wedge \quad \tan \theta = S_0 \quad \vee \quad \cos \alpha = \frac{dy}{[(dy)^2 + (dz)^2]^{0.5}} \quad (4.164)$$

where S_0 is the streamwise bed slope. At the central plane of symmetry of the channel (last assumption), the bed shear stress becomes $\tau_0(z = h, \alpha = 0) = \rho g h S_0$, where h is the flow depth. The channel section is stable, if $\tau_{0c} \geq \tau_{0cz}$.

Therefore, using Eqs. (4.122) and (4.164), the following expressions can be obtained:

$$\rho g z S_0 \cos \alpha = \rho g h S_0 \tilde{\Theta}_{cz} \quad \wedge \quad z(y = 0) = h \quad \vee \quad \alpha = \arctan \frac{dz}{dy} \quad (4.165a)$$

$$\left(\frac{dz}{dy}\right)^2 + \left(\frac{z}{h}\right)^2 \tan^2 \phi - \tan^2 \phi = 0 \quad (4.165b)$$

The solution of Eq. (4.165b) using the boundary condition $z(y = 0) = h$ yields the equation of threshold channel profile

$$z = h \cos\left(\frac{\tan \phi}{h} y\right) \quad (4.166)$$

Equation (4.166) can be used to define the geometry of a stable-ideal channel section by a simple cosine curve. For a stable-ideal channel section, the USBR (1951) gave the following recommendation for the flow area A , the average flow velocity U , and the top width T of flow:

$$A = \frac{2h^2}{\tan \phi} \quad \wedge \quad h = \frac{\tau_{0c}}{\rho g S_0} \quad (4.167a)$$

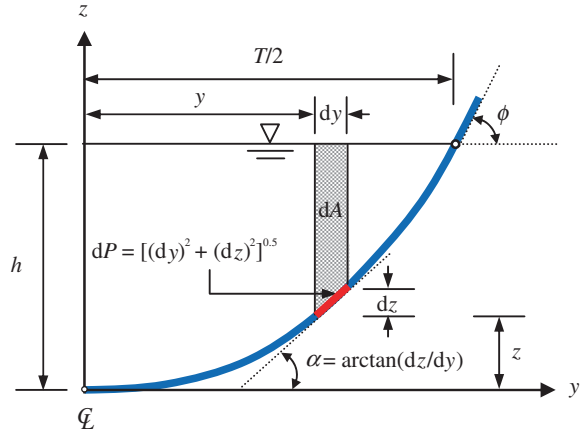
$$U = \frac{1}{n} \left[\frac{h \cos \phi}{E(\sin \phi)} \right]^{2/3} S_0^{0.5} \quad \wedge \quad E(\sin \phi) = \frac{\pi}{2} \left(1 - \frac{1}{4} \sin^2 \phi \right) \quad (4.167b)$$

$$T = \frac{\pi h}{\tan \phi} \quad (4.167c)$$

where n is the Manning roughness coefficient. The theoretical discharge Q_{th} of the stable-ideal channel section is thus obtained as $Q_{th} = UA$.

In practice, the design discharges Q_d in most of the cases differ from the theoretical ones. When $Q_d > Q_{th}$, a flat central base T_0 at a depth h is added to the channel section in order to accommodate extra discharge $Q_d - Q_{th}$ as

Fig. 4.25 Schematic of stable-ideal section of a self-formed threshold channel (Dey 2001)



$$T_0 = \frac{n}{h^{5/3} S_0^{0.5}} (Q_d - Q_{th}) \quad (4.168)$$

On the other hand, when $Q_d < Q_{th}$, the value of h can be altered and the corresponding new theoretical discharge can be estimated. The procedure is repeated until design, and theoretical discharges are equal ($Q_d = Q_{th}$).

Dey (2001) developed a simplified model for the computation of shape and dimensions of the cross-section of a self-formed straight threshold channel. The model was based on the equilibrium of the individual sediment particles lying on the channel bed at the threshold condition due to the hydrodynamic force acting on it. The transverse momentum diffusion, caused by the Reynolds shear stress, was assumed as a function of the transverse distance from the center. As the transverse bed slope of a channel is much greater than the streamwise slope, the streamwise component of gravity force is ignored in analyzing the forces acting on an individual sediment particle at threshold condition.

The schematic of a stable-ideal section of self-formed threshold channel considered by Dey (2001) is shown in Fig. 4.25, where y -axis lies on the bottom of the channel running transverse to the flow direction and z -axis is positive vertically upward. The origin of the coordinate system (that follows a right-hand rule) lies on the bottom of the channel (that is on the axis of symmetry of the flow section). Based on the modified area method of Lundgren and Jonsson (1964), the following expression for the bed shear stress acting along the wetted perimeter dP can be obtained considering the balance of downstream momentum for the area dA as shown in Fig. 4.25:

$$[\tau_0]_{\alpha=\alpha} = \rho g S_0 \frac{dA}{dP} + \frac{d}{dP} \left(\int_{h-z}^h -\rho \overline{u'v'} dz \right) \quad (4.169)$$

where $[\tau_0]_{\alpha=\alpha}$ is the bed shear stress acting on the elementary area of the channel bed, and z is the vertical distance from the mid-point of the channel bed. The second term of the right-hand side of Eq. (4.169) refers to the transverse momentum diffusion caused by the Reynolds shear stress due to turbulence. The transverse transport of momentum by the turbulence acts to diffuse momentum from the areas of high concentration (faster flow) to the areas of low concentration (slower flow). The depth integrated transport is given by $\xi_t(y)$ as

$$\xi_t(y) = \int_{h-z}^h -\rho \overline{u'v'} dz \quad (4.170)$$

Ignoring secondary currents, the local momentum balance is obtained from Eq. (4.169) as

$$[\tau_0]_{\alpha=\alpha} = \left[\rho g S_0 (h - z) + \frac{d\xi_t}{dy} \right] \cos \alpha \quad (4.171)$$

Using $[\tau_0]_{\alpha=0} = \rho g h S_0$, Eq. (4.171) is expressed in nondimensional form as

$$\tilde{\Theta}_\alpha = \frac{[\tau_0]_{\alpha=\alpha}}{[\tau_0]_{\alpha=0}} = \left(1 - \tilde{z} + \frac{d\tilde{\xi}_t}{d\tilde{y}} \right) \cos \alpha \quad (4.172)$$

where $\tilde{z} = z/h$, $\tilde{y} = y/h$, and $\tilde{\xi}_t = \xi_t/[h(\rho g h S_0)]$. According to Parker (1979), as the bed stress shear varies monotonically with y , ξ_t should have a monotonic variation with y . Hence, $\tilde{\xi}_t$ was assumed as a function of y in the form of a power law:

$$\tilde{\xi}_t = C_\xi \tilde{y}^{m_1} \quad (4.173)$$

where C_ξ and m_1 are the coefficient and exponent, respectively. By using the experimental data of Stebbings (1963), the values of C_ξ and m_1 were obtained as 0.0027 and 4.5, respectively.

In case of a threshold channel, the sediment particles on the channel bed are at threshold of motion, that is, $[\tau_0]_{\alpha=\alpha} \rightarrow [\tau_{0c}]_{\alpha=\alpha}$. Using $\cos \alpha = [1 + (dz/dy)^2]^{-0.5}$ and Eq. (4.173), and then equating Eqs. (4.121) and (4.172), the following differential equation for the channel profile of a threshold channel is obtained:

$$\sqrt{1 - \eta^2 \tan^2 \phi} \frac{d\tilde{z}}{d\tilde{y}} = \tan \phi \sqrt{1 - [(1 - \tilde{z} + C_\xi m_1 \tilde{y}^{m_1-1})(1 - \eta \tan \phi) + \eta \tan \phi]^2} \quad (4.174)$$

Equation (4.174) is a first-order differential equation, which can be solved numerically by the fourth-order Runge–Kutta method to determine the variation of \tilde{z} with \tilde{y} , that is, the nondimensional channel profile of a threshold channel. The values

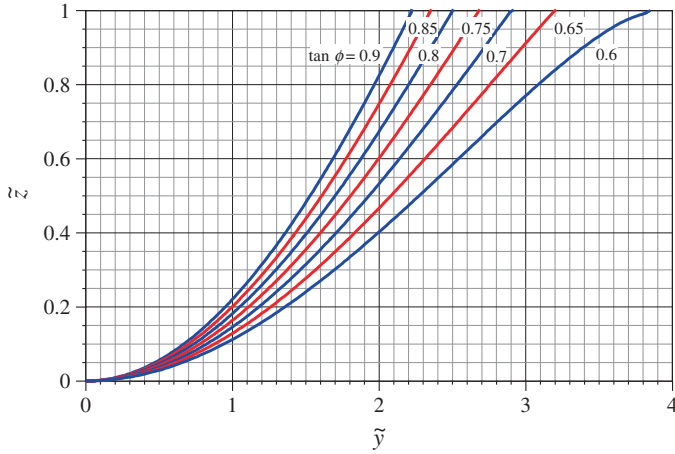


Fig. 4.26 Nondimensional channel profiles of threshold channel for $d_{50} = 45$ mm and different values of $\tan\phi$

of d_{50} , S_0 , and ϕ are required as input data. The $\eta = 0.85$ can be considered, as proposed by Chepil (1958). The steps involved in the computation are as follows:

1. Compute $D_* = k_s(\Delta g/v^2)^{1/3}$, assuming $k_s = 2d_{50}$.
2. Compute Θ_c from the following equation that provides an explicit version of the threshold curve given by Dey (1999):

$$\begin{aligned}
 \Theta_c(D_* \leq 1) &= 0.142D_*^{-0.35} \\
 \Theta_c(1 < D_* \leq 15) &= 0.148D_*^{-0.6} \\
 \Theta_c(15 < D_* \leq 50) &= 0.013D_*^{0.32} \\
 \Theta_c(D_* > 50) &= 0.045
 \end{aligned} \tag{4.175}$$

3. Compute $[\tau_{0c}]_{z=0}$, using $[\tau_{0c}]_{z=0} = \Theta_c(\rho g \Delta d_{50})$.
4. Compute h , using $h = [\tau_{0c}]_{z=0}/(\rho g S_0)$.
5. Compute the variation of \tilde{z} with \tilde{y} from Eq. (4.174) by using the fourth-order Runge–Kutta method.
6. Compute the area A and the top width T of flow numerically using the variation of $z(= \tilde{z}h)$ with $y(= \tilde{y}h)$. The wetted perimeter P can also be computed from the length of the curve representing the channel profile.
7. Compute Q from the following relationship:

$$Q = AU = 2.5A \left(g S_0 \frac{A}{T} \right)^{0.5} \ln \left(11 \frac{A}{d_{50}T} \right) \tag{4.176}$$

The above relationship for the estimation of discharge was proposed by Diplas and Vigilar (1992). Figure 4.26 shows the nondimensional channel profiles for $d_{50} = 45$ mm and different values of $\tan\phi$.

4.10 Examples

Example 4.1 Use Shields diagram to determine the threshold shear velocity for the median sediment size of 1.1 mm. Consider coefficient of kinematic viscosity of water $\nu = 10^{-6} \text{ m}^2 \text{ s}^{-1}$ and relative density of sediment $s = 2.65$.

Solution

Given data are as follows:

Size of the sediment, $d_{50} = 1.1$ mm; relative density, $s = 2.65$; and kinematic viscosity of water, $\nu = 10^{-6} \text{ m}^2 \text{ s}^{-1}$. Assume acceleration due to gravity $g = 9.81 \text{ m s}^{-2}$

First trial: Assume a trial value of $u_{*c}|_{\text{trial}} = 0.05 \text{ m s}^{-1}$

Calculate R_{*c} :

$$R_{*c} = \frac{u_{*c}|_{\text{trial}} d_{50}}{\nu} = \frac{0.05 \times 1.1 \times 10^{-3}}{10^{-6}} = 55$$

Use $R_{*c} = 55$ to determine Θ_c from the Shields diagram (Fig. 4.5). It is $\Theta_c = 0.038$.

Calculate new $u_{*c}|_{\text{new}}$:

$$u_{*c}|_{\text{new}} = (\Theta_c \Delta g d)^{0.5} = (0.038 \times 1.65 \times 9.81 \times 1.1 \times 10^{-3})^{0.5} = 0.026 \text{ m s}^{-1}$$

Therefore, $u_{*c}|_{\text{new}} \neq u_{*c}|_{\text{trial}}$.

Second trial: Retry with $u_{*c}|_{\text{trial}} = 0.026 \text{ m s}^{-1}$

Calculate R_{*c} :

$$R_{*c} = \frac{u_{*c}|_{\text{trial}} d_{50}}{\nu} = \frac{0.026 \times 1.1 \times 10^{-3}}{10^{-6}} = 28.6$$

Use $R_{*c} = 28.6$ to determine Θ_c from the Shields diagram (Fig. 4.5). It is $\Theta_c = 0.037$.

Calculate new $u_{*c}|_{\text{new}}$:

$$u_{*c}|_{\text{new}} = (\Theta_c \Delta g d)^{0.5} = (0.037 \times 1.65 \times 9.81 \times 1.1 \times 10^{-3})^{0.5} = 0.0257 \text{ m s}^{-1}$$

Therefore, $u_{*c}|_{\text{new}} \approx u_{*c}|_{\text{trial}}$.

Hence, the threshold shear velocity $u_{*c} = 0.0257 \text{ m s}^{-1}$

Example 4.2 A straight unlined trapezoidal channel is to be designed to convey a water discharge of $30 \text{ m}^3 \text{ s}^{-1}$. The median size of bed sediment is 25 mm for which Manning roughness coefficient is 0.015 SI units. The bed sediment is approximately rounded quartz particles having an angle of repose of 36° and a relative density of 2.65. It is proposed the channel to be laid on with a longitudinal slope of 1.2×10^{-3} . Compute the dimensions of the channel.

Solution

Given data are as follows:

Flow discharge, $Q = 30 \text{ m}^3 \text{ s}^{-1}$; size of the bed sediment, $d_{50} = 25 \text{ mm}$; Manning roughness coefficient, $n = 0.015 \text{ SI units}$; angle of repose, $\phi = 36^\circ$; relative density, $s = 2.65$; and longitudinal slope, $S_0 = 1.2 \times 10^{-3}$.

To determine the threshold bed shear stress τ_{0c} on a horizontal bed, the explicit equation given by Cao et al. (2006) for the curve of Yalin and Karahan (1979) is used:

$$S_* = d_{50}(\Delta g d_{50})^{0.5}/v = 25 \times 10^{-3}(1.65 \times 9.81 \times 25 \times 10^{-3})^{0.5}/10^{-6} = 15903.3$$

$$\Theta_c(S_* \geq 282.84) = 0.045 \Leftarrow \text{Eq. (4.108)}$$

$$\tau_{0c} = \Theta_c \Delta \rho g d_{50} = 0.045 \times 1.65 \times 10^3 \times 9.81 \times 25 \times 10^{-3} = 18.21 \text{ Pa}$$

The side slope of the channel should be less than the angle of repose of the bed sediment. Therefore, a side slope of the channel of 1.5 horizontal to 1 vertical (that is, $m:1$), which has an angle $\alpha = 33.7^\circ$, is assumed.

Next, the threshold bed shear stress on side slope can be calculated as follows:

$$\tilde{\Theta}_{c\alpha} = \left(1 - \frac{\sin^2 33.7^\circ}{\sin^2 36^\circ}\right)^{0.5} = 0.33 \Leftarrow \text{Eq. (4.122)}$$

$$\tau_{0c\alpha} = \tilde{\Theta}_{c\alpha} \tau_{0c} = 0.33 \times 18.21 = 6.01 \text{ Pa}$$

Determination of flow depth h :

$$h = \frac{\tau_{0c}}{\rho g S_0} = \frac{18.21}{10^3 \times 9.81 \times 1.2 \times 10^{-3}} = 1.55 \text{ m (from bottom shear stress criterion)}$$

$$h = \frac{\tau_{0c\alpha}}{0.77 \rho g S_0} = \frac{6.01}{0.77 \times 10^3 \times 9.81 \times 1.2 \times 10^{-3}} = 0.66 \text{ m (from side shear stress criterion)}$$

The flow depth is adopted as 0.66 m that provides a bed shear stress of 7.77 Pa at the bottom being less than the threshold bed shear stress $\tau_{0c} = 18.21 \text{ Pa}$

The bottom width b of the channel can be determined by solving the Manning equation numerically:

$$Q = \frac{A}{n} \left(\frac{A}{P} \right)^{2/3} S_0^{0.5} \quad \wedge \quad A = (b + mh)h \quad \vee \quad P = b + 2(1 + m^2)^{0.5}h$$

$$30 = \frac{(b + 1.5 \times 0.66)0.66}{0.015} \left[\frac{(b + 1.5 \times 0.66)0.66}{b + 2(1 + 1.5^2)^{0.5} \times 0.66} \right]^{2/3} (1.2 \times 10^{-3})^{0.5} \Rightarrow b = 25.86 \text{ m}$$

Therefore, the dimensions of the trapezoidal channel are as follows:

Side slope = 1.5:1

Flow depth = 0.66 m

By using a freeboard of 0.15 m, the design depth of the channel is 0.81 m (=0.66 + 0.15 m).

Width = 25.86 m

Example 4.3 Determine stable-ideal section of a threshold channel for the data given in Example 4.2.

Solution

Given data are as follows:

Design flow discharge, $Q_d = 30 \text{ m}^3 \text{ s}^{-1}$; size of bed sediment, $d_{50} = 25 \text{ mm}$; Manning roughness coefficient, $n = 0.015$ SI units; angle of repose, $\phi = 36^\circ$; relative density, $s = 2.65$; longitudinal slope, $S_0 = 1.2 \times 10^{-3}$; and threshold bed shear stress, $\tau_{0c} = 18.21 \text{ Pa}$

$$\text{Flow depth } h = \frac{\tau_{0c}}{\rho g S_0} = \frac{18.21}{10^3 \times 9.81 \times 1.2 \times 10^{-3}} = 1.55 \text{ m}$$

$$\text{Equation of threshold channel is } z = 1.55 \cos \left(\frac{\tan 36^\circ}{1.55} y \right) = 1.55 \cos(0.469y)$$

\Leftarrow Eq. (4.166)

$$A = \frac{2 \times 1.55^2}{\tan 36^\circ} = 6.614 \text{ m}^2 \Leftarrow \text{Eq. (4.167a)}$$

$$E(\sin 36^\circ) = \frac{\pi}{2} \left(1 - \frac{1}{4} \sin^2 36^\circ \right) = 1.435$$

$$U = \frac{1}{0.015} \left(\frac{1.55 \cos 36^\circ}{1.435} \right)^{2/3} (1.2 \times 10^{-3})^{0.5} = 2.111 \text{ m s}^{-1} \Leftarrow \text{Eq. (4.167b)}$$

$$T = \frac{\pi \times 1.55}{\tan 36^\circ} = 6.7 \text{ m} \Leftarrow \text{Eq. (4.167c)}$$

$$Q_{th} = UA = 2.111 \times 6.614 = 13.96 \text{ m}^3 \text{ s}^{-1} < Q_d (= 30 \text{ m}^3 \text{ s}^{-1})$$

Therefore, an extra flat channel base T_0 is to be provided. It is

$$T_0 = \frac{0.015}{1.55^{5/3} (1.2 \times 10^{-3})^{0.5}} (30 - 13.96) = 3.346 \text{ m} \Leftarrow \text{Eq. (4.168)}$$

References

- Aksoy S (1973) Fluid forces acting on a sphere near a solid boundary. In: Proceedings of the fifteenth congress of International Association for Hydraulic Research, vol 1, Istanbul, pp 217–224
- Allen JRL (1982) Simple models for the shape and symmetry of tidal sand wave: (1) statically stable equilibrium forms. *Mar Geol* 48(1–2):31–49
- Apperley LW (1968) Effect of turbulence on sediment entrainment. PhD thesis, University of Auckland, Auckland
- Ashida K, Michiue M (1971) An investigation of river bed degradation downstream of a dam. In: Proceedings of the fourteenth congress of International Association for Hydraulic Research, vol 3, Paris, pp 247–256
- Bagnold RA (1974) Fluid forces on a body in shear flow; experimental use of stationary flow. *Proc R Soc London A* 340(1621):147–171
- Bose SK, Dey S (2010) Universal probability distributions of turbulence in open channel flows. *J Hydraul Eng* 48(3):388–394
- Brayshaw AC, Frostick LE, Reid I (1983) The hydrodynamics of particle clusters and sediment entrainment in coarse alluvial channels. *Sedimentology* 30(1):137–143
- Brownlie WR (1981) Prediction of flow depth and sediment discharge in open channels. Report number KH-R-43A, Keck Laboratory of Hydraulics and Water Resources, California Institute of Technology, Pasadena, California
- Buffington JM (1999) The legend of A. F. Shields. *J Hydraul Eng* 125(4):376–387
- Buffington JM, Montgomery DR (1997) A systematic analysis of eight decades of incipient motion studies, with special reference to gravel-bedded rivers. *Water Resour Res* 33(8):1993–2029
- Calantoni J, Drake TG (1999) Bedload transport on sloping beds in the surf zone. *Trans Am Geophys Union* 80(17). Spring Meeting Supplementary, S194
- Cao Z (1997) Turbulent bursting-based sediment entrainment function. *J Hydraul Eng* 123(3):233–236
- Cao Z, Pender G, Meng J (2006) Explicit formulation of the Shields diagram for incipient motion of sediment. *J Hydraul Eng* 132(10):1097–1099
- Carstens MR (1966) An analytical and experimental study of bed ripples under water waves. Quarter reports 8 and 9, Georgia Institute of Technology, School of Civil Engineering, Atlanta
- Casey HJ (1935) Ueber geschiebewegung. *Mitteilungen Preuss Versuchsanstalt für Wasserbau und Schiffbau*, Berlin
- Chen X, Ma J, Dey S (2010) Sediment transport on arbitrary slopes: a simplified model. *J Hydraul Eng* 136(5):311–317
- Cheng N-S, Chiew Y-M (1998) Pickup probability for sediment entrainment. *J Hydraul Eng* 124(2):232–235
- Chepil WS (1958) The use of evenly spaced hemispheres to evaluate aerodynamic force on a soil surface. *Trans Am Geophys Union* 39(3):397–404
- Chepil WS (1961) The use of spheres to measure lift and drag on wind-eroded soil grains. *Proc Soil Sci Soc Am* 25(5):343–345
- Chiew YM, Parker G (1994) Incipient sediment motion on non-horizontal slopes. *J Hydraul Res* 32(5):649–660
- Chow VT (1959) Open channel hydraulics. McGraw-Hill Book Company, New York
- Clifford NJ, McClatchey J, French JR (1991) Measurements of turbulence in the benthic boundary layer over a gravel bed and comparison between acoustic measurements and predictions of the bedload transport of marine gravels. *Sedimentology* 38(1):161–171
- Coleman NL (1967) A theoretical and experimental study of drag and lift forces acting on a sphere resting on a hypothetical stream bed. In: Proceedings of the twelfth congress of International Association for Hydraulic Research, vol 3, Fort Collins, Colorado, pp 185–192

- Dancey CL, Diplas P, Papanicolaou A, Bala M (2002) Probability of individual grain movement and threshold condition. *J Hydraul Eng* 128(12):1069–1075
- Davies TRH, Samad MFA (1978) Fluid dynamic lift on a bed particle. *J Hydraul Div* 104(8):1171–1182
- Dey S (1999) Sediment threshold. *Appl Math Model* 23(5):399–417
- Dey S (2001) Bank profile of threshold channels: a simplified approach. *J Irrig Drainage Eng* 127(3):184–187
- Dey S (2003) Threshold of sediment motion on combined transverse and longitudinal sloping beds. *J Hydraul Res* 41(4):405–415
- Dey S (2004) Critical bed shear for initial movement of sediments on a combined lateral and longitudinal slope. *Nord Hydrol* 35(2):153–164
- Dey S, Das R, Gaudio R, Bose SK (2012) Turbulence in mobile-bed streams. *Acta Geophys* 60(6):1547–1588
- Dey S, Debnath K (2000) Influence of stream-wise bed slope on sediment threshold under stream flow. *J Irrig Drainage Eng* 126(4):255–263
- Dey S, Dey Sarker HK, Debnath K (1999) Sediment threshold under stream flow on horizontal and sloping beds. *J Eng Mech* 125(5):545–553
- Dey S, Papanicolaou A (2008) Sediment threshold under stream flow: a state-of-the-art review. *KSCE J Civ Eng* 12(1):45–60
- Dey S, Sarkar S, Solari L (2011) Near-bed turbulence characteristics at the entrainment threshold of sediment beds. *J Hydraul Eng* 137(9):945–958
- Dinkelacker A, Hessel M, Meier GEA, Schewe G (1977) Investigation of pressure fluctuations beneath a turbulent boundary layer by means of optical method. *Phys Fluids* 20(10):S216–S224
- Diplas P, Vigilar G (1992) Hydraulic geometry of threshold channels. *J Hydraul Eng* 118(4):597–614
- Drake TG, Shreve RL, Dietrich WE, Whiting PJ, Leopold LB (1988) Bedload transport of fine gravel observed by motion picture photography. *J Fluid Mech* 192:193–217
- Duan JG, Julien PY (2005) Numerical simulation of the inception of channel meandering. *Earth Surf Proc Land* 30(9):1093–1110 (Special issue on quantifying rates of geomorphic processes)
- Duan JG, Wang SSY, Jia Y (2001) The application of the enhanced CCHE2D model to study the alluvial channel migration processes. *J Hydraul Res* 39(5):469–480
- Egiazaroff JV (1965) Calculation of non-uniform sediment concentrations. *J Hydraul Div* 91(4):225–247
- Einstein HA (1950) The bed-load function for sediment transportation in open channel flows. Technical bulletin number 1026, United States Department of Agriculture, Soil Conservation Service, Washington, DC
- Einstein HA, El-Samni EA (1949) Hydrodynamic forces on rough wall. *Rev Mod Phys* 21(3):520–524
- Emmerling R (1973) The instantaneous structure of the wall pressure under a turbulent boundary layer flow. Max-Planck Institut für Strömungsforschung, Bericht 9
- Fernandez Luque R, van Beek R (1976) Erosion and transport of bed-load sediment. *J Hydraul Res* 14(2):127–144
- Garde RJ (1970) Initiation of motion on a hydrodynamically rough surface—Critical velocity approach. *J Irrig Power* 27(3):271–282
- Gessler J (1966) Geschiebetrieb bei mischungen untersucht an natürlichen, abpflasterungserscheinungen in kanälen. Number 69, Mitteilungen der Versuchsanstalt für Wasserbau und Erdbau, ETH Zürich
- Gessler J (1970) Self-stabilizing tendencies of alluvial channels. *J Waterways Harbors Div* 96(2):235–249
- Gilbert GK (1914) Transportation of debris by running water. Professional paper number 86, United States Geological Survey, Washington DC

- Glover RE, Florey QL (1951) Stable channel profiles. United States Bureau of Reclamation, Washington, DC
- Goncharov VN (1964) Dynamics of channel flow. Israel Programme for Scientific Translation, Moscow
- Grass AJ (1970) Initial instability of fine bed sand. *J Hydraul Div* 96(3):619–632
- Grass AJ (1971) Structural features of turbulent flow over smooth and rough boundaries. *J Fluid Mech* 50:233–255
- Gyr A, Hoyer K (2006) Sediment transport: a geophysical phenomenon. Springer, Dordrecht
- Heathershaw AD, Thorne PD (1985) Sea-bed noises reveal role of turbulent bursting phenomenon in sediment transport by tidal currents. *Nature* 316:339–342
- Hjulström F (1935) Studies in the morphological activity of rivers as illustrated by the river Fyris. *Bull Geol Inst Uppsala* 25:221–527
- Ikeda S (1982) Incipient motion of sand particles on side slopes. *J Hydraul Div* 108(1):95–114
- Ippen AT, Eagleson PS (1955) A study of sediment sorting by waves shoaling on a plane beach. Technical Memorandum 63, Beach Erosion Board, United States Army Corps Engineers
- Iversen JD, Rasmussen KR (1994) The effect of surface slope on saltation threshold. *Sedimentology* 41(4):721–728
- Iwagaki Y (1956) Fundamental study on critical tractive force. *Trans Japan Soc Civ Eng* 41:1–21
- Jeffreys H (1929) On the transport of sediments in stream. *Proc Cambridge Philos Soc* 25:272–276
- Karahan E (1975) Initiation of motion for uniform and non-uniform materials. PhD thesis, Technical University, Istanbul
- Kennedy JF (1995) The Albert Shields story. *J Hydraul Eng* 121(11):766–772
- Keshavarzy A, Ball JE (1996) Characteristics of turbulent shear stress applied to bed particles in an open channel flow. In: Proceedings of the seventh international of symposium of International Association for Hydraulic Research on stochastic hydraulics, Mackay, pp 451–458
- Kline SJ, Reynolds WC, Straub FA, Runstadler PW (1967) The structure of turbulent boundary layers. *J Fluid Mech* 30:741–773
- Kovacs A, Parker G (1994) A new vectorial bedload formulation and its application to the time evolution of straight river channels. *J Fluid Mech* 267:153–183
- Kramer H (1935) Sand mixtures and sand movement in fluvial model. *Trans Am Soc Civ Eng* 100:798–838
- Krey H (1925) Grenzen der übertragbarkeit der versuchsergebnisse und modellähnlichkeit bei praktischen flussbauversuchen. *Zeitschrift für Angewandte Mathematik und Mechanik* 5:484–486
- Kurihara M (1948) On the critical tractive force. Report number 3, vol 4, Research Institute for Hydraulic Engineering, Kyushu University, Japan
- Lane EW (1953) Progress report on studies on the design of stable channels of the Bureau of Reclamation. *Proc Am Soc Civ Eng* 79:246–261
- Lane EW (1955) Design of stable channels. *Trans Am Soc Civ Eng* 120:1234–1260
- Lane EW, Kalinske AA (1939) The relation of suspended to bed materials in river. *Trans Am Geophys Union* 20(4):637–641
- Lavy EE (1956) River mechanics. National Energy Press, Moscow
- Leliavsky S (1966) An introduction to fluvial hydraulics. Dover, New York
- Ling CH (1995) Criteria for incipient motion of spherical sediment particles. *J Hydraul Eng* 121(6):472–478
- Lundgren H, Jonsson GI (1964) Shear and velocity distribution in shallow channels. *J Hydraul Div* 90(1):1–21
- Mantz PA (1977) Incipient transport of fine grains and flakes by fluids-extended Shields diagram. *J Hydraul Div* 103(6):601–615
- Mavis FT, Laushey LM (1966) Discussion of ‘Sediment transportation mechanics: Initiation of motion’. *J Hydraul Div* 92(5):288–291

- Meyer-Peter E, Müller R (1948) Formulas for bed-load transport. In: Proceedings of the second meeting of International Association for Hydraulic Research, vol 3, Stockholm, pp 39–64
- Miller MC, McCave IN, Komar PD (1977) Threshold of sediment motion under unidirectional currents. *Sedimentology* 24(4):507–527
- Miller RL, Byrne RJ (1966) The angle of repose for a single grain on a fixed rough bed. *Sedimentology* 6(4):303–314
- Mingmin H, Qiwei H (1982) Stochastic model of incipient sediment motion. *J Hydraul Div* 108(2):211–224
- Morsi SA, Alexander AJ (1972) An investigation of particle trajectories in two-phase flow systems. *J Fluid Mech* 55:193–208
- Neill CR (1967) Mean velocity criterion for scour of coarse uniform bed material. In: Proceedings of the twelfth congress of International Association for Hydraulic Research, vol 3, Fort Collins, Colorado, pp 46–54
- Neill CR (1968) Note on initial movement of coarse uniform bed-material. *J Hydraul Res* 6(2):173–176
- Nelson J, Shreve RL, McLean SR, Drake TG (1995) Role of near-bed turbulence structure in bed load transport and bed form mechanics. *Water Resour Res* 31(8):2071–2086
- Paintal A (1971) Concept of critical shear stress in loose boundary open channels. *J Hydraul Res* 9(1):91–113
- Papanicolaou A, Diplas P, Dancy C, Balakrishnan M (2001) Surface roughness effects in near-bed turbulence: implications to sediment entrainment. *J Eng Mech* 127(3):211–218
- Papanicolaou AN, Diplas P, Evaggelopoulos N, Fotopoulos S (2002) Stochastic incipient motion criterion for spheres under various bed packing conditions. *J Hydraul Eng* 128(4):369–380
- Paphitis D (2001) Sediment movement under unidirectional flows: an assessment of empirical threshold curves. *Coast Eng* 43(3–4):227–245
- Parker G (1979) Hydraulic geometry of active gravel rivers. *J Hydraul Div* 105(9):1185–1201
- Parker G, Kilingeman PC, McLean DG (1982) Bed load and size distribution in paved gravel-bed streams. *J Hydraul Div* 108(4):544–571
- Qin YY (1980) Incipient motion of nonuniform sediment. *J Sediment Res* 1:83–91
- Reichardt H (1951) Vollständige darstellung der turbulenten geschwindigkeitsverteilung in glatten leitungen. *Zeitschrift für Angewandte Mathematik und Mechanik* 31(7):208–219
- Reitz W (1936) Über geschiebebewegung. *Wasserwirtschaft und Technik* 28–30
- Rubinow SI, Keller JB (1961) The transverse force on a spinning sphere moving in a viscous fluid. *J Fluid Mech* 11:447–459
- Saffman PG (1965) The lift on a small sphere in a slow shear flow. *J Fluid Mech* 22:385–400
- Saffman PG (1968) Corrigendum, the lift on a small sphere in a slow shear flow. *J Fluid Mech* 31:624
- Schiller L, Naumann A (1933) Über die grundlegenden berechnungen bei der schwerkraftaufbereitung. *Zeitschrift des Vereines Deutscher Ingenieure* 77(12):318–320
- Schlichting H (1979) Boundary layer theory. McGraw-Hill Book Company, New York
- Schmid A (1985) Wandnahe turbulente bewegungsabläufe und ihre bedeutung für die riffelbildung. PhD thesis and report R22-85, Institute for Hydromechanics and Water Resources Management, ETH Zürich
- Schoklitsch A (1914) Über schleppkraft und geschiebebewegung. Engelmann, Leipzig
- Sechet P, Le Guennec B (1999) Bursting phenomenon and incipient motion of solid particles in bed-load transport. *J Hydraul Res* 37(5):683–696
- Seminara G, Solari L, Parker G (2002) Bed load at low Shields stress on arbitrarily sloping beds: failure of the Bagnold hypothesis. *Water Resour Res* 38(11). doi:10.1029/2001WR000681
- Shields AF (1936) Application of similarity principles and turbulence research to bed-load movement. *Mitteilungen der Preussischen Versuchsanstalt für Wasserbau und Schiffbau*, Berlin 26:5–24

- Soulsby RL, Whitehouse RJS (1997) Threshold of sediment motion in coastal Environments. In: Proceedings of the combined Australasian coastal engineering and port conference, Christchurch, pp 149–154
- Stebbins J (1963) The shape of self-formed model alluvial channels. *Proc Inst Civ Eng (London)* 25(4):485–510
- Stevens MA, Simons DB, Lewis GL (1976) Safety factor for riprap protection. *J Hydraul Div* 102(5):637–655
- Sutherland AJ (1967) Proposed mechanism for sediment entrainment by turbulent flows. *J Geophys Res* 72(24):6183–6194
- Task Committee (1966) Sediment transportation mechanics: initiation of motion. *J Hydraul Div* 92(2):291–314
- Thorne PD, Williams JJ, Heathershaw AD (1989) In situ acoustic measurements of marine gravel threshold and transport. *Sedimentology* 36(1):61–74
- USBR (1951) Stable channel profiles. Hydraulic Laboratory report number HY 325, United States Bureau of Reclamation, Denver, Colorado
- USWES (1936) Flume tests made to develop a synthetic sand which will not form ripples when used in movable bed models. Technical Memorandum 99-1, United States Waterways Experiment Station, Vicksburg, Mississippi
- van Rijn LC (1984) Sediment transport, part I: bed load transport. *J Hydraul Eng* 110(10):1431–1456
- van Rijn LC (1993) Principles of sediment transport in rivers, estuaries and coastal seas. Aqua Publications, The Netherlands
- Vanoni VA (1946) Transportation of suspended sediment by water. *Trans Am Soc Civ Eng* 111:67–102
- Vanoni VA (1964) Measurements of critical shear stress. Report number KH-R-7, California Institute of Technology, California
- Vanoni VA (1977) Sedimentation engineering. ASCE Manual number 54, American Society of Civil Engineers, New York
- Velikanov MA (1955) Dynamics of alluvial stream, vol 2. State Publishing House of Theoretical and Technical Literature, Russia
- Watters GZ, Rao MVP (1971) Hydrodynamic effects of seepage on bed particles. *J Hydraul Div* 97(3):421–439
- White CM (1940) The equilibrium of grains on the bed of a stream. *Philos Trans R Soc London A* 174(958):322–338
- White SJ (1970) Plane bed thresholds of fine grained sediments. *Nature* 228(October):152–153
- Whitehouse RJS, Hardisty J (1988) Experimental assessment of two theories for the effect of bed slope on the threshold of bed-load transport. *Mar Geol* 79(1–2):135–139
- Wiberg PL, Smith JD (1987) Calculations of the critical shear stress for motion of uniform and heterogeneous sediments. *Water Resour Res* 23(8):1471–1480
- Wu F-C, Chou YJ (2003) Rolling and lifting probabilities for sediment entrainment. *J Hydraul Eng* 129(2):110–119
- Wu F-C, Lin Y-C (2002) Pickup probability of sediment under log-normal velocity distribution. *J Hydraul Eng* 128(4):438–442
- Wu W, Wang SSY (1999) Movable bed roughness in alluvial rivers. *J Hydraul Eng* 125(12):1309–1312
- Wu W, Wang SSY, Jia Y (2000) Nonuniform sediment transport in alluvial rivers. *J Hydraul Res* 38(6):427–434
- Yalin MS (1963) An expression for bed-load transportation. *J Hydraul Div* 89(3):221–250
- Yalin MS, Karahan E (1979) Inception of sediment transport. *J Hydraul Div* 105(11):1433–1443
- Yang CT (1973) Incipient motion and sediment transport. *J Hydraul Div* 99(10):1679–1704

- Zanke UCE (1977) Neuer ansatz zur berechnung des transportbeginns von sedimenten unter stromungseinfluss. Mitteilungen Des Franzius-Institut, Technical University Hannover, Heft 46:156–178
- Zanke UCE (2003) On the influence of turbulence on the initiation of sediment motion. *Int J Sediment Res* 18(1):17–31
- Zhang H, Nakagawa H, Ishigaki T, Moto Y (2005) Prediction of 3D flow field and local scouring around spur dikes. *Ann J Hydraul Eng* 49(2):1003–1008 (Japan Soc Civ Eng)

Chapter 5

Bed-Load Transport

5.1 General

The transport of sediment in rivers, by which the river morphological changes are closely related, is an important aspect in fluvial processes. The term *load*, as often used to define the sediment transport, refers to the quantity of sediment that is transported in a stream. More specifically, it is used to define the rate (volume or weight per unit time and width) at which the sediment is transported.

When the bed shear stress τ_0 induced by the flow exceeds the threshold bed shear stress τ_{0c} for the initiation of sediment motion, the sediment particles forming the bed are set in motion. The *bed-load transport* is the mode of sediment transport where the sediment particles slide, roll, or travel in succession of low jumps, termed *saltation*, but belong close to the bed, from where they may leave temporarily. The dislodgment of the sediment particles is rather intermittent, as turbulence (velocity fluctuations) interacts with the bed particles randomly to play an important role in transporting them. It is, however, convenient to distinguish the modes of sediment transport as *bed load* (*slide*, *roll*, and *saltation*) and *suspended load*. Figure 5.1 presents a schematic of different modes of sediment transport.

At relatively small *excess bed shear stress* ($\tau_0 - \tau_{0c}$), the bed-load transport takes place in a sliding and/or rolling mode. It therefore describes a sediment motion generally in contact with the bed; while individual sediment particles have intermittent motion, but substantially continuous. The bed-load transport in this mode is known as *contact load*. With an increase in excess bed shear stress, increasingly sediment particles are driven streamwise in a short succession of jumping or bouncing mode of motion, as the particles lose contact with the bed for a short while to attain a mean height in water of a number of particle diameters. The bed-load transport in this mode is called *saltation*. According to Einstein (1942, 1950), the bed-load transport is defined as the transport of sediment particles within a thin layer having a thickness of two particle diameters above the bed by sliding, rolling, or traveling in succession of jumps with a streamwise distance of a few particle diameters. On the other hand, Bagnold (1956) defined the

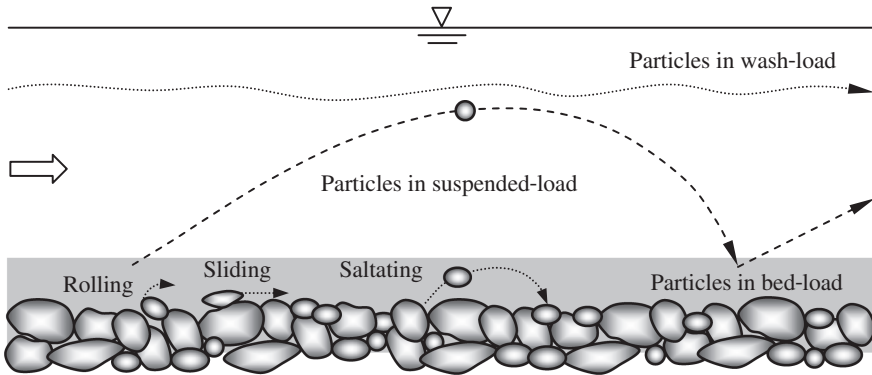


Fig. 5.1 Schematic of different modes of sediment transport

bed-load transport that takes place by successive contacts of the particles with the bed being limited by the gravity effect.

With a further increase in excess bed shear stress, the production of turbulence near the bed and its diffusion in upward direction lift up relatively finer sediment particles from the bed keeping them in suspension, as they are transported by the flow. The upward diffusion of turbulence retains the particles in the fluid domain against the gravity; while relatively coarser particles are still transported as bed load. In reality, the particles stay occasionally in contact with the bed and are displaced by making more or less large jumps to remain often surrounded by the fluid. The sediment transport in suspension mode is termed *suspended load*. Bagnold (1956) defined the suspended-load transport that takes place by balancing submerged weight of the particles with upward diffusion of turbulent eddies. In both bed-load and suspended-load transports, the sediment transport is established by the action of gravity on the fluid phase driving the sediment particles by the induced drag.

It is useful to provide approximate limiting values to separate different modes of sediment transport:

$$6 > w_s/u_* \geq 2 \text{ contact-load, bed-load} \quad (5.1a)$$

$$2 > w_s/u_* \geq 0.6 \text{ saltation, bed-load} \quad (5.1b)$$

$$0.6 > w_s/u_* \text{ suspended-load} \quad (5.1c)$$

where u_* is the shear velocity and w_s is the settling or terminal velocity of particles. Generally, the amount of bed load transported through a large deep river is approximately 5–25 % of the suspended load.

In natural stream, *wash load* is the portion of sediment that is carried by the flow such that it always remains close to the free surface. It is in near-permanent suspension and transported without deposition, essentially passing straight through

the stream. It consists of very fine sediment particles, such as silt and clay. The composition of wash load is distinct because it is almost entirely made up of particles that are only found in small quantities in the bed. Nevertheless, wash-load particles are also brought in by the overland flow or from the cohesive stream banks. As the wash-load particles tend to be very fine, they have a small settling velocity, being easily kept in suspension by the turbulence in flow. A physical characterization of the wash load is a difficult proposition, as the wash load, by definition, cannot be determined by the given flow characteristics of a river.

5.2 Definition of Bed-Load Transport

The term *bed-load transport* is defined as the sediment particles, such as silt, sand, gravel, etc., carried by the stream flow in the streamwise direction immediately above the bed as sliding, rolling, and/or saltating at a velocity less than that of the stream flow. The bed-load transport rate q_b is generally expressed as the solid volume of sediment transported per unit time and width. It is also expressed as the weight of sediment transported per unit time and width, denoted by g_b , or the submerged weight of sediment transported per unit time and width, denoted by g_{bs} . However, in nondimensional form, the bed-load transport rate is designated as *bed-load transport intensity* and denoted by Φ_b . The bed-load transport intensity Φ_b is related with q_b , g_b , and g_{bs} as follows:

$$\Phi_b = \frac{q_b}{(\Delta g d^3)^{0.5}} = \frac{g_b}{\rho_s g (\Delta g d^3)^{0.5}} = \frac{g_{bs}}{\Delta \rho g (\Delta g d^3)^{0.5}} \quad (5.2)$$

where Δ is the submerged relative density ($= s - 1$), s is the relative density of sediment ($= \rho_s/\rho$), ρ_s is the mass density of sediment, ρ is the mass density of water, g is the acceleration due to gravity, and d is the representative sediment size, that is the median or weighted mean diameter.

The bed-load transport rate q_b can be defined as the product of the particle velocity u_b in streamwise direction, the volumetric concentration C of particles transported as bed-load, and the thickness δ_b of bed-load transport layer. It is therefore given by

$$q_b = u_b C \delta_b \quad (5.3)$$

The bed-load transport rate q_b can also be defined as the product of the particle velocity u_b in streamwise direction, the number of particles in motion N_b per unit area, and the volume of particles V_b . It is thus

$$q_b = u_b N_b V_b \quad (5.4)$$

Further, by defining the particle velocity u_b as the ratio of saltation or step length λ_s to saltation or step period t_e , that is $u_b = \lambda_s/t_e$, Eq. (5.4) can be rewritten as

$$q_b = \frac{\lambda_s}{t_e} N_b V_b = \lambda_s E_b = \lambda_s D_b \quad \wedge \quad E_b = D_b = \frac{N_b V_b}{t_e} \quad (5.5)$$

where E_b and D_b are the degraded or aggraded volume of particles per unit time and area.

Another way of defining bed-load transport rate is the *pickup rate*. It is, in fact basically, defined as the number of particles picked up per unit time and area. Later, the definition of pickup rate E_p has been modified to the mass of particles picked up per unit time and area. The nondimensional pickup rate, known as the *sediment pickup function* Φ_p , is defined according to Einstein (1950) as

$$\Phi_p = \frac{E_p}{\rho_s (\Delta g d)^{0.5}} \quad (5.6)$$

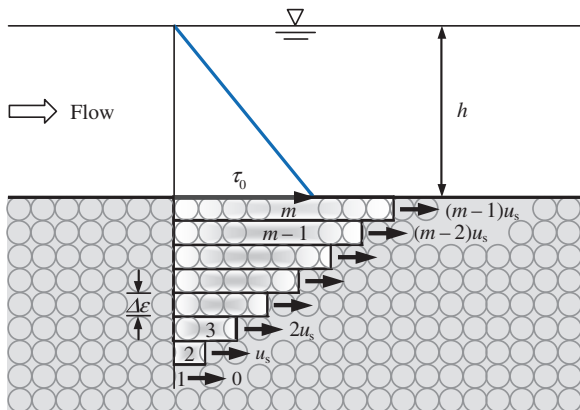
Although different researchers studied pickup rate (Einstein 1950; Fernandez Luque 1974; Yalin 1977; Nakagawa and Tsujimoto 1980; de Ruiter 1982, 1983; van Rijn 1984b; Dey and Debnath 2001), it, however, remains almost unclear whether contact load or saltation contributes to pickup rate.

5.3 Bed Shear Stress Concept for Bed-Load Transport

5.3.1 du Boys' Approach

The pioneering attempt to predict the bed-load transport rate was due to MP du Boys in 1879, who was a French engineer. His analysis was based on the force balance between the force applied to the top layer of sediment bed by the flowing fluid and the frictional resistance between the top layer of sediment particles and the layers beneath it.

du Boys (1879) assumed that the sediment particles move in series of superimposed layers of individual thickness $\Delta \varepsilon$ by the tractive force offered by the uniform flow as given by the bed shear stress $\tau_0 = \rho g h S_0$ applied to the surface of the top layer; where h is the flow depth and S_0 is the streamwise bed slope. The mean velocity of the successive layers that are sliding over each other increases linearly toward the bed surface. It implies that the velocity is highest at the top layer forming the bed surface and zero (minimum) at the lowest layer at a depth of $\Delta \varepsilon m$; where m is the number of layers. Figure 5.2 illustrates the definition sketch of du Boys model. Under the equilibrium condition, the top layer is one where the tractive force balances the frictional resistance force between these layers.

Fig. 5.2 Definition sketch of du Boys' bed-load model

The coefficient of frictional resistance μ_f between successive layers is assumed to be constant, such that the force balance is

$$\tau_0 = \rho g h S_0 = \mu_f \cdot \Delta \varepsilon \cdot m (\rho_s - \rho) g \quad (5.7)$$

The fastest moving layer being the top layer moves with a velocity of $(m-1)u_s$, where u_s is the velocity of the second lowest layer. As the layers between the first and the m -th move according to a linear velocity distribution, the sediment transport rate (in volume per unit time and width, that is, $\text{m}^3 \text{s}^{-1} \text{m}^{-1}$) is given by

$$q_b = \Delta \varepsilon \cdot m \frac{(m-1)u_s}{2} \quad (5.8)$$

The threshold condition at which sediment motion is just about to begin can be obtained by setting $m = 1$. Then, from Eq. (5.7), threshold bed shear stress τ_{0c} can be determined, and thus, m is obtained as the ratio of applied bed shear stress to threshold bed shear stress as follows:

$$\tau_{0c} = \mu_f \cdot \Delta \varepsilon (\rho_s - \rho) g \Rightarrow m = \frac{\tau_0}{\tau_{0c}} \quad (5.9)$$

It is introduced into Eq. (5.8) and then

$$q_b = \left(\frac{\Delta \varepsilon \cdot u_s}{2 \tau_{0c}^2} \right) \tau_0 (\tau_0 - \tau_{0c}) \quad (5.10)$$

du Boys referred the first term within the parenthesis in right-hand side of Eq. (5.10) as a characteristic of sediment coefficient and denoted by χ . Thus, the equation becomes

$$q_b = \chi \tau_0 (\tau_0 - \tau_{0c}) \quad (5.11)$$

The sediment coefficient χ was determined from the experimental data obtained by Schoklitsch (1914). According to Graf (1971), it is

$$\chi = \frac{0.54}{\Delta \rho g} \text{ (in metric units)} \quad (5.12)$$

Straub (1935) related χ with the particle size d (in mm) ($0.125 < d < 4$ mm) as

$$\chi = \frac{6.89 \times 10^{-6}}{d^{0.75}} \text{ (in SI units)} \quad (5.13)$$

5.3.2 du Boys Type Equations

du Boys equation that is characterized by the excess bed shear stress is one of the classical equations of bed-load transport. Later, investigators have tried to put forward improved version of bed-load transport equations, known as *du Boys type equations*, based on excess bed shear stress. They are discussed below:

Shields (1936) obtained the threshold bed shear stress that had a value for which the extrapolated sediment flux (bed-load transport) became zero. Therefore, he basically studied the flow conditions corresponding to the bed-load transport rate greater than zero. He obtained an empirical equation of bed load as

$$q_b = \frac{10qS_0}{s\Delta^2\rho gd}(\tau_0 - \tau_{0c}) \Rightarrow \Phi_b = \frac{10U}{s(\Delta gd)^{0.5}}(\Theta - \Theta_c)\Theta \quad (5.14)$$

where Θ and Θ_c are the Shields and threshold Shields parameters, respectively, q is the flow rate per unit width ($= Uh$), and U is the depth-averaged flow velocity. The Shields parameter is given by $\Theta = \tau_0/(\Delta\rho gd)$ and Θ_c corresponds to τ_{0c} .

Meyer-Peter and Müller (1948) gave the following equation of bed load including the effects of particle roughness:

$$q_b = \frac{8}{\Delta\rho^{1.5}g} \left[\left(\frac{C_R}{C'_R} \right)^{1.5} \tau_0 - \tau_{0c} \right]^{1.5} \Rightarrow \Phi_b = 8(\eta_c\Theta - \Theta_c)^{1.5} \quad \wedge \quad \eta_c = \left(\frac{C_R}{C'_R} \right)^{1.5} \quad (5.15)$$

where C_R is the total Chézy coefficient due to effective bed roughness k_s , that is $18\log(12 h/k_s)$ or $U/(R_b S_0)^{0.5}$, R_b is the hydraulic radius, and C'_R is the Chézy coefficient due to particle roughness d_{90} , that is $18\log(12 h/d_{90})$. In Eq. (5.15), Meyer-Peter and Müller recommended the value of $\Theta_c = 0.047$. Their formula

corresponded well with the experimental data for coarse sands and gravels. The η_C was reported to vary from 0.5 to 1 that corresponds to coarse sand and a small form drag. Considering $k_s \approx d_{90}$, the η_C becomes unity; and the Meyer-Peter and Müller formula can be simplified to

$$\Phi_b = 8(\Theta - \Theta_c)^{1.5} \quad (5.16)$$

Subsequently, Frijlink (1952) proposed a formula that can approximate Meyer-Peter and Müller formula, but it is not a du Boys type equation. It is

$$\Phi_b = 5(\eta_C \Theta_c)^{0.5} \exp\left(-\frac{0.27}{\eta_C \Theta}\right) \quad (5.17)$$

However, Chien (1954) showed that the Meyer-Peter and Müller formula can be replaced by

$$\Phi_b = (4\Theta - 0.188)^{1.5} \quad (5.18)$$

Further, Wong and Parker (2006) reanalyzed the experimental data used by Meyer-Peter and Müller and found a better fitting for the Meyer-Peter and Müller formula with the following equation:

$$\Phi_b = 3.97(\Theta - 0.0495)^{1.5} \quad (5.19)$$

For the high bed-load transport rate, Wilson (1966) put forward an empirical equation as

$$\Phi_b = 12(\Theta - \Theta_c)^{1.5} \quad (5.20)$$

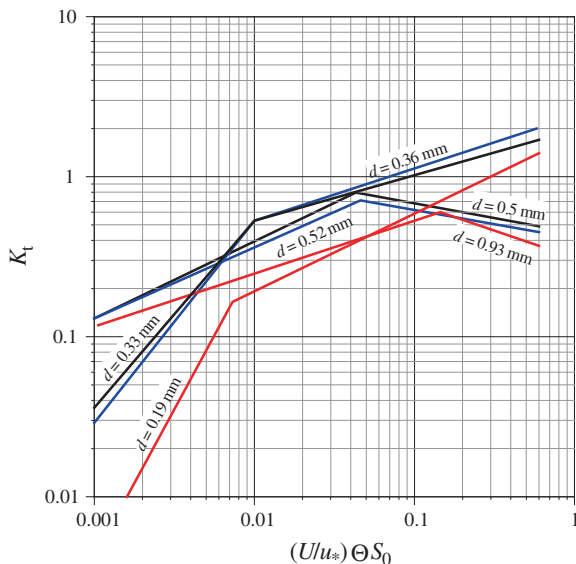
Chang et al. (1967) suggested that the bed-load transport can be determined from the following relationship:

$$\Phi_b = K_t \frac{\Delta}{s} \cdot \frac{U}{(\Delta g d)^{0.5}} (\Theta - \Theta_c) \quad \wedge \quad K_t = K_b \frac{s}{\Delta} \cdot \frac{1}{\tan \phi} \quad (5.21)$$

where K_b is a constant and ϕ is the angle of repose of the sediment. In the above, K_t represents a constant defining the bed-load transport and can be determined using Fig. 5.3.

Ashida and Michiue (1972) analyzed micro-mechanical particle collision with the bed, but not considered the saltation. They obtained the following equation of bed-load transport intensity for the range of particle size $0.3 \leq d \leq 7$ mm:

Fig. 5.3 Variation of K_t with $(U/u_*)\Theta S_0$ for different sediment sizes (Chang et al. 1967)



$$\Phi_b = 17(\Theta - \Theta_c)(\Theta^{0.5} - \Theta_c^{0.5}) \quad (5.22)$$

In the above, Ashida and Michiue recommended the value $\Theta_c = 0.05$.

Fernandez Luque and van Beek (1976) used laboratory experimental data to suggest bed-load transport intensity as

$$\Phi_b = 5.7(\Theta - \Theta_c)^{1.5} \quad (5.23)$$

They considered a range of Θ_c within $0.05 \leq \Theta_c \leq 0.058$ for $0.9 \leq d \leq 3.3$ mm. For gravel-bed rivers, Parker (1979) proposed

$$\Phi_b = 11.2 \frac{(\Theta - 0.03)^{4.5}}{\Theta^3} \quad (5.24)$$

Smart (1984) measured bed-load transport rate in steep channels ($0.03 \leq S_0 \leq 0.2$) for the gravel sizes $2 \leq d \leq 10.5$ mm. Based on his data and the data of Meyer-Peter and Müller, he proposed

$$\Phi_b = 4 \frac{C_R}{g^{0.5}} \left(\frac{d_{90}}{d_{30}} \right)^{0.2} S_0^{0.6} (\Theta - \Theta_c) \Theta^{0.5} \quad (5.25)$$

The bed-load transport intensity equation derived by van Rijn (1984a) for $0.2 \leq d \leq 2$ mm is

$$\Phi_b = \frac{0.053}{D_*^{0.3}} \left(\frac{\Theta}{\Theta_c} - 1 \right)^{2.1} \quad (5.26)$$

where D_* is the particle parameter, that is $d(\Delta g/v^2)^{1/3}$, and v is the kinematic viscosity of water.

Graf and Suszka (1987) gave a bed-load transport intensity formula for steep bed slopes as

$$\Phi_b(\Phi_b \leq 10^{-2}) = 10.4 \left(1 - \frac{0.045}{\Theta} \right)^{2.5} \Theta^{1.5} \quad (5.27a)$$

$$\Phi_b(\Phi_b > 10^{-2}) = 10.4 \Theta^{1.5} \quad (5.27b)$$

Madsen (1991) recommended

$$\Phi_b = K_b(\Theta - \Theta_c)(\Theta^{0.5} - 0.7\Theta_c^{0.5}) \quad (5.28)$$

where $K_b = 8/\tan\phi$ for sliding and rolling sand particles, and $K_b = 9.5$ for saltating sand particles in water. However, Niño and García (1998) proposed a similar equation with $K_b = 12/\mu_d$ for saltating particles. They determined a dynamic coefficient of friction $\mu_d = 0.23$.

Nielsen's (1992) equation for sand and gravel ($0.69 \leq d \leq 28.7$ mm) transport is

$$\Phi_b = 12(\Theta - 0.05)\Theta^{0.5} \quad (5.29)$$

Damgaard et al. (1997) conducted experiments for the wide variation of streamwise bed slope ($-32^\circ \leq \theta \leq 32^\circ$; where θ is the streamwise bed angle with the horizontal). They introduced a correction factor f_θ to Meyer-Peter and Müller formula as

$$\Phi_b = 8(\Theta - \Theta_c)^{1.5} f_\theta \quad (5.30)$$

where

$$\begin{aligned} f_\theta(-32^\circ < \theta \leq 0) &= 1 + 0.8 \left(\frac{\Theta_c}{\Theta} \right)^{0.2} \left(1 - \frac{\Theta_{c\theta}}{\Theta_c} \right)^{1.5 + \frac{\Theta}{\Theta_c}} \\ f_\theta(0 < \theta \leq 32^\circ) &= 1 \end{aligned} \quad (5.31)$$

where $\Theta_{c\theta}$ is the threshold Shields parameter on streamwise bed slope.

Lajeunesse et al. (2010) suggested

$$\Phi_b = 10.6(\Theta - \Theta_c)(\Theta^{0.5} - \Theta_c^{0.5} + 0.025) \quad (5.32)$$

5.3.3 Other Empirical Relationships Involving Bed Shear Stress

Kalinske (1947) emphasized on the near-bed turbulence that plays an important role in analyzing bed particle motion. The time-averaged bed-load transport rate q_b was expressed as a product of three quantities: volume of a particle, number of particles in motion per unit area, and time-averaged particle velocity \bar{u}_b . It is

$$q_b = \frac{\pi d^3}{6} \cdot \frac{4p_n}{\pi d^2} \cdot \bar{u}_b \quad (5.33)$$

where p_n is the fraction of moving particles. The time-averaged particle velocity \bar{u}_b can be obtained as

$$\bar{u}_b = c_0 \int_{u_{cr}}^{\infty} (u_d - u_{cr}) f(u_d) du_d \quad (5.34)$$

where c_0 is the constant of proportionality, u_d is the instantaneous flow velocity at the particle level, u_{cr} is the threshold velocity (at the particle level) for the particle motion, and $f(u_d)$ is the frequency distribution of u_d . The $f(u_d)$ is given by

$$f(u_d) = \frac{1}{(2\pi)^{0.5} \sigma_u} \exp \left[-\frac{(u_d - \bar{u}_d)^2}{2\sigma_u^2} \right] \quad (5.35)$$

where σ_u is the standard deviation of u_d . Assuming $\tau_{0c}/\tau_0 = (u_{cr}/\bar{u}_d)^2$, where \bar{u}_d is the time-averaged value of u_d , the following functional relationship is obtained:

$$\frac{\bar{u}_b}{u_*} = f \left(\frac{\tau_{0c}}{\tau_0} \right) \quad (5.36)$$

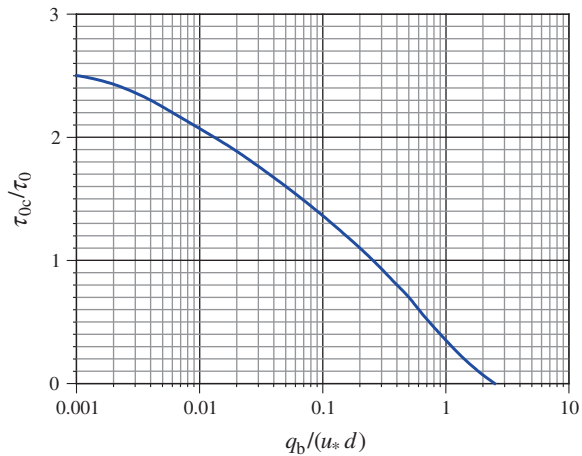
Using Eq. (5.36), Eq. (5.33) can be expressed a functional relationship as

$$\frac{q_b}{u_* d} = f_1 \left(\frac{\tau_{0c}}{\tau_0} \right) \quad (5.37)$$

Figure 5.4 shows this relationship.

Frijlink (1952) formula, as already given by Eq. (5.17) that can approximate Meyer-Peter and Müller formula, was one that falls under the category to involve bed shear stress. Further, the bed-load transport formula that was widely used by Engelund and Hansen (1967) for sand transport in terms of bed shear stress is

Fig. 5.4 Variation of τ_{0c}/τ_0 with $q_b/(u_* d)$ (Kalinske 1947)



$$\Phi_b = 0.05 \frac{U^2}{\Delta g d} \Theta^{1.5} \quad (5.38)$$

In case of weak bed-load transport rate, Paintal (1971) obtained a bed-load transport formula for $1 \leq d \leq 25$ mm as

$$\Phi_b(0.007 < \Theta < 0.06) = 6.56 \times 10^{18} \Theta^{16} \quad (5.39)$$

The relationships proposed by Misri et al. (1984) to involve bed shear stress due to particle roughness are as follows:

$$\Phi_b(\Theta' \leq 0.065) = 4.6 \times 10^7 \Theta'^8 \quad (5.40a)$$

$$\Phi_b(\Theta' > 0.065) = \frac{0.85 \Theta'^{1.8}}{(1 + 5.95 \times 10^{-6} \Theta'^{-4.7})^{1.43}} \quad (5.40b)$$

where Θ' is the Shields parameter due to particle roughness, that is $\tau'_0/(\Delta \rho g d)$, and τ'_0 is the bed shear stress due to particle roughness.

On the other hand, Cheng (2002) gave a relationship for moderate bed-load transport rate as

$$\Phi_b = 13 \Theta^{1.5} \exp\left(-\frac{0.05}{\Theta^{1.5}}\right) \quad (5.41)$$

The above equation yields results similar to those obtained from Meyer-Peter and Müller formula for moderate transport rate and Paintal formula for weak transport rate.

For high bed-load transport rate, Rickenmann (1991) reported that the particles transport like a sheet flow, when $\Theta > 0.4$. Hanes (1986) suggested that under a sheet flow type transport, the intense bed-load transport can be approximated as

$$\Phi_b = 6\Theta^{2.5} \quad (5.42)$$

5.4 Discharge Concept for Bed-Load Transport

Schoklitsch (1934) was the pioneer to use discharge for the estimation of bed load. He used the data of Gilbert (1914) with his own to propose a bed-load transport rate formula for particle size $0.305 \leq d \leq 7.02$ mm as

$$g_b = \frac{7000}{d^{0.5}} S_0^{1.5} (q - q_c) \quad (5.43)$$

where g_b is the bed-load transport rate in mass per unit time and width ($\text{kg s}^{-1} \text{m}^{-1}$), d is in mm, and q_c is the discharge per unit width corresponding to sediment threshold. Schoklitsch determined $q_c = 1.944 \times 10^{-5} / S_0^{4/3} (\text{m}^2 \text{s}^{-1})$ by plotting a curve of bed-load transport rate versus bed slope. He then extrapolated the curve to zero transport rate ($g_b = 0$) to determine the corresponding value of q as q_c . Schoklitsch later modified the equation for $d \geq 6$ mm as

$$g_b = 2500 S_0^{1.5} (q - q_c) \quad (5.44)$$

He redefined the threshold discharge as $q_c = h_c^{5/3} S_0^{0.5} / n = 0.26 \Delta^{5/3} d^{1.5} / S_0^{7/6} (\text{m}^3 \text{s}^{-1} \text{m}^{-1})$; where d is in m, n is the Manning coefficient, and h_c is the flow depth corresponding to sediment threshold.

5.5 Velocity Concept for Bed-Load Transport

Donat (1929) used the Chézy equation in Eq. (5.11) and obtained the following equation of bed-load transport using average flow velocity:

$$q_b = \chi \frac{(\rho g U)^2}{C_R^4} (U^2 - U_{cr}^2) \quad \wedge \quad U^2 = C_R^2 \frac{\tau_0}{\rho g} \quad \vee \quad U_{cr}^2 = C_R^2 \frac{\tau_{0c}}{\rho g} \quad (5.45)$$

where U_{cr} is the average threshold velocity.

Barekryan (1962) proposed bed-load transport equation using average flow velocity as

$$q_b = 0.187 \rho_s g \frac{q S_0}{\Delta} \left(\frac{U}{U_{cr}} - 1 \right) \quad (5.46)$$

Based on the stream power concept, Dou (1964) established an empirical equation of bed-load transport for sand as

$$g_b = 0.01 \frac{s}{\Delta} \tau_0 (U - U_{cr}) \frac{U}{w_s} \quad (5.47)$$

5.6 Bedform Concept for Bed-Load Transport

Bedforms are discussed comprehensively in Chap. 8. Note that the bed load is the mode of sediment transport in lower flow regime when the bed is covered by ripples and/or dunes. The particles transport up the face of the mild slope of the ridge of a bedform and then drop down the steep slope being deposited on the downstream face and in the trough. As a result of sediment removal from the upstream and deposition on the downstream slope, the bedforms move downstream (Fig. 5.5). The bed-load transport can therefore be calculated directly from the movement of the bedforms. The continuity equation of sediment transport resulting in a change of bed level was given by Exner (1925) as

$$(1 - \rho_0) \frac{\partial \eta}{\partial t} + \frac{\partial q_b}{\partial x} = 0 \quad (5.48)$$

where η is the elevation of the sand-bed with respect to a horizontal reference, t is the time, x is the horizontal distance from a reference point, and ρ_0 is the porosity of sediment.

Assuming that the bedforms migrate with a velocity of U_b being independent of time, the following transformation can be used:

$$\xi = x - U_b t \quad (5.49)$$

By using Eq. (5.49), Eq. (5.48) yields

$$(1 - \rho_0) \frac{\partial \eta}{\partial \xi} \cdot \frac{\partial \xi}{\partial t} + \frac{\partial q_b}{\partial \xi} \cdot \frac{\partial \xi}{\partial x} = 0 \Rightarrow -(1 - \rho_0) U_b \frac{\partial \eta}{\partial \xi} + \frac{\partial q_b}{\partial \xi} = 0 \quad (5.50)$$

Integrating Eq. (5.50) yields

$$q_b = (1 - \rho_0) U_b \eta + A \quad (5.51)$$

Assuming that the simplified bedforms are triangular shaped with an average height or pick-to-pick amplitude of a_m and noting that the constant of integration $A = 0$ for the initial boundary condition, Eq. (5.51) becomes

$$q_b = (1 - \rho_0) U_b \frac{a_m}{2} \quad (5.52)$$

The above equation can be used to determine the bed-load transport rate from the information of the bedform migration velocity and its height.

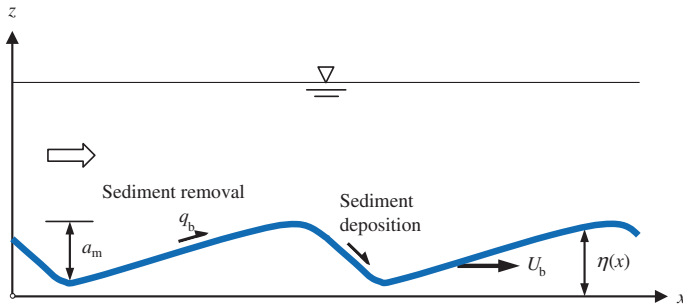


Fig. 5.5 Bed-load transport with migration of bedforms

5.7 Probabilistic Concept for Bed-Load Transport

5.7.1 Einstein's Approach

Einstein (1942, 1950) was the pioneer to develop a bed-load transport model based on the probabilistic concept. Primarily, he had two fundamental considerations that departed from the then earlier concepts. Firstly, the threshold criterion was avoided, as it is always a difficult proposition to define, if not impossible. Secondly, the transport of sediment particles was related to the velocity fluctuations instead of the time-averaged velocity. As a result of which, the beginning and the ceasing of sediment motion are expressed with probabilistic concept that relates to the ratio of submerged weight of the particle to instantaneous hydrodynamic lift induced to the particle. Some of the key issues toward the bed-load transport of sediment particles, as experimentally observed by Einstein, are as follows:

- A rigorous, but steady, exchange of sediment particles is prevalent between the bed surface and mobile bed-load layer.
- The particles travel along the bed in a series of quick steps. A particle does not, however, remain in motion continuously, but temporarily deposited on the bed after some steps with comparatively long intermediate resting periods.
- The average step, which is always the same and about 100 times the particle diameter, is simply proportional to the particle diameter and independent of the hydraulic condition and the transport rate.
- The transport rate is dependent on the average time period between two steps and the thickness of the mobile bed-load layer.

Einstein's (1942, 1950) bed-load transport model was based on the aforementioned aspects. He first presented an empirical relationship in 1942, which was then replaced by a semitheoretical approach in 1950.

Dynamic equilibrium during the bed-load transport is established by exchanging the particles from the bed within the bed-load transport layer. Thus,

the conservation of sediment mass is maintained balancing the number of particles removal (washed out by the flow) per unit time and area by those deposited (put down by the flow) per unit time and area.

Rate of deposition: The average traveling distance L_x of a particle is defined by the distance that a particle travels from its starting point until it is deposited on the bed. The single step length of a particle having diameter d can be expressed as $\lambda_s d$ and for spherical particles, $\lambda_s = 100$. As a particle travels a step by a brief jump (Fig. 5.6), it goes down on the bed at a location where a local lift force exceeds the submerged weight of the particle. Thus, the particle does not stop moving but travels for a second step and so on until it is temporarily deposited on the bed with comparatively long intermediate resting periods. In this way, the sediment particles passing a section (across the flow) per unit time deposit within a length of the channel that is equal to L_x , regardless from where they have started to move. If g_b represents the bed-load transport rate in dry weight and i_{bs} is the fraction of bed load to be deposited of a given sediment size d , then the rate at which the particles of a size d are deposited per unit time and width is $g_b i_{bs}$. Therefore, the number of particles N_d deposited per unit time and area is given by

$$N_d = \frac{g_b i_{bs}}{L_x (\rho_s g k_1 d^3)} \quad (5.53)$$

where k_1 is the factor related to particle volume. The term within the parenthesis in the denominator defines the weight of a particle.

If p is the probability of lift force to exceed the submerged weight of the particles, then $n(1 - p)$ particles deposit on the bed after traveling a step length, where n is the number of particles in motion. Thus, only np particles continue to move. Subsequently, the $np(1 - p)$ more particles deposit and only np^2 particles remain in motion after traveling the second step length, and so on. In this way, all n particles deposit on the bed after elapsing some time. The average traveling distance¹ can therefore be determined as

$$L_x = \sum_{n=0}^{\infty} (1 - p)p^n (n + 1) \lambda_s d = \frac{\lambda_s d}{1 - p} \quad (5.54)$$

¹ The probability of a particle performing $(n + 1)$ number of jumps is $(1 - p)p^n(n + 1)$. Then,

$$\sum_{n=0}^{\infty} (1 - p)p^n (n + 1) = 1 + p + p^2 + p^3 + \dots + p^n = (1 - p)^{-1}.$$

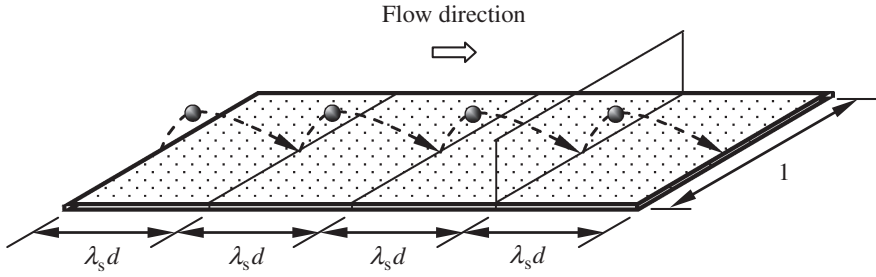


Fig. 5.6 Sketch of a particle traveling along the bed in a series of steps

Using Eq. (5.54) into Eq. (5.53), the number of particles deposited per unit time and area becomes

$$N_d = \frac{g_b i_{bs} (1-p)}{\lambda_s \rho_s g k_1 d^4} \quad (5.55)$$

Rate of removal: Depending on the availability of the particles and the flow conditions, a particle of a given size d is removed. If the fraction of sediment of a given size d to be removed is i_{br} , then the number of such particles per unit area can be given by $i_{br}/(k_2 d^2)$; where k_2 is the factor related to the projected area of the particle. If p is the probability of a particle to begin to move at any location, then p/t_e is the probability of removal per unit time. Here, t_e is the time consumed by each exchange. Therefore, the number of particles removed N_r per unit time and area is given by

$$N_r = \frac{i_{br}}{k_2 d^2} \cdot \frac{p}{t_e} \quad (5.56)$$

The exchange time t_e or the time for a particle to remove is assumed to be proportional to the time for a particle to fall a height of one diameter with a terminal velocity w_s in a still water. Thus, it is

$$t_e \sim \frac{d}{w_s} = k_3 \left(\frac{d}{\Delta g} \right)^{0.5} \quad (5.57)$$

where k_3 is a constant for time scale. Using Eq. (5.57) into Eq. (5.56), the number of particles removed per unit time and area is

$$N_r = \frac{i_{br}}{k_2 d^2} \cdot \frac{p}{k_3} \left(\frac{\Delta g}{d} \right)^{0.5} \quad (5.58)$$

Equilibrium of bed-load transport: Sediment transport is in equilibrium if the rate of sediment deposition on the bed is balanced by the rate of sediment removal

from the bed. Thus, equating Eqs. (5.55) and (5.58), the equation of dynamic equilibrium is obtained as

$$N_d = N_r \Rightarrow \frac{g_b i_{bs}(1-p)}{\lambda_s \rho_s g k_1 d^4} = \frac{i_{br}}{k_2 d^2} \cdot \frac{p}{k_3} \left(\frac{\Delta g}{d} \right)^{0.5} \quad (5.59)$$

The bed-load transport equation is therefore obtained from Eq. (5.59) as

$$\frac{p}{1-p} = A_* \left(\frac{i_{bs}}{i_{br}} \right) \Phi_b = A_* \Phi_{b*} \quad \wedge \quad A_* = \frac{k_2 k_3}{\lambda_s k_1} \quad \vee \quad \Phi_{b*} = \left(\frac{i_{bs}}{i_{br}} \right) \Phi_b \quad (5.60)$$

The parameter Φ_{b*} is called *bed-load transport intensity*, and the probability p of rate of sediment removal is given by

$$p = \frac{A_* \Phi_{b*}}{1 + A_* \Phi_{b*}} \quad (5.61)$$

Probability determination: The probability p of a sediment particle removal is a function of the ratio of submerged weight F_G of the particle to instantaneous hydrodynamic lift F_L induced to the particle. The condition of removal is therefore $p(F_G/F_L) < 1$. It can therefore be expressed as

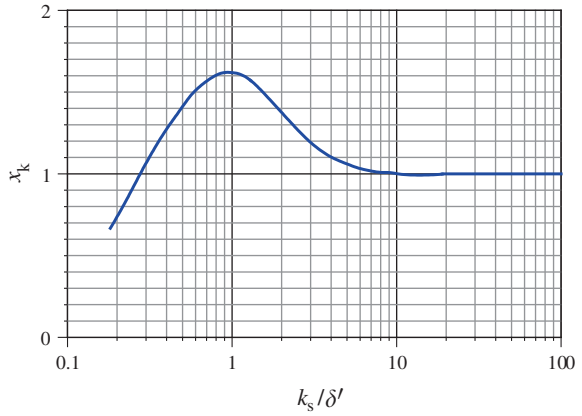
$$p = p\left(\frac{F_G}{F_L}\right) = p\left(\frac{\Delta g k_1 d}{C_L k_2 u_{\delta'}^2 / 2}\right) \quad \wedge \quad F_G = \Delta \rho g k_1 d^3 \quad \vee \quad F_L = C_L \frac{\rho}{2} k_2 d^2 u_{\delta'}^2 \quad (5.62)$$

where C_L is the lift coefficient and $u_{\delta'}$ is the effective instantaneous flow velocity at the edge of the viscous sublayer. Einstein and El-Samni (1949) observed that for uniform sediment particles, if the flow velocity at an elevation $z = 0.35X$ is taken as the effective flow velocity $u_{\delta'}$, the distribution of lift force fluctuations follows the Gaussian distribution with a standard deviation equaling half of the mean value and the lift coefficient as $C_L = 0.178$ (a constant value). Here, X is the characteristic size of the bed sediment particles. The random function parameter $\eta_t(t)$ represents the lift force fluctuations with time t being distributed according to the normal error law, where the standard deviation η_0 is a universal constant having a value $\eta_0 = 0.5$. Using a nondimensional number η_* that represents the lift force fluctuations, it can be written as $\eta_t = \eta_0 \eta_*$.

The effective instantaneous flow velocity $u_{\delta'}$ is expressed as

$$\frac{u_{\delta'}}{u_*} = \frac{1}{\kappa} \ln \left(\frac{0.35X}{\Delta_k / 30.2} \right) \quad \wedge \quad \begin{aligned} X \left(\frac{\Delta_k}{\delta'} \geq 1.8 \right) &= 0.77 \Delta_k \\ X \left(\frac{\Delta_k}{\delta'} < 1.8 \right) &= 1.39 \delta' \end{aligned} \quad (5.63)$$

Fig. 5.7 Variation of correction factor x_k with k_s/δ' , where Nikuradse's equivalent sand roughness $k_s = d_{65}$



where κ is the von Kármán constant, Δ_k is the apparent roughness ($= k_s/x_k$), x_k is a correction factor, u'_* is the shear velocity due to particle roughness, that is $(gR'_b S_0)^{0.5}$, R'_b is the hydraulic radius due to particle roughness, and δ' is the viscous sublayer thickness ($= 11.6\nu/u'_*$). Einstein (1950) considered Nikuradse's equivalent sand roughness as $k_s = d_{65}$. The correction factor x_k can be obtained from the curve given by Einstein (1950) (Fig. 5.7), and thus, apparent roughness $\Delta_k (= k_s/x_k)$ can be determined.

Hence, the lift force can be expressed as

$$F_L = (1 + \eta_0 \eta_*) 0.178 \frac{\rho}{2} k_2 d^2 \frac{1}{\kappa^2} g R'_b S_0 \ln^2 \left(\frac{10.6X}{\Delta_k} \right) \quad (5.64)$$

The probability p of sediment removal is expressed as the probability of the ratio of the submerged weight F_G to the instantaneous lift F_L . The ratio has to be smaller than unity, that is

$$1 > \frac{F_G}{F_L} = \frac{1}{1 + \eta_0 \eta_*} \cdot \frac{\Delta d}{R'_b S_0} \cdot \frac{2k_1 \kappa^2}{0.178 k_2} \cdot \frac{1}{\beta_x^2} \quad \wedge \quad \beta_x = \ln \left(\frac{10.6X}{\Delta_k} \right) \quad (5.65)$$

Using symbols, Eq. (5.65) can be reduced to

$$1 > \frac{1}{1 + \eta_0 \eta_*} \cdot \frac{\Psi'_b B}{\beta_x^2} \quad \wedge \quad \Psi'_b = \frac{\Delta d}{R'_b S_0} \quad \vee \quad B = \frac{2k_1 \kappa^2}{0.178 k_2} \quad (5.66)$$

In the above, Ψ'_b is known as *flow intensity parameter* due to particle roughness, which is reciprocal of the Shields parameter.

Einstein (1950) proposed two correction factors ξ and Y termed *hiding factor* and *lift correction factor*, respectively, which were determined experimentally (Figs. 5.8 and 5.9). Particles in the sediment mass smaller than X likely to hide

Fig. 5.8 Variation of hiding factor ξ with d/X (Einstein 1950)

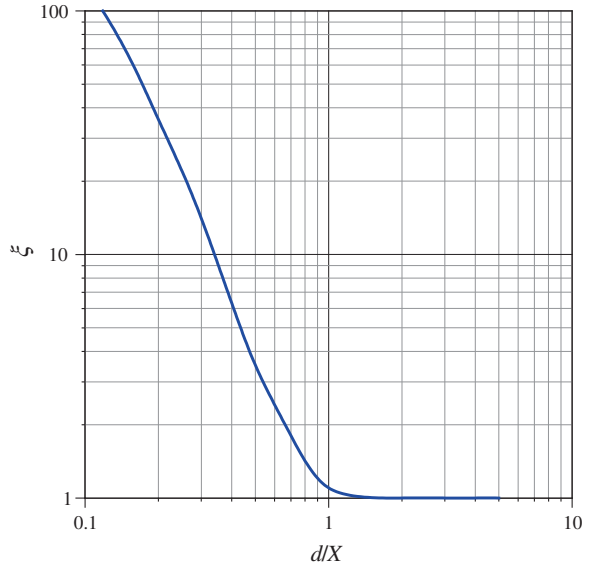
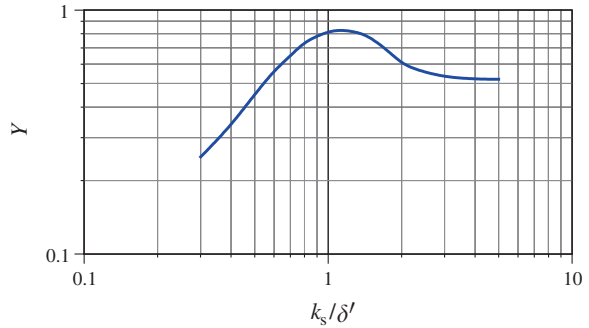


Fig. 5.9 Variation of lift correction factor Y with k_s/δ' (Einstein 1950)



between larger ones or within the viscous sublayer, as such the lift experienced by the smaller particles is to be corrected by a factor ξ^{-1} . Einstein gave a curve for the hiding factor ξ as a function of d/X (see Fig. 5.8). The lift correction factor Y takes care of the change of lift coefficient in the sediment mass due to different roughness and is expressed as a function of k_s/δ' (see Fig. 5.9).

The fluctuations of lift force are caused by the velocity fluctuations. The lift force is always positive regardless of the velocity fluctuations to be positive or negative. Thus, the inequality for the lift force can be modified as

$$\left| \eta_* + \frac{1}{\eta_0} \right| > B_* \Psi_{b*} \quad \wedge \quad B_* = \frac{B}{\eta_0 \ln^2(10.6)} \quad \vee \quad \Psi_{b*} = \Psi'_b \xi Y \frac{\ln^2(10.6)}{\beta_x^2} \quad (5.67)$$

Therefore, the threshold condition for the bed particle motion is as follows:²

$$\eta_* = \pm B_* \Psi_{b*} - \frac{1}{\eta_0} \quad (5.68)$$

It implies that between these two values of η_* , no sediment transport takes place. Therefore, the probability p of sediment motion, as the lift force fluctuations follow Gaussian distribution, is

$$p = 1 - \frac{1}{\pi^{0.5}} \int_{-B_* \Psi_{b*} - \eta_0^{-1}}^{B_* \Psi_{b*} - \eta_0^{-1}} \exp(-t^2) dt \quad (5.69)$$

Using Eq. (5.69) into Eq. (5.60), Einstein's bed-load transport equation is

$$\Phi_{b*} = \frac{1}{A_*} \cdot \frac{1 - \frac{1}{\pi^{0.5}} \int_{-B_* \Psi_{b*} - \eta_0^{-1}}^{B_* \Psi_{b*} - \eta_0^{-1}} \exp(-t^2) dt}{\frac{1}{\pi^{0.5}} \int_{-B_* \Psi_{b*} - \eta_0^{-1}}^{B_* \Psi_{b*} - \eta_0^{-1}} \exp(-t^2) dt} \quad (5.70)$$

Einstein experimentally obtained the values of the constants that are $\eta_0 = 0.5$, $A_* = 43.5$ and $B_* = 1/7$. The variation of Ψ_{b*} with Φ_{b*} from Eq. (5.70) is shown in Fig. 5.10.³ The $\Psi_{b*}(\Phi_{b*})$ curve matches well with the experimental data of Gilbert (1914), Meyer-Peter et al. (1934) and Chien and Wan (1999).

5.7.2 Empirical Refinement of Einstein Formula

Brown (1950) refined the Einstein formula by curve fitting and showed that the majority of flume data of Gilbert and Meyer-Peter et al. could be expressed by the following relationships:

² To minimize the errors, the standard deviation of lift force fluctuations given by Eq. (5.68) should be small, then $B_* \rightarrow \infty$ as $\eta_0 \rightarrow \infty$. Hence,

$$-B_* \Psi_{b*} - \frac{1}{\eta_0} = -\infty \text{ and } B_* \Psi_{b*} - \frac{1}{\eta_0} \neq 0$$

³ The use of Einstein's $\Psi_{b*}(\Phi_{b*})$ curve as shown in Fig. 5.10 is as follows:

Step 1: From the given bed sediment and flow conditions, compute Ψ_{b*} from Eq. (5.67). Then, the correction factors ξ and Y can be obtained from Figs. 5.8 and 5.9, respectively. The other parameters required to be computed are B_* from Eq. (5.67), $\Delta_k = k_s/x_k$, x_k from Fig. 5.7, $u'_* = (gR'_b S_0)^{0.5}$, $\delta' = 11.6\nu/u'_*$, and Ψ_b and B from Eq. (5.66).

Step 2: From Fig. 5.10, determine Φ_{b*} for the computed Ψ_{b*} . Thus, q_b or g_b can be obtained from Eq. (5.2).

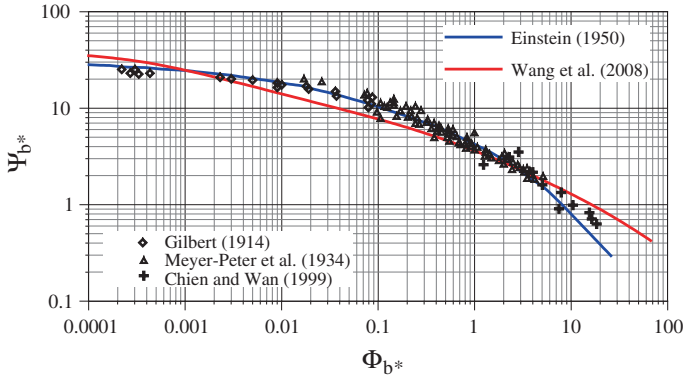


Fig. 5.10 Variations of Ψ_b^* with Φ_b^* obtained from the models of Einstein (1950) and Wang et al. (2008)

$$\Phi_b(1.92 < \Psi_b \leq 5.56) = 40K_f \frac{1}{\Psi_b^3} \quad \wedge \quad K_f = \left(\frac{2}{3} + \frac{36v^2}{\Delta g d^3} \right)^{0.5} - \left(\frac{36v^2}{\Delta g d^3} \right)^{0.5} \quad (5.71a)$$

$$\Phi_b(\Psi_b > 5.56) = 2.15K_f \exp(-0.391\Psi_b) \quad (5.71b)$$

For the sediment transport at higher Shields parameter ($\Psi_b \leq 1.92$), Julien (1998) suggested

$$\Phi_b(\Psi_b \leq 1.92) = 15K_f \frac{1}{\Psi_b^{1.5}} \quad (5.72)$$

In the above equations, the parameter K_f that appears in Rubey (1933) formula for terminal fall velocity was introduced by Brown to account for the effects of fall velocity of the sediment particles.

5.7.3 Modified Einstein's Approach

The derivation of Einstein's bed-load formula involves some oversimplified assumptions concerning the step length of a particle, exchange time, and probability of particle removal. Later, Wang et al. (2008) proposed a modification of the Einstein formula.

They argued that conceptually, the step length of a particle increases with the magnitude of the lift force exerted by the flow, but decreases with the submerged

weight of the particle. The step length can thus be given by $\lambda_s d / \Psi_b$. The rate of particle deposition g_{dep} per unit area is obtained as

$$g_{\text{dep}} = \frac{g_b}{L_x} = \frac{g_b}{\lambda_s d} (1 - p) \Psi_b \quad \wedge \quad L_x = \frac{\lambda_s d}{(1 - p) \Psi_b} \quad (5.73)$$

The number of particles per unit area can be estimated as $1/(k_2 d^2)$, and their total weight is $k_1 \rho_s g d^3 / (k_2 d^2)$. If p is the probability of a particle to begin to move, sediment with a total weight of $(k_1/k_2) \rho_s g d p$ is removed from the bed per unit time and area.

Based on the finding by Hu and Hui (1996) that the upward velocity of a particle is approximated by a linear relationship of shear velocity u_* , the time for a particle to be removed from the bed is inversely proportional to u_* . Wang et al., therefore, suggested that the exchange time t_e can be expressed as

$$t_e \sim \frac{d}{u_*} = k_3 \frac{d}{u_*} \quad (5.74)$$

The rate of particle removal g_{rem} per unit area is obtained as

$$g_{\text{rem}} = \frac{1}{t_e} \cdot \frac{k_1}{k_2} \rho_s g d p = \frac{k_1}{k_2 k_3} \rho_s g p u_* \quad (5.75)$$

Equilibrium is reached when the rate of sediment removal from the bed equals the rate of deposition on the bed. Equating Eqs. (5.73) and (5.75) yields

$$p = \frac{A_* \Phi_b}{\Psi_b^{-1.5} + A_* \Phi_b} \quad \wedge \quad A_* = \frac{k_2 k_3}{\lambda_s k_1} \quad (5.76)$$

Wang et al. assumed that a particle is removed only if the lift force exceeds the submerged weight of the particle, that is

$$1 + \eta_0 \eta_* > B' \Psi_b \quad (5.77)$$

where B' is the coefficient. The probability p of particle removal is given by

$$p = \frac{1}{\pi^{0.5}} \int_{(B' \Psi_b - 1)/\eta_0}^{\infty} \exp(-t^2) dt \quad (5.78)$$

Combining Eqs. (5.76) and (5.78) and introducing nonuniformity of sediments, the following relationship is obtained

$$\frac{1}{\pi^{0.5}} \int_{(B'\Psi_b - 1)/\eta_0}^{\infty} \exp(-t^2) dt = \frac{A_* \Phi_{b*}}{\Psi_b^{-1.5} + A_* \Phi_{b*}} \quad \wedge \quad \Phi_{b*} = \left(\frac{i_{bs}}{i_{br}} \right) \Phi_b \quad (5.79)$$

Based on the measured data used by Einstein (1950), the values of the constants were determined as $B'/\eta_0 = 0.07$, $\eta_0 = 0.5$ and $A_* = 20$. The variation of Ψ_b (read Ψ_{b*} as Ψ_b) with Φ_{b*} obtained from Eq. (5.79) is shown in Fig. 5.10. The $\Psi_b(\Phi_{b*})$ curve departs to some extent from the experimental data plots of Gilbert (1914), Meyer-Peter et al. (1934) and Chien and Wan (1999), and the curve of Einstein (1950).

5.7.4 Engelund and Fredsøe's Approach

Engelund and Fredsøe (1976) developed a bed-load transport model for the flow conditions close to the threshold of sediment motion. In this type of flow, the superficial bed particles are only transported. The model is based on the concept of Fernandez Luque and van Beek (1976), who hypothesized that the transported bed particles are to reduce the maximum fluid bed shear stress to its threshold value for the bed particle motion by exerting an average reaction force on the ambient fluid.

If the particles are transported with a mean velocity \bar{u}_b , when they are in motion, the hydrodynamic drag force F_D acting on a transported particle is given by

$$F_D = \frac{1}{2} \rho C_D \frac{\pi}{4} d^2 (\alpha u_* - \bar{u}_b)^2 \quad (5.80)$$

where C_D is the drag coefficient and αu_* is the flow velocity at the bed particle level. If the particle is at a distance of one to two particle diameters above the mean bed level, then $\alpha = 6-10$.

The stabilizing resistance F_R on the moving particle is

$$F_R = \Delta \rho g \frac{\pi}{6} d^3 \mu_d \quad (5.81)$$

where μ_d is the dynamic coefficient of friction for the bed particles.

At dynamic equilibrium, the hydrodynamic drag force is balanced by the stabilizing resistance ($F_D = F_R$). Thus, equating Eqs. (5.80) and (5.81) and then simplifying yield

$$\frac{\bar{u}_b}{u_*} = \alpha \left[1 - \left(\frac{\Theta_{0c}}{\Theta} \right)^{0.5} \right] \quad \wedge \quad \Theta_{0c} = \frac{4\mu_d}{3\alpha^2 C_D} \quad (5.82)$$

where Θ_{0c} is the threshold Shields parameter for a particle protruding from the bed surface. In fact, Θ_{0c} differs from Θ_c , which is the conventional threshold Shields parameter for the initiation of particle motion in a compactly arranged bed. As a particle lying on the bed is easier to move than a particle within the bed, it implies that $\Theta_c > \Theta_{0c}$. From the experimental data, Fernandez Luque and van Beek (1976) found $\Theta_{0c} = 0.5\Theta_c$. Thus, Eq. (5.82) becomes

$$\frac{\bar{u}_b}{u_*} = \alpha \left[1 - 0.7 \left(\frac{\Theta_c}{\Theta} \right)^{0.5} \right] \quad (5.83)$$

For a sandy bed, $\alpha \approx 9.3$. Engelund and Fredsøe treated sediment particles as spheres of diameter d , so that the number of spherical particles per unit area of bed surface is approximately $1/d^2$. For a given flow intensity, the probability of the particles on the bed surface to move is p . Hence, the bed-load transport rate g_b is

$$g_b = \frac{\pi}{6} d^3 \rho_s g \frac{p}{d^2} \bar{u}_b \quad (5.84)$$

Using Eq. (5.83) into Eq. (5.84) yields

$$g_b = 9.3 \frac{\pi}{6} d \rho_s g p \left[1 - 0.7 \left(\frac{\Theta_c}{\Theta} \right)^{0.5} \right] u_* \quad (5.85)$$

According to Bagnold, the applied bed shear stress τ_0 by the flow is composed of dispersive particle bed shear stress τ_{0b} and interfacial (intergranular) fluid bed shear stress τ_{0f} . Furthermore, he suggested that during bed-load transport, the interfacial fluid bed shear stress τ_{0f} equals the threshold bed shear stress τ_{0c} for the initiation of particle motion. This phenomenon is further discussed in the following section using a shear stress diagram. The estimation of probability p of surface bed particle removal is based on the assumption that only τ_{0c} of the applied bed shear stress τ_0 by the flow is transmitted directly to the immobile-bed particles as a skin frictional stress; whereas the residual fluid bed shear stress $(\tau_0 - \tau_{0c})$ is directly transmitted to the mobile particles as a drag induced bed shear τ_{0b} ($= nF_D$) and indirectly transmitted to the bed by intermittent surface creep. Hence,

$$\tau_0 = \tau_{0c} + nF_D \quad (5.86)$$

where n is the number of particles moving per unit area of bed surface. As $F_D = F_R$, inserting Eq. (5.81) into Eq. (5.86) leads to an estimation of p as

$$\Theta = \Theta_c + \frac{\pi}{6} \mu_d (nd^2) = \Theta_c + \frac{\pi}{6} \mu_d p \Rightarrow p = \frac{6}{\pi \mu_d} (\Theta - \Theta_c) \quad \wedge \quad p = nd^2 \quad (5.87)$$

Using Eq. (5.87) into Eq. (5.85), the bed-load transport rate, expressed as bed-load transport intensity Φ_b , is obtained as follows:

$$\Phi_b = \frac{9.3}{\mu_d} (\Theta - \Theta_c)(\Theta^{0.5} - 0.7\Theta_c^{0.5}) \quad (5.88)$$

For an intense bed-load transport rate $\Theta \gg \Theta_c$, Eq. (5.88) can be approximated as $\Phi_b = 9.3\Theta^{1.5}/\mu_d$.

5.8 Deterministic Concept for Bed-Load Transport

5.8.1 Bagnold's Approach

Bagnold (1954) identified the limitation in Einstein's approach by revealing an inconsistency toward the stability criterion of the bed during bed-load transport. Let it be discussed with an ideal example of the flow over a plane bed formed by uniform spherical sediment particles. This situation of a streambed leads to an equal exposure of all the bed particles to the flow; and hence, the stochastic variations due to turbulence can be ignored. When the applied bed shear stress exceeds its threshold value for the particle motion, all particles in the uppermost layer are in motion simultaneously and removed by the flow. As a result, the next layer of particles comes in contact with the flow and is subsequently also removed and so on. In this way, all the subsequent underlying layers of particles are removed and equilibrium toward a stable bed never exits as long as the bed shear stress exceeds the threshold value. Bagnold, however, argued this inconsistency by decomposing the applied shear stress τ by the flow into the dispersive particle shear stress τ_b that is the shear stress transmitted due to exchange of momentum for the collision of moving particles and the interfacial fluid shear stress τ_f that is the shear stress transmitted by the interfacial fluid (Fig. 5.11). The background of the idea was that the sediment-laden flows are a result of shear that includes shear between the layers of the particles and that between the sediment and the surrounding fluid. An applied bed shear stress τ_0 induced by the fluid tractive force that acts in the streamwise direction to sustain such a shear is developed by the gravity in the streamwise direction (Fig. 5.11).

The bed shear stress decomposition is therefore

$$\tau_0 = \tau_{ob} + \tau_{of} \quad (5.89)$$

Bagnold further argued that with the removal of a layer of particles, a dispersive pressure on the subsequent layer of particles is developed as a stabilizing force. The number of layers to be removed is governed by the interfacial fluid bed shear stress τ_{of} until it equals the threshold bed shear stress τ_{oc} that acts on the first immobile layer. The applied bed shear stress τ_0 induced by the fluid tractive force

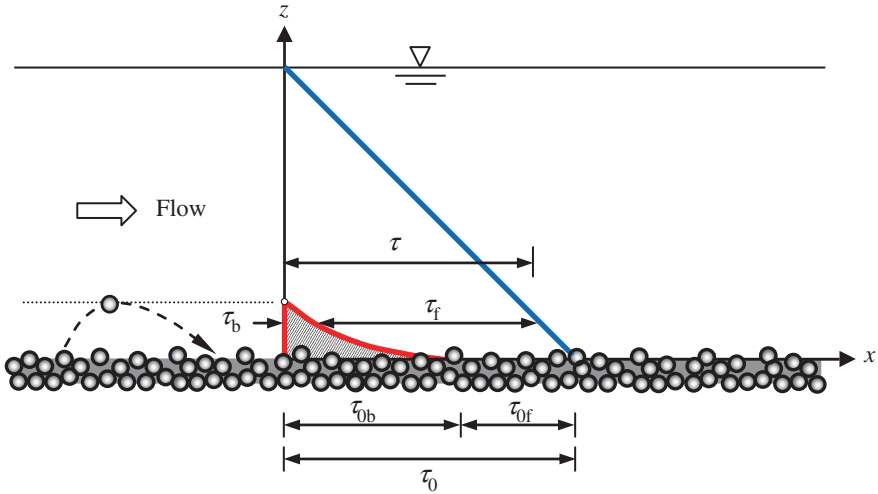


Fig. 5.11 Decomposition of applied shear stress into dispersive particle shear stress and interfacial fluid shear stress

is therefore greater than the threshold bed shear stress τ_{0c} . Hence, the τ_0 is partially transmitted to the moving particle as τ_{0b} and rest to the immobile bed as τ_{0c} .

Bagnold (1956) assumed that the saltation is the primary mode of bed-load transport. The momentum component in the streamwise direction when a saltating particle drops down to the bed is $m_G u_1$. Here, m_G is the submerged mass of the particle, and u_1 is the velocity component of the particle in the streamwise direction when it collides with the bed. The particle at the same time is acted on by a force from the bed particles producing a momentum component $m_G(-u_0)$ opposite to the streamwise direction. Here, $-u_0$ is the reduction of particle velocity component in the streamwise direction due to collision with the bed particles. To maintain the saltation of a particle, the flowing fluid therefore must act on the particle to provide a momentum component $m_G u_0$ in the time interval Δt between successive collisions of the saltating particle with the bed particles.

Therefore, the fluid flow exerts a force on the particle with a component in the streamwise direction as

$$F_x = \frac{m_G u_0}{\Delta t} = \frac{F_G u_0}{g \Delta t} \quad (5.90)$$

If \bar{u}_b is the average velocity of the particle, then the work done per unit time by the flowing fluid on the particle is $F_x \bar{u}_b$. Also, the energy consumed per unit time by the flow is $F_G \bar{u}_b \tan \phi_d$; where ϕ_d is the dynamic frictional angle. Equating them and using Eq. (5.90) yield

$$\frac{F_x}{F_G} = \tan \phi_d = \frac{u_0}{g \Delta t} \quad (5.91)$$

The vertical distance z_n is the location at which the particle is acted upon by a force F_x to accelerate the particle from $u_1 - u_0$ to u_0 . If the flow velocity at z_n is \bar{u}_n , then the $u_r (= \bar{u}_n - \bar{u}_b)$ exists at an elevation $z = z_n$. As a number of particles are in motion along the bed during bed-load transport, then

$$\tau_{bn} \bar{u}_b = F_G \bar{u}_b \tan \phi_d = g_{bs} \tan \phi_d \quad (5.92)$$

where τ_{bn} is the shear stress for maintaining sediment motion at $z = z_n$. So, the bed-load transport rate g_{bs} (in submerged weight per unit time and width) is

$$g_{bs} = \frac{\tau_{bn}}{\tan \phi_d} (\bar{u}_n - u_r) \quad (5.93)$$

Using a coefficient a , the shear stress τ_{bn} is given by

$$\tau_{bn} = a \tau_0 \quad (5.94)$$

The flow velocity is considered to follow the logarithmic law in the flow region $z \geq z_n$, and the velocity at $z = 0.4h$ is considered to be equal to the depth-averaged flow velocity U . Then,

$$\bar{u}_n = U - \frac{u_*}{\kappa} \ln \frac{0.4h}{z_n} \quad (5.95)$$

Using Eqs. (5.94) and (5.95) into Eq. (5.93) yields

$$g_{bs} = \frac{a \tau_0}{\tan \phi_d} \left[U - \frac{u_*}{\kappa} \ln \left(\frac{0.4h}{z_n} \right) - u_r \right] \quad (5.96)$$

Determination of a : Bagnold argued $a = 0$ at the threshold condition and $a \rightarrow 1$ for the high flow velocity corresponding to intense bed-load transport. It is thus given by

$$a = \frac{u_* - u_{*c}}{u_*} \quad (5.97)$$

Determination of u_r : The hydrodynamic drag force exerted by the flow on a particle is balanced by the bed resistance. It can be expressed as

$$F_x = \frac{1}{2} C_{Dx} \frac{\pi}{4} d^2 \rho u_r^2 = F_G \tan \phi_d \quad (5.98)$$

where C_{Dx} is the drag coefficient for the drag force acting in the streamwise direction.

When a particle falls with a terminal fall velocity w_s in a still fluid, the drag force F_{Dz} acting on the particle is balanced by the submerged weight F_G of the particle. Then,

$$F_{Dz} = \frac{1}{2} C_{Dz} \frac{\pi}{4} d^2 \rho w_s^2 = F_G \quad (5.99)$$

where C_{Dz} is the drag coefficient for a settling particle. From Eqs. (5.98) and (5.99), the following relationship is obtained:

$$u_r = w_s \left(\frac{C_{Dz} \tan \phi_d}{C_{Dx}} \right)^{0.5} \quad (5.100)$$

It was found from the measured data that $C_{Dx} \approx C_{Dz}$ and $\tan^{0.5} \phi_d \approx 1$. Therefore, Eq. (5.100) becomes

$$u_r = w_s \quad (5.101)$$

Determination of z_n : In the absence of any bedforms, the average elevation of the saltating particles is proportional to their diameter. Thus,

$$z_n = m_1 d \quad \wedge \quad m_1 = K_1 \left(\frac{u_*}{u_{*c}} \right)^{0.6} \quad (5.102)$$

where K_1 is a coefficient. In laboratory experiments, $K_1 = 0.4$ was found by Francis (1973); but in rivers, it becomes 2.8 for sands and 7.3–9.1 for gravels (Bagnold 1977).

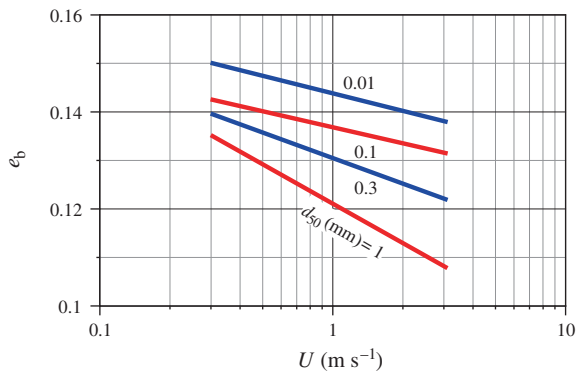
Equation of bed-load transport rate: Using Eqs. (5.97), (5.101) and (5.102) into Eq. (5.96), the equation of bed-load transport rate obtained by Bagnold in terms of submerged weight is given by

$$g_{bs} = \frac{u_* - u_{*c}}{u_*} \cdot \frac{\tau_0 U}{\tan \phi_d} \left[1 - \frac{1}{\kappa} \left(\frac{u_*}{U} \right) \ln \left(\frac{0.4h}{m_1 d} \right) - \left(\frac{w_s}{U} \right) \right] \quad (5.103)$$

Later, Bagnold (1966) simplified the analysis introducing an efficiency factor e_b for the bed-load transport. He balanced the available fraction of flow energy per unit time and area (that is the stream power) $\tau_0 U e_b$ with the work done required to move the bed-load particles $F_G \bar{u}_b \tan \phi_d (= g_{bs} \tan \phi_d)$. Thus, equation of bed-load transport rate is

$$g_{bs} = \frac{\tau_0 U}{\tan \phi_d} e_b \quad \wedge \quad g_b = \frac{s}{\Delta} g_{bs} \Rightarrow g_b = \frac{\tau_0 U s}{\Delta \tan \phi_d} e_b \quad (5.104)$$

Fig. 5.12 Variation of bed-load transport efficiency e_b with U for different particle sizes d



The variation of bed-load transport efficiency e_b with U for different particle sizes d given by Bagnold is shown in Fig. 5.12. The prediction of e_b is possible for $d = 0.01$ – 1 mm.

5.8.2 Yalin's Approach

Yalin (1977) proposed a bed-load transport model based on the analysis of forces acting on a sediment particle. The equations of force acting on a moving sediment particle in the streamwise and normal directions are

$$F_x = m_G \frac{du_b}{dt} \quad (5.105a)$$

$$-F_z - F_G = m_G \frac{dw_b}{dt} \quad (5.105b)$$

where F_x and F_z are the force components of flow acting on a particle in the streamwise and normal directions, respectively, and u_b and w_b are the velocity components of a sediment particle in the streamwise and normal directions, respectively. The force components F_x and F_z are given by

$$F_x = \frac{\pi}{8} C_{Dx} \rho d^2 (u_d - u_b)^2 \quad (5.106a)$$

$$F_z = \frac{\pi}{8} C_{Dz} \rho d^2 w_b^2 \quad (5.106b)$$

where u_d is the instantaneous streamwise flow velocity at the particle level.

A particle detaches from the bed by the action of hydrodynamic lift force F_L . The difference $F_L - F_G > 0$ near the bed reduces with distance from the bed and becomes $F_L - F_G = 0$ at an elevation where the particle reaches its maximum

vertical velocity component $[w_b]_{\max}$. The $[w_b]_{\max}$ can be determined from the following equation:

$$-F_z - F_G + F_L = m_G \frac{dw_b}{dt} \quad (5.107)$$

Equation (5.107) represents the initial condition of Eq. (5.105b). To solve these equations, Yalin made the assumptions: (1) The F_L/F_G ratio decreases with z/d according to the exponential law, that is $F_L/F_G \sim \exp(-z/d)$, (2) the drag coefficients C_{Dx} and C_{Dz} are constants, and (3) the nondimensional flow velocity u/u_* in the vicinity of the bed is constant.

As a result, he obtained an expression for u_b and then its average value \bar{u}_b over the time when the particle is in motion. It is given by

$$\bar{u}_b = u_* C_1 \left\{ 1 - \frac{\Theta_c}{a_1(\Theta - \Theta_c)} \ln \left[1 + a_1 \left(\frac{\Theta}{\Theta_c} - 1 \right) \right] \right\} \quad (5.108)$$

where $a_1 = 2.45\Theta_c^{0.5}/s^{0.4}$ and C_1 is a constant to be determined. He determined the submerged weight of the bed-load transport per unit area W_s from the dimensional analysis. It follows

$$\frac{W_s}{\Delta \rho g d} = f_1(\Theta, R_{*d}) \quad (5.109)$$

where $\Theta = R_b S_0/(\Delta d)$, R_b is the hydraulic radius, and $R_{*d} = u_* d/v$. Equation (5.109) can be rewritten as

$$\frac{W_s}{\Delta \rho g d} = f_2 \left(\Theta, \frac{\Delta g d^3}{v^2} \right) \quad \wedge \quad R_{*d} = \left(\frac{\Delta g d^3}{v^2} \Theta \right)^{0.5} \quad (5.110)$$

At the threshold of particle motion, $\Theta(W_s = 0) = \Theta_c$, and thus

$$f_2 \left(\Theta_c, \frac{\Delta g d^3}{v^2} \right) = 0 \quad (5.111)$$

Equations (5.110) and (5.111) are combined to

$$\frac{W_s}{\Delta \rho g d} = f_2(\Theta, \Theta_c) \quad (5.112)$$

Yalin assumed that the left-hand side of Eq. (5.112) is linearly proportional to nondimensional excess bed shear stress. Hence,

$$\frac{W_s}{\Delta \rho g d} = C_2 \left(\frac{\Theta}{\Theta_c} - 1 \right) \quad (5.113)$$

where C_2 is a constant to be determined.

Substituting Eqs. (5.108) and (5.113) into Eqs. (5.105a, b) and determining the constants from the measured data, the bed-load transport rate g_b in weight per unit time and width is given by $g_b = (s/\Delta)g_{bs} = (s/\Delta)W_s\bar{u}_b$. Thus, the bed-load equation of Yalin is

$$g_b = 0.635 \rho_s g d u_* \left(\frac{\Theta}{\Theta_c} - 1 \right) \left\{ 1 - \frac{\Theta_c}{a_1(\Theta - \Theta_c)} \ln \left[1 + a_1 \left(\frac{\Theta}{\Theta_c} - 1 \right) \right] \right\} \quad (5.114)$$

Equation (5.114) can be expressed in nondimensional form as

$$\Phi_b = 0.635 \Theta^{0.5} \left(\frac{\Theta}{\Theta_c} - 1 \right) \left\{ 1 - \frac{\Theta_c}{a_1(\Theta - \Theta_c)} \ln \left[1 + a_1 \left(\frac{\Theta}{\Theta_c} - 1 \right) \right] \right\} \quad (5.115)$$

For initiation of bed-load transport, $\Theta \rightarrow \Theta_c$ and $a_1[(\Theta/\Theta_c) - 1] \approx 0$. Hence, one can write

$$\frac{\Theta_c}{a_1(\Theta - \Theta_c)} \ln \left[1 + a_1 \left(\frac{\Theta}{\Theta_c} - 1 \right) \right] \approx 1 - \frac{1}{2} \cdot a_1 \left(\frac{\Theta}{\Theta_c} - 1 \right) \quad (5.116)$$

The bed-load transport rate equation, Eq. (5.115), becomes

$$\Phi_b = 0.635 a_1 \frac{\Theta^{0.5}}{2} \left(\frac{\Theta}{\Theta_c} - 1 \right)^2 \quad (5.117)$$

For high intensity bed-load transport rate, $\Theta \gg \Theta_c$ and $(\Theta - \Theta_c) \rightarrow \infty$. Hence, it is given by

$$\frac{\Theta_c}{\Theta - \Theta_c} \rightarrow 0 \quad (5.118)$$

The bed-load transport rate equation, Eq. (5.115), then becomes

$$\Phi_b = 0.635 \Theta^{0.5} \left(\frac{\Theta}{\Theta_c} - 1 \right) \quad (5.119)$$

5.9 Equal Mobility Concept for Bed-Load Transport

Parker et al. (1982) developed a concept of equal mobility assuming that the bed-load transport of gravels can be accomplished through mobility of the particles exposed to the flow. The participation of the underneath particles in bed-load transport can only be possible up to the extent of the degradations that can result in an exposure of those particles to the flow. They referred coarser surface layer with bed-load transport as *pavement*; however, it is different from an *armor layer*. In this concept, the particle size distribution of bed load is approximated by that of underneath particles for all flows capable of mobilizing the majority of available gravel sizes.

Based on the equal mobility concept, Parker et al. (1982) developed a functional relationship between a bed-load transport function Φ_{bi}^+ and a bed shear stress parameter Θ_i^+ for a gravel size of d_i . The Φ_{bi}^+ and Θ_i^+ are given by

$$\Phi_{bi}^+ = \frac{\Delta g_{bi}}{p_i (ghS_0)^{0.5} hS_0} \quad (5.120a)$$

$$\Theta_i^+ = \frac{hS_0}{\Delta d_i \tau_{0i}^+} \quad (5.120b)$$

where g_{bi} is the bed-load transport rate per unit width for the fractional particle size d_i , p_i is the fraction by weight of size d_i , and $\tau_{0i}^+ = 0.0875(d_{50}/d_i)$.

Due to equal mobility of all sizes, a specific particle size, termed *subpavement size* and denoted by d_{50} , is used to characterize the bed-load transport. Based on the field data of gravel-bed streams with sizes from 18 to 28 mm, Parker et al. (1982) proposed

$$\Phi_b^+ (0.95 < \Theta_{50}^+ < 1.65) = 2.5 \times 10^{-3} \exp[14.2(\Theta_{50}^+ - 1) - 9.28(\Theta_{50}^+ - 1)^2] \quad (5.121a)$$

$$\Phi_b^+ = 11.2 \left(1 - \frac{0.822}{\Theta_{50}^+} \right)^{4.5} \quad (5.121b)$$

where Θ_{50}^+ is the bed shear stress parameter defined in Eq. (5.120b) corresponding to subpavement size d_{50} .

5.10 Sediment Pickup Function

Pickup rate, defined as volume rate of sediment removal per unit area, was studied by different investigators. Although the mode of bed-load transport according to the concept of pickup is not clear, there are three concepts of sediment pickup. As

already discussed, Einstein (1950) hypothesized that after a period of rest, a sediment particle can only be picked up. The period of rest is longer than that of pickup. In his hypothesis, the total distance between two successive periods of rest can be traveled by a particle by performing several brief jumps. A particle covers an average step length of $100d$ by performing a jump. However, the pickup definition of Yalin (1977) is different from that of Einstein. Yalin hypothesized that a particle can be picked up when it detaches the bed surface to perform a jump. It implies that a jump by a particle involves a pickup and then deposition. According to de Ruiter (1982, 1983), the period of pickup equals the time period required to travel (from rest) by a particle over a distance of its half the diameter.

The approach of Einstein (1950) was stochastic. He assumed that a sediment particle is lifted when the instantaneous lift having a Gaussian distribution exceeds the submerged weight of the particle. His sediment pickup formula is

$$\Phi_p = \alpha_p p \quad (5.122)$$

where α_p is the coefficient and p is pickup or removal probability, that is the time fraction during which a sediment particle is picked up by the flow, which has already been discussed in Einstein's approach.

Fernandez Luque (1974) used experimental data for $0.9 \leq d \leq 1.8$ mm and proposed

$$\Phi_p(0.05 \leq \Theta \leq 0.11) = \alpha_p (\Theta - \Theta_c)^{1.5} \quad (5.123)$$

According to Yalin (1977), the period of pickup is proportional to the ratio of the particle diameter to shear velocity. Using a stochastic approach, he obtained a sediment pickup formula as

$$\Phi_p = \alpha_p p \Theta \quad (5.124)$$

Based on experimental data ($3 \leq d \leq 13.5$ mm), Nakagawa and Tsujimoto (1980) suggested

$$\Phi_p(0.03 \leq \Theta \leq 0.2) = \alpha_p \left(1 - \frac{0.035}{\Theta}\right)^3 \Theta \quad (5.125)$$

They recommended $\alpha_p = 0.02$ for spherical particles.

According to de Ruiter (1982, 1983), the pickup time period was found to be much smaller than that of instantaneous bed shear stress exceeding its threshold value. Based on stochastic approach, he proposed

$$\Phi_p = \alpha_p p_p \left(\frac{\sigma_0}{\Delta \rho g d} \cdot \frac{\tan \phi}{\Theta_c} \right)^{0.5} \quad (5.126)$$

where p_p is the pickup probability function and σ_0 is the standard deviation of instantaneous bed shear stress. The value of coefficient α_p , recommended by de Ruiter, is 0.016.

van Rijn (1984b) conducted experiments with different sand sizes ($0.13 \leq d \leq 1.5$ mm) and proposed an empirical equation of pickup function as

$$\Phi_p = 3.3 \times 10^{-4} D_*^{0.3} \left(\frac{\Theta}{\Theta_c} - 1 \right)^{1.5} \quad (5.127)$$

Dey and Debnath (2001) performed experiments with various uniform and nonuniform sand sizes ($0.24 \leq d \leq 1.55$ mm). Considering the effects of sediment nonuniformity, they proposed

$$\Phi_p = 6 \times 10^{-4} D_*^{0.24} \left(\frac{\Theta}{\Theta_c} - 1 \right) \sigma_g^{1.9} \quad (5.128)$$

where σ_g is the geometric standard deviation of particle size distribution.

5.11 Saltation

5.11.1 Characteristics of Saltation

When the bed shear stress just exceeds the threshold value for the initiation of particle motion, the particles roll and/or slide in contact with the bed. As the bed shear stress increases further, the particles move along the bed by a series of short jumps with approximately same step lengths. This phenomenon is called *saltation*. The saltation of a particle is governed by the hydrodynamic drag and lift forces and also the bed roughness. Due to the gravity, the particle begins to descend and returns to the bed when it is lifted by the hydrodynamic force to a certain height. In this way, the particle undergoes a saltation process as shown in Fig. 5.13. Subsequently, a new step of saltation may begin as a result of an impact against the bed and the lift force. According to the laboratory experimental observations by Francis (1973) and Abbott and Francis (1977), the characteristics of a saltating particle are described as follows:

The particle transport in saltation mode is limited to a maximum height of about ten times the particle diameter. The particle motion is dominated by the gravitational force, although it can be set off by the impulses of velocity fluctuations (near-bed turbulence agitations) during bursting events or by the effects of wall shear flow that a particle experiences a shear lift due to the velocity gradient in the vicinity of the bed. The hydrodynamic pressure and the viscous skin friction can also be the sources to provide momentum to the particles. In the rising stage of particle trajectory, the vertical component of the drag force and the gravitational

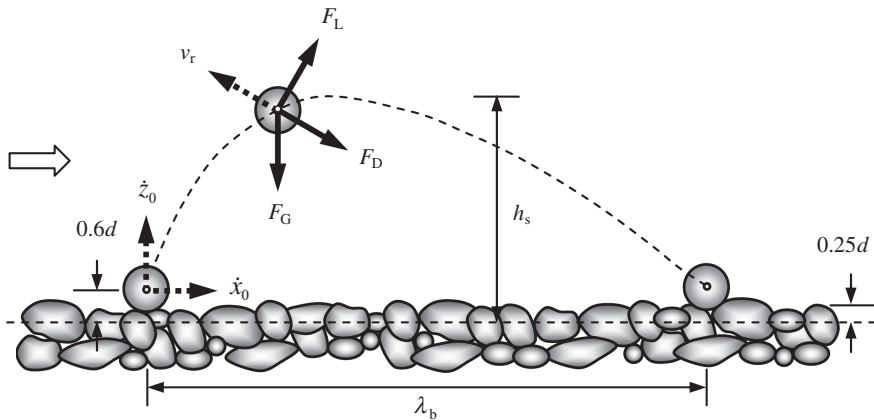


Fig. 5.13 Schematic of a particle saltation

force are together directed downwards; while in the falling stage of particle trajectory, the vertical component of drag force being directed upwards opposes the gravitational force. The lift force is always directed upwards provided the particle velocity to lag behind the fluid velocity at the saltating particle.

It is observed that some particles move in the form of series of saltations. It means that after the particles coming back to the bed performing a saltation, they immediately perform next saltation without any pause on the bed. It is obvious that the lift force is the main cause of lifting up the particles from the bed. However, the effects of the bed impact force by no means can be neglected. As a saltating particle strikes the bed particles, it may either ricochet off the bed particles or impact against them. During the impact of the particles with the bed particles, majority of the momentum, that they possess, is transferred to the bed particles in a succession of horizontal impulses. It may cause to initiate a rolling motion of the surface particles, termed *surface creep*. However, a saltating particle may cease motion, if it falls within one of the local depressions on the bed surface.

5.11.2 Particle Trajectory and Characteristic Parameters (van Rijn's Approach)

The forces acting on a saltating particle, as shown in Fig. 5.13, were analyzed by van Rijn (1984a). In fact, he analyzed the problem deterministically in the context of estimation of bed-load transport rate. In Fig. 5.13, the forces are the submerged weight of the particle F_G acting downwards and the hydrodynamic force components in the form of drag and lift. The direction of drag force F_D is opposite to the direction of the particle velocity v_r relative to the fluid flow; whereas the lift force is in the normal direction.

Equations of motion: The trajectory of a saltating particle can be determined by solving the equations of motion. Assuming a spherical saltating particle and the forces due to fluid accelerations to be of a second order, the equations of motion, according to White and Schultz (1977), can be written as

$$m_a \ddot{x} - F_L \left(\frac{\dot{z}}{v_r} \right) - F_D \left(\frac{\bar{u} - \dot{x}}{v_r} \right) = 0 \quad (5.129a)$$

$$m_a \ddot{z} - F_L \left(\frac{\bar{u} - \dot{x}}{v_r} \right) + F_D \left(\frac{\dot{z}}{v_r} \right) + F_G = 0 \quad (5.129b)$$

where m_a is the particle mass plus *added fluid mass*, v_r is the particle velocity relative to the fluid flow, that is $[(\bar{u} - \dot{x})^2 + \dot{z}^2]^{0.5}$, \bar{u} is the local time-averaged flow velocity in x -direction, \dot{x} and \dot{z} are the streamwise and vertical velocities of particle, respectively, and \ddot{x} and \ddot{z} are the streamwise and vertical accelerations of particle, respectively.

The *added fluid mass* or *virtual mass* is the inertia added to a system. An accelerating or decelerating particle is to move some volume of surrounding fluid, as it moves through it, since the particle and fluid cannot occupy the same physical space simultaneously. For simplicity, this can be assumed as some volume of fluid moving with the particle, though in reality all the fluid is accelerated to various degrees. Therefore, the total mass of a spherical particle can be given by

$$m_a = \frac{1}{6}(\rho_s + \alpha_m \rho) \pi d^3 \quad (5.130)$$

where α_m is the added mass coefficient. Assuming a potential flow, the added mass of a sphere is obtained as the half of the fluid mass displaced by the sphere. However, in real fluid flow, the flow is separated from the sphere and α_m may be different from that for a potential flow. The value $\alpha_m = 0.5$ was considered by van Rijn.

The drag force F_D , which is resulted from the pressure and the viscous skin frictional effects, can be expressed as

$$F_D = C_D \frac{\rho}{2} v_r^2 \frac{\pi}{4} d^2 \quad (5.131)$$

The drag coefficient C_D can be determined from the empirical expressions given by Morsi and Alexander (1972).

The lift on a particle in the wall shear layer of flow is induced by two ways. They are due to (1) velocity gradient in the shear layer and (2) spinning motion of the particle as a *Magnus effect*. For a sphere moving in a viscous fluid flow, Saffman (1968) determined the lift F_{Ls} due to shear as

$$F_{Ls} = C_L \rho v^{0.5} d^2 v_r \left(\frac{\partial u}{\partial z} \right)^{0.5} \quad (5.132)$$

The Magnus lift F_{Lm} due to spinning motion in a viscous fluid flow obtained by Rubinow and Keller (1961) is given by

$$F_{Lm} = C_L \rho d^3 v_r \omega \quad (5.133)$$

where ω is the angular velocity of the particle. The total lift force F_L is therefore

$$F_L = F_{Ls} + F_{Lm} \quad (5.134)$$

The submerged weight of the spherical particle is given by Eq. (4.9). The velocity distribution in the wall shear layer is assumed to follow the logarithmic law given by Eq. (4.27), where the zero-velocity level can be considered as $z_0 = 0.11(v/u_*) + 0.03k_s$.

Boundary conditions and solution scheme: The virtual bed level is assumed to be at $0.25d$ below the top of the bed particles, as shown in Fig. 5.13. The initial position of the particle lying on closely packed bed particles is $0.6d$ above the virtual bed level. Here, d is the representative particle size, assumed to be d_{50} . According to the experimental observations by Francis (1973) and Abbott and Francis (1977), $\dot{x} = \dot{z} = 2u_*$. Equations (5.129a, b) were first transformed⁴ by van Rijn to a system of ordinary simultaneous differential equations of the first order. Then, he solved them by a numerical method known as automatic step-change differential equation solver. The characteristic parameters of saltating particles were computed for the range $u_* = 0.04\text{--}0.14 \text{ m s}^{-1}$ and $d_{50} = 0.1\text{--}2 \text{ mm}$. He assumed $k_s = 2d_{50}$ and calibrated C_L as $C_L(R_{*d} \leq 5) = 1.6$, $C_L(5 < R_{*d} < 70) = 1.6\text{--}20$ varying linearly, and $C_L(R_{*d} \geq 70) = 20$.

Characteristic parameters of saltating particles: The saltation length λ_b and height h_s were first computed. Then, they are empirically correlated with the nondimensional particle parameter $D_* [= d(\Delta g/v^2)^{1/3}]$ and the nondimensional excess bed shear stress $(\Theta/\Theta_c) - 1$ as follows (van Rijn 1984a):

$$\frac{\lambda_b}{d_{50}} = 3D_*^{0.6} \left(\frac{\Theta}{\Theta_c} - 1 \right)^{0.9} \quad (5.135a)$$

$$\frac{h_s}{d_{50}} = 0.3D_*^{0.7} \left(\frac{\Theta}{\Theta_c} - 1 \right)^{0.5} \quad (5.135b)$$

⁴ The procedure of transformation of second order differential equation to first order and the numerical solution methodology of a system of ordinary simultaneous differential equations can be found in Bose (2009).

Table 5.1 Formulas of saltation length λ_b and height h_s proposed by different investigators

References	Saltation length	Saltation height
Fernandez Luque and van Beek (1976)	$\lambda_b/d_{50} = 16$	–
Abbott and Francis (1977)	$\lambda_b = \lambda_b(\Theta)$	$h_s = h_s(d_{50}, \Theta)$
Sekine and Kikkawa (1992)	$\lambda_b/d_{50} = 3000(u_*/w_s)^{1.5}$ $\times (u_* - u_{*c})/u_*$ where u_{*c} = threshold shear velocity	–
Niño et al. (1994)	$\lambda_b/d_{50} = 2.3\Theta/\Theta_c$	$h_s = h_s(d_{50}, \Theta/\Theta_c)$
Lee and Hsu (1994)	$\lambda_b/d_{50} = 196.3(\Theta - \Theta_c)^{0.788}$	$h_s/d_{50} = 14.3(\Theta - \Theta_c)^{0.575}$
Hu and Hui (1996)	$\lambda_b/d_{50} = 27.5 s^{0.94}\Theta^{0.9}$	$h_s/d_{50} = 1.78 s^{0.86}\Theta^{0.69}$
Lajeunesse et al. (2010)	$\lambda_b/d_{50} = 70(u_* - u_{*c})/w_s$	–

The above equations suggest that the saltation length and height increase with an increase in particle parameter and excess bed shear stress, but independent of flow depth. Experimental observations by Poreh et al. (1970) on saltation length and Williams (1970) on saltation height confirmed that $\lambda_b \approx 8d_{50}$ for $d_{50} = 1.35$ mm and $h_s = 5\text{--}40d_{50}$ for $d_{50} = 1.9$ mm. The results obtained from Eqs. (5.135a, b) are more or less in conformity with these experimental results. Besides van Rijn's Eqs. (5.135a, b), Table 5.1 furnishes the formulas of saltation length λ_b and height h_s proposed by different investigators. It is obvious that their results are quite varying from one another.

For a saltating particle, van Rijn (1984a) computed the mean velocity \bar{u}_b as a function of nondimensional particle parameter and nondimensional bed shear stress as

$$\frac{\bar{u}_b}{u_*} = 9 + 2.6 \log D_* - 8 \left(\frac{\Theta_c}{\Theta} \right)^{0.5} \quad (5.136)$$

Further, van Rijn (1984a) approximated Eq. (5.136) in a simpler form as

$$\frac{\bar{u}_b}{(\Delta g d_{50})^{0.5}} = 1.5 \left(\frac{\Theta}{\Theta_c} - 1 \right)^{0.6} \quad (5.137)$$

Besides Eqs. (5.136) and (5.137), Table 5.2 furnishes the formulas of mean velocity \bar{u}_b of a saltating particle given by different investigators.

Bed-load transport rate: van Rijn (1984a) defined the bed-load transport rate q_b as a product of the particle velocity \bar{u}_b , the volumetric concentration C of transported particles, and the saltation height h_s . It is therefore given by

Table 5.2 Formulas of mean velocity \bar{u}_b of a saltating particle given by different investigators

References	Mean velocity of particle
Fernandez Luque and van Beek (1976)	$\bar{u}_b = 11.5(u_* - 0.7u_{*c})$
Engelund and Fredsøe (1976)	$\bar{u}_b = u_* [10 - 0.7(\Theta_c/\Theta)^{0.5}]$
Abbott and Francis (1977)	$\bar{u}_b = a(u_* - u_{*c}) \quad \wedge \quad a = 13.4 - 14.3$
Sekine and Kikkawa (1992)	$\bar{u}_b = 8(u_*^2 - u_{*c}^2)^{0.5}$
Niño et al. (1994)	$\bar{u}_b = a(u_* - u_{*c}) \quad \wedge \quad a = 6.8 - 8.5$
Lee and Hsu (1994)	$\bar{u}_b = 11.53u_* (\Theta - \Theta_c)^{0.174}$
Hu and Hui (1996)	$\bar{u}_b = 11.9(u_* - 0.44u_{*c})$

$$q_b = \bar{u}_b C h_s \quad (5.138)$$

Note that if the saltation height h_s is replaced by the thickness δ_b of bed-load transport layer, then Eq. (5.138) becomes Eq. (5.3). Analysis of the experimental data by van Rijn (1981) showed that the bed-load concentration C (by volume) can be represented by

$$\frac{C}{C_0} = \frac{0.18}{D_*} \left(\frac{\Theta}{\Theta_c} - 1 \right) \quad (5.139)$$

where C_0 is the maximum bed-load concentration. He determined $C_0 = 0.65$. It is interesting to note that the bed-load concentration C is inversely proportional to the nondimensional particle parameter and directly proportional to the nondimensional excess bed shear stress. Using Eqs. (5.135b), (5.137) and (5.139) into Eq. (5.138), van Rijn (1984a) obtained a bed-load transport equation, which has already been given as Eq. (5.26) as a du Boys type equation.

5.12 Fractional Bed Load of Nonuniform Sediments

Natural streams are typically made up of nonuniform sediment mixtures, whose transport phenomenon is therefore of immense importance. Unlike the transport of uniform sediment, the problems related to fractional nonuniform sediment transport are rather complex, especially when the consideration is given to the shelter-exposure interactions of bed particles of different sizes. Einstein (1950) was the pioneer to develop fractional transport rate of nonuniform sediments. Since then, Ashida and Michiue (1972), Parker et al. (1982), Patel and Ranga Raju (1996), Wu et al. (2000), and some other investigators put forward different methods to calculate the fractional bed-load transport rate of nonuniform sediments. Besides, Hsu and Holly (1992) proposed a method to determine the size fractional composition of nonuniform bed load aided by probability and availability of mobile sediments. The probabilistic approach by Einstein (1950) and the equal mobility approach by

Parker et al. (1982) taking into the fractional transport rate have already been discussed. Here, some other important methods are introduced.

Ashida and Michiue's (1972) bed-load transport formula for uniform sediment is given by Eq. (5.22). This formula was found to overestimate the individual size fractions of bed-load transport rate when compared with the experimental data for nonuniform sediment mixtures. They recommended the values of Shields parameters to be corrected for the fractional size of sediment. Thus, the equation of fractional bed-load transport intensity is given by

$$\Phi_{bi} = 17(\Theta_i - \Theta_{ci})(\Theta_i^{0.5} - \Theta_{ci}^{0.5}) \quad \wedge \quad \Phi_{bi} = \frac{q_{bi}}{p_i(\Delta g d_i^3)^{0.5}} \quad \vee \quad q_{bi} = i_b q_b \quad (5.140)$$

where Θ_i and Θ_{ci} are the Shields parameter and threshold Shields parameter corresponding to a fraction p_i of size d_i , respectively, and i_b is the fraction of bed-load transport. Equation (5.140) thus can be used to compute total bed-load transport for the entire range of particle size distribution of the bed sediment.⁵

Hsu and Holly's (1992) method begins with the determination of the size distribution of transported sediment and then ends with the estimation of bed-load transport rate. The each fractional size d_i in the transported sediment is hypothesized to be proportional to the joint probability of its mobility under the prevailing hydraulic condition and its availability on the bed surface within the active layer. If the flow velocity fluctuations follow the Gaussian probability distribution, the probability p_{ri} of removal of size d_i is derived as

$$p_{ri} = \frac{1}{(2\pi)^{0.5} \sigma_{\tilde{u}_d}} \int_{(u_{cri}/\tilde{u}_d)-1}^{\infty} \exp\left(-\frac{\tilde{u}_d^2}{2\sigma_{\tilde{u}_d}^2}\right) d\tilde{u}_d = 0.5 - 0.5\text{erf}\left(\frac{(u_{cri}/\tilde{u}_d) - 1}{2^{0.5} \sigma_{\tilde{u}_d}}\right) \quad (5.141)$$

⁵ The procedure of computation of total bed-load transport for the entire range of particle size distribution of the bed sediment is as follows:

Step 1: Compute Φ_{bi} for the fraction p_i of sediment size d_i by using Einstein's approach or Ashida and Michiue's bed-load transport formula or by any other standard method given in this chapter.

Step 2: Compute $i_b q_b$ by using Eq. (5.140) as

$$\Phi_{bi} = \frac{q_{bi}}{p_i(\Delta g d_i^3)^{0.5}} \quad \wedge \quad q_{bi} = i_b q_b \Rightarrow i_b q_b = \Phi_{bi} \times p_i(\Delta g d_i^3)^{0.5}$$

Step 3: For each size fraction, the $i_b q_b$ can be computed in this way. The total bed-load transport can therefore be obtained by summing up the results over the entire range of particle size distribution.

Note: In case of a mixture of small size of sediment spread, the size d_{35} can be approximated as an effective sediment size for the approximate estimation of total bed-load.

where $\tilde{u}_d = u' / \bar{u}_d$, u' is the fluctuations of instantaneous streamwise velocity at the bed particle level, \bar{u}_d is the time-averaged streamwise velocity at the bed particle level, $\sigma_{\tilde{u}_d}$ is the standard deviation of \tilde{u}_d , and u_{cri} is the near-bed threshold velocity for the initiation of motion of sediment size d_i . They employed Qin's (1980) formula given by Eq. (4.160) for the computation of u_{cri} for a given size d_i , and used $\sigma_{\tilde{u}_d} = 0.2$, as suggested by Yen et al. (1988).

The availability of fractional size d_i is equivalent to its fractional representation β_{bi} on the bed surface within the active layer. Therefore, the fraction p_i of size d_i in the transported sediment is

$$p_i = \frac{p_{ri} \beta_{bi}}{\int_{d_{\min}}^{d_{\max}} p_{ri} \beta_{bi} dd} \quad (5.142)$$

In this way, the particle size distribution of the transported sediment in bed load is determined. Then, the weighted mean sediment size d_m and mean near-bed threshold velocity u_{crm} are estimated. For the estimation of bed-load transport rate for all fractional sizes, Hsu and Holly used Shamov's formula (Zhang et al. 1989):

$$g_b = 12.5g d_m^{0.5} \left(\bar{u}_d - u_{cr}|_{d_{\min}} \right) \left(\frac{\bar{u}_d}{u_{crm}} \right)^3 \left(\frac{d_m}{h} \right)^{0.25} \quad \wedge \quad u_{cr}|_{d_{\min}} = u_{cr}(d_{\min}) \quad (5.143)$$

Hsu and Holly originally expressed g_b in mass of bed-load transport rate per unit width. The right-hand side of Eq. (5.143) is multiplied by g (acceleration due to gravity) to convert the unit to $\text{N m}^{-1} \text{s}^{-1}$.

Patel and Ranga Raju (1996) expressed the fractional bed-load transport intensity Φ_{bi} as a function of $\Theta_{ci} \zeta_b$. In fact, they corrected the threshold Shields parameter Θ_{ci} corresponding to fractional size d_i by a factor ζ_b , termed *hiding-exposure correction factor*. The estimation of ζ_b is as follows:

$$\zeta_b = \frac{0.0713}{C_m (C_s \Theta_{ci})^{0.75144}} \quad \wedge \quad \Theta_{ci} = \frac{\tau'_{0i}}{\Delta \rho g d_i} \quad (5.144a)$$

$$C_m(M > 0.38) = 1, C_m(0.05 < M \leq 0.38) = 0.7092 \log M + 1.293 \quad (5.144b)$$

$$\log C_s = 0.0644\tau^{*3} - 0.1949\tau^{*2} - 0.9571\tau^* - 0.1957 \quad \wedge \quad \tau^* = \log \left(\frac{\tau'_{0i}}{\tau_{0cg}} \right) \quad (5.144c)$$

where M is the Kramer's uniformity parameter, $\tau'_{0i} = \rho g R'_b S_0$, $R'_b = (Un'/S_0^{0.5})^{1.5}$, $n' = d_{65}^{1/6}/24$, and τ_{0cg} is the threshold bed shear stress for the geometric mean size d_g [$\approx (d_{84.1} d_{15.9})^{0.5}$] of the nonuniform sediment mixture as per Shields. The variation of fractional bed-load transport intensity Φ_{bi} with $\Theta_{ci} \zeta_b$ obtained by Patel and Ranga Raju (1996) is illustrated in Fig. 5.14.

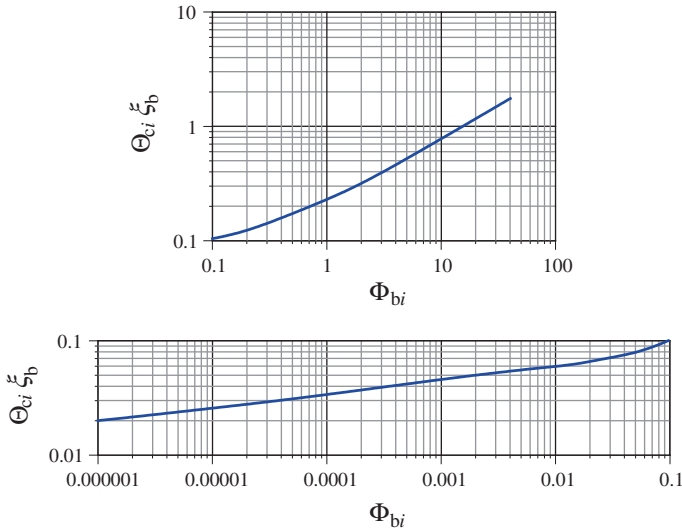


Fig. 5.14 Curve to estimate fractional bed-load transport rate (Patel and Ranga Raju 1996)

Wu et al. (2000) presented a relationship of fractional bed-load transport intensity Φ_{bi} as a function of nondimensional excess particle bed shear stress. It is

$$\Phi_{bi} = 5.3 \times 10^{-3} \left[\left(\frac{n'}{n} \right)^{1.5} \left(\frac{\tau_0}{\tau_{0ci}} \right) - 1 \right]^{2.2} \quad (5.145)$$

where $n' = d_{50}^{1/6}/20$, τ_{0ci} is the threshold bed shear stress corresponding to size d_i , $\tau_0 = \rho g R_b S_0$, R_b is the total hydraulic radius, and n is the Manning roughness coefficient ($= R_b^{2/3} S_0^{0.5}/U$).

Note that one can use Meyer-Peter and Müller (1948) formula for the estimation of fractional bed-load transport intensity Φ_{bi} (van Rijn 1993). The threshold bed shear stress is corrected to account for the nonuniformity effect as $\zeta_i \Theta_c$. Then,

$$q_{bi} = 8p_i (\Delta g d_i^3)^{0.5} \left[\left(\frac{C_R}{C'_R} \right)^{1.5} \Theta_i - \zeta_i \Theta_c \right]^{1.5} \Rightarrow \Phi_{bi} = 8(\eta_c \Theta_i - \zeta_i \Theta_c)^{1.5} \quad (5.146)$$

In the above, the correction factor ζ_i given by Egiazaroff (1965) is

$$\zeta_i = \frac{\log^2 19}{\log^2 (19d_i/d_m)} \quad \wedge \quad d_m = \sum p_i d_i \quad (5.147)$$

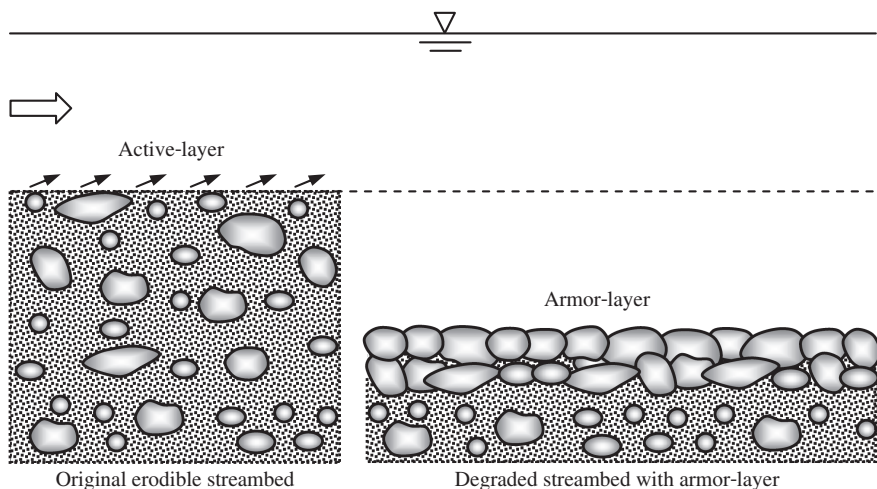


Fig. 5.15 Definition sketch of streambed armoring

5.13 Sediment Sorting and Streambed Armoring

The time-dependent transport rate of nonuniform sediment mixture is a complicated process due to sorting of a sediment bed in addition to sediment diffusion as suspension. In a sediment mixture, the resistance to an individual particle motion depends upon particle size and shape, as well as sheltering and exposure to the flow. *Sediment sorting* is defined as a selective transport of different fractional sizes of sediment particles. When the sediment transport rate of a bed exceeds the rate of sediment supply by the approaching flow, the sediment bed starts to degrade. *Active layer* refers to the surface layer of the sediment bed from which the sediment can be entrained to the flow. Because of the nonuniformity of the sediment, typically, exposed finer particles are transported easily at a faster rate than the coarser ones, and the remaining bed particles are being coarsened. Thus, the size of particles' sorting takes place. The weakly entrained or unentrained coarse particles tend to accumulate in the surface layer, forming a band of coarser particles. Gradually, this coarsening process stops until a layer of coarse particles is completely developed to cover the streambed protecting the underneath finer sediment particles from being transported. Once this process is completed, the streambed is called *armored* and the layer of coarsest particles is called the *armor layer* (Fig. 5.15).

Due to variable nature of flow condition of a natural streambed, typically one or more than one layers of armor particles are required to protect the underneath finer sediment particles (Fig. 5.16). Borah (1989) and Froehlich (1995) reported that the natural armor-layer thickness is one to three times the armor-particle sizes. However, the thickness, porosity, and particle size distribution of an armor layer

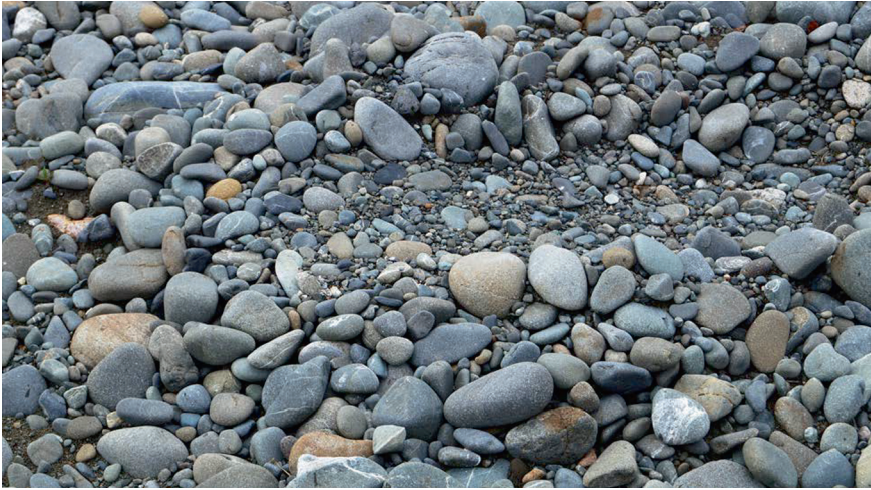


Fig. 5.16 Natural streambed armoring. Photograph by the author

vary with flow and bed evolution. Importantly, fine sediment can still be winnowed at a very feeble rate through the interstices of armored particles.

Borah et al. (1982) considered an active layer to be homogeneous within itself at any given time and proposed estimation for the thickness of the active layer t_a from the volumetric consideration as

$$t_a = \frac{1}{\sum_{i=M}^n p_i} \cdot \frac{d_M}{1 - \rho_{0M}} \quad (5.148)$$

where M is the fraction of the size d_M or larger than d_M , that cannot be transported by the flow, d_M is the size for the fraction M , and ρ_{0M} is the porosity for the fraction M . Thus, the fractional size d_M and larger sizes contribute to an armor layer.

In an active layer, the rate of transport from the bed surface decreases with time but does not truly go to zero even after a long time (several days). It implies that the development of an armor layer is an asymptotic process. When the bed shear stress increases, the finer particles are transported and coarser ones stay in place. Eventually, an upper limiting condition of the streambed is reached, which is called the *threshold armoring condition*. The corresponding bed shear stress is used to define the *threshold bed shear stress for armoring* τ_{0ca} . Hence, a sediment mixture has a range of bed shear stress over which its bed surface can be armored. The armor layer is thus now formed by the near-coarsest particles d_{90} or even coarser than d_{90} , which are found in a particle size distribution curve of nonuniform sediment. However, for a higher flow rate, when $\tau_0 > \tau_{0ca}$, the armor layer becomes unstable and subsequently is destroyed. Correia and Graf (1988) suggested the median size of armor particles: $d_{50a} \approx 1.4d_{50}$ and $d_{50a} \leq 0.6d_{90}$.

Raudkivi (1990) gave an empirical relationship for the estimation of stability of particles in an armor layer as

$$\frac{\Theta_{ca}}{\Theta_c} = \left[0.4 \left(\frac{d_{50}}{d_{50a|_{\max}}} \right)^{0.5} + 0.6 \right]^2 \quad \wedge \quad \Theta_{ca} = \frac{\tau_{0ca}}{\Delta \rho g d_{50a|_{\max}}} \quad \vee \quad \frac{d_{50a|_{\max}}}{d_{100}} \leq 0.55 \quad (5.149)$$

where Θ_{ca} is the threshold Shields parameter for the armoring particles and $d_{50a|_{\max}}$ is the maximum size of the armoring particles, being determined by extrapolating the particle size distribution curve on the basis of last two or three points. Importantly, no armoring takes place for uniform sediments.

In case of a nonuniform sediment sample with a mixture of fine and large particles (for example, sand and gravel), Chin et al. (1994) observed that the stability of individual large particles and their number in the bed govern the process of formation of a stable armor layer. The removal of finer particles from the bed surface exposes individual large particles. As a large particle is exposed considerably to the flow, it leads to the formation of an erosion pit in the front and a deposition of finer particles at the rear. The large particle may then slide into the erosion pit, reducing its exposure to the flow and becoming more stable. Medium and relatively coarse particles may also be accumulated within the scour pit and finer particles may hide behind and in between the larger ones. Gradually, this rearrangement of the surface particles leads to the formation of clusters of particles of various sizes. A cluster may slowly collapse with an erosion of the bed at its periphery. The anchor large particle may then be moved downstream to another stable position; and the process of cluster formation may be repeated. Thus, the formation of an armor layer in a nonuniform sediment mixture with fine and large particles is a continuous process involving formation and collapse of clusters. In Sect. 8.6, formation of cluster is further discussed.

5.14 Sediment Entrainment Probability to Bed Load

Determination of sediment entrainment probability to bed load is an essential prerequisite in developing a probabilistic theory of bed-load transport. Einstein (1942) laid the foundation of the probabilistic concept to study the bed-load transport, in which the probability of sediment removal was introduced. The most innovative development was due to Einstein (1950) to introduce a formula for the probability of sediment transport [see Eq. (5.70)]. It was based on the probability of hydrodynamic lift induced by the fluctuating velocity to exceed submerged particle weight, using the Gaussian distribution, as already discussed. The probability function p that is given by Eq. (5.69) can be written in a simplified form as

$$p = 1 - \frac{1}{\pi^{0.5}} \int_{-0.143\Theta^{-1}-2}^{0.143\Theta^{-1}-2} \exp(-t^2) dt \quad (5.150)$$

Subsequent investigations by other researchers viewed the probability of sediment removal in different ways and put forward formulation for probability in terms of entrainment or pickup probability function. The *entrainment probability function* is a function of Shields parameter Θ . Engelund and Fredsøe (1976) gave an empirical formula for the entrainment probability function [see Eq. (5.87)] by using experimental data of Guy et al. (1966) and Fernandez Luque (1974). The formula was subsequently modified by Fredsøe and Deigaard (1992) in the form

$$p = \left[1 + \left(\frac{\mu_d \pi / 6}{\Theta - \Theta_c} \right)^4 \right]^{-0.25} \quad (5.151)$$

However, following Einstein's concept of bed-load transport, Cheng and Chiew (1998) obtained an expression for the entrainment probability function, based on the assumption of the Gaussian distribution for the streamwise velocity fluctuations. They expressed the sediment entrainment probability in hydraulically rough flow regime as

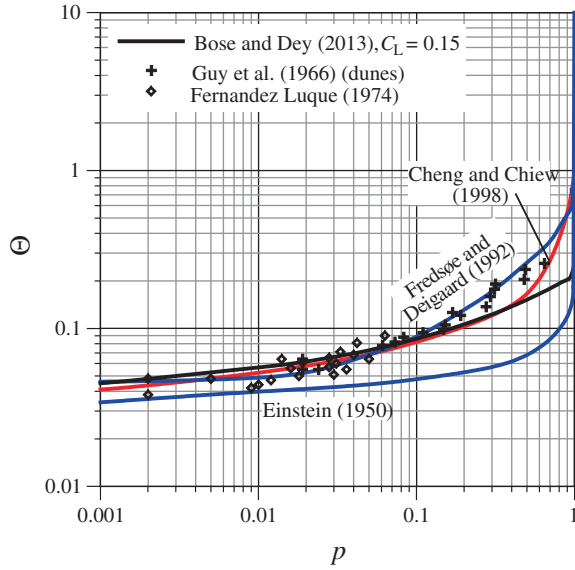
$$p = p(F_L > F_G) = p(u_d^2 > B^2) = p(u_d > B) + p(u_d < -B) \quad (5.152)$$

where u_d is the instantaneous near-bed velocity and $B = [4\Delta g d / (3C_L)]^{0.5}$. They estimated the time-averaged near-bed velocity \bar{u}_d , using the logarithmic law and fixing the zero-plane displacement level at $0.25d$ and the zero-velocity level z_0 at $k_s/30$ below the top of the closely packed bed particles. Here, k_s was considered as $2d$. They assumed that a particle placed in an interstice between two bed particles is about to move. In this way, they estimated $\bar{u}_d = 5.52u_*$ acting on the particle in an initial position at $z = 0.6d$. Quoting Kironoto and Graf (1994), Cheng and Chiew (1998) assumed $\sqrt{u'^2} = 2u_*$ and finally obtained the entrainment probability as

$$p = 1 - 0.5 \frac{0.21 - \sqrt{\Theta C_L}}{|0.21 - \sqrt{\Theta C_L}|} \sqrt{1 - \exp \left[- \left(\frac{0.46}{\sqrt{\Theta C_L}} - 2.2 \right)^2 \right]} - 0.5 \sqrt{1 - \exp \left[- \left(\frac{0.46}{\sqrt{\Theta C_L}} + 2.2 \right)^2 \right]} \quad (5.153)$$

Cheng and Chiew (1998) selected a value of $C_L = 0.25$ to fit Eq. (5.153) with the previous experimental data, as shown in Fig. 5.17.

Fig. 5.17 Variation of Shields parameter Θ with probability p of sediment entrainment (Bose and Dey 2013). The $\Theta(p)$ curves obtained from the approaches given by Einstein (1950), Fredsøe and Deigaard (1992) and Cheng and Chiew (1998), and the experimental data of Guy et al. (1966) and Fernandez Luque (1974) are shown for the comparison



Later, Wu and Lin (2002) noted that since only positive fluctuations in the streamwise velocity could cause entrainment of bed particles, a log-normal distribution could be better suited to derive an expression for the entrainment probability. They therefore modified the concept of entrainment probability as

$$p = p(u_d > B) = p(\ln u_d > \ln B) = 1 - p(-\infty < \ln u_d < \ln B) \quad (5.154)$$

Wu and Lin (2002) finally expressed the entrainment probability as

$$p = 0.5 - 0.5 \frac{\ln(0.044\Theta^{-1}C_L^{-1})}{|\ln(0.044\Theta^{-1}C_L^{-1})|} \sqrt{1 - \exp\left\{-\frac{2}{\pi} \left[\frac{\ln(0.044\Theta^{-1}C_L^{-1})}{0.724}\right]^2\right\}} \quad (5.155)$$

Bose and Dey (2013) argued that the Gaussian and the log-normal distributions primarily occur when there is additive and multiplicative accumulation of errors. This is, however, not the case of turbulent velocity fluctuations in open channel flow. *Bose–Dey universal probability theory* (see Sect. 3.17.1), on the other hand, gave the Gram–Charlier series expansion of the probability densities based on the two-sided exponential or Laplace distribution. They explained that the probability density function (henceforth pdf) $p_{\hat{u}}(\hat{u})$ for the nondimensional streamwise velocity fluctuations \hat{u} can be given by

$$p_{\hat{u}}(\hat{u}) = \frac{1}{2} \left[1 + \frac{1}{2} C_{10} \hat{u} - \frac{1}{8} C_{20} (1 + |\hat{u}| - \hat{u}^2) - \frac{1}{48} C_{30} \hat{u} (3 + 3|\hat{u}| - \hat{u}^2) \right. \\ \left. + \frac{1}{384} C_{40} (9 + 9|\hat{u}| - 3\hat{u}^2 - 6|\hat{u}^3| + \hat{u}^4) + \dots \right] \exp(-|\hat{u}|) \quad \wedge \quad \hat{u} = \frac{u'}{\sqrt{u'^2}} \quad (5.156)$$

Dey et al. (2012) obtained that the coefficients C_{10} and C_{30} are of the order of 0.001; while $C_{20} \approx -0.5$ and $C_{40} \approx 0.6$. Thus, it was assumed that $C_{20} \approx -0.5$ and the rest of the coefficients are effectively negligible due to their smallness or division by a large number, such as 384. Then, Eq. (5.156) reduces to

$$p_{\hat{u}}(\hat{u}) = \frac{1}{32} (17 + |\hat{u}| - \hat{u}^2) \exp(-|\hat{u}|) \quad (5.157)$$

The instantaneous near-bed streamwise velocity u_d , which can be decomposed as $u_d = \bar{u}_d + u'$, is the cause of an entrainment of particles lying on the bed. Wu and Lin (2002), following Nelson et al. (1995), argued that the entrainment is only possible when the velocity fluctuations $u' > 0$, for which the pdf according to Eq. (5.157) becomes the one-sided exponential based Gram–Charlier series. Therefore,

$$\left. \begin{aligned} p_{u'}(u' \geq 0) &= \frac{1}{16\sqrt{u'^2}} (17 + \hat{u} - \hat{u}^2) \exp(-\hat{u}) \\ p_{u'}(u' < 0) &= 0 \end{aligned} \right\} \quad (5.158)$$

where $p_{u'}(u')$ is the pdf for u' . It satisfies the condition

$$\int_{-\infty}^{\infty} p_{u'}(u') du' = \int_0^{\infty} p_{u'}(u') du' = 1$$

Following Einstein (1950), a particle placed on the bed is likely to be lifted by the flowing fluid provided $F_L > F_G$. Importantly, the instantaneous lift force F_L acting on a particle fluctuates in accordance with the velocity fluctuations u' of the near-bed velocity u_d ; while the submerged weight F_G of a particle is a constant for a given particle size. Therefore, $F_L > F_G$ implies that $u_d > B$ or $u' > B - \bar{u}_d$, where $B = [4\Delta g d / (3C_L)]^{0.5}$. Thus, using Eq. (5.158), the total entrainment probability p is

$$p = \int_{B - \bar{u}_d}^{\infty} p_{u'}(u') du' = \frac{1}{16} (16 - a - a^2) \exp(-a) \quad \wedge \quad a = \frac{B - \bar{u}_d}{\sqrt{u'^2}} \quad (5.159)$$

It is pertinent to mention that Dey et al. (2012) found that when the bed particles move, the von Kármán constant κ diminishes from its universal value 0.41, and the zero-plane displacement level and the zero-velocity level move up as compared to their values in immobile beds [also available in Dey and Raikar (2007), Gaudio et al. (2010), Dey et al. (2011), and Gaudio and Dey (2012)]. These modify the estimation of near-bed velocity from the logarithmic law as $\bar{u}_d = 6.4u_*$, which was used by Bose and Dey. Quoting Kironoto and Graf (1994), Cheng and Chiew (1998) estimated $\sqrt{u'^2} = 2u_*$. Using these results, the a can be expressed as

$$a = \frac{B - \bar{u}_d}{\sqrt{u'^2}} = \frac{1}{2\sqrt{\Delta g d \Theta}} \left(\sqrt{\frac{4\Delta g d}{3C_L}} - 6.4\sqrt{\Delta g d \Theta} \right) = \frac{1}{\sqrt{3C_L \Theta}} - 3.2 \quad (5.160)$$

Figure 5.17 depicts the theoretical $\Theta(p)$ curve for $C_L = 0.15$ obtained by solving Eq. (5.159) using Eq. (5.160). The theoretical curve matches well with the experimental data of Guy et al. (1966) and Fernandez Luque (1974). The data of Guy et al. (1966) that correspond to dunes have less agreement, because the analysis by Bose and Dey (2013) did not include the flow resistance due to bedforms. However, the curve obtained by Bose and Dey (2013) corresponds closely with the curves of Fredsøe and Deigaard (1992) and Cheng and Chiew (1998) for $p < 0.2$. The Shields parameter Θ for rough flow regime ($R_* > 70$, where R_* is the shear Reynolds number, $u_* k_s/\nu$) according to Yalin and Karahan's (1979) diagram is 0.046, for which the probability of entrainment is 0.1 % as obtained from Fig. 5.17. It implies that 0.1 % of all the particles on a given bed area are in motion under the threshold of sediment entrainment.

5.15 Effects of Bed Load on Velocity Distribution

Dey et al. (2012) conducted experiments to measure the velocity distributions and turbulence parameters in mobile-bed flow with bed-load transport and to compare them with those in a clear-water (immobile bed) flow. The experimental data for clear-water flow were used as a reference. For each sediment sample, an experimental set comprised of two different runs, such as clear-water and mobile-bed flow conditions. Fixed-bed roughness for a clear-water flow was prepared by gluing sediment on the flume bottom. The mobile-bed experiments were conducted to simulate the bed-load transport at a certain rate corresponding to the same flow condition as that of the clear-water flow. In mobile-bed experiments, the same sediment that was glued on the flume bottom was fed in the flow at a uniform rate to achieve a dynamic equilibrium condition of the mobile bed. A continuous weak sediment transport (as bed load) was established by the flow in the form of a thin sediment layer disallowing any bedforms to develop.

Figure 5.18 shows the vertical distributions of nondimensional time-averaged streamwise velocity u^+ for clear-water and mobile-bed flows. In order to fit the data points in the inner layer ($z \leq 0.2h$) to the universal logarithmic law of wall, the time-averaged streamwise velocity \bar{u} and the vertical distance z are scaled by u_* and d_{50} , such that $u^+ = \bar{u}/u_*$ and $z^+ = z/d_{50}$. For the convenience, the origin of z -axis is set at the top of the bed particles (that is the bed surface). As the flow regime was the rough-turbulent flow, it is customary to use d_{50} to scale z . Dey et al. used the values of u_* that were obtained from the Reynolds shear stress plots by extrapolating a linear curve fitting onto the bed surface. To plot the experimental data, they consider the logarithmic law expressed in nondimensional form. It is

$$u^+ = \frac{1}{\kappa} \ln \left(\frac{z^+ + \Delta z^+}{\zeta^+} \right) \quad (5.161)$$

where $\Delta z^+ = \Delta z/d_{50}$, Δz is the depth of the virtual bed level from the bed surface, $\zeta^+ = z_0/d_{50}$, and z_0 is the zero-velocity level. Figure 5.18 describes the logarithmic law showing the variations of u^+ with $z^+ + \Delta z^+$ for the experimental datasets. It is clear that a prior estimation of Δz^+ was an essential prerequisite to plot the data, and subsequent determination of κ and ζ^+ was required to fit the data to the logarithmic law given by Eq. (5.161). The determination of these parameters was done independently, as described below:

- Step 1: Having obtained u_* from the Reynolds shear stress plots by projecting straight line on the bed surface [see Eq. (3.20) and Fig. 3.11], such that $u_* = (-\overline{u'w'})^{0.5} \Big|_{z=0}$, the dataset $u^+(z^+)$ for the range $z \leq 0.2h$ were prepared for the data analysis.
- Step 2: As an initial trial, considering $\Delta z^+ = 0$, the values of κ and ζ^+ were determined from Eq. (5.161) by the regression analysis, and then, the regression coefficient RC was evaluated.
- Step 3: The values Δz^+ were increased at a regular interval by a small magnitude (say 0.001), and the values of κ and ζ^+ were determined in the same way as in step 2. The values of RC for each value of Δz^+ were checked, till RC became the maximum. Then, the corresponding values of Δz^+ , κ and ζ^+ were considered as parameters for Eq. (5.161).

The average values of $\Delta z^+ = 0.39$, $\kappa = 0.413$, and $\zeta^+ = 0.034$ obtained for clear-water flow are in agreement with those for the traditional logarithmic law over rough boundary. Typically, the customary values of these parameters for the rough beds are $\Delta z^+ = 0.25$, $\kappa = 0.41$, and $\zeta^+ = 0.033$ (van Rijn 1984a). Thus, for clear-water flow, the data collapse well on the average logarithmic law curve shown by a solid line in Fig. 5.18. On the other hand, the average values of $\Delta z^+ = 0.21$, $\kappa = 0.37$, and $\zeta^+ = 0.04$ obtained for mobile-bed flow suggest the modified values of the parameters for the logarithmic law over a rough mobile bed. It is obvious that for mobile-bed flow, the data exhibit some degree of scatter about the average logarithmic law curve. A comparison of the values of Δz^+ and ζ^+ for

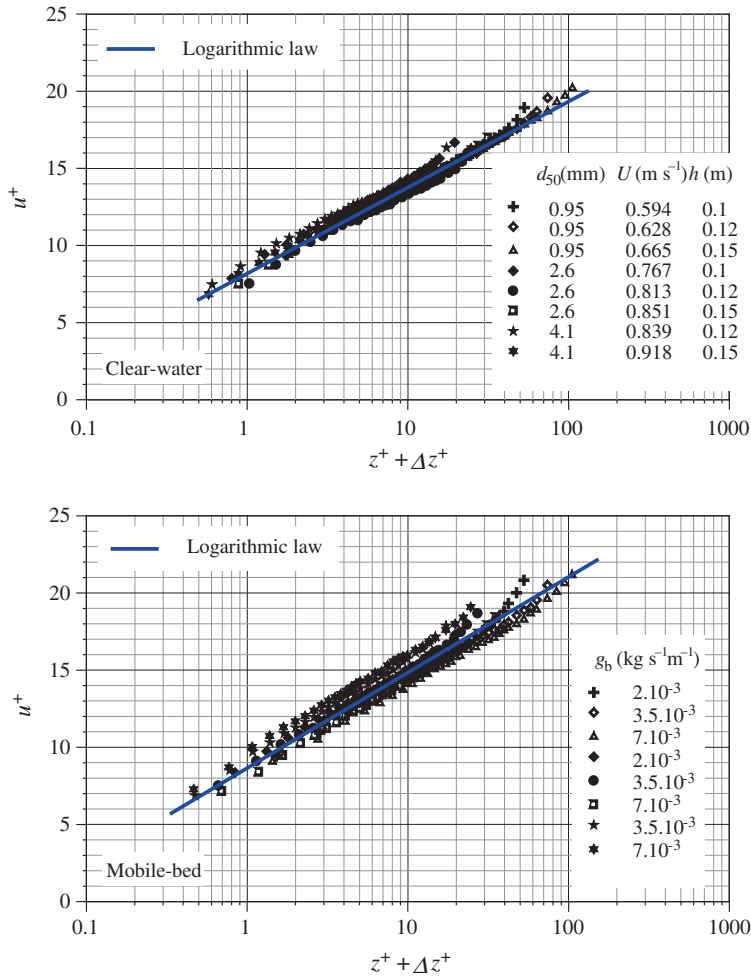


Fig. 5.18 Vertical distributions of nondimensional time-averaged streamwise velocity u^+ for clear-water and mobile-bed flows (Dey et al. 2012)

clear-water and mobile-bed flows reveals that the virtual bed and zero-velocity levels move up in the presence of bed-load transport. Although the data analysis related to the logarithmic law was done considering the data range $z \leq 0.2h$, Fig. 5.18 displays all the data plots for $z \leq 0.2h$ and $z > 0.2h$. Thus, the data plots depart from the logarithmic law in the outer layer to some extent. Additionally, the values of Nikuradse’s equivalent sand roughness k_s can be determined from the relationship of zero-velocity level as $k_s = 30\zeta^+d_{50}$. Finally, it can be concluded that for mobile-bed flow, (1) the von Kármán constant decreases and (2) the virtual bed and the zero-velocity levels move up.

5.16 Effects of Bed Load on Length Scales of Turbulence

According to Prandtl, the mixing length l , which defines a distance that a fluid parcel (eddy) keeps its original characteristics before dispersing into the surrounding fluid, is given by

$$l = \frac{(-\overline{u'w'})^{0.5}}{d\bar{u}/dz} \quad (5.162)$$

To calculate the mixing length l from Eq. (5.162), Dey et al. (2012) used the measured velocity profiles to determine the velocity gradients $d\bar{u}/dz$ by a smooth curve fitting to the data plots. They obtained the values of $-\overline{u'w'}$ directly from the measured Reynolds shear stress distributions. The variations of nondimensional mixing length $\tilde{l}(=l/h)$ with $\tilde{z}(=z/h)$ for clear-water and mobile-bed flows as obtained by Dey et al. are shown in Fig. 5.19. Within the wall shear layer ($z \leq 0.2h$), \tilde{l} varies linearly with \tilde{z} . All the experimental data points for clear-water and mobile-bed flows collapse reasonably on a single band, which is in conformity with Prandtl's mixing length hypothesis. Also, the data points collapse satisfactorily on the curves obtained from the theoretical equation of $\tilde{l} = \kappa\tilde{z}(1-\tilde{z})^{0.5}$ given by Nezu and Nakagawa (1993). The slope of the linear portion defining von Kármán constant $\kappa(=\tilde{l}/\tilde{z} = l/z)$ for mobile-bed flow is smaller than that for clear-water flow. It suggests that the traversing length of an eddy decreases with bed-load transport and increases more rapidly with z in a clear-water flow. A detailed discussion on nonuniversality of von Kármán constant κ is given in next section.

Studies by Gore and Crowe (1991), Hetsroni (1993), Crowe (1993), Best et al. (1997) argued that in flow with transported particles, the ratio of the size of transported particles to the length scale of turbulence is involved in influencing the enhancement or attenuation of the streamwise turbulence intensity. Taylor microscale λ_T , which defines the eddy size in the inertial subrange, is the relevant length scale of turbulence and is given by

$$\lambda_T = \left(\frac{15v\overline{u'^2}}{\varepsilon} \right)^{0.5} \quad (5.163)$$

where ε is the turbulent kinetic energy dissipation rate. The estimation of ε is done by using Kolmogorov second hypothesis that predicts the following equality describing the true inertial subrange (Pope 2001):

$$k_w^{5/3} S_{uu} = C\varepsilon^{2/3} \quad (5.164)$$

where k_w is the wave number, S_{uu} is the spectral density function for u' , and C is the constant approximately equaling 0.5 (Monin and Yaglom 2007).

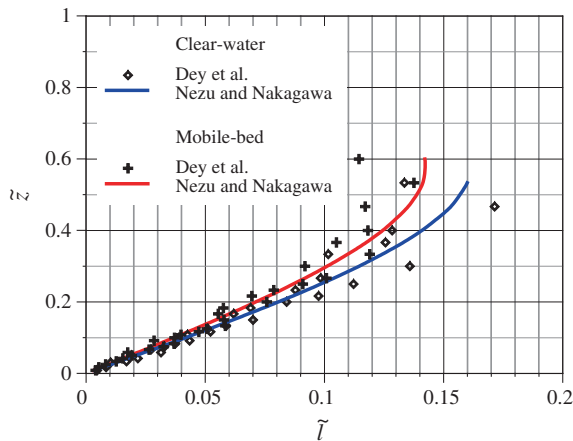


Fig. 5.19 Nondimensional mixing length \tilde{l} as a function of nondimensional vertical distance \tilde{z} for clear-water and mobile-bed flows (Dey et al. 2012)

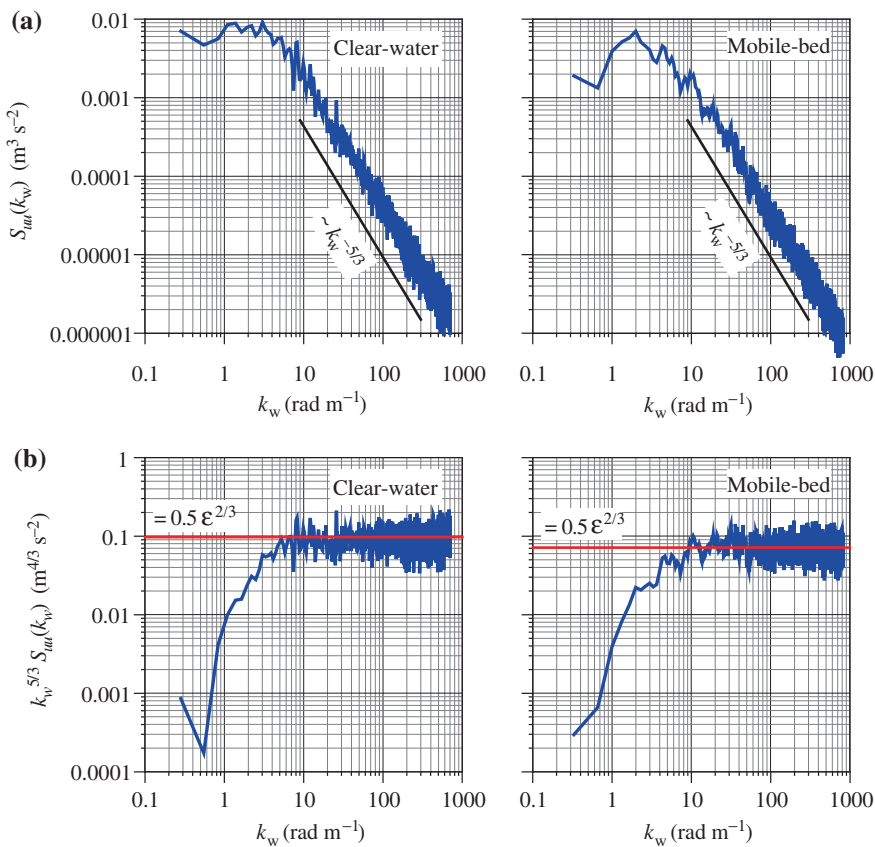
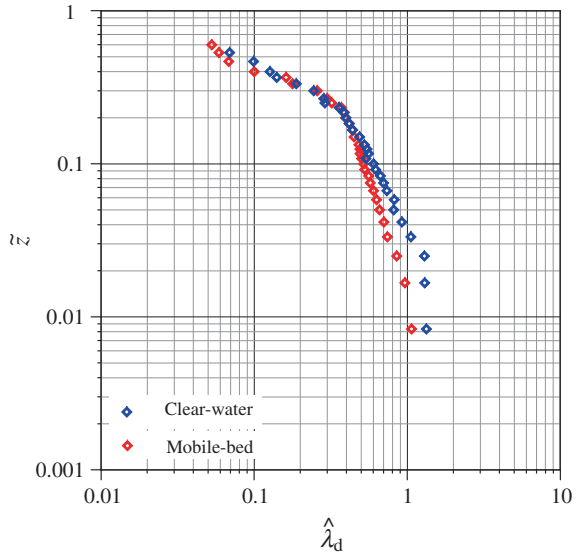


Fig. 5.20 **a** Velocity power spectra $S_{uu}(k_w)$. **b** Estimation of turbulent dissipation rate ε for clear-water and mobile-bed flows (Dey et al. 2012)

Fig. 5.21 Ratio of particle size to Taylor microscale $\hat{\lambda}_d$ as a function of nondimensional vertical distance \tilde{z} for clear-water and mobile-bed flows (Dey et al. 2012)



In Fig. 5.20a, the spectra $S_{uu} [= (0.5\bar{u}/\pi)F_{uu}(f)]$ as a function of $k_w [= (2\pi/\bar{u})f]$ are drawn using the despiked instantaneous velocity data at $z = 2$ mm (near-bed point) from the bed surface having $d_{50} = 2.6$ mm for clear-water and mobile-bed flows. For both flow conditions, the depth-averaged flow velocity was 0.851 m s^{-1} and the flow depth 0.15 m . The bed-load transport rate in mobile-bed experiment was $7 \times 10^{-3} \text{ kg s}^{-1} \text{ m}^{-1}$. The inertial subranges in clear-water and mobile-bed flows are characterized by Kolmogorov's $-5/3$ -th power law. It corresponds to a subrange of k_w , where the average value of $k_w^{5/3} S_{uu}$ is relatively constant (that is independent of k_w), as shown in Fig. 5.20b. Then, the ε was estimated from Eq. (5.164) and λ_T from Eq. (5.163).

Figure 5.21 shows the variations of the ratio of sediment size to Taylor microscale, that is $\hat{\lambda}_d = d_{50}/\lambda_T$, with \tilde{z} obtained by Dey et al. (2012) for the same flow condition mentioned above (clear-water and mobile-bed cases). Near the bed ($z \leq 0.1 h$), $\hat{\lambda}_d$ for mobile-bed flow is smaller than that for a clear-water flow. In the outer layer, $\hat{\lambda}_d$ for both the cases, the variation being almost same decreases away from the bed. The values of λ_T near the bed are 2 and 2.44 mm in clear-water and mobile-bed flows, respectively. Hence, the eddy size close to the bed increases in the presence of bed-load transport. Other studies on two-phase flows reported that the range $\hat{\lambda}_d \approx 0.2\text{--}1.2$ corresponds to the turbulence enhancement; while the range $\hat{\lambda}_d \approx 0.2\text{--}0.065$ corresponds to the turbulence attenuation (Gore and Crowe 1991; Hetsroni 1993; Best et al. 1997).

Figure 5.22 presents the data plots of the ratio of particle size to Taylor microscale, $\hat{\lambda}_d$, for mobile-bed flow as a function of relative difference of streamwise turbulence intensities $\Delta\sigma_{uu} [= (\overline{u^2})^{0.5}|_{\text{mb}}/(\overline{u^2})^{0.5}|_{\text{cw}} - 1]$. Here, subscripts “cw” and

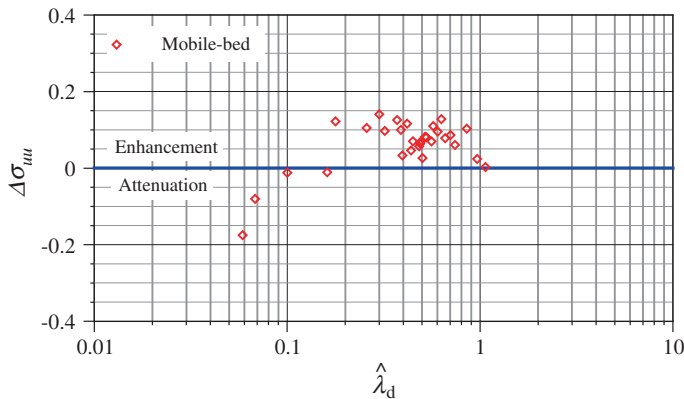


Fig. 5.22 Ratio of particle size to Taylor microscale $\hat{\lambda}_d$ for mobile-bed flow as a function of relative difference of streamwise turbulence intensities $\Delta\sigma_{uu}$ between clear-water and mobile-bed flows (Dey et al. 2012)

“mb” refer to clear-water and mobile-bed flows, respectively. The positive values of $\Delta\sigma_{uu}$ ($\tilde{z} < 0.2$) indicate that the streamwise turbulence intensity in mobile bed is greater than that in clear-water flow. This is in conformity to the findings of Sumer et al. (2003), who studied the role of externally induced turbulence fields on bed-load transport and argued that the sediment transport rate increases considerably with an increase in streamwise turbulence intensity $(\overline{u'^2})^{0.5}$.

5.17 Effects of Bed Load on von Kármán Constant κ

During bed-load transport, the sediment motion (by rolling, sliding, and saltation) produces an expansion of the roughness layer. Recking et al. (2008) reported that the Nikuradse’s equivalent sand roughness k_s increases from the particle size d_{50} for immobile-bed condition to $2.6d_{50}$ for intense bed-load transport condition. The expansion of the roughness layer modifies the logarithmic wall shear layer, resulting in the variation of von Kármán constant κ from its universal value 0.41. Gaudio et al. (2010) and Gaudio and Dey (2012) reviewed the studies on the effects of sediment transport on κ , which is discussed below:

Gust and Southard (1983) analyzed the velocity data in the wall shear layer ($z/h \leq 0.2$) measured by a hot-wire anemometer. They observed a decrease in κ from its universal value with an increase in bed-load transport rate. After a transitional regime corresponding to the entrainment threshold of sediment, κ adjusted to a constant value of 0.32 ± 0.04 for all the experiments with bed-load transport, in which the transport rate varied by a factor 10. Best et al. (1997) used a phase Doppler anemometer to differentiate the characteristics of the fluid from those of the sediment particles and to quantify the influence of the sediments on the carrier

fluid turbulence. They observed that the average value of κ was 0.385 in the presence of bed-load transport. Nikora and Goring (2000) reported a study on the characteristics of turbulent structure of high Reynolds number in quasi-two-dimensional flow with fixed and weakly mobile gravel-beds. The flow measurements by an acoustic Doppler velocimeter in an irrigation field canal were carried out for two bed conditions: fixed and weakly mobile beds. Measurements were first taken with a weakly mobile-bed flow (WMBF) and then repeated for a fixed-bed flow (FBF). They obtained $\kappa \approx 0.29$ for the WMBF being significantly smaller than $\kappa \approx 0.4$ for the FBF. They argued that the value $\kappa \approx 0.4$ with the WMBF would have been achieved with an adjustment of the virtual bed level if the bed level was shifted by 30 mm upwards. Since such a shift is physically unjustifiable, it corroborates that the difference of κ values between the WMBF and the FBF is possible due to the effects of bed-load transport. Bennett and Bridge (1995), Nikora and Goring (1999), and Gallagher et al. (1999) also revealed an appreciable decrease in κ under bed-load transport. Nikora and Goring (1999) anticipated that the reduction in κ might reflect the special turbulence characteristics within a narrow range of the Shields parameter when the bed shear stress is approximately equal to the threshold bed shear stress. In Nikora and Goring (2000), the drag reduction effects were expressed as decreased values of κ . The general concept is that the drag reduction prevails when the spacing between turbulent bursting events increases in comparison to the spacing in flow with no sediment (Tiederman et al. 1985). However, it is revealed that the κ reduces when spanwise (lateral) spacing between bursting events increases; while streamwise spacing remains unchanged (Hetsroni et al. 1997). Nikora and Goring (2000) found that the streamwise spacing between bursting events was approximately the same for both the WMBF and the FBF, referring to an increase in spanwise spacing for the WMBF. Dey and Raikar (2007) reported the laboratory experimental results on the turbulent flow characteristics measured by an acoustic Doppler velocimeter. The primary endeavor was to investigate the response of the turbulent flow field, having zero-pressure gradient, to the uniform gravel-beds at the near-threshold of sediment of motion. They observed that the variation of mixing length is considerably linear with the distance from the bed within the wall shear layer, whose thickness was obtained as 0.23 times the boundary layer thickness; and von Kármán κ was estimated as 0.35.

Gaudio et al. (2011) performed laboratory tests in a narrow flume with sediment feeding to simulate bed load on a rough bed and measured the velocity within the wall shear layer ($z/h \leq 0.2$) by using a Pitot-Prandtl tube. They obtained a decrease in κ , that κ varied from 0.3 with bed load ($0.0334 \leq g_b \leq 0.0649 \text{ kg s}^{-1} \text{ m}^{-1}$) to 0.4 with clear-water flow condition. Further, Dey et al. (2012) fitted a logarithmic law for mobile-bed flow to obtain $\kappa = 0.37$ for bed-load transport rates ($2 \times 10^{-3} \leq g_b \leq 7 \times 10^{-3} \text{ kg s}^{-1} \text{ m}^{-1}$), as already discussed. Table 5.3 furnishes a summary of the results on κ in flow with bed-load transport. The available experimental data are so limited that the variation of κ with bed-load transport rate (q_b or g_b) is not so specific, although it has been well-recognized that the κ values with bed-load transport are less than its universal value 0.41.

Table 5.3 Experimental results on the effects of bed-load transport on κ

References	d_{50} (mm)	R_*	g_b ($\text{kg s}^{-1} \text{m}^{-1}$)	κ
Gust and Southard (1983)	0.16	—	$0.15 - 1.5 \times 10^{-5}$	$0.32 \pm 12.5 \%$
Best et al. (1997)	0.22	8.9	$9 - 22 \times 10^{-3}$	0.385
Nikora and Goring (2000)	6.4	429	0.0138	$0.29 \pm 10.3 \%$
Dey and Raikar (2007)	4.1–14.25	210–1,573	$1.23 - 0.09$	$0.35 \pm 0.86 \%$
Gaudio et al. (2011)	1	101–120	$3.34 - 0.0649$	$0.3 - 0.39 \pm 10.7 \%$
Dey et al. (2012)	0.95, 2.6, 4.1	63–508	$2-7 \times 10^{-3}$	$0.35 - 0.42$

5.18 Examples

Example 5.1 The flow velocity in a wide river is 1.65 m s^{-1} , flow depth 3.2 m, and energy slope 5×10^{-4} . The flow is uniform within the measuring reach. The bed sediment has a median size $d_{50} = 1.5 \text{ mm}$, $d_{65} = 1.8 \text{ mm}$, and $d_{90} = 3 \text{ mm}$, a static angle of repose of 32° , a dynamic angle of repose of 20° , and a relative density of 2.65. Consider coefficient of kinematic viscosity of water $\nu = 10^{-6} \text{ m}^2 \text{ s}^{-1}$ and mass density of water $\rho = 10^3 \text{ kg m}^{-3}$.

Compute the bed-load transport rate (in volume per unit time and width) by using formulas/methodologies proposed by du Boys, Shields, Schoklitsch, Meyer-Peter and Müller, Einstein, Brown/Julien (empirical form of Einstein's method), Bagnold, Engelund and Fredsøe, Yalin, and van Rijn.

Also, compute the saltation characteristics of the particle.

Solution

Given data are as follows:

Flow velocity, $U = 1.65 \text{ m s}^{-1}$; flow depth, $h = 3.2 \text{ m}$; energy slope, $S_f = 5 \times 10^{-4}$; sediment size, $d_{50} = 1.5 \text{ mm}$, $d_{65} = 1.8 \text{ mm}$, and $d_{90} = 3 \text{ mm}$; static angle of repose, $\phi = 32^\circ$; dynamic angle of repose, $\phi_d = 20^\circ$; relative density, $s = 2.65$; kinematic viscosity of water, $\nu = 10^{-6} \text{ m}^2 \text{ s}^{-1}$; and mass density of water, $\rho = 10^3 \text{ kg m}^{-3}$

For uniform flow, the energy slope equals the streamwise bed slope. Thus, $S_f = S_0 = 5 \times 10^{-4}$

Applied bed shear stress, $\tau_0 = \rho g h S_0 = 10^3 \times 9.81 \times 3.2 \times 5 \times 10^{-4} = 15.7 \text{ Pa}$

Shear velocity, $u_* = (\tau_0/\rho)^{0.5} = (15.7/10^3)^{0.5} = 0.125 \text{ m s}^{-1}$

Shields parameter, $\Theta = \tau_0/(\Delta \rho g d_{50}) = 15.7/(1.65 \times 10^3 \times 9.81 \times 1.5 \times 10^{-3}) = 0.647$

Use van Rijn's empirical formula for the determination of threshold bed shear stress and threshold shear velocity (see Table 4.1):

Particle parameter, $D_* = d_{50}(\Delta g/v^2)^{1/3} = 1.5 \times 10^{-3}[1.65 \times 9.81/(10^{-6})^2]^{1/3} = 37.94$

Threshold Shields parameter, $\Theta_c(20 < D_* \leq 150) = 0.013D_*^{0.29} = 0.013 \times 37.94^{0.29} = 0.037$

Threshold bed shear stress, $\tau_{0c} = \Theta_c \Delta \rho g d_{50} = 0.037 \times 1.65 \times 10^3 \times 9.81 \times 1.5 \times 10^{-3} = 0.898 \text{ Pa}$

Threshold shear velocity, $u_{*c} = (\tau_{0c}/\rho)^{0.5} = (0.898/10^3)^{0.5} = 0.03 \text{ m s}^{-1}$

Computation of bed load by du Boys formula

$$\chi = 6.89 \times 10^{-6} / 1.5^{0.75} = 5.083 \times 10^{-6} \text{ kg}^{-2} \text{ m}^4 \text{ s}^3$$

\Leftarrow Eq. (5.13) (Note: d_{50} is in mm)

$$q_b = 5.083 \times 10^{-6} \times 15.7(15.7 - 0.898) = 1.181 \times 10^{-3} \text{ m}^2 \text{ s}^{-1}$$

\Leftarrow Eq. (5.11)

Computation of bed load by Shields formula

$$q = Uh = 1.65 \times 3.2 = 5.28 \text{ m}^2 \text{ s}^{-1}$$

$$q_b = \frac{10 \times 5.28 \times 5 \times 10^{-4}}{2.65 \times 1.65^2 \times 10^3 \times 9.81 \times 1.5 \times 10^{-3}} (15.7 - 0.898) \\ = 3.681 \times 10^{-3} \text{ m}^2 \text{ s}^{-1} \Leftarrow \text{Eq. (5.14)}$$

Computation of bed load by Schoklitsch formula

$$q_c = 1.944 \times 10^{-5} / S_0^{4/3} = 1.944 \times 10^{-5} / (5 \times 10^{-4})^{4/3} = 0.49 \text{ m}^2 \text{ s}^{-1}$$

$$g_b = \frac{7000}{(1.5 \times 10^{-3})^{0.5}} (5 \times 10^{-4})^{1.5} (5.28 - 0.49) = 9.679 \text{ N s}^{-1} \text{ m}^{-1} \Leftarrow \text{Eq. (5.43)}$$

$$q_b = g_b / (\rho_s g) = 9.679 / (2.65 \times 10^3 \times 9.81) = 3.723 \times 10^{-4} \text{ m}^2 \text{ s}^{-1}$$

Computation of bed load by Meyer-Peter and Müller formula

$$C_R = U / (hS_0)^{0.5} = 1.65 / (3.2 \times 5 \times 10^{-4})^{0.5} = 41.25 \text{ m}^{0.5} \text{ s}^{-1}$$

$$C'_R = 18 \log(12h/d_{90}) = 18 \log[12 \times 3.2 / (3 \times 10^{-3})] = 73.93 \text{ m}^{0.5} \text{ s}^{-1}$$

$$\eta_C = (C_R / C'_R)^{1.5} = (41.25 / 73.93)^{1.5} = 0.417$$

Meyer-Peter and Müller recommended $\Theta_c = 0.047$ and corresponding $\tau_{0c} = \Theta_c \Delta \rho g d_{50} = 0.047 \times 1.65 \times 10^3 \times 9.81 \times 1.5 \times 10^{-3} = 1.14 \text{ Pa}$

$$q_b = \frac{8}{1.65(10^3)^{1.5} \times 9.81} (0.417 \times 15.7 - 1.14)^{1.5} = 1.965 \times 10^{-4} \text{ m}^2 \text{ s}^{-1} \\ \Leftarrow \text{Eq. (5.15)}$$

Computation of bed load by Einstein's method

Assume $R'_b = R_b = h = 3.2$ m (for the wide channel)

$$\Psi_b = \Delta d_{65} / (R'_b S_0) = 1.65 \times 1.8 \times 10^{-3} / (3.2 \times 5 \times 10^{-4}) = 1.86$$

From Fig. 5.10, $\Phi_b (\Psi_b = 1.86) = 4$

$$q_b = \Phi_b (\Delta g d_{50}^3)^{0.5} = 4 [1.65 \times 9.81 (1.5 \times 10^{-3})^3]^{0.5} = 0.349 \times 10^{-4} \text{ m}^2 \text{ s}^{-1}$$

Computation of bed load by empirical form of Einstein's method

$\Psi_b = 1.86 \leq 1.92$; thus, Julien formula, given by Eq. (5.72), is applicable.

$$K_f = \left[\frac{2}{3} + \frac{36(10^{-6})^2}{1.65 \times 9.81 (1.5 \times 10^{-3})^3} \right]^{0.5} - \left[\frac{36(10^{-6})^2}{1.65 \times 9.81 (1.5 \times 10^{-3})^3} \right]^{0.5} = 0.791 \Leftarrow \text{Eq. (5.71a)}$$

$$\Phi_b (\Psi_b \leq 1.92) = 15 \times 0.791 \times \frac{1}{1.86^{1.5}} = 4.677 \Leftarrow \text{Eq. (5.72)}$$

$$q_b = \Phi_b (\Delta g d_{50}^3)^{0.5} = 4.677 [1.65 \times 9.81 (1.5 \times 10^{-3})^3]^{0.5} = 1.093 \times 10^{-3} \text{ m}^2 \text{ s}^{-1}$$

Computation of bed load by Bagnold formula

Assume $e_b = 0.1$

$$g_{bs} = 15.7 \times 1.65 \times 0.1 / \tan 20^\circ = 7.12 \text{ N s}^{-1} \text{ m}^{-1} \Leftarrow \text{Eq. (5.104)}$$

$$g_b = (s/\Delta) g_{bs} = (2.65/1.65) 7.12 = 11.44 \text{ N s}^{-1} \text{ m}^{-1}$$

$$q_b = g_b / (\rho_s g) = 11.44 / (2.65 \times 10^3 \times 9.81) = 4.4 \times 10^{-4} \text{ m}^2 \text{ s}^{-1}$$

Computation of bed load by Engelund and Fredsøe formula

Dynamic coefficient of friction, $\mu_d = \tan 20^\circ$

$$\Phi_b = \frac{9.3}{\tan 20^\circ} (0.647 - 0.037) (0.647^{0.5} - 0.7 \times 0.037^{0.5}) = 10.44 \Leftarrow \text{Eq. (5.88)}$$

$$q_b = \Phi_b (\Delta g d_{50}^3)^{0.5} = 10.44 [1.65 \times 9.81 (1.5 \times 10^{-3})^3]^{0.5} = 2.44 \times 10^{-3} \text{ m}^2 \text{ s}^{-1}$$

The formula of Engelund and Fredsøe seems to produce a higher estimation.

Computation of bed load by Yalin formula

$$a_1 = 2.45 \Theta_c^{0.5} / s^{0.4} = 2.45 \times 0.037^{0.5} / 2.65^{0.4} = 0.319$$

$$(\Theta / \Theta_c) - 1 = (0.647 / 0.037) - 1 = 16.49$$

$$\Phi_b = 0.635 \times 0.647^{0.5} \times 16.49 \left[1 - \frac{1}{0.319 \times 16.49} \ln(1 + 0.319 \times 16.49) \right]$$

$$= 5.486 \Leftarrow \text{Eq. (5.115)}$$

$$q_b = \Phi_b (\Delta g d_{50}^3)^{0.5} = 5.486 [1.65 \times 9.81 (1.5 \times 10^{-3})^3]^{0.5} = 1.282 \times 10^{-3} \text{ m}^2 \text{ s}^{-1}$$

Table 5.4 Saltation length λ_b , height h_s and particle velocity \bar{u}_b obtained from different formulas

References	λ_b (m)	h_s (m)	\bar{u}_b (m s ⁻¹)	Remark
Fernandez Luque and van Beek (1976)	0.024	–	1.196	
Engelund and Fredsøe (1976)	–	–	1.229	
Abbott and Francis (1977)	–	–	1.33	$a = 14$
Sekine and Kikkawa (1992)	2.55	–	0.971	From Cheng formula, $w_s = 0.15$ m s ⁻¹ (Table 1.3)
Niño et al. (1994)	0.06	–	0.71	$a = 7.5$
Lee and Hsu (1994)	0.2	0.016	1.322	
Hu and Hui (1996)	0.07	0.005	1.33	
Lajeunesse et al. (2010)	0.066	–	–	

Computation of bed load by van Rijn formula

$$\Phi_b = (5.3 \times 10^{-2} / 37.94^{0.3}) 16.49^{2.1} = 6.41 \Leftarrow \text{Eq. (5.26)}$$

$$q_b = \Phi_b (\Delta g d_{50}^3)^{0.5} = 6.41 [1.65 \times 9.81 (1.5 \times 10^{-3})^3]^{0.5} = 1.498 \times 10^{-3} \text{ m}^2 \text{ s}^{-1}$$

Computation of saltation characteristics

By van Rijn formulas:

$$\text{Saltation length, } \lambda_b / d_{50} = 3 \times 37.94^{0.6} \times 16.49^{0.9} \Rightarrow \lambda_b = 0.497 \text{ m} \Leftarrow \text{Eq. (5.135a)}$$

$$\text{Saltation height, } h_s / d_{50} = 0.3 \times 37.94^{0.7} \times 16.49^{0.5} \Rightarrow h_s = 0.023 \text{ m} \Leftarrow \text{Eq. (5.135b)}$$

$$\text{Particle velocity, } \bar{u}_b / (\Delta g d_{50})^{0.5} = 1.5 \times 16.49^{0.6} \Rightarrow \bar{u}_b = 1.256 \text{ m s}^{-1} \Leftarrow \text{Eq. (5.137)}$$

Further, estimates of saltation length λ_b , height h_s , and particle velocity \bar{u}_b by using the formulas (see Tables 5.1 and 5.2) proposed by different investigators are given in Table 5.4.

Example 5.2 Water flows with a depth-averaged velocity of 1.5 m s^{-1} through a wide channel having a uniform flow depth of 3 m. The channel has a streamwise bed slope of 8×10^{-4} . The size classes of nonuniform sediment obtained from the sieve analysis are 35 % between 0.1 and 0.5 mm, 30 % between 0.5 and 1 mm, 20 % between 1 and 2 mm, 10 % between 2 and 3 mm, and 5 % between 3 and 4 mm. Relative density of sediment is 2.65; and sediment size, $d_{50} = 0.75 \text{ mm}$ and $d_{90} = 3 \text{ mm}$.

Find the bed-load transport rate by using the methods of (1) Meyer-Peter and Müller and (2) Ashida and Michiue.

Table 5.5 Calculation by Meyer-Peter and Müller's method

Size class (mm)	d_i (mm)	p_i	$p_i d_i$ (m)	ξ_i	$\eta_c \Theta_i$	$\xi_i \Theta_c$	q_{bi} (m ² s ⁻¹)
0.1–0.5	0.3	0.35	1.05×10^{-4}	3.064	1.304	0.104	7.695×10^{-5}
0.5–1	0.75	0.3	2.25×10^{-4}	1.284	0.522	0.0437	6.555×10^{-5}
1–2	1.5	0.2	3×10^{-4}	0.8	0.261	0.0272	4.223×10^{-5}
2–3	2.5	0.1	2.5×10^{-4}	0.6	0.157	0.0204	2.021×10^{-5}
3–4	3.5	0.05	1.75×10^{-4}	0.506	0.112	0.0172	9.693×10^{-6}
			$\sum 1.06 \times 10^{-3}$				$\sum 2.146 \times 10^{-4}$

Solution

Given data are as follows:

Flow velocity, $U = 1.5 \text{ m s}^{-1}$; flow depth, $h = 3 \text{ m}$; bed slope, $S_0 = 8 \times 10^{-4}$; bed sediment size, $d_{50} = 0.75 \text{ mm}$ and $d_{90} = 3 \text{ mm}$; and relative density, $s = 2.65$

1. Meyer-Peter and Müller's method

Weighted mean size, $d_m = \sum p_i d_i = 1.06 \text{ mm}$ (see Table 5.5)

$$C_R = U/(hS_0)^{0.5} = 1.5/(3 \times 8 \times 10^{-4})^{0.5} = 30.62 \text{ m}^{0.5} \text{ s}^{-1}$$

$$C'_R = 18 \log(12h/d_{90}) = 18 \log[12 \times 3/(3 \times 10^{-3})] = 73.43 \text{ m}^{0.5} \text{ s}^{-1}$$

$$\eta_c = (C_R/C'_R)^{1.5} = 0.269$$

Applied bed shear stress, $\tau_0 = \rho ghS_0 = 10^3 \times 9.81 \times 3 \times 8 \times 10^{-4} = 23.54 \text{ Pa}$

$$\Theta_i = \tau_0/(\Delta \rho g d_i) = 23.54/(1.65 \times 10^3 \times 9.81 \times d_i) = 1.454 \times 10^{-3}/d_i$$

Threshold Shields parameter, $\Theta_c = 0.034$ that is obtained from van Rijn's empirical formula (Table 4.1) for the sediment size $d_m = 1.06 \text{ mm}$. Bed-load transport rate for fractional size d_i is $q_{bi} = 8(\Delta g)^{0.5} p_i d_i^{1.5} (\eta_c \Theta_i - \xi_i \Theta_c)^{1.5}$ [see Eq. (5.146)]

Therefore, the total bed-load transport rate for all size fractions, $q_b = 2.146 \times 10^{-4} \text{ m}^2 \text{ s}^{-1}$ (Table 5.5)

However, one can check the difference in estimation of bed-load transport rate obtained using the weighted mean size d_m .

$$\Theta = \tau_0/(\Delta \rho g d_m) = 23.54/(1.65 \times 10^3 \times 9.81 \times 1.06 \times 10^{-3}) = 1.372$$

$$q_b = 8(\Delta g d_m^3)^{0.5} (\eta_c \Theta - \Theta_c)^{1.5} = 8[1.65 \times 9.81 (1.06 \times 10^{-3})^3]^{0.5} (0.269 \times 1.372 - 0.034)^{1.5} = 2.154 \times 10^{-4} \text{ m}^2 \text{ s}^{-1}$$

which is almost equaling the estimate of total bed-load transport rate for all size fractions.

Table 5.6 Calculation by Ashida and Michiue's method

Size class (mm)	d_i (mm)	p_i	Θ_i	Θ_{ci}	$\Theta_i - \Theta_{ci}$	$\Theta_i^{0.5} - \Theta_{ci}^{0.5}$	$q_{bi} \text{ (m}^2 \text{ s}^{-1}\text{)}$
0.1–0.5	0.3	0.35	4.85	0.039	4.811	2.005	1.2×10^{-3}
0.5–1	0.75	0.3	1.94	0.03	1.91	1.22	9.82×10^{-4}
1–2	1.5	0.2	0.97	0.037	0.933	0.793	5.88×10^{-4}
2–3	2.5	0.1	0.582	0.043	0.539	0.556	2.56×10^{-4}
3–4	3.5	0.05	0.416	0.048	0.368	0.426	1.11×10^{-4}
							$\Sigma 3.14 \times 10^{-3}$

2. Ashida and Michiue's method

Bed-load transport rate for fractional size d_i is $q_{bi} = 17(\Delta g)^{0.5} p_i d_i^{1.5} (\Theta_i - \Theta_{ci}) \times (\Theta_i^{0.5} - \Theta_{ci}^{0.5})$ [see Eq. (5.140)]

Threshold Shields parameter Θ_{ci} for the fractional size d_i can be obtained by using van Rijn's empirical formula (Table 4.1) for the size d_i (Table 5.6).

Therefore, the total bed-load transport rate for all size fractions, $q_b = 3.14 \times 10^{-3} \text{ m}^2 \text{ s}^{-1}$ (Table 5.6)

However, one can check the difference in estimation of bed-load transport rate obtained using the weighted mean size d_m .

$$q_b = 17(\Delta g d_m^3)^{0.5} (\Theta - \Theta_c) (\Theta^{0.5} - \Theta_c^{0.5}) = 17[1.65 \times 9.81(1.06 \times 10^{-3})^3]^{0.5} \times (1.372 - 0.034)(1.372^{0.5} - 0.034^{0.5}) = 3.12 \times 10^{-3} \text{ m}^2 \text{ s}^{-1}$$

which is very close to the estimate of total bed-load transport rate for all size fractions.

References

- Abbott JE, Francis JRD (1977) Saltation and suspension trajectories of solid grains in a water stream. *Proc R Soc London A* 284(1321):225–254
- Ashida K, Michiue M (1972) Study on hydraulic resistance and bed-load transport rate in alluvial streams. *Trans Japan Soc Civ Eng* 206:59–69
- Bagnold RA (1954) Experiments on a gravity-free dispersion of large solid spheres in a Newtonian fluid under shear. *Proc R Soc London A* 255(1160):49–63
- Bagnold RA (1956) The flow of cohesionless grains in fluids. *Philos Trans R Soc London A* 249(964):315–319
- Bagnold RA (1966) An approach to the sediment transport problem from general physics. Geological survey professional paper 422-I, Washington, DC
- Bagnold RA (1977) Bed load transport by natural rivers. *Water Resour Res* 13(2):303–312
- Barekyan AS (1962) Discharge of channel forming sediments and elements of sand waves. *Trans Am Geophys Union* 2:128–130
- Bennett SJ, Bridge JS (1995) The geometry and dynamics of low-relief bed forms in heterogeneous sediment in a laboratory channel, and their relationship to water flow and sediment transport. *J Sediment Res* 65A(1):29–39

- Best J, Bennett S, Bridge J, Leeder M (1997) Turbulence modulation and particle velocities over flat sand beds at low transport rates. *J Hydraul Eng* 123(12):1118–1129
- Borah DK (1989) Scour-depth prediction under armoring conditions. *J Hydraul Eng* 115(10):1421–1425
- Borah DK, Alonso CV, Prasad SN (1982) Routing graded sediment in streams: formation. *J Hydraul Div* 108(12):1486–1503
- Bose SK (2009) Numeric computing in Fortran. Narosa, New Delhi
- Bose SK, Dey S (2013) Sediment entrainment probability and threshold of sediment suspension: Exponential-based approach. *J Hydraul Eng* 139(10):1099–1106
- Brown CB (1950) Sediment transportation. In: Rouse H (ed) *Engineering hydraulics*. Wiley, New York, pp 769–857
- Chang FM, Simons DB, Richardson EV (1967) Total bed-material discharge in alluvial channels. In: *Proceedings of the twelfth congress of International Association for Hydraulic Research*, Fort Collins, Colorado, pp 132–140
- Cheng N-S (2002) Exponential formula for bedload transport. *J Hydraul Eng* 128(10):942–946
- Cheng N-S, Chiew Y-M (1998) Pickup probability for sediment entrainment. *J Hydraul Eng* 124(2):232–235
- Chien N (1954) Meyer-Peter formula for bed load transport and Einstein bed load function. Missouri River division sediment series number 7, University of California-Berkeley and Missouri River Division, United States Army Corps of Engineers, Berkeley, California
- Chien N, Wan Z (1999) *Mechanics of sediment transport*. ASCE Press, Reston
- Chin CO, Melville BW, Raudkivi AJ (1994) Streambed armoring. *J Hydraul Eng* 120(8):899–918
- Correia L, Graf WH (1988) Grain-size distribution and armoring in gravel-bed rivers. *Activities report of the hydraulics research laboratory, École Polytechnique Fédérale de Lausanne, Lausanne*
- Crowe CT (1993) Modelling turbulence in multiphase flows. In: Rodi W, Martelli F (eds) *Engineering turbulence modelling and experiments*, vol 2., Elsevier, Amsterdam, pp 899–913
- Damgaard JS, Whitehouse RJS, Soulsby RL (1997) Bedload sediment transport on steep longitudinal slopes. *J Hydraul Eng* 123(12):1130–1138
- de Ruiter JCC (1982) The mechanism of sediment transport on bed forms. In: *Proceedings of the Euromech conference*, vol 156, Technical University of Istanbul, Istanbul
- de Ruiter JCC (1983) Incipient motion and pick-up of sediment as function of local variables. Report R 657-XI, Delft Hydraulics Laboratory, Delft
- Dey S, Das R, Gaudio R, Bose SK (2012) Turbulence in mobile-bed streams. *Acta Geophys* 60(6):1547–1588
- Dey S, Debnath K (2001) Sediment pick-up on stream-wise sloping beds. *J Irrig Drainage Eng* 127(1):39–43
- Dey S, Raikar RV (2007) Characteristics of loose rough boundary streams at near-threshold. *J Hydraul Eng* 133(3):288–304
- Dey S, Sarkar S, Solari L (2011) Near-bed turbulence characteristics at the entrainment threshold of sediment beds. *J Hydraul Eng* 137(9):945–958
- Donat J (1929) Über sohlgriff und geschiebetrieb. *Wasserwirtschaft* 26:27–36
- Dou GR (1964) Bed-load transport. Report, Nanjing Hydraulic Research Institute, Nanjing
- du Boys MP (1879) Le rhone et les rivières a lit affouillable. *Annales des Ponts et Chaussées* 18(5):141–195
- Egiazaroff JV (1965) Calculation of non-uniform sediment concentrations. *J Hydraul Div* 91(4):225–247
- Einstein HA (1942) Formulas for the transportation of bed load. *Trans Am Soc Civ Eng* 107:561–577
- Einstein HA (1950) The bed-load function for sediment transportation in open channel flows. Technical bulletin number 1026, United States Department of Agriculture, Soil Conservation Service, Washington, DC
- Einstein HA, El-Samni EA (1949) Hydrodynamic forces on rough wall. *Rev Modern Phys* 21(3):520–524

- Engelund F, Fredsøe J (1976) A sediment transport model for straight alluvial channels. *Nord Hydrol* 7(5):293–306
- Engelund F, Hansen E (1967) A monograph on sediment transport in alluvial streams. Technical Press (Teknisk Forlag), Copenhagen
- Exner FM (1925) Über die wechselwirkung zwischen wasser und geschiebe in flüssen. *Sitzungsberichte der Akademie der Wissenschaften* 134(2a):165–203
- Fernandez Luque R (1974) Erosion and transport of bed-load sediment. PhD thesis, Delft University of Technology, Meppel
- Fernandez Luque R, van Beek R (1976) Erosion and transport of bed-load sediment. *J Hydraul Res* 14(2):127–144
- Francis JRD (1973) Experiments on the motion of solitary grains along the bed of a water stream. *Proc R Soc London A* 332(1591):443–471
- Fredsøe J, Deigaard R (1992) *Mechanics of coastal sediment transport*. World Scientific, Singapore
- Frijlink HC (1952) Discussion of bed load transport formulas. Report number X2344/LV, Delft Hydraulics, Delft
- Froehlich DC (1995) Armor-limited clear-water contraction scour at bridges. *J Hydraul Eng* 121(6):490–493
- Gallagher M, McEwan I, Nikora V (1999) The changing structure of turbulence over a self-stabilising sediment bed. Internal report number 21, Department of Engineering, University of Aberdeen, Aberdeen
- Gaudio R, Dey S (2012) Evidence of non-universality of von Kármán's κ . In: Rowinski P (ed) *Experimental and computational solutions of hydraulic problems*. Springer, Heidelberg, pp 71–83
- Gaudio R, Miglio A, Calomino F (2011) Friction factor and von Kármán's κ in open channels with bed-load. *J Hydraul Res* 49(2):239–247
- Gaudio R, Miglio A, Dey S (2010) Non-universality of von Kármán's κ in fluvial streams. *J Hydraul Res* 48(5):658–663
- Gilbert GK (1914) *Transportation of debris by running water*. Professional paper number 86, United States Geological Survey, Washington DC
- Gore RA, Crowe CT (1991) Modulation of turbulence by a dispersed phase. *J Fluids Eng* 113(6):304–307
- Graf WH (1971) *Hydraulics of sediment transport*. McGraw-Hill Book Company, New York
- Graf WH, Suszka L (1987) Sediment transport in steep channels. *J Hydrosci Hydraul Eng* 5(1):11–26
- Gust G, Southard JB (1983) Effects of weak bed load on the universal law of the wall. *J Geophys Res* 88(C10):5939–5952
- Guy HP, Simons DB, Richardson EV (1966) Summary of alluvial channel data from flume experiments, 1956–1961. United States Geological survey professional paper, 462-1, Washington, DC
- Hanes DM (1986) Grain flows and bed-load sediment transport: review and extension. *Acta Mech* 63(1–4):131–142
- Hetsroni G (1993) The effect of particles on the turbulence in a boundary layer. In: Raco MC (ed) *Particulate two-phase flow*. Butterworth-Heinemann, pp 244–264
- Hetsroni G, Zakin JL, Mosyak A (1997) Low-speed streaks in drag-reduced turbulent flow. *Phys Fluids* 9(8):2397–2404
- Hsu SM, Holly FM (1992) Conceptual bed-load transport model and verification for sediment mixtures. *J Hydraul Eng* 118(8):1135–1152
- Hu CH, Hui YJ (1996) Bed-load transport. I: mechanical characteristics. *J Hydraul Eng* 122(5):245–254
- Julien PY (1998) *Erosion and sedimentation*, 1st edn. Cambridge University Press, Cambridge
- Kalinske AA (1947) Movement of sediment as bed-load in rivers. *Trans Am Geophys Union* 28(4):615–620

- Kironoto BA, Graf WH (1994) Turbulence characteristics in rough uniform open-channel flow. *Water Marit Eng Proc Inst Civ Eng (London)* 106(4): 333–344
- Lajeunesse E, Malverti L, Charru F (2010) Bed load transport in turbulent flow at the grain scale: Experiments and modeling. *J Geophys Res* 115(F04001). doi:10.1029/2009JF001628
- Lee HY, Hsu I-S (1994) Investigation saltating particle motions. *J Hydraul Eng* 120(7):831–845
- Madsen OS (1991) Mechanics of cohesionless sediment transport in coastal waters. In: Kraus NC, Gingerich KJ, Kriedel DL (eds) *Coastal sediment '91*. American Society of Civil Engineers, New York, pp 15–27
- Meyer-Peter E, Favre H, Einstein HA (1934) Neuere versuchsergebnisse über den geschiebetrieb. *Schweizerische Bauzeitung* 103(13):147–150
- Meyer-Peter E, Müller R (1948) Formulas for bed-load transport. In: *Proceedings of the second meeting of International Association for Hydraulic Research*, vol 3. Stockholm, pp 39–64
- Misri RL, Garde RJ, Ranga Raju KG (1984) Bed load transport of coarse nonuniform sediment. *J Hydraul Eng* 110(3):312–328
- Monin AS, Yaglom AM (2007) *Statistical fluid mechanics, volume II: mechanics of turbulence*. Dover Publications, New York
- Morsi SA, Alexander AJ (1972) An investigation of particle trajectories in two-phase flow systems. *J Fluid Mech* 55:193–208
- Nakagawa H, Tsujimoto T (1980) Sand bed instability due to bed load motion. *J Hydraul Div* 106(12):2029–2051
- Nelson J, Shreve RL, McLean SR, Drake TG (1995) Role of near-bed turbulence structure in bed load transport and bed form mechanics. *Water Resour Res* 31(8):2071–2086
- Nezu I, Nakagawa H (1993) *Turbulence in open-channel flows*. Balkema, Rotterdam
- Nielsen P (1992) *Coastal bottom boundary layers and sediment transport*. World Scientific, Singapore
- Nikora VI, Goring DG (1999) Effects of bed mobility on turbulence structure. NIWA internal report number 48, National Institute of Water & Atmospheric Research (NIWA), Christchurch
- Nikora V, Goring D (2000) Flow turbulence over fixed and weakly mobile gravel beds. *J Hydraul Eng* 126(9):679–690
- Niño Y, García M, Ayala L (1994) Gravel saltation: 1. experiments. *Water Resour Res* 30(6):1907–1914
- Niño Y, García MH (1998) Using Lagrangian particle saltation observations for bedload sediment transport modelling. *Hydrol Process* 12(8):1197–1218
- Paintal A (1971) Concept of critical shear stress in loose boundary open channels. *J Hydraul Res* 9(1):91–113
- Parker G (1979) Hydraulic geometry of active gravel rivers. *J Hydraul Div* 105(9):1185–1201
- Parker G, Kilingeman PC, McLean DG (1982) Bed load and size distribution in paved gravel-bed streams. *J Hydraul Div* 108(4):544–571
- Patel PL, Ranga Raju KG (1996) Fractionwise calculation of bed load transport. *J Hydraul Res* 34(3):363–379
- Pope SB (2001) *Turbulent flows*. Cambridge University Press
- Poreh M, Sagiv A, Seginer J (1970) Sediment sampling efficiency of slots. *J Hydraul Div* 96(10):2065–2078
- Qin YY (1980) Incipient motion of nonuniform sediment. *J Sediment Res* 1:83–91
- Raudkivi AJ (1990) *Loose boundary hydraulics*. Pergamon, New York
- Recking A, Frey P, Paquier A, Belleudy P, Champagne JY (2008) Feedback between bed load transport and flow resistance in gravel and cobble bed rivers. *Water Resour Res* 44(W05412). doi:10.1029/2007WR006219
- Rickenmann D (1991) Bed load transport and hyperconcentrated flow at steep slopes. *Fluvial hydraulics of mountain regions, Lecture notes in earth sciences*, vol 37, pp 429–441
- Rubey W (1933) Settling velocities of gravel, sand and silt particles. *Am J Sci* 225(148):325–338
- Rubinow SI, Keller JB (1961) The transverse force on a spinning sphere moving in a viscous fluid. *J Fluid Mech* 11:447–459

- Saffman PG (1968) Corrigendum, the lift on a small sphere in a slow shear flow. *J Fluid Mech* 31:624
- Schoklitsch A (1914) Über schleppkraft und geschiebebewegung. Engelmann, Leipzig
- Schoklitsch A (1934) Geschiebetrieb und die geschiebefracht. *Wasserkraft und Wasserwirtschaft* 39(4):1–7
- Sekine M, Kikkawa H (1992) Mechanics of saltating grains.II. *J Hydraul Eng* 118(4):536–558
- Shields AF (1936) Application of similarity principles and turbulence research to bed-load movement. *Mitteilungen der Preussischen Versuchsanstalt für Wasserbau und Schiffbau* 26:5–24
- Smart GM (1984) Sediment transport formula for steep channels. *J Hydraul Eng* 110(3):267–276
- Straub LG (1935) Missouri river report. In-House document 238, Seventy-third Congress, Second Session, United States Government Printing office, Washington, DC
- Sumer BM, Chua LHC, Cheng N-S, Fredsøe J (2003) Influence of turbulence on bed load sediment transport. *J Hydraul Eng* 129(8):585–596
- Tiederman WG, Luchik TS, Bogard DG (1985) Wall layer structure and drag reduction. *J Fluid Mech* 156:419–437
- van Rijn LC (1981) Computation of bed-load concentration and bed-load transport. Research report S 487-1, Delft Hydraulics Laboratory, Delft
- van Rijn LC (1984a) Sediment transport, part I: bed load transport. *J Hydraul Eng* 110(10):1431–1456
- van Rijn LC (1984b) Sediment pick-up function. *J Hydraul Eng* 110(10):1494–1502
- van Rijn LC (1993) Principles of sediment transport in rivers, estuaries and coastal seas. Aqua Publications, The Netherlands
- Wang X, Zheng J, Danxun L, Qu Z (2008) Modification of the Einstein bed-load formula. *J Hydraul Eng* 134(9):1363–1369
- White BR, Schultz JC (1977) Magnus effect in saltation. *J Fluid Mech* 81:497–512
- Williams PG (1970) Flume width and water depth effects in sediment transport experiments. Geological survey professional paper 562-H, Washington, DC
- Wilson KC (1966) Bedload transport at high shear stresses. *J Hydraul Div* 92(6):49–59
- Wong M, Parker G (2006) Re-analysis and correction of bedload relation of Meyer-Peter and Muller using their own database. *J Hydraul Eng* 132(11):1159–1168
- Wu F-C, Lin Y-C (2002) Pickup probability of sediment under log-normal velocity distribution. *J Hydraul Eng* 128(4):438–442
- Wu W, Wang SSY, Jia Y (2000) Nonuniform sediment transport in alluvial rivers. *J Hydraul Res* 38(6):427–434
- Yalin MS (1977) *Mechanics of sediment transport*. Pergamon, Oxford
- Yalin MS, Karahan E (1979) Inception of sediment transport. *J Hydraul Div* 105(11):1433–1443
- Yen CL, Lee HY, Chang SY, Hsu SH (1988) A study on aggradation/degradation of coarse sediment in alluvial stream. Research report number 88, Hydraulic Research Laboratory, National Taiwan University, Taipei (in Chinese)
- Zhang RJ, Xie JH, Wang MF, Huang JT (1989) *Dynamics of river sedimentation*. Water and Power Press, Beijing

Chapter 6

Suspended-Load Transport

6.1 General

If and when the motion of sediment particles in a flowing fluid is such that they are surrounded by the fluid over an appreciably long period of time, the sediment particles are said to be in *suspension* and the transport mode is termed *suspended load*. In natural streams, large amount of sediment is transported as suspended load. The mechanism of sediment to come in suspension and being transported by the stream flow is rather complex in details. *Convection*¹ of turbulence in flow results in exchanges of both mass and momentum (including suspended sediment particles) between layers of fluid flow. However, suspended load of sediment particles that are diffused and supported by the advection of turbulence throughout the column of fluid differs from the bed load. The spreading of suspended sediment particles by random motion and by turbulence is termed *diffusion*, while that due to gradients of time-averaged velocity components is termed *advection*. In reality, when the tendency for settling sediment particles with their terminal fall velocity is counterbalanced by the diffusion induced by the turbulence, sediment particles remain in suspension and are transported by the time-averaged flow velocity. There exists an active interchange of sediment particles between bed load and suspended load. The upper extremity of sediment suspension is the free surface, where suspension comes to an end; while the lower extremity is up to the top of the bed-load layer, whose determination is a difficult proposition. Therefore, suspended load is always accompanied by the bed-load transport.

The *suspended-load transport rate* is calculated by the depth integration of the product of sediment concentration and flow velocity and expressed as

¹ Technically, *convection* means a transport governed by *diffusion* together with *advection*. *Diffusion* results in mixing or mass transport mechanism of a substance without requiring bulk motion, while *advection* is the transport by a fluid due to the bulk motion of fluid.

$$q_s = \int_a^h C\bar{u} dz, \quad g_s = \rho_s g \int_a^h C\bar{u} dz, \quad g_{ss} = \Delta\rho g \int_a^h C\bar{u} dz \quad (6.1a)$$

$$\Phi_s = \frac{q_s}{(\Delta g d^3)^{0.5}} = \frac{g_s}{\rho_s g (\Delta g d^3)^{0.5}} = \frac{g_{ss}}{\Delta\rho g (\Delta g d^3)^{0.5}} \quad (6.1b)$$

where q_s is the suspended-load transport rate in volume per unit time and width, g_s is the suspended-load transport rate in weight per unit time and width, g_{ss} is the suspended-load transport rate in submerged weight per unit time and width, Φ_s is the nondimensional suspended-load transport rate, called *suspended-load transport intensity*, \bar{u} is the time-averaged velocity at an elevation z , C is the time-averaged concentration by volume at an elevation z , a is the thickness of bed-load layer, h is the flow depth, ρ_s is the mass density of sediment, and g is the acceleration due to gravity. The integration of Eq. (6.1a) is possible, if mathematical expressions of $C(z)$ and $\bar{u}(z)$ are known. Several attempts have so far been made for the determination of the relationship $C(\bar{u})$ both analytically and empirically.

The theoretical analyses for sediment suspension are based on diffusion, energy, and stochastic concepts. However, the diffusion concept has so far been the most acceptable one for practical applications and also the basis of most of the numerical exercises.

6.2 Diffusion Concept

6.2.1 Background

The concept developed for molecular diffusion, which is based on the continuum hypothesis and *Fick's law*, is by analogy important for turbulent diffusion. *Fick's first law* defines the diffusive flux that goes from high-concentration zone to low-concentration zone with a magnitude that is proportional to the concentration gradient. The transport is postulated down the concentration gradient. The law in the context of diffusion of small amount of dye in still water is therefore

$$J = -\varepsilon_m \frac{\partial C}{\partial z} \quad (6.2)$$

where J is rate at which the dye transports across a unit area normal to z -direction, ε_m is the molecular diffusivity, and C is the concentration of dye.

Fick's second law defines how diffusion causes the concentration to change with time

$$\frac{\partial C}{\partial t} = -\frac{\partial J}{\partial z} = \varepsilon_m \frac{\partial^2 C}{\partial z^2} \quad (6.3)$$

where t is the time. The molecular diffusivity ε_m is assumed not to vary with concentration C , being satisfied with the condition for a dilute concentration. Equation (6.3) has a solution

$$C(z, t) = \frac{B}{t^{0.5}} \exp\left(-\frac{z^2}{4\varepsilon_m t}\right) \quad (6.4)$$

where B is an integration constant.

6.2.2 Generalized Advection–Diffusion Equation of Suspended Sediment Motion

To derive three-dimensional continuity equation of suspended sediment motion by the fluid flow, a control volume element of fluid $dx dy dz$, containing a sediment concentration C having a mass density ρ_s , with center at (x, y, z) in a Cartesian coordinate system is considered, as shown in Fig. 6.1. The velocity components in x -, y -, and z -direction are u , v , and w , respectively. Note that for the simplicity of the derivation, the velocity components are initially assumed to be nonfluctuating in nature. However, the velocity fluctuations due to turbulence are introduced subsequently in the analysis. The mass flux of sediment entering through the back face of the control volume by advection in x -direction is given by

$$\left[\rho_s C u - \frac{\partial}{\partial x} (\rho_s C u) \cdot \frac{dx}{2} \right] dy dz$$

In the above expression, the first term, $(\rho_s C u) dy dz$, is the mass flux through a central plane normal to the x -axis, as shown by the broken line (Fig. 6.1). The second term, $[\partial(\rho_s C u)/\partial x](dx/2) dy dz$, is the rate of change of mass flux with respect to distance in x -direction multiplied by the distance $dx/2$ from the central plane to the back face. Similarly, the mass flux leaving through the front face of the control volume in x -direction is given by

$$\left[\rho_s C u + \frac{\partial}{\partial x} (\rho_s C u) \cdot \frac{dx}{2} \right] dy dz$$

Therefore, the net mass flux out in x -direction through these two faces is

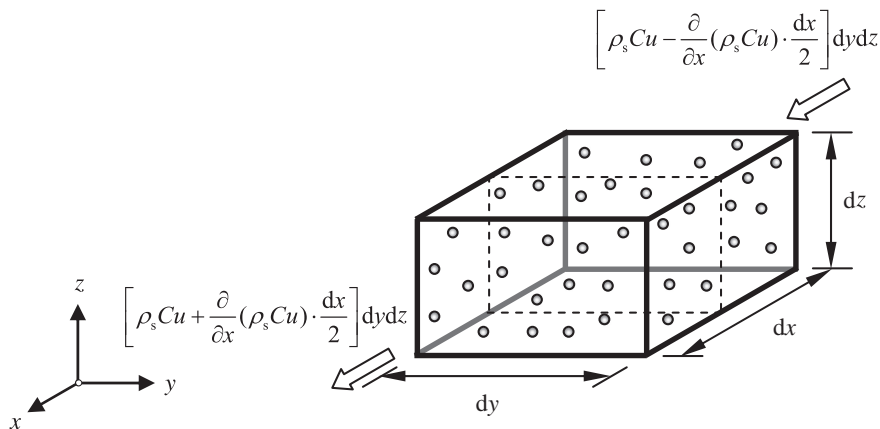


Fig. 6.1 Definition sketch for derivation of three-dimensional continuity equation of sediment suspension in a control volume element

$$\frac{\partial}{\partial x}(\rho_s Cu) dx dy dz$$

The other two directions yield similar expressions, and hence, the net mass flux out of the control volume is

$$\left[\frac{\partial}{\partial x}(\rho_s Cu) + \frac{\partial}{\partial y}(\rho_s Cv) + \frac{\partial}{\partial z}(\rho_s Cw) \right] dx dy dz$$

By definition of the principle of conservation of mass, the net sediment mass flux out of the control volume plus the rate of change of mass in the control volume, given by $[\partial(\rho_s C)/\partial t] dx dy dz$, equals the rate of production of mass in the control volume, that is

$$\frac{d}{dt}(\rho_s C) dx dy dz$$

Thus, the three-dimensional continuity equation of suspended sediment motion is given by

$$\frac{\partial}{\partial t}(\rho_s C) + \frac{\partial}{\partial x}(\rho_s Cu) + \frac{\partial}{\partial y}(\rho_s Cv) + \frac{\partial}{\partial z}(\rho_s Cw) = \frac{d}{dt}(\rho_s C) \quad (6.5)$$

For suspended sediment motion in turbulent flow, the velocity and concentration fluctuate with time. Hence, Eq. (6.5), which has been derived for nonfluctuating velocity and concentration, is modified by replacing the nonfluctuating quantities

by the instantaneous quantities. Now, C is replaced by C_t , that represents the instantaneous concentration, and u , v , and w represent the instantaneous velocity components in x -, y -, and z -direction, respectively. Thus, for a constant mass density ρ_s of sediment, Eq. (6.5) is rewritten as

$$\frac{\partial C_t}{\partial t} + \frac{\partial}{\partial x}(C_t u) + \frac{\partial}{\partial y}(C_t v) + \frac{\partial}{\partial z}(C_t w) = \frac{dC_t}{dt} = \dot{C} \quad (6.6)$$

Applying Reynolds decomposition, the instantaneous velocity components and the suspended sediment concentration are split into time-averaged and fluctuation parts as

$$\left. \begin{aligned} u &= \bar{u} + u' \\ v &= \bar{v} + v' \\ w &= \bar{w} + w' \\ C_t &= C + C' \end{aligned} \right\} \quad (6.7)$$

Using Reynolds conditions, the time-averaging of the product of C_t and u is

$$\begin{aligned} \overline{C_t u} &= \overline{(C + C')(\bar{u} + u')} = \overline{C\bar{u}} + \overline{C'u'} = C\bar{u} + \overline{C'u'} \\ \wedge \quad \overline{u'} &= \overline{C'} = 0 \quad \vee \quad \overline{C\bar{u}} = C\bar{u} \end{aligned} \quad (6.8a)$$

Similarly,

$$\overline{C_t v} = C\bar{v} + \overline{C'v'} \quad (6.8b)$$

$$\overline{C_t w} = C\bar{w} + \overline{C'w'} \quad (6.8c)$$

In the above, the first term of right-hand side of each equation represents advective flux and the second term characterizes diffusive and mixing flux.

Then, introducing Prandtl's mixing length theory, it can be hypothesized that the fluid parcel, as it is generated by the turbulence, containing suspended sediment moves randomly in turbulent flow. As the fluid parcel moves, it travels over a distance l , well known as mixing length, before it mixes (degenerates or loses its identity) with the local fluid body. The change in magnitude of suspended sediment concentration in the fluid parcel between its generation and degeneration points produces a temporal fluctuation. Thus,

$$C' = -l_x \frac{\partial C}{\partial x} \quad (6.9)$$

In the above, the subscript x denotes the quantity in x -direction. By definition of turbulent diffusivity or eddy viscosity, the following expression can be written:

$$\varepsilon_{tx} = |u'|l_x = \varepsilon_{sx} \quad (6.10)$$

where ε_t is the turbulent diffusivity or eddy viscosity and ε_s is the solid diffusivity. In the above expression, the turbulent diffusivity is considered to be identical with the solid diffusivity, which is the governing mechanism of diffusion of suspended sediment particles. The Reynolds analogy, which relates solid diffusivity for mass transfer to turbulent diffusivity for momentum transfer, is valid if the mechanisms controlling both mass and momentum transfer are identical, that is, $\varepsilon_s = \varepsilon_t$. However, its validity was tested by Brush et al. (1962), Majumdar and Carstens (1967) and Jobson and Sayre (1970). They found $\varepsilon_s < \varepsilon_t$ and expressed the inequality as $\varepsilon_s = \beta \varepsilon_t$, where β is the *proportionality factor*. For suspended sediment in turbulent flow of water, β depends on centrifugal acceleration induced on a particle having a particle size d . As a result of which, evaluating β even under simplified assumption is a difficult proposition. Using Eq. (6.10) into Eq. (6.9) and then time-averaging yield

$$\overline{C'u'} = -\varepsilon_{sx} \frac{\partial C}{\partial x} = -\beta_x \varepsilon_{tx} \frac{\partial C}{\partial x} \quad \wedge \quad \varepsilon_{sx} = \beta_x \varepsilon_{tx} \quad (6.11)$$

Recollecting Fick's second law, suspended particles can also be transported by the molecular diffusion process, although it is a weak process as compared to turbulent or solid diffusion. Equation (6.11) is therefore generalized as

$$\overline{C'u'} = -(\varepsilon_m + \varepsilon_{sx}) \frac{\partial C}{\partial x} = -(\varepsilon_m + \beta_x \varepsilon_{tx}) \frac{\partial C}{\partial x} \quad (6.12a)$$

Similarly, for other two directions, the expressions are

$$\overline{C'v'} = -(\varepsilon_m + \varepsilon_{sy}) \frac{\partial C}{\partial y} = -(\varepsilon_m + \beta_y \varepsilon_{ty}) \frac{\partial C}{\partial y} \quad \wedge \quad \varepsilon_{sy} = \beta_y \varepsilon_{ty} \quad (6.12b)$$

$$\overline{C'w'} = -(\varepsilon_m + \varepsilon_{sz}) \frac{\partial C}{\partial z} = -(\varepsilon_m + \beta_z \varepsilon_{tz}) \frac{\partial C}{\partial z} \quad \wedge \quad \varepsilon_{sz} = \beta_z \varepsilon_{tz} \quad (6.12c)$$

Inserting Eq. (6.7), then averaging and using Eqs. (6.8a–c) and (6.12a–c) into Eq. (6.6), the *generalized three-dimensional advection–diffusion equation* for a low concentration of suspended sediment motion in incompressible fluid flow is obtained as

$$\underbrace{\frac{\partial C}{\partial t}}_I + \underbrace{\bar{u} \frac{\partial C}{\partial x} + \bar{v} \frac{\partial C}{\partial y} + \bar{w} \frac{\partial C}{\partial z} + C \left(\frac{\partial \bar{u}}{\partial x} + \frac{\partial \bar{v}}{\partial y} + \frac{\partial \bar{w}}{\partial z} \right)}_{II} = \underbrace{\dot{C}}_{III} \quad (6.13)$$

$$+ \underbrace{\frac{\partial}{\partial x} \left[(\epsilon_m + \epsilon_{sx}) \frac{\partial C}{\partial x} \right] + \frac{\partial}{\partial y} \left[(\epsilon_m + \epsilon_{sy}) \frac{\partial C}{\partial y} \right] + \frac{\partial}{\partial z} \left[(\epsilon_m + \epsilon_{sz}) \frac{\partial C}{\partial z} \right]}_{IV}$$

In Eq. (6.13), the term denoted by *I* represents the local change of concentration due to time, the terms denoted by *II* correspond to the advection of concentration, the term denoted by *III* signifies the rate of change of state of concentration, and the terms denoted by *IV* characterize the diffusion and the mixing of concentration. Importantly, according to the law of the conservation of mass, \dot{C} that is in fact the sediment production rate or dissipation rate per unit volume is zero. In viscous flow, the molecular diffusion is prevalent ($\epsilon_m \neq 0$) and the turbulent diffusion does not exist ($\epsilon_{tx} = \epsilon_{ty} = \epsilon_{tz} = 0$). In contrast, in turbulent flow, molecular diffusion is negligible ($\epsilon_m \approx 0$) in comparison to turbulent diffusion ($\epsilon_{tx}, \epsilon_{ty}, \epsilon_{tz} \gg \epsilon_m$).

6.2.3 Governing Equation of Vertical Distribution of Sediment Concentration

The mechanism of suspended sediment motion occurs in a turbulent flow through the transport of sediment particles by the velocity fluctuations and the mixing of sediment particles with the surrounding fluid body. For two-dimensional steady-uniform flow (zero-pressure gradient) under consideration, the streamwise velocity, being the main flow velocity, is in the downstream direction, and the time-averaged vertical velocity component is zero, but the fluctuations of vertical velocity component is nonzero. Therefore, the convection of suspended sediment particles cannot be governed by the time-averaged velocity, but it should be attributed to the complex diffusion process. Convective transport of the suspended particles occurs when a fluid parcel containing suspended particles is transported by the vertical velocity fluctuations to a zone of lower sediment concentration and mixes with the surrounding fluid body with lower sediment concentration. Therefore, the diffusion is toward the direction of decreasing concentration tending to equalize the concentration. The transport rate of suspended sediment should therefore be directly related to the gradient of its concentration.

In a two-dimensional steady-uniform flow, the sediment concentration varies with and diffuses in the vertical direction only, but not in the streamwise or transverse directions. Because of the gravitational effects on suspended sediment particles, the concentration usually decreases in the upward direction. Under this consideration, the advection–diffusion equation, given $\partial C / \partial t = 0$, $\partial C / \partial x = 0$,

$\partial C/\partial y = 0$, $\partial^2 C/\partial x^2 = 0$, $\partial^2 C/\partial y^2 = 0$, $\bar{v} = 0$, $\partial \bar{u}/\partial x + \partial \bar{v}/\partial y + \partial \bar{w}/\partial z = 0$, $\varepsilon_m = 0$ and $\bar{C} = 0$, reduces to

$$\bar{w} \frac{\partial C}{\partial z} = \frac{\partial}{\partial z} \left(\varepsilon_{sz} \frac{\partial C}{\partial z} \right) \quad (6.14)$$

In Eq. (6.14), the vertical velocity component \bar{w} is substituted by the terminal fall velocity $-w_s$ (negative sign is due to downwards motion) of sediment and the notation of solid or sediment diffusivity in z -direction ε_{sz} by ε_s . Integrating Eq. (6.14) yields

$$\underbrace{\varepsilon_s \frac{\partial C}{\partial z}}_{\text{Entrainment flux}} + \underbrace{C w_s}_{\text{Depositional flux}} = 0 \quad (6.15)$$

The integration constant, which is determined from the boundary condition $\partial C/\partial z = 0$ for $C = 0$, is zero. Equation (6.15) represents that in a steady turbulent flow, the equilibrium of the sediment suspension exists by balancing the upward rate of sediment motion (entrainment flux) due to turbulent diffusion and the downward volumetric rate of sediment settling (depositional flux) per unit area (parallel to the bed) due to gravity. Schmidt (1925) was the first to derive Eq. (6.15) and used it to describe the distribution of fine dust particles in atmosphere. An interpretation of Eq. (6.15) is illustrated in Fig. 6.2.

The vertical distribution of suspended sediment concentration C can be determined from the solution of Eq. (6.15). Considering the importance of Eq. (6.15), for better understanding of the readers, the mechanism of sediment diffusion, as it occurs in an open-channel flow, can be explained further in an analytical way as follows:

In a steady flow, as sediment particles are kept in suspension in fluid by the turbulent fluctuations, they settle by their terminal fall velocity w_s . Following the Prandtl's mixing length theory, fluid containing sediment particles are transported from the lower level I , where the concentration (volumetric) of suspended sediment is $C - dC$, to the higher level II , where the concentration is $C + dC$ (see Fig. 6.3).

The fluid transports up with the amount of sediment q_u (volume rate per unit area) through the section AA (having a length of unity), which is a section in between I and II . It is

$$q_u = (w' - w_s)(C - dC) = (w' - w_s) \left(C - l_z \frac{\partial C}{\partial z} \right) \quad (6.16)$$

The upward transport is reciprocated by a corresponding downward transport of fluid with sediment. Analogous to Eq. (6.16), the downward sediment transport q_d is given by

Fig. 6.2 Equilibrium of sediment suspension by settling and diffusion

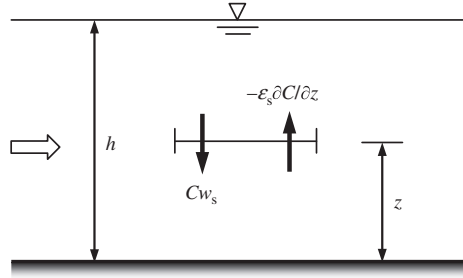
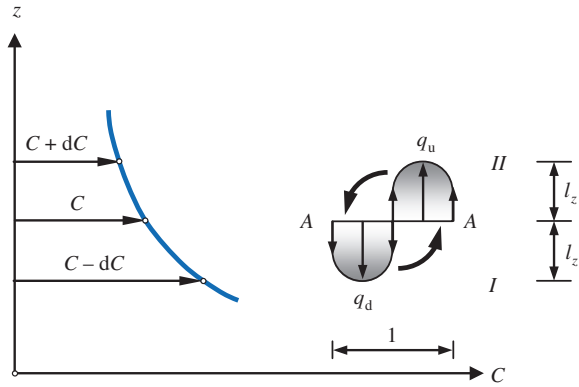


Fig. 6.3 Mechanism of sediment suspension in turbulent flow



$$q_d = (w' + w_s)(C + dC) = (w' + w_s) \left(C + l_z \frac{\partial C}{\partial z} \right) \quad (6.17)$$

In case of a steady flow, the upward transport q_u and the downward transport q_d are balanced (that is, $q_u = q_d$), which yields

$$Cw_s + w'l_z \frac{\partial C}{\partial z} = 0 \quad (6.18)$$

Analogous to Eq. (6.10) and introducing β [see Eq. (6.12c)], one can write, $w'l_z \approx \beta \epsilon_{tz} = \epsilon_{sz}$; and thus, Eq. (6.18) becomes Eq. (6.15).

Here, it is important to have a discussion on β -factor. The β -factor in fact describes diffusion of discrete sediment particles relative to that of a fluid parcel in which sediment particles belong to. In the analysis, β is in general assumed to be constant over entire flow depth. However, experimental results were interpreted to show $\beta \approx 1$ for fine sediment particles that correspond to $\epsilon_t \approx \epsilon_s$; and $\beta < 1$ for coarse sediment particles that correspond to $\epsilon_t > \epsilon_s$. On the other hand, using experimental results of Coleman (1970), van Rijn (1984b) represented

$$\beta \left(0.1 < \frac{w_s}{u_*} < 1 \right) = 1 + 2 \left(\frac{w_s}{u_*} \right)^2 \quad (6.19)$$

where u_* is the shear velocity. Equation (6.19) suggests $\beta > 1$ (contradictory to the previous findings), which signifies a predominating influence of centrifugal acceleration causing the particles to be moved outwards of an eddy. Thus, it results in an increase in the effective mixing length of eddies.

6.2.4 Distribution of Sediment Concentration

For uniform turbulence, the solution of Eq. (6.15) with a simplest approximation ε_t (or in turn ε_s) to be invariant of z can be obtained through integration, such that

$$\frac{C}{C_a} = \exp \left[-\frac{w_s}{\varepsilon_s} (z - a) \right] \quad (6.20)$$

where C_a is the *reference concentration* (by volume) at an elevation $z = a$ from the bed level and a is the *reference level*. According to Eq. (6.20), the concentration distribution is an exponential. The concentration varies with distance from the bed being maximum at $z = a$ and decreasing with an increase in z . Importantly, the diffusivity varies with the vertical distance in an open-channel flow or in a natural stream. Therefore, the concentration distribution obtained from Eq. (6.20), which is based on ε_t as a constant, is merely approximate one and can hardly be used for any problem dealing with realistic situation.

6.2.4.1 Rouse Equation

Separating the variables and replacing the partial differential by the total differential sign, Eq. (6.15) can be rearranged as

$$\frac{dC}{C} + w_s \frac{dz}{\varepsilon_s} = 0 \quad (6.21)$$

In the above equation, the diffusivity of sediment particles ε_s is given as a function of z , that is, $\varepsilon_s = \varepsilon_s(z)$. Integration of Eq. (6.21) yields

$$C = C_a \exp \left(-w_s \int_a^z \frac{dz}{\varepsilon_s} \right) \quad (6.22)$$

For turbulent flow, the Reynolds shear stress τ , according to Boussinesq hypothesis, can be expressed as

$$\tau = \varepsilon_t \rho \frac{d\bar{u}}{dz} \quad (6.23)$$

The shear stress distribution along z in turbulent flow is given by

$$\tau = \tau_0 \left(1 - \frac{z}{h}\right) \quad (6.24)$$

where τ_0 is the bed shear stress.

Assuming that the logarithmic law of velocity distribution is preserved over the entire flow depth, one can write

$$\frac{d\bar{u}}{dz} = \frac{u_*}{\kappa} \cdot \frac{1}{z} \quad (6.25)$$

where κ is the von Kármán constant. From Eqs. (6.23)–(6.25), one gets

$$\varepsilon_t = \kappa u_* z \left(1 - \frac{z}{h}\right) \quad \wedge \quad \varepsilon_s = \beta \varepsilon_t = \beta \kappa u_* z \left(1 - \frac{z}{h}\right) \quad (6.26)$$

Inserting ε_s from Eq. (6.26) into Eq. (6.22) and performing the integration yield

$$\frac{C}{C_a} = \left(\frac{1 - \tilde{z}}{\tilde{z}} \cdot \frac{\tilde{a}}{1 - \tilde{a}} \right)^\zeta \quad \wedge \quad \tilde{z} = \frac{z}{h} \quad \vee \quad \tilde{a} = \frac{a}{h} \quad \wedge \quad \zeta = \frac{w_s}{\beta \kappa u_*} \quad (6.27)$$

The exponent ζ is called *Rouse number or suspension number*. This equation of concentration distribution, known as *Rouse equation* of concentration, was introduced by Rouse (1937), who assumed $\beta = 1$ as an approximation. Equation (6.27) can be used to calculate the concentration C at any distance z from the bed for a given terminal fall velocity w_s of the sediment size if a reference concentration C_a at a reference level a is known.

The vertical distribution of suspended sediment concentration (C/C_a versus z_1) for different values of ζ according to Rouse equation is presented in Fig. 6.4, where $z_1 = (z - a)/(h - a)$ and \tilde{a} is assumed as 0.05. Note that the concentration C decreases with the distance z from the bed. Mathematically, at the bed ($z = 0$), the concentration C becomes infinity breaking down Eq. (6.27). Einstein et al. (1940) pointed out that the sediment suspension cannot be feasible in the so-called *bed layer*, which has a thickness of two particle diameters. However, at the free surface ($z = h$), the concentration C becomes zero, and at the reference level $z = a$ or $z_1 = 0$, $C = C_a$, as already mentioned. It is attributed to the fact that Eq. (6.26) that is known as *Rousean formulation* of vertical turbulent diffusivity ε_t predicts a parabolic form of distribution (Fig. 6.5).

Fig. 6.4 Vertical distribution of suspended sediment concentration according to Rouse equation

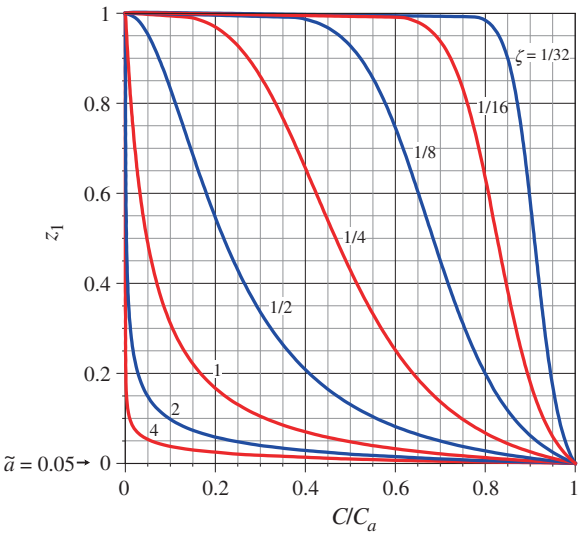
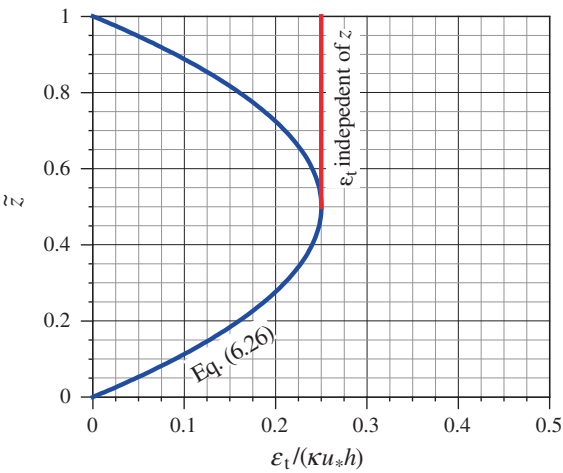


Fig. 6.5 Vertical distribution of turbulent diffusivity



Coleman (1970) was the first to present the experimental variation of turbulent diffusivity ε_t with distance z from the bed. The observation was that the turbulent diffusivity becomes invariant of z for the upper half ($z > 0.5h$) of the flow depth and is no longer a parabolic distribution; while for the lower half ($z \leq 0.5h$) of the flow depth, the distribution of turbulent diffusivity is reasonably parabolic, as shown in Fig. 6.5. It is pertinent to mention that van Rijn (1984b), among others, introduced the variation of turbulent diffusivity obtained by Coleman (1970) in his model, as discussed in succeeding subsection.

Reverting to the Rouse equation, Fig. 6.6 shows that the computed distributions of concentration using Eq. (6.27) with $\tilde{a} = 0.05$ corresponded well with the experimental data of Vanoni (1946). For small values of Rouse number ζ , the concentration varies slowly with an increase in vertical distance z ; while for large values of ζ , the concentration varies rapidly with z . It is important to mention that the distributional pattern of concentration C is primarily governed by the particle size, expressed by the terminal fall velocity $w_s(d)$, and the flow, expressed by the shear velocity u_* . Therefore, small and large values of ζ correspond to fine and coarse sediment sizes, respectively. Alternatively, for a given sediment size, an increase in u_* leads to a decrease in ζ and results in a slow variation C with z . Although Rouse equation is widely used in prediction of concentration distribution for given sediment size and flow condition, the primary shortcoming of the equation is that it is derived from the logarithmic law of velocity distribution, notwithstanding that the logarithmic law is legitimate only for the wall shear layer ($z \leq 0.2h$) of flow having a universal von Kármán constant κ ($=0.41$). Whether κ to be a universal constant in a sediment-laden flow is still in debate and is discussed further in Sect. 6.7.

Note that in this book, the symbol ζ with $\beta \neq 1$ is not differentiated from that with $\beta = 1$. Rather symbol ζ [$= w_s/(\beta \kappa u_*)$] has been used all throughout mentioning explicitly if $\beta \neq 1$ or $\beta = 1$. However, in literature, different symbols were sometimes used for $\zeta|_{\beta \neq 1}$ and $\zeta|_{\beta=1}$, where they can be easily be related to $\zeta|_{\beta=1}/\zeta|_{\beta \neq 1} = \beta$. In an attempt to obtain the relationship for β , Chien (1954) suggested

$$\beta = \frac{\zeta|_{\beta=1}}{\zeta|_{\beta \neq 1}} = \exp\left(-\frac{L^2 \zeta|_{\beta=1}^2}{\pi}\right) + \left(\frac{2}{\pi}\right)^{0.5} L \zeta|_{\beta=1} \int_0^{(2/\pi)^{0.5} L \zeta|_{\beta=1}} \exp[-0.5(\ln z)^2] d(\ln z) \quad \wedge \quad L = \ln(1 + R\kappa) \quad (6.28)$$

where R is the coefficient that modifies universal κ as $R\kappa$ for defining mixing length ($l = R\kappa z$). If $\zeta|_{\beta=1}$ is very large, then

$$\left(\frac{2}{\pi}\right)^{0.5} L \zeta|_{\beta=1} \int_0^{(2/\pi)^{0.5} L \zeta|_{\beta=1}} \exp[-0.5(\ln z)^2] d(\ln z) \rightarrow 1 \Rightarrow \zeta|_{\beta \neq 1} \rightarrow L^{-1}$$

It means that $\zeta|_{\beta \neq 1}$ approaches a constant. Alternatively, if $\zeta|_{\beta=1}$ is very small, then

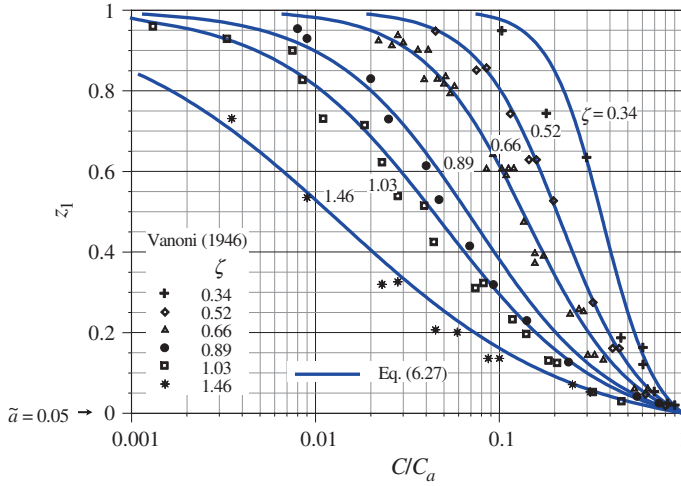


Fig. 6.6 Comparison of vertical distribution of suspended sediment concentration obtained from Rouse equation with experimental data of Vanoni (1946)

$$\left(\frac{2}{\pi}\right)^{0.5} L\zeta|_{\beta=1} \int_0^{(2/\pi)^{0.5} L\zeta|_{\beta=1}} \exp[-0.5(\ln z)^2] d(\ln z) \rightarrow 0 \Rightarrow \zeta|_{\beta \neq 1} \rightarrow \zeta|_{\beta=1}$$

From the curve fitting with the experimental data, $R\kappa$ was found as 0.3. In later period, van Rijn (1984b) suggested a refined expression for β in the context to relate turbulent and sediment diffusivities [see Eq. (6.19)].

6.2.4.2 Lane and Kalinske Equation

Lane and Kalinske (1941) assumed $\varepsilon_s = \varepsilon_t$ for $\beta = 1$. Equation (6.26) then becomes

$$\varepsilon_s = \kappa u_* h (1 - \tilde{z}) \tilde{z} \quad (6.29)$$

The average value of ε_s over flow depth h is given by

$$\bar{\varepsilon}_s = \frac{1}{h} \int_0^h \varepsilon_s dz = \int_0^1 \varepsilon_s d\tilde{z} = \kappa u_* h \int_0^1 (1 - \tilde{z}) \tilde{z} d\tilde{z} \quad (6.30)$$

Performing the integration of Eq. (6.30) and using the value of von Kármán constant $\kappa = 0.41$ yield

$$\bar{\varepsilon}_s = \frac{1}{15} u_* h \quad (6.31)$$

Introducing Eq. (6.31) into Eq. (6.22), the equation of concentration is obtained as

$$\frac{C}{C_a} = \exp \left[-15 \frac{w_s}{u_*} (\tilde{z} - \tilde{a}) \right] \quad (6.32)$$

Note that Eq. (6.32) is characterized by a depth invariant quantity $\bar{\varepsilon}_s$. It is therefore quite similar to Eq. (6.20). However, this simple exponential distribution is capable to provide a reasonable estimation of concentration distribution in wide streams. Additionally, Eq. (6.32) produces a finite estimate of sediment concentration at the free surface; while the Rouse equation is unable to do so.

6.2.4.3 Hunt Equation

Hunt (1954) considered the state of equilibrium of solid (suspended sediment) and fluid phases, as was done to derive Eq. (6.13). For steady-uniform flow, he reduced Eq. (6.13), that is applicable for both the phases, with $\varepsilon_m = 0$ and the time-averaged concentration to be constant over time and varying only with the vertical distance. The equation of solid phase is obtained as follows:

$$-w_b \frac{\partial C}{\partial z} - C \frac{\partial w_b}{\partial z} + \frac{\partial}{\partial z} \left(\varepsilon_{sz} \frac{\partial C}{\partial z} \right) = 0 \quad (6.33)$$

where w_b is the velocity of suspended solid particle in z -direction. Likewise, for the fluid phase, the equation is given by

$$-\bar{w} \frac{\partial C}{\partial z} + (1 - C) \frac{\partial \bar{w}}{\partial z} + \frac{\partial}{\partial z} \left(\varepsilon_{tz} \frac{\partial C}{\partial z} \right) = 0 \quad (6.34)$$

The time-averaged vertical velocity component w_b of sediment particles is equal to the sum of the fluid velocity \bar{w} together with the terminal fall velocity of the sediment particles in still water $-w_s$. Thus, the velocity relationship is given by

$$w_b = \bar{w} - w_s \quad (6.35)$$

Eliminating w_b and \bar{w} from Eqs. (6.33) and (6.34) with Eq. (6.35) yields

$$\varepsilon_{sz} \frac{\partial C}{\partial z} + C \frac{\partial C}{\partial z} (\varepsilon_{tz} - \varepsilon_{sz}) + (1 - C) C w_s = 0 \quad (6.36)$$

The above equation is regarded as the most generalize governing equation for suspended sediment motion. However, to simplify the solution, the solid and turbulent diffusivities were assumed same, that is, $\varepsilon_{sz} = \varepsilon_{tz} = \varepsilon_s$. Thus, one gets

$$\varepsilon_s \frac{dC}{dz} + (1 - C)Cw_s = 0 \quad (6.37)$$

The quantity $(1 - C)$ that appears as a product in the second term of the left-hand side of Eq. (6.37) makes Eq. (6.37) to differ from Eq. (6.15). The $(1 - C)$ results by accounting for the volume of sediment in setting the expression for the sediment flux similar to those as shown in Fig. 6.2.

He hypothesized the distribution of streamwise velocity u_b of suspended sediment from the defect law

$$\frac{U - u_b}{u_*} = -\frac{1}{\kappa_s} \left\{ (1 - \tilde{z})^{0.5} + B_s \ln \left[1 - \frac{1}{B_s} (1 - \tilde{z})^{0.5} \right] \right\} \quad (6.38)$$

where U is the depth-averaged velocity, B_s is the constant of integration in the velocity distribution law ($B_s \leq 1$), and κ_s is the constant similar to the von Kármán constant. Substituting Eq. (6.38) into Eq. (6.23) and using Eq. (6.24), the sediment diffusivity ε_s ($= \varepsilon_t$ for $\beta = 1$) is derived as

$$\varepsilon_s = 2\kappa_s h u_* (1 - \tilde{z}) [B_s - (1 - \tilde{z})^{0.5}] \quad (6.39)$$

The solution of Eq. (6.37) using Eq. (6.39) is obtained as follows:

$$\frac{C}{1 - C} \cdot \frac{1 - C_a}{C_a} = \left(\sqrt{\frac{1 - \tilde{z}}{1 - \tilde{a}}} \cdot \frac{B_s - \sqrt{1 - \tilde{a}}}{B_s - \sqrt{1 - \tilde{z}}} \right)^{\zeta_0} \quad \wedge \quad \zeta_0 = \frac{w_s}{\kappa_s B_s u_*} \quad (6.40)$$

It is known as *Hunt equation*. Equation (6.40) agrees well with Rouse equation (Eq. 6.27) for the values of B_s between 0.99 and 1 and κ_s between 0.31 and 0.44, that Hunt determined using the experimental data of Vanoni (1946). However, due to complex form of Eq. (6.40), it has not been widely used so far, because Eq. (6.40) requires two unknown parameters (B_s and ζ_0) to be determined; while Eq. (6.27) consists of a single unknown (ζ) that makes possible for a better fitting of experimental data.

Importantly, for large sediment concentration, Eq. (6.34) should be used. If the sediment diffusivity is obtained from the relationship given by Einstein and Chien (1955) as

$$\tau = (1 + \Delta C) \rho \varepsilon_t \frac{d\bar{u}}{dz} \quad (6.41)$$

then the governing equation of large sediment concentration is

$$\frac{dC}{dz} + (1 + \Delta C)(1 - C)Cw_s \frac{\rho}{\tau} \cdot \frac{d\bar{u}}{dz} = 0 \quad (6.42)$$

where Δ is the submerged relative density ($=s - 1$), s is the relative density of sediment ($=\rho_s/\rho$), ρ_s is the mass density of sediment, and ρ is the mass density of water.

However, for small sediment concentration, Eq. (6.15) can be effectively used.

6.2.4.4 Zagustin Equation

According to Rouse equation (Eq. 6.27), the magnitude of sediment concentration C at the free surface $z = h$ vanishes. However, this result does not correspond to that observed in the stream flows with suspended sediment. The turbulent diffusion does not exist at the free surface ($\varepsilon_{tz} = 0$), but the sediment diffusion persists there ($\varepsilon_s > 0$). For turbulent diffusion, according to the mixing length theory [see Eq. (3.24)], the relationship of the Reynolds shear stress $-\rho\overline{u'w'}$ holds; and it shows that the shear stress is generated by the diffusion of eddies only at the position where u' and w' have a certain degree of correlation. On the other hand, sediment suspension is primarily governed by $|w'|$ that is smaller than $|u'|$, as turbulence in a stream flow is anisotropic in nature. Thus, even if u' and w' are not correlated, sediment can still be moved. Therefore, although the turbulent diffusion does not persist at $z = h$, sediment exchange can be possible at that level. Importantly, at the free surface, the logarithmic law of velocity distribution does not hold. Instead, the following equation makes possible to estimate the velocity near the free surface

$$\frac{u_{\max} - \bar{u}}{u_*} = \frac{2}{\kappa} \arctanh(1 - \tilde{z})^{1.5} \quad (6.43)$$

where u_{\max} is the maximum value of \bar{u} which occurs at $z = h$. The mixing length l and the turbulent diffusivity ε_{tz} are then

$$l = \frac{\kappa}{3} h [1 - (1 - \tilde{z})^3] \quad (6.44)$$

$$\varepsilon_t = \frac{\kappa}{3} u_* h (1 - \tilde{z})^{0.5} [1 - (1 - \tilde{z})^3] \quad (6.45)$$

Remembering the relationship $\varepsilon_s = \beta \varepsilon_t$, the differential equation of the vertical distribution of sediment concentration can be obtained as

$$Cw_s + \beta \frac{\kappa}{3} u_* (1 - \tilde{z})^{0.5} [1 - (1 - \tilde{z})^3] \frac{dC}{d\tilde{z}} = 0 \quad (6.46)$$

The solution of Eq. (6.46) that was obtained by Zagustin (1968) is given by

$$\frac{C}{C_a} = \exp(-\zeta \Omega) \quad (6.47)$$

where

$$\Omega = \frac{1}{2} \ln \left[\frac{[(1-\tilde{z})^{1.5} + 1][(1-\tilde{z})^{0.5} - 1]^3}{[(1-\tilde{z})^{1.5} - 1][(1-\tilde{z})^{0.5} + 1]^3} \right] \Bigg|_{\tilde{z}=\tilde{a}}^{\tilde{z}=\tilde{z}} + \sqrt{3} \arctan \left[-\sqrt{3} \frac{(1-\tilde{z})^{0.5}}{\tilde{z}} \right] \Bigg|_{\tilde{z}=\tilde{a}}^{\tilde{z}=\tilde{z}} \quad (6.48)$$

In Fig. 6.7, a comparison is presented between the distributions of suspended sediment concentration obtained from Eqs. (6.27) and (6.47). It is evident that Eq. (6.47) provides a finite (nonzero) estimation of concentration at the free surface. However, Eq. (6.47) underestimates Rouse equation to some extent in most of the portions of the flow depth.

6.2.4.5 van Rijn Equation

The differential equation of sediment concentration that was used by van Rijn (1984b) is similar to Eq. (6.37), but in slightly modified form with a replacement of w_s by w_{sc} . It is

$$\varepsilon_s \frac{dC}{dz} + (1 - C)Cw_{sc} = 0 \quad (6.49)$$

where w_{sc} is the terminal fall velocity of sediment particles in sediment-laden water. It is less than the terminal fall velocity w_s of sediment particles in the clear water. The relationship used by him was $w_{sc} = w_s(1 - C)^4$, which was proposed by Richardson and Zaki (1954) [see Eq. (1.44)].

He divided the flow into two layers, namely the lower and the upper half. As was experimentally observed by Coleman (1970), he considered a parabolic-constant distribution of ε_t that gives a parabolic variation in the lower half ($z < 0.5h$) and a constant value in the upper half ($z \geq 0.5h$) (Fig. 6.5), such that

$$\varepsilon_t(\tilde{z} < 0.5) = 4\tilde{z}(1 - \tilde{z})\varepsilon_t|_{\max} \quad (6.50a)$$

$$\varepsilon_t|_{\max}(\tilde{z} \geq 0.5) = 0.25\kappa u_* h \quad (6.50b)$$

The sediment diffusivity is described by

$$\varepsilon_s = \beta \phi \varepsilon_t \quad (6.51)$$

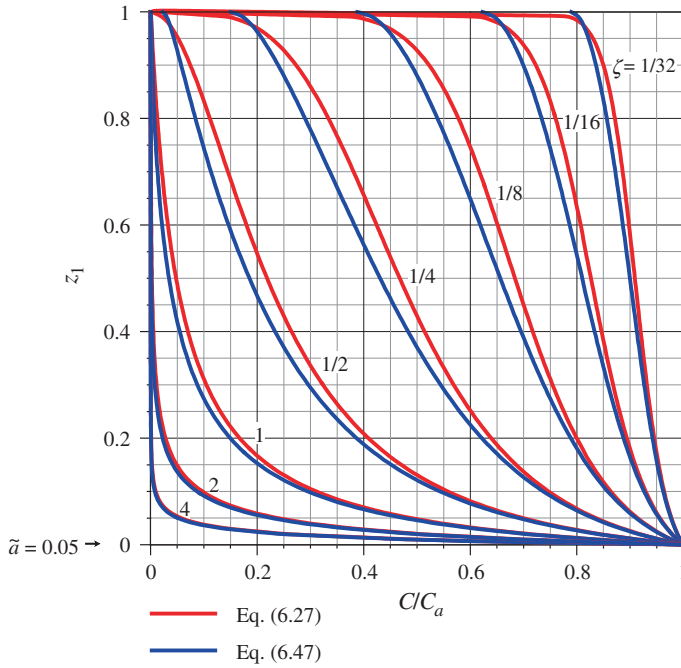


Fig. 6.7 Comparison between the vertical distributions of suspended sediment concentration obtained from Eqs. (6.27) and (6.47)

where ϕ is a factor accounting for the damping of fluid turbulence in the presence of suspended sediment particles. However, van Rijn (1984b) suggested an empirical relationship as $\phi = 1 + (C/C_{\max})^{0.8} - 2(C/C_{\max})^{0.4}$.

Setting $\phi = 1$ (that is, negligible damping effect) and concentration depended terminal fall velocity of sediment, the concentration distribution is obtained by integrating Eq. (6.49) as

$$\left[\ln\left(\frac{C}{1-C}\right) + \sum_{n=1}^4 \frac{1}{n(1-C)^n} \right] \Bigg|_{C=C_a}^{C=C} = \ln\left(\frac{1-\tilde{z}}{\tilde{z}} \cdot \frac{\tilde{a}}{1-\tilde{a}}\right)^{\zeta} \quad \text{for } \tilde{z} < 0.5 \quad (6.52a)$$

$$\left[\ln\left(\frac{C}{1-C}\right) + \sum_{n=1}^4 \frac{1}{n(1-C)^n} \right] \Bigg|_{C=C_a}^{C=C} = -\zeta \left[\ln\left(\frac{\tilde{a}}{1-\tilde{a}}\right) + 4(\tilde{z} - 0.5) \right] \quad \text{for } \tilde{z} \geq 0.5 \quad (6.52b)$$

For small concentration ($C < C_a < 0.001$), Eqs. (6.52a) and (6.52b) reduce to

$$\frac{C}{C_a}(\tilde{z} < 0.5) = \left(\frac{1 - \tilde{z}}{\tilde{z}} \cdot \frac{\tilde{a}}{1 - \tilde{a}} \right)^\zeta \quad (6.53a)$$

$$\frac{C}{C_a}(\tilde{z} \geq 0.5) = \left(\frac{\tilde{a}}{1 - \tilde{a}} \right)^\zeta \exp[-4\zeta(\tilde{z} - 0.5)] \quad (6.53b)$$

6.2.4.6 Ni and Wang Equation

Ni and Wang (1991) started the analysis with Eq. (6.15), as governing equation, with the assumption that ε_s ($=\varepsilon_t$ for $\beta = 1$) is characterized by the vertical component of the Lagrangian trajectory of particle, called *sediment mixing length* l_s being different from the so-called Prandtl's mixing length l . Hence,

$$\varepsilon_s = \frac{l_s}{2} \overline{|w'|} \quad (6.54)$$

As w' is assumed to follow the Gaussian distribution, then

$$f(w') = \frac{1}{\sqrt{2\pi}\sqrt{w'^2}} \exp\left(-\frac{w'^2}{2w'^2}\right), \quad f(\overline{|w'|} \geq 0) = \frac{2}{\sqrt{2\pi}\sqrt{w'^2}} \exp\left(-\frac{w'^2}{2w'^2}\right) \quad (6.55a)$$

therefore

$$\overline{|w'|} = \int_0^\infty f(\overline{|w'|}) w' dw' = \sqrt{\frac{2}{\pi}} \sqrt{w'^2} \quad (6.55b)$$

The relationship that was used by them for the terminal fall velocity w_{sc} of sediment particles in sediment-laden water was $w_{sc} = w_s(1 - C)^\alpha$, where α is an exponent dependent on particle size.

Replacing w_s by w_{sc} and using the above relationships into Eq. (6.15), the differential equation of sediment diffusion is given by

$$\frac{dC}{dz} = -\sqrt{2\pi} \frac{w_s}{u_*} (1 - C)^\alpha C \frac{u_*}{l_s \sqrt{w'^2}} \quad \wedge \quad \zeta|_{\beta=1} \approx \sqrt{2\pi} \frac{w_s}{u_*} \quad (6.56)$$

Since the experiments by Grass (1971) proved that $\overline{w'^2} \approx u_*^2$ for almost entire flow depth (except in near-bed region), the characteristic Eulerian length l_0 related to vertical motion of sediment can be shown identical with l_s as follows:

$$l_0 = l_s \frac{\sqrt{w'^2}}{u_*} = l_s \quad \wedge \quad \sqrt{w'^2} \approx u_* \quad (6.57)$$

Analogous to Prandtl's mixing length l , a typical expression for l_0 can be put forward considering the effects of sediment suspension as

$$\frac{l_0}{z} = \tilde{z}(1 - \tilde{z})^m \quad (6.58)$$

where m is an exponent accounting for the effects of sediment–water interaction on the length scale of vertical motion of sediment. Equation (6.58) is quite similar to the traditional expression for turbulent diffusivity or eddy viscosity.

Using Eqs. (6.57) and (6.58) into Eq. (6.56) and then integrating yield

$$\int_{C_a}^C \frac{dC}{(1 - C)^\alpha C} = - \int_{\tilde{a}}^{\tilde{z}} \zeta \cdot \frac{1}{\tilde{z}(1 - \tilde{z})^m} d\tilde{z} \quad (6.59)$$

For low concentration, Eq. (6.59) with $\alpha = 0$ becomes

$$\frac{C}{C_a} = \exp \left[-\zeta \int_{\tilde{a}}^{\tilde{z}} \frac{1}{\tilde{z}(1 - \tilde{z})^m} d\tilde{z} \right] \quad (6.60)$$

For m taking positive integer values, a progressional solution is obtained as

$$\frac{C}{C_a} = \left(\frac{\tilde{a}}{\tilde{z}} \cdot \frac{1 - \tilde{z}}{1 - \tilde{a}} \right)^\zeta \cdot \exp \left\{ \zeta \left[\sum_{n=1}^{n=m-1} \frac{1}{n(1 - \tilde{z})^n} \right] \right\} \bigg|_{\tilde{z}=\tilde{a}}^{\tilde{z}=\tilde{z}} \quad (6.61)$$

On the other hand, for $m \leq 1$ taking integer values, another progressional solution is obtained as

$$\frac{C}{C_a} = \left(\frac{\tilde{a}}{\tilde{z}} \right)^\zeta \cdot \exp \left\{ \zeta \sum_{i=1}^{i=m} \left[\frac{(-1)^i}{i} \cdot \frac{m(m-1) \cdots (m-i+1)}{i!} (-\tilde{z}) \right] \right\} \bigg|_{\tilde{z}=\tilde{a}}^{\tilde{z}=\tilde{z}} \quad (6.62)$$

where m takes absolute values. However, Ni and Wang (1991) also used the following progressional method for the integration of Eq. (6.60):

$$f(1 - \tilde{z}) = \int \frac{1}{\tilde{z}(1 - \tilde{z})^m} d\tilde{z} = \sum_{m=0}^{m=n} \frac{\tilde{z}^{1+n-m}}{1 + n - m} \quad (6.63a)$$

$$f(\tilde{z}) = \int \frac{1}{\tilde{z}^m(1-\tilde{z})} d\tilde{z} = - \sum_{m=0}^{m=n} \frac{(1-\tilde{z})^{1+n-m}}{1+n+m} \quad (6.63b)$$

Therefore, the generalized equation of concentration distribution can be obtained as

$$\frac{C}{C_a} = \exp \left[\zeta f(\tilde{z}) \Big|_{\tilde{z}=\tilde{a}}^{\tilde{z}=\tilde{z}} \right] \quad (6.64)$$

Some of the interesting features of the integral equation of concentration (Eq. 6.60) can be furnished as follows:

1. With $m = 0$, Laursen (1980) equation can be obtained from Eq. (6.60). It is

$$\frac{C}{C_a} = \left(\frac{a}{z} \right)^\zeta \quad (6.65)$$

2. With $m = 1$, Rouse (1937) equation (Eq. 6.27) is obtained.
3. With $m = 0.8$, Barenblatt (1956) equation can be obtained with equivalent substitution of $2(1-\tilde{z})[1-(1-\tilde{z})^{0.5}]$ and $(1-\tilde{z})^{0.8}$ from Eq. (6.60) as

$$\frac{C}{C_a} = \left(\frac{\sqrt{1-\tilde{z}}}{\sqrt{1-\tilde{a}}} \cdot \frac{1-\sqrt{1-\tilde{a}}}{1-\sqrt{1-\tilde{z}}} \right)^\zeta \quad (6.66)$$

4. With $m = 0.5$, Tanaka and Sugimoto (1958) equation can be obtained from Eq. (6.60) as

$$\frac{C}{C_a} = \left(\frac{1+\sqrt{1-\tilde{z}}}{1+\sqrt{1-\tilde{a}}} \cdot \frac{1-\sqrt{1-\tilde{a}}}{1-\sqrt{1-\tilde{z}}} \right)^\zeta \quad (6.67)$$

6.2.4.7 Umeyama Equation

From the data analysis, Umeyama and Gerritsen (1992) observed that the Prandtl's mixing length theory, used to derive the velocity equation, fails to agree with the experimental data for sediment-laden flows in the flow region outside the near-bed layer. Therefore, in order to improve mixing length hypotheses, Umeyama (1992) proposed a new mixing length l_u , that is

$$l_u = \kappa h \tilde{z} (1 - \tilde{z})^{0.5[1+\beta(C/C_a)]} \quad (6.68)$$

Analogous to other theoretical development in sediment-laden flows, the Reynolds shear stress τ is expressed as

$$\tau = (1 + \Delta C) \rho l_u^2 \left| \frac{d\bar{u}}{dz} \right| \left| \frac{d\bar{u}}{dz} \right| \quad (6.69)$$

Equating the right-hand side of Eq. (6.69) with that of Eq. (6.24), it leads to

$$\frac{d\bar{u}}{dz} = \frac{(\tau_0/\rho)^{0.5}}{\kappa z} \cdot \frac{1}{(1 - \tilde{z})^{0.5\beta(C/C_a)} (1 + \Delta C)^{0.5}} \quad \wedge \quad u_* = \left(\frac{\tau_0}{\rho} \right)^{0.5} \quad (6.70)$$

Using Eq. (6.70), the turbulent diffusivity ε_t is obtained from Eq. (6.23) as

$$\varepsilon_t = \kappa u_* h \tilde{z} (1 - \tilde{z})^{1+0.5\beta(C/C_a)} (1 + \Delta C)^{0.5} \quad (6.71)$$

The new mixing length l_u is assumed to be independent of the sediment concentration C . So, l_u is a function of z alone. Then, the turbulent diffusivity ε_t is modified as

$$\varepsilon_t = \kappa u_* h \tilde{z} (1 - \tilde{z})^{1+0.5\beta(C_{0.1h}/C_a)} (1 + \Delta C_{0.1h})^{0.5} \quad (6.72)$$

where $C_{0.1h}$ is the suspended sediment concentration at $z = 0.1h$.

Substituting Eq. (6.72) into Eq. (6.15) with $\varepsilon_s = \beta \varepsilon_t$ and then integrating yield

$$\begin{aligned} \frac{C}{C_a} = A \exp \left\{ - \frac{\zeta}{(1 + \Delta C_{0.1h})^{0.5}} \left[\ln \tilde{z} + \left(1 + \frac{\beta}{2} \cdot \frac{C_{0.1h}}{C_a} \right) \tilde{z} \right. \right. \\ \left. \left. + \cdots + \frac{1}{n!} \left(1 + \frac{\beta}{2} \cdot \frac{C_{0.1h}}{C_a} \right) \left(2 + \frac{\beta}{2} \cdot \frac{C_{0.1h}}{C_a} \right) \cdots \left(n + \frac{\beta}{2} \cdot \frac{C_{0.1h}}{C_a} \right) \frac{\tilde{z}^n}{n} \right] \right\} \end{aligned} \quad (6.73)$$

where A is a constant to be determined from the boundary condition.

6.2.4.8 Other Equations

Lavelle and Thacker (1978) assumed that the turbulent diffusivity ε_t ($=\varepsilon_s$ for $\beta = 1$) is a function of distance from the bed. It is

$$\varepsilon_t = (a_e + b_e h \tilde{z})(1 - \tilde{z}) \quad (6.74)$$

where a_e and b_e are the empirical constants. Using Einstein and Chien's (1955) flume data, the ranges of a_e and b_e for $u_* = 0.1009 - 0.1245 \text{ m s}^{-1}$ were evaluated as $5.8 \times 10^{-8} - 1.5 \times 10^{-6} \text{ m}^2 \text{ s}^{-1}$ and $0.0146 - 0.401 \text{ m s}^{-1}$, respectively. The relationship used by them for the terminal fall velocity w_{sc} of sediment particles in sediment-laden flows is $w_{sc} = w_s(1 - C)^5$.

Replacing w_s by w_{sc} [and expressing $w_{sc} = w_s(1 - C)^5$] and using Eq. (6.74) into Eq. (6.15), the concentration distribution is obtained as

$$\left[\ln\left(\frac{C}{1-C}\right) - \sum_{n=2}^{\infty} \frac{(1-C)^{1-n}}{1-n} \right] \Big|_{C=C_a}^{C=C} = -\frac{w_s}{b_e + (a_e/h)} \ln \left\{ \frac{[a_e/(b_e h)] + \tilde{z}}{1 - \tilde{z}} \right\} \Big|_{\tilde{z}=\tilde{a}}^{\tilde{z}=\tilde{z}} \quad (6.75)$$

Willis (1979) argued that the turbulent diffusivity ε_t ($=\varepsilon_s$ for $\beta = 1$) can be expressed by an error function as

$$\varepsilon_t = \sqrt{2} \frac{\kappa u_* h}{6} \exp\left(-\frac{P^2}{2}\right) \quad (6.76)$$

where quantity P can be obtained from the following relationship:

$$\int_{-\infty}^P \exp(-0.5r^2) dr = \sqrt{2\pi} \tilde{z} \quad (6.77)$$

Then, the concentration distribution is obtained as

$$\frac{C}{C_a} = \exp\left[\left(-\frac{3\zeta}{\sqrt{\pi}}\right)(P - P_a)\right] \quad (6.78)$$

where $P_a = Pl_{z=a}$.

Antsyferov and Kos'yan (1980), who argued that the Rouse equation of concentration cannot describe the concentration distribution if $w_s > 0.27u_*$, proposed a two-layer model for the distribution of suspended sediment concentration. They pointed out that in the vicinity of the bed, $\sqrt{w'^2}$ approximately equals u_* , and therefore, ε_t and ε_s differ significantly from each other. Based on the analysis of experimental data, ε_s is proposed as

$$\frac{\varepsilon_s}{u_* \tilde{z}} = \frac{R_{*z}(1 - \tilde{z})}{2.8R_{*z} + 15.7} \tanh\left(\frac{u_*}{w_s} \tilde{z}\right) + \frac{1}{0.14\Delta s} \cdot \frac{v^{2/3}}{g^{1/3} \tilde{z}} \left(\frac{\bar{u}_d}{u_*} - \frac{w_s}{u_*}\right) \exp\left(-30 \frac{\tilde{z}}{d}\right) \quad (6.79)$$

where $R_{*z} = u_* \tilde{z}/v$, v is the coefficient of kinematic viscosity of water, \bar{u}_d is the time-averaged flow velocity close to the bed, given by $1.25U[\log(8.8 h/d)]^{-1}$, and

d is the sediment size. The concentration distribution can be determined from numerical integration of the following integration obtained from Eq. (6.22):

$$\frac{C}{C_a} = \exp \left(-w_s h \int_{\tilde{a}}^{\tilde{z}} \frac{1}{\varepsilon_s} d\tilde{z} \right) \quad (6.80)$$

Itakura and Kishi (1980) recognized that the logarithmic law of velocity distribution does not satisfactorily hold in sediment-laden flows. Instead, the following velocity defect law makes it possible to estimate the velocity distribution in sediment-laden flows:

$$\frac{\bar{u} - u_{\max}}{u_*} = \frac{2}{\kappa} [\ln(\tilde{z}) + h_*(\tilde{z} - 1)] \quad \wedge \quad h_* = \frac{2.8 \Delta g s h w_s \bar{C}}{u_*^2} \quad (6.81)$$

where \bar{C} is the depth-averaged sediment concentration. Using Eqs. (6.26) and (6.81) into Eq. (6.22), the concentration distribution is derived as

$$\frac{C}{C_a} = \left[\frac{\tilde{a}}{\tilde{z}} \left(\frac{1 - \tilde{z}}{1 - \tilde{a}} \right)^{1+h_*} \right]^{\zeta} \quad (6.82)$$

As \bar{C} remains unknown a priori, Eq. (6.82) is to be solved by trial and error method.

McTigue (1981) divided the flow into two layers, such as an inner layer ($z \leq 0.2h$) and an outer layer ($z > 0.2h$). The sediment diffusivity is assumed as

$$\varepsilon_s(z \leq 0.2h) = k_1 u_* z, \quad \varepsilon_s(z > 0.2h) = k_2 u_* h \quad (6.83)$$

where k_1 and k_2 are the coefficients and were evaluated using a lone experimental run as 0.35 and 0.11, respectively. The concentration distribution is given by

$$\frac{C}{C_a}(\tilde{z} \leq 0.2) = \left(\frac{\tilde{z}}{\tilde{a}} \right)^{-w_s/(k_1 u_*)} \quad (6.84a)$$

$$\frac{C}{C_a}(\tilde{z} > 0.2) = \exp \left[-\frac{w_s}{k_2 u_*} (\tilde{z} - \tilde{a}) \right] \quad (6.84b)$$

Bose and Dey (2009b) proposed that it is convenient to fit a concentration distribution by an empirical equation as

$$\frac{C}{C_a} = \left(\frac{\tilde{z}}{\tilde{a}} \right)^{-p_0} + \eta_0 \left(\frac{\tilde{z}}{\tilde{a}} \right)^{p_1} \quad (6.85)$$

The exponents p_0 , p_1 and coefficient η_0 being dependent on sediment size and flow condition were determined empirically.

6.2.5 Stratification Effects on Concentration Distribution

Stream flows carrying suspended sediment are subjected to a variable sediment concentration in the vertical. The concentration C of suspended sediment decreases with an increase in elevation z above the bed. It implies that the mass density of the fluid–sediment mixture ρ_m , given by $\rho_m = (1 + \Delta C)\rho$, also decreases with an increase in z . In particular, the flow region close to the bed, where the sediment concentration is high behaving as a concentrated fluid, is referred to as a *heavy-fluid zone*. The remaining portion of the flow having relatively low sediment concentration has a little change of mass density of the fluid–sediment mixture from that of fluid and is called *light-fluid zone*. The heavy-fluid zone is much shallow as compared to the light-fluid zone. This stable stratification slows down the process of turbulent mixing of the fluid momentum and the sediment mass in the vertical. To be more explicit, turbulence is produced in the vicinity of the bed and the heavy-fluid zone acts as a filter to dissipate the turbulence level because the turbulent kinetic energy is spent to retain the sediment particles in suspension in this zone. As a result of which, the vertical distributions of both streamwise flow velocity and suspended sediment concentration are modified, as the former becomes faster in the vertical than the logarithmic law distribution and the latter decreases more rapidly in the vertical than the distribution obtained from the Rouse equation. It is, however, pertinent to mention that both the logarithmic law and the Rouse equation are devoid from the consideration of the stratification concept.

The concept of self-stratification formed by the suspended sediment in sediment-laden flows was brought in by Smith and McLean (1977a, b) and McLean (1991, 1992). Following the concept of self-stratification, García (2008) modified the sediment diffusivity ε_{sd} due to stratification effects by introducing a function of the gradient Richardson number $\phi_R(R_G)$ as a product of ε_s (without stratification effects) and obtained the gradient Richardson number R_G as follows:

$$\varepsilon_{sd} = \varepsilon_s \phi_R(R_G) \quad \wedge \quad \varepsilon_s(\beta = 1) = \kappa u_* z \left(1 - \frac{z}{h}\right) \Rightarrow R_G = -\frac{\Delta g(dC/dz)}{(\bar{u}/dz)^2} \quad (6.86)$$

where \bar{u} is the streamwise time-averaged flow velocity at an elevation z .

The function of the gradient Richardson number, $\phi_R(R_G)$, which reduces with an increase in gradient Richardson number R_G as an effect of damping of turbulence due to flow stratification, was introduced by Smith and McLean (1977a, b) as

$$\phi_R(R_G) = 1 - 4.7R_G = 1 + 4.7 \frac{\Delta g(dC/dz)}{(\bar{u}/dz)^2} \quad (6.87)$$

In the above equation, $\phi_R(R_G \rightarrow 0) \rightarrow 1$ corresponds to no stratification effects, and $\phi_R(R_G = 0.21) = 0$ refers to no turbulent mixing (that is, a viscous flow).

Using Eqs. (6.86) and (6.87) into Eq. (6.22) yields the concentration equation

$$\frac{C}{C_a} = \exp \left\{ -w_s \int_a^z \left[\kappa u_* z \left(1 - \frac{z}{h} \right) \right]^{-1} \left[1 + 4.7 \frac{\Delta g(dC/dz)}{(\bar{u}/dz)^2} \right]^{-1} dz \right\} \quad (6.88)$$

Equation (6.88) converges to the Rouse equation (nonstratification case), as $\phi_R(R_G \rightarrow 0) \rightarrow 1$. However, Eq. (6.88) can be solved, if the term \bar{u}/dz is known for the self-stratification case.

Smith and McLean (1977a) approximated the equation of Reynolds shear stress in an open-channel flow with a zero-pressure gradient as

$$\varepsilon_{sd} \frac{d\bar{u}}{dz} = \tau_0 \left(1 - \frac{z}{h} \right) \quad (6.89)$$

The flow velocity at the reference level can be obtained from the logarithmic law as

$$\bar{u}|_{z=a} = \frac{u_*}{\kappa} \ln \left(\frac{z}{z_0} \right) \bigg|_{z=a} = \frac{u_*}{\kappa} \ln \left(30 \frac{a}{k_s} \right) \quad \wedge \quad z_0 = \frac{k_s}{30} \quad (6.90)$$

where z_0 is the zero-velocity level and k_s is the Nikuradse's equivalent sand roughness.

Using Eq. (6.86) into Eq. (6.89) and then integrating Eq. (6.89) with boundary condition given by Eq. (6.90) yield the equation of velocity distribution as

$$\bar{u} = \frac{u_*}{\kappa} \left\{ \ln \left(\frac{a}{z_0} \right) + \int_a^z z^{-1} \left[1 + 4.7 \frac{\Delta g(dC/dz)}{(\bar{u}/dz)^2} \right]^{-1} dz \right\} \quad (6.91)$$

Note that Eq. (6.91) converges to the universal logarithmic law (nonstratification case), as $\phi_R(R_G \rightarrow 0) \rightarrow 1$.

Equations (6.88) and (6.91) constitute an implicit solution for the concentration and the velocity distributions. García (2008) proposed an iterative method of solution² for the concentration C and the velocity \bar{u} from Eqs. (6.88) and (6.91).

² The iterative method is as follows:

Step 1: To initiate the computation, calculate $C|_{i=0}$ and $\bar{u}|_{i=0}$ from the Rouse equation (Eq. 6.27) and the logarithmic law (Eq. 4.27), respectively.

Step 2: The values of $C|_{i=0}$ and $\bar{u}|_{i=0}$ obtained in Step 1 are used in Eqs. (6.88) and (6.91) with stratification effects, as given by Eq. (6.87) that is introduced to Eqs. (6.88) and (6.91).

Step 3: Continue the iterations for $C|_{i=i}$ and $\bar{u}|_{i=i}$, until the solutions for C and \bar{u} converge to a minimum error (say 0.1 %).

Wright and Parker (2004) used an approach similar to that of García (2008) for the estimation of concentration and velocity distributions. The computational results agreed well with the observed data.

6.2.6 Nonequilibrium Sediment Concentration Distribution

Brown (2008) introduced a formulation for the nonequilibrium distribution of sediment concentration, using the approach used by Nielsen (1992) and Fujita and Mizuyama (2000) to describe the effects of convective flux on the equilibrium distribution of sediment concentration. He considered a generalized quasi-steady flow condition with nonequilibrium suspended sediment flux, which is liable to net erosion or deposition. It was assumed that on the horizontal plane, the spatial variation of concentration is dominant over temporal variation. Hence, the temporal derivative of concentration was neglected. Figure 6.8, which is modified form of Fig. 6.3, illustrates the relevant contributions to the vertical sediment flux (positive in upwards) balance.

According to Prandtl's mixing length theory, fluid parcel containing sediment particles having concentration $C - dC$ are transported from the lower level I up to the higher level II , where the concentration is $C + dC$ (see Fig. 6.8). In addition, in case of nonequilibrium suspended sediment flux, q_z is the nonequilibrium sediment flux transported in the upward direction through lower level I and $q_z + dq_z$ is the nonequilibrium flux transported in the upward direction through upper level II . The nonequilibrium flux was assumed to vary linearly with mixing length.

The fluid (volume per unit time and area) moves up with the amount of sediment q_u through the section AA (having a length of unity), which is a section in between I and II . It is

$$q_u = (w' - w_s) \underbrace{\left(C - l_z \frac{\partial C}{\partial z} \right)}_{C-dC} \quad (6.92)$$

The downward sediment flux q_d through the section AA is given by

$$q_d = (w' + w_s) \underbrace{\left(C + l_z \frac{\partial C}{\partial z} \right)}_{C+dC} \quad (6.93)$$

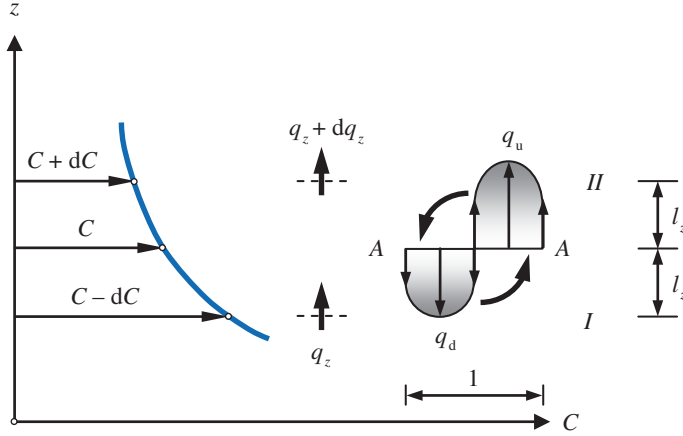


Fig. 6.8 Schematic of nonequilibrium sediment flux in turbulent flow

The dynamic equilibrium exists balancing the net upward sediment flux ($q_u - q_d$) by the total nonequilibrium suspended sediment flux. Hence,

$$(w' - w_s) \left(C - l_z \frac{\partial C}{\partial z} \right) - (w' + w_s) \left(C + l_z \frac{\partial C}{\partial z} \right) = q_z + \underbrace{\left(q_z + 2l_z \frac{\partial q_z}{\partial z} \right)}_{q_z + dq_z} \quad (6.94)$$

Simplifying Eq. (6.94), it gives

$$Cw_s + w'l_z \frac{\partial C}{\partial z} + q_z + l_z \frac{\partial q_z}{\partial z} = 0 \quad (6.95)$$

Nielsen (1992) and Fujita and Mizuyama (2000) also obtained an equation, which was analogous to Eq. (6.95), in describing the contribution from convective flux. Remembering that $lw'l_z \approx \beta \varepsilon_t = \varepsilon_s$ and $\overline{w'^2} \approx u_*^2$ (Grass 1971), Eq. (6.95), by replacing partial differential to total differential sign, becomes

$$Cw_s + \varepsilon_s \frac{dC}{dz} + q_z + \frac{\varepsilon_s}{u_*} \cdot \frac{dq_z}{dz} = 0 \quad (6.96)$$

As $q_z(\varepsilon_s = 0) = -Cw_s$ from Eq. (6.96), one can establish the ratio of q_z (at any elevation z) to $q_z|_{z=a}$ (that is, at $z = a$) and express dq_z/dz as

$$\frac{q_z}{q_z|_{z=a}} = \frac{C}{C_a} \Rightarrow \frac{dq_z}{dC} = \frac{q_z|_{z=a}}{C_a}, \quad \therefore \frac{dq_z}{dz} = \frac{dq_z}{dC} \cdot \frac{dC}{dz} = \frac{q_z|_{z=a}}{C_a} \cdot \frac{dC}{dz} \quad (6.97)$$

Using Eq. (6.97) into Eq. (6.96), the following differential equation of concentration can be obtained

$$\frac{dC}{C} = - \frac{\left(w_s + \frac{q_z|_{z=a}}{C_a} \right)}{\varepsilon_s \left(1 + \frac{1}{u_*} \cdot \frac{q_z|_{z=a}}{C_a} \right)} dz \quad \wedge \quad \varepsilon_s = \beta \kappa u_* z \left(1 - \frac{z}{h} \right) \quad (6.98)$$

Integrating Eq. (6.98) within limit $z(C = C_a) = a$ to $z(C = C) = z$ and expressing the resulting equation in nondimensional form yield

$$\begin{aligned} \frac{C}{C_a} &= \left(\frac{1 - \tilde{z}}{\tilde{z}} \cdot \frac{\tilde{a}}{1 - \tilde{a}} \right)^{\zeta_N} \quad \wedge \quad \zeta_N = \frac{1 + \tilde{q}_z|_{\tilde{z}=\tilde{a}}}{\beta \kappa} \left(\frac{u_*}{w_s} + \tilde{q}_z|_{\tilde{z}=\tilde{a}} \right)^{-1} \\ \vee \quad \tilde{q}_z|_{\tilde{z}=\tilde{a}} &= \frac{q_z|_{z=a}}{C_a w_s} \end{aligned} \quad (6.99)$$

Note that if the equilibrium of suspended sediment exists, then $q_z|_{z=a} = 0$ and Eq. (6.99) becomes the Rouse equation (Eq. 6.27).

6.2.7 Vertical Distribution of Sediment Concentration Due to Nonuniform Streamwise Variation of Concentration

For nonuniform sediment transport, the spatial variation of sediment flux is associated with changes in sediment bed elevation that reflects aggradations or degradations. The rate of aggradations or degradations is related to the spatial variation of sediment flux by the continuity equation of sediment transport given by Exner (1925). The Exner equation corresponding to the bed-load transport with migration of bedforms is given by Eq. (5.48), which is modified here in presence of sediment suspension as

$$\frac{\partial(q_b + q_s)}{\partial x} + \frac{\partial}{\partial t} \int_{\eta}^z C dz + (1 - \rho_0) \frac{\partial \eta}{\partial t} = 0 \quad (6.100)$$

where q_b is the bed-load transport rate in volume per unit time and width, η is the elevation of the sediment bed with respect to a horizontal reference, x is the streamwise direction, and ρ_0 is the porosity of sediment. Note that the term $(1 - \rho_0)$ converts the bulk volume of bed elevation change per unit length into the net volume of sediment that is used for q_b and q_s . Equation (6.100) was used by Bose and Dey (2009a) in analyzing the formation of sand waves.

For nonuniform sediment transport, the diffusion phenomenon influences suspended sediment entrainment or deposition. The finer fractions of suspended

sediment particles involve considerable time period and long distance in settling or in attaining its transport capacity. As a result of which the suspended sediment may not respond and adjust immediately according to the flow condition. The spatial variation of concentration of suspended sediment over a sediment bed downstream of a rigid boundary following an introduction of a clear-water flow is depicted schematically in Fig. 6.9. When there is a rapid streamwise variation of suspended sediment concentration, the diffusion effects become pronounced. Due to which, a certain development length is required to attain the equilibrium concentration. For a mathematical treatment of such problems, the development length for suspended sediment flux is thus required to be included.

The nonuniform suspended sediment concentration can be computed from the advection–diffusion equation (Eq. 6.13), which reads for time-averaged variables on the vertical plane (xz) after replacing \bar{w} by $\bar{w} - w_s$ and using $\varepsilon_{sx} = \varepsilon_{sz} = \varepsilon_s$ as follows (van Rijn 1986):

$$\begin{aligned} \frac{\partial C}{\partial t} + \bar{u} \frac{\partial C}{\partial x} + (\bar{w} - w_s) \frac{\partial C}{\partial z} + C \left[\frac{\partial \bar{u}}{\partial x} + \frac{\partial}{\partial z} (\bar{w} - w_s) \right] - \frac{\partial}{\partial x} \left(\varepsilon_s \frac{\partial C}{\partial x} \right) - \frac{\partial}{\partial z} \left(\varepsilon_s \frac{\partial C}{\partial z} \right) \\ = 0 \end{aligned} \quad (6.101)$$

For a steady sediment transport rate, $\partial C / \partial t = 0$, the derivatives in streamwise direction are $\partial \varepsilon_s / \partial x \ll \partial \varepsilon_s / \partial z \approx 0$ and $\partial^2 C / \partial x^2 \ll \partial^2 C / \partial z^2 \approx 0$. Hence, considering a steady transport rate and neglecting the streamwise diffusive transport that has a smaller order of magnitude in comparison to other terms in Eq. (6.101), Eq. (6.101) reduces to

$$\bar{u} \frac{\partial C}{\partial x} + (\bar{w} - w_s) \frac{\partial C}{\partial z} + C \left[\frac{\partial \bar{u}}{\partial x} + \frac{\partial}{\partial z} (\bar{w} - w_s) \right] - \frac{\partial}{\partial z} \left(\varepsilon_s \frac{\partial C}{\partial z} \right) = 0 \quad (6.102)$$

The solutions of the above advection–diffusion equation (Eq. 6.102) have been mainly obtained numerically for one- and two-dimensional approaches. In a one-dimensional approach, the depth-averaged streamwise variation of suspended sediment concentration is considered (Mei 1969; Hjelmfelt and Lenau 1970; Zhang et al. 1983; Cheng 1985). In an attempt to determine depth-averaged suspended sediment concentration \bar{C} , Zhang et al. (1983) started with following equation:

$$\bar{u} \frac{\partial C}{\partial x} = \frac{\partial}{\partial z} \left(\varepsilon_s \frac{\partial C}{\partial z} + C w_s \right) \quad (6.103)$$

Then, integrating across the flow depth for depth-averaging, they obtained

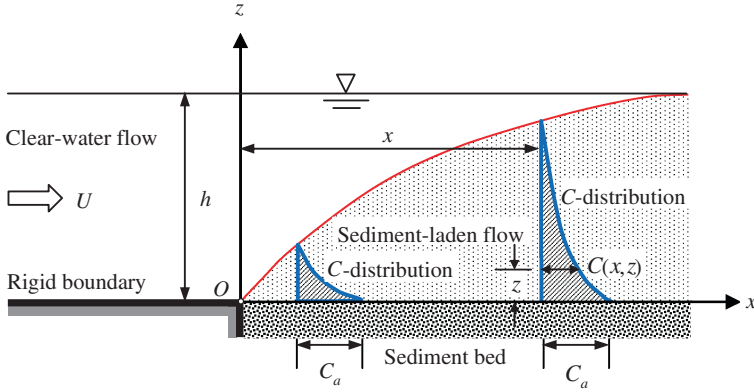


Fig. 6.9 Schematic of nonuniform streamwise variation of sediment concentration as a clear-water flowing over a rigid boundary and entering a sediment bed

$$\frac{d\bar{C}}{dx} = -\frac{\alpha_e w_s}{q} (\bar{C} - \bar{C}_e) \quad (6.104)$$

where q is the flow discharge per unit width, \bar{C}_e is the depth-averaged equilibrium concentration of sediment or the transport capacity of a specific flow, and α_e is the coefficient characterizing the rate of attaining the transport capacity. The general solution is

$$\bar{C} = \left[A + \int \frac{\alpha_e w_s}{q} \exp\left(\int \frac{\alpha_e w_s}{q} dx\right) dx \right] \exp\left(-\int \frac{\alpha_e w_s}{q} dx\right) \quad (6.105)$$

where A is a constant of integration, which can be obtained from the initial value of the concentration ($C|_{x=0}$) at the starting point ($x = 0$) of the sediment bed. Zhang et al. (1983) gave an approximate numerical solution for Eq. (6.105) for a given particle size as

$$(\bar{C})_{j+1} - (\bar{C}_e)_{j+1} = \exp\left(-\frac{\alpha_e w_s}{q} \Delta x\right) [(\bar{C})_j - (\bar{C}_e)_{j+1}] \quad (6.106)$$

where j is the cross section index counted from upstream to downstream and Δx is the spacing of grids. The coefficient α_e should be determined separately for the cases of deposition and entrainment due to different processes. According to Zhang et al. (1983), they were

$$\alpha_e(\text{deposition}) = 1 + \frac{1}{2} \cdot \frac{6w_s}{\kappa u_*}, \quad \alpha_e(\text{entrainment}) = \pi^2 \frac{\kappa u_*}{6w_s} + \frac{1}{4} \cdot \frac{6w_s}{\kappa u_*} \quad (6.107)$$

However, Chang (1988) gave a finite difference form of Eq. (6.105) in terms of size fractions for sediment having a size fraction index i as

$$(\bar{C}_i)_{j+1} = \left[(\bar{C}_i)_j + \frac{\alpha_e w_{si} (\bar{C}_{ei})_{j+1/2}}{q_{i+1/2}} \exp\left(-\frac{\alpha_e w_{si}}{q_{i+1/2}} \Delta x\right) \Delta x \right] \exp\left(-\frac{\alpha_e w_{si}}{q_{i+1/2}} \Delta x\right) \quad (6.108)$$

On the other hand, in a two-dimensional approach, the vertical distributions of suspended sediment concentration and streamwise flow velocity under accelerated ($\partial U/\partial x > 0$) and decelerated ($\partial U/\partial x < 0$) conditions are employed (van Rijn 1986).

6.2.8 Reference Level and Reference Concentration

The depth a and the concentration C_a that appear in equations of concentration distribution proposed by various investigators are called *reference level* and *reference concentration*, respectively. The reference level a , in fact, is the demarcation line between the bed-load and the suspended-load transport.

Einstein (1950) assumed that the bed-layer thickness, which is denoted by δ_b in Chap. 5, is twice the bed particle size and set as $z = a = 2d$. The average particle velocity within the bed layer \bar{u}_b can be found to be $\bar{u}_b = 11.6u_*$. By definition of bed-load transport rate [see Eq. (5.3)], $q_b = C_a \bar{u}_b a$, the reference concentration C_a is then

$$C_a = \frac{q_b}{\bar{u}_b a} = \frac{q_b}{23.2 u_* d} = \frac{\Phi_b}{23.2 \Theta^{0.5}} \quad \wedge \quad \Theta = \frac{\tau_0}{\Delta \rho g d} \quad \vee \quad \Phi_b = \frac{q_b}{(\Delta g d^3)^{0.5}} \quad (6.109)$$

where Θ is the Shields parameter and Φ is the bed-load transport intensity.

Bijker (1971) suggested that a could be taken as the bed roughness height k_s and C_a could be the concentration of the bed-load transport rate q_b . He assumed that the bed-load transport takes place in the bed layer from $z = 0$ to $a (=k_s)$ with a constant sediment concentration C_a . He argued that in a hydraulically rough flow, there is still a viscous sublayer, which starts from $z = 0$ extending up to δ' where the linear velocity distribution matches tangentially with the logarithmic law of velocity distribution. The hypothesis therefore relies on a thickness of the viscous sublayer in hydraulically rough flow which is much smaller than that in hydraulically smooth flow, although the hypothesis seems to be questionable if the viscous sublayer at all exists in a hydraulically rough flow. However, he obtained streamwise velocity as $\bar{u}(z = \delta') = u_*/\kappa$ at the top of the viscous sublayer. The depth-averaged velocity within the bed layer \bar{u}_b is obtained as

$$\bar{u}_b = \frac{1}{k_s} \left[\frac{1}{2} \cdot \frac{u_* \delta'}{\kappa} + \int_{\delta'}^{k_s} \frac{u_*}{\kappa} \ln \left(\frac{z}{z_0} \right) dz \right] \approx 6.34 u_* \quad (6.110)$$

Given the bed-load transport rate $q_b = C_a \bar{u}_b k_s$, the sediment concentration C_a is estimated as

$$C_a = \frac{q_b}{\bar{u}_b k_s} = \frac{q_b}{6.34 u_* k_s} \quad (6.111)$$

Engelund and Fredsøe (1976) proposed a bed-layer thickness $z = a = 2d$ and obtained the reference concentration C_a as

$$C_a = \frac{0.65 \lambda_\Theta^3}{(1 + \lambda_\Theta)^3} \quad \wedge \quad \lambda_\Theta = \left[\frac{\Theta - \Theta_c - (\beta_1 \pi p / 6)}{0.027(\Delta + 1)\Theta} \right]^{0.5} \quad (6.112)$$

$$\vee \quad p = \left[1 + \left(\frac{\beta_1 \pi / 6}{\Theta - \Theta_c} \right)^4 \right]^{-0.25}$$

where p is the probability of the particles to move in the bed layer, β_1 is a coefficient, Θ_c is the threshold Shields parameter, that is $\tau_{0c}/(\Delta \rho g d)$, and τ_{0c} is the threshold bed shear stress. Engelund and Fredsøe (1976) originally set $\beta_1 = 0.51$, but later they modified it as $\beta_1 = 1$ (Engelund and Fredsøe 1982). The Shields parameter was obtained as follows:

$$\Theta = \frac{\tau_0}{\Delta \rho g d} = \frac{u_*^2}{\Delta g d} \quad \wedge \quad u_* = U \left[6 + 2.5 \ln \left(\frac{h}{2.5d} \right) \right]^{-1} \quad (6.113)$$

Smith and McLean (1977a) argued that the bed-layer thickness is equal to the thickness of the zero-velocity level z_0 . They recommended

$$a = k'_s + 26.3(\Theta - \Theta_c)d \quad \wedge \quad k'_s = 3d_{90} \quad (6.114)$$

where k'_s is the particle roughness. They proposed the reference concentration C_a at the top of the bed layer $z = a$ as

$$C_a = 0.65 \gamma_0 \left[\frac{\Theta - \Theta_c}{\Theta_c + \gamma_0(\Theta - \Theta_c)} \right] \quad (6.115)$$

where γ_0 is a constant ($\approx 2.4 \times 10^{-3}$).

Itakura and Kishi (1980) set a reference level $z = a = 0.05h$ and determined the reference concentration C_a as

$$C_a = 8 \times 10^{-3} \left(0.14 \frac{u_*}{w_s} \cdot \frac{\Xi}{\Theta} - 1 \right) \quad (6.116)$$

where

$$\Xi = \frac{\Theta}{0.143} \left[2 + \frac{\exp(-r_\Theta^2)}{\int_{r_\Theta}^{\infty} \exp(-r^2) dr} \right] - 1 \quad \wedge \quad r_\Theta = \frac{0.143}{\Theta} - 2 \quad (6.117)$$

In case of a flat bed (without bedforms), van Rijn (1984b) suggested that the bed-layer thickness can be obtained from the saltation height (denoted by h_s in Chap. 5) of the bed-load particles, given by Eq. (5.135b) that estimates a value in the range 2–10 times particle diameter (median size). The reference level a and the reference concentration C_a , as a depth-averaged sediment concentration within the bed layer, are given by

$$a = 0.3dD_*^{0.7} \left(\frac{\Theta}{\Theta_c} - 1 \right)^{0.5} \quad \wedge \quad D_* = d \left(\frac{\Delta g}{v^2} \right)^{1/3} \quad (6.118a)$$

$$C_a = 0.18C_{\max}D_*^{-1} \left(\frac{\Theta}{\Theta_c} - 1 \right) = 0.015 \frac{d}{a} D_*^{-0.3} \left(\frac{\Theta}{\Theta_c} - 1 \right)^{1.5} \quad (6.118b)$$

The maximum concentration C_{\max} was taken as 0.65. In case of bedforms, the reference level a is assumed to be equaling the half of the bedform height η_d . If the dimensions of the bedforms are not known, then a minimum value of a can be taken as $0.01h$.

Celik and Rodi (1984) obtained the reference concentration C_a at an elevation $z = a = 0.05h$ as

$$C_a = 1.13 \frac{\bar{C}}{I_0} \quad \wedge \quad \bar{C} = 0.034 \left[1 - \left(\frac{k_s}{h} \right)^{0.06} \right] \frac{u_*^2}{\Delta gh} \cdot \frac{U}{w_s} \quad \vee \quad I_0 = \int_{\tilde{a}}^1 \left(\frac{\tilde{a}}{\tilde{z}} \cdot \frac{1 - \tilde{z}}{1 - \tilde{a}} \right)^\zeta d\tilde{z} \quad (6.119)$$

Akiyama and Fukushima (1986) put forward the reference concentration C_a as a nondimensional coefficient of bed sediment entrainment in suspension at a reference level $z = a = 0.05h$. It is

$$\begin{aligned} C_a(\Re \leq 5) &= 0 \\ C_a(5 < \Re < 13.2) &= 3 \times 10^{-12} \Re^{10} \left(1 - \frac{5}{\Re} \right) \quad \wedge \quad \Re = \frac{u_*}{w_s} \left[\frac{d(\Delta g d)^{0.5}}{v} \right]^{0.5} \\ C_a(\Re \geq 13.2) &= 0.3 \end{aligned} \quad (6.120)$$

García and Parker (1991) suggested the reference concentration C_a at a reference level $z = a = 0.05h$ as

$$C_a = \frac{1.3 \times 10^{-7} \Re_u^5}{1 + 4.33 \times 10^{-7} \Re_u^5} \quad \wedge \quad \Re_u = \frac{u_{*s}}{w_s} \left[\frac{d(\Delta g d)^{0.5}}{v} \right]^{0.6} \quad \vee \quad u_{*s} = U \frac{g^{0.5}}{C'_R} \quad (6.121)$$

where C'_R is the Chézy coefficient due to particle roughness ($k_s \approx 3d$), that is $18 \log(12h/k_s)$.

Zyserman and Fredsøe (1994) gave an empirical relationship for the reference concentration C_a assuming a bed-layer thickness $z = a = 2d$. It is

$$C_a = \frac{0.331(\Theta' - \Theta_c)^{1.75}}{1 + 0.72(\Theta' - \Theta_c)^{1.75}} \quad (6.122)$$

where Θ' is the Shields parameter due to particle roughness. For a flat sediment bed, $\Theta' = \Theta$.

It can be concluded that the formulations for the reference level and the reference concentration were developed on the basis of a certain assumption of reference level $z = a$ and the corresponding concentration. They are

$$(i) a \sim h, (ii) a \sim d, (iii) a \sim \eta_d, \text{ and } (iv) a = h_s$$

In reality, it is not feasible to experimentally quantify the suspended sediment concentration at a few particle sizes above the bed. Therefore, from the viewpoint of verification of the concentration distribution, the reference level proportional to the flow depth, that is $a \sim h$, could provide a reliable experimental verification, as the near-bed concentration C_a at a level $z = a = 0.05h$ was possible with some interpolation or a slight extrapolation.

6.2.9 Suspended Load by Diffusion Approach

6.2.9.1 Lane and Kalinske's Approach

Equation (6.32) for the distribution of suspended sediment concentration C given by Lane and Kalinske (1941) can be integrated over the flow depth to obtain the depth-averaged concentration \bar{C} provided the reference concentration C_a at $z = a$ to be known. Then, the ratio \bar{C} to C_a is given by P_C .

The following equation of suspended-load transport rate q_s was suggested by Lane and Kalinske (1941):

$$q_s = q C_a P_C \exp\left(\frac{15 w_s a}{u_* h}\right) \quad (6.123)$$

where P_C is \bar{C}/C_a being a function of w_s/u_* and relative roughness $n/h^{1/6}$, as shown in Fig. 6.10, and n is the Manning roughness coefficient. Here, h is in inches.

As Eq. (6.123) is applicable for a single particle size with a terminal fall velocity w_s , the equation is to be solved for each particle size range to estimate corresponding suspended-load transport rate. Note that Eq. (6.123) provides an estimation of suspended-load transport rate in volume per unit time and width in metric units ($\text{ft}^2 \text{ s}^{-1}$). To convert the suspended-load transport rate (g_s) in weight per unit time and width, the right-hand side of the equation is to be multiplied by $\rho_s g$.

6.2.9.2 Einstein's Approach

Einstein (1950) obtained the suspended-load transport rate q_s from the integral equation, Eq. (6.1a), by using the distribution of sediment concentration given by the Rouse equation and the logarithmic law of streamwise velocity distribution. He assumed $\beta = 1$ and $\kappa = 0.4$. Replacing the shear velocity u_* with the shear velocity due to particle roughness u'_* , the Rouse number ζ is

$$\zeta = \frac{w_s}{\kappa u'_*} \quad (6.124)$$

He used the logarithmic law of velocity distribution given by Keulegan (1938)

$$\bar{u} = \frac{u'_*}{\kappa} \ln \left(30.2 \frac{z}{\Delta_k} \right) \quad (6.125)$$

where Δ_k is the apparent roughness, that is k_s/x_k , and x_k is a correction factor. The particle shear velocity can be obtained from $u'_* = (gR'_b S_0)^{0.5}$, where R'_b is the hydraulic radius due to particle roughness and S_0 is the streamwise bed slope. Einstein (1950) assumed $k_s = d_{65}$ and gave a curve for the determination of correction factor x_k (Fig. 5.7). Hence, the apparent roughness $\Delta_k (=k_s/x_k)$ can be determined.

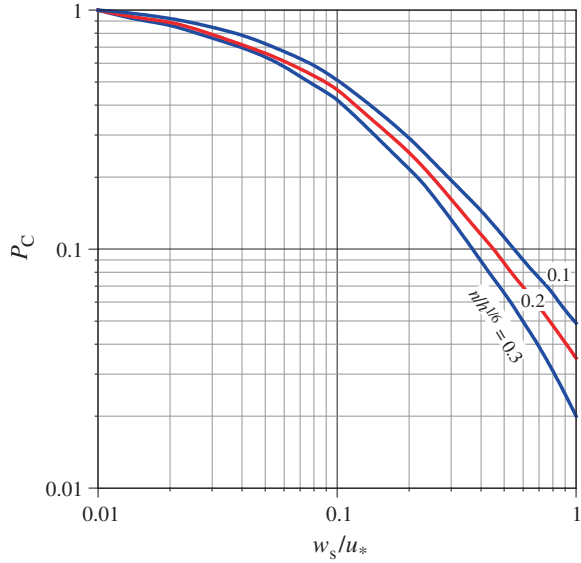
Substituting Eqs. (6.27) and (6.125) into Eq. (6.1a), the suspended-load transport rate q_s is

$$q_s = \int_a^h C_a \left(\frac{1-\tilde{z}}{\tilde{z}} \cdot \frac{\tilde{a}}{1-\tilde{a}} \right)^{\zeta} \frac{u'_*}{\kappa} \ln \left(30.2 \frac{z}{\Delta_k} \right) dz \quad (6.126)$$

After simplification, Eq. (6.126) becomes

$$q_s = \frac{C_a u'_* h}{\kappa} \left(\frac{\tilde{a}}{1-\tilde{a}} \right)^{\zeta} \int_{\tilde{a}}^1 \left(\frac{1-\tilde{z}}{\tilde{z}} \right)^{\zeta} \ln \left(\frac{30.2 \tilde{z}}{\Delta_k/h} \right) d\tilde{z} \quad (6.127)$$

Fig. 6.10 Relationship of P_C
(Lane and Kalinske 1941)



Rearranging Eq. (6.127) yields

$$q_s = \frac{C_a u_*' h}{\kappa} \left(\frac{\tilde{a}}{1 - \tilde{a}} \right)^\zeta \left[\ln \left(\frac{30.2h}{A_k} \right) \int_{\tilde{a}}^1 \left(\frac{1 - \tilde{z}}{\tilde{z}} \right)^\zeta d\tilde{z} + \int_{\tilde{a}}^1 \left(\frac{1 - \tilde{z}}{\tilde{z}} \right)^\zeta \ln \tilde{z} d\tilde{z} \right] \quad (6.128)$$

As the closed-form integration of Eq. (6.128) could not be possible, Einstein (1950) expressed it as

$$q_s = \frac{C_a u_*' a}{\kappa} (P_E J_1 + J_2) \quad \wedge \quad P_E = \ln \left(\frac{30.2h}{A_k} \right) \quad (6.129)$$

where

$$J_1 = \frac{I_1}{0.216} \quad \wedge \quad I_1 = 0.216 \frac{\tilde{a}^{\zeta-1}}{(1 - \tilde{a})^\zeta} \int_{\tilde{a}}^1 \left(\frac{1 - \tilde{z}}{\tilde{z}} \right)^\zeta d\tilde{z} \quad (6.130a)$$

$$J_2 = \frac{I_2}{0.216} \quad \wedge \quad I_2 = 0.216 \frac{\tilde{a}^{\zeta-1}}{(1 - \tilde{a})^\zeta} \int_{\tilde{a}}^1 \left(\frac{1 - \tilde{z}}{\tilde{z}} \right)^\zeta \ln \tilde{z} d\tilde{z} \quad (6.130b)$$

The values of integral functions I_1 and I_2 , called *Einstein's integrals*, were given by Einstein in graphical form in terms of \tilde{a} for different values of ζ (see

Figs. 6.11 and 6.12). However, these integral functions can also be computed numerically by using Simpson's rule through a simple algorithm (Bose 2009).

Einstein (1950) emphasized on the *bed layer*, which has a thickness of $a = 2d$, being the source of supplying sediment to suspended load. Then, the reference concentration C_a that is the most important parameter can be obtained.

If q_b represents the rate of bed-load transport and i_b is the fraction of bed-load transport for a given sediment size d_i , then the rate at which the particles of a size d_i are transported per unit time and width is $i_b q_b$. If the velocity of bed particles is u_b , then the volume of the particles for a given particle size d_i per unit area is $i_b q_b / u_b$. The average concentration in the bed layer can be obtained from Eq. (6.109) as

$$C_a = \frac{1}{11.6} \cdot \frac{i_b q_b}{u'_s a} \quad (6.131)$$

Therefore, the suspended-load transport rate, where the bed-load transport exists, can be obtained for a given sediment size fraction d_i as

$$i_s q_s = 0.216 i_b q_b (P_E J_1 + J_2) = i_b q_b (P_E I_1 + I_2) \quad (6.132)$$

where i_s is the fraction of suspended load.

There were number of attempts to propose analytical expressions and expansion series for Einstein's integrals I_1 and I_2 . Nakato (1984) expressed the integral portion of I_1 , that is G_1 , as

$$\begin{aligned} G_1 &= \int_{\tilde{a}}^1 \left(\frac{1-\tilde{z}}{\tilde{z}} \right)^{\zeta} d\tilde{z} = \int_{\tilde{a}}^{\varepsilon} \left(\frac{1-\tilde{z}}{\tilde{z}} \right)^{\zeta} d\tilde{z} + \int_{\varepsilon}^1 \left(\frac{1-\tilde{z}}{\tilde{z}} \right)^{\zeta} d\tilde{z} \\ &= G_{1a} + G_{1b} + G_{1c} + \cdots + \int_{\varepsilon}^1 \left(\frac{1-\tilde{z}}{\tilde{z}} \right)^{\zeta} d\tilde{z} \end{aligned} \quad (6.133)$$

where ε is a small value ($\varepsilon > \tilde{a}$) and G_{1a} , G_{1b} , and G_{1c} are

$$\begin{aligned} G_{1a}(\zeta \neq 1) &= \frac{1}{1-\zeta} (\varepsilon^{1-\zeta} - \tilde{a}^{1-\zeta}) \\ G_{1a}(\zeta = 1) &= \ln \varepsilon - \ln \tilde{a} \end{aligned} \quad (6.134a)$$

$$\begin{aligned} G_{1b}(\zeta \neq 2) &= \frac{\zeta}{\zeta-2} (\varepsilon^{2-\zeta} - \tilde{a}^{2-\zeta}) \\ G_{1b}(\zeta = 2) &= -2(\ln \varepsilon - \ln \tilde{a}) \end{aligned} \quad (6.134b)$$

$$\begin{aligned} G_{1c}(\zeta \neq 3) &= \frac{\zeta(\zeta-1)}{2(3-\zeta)} (\varepsilon^{3-\zeta} - \tilde{a}^{3-\zeta}) \\ G_{1c}(\zeta = 3) &= 3(\ln \varepsilon - \ln \tilde{a}) \end{aligned} \quad (6.134c)$$

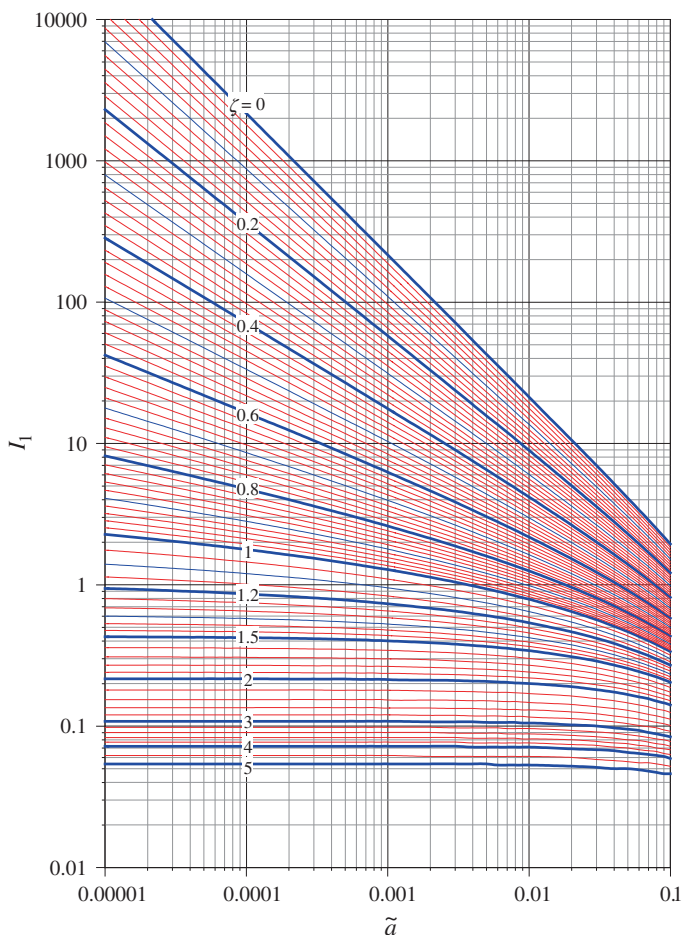


Fig. 6.11 Integral function I_1 in terms of \tilde{a} for different ζ (Einstein 1950)

He expressed the integral portion of I_2 , that is G_2 , in a similar way as

$$\begin{aligned}
 G_2 &= \int_{\tilde{a}}^1 \left(\frac{1-\tilde{z}}{\tilde{z}} \right)^{\zeta} \ln \tilde{z} d\tilde{z} = \int_{\tilde{a}}^{\varepsilon} \left(\frac{1-\tilde{z}}{\tilde{z}} \right)^{\zeta} \ln \tilde{z} d\tilde{z} + \int_{\varepsilon}^1 \left(\frac{1-\tilde{z}}{\tilde{z}} \right)^{\zeta} \ln \tilde{z} d\tilde{z} \\
 &= G_{2a} + G_{2b} + G_{2c} + \cdots + \int_{\varepsilon}^1 \left(\frac{1-\tilde{z}}{\tilde{z}} \right)^{\zeta} \ln \tilde{z} d\tilde{z}
 \end{aligned} \tag{6.135}$$

where G_{2a} , G_{2b} , and G_{2c} are

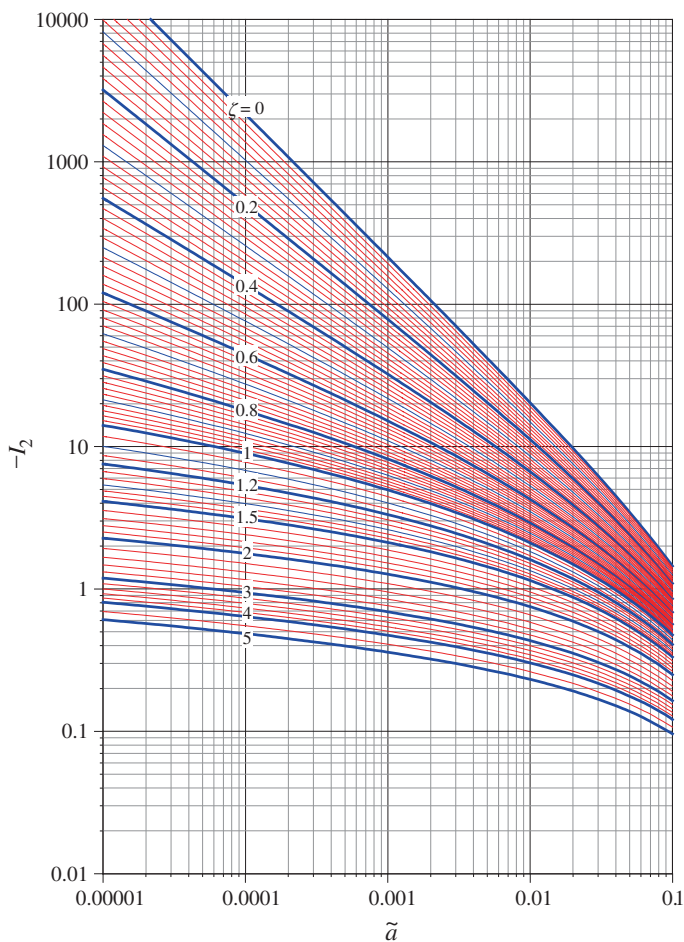


Fig. 6.12 Integral function $-I_2$ in terms of \tilde{a} for different ζ (Einstein 1950)

$$G_{2a}(\zeta \neq 1) = \frac{1}{1-\zeta} \left[\varepsilon^{1-\zeta} \left(\ln \varepsilon - \frac{1}{1-\zeta} \right) - \tilde{a}^{1-\zeta} \left(\ln \tilde{a} - \frac{1}{1-\zeta} \right) \right] \quad (6.136a)$$

$$G_{2a}(\zeta = 1) = \frac{1}{2} [(\ln \varepsilon)^2 - (\ln \tilde{a})^2]$$

$$G_{2b}(\zeta \neq 2) = \frac{\zeta}{\zeta-2} \left[\varepsilon^{2-\zeta} \left(\ln \varepsilon - \frac{1}{2-\zeta} \right) - \tilde{a}^{1-\zeta} \left(\ln \tilde{a} - \frac{1}{2-\zeta} \right) \right] \quad (6.136b)$$

$$G_{2b}(\zeta = 2) = -(\ln \varepsilon)^2 + (\ln \tilde{a})^2$$

$$\begin{aligned}
 G_{2c}(\zeta \neq 3) &= \frac{\zeta(\zeta-1)}{2(3-\zeta)} \left[\varepsilon^{3-\zeta} \left(\ln \varepsilon - \frac{1}{3-\zeta} \right) - \tilde{a}^{3-\zeta} \left(\ln \tilde{a} - \frac{1}{3-\zeta} \right) \right] \\
 G_{2c}(\zeta = 3) &= \frac{3}{2} \left[(\ln \varepsilon)^2 - (\ln \tilde{a})^2 \right]
 \end{aligned} \tag{6.136c}$$

Nakato's (1984) suggested that the second integral in Eqs. (6.133) and (6.135) can be evaluated by a simple numerical exercise (for example, Simpson's rule). So, the solutions proposed by him could not give complete analytical solutions for Einstein's integrals.

On the other hand, Guo and Julien (2004) who gave complete analytical solutions, although approximate, for Einstein's integrals expressed the integral portions G_1 and G_2 as

$$G_1 = \int_{\tilde{a}}^1 \left(\frac{1-\tilde{z}}{\tilde{z}} \right)^{\zeta} d\tilde{z} = \int_0^1 \left(\frac{1-\tilde{z}}{\tilde{z}} \right)^{\zeta} d\tilde{z} - \int_0^{\tilde{a}} \left(\frac{1-\tilde{z}}{\tilde{z}} \right)^{\zeta} d\tilde{z} \tag{6.137a}$$

$$G_2 = \int_{\tilde{a}}^1 \left(\frac{1-\tilde{z}}{\tilde{z}} \right)^{\zeta} \ln \tilde{z} d\tilde{z} = \int_0^1 \left(\frac{1-\tilde{z}}{\tilde{z}} \right)^{\zeta} \ln \tilde{z} d\tilde{z} - \int_0^{\tilde{a}} \left(\frac{1-\tilde{z}}{\tilde{z}} \right)^{\zeta} \ln \tilde{z} d\tilde{z} \tag{6.137b}$$

Using the results based on Γ -function obtained by Guo and Wood (1995) for $\zeta < 1$, first integral parts of the right-hand side of Eqs. (6.137a, b) are solved. The second integral parts of the right-hand side of Eqs. (6.137a, b) can be expressed by the infinite series. Then, Guo and Julien gave

$$G_1 = \frac{\zeta \pi}{\sin \zeta \pi} - \underbrace{\left[\frac{(1-\tilde{a})^{\zeta}}{\tilde{a}^{\zeta-1}} - \zeta \sum_{n=1}^{\infty} \frac{(-1)^n}{n-\zeta} \left(\frac{\tilde{a}}{1-\tilde{a}} \right)^{n-\zeta} \right]}_{F_1(\zeta)} \tag{6.138a}$$

$$\begin{aligned}
 G_2 &= \frac{\zeta \pi}{\sin \zeta \pi} \left[\pi \cot \zeta \pi - 1 - \frac{1}{\zeta} + \sum_{n=1}^{\infty} \left(\frac{1}{n} - \frac{1}{n+\zeta} \right) \right] \\
 &\quad - \left[F_1(\zeta) \left(\ln \tilde{a} + \frac{1}{\zeta-1} \right) + \zeta \sum_{n=1}^{\infty} \frac{(-1)^n F_1(\zeta-n)}{(\zeta-n)(\zeta-n-1)} \right]
 \end{aligned} \tag{6.138b}$$

They suggested the following approximation:

$$\sum_{n=1}^{\infty} \left(\frac{1}{n} - \frac{1}{n+\zeta} \right) \approx \frac{\pi^2}{6} \cdot \frac{\zeta}{(1+\zeta)^{0.7162}} \tag{6.139}$$

6.2.9.3 Brooks' Approach

Brooks (1963) assumed that the logarithmic law of velocity distribution is applicable and the sediment concentration follows the Rouse equation (Eq. 6.27). Taking $\beta = 1$, that is, $\zeta = w_s/(\kappa u_*)$ and the velocity defect relationship of logarithmic law, he obtained

$$q_s = qC_{0.5h} \left[1 + \frac{u_*}{\kappa U} \int_{\tilde{a}}^1 \left(\frac{1-\tilde{z}}{\tilde{z}} \right)^\zeta d\tilde{z} + \frac{u_*}{\kappa U} \int_{\tilde{a}}^1 \left(\frac{1-\tilde{z}}{\tilde{z}} \right)^\zeta \ln \tilde{z} d\tilde{z} \right] \quad (6.140)$$

where $C_{0.5h}$ is the reference concentration at $z = 0.5h$. Having performed the integration, Eq. (6.140) is expressed in terms of a transport function T_B as

$$\frac{q_s}{qC_{0.5h}} = T_B \left(\frac{\kappa U}{u_*}, \zeta, \tilde{a} \right) \quad (6.141)$$

Taking a lower limit of integration at zero-velocity level and the nondimensional reference level as $\tilde{a} = \exp\{-(\kappa U/u_* + 1)\}$, Eq. (6.141) is given by

$$\frac{q_s}{qC_{0.5h}} = T_{B1} \left(\frac{\kappa U}{u_*}, \zeta \right) \quad (6.142)$$

The functional relationship is illustrated in Fig. 6.13.

6.2.9.4 Chang et al.'s Approach

Chang et al. (1965) assumed that for sediment diffusivity, Eq. (6.26) holds and is given by

$$\varepsilon_s = \beta \kappa u_* h \tilde{z} (1 - \tilde{z}) \quad (6.143)$$

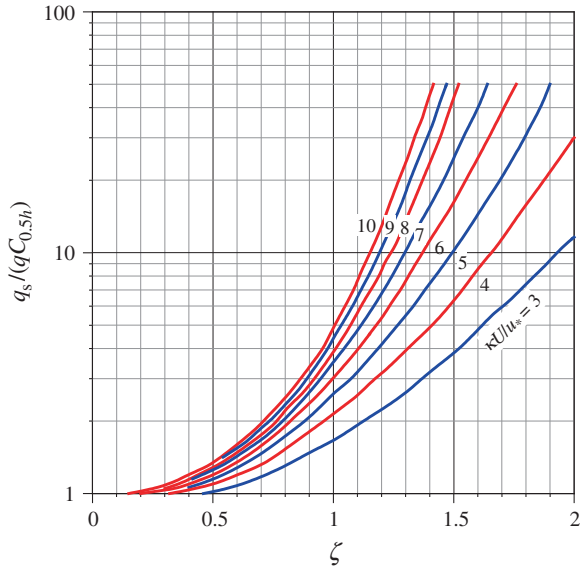
Substituting Eq. (6.143) into Eq. (6.22) yields

$$\frac{C}{C_a} = \left[\frac{1 - (1 - \tilde{a})^{0.5}}{\tilde{a}^{0.5}} \right]^{\zeta_1} \left[\frac{\tilde{z}^{0.5}}{1 - (1 - \tilde{z})^{0.5}} \right]^{\zeta_1} \quad \wedge \quad \zeta_1 = \frac{2w_s}{\beta \kappa u_*} \quad (6.144)$$

Using Eq. (6.144) into Eq. (6.1a), the equation of suspended load is expressed as

$$q_s = \int_a^h C \bar{u} dz = C_a h \left(UI_3 - \frac{2u_*}{\kappa} I_4 \right) \quad (6.145)$$

Fig. 6.13 Brooks' (1963) suspended-load transport function $q_s/(qC_{0.5h})$ in terms of ζ for different values of $\kappa U/u_*$



In the above, I_3 and I_4 are the integrals that are given by

$$I_3 = \left[\frac{1 - (1 - \tilde{a})^{0.5}}{\tilde{a}^{0.5}} \right]^{\zeta_1} \int_{\tilde{a}}^1 \left[\frac{\tilde{z}^{0.5}}{1 - (1 - \tilde{z})^{0.5}} \right]^{\zeta_1} d\tilde{z} \quad (6.146a)$$

$$I_4 = \left[\frac{1 - (1 - \tilde{a})^{0.5}}{\tilde{a}^{0.5}} \right]^{\zeta_1} \int_{\tilde{a}}^1 \left[\frac{\tilde{z}^{0.5}}{1 - (1 - \tilde{z})^{0.5}} \right]^{\zeta_1} \left\{ \ln \left[\frac{\tilde{z}^{0.5}}{1 - (1 - \tilde{z})^{0.5}} \right] - (1 - \tilde{z})^{0.5} - \frac{1}{3} \right\} d\tilde{z} \quad (6.146b)$$

In Figs. 6.14 and 6.15, the variations of integral functions I_3 and I_4 with \tilde{a} for different values of ζ_1 are presented.

It was assumed the bed sediment velocity as $u_b = 0.8U$. Using the definition of bed-load transport given by Eq. (5.3), the reference concentration C_a is

$$C_a = \frac{q_b}{0.8Ua} \quad (6.147)$$

Substituting C_a into Eq. (6.15) yields

$$q_s = \frac{q_b h}{0.8Ua} \left(UI_3 - \frac{2u_*}{\kappa} I_4 \right) \quad (6.148)$$

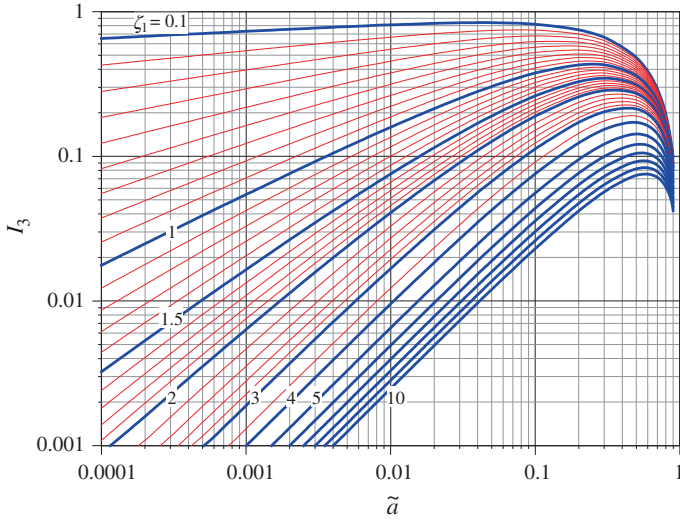


Fig. 6.14 Integral function I_3 in terms of \tilde{a} for different ζ_1 (Chang et al. 1965)

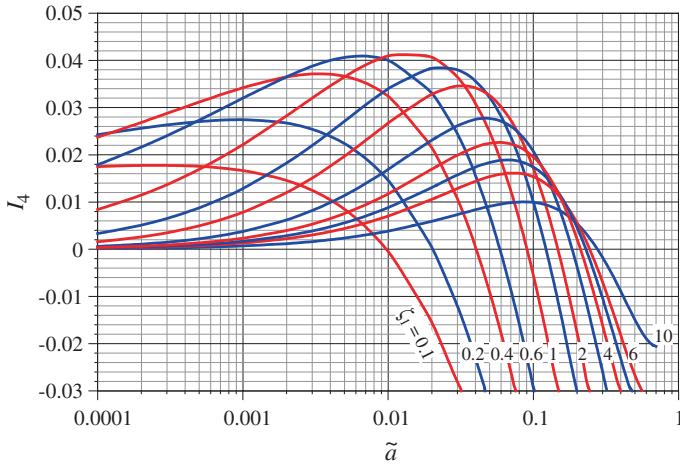


Fig. 6.15 Integral function I_4 in terms of \tilde{a} for different ζ_1 (Chang et al. 1965)

Based on du Boys' (1879) assumption, the bed-layer thickness a is obtained as

$$a = c_j \frac{\tau_0 - \tau_{0c}}{(1 - \rho_0)\Delta\rho g \tan \phi} \quad (6.149)$$

where c_j is a constant determined empirically as 10 and ϕ is the angle of repose.

6.2.9.5 Bijker's Approach

Based on Einstein's (1950) approach, Bijker (1971) proposed an equation of suspended-load transport rate. He assumed the reference level at $z = a = k_s$. He used the Rouse equation for concentration distribution (Eq. 6.27) with $\beta = 1$ and the logarithmic law of velocity distribution (Eq. 4.27) with zero-velocity level $z_0 = k_s/33 = a/33$, into Eq. (6.1a) to obtain

$$q_s = \frac{C_a u_* a}{\kappa} (P_{E1} J_1 + J_2) \quad \wedge \quad P_{E1} = \ln \left(\frac{33h}{a} \right) \quad (6.150)$$

Using the relationship of reference concentration C_a (Eq. 6.111) and the bed-load transport rate q_b given by him, Eq. (6.150) is rewritten as

$$q_s = 0.158 \frac{q_b}{\kappa} (P_{E1} J_1 + J_2) \quad (6.151)$$

6.2.9.6 van Rijn's Approach

Further, van Rijn (1984b) expressed the suspended-load transport rate by using the concentration distribution given by Eqs. (6.53a, b) and the logarithmic law given by Eq. (4.27) with zero-velocity level $z_0 = 0.03k_s$ in Eq. (6.1a). It is

$$q_s = F_{\bar{z}} C_a U h \quad (6.152)$$

where

$$F_{\bar{z}} = \frac{1}{\kappa} \cdot \frac{u_*}{U} \left(\frac{1 - \bar{a}}{\bar{a}} \right)^{\zeta_\psi} \left\{ \int_{\bar{a}}^{0.5} \left(\frac{1 - \bar{z}}{\bar{z}} \right)^{\zeta_\psi} \ln \left(\frac{\bar{z}}{\bar{z}_0} \right) d\bar{z} + \int_{0.5}^1 \exp \left[-4\zeta_\psi \left(\bar{z} - \frac{1}{2} \right) \right] \ln \left(\frac{\bar{z}}{\bar{z}_0} \right) d\bar{z} \right\} \quad (6.153)$$

where ζ_ψ is the modified Rouse number and $\bar{z}_0 = z_0/h$. He expressed ζ_ψ as

$$\zeta_\psi = \zeta + \psi \quad \wedge \quad \zeta = \frac{w_s}{\beta \kappa u_*} \quad (6.154)$$

where ψ is the correction factor and is empirically given by

$$\psi \left(0.01 \leq \frac{w_s}{u_*} \leq 1 \right) = 2.5 \left(\frac{w_s}{u_*} \right)^{0.8} \left(\frac{C_a}{C_{\max}} \right)^{0.4} \quad (6.155)$$

In the above equations, the values of β , a , and C_a can be obtained from Eqs. (6.19) and (6.118a, b), respectively, as proposed by van Rijn (1984b).

Further, van Rijn (1984b) proposed a simplified empirical expression as

$$q_s = 0.012Uh \left[\frac{U - U_{cr}}{(\Delta g d)^{0.5}} \right]^{2.4} \left(\frac{d}{h} \right) \frac{1}{D_*^{0.6}} \quad (6.156)$$

where U_{cr} is the average threshold velocity. Equation (6.156) was obtained for $1 \leq h \leq 20$ m, $0.5 \leq U \leq 2.5$ m s⁻¹, and $0.1 \leq d \leq 2$ mm.

6.3 Energy Concept

6.3.1 Velikanov's Approach

Based on the principle of conservation of energy, Velikanov (1954, 1958) developed a theory, named the *gravitational theory*, for the distribution of suspended sediment particles. He considered the work done per unit time of a unit volume of fluid and suspended sediment mixture to transfer from one layer to another layer. The fluid and sediment phases were treated separately with an idea that they together completely occupy the entire space within a unit volume. The fluid phase was regarded as the active component of dispersion performing work in taking the sediment particles in suspension and transporting them. In contrast, the sediment phase is the passive component, as the sediment particles are picked up into a suspension to consume the energy from the fluid. The energy dissipation along a unit streamwise distance was assumed to take into account the sum of the energy dissipation due to momentum exchange between fluid layers and the energy required to transport the sediment. The conservation of energy is maintained separately in the fluid and sediment phases by balancing the energy supplied and the energy dissipated. His mathematical analysis is as follows:

For two-dimensional steady-uniform flow, Velikanov expressed the energy balance for fluid phase as

$$\underbrace{\rho g(1-C)\bar{u}S_f}_{E1} = \underbrace{-\bar{u} \frac{d}{dz} [(1-C)\tau]}_{E2} + \underbrace{\Delta \rho g(1-C)Cw_s}_{E3} \quad \wedge \quad \tau = -\rho \overline{u'w'} \quad (6.157)$$

$$\Rightarrow g(1-C)\bar{u}S_f = \bar{u} \frac{d}{dz} [(1-C)\overline{u'w'}] + \Delta g(1-C)Cw_s$$

where S_f is the energy slope and τ is the Reynolds shear stress ($= -\rho \overline{u'w'}$). In Eq. (6.157), the term $E1$ represents the amount of energy (work done per unit time due to energy slope) supplied by the fluid phase, the term $E2$ denotes the energy dissipated (work done per unit time due to internal shear) for the momentum

exchange in the fluid phase, and the term $E3$ refers to the amount of energy required to keep the sediment particles in suspension.

On the other hand, he expressed the energy balance for sediment phase as

$$\underbrace{\rho_s g C \bar{u} S_f}_{E4} = \underbrace{-s \bar{u} \frac{d}{dz} (C \tau)}_{E5} \quad (6.158)$$

$$\Rightarrow g C S_f = \frac{d}{dz} (C \bar{u} w')$$

In the above, the term $E4$ represents the amount of energy supplied (work done per unit time due to energy slope) by the sediment phase and the term $E5$ denotes the energy dissipated (work done per unit time due to internal shear) for the momentum exchange in the sediment phase. As the water–sediment interaction is the present case, the ρ_s and ρ are combined to ρ_s/ρ ratio being traditionally denoted by the relative density s ; where ρ represents the mass density of water.

Velikanov assumed a sediment particle to fall in a flowing fluid with a velocity $w - w_s$. Note that subscript t of a quantity denotes the instantaneous condition of the quantity. In a two-dimensional, two-phase flow (steady-uniform), the vertical net flux of each phase must be zero. Applying the Reynolds decomposition [see Eq. (6.7)] and the Reynolds conditions, the continuity of suspended sediment passing through a unit area (parallel to the bed) at an elevation z from the bed is

$$\rho_s \overline{C_t(w - w_s)} = 0 \Rightarrow C \bar{w} - C w_s + \overline{w' C'} = 0 \quad (6.159)$$

and the continuity of fluid is

$$\overline{\rho w(1 - C_t)} = 0 \Rightarrow \bar{w} - C \bar{w} - \overline{w' C'} = 0 \quad (6.160)$$

Combining Eqs. (6.159) and (6.160) yields

$$\bar{w} = C w_s, \quad -C(\bar{w} - w_s) = \overline{w' C'} \quad (6.161)$$

In the above, the first equation implies that the time-averaged vertical velocity component \bar{w} of fluid is finite and directed upwards, as both C and w_s are finite and positive. The second equation suggests that the downward flux (with negative sign) of falling particles is equal to the upward flux of lifting particles by the fluid through a unit area parallel to the bed.

Velikanov adopted the logarithmic law of velocity distribution for rough flow regime given by Nikuradse

$$\bar{u} = \frac{u_*}{\kappa} \ln \left(1 + \frac{z}{\Delta_k} \right) = \frac{(ghS_f)^{0.5}}{\kappa} \ln \left(1 + \frac{\tilde{z}}{\alpha} \right) \quad \wedge \quad u_* = (ghS_f)^{0.5} \quad \vee \quad \alpha = \frac{\Delta_k}{h} \quad (6.162)$$

where Δ_k is the roughness parameter. Dividing Eq. (6.157) by \bar{u} and then adding it to Eq. (6.158), the resulting equation is integrated within limits z to h . Then,

$$\int_z^h g S_f dz = \int_z^h \frac{d}{dz} (\overline{u'w'}) dz + \Delta g w_s \int_z^h \frac{(1-C)C}{\bar{u}} dz \quad (6.163)$$

Performing integration except the second term of the right-hand side of Eq. (6.163) yields

$$g S_f (h - z) = -\overline{u'w'} + \Delta g w_s \int_z^h \frac{(1-C)C}{\bar{u}} dz \quad (6.164)$$

As C is small and \bar{u} is large, the ratio C/\bar{u} is very small, which makes the second term of the right-hand side of Eq. (6.164) to be negligibly small as compared to the first term, that is, Reynolds shear stress divided by ρ . The equation is then approximated as

$$\overline{u'w'} = -g S_f (h - z) \Rightarrow \frac{d(\overline{u'w'})}{dz} = g S_f \quad \wedge \quad \overline{u'w'} \gg \Delta g w_s \int_z^h \frac{(1-C)C}{\bar{u}} dz \approx 0 \quad (6.165)$$

For small suspended sediment concentration, $1 - C \approx 1$; and the substitution of Eqs. (6.162) and (6.165) into Eq. (6.157) yields the differential equation of suspended sediment concentration as

$$\frac{dC}{C} = -\beta_v \frac{d\tilde{z}}{(1 - \tilde{z}) \ln[1 + (\tilde{z}/\alpha)]} \quad \wedge \quad \beta_v = \frac{\Delta \kappa w_s}{S_f (gh S_f)^{0.5}} \quad (6.166)$$

The distribution of suspended sediment concentration is obtained from the solution of Eq. (6.166) as

$$\frac{C}{C_a} = \exp(-\beta_v \zeta_v) \quad \wedge \quad \zeta_v = \int_{\tilde{a}}^{\tilde{z}} \frac{d\tilde{z}}{(1 - \tilde{z}) \ln[1 + (\tilde{z}/\alpha)]} \quad (6.167)$$

The weakness of the gravitational theory is that the energy balance seems to be not scientifically sound. This is the reason why the theory has become disputed one. The primary objection lies on the principle of treating the fluid and sediment phases separately; while both occupy the entire space at the same time.

To determine depth-averaged concentration \bar{C} , Velikanov (1954, 1958) expressed Eq. (6.157) to integrate over the entire flow depth with an approximation $1 - C \approx 1$ for a small suspended sediment concentration as

$$\int_0^h g\bar{u}S_f dz = \int_0^h \bar{u} \frac{d}{dz} (\overline{u'w'}) dz + \int_0^h \Delta g C w_s dz \quad (6.168)$$

Since $-\rho \overline{u'w'} = \tau_0(1 - \bar{z})$ and $\tau_0 \sim U^2$, he expressed

$$\int_0^h \bar{u} \frac{d}{dz} (\overline{u'w'}) dz = k_h U^3 \quad (6.169)$$

where k_h is the coefficient. Then, Eq. (6.168) is integrated and simplified by using Eq. (6.169). Rearranging, the resulting equation is given by

$$\frac{k_h}{\lambda_k} + \Delta \frac{\bar{C} w_s}{U S_f} = 1 \quad \wedge \quad \lambda_k = \frac{g h S_f}{U^2} \quad (6.170)$$

where λ_k is the bed friction coefficient.

For clear-water flow ($\bar{C} = 0$), Eq. (6.170) provides

$$k_h = \lambda_{k0} \quad (6.171)$$

where λ_{k0} is the bed friction coefficient corresponding to $\bar{C} = 0$. Importantly, under a certain flow condition for a given sediment size, the sediment concentration in the flow may attain the state of saturation, which corresponds to the maximum sediment carrying capacity by the flow. Here, the corresponding bed friction coefficient is denoted by λ_{km} .

Velikanov argued that the ratio $\lambda_{k0}/\lambda_{km}$ is approximately a constant. Substituting the ratio into Eq. (6.170) yields

$$\Delta \frac{\bar{C} w_s}{U S_f} = 1 - \frac{\lambda_{k0}}{\lambda_{km}} \quad (6.172)$$

Here, \bar{C} is thus the saturated depth-averaged sediment concentration defining *suspended-load transport capacity*.

The depth-averaged velocity can be given by

$$\begin{aligned} U &= \frac{1}{h} \int_0^h \bar{u} dz = \frac{1}{h} \int_0^h \frac{(g h S_f)^{0.5}}{\kappa} \ln \left(1 + \frac{z}{\Delta_k} \right) dz \\ \Rightarrow U &= f(\alpha) \frac{(g h S_f)^{0.5}}{\kappa} \quad \wedge \quad f(\alpha) = (1 + \alpha) [\ln(1 + \alpha) - 1] \end{aligned} \quad (6.173)$$

Substituting Eq. (6.173) into Eq. (6.172) yields

$$\frac{\Delta\kappa\bar{C}w_s}{f(\alpha)S_f(ghS_f)^{0.5}} = 1 - \frac{\lambda_{k0}}{\lambda_{km}} \Rightarrow \frac{\beta_v\bar{C}}{f(\alpha)} = 1 - \frac{\lambda_{k0}}{\lambda_{km}} = \text{constant} \quad (6.174)$$

Hence,

$$\bar{C} \sim \frac{f(\alpha)}{\beta_v} = \frac{\kappa^2 U^3}{\Delta f^2(\alpha)ghw_s} \quad (6.175)$$

Therefore, the general form of suspended-load transport capacity equation obtained from Eq. (6.175) is given by

$$\bar{C} = K \frac{U^3}{ghw_s} \quad (6.176)$$

where K is a coefficient. A group of investigators from the Wuhan Institute of Hydraulic and Electric Engineering, China, made an extensive analysis of the field data collected from different rivers and canals in China (WIHEE 1981). They proposed that Eq. (6.176) should be modified to

$$\bar{C} = K \left(\frac{U^3}{ghw_s} \right)^{m_1} \quad (6.177)$$

The variations of coefficient K (in kg m^{-3}) and exponent m_1 with $U^3/(ghw_s)$, obtained by WIHEE (1981), are shown in Fig. 6.16.

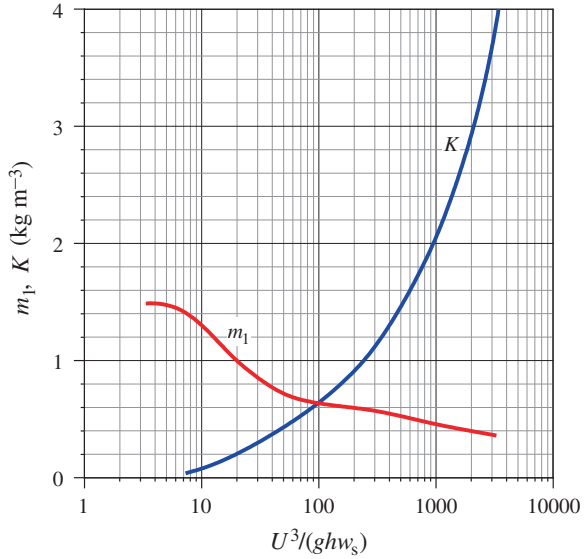
In another attempt, based on the energy concept, Zhang (1961) and Zhang and Xie (1993) also established a relationship between the suspended-load transport capacity \bar{C} and the parameter $U^3/(ghw_s)$, using the field data from different Chinese rivers. Later, Guo (2002) approximated their results by a convenient relationship as

$$\bar{C} = \frac{1}{20} \left(\frac{U^3}{ghw_s} \right)^{1.5} \left[1 + \left(\frac{1}{45} \cdot \frac{U^3}{ghw_s} \right)^{1.15} \right]^{-1} \quad (6.178)$$

6.3.2 Bagnold's Approach

Bagnold (1966) hypothesized that the suspended sediment particles in fluid are settled with their terminal fall velocity w_s , despite the distribution of sediment concentration across the fluid column is still preserved. It implies that to establish a dynamic equilibrium of sediment exchange, the flow must continuously pick up the sediment at the same rate with an upward velocity equaling w_s .

Fig. 6.16 Variations of K (in kg m^{-3}) and m_1 with $U^3/(ghw_s)$ (WIHEE 1981)



According to Bagnold (1966), in the fluid column resting over a unit area of bed, the power (work done per unit time) by the turbulent flow to keep sediment in suspension is expressed as $W_G w_s$, where W_G is the total submerged weight of suspended sediment in the fluid column. He argued that the potential energy of the flow is the source toward the turbulent kinetic energy required to maintain the motion of suspended particles. Thus, the energy required for sediment particles to keep in suspension is related to the potential energy loss. Hence, the work done per unit time for sediment suspension is equated to the net stream power used for the suspended-load transport

$$W_G w_s = \tau_0 U (1 - e_b) e_s \quad (6.179)$$

where e_b and e_s are the efficiencies for bed-load and suspended-load transports, respectively. The idea to introduce the efficiency terms is that a portion of total stream power $\tau_0 U e_b$ is dissipated into heat by the process of bed friction leaving the available power $\tau_0 U (1 - e_b)$ for suspended-load transport. Thus, when the available power $\tau_0 U (1 - e_b)$ is multiplied by e_s , it provides the net stream power used for the suspended-load transport.

The suspended-load transport rate g_{ss} in submerged weight per unit time and width is expressed as

$$g_{ss} = W_G U_s \quad (6.180)$$

where U_s is the depth-averaged velocity of suspended load. Using Eq. (6.179) to substitute W_G in Eq. (6.180) yields

$$g_{ss} = \tau_0 U \frac{U_s}{w_s} (1 - e_b) e_s \quad (6.181)$$

Bagnold assumed that at a certain elevation, the suspended sediment particles transport with the velocity that equals the flow velocity at that location. Thus, the depth-averaged velocity of the suspended load can be compared with that of the flow as follows:

$$U_s = \frac{1}{h-a} \int_a^h C \bar{u} dz, \quad U = \frac{1}{h} \int_0^h \bar{u} dz, \quad \therefore U_s < U \quad (6.182)$$

Note that the velocity \bar{u} increases with an increase in elevation z , while the sediment concentration C decreases with z . Therefore, the depth-averaged velocity of suspended load U_s is usually smaller than that of flow velocity U . Setting $r = U_s/U < 1$, Eq. (6.181) becomes

$$g_{ss} = \tau_0 \frac{U^2}{w_s} r (1 - e_b) e_s \quad (6.183)$$

However, the suspended-load transport rate g_s in weight per unit time and width can be given by

$$g_s = \tau_0 \frac{s}{\Delta} \cdot \frac{U^2}{w_s} r (1 - e_b) e_s \quad (6.184)$$

Bagnold used the laboratory data to evaluate $r(1 - e_b)e_s = 0.01$. Thus, the suspended-load transport rate is

$$g_s = 0.01 \tau_0 \frac{s}{\Delta} \cdot \frac{U^2}{w_s} \quad (6.185)$$

6.3.3 Wu *et al.*'s Approach

Following Bagnold's (1966) stream power approach, Wu *et al.* (2000) related the suspended-load transport rate to the rate of energy available in the flow, that is, $\tau_0 U$. They argued that the suspended-load transport rate is also influenced by the gravity that is accounted for by introducing the terminal fall velocity w_s and the threshold bed shear stress τ_{0c} . They conducted the dimensional analysis to determine the nondimensional dependent parameter $q_s/(\Delta g d^3)^{0.5}$ and the independent parameter $(\tau_0/\tau_{0c})(U/w_s)$. The τ_0/τ_{0c} ratio was logically modified by reformatting to $(\tau_0 - \tau_{0c})/\tau_{0c}$. By using the experimental data of nonuniform

suspended load measured by Samaga et al. (1986) and the field data of the Yampa River and the Yellow River, the relation for the fractional transport rate Φ_{si} was obtained. It is

$$\Phi_{si} = 2.62 \times 10^{-5} \left[\left(\frac{\tau_0}{\tau_{0ci}} - 1 \right) \frac{U}{w_{si}} \right]^{1.74} \quad \wedge \quad \Phi_{si} = \frac{q_{si}}{p_i (\Delta g d_i^3)^{0.5}} \quad (6.186)$$

where p_i is the fraction of sediment size d_i , τ_{0ci} is the threshold bed shear stress for sediment size fraction d_i , and w_{si} is the terminal fall velocity of sediment size d_i . The threshold bed shear stress τ_{0ci} was determined using Eq. (4.163) that takes into account the hiding and exposure effects in nonuniform sediment transport. The terminal fall velocity of sediment was obtained by using the Zhang (1961) equation (see Table 1.3).

6.4 Threshold Condition for Sediment Suspension

The threshold of sediment suspension is defined as the flow condition required for the mass exchange process of sediment particles of a given size at the lower boundary of the suspended load, that is at the top of the bed layer. In other words, the threshold refers to the flow condition at which the initiation of sediment suspension occurs.

Bagnold (1966) stated that sediment particles are lifted in suspension if the upward velocity of turbulence induced eddies exceeds the terminal fall velocity w_s of the particles. He obtained the upward velocity of eddies to be 1.25 times the shear velocity. This leads to the following threshold condition for sediment suspension:

$$\frac{w_s}{u_*} = 1.25 \quad (6.187)$$

It means that the particles are kept in suspension if $u_* > 0.8w_s$.

Xie (1981) obtained the threshold condition for sediment suspension from the Rouse equation (Eq. 6.27). As the Rouse number ζ increases, the distribution of sediment concentration becomes progressively inclined toward the abscissa, as shown in Fig. 6.4; and the sediment transport rate in the form of suspended load decreases. Xie defined the threshold of suspension to occur at the condition $\zeta = 5$, for which the suspended-load transport rate becomes very small. Hence,

$$\zeta = \frac{w_s}{\kappa u_*} = 5 \quad (6.188)$$

The threshold condition for the sediment suspension identified by van Rijn (1984b) is the instantaneous upward motion of the sediment particle that has a

jump length of 100 particle diameters. He used the experimental results to represent the following relationships:

$$\frac{u_*}{w_s}(1 < D_* \leq 10) = \frac{4}{D_*} \quad \wedge \quad D_* = d \left(\frac{\Delta g}{v^2} \right)^{1/3} \quad (6.189a)$$

$$\frac{u_*}{w_s}(D_* > 10) = 0.4 \quad (6.189b)$$

Sumer (1986) proposed the threshold condition for the sediment suspension in terms of Shields parameter as a function of shear Reynolds number R_* . The formulas are

$$\Theta(R_* \leq 70) = \frac{17}{R_*} \quad \wedge \quad R_* = \frac{u_* k_s}{v} \quad \vee \quad k_s = d \quad (6.190a)$$

$$\Theta(R_* > 70) = 0.27 \quad (6.190b)$$

Celik and Rodi (1991) gave the following empirical relationships to determine the bed shear stress for the initiation of sediment suspension:

$$\Theta(R_* \leq 0.6) = \frac{0.15}{R_*} \quad (6.191a)$$

$$\Theta(R_* > 0.6) = 0.25 \quad (6.191b)$$

Both Sumer (1986) and Celik and Rodi (1991) considered sediment particles to be in suspension from the sediment bed with no motion rather than from the top of the bed layer. Note that the above expressions defining the threshold criterion for sediment suspension are empirical and devoid of probabilistic considerations.

6.4.1 Cheng and Chiew's Probabilistic Approach

Cheng and Chiew (1999), however, brought the probabilistic consideration for the first time to determine the threshold of sediment suspension. They defined the threshold condition as the fluctuations of vertical velocity component w' exceeds the terminal fall velocity w_s of the particles, that is, $w' > w_s$. In contrast, the condition of $w' < w_s$ was used for the termination of suspension of sediment particles at any location in the suspension zone. They expressed the probability of suspension p to be given by $p = p(w' > w_s)$. They adopted the concept of Nezu (1977) that the probability of fluctuations of vertical velocity component near the bed could be considered, as a first approximation, to follow the Gaussian distribution. Thus

$$p = \frac{1}{\sqrt{2\pi}\sqrt{w'^2}} \int_{w_s}^{\infty} \exp\left(-\frac{1}{2} \cdot \frac{w'^2}{w'^2}\right) dw' \quad (6.192)$$

where $\sqrt{w'^2}$ is the root-mean-square (rms) of w' . Using the approximate solution of the error function (Cheng and Chiew 1998), they approximated Eq. (6.192) to

$$p = \frac{1}{2} - \frac{1}{2} \left[1 - \exp\left(-\frac{2}{\pi} \cdot \frac{w_s^2}{w'^2}\right) \right]^{0.5} \quad (6.193)$$

The terminal fall velocity w_s was obtained from Cheng's (1997) equation (Table 1.3). The root-mean-square of w' for hydraulically rough flow regime can be obtained from the experimental results of Grass (1971) and Nezu (1977). It is

$$\sqrt{w'^2} = u_* \quad (6.194)$$

For hydraulically smooth flow regime, Cheng and Chiew (1999) proposed following equation obtained using the experimental data of Grass (1971):

$$\sqrt{w'^2} = u_* \left\{ 1 - \exp\left[-0.025 \left(\frac{2.75u_*d}{v}\right)^{1.3}\right] \right\} \quad (6.195)$$

They computed and compared with experimental results to conclude the probability of threshold of sediment suspension to be 0.01, that is, one percent.

6.4.2 Bose and Dey's Probabilistic Approach

Bose and Dey (2013) argued that the Gaussian distribution primarily occurs when there is an additive accumulation of errors. This is, however, not the case of turbulent velocity fluctuations. Bose and Dey, on the other hand, drawing a similarity with the random signals on a computer monitor for the fluctuating velocity to be regarded analogous to the service arriving in a queue, gave the Gram-Charlier series expansion of the probability densities based on the two-sided exponential or Laplace distribution. They explained that the probability density function (pdf) $p_{\hat{w}}(\hat{w})$ for the nondimensional vertical velocity fluctuations \hat{w} can be given by

$$p_{\hat{w}}(\hat{w}) = \frac{1}{2} \left[1 + \frac{1}{2} C_{01} \hat{w} - \frac{1}{8} C_{02} (1 + |\hat{w}| - \hat{w}^2) - \frac{1}{48} C_{03} \hat{w} (3 + 3|\hat{w}| - \hat{w}^2) + \frac{1}{384} C_{04} (9 + 9|\hat{w}| - 3\hat{w}^2 - 6|\hat{w}^3| + \hat{w}^4) + \dots \right] \exp(-|\hat{w}|) \quad \wedge \quad \hat{w} = \frac{w'}{\sqrt{w'^2}} \quad (6.196)$$

Dey et al. (2012) obtained that the coefficients C_{01} and C_{03} are of the order of 0.001; while $C_{02} \approx -0.5$ and $C_{04} \approx 0.6$. Thus, it was assumed that $C_{02} \approx -0.5$ and the rest of the coefficients are effectively negligible due to their smallness or division by a large number, such as 384. Then, Eq. (6.196) reduces to

$$p_{\hat{w}}(\hat{w}) = \frac{1}{32} (17 + |\hat{w}| - \hat{w}^2) \exp(-|\hat{w}|) \quad (6.197)$$

The vertical velocity fluctuations w' are random to follow Eq. (6.197); and their pdf for positive values can be given by

$$\left. \begin{aligned} p_{w'}(w' \geq 0) &= \frac{1}{16\sqrt{w'^2}} (17 + \hat{w} - \hat{w}^2) \exp(-\hat{w}) \\ p_{w'}(w' < 0) &= 0 \end{aligned} \right\} \quad (6.198)$$

where $p_{w'}(w')$ is the pdf for w' . It satisfies the condition

$$\int_{-\infty}^{\infty} p_{w'}(w') dw' = 1$$

The total probability p of a particle to remain in suspension is thus given by

$$p = \int_{w_s}^{\infty} p_{w'}(w') dw' = \frac{1}{16} (16 - b - b^2) \exp(-b) \quad \wedge \quad b = \frac{w_s}{\sqrt{w'^2}} \quad (6.199)$$

Given the values of w_s and $\sqrt{w'^2}$, the total probability p depends on the value of $\sqrt{w'^2}$ at a given point in the fluid, as w_s is a constant for a given particle size.

Near the bed, if the bed layer is very thin, the bed is regarded as hydraulically rough. Using the condition for a hydraulically rough flow given by Eq. (6.194), the p can be given by

$$p = \frac{1}{16} \left(16 - \frac{w_s}{u_*} - \frac{w_s^2}{u_*^2} \right) \exp\left(-\frac{w_s}{u_*}\right) \quad (6.200)$$

For a comparatively thicker bed layer, the bed is regarded as hydraulically smooth, for which the empirical formula, that is Eq. (6.195), given by Grass (1971) can be used. Hence, in this case, the p can be given by

$$p = \frac{1}{16} \left(16 - \frac{u_*}{\sqrt{w'^2}} \cdot \frac{w_s}{u_*} - \frac{u_*^2}{w'^2} \cdot \frac{w_s^2}{u_*^2} \right) \exp \left(- \frac{u_*}{\sqrt{w'^2}} \cdot \frac{w_s}{u_*} \right) \quad (6.201)$$

Equations (6.200) and (6.201) for hydraulically rough and smooth flow regimes, respectively, can be represented in terms of Shields parameter Θ and shear Reynolds number R_* with the introduction of the particle parameter D_* that gives

$$\Theta = \frac{R_*^2}{D_*^3} \quad (6.202)$$

The expression of D_* can be related to w_s/u_* as follows [see Eq. (1.40) and Table 1.3] (Cheng 1997):

$$D_* = \sqrt{\frac{1}{1.2} \left(\frac{R_* w_s}{u_*} \right)^{2/3} \left[\left(\frac{R_* w_s}{u_*} \right)^{2/3} + 10 \right]} \quad (6.203)$$

Using Eq. (6.200) for a given value of p and a range of R_* from 0.03 to 10^4 , w_s/u_* was first computed from Eqs. (6.195) and (6.201) by numerical method of solving equations. Following this step, D_* was obtained from Eq. (6.203), and then, Θ was computed from Eq. (6.202). The computational results in terms of $\Theta(R_*)$ for different values of $p = 0.001, 0.01, 0.05$, and 0.1 are presented in Fig. 6.17. The entrainment threshold curve given by Yalin and Karahan (1979) is also superimposed for the comparison. Note that Yalin and Karahan's curve is often used for the comparison, as it is regarded as superior to well-known Shields diagram (Dey 1999; Dey et al. 1999).

The Rouse number ζ [$=w_s/(\kappa u_*)$] is an essential parameter that provides a measure of the relative effect of the gravity and the turbulence on a sediment particle in suspension. It can therefore be used to examine the condition of suspended sediment concentration. Regarding the computation of Rouse number ζ , the related conversion can be made by using Eqs. (6.202) and (6.203). In Fig. 6.18, the $\zeta(D_*)$ curve for probability of suspension $p = 0.05$ was plotted by Bose and Dey using Eqs. (6.195) and (6.101). For $p = 0.05$, the $\zeta(D_*)$ curve completely matches with that proposed by Cheng and Chiew (1999). The value $p = 0.05$ was used as an index for the threshold of sediment suspension. It means that the sediment suspension begins with bringing 5 % of particles in suspension from a given area at the top of bed layer. Note that Cheng and Chiew (1999) who used the Gaussian probability distribution obtained such a curve for $p = 0.1$. It implies that the exponential based probability distribution yields the threshold criterion for suspension at a lower value of probability. Importantly, Bose and Dey (2010)

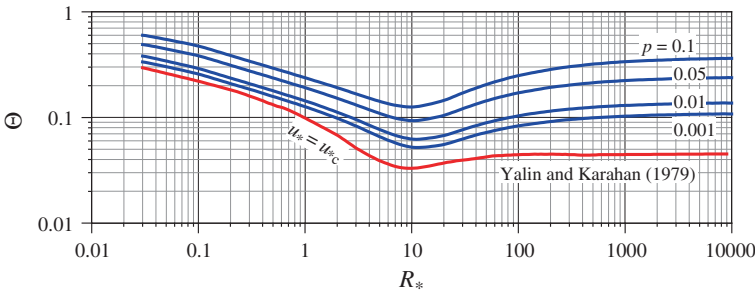


Fig. 6.17 Curves for the threshold of suspension in terms of $\Theta(R_*)$ for different values of $p = 0.001, 0.01, 0.05$, and 0.1 obtained by Bose and Dey (2013). Entrainment threshold curve given by Yalin and Karahan (1979) is superimposed for the comparison

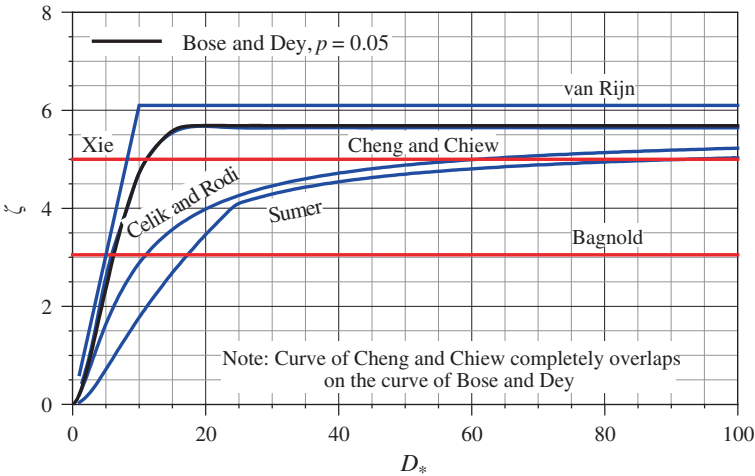
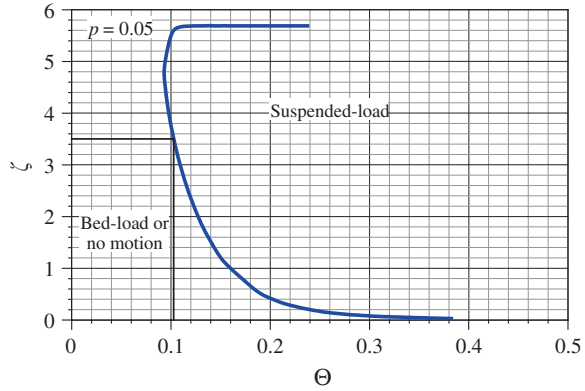


Fig. 6.18 Variation of Rouse number ζ with particle parameter D_* obtained by Bose and Dey (2013). The curves of ζ versus D_* drawn from the formulas given by Bagnold (1966), Xie (1981), van Rijn (1984b), Sumer (1986), Celik and Rodi (1991), and Cheng and Chiew (1999) are superimposed for the comparison

showed that the exponential based probability distributions for the velocity fluctuations are universal. Reverting to Fig. 6.18, it is evident that ζ increases sharply with D_* up to $D_* = 15$ and then ζ becomes independent of D_* for $D_* > 15$. The $\zeta(D_*)$ curves drawn from the threshold criterion of suspension given by Bagnold (1966), Xie (1981), van Rijn (1984b), Sumer (1986), Celik and Rodi (1991) and Cheng and Chiew (1999) are superimposed for the comparison. The curves of various investigators yield widely varying results for $D_* < 50$, while the threshold criterion lies in between $\zeta \approx 4.8$ and 6.1 for $D_* \geq 50$. However, Bagnold's (1966) curve provides a much reduced value of $\zeta = 3.05$.

Fig. 6.19 Diagram for the prediction of threshold of suspended load from bed load in terms of Rouse number ζ as a function of Θ obtained by Bose and Dey (2013)



Further, in Fig. 6.19, Rouse number ζ is plotted against Θ for $p = 0.05$. This curve clearly illustrates that for the given values of ζ and Θ whether the sediment particles of a given size in a flow can be in suspension. In fact, this curve can be used as a predication curve for the determination of threshold criterion for sediment suspension in terms of ζ and Θ . For instance, a particle can be in suspension if $\Theta(\zeta = 3.5) > 0.103$, as shown in Fig. 6.19.

6.5 Effects of Suspended Load on Bed-Load Transport

Fredsøe and Deigaard (1992) developed a method to quantify the effects of sediment suspension on bed-load transport. They first distinguish the bed load, according to the definition of Wilson (1966), from the suspended-load transport, according to their own definition: The bed load is the portion of sediment load that is transported immediately over the bed and supported by the effects of random particle interactions rather than by the effects of fluid turbulence (Wilson 1966), while suspended load is then the portion of the load that is primarily supported by the effects of fluid turbulence.

Fredsøe and Deigaard (1992) extended the applied bed shear stress τ_0 equation given by Bagnold (1954) [see Eqs. (5.86) and (5.89)] including the dispersive bed shear stress τ_{0s} from the suspended load. It is

$$\tau_0 = \tau_{0c} + nF_D + \tau_{0s} \quad (6.204)$$

According to Bagnold (Fredse and Deigaard 1992), the dispersive bed shear stress τ_{0s} is

$$\tau_{0s} = 0.013 \rho_s A_c^2 d^2 \left(\frac{d\bar{u}}{dz} \right)^2 \quad (6.205)$$

where A_c is the linear concentration related to sediment concentration as $C = C|_{\max} (1 + \vartheta_c^{-1})^{-3}$. It was approximated that the velocity gradient is unaffected by the sediment load. As the dispersive bed shear stress acts at an elevation z that is in the order of a particle size, $z = a_0 d$, where a_0 is an order of unity, the velocity gradient at that point is defined by

$$\left. \frac{d\bar{u}}{dz} \right|_{z=a_0 d} = \frac{(\tau_0 / \rho)^{0.5}}{\kappa a_0 d} \quad (6.206)$$

Using Eqs. (6.205) and (6.206) into Eq. (6.204) and rearranging lead to

$$\tau_0 = (\tau_{0c} + nF_D) \left(1 + \frac{0.013}{\kappa^2 a_0^2} s A_{c0}^2 \right)^{-1} \quad (6.207)$$

where A_{c0} is the value of A_c at the bed level. With Eq. (5.87), Eq. (6.207) can be expressed in nondimensional form as

$$\Theta = \left(\Theta_c + \frac{\pi}{6} \mu_d p \right) \left(1 + \frac{0.013}{\kappa^2 a_0^2} s A_{c0}^2 \right)^{-1} \quad (6.208)$$

where p is the probability of the particles to move and μ_d is the dynamic coefficient of friction. Fredsøe and Deigaard (1992) tested Eq. (6.208) for the case of large transport rate (that is, $\Theta \gg \Theta_c$ or $\Theta - \Theta_c \approx \Theta$) that corresponds to $p \rightarrow 1$. They estimated A_{c0} from Eq. (6.208) as $A_{c0} = 4.32$ and corresponding $C|_{\max} = 0.35$. The estimation was done for $\mu_d = 0.57$, $s = 2.65$, $\kappa = 0.41$, and $a_0 = 2$.

6.6 Effects of Suspended Load on Velocity Distribution

It has already been discussed in Sect. 6.2.2 that in the flow region close to the bed, the sediment concentration is high; while in the remaining portion of the flow, the sediment concentration is relatively low. This stratification retards turbulent mixing process of fluid momentum and sediment mass. As a result of which, the velocity distribution in sediment-laden flows is modified from the logarithmic law distribution in a clear-water flow. As already discussed, García (2008) proposed an iterative solution for the velocity \bar{u} in sediment-laden flows using Eqs. (6.88) and (6.91). Besides, there are number of contributions that are discussed as follows:

6.6.1 Einstein and Chien's Contribution

Einstein and Chien (1955) modified the logarithmic law of velocity distribution due to the effects of sediment suspension. They argued that in sediment-laden flows, a more realistic velocity distribution could be obtained by the introduction of the participation of suspended sediment particles in the exchange mechanism. They modified the traditional Reynolds shear stress τ relationship according to Boussinesq hypothesis given by Eq. (3.24) or (6.23). The modified equation is

$$\tau = (1 + \Delta C)\rho\epsilon_t \frac{d\bar{u}}{dz} \quad (6.209)$$

In the zone of small concentration, that is, $1 + \Delta C \approx 1$, Eq. (6.209) becomes Eq. (6.23). In this case, an equation similar to the universal logarithmic law, but with different values of constants, could be applied. Experimental data analysis suggested the following relationship:

$$\frac{\bar{u}}{u_*} = 17.66 + \frac{1}{\kappa} \ln \left(\frac{z}{35.45k_s} \right) \quad (6.210)$$

Experiments revealed that when the local sediment concentration reaches $C = 981 \text{ N m}^{-3}$ in the near-bed flow region or when the flow region is $z < 0.1h$, Eq. (6.210) proved to be inadequate. In this flow region, the suspended sediment concentration is high, and the shear stress given by Eq. (6.209) can be approximated by the bed shear stress τ_0 as

$$\tau_0 = \int_0^h (1 + \Delta C)\rho g S_0 dz \quad (6.211)$$

The velocity distribution is thus obtained as

$$\frac{\bar{u}}{u_*} = \frac{1}{\kappa} \left(\frac{1 + \Delta h^{-1} \int_0^h C dz}{1 + \Delta C|_{z=0}} \right)^{0.5} \ln \left(B_e \frac{z}{k_s} \right) \quad (6.212)$$

where B_e is a constant to be determined empirically. However, the depth-averaged velocity U can be obtained from the following equation with a minimal error

$$\frac{U}{u_*} = 17.66 + \frac{1}{\kappa} \ln \left(\frac{z}{96.5k_s} \right) \quad (6.213)$$

6.6.2 Umeyama and Gerritsen's Contribution

Using a modified mixing length concept, Umeyama and Gerritsen (1992) developed a theoretical model to predict the velocity distribution in a sediment-laden flow. They introduced a modified mixing length l for sediment-laden flows as

$$l = \kappa z(1 - \tilde{z})^{\alpha_1} \quad \wedge \quad \alpha_1 = 0.5 \left(1 + \beta_1 \frac{C}{C_a} \right) \quad (6.214)$$

where β_1 is a coefficient to be determined empirically. Substituting Eq. (6.214) into the traditional Reynolds shear stress equation obtained from Prandtl's mixing length theory provides

$$\tau \left(= \rho_m l^2 \left| \frac{\partial \bar{u}}{\partial z} \right| \frac{\partial \bar{u}}{\partial z} \right) = (1 + \Delta C) \rho [\kappa z(1 - \tilde{z})^{\alpha_1}]^2 \left| \frac{\partial \bar{u}}{\partial z} \right| \frac{\partial \bar{u}}{\partial z} \quad (6.215)$$

In the above, the mass density ρ of a clear-water fluid is replaced by that of fluid–sediment mixture ρ_m , given by $\rho_m = (1 + \Delta C)\rho$ (Eq. 1.29). Remembering that the Reynolds shear stress distribution in a zero-pressure gradient (uniform) flow is linear and can be given by $\tau = \tau_0(1 - \tilde{z})$, it can be equated to Eq. (6.215) to get

$$\frac{d\bar{u}}{dz} = \frac{u_*}{\kappa z} (1 + \Delta C)^{-0.5} (1 - \tilde{z})^{-0.5\beta_1(C/C_a)} \quad (6.216)$$

In Eq. (6.216), the partial differential form is replaced by the total differential, as both \bar{u} and C are functions of z . The Rouse equation, Eq. (6.27), can be used as a first approximation for C . Then, the velocity distribution in a sediment-laden flow can be determined numerically from Eq. (6.216).

6.6.3 Castro-Orgaz et al.'s Contribution

The study of Castro-Orgaz et al. (2012) proposed a physical interpretation of the turbulent momentum transfer in sediment-laden flows by using a modified mixing length theory. They considered a steady two-dimensional turbulent flow having the distributions of mass density of fluid–sediment mixture $\rho_m(z)$, induced by the sediment suspension, and velocity $\bar{u}(z)$ as shown in Fig. 6.20. Note that there exists a mass density gradient due to differential sediment concentration along vertical. The flow momentum per unit volume $M(=\rho_m \bar{u})$ at an elevation z from the bed is expanded by a Taylor series up to the first-order term.

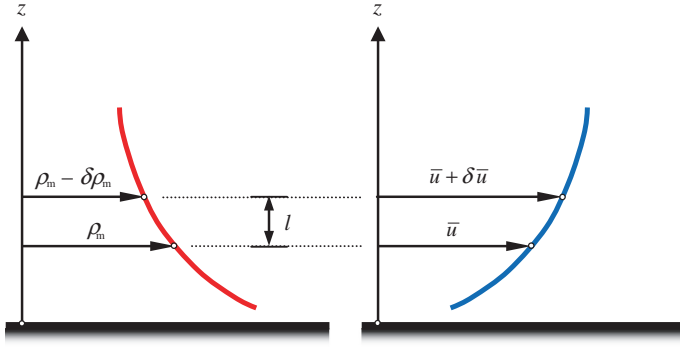


Fig. 6.20 Distributions of mass density ρ_m and velocity \bar{u} in a sediment-laden flow, as components of momentum transfer, $M = \rho_m \bar{u}$, between two layers separated by the mixing length l (Castro-Orgaz et al. 2012)

$$M(z + \delta z) = M(z) + \delta z \frac{dM}{dz} \quad (6.217)$$

Analogous to Prandtl's mixing length theory, it was assumed that δz is the length scale l , termed the *mixing length* for the sediment-laden flows. Thus, from Eq. (6.217), it can be obtained as

$$\delta M = M(z + \delta z) - M(z) = l \frac{d}{dz} (\rho_m \bar{u}) = l \left(\bar{u} \frac{d\rho_m}{dz} + \rho_m \frac{d\bar{u}}{dz} \right) \quad (6.218)$$

Further, from the definition sketch (Fig. 6.20), δM is obtained as

$$\delta M = (\rho_m - \delta\rho_m)(\bar{u} + \delta\bar{u}) - \rho_m \bar{u} = \rho_m \delta\bar{u} - \bar{u} \delta\rho_m \quad \wedge \quad \delta\bar{u} \delta\rho_m \rightarrow 0 \quad (6.219)$$

Equating Eqs. (6.218) and (6.219) gives

$$\delta\bar{u} = l \frac{\bar{u}}{\rho_m} \cdot \frac{d\rho_m}{dz} + l \frac{d\bar{u}}{dz} + \bar{u} \frac{\delta\rho_m}{\rho_m} \quad (6.220)$$

The mass density difference can also be expanded in terms of l as

$$\delta\rho_m = l \frac{d\rho_m}{dz} + \frac{l^2}{2} \cdot \frac{d^2\rho_m}{dz^2} \quad (6.221)$$

Using Eq. (6.221) into Eq. (6.220) yields

$$\delta \bar{u} = l \frac{d\bar{u}}{dz} \left[1 + \frac{\bar{u}}{\rho_m} \left(\frac{d\bar{u}}{dz} \right)^{-1} \left(2 \frac{d\rho_m}{dz} + \frac{l}{2} \cdot \frac{d^2 \rho_m}{dz^2} \right) \right] \quad (6.222)$$

The above equation that was originally developed by Montes (1973) represents the influence of mass density of suspended sediment on the momentum transfer. The turbulent momentum transfer is therefore not only influenced by the local values of ρ_m and \bar{u} , but also by their gradients. Therefore, Eq. (6.222) implies that the influence of suspended sediment is pronounced in the flow region with large gradients of mass and momentum transfer, as in the near-bed flow region; both $d\rho_m/dz$ and $d\bar{u}/dz$ are substantial.

The mass density ρ_m of fluid-sediment mixture is given by [see Eq. (1.29)]

$$\rho_m = \rho + (\rho_s - \rho)C = \rho(1 + \Delta C) \quad (6.223)$$

An accelerating or decelerating particle is to move some volume of surrounding fluid as it transports through it, since the particle and fluid cannot occupy the same physical space simultaneously. Therefore, it was required to include the *added fluid mass* or *virtual mass*, that is the inertia added to a system, through a modification of the mass density of a particle ρ_p as follows (Montes 1973; Liggett 1994):

$$\rho_p = \rho_s + \alpha_m \rho \quad (6.224)$$

where α_m is the added mass coefficient, which can be approximated as $\alpha_m = 0.5$ (van Rijn 1984a). Using Eq. (6.224), Eq. (6.223) can be reformed as

$$\rho_m = \rho[1 + (1 + \Delta - \beta_m)C] \quad (6.225)$$

where $\beta_m = 1 - \alpha_m$. Differentiating Eq. (6.225) once and twice with respect to z yields

$$\frac{d\rho_m}{dz} = \rho(1 + \Delta - \beta_m) \frac{dC}{dz}, \quad \frac{d^2 \rho_m}{dz^2} = \rho(1 + \Delta - \beta_m) \frac{d^2 C}{dz^2} \quad (6.226)$$

Then, inserting Eq. (6.226) into Eq. (6.222), the resulting equation is

$$\delta \bar{u} = l \frac{d\bar{u}}{dz} \left[1 + \frac{\rho}{\rho_m} \bar{u}(1 + \Delta - \beta_m) \left(\frac{d\bar{u}}{dz} \right)^{-1} \frac{dC}{dz} \left(2 + \frac{l}{2} \cdot \frac{d^2 C/dz^2}{dC/dz} \right) \right] \quad (6.227)$$

Differentiating the diffusion equation Eq. (6.37) that was obtained by Hunt (1954), with respect to z , yields:

$$\varepsilon_s \frac{d^2 C}{dz^2} + w_s(1 - 2C) \frac{dC}{dz} = 0 \quad (6.228)$$

Inserting Eq. (6.228) into Eq. (6.227) produces

$$\delta \bar{u} = l \frac{d\bar{u}}{dz} \left\{ 1 + \frac{\rho}{\rho_m} \bar{u}(1 + \Delta - \beta_m) \left(\frac{d\bar{u}}{dz} \right)^{-1} \frac{dC}{dz} \left[2 - \frac{lw_s}{2\varepsilon_s} (1 - 2C) \right] \right\} \quad (6.229)$$

In turbulent momentum transfer, the term dC/dz represents the stratification effect that is predominant in the near-bed flow region (Smith and McLean 1977a). In order to simplify, the sediment diffusivity ε_s in near-bed flow can be approximated by (Montes 1973):

$$\varepsilon_s = lu_* \quad (6.230)$$

However, besides the near-bed approximation, its application to the entire flow depth was hypothesized, as in the upper flow layer, the mass and momentum transfer is less affected by the suspended particles (Smith and McLean 1977a). Further, the mixing length l in a sediment-laden flow which is different from the mixing length l_0 in a clear-water flow was assumed as $l = l_0$ based on the asymptotic considerations. Note that if $C \rightarrow 0$, then $dC/dz \rightarrow 0$ by Eq. (6.37); and if $l \rightarrow l_0$, then Eq. (6.229) tends to be the classical Prandtl equation, $\delta \bar{u} = l_0 d\bar{u}/dz$. With this approximation and that given by Eq. (6.230), Eq. (6.229) is rewritten as

$$\begin{aligned} \delta \bar{u} &= l_0 \frac{d\bar{u}}{dz} \underbrace{\left\{ 1 + \frac{\rho}{\rho_m} \bar{u}(1 + \Delta - \beta_m) \left(\frac{d\bar{u}}{dz} \right)^{-1} \frac{dC}{dz} \left[2 - \frac{w_s}{2u_*} (1 - 2C) \right] \right\}}_{\phi} \\ \Rightarrow \delta \bar{u} &= \underbrace{\phi l_0}_{l_m} \frac{d\bar{u}}{dz} \end{aligned} \quad (6.231)$$

where ϕ is a sediment damping factor, which modifies the clear-water mixing length l_0 to $l_m = \phi l_0$ for sediment-laden flows. The damping factor ϕ is therefore dependent on $\bar{u}(z)$, $C(z)$, $d\bar{u}/dz$, and dC/dz .

In order to analytically relate the mixing length l_0 in a clear-water flow with the mixing length l_m in a sediment-laden flow, Castro-Orgaz et al. derived l_0 by balancing the Reynolds shear stress equation obtained from the Prandtl's mixing length theory with the linear Reynolds shear stress distribution in a zero-pressure gradient flow given by $\tau = \tau_0(1 - \tilde{z})$:

$$\tau = \rho l_0^2 \left| \frac{d\bar{u}}{dz} \right| \frac{d\bar{u}}{dz} = \tau_0(1 - \tilde{z}) \quad (6.232)$$

To determine the velocity gradient, they used the wall-wake velocity distribution in a clear-water flow as follows (White 1991):

$$\frac{U - \bar{u}}{u_*} = -\frac{1}{\kappa} \ln \tilde{z} + \frac{2\Pi}{\kappa} (1 - \varpi) \quad \wedge \quad u_* = \left(\frac{\tau_0}{\rho} \right)^{0.5} \quad \vee \quad \varpi = \sin^2 \left(\frac{\pi}{2} \tilde{z} \right) \quad (6.233)$$

where Π is the Coles' wake parameter. Using Eq. (6.233) into Eq. (6.232), the l_0 and l_m are obtained as

$$\frac{l_0}{h} = \kappa \tilde{z} (1 - \tilde{z})^{0.5} \left(1 + 2\Pi \tilde{z} \frac{d\varpi}{d\tilde{z}} \right)^{-1} \quad \wedge \quad \frac{d\varpi}{d\tilde{z}} = \frac{\pi}{2h} \sin(\pi \tilde{z}) \quad (6.234a)$$

$$\frac{l_m}{h} \left(= \phi \frac{l_0}{h} \right) = \phi \kappa \tilde{z} (1 - \tilde{z})^{0.5} \left(1 + 2\Pi \tilde{z} \frac{d\varpi}{d\tilde{z}} \right)^{-1} \quad (6.234b)$$

Therefore, von Kármán constant κ_s for sediment-laden flows is defined by

$$\kappa_s = \phi \kappa \quad (6.235)$$

The above equation suggests that κ_s is a function of z , as $\phi = \phi(z)$.

For sediment-laden flows, Eq. (6.232) was expressed as follows (Lyn 1986; Umeyama and Gerritsen 1992):

$$\tau = \rho l_m^2 \left| \frac{d\bar{u}}{d\tilde{z}} \right| \frac{d\bar{u}}{d\tilde{z}} = \tau_0 \left(1 - \tilde{z} + \Delta \int_{\tilde{z}}^1 C d\tilde{z} \right) \quad (6.236)$$

Equation (6.236) produces a differential equation of velocity distribution, that is

$$\frac{du^+}{d\tilde{z}} = \frac{h}{l_m (1 + \Delta C)^{0.5}} \left(1 - \tilde{z} + \Delta \int_{\tilde{z}}^1 C d\tilde{z} \right)^{0.5} \quad \wedge \quad u^+ = \frac{\bar{u}}{u_*} \quad (6.237)$$

However, the term ϕ in Eq. (6.231) is further simplified with the assumption that w_s/u_* in pure suspension is less than unity leading to $w_s(1 - 2C)/(2u_*) \ll 2$. Therefore, the ϕ is approximated as

$$\phi = 1 + 2u^+ \cdot \frac{1 + \Delta - \beta_m}{1 + \Delta C} \cdot \frac{dC}{d\tilde{z}} \left(\frac{du^+}{d\tilde{z}} \right)^{-1} \quad (6.238)$$

The solution for velocity distribution from Eq. (6.237) can be obtained if the concentration distribution is known. Castro-Orgaz et al. adopted a simplified exponential distribution for sediment concentration as follows (Montes 1973):

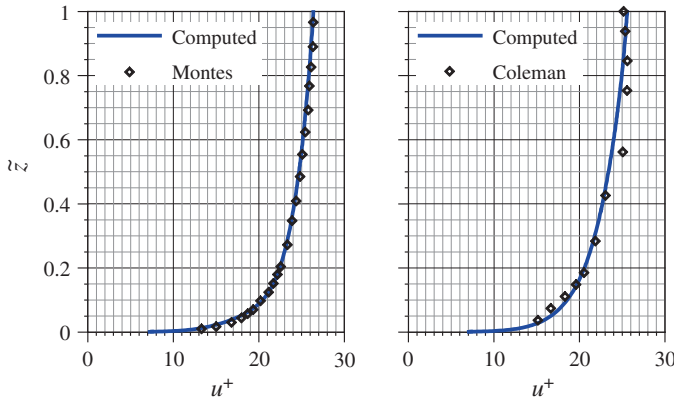


Fig. 6.21 Comparison of velocity distributions computed from Castro-Orgaz et al.'s (2012) approach with the experimental data of Montes (1973) and Coleman (1981)

$$\frac{C}{C_{\max}} = \exp \left\{ -A\tilde{z} \left[\frac{1 + \exp(-2B\tilde{z})}{2} \right]^{-A/B} \right\} \quad (6.239)$$

where A and B are empirical coefficients. According to Montes (1973), A could be determined by fitting Eq. (6.239) and $B \approx 30$. In the above, C_{\max} is C at the interface of bed load and suspended load.

Equation (6.237) was solved in velocity defect form, $d\vartheta/d\tilde{z} = -du^+/d\tilde{z}$ [where $\vartheta = (U - \bar{u})/u_*$], using l_m from Eq. (6.234b) and ϕ from Eq. (6.238). The $C(z)$ and dC/dz were determined from Eq. (6.239), once A was obtained by fitting the experimental data of C . Equation (6.237) was then solved numerically using a fourth-order Runge–Kutta method, with an initial value of $\vartheta(\tilde{z} = 0.999) = 0$. To avoid a singularity, $\tilde{z} = 0.999$ was used in place of $\tilde{z} = 1$ for the computation. Note that Eq. (6.237) was implicit in $du^+/d\tilde{z}$. The value $du^+/d\tilde{z}$ in a given computational step for the computation of ϕ was used from the previous step. The computation was continued until no significant variation between the assumed $du^+/d\tilde{z}$ in ϕ and that computed from Eq. (6.237) were detected. Figure 6.21 compares the computed velocity $u^+(\tilde{z})$ distributions obtained from Castro-Orgaz et al.'s approach with the experimental data of Montes (1973) and Coleman (1981) having reference concentrations $C_a = 9 \times 10^{-3}$ and 0.0246, respectively.

6.7 Effects of Suspended Load on von Kármán Constant κ

Gaudio et al. (2010) [also Gaudio and Dey (2012)] gave a comprehensive review of the studies on the influence of sediment suspension on von Kármán constant κ . In fact, von Kármán constant κ has been a long disputed parameter, involved in the

velocity data analysis of the logarithmic law distribution in the wall shear layer, to report the results of sediment-laden flows. In the past, pioneering research contributions were due to Vanoni (1946), Brooks (1954), Einstein and Chien (1955) and Elata and Ippen (1961) to study the influence of suspended sediment concentration C on the distributions of streamwise velocity \bar{u} by fitting the logarithmic law to match the experimental results. One of the important findings was that κ decreases from its universal value ($\kappa = 0.41$) with an increase in C as suspended sediment in the flow induces a damping effect on the turbulence momentum transfer, as hypothesized by Vanoni (1946). It may be attributed to the energy that comes from the turbulence to keep sediment particles in suspension. In fact, it was seen that an increase in velocity gradient $d\bar{u}/dz$ for a given u_* was associated with a decrease in κ . However, Coleman (1981, 1986) argued strongly against this issue. He believed that the results of Vanoni were an artifact of the erroneous method of evaluating κ that was generally accepted at the time when he did the work. According to Coleman, the experimental findings of Einstein and Chien (1955) were also unreliable, as the velocities were measured only within the lower 40 % of the flow depth. Thus, it was hard to obtain the general information of the flow characteristics, such as boundary layer thickness, and maximum velocity. In experiments by Elata and Ippen (1961), they used virtually neutral buoyant polystyrene particles to simulate the sediment suspension. The \bar{u} distributions were plotted as velocity defect distributions; and the apparent reduction of κ was due to its erroneous evaluation, as emphasized by Coleman. However, in sediment-laden flows, Coleman (1981) studied \bar{u} distributions using the wake law and argued that the wake coefficient rather than κ is influenced by sediment suspension. The wake law that can describe the logarithmic law distribution in sediment-laden flows only near the bed has the same value of $\kappa = 0.41$ as that in a clear-water flow. Lyn (1986) pointed out that in the variation of κ with C , the application of the logarithmic law results in a decreased value of κ ; while the application of the log-wake law yields a universal value of κ . Cioffi and Gallerano (1991) conducted an experimental study to determine \bar{u} and C distributions by using the phase difference method. Without examining κ in the logarithmic law layer, they only demonstrated that the measured \bar{u} distributions were reasonably interpolated with $\kappa = 0.4$ if $\bar{z} < 0.15$. Cellino and Graf (1999) studied the effects of sediment suspension in flows under noncapacity (unsaturated) and capacity (saturated) conditions. They reported that $\kappa = 0.4$ was an acceptable value for describing \bar{u} distributions using the velocity defect law. According to Muste (2002), $\kappa = 0.41$ could be an appropriate value for sediment-laden flows involving only small values of C (< 0.05). The above discussion is made on the studies by the investigators who opposed the changed value of κ from its universal value.

On the other hand, other investigators believed that κ is nonuniversal in sediment-laden flows. Besides Vanoni (1946), Einstein and Chien (1955), and Elata and Ippen (1961), many others during the 1960s and 1970s reported that κ diminishes as C increases, primarily owing to an increase in velocity gradient $d\bar{u}/dz$ in presence of sediment suspension (Vanoni and Nomicos 1960; Hino 1963; Ippen 1971). In 1980s, Nouh (1989) analyzed the velocity data in logarithmic law

layer ($\bar{z} \leq 0.15$). He argued that the variation of κ with depth-averaged suspended sediment concentration \bar{C} depends on the flow Reynolds number Re ($= 4Uh/\nu$). The \bar{C} increases with a decrease in κ if $Re < 7 \times 10^5$, but increases if $Re > 7 \times 10^5$. The variation of κ with \bar{C} is insignificant in flow with Re nearly equaling the critical value $Re_c = 7 \times 10^5$. Noh (1989) hypothesized that the turbulence level (Reynolds stresses) in the flow region of the proximity of the bed decreases if $Re < Re_c$ and increases if $Re > Re_c$, as \bar{C} increases. Additionally, he argued that the near-bed turbulence level in sediment-laden flows increases as \bar{C} decreases and Re increases, with a rate depending on \bar{C} and Re . For $Re < Re_c$, the \bar{C} influences the turbulence level more than Re , and vice versa for $Re > Re_c$. These two effects balance each other for $Re \approx Re_c$. Noh (1989) also observed that the amplified values of κ in flow with fine suspended particles are larger than those in flow with relatively coarse suspended particles. Also, the amplified values of κ in flow with high \bar{C} are larger than those in flow with low \bar{C} . In a clear-water flow, κ is invariant of Re for $4 \times 10^5 < Re < 2 \times 10^6$. Wang and Qian (1992) explained that in the far-bed flow region ($0.1 < \bar{z} < 1$), the values of κ in sediment-laden flows are less than $\kappa = 0.41$ in clear-water flow. Guo and Julien (2001) argued that the reduction of κ in sediment-laden flows is due to \bar{C} ; and the mass density gradient should be given by the Richardson number. In sediment-laden flows, Wang et al. (2001) modified the von Kármán constant separately as κ_p for the logarithmic law and κ_w for the wake law. For the logarithmic law, they proposed $\kappa_p = 2.08\kappa/(\Delta u^+ \kappa + 2.08)$, where $\Delta u^+ = (\bar{u}_{cw} - \bar{u}_{sf})/u_*$, and \bar{u}_{cw} and \bar{u}_{sf} are the time-averaged velocities at $\bar{z} = 0.05$ in clear-water and sediment-laden flows, respectively. It is obvious that the κ_p (evaluated within the flow region $z < \delta$; where δ is the boundary layer thickness) decreases with an increase in Δu^+ . For the wake law, they obtained an average value of κ_w as 0.346 with a relative error of 229 %. Nezu and Azuma (2004) conducted measurements in the logarithmic law layer for both particles and fluid in particle-laden flow by means of a discriminator particle-tracking velocimeter. They observed that κ decreases with an increase in \bar{C} . They detected increased near-bed turbulence intensity in flow with particle suspension. Bose and Dey (2009b) also reported a reduction of κ in sediment-laden flows. It can therefore be concluded that κ decreases due to an increase in near-bed turbulence intensity that is augmented by suspended sediment particles. In a recent attempt, a rational approach to study the effects of sediment suspension on turbulent momentum transfer was put forward by Castro-Orgaz et al. (2012). It has already been discussed in Sect. 6.6. An improved definition of the von Kármán constant κ_s as a local turbulent variable was proposed, arising from a modified mixing length theory for sediment-laden flows. The analysis showed that the κ_s is not constant in turbulent sediment-laden flows, but a function of distance from the wall, as the turbulent momentum transfer is influenced by the stratification. In investigating the log-wake data fitting by their approach, it was observed that if near-wall data were used, the conclusion of Coleman (1981) was generally supported, resulting in $\kappa \approx 0.41$. Nevertheless, it was recognized that it did not corroborate that the suspended sediment influences the turbulence structure of the

outer layer. Further, if the data over entire flow depth were taken into account, then the fitted κ_s by a log-wake approach reduced considerably from 0.41, because $\kappa_s (= \phi\kappa)$, where $\phi < 1$) in a sediment-laden flow is less than κ in a clear-water flow.

The researchers supporting the universality of κ in sediment-laden flows referred to Coleman's (1981, 1986) data and analysis. In this context, it is pertinent to mention that Gust (1984) severely criticized the method of data analysis by Coleman's (1981). One of the reasons for the critique was the lack of data in the near-wall flow region, typically four data points, which might lead to inaccurate fittings for the corresponding κ values. Subsequent work by Parker and Coleman (1986) corroborated the results presented by Coleman (1981, 1986) regarding the strength of the wake, but it did not provide enough additional information to support the value $\kappa = 0.41$. Further, criticizing the approach of Coleman (1981, 1986), Lyn (1986, 1988), and Valiani (1988) argued that statistically rigorous fittings by the log-wake law suggest that both κ and wake function are influenced by the suspended sediment. Valiani (1988) adopted the log-wake law for sediment-laden flows reanalyzing Coleman's (1986) data. He proposed that rather than determining κ from the near-wall data, the entire velocity distribution could be used with values weighted inversely with the distance from the wall. Surprisingly, using this weighted values, Valiani (1988) recognized a pronounced effect of sediment suspension reducing the value of κ and a less significant effect on wake function, which yielded smaller values from those obtained by Coleman (1986).

Owing to the available evidence where κ varies in flow with suspended sediment concentration C , a reanalysis of Coleman's dataset was carried out by Gaudio et al. (2010) [also Gaudio and Dey (2012)] to verify the constancy of κ . Using the velocity defect law as in the original work, the data $(\bar{u}_{\max} - \bar{u})/u_*$ versus z/δ were plotted in a semilog graph (Fig. 6.22). The slopes representing $-\kappa^{-1}$ were determined from a straight line fitting within the logarithmic law layer ($z \leq 0.15\delta$). The newly obtained values of κ were different from those originally obtained by Coleman (1981, 1986). Figure 6.22 depicts the reanalyzed plots for κ versus C . The mean trend shown by the solid line confirms a progressively diminishing trend of κ with an increase in C . In general, the values of κ are less than 0.41 for $C > 0.0008$.

6.8 Effects of Sediment Suspension on Turbulence Characteristics

6.8.1 Effects on Turbulent Stresses

Suspended sediment particles are known to modify the turbulence structure in a fluid flow by which they are transported, which in turn affects the sediment transport. The interaction between turbulent flow and suspended particles is of primary attention in the mechanics of sediment transport. There has been much controversy

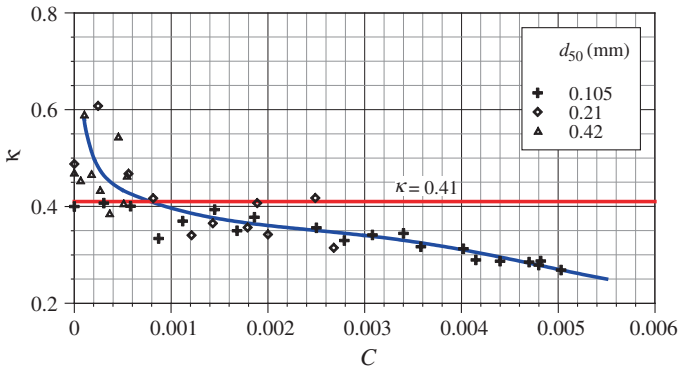


Fig. 6.22 Variation of κ with C obtained by Gaudio et al. (2010) [also Gaudio and Dey (2012)] reanalyzing the data of Coleman (1981, 1986)

over the effects of suspended sediment on turbulent flow. The major controversy is related to the turbulence intensities or Reynolds stresses, if they increase or decrease, and the turbulence modulation, if it enhances or attenuates. Present understanding of these issues is not at all comprehensive but far from complete.

Elata and Ippen (1961), who conducted experiments on neutrally buoyant suspension of high concentrations, argued that the turbulence structure is modified primarily at scales comparable to suspended particle size. Wang and Qian (1989) performed experiments with both fine sand and neutrally buoyant plastic particles having average concentrations to be greater than 1 %. In contrast to Elata and Ippen, they observed a noticeable reduction in streamwise turbulence intensity. Examining streamwise turbulence intensity in sediment-laden flows with fine sand ($d \approx 0.24$ mm), van Ingen (1983) concluded that the sediment-laden flows did not exhibit substantially different streamwise turbulence intensity from that in a clear-water flow. Lyn (1992) examined flows with well-sorted sand ($d = 0.15 - 0.24$ mm) suspension under both equilibrium sediment bed and rigid bed conditions. The streamwise turbulence intensity was found to increase slightly in the upper half and the near-bed flow regions, separated by a flow region where no distinction was observed. Power spectra of the streamwise velocity fluctuations at about half the flow depth revealed a relative attenuation of small scales and a relative enhancement of larger scales. He, however, did not observe any evidence to support the traditional inference of turbulence damping. Nezu and Azuma (2004) reported that the turbulence intensities are enhanced substantially by the presence of particles in the near-bed flow region. The turbulence intensities of particles become further larger than those of fluid in that region. Cellino and Lemmin (2004) measured enhanced turbulence intensities corresponding to ejections that are involved in suspended sediment transport.

6.8.2 Response of Turbulent Bursting to Sediment Suspension

As a latest development of research in sediment transport by turbulent flow, the dynamics of coherent structures in sediment-laden flows has been studied in great detail to explore their generation mechanism and role in bringing the sediment particles in suspension and transporting them. Investigations were primarily concerned with the quantification of the conditional shear stress in hydraulically smooth and rough boundary layer flows. They, however, documented the presence of a dominant turbulence to generate bursting events. Figures 6.23a, b show the near-bed flow visualization by Mao (2003) illustrating a single ejection and sweep in smooth boundary layer flow. These events that were well recognized are characterized by highly intermittent with large amplitudes and turbulent time-scales. However, no consensus has so far been achieved concerning a formal scaling law for these structures, because the complex mutual interaction between bursts and suspended particles is far from being understood.

Attempts were primarily made to determine the link between the coherent structures and sediment transport. Sediment particles are found to respond to different flow structures in bed- and suspended-load transports. The general opinion is that the bed-load transport arises from pressure fluctuations induced by sweeps at the bed; while ejections lift the particles in suspension in turbulent flow. Sumer and Oguz (1978) and Sumer and Deigaard (1981) experimentally studied the near-bed motion of sediment particles in hydraulically smooth and rough flow regimes. They observed that the kinematics in connection with the particle motion is in good agreement with the bursting events in both flow regimes. The underlying mechanism is that the lifting up of the particles is strongly governed by the ejections. The process continues until the accompanying bursting structure breaks up. The lifting of particles then terminates, and they start to move (fall) toward the bed. On the way back to the bed, a particle may interact with newly generated ejecting fluid streaks due to other bursts, and then, the particle again starts to rise. In the case, where the particles turn back to reach the bed, they are lifted up again by the same mechanism. Sediment particles are thus suspended in this way. Nezu and Nakagawa (1993) documented that the vertical movements of the particles coincide with ejection and sweep velocities observed in bursting. They also argued that in a hydraulically rough flow, sweeps dominate over ejections. The sweeps are important in the near-bed shear layer for the re-suspension of the sediment particles. Soulsby et al. (1994) observed in a tidal flow, the vertical sediment flux to dominate by the dynamics of large-scale turbulent structures. They also argued that the damping of the turbulent kinetic energy is the cause of suspension, as was identified by Barenblatt (1955) and Smith and McLean (1977a). Niño and García (1996) and García et al. (1997) showed that in hydraulically smooth and rough flow regimes, ejections are responsible for particle entrainment into suspension if the particles are completely immersed in the viscous sublayer. This mechanism is independent of the relative roughness and in conformity with the previous findings by Grass (1971) and Grass

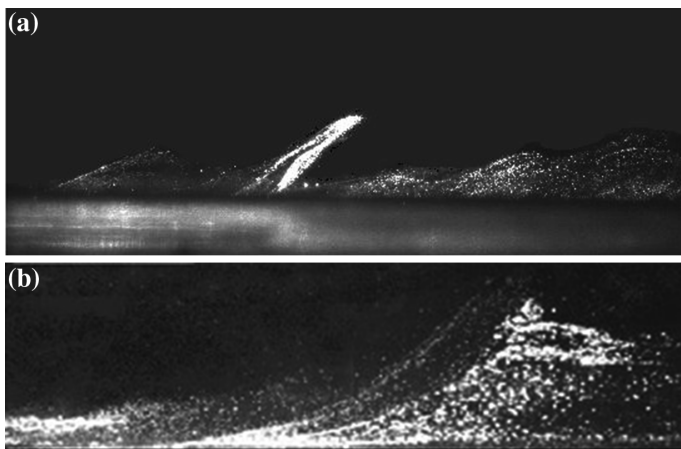


Fig. 6.23 **a** Single ejection, and **b** sweep over a bed having $k_s \approx 0.1$ mm (Mao 2003)

et al. (1993), who also reported that ejections and sweeps occur in a similar manner in both smooth and rough shear flows. Hurther and Lemmin (2003) observed that the coherent structures are important contributors to suspended sediment transport. Strong structures that persist for 30 % of the time carry about 50 % of the vertical sediment flux. This indicates that the suspended-load transport is strongly intermittent and that the sediment concentration along vertical varies strongly. Nezu and Azuma (2004) found that the vertical component of turbulence intensities of particles are more marked than the streamwise ones. It infers that the vertical motion of particles is more enhanced due to the bursting events. Cellino and Lemmin (2004) argued that the upward sediment flux $\overline{C'w'}$ is generally generated by ejections. The contribution of sweeps directed toward the sediment bed is always smaller than that of ejections. They noticed that the emergence of sediment clouds from the bed corresponds to the strong events of vertical velocity fluctuations, in general, and the strong ejections, in particular. The sediment cloud is coherent over entire flow depth with nearly invariant concentration. They also observed that in the events of downward vertical velocity fluctuations, the sediment cloud frequently disappears. Lelouvetel et al.'s (2009) study focused on the kind and the strength of turbulence structures involved in particle suspension. By applying the quadrant analysis to the flow in the vicinity of moving particles, they found that an upward motion of a particle is strongly correlated to the presence of ejections in the vicinity of the particle. For a given study, all particles surrounded by ejections with an instantaneous magnitude of momentum flux greater than a threshold value are lifted with a positive vertical velocity.

Mao (2003) used the particle image velocimetry (PIV) and the hydrogen bubble generator to study the bursting phenomenon over sediment beds. He observed the occurrence of quite a few ejections, termed a *multi-ejection* (Fig. 6.24a). It was found that with an increase in Re , when $R_* > 0.5$, the occurrence of multi-ejection

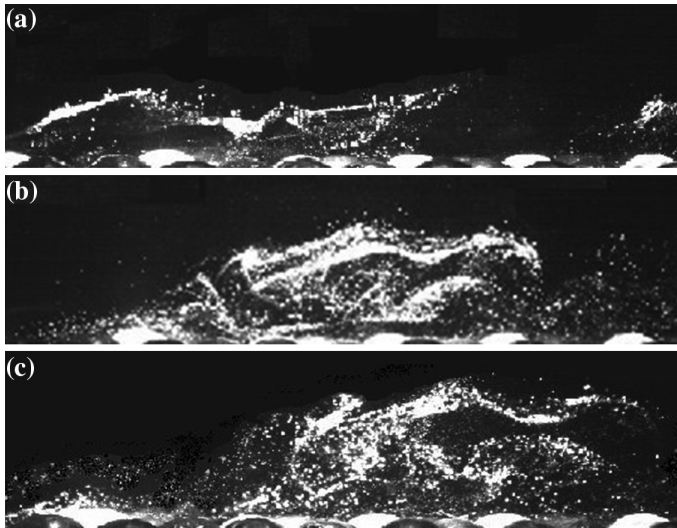


Fig. 6.24 **a** Beginning of multi-ejection, **b** beginning of sweeps, and **c** sweeping fluid streaks coming across an ejection cushion over a bed having $k_s \approx 6$ mm (Mao 2003)

becomes more common instead of a single ejection; and the sweeps are reduced. For larger roughness k_s , multi-ejection plays a leading role. With an increase in R_* , the magnitude of kinetic energy in the main flow and the turbulent kinetic energy near the bed increase, and thus, the ejection density increases as well. In contrast, the sweeps encounter the resistance from the so-called *ejection cushion* formed by the multi-ejection (Figs. 6.24b, c). Sediment particles from the bed are ejected to a certain height to start their movement in suspension. As the flow velocity increases, multi-ejection becomes more frequent, for which fluid streaks are ejected at a higher elevation with a longer period of ejection. On the other hand, the sediment particles in suspension may fall by the gravity, but the ejection cushion may prevent them from falling. The relative thickness of the ejection cushion increases with R_* , implying the particles in suspension to move further.

Breugem (2012) conducted experiments to study the vertical transport process of suspended sediment particles and the role of turbulence in transporting them under a fully developed flow condition. Experiments were performed by feeding sediment into the flow at the far upstream of the measuring zone. The flow velocity was measured by a particle image velocimetry (PIV), and the velocities of individual sediment particles were detected by a particle tracking velocimetry (PTV).

His observation is shown schematically in Fig. 6.25 that illustrates the occurrence of a hairpin vortex parcel, consisting of multiple aligned hairpin vortices separated each other by an internal shear layer, and the trajectories of two particles. From the near-bed flow region, particles are transported upwards by ejection events ($Q2$), leading to an increase in number of upward moving particles in ejections. Some of these particles are also transported above the hairpin vortex.

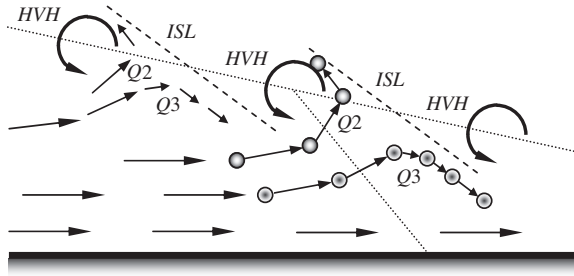


Fig. 6.25 Schematic of the mechanism of particle transport in a fully developed boundary layer flow illustrating a hairpin vortex parcel and two typical particles in a frame moving with the convective velocity of hairpin vortex parcel. *ISL* is the internal shear layer and *HVH* is the hairpin vortex head (Breugem 2012)

Only those particles end up in sweep events ($Q4$), leading to a decrease in number of particles in sweeps. Other particles end up in inward interaction events ($Q3$) induced by an upstream hairpin vortex, leading to an increase in number of downward moving particles in inward interactions.

As the sediment particles were observed more frequently in ejections and inward interactions and less frequently in sweeps, they encounter more frequently with low velocity flow structures. This is the governing mechanism to have an average streamwise particle velocity that is lower than the average streamwise flow velocity. To be more explicit, a net upward velocity, that the particles encounter, is resulted from an increased occurrence in ejections and is correlated with a flow velocity to be lower than the average flow velocity. In addition, due to an increased occurrence of inward interactions, the particles arrive from the near-bed flow region where the mean flow velocity is lower.

He recognized that the individual coherent structures transport particles in different modes than the way they transport momentum. Particles are transported upwards from higher to lower concentration zone by ejections and downwards by sweeps and inward interactions. Thus, sweeps have a different effect on momentum transport than on sediment transport. He also identified that each individual quadrant event is more efficient in transporting particles than momentum. In particular, ejections are more efficient in transporting particles than others. The net transport of sediment particles and momentum is the collective effect of all quadrant events.

6.9 Wash Load

Wash load is the portion of sediment that is transported by the stream flows, usually in a river, such that it always remains near the free surface as a near-permanent suspension (see Fig. 5.1). It is therefore transported without deposition,

essentially passing straight through the stream. It consists of the finest sediment particles and can approximately be defined by those having a Rouse number $\zeta < 0.8$, implying that the vertical turbulence intensity, that is root-mean-square of w' ($\sqrt{w'^2}$ being nearly equal to u_*), to retain the sediment is far greater than the terminal fall velocity w_s of the sediment.

Einstein et al. (1940) introduced a concept of wash load and defined as the finest size fractions of the total sediment-load, not at all present or hardly present in significant amounts in the streambed and banks. These size fractions are transported as suspended load through the channel over a long distance and scarcely deposited on the bed. The transport rate of wash load could be considered to depend upon the supply rate from the upstream catchment and that might not be uniquely related to the hydraulic parameters of the flow. Einstein (1950) recommended that the limiting (largest) size of sediment for the wash load could be arbitrarily chosen as that particle size d_{10} for which 10 % of the bed sediment is finer. However, the *Subcommittee of Sediment Terminology* of the *American Geophysical Union* formally introduced a definition of wash load (Lane 1947): *Wash load is the part of the sediment load of a stream which is composed of particle sizes smaller than those found in appreciable quantities in the sifting portions of the streambed.* It is therefore not appropriate to identify wash load with suspended load, as the primary difference is that the former carries sediment particles that never come in contact with the bed or bed layer and the latter has a continuous exchange of sediment with the bed layer.

Besides Einstein and Lane, some other researchers also attempted to put forward the definition of wash load. Einstein and Chien (1953a, b) argued against the general belief that the sediment transported by wash load is never deposited on the riverbed. They also argued that the wash load could not be predicted from Einstein's bed-load approach. Shen (1970) defined the wash load as the sediment transport rate of a given size for which the sediment supply rate is less than the sediment transport capacity by the flow for a given hydraulic condition. According to Partheniades (1977), the wash load may be governed by two different types of sediment transport processes. They may either exist separately or coexist. The first type refers to a bed-load function for a limited range of discharge. For a higher discharge, it may behave as a wash load without depositing particles over the bed; while for a lower discharge, the sediment can simply be deposited over the river bed. On the other hand, the second type of sediment transport does correspond to a bed-load function. The sediment in wash load is either transported as suspension without leaving any signature over the bed, or it is deposited on the bed in the enlarged zones, where considerably low bed shear stresses exist, such as in estuarine reaches of a channel or in a reservoir zone. Woo et al. (1986) stated that it was not feasible to specify the sediment size limit for the wash load. Nevertheless, many researchers assumed the limiting size of sediment carried by the wash load being approximately 0.0625 mm, which corresponds to the silt size.

Diplas and Parker (1992) recognized that when the sediment-laden flows containing fine sediment in suspension pass over a gravel-bed, the suspended fine

sediment interacts with the macro-roughness of the gravel-bed, infiltrates into the substrate, and becomes trapped within the interstices of gravels forming the bed. The fines deposited within the interstices of gravels can be re-entrained and washed out as a wash load by the subsequent clear-water flow. The condition of equilibrium between sediment concentration of wash load in the flow and the fraction of washed material (fine sediment) in the bed sediment was experimentally investigated by Khullar et al. (2010). They gave the suspended wash-load transport intensity Φ_{wi} relationship for such sediments as

$$\Phi_{wi} = 28(\zeta_{si}\Theta_i)^6 \quad (6.240a)$$

$$\log \left[\zeta_{si} \left(\frac{\tau_0}{\tau_{0av|c}} \right)^{0.62} \right] = 0.703 + 0.54 \log \left(\frac{d_i}{d_a} \right) + 0.0308 \left[\log \left(\frac{d_i}{d_a} \right) \right]^3 \quad (6.240b)$$

where ζ_{si} is the sheltering factor and $\tau_{0av|c}$ is the threshold bed shear stress for the average size d_a of a sediment mixture.

In conclusion, the prediction of wash-load transport rate still remains an elusive issue. It is generally acknowledged that the wash load is originated in the watershed and conveyed to the watercourse by an overland flow. It consists of very fine sediment that is mostly washed through the watercourse without contributing much to its sedimentation processes, but that generally provides the bulk of the contribution to estuarine sedimentation, lake and reservoir deposits. It is generally accepted that the wash load cannot be related to the traditional hydraulics of two-phase flow. However, aerial precipitation could be an important cause in producing the overland flow that brings the wash load to the watercourse contributing to the main stream flow.

6.10 Examples

Example 6.1 A natural stream has a bed slope of 5×10^{-3} and the flow depth of 1.2 m. The bed consists of fine sand with median size of 0.45 mm. Consider the sediment concentration at an elevation 0.06 m from the bed is 0.55. (1) Calculate the Rouse number and (2) plot the sediment concentration distribution between 0.06 mm and the free surface. Assume that the sediment concentration distribution follows the Rouse equation.

Solution

Given data are as follows:

Bed slope, $S_0 = 5 \times 10^{-3}$; flow depth, $h = 1.2$ m; reference level, $a = 0.06$ m; reference concentration, $C_a = 0.55$, and median size of sediment, $d_{50} = 0.45$ mm. Nominal diameter, $d_n = d_{50}/0.9 = 0.45/0.9 = 0.5$ mm

For $d_n = 0.5$ mm, the terminal fall velocity w_s has been calculated in Example 1.4.

Considering Cheng's formula (see Table 1.5), $w_s = 0.0611 \text{ m s}^{-1}$

Bed shear stress, $\tau_0 = \rho g h S_0 = 10^3 \times 9.81 \times 1.2 \times 5 \times 10^{-3} = 58.86 \text{ Pa}$

Shear velocity, $u_* = (\tau_0 / \rho)^{0.5} = (58.86 / 10^3)^{0.5} = 0.243 \text{ m s}^{-1}$

1. *Calculation of Rouse number:*

Considering $\beta = 1$ and $\kappa = 0.41$, calculate Rouse number

$$\zeta = \frac{0.0611}{1 \times 0.41 \times 0.243} = 0.613 \Leftarrow \text{Eq. (6.27)}$$

2. *Plotting of sediment concentration distribution:*

Using Rouse equation (Eq. 6.27), calculate sediment concentration distribution

$$\begin{aligned} C &= C_a \left(\frac{h-z}{z} \cdot \frac{a}{h-a} \right)^\zeta = 0.55 \left(\frac{1.2-z}{z} \cdot \frac{0.06}{1.2-0.06} \right)^{0.613} \\ &= 0.0905 \left(\frac{1.2-z}{z} \right)^{0.613} \end{aligned}$$

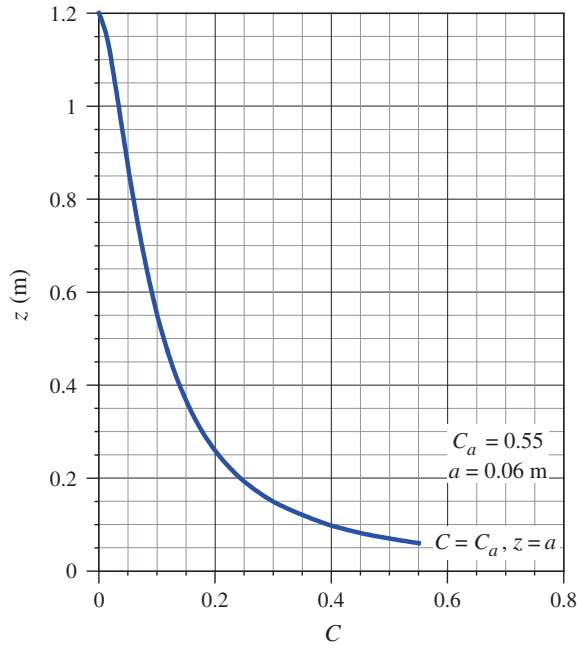
The sediment concentration distribution curve plotted using the above equation is shown in Fig. E6.1.

Example 6.2 Water flows through a wide channel with a flow rate per unit width of $12 \text{ m}^2 \text{ s}^{-1}$ having a uniform flow depth of 7 m. The channel has a streamwise bed slope of 2×10^{-4} . Relative density of sediment forming the bed is 2.65; sediment size, $d_{50} = 0.5$ mm and $d_{65} = 0.6$ mm, for which Manning roughness coefficient is 0.02 SI units. The terminal fall velocity of sediment particles is 0.072 m s^{-1} , static angle of repose is 32° , and porosity is 0.4. Assume coefficient of kinematic viscosity of water as $10^{-6} \text{ m}^2 \text{ s}^{-1}$.

Find the suspended-load transport rate by using the methods of (1) Lane and Kalinske,³ (2) Einstein, (3) Brooks, (4) Chang et al., (5) Bijker, (6) van Rijn, (7) Bagnold, and (8) Wu et al.

³ For Lane and Kalinske's method, they did not clearly define the reference level and its corresponding concentration. It is therefore suggested that one can consider reference level at 0.05 times the flow depth. However, the concentration at that level may be assumed as 10^{-3} , for solving this problem. Essentially, in practice, these two parameters are to be obtained from the measured concentration distributions.

Fig. E6.1 Sediment concentration distribution curve



Solution

Given data are as follows:

Flow rate per unit width, $q = 12 \text{ m}^2 \text{ s}^{-1}$; flow depth, $h = 7 \text{ m}$; bed slope, $S_0 = 2 \times 10^{-4}$; relative density of sediment, $s = 2.65$; sediment size, $d_{50} = 0.5 \text{ mm}$ and $d_{65} = 0.6 \text{ mm}$; Manning roughness coefficient, $n = 0.02$ SI units; terminal fall velocity of sediment, $w_s = 0.072 \text{ m s}^{-1}$; static angle of repose, $\phi = 32^\circ$; porosity of sediment, $\rho_0 = 0.4$; and coefficient of kinematic viscosity of water, $\nu = 10^{-6} \text{ m}^2 \text{ s}^{-1}$

Average flow velocity, $U = q/h = 12/7 = 1.714 \text{ m s}^{-1}$

Bed shear stress, $\tau_0 = \rho g h S_0 = 10^3 \times 9.81 \times 7 \times 2 \times 10^{-4} = 13.734 \text{ Pa}$

Shear velocity, $u_* = (\tau_0/\rho)^{0.5} = (13.734/10^3)^{0.5} = 0.117 \text{ m s}^{-1}$

Shields parameter, $\Theta = u_*^2/(\Delta g d_{50}) = 0.117^2/(1.65 \times 9.81 \times 0.5 \times 10^{-3}) = 1.691$

Use van Rijn's empirical formula for the determination of threshold bed shear stress and threshold shear velocity (see Table 4.1):

Particle parameter, $D_* = d_{50}(\Delta g/\nu^2)^{1/3} = 0.5 \times 10^{-3}[1.65 \times 9.81/(10^{-6})^2]^{1/3} = 12.648$

Threshold Shields parameter, $\Theta_c(10 < D_* \leq 20) = 0.04 D_*^{-0.1} = 0.04 \times 12.648^{-0.1} = 0.031$

Threshold bed shear stress, $\tau_{0c} = \Theta_c \Delta \rho g d_{50} = 0.031 \times 1.65 \times 10^3 \times 9.81 \times 0.5 \times 10^{-3} = 0.251 \text{ Pa}$

Threshold shear velocity, $u_{*c} = (\tau_{0c}/\rho)^{0.5} = (0.251/10^3)^{0.5} = 0.016 \text{ m s}^{-1}$

Use Zanke's formula to calculate threshold flow velocity [see Eq. (4.7)]:

Consider $c_1 = 1$ for noncohesive sediment.

Threshold flow velocity, $U_{cr} = 2.8(1.65 \times 9.81 \times 0.5 \times 10^{-3})^{0.5} + 14.7 \times 1[10^{-6}/(0.5 \times 10^{-3})] = 0.281 \text{ m s}^{-1} \Leftarrow \text{Eq. (4.7)}$

Calculation for other parameters:

Rouse number, $\zeta(\beta = 1) = w_s/(\kappa u_*) = 0.072/(0.41 \times 0.117) = 1.5 \Leftarrow \text{Eq. (6.27)}$

Ratio w_s to u_* , $w_s/u_* = 0.072/0.117 = 0.615$

Hence, $0.1 < w_s/u_* < 1$; and factor $\beta = 1 + 2(0.072/0.117)^2 = 1.757 \Leftarrow \text{Eq. (6.19)}$

Exponent of Chang et al. equation, $\zeta_1 = 2w_s/(\beta \kappa u_*) = 2 \times 0.072/(1.757 \times 0.41 \times 0.117) = 1.71 \Leftarrow \text{Eq. (6.144)}$

Note: Regarding the choice of reference level a and the corresponding estimation of reference concentration C_a , there are several formulas given in Sect. 6.2.8. In the following, the solutions are obtained from the consideration of a and C_a as given by respective investigators.

1. *Lane and Kalinske's method:*

For $w_s/u_* = 0.615$ and $n/h^{1/6} = 0.02/(275.6)^{1/6} = 7.84 \times 10^{-3}$

In the above, n is in SI units and h in inches, $h = 7 \text{ m} = 275.6$

Note that Fig. 6.10 does not provide a curve for $n/h^{1/6} = 0.00784$. Therefore, an approximate extrapolated value of P_C is considered as 0.15 for $w_s/u_* = 0.615$ and $n/h^{1/6} = 7.84 \times 10^{-3}$

Given $a = 0.05 \times 7 = 0.35 \text{ m}$ and $C_a = 10^{-3}$

$$\frac{15w_s a}{u_* h} = \frac{15 \times 0.072 \times 0.35}{0.117 \times 7} = 0.462$$

$$\begin{aligned} q_s &= 129.1 \times 10^{-3} \times 0.15 \times \exp(0.462) = 0.031 \text{ ft}^2 \text{ s}^{-1} \\ &= 2.88 \times 10^{-3} \text{ m}^2 \text{ s}^{-1} \Leftarrow \text{Eq. (6.123)} \end{aligned}$$

In the above, q is in $\text{ft}^2 \text{ s}^{-1}$, $q = 12 \text{ m}^2 \text{ s}^{-1} = 129.1 \text{ ft}^2 \text{ s}^{-1}$

$$g_s = 2.88 \times 10^{-3} \times 2.65 \times 10^3 \times 9.81 = 70.632 \text{ N s}^{-1} \text{ m}^{-1}$$

2. *Einstein's method:*

$a = k_s = 2d_{50} = 2 \times 0.5 \times 10^{-3} = 10^{-3} \text{ m}$ (according to Einstein), $\tilde{a} = a/h = 10^{-3}/7 = 1.429 \times 10^{-4}$

From Figs. 6.11 and 6.12, $I_1 = 0.42$ and $I_2 = -2.95$ for $\tilde{a} = 1.429 \times 10^{-4}$ and $\zeta = 1.5$

$$J_1 = I_1/0.216 = 0.42/0.216 = 1.94$$

$$J_2 = I_2/0.216 = -2.95/0.216 = -13.657$$

$$\Psi_b = 1/\Theta [\text{or } \Delta d_{50}/(hS_0)] = 1/1.691 = 0.591$$

From Fig. 5.10, $\Phi_b(\Psi_b = 0.591) = 12$

$$C_a = 12/(23.2 \times 1.691^{0.5}) = 0.4 \Leftarrow \text{Eq. (6.109)}$$

Note, it is assumed that $u'_* = u_*$

The viscous sublayer thickness, $\delta' = 11.6\nu/u'_* = 11.6 \times 10^{-6}/0.117 = 9.915 \times 10^{-5} \text{ m}$
 $d_{65}/\delta' = 0.6 \times 10^{-3}/9.915 \times 10^{-5} = 6.05$

From Fig. 5.7, correction factor $x_k = 1.03$ for $d_{65}/\delta' = 6.05$. The apparent roughness $\Delta_k = d_{65}/x_k = 0.6 \times 10^{-3}/1.03 = 5.825 \times 10^{-4} \text{ m}$

$$P_E = \ln\left(\frac{30.2 \times 7}{5.825 \times 10^{-4}}\right) = 12.802 \Leftarrow \text{Eq. (6.129)}$$

$$q_s = \frac{0.4 \times 0.117 \times 10^{-3}}{0.41} (12.802 \times 1.94 - 13.657) = 1.276 \times 10^{-3} \text{ m}^2 \text{ s}^{-1}$$

$\Leftarrow \text{Eq. (6.129)}$

$$g_s = 1.276 \times 10^{-3} \times 2.65 \times 10^3 \times 9.81 = 33.17 \text{ N s}^{-1} \text{ m}^{-1}$$

3. Brooks' method:

$$\kappa U/u_* = 0.41 \times 1.714/0.117 = 6.006$$

From Fig. 6.13, $q_s/(qC_{0.5h}) = 17$, for $\zeta = 1.5$ and $\kappa U/u_* = 6.006$

$$\tilde{a} = 1.429 \times 10^{-4} \quad \text{and} \quad C_a = 0.4$$

$$C_{0.5h} = 0.4 \left(\frac{1 - 0.5}{0.5} \cdot \frac{1.429 \times 10^{-4}}{1 - 1.429 \times 10^{-4}} \right)^{1.5} = 6.831 \times 10^{-7} \Leftarrow \text{Eq. (6.27)}$$

$$q_s = 17(qC_{0.5h}) = 17(12 \times 6.831 \times 10^{-7}) = 1.394 \times 10^{-4} \text{ m}^2 \text{ s}^{-1}$$

$$g_s = 1.394 \times 10^{-4} \times 2.65 \times 10^3 \times 9.81 = 3.624 \text{ N s}^{-1} \text{ m}^{-1}$$

4. Chang et al.'s method:

$$\zeta_1 = 1.71$$

$$c_j = 10$$

$$a = 10 \frac{13.734 - 0.251}{(1 - 0.4)1.65 \times 10^3 \times 9.81 \times \tan 32^\circ} = 0.022 \text{ m} \Leftarrow \text{Eq. (6.149)}$$

$$\tilde{a} = a/h = 0.022/7 = 3.143 \times 10^{-3}$$

From Figs. 6.14 and 6.15, $I_3 = 0.0252$ and $I_4 = 0.0191$ for $\tilde{a} = 3.143 \times 10^{-3}$ and $\zeta = 1.71$

$$q_b = \Phi_b(\Delta g d_{50}^3)^{0.5} = 12[1.65 \times 9.81(0.5 \times 10^{-3})^3]^{0.5} = 5.398 \times 10^{-4} \text{ m}^2 \text{ s}^{-1}$$

$$\begin{aligned} q_s &= \frac{5.398 \times 10^{-4} \times 7}{0.8 \times 1.714 \times 0.022} \left(1.714 \times 0.0252 - \frac{2 \times 0.117}{0.41} 0.0191 \right) \\ &= 4.045 \times 10^{-3} \Leftarrow \text{Eq. (6.148)} \end{aligned}$$

$$g_s = 4.045 \times 10^{-3} \times 2.65 \times 10^3 \times 9.81 = 105.16 \text{ N s}^{-1} \text{ m}^{-1}$$

5. *Bijker's method:*

$$J_1 = 1.94$$

$$J_2 = -13.657$$

$$q_b = 5.398 \times 10^{-4} \text{ m}^2 \text{ s}^{-1}$$

$$C_a = 5.398 \times 10^{-4} / (6.34 \times 0.117 \times 10^{-3}) = 0.728 \Leftarrow \text{Eq. (6.111)}$$

$$P_{\text{EI}} = \ln \left(\frac{33 \times 7}{10^{-3}} \right) = 12.35 \Leftarrow \text{Eq. (6.150)}$$

$$\begin{aligned} q_s &= \frac{0.728 \times 0.117 \times 10^{-3}}{0.41} (12.35 \times 1.94 - 13.657) = 2.14 \times 10^{-3} \text{ m}^2 \text{ s}^{-1} \\ &\Leftarrow \text{Eq. (6.150)} \end{aligned}$$

$$g_s = 2.14 \times 10^{-3} \times 2.65 \times 10^3 \times 9.81 = 55.63 \text{ N s}^{-1} \text{ m}^{-1}$$

6. *van Rijn's method:*

$$\begin{aligned} q_s &= 0.012 \times 1.714 \times 7 \left[\frac{1.714 - 0.281}{(1.65 \times 9.81 \times 0.5 \times 10^{-3})^{0.5}} \right]^{2.4} \left(\frac{0.5 \times 10^{-3}}{7} \right) \frac{1}{12.648^{0.6}} \\ &= 1.723 \times 10^{-3} \text{ m}^2 \text{ s}^{-1} \Leftarrow \text{Eq. (6.156)} \end{aligned}$$

$$g_s = 1.723 \times 10^{-3} \times 2.65 \times 10^3 \times 9.81 = 44.792 \text{ N s}^{-1} \text{ m}^{-1}$$

7. *Bagnold's method:*

$$g_s = 0.01 \times 13.734 \frac{2.65}{1.65} \cdot \frac{1.714^2}{0.072} = 9 \text{ N s}^{-1} \text{ m}^{-1} \Leftarrow \text{Eq. (6.185)}$$

8. *Wu et al.'s method:*

$$\Phi_s = 2.62 \times 10^{-5} \left[\left(\frac{13.734}{0.251} - 1 \right) \frac{1.714}{0.072} \right]^{1.74} = 6.67 \Leftarrow \text{Eq. (6.186)}$$

$$q_s = 6.67 [1.65 \times 9.81 (0.5 \times 10^{-3})^3]^{0.5} = 3 \times 10^{-4} \text{ m}^2 \text{ s}^{-1}$$

$$g_s = 3 \times 10^{-4} \times 2.65 \times 10^3 \times 9.81 = 7.8 \text{ N s}^{-1} \text{ m}^{-1}$$

References

- Akiyama J, Fukushima Y (1986) Entrainment of noncohesive sediment into suspension. In: Wang SY, Shen HW, Ding LZ (eds) Proceedings of the third symposium on river sedimentation. University of Mississippi, Mississippi, pp 804–813
- Antsyferov SM, Kos'yan RD (1980) Sediment suspended in stream flow. *J Hydraul Div* 106(2):313–330
- Bagnold RA (1954) Experiments on a gravity-free dispersion of large solid spheres in a Newtonian fluid under shear. *Proc R Soc London A* 255(1160):49–63
- Bagnold RA (1966) An approach to the sediment transport problem from general physics. Geological survey professional paper 422-I, Washington, DC
- Barenblatt GI (1955) On the motions of suspended particles in a turbulent flow occupying a half-space or a plane open channel of finite depth. *Prikladnaya Matematika i Mekhanika* 19(1):61–88 (in Russian)
- Barenblatt GN (1956) The suspended sediment movement in turbulent flow. Water Conservancy Press, Beijing
- Bijker EW (1971) Longshore transport computations. *J Waterways Harbors Coast Eng Div* 97(4):687–701
- Bose SK (2009) Numeric computing in Fortran. Narosa, New Delhi
- Bose SK, Dey S (2009a) Reynolds averaged theory of turbulent shear flow over undulating beds and formation of sand waves. *Phys Rev E* 80:036304
- Bose SK, Dey S (2009b) Suspended-load of sediment in flow on erodible beds. *Int J Sediment Res* 24(3):315–324
- Bose SK, Dey S (2010) Universal probability distributions of turbulence in open channel flows. *J Hydraul Res* 48(3):388–394
- Bose SK, Dey S (2013) Sediment entrainment probability and threshold of sediment suspension: exponential-based approach. *J Hydraul Eng* 139(10):1099–1106
- Breugem A (2012) Transport of suspended particles in turbulent open channel flows. PhD thesis, Delft University of Technology, Meppel
- Brooks NH (1954) Laboratory studies of the mechanics of streams flowing over a movable bed of fine sand. Doctoral thesis, California Institute of Technology, Pasadena
- Brooks NH (1963) Calculation of suspended load discharge from velocity concentration parameters. In: Proceedings of the federal interagency sediment conference, United States Department of Agriculture, pp 229–237
- Brown GL (2008) Approximate profile of nonequilibrium suspended sediment. *J Hydraul Eng* 134(7):1010–1014

- Brush LM, Ho HW, Singamsetti SR (1962) A study of sediment in suspension. Publication number 59, International Association for the Science of Hydraulics, IASH Commission of Land Erosion, Bari
- Castro-Organ O, Giráldez JV, Mateos L, Dey S (2012) Is the von Kármán constant affected by sediment suspension? *J Geophys Res* 117(F04002). doi:10.1029/2011JF002211
- Celik I, Rodi W (1984) A deposition entrainment model for suspended sediment transport. Report SFB 210/T/6, University of Karlsruhe, Karlsruhe
- Celik I, Rodi W (1991) Suspended sediment-transport capacity for open channel flow. *J Hydraul Eng* 117(2):191–204
- Cellino M, Graf WH (1999) Sediment-laden flow in open-channels under noncapacity and capacity conditions. *J Hydraul Eng* 125(5):455–462
- Cellino M, Lemmin U (2004) Influence of coherent flow structures on the dynamics of suspended sediment transport in open-channel flow. *J Hydraul Eng* 130(11):1077–1088
- Chang FM, Simons DB, Richardson EV (1965) Total bed-material discharge in alluvial channels. Paper 1498-I, United States Geological Survey Water Supply, Washington, DC
- Chang HH (1988) Fluvial processes in river engineering. Wiley, New York
- Cheng KJ (1985) An integrated suspended load equation for non-equilibrium transport of non-uniform sediment. *J Hydrol* 79(3–4):359–364
- Cheng N-S (1997) Simplified settling velocity formula for sediment particle. *J Hydraul Eng* 123(2):149–152
- Cheng N-S, Chiew Y-M (1998) Pickup probability for sediment entrainment. *J Hydraul Eng* 124(2):232–235
- Cheng N-S, Chiew Y-M (1999) Analysis of initiation of sediment suspension from bed load. *J Hydraul Eng* 125(8):855–861
- Chien N (1954) The present status of research on sediment transport. *Proc Am Soc Civ Eng* 80:565–1–565–33
- Cioffi F, Gallerano F (1991) Velocity and concentration profiles of solid particles in a channel with movable and erodible bed. *J Hydraul Res* 29(3):387–401
- Coleman NL (1970) Flume studies of the sediment transfer coefficient. *Water Resour Res* 6(3):801–809
- Coleman NL (1981) Velocity profiles with suspended sediment. *J Hydraul Res* 19(3):211–227
- Coleman NL (1986) Effects of suspended sediment on the open-channel velocity distribution. *Water Resour Res* 22(10):1377–1384
- Dey S (1999) Sediment threshold. *Appl Math Model* 23(5):399–417
- Dey S, Das R, Gaudio R, Bose SK (2012) Turbulence in mobile-bed streams. *Acta Geophys* 60(6):1547–1588
- Dey S, Dey Sarker HK, Debnath K (1999) Sediment threshold under stream flow on horizontal and sloping beds. *J Eng Mech* 125(5):545–553
- Diplas P, Parker G (1992) Deposition and removal of fines in gravel bed streams. In: Hey RD, Thorne CR, Billi P (eds) *Dynamics of gravel bed rivers*. Wiley, New York, pp 313–329
- du Boys MP (1879) Le rhone et les rivieres a lit affouillable. *Annales des Ponts et Chaussées* 18(5):141–195
- Einstein HA (1950) The bed-load function for sediment transportation in open channel flows. Technical bulletin number 1026, United States Department of Agriculture, Soil Conservation Service, Washington, DC
- Einstein HA, Anderson AG, Johnson JW (1940) A distinction between bed-load and suspended load in natural streams. *Trans Am Geophys Union* 21(2):628–633
- Einstein HA, Chien N (1953a) Transport of sediment mixtures with large range of grain sizes. Missouri River Division series number 2, Institute of Engineering Research, University of California, Berkeley, California
- Einstein HA, Chien N (1953b) Can the rate of wash load be predicted from the bed load function? *Trans Am Geophys Union* 34(6):876–882

- Einstein HA, Chien N (1955) Effects of heavy sediment concentration near the bed on the velocity and sediment distribution. Institute of Engineering Research, Report number 8, University of California, Berkeley, California
- Elata C, Ippen AT (1961) The dynamics of open channel flow with suspensions of neutrally buoyant particles. Technical report number 45, Massachusetts Institute of Technology, Boston
- Engelund F, Fredsøe J (1976) A sediment transport model for straight alluvial channels. *Nord Hydrol* 7(5):293–306
- Engelund F, Fredsøe J (1982) Hydraulic theory of alluvial rivers. In: Chow VT (ed) *Advances in hydrosociences*, vol 13. Academic Press, San Diego, California, pp 187–215
- Exner FM (1925) Über die wechselwirkung zwischen wasser und geschiebe in flüssen. *Sitzungsberichte der Akademie der Wissenschaften* 134(2a):165–203
- Fredsøe J, Deigaard R (1992) *Mechanics of coastal sediment transport*. World Scientific, Singapore
- Fujita M, Mizuyama T (2000) A diffusion model for suspended sediment in mountain streams. In: *Proceedings of the twelfth congress of the Asia Pacific Division of the International Association of Hydraulic Engineering and Research*, Bangkok, pp 255–264
- García MH (2008) Sediment transport and morphodynamics. In: García MH (ed) *Sedimentation engineering: processes, measurements, modeling, and practice*. Manuals and reports on engineering practice number 110, American Society of Civil Engineers, Reston, pp 21–163
- García MH, Parker G (1991) Entrainment of bed sediment into suspension. *J Hydraul Eng* 117(4):414–434
- García MH, Niño Y, López F (1997) *Coherent flow structures in open channels*. Wiley, New York
- Gaudio R, Dey S (2012) Evidence of non-universality of von Kármán's κ . In: Rowinski P (ed) *Experimental and computational solutions of hydraulic problems*. Springer, Heidelberg, pp 71–83
- Gaudio R, Miglio A, Dey S (2010) Non-universality of von Kármán's κ in fluvial streams. *J Hydraul Res* 48(5):658–663
- Grass AJ (1971) Structural features of turbulent flow over smooth and rough boundaries. *J Fluid Mech* 50:233–255
- Grass AJ, Stuart RJ, Mansour-Tehrani M (1993) Common vertical structure of turbulent flows over smooth and rough boundaries. *Am Inst Aeronaut Astronaut J* 31(5):837–847
- Guo J (2002) Logarithmic matching and its applications in computational hydraulics and sediment transport. *J Hydraul Res* 40(5):555–565
- Guo J, Julien PY (2001) Turbulent velocity profiles in sediment-laden flows. *J Hydraul Res* 39(1):11–23
- Guo J, Julien PY (2004) Efficient algorithm for computing Einstein integrals. *J Hydraul Eng* 130(12):1198–1201
- Guo J, Wood WL (1995) Fine suspended sediment transport rates. *J Hydraul Eng* 121(12):919–922
- Gust G (1984) Discussion of 'Velocity profile with suspended sediment'. *J Hydraul Res* 22(4):263–289
- Hino M (1963) Turbulent flow with suspended particles. *J Hydraul Div* 89(4):161–185
- Hjelmfelt A, Lenau C (1970) Nonequilibrium transport of suspended sediment. *J Hydraul Div* 96(7):1567–1586
- Hunt JN (1954) The turbulent transport of suspended sediment in open channels. *Proc R Soc London A* 224(1158):322–335
- Hurth D, Lemmin U (2003) Turbulent particle flux and momentum flux statistics in suspension flow. *Water Resour Res* 39(5):1139. doi:10.1029/2001WR001113
- Ippen AT (1971) A new look at sedimentation in turbulent streams. *J Boston Soc Civ Eng* 58(3):131–163
- Itakura T, Kishi T (1980) Open channel flow with suspended sediments. *J Hydraul Div* 106(8):1325–1343

- Jobson JE, Sayre WW (1970) Vertical transfer in open channel flow. *J Hydraul Div* 96(3):703–724
- Keulegan GH (1938) Laws of turbulent flow in open channels. *J Res Natl Bur Stand* 21(6):707–741
- Khullar NK, Kothiyari UC, Ranga Raju KG (2010) Suspended wash load transport of nonuniform sediments. *J Hydraul Eng* 136(8):534–543
- Lane EW (1947) Report of the subcommittee on sediment terminology. *Trans Am Geophys Union* 28(6):936–938
- Lane EW, Kalinske AA (1941) Engineering calculations of suspended sediment. *Trans Am Geophys Union* 20(3):603–607
- Laursen EM (1980) A concentration distribution formula from the revised theory of Prandtl mixing length. In: *Proceedings of the first international symposium on river sedimentation*. Guanghua Press, Beijing, pp 237–244
- Lavelle JW, Thacker WC (1978) Effects of hindered settling on sediment concentration profiles. *J Hydraul Res* 16(4):347–355
- Lelouvetel J, Bigillon F, Doppler D, Vinkovic I, Champagne J-Y (2009) Experimental investigation of ejections and sweeps involved in particle suspension. *Water Resour Res* 45:W02416. doi:10.1029/2007WR006520
- Liggett JA (1994) *Fluid mechanics*. McGraw-Hill, New York
- Lyn DA (1986) Turbulence and turbulent transport in sediment-laden open-channel flows. Report number KH-R-49, WM Keck Laboratory of Hydraulic and Water Resources, California Institute of Technology, Pasadena
- Lyn DA (1988) A similarity approach to turbulent sediment laden flows in open channels. *J Fluid Mech* 193:1–26
- Lyn DA (1992) Turbulence characteristics of sediment-laden flows in open channels. *J Hydraul Eng* 118(7):971–988
- Majumdar H, Carstens MR (1967) Diffusion of particles by turbulence: effect on particle size. WRC-0967, Water Resources Center, Georgia Institute of Technology, Atlanta
- Mao Y (2003) The effects of turbulent bursting on the sediment movement in suspension. *Int J Sediment Res* 18(2):148–157
- McLean SR (1991) Depth-integrated suspended-load calculations. *J Hydraul Eng* 117(11):1440–1458
- McLean SR (1992) On the calculation of suspended load for noncohesive sediments. *J Geophys Res* 97(C4):5759–5770
- McTigue DF (1981) Mixture theory for suspended sediment transport. *J Hydraul Div* 107(6):659–673
- Mei CC (1969) Nonuniform diffusion of suspended sediment. *J Hydraul Div* 95(1):581–584
- Montes JS (1973) Interaction of two dimensional turbulent flow with suspended particles. PhD thesis, Massachusetts Institute of Technology, Cambridge
- Muste M (2002) Sources of bias errors in flume experiments on suspended-sediment transport. *J Hydraul Res* 40(6):695–708
- Nakato T (1984) Numerical integration of Einstein's integrals, I_1 and I_2 . *J Hydraul Eng* 110(12):1863–1868
- Nezu I (1977) Turbulent structure in open channel flow. PhD thesis, Kyoto University, Kyoto
- Nezu I, Azuma R (2004) Turbulence characteristics and interaction between particles and fluid in particle-laden open channel flows. *J Hydraul Eng* 130(10):988–1001
- Nezu I, Nakagawa H (1993) *Turbulence in open-channel flows*. Balkema, Rotterdam
- Ni JR, Wang GQ (1991) Vertical sediment distribution. *J Hydraul Eng* 117(9):1184–1194
- Nielsen P (1992) *Coastal bottom boundary layers and sediment transport*. World Scientific, Singapore
- Niño Y, García MH (1996) Experiments on particle-turbulence interactions in the near-wall region of an open channel flow: implications for sediment transport. *J Fluid Mech* 326:285–319

- Nouh M (1989) The von-Kármán coefficient in sediment laden flow. *J Hydraul Res* 27(4):477–499
- Parker G, Coleman NL (1986) Simple model for sediment laden flows. *J Hydraul Eng* 112(5):356–375
- Partheniades E (1977) Unified view of wash load and bed material load. *J Hydraul Eng* 103(9):1037–1057
- Richardson JF, Zaki WN (1954) Sedimentation and fluidisation, part I. *Trans Inst Chem Eng* 32(1):35–53
- Rouse H (1937) Modern conceptions of the mechanics of turbulence. *Trans Am Soc Civ Eng* 102:463–505
- Samaga BR, Ranga Raju KG, Garde RJ (1986) Suspended load transport rate of sediment mixture. *J Hydraul Eng* 112(11):1019–1038
- Schmidt W (1925) Der massenaustausch in freier luft und verwandte erscheinungen. *Probleme der Kosmischen Physik*, vol 7, Hamburg
- Shen HW (1970) Wash load and bed load. In: Shen HW (ed) *River mechanics*, vol I. Fort Collins, Colorado, pp 11.1–11.30
- Smith JD, McLean SR (1977a) Spatially averaged flow over a wavy surface. *J Geophys Res* 82(12):1735–1746
- Smith JD, McLean SR (1977b) Boundary layer adjustments to bottom topography and suspended sediment. In: Nihoul JCJ (ed) *Bottom turbulence*, vol 112., *Proceedings of the eighth international liege colloquium on ocean hydrodynamics*, Elsevier Scientific Publishing Company, Liege, pp 123–151
- Soulsby RL, Atkins R, Salkield AP (1994) Observations of the turbulent structures of a suspension of sand in a tidal current. *Cont Shelf Res* 14(4):429–435
- Sumer BM (1986) Recent developments on the mechanics of sediment suspension. In: Bechteler W (ed) *Transport of suspended solids in open channels*, Euromech 192, Neubiberg. Balkema, Rotterdam, pp 3–13
- Sumer BM, Deigaard R (1981) Particle motions near the bottom in turbulent flow in an open channel, Part 2. *J Fluid Mech* 109:311–337
- Sumer BM, Oguz B (1978) Particle motions near the bottom in turbulent flow in an open channel. *J Fluid Mech* 86:109–127
- Tanaka S, Sugimoto S (1958) On the distribution of suspended sediment in experimental flume flow. *Mem Fac Eng Kobe Univ* 5:61–71
- Umeiyama M (1992) Vertical distribution of suspended sediment in uniform open-channel flow. *J Hydraul Eng* 118(6):936–941
- Umeiyama M, Gerritsen F (1992) Velocity distribution in uniform sediment-laden flow. *J Hydraul Eng* 118(2):229–245
- Valiani A (1988) An open question regarding shear flow with suspended sediments. *Meccanica* 23(1):36–43
- van Ingen C (1983) A signal-processing system for laser-Doppler velocimetry in solid-liquid flows. Report UCBIHEL-83102, Hydraulic Engineering Laboratory, University of California, Berkeley, California
- van Rijn LC (1984a) Sediment transport, part I: bed load transport. *J Hydraul Eng* 110(10):1431–1456
- van Rijn LC (1984b) Sediment transport, part II: suspended load transport. *J Hydraul Eng* 110(11):1613–1641
- van Rijn LC (1986) Mathematical modeling of suspended sediment in nonuniform flows. *J Hydraul Eng* 112(6):433–455
- Vanoni VA (1946) Transportation of suspended sediment by water. *Trans Am Soc Civ Eng* 111:67–102
- Vanoni VA, Nomicos GN (1960) Resistance properties of sediment-laden streams. *Trans Am Soc Civ Eng* 125:1140–1167
- Velikanov MA (1954) Principle of the gravitational theory of the movement of sediments. *Acad Sci Bull, Geophys Ser* 4

- Velikanov MA (1958) Alluvial process (fundamental principles). State Publishing House of Theoretical and Technical Literature, Russia
- Wang X, Qian N (1989) Turbulence characteristics of sediment-laden flow. *J Hydraul Eng* 115(6):781–800
- Wang X, Qian N (1992) Velocity profiles of sediment-laden flow. *Int J Sediment Res* 7(1):27–58
- Wang X, Wang ZY, Yu M, Li D (2001) Velocity profile of sediment suspensions and comparison of log-law and wake-law. *J Hydraul Res* 39(2):211–217
- White FM (1991) Viscous fluid flow. McGraw-Hill, New York
- WIHEE (1981) River sedimentation engineering. Hydraulic and Electric Press, Wuhan Institute of Hydraulic and Electric Engineering, China
- Willis JC (1979) Suspended load from error-function models. *J Hydraul Div* 105(7):801–816
- Wilson KC (1966) Bedload transport at high shear stresses. *J Hydraul Div* 92(6):49–59
- Woo HS, Julien PY, Richardson EV (1986) Wash load and fine sediment load. *J Hydraul Eng* 112(6):541–545
- Wright S, Parker G (2004) Flow resistance and suspended load in sand-bed rivers: simplified stratification model. *J Hydraul Eng* 130(8):796–805
- Wu W, Wang SSY, Jia Y (2000) Nonuniform sediment transport in alluvial rivers. *J Hydraul Res* 38(6):427–434
- Xie JH (1981) River sediment engineering, vol 1. Water Resources Press, Beijing (in Chinese)
- Yalin MS, Karahan E (1979) Inception of sediment transport. *J Hydraul Div* 105(11):1433–1443
- Zagustin K (1968) Sediment distribution in turbulent flow. *J Hydraul Res* 6(2):163–172
- Zhang Q, Zhang Z, Yue J, Duan Z, Dai M (1983) A mathematical model for prediction of the sedimentation process in rivers. In: Proceedings of the second international symposium on river sedimentation, Nanjing
- Zhang RJ (1961) River dynamics. Industry Press, Beijing (in Chinese)
- Zhang RJ, Xie JH (1993) Sedimentation research in China: systematic selections. Water and Power Press, Beijing
- Zyserman J, Fredsøe J (1994) Data analysis of bed concentration of suspended sediment. *J Hydraul Eng* 120(9):1021–1042

Chapter 7

Total-Load Transport

7.1 General

Quantification of the total sediment transport rate is necessary in studying the fluvial processes in a river. In fact, the sediment transport and the water discharge govern the dynamic stability or instability of the streambeds, such as aggradations and degradations. The total amount of sediment transported per unit time and width through a given section of a river for the given flow and sediment bed conditions is termed *total load*. Based on the mode of sediment transport, the total load is the sum of the bed load, suspended load, and wash load. In laboratory experimental studies, the wash load cannot be usually simulated; while it generally exists in natural streams and is often not insignificant, although it is a difficult proposition to separate out the wash load from the suspended load. To date, there are many formulas proposed by various investigators for the calculation of bed load, suspended load, and total load. As an informal way, the total load is also simply called the *bed-material load*¹ as it is made up of only those sediment particles consisting of sizes represented in the bed; and the wash load remains usually excluded in those formulas. This is the reason why the actual total load in a stream does not necessarily have to be exactly identical with the bed-material load. As discussed in Sect. 6.9, the amount of wash load depends mainly on the supply of very fine sediment from the watershed, being independent of the river hydraulics. Consequently, it is not possible to predict the wash load from the hydraulic characteristics of a river. Most of the total-load prediction formulas are therefore actually the total bed-material load prediction formulas. There are two general approaches to determine the total load:

Indirect approach: The total-load transport rate can be determined as the sum of bed load and suspended load transport rates, estimated separately by using appropriate bed-load and suspended-load formulas. It is therefore someway an indirect approach of the addition of two fractional sediment loads.

¹ By definition, the bed-material load is the total load minus the wash load.

Direct approach: The total-load transport rate can also be determined directly without dividing it into bed-load and suspended-load components. This approach is rather useful for river engineers or practitioners, because in some cases, they only want to estimate the total load in a river section. In addition, the distinction between the bed-load and the suspended-load transports is sometimes very difficult in measurement for both of them, as they are often interchangeable. For instance, particularly at a high rate of suspended-load transport, the bed load is hardly separated from the suspended load (Chien and Wan 1999).

The equations of total-load transport rate q_t in volume per unit time and width and g_t in weight per unit time and width are given as follows:

$$q_t = \underbrace{q_b + q_s}_{\text{Bed-material load}} \left(+ \underbrace{q_w}_{\text{Wash-load}} \right) \quad (7.1a)$$

$$g_t = \underbrace{g_b + g_s}_{\text{Bed-material load}} \left(+ \underbrace{g_w}_{\text{Wash-load}} \right) \quad (7.1b)$$

where q_b , q_s , and q_w are the bed-load, suspended-load, and wash-load transport rates in volume per unit time and width, respectively, and g_b , g_s , and g_w are the bed-load, suspended-load, and wash-load transport rates in weight per unit time and width, respectively. In non-dimensional form, the *total-load transport intensity* Φ_t is expressed as

$$\Phi_t = \frac{q_t}{(\Delta g d^3)^{0.5}} = \frac{g_t}{\rho_s g (\Delta g d^3)^{0.5}} \quad (7.2)$$

7.2 Indirect Approach

7.2.1 Einstein's Approach

Einstein (1950) advanced the bed-load and the suspended-load concepts for the computation of total load as the summation of these two loads. The bed load and suspended load for sediment size fractions are given by $i_b q_b$ and $i_s q_s$, respectively. Here, i_b and i_s are the fractions of bed-load and suspended-load transport rates, respectively. Therefore, using Eq. (7.1a) and excluding wash load ($q_w = 0$), the total-load transport rate q_{ti} for a given sediment size fraction d_i is expressed as

$$i_t q_t = i_b q_b + i_s q_s \quad \wedge \quad q_{ti} = i_t q_t \Rightarrow q_{ti} = i_b q_b + i_s q_s \quad (7.3)$$

Using Eq. (6.132) into Eq. (7.3), the total-load transport rate q_{ti} can be obtained as

$$q_{ti} = i_b q_b (1 + P_E I_1 + I_2) \quad \wedge \quad P_E = \ln \left(\frac{30.2h}{\Delta_k} \right) \quad (7.4)$$

where h is the flow depth, P_E is transport parameter, and Δ_k is the apparent roughness. In the above, I_1 and I_2 are the Einstein's integrals given by Eqs. (6.130a, b), respectively. It is pertinent to mention that Einstein's approach is rather complicated and lengthy for a practical use, although it involves considerable fundamental concepts of sediment transport from the theoretical viewpoint. The total-load transport rate g_{ti} is $g_{ti} = i_b g_b (1 + P_E I_1 + I_2)$.

7.2.2 Modified Einstein Procedure

In the above, original Einstein's (1950) approach calculates the total load excluding wash load for the given flow and bed conditions. Colby and Hembree (1955) and afterward others proposed some modifications of the original Einstein's approach, termed *modified Einstein procedure*, for the estimation of total load including wash load for a given flow rate. Here, the total load is obtained from the depth-integrated suspended sediment concentration samples, the flow and the bed sediment characteristics. For the reason of several information related to the field measurement required to estimate the total load by the modified Einstein procedure, the approach cannot be used for the design purposes; while the original Einstein approach can be used for the said purposes.² Simons and Sentürk (1977) and Yang (1996) provided an outline of the application of modified Einstein procedure as proposed by Colby and Hembree (1955).

The information required for the application of the modified Einstein procedure is the flow discharge Q , the flow area A , the channel width B , the average flow depth h_m at the location of suspended sediment sampling, the measured suspended sediment concentrations C_{lm} , the fraction of measured suspended sediment i_s , the

² Besides, the major differences between the original Einstein's approach (Einstein 1950) and the modified Einstein procedure (Colby and Hembree 1955) are as follows:

1. The modified approach requires information of the measured mean velocity U , rather than computed velocity for a given bed slope S_0 . The flow depth h is also to be measured in each vertical where the velocity is measured.
2. The exponent of Rouse equation or the Rouse number ζ is to be determined from the observed ζ value for a dominantly prevailing suspended sediment particle size. The ζ values for other particles are to be calculated from the ζ value for dominant size and are assumed to vary with a law of $w_s^{0.7}$, where w_s is the terminal fall velocities of the other particles.
3. The hiding factor ξ was introduced with a minor change.
4. The hydraulic radius R_b of the channel was replaced by the flow depth h .
5. The bed-load transport intensity Φ_b originally proposed by Einstein (1950) was arbitrarily multiplied by a factor 0.5 for an improved fitting of the observed bed-load transport data.

fraction of measured bed-load sediment i_b at the measuring section and the temperature t of flowing water.

Step 1: The first step is to compute the suspended-load transport rate $q_{si}|_m (=i_s q_s|_m)$ for a given size fraction in the sampling zone of cross section. The sediment transport rate through a unit width of sampling zone is

$$q_s|_m = \sum_i q_{si}|_m = \frac{C|_m Q|_m}{B} = C|_m q|_m \quad (7.5)$$

where $Q|_m$ and $q|_m$ are the total flow discharge and the flow discharge per unit width in the sampling zone.

Assuming the streamwise velocity to follow the logarithmic law of velocity distribution given by Keulegan (1938) [see Eq. (6.125)], the ratio of $q|_m$ to q is therefore given by

$$\begin{aligned} \frac{q|_m}{q} &= \frac{a_m}{h_m} \frac{\int_0^{h_m} \bar{u} dz}{\int_0^{h_m} \bar{u} dz} = 1 - \tilde{a}_m \left(1 + \frac{\ln \tilde{a}_m}{P_m - 1} \right) \quad \wedge \quad \tilde{a}_m = \frac{a_m}{h_m} \\ \vee \quad P_m &\approx \ln \left(\frac{30.2 x_k h}{d_{65}} \right) \end{aligned} \quad (7.6)$$

where q is the flow discharge per unit width, a_m is the distance from the streambed to the sampling point which should be as close as possible to the bed, and x_k is a correction factor, which can be obtained by trial and error using the curve x_k versus k_s/δ' as shown in Fig. 5.7 and the resistance equation given by Einstein (1950) as

$$\frac{U}{u_*} = \ln \left(12.27 R'_b \frac{x_k}{k_s} \right) \quad \wedge \quad x_k = x_k \left(\frac{k_s}{\delta'} \right) \quad \vee \quad \delta' = 11.6 \frac{\nu}{u_*} \quad (7.7)$$

where R'_b is the hydraulic radius due to particle roughness, k_s is the Nikuradse's equivalent sand roughness, δ' is the viscous sublayer thickness, u_* is the shear velocity, and ν is the coefficient of kinematic viscosity. Using Eqs. (7.5) and (7.6) yields

$$q_{si}|_m (=i_s q_s|_m) = i_s C|_m q \left[1 - \tilde{a}_m \left(1 + \frac{\ln \tilde{a}_m}{P_m - 1} \right) \right] \quad (7.8)$$

Step 2: The next step is to compute the bed-load transport rate q_{bi} ($=i_b q_b$) for a given size fraction in the sampling zone of cross section. The flow intensity parameter due to particle roughness is determined as

$$\Psi'_b = \frac{\Delta d_{35}}{R'_b S_0} \quad \wedge \quad d_{35} \approx 0.4 d_g \quad (7.9)$$

where Δ is the submerged relative density ($= s - 1$), s is the relative density of sediment ($= \rho_s / \rho$), ρ_s is the mass density of sediment, ρ is the mass density of water, d_{35} is the 35 % finer sediment size, d_g is the geometric mean size, and S_0 is the bed slope.

The computed value of Ψ'_b is used to determine Φ_b ($\approx \Phi_{b*}$) from Einstein's curve, as shown in Fig. 5.10, where Ψ_{b*} is replaced by Ψ'_b . Then, by definition of Φ_b given by Eq. (5.2), the following bed-load transport rate for a given size fraction d_i is obtained:

$$q_{bi}(=i_b q_b) = 0.5 \Phi_b p_i (\Delta g d_i^3)^{0.5} \quad (7.10)$$

where p_i is the fraction of size d_i . In the above, the bed-load transport intensity Φ_b is arbitrarily multiplied by a factor 0.5 to fit the measured field data.

Step 3: The final step is to compute the Rouse number ζ_{mi} by trial and error for a given fractional sediment size d_i . If $q_{si}|_m$ is expressed as

$$q_{si}|_m = \int_{a_m}^{h_m} C_i \bar{u} dz \quad (7.11)$$

then the ratio of $q_{si}|_m$ to $i_b q_b$, that is analogous to Eq. (6.132), is given by

$$\frac{q_{si}|_m}{i_b q_b} = \frac{I_1(\tilde{a}, \zeta_m)}{J_a(\tilde{a}, \zeta_m)} [P_m J_a(\tilde{a}_m, \zeta_m) + J_b(\tilde{a}_m, \zeta_m)] \quad (7.12)$$

where $\tilde{a} = a/h$,

$$J_a(\tilde{a}_m, \zeta_m) = \int_{\tilde{a}_m}^1 \left(\frac{1-\tilde{z}}{\tilde{z}} \right)^{\zeta_m} d\tilde{z} \quad (7.13a)$$

$$J_b(\tilde{a}_m, \zeta_m) = \int_{\tilde{a}_m}^1 \left(\frac{1-\tilde{z}}{\tilde{z}} \right)^{\zeta_m} \ln \tilde{z} d\tilde{z} \quad (7.13b)$$

$$I_1(\tilde{a}, \zeta_m) = 0.216 \frac{\tilde{a}^{\zeta_m-1}}{(1-\tilde{a})^{\zeta_m}} J_a(\tilde{a}, \zeta_m) \quad \wedge \quad J_a(\tilde{a}, \zeta_m) = \int_{\tilde{a}}^1 \left(\frac{1-\tilde{z}}{\tilde{z}} \right)^{\zeta_m} d\tilde{z} \quad (7.13c)$$

Equation (7.13c) is identical to Eq. (6.130a); hence, $I_1 = I_1(\tilde{a}, \zeta_m)$. Then, Eq. (7.12) becomes

$$\frac{Q_{si}|_m}{i_b Q_b} = \frac{Bq_{si}|_m}{Bi_b q_b} = \frac{I_1}{J_a(\tilde{a}, \zeta_m)} [P_m J_a(\tilde{a}_m, \zeta_m) + J_b(\tilde{a}_m, \zeta_m)] \quad (7.14)$$

The values of I_1 , J_a , and J_b can be obtained from Figs. 6.11, 7.1 and 7.2, respectively. From Eq. (7.14), the Rouse number ζ_{mi} for a given fractional size d_i can be solved by trial and error, as $Q_{si}|_m/(i_b Q_b)$ is known for a given d_i . In this way, ζ_{mi} can be obtained for all sediment size fractions.

Colby and Hembree (1955) recognized that there exists a relationship between the Rouse number ζ_{mi} and the terminal fall velocity w_{si} for a given fractional size d_i as

$$\frac{\zeta_{mi}}{\zeta_{m1}} = \left(\frac{w_{si}}{w_{s1}} \right)^{0.7} \quad (7.15)$$

where ζ_{m1} is the Rouse number obtained from Eq. (7.14) for the dominantly prevailing suspended particle size that has a terminal fall velocity w_{s1} .

Therefore, the total-load transport rate Q_{ti} through the channel cross section for a given fractional size d_i is estimated from

$$Q_{ti} = Q_{si}|_m \frac{P_m J_a(\tilde{a}, \zeta_m) + J_b(\tilde{a}, \zeta_m)}{P_m J_a(\tilde{a}_m, \zeta_m) + J_b(\tilde{a}_m, \zeta_m)} \quad (7.16)$$

for the range of fine particle sizes.

To calculate the total-load transport rate for the coarse sediment particles, the following equation obtained from Eq. (7.4) is used

$$Q_{ti} = i_b Q_{bi} (1 + P_m I_1 + I_2) \quad (7.17)$$

where Q_{bi} is the bed-load transport rate through the channel cross section for a given fractional size d_i ($=Bq_{bi}$). The Q_{ti} is in volume per unit time. To convert the units to total load G_{ti} in weight per unit time, Q_{ti} is to be multiplied by $\rho_s g$; where g is the acceleration due to gravity. One of the equations, Eq. (7.16) or (7.17), can be used to calculate the total load for the entire range of particle size fractions. In practical applications, Eq. (7.16) is restricted to the range of particle sizes due to which $Q_{si}|_m$ can be found with a reasonable accuracy. Besides, Eq. (7.17) is restricted to the range of particle sizes due to which $i_b Q_{bi}$ can be determined with a reasonable accuracy. Further, there is a limitation on the selection of equations that a given variation of ζ_m changes the estimated total load more than that obtained from Eq. (7.16) when ζ_m is large and more than that obtained from Eq. (7.17) when ζ_m is small.

Therefore, the modified Einstein procedure estimates unmeasured sediment load from the measured load. The total-load transport rate is determined from the measurements by a depth-integrated suspended sediment sampler and a sample of

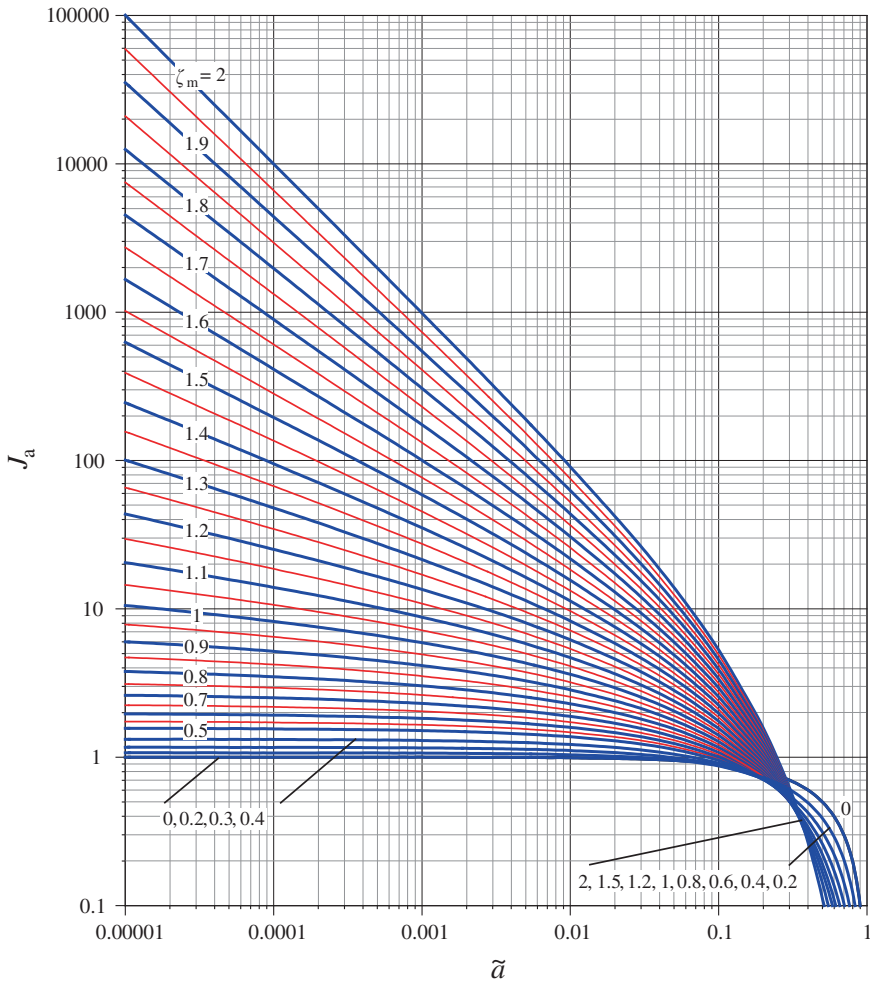


Fig. 7.1 Integral function J_a in terms of \tilde{a} for different ζ_m (Colby and Hembree 1955)

bed load. The method was developed based on the data from the Niobrara River, Nebraska, USA. The US Bureau of Reclamation (USBR 1955) provided a step-by-step method for computing total load by the modified Einstein procedure that was put forward by Colby and Hembree (1955).

Further development of the modified Einstein procedure was based on the series expansion of the Einstein integrals given by Guo and Julien (2004) [see Eqs. (6.137)–(6.139)]. The series expansion of the modified Einstein procedure was developed by Shah-Fairbank (2009) and Shah-Fairbank et al. (2011) and tested on various laboratory experimental and field (sand-bed) data from the Niobrara to the Mississippi River, USA.

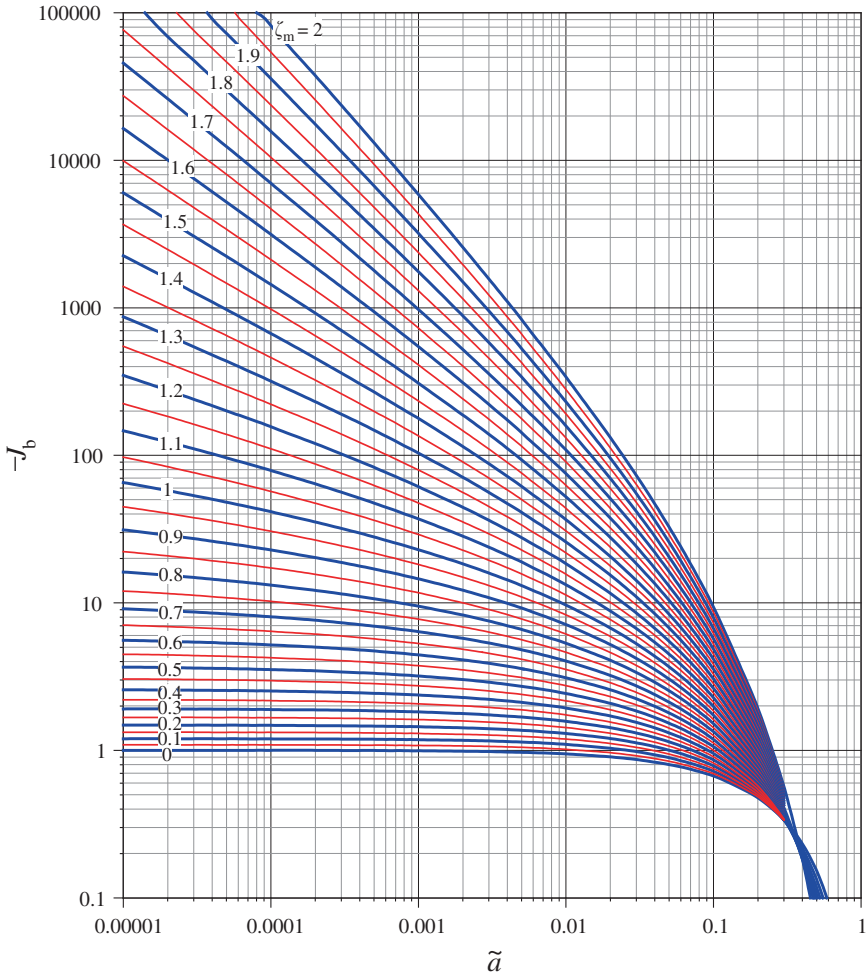


Fig. 7.2 Integral function $-J_b$ in terms of \tilde{a} for different ζ_m (Colby and Hembree 1955)

7.2.3 Bagnold's Approach

Bagnold (1966) considered the energy balance concept that led to the relationship between the rate of energy available to a fluvial system and the rate of work done by the system in transporting sediment. He obtained the equation of bed-load transport rate g_b that is given by Eq. (5.104).

Further, to derive the equation of suspended-load transport rate g_s , Bagnold equated the work done per unit time for sediment suspension to the net stream power used for the suspended-load transport. He then proposed Eq. (6.185) for suspended-load transport rate g_s .

Using Eqs. (5.104) and (6.185) into Eq. (7.1b), the total-load transport rate $g_t (=g_b + g_s)$ can be obtained as

$$g_t = \frac{\tau_0 U s}{\Delta} \left(\frac{e_b}{\tan \phi_d} + 0.01 \frac{U}{w_s} \right) \quad (7.18)$$

where τ_0 is the bed shear stress and e_b is the efficiency for bed-load transport. In Eq. (7.18), the product $\tau_0 U$ is the stream power or the power per unit area acting along the bed surface. The variation of efficiency e_b given by Bagnold is shown in Fig. 5.12. Equation (7.18) can be applicable for $u_*/w_s < 2$ for the best results.

7.2.4 Chang et al.'s Approach

Chang et al. (1965, 1967) computed the total load as a summation of the bed load and the suspended load. So, wash load was excluded.

They suggested a bed-load transport relationship given by Eq. (5.21) that can be expressed in terms of g_b (weight per unit time and width) as follows:

$$g_b = K_t U (\tau_0 - \tau_{0c}) \quad (7.19)$$

where K_t is a constant, which can be determined using Fig. 5.3, and τ_{0c} is the threshold bed shear stress.

They also derived the suspended-load transport equation, given by Eq. (6.148), which can be rearranged as

$$g_s = g_b R_s \quad \wedge \quad R_s = \frac{h}{0.8 U a} \left(U I_3 - \frac{2 u_*}{\kappa} I_4 \right) \quad (7.20)$$

where a is the level given by Eq. (6.149), κ is the von Kármán constant, and I_3 and I_4 are the Chang et al.'s integrals. Figures 6.14 and 6.15 can be used to determine I_3 and I_4 , respectively.

Using Eqs. (7.19) and (7.20) into Eq. (7.1b), the total-load transport rate $g_t (=g_b + g_s)$ can therefore be obtained as

$$g_t = K_t U (\tau_0 - \tau_{0c}) (1 + R_s) \quad (7.21)$$

7.3 Direct Approach

7.3.1 Laursen's Approach

Laursen (1958) used his laboratory experimental data to develop a functional relationship for the total load of sediment transport in terms of sediment

concentration (by volume) taking into account the summation of each size fraction of sediment for the given particle size distribution and flow condition. It is

$$\bar{C}_t = 0.01 \sum_i p_i \underbrace{\left(\frac{d_i}{h} \right)^{7/6} \left(\frac{\tau'_0}{\tau_{0ci}} - 1 \right)}_I \underbrace{f\left(\frac{u_*}{w_{si}} \right)}_{II} \Rightarrow q_t = q \bar{C}_t \quad (7.22)$$

where p_i is the percentage of sediment size d_i , τ'_0 is the bed shear stress due to particle roughness, and τ_{0ci} is the threshold bed shear stress for size fraction d_i . In Eq. (7.22), the portion *I* corresponds to the bed load, as it contains an excess bed shear stress expression; while the portion *II* expressing a function of the ratio of shear velocity to terminal fall velocity of sediment involves in turbulence mixing that sustains sediment in suspension. In this way, Eq. (7.22) involves both bed load and suspended load in expressing the total load, although wash load is excluded.

The functional relationship $f(u_*/w_{si})$ that was proposed by Laursen based on the flume data is shown in Fig. 7.3. He expressed the bed shear stress τ'_0 due to particle roughness with the aid of Manning-Strickler formula, $U/u_* = 7.66(h/d_{65})^{1/6}$, as

$$\tau'_0 \approx \frac{\rho U^2}{58} \left(\frac{d_i}{h} \right)^{1/3} \quad (7.23)$$

7.3.2 Bishop et al.'s Approach

Bishop et al. (1965) argued that the flow intensity parameter Ψ'_b could be used to predict total-load transport intensity Φ_t (excluding wash load) as

$$\Phi_t = f(\Psi'_b) \quad (7.24)$$

According to them, the Φ_t and Ψ'_b are given by

$$\Phi_t = \frac{q_t}{(\Delta g d_{50}^3)^{0.5}} = \frac{g_t}{\rho_s g (\Delta g d_{50}^3)^{0.5}} \quad \text{and} \quad \Psi'_b = \frac{\Delta d_{35}}{R'_b S_0} \quad (7.25)$$

Based on the experimental data for sand sizes 0.19, 0.27, 0.47, and 0.93 mm, they established the functional relationship given by Eq. (7.24), which is shown in Fig. 7.4. The trend of variation of individual curves for different sand sizes is quite identical, although their magnitudes are considerably dissimilar. The portion of the curves $\Phi_t \leq 5$ are almost similar to Einstein's $\Psi_{b*}(\Phi_{b*})$ curve (Fig. 5.10). Therefore, for this portion, the theoretical probability curve represented by Eq. (5.69) was fitted with the data by selecting different values of A_* and B_* for different sand sizes. Variations of A_* and B_* with sand size d_{50} are shown in Fig. 7.5, which suggests

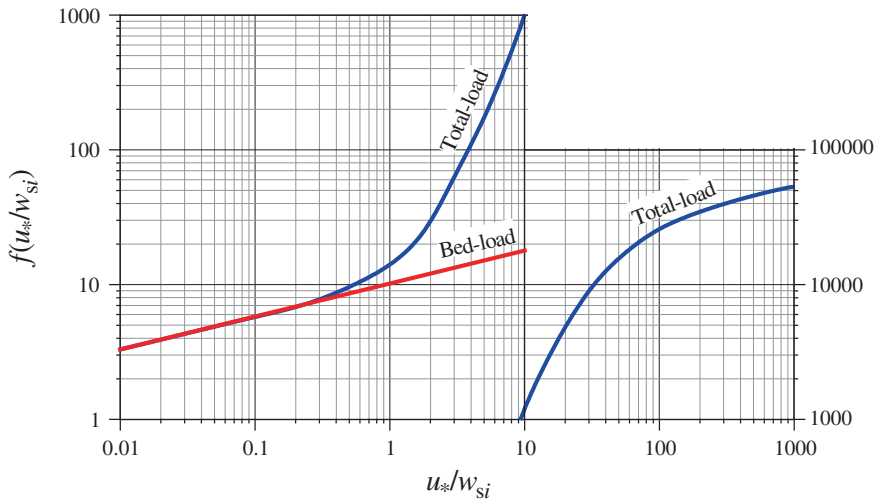


Fig. 7.3 Total-load functional relationship $f(u_*/w_{si})$ (Laursen 1958)

that A_* and B_* are not constant as considered by Einstein (1950), but are a function of particle size. Note that the portions of curves $\Phi_t > 5$ cannot be predicted by Einstein's approach, since a large portion of sediment is transported as suspended load that was beyond the scope of Einstein's bed-load transport equation. In fact, in Fig. 7.4, the band of the curves forming a trend has three segments. The portions of the curves $\Phi_t > 20$ correspond to the upper flow regime with plane beds and antidunes, while the portions of the curves $\Phi_t < 5$ represent the data of the lower flow regime with bedforms as ripples and/or dunes. Besides, the portions of the curves $5 < \Phi_t < 20$ show an inflectional pattern corresponding to transitional flow regime such as dunes to plane beds or starting to form antidunes.

7.3.3 Engelund and Hansen's Approach

Engelund and Hansen (1967) applied Bagnold's stream power concept and the similarity principle to obtain the total-load transport equation over a bed with bedforms. They did not take into account the wash load in estimation of total load.

The energy (work done per unit time and width) consumed E_s to lift the sediment particles from the bed over an elevation equaling bedform height η_d is

$$E_s = \underbrace{(\Delta\rho g)q_t}_{\text{Submerged weight of solid flux}} \times \eta_d \quad (7.26)$$

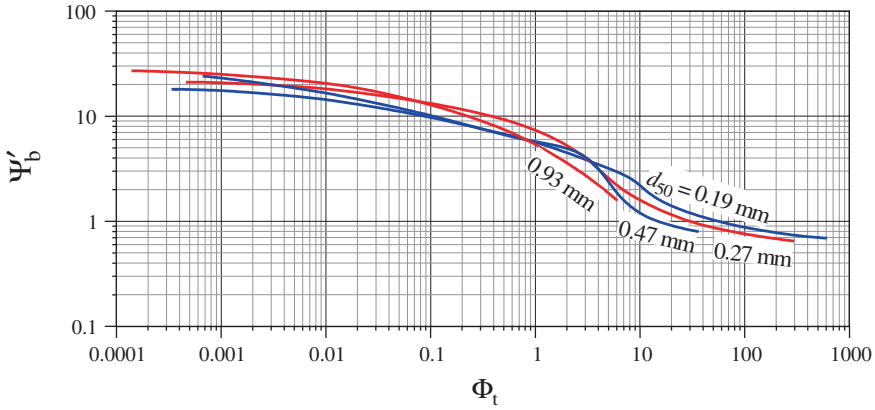


Fig. 7.4 Variation of Ψ'_b with Φ_t for different sand sizes d_{50} (Bishop et al. 1965)

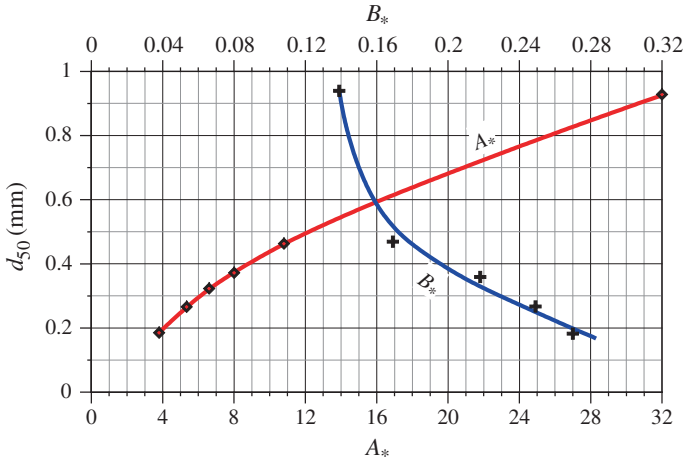


Fig. 7.5 Variations of A_* and B_* with sand size d_{50} (Bishop et al. 1965)

On the other hand, the energy (work done per unit time and width) supplied E_f by the flowing fluid to the particles to move over a distance equaling bedform length λ_d is

$$E_f = \underbrace{k_1(\tau'_0 - \tau_{0c})u_*}_{\text{Effective stream power}} \times \lambda_d \quad (7.27)$$

where k_1 is a constant. Applying the principle of conservation of energy ($E_s = E_f$) yields

$$q_t = k_1(\tau'_0 - \tau_{0c}) \frac{u_*}{\Delta \rho g} \cdot \frac{k_2}{\lambda_f} \quad \wedge \quad k_2 = \frac{\lambda_d \lambda_f}{\eta_d} \quad \vee \quad \lambda_f = \frac{2gR_b S}{U^2} = \frac{2g}{C_R^2} \quad (7.28)$$

where λ_f is the friction parameter and C_R is the Chézy coefficient. From the experimental data, Engelund and Hansen found that the quantity $\lambda_d \lambda_f / \eta_d (= k_2)$ is approximately a constant. Using Eq. (7.2), Eq. (7.28) is expressed in non-dimensional form as

$$\Phi_t = \frac{k_3}{\lambda_f} (\Theta' - \Theta_c) \Theta^{0.5} \quad \wedge \quad k_3 = k_1 k_2 \quad \vee \quad \Theta' = \frac{\tau'_0}{\Delta \rho g d} \quad (7.29)$$

where Θ is the Shields parameter given by Eq. (4.31) and Θ' is the Shields parameter corresponding to particle roughness. For lower flow regime ($\Theta \leq 0.7$), they defined $\Theta' = 0.06 + 0.4\Theta^2$ and $\Theta_c \approx 0.06$ and also found empirically $k_3 = 0.25$.³ Using these conditions, Eq. (7.29) is expressed as

$$\Phi_t = \frac{0.1}{\lambda_f} \Theta^{2.5} \quad (7.30)$$

The above equation can also be expressed as the volume of total load per unit time and width q_t and the depth-averaged concentration \bar{c}_t (by weight) as follows:

$$q_t = 0.05 U^2 \left(\frac{d}{\Delta g} \right)^{0.5} \Theta^{1.5} \quad (7.31a)$$

$$\bar{c}_t = \frac{s \bar{C}_t}{1 + \Delta \bar{C}_t} \quad \wedge \quad \bar{C}_t = \frac{q_t}{q} \quad (7.31b)$$

Note that the relationship between \bar{c}_t and \bar{C}_t is given by Eq. (1.28). Categorically, Eq. (7.30) or (7.31a) or (7.31b) should be applicable to the flows over dune beds in accordance with the similarity principle. However, they found that it can also be applied to the upper flow regime ($\Theta > 0.7$) with particle size greater than 0.15 mm without severe deviation from the theory.

7.3.4 Graf and Acaroglu's Approach

Graf and Acaroglu (1968) used hydraulic radius R_b , without separating it to R'_b and R''_b , where R''_b is the hydraulic radius due to bedforms. They developed a flow

³ For upper flow regime, Θ' is as follows:

$$\begin{aligned} \Theta'(0.7 < \Theta \leq 1) &= \Theta \\ \Theta'(\Theta > 1) &= \left(0.298 + \frac{0.702}{\Theta^{1.8}} \right)^{-0.56} \end{aligned}$$

intensity parameter Ψ_b as a transport criterion. It is given as in Eq. (5.66) with $R_b = R'_b$ as follows:

$$\Psi_b = \frac{\Delta d}{R_b S_0} \quad (7.32)$$

Based on the work done rate concept, a *transport parameter* was established as

$$\Phi_t = \frac{\bar{C}_t U R_b}{(\Delta g d^3)^{0.5}} \quad (7.33)$$

Using experimental data of different investigators, Graf and Acaroglu obtained the following empirical relationship between Φ_t and Ψ_b :

$$\Phi_t = \frac{10.39}{\Psi_b^{2.52}} \quad (7.34)$$

It is pertinent to mention that Eq. (7.34) was obtained from the laboratory experimental and field data with open channels and closed conduits, and hence, it is applicable for both the cases.

7.3.5 Ackers and White's Approach

On the basis of Bagnold's (1966) stream power approach, Ackers and White (1973) carried out the dimensional analysis to express the total-load transport rate in terms of a newly introduced mobility number and some other non-dimensional parameters. They hypothesized that a portion of bed shear stress is effective in causing the motion of coarse sediment particles. On the other hand, suspended-load transport is predominant for fine sediment particles, in which total bed shear stress is effective in causing the motion of the fine sediment particles. Their empirical equation of total-load transport rate can be expressed as the volume of total load per unit time and width q_t and the depth-averaged concentration \bar{c}_t :

$$q_t = K U d_{35} \left(\frac{U}{u_*} \right)^n \left(\frac{F_{gr}}{A} - 1 \right)^m \quad (7.35a)$$

$$\bar{c}_t = K_s \frac{d_{35}}{h} \left(\frac{U}{u_*} \right)^n \left(\frac{F_{gr}}{A} - 1 \right)^m \quad (7.35b)$$

where K and A are the coefficients, n and m are the exponents, and F_{gr} is called the *mobility number*, which is

Table 7.1 Coefficients and exponents (Ackers and White 1973)

Parameter	$D_* > 60$	$60 \geq D_* > 1$
K	0.025	$\log K = 2.86 \log D_* - (\log D_*)^2 - 3.53$
A	0	$0.23 D_*^{-0.5} + 0.14$
n	0.17	$1 - 0.56 \log D_*$
m	1.5	$9.66 D_*^{-1} + 1.34$

$$F_{\text{gr}} = \underbrace{\frac{u_*^n}{(\Delta g d_{35})^{0.5}}}_I \underbrace{\left[\frac{U}{5.66 \log(\alpha h/d_{35})} \right]^{1-n}}_{II} \quad (7.36)$$

where α is a coefficient determined for the turbulent shear flow as 10. Further, their hypothesis is reflected in the mobility factor F_{gr} (Eq. 7.36), as the bed load and the suspended load are distinguishable. For instance, coarse sediment transports as a bed load, which is attributed to the stream power $\tau'_0 U$ generated by the bed shear stress due to particle roughness. It involves in the portion II of Eq. (7.36). On the other hand, fine sediment transports mainly as suspension. The fluctuations of vertical velocity component, given by $(\overline{w'w'})^{0.5}$, that sustains the sediment suspension is a function of the stream power $\tau_0 U$ generated by the total bed shear stress. Therefore, the portion I of Eq. (7.36) reflects stream power consumption associated with the turbulence intensity to bring the fine sediment in suspension. However, Eq. (7.35) was basically made for the bed-material load.

The coefficients and exponents suggested by them for different ranges of particle parameter $D_* [=d_{35}(\Delta g/v^2)^{1/3}]$ are given in Table 7.1.

The coefficient K and exponent m were later revised by Ackers (1990) given in Table 7.2.

Note that for fine sediments, $D_* < 1$ and $n = 1$, it leads to $F_{\text{gr}} = \Theta^{0.5}$.

7.3.6 Yang's Approach

Yang (1972) assumed that the total load of sediment transport is caused by the rate of energy dissipation of flow. In a steady uniform flow, as the kinetic energy of flow does not vary, the rate of energy dissipation is due to the rate of change of potential energy,⁴ which is expressed as the product of velocity and bed slope, US_0 , termed *unit stream power*. As the sediment transport mainly occurs in turbulent flow condition, Yang and Molinas (1982) made a derivation to show that

⁴ The rate of potential energy dissipation per unit weight of flow over an elementary reach dx having a drop of dz is

$$\frac{dz}{dt} = \frac{dx}{dt} \cdot \frac{dz}{dx} = US_0 \quad \wedge \quad \frac{dx}{dt} = U \quad \vee \quad \frac{dz}{dx} = S_0.$$

Table 7.2 Coefficient K and exponent m (Ackers 1990)

Parameter	$D_* > 60$	$60 \geq D_* > 1$
K	0.025	$\log K = 2.79 \log D_* - 0.98(\log D_*)^2 - 3.46$
m	1.78	$6.83 D_*^{-1} + 1.67$

the average concentration \bar{c}_{pt} [in parts per million (or ppm) by weight] can be directly related to the unit stream power. The generalized stream power equation is

$$\log \bar{c}_{pt} = M + N \log P_s \quad (7.37)$$

where M , N , and P_s are the coefficients (see Table 7.3).

Yang and Simões (2005) used Yang's unit stream power approach (Yang 1979; Yang et al. 1996) to predict the total bed-material load and the wash load in the Yellow River in China.⁵

7.3.7 Brownlie's Approach

Brownlie (1981) used more than 1,000 flume experimental and field data to propose an empirical equation of average concentration \bar{c}_{pt} (in ppm by weight) as

$$\bar{c}_{pt} = 7115 c_f (F_d - F_{dc})^{1.978} S_0^{0.6601} \left(\frac{R_b}{d_{50}} \right)^{-0.3301} \quad (7.38)$$

⁵ Steps involved in predicting the total load by Yang and Simões's approach are as follows:

Step 1: Compute \bar{c}_{pt} from Eq. (7.37) using M , N , and P_s given by Yang (1979) (Table 7.3).

Step 2: Compute \bar{C}_{bm} (by volume) for bed-material load from the equation:

$$\bar{C}_{bm} = \frac{\bar{c}_{pt} \times 10^{-6}}{s - \Delta \bar{c}_{pt} \times 10^{-6}}$$

Step 3: Compute average concentration of suspended load \bar{C}_t including wash load from $\bar{C}_t = \alpha \bar{C}_{bm}$, where α is the proportionality factor (≈ 1.5).

Step 4: Compute mass density of sediment-laden flow ρ_m from Eq. (1.29) and kinematic viscosity of sediment laden flow ν_m from $\nu_m = (\nu \rho / \rho_m) \exp(5.06 \bar{C}_t)$.

Step 5: Compute new \bar{c}_{pt} (say, $\bar{c}_{pt}|_{new}$) from Eq. (7.37) with M , N , and P_s given by Yang (1979) (Table 7.3) replacing w_s by $w_{sc} [= w_s(1 - \bar{C}_t)^7]$, ν by $\nu_m [= (\nu \rho / \rho_m) \exp(5.06 \bar{C}_t)]$ and US_0/w_s by $(US_0/w_s)[(\rho/\rho_m) - 1]^{-1}(1 - \bar{C}_t)^{-7}$.

Step 6: Compute new \bar{C}_{bm} (say, $\bar{C}_{bm}|_{new}$) for bed-material load from the equation:

$$\bar{C}_{bm}|_{new} = \frac{\bar{c}_{pt}|_{new} \times 10^{-6}}{s - \Delta \bar{c}_{pt}|_{new} \times 10^{-6}}$$

Step 7: Compute new \bar{C}_t (say, $\bar{C}_t|_{new}$) from $\bar{C}_t|_{new} = \alpha \bar{C}_{bm}|_{new}$.

Step 8: If $\bar{C}_t \approx \bar{C}_{bm}|_{new}$ within acceptable accuracy, then no further iteration is required. Otherwise, if $\bar{C}_t \neq \bar{C}_{bm}|_{new}$, then repeat the iteration from Step 4 to Step 8 until $\bar{C}_t \approx \bar{C}_{bm}|_{new}$.

Table 7.3 Coefficients M , N , and P_s

M	N	P_s
<i>Sand transport</i> (Yang 1973)		
$5.435 - 0.286 \log R_e + 0.457 \log w_s^+$	$1.799 - 0.409 \log R_e + 0.314 \log w_s^+$	$(U - U_{cr})(S_0/w_s)$
<i>Sand and silt transport at high concentration</i> (Yang 1979)		
$5.165 - 0.153 \log R_e + 0.297 \log w_s^+$	$1.78 - 0.36 \log R_e + 0.48 \log w_s^+$	US_0/w_s
<i>Gravel transport</i> (Yang 1984)		
$6.681 - 0.633 \log R_e + 4.816 \log w_s^+$	$2.784 - 0.305 \log R_e + 0.282 \log w_s^+$	$(U - U_{cr})(S_0/w_s)$
<i>Note</i> R_e is the particle Reynolds number ($=w_s d_{50}/\nu$), $w_s^+ = w_s/u_*$, and U_{cr} is the depth-averaged flow velocity corresponding to the sediment threshold, which can be determined from Eqs. (4.17a, b)		

where c_f is the coefficient depending on experimental conditions, F_d is the densimetric Froude number, and F_{dc} is the densimetric Froude number corresponding to sediment threshold. In Eq. (7.38), c_f is 1 for laboratory flumes and 1.268 for field channels. Equation (7.38) includes the wash load. Note that the relationship between \bar{c}_{pt} and \bar{c}_t is $\bar{c}_t = 10^{-6} \bar{c}_{pt}$. The F_d and F_{dc} are given by

$$F_d = \frac{U}{(\Delta g d_{50})^{0.5}} \quad (7.39a)$$

$$F_{dc} \left[\frac{U_c}{(\Delta g d_{50})^{0.5}} \right] = 4.596 \frac{\Theta_c^{0.5295}}{S_0^{0.1045} \sigma_g^{0.1606}} \quad \wedge \quad \Theta_c = 0.22\Upsilon - \frac{0.06}{10^{7.7\Upsilon}} \quad \vee \quad \Upsilon = \frac{1}{S_*^{0.6}} \quad (7.39b)$$

where $S_* = d(\Delta g d)^{0.5}/\nu$.

7.3.8 Karim and Kennedy's Approach

Karim and Kennedy (1990) used non-linear multiple regression analysis to relate flow velocity, total-load transport rate, bedform configuration, and friction factor of sediment bed. The uncoupled relationships for total load and flow resistance proposed by them are

$$\begin{aligned} \log \Phi_t &= -2.279 + 2.972 \log F_d \\ &+ \left[1.06 \log F_d + 0.299 \log \left(\frac{h}{d_{50}} \right) \right] \log \left[\frac{u_* - u_{*c}}{(\Delta g d_{50})^{0.5}} \right] \end{aligned} \quad (7.40a)$$

$$F_d \left[\frac{U}{(\Delta g d_{50})^{0.5}} \right] = 2.822 \left[\frac{q}{(\Delta g d_{50}^3)^{0.5}} \right]^{0.376} S_0^{0.31} \quad (7.40b)$$

Equation (7.40b) that is used for the flow condition well above the threshold of sediment motion does not take into account the resistance due to bedforms. Hence, for the bed with bedforms, a modified resistance equation was proposed as

$$F_d \left[\frac{U}{(\Delta g d_{50})^{0.5}} \right] = 9.82 \Phi_t^{0.216} \left(\frac{\lambda_D}{\lambda'_D} \right)^{-0.164} \quad (7.41)$$

where λ_D is the Darcy-Weisbach friction factor and λ'_D is the friction factor due to particle roughness, which was expressed as

$$\lambda'_D = 8 \left[2.5 \ln \left(\frac{h}{2.5 d_{50}} \right) + 6.25 \right]^{-2} \quad (7.42)$$

They suggested that the ratio of λ_D to λ'_D could be computed as

$$\frac{\lambda_D}{\lambda'_D} (\Theta \geq 1.5) = 1.914 + 6.66\Theta - 17.969\Theta^2 + 23.423\Theta^3 - 0.982\Theta^4 \quad (7.43a)$$

$$\frac{\lambda_D}{\lambda'_D} (\Theta < 1.5) = 1.2 \quad (7.43b)$$

Later, Karim (1998) suggested a simpler empirical equation for total-load transport using the same data set used by Karim and Kennedy (1990) in their analysis. It is

$$\Phi_t = 1.39 \times 10^{-3} F_d^{2.97} \left(\frac{u_*}{w_s} \right)^{1.47} \quad (7.44)$$

The above equation was also used by Karim to laboratory experimental and field data for nonuniform sediment by dividing sediment into size fractions. However, both Eqs. (7.40a) and (7.44) could produce almost same results, but latter equation is easier to use than the former.

Equations (7.40a), (7.41) and (7.43) constitute a set of coupled total-load transport rate, flow resistance due to friction, and bedforms relationship. The solution of them can be obtained by an iterative scheme.⁶

⁶ Procedure for the determination of total-load transport rate q_t for the given q , S_0 and d_{50} is as follows:

- Step 1: Assume a suitable trial value for h , say h_{trial}
- Step 2: Compute $U = q/h_{\text{trial}}$.
- Step 3: Compute q_t from Eq. (7.40a).
- Step 4: Compute λ_D/λ'_D from Eq. (7.43).
- Step 5: Compute U from Eq. (7.41).

7.3.9 Molinas and Wu's Approach

Molinas and Wu (2001) expressed concerns over the field applicability of the predictors proposed by Engelund and Hansen (1967), Ackers and White (1973), and Yang (1973), as they were developed using the flume experimental data on shallow flow depths being less than 1 m, in general. Therefore, the flow depths used in the laboratory flume experiments were very limited as compared to the large natural rivers. For instance, the average depths vary from 12 to 68 m for Amazon River and from 3 to 22 m for Mississippi River (Posada 1995). Likewise, in laboratory conditions, the flow Reynolds numbers are much smaller, the flow Froude numbers are much larger, and the energy gradients are steeper than those conditions in large natural rivers. Thus, in developing an empirical equation of average concentration \bar{c}_t , they applied the stream power and the energy concepts together with the data of large sand-bed rivers (namely, Amazon, Atchafalaya, Mississippi, Orinoco, Red River, etc.). The equation of \bar{c}_{pt} (in ppm by weight) is

$$\bar{c}_{pt} = \frac{1430(0.86 + \Psi_s^{0.5})\Psi_s^{1.5}}{0.016 + \Psi_s} \quad \wedge \quad \Psi_s = \frac{U^3}{\Delta gh w_s} \left[\log \left(\frac{h}{d_{50}} \right) \right]^{-2} \quad (7.45)$$

where Ψ_s is the *non-dimensional stream power*. The above equation takes into account the wash load.

7.3.10 Yang and Lim's Approach

Yang and Lim (2003) and Yang (2005) conducted a dimensional analysis to derive the following equation of total-load transport rate including the wash load:

$$g_t = k \frac{s\tau_0}{\Delta w_s} \cdot (u_*'^2 - u_{*c}^2) \quad (7.46)$$

where k is an empirical coefficient ($=12.5$), u_*' is the shear velocity due to particle roughness, and u_{*c} is the threshold shear velocity. They used experimental data of

(Footnote 6 continued)

Step 6: If computed values of U from Step 2 and Step 5 are within an acceptable accuracy, then go to Step 7. Otherwise, retry Step 1 to Step 6 with a new value for h until a convergence on U is obtained.

Step 7: Compute $h = q/U$.

Step 8: Compute $\lambda_D = 8ghS_0/U^2$ and $\Theta = hS_0/(\Delta d_{50})$.

Step 9: Determine flow regime: Lower regime $\Theta \leq 1.1$; transition $1.1 < \Theta < 1.5$; upper regime $\Theta \geq 1.5$.

Step 10: Compute q_t from Eq. (7.40a).

USWES (1936) to validate Eq. (7.46), which is quite simple and can produce reasonably good estimations.

7.3.11 Sinnakaudan et al.'s Approach

Sinnakaudan et al. (2006) proposed an empirical equation of total-load transport rate in terms of average concentration \bar{C}_t (by volume) that could be applicable for the uniform sediment sizes ranging from 0.37 to 4 mm and provided best results for the rivers in Malaysia. It is

$$\bar{C}_t = 1.811 \times 10^{-4} \frac{(\Delta g d^3)^{0.5}}{UR_b} \left(\frac{US_0}{w_s} \right)^{0.293} \left(\frac{R_b}{d} \right)^{1.39} \quad (7.47)$$

Equation (7.47) does not take into account the wash load.

7.4 Total-Load Transport of Nonuniform Sediments

Natural riverbeds are usually composed of nonuniform sediment mixtures and the corresponding particle size distribution of transported sediment is generally finer than the distribution of bed sediment, because of the selective transport process. The nonuniformity of bed sediments affects the total-load transport rate calculations based on median size d_{50} . Wu et al. (2004) analyzed the relationship between total-load transport calculation by particle size fractions d_i and calculations based on the median size d_{50} of particle for sediment transport. A size gradation correction factor K_d was introduced to account for the lognormal distribution of bed sediments. The use of K_d in conjunction with total-load equations originally developed for single particle sizes improved the accuracy of transport calculations for sediment mixtures. This method is applicable to laboratory flumes and natural rivers with median size of bed sediment in the sand size ranges. They found that the results depend on the geometric standard deviation of particle size distribution given by $\sigma_g = (d_{84}/d_{16})^{0.5}$, which is one of the measures of the nonuniformity of sediments. Data plots showed that the measured total-load transport rate g_{ti} for a fractional particle size d_i varies inversely with d_i according to

$$K_d \approx \left(\frac{d_i}{d_{50}} \right)^{-1.2} \quad \wedge \quad K_d = \frac{g_{ti}}{g_{t|d_{50}}} \quad (7.48)$$

where g_{ti} is the total-load transport rate in weight per unit time and width for particle size d_i , and $g_{t|d_{50}}$ is the total-load transport rate in weight per unit time and width for particle size d_{50} . Wu et al. (2004) then defined the ratio of the transport rate by size fraction g_{ti} to the transport rate $g_{t|d_{50}}$ based on the median particle size d_{50} as a function of σ_g . The K_d is given by

$$K_d = \exp \left[\frac{1}{2} (1.2 \ln \sigma_g)^2 \right] \quad (7.49)$$

Similarly, the d_{50s} of the sediment in suspension was expressed as a function of σ_g and d_{50} of the total load as

$$\frac{d_{50s}}{d_{50}} = \sigma_g^{-1.2 \ln \sigma_g} \quad (7.50)$$

In practice, it was found that this correction due to sediment nonuniformity is quite significant when $\sigma_g > 2$ and negligible for $\sigma_g < 1.5$. Note that Wu et al. did not take into account the wash load.

7.5 Examples

Example 7.1 A wide natural stream flows with an average velocity of 1.1 m s^{-1} , having a bed slope of 2×10^{-3} and an average flow depth of 0.55 m . The bed consists of uniform fine sand of median size $d_{50} = 0.25 \text{ mm}$ and $d_{35} = 0.2 \text{ mm}$, having a relative density of 2.65 . Calculate the total-load transport rate in volume per unit time and width by the following methods:

(i) Laursen, (ii) Bishop et al., (iii) Bagnold, (iv) Engelund and Hansen, (v) Graf and Acaroglu, (vi) Yang (1973), (vii) Ackers and White, (viii) Brownlie, (ix) Karim, (x) Molinas and Wu, (xi) Yang and Lim, and (xii) Sinnakaudan et al.

Solution

Given data are as follows:

Average flow velocity, $U = 1.1 \text{ m s}^{-1}$; bed slope, $S_0 = 2 \times 10^{-3}$; average flow depth, $h = 0.55 \text{ m}$; median size of sediment, $d_{50} = 0.25 \text{ mm}$; $d_{35} = 0.2 \text{ mm}$; and relative density, $s = 2.65$

Discharge per unit width, $q = Uh = 1.1 \times 0.55 = 0.605 \text{ m}^2 \text{ s}^{-1}$

Bed shear stress, $\tau_0 = \rho gh S_0 = 10^3 \times 9.81 \times 0.55 \times 2 \times 10^{-3} = 10.791 \text{ Pa}$

Shear velocity, $u_* = (\tau_0/\rho)^{0.5} = (10.791/10^3)^{0.5} = 0.104 \text{ m s}^{-1}$

Shields parameter, $\Theta = \tau_0/(\Delta \rho g d_{50}) = 10.791/(1.65 \times 10^3 \times 9.81 \times 0.25 \times 10^{-3}) = 2.667$

Shear Reynolds number, $R_* = u_* d_{50}/\nu = 0.104 \times 0.25 \times 10^{-3}/10^{-6} = 26$ (assume $\nu = 10^{-6} \text{ m}^2 \text{ s}^{-1}$).

The empirical relationship proposed by van Rijn is used to determine threshold bed shear stress and threshold shear velocity (see Table 4.1):

Particle parameter, $D_* = d_{50}(\Delta g/\nu^2)^{1/3} = 0.25 \times 10^{-3} [1.65 \times 9.81/(10^{-6})^2]^{1/3} = 6.324$

Threshold Shields parameter, $\Theta_c(4 < D_* \leq 10) = 0.14D_*^{-0.64} = 0.14 \times 6.324^{-0.64} = 0.043$

Threshold bed shear stress, $\tau_{0c} = \Theta_c \Delta \rho g d_{50} = 0.043 \times 1.65 \times 10^3 \times 9.81 \times 0.25 \times 10^{-3} = 0.174 \text{ Pa}$

Threshold shear velocity, $u_{*c} = (\tau_{0c}/\rho)^{0.5} = (0.174/10^3)^{0.5} = 0.013 \text{ m s}^{-1}$.

The terminal fall velocity is calculated by the formula given by Cheng (1997) [see Eq. (1.40) and Table 1.3], considering shape factor $S_p = 0.7$ and nominal diameter $d_n \approx d_{50}$ as

$$w_s = \frac{v}{d} [(25 + 1.2D_*^2)^{0.5} - 5]^{1.5} = \frac{10^{-6}}{0.25 \times 10^{-3}} [(25 + 1.2 \times 6.324^2)^{0.5} - 5]^{1.5} \\ = 0.027 \text{ m s}^{-1}$$

Threshold average velocity is obtained from Yang's (1973) formula, Eq. (4.17):

$$U_{cr}(0 < R_* < 70) = w_s \left(\frac{2.5}{\log R_* - 0.06} + 0.66 \right) = 0.027 \left(\frac{2.5}{\log 26 - 0.06} + 0.66 \right) \\ = 0.068 \text{ m s}^{-1}$$

(i) *Laursen's method*:

For uniform bed sand, Eq. (7.22) is reduced to

$$\bar{C}_t = 0.01 \left(\frac{d}{h} \right)^{7/6} \left(\frac{\tau'_0}{\tau_{0c}} - 1 \right) f \left(\frac{u_*}{w_s} \right)$$

The bed shear stress τ'_0 due to particle roughness is obtained from Eq. (7.23) as

$$\tau'_0 = \frac{10^3 \times 1.1^2}{58} \left(\frac{0.25 \times 10^{-3}}{0.55} \right)^{1/3} = 1.604 \text{ Pa} \Leftarrow \text{Eq. (7.23)}$$

Note: In the above equation, it is assumed that $d_{65} \approx d_{50}$

For $u_*/w_s = 0.104/0.027 = 3.852$, the parameter $f(u_*/w_s)$ is determined from Fig. 7.3 as $f(u_*/w_s) = 90$

Therefore, the average sediment concentration is

$$\bar{C}_t = 0.01 \left(\frac{0.25 \times 10^{-3}}{0.55} \right)^{7/6} \left(\frac{1.604}{0.174} - 1 \right) 90 = 9.323 \times 10^{-4}$$

The total-load transport rate is

$$q_t = q \bar{C}_t = 0.605 \times 9.323 \times 10^{-4} = 5.64 \times 10^{-4} \text{ m}^2 \text{ s}^{-1}$$

(ii) *Bishop et al.'s method:*

The flow intensity parameter is obtained as

$$\Psi'_b = \frac{\Delta d_{35}}{R'_b S_0} = \frac{1.65 \times 0.2 \times 10^{-3}}{0.55 \times 2 \times 10^{-3}} = 0.3 \text{ (Note: It is assumed that } R'_b \approx h \text{)}$$

For $\Psi'_b = 0.3$, total-load transport intensity Φ_t cannot be determined from Fig. 7.4, as the individual curves for different d_{50} are limited to $0.6 < \Psi'_b < 25$. Therefore, Bishop et al.'s method does not produce any result for the given data.

(iii) *Bagnold's method:*

For $U = 1.1 \text{ m s}^{-1}$ and $d_{50} = 0.25 \text{ mm}$, the bed-load transport efficiency e_b is obtained from Fig. 5.12 as $e_b = 0.132$. Also, it is assumed that $\phi_d = 25^\circ$. The total-load transport rate (in weight per unit time and width) is

$$g_t = \frac{10.791 \times 1.1 \times 2.65}{1.65} \left(\frac{0.132}{\tan 25^\circ} + 0.01 \frac{1.1}{0.027} \right) = 13.163 \text{ N s}^{-1} \Leftarrow \text{Eq. (7.18)}$$

Then, the total-load transport rate (in volume per unit time and width) is

$$q_t = \frac{g_t}{\rho_s g} = \frac{13.163}{2.65 \times 10^3 \times 9.81} = 5.063 \times 10^{-4} \text{ m}^2 \text{ s}^{-1}$$

(iv) *Engelund and Hansen's method:*

The total-load transport rate obtained using Eq. (7.31a) as

$$q_t = 0.05 \times 1.1^2 \left(\frac{0.25 \times 10^{-3}}{1.65 \times 9.81} \right)^{0.5} 2.667^{1.5} = 1.036 \times 10^{-3} \text{ m}^2 \text{ s}^{-1} \\ \Leftarrow \text{Eq. (7.31a)}$$

(v) *Graf and Acaroglu's method:*

The total-load transport intensity is obtained from Eq. (7.34) as

$$\Phi_t = \frac{10.39}{0.3^{2.52}} = 215.91 \Leftarrow \text{Eq. (7.34)}$$

Then, the total-load transport rate (in volume per unit time and width) is

$$q_t = \Phi_t (\Delta g d_{50}^3)^{0.5} = 215.91 [1.65 \times 9.81 (0.25 \times 10^{-3})^3]^{0.5} \\ = 3.434 \times 10^{-3} \text{ m}^2 \text{ s}^{-1}$$

(vi) *Yang's method:*

For $w_s^+ = w_s/u_* = 0.027/0.104 = 0.26$, $R_e = w_s d_{50}/\nu = 0.027 \times 0.25 \times 10^{-3}/10^{-6} = 6.75$, the values of M , N , and P_s are obtained from Table 7.3 as follow:

$$\begin{aligned} M &= 5.435 - 0.286 \log R_e + 0.457 \log w_s^+ = 5.435 - 0.286 \log 6.75 \\ &\quad + 0.457 \log 0.26 = 4.93 \\ N &= 1.799 - 0.409 \log R_e + 0.314 \log w_s^+ = 1.799 - 0.409 \log 6.75 \\ &\quad + 0.314 \log 0.26 = 1.276 \\ P_s &= (U - U_{cr}) \frac{S_0}{w_s} = (1.1 - 0.068) \frac{2 \times 10^{-3}}{0.027} = 0.076 \end{aligned}$$

The average concentration \bar{c}_t (by weight) is calculated from Eq. (7.37) as

$$\begin{aligned} \bar{c}_{pt} &= 10^{M+N \log P_s} = 10^{4.93+1.276 \log 0.076} = 3176.28 \Leftarrow \text{Eq. (7.37)} \\ \bar{c}_t &= 10^{-6} \bar{c}_{pt} = 10^{-6} \times 3176.28 = 3.176 \times 10^{-3} \end{aligned}$$

The average concentration \bar{C}_t (by volume) is

$$\bar{c}_t = \frac{s \bar{C}_t}{1 + \Delta \bar{C}_t} (\text{Eq. 1.28}) \Rightarrow \bar{C}_t = \frac{\bar{c}_t}{s - \Delta \bar{c}_t} \approx \frac{\bar{c}_t}{s} = \frac{3.176 \times 10^{-3}}{2.65} = 1.198 \times 10^{-3}$$

The total-load transport rate (in volume per unit time and width) is

$$q_t = q \bar{C}_t = 0.605 \times 1.198 \times 10^{-3} = 7.248 \times 10^{-4} \text{ m}^2 \text{ s}^{-1}$$

(vii) *Ackers and White's method:*

For $D_* = 6.324$ (that is $60 \geq D_* > 1$), the values of A and n from Table 7.1 and K and m from Table 7.2 can be obtained as follows:

$$\begin{aligned} A &= \frac{0.23}{D_*^{0.5}} + 0.14 = \frac{0.23}{6.324^{0.5}} + 0.14 = 0.231 \\ n &= 1 - 0.56 \log D_* = 1 - 0.56 \log 6.324 = 0.551 \\ K &= 10^{2.79 \log D_* - 0.98 (\log D_*)^2 - 3.46} = 10^{2.79 \log 6.324 - 0.98 (\log 6.324)^2 - 3.46} = 0.014 \\ m &= \frac{6.83}{D_*} + 1.67 = \frac{6.83}{6.324} + 1.67 = 2.75 \end{aligned}$$

The mobility number F_{gr} is determined from Eq. (7.36) as

$$F_{gr} = \frac{0.104^{0.551}}{(1.65 \times 9.81 \times 0.2 \times 10^{-3})^{0.5}} \left[\frac{1.1}{5.66 \log(10 \times 0.55/0.2 \times 10^{-3})} \right]^{1-0.551}$$

$$= 1.239 \Leftarrow \text{Eq. (7.36)}$$

The total-load transport rate is obtained from Eq. (7.35a) as

$$q_t = 0.014 \times 1.1 \times 0.2 \times 10^{-3} \left(\frac{1.1}{0.104} \right)^{0.551} \left(\frac{1.239}{0.231} - 1 \right)^{2.75}$$

$$= 6.495 \times 10^{-4} \text{ m}^2 \text{ s}^{-1} \Leftarrow \text{Eq. (7.35a)}$$

(viii) *Brownlie's method:*

The densimetric Froude number F_d is calculated from Eq. (7.39a) as

$$F_d = \frac{1.1}{(1.65 \times 9.81 \times 0.25 \times 10^{-3})^{0.5}} = 17.292 \Leftarrow \text{Eq. (7.39a)}$$

For $S_* = d_{50}(\Delta g d_{50})^{0.5}/\nu = 0.25 \times 10^{-3}(1.65 \times 9.81 \times 0.25 \times 10^{-3})^{0.5}/10^{-6} = 15.903$, the parameter Υ and the threshold Shields parameter Θ_c according to Brownlie are calculated from Eq. (7.39b) as

$$\Upsilon = \frac{1}{S_*^{0.6}} = \frac{1}{15.903^{0.6}} = 0.19 \text{ and } \Theta_c = 0.22\Upsilon - \frac{0.06}{10^{7.7\Upsilon}}$$

$$= 0.22 \times 0.19 - \frac{0.06}{10^{7.7 \times 0.19}} = 0.04$$

Then, the densimetric Froude number F_{dc} corresponding to threshold condition is calculated from Eq. (7.39b) as

$$F_{dc} = 4.596 \frac{0.043^{0.5295}}{(2 \times 10^{-3})^{0.1045} \times 10^{1.606}}$$

$$= 1.663 \Leftarrow \text{Eq. (7.39b)}$$

(Note: $\sigma_g = 1$ for uniform sediment)

The average concentration \bar{c}_t (by weight) is calculated from Eq. (7.38) as

$$\bar{c}_{pt} = 7115 \times 1.268(17.292 - 1.663)^{1.978} (2 \times 10^{-3})^{0.6601} \left(\frac{0.55}{0.25 \times 10^{-3}} \right)^{-0.3301}$$

$$= 2703.75 \Leftarrow \text{Eq. (7.38)}$$

$$\bar{c}_t = 10^{-6} \bar{c}_{pt} = 10^{-6} \times 2703.75 = 2.704 \times 10^{-3}$$

Note: In the above, it is assumed that $R_b = h$ and $c_f = 1.268$.

The average concentration \bar{C}_t (by volume) is

$$\bar{c}_t = \frac{s\bar{C}_t}{1 + \Delta\bar{C}_t} \text{ (Eq. 1.28)} \Rightarrow \bar{C}_t = \frac{\bar{c}_t}{s - \Delta\bar{c}_t} \approx \frac{\bar{c}_t}{s} = \frac{2.704 \times 10^{-3}}{2.65} = 1.02 \times 10^{-3}$$

The total-load transport rate (in volume per unit time and width) is

$$q_t = q\bar{C}_t = 0.605 \times 1.02 \times 10^{-3} = 6.171 \times 10^{-4} \text{ m}^2 \text{ s}^{-1}$$

(ix) *Karim's method:*

The total-load transport intensity is obtained from Eq. (7.44) as

$$\Phi_t = 1.39 \times 10^{-3} \times 17.292^{2.97} \left(\frac{0.104}{0.027} \right)^{1.47} = 47.902 \Leftarrow \text{Eq. (7.44)}$$

Then, the total-load transport rate (in volume per unit time and width) is

$$\begin{aligned} q_t &= \Phi_t (\Delta g d_{50}^3)^{0.5} = 47.902 [1.65 \times 9.81 (0.25 \times 10^{-3})^3]^{0.5} \\ &= 7.618 \times 10^{-4} \text{ m}^2 \text{ s}^{-1} \end{aligned}$$

(x) *Molinas and Wu's method:*

The non-dimensional stream power is computed from Eq. (7.45) as

$$\begin{aligned} \Psi_s &= \frac{U^3}{\Delta g h w_s} \left[\log \left(\frac{h}{d_{50}} \right) \right]^{-2} \\ &= \frac{1.1^3}{1.65 \times 9.81 \times 0.55 \times 0.027} \left[\log \left(\frac{0.55}{0.25 \times 10^{-3}} \right) \right]^{-2} = 0.496 \end{aligned}$$

The average concentration \bar{c}_t (by weight) is calculated from Eq. (7.45) as

$$\begin{aligned} \bar{c}_{pt} &= \frac{1430(0.86 + 0.496^{0.5})0.496^{1.5}}{0.016 + 0.496} = 1526.16 \Leftarrow \text{Eq. (7.45)} \\ \bar{c}_t &= 10^{-6} \bar{c}_{pt} = 10^{-6} \times 1526.16 = 1.526 \times 10^{-3} \end{aligned}$$

The average concentration \bar{C}_t (by volume) is

$$\bar{c}_t = \frac{s\bar{C}_t}{1 + \Delta\bar{C}_t} \text{ (Eq. 1.28)} \Rightarrow \bar{C}_t = \frac{\bar{c}_t}{s - \Delta\bar{c}_t} \approx \frac{\bar{c}_t}{s} = \frac{1.526 \times 10^{-3}}{2.65} = 5.758 \times 10^{-4}$$

The total-load transport rate (in volume per unit time and width) is

$$q_t = q\bar{C}_t = 0.605 \times 5.758 \times 10^{-4} = 3.484 \times 10^{-4} \text{ m}^2 \text{ s}^{-1}$$

(xi) *Yang and Lim's method:*

The total-load transport rate (in weight per unit time and width) is calculated from Eq. (7.46) as

$$g_t = 12.5 \frac{2.65 \times 10.791}{1.65 \times 0.027} (0.104^2 - 0.013^2) = 85.427 \text{ N s}^{-1} \Leftarrow \text{Eq. (7.46)}$$

Note: In the above, it is assumed that $k = 12.5$ and $u'_* = u_*$.

Then, the total-load transport rate (in volume per unit time and width) is

$$q_t = \frac{g_t}{\rho_s g} = \frac{85.427}{2.65 \times 10^3 \times 9.81} = 3.286 \times 10^{-3} \text{ m}^2 \text{ s}^{-1}$$

(xii) *Sinnakaudan et al.'s method:*

The average concentration \bar{C}_t (by volume) is calculated from Eq. (7.47) as

$$\begin{aligned} \bar{C}_t &= 1.811 \times 10^{-4} \frac{[1.65 \times 9.81(0.25 \times 10^{-3})^3]^{0.5}}{1.1 \times 0.55} \\ &\quad \left(\frac{1.1 \times 2 \times 10^{-3}}{0.027} \right)^{0.293} \left(\frac{0.55}{0.25 \times 10^{-3}} \right)^{1.39} \\ &= 1.011 \times 10^{-4} \text{ m}^2 \text{ s}^{-1} \Leftarrow \text{Eq. (7.47)} \end{aligned}$$

Note: In the above, it is assumed that $R_b = h$.

The total-load transport rate (in volume per unit time and width) is

$$q_t = q \bar{C}_t = 0.605 \times 1.011 \times 10^{-4} = 6.117 \times 10^{-5} \text{ m}^2 \text{ s}^{-1}.$$

Example 7.2 Given the cross section of an alluvial channel (Fig. E7.1) and the following data, compute the total-load transport rate in weight per unit time by using Einstein's approach: Bed slope $S_0 = 9 \times 10^{-4}$; relative density of sediment $s = 2.65$; maximum flow discharge $Q_{\max} = 63.2 \text{ m}^3 \text{ s}^{-1}$; and coefficient of kinematic viscosity of water $\nu = 10^{-6} \text{ m}^2 \text{ s}^{-1}$.

The sieve analysis results and particle size distribution curve (Fig. E7.2) are as follows:

Size fraction (mm)	Percentage retained	Mean size, d_i (mm)	Terminal fall velocity, w_s (m s^{-1})
$0.6 < d$	0.5	—	—
$0.425 < d < 0.6$	16.8	0.5125	0.058
$0.25 < d < 0.425$	39.3	0.3375	0.041
$0.15 < d < 0.25$	35.6	0.2	0.022
$0.125 < d < 0.15$	7.1	0.1375	0.012
$d < 0.125$	0.7	—	—

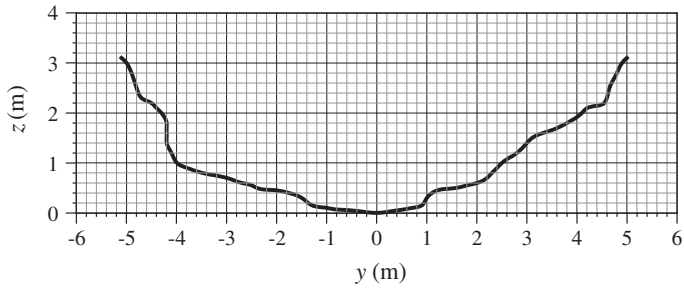
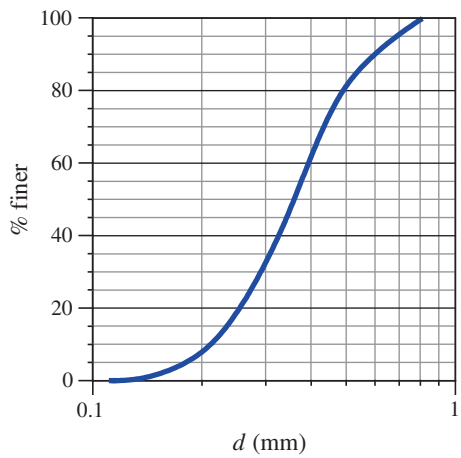


Fig. E7.1 Channel cross section

Fig. E7.2 Particle size distribution curve



Solution

From the given channel cross section (Fig. E7.1), the variations of flow area A , wetted perimeter P , and hydraulic radius R_b with flow depth h are estimated and shown in Figs. E7.3a, b:

In the table of the sieve analysis results, the mean size of sediment actually corresponds to the geometric mean size, which is approximately equal to the arithmetic mean size for a small difference in size fractions. Consider the mean

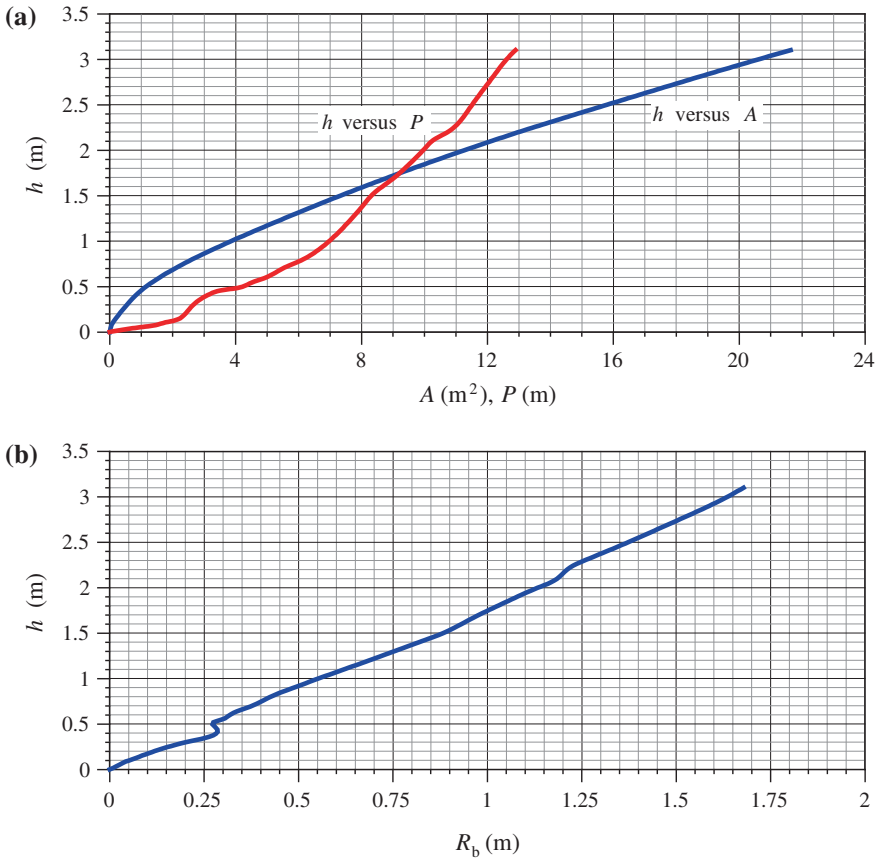


Fig. E7.3 **a** Flow depth h versus flow area A and wetted perimeter P curves and **b** flow depth h versus hydraulic radius R_b curve

size d_i being the representative size for the size fractions. From the particle size distribution curve (Fig. E7.2), $d_{35} = 0.303$ mm, $d_{50} = 0.35$ mm, and $d_{65} = 0.415$ mm are obtained.

The computation is performed in two phases: (i) hydraulic computation for the flow (Table 7.4) and (ii) total-load transport rate computation (Table 7.5).

(i) *Hydraulic computation for the flow:*

Following steps are involved in computation of various parameters in Table 7.4

1. Various values of hydraulic radius due to particle roughness R'_b are assumed covering the entire range of maximum discharge, $Q_{\max} = 63.2 \text{ m}^3 \text{ s}^{-1}$
2. Calculate the shear velocity due to particle roughness, $u'_* = (gR'_b S_0)^{0.5}$
3. Calculate the viscous sublayer thickness, $\delta' = 11.6\nu/u'_*$

Table 7.4 Summary of hydraulic computation

R'_b (m)	u'_* (m s ⁻¹)	δ' (m)	k_s/δ'	x_k	Δ_k (m)	U (m s ⁻¹)
1	2	3	4	5	6	7
0.1	0.0297	3.9×10^{-4}	1.063	1.62	2.56×10^{-4}	0.629
0.2	0.042	2.76×10^{-4}	1.503	1.5	2.77×10^{-4}	0.954
0.4	0.0594	1.95×10^{-4}	2.126	1.31	3.17×10^{-4}	1.432
0.6	0.0728	1.59×10^{-4}	2.604	1.24	3.35×10^{-4}	1.817
0.9	0.0891	1.3×10^{-4}	3.189	1.16	3.58×10^{-4}	2.301
1.2	0.103	1.13×10^{-4}	3.682	1.12	3.71×10^{-4}	2.722
1.6	0.119	9.76×10^{-5}	4.252	1.07	3.88×10^{-4}	3.215
Ψ'_b	U/hu''_*	u''_* (m s ⁻¹)	R''_b (m)	R_b (m)	u_w (m s ⁻¹)	h (m)
8	9	10	11	12	13	14
5.555	10.1	0.062	0.436	0.5356	0.0688	1
2.778	15.2	0.0624	0.4405	0.6405	0.0752	1.1
1.389	28	0.051	0.2954	0.6954	0.0784	1.2
0.926	40.5	0.0448	0.2274	0.8274	0.0855	1.4
0.617	71	0.0324	0.1186	1.0186	0.0948	1.76
0.463	112	0.0243	0.0667	1.2667	0.1058	2.32
0.347	135	0.0238	0.0641	1.6641	0.1212	2.9
A (m ²)	P (m)	Q (m ³ s ⁻¹)	X (m)	Y	β_x	P_E
15	16	17	18	19	20	21
3.9	7.211	2.443	5.43×10^{-4}	0.83	3.111	11.678
4.5	7.026	4.265	3.84×10^{-4}	0.74	2.688	11.696
5.1	7.334	7.292	2.71×10^{-4}	0.58	2.206	11.647
6.8	8.218	12.341	2.58×10^{-4}	0.55	2.099	11.747
9.3	9.099	21.371	2.75×10^{-4}	0.53	2.099	11.909
14	11.052	38.056	2.85×10^{-4}	0.525	2.099	12.15
19.7	11.839	63.248	2.99×10^{-4}	0.52	2.099	12.327

Table 7.5 Summary of total-load transport rate computation

R'_b (m)	Ψ'_b	d_i/X	ξ	Ψ_{b^*}	Φ_{b^*}	i_{b8b} (N s ⁻¹ m ⁻¹)	$i_b G_b$ (N s ⁻¹)	$\sum i_b G_b$ (N s ⁻¹)
1	2	3	4	5	6	7	8	9
Fractional size $d_i = 5.125 \times 10^{-4}$ m and fraction $p_i = 16.8$ % or 0.168								
0.1	9.396	0.944	1.12	5.029	0.7	0.143	1.039	1.039
0.2	4.698	1.336	1	2.682	2.65	0.54	3.796	3.796
0.4	2.349	1.889	1	1.561	4.8	0.979	7.177	7.177
0.6	1.566	1.989	1	1.089	6.8	1.386	11.393	11.393
0.9	1.044	1.86	1	0.7	10.8	2.202	20.101	20.101
1.2	0.783	1.796	1	0.52	14.5	2.956	32.671	32.671
1.6	0.587	1.716	1	0.386	20	4.077	48.269	48.269
Fractional size $d_i = 3.375 \times 10^{-4}$ m and fraction $p_i = 39.3$ % or 0.393								
0.1	6.188	0.622	2.15	6.357	0.4	0.102	0.742	1.781
0.2	3.094	0.88	1.2	2.119	3.25	0.828	5.82	9.616
0.4	1.547	1.244	1.05	1.079	7.5	1.911	14.019	21.196
0.6	1.031	1.31	1	0.717	10.6	2.701	22.201	33.594
0.9	0.688	1.225	1.05	0.484	15.5	3.95	36.065	56.166
1.2	0.516	1.183	1.04	0.356	20.5	5.225	57.743	90.413
1.6	0.387	1.13	1.02	0.259	27	6.881	81.462	129.731
Fractional size $d_i = 2 \times 10^{-4}$ m and fraction $p_i = 35.6$ % or 0.356								
0.1	3.667	0.369	8	14.017	0.035	3.686×10^{-3}	0.0268	1.808
0.2	1.833	0.521	2.95	3.087	1.75	0.184	1.295	10.911
0.4	0.917	0.737	1.6	0.974	8	0.843	6.179	27.376
0.6	0.611	0.776	1.4	0.595	12	1.264	10.386	43.98
0.9	0.407	0.726	1.7	0.464	16	1.685	15.384	71.55
1.2	0.306	0.701	1.8	0.365	21	2.212	24.443	114.856
1.6	0.229	0.67	2	0.301	24	2.528	29.922	159.653

(continued)

Table 7.5 (continued)

R'_b (m)	Ψ'_b	d_i/X	ξ	Ψ_{b^*}	Φ_{b^*}	i_{bgb} (N s ⁻¹ m ⁻¹)	$i_b G_b$ (N s ⁻¹)	$\sum i_b G_b$ (N s ⁻¹)
1	2	3	4	5	6	7	8	9
Fractional size $d_i = 1.375 \times 10^{-4}$ m and fraction $p_i = 7.1$ % or 0.07								
0.1	2.521	0.253	20	24.091	1×10^{-3}	1.197×10^{-5}	8.72×10^{-5}	1.808
0.2	1.26	0.358	8.9	6.404	0.44	5.268×10^{-3}	0.037	10.948
0.4	0.63	0.507	3.2	1.34	5.5	0.066	0.483	27.859
0.6	0.42	0.534	2.8	0.818	9.8	0.117	0.964	44.945
0.9	0.28	0.499	3.23	0.606	12.1	0.145	1.323	72.873
1.2	0.21	0.482	4	0.558	13.5	0.162	1.786	116.643
1.6	0.158	0.46	4.2	0.435	17	0.204	2.41	162.063
\bar{a}	ξ	I_1	$-I_2$	$1 + P_E I_1 + I_2$	i_{sgst} (N s ⁻¹ m ⁻¹)	i_{sgst} (N s ⁻¹)	$\sum i_{sgst}$ (N s ⁻¹)	
10	11	12	13	14	15	16	17	
Fractional size $d_i = 5.125 \times 10^{-4}$ m and fraction $p_i = 16.8$ % or 0.168								
1.91×10^{-3}	4.88	0.054	0.333	1.298	0.185	1.348	1.348	1.348
1.6×10^{-3}	3.451	0.088	0.53	1.499	0.81	5.691	5.691	5.691
1.47×10^{-3}	2.44	0.149	0.868	1.867	1.827	13.403	13.403	13.403
1.24×10^{-3}	1.992	0.214	1.227	2.287	3.17	26.053	26.053	26.053
1×10^{-3}	1.627	0.335	1.81	3.179	7	63.911	63.911	63.911
8.09×10^{-4}	1.409	0.475	2.493	4.278	12.647	139.773	139.773	139.773
6.16×10^{-4}	1.22	0.727	3.579	6.383	26.026	308.104	308.104	308.104
Fractional size $d_i = 3.375 \times 10^{-4}$ m and fraction $p_i = 39.3$ % or 0.393								
1.26×10^{-3}	3.45	0.088	0.551	1.477	0.151	1.096	1.096	2.444
1.05×10^{-3}	2.439	0.149	0.92	1.823	1.51	10.608	10.608	16.298
9.71×10^{-4}	1.725	0.29	1.639	2.739	5.235	38.395	38.395	51.798
8.16×10^{-4}	1.408	0.475	2.49	4.09	11.048	90.796	90.796	116.849

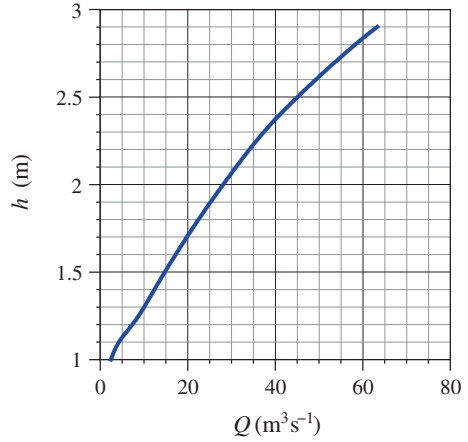
(continued)

(continued)

Table 7.5 (continued)

\tilde{a}	ζ	I_1	$-I_2$	$1 + P_E I_1 + I_2$	$i_{st} g_{st}$ (N s ⁻¹ m ⁻¹)	$i_{st} G_{st}$ (N s ⁻¹)	$\sum i_{st} G_{st}$ (N s ⁻¹)
10	11	12	13	14	15	16	17
6.63×10^{-4}	1.15	0.868	4.022	7.315	28.896	263.809	327.72
5.33×10^{-4}	0.996	1.433	5.965	12.446	65.0242	718.659	858.431
4.06×10^{-4}	0.862	2.523	9.291	22.811	156.966	1858.24	2166.35
Fractional size $d_i = 2 \times 10^{-4}$ m and fraction $p_i = 35.6$ % or 0.356							
7.47×10^{-4}	1.851	0.25	1.518	2.401	8.85×10^{-3}	0.064	2.509
6.25×10^{-4}	1.309	0.59	3.059	4.842	0.892	6.27	22.568
5.75×10^{-4}	0.926	1.823	6.965	15.268	12.864	94.348	146.145
4.83×10^{-4}	0.756	3.886	12.238	34.41	43.486	357.377	474.226
3.93×10^{-4}	0.617	8.484	22.19	79.844	134.54	1228.31	1556.03
3.16×10^{-4}	0.534	15.103	35.165	149.336	330.271	3650.21	4508.64
2.4×10^{-4}	0.463	27.416	57.379	281.59	711.73	8425.82	10592.17
Fractional size $d_i = 1.375 \times 10^{-4}$ m and fraction $p_i = 7.1$ % or 0.07							
5.13×10^{-4}	1.01	1.375	5.829	11.228	1.34×10^{-4}	9.79×10^{-4}	2.51
4.29×10^{-4}	0.714	4.936	14.825	43.906	0.231	1.625	24.193
3.96×10^{-4}	0.505	16.156	3.644	185.532	12.218	89.609	235.754
3.32×10^{-4}	0.412	31.853	61.034	314.132	36.859	302.916	777.143
2.7×10^{-4}	0.337	60.811	103.81	621.377	90.021	821.869	2377.901
2.17×10^{-4}	0.291	98.002	156.03	1035.688	167.404	1850.18	6358.822
1.65×10^{-4}	0.252	161.21	241.56	1746.71	355.528	4208.92	14801.09

Fig. E7.4 Variation of discharge Q with flow depth h



4. Obtain the ratio k_s/δ' , where $k_s = d_{65}$
5. Find the correction factor x_k from Fig. 5.7 for the value of k_s/δ'
6. Obtain the apparent roughness, $\Delta_k = k_s/x_k$
7. Calculate the depth-averaged velocity, $U = (u_*'/\kappa)\ln(12.27R_b'/\Delta_k)$ [see Eq. (7.7)]
8. Estimate the flow intensity parameter, $\Psi'_b = \Delta d_{35}/(R_b'S_0)$
9. Find the ratio U/u_*'' from Fig. 8.35 for the value of Ψ'_b
10. Obtain the shear velocity due to bedforms u_*'' from the ratio U/u_*''
11. Calculate the hydraulic radius due to bedforms, $R_b'' = u_*''^2/(gS_0)$
12. Calculate the total hydraulic radius, $R_b = R_b' + R_b''$
13. Calculate the total shear velocity, $u_* = (gR_bS_0)^{0.5}$
14. Using Fig. E7.3b, determine the flow depth h for the value of R_b
15. Determine the flow area A from Fig. E7.3a
16. Determine the wetted perimeter P from Fig. E7.3a or simply from $P = A/R_b$
17. Obtain the flow discharge, $Q = UA$. The variation of discharge Q with flow depth h is shown in Fig. E7.4
18. Find the characteristic particle size, $X(\Delta_k/\delta' \geq 1.8) = 0.77\Delta_k$ and $X(\Delta_k/\delta' < 1.8) = 1.39\delta'$
19. Find the lift correction factor Y from Fig. 5.9 for the value of k_s/δ'
20. Calculate β_x from $\beta_x = \ln(10.6X/\Delta_k)$ [see Eq. (5.65)]
21. Calculate the transport parameter, $P_E = \ln(30.2h/\Delta_k)$ [see Eq. (6.129) or (7.4)]

(ii) *Total-load transport rate computation:*

Following steps are involved in computation of various parameters in Table 7.5

1. Get the hydraulic radius due to particle roughness R_b' from Table 7.4.
2. Obtain the flow intensity parameter for a fractional particle size d_i (mean value of fractional size), $\Psi'_b = \Delta d_i/(R_b'S_0)$
3. Find the ratio d/X , where X is obtained from Table 7.4.

4. Find the hiding factor ζ from Fig. 5.8 for the value of d/X
5. Calculate the flow intensity parameter due to individual particle roughness, $\Psi_{b*} = \Psi'_b \zeta Y [\ln(10.6)/\beta_x]^2$, where Y and β_x are obtained from Table 7.4
6. Obtain the bed-load transport intensity Φ_{b*} due to individual particle roughness from Fig. 5.10 for the value of Ψ_{b*}
7. Calculate the bed-load transport rate (in weight per unit time and width) for a particle size fraction, $i_b g_b = p_i \Phi_{b*} \rho_s g (\Delta g d_i^3)^{0.5}$
8. Calculate the bed-load transport rate (in weight per unit time) for a particle size fraction for the entire cross section, $i_b G_b = (i_b g_b) P$
9. Calculate the bed-load transport (in weight per unit time) for all particle size fractions for the entire cross section, $\sum i_b G_b$
10. Obtain the ratio $\tilde{a} = a/R_b$, where $a = 2d_i$
11. Calculate the Rouse number, $\zeta = w_s/(0.4u'_*)$, where w_s and u'_* are obtained from sieve analysis table and Table 7.4, respectively
12. Read the Einstein integral I_1 from Fig. 6.11 or compute I_1 numerically from Eq. (6.130a)
13. Read the Einstein integral I_2 from Fig. 6.12 or compute I_2 numerically from Eq. (6.130b)
14. Calculate $1 + P_E I_1 + I_2$, where P_E is obtained from Table 7.4
15. Calculate the total-load transport rate (in weight per unit time and width) for a particle size fraction, $i_{st} g_{st} = i_b g_b (1 + P_E I_1 + I_2)$
16. Calculate the total-load transport rate (in weight per unit time) for a particle size fraction for the entire cross section, $i_{st} G_{st} = (i_{st} g_{st}) P$
17. Calculate the total-load transport (in weight per unit time) for all particle size fractions for the entire cross section, $\sum i_s G_{st}$

References

- Ackers P (1990) Sediment transport: the Ackers and White theory revised. Report SR 237, HR Wallingford, Wallingford, Oxfordshire
- Ackers P, White WR (1973) Sediment transport: new approach and analysis. J Hydraul Div 99(11):2041–2060
- Bagnold RA (1966) An approach to the sediment transport problem from general physics. Geological survey professional paper 422-I, Washington, DC
- Bishop AA, Simons DB, Richardson EV (1965) Total bed material transport. J Hydraul Div 91(2):175–191
- Brownlie WR (1981) Prediction of flow depth and sediment discharge in open channels. Report number KH-R-43A, Keck Laboratory of Hydraulics and Water Resources, California Institute of Technology, Pasadena
- Chang FM, Simons DB, Richardson EV (1965) Total bed-material discharge in alluvial channels. Paper 1498-I, United States Geological Survey Water Supply, Washington, DC
- Chang FM, Simons DB, Richardson EV (1967) Total bed-material discharge in alluvial channels. In: Proceedings of the twelfth congress of International Association for Hydraulic Research, Fort Collins, pp 132–140
- Cheng N-S (1997) Simplified settling velocity formula for sediment particle. J Hydraul Eng 123(2):149–152

- Chien N, Wan Z (1999) *Mechanics of sediment transport*. ASCE Press, Reston
- Colby BR, Hembree CH (1955) Computations of total sediment discharge Niobrara River near Cody, Nebraska. Water-Supply Paper 1357, United States Geological Survey, Washington, DC
- Einstein HA (1950) The bed-load function for sediment transportation in open channel flows. Technical Bulletin number 1026, United States Department of Agriculture, Soil Conservation Service, Washington, DC
- Engelund F, Hansen E (1967) A monograph on sediment transport in alluvial streams. Technical Press (Teknisk Forlag), Copenhagen
- Graf WH, Acaroglu ER (1968) Sediment transport in conveyances systems, part 1. *Bull Int Assoc Sci Hydrol* 13(2):20–39
- Guo J, Julien PY (2004) Efficient algorithm for computing Einstein integrals. *J Hydraul Eng* 130(12):1198–1201
- Karim F (1998) Bed material discharge prediction for nonuniform bed sediments. *J Hydraul Eng* 124(6):597–604
- Karim MF, Kennedy JF (1990) Menu of coupled velocity and sediment-discharge relations for rivers. *J Hydraul Eng* 116(8):978–996
- Keulegan GH (1938) Laws of turbulent flow in open channels. *J Res National Bur Stand* 21(6):707–741
- Laursen EM (1958) The total sediment load of streams. *J Hydraul Div* 84(1):1–36
- Molinas A, Wu B (2001) Transport of sediment in large sand-bed rivers. *J Hydraul Res* 39(2):135–146
- Posada GL (1995) Transport of sands in deep rivers. PhD thesis, Colorado State University, Fort Collins, Colorado
- Shah-Fairbank SC (2009) Series expansion of the modified Einstein procedure. Colorado State University, Fort Collins
- Shah-Fairbank SC, Julien PY, Baird DC (2011) Total sediment load from SEMEP using depth-integrated concentration measurements. *J Hydraul Eng* 137(12):1606–1614
- Simons DB, Sentürk F (1977) *Sediment transport technology*. Water Resources Publication, Fort Collins
- Sinnakaudan SK, Ghani AA, Ahmad MSS, Zakaria NA (2006) Multiple linear regression model for total bed material load prediction. *J Hydraul Eng* 132(5):521–528
- USBR (1955) Step method for computing total sediment load by the modified Einstein procedure. Sedimentation Section, Hydrology Branch, Project Investigations Division, United States Bureau of Reclamation, Denver, Colorado
- USWES (1936) Studies of light-weight materials with special reference to their movement and use as model bed material. Technical Memorandum 103-1, United States Waterways Experiment Station, Vicksburg, Mississippi
- Wu B, Molinas A, Julien PY (2004) Bed-material load computations for sediment mixtures. *J Hydraul Eng* 130(10):1002–1012
- Yang CT (1972) Unit stream power and sediment transport. *J Hydraul Div* 98(10):1805–1826
- Yang CT (1973) Incipient motion and sediment transport. *J Hydraul Div* 99(10):1679–1704
- Yang CT (1979) Unit stream power equations for total load. *J Hydrol* 40(1–2):123–138
- Yang CT (1984) Unit stream power equation for gravels. *J Hydraul Eng* 110(12):1783–1797
- Yang CT (1996) *Sediment transport: theory and practice*. McGraw-Hill, New York
- Yang CT, Molinas A (1982) Sediment transport and unit stream power function. *J Hydraul Div* 108(6):774–793
- Yang CT, Molinas A, Wu B (1996) Sediment transport in the Yellow River. *J Hydraul Eng* 122(5):237–244
- Yang CT, Simões FJM (2005) Wash load and bed-material load transport in the Yellow River. *J Hydraul Eng* 131(5):413–418
- Yang S-Q (2005) Prediction of total bed material discharge. *J Hydraul Res* 43(1):12–22
- Yang S-Q, Lim S-Y (2003) Total load transport formula for flow in alluvial channels. *J Hydraul Eng* 129(1):68–72

Chapter 8

Bedforms

8.1 General

In nature, sediment beds are almost always characterized by bed undulations resulting from the flow associated with sediment transport. The processes of local sediment removal and deposition govern the configuration of bed undulations. The undulation may be only a few centimeters to several meters high, displaying relatively regular features in statistical sense. This is the reason why the sediment bed surface is rarely found plane and the bed configuration usually exhibits somewhat distinctive geometric features.

When the bed shear stress τ_0 of flow over a sediment bed exceeds its threshold value τ_{0c} , the sediment starts moving and the bed surface does not remain stable but takes different geometric configurations known as *bedforms*. As the bed shear stress increases in accordance with an increase in flow velocity, the bedforms grow to a certain size and then decrease to a state where the sediment transport essentially takes place on a relatively plane bed. With further increase in bed shear stress (or in turn, flow velocity), a strong interaction between the bed undulations and the water surface takes place. Therefore, the shape, size, and spacing of the bedforms, which are uniform in statistical sense, depend on the flow (velocity and depth) and the bed sediment characteristics (size and grading). Due to sediment transport, the bedforms (except antidune propagating upstream) usually migrate in the downstream direction with a velocity that is much slower than the average flow velocity, while their shape is preserved for the given flow condition and sediment size. The interaction between the flow and the bedforms in addition to sediment transport (bed load and/or suspended load) is extremely complex. On the one hand, the intensity of flow controls the bedforms. On the other hand, the bedforms significantly influence the characteristics of flow field. Detailed description of various bedforms was given by Allen (1968).

To classify bedforms, three flow regimes are distinguished according to the flow Froude number $Fr [= U/(gh_d)^{0.5}]$, where U is the depth-averaged flow velocity, g is the acceleration due to gravity, h_d is the hydraulic depth ($= A/T$), A is the flow area, and T is the top width of flow] (Simons et al. 1961):

1. *Lower flow regime* for $Fr < 1$ (subcritical flow), namely *ripples*, *ripples on dunes*, and *dunes*.
2. *Transition* for $Fr \approx 1$ (about critical flow), namely *washed-out dunes*.
3. *Upper flow regime* for $Fr > 1$ (supercritical flow), namely *plane bed*, *antidunes*, *chutes*, and *pools*.

According to Simons and Richardson (1966), Figs. 8.1(a–h) illustrate different bedforms. As Froude number increases, a plane bed is modified to different bedforms with a sequence: plane bed \Rightarrow ripples \Rightarrow ripples on dunes \Rightarrow dunes \Rightarrow transition or washed-out dunes \Rightarrow plane bed \Rightarrow antidune standing waves \Rightarrow antidune breaking waves \Rightarrow chutes and pools [also see Engelund and Fredsøe (1982)].

8.2 Bedforms

8.2.1 Ripples

Small skewed delta-shaped (asymmetrical triangular) bedforms having a relatively long gentle upstream slope (approximately 6°) and a short steep downstream slope (approximately angle of repose of bed sediment, $\phi \approx 32^\circ$) are called *ripples* (Figs. 8.1a and 8.2). Ripples can only be observed on a bed of fine sediments having median size d less than 0.7 mm and at shear Reynolds number R_* ($= u_* k_s / \nu$, where u_* is the shear velocity, k_s is the Nikuradse's equivalent sand roughness, and ν is the coefficient of kinematic viscosity), ranging less than 11.6.¹ The length λ_r of ripples is usually shorter than 600 mm and the height η_r shorter than 60 mm. According to Yalin (1985), $\lambda_r = 500\text{--}1000d$ and $\eta_r = 50\text{--}200d$.

It is understood that the ripples are developed in the presence of viscous sub-layer (hydraulically smooth flow) in which the bed shear stress induced by the flow exceeds its threshold value for the sediment motion, while dunes are formed in hydraulically rough flow. The length of the ripples depends on the sediment size and the flow velocity, but is believed to be independent of the flow depth (Raudkivi 1990). Ripples may be superimposed on the upstream slope of dunes (Fig. 8.1b); this condition usually prevails when there is a transition between ripples and dunes. It is therefore concluded that the ripples are the bed configuration that is developed in a shear layer of smooth flow at small excess bed shear stress (that is, $\tau_0 - \tau_{0c}$), while dunes interact with the main flow. However, at a

¹ In terms of Shields parameter, ripples can occur at about $\Theta = 10\text{--}14\Theta_c$, where Θ and Θ_c are the Shields parameter and the threshold Shields parameter, respectively. The Shields parameter is defined as $\Theta = \tau_0 / (\Delta \rho g d)$, and the threshold Shields parameter Θ_c corresponds to the threshold bed shear stress τ_{0c} . Here, τ_0 is the bed shear stress ($= \rho u_*^2$), Δ is the submerged relative density ($= s - 1$), s is the relative density of sediment ($= \rho_s / \rho$), ρ_s is the mass density of sediment, ρ is the mass density of water, g is the acceleration due to gravity, and d is the median particle size.

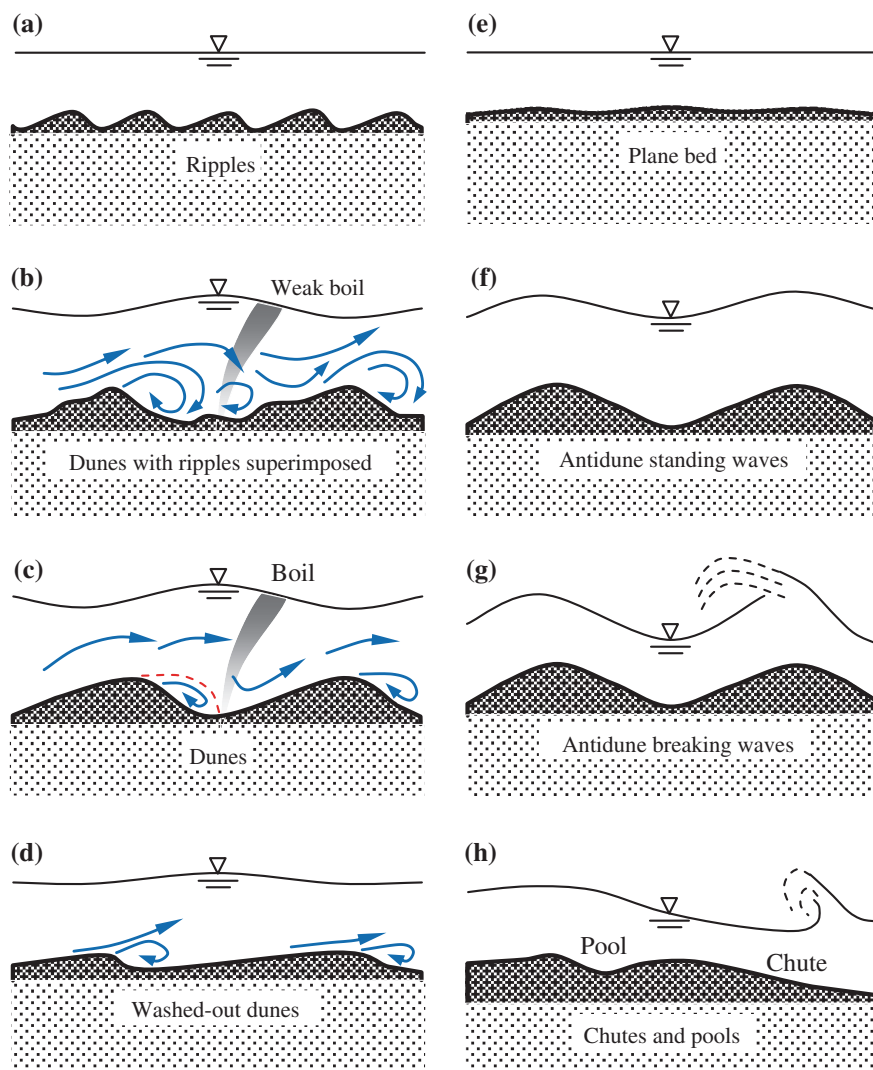


Fig. 8.1 Schematic of bedforms (Simons and Richardson 1966): **a** ripples, **b** ripples on dunes, **c** dunes, **d** transition or washed-out dunes, **e** plane bed, **f** antidune standing waves, **g** antidune breaking waves, and **h** chutes and pools

low flow intensity, ripples are more or less uniform, but they become three-dimensional at an increased flow intensity. Further, in developing state, the ripples undergo the process of *coarsening* with a progressive increase in length as time goes by due to the merger of two adjacent ripples (Raudkivi 1997; Baas 1999; Valance 2005).



Fig. 8.2 Photograph of two-dimensional ripples (courtesy of JH Baas, Bangor University, UK)

The mechanism of ripple formation is not so well understood, as there is no general consensus of opinions as yet. The concepts, in this regard, are broadly divided into two categories: stability concept and initial disturbance concept. Bagnold (1956) studied the stability of the sediment bed in a steam flow. He defined the threshold Shields parameter and above which all the surface particles to be in a saltating motion (see Sect. 5.11). At slightly lower values of the Shields parameter, he argued that the plane bed that becomes unstable is unable to resist the applied bed shear stress. Primary ripples are then formed to introduce form drag and thus to reduce the resistance due to skin friction. In increased flow intensities, these primary ripples become unstable and form secondary ripples with a larger form drag. Liu (1957), however, argued that the sediment bed acts as a viscous fluid and ripples are formed due to a type of *Kelvin–Helmholtz instability*² of two sheared fluids of different densities. It seems to be not a successful attempt. In contrast, according to the initial disturbance concept, the genesis of the formation of ripples lies on the local intermittent action of turbulence or a disturbance that causes a deviation from a perfectly plane sediment bed (Raudkivi 1963, 1966; Williams and Kemp 1971). In particular, Raudkivi (1966) attributed the ripples to a downstream propagation of a possible initial piling up of the bed sediment, while Williams and Kemp (1971) believed that the small bed disturbances are resulted from the random action of near-bed turbulent bursts. The disturbed bed then causes the near-bed flow to separate with subsequent building up of the bed disturbances into ripples. The propagation of ripples proceeds with an erosion and deposition process.

² The *Kelvin–Helmholtz instability* may occur when there is shear at the interface between two flowing fluids.

Richards (1980) gave the criterion for the formation of ripples in terms of the product of wave number and roughness parameter as

$$7 \times 10^{-4} < k_w \varepsilon_0 < 0.16 \quad (8.1)$$

where k_w is the wave number ($= 2\pi/\lambda_r$), λ_r is the wavelength of ripple, and ε_0 is the roughness parameter given by

$$\varepsilon_0 = 26.3d(\Theta - \Theta_c) + z_0 \quad \wedge \quad z_0 = \frac{k_s}{30}$$

where k_s is the Nikuradse's equivalent sand roughness.

Using the laboratory data of Guy et al. (1966), Karim (1999) proposed the criterion for the formation of ripples as

$$N_* < 80 \quad \wedge \quad N_* = R_* F_d \quad \vee \quad F_d = \frac{U}{(\Delta g d)^{0.5}} \quad (8.2)$$

where F_d is the densimetric Froude number and U is the depth-averaged velocity.

According to Julien (2010), the conditions for the formation of ripples are

$$(1) \ 2 < D_* < 6, \ (2) \ 4 < R_* < 11.6, \ (3) \ \tau_0 < \frac{4}{D_*} \text{ or } \tau_0 < 1 \quad \wedge \quad D_* = d \left(\frac{\Delta g}{v^2} \right)^{1/3} \quad (8.3)$$

It is also important to discuss the dimensions of ripples. Yalin (1985) gave the range of equilibrium length λ_r of ripples as

$$\lambda_r|_{\min} < \lambda_r < \lambda_r|_{\max} \quad \wedge \quad \lambda_r|_{\min} = 2096 \frac{d}{D_*^{0.75}} \quad \vee \quad \lambda_r|_{\max} = 2000d \quad (8.4)$$

Both $\lambda_r|_{\min}$ and d are in mm. Equation (8.4) is applicable for $d = 0.105$ – 0.26 mm.

On the other hand, Baas (1993) proposed empirical equations for the length λ_r and height η_r of ripples in equilibrium condition as

$$\lambda_r = 75.4 \log d + 197, \quad \eta_r = 18.16d^{0.097} \quad (8.5)$$

Both η_r and d are in mm.

Raudkivi (1997) related ripple length to particle size as

$$\lambda_r = 245d^{0.35} \quad (8.6)$$

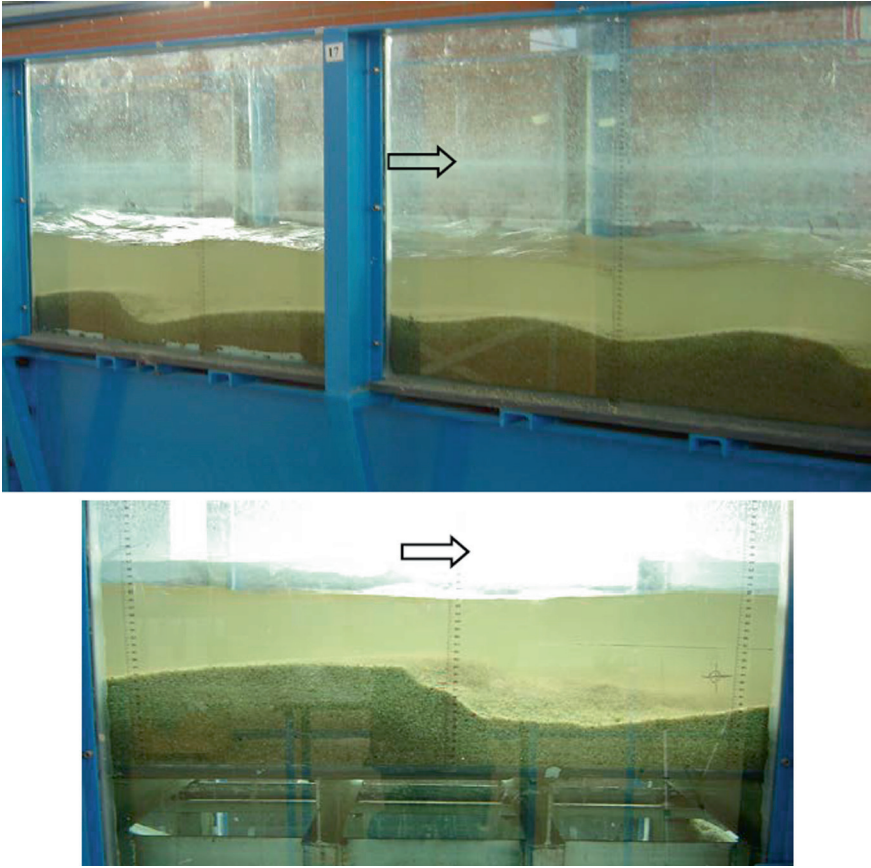


Fig. 8.3 Photographs of dunes (Núñez-González 2012)

8.2.2 Dunes

Dunes are the larger bedforms as compared to ripples. The streamwise profile of a dune is roughly asymmetrical triangular with a mild, but a little convexly curved, stoss-side (upstream) slope and a leeside (downstream) slope approximately equaling the angle of repose of bed sediment (Figs. 8.1c and 8.3). Dunes are formed in relatively coarse sediments ($d > 0.6$ mm), as compared to ripple-forming sediments and at larger excess bed shear stresses ($\tau_0 - \tau_{0c}$) than those for the case of ripples.

The dune profile is out of phase with the free surface profile. Flow separation that originates at the dune crest reattaches to the trough (Fig. 8.1c). Thus, a roller is formed on the leeside of dunes. In the flow zone above the roller, high turbulent mixing occurs, where the turbulent kinetic energy production, as well as dissipation, takes place to a large extent. The presence of flow separation is also

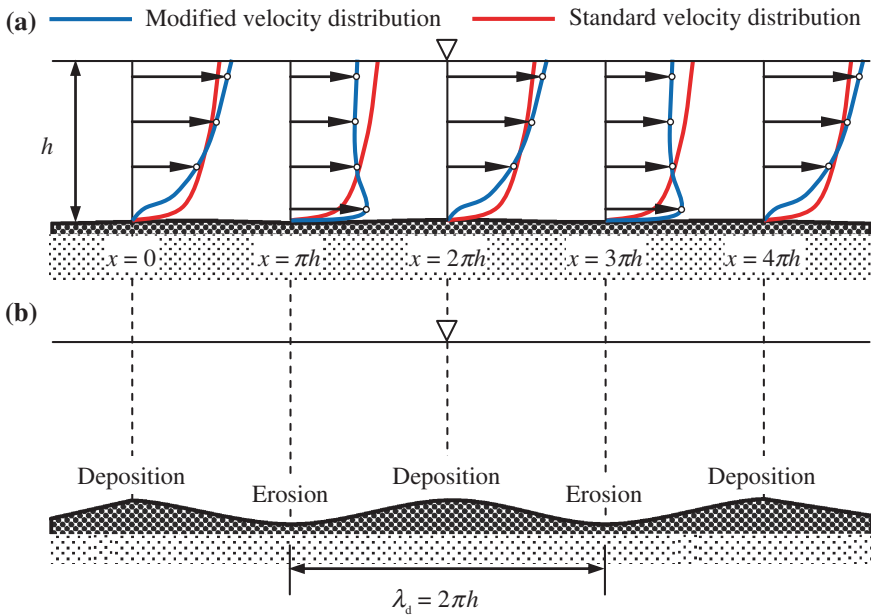


Fig. 8.4 Formation of dunes according to Yalin (1977): **a** Modified velocity distributions and **b** zones of sediment deposition and erosion

observed at the free surface in the form of *boils* rising up to the surface (Fig. 8.1c). Near the reattachment zone, the sediment particles are removed by the turbulence, even though the local bed shear stress is less than its threshold value. On the stoss side of dunes, the bed shear stress drives the sediment particles uphill until they roll over the crest and eventually are deposited on the leeward side and buried by the succession of sediment deposition. In fact, the flow roller favors sediment deposition. As sediment is transported from the stoss side and deposited on the leeward side, dunes continuously migrate downstream at a slow speed.

Yalin (1977) argued that the formation of dunes may be caused by the large-scale oscillations. Large, but low-frequency, eddies appear at a relatively regular interval, resulting in decrease and increase in bed shear stress. This is the reason for local deposition and erosion of sediment particles on leeward and stoss side, respectively. Yalin explained the decrease and increase in bed shear stress corresponding to near-bed decrease and increase (with respect to standard distribution) in velocity gradients (du/dz) (Fig. 8.4a). It leads to a relatively similar kind of sediment deposition at $x = 2\pi h$, $4\pi h$, ... and erosion at $x = \pi h$, $3\pi h$, ... (Fig. 8.4b). Thus, the dunes that are developed, in this way, have a wavelength $\lambda_d \approx 2\pi h$, which shows that the geometry of dunes depends on flow depth h .

According to Julien (2010), dunes can be formed, if the following conditions are satisfied:

$$(1) 3 < D_* < 70, \quad (2) 11.6 < R_* < 70, \quad (3) \tau'_0 < \frac{1}{D_* \kappa} \ln \left(\frac{h}{20d} \right) \quad (8.7)$$

where τ'_0 is the bed shear stress due to particle roughness, κ is the von Kármán constant, and h is the mean flow depth.

Performing a detailed potential flow analysis (see Sect. 8.5.3), Kennedy (1963) proposed the criterion for the formation of dunes as follows:

$$Fr^2 < \frac{1}{k_w h} \tanh(k_w h) \quad \wedge \quad k_w = \frac{2\pi}{\lambda_d} \quad (8.8)$$

where λ_d is the wavelength of dune.

Regarding the dimensions of dunes, Fredsøe (1975) expressed the steepness (ratio of dune height η_d to dune length λ_d) of dunes using the data reported by Guy et al. (1966) as

$$\frac{\eta_d}{\lambda_d} = 0.119 \left(1 - \frac{0.06}{\Theta} - 0.4\Theta \right)^2 \quad (8.9)$$

In this context, it is pertinent to mention that the steepness of a dune can be approximately calculated considering the dune shape a triangular with an upstream slope α ($\approx 6^\circ$, say) and a downstream slope β ($\approx 33^\circ$, say). Then, the steepness is as follows:

$$\frac{\eta_d}{\lambda_d} = \frac{\sin \alpha \sin \beta}{\sin(\alpha + \beta)} \approx \frac{1}{11}$$

On the other hand, van Rijn (1984b) gave empirical equations for the determination of dune height η_d and length λ_d :

$$\eta_d = 0.11h \left(\frac{d}{h} \right)^{0.3} \left[1 - \exp \left(-0.5 \frac{\tau'_0 - \tau_{0c}}{\tau_{0c}} \right) \right] \left(25 - \frac{\tau'_0 - \tau_{0c}}{\tau_{0c}} \right), \quad \lambda_d = 7.3h \quad (8.10)$$

Note that Yalin (1964) proposed $\lambda_d = 2\pi h$, which is very close to the value of λ_d in Eq. (8.10). However, it was recognized that both the equations tend to underestimate the dune height and length of the field data. To overcome this discrepancy, Julien and Klaassen (1995) compiled a large number of field data to propose average dune height and length, which can be used at least as a first approximation. They are as follows:

$$\bar{\eta}_d \approx 2.5h^{0.7}d^{0.3}, \quad \bar{\lambda}_d = 6.5h \quad (8.11)$$

Table 8.1 Dimensions of dunes

References	Dune height	Dune length
Allen (1968)	$\eta_d = 0.086 h^{1.19}$	$\lambda_d = h^{0.6}$
Gill (1971)	$\eta_d = \frac{(1 - Fr^2)h}{2n\alpha} \left(1 - \frac{\tau_{0c}}{\tau_0}\right)$ where n is the exponent of velocity power law (= 3–6) and α is the shape coefficient of dunes (= 0.5–0.7)	–
Orgis (1974)	$\eta_d _{\max} = 2h \left(1 - \frac{Fr^2}{2} - \frac{3Fr^{2/3}}{2}\right)$	–
Ranga Raju and Soni (1976)	$\eta_d = 6500 \frac{d}{Fr^3 F_d} \Theta^{8/3}$ where Θ' is the Shields parameter due to particle roughness	$\lambda_d = 3 \times 10^8 \frac{d^2}{Fr^3 F_d h} \Theta'^{10/3}$
Yalin (1977)	$\eta_d = \frac{h}{6} \left(1 - \frac{\tau_{0c}}{\tau_0}\right)$	$\lambda_d = 6.3 h$
Allen (1978)	$\eta_d = h(0.08 + 0.747\Theta - 2.014\Theta^2 + 2.626\Theta^3 - 1.09\Theta^4)$	–
Watannabe (1989)	$\eta_d = 2000d(1 - Fr^2)(\Theta - \Theta_c)^{1.5}$	–

According to García (2008) [also Yalin (1964)], a dune in a fully developed stage has a height up to one-sixth of the flow depth, that is, $\eta_d = h/6$. The wavelength of dunes can be given in terms of the product of the wave number and the flow depth ranging $0.25 < k_w h < 4$. Other relationships for the dimensions of dunes are given in Table 8.1.

Tjerry and Fredsøe (2005) gave an analytical solution for the migration of dunes. They considered two-dimensional dunes, as shown in Fig. 8.5, migrating with a velocity U_b in the x -direction without changing the shape (Fig. 8.6). The dunes migrate due to erosion of stoss side and deposition on leeside.

Referring to Fig. 8.5, the dune shape $\eta(x, t)$ at a given distance x and time t and its differential form are given by

$$\eta(x, t) = \eta(x - U_b t) \Rightarrow U_b \frac{\partial \eta}{\partial x} + \frac{\partial \eta}{\partial t} = 0 \quad (8.12)$$

If the amount of sediment deposited is q_{b1} , then the migration velocity U_b is obtained as

$$U_b = \frac{q_{b1}}{(1 - \rho_0)\eta_d} \quad (8.13)$$

where ρ_0 is the porosity of the sediment. The continuity equation of sediment transport resulting in a change in bed level was given by Exner (1925). It is as follows:

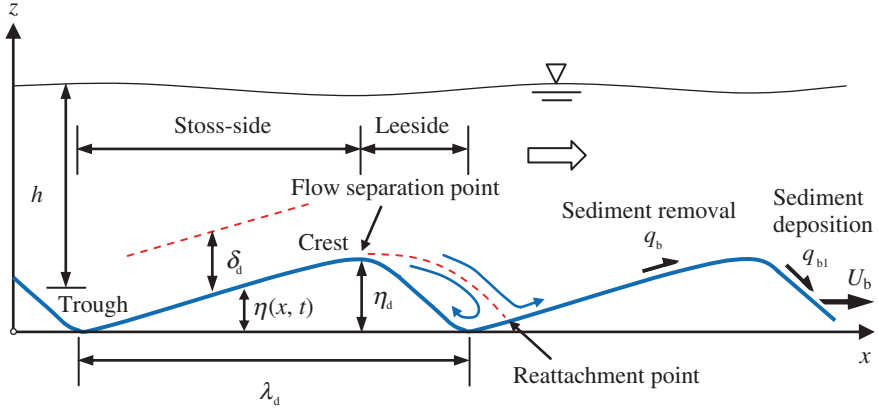


Fig. 8.5 Schematic profile of dunes (enlarged vertical scale)

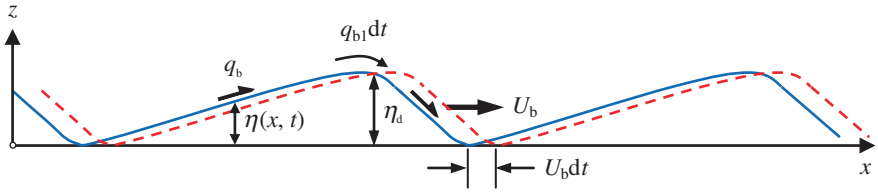


Fig. 8.6 Migration of dunes (enlarged vertical scale) (Tjerry and Fredsøe 2005)

$$(1 - \rho_0) \frac{\partial \eta}{\partial t} + \frac{\partial q_b}{\partial x} = 0 \quad (8.14)$$

Using Eqs. (8.12) (the differential form of η) and (8.14) yields

$$\frac{\partial q_b}{\partial x} = (1 - \rho_0) U_b \frac{\partial \eta}{\partial x} \quad (8.15)$$

By integration of Eq. (8.15), the following equation is obtained:

$$q_b = q_{b0} + (1 - \rho_0) U_b \eta \quad (8.16)$$

where q_{b0} is a constant sediment transport rate at the trough ($\eta = 0$). Tjerry and Fredsøe assumed the bed load to be the only mode of sediment transport and no sediment to be transported at the trough. Hence, q_{b0} becomes zero. Then, Eq. (8.13) and Eq. (8.16) produce

$$\frac{\eta}{\eta_d} = \frac{q_b}{q_b|_{\eta=\eta_d}} \quad (8.17)$$

Recalling Meyer-Peter and Müller formula for a horizontal bed, $\Phi_b = 8(\Theta - \Theta_c)^{1.5}$ [see Eq. (5.16)], Fredsøe and Deigaard (1992) suggested the modification of Meyer-Peter and Müller formula due to streamwise bed slope as

$$\Phi_b = 8 \left(\Theta - \mu \frac{\partial \eta}{\partial x} - \Theta_c \right)^{1.5} \quad (8.18)$$

where Φ_b is the bed-load transport intensity [see Eq. (5.2)] and μ is the particle frictional coefficient, which is of the order of 0.1, according to Fredsøe and Deigaard. They also specified $\Theta_c = 0.047$. Both Eqs. (8.17) and (8.18) lead to a differential equation of dune shape:

$$\frac{\partial \eta}{\partial x} = \left(\frac{\Theta_c - \Theta|_{\eta=\eta_d}}{\mu} \right) \left(\frac{\eta}{\eta_d} \right)^{2/3} + \frac{\Theta - \Theta_c}{\mu} \quad (8.19)$$

The above equation provides a relationship of dune shape with the local bed shear stress.

The continuity of fluid flow between a flow section at x over the dune (that is, over $\eta = \eta$) and a flow section right over the dune crest (that is, over $\eta = \eta_d$) is given by

$$U \left(1 - \frac{\eta}{h} \right) = U|_{\eta=\eta_d} \left(1 - \frac{\eta_d}{h} \right) \quad (8.20)$$

where U is the average flow velocity over a dune where the bed elevation is $\eta = \eta$. Using the expression for bed shear stress that is expressed as a function of dynamic pressure due to an average flow velocity, it leads to the following equations:

$$\tau_0 = \frac{f_D}{8} \rho U^2, \quad \tau_0|_{\eta=\eta_d} = \frac{f_D|_{\eta=\eta_d}}{8} \rho U|_{\eta=\eta_d}^2 \quad (8.21)$$

where f_D is the Darcy–Weisbach friction factor. Inserting Eq. (8.21) into Eq. (8.20) yields

$$\Theta = \Theta|_{\eta=\eta_d} \frac{f_D}{f_D|_{\eta=\eta_d}} \left[\frac{1 - (\eta_d/h)}{1 - (\eta/h)} \right]^2 \quad (8.22)$$

Differentiating Eq. (8.22) with respect to x and assuming no variation of Darcy–Weisbach friction factor over the dune (that is, $f_D = f_D|_{\eta=\eta_d}$), it gives

$$\frac{\partial \Theta}{\partial x} = \Theta|_{\eta=\eta_d} \frac{1/h}{1 - (\eta_d/h)} \cdot \frac{\partial \eta}{\partial x} \quad (8.23)$$

With $q_{b0} = 0$ and using Eqs. (8.16) and (8.17) into Eq. (8.15) yield

$$\frac{\partial q_b}{\partial x} = \frac{q_{b1}}{\eta_d} \cdot \frac{\partial \eta}{\partial x} \quad \wedge \quad \frac{\partial q_b}{\partial x} = \frac{\partial q_b}{\partial \Theta} \cdot \frac{\partial \Theta}{\partial x} \quad (8.24)$$

Then, inserting Eq. (8.24) into Eq. (8.23), the following equation is obtained:

$$\frac{\eta_d/h}{1 - (\eta_d/h)} = \frac{\Phi_b|_{\eta=\eta_d}}{2\Theta} \left(\frac{d\Phi_b}{d\Theta} \right)^{-1} \quad (8.25)$$

Using Meyer-Peter and Müller formula, Eq. (8.25) becomes

$$\frac{\eta_d/h}{1 - (\eta_d/h)} = \frac{1}{3} \left(\frac{\Theta - \Theta_c}{\Theta} \right)^{1.5} \quad (8.26)$$

The above equation, which was obtained by Tjerry and Fredsøe (2005), can be used to determine dune height.

In case of dominant bed-load transport, Fredsøe and Deigaard (1992) argued that the maximum bed shear stress is located at approximately $16\eta_d$ downstream the former crest of dune. Also, the maximum sediment transport rate, with the exception of very small values of Shields parameter, occurs at the crest of the dunes. Then, the dune length λ_d can be obtained from Eq. (8.17) as

$$\lambda_d = 16\eta_d \quad (8.27)$$

On the other hand, at a very large bed shear stress, where suspended-load transport becomes the dominant mechanism of sediment transport, Fredsøe and Deigaard (1992) argued that the maximum bed shear stress and the maximum suspended-load transport rate are not located at the same section, as the suspended load requires a distance to reach its maximum value. They introduced a spatial phase lag L_s between the locations of the maximum bed shear stress and the maximum suspended-load transport rate. Thus, in such a case, the dune length λ_d is given by

$$\lambda_d = 16\eta_d + \frac{q_s}{q_b + q_s} L_s \quad (8.28)$$

where q_s is the suspended-load transport rate. They deduced the spatial phase lag L_s formulation as

$$L_s = z_c \frac{u|_{z=z_c}}{w_s} \quad \wedge \quad z_c = \frac{\int_0^h C_z dz}{\int_0^h C dz} \quad (8.29)$$

where z_c is the height of the centroid of concentration distribution above the bed, $u|_{z=z_c}$ is the velocity at an elevation $z = z_c$, w_s is the terminal fall velocity of sediment, and C is the sediment concentration at an elevation z .

8.2.3 Transition and Plane Bed

With an increase in flow Froude number, which is still less than unity (that is a subcritical flow), the stream power, $U\tau_0$, increases and the dunes are gradually washed out, which is called a *transition* from dunes to a plane bed (Fig. 8.1d). In the process of washing out of dunes, the dunes become progressively elongated and flattened lowering the amplitude. Eventually they almost disappear attaining a relatively *plane bed* (Fig. 8.1e). Both the flow resistance and the flow depth are reduced drastically due to the change in bed feature from dunes to a plane bed. However, in some cases, a part of the plane bed may be covered by distorted dunes (which is also found in case of a transition), although in most of the cases, the plane beds are devoid of any distinct bedforms. Note that in lower flow regime, washed-out ripples also exist (Baas and de Koning 1995).

8.2.4 Antidunes

Of the bedforms developed by unidirectional flows, the bedforms classed as *antidunes* occur in the so-called upper flow regime ($Fr > 1$). Contrary to the bedforms (ripples and dunes) that can only migrate in the downstream in lower flow regime ($Fr < 1$), antidunes can remain stationary or migrate upstream or downstream.

For antidunes, the bed and the free surface profiles are almost in phase (Figs. 8.1f, g, and 8.7). The streamwise profile of antidunes is nearly sinusoidal and so is free surface profile, but usually with much larger amplitude. Antidunes do exist as a continuous train of bed waves having a wavelength of approximately ten times the flow depth. While the flow and the sediment transport are in downstream direction, the antidunes and the free surface undulations may remain stationary or migrate upstream or downstream. At a higher flow Froude number, which is more than unity (that is a supercritical flow), antidunes appear as *standing waves* (Fig. 8.1f). However, with a further increase in Froude number, the antidunes that appear as *breaking waves* may grow, becoming unstable and breaking in the upstream direction. They move upstream just before breaking (Fig. 8.1g). If the breaking waves occur, the antidunes are destroyed and the bed becomes relatively plane. However, the formation of antidunes resumes all over the bed. After breaking, the reformed antidunes may be small for the time being, but the process of growing and breaking is repeated.

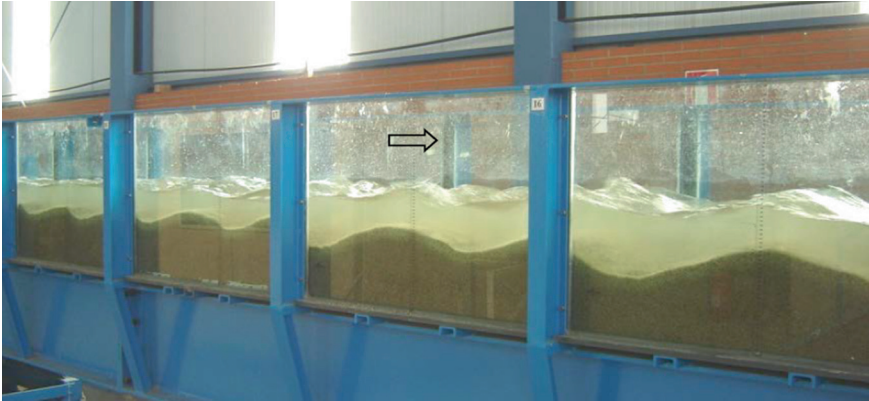


Fig. 8.7 Photograph of antidunes appearing as standing waves (Núñez-González 2012)

Antidune migration may be related to the flow detachment at the crest, so that the flow separation over the stoss side may be associated with an upstream migration, while the flow separation over the leeside may be associated with a downstream migration. In contrast to dunes, the flow detachment over antidunes may be intermittent and irregular in position. This unsteadiness is attributed to the strong interaction between the bed and the free surface. The antidunes, especially to migrate upstream, tend to be very symmetrical with a curved crest in their profile parallel to the flow. However, from the viewpoint of sediment transport, the upstream migration of antidunes occurs due to strong leeside erosion and stoss-side deposition. Following a potential flow analysis, Kennedy (1963) proposed the criterion for the upstream migration of antidunes as

$$Fr^2 \geq \frac{1}{k_w h} \tanh(k_w h) \quad (8.30)$$

8.2.5 Chutes and Pools

Very strong antidunes actively lead to *chutes* and *pools* flow, which occur at relatively steep slopes with high flow velocities and sediment concentrations. The bedforms consist of large elongated sediment heaps forming *chutes* in which the flow is shooting or supercritical. Shooting flow on the sediment heaps rushes into a *pool*, where the flow is generally tranquil or subcritical (Fig. 8.1h). In this way, a chute is normally connected to a pool and vice versa. The flow is supercritical at the chutes and subcritical in the pools. The transition from the supercritical flow to the subcritical flow occurs through a weak hydraulic jump. The sediment is eroded severely at the chutes and deposited into the pools. In this way, the entire bedforms slowly migrate downstream. In natural rivers on plains, the flow velocity is seldom high enough for this phenomenon to occur.

8.3 Bars

It is pertinent to mention that the larger type of bedforms, which are not necessarily very much linked with a specific flow regime but potentially featuring more than any other bedforms with a flow three-dimensionality, is called *bar*. Bars appear as a large sediment depositional feature with a length dimension of in the order of a channel width or a height dimension of a flow depth. Seemingly, they have the geometry of a dune, but are large enough. In most of the cases, bars are formed at high flow discharges and may appear as small islands or peninsulas during a low-stage flow in rivers.

There are different types of bars, as shown in Fig. 8.8. Among them, *point bars* are the sediment deposits that take place on the inner side of a curved channel. Depending on the flow condition, their shape may vary; however, they remain unmoved relative to the channel curvature. *Alternate bars* generally appear periodically along the straight channels with bars near alternate channel banks (Fig. 8.8). The wavelength of alternate bars is approximately six to ten times the channel width, while the width is much less than the channel width. These bars may slowly migrate downstream.

Sukegawa (1973) proposed the condition for the formation of alternate bars as

$$\frac{u_*}{u_{*c}} \leq 2.236 \left[\frac{(gB)^{0.5} S_0}{u_{*c}} \right]^{1/3} \quad (8.31)$$

where u_* is the shear velocity, u_{*c} is the threshold shear velocity for the sediment motion, B is the channel width, and S_0 is the streamwise bed slope.

Further, Jaeggi (1984) put forward the minimum bed slope required for the formation of alternate bars as

$$S_0 > \frac{\exp(1.07\hat{B}^{0.15} + M)}{12.9\hat{B}} \quad \wedge \quad \hat{B} = \frac{B}{\sigma_g} \quad (8.32)$$

where M is a parameter being 0.34 for uniform sediments and 0.7 for nonuniform sediments and σ_g is the geometric standard deviation of particle size distribution.

On the other hand, *middle bars* appear in the mid portion of the straight channels as isolated bars. *Tributary bars* that are approximately triangular are sometimes found at the confluence of the tributaries and the main channels. While the middle bars may migrate, the tributary bars remain almost stationary. However, the shape of both bars may vary depending on the flow condition.

Fig. 8.8 Schematic of different types of bars: 1-point bar, 2-alternate bar, 3-middle bar, and 4-tributary bar

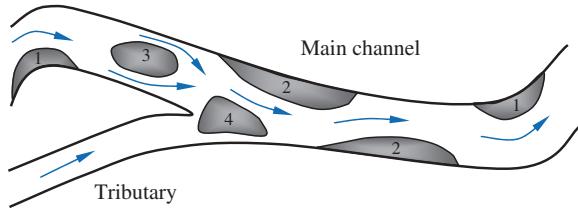
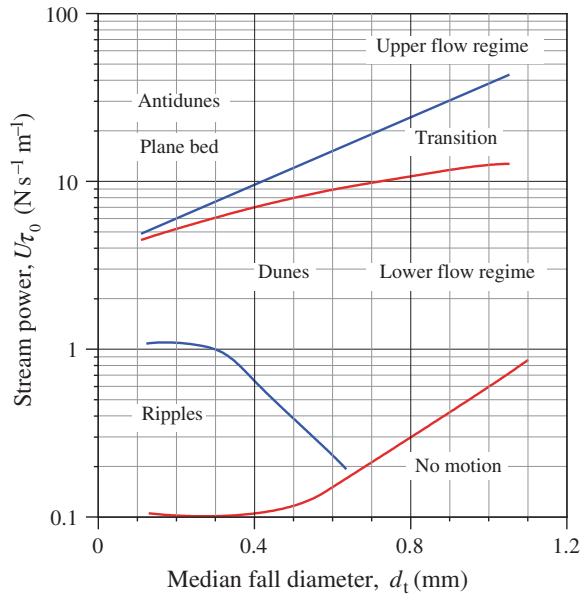


Fig. 8.9 Bedform predictor after Simons and Richardson (1961, 1966)



8.4 Prediction of Bedforms

Important studies on bedforms were carried out by various investigators to predict the occurrence of bedforms and their types. However, a universally acceptable predictor is still lacking, as the mechanism of formation of bedforms is yet to be well understood. Predictors are mainly empirical and are discussed here.

Based on the experimental and field data, Simons and Richardson (1961, 1966) proposed a bedform predictor in graphical form (curves for stream power $U\tau_0$ versus median fall diameter d_t), as shown in Fig. 8.9. The zones in between the curves delineate the range of formation of different bedforms. The lower flow regime changes to upper flow regime via transition with an increase in stream power. It implies that the bedforms are well correlated with the rate of flow energy expenditure per unit area. For instance, a threshold stream power as $0.1 \text{ N s}^{-1} \text{ m}^{-1}$ for $d_t < 0.4 \text{ mm}$ is required for the formation of ripples. Figure 8.9 is applicable only for the sands.

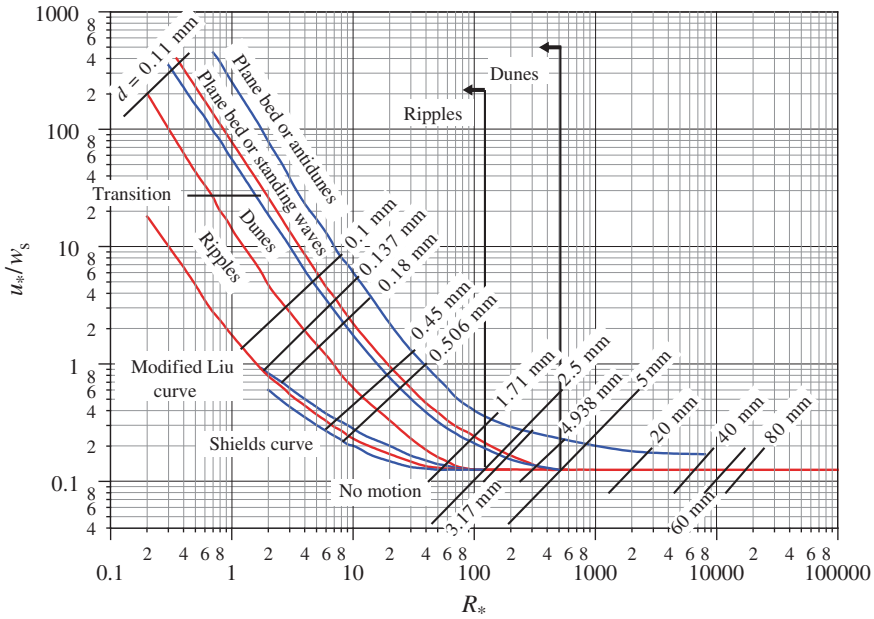


Fig. 8.10 Bedform predictor after Liu (1957), as extended by Simons and Richardson (1961)

Liu (1957) prepared the bedform predictor in graphical form (curves for shear velocity to terminal fall velocity ratio u_*/w_s versus shear Reynolds number R_*) that was extended later by Simons and Richardson (1961), as shown in Fig. 8.10. The predictor covers a wide range of sediment particle sizes. It is evident that the curves discriminating various bedforms tend to collapse (except in the upper flow regime) with an increase in R_* becoming independent of R_* at higher R_* .

Chabert and Chauvin (1963) put forward a bedform predictor based on the Shields diagram (Θ versus R_*), as shown in Fig. 8.11. They used $D_* [= d(\Delta g/v^2)^{1/3}]$ as a third parameter. Ripples form when $D_* < 20$, which corresponds to $R_* < 15$, or when flow regime changes from a transition to hydraulically smooth flow. However, their diagram is not suitable for the description of upper flow regime.

Athallah (1968) used flow Froude number Fr versus relative submergence R_b/d plots to prepare the bedform predictor, as shown in Fig. 8.12. Here, R_b is the hydraulic radius. It means that one can predict bedforms if mean flow velocity, flow depth, and sediment size are known. The diagram shows that at small relative submergence, lower flow regime prevails at higher Froude numbers. On the other hand, the transition from lower flow regime to plane bed is persistent at relatively small Froude numbers.

Based on the experimental and field data, Brownlie (1983) argued that the transitional flow regime can be defined by the densimetric Froude number F_d and the ratio of particle size d to viscous sublayer thickness δ' ($=11.6\nu/u_*$). He asserted

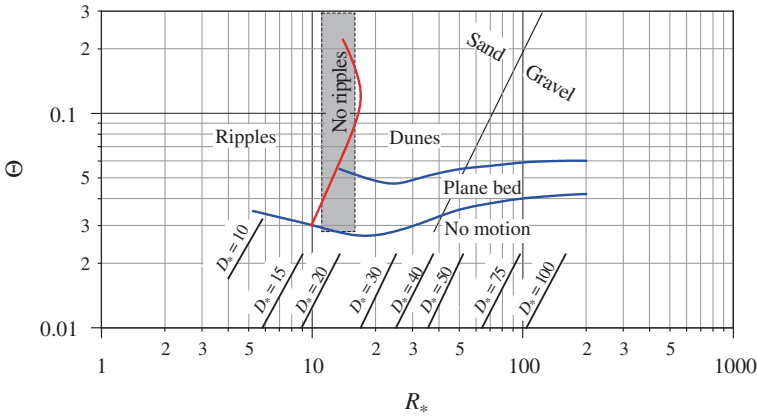


Fig. 8.11 Bedform predictor after Chabert and Chauvin (1963)

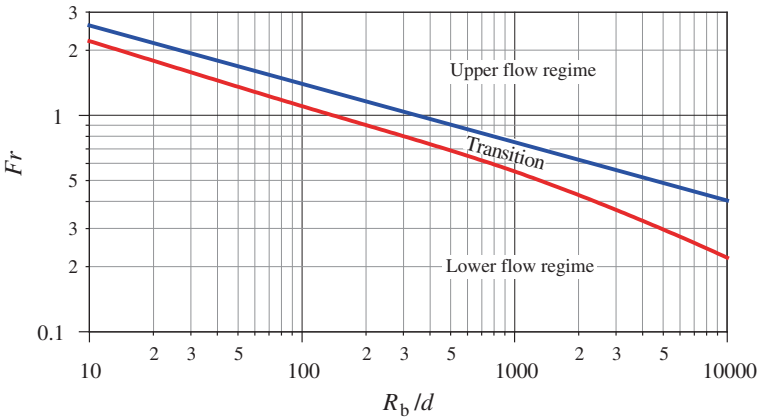


Fig. 8.12 Bedform predictor after Athaullah (1968)

that all bedforms for bed slopes S_0 greater than 0.006 are in the upper flow regime. However, for $S_0 < 0.006$, he proposed the following relationships for the lower limit of the upper flow regime:

$$\log(F_d S_0^{1/3}) = 0.2159 + 0.1517 \log \frac{d}{\delta'} + 0.8381 \left(\log \frac{d}{\delta'} \right)^2 \quad \text{for } \frac{d}{\delta'} < 2 \quad (8.33a)$$

$$F_d S_0^{1/3} = 2.175 \quad \text{for } \frac{d}{\delta'} \geq 2 \quad (8.33b)$$

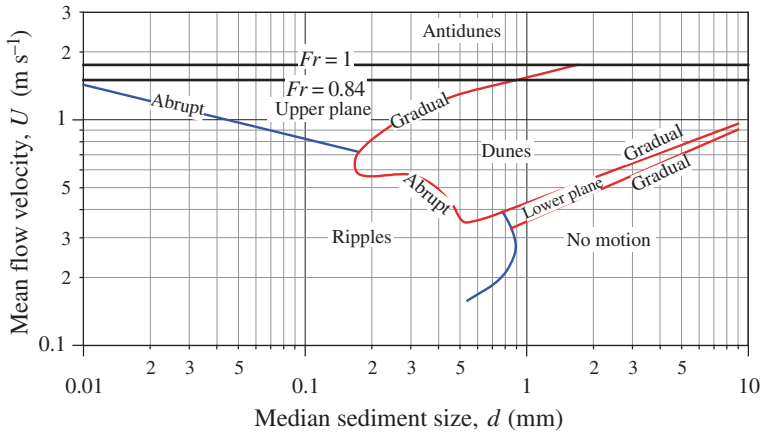


Fig. 8.13 Bedform predictor after Southard and Boguchwal (1990) (Ashley 1990)

For the upper limit of lower flow regime, Brownlie proposed

$$\log(F_d S_0^{1/3}) = 0.0379 + 0.07026 \log \frac{d}{\delta'} + 0.933 \left(\log \frac{d}{\delta'} \right)^2 \quad \text{for } \frac{d}{\delta'} < 2 \quad (8.34a)$$

$$F_d S_0^{1/3} = 1.392 \quad \text{for } \frac{d}{\delta'} \geq 2 \quad (8.34b)$$

Southard and Boguchwal (1990) proposed a bedform predictor in graphical form. As reorganized by Ashley (1990), the bedform predictor is shown in Fig. 8.13. It shows a plot of mean flow velocity U versus median size d of sediment (covering the range of fine to coarse sands and gravels) at 10 °C water temperature for the flow depths of 0.25–0.4 m. Several limiting curves provide demarcation of different types of bedforms. It is evident that the ripples are stable for sediment size range $d < 0.8$ mm. The range of U for ripples narrows down with an increase in d to end up against the zones for the plane beds with and without sediment motion. For medium sands, ripples give way abruptly to dunes with an increase in U , while for finer sands, ripples yield abruptly to plane beds without appearance of dunes. On the other hand, dunes are rather stable over a wide range of U with sediment sizes ranging from medium to coarse sands and gravels. Both the lower and the upper limiting curves of the dune zone rise with an increase in U . For sediments $d > 0.8$ mm, there is a narrow zone below the dune zone for a lower flow regime plane bed. The lower limiting curve of this zone is represented by the Shields curve for the threshold of sediment motion on a plane bed. The antidune zone exists at higher mean flow velocities ($U > 1.5 \text{ m s}^{-1}$). It indicates that the transition to the upper flow regime occurs for Froude numbers smaller than unity.

Table 8.2 Bedform prediction scheme after van Rijn (1993)

Flow regime	Transport stage parameter	Particle parameter and corresponding bedforms	
		$1 \leq D_* \leq 10$	$D_* > 10$
Lower	$0 < T_* \leq 3$	Small ripples	Dunes
	$3 < T_* \leq 10$	Large ripples and dunes	Dunes
	$10 < T_* \leq 15$	Dunes	Dunes
Transition	$15 < T_* < 25$	Washed-out dunes and sand waves (asymmetrical)	
Upper	$T_* \geq 25, Fr < 0.8$	Sand waves (symmetrical)	
	$T_* \geq 25, Fr \geq 0.8$	Plane bed and/or antidunes	

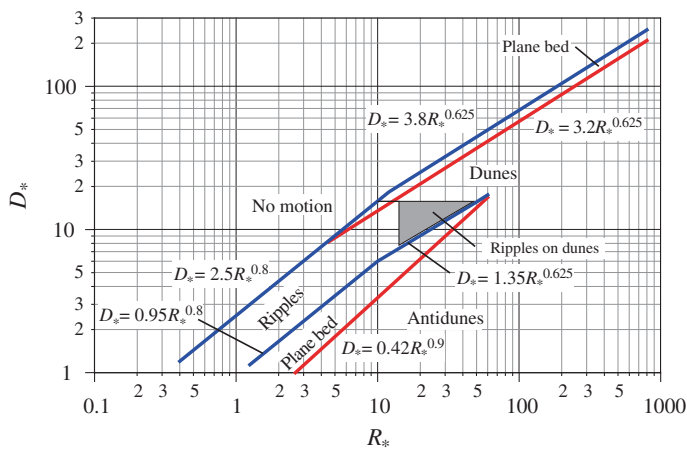


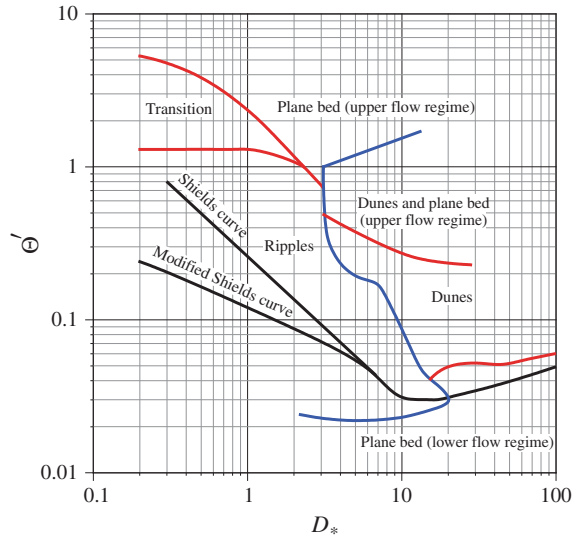
Fig. 8.14 Bedform predictor after Bonnefille–Pernecker (Bechteler et al. 1991)

Using both laboratory experimental and field data, van Rijn (1984b, 1993) advanced significantly the bedform prediction scheme. The scheme is based on the $(\tau_0 - \tau_{0c})/\tau_{0c}$, known as *transport stage parameter* T_* , and the particle parameter D_* . The prediction scheme is given in Table 8.2.

According to van Rijn, in lower flow regime, the small ripples have a length scale of the order of turbulence length scale near the bed. Also, it means that the length scale is much smaller than the flow depth ($\lambda_r \ll h$). In contrast, the large ripples, which could be superimposed on the dunes, have a length scale of the order of flow depth [$\lambda_r \approx O(h)$]. On the other hand, in the upper flow regime, the sand waves have a length scale much larger than the flow depth ($\lambda_d \gg h$). Due to the involvement of large number of laboratory experimental and field data and methodical use of important parameters, T_* and D_* , this method is perhaps superior to other ones, although it is very sensitive to any inaccuracy in determining the values of threshold bed shear stress.

The bedform predictor that was proposed by Bonnefille–Pernecker in a graphical form, as modified and prepared by Bechteler et al. (1991), is shown in Fig. 8.14. It shows a plot of particle parameter D_* versus shear Reynolds number R_* . For finer

Fig. 8.15 Bedform predictor after van der Berg and van Gelder (1993)



sediments ($D_* < 20$), the transition from ripples to plane bed in the upper flow regime and then antidunes occurs with an increase in R_* . In contrast, for coarser sediments, dunes follow a narrow strip of plane bed in lower flow regime. Further, ripples superimposed on dunes, that is a transition from ripples to dunes, are observed for $20 < R_* < 45$ and $7 < D_* < 20$.

In another attempt, van den Berg and van Gelder (1993) proposed a diagram for bedform prediction that provides a plot of Shields parameter Θ' due to particle roughness as a function of particle parameter D_* (Fig. 8.15). As proposed by van Rijn (1984b), Θ' can be given by

$$\Theta' = \frac{U^2}{\Delta g d C_R'^2} \quad \wedge \quad C_R' = 18 \log \left(\frac{4h}{d_{90}} \right)$$

It is evident from Fig. 8.15 that the transition from ripples to plane bed in the upper flow regime takes place for $D_* < 20$. The discriminator curves are compared with the Shields diagram.

Karim (1995) used limiting Froude numbers to define various regimes and types of bedforms as (1) for lower flow regime (ripples and dunes), $Fr \leq F_T$, (2) for transitional flow regime (washed-out dunes), $F_T \leq Fr \leq F_U$, and (3) for upper flow regime (plane bed and antidunes), $Fr \geq F_U$. Here, F_T is the beginning of transitional flow regime from lower flow regime, and F_U is the beginning of upper flow regime. They are given by

$$F_T = 2.716 \left(\frac{d}{h} \right)^{0.25}, \quad F_U = 4.785 \left(\frac{d}{h} \right)^{0.27} \quad (8.35)$$

Karim additionally used a limit $Fr \geq 0.8$ for the prediction of antidunes.

Julien and Raslan (1998), however, reported that the transport stage parameter T_* for the plane bed in the upper flow regime increases with an increase in relative submergence h/d . They identified two separate regimes for the transition to upper flow regime with

$$\Theta(R_* < 11.6) \approx \frac{4}{D_*}, \quad \Theta(R_* \geq 11.6) = \frac{1}{D_*} \cdot \frac{1}{\kappa} \ln \left(\frac{h}{20d} \right)$$

where κ is the von Kármán constant ($= 0.4$). Therefore, according to them, the ripples are formed when

$$2 < D_* < 6, \quad 4 < R_* < 11.6, \quad \Theta < \frac{4}{D_*}$$

On the other hand, the dunes are formed when

$$3 < D_* < 70, \quad 11.6 < R_* < 70, \quad \Theta < \frac{1}{D_*} \cdot \frac{1}{\kappa} \ln \left(\frac{h}{20d} \right)$$

8.5 Mathematical Developments

8.5.1 Exner's Model

Based on sediment continuity, a classical model that can predict the profile and migration velocity of bedforms was developed by Exner (1925). He initially derived the model without considering friction. Referring to Fig. 8.16, the continuity equation of sediment transport resulting in a change of bed level, as given by Eq. (5.48), can be rearranged as follows:

$$(1 - \rho_0) \frac{\partial \eta}{\partial t} + \frac{\partial q_b}{\partial x} = 0 \Rightarrow \frac{\partial \eta}{\partial t} + \alpha_E \frac{\partial U}{\partial x} = 0 \quad \wedge \quad q_b = (1 - \rho_0) \alpha_E U \quad (8.36)$$

where η is the elevation of the sand-bed with respect to a horizontal reference, t is the time, q_b is the bed-load transport, x is the streamwise direction, ρ_0 is the porosity of the sediment, U is the depth-average flow velocity, and α_E is the erosion coefficient. Exner considered q_b proportional to U , as given by Eq. (8.36).

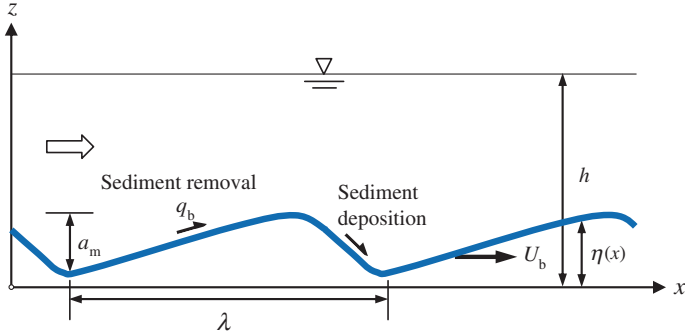


Fig. 8.16 Definition sketch of Exner's model

Considering the flow depth over the bedforms as $h - \eta$ and the flow discharge per unit width q (constant), the continuity equation of flow is given by

$$U = \frac{q}{h - \eta} \quad (8.37)$$

where h is the depth from x -axis or datum being approximated as a constant. Inserting U from Eq. (8.37) into Eq. (8.36) yields

$$\frac{\partial \eta}{\partial t} + \frac{\alpha_E q}{(h - \eta)^2} \cdot \frac{\partial \eta}{\partial x} = 0 \quad (8.38)$$

The solution of the above equation at initial time $t = 0$ can be sought as a cosine function

$$\eta = a_0 + a_m \cos(k_w x) \quad (8.39)$$

where a_m is the amplitude, $k_w = 2\pi/\lambda$, and λ is the wavelength of bedforms. The equation of a bedform for a given time t is

$$\eta = a_0 + a_m \cos[k_w(x - U_b t)] \quad \wedge \quad U_b = \frac{\alpha_E q}{(h - \eta)^2} \quad (8.40)$$

where U_b is the bedform migration velocity. An examination of the above expression of U_b reveals that the crest of bedforms moves faster than the trough, and as a result, the sinusoidal bed becomes an asymmetrical wave with gentle upstream slope. However, the theoretical solution produces the bedform profiles that have an overhanging crest portion (on downstream slope) with time. It does not occur in nature.

In developing a model considering a friction, the dynamic equation of gradually varied unsteady flow, given by Eq. (2.64), can be rearranged as follows:

$$S_f = S_0 - \frac{\partial h}{\partial x} - \frac{U}{g} \cdot \frac{\partial U}{\partial x} - \frac{1}{g} \cdot \frac{\partial U}{\partial t} \Rightarrow \frac{\partial U}{\partial t} = -gS_f + gS_0 - g \frac{\partial h}{\partial x} - U \frac{\partial U}{\partial x} \quad (8.41)$$

Considering horizontal bed ($S_0 = 0$) and approximating frictional effects as $gS_f \approx k_f U$, Eq. (8.41) together with Eqs. (8.36) and (8.37) can be rearranged and then differentiated to yield

$$\frac{\partial^2 \eta}{\partial t^2} - m \frac{\partial^2 \eta}{\partial x \partial t} + k_f \frac{\partial \eta}{\partial t} - \alpha_E g \frac{\partial^2 \eta}{\partial x^2} = 0 \quad \wedge \quad m = \frac{gq}{U^2} - U \quad (8.42)$$

where k_f is the friction parameter (per unit time). The solution of Eq. (8.42) is obtained with the initial condition in terms of a cosine function, given by Eq. (8.39). It is as follows:

$$\eta = a_0 + a_m \exp \left[- \left(\frac{k_f}{2} - p \right) t \right] \cos \left\{ k_w \left[x - \frac{m}{2p} \left(\frac{k_f}{2} - p \right) t \right] \right\} \quad (8.43)$$

where p is a function depending on k_f , m , λ , and α_E . In Eq. (8.43), if $0.5k_f - p > 0$, then the amplitude of the bedforms decreases with an increase in time due to frictional resistance. The bedforms with longer wavelength have a migrating velocity slower than the shorter ones, and also the rate of decrease in amplitude is slower than the shorter ones.

8.5.2 Kinematic Model

Song (1983) proposed a simple model that enables us to predict the migration velocity and direction of bedforms. Referring to Fig. 8.17, the energy and the continuity equations of flow are

$$\frac{U^2}{2g} + h + \xi = E \quad (8.44a)$$

$$U(h + \xi - \eta) = q \quad (8.44b)$$

where ξ is the free surface elevation with respect to mean flow level (that is, x -axis), η is the bed elevation with respect to mean bed level, and E is the total energy. Following the usual assumption of bed-load transport q_b as a function of average flow velocity U , the expression can be written as:

$$\frac{\partial q_b}{\partial \eta} = \frac{\partial q_b}{\partial U} \cdot \frac{\partial U}{\partial \eta} \quad (8.45)$$

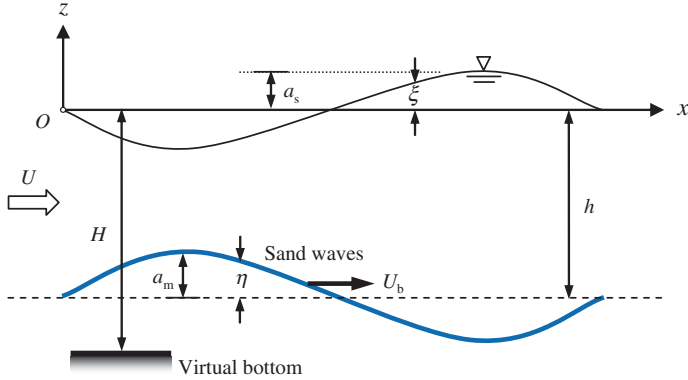


Fig. 8.17 Definition sketch of flow over sand waves

Noting that E and q are constants and using Eqs. (8.44a, b) yields

$$\frac{\partial U}{\partial \eta} = \frac{U^2}{q(1 - Fr^2)} \quad \wedge \quad Fr = \frac{U}{(gh)^{0.5}} \quad (8.46)$$

The bedform (sand wave) migration velocity U_b is given by

$$U_b = \frac{\partial q_b}{\partial \eta} = \frac{\partial q_b}{\partial U} \cdot \frac{\partial U}{\partial \eta} = \frac{\partial q_b}{\partial U} \cdot \frac{U^2}{q(1 - Fr^2)} \quad (8.47)$$

Since $\partial q_b / \partial U$ is always positive, the direction of bedform migration that depends on its sign is governed by the term $(1 - Fr^2)$. For $Fr < 1$ (subcritical flow), $U_b > 0$ implies a downstream migration, and for $Fr > 1$ (supercritical flow), $U_b < 0$ suggests an upstream migration. These are in conformity with the reality.

In another attempt, Núñez-González and Martín-Vide (2011) developed a model for antidune migration. The underlying phenomenon is that antidunes propagate in the downstream direction if the sediment is predominantly eroded over the stoss side and deposited over the leeside. Conversely, antidunes migrate upstream if most of the sediment is deposited over the stoss side and eroded over the leeside. To relate these two conditions to the near-bed flow features and the flow depth, it can be stated that the sediment deposition occurs where the near-bed flow decelerates and the flow depth increases, and the erosion occurs where the near-bed flow accelerates and the flow depth decreases. In this way, if it is considered that the flow depth variation along the antidune profile is the most important property for defining the direction of antidune migration, the following conditions can be established, according to Fig. 8.18: (1) If $h_1/h_2 < 1$, the antidunes migrate downstream; (2) if $h_1/h_2 = 1$, the antidunes remain stationary; and (3) if $h_1/h_2 > 1$, the antidunes migrate upstream. Here, h_1 and h_2 are the flow depths above the crest and the trough, respectively.

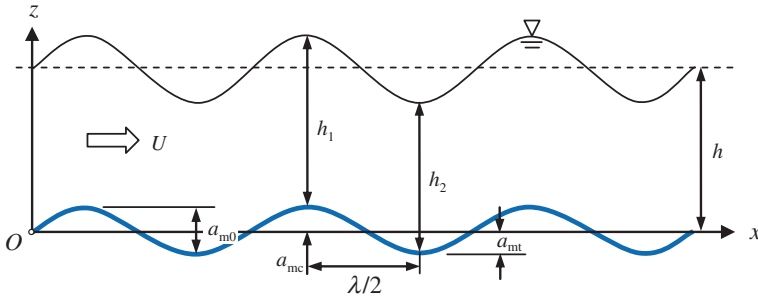


Fig. 8.18 Definition sketch of flow over antidunes. Note that the free surface profile and the antidune profile are in phase (Núñez-González and Martín-Vide 2011)

Considering that the idealized train of sinusoidal antidunes, as shown in Fig. 8.18, is stable, the continuity of flow over a crest and an immediate downstream trough can be related to the average flow condition as

$$q = Uh = U_1 h_1 = U_2 h_2 \quad (8.48)$$

where subscripts 1 and 2 refer to the flow over the crest and the trough, respectively. The average flow depth h is defined as a geometric mean of the flow depths over the crest and the trough. Then, it is as follows:

$$h = (h_1 h_2)^{0.5} \quad (8.49)$$

If energy losses are considered negligible, the total energy head at the upstream section over the crest should be equal to the total energy head at the downstream section over the trough (Fig. 8.18). Then,

$$a_{mc} + h_1 + \frac{U_1^2}{2g} = -a_{mt} + h_2 + \frac{U_2^2}{2g} \quad (8.50)$$

where a_{mc} and a_{mt} are the average elevations of crest and trough of antidunes from the mean bed level. Further, the hydrostatic (that is, piezometric) pressure head over the crest and the trough must be corrected to account for the centrifugal effects due to curvilinear flow. Including the correction as a function of flow depth, flow velocity, gravity, and radius of curvature, Eq. (8.50) can be modified as

$$a_{mc} + h_1 \left(1 - \frac{1}{g} \cdot \frac{U_1^2}{r_1} \right) + \frac{U_1^2}{2g} = -a_{mt} + h_2 \left(1 + \frac{1}{g} \cdot \frac{U_2^2}{r_2} \right) + \frac{U_2^2}{2g} \quad (8.51)$$

If the profiles of antidunes are symmetrical, then the following relationships hold

$$a_{m0} = 2a_{mc} = 2a_{mt} = a_{mc} + a_{mt}, \quad r = r_1 = r_2 \quad (8.52)$$

Using Eqs. (8.48), (8.49) and (8.52), Eq. (8.51) can be rewritten as

$$\begin{aligned} a_{m0} + h_1 - h_2 &= Fr^2 h^3 \left(\frac{1}{h_1} + \frac{1}{h_2} \right) \left[\frac{1}{r} + \frac{1}{2} \left(\frac{1}{h_2} - \frac{1}{h_1} \right) \right] \\ \wedge \quad Fr &= \frac{U}{(gh)^{0.5}} = \frac{q}{(gh^3)^{0.5}} \end{aligned} \quad (8.53)$$

where q is the discharge per unit width ($= Uh$).

For a stationary train of antidunes ($h_1 = h_2 = h$), Eq. (8.53) reduces to the following nondimensional number, defined as *antidune mobility number*

$$F_a = Fr \cdot h \left(\frac{2}{ra_{m0}} \right)^{0.5} = 1 \quad (8.54)$$

By definition, the curvature of a sinusoidal function is equal to

$$r = \frac{1}{2a_{m0}} \left(\frac{\lambda}{\pi} \right)^2 = \frac{1}{2a_{m0}} \left(\frac{2}{k_w} \right)^2 \quad \wedge \quad k_w = \frac{2\pi}{\lambda} \quad (8.55)$$

where λ is the wavelength of antidunes.

Inserting Eq. (8.55) into Eq. (8.54), the antidune mobility number can be defined solely as a product of flow Froude number Fr , average flow depth h , and wave number k_w . Thus,

$$F_a = Fr \cdot h \cdot k_w \quad (8.56)$$

The solution of Eq. (8.53), as F_a a function of h_1/h_2 for different Froude numbers Fr and a value of $a_{m0}/\lambda = 0.05$, is shown in Fig. 8.19. It is found that for $Fr > 1$ (that is the supercritical flow, when antidunes occur), the relationship between F_a and h_1/h_2 is *biunivocal*.³ Besides, it is always fulfilled that if $F_a < 1$, then $h_1/h_2 > 1$, and if $F_a > 1$, then $h_1/h_2 < 1$. The biunivocal characteristic of the deduced function for the supercritical flow range allows for the establishment of a criterion to identify the preferential direction of antidune migration according to antidune mobility number F_a . Due to this, the criterion for the direction of antidune migration can be stated as (1) if $F_a < 1$, the antidunes migrate downstream, (2) if $F_a = 1$, the antidunes remain stationary, and (3) if $F_a > 1$, the antidunes migrate upstream.

³ *Biunivocal* is a type of relationship that exclusively links two terms to one another on the basis of one of the two terms.

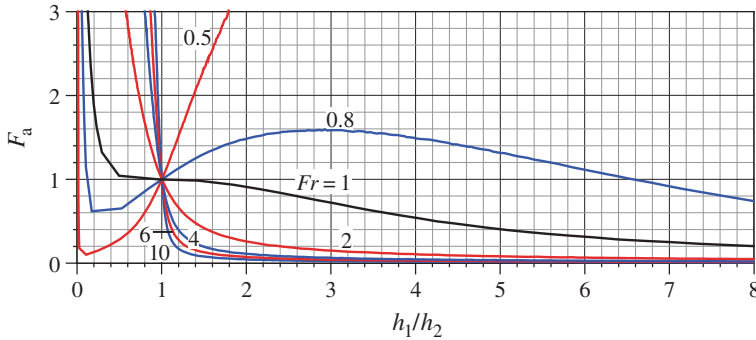


Fig. 8.19 Antidune mobility number F_a as a function of h_1/h_2 for different flow Froude numbers Fr and $a_{m0}/\lambda = 0.05$ (Núñez-González and Martín-Vide 2011)

8.5.3 Potential Flow Model

At first, the potential flow theory is discussed briefly. In Sect. 2.3.1, the introduction to stream function ψ has been given through Eqs. (2.25)–(2.27). There is another function known as *velocity potential function*, which is a fictitious continuous function $\phi(x, y, z)$, defining the components of the velocity vector as the gradient of scalar velocity potential function ϕ . In hydrodynamics, the *potential flow* therefore describes the velocity field as the gradient of velocity potential function. As a result, the potential flow is characterized by an irrotational flow field. Thus, velocity components are

$$u = \frac{\partial \phi}{\partial x}, \quad v = \frac{\partial \phi}{\partial y}, \quad w = \frac{\partial \phi}{\partial z}$$

Substituting them into three-dimensional continuity equation (Eq. 2.22), the *Laplace equation* is obtained. It is as follows:

$$\frac{\partial^2 \phi}{\partial x^2} + \frac{\partial^2 \phi}{\partial y^2} + \frac{\partial^2 \phi}{\partial z^2} = 0 \Rightarrow \nabla^2 \phi = 0$$

Potential flow in two dimensions is analyzed using the *conformal mapping*, by using transformations of the complex plane. The idea is to use an *analytic function* f , which maps the physical domain (x, z) to the transformed domain (ϕ, ψ) . While x, z, ϕ , and ψ are all real variables, it is convenient to define the complex quantities as

$$Z = x + iz, \quad W = \phi + i\psi \Rightarrow f(x + iz) = \phi + i\psi \Rightarrow f(Z) = W$$

where f is an analytic function that should satisfy the following equation called the *Cauchy–Riemann equations*:

$$\frac{\partial \phi}{\partial x} = \frac{\partial \psi}{\partial z}, \quad \frac{\partial \phi}{\partial z} = -\frac{\partial \psi}{\partial x}$$

Then, differentiating f with respect to Z yields

$$\frac{df}{dZ} = u - iw \Rightarrow u = \frac{\partial \phi}{\partial x} = \frac{\partial \psi}{\partial z}, \quad w = \frac{\partial \phi}{\partial z} = -\frac{\partial \psi}{\partial x}$$

8.5.3.1 Kennedy's Model

Based on the potential flow theory, Kennedy (1963) developed an analytical model to examine the stability of the fluid-bed interface and the bedform characteristics. Referring to Fig. 8.17 where the flow over a mobile sinusoidal bed is considered, the free surface profile and the bed profile are represented by

$$z = \zeta(x, t) \quad \wedge \quad \zeta = \alpha_s \sin[k_w(x - U_b t)] \quad (8.57a)$$

$$z = -h + \eta(x, t) \quad \wedge \quad \eta = \alpha_m \sin[k_w(x - U_b t)] \quad (8.57b)$$

where ζ and η are the fluctuations of free surface and bed waves, respectively, and α_s and α_m are the amplitudes of free surface and bed waves, respectively. The amplitudes are small in comparison to wavelength.

The kinematic boundary condition that the streamline follows the free surface ($z = 0$) yields

$$U \frac{\partial \zeta}{\partial x} + \frac{\partial \zeta}{\partial t} = \frac{\partial \phi}{\partial z} \quad (8.58)$$

where t is the time. The dynamic boundary condition that the pressure at the free surface ($z = 0$) is constant yields

$$U \frac{\partial \phi}{\partial x} + \frac{\partial \phi}{\partial t} = -g\zeta \quad (8.59)$$

Another condition is that for the limiting streamline at the bed ($z = -h$), the velocity component normal to the bed vanishes. It produces

$$U \frac{\partial \eta}{\partial x} + \frac{\partial \eta}{\partial t} = \frac{\partial \phi}{\partial z} \quad (8.60)$$

Also, considering both bed and suspended load of sediment transport, the continuity equation of sediment transport given by Eq. (5.48) can be rearranged as follows:

$$(1 - \rho_0) \frac{\partial \eta}{\partial t} + \frac{\partial q_t}{\partial x} = 0 \Rightarrow \beta_E \frac{\partial \eta}{\partial t} + \frac{\partial g_t}{\partial x} = 0 \quad \wedge \quad \beta_E = \rho_s g (1 - \rho_0) \quad (8.61)$$

$$\vee \quad g_t = \rho_s g q_t$$

where q_t is the solid volume of sediment transported per unit time and width, g_t is the weight of sediment transported per unit time and width, and β_E is the bulk specific weight of sediment.

The complex velocity potential satisfying the kinematic conditions required by Eqs. (8.57a, b) can be given as follows (Milne-Thompson 1960):

$$W = U \left\{ Z + \frac{\alpha_s}{\sinh(k_w H)} \cos[k_w(Z + iH - U_b t)] \right\} \quad (8.62)$$

where $Z = x + iz$, which is the complex coordinate and H is the depth of virtual bottom so that at $z = -H$ (Fig. 8.17), a streamline has a stream function $\psi = -UH$. For celerity of wave with small amplitude, it can be written

$$U^2 = \frac{g}{k_w} \tanh(k_w H) \quad (8.63)$$

Separating the real and the imaginary parts of Eq. (8.62), the velocity potential function ϕ and the stream function ψ can be given by

$$\phi = U \left\{ x + \alpha_s \frac{\cosh[k_w(z + H)]}{\sinh(k_w H)} \cos[k_w(x - U_b t)] \right\} \quad (8.64a)$$

$$\psi = U \left\{ z - \alpha_s \frac{\sinh[k_w(z + H)]}{\sinh(k_w H)} \sin[k_w(x - U_b t)] \right\} \quad (8.64b)$$

The bed corresponds to the stream function $\psi_0 = -Uh$ with a position $z = -h + \eta(x, t)$. Thus, neglecting the higher-order quantities and using Eq. (8.64b) yield

$$\eta = \alpha_s \frac{\sinh[k_w(H - h)]}{\sinh(k_w H)} \sin[k_w(x - U_b t)] \quad (8.65)$$

Introducing the concept of slowly varying amplitude $\alpha(t)$ of bed waves with time t such that $\partial \alpha / \partial t \ll U k_w \alpha$, the velocity potential function ϕ for the flow over bed waves with slowly varying amplitude is

$$\phi(U_b \ll U) = U \left\{ x + \alpha(t) \frac{\cosh[k_w(z + H)]}{\sinh(k_w H)} \cos[k_w(x - U_b t)] \right\} \quad (8.66)$$

Equating Eqs. (8.57b) and (8.65) and using Eq. (8.63), the relationship of amplitude of bed waves is related to that of free surface waves

$$\alpha_m(t) = \alpha(t) \frac{\sinh[k_w(H-h)]}{\sinh(k_w H)} \quad (8.67)$$

$$\therefore \alpha_m(t) = \alpha(t) \left[1 - \frac{g}{k_w U^2} \tanh(k_w h) \right] \cosh(k_w h)$$

Kennedy assumed the sediment transport rate as a function of flow velocity and suggested

$$g_t(x, t) = m \left(\frac{\partial \phi}{\partial x} \right)^n \quad \wedge \quad \phi = \phi(x - L_s, -h, t) \quad (8.68)$$

where m , n , and L_s are the parameters being dependent on h , U , d , ρ , ρ_s , and v . The L_s is the distance by which the local sediment transport rate lags the local bed shear stress.

Substituting Eq. (8.66) into Eq. (8.68) and expressing into binomial series yield

$$g_t(x, t) = mU^n - k_w m n U^n \alpha \frac{\cosh[k_w(H-h)]}{\sinh(k_w H)} \sin[k_w(x - L_s - U_b t) + O(u^2)] \quad (8.69)$$

Neglecting the higher-order terms, the streamwise sediment transport rate $g_{t|x}$ is given as

$$g_{t|x} = mU^n \quad (8.70)$$

Substituting Eqs. (8.57b), (8.67), (8.69) and (8.70) into Eq. (8.61) and neglecting terms of $O(u^2)$ yield the following differential equation for $\alpha(t)$:

$$\begin{aligned} \frac{\partial \alpha}{\partial t} \sin[k_w(x - U_b t)] - \alpha k_w U_b \cos[k_w(x - U_b t)] \\ + \alpha \frac{nk_w^2 g_{t|x}}{\beta_E} \coth[k_w(H-h)] \cos[k_w(x - L_s - U_b t)] = 0 \end{aligned} \quad (8.71)$$

The solution is

$$\alpha(t) = \alpha(0) \exp \left\{ \underbrace{t \frac{nk_w^2 g_{t|x}}{\beta_E} \coth[k_w(H-h)] \sin(k_w L_s)}_I - \underbrace{\left\langle \frac{nk_w g_{t|x}}{\beta_E U_b} \coth[k_w(H-h)] \cos(k_w L_s) + 1 \right\rangle \ln |\sin[k_w(x - U_b t)]|}_H \right\} \quad (8.72)$$

As $\alpha(t)$ is a function of t only, the term II is zero. Hence, the velocity of bed wave migration is

$$U_b = -\frac{nk_w g t|_x}{\beta_E} \coth[k_w(H-h)] \cos(k_w L_s) \quad (8.73)$$

Substituting Eq. (8.72) into Eq. (8.67) and eliminating x dependent term by Eq. (8.73), the amplitude of bed waves is obtained as

$$\alpha_m(t) = \alpha(0) \frac{\sinh[k_w(H-h)]}{\sinh(k_w H)} \exp \left\{ t \frac{nk_w^2 g t|_x}{\beta_E} \coth[k_w(H-h)] \sin(k_w L_s) \right\} \quad (8.74)$$

Equation (8.74) suggests that the amplitude of small waves (perturbations) on an otherwise plane bed initiated by an arbitrary disturbance increases exponentially with time, provided k_w and L_s are such that the exponential term in Eq. (8.74) is positive, and under such condition, a flat bed becomes unstable. On the other hand, the amplitude of bed waves cannot continue to grow indefinitely. As the amplitude increases, it gives rise to the nonlinear effects which govern the equilibrium height of fully developed dunes and antidunes.

Using Eqs. (8.67), (8.73) and (8.74), the various bedforms and the criteria for their occurrence are furnished in Table 8.3, as was given by Kennedy (1963).

From Eq. (8.74), the initial growth rate α_{m0} is obtained as

$$\alpha_{m0}(0) = \alpha(0) \frac{nk_w^2 g t|_x}{\beta_E} \cdot \frac{\cosh[k_w(H-h)]}{\sinh(k_w H)} \sin(k_w L_s) \quad (8.75)$$

To determine k_w corresponding to maximum α_{m0} , Eq. (8.75) is differentiated with respect to k_w and then equated to zero. Hence, eliminating H using Eq. (8.63), the following can be obtained:

$$\begin{aligned} \frac{d\alpha_{m0}(0)}{dk_w} = \alpha(0) \frac{ng t|_x}{\beta_E} \left\{ [2k_w \sin(k_w L_s) + k_w^2 L_s \cos(k_w L_s)] \left[\frac{g \cosh(k_w h)}{k_w U^2} - \sinh(k_w h) \right] \right. \\ \left. + k_w^2 \sin(k_w L_s) \left[-\frac{g \cosh(k_w h)}{k_w^2 U^2} + \frac{gh \sinh(k_w h)}{k_w U^2} - h \cosh(k_w h) \right] \right\} = 0 \end{aligned} \quad (8.76)$$

The solution given by Kennedy is as follows:

$$Fr^2 = \frac{1 + k_w h \tanh(k_w h) + j k_w h \cot(j k_w h)}{(k_w h)^2 + [2 + j k_w h \cot(j k_w h)] k_w h \tanh(k_w h)} \quad \wedge \quad L_s = j h \quad (8.77)$$

Table 8.3 Summary of bedforms and the criteria for their occurrence (Kennedy 1963)

Case	Bed and free surface profiles	$H-h$	$k_w L_s$	$\sin(k_w L_s)$	$\cos(k_w L_s)$	Direction of bedform migration	Bedforms
1	In phase	+ve	$0-0.5\pi$	+ve	+ve	Upstream	Antidunes
2		+ve	0.5π	+ve	0	None	
3		+ve	$0.5\pi-\pi$	+ve	-ve	Downstream	
4a	No bed wave	-ve	$\pi-1.5\pi$	-ve	+ve	—	Plane bed
4b		-ve	$0-\pi$	+ve	—	—	
4c		+ve	$\pi-2\pi$	-ve	—	—	
5	Out of phase	-ve	$1.5\pi-2\pi$	-ve	+ve	Downstream	Dunes

For the limiting case ($L_s \ll h$ or $j \rightarrow 0$), Eq. (8.77) becomes

$$\lim_{j \rightarrow 0} Fr^2 = \frac{2 + k_w h \tanh(k_w h)}{(k_w h)^2 + 3k_w h \tanh(k_w h)} \quad (8.88)$$

The shortest wavelength λ_{\min} for the bed waves can be obtained by setting $H \rightarrow \infty$ in Eq. (8.63). It is as follows:

$$\lambda_{\min}(H \rightarrow \infty) = \frac{2\pi}{g} U^2 \quad (8.89)$$

Note that the wavelength λ of bed waves can have any value greater than λ_{\min} . The relationship between Fr and $k_w h$ for the shortest possible long-crested waves (two-dimensional) can be obtained from Eq. (8.89) as

$$Fr_m^2 = \frac{U^2}{gh} = \frac{\lambda_{\min}}{2\pi h} = \frac{1}{k_w h} \quad (8.90)$$

Here, Fr_m is the maximum possible Froude number for the given k_w and h , provided the surface waves and bed profiles are two-dimensional. Therefore, for long-crested waves (two-dimensional), the $k_w h$ belongs to the range $0 < k_w h < Fr_m^{-2}$, while for short-crested waves (three-dimensional), the $k_w h$ can exceed Fr_m^{-2} , provided for the given values of U and H , these waves are shorter than two-dimensional waves (Fuchs 1951).

Another case is that for $H = h$, the relationship between Fr and $k_w h$ can be obtained replacing H by h in Eq. (8.63) and then dividing by gh as

$$Fr_a^2(H = h) = \frac{U^2}{gh} = \frac{\tanh(k_w h)}{k_w h} \quad (8.91)$$

Here, Fr_a is the minimum Froude number for the formation of antidunes. It means that the above equation holds for all values of j provided $H = h$.

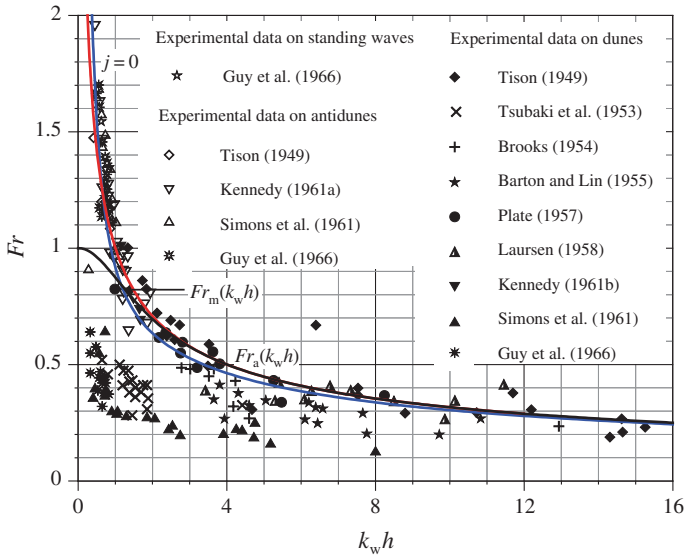


Fig. 8.20 Flow Froude number Fr as a function of $k_w h$ obtained by Kennedy (1963) and comparison with the experimental data (Tison 1949; Tsubaki et al. 1953; Brooks 1954; Barton and Lin 1955; Plate 1957; Laursen 1958; Simons et al. 1961; Kennedy 1961a, b; Guy et al. 1966)

Figure 8.20 shows the variation of flow Froude number Fr with $k_w h$ obtained from Eqs. (8.88), (8.90) and (8.91). For a given value of $k_w h$, the Fr is either greater than $Fr_a(H > h)$ or less than $Fr_a(H < h)$. It is found that the condition $H > h$ corresponds to the formation of antidunes and the condition $H < h$ to the formation of dunes. As a result of this, the antidunes occur in the region above the $Fr_a(k_w h)$ curve (Eq. 8.91). It implies that for a given value of $k_w h$, the Fr_a is the minimum Froude number for the formation of antidunes and at the same time the maximum Froude number for the formation of dunes. The available experimental data that are used for the comparison are due to Tison (1949), Tsubaki et al. (1953), Brooks (1954), Barton and Lin (1955), Plate (1957), Laursen (1958), Kennedy (1961a, b), Simons et al. (1961) and Guy et al. (1966). From Fig. 8.20, it is noticeable that the antidune data plots are in satisfactory agreement, while particularly most of the dune data plots fall below the $Fr_a(k_w h)$ curve. However, the overall performance of the model is apparently encouraging in predicting the formation of dunes and antidunes.

8.5.3.2 Hayashi's Model

Hayashi (1970) initiated to develop a model considering almost similar boundary conditions [Eqs. (8.57a, b), (8.58) and (8.60)] assumed by Kennedy (1963). However, he used a modified form of Eq. (8.59) as

$$\frac{1}{2} \left[\left(\frac{\partial \phi}{\partial x} \right)^2 + \left(\frac{\partial \phi}{\partial z} \right)^2 \right] + \frac{\partial \phi}{\partial t} + g\zeta = \text{constant (on } z = 0)$$

Using the boundary conditions and the Laplace equation, the velocity potential function is obtained as

$$\phi = U \left\{ x - \alpha_m \frac{\cosh(k_w z) + Fr^2 k_w h \sinh(k_w z)}{\sinh(k_w h) - Fr^2 k_w h \cosh(k_w h)} \cos[k_w(x - U_b t)] \right\} \quad (8.92)$$

provided that the slowly varying amplitude $\alpha(t)$ with time t is prevalent such that $\partial \alpha / \partial t \ll U k_w \alpha$ and $U_b \ll U$. Using Eqs. (8.58) and (8.92), the following relationship between amplitudes of free surface and bed waves is obtained:

$$\alpha_s(t) = \alpha(t) \frac{Fr^2 k_w h}{[\tanh(k_w h) - Fr^2 k_w h] \cosh(k_w h)} \quad (8.93)$$

provided that $\alpha_s(t)$ is also a slowly varying function of t such that $\partial \alpha_s / \partial t \ll U k_w \alpha_s$. The continuity equation of sediment transport given by Eq. (5.48) was rearranged by Hayashi as follows:

$$(1 - \rho_0) \frac{\partial \eta}{\partial t} + \frac{\partial q_t}{\partial x} = 0 \Rightarrow \frac{\partial \eta}{\partial t} + \frac{\partial q_T}{\partial x} = 0 \quad \wedge \quad q_T = \frac{q_t}{1 - \rho_0} \quad (8.94)$$

where q_T is the sediment transport rate in bulk volume per unit time and width. Hayashi expressed it as

$$q_T(x, t) = m \left(1 + a \frac{\partial \eta}{\partial x} \right) \left(\frac{\partial \phi}{\partial x} \right)^4 \quad \wedge \quad \eta = \eta(x - L_s, t) \quad \vee \quad \phi = \phi(x - L_s, -h, t) \quad (8.95)$$

where m is a dimensional coefficient and a is a nondimensional constant.

Substituting Eq. (8.95) into Eq. (8.94) and expressing $\partial \phi(x, z, t) / \partial x = U + u(x, z, t)$ yield

$$\frac{\partial \eta(x, t)}{\partial t} + q_T|_x \left[\frac{\partial^2 \eta(x - L_s, t)}{\partial x^2} + \frac{4}{U} \cdot \frac{\partial u(x - L_s, -h, t)}{\partial x} + O(u^2) \right] = 0 \quad (8.96)$$

where $q_T|_x = mU^4$, which is the net streamwise sediment transport rate.

Substituting Eq. (8.57b) and the expression of u obtained from Eq. (8.92) into Eq. (8.96), the following differential equation of $\alpha(t)$ is obtained:

$$\begin{aligned} \frac{\dot{\alpha}(t)}{\alpha(t)} - k_w^2 q_T|_x \left[a \cos(k_w L_s) - 4 \frac{1 - Fr^2 k_w h \tanh(k_w h)}{\tanh(k_w h) - Fr^2 k_w h} \sin(k_w L_s) \right] - \frac{k_w}{\tan[k_w(x - U_b t)]} \\ \times \left\{ U_b - q_T|_x k_w \left[a \sin(k_w L_s) + 4 \frac{1 - Fr^2 k_w h \tanh(k_w h)}{\tanh(k_w h) - Fr^2 k_w h} \cos(k_w L_s) \right] \right\} = 0 \end{aligned} \quad (8.97)$$

As $\alpha(t)$ is a function of t , the third term of the left-hand side of Eq. (8.97) must vanish. Hence, assuming $k_w L_s \ll 1$, Eq. (8.97) reduces to

$$\alpha(t) = \alpha(0) \exp\left(\frac{mg^2 a}{C} Fr^4 k_w^2 h^2 \vartheta t\right) \quad (8.98)$$

where

$$C = \frac{a}{L_s} \left(\frac{U^2}{2g}\right)^{-1}, \quad \vartheta = C - 2Fr^2 k_w h \frac{1 - Fr^2 k_w h \tanh(k_w h)}{\tanh(k_w h) - Fr^2 k_w h} \quad (8.99)$$

Equation (8.98) produces an increase in amplitude of bed waves if $\vartheta > 0$, which is the condition for a plane bed to become unstable. It implies that $\vartheta > 0$ is the criterion for the formation of bed waves and $\vartheta < 0$ is the criterion for a plane bed. Therefore, the limits of the formation of bed waves are as follows: (1) $\vartheta = 0$ and (2) $\tanh(k_w h) - Fr^2 k_w h = 0$. Thus, the limiting values of Fr^2 are obtained as

$$Fr^2 = \left[\frac{Fr_2^2}{Fr_1^2} \right] = \frac{1}{4k_w h \tanh(k_w h)} \{C + 2 \pm [(C + 2)^2 - 8C \tanh^2(k_w h)]^{0.5}\} \quad (8.100a)$$

$$Fr^2 = Fr_a^2 = \frac{\tanh(k_w h)}{k_w h} \quad (8.100b)$$

Figure 8.21 shows the variation of flow Froude number Fr with $k_w h$ for $C = 0$ and the experimental data plots for the comparison. Hayashi defined the dunes and the antidunes as bed waves correspond to $\alpha_s < \alpha_m$ and $\alpha_s > \alpha_m$, respectively. In Fig. 8.21, the regions of occurrence of different bedforms in terms of Froude number are furnished in Table 8.4, which provides an understanding on the criteria for the formation of bedforms.

Table 8.4 suggests that

1. Fr_1 is the maximum Froude number for the formation of dunes,
2. Fr_a is the minimum Froude number for the formation of antidunes, and
3. Fr_2 is the maximum Froude number for the formation of antidunes.

In Eq. (8.98), the instability occurs for $C = 0$ only in the region whose limits are given by Eq. (8.100b) and

$$Fr^2 = Fr_m^2 = \frac{1}{k_w h \tanh(k_w h)} \quad (8.101)$$

The curves obtained from these two equations are shown in Fig. 8.21. The bed waves formed in the region bounded by the two curves are antidunes. Hence, for $C = 0$, only antidunes can occur.

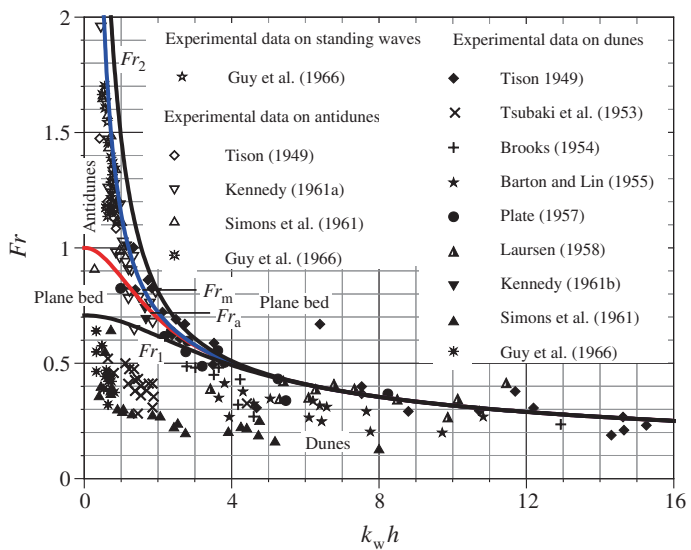


Fig. 8.21 Flow Froude number Fr as a function of $k_w h$ obtained by Hayashi (1970) and comparison with the experimental data (Tison 1949; Tsubaki et al. 1953; Brooks 1954; Barton and Lin 1955; Plate 1957; Laursen 1958; Simons et al. 1961; Kennedy 1961a, b; Guy et al. 1966)

Table 8.4 Criteria for the formation of bedforms (Hayashi 1970)

Bedform	Criterion
Dunes	$Fr < Fr_1$
Antidunes	$Fr_a < Fr < Fr_2$
Plane bed	$Fr_1 < Fr < Fr_a$ and $Fr_2 < Fr$

8.5.3.3 Song’s Model

Song (1983) advanced the methodology developed by Milne-Thompson (1960) for the solution of flow over a sinusoidal wavy bed to explain the bedform phenomenon.

He expressed the complex velocity potential satisfying the kinematic conditions required by Eqs. (8.57a, b) as

$$W = U_m \left\{ Z + \frac{\alpha_s}{\sinh(k_w H)} \cos[k_w (Z + iH - U_b t)] \right\} \tag{8.102}$$

where U_m is the mean flow velocity over the entire flow field. At $z = -H$, a streamline has a stream function $\psi = -U_m H$. The complex velocity potential is to satisfy the condition of the constant pressure at the free surface. It is therefore required

$$U_m^2 = \frac{g}{k_w} \tanh(k_w H) \quad (8.103)$$

There also exists a relationship between the amplitudes of free surface waves and bed waves as

$$\alpha_m = \alpha_s \left[1 - \frac{g}{k_w U_m^2} \tanh(k_w h) \right] \cosh(k_w h) \quad (8.104)$$

Noting that the celerity C of gravity waves having a small amplitude is given by

$$C^2 = \frac{g}{k_w} \tanh(k_w h) \quad (8.105)$$

Equation (8.104) suggests that the free surface waves and the bed waves are in phase if the flow is supercritical and out of phase if the flow is subcritical.

To estimate the velocity of bedform migration, it is assumed that the bed-load transport is a function of near-bed flow velocity. This assumption is applicable in case of no flow separation and a thin boundary layer. Some error is expected for fully developed dunes, as the flow is separated on the leeside.

Differentiating Eq. (8.102) with respect to Z and setting $z = -h$, the component of near-bed flow velocity u_0 in streamwise direction is obtained as

$$u_0 = U_m \left\{ 1 - \frac{\alpha_s k_w}{\sinh(k_w H)} \cosh[k_w (H - h)] \sin[k_w (x - U_b t)] \right\} \quad (8.106)$$

Using Eqs. (8.57a, b), (8.103) and (8.104), Eq. (8.106) is simplified as

$$u_0 = U_m (1 + k_w U^* \eta) \quad \wedge \quad U^* = \frac{1 - Fr^2 k_w h \tanh(k_w h)}{\tanh(k_w h) - Fr^2 k_w h} \quad (8.107)$$

where U^* is a nondimensional parameter.

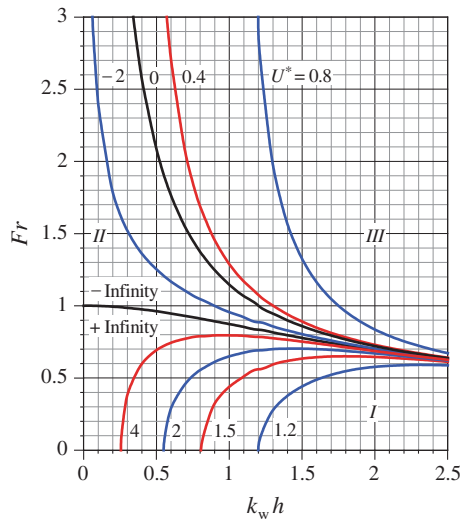
If the amplitude of bedforms is small, then the vertical velocity component of the near-bed flow is small as compared to streamwise velocity component u_0 . Thus, it can be approximated as $u_0 \approx U$. Then, the migration velocity U_b of bedforms (sand waves) using Eq. (8.47) is obtained as

$$U_b = \frac{\partial q_b}{\partial \eta} = \frac{\partial q_b}{\partial U} \cdot \frac{\partial U}{\partial \eta} = \frac{\partial q_b}{\partial U} \cdot k_w U_m U^* \Rightarrow U^* = U_b \left(\frac{\partial q_b}{\partial U} \cdot k_w U_m \right)^{-1} \quad (8.108)$$

Therefore, the nondimensional parameter U^* represents the nondimensional velocity of bedform migration.

Figure 8.22 shows $Fr_a(k_w h)$ curves for different U^* . The plane $Fr-k_w h$ is divided into three regions by the curves represented by

Fig. 8.22 Flow Froude number Fr as a function of $k_w h$ for different U^* (Song 1983)



$$Fr^2 = \frac{\tanh(k_w h)}{k_w h}, \quad Fr^2 = \frac{1}{k_w h \tanh(k_w h)}$$

In Fig. 8.22, these curves represent the demarcation lines across which the migration of bedforms changes the direction. Zone *I*, in which $U_m \leq C$ and $U^* \geq 1$, is the zone where dunes occur. On the other hand, antidunes occur in Zone *II*, in which $U_m \geq C$ and $U^* < 0$. The occurrence of a downstream migration of bedforms in Zone *III* is rather interesting. Kennedy (1963) who used the lag as the mechanism of growth of the bedforms found Zone *III* to be the unstable zone. In contrast, Engelund (1970) and Fredsøe (1974) argued that the antidunes moving downstream could potentially occur in this zone, if the mode of sediment transport is predominantly the bed load.

8.5.4 Bose–Dey Instability Theory

8.5.4.1 Instability of Sand-Bed Leading to Formation of Dunes and Antidunes

Based on the Reynolds-averaged Navier–Stokes (RANS) equations, Bose and Dey (2009) developed a theory of turbulent shear flow over bed waves addressing the instability criterion for a plane bed leading to the formation of bedforms. Under consideration is a curvilinear flow over a sinusoidal bed (Fig. 8.23). The z -axis is vertically upward. For bed waves, the bed elevation is $z = \eta(x, t)$ with respect to

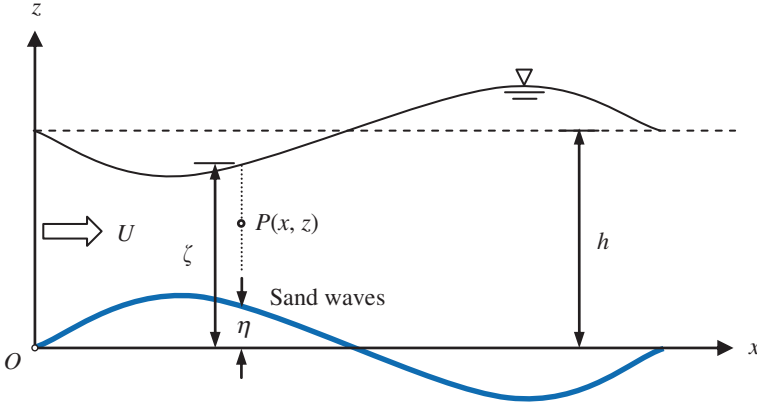


Fig. 8.23 Definition sketch of flow over sand waves (Bose and Dey 2009)

the mean bed level (that is, x -axis). The bed waves cause a wavy profile of the free surface of flow being defined by $z = \zeta(x, t)$ above the mean bed level. However, the mean flow depth, that is the height from the mean bed level to the mean free surface is h being approximately a constant. According to the Reynolds decomposition in two-dimensional turbulent flow, the instantaneous velocity components (u, w) at a point $P(x, z)$ at time t can be split into the time-averaged part (\bar{u}, \bar{w}) and the fluctuating part (u', w').

The continuity equations are

$$\frac{\partial \bar{u}}{\partial x} + \frac{\partial \bar{w}}{\partial z} = 0, \quad \frac{\partial u'}{\partial x} + \frac{\partial w'}{\partial z} = 0 \quad (8.109)$$

The RANS equations are

$$\frac{\partial \bar{u}}{\partial t} + \bar{u} \frac{\partial \bar{u}}{\partial x} + \bar{w} \frac{\partial \bar{u}}{\partial z} = \frac{1}{\rho} \left(-\frac{\partial \bar{p}}{\partial x} + \frac{\partial \tau}{\partial z} \right) + \nu \frac{\partial^2 \bar{u}}{\partial z^2} - \frac{\partial (\overline{u'^2})}{\partial x} \quad (8.110a)$$

$$\frac{\partial \bar{w}}{\partial t} + \bar{u} \frac{\partial \bar{w}}{\partial x} + \bar{w} \frac{\partial \bar{w}}{\partial z} = \frac{1}{\rho} \left(-\frac{\partial \bar{p}}{\partial z} + \frac{\partial \tau}{\partial x} \right) + \nu \frac{\partial^2 \bar{w}}{\partial x^2} - \frac{\partial (\overline{w'^2})}{\partial z} - g \quad (8.110b)$$

where $\bar{p}(x, z, t)$ is the time-averaged hydrostatic pressure and τ is the Reynolds shear stress.

The power law of velocity distribution is given by

$$\bar{u} = U_{\max}(x, t) \left(\frac{z - \eta}{\zeta - \eta} \right)^{1/m} \quad (8.111)$$

where m is an exponent and $U_{\max} = \bar{u}(z = \zeta)$. The U_{\max} can be related to the depth-averaged velocity $U(x, t)$ of the flow section, and then, \bar{u} is expressed as

$$U(x, t) = \frac{1}{\zeta - \eta} \int_{\eta}^{\zeta} \bar{u} dz = \frac{m}{1+m} U_{\max}(x, t) \Rightarrow \bar{u} = \frac{1+m}{m} U \left(\frac{z - \eta}{\zeta - \eta} \right)^{1/m} \quad (8.112)$$

Equation (8.109) then yields

$$\bar{w} = -(\zeta - \eta) \frac{\partial U}{\partial x} \left(\frac{z - \eta}{\zeta - \eta} \right)^{(1+m)/m} \quad (8.113)$$

The free surface waves and the bed waves have small amplitude and long wavelength, so $|\partial \zeta / \partial x| \approx 0$ and $|\partial \eta / \partial x| \approx 0$. Moreover, along a curvilinear streamline with a small curvature, the normal acceleration is essentially convective for vanishing local acceleration ($\partial \bar{w} / \partial t \approx 0$). By Eq. (8.109), the convective vertical acceleration can be given by

$$\bar{u} \frac{\partial \bar{w}}{\partial x} + \bar{w} \frac{\partial \bar{w}}{\partial z} = \bar{u} \frac{\partial \bar{w}}{\partial x} - \bar{w} \frac{\partial \bar{u}}{\partial x} = \bar{u}^2 \frac{\partial (\tan \psi)}{\partial x} \approx \bar{u}^2 k \quad (8.114)$$

where $\psi = \arctan(\bar{w} / \bar{u})$, that is the slope of the streamline through the point $P(x, z)$, and k is the curvature of the streamline through the point P , such that $k(\zeta) \approx \partial^2 \zeta / \partial x^2$ and $k(\eta) \approx \partial^2 \eta / \partial x^2$, in which the slopes are negligible. Following the Boussinesq approximation, a linear variation of k with z exists, so that

$$k = k(\eta) + [k(\zeta) - k(\eta)] \frac{z - \eta}{\zeta - \eta} \quad (8.115)$$

With this expression of k in Eq. (8.114) and \bar{u} given by Eq. (8.112), Eq. (8.110b) is integrated over the depth z and the resulting equation is

$$\begin{aligned} \frac{\bar{p}}{\rho} = \frac{\bar{p}_0}{\rho} + g(\zeta - z) - U^2(\zeta - \eta) \left(\frac{1+m}{m} \right)^2 \left\{ \frac{m}{2+m} k(\eta) \left[\left(\frac{z - \eta}{\zeta - \eta} \right)^{(2+m)/m} - 1 \right] \right. \\ \left. + \frac{m}{2(m+1)} [k(\zeta) - k(\eta)] \left[\left(\frac{z - \eta}{\zeta - \eta} \right)^{2(1+m)/m} - 1 \right] \right\} - \overline{w'^2} \end{aligned} \quad (8.116)$$

where $\bar{p}_0 = \bar{p}(z = \zeta)$. Equation (8.116) yields $\partial \bar{p} / \partial x$, noting that the contribution from $\overline{w'^2}$ is negligible due to insignificant streamwise variation of turbulence stresses. Thus, the gravity, the curvature of streamlines, and the $1/m$ -th power law of streamwise velocity contribute to the expression for $\partial \bar{p} / \partial x$. The resulting expression for $\partial \bar{p} / \partial x$ is used in Eq. (8.110a).

Integrating the continuity equation (Eq. 8.109) and using Eq. (8.112), the depth-averaged continuity equation is obtained as

$$\begin{aligned} \frac{d\zeta}{dt} - \frac{d\eta}{dt} = \bar{w}|_{\eta}^{\zeta} &= - \int_{\eta}^{\zeta} \frac{\partial \bar{u}}{\partial x} dz = - \frac{\partial}{\partial x} [(\zeta - \eta)U] + \bar{u}(x, \zeta, t) \frac{\partial \zeta}{\partial x} - \bar{u}(x, \eta, t) \frac{\partial \eta}{\partial x}, \\ \therefore \quad \frac{\partial}{\partial t} (\zeta - \eta) + \frac{\partial}{\partial x} [(\zeta - \eta)U] &= 0 \end{aligned} \quad (8.117)$$

From Eq. (8.116), it yields

$$\frac{1}{\rho} \int_{\eta}^{\zeta} \frac{\partial \bar{p}}{\partial x} dz = g(\zeta - \eta) \frac{\partial h}{\partial x} + \beta \frac{\partial}{\partial x} \left\{ U^2 (\zeta - \eta)^2 \left[k(\zeta) + \frac{m}{2(m+1)} k(\eta) \right] \right\} \quad (8.118)$$

where $\beta = (m+1)^2/[m(3m+2)]$. Similarly, for the convective acceleration, partially integrating the terms of the left-hand side of Eq. (8.110a) using Eqs. (8.109) and (8.112) yields

$$\begin{aligned} \int_{\eta}^{\zeta} \left(\frac{\partial \bar{u}}{\partial t} + \bar{u} \frac{\partial \bar{u}}{\partial x} + \bar{w} \frac{\partial \bar{u}}{\partial z} \right) dz &= \frac{\partial}{\partial t} [(\zeta - \eta)U] + \frac{\partial}{\partial x} \int_{\eta}^{\zeta} \bar{u}^2 dz \\ &= \frac{\partial}{\partial t} [(\zeta - \eta)U] + \alpha \frac{\partial}{\partial x} [(\zeta - \eta)U^2] \end{aligned} \quad (8.119)$$

where $\alpha = (m+1)^2/[m(m+2)]$. Neglecting the variation of Reynolds stresses in x -direction, the integration of Eq. (8.110a) over z produces

$$\begin{aligned} \frac{\partial}{\partial t} [(\zeta - \eta)U] + \alpha \frac{\partial}{\partial x} [(\zeta - \eta)U^2] + \beta \frac{\partial}{\partial x} \left\{ (\zeta - \eta)^2 U^2 \left[k(\zeta) + \frac{m}{2(m+1)} k(\eta) \right] \right\} \\ + g(\zeta - \eta) \frac{\partial \zeta}{\partial x} + gn^2 \frac{U^2}{(\zeta - \eta)^{1/3}} = 0 \end{aligned} \quad (8.120)$$

where n is the Manning roughness coefficient. The Manning equation used for the estimation of local flow resistance is given by $\rho u_*^2 = \tau_0 = \rho g n^2 U^2 (\zeta - \eta)^{-1/3}$ where u_* is the shear velocity at a distance x . Rearranging Eq. (8.120), an alternative form of Eq. (8.120) can be obtained as

$$\begin{aligned}
& \frac{\partial U}{\partial t} + (2\alpha - 1)U \frac{\partial U}{\partial x} + (\alpha - 1) \frac{U^2}{\zeta - \eta} \cdot \frac{\partial}{\partial x} (\zeta - \eta) + \beta(\zeta - \eta)U^2 \\
& \times \left[\frac{\partial k(\zeta)}{\partial x} + \frac{m}{2(m+1)} \cdot \frac{\partial k(\eta)}{\partial x} \right] + 2\beta U \left[k(\zeta) + \frac{m}{2(m+1)} k(\eta) \right] \frac{\partial}{\partial x} [(\zeta - \eta)U] \\
& + g \frac{\partial \zeta}{\partial x} + gn^2 \frac{U^2}{(\zeta - \eta)^{4/3}} = 0
\end{aligned} \tag{8.121}$$

Equation (8.120) or (8.121) is a generalization of the *de Saint-Venant equation*, where the variability of \bar{u} is in accordance with $1/m$ -th power law including the curvature effects of streamlines.

The total load sediment transport rate q_t (by volume) per unit time and width is given by

$$q_t = q_b + \int_{\eta}^{\zeta} \bar{u} C \, dz \tag{8.122}$$

where q_b is the bed-load transport rate and C is the concentration of sediment suspension. The total load satisfies the Exner's equation. It is as follows:

$$\frac{\partial q_t}{\partial x} = -(1 - \rho_0) \frac{\partial \eta}{\partial t} - \frac{\partial}{\partial t} \int_{\eta}^{\zeta} C(x, z, t) dz = -(1 - \rho_0) \frac{\partial \zeta}{\partial t} - \frac{\partial}{\partial t} [(\zeta - \eta) \bar{C}] \tag{8.123}$$

where $\bar{C}(x, t)$ is the depth-averaged concentration, which is given by

$$\bar{C}(x, t) = \frac{1}{\zeta - \eta} \int_{\eta}^{\zeta} C(x, z, t) dz \tag{8.124}$$

Including the effects of bed slope in the bed-load transport equation, the original equation of Meyer-Peter and Müller (1948) was modified by Fredsøe (1974). It is then expressed as

$$q_b = 8d(\Delta g d)^{0.5} \left(\frac{\tau_0}{\Delta \rho g d} - \mu \frac{\partial \eta}{\partial x} - 0.047 \right)^{1.5} \tag{8.125}$$

where μ is the frictional coefficient of particles (of the order of 0.1). The bed shear stress is obtained from the Manning equation of flow resistance as $\tau_0 = \rho g n^2 U^2 (\zeta - \eta)^{-1/3}$. Consequently, the sediment transport rate is higher near the crest of the bed waves. The sediment concentration C in suspension satisfies

the fluid–sediment continuity equation (Engelund 1970). The equation is an advection–diffusion equation [see Eq. (6.13)], which is given by

$$\frac{dC}{dt} = w_s \frac{\partial C}{\partial z} + \left(\varepsilon_{sx} \frac{\partial^2 C}{\partial x^2} + \varepsilon_{sz} \frac{\partial^2 C}{\partial z^2} \right) \quad (8.126)$$

where w_s is the terminal fall velocity of sand, and ε_{sx} and ε_{sz} are the turbulent diffusivities in x - and z -direction, respectively. Thackston and Krenkel (1967) gave an estimate of ε_{sx} as

$$\varepsilon_{sx} = 7.25 u_* h \left(\frac{U}{u_*} \right)^{0.25} = 7.25 g^{0.375} n^{0.75} U h^{0.875} \quad (8.127)$$

On the other hand, Lane and Kalinske (1941) expressed ε_{sz} as

$$\varepsilon_{sz} = \frac{1}{15} u_* h = 0.066 g^{0.5} n U h^{5/6} \quad (8.128)$$

Using Eq. (8.109) into Eq. (8.126) and integrating between limits η to ζ yield

$$\int_{\eta}^{\zeta} \frac{dC}{dt} dz = \frac{\partial}{\partial t} [(\zeta - \eta) \bar{C}] + \frac{\partial}{\partial x} \int_{\eta}^{\zeta} \bar{u} C dz \quad (8.129)$$

The time-averaged velocity \bar{u} increases with z , while C diminishes. Hence, in Eq. (8.129), it can be assumed that $\bar{u} C \approx U \bar{C}$, replacing the velocity and the concentration by their averaged values. The integral of the right-hand side of Eq. (8.126) is

$$\left(w_s C + \varepsilon_{sz} \frac{\partial C}{\partial z} \right)_{\eta}^{\zeta} + \varepsilon_{sx} \int_{\eta}^{\zeta} \frac{\partial^2 C}{\partial x^2} dz \approx \varepsilon_{sx} \frac{\partial^2}{\partial x^2} [(\zeta - \eta) \bar{C}] \quad (8.130)$$

In Eq. (8.130), the first term of the left-hand side vanishes, as there is no net vertical sediment flux across the extremities ($z = \eta$ and ζ). Equation (8.126) thus leads to

$$\frac{\partial}{\partial t} [(\zeta - \eta) \bar{C}] + \frac{\partial}{\partial x} [(\zeta - \eta) U \bar{C}] = \varepsilon_{sx} \frac{\partial^2}{\partial x^2} [(\zeta - \eta) \bar{C}] \quad (8.131)$$

It is pertinent to mention that Eq. (8.131) is approximately legitimate. Thus, using Eqs. (8.122), (8.125) and (8.131) into the Exner equation (Eq. 8.123) yields

$$\begin{aligned}
& (1 - \rho_0) \frac{\partial \eta}{\partial t} + \varepsilon_{sx} \frac{\partial^2}{\partial x^2} [(\zeta - \eta) \bar{C}] + 12d(\Delta g d)^{0.5} \left[\frac{n^2 U^2}{\Delta d (\zeta - \eta)^{1/3}} - \mu \frac{\partial \eta}{\partial x} - 0.047 \right]^{0.5} \\
& \times \left\{ \frac{n^2}{\Delta d (\zeta - \eta)^{1/3}} \left[2U \frac{\partial U}{\partial x} - \frac{1}{3} \cdot \frac{U^2}{\zeta - \eta} \left(\frac{\partial \zeta}{\partial x} - \frac{\partial \eta}{\partial x} \right) \right] - \mu \frac{\partial^2 \eta}{\partial x^2} \right\} = 0
\end{aligned} \tag{8.132}$$

Equations (8.117), (8.121) (with $\alpha = 1$ and $\beta = 2/5$), (8.131) and (8.132) constitute the governing equation of perturbed flow due to erosion of bed. In Eq. (8.121), $k(\zeta) = \partial^2 \zeta / \partial x^2$ and $k(\eta) = \partial^2 \eta / \partial x^2$ are taken.

In analogy of propagation of waves along the interface of two immiscible fluids, the conditions for propagation of sand waves are investigated for a mean flow depth h and a mean flow velocity U_m over an undisturbed plane bed. The above set of equations to the first order is then linearized as

$$\frac{\partial \zeta}{\partial t} - \frac{\partial \eta}{\partial t} + h \frac{\partial U}{\partial x} + U_m \left(\frac{\partial \zeta}{\partial x} - \frac{\partial \eta}{\partial x} \right) = 0 \tag{8.133a}$$

$$\frac{\partial U}{\partial t} + U_m \frac{\partial U}{\partial x} + \frac{2}{5} h U_m^2 \left(\frac{\partial^3 \zeta}{\partial x^3} + \frac{7}{16} \cdot \frac{\partial^3 \eta}{\partial x^3} \right) + g \frac{\partial \zeta}{\partial x} + \frac{g n^2 U_m^2}{h^3} = 0 \tag{8.133b}$$

$$\frac{\partial \bar{C}}{\partial t} + U_m \frac{\partial \bar{C}}{\partial x} + C_0 \frac{\partial U}{\partial x} = \varepsilon_{sx} \frac{\partial^2 \bar{C}}{\partial x^2} \tag{8.133c}$$

$$(1 - \rho_0) \frac{\partial \eta}{\partial t} + \varepsilon_{sx} h \frac{\partial^2 \bar{C}}{\partial x^2} + G \left\{ \frac{n^2 U_m}{\Delta d h^{1/3}} \left[2 \frac{\partial U}{\partial x} - \frac{1}{3} \cdot \frac{U_m}{h} \left(\frac{\partial \zeta}{\partial x} - \frac{\partial \eta}{\partial x} \right) \right] - \mu \frac{\partial^2 \eta}{\partial x^2} \right\} = 0 \tag{8.133d}$$

where $G = 12(n^2 g d^2 U_m^2 h^{-1/3} - 0.047 \Delta g d^3)^{0.5}$ and C_0 is the initial average concentration resulting from the mean flow velocity U_m . According to Engelund (1970), if an exponential distribution of C_0 is assumed with ε_{sz} given by Eq. (8.128), then the average concentration C_0 is

$$C_0 = 4.853 \times 10^{-4} \frac{g^2 n^4 U_m^4}{w_s^4 h^{2/3}} \tag{8.134}$$

A system of linear differential equations is constituted by Eqs. (8.133a–d) with Eq. (8.134). For propagating waves, such as dunes and antidunes, the solution must be of the form

$$(\zeta, \eta, U, \bar{C}) = (\tilde{H}, \tilde{E}, \tilde{U}, \tilde{C}) \exp(-\hat{\lambda} t) \exp(ik_w x) \tag{8.135}$$

where $\hat{\lambda}$ is a complex number, whose imaginary part $\text{Im}(\hat{\lambda})$ and real part $\text{Re}(\hat{\lambda})$ represent circular frequency and exponential decay rate, respectively. The constants \tilde{H} , \tilde{E} , \tilde{U} and \tilde{C} are the complex constants involving amplitude and possible phase differences between two different components in Eq. (8.135). For an unstable bed resulting in a moving bedform $\eta = \tilde{E} \exp[-\text{Re}(\hat{\lambda})t] \exp\{i[k_w x - \text{Im}(\hat{\lambda})t]\}$ which grows with time $t > 0$, if $\text{Re}(\hat{\lambda}) < 0$. The exponential growth with time is actually inhibited by the nonlinear nature of the parent flow equations [Eqs. (8.117), (8.121), (8.131) and (8.132)] that are lost in the linear instability analysis. Under unstable conditions, therefore, saturation of amplitude sets in resulting in bedforms for all time. Thus, for unstable bedforms, $\text{Re}(\hat{\lambda}) < 0$, and for stable beds, $\text{Re}(\hat{\lambda}) > 0$. By substitution of Eq. (8.135), noting that the constant term (last term) in Eq. (8.133b) has no role in such an unstable solution analysis; the following linear algebraic equations are obtained:

$$(-\hat{\lambda} + ik_w U_m)(\tilde{H} - \tilde{E}) + ik_w h \tilde{U} = 0 \quad (8.136a)$$

$$i \left(k_w g - \frac{2}{5} k_w^3 h U_m^2 \right) \tilde{H} - \frac{7}{40} ik_w^3 h U_m^2 \tilde{E} + (-\hat{\lambda} + ik_w U_m) \tilde{U} = 0 \quad (8.136b)$$

$$ik_w C_0 \tilde{U} + (-\hat{\lambda} + ik_w U_m + \varepsilon_{sx} k_w^2) \tilde{C} = 0 \quad (8.136c)$$

$$-(1 - \rho_0) \hat{\lambda} \tilde{E} - \varepsilon_{sx} h k_w^2 \tilde{C} + G \left\{ \frac{ik_w h^2 U_m}{\Delta d h^{4/3}} \left[2h \tilde{U} - \frac{1}{3} U_m (\tilde{H} - \tilde{E}) \right] + \mu k_w^2 \tilde{E} \right\} = 0 \quad (8.136d)$$

Eliminating \tilde{H} , \tilde{E} , \tilde{U} , and \tilde{C} from Eqs. (8.136a–d), the quartic equation for $\hat{\lambda}$ is obtained as

$$\begin{aligned} (\hat{\lambda} - ik_w U_m - \varepsilon_{sx} k_w^2) & \left\{ \left[(1 - \rho_0) \frac{\hat{\lambda}}{G} - \mu k_w^2 \right] \left[(\hat{\lambda} - ik_w U_m)^2 + k_w^2 h \left(-\frac{2}{5} h k_w^2 U_m^2 + g \right) \right] \right. \\ & + \frac{n^2 k_w^2 U_m}{\Delta d h^{1/3}} \left(2\hat{\lambda} - \frac{7}{3} ik_w U_m \right) \left(-\frac{23}{40} h k_w^2 U_m^2 + g \right) \Big\} \\ & - \varepsilon_{sx} \frac{k_w^4 C_0 h}{G} (\hat{\lambda} - ik_w U_m) \left(-\frac{23}{40} h k_w^2 U_m^2 + g \right) = 0 \end{aligned} \quad (8.137)$$

Equation (8.137) has four complex roots. For the formation of sand waves, the real part of at least one root in Eq. (8.137) must be negative. If a root simultaneously possesses a positive real part, it represents a rapidly decaying mode without altering overall instability. Using nondimensional quantities $X = (h/g)^{0.5} \hat{\lambda}$, $\hat{k}_w = k_w h$, $Fr = U_m / (gh)^{0.5}$, $\varphi_0 = h\varphi / (\Delta d)$, φ is the bed characteristic parameter

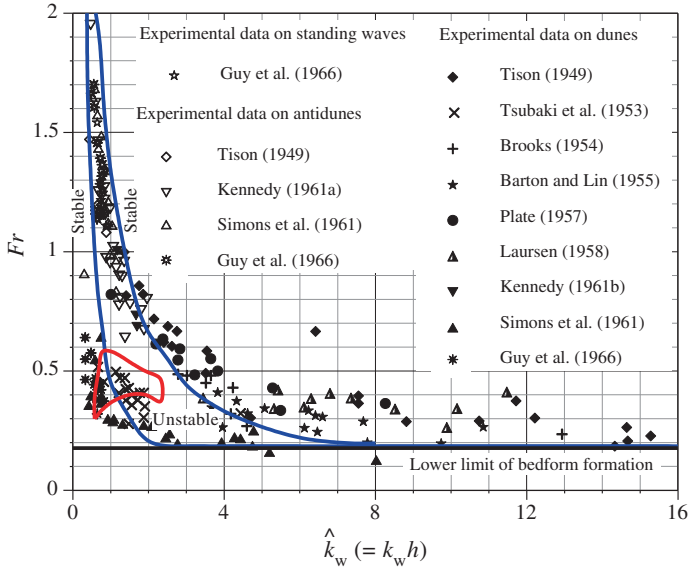


Fig. 8.24 Bose–Dey stability diagram [Froude number Fr versus $\hat{k}_w (= k_w h)$] (Bose and Dey 2009) and its comparison with the experimental data (Tison 1949; Tsubaki et al. 1953; Brooks 1954; Barton and Lin 1955; Plate 1957; Laursen 1958; Simons et al. 1961; Kennedy 1961a, b; Guy et al. 1966)

($= n^2 g/h^{1/3}$), $\varphi_A = 12(Fr^2 \varphi_0 - 0.047)^{0.5} / [\Delta(\varphi_0/\varphi)^{1.5}]$, $\varepsilon = \varepsilon_{sx}/(gh^3)^{0.5} = 7.25\varphi^{3/8} Fr$ and $C_0 = 4.853 \times 10^{-4}(Fr^2/\varphi^2)(u_*/w_s)^4$, Eq. (8.137) is expressed as a quartic equation of X :

$$\begin{aligned}
 (-X + i\hat{k}_w Fr + \varepsilon\hat{k}_w^2) & \left\{ \left[(1 - \rho_0) \frac{X}{\varphi_A} - \mu\hat{k}_w^2 \right] \left[(X - i\hat{k}_w Fr)^2 + \hat{k}_w^2 \left(-\frac{2}{5}\hat{k}_w^2 Fr^2 + 1 \right) \right] \right. \\
 & + \varphi_0 \hat{k}_w^2 Fr \left(2X - \frac{7}{3}i\hat{k}_w Fr \right) \left(-\frac{23}{40}\hat{k}_w^2 Fr^2 + 1 \right) \Big\} \\
 & + \varepsilon \frac{C_0 \hat{k}_w^4}{\varphi_A} (X - i\hat{k}_w Fr) \left(-\frac{23}{40}\hat{k}_w^2 Fr^2 + 1 \right) = 0
 \end{aligned} \tag{8.138}$$

Equation (8.138), which is an implicit equation of X , is amenable to solution by the numerical method for the given values of the parameters. Possible values of the parameters as $\rho_0 = 0.4$, $\Delta = 1.65$, $\varphi = 2.5 \times 10^{-3}$, $\varphi_0 = 600\varphi$, and $u_*/w_s = 0.6$ are chosen for the computation of the four roots of X for different values of nondimensional wave number $\hat{k}_w (= k_w h)$ and Froude number Fr .

It transpires that there is at least one root with negative real part when the $Fr(\hat{k}_w)$ plots, as shown in Fig. 8.24, lie in a curved band forming a zone in which bedforms

propagate with time. In this zone, if $Fr > 0.8$, there exists one root with negative real part, while if $Fr \leq 0.8$, there are two roots with negative real part. On the left side of and below the left bounding curve, all the roots possess either positive real part or do not exist at all, forming a stable zone. In contrast, on the right bounding curve, the roots cease to exist indicating stability, and beyond for higher values of \hat{k}_w , only one root possesses negative real part. The crescent-shaped unstable zone in Fig. 8.24, where significant sediment transport takes place as both bed load and suspended load, is replete with the experimental data of antidunes and also standing waves, having higher Froude numbers (> 0.8), reported by various investigators. The zone shrinks to an asymptotic limiting line at $Fr = 0.177$, when \hat{k}_w becomes large. Below this line, no root of Eq. (8.138) exists, as the sediment transport is inhibited due to significant decrease in flow velocity. If $C_0 = 0$, the transport mode is due to bed load only. In this case, the boundary of the unstable zone degenerates into a small enclosed zone above $Fr = 0.3$. The asymptotic line defined by $Fr = 0.177$ could therefore be called the *lower limit of bedform formation*. The usual practice is that the threshold of sediment transport is defined by the Shields parameter, $\Theta = \tau_o/(\Delta\rho gd)$. The relationship $\Theta = \varphi_0 Fr^2$ produces the Shields parameter $\Theta = 0.047$, corresponding to $Fr = 0.177$ for the lower limit of bedform formation. However, in Fig. 8.24, the stability limits in the zone of formation of dunes change considerably by the influence of gravity. This is attributed to the fact that the bed-load transport is the principal sediment transport mechanism in the dunal regime, while the formation of antidunes is associated with the bed load and suspended load of sediment transport.

8.5.4.2 Instability of Sand-Bed Leading to Formation of Ripples

Bose and Dey (2012) extended the preceding instability theory (for dunes and antidunes) of them (Bose and Dey 2009) to predict the formation of ripples. The primary modifications in the governing equations are the considerations of (1) the near-bed flow layer influenced by the ripples being 3.5 times the ripple height (η_r) and (2) the sediment transport mode being solely the bed-load transport for the rolling particle ripples (in the range of fine sand sizes), as defined by Bagnold (1946). Formation of ripples on the sand-bed is envisaged as an instability phenomenon of the fluid-bed-particle interface, and as such, a moderately thick layer of flow above the bed is needed to be considered.

Figure 8.25 shows a schematic of steady flow over an erodible sinusoidal sand-bed. Let D be the thickness of the near-bed flow layer which is influenced by the roughness due to ripples. According to Raupach et al. (1991), the extent of the near-bed disturbed layer could be in the order of 2 to 5 times the perturbation height. Thus, D as 3.5 times ripple height (that is, $D \approx 3.5\eta_r$) can be considered as an average value of that recommended by Raupach et al. (1991). Taking the x -axis

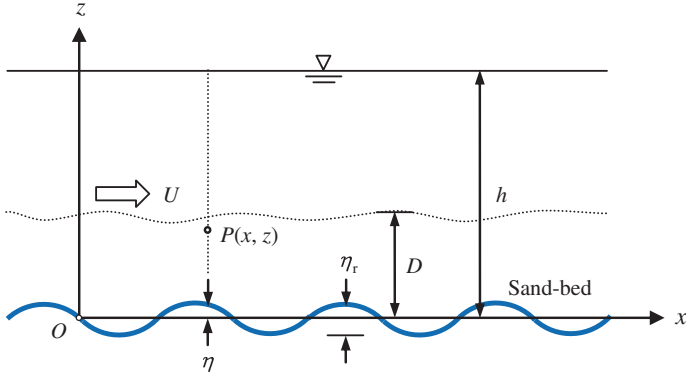


Fig. 8.25 Definition sketch of flow over a rippled (sinusoidal) bed (Bose and Dey 2012)

along the undisturbed bed level in the direction of flow and the z -axis in the vertically upward direction, let the perturbed ripple height at a point $(x, 0)$ at time t be $\eta(x, t)$, where $|\eta| \ll h$. Here, h is the flow depth. In a two-dimensional turbulent flow over a sinusoidal sand-bed under consideration, instantaneous velocity components at a point $P(x, z)$ at time t are (u, w) , whose time-averaged and fluctuating parts are (\bar{u}, \bar{w}) and (u', w') , respectively. It is assumed that the Reynolds stresses in the x -direction are almost invariant.

Integrating the two-dimensional continuity equation [see Eq. (8.117)] yields

$$\frac{\partial \eta}{\partial t} = \frac{\partial}{\partial x} [(D - \eta)U] \quad (8.139)$$

Then, adopting the Boussinesq approximation for curvilinear streamlines and integrating the RANS equation in z -direction yield

$$\begin{aligned} & \frac{ik_w U_m}{8\Delta g d} \left(2\lambda_{Dm} - \frac{2.698\nu\lambda_{Dm}^{1.5}}{U_m D C_m} \right) \tilde{U} \\ & + \left[\frac{(1 - \rho_0)\hat{\lambda}}{12d(gD)^{0.5}A_m} - \frac{0.195ik_w B_m \lambda_{Dm}^{1.5} U_m^2}{\Delta g d D} - \mu_d k_w^2 \right] \tilde{Z} = 0 \end{aligned} \quad (8.140)$$

where $\bar{p}_0 = \bar{p}(z = D)$ and m is an exponent of $1/m$ -th power law of velocity distribution. Unlike $\bar{p}_0 = 0$ (gauge pressure) as in Bose and Dey (2009) in the preceding analysis, \bar{p}_0 is nonzero here, representing the pressure at $z = D$. However, as a result of differentiation with respect to x in the following steps [also see Eq. (8.118)], the effect of \bar{p}_0 is not carried out.

For integrating the RANS equation in x -direction, the assumption of the invariant Reynolds stresses in x -direction is applied. For the convective acceleration in x -direction, Eq. (8.119) is used. The RANS equation in x -direction is therefore

$$\begin{aligned} \frac{\partial}{\partial t} [(D - \eta)U] + \alpha \frac{\partial}{\partial x} [(D - \eta)U^2] + \beta \left[(D - \eta)U^2 \frac{\partial^2 \eta}{\partial x^2} \right] \\ - \chi \frac{\partial^3}{\partial t \partial x^2} [(D - \eta)^3 U] + \frac{\tau_0}{\rho} = 0 \end{aligned} \quad (8.141)$$

where $\alpha = (1 + m)^2/[m(2 + m)]$, $\beta = (1 + m)/[2(2 + 3m)]$, and $\chi = m/(1 + 3m)$. For $m = 7$, the values of $\alpha \approx 1$, $\beta \approx 4/23$, and $\chi \approx 7/22$. Using Eq. (8.139), Eq. (8.141) reduces to

$$\frac{\partial U}{\partial t} + U \frac{\partial U}{\partial x} - \frac{4}{23} \zeta U^2 \frac{\partial^3 \zeta}{\partial x^3} - \frac{8}{23} U \frac{\partial^2 \zeta}{\partial x^2} \cdot \frac{\partial}{\partial x} (\zeta U) - \frac{7}{22 \zeta} \cdot \frac{\partial^3}{\partial t \partial x^2} (\zeta^3 U) + \frac{\tau_0}{\rho} = 0 \quad (8.142)$$

where $\zeta = D - \eta$, that is the thickness of the flow layer influenced by the perturbed bed.

When the bed shear stress τ_0 induced by the flow just exceeds its threshold value τ_{0c} , the sediment begins to transport as bed load, and the ripples are gradually formed on the bed, if the bed sand is fine. If q_b is the volumetric bed-load transport per unit time and width, the Exner's sediment continuity equation is as follows:

$$\frac{\partial q_b}{\partial x} = -(1 - \rho_0) \frac{\partial \eta}{\partial t} = (1 - \rho_0) \frac{\partial \zeta}{\partial t} \quad (8.143)$$

The well-known Meyer-Peter and Müller (1948) formula [see Eq. (5.16)] for the bed-load transport q_b is used here. Equation (5.16) is expressed as

$$q_b = 8d(\Delta g d)^{0.5} (\Theta - \Theta_c)^{1.5}$$

The threshold Shields parameter Θ_c is dependent on the local bed slope $\partial \eta / \partial x$ and the sand size forming ripples. During the instability, the bed accrues a slope, for which Fredsøe (1974) gave the bed-load transport formula [see Eq. (8.125), which is explained here explicitly], taking $\Theta_c = \Theta_{c0} + \mu_d \partial \eta / \partial x$. Here, Θ_{c0} is the threshold Shields parameter for horizontal bed and $\mu_d (0 < \mu_d < 1)$ is the coefficient of dynamic friction. The value of Θ_{c0} for a given d can be obtained from the set of empirical formulas given by van Rijn (1984a) (see Table 4.1). The average value of μ_d for equivalent sinusoidal sand wave form is approximated as $\mu_d \approx \tan 30^\circ = 0.577$.

The equation of the bed shear stress τ_0 on a plane rough bed expressed as a function of dynamic pressure is

$$\tau_0 = \frac{\lambda_D}{8} \rho U^2 \quad (8.144)$$

where λ_D is the Darcy–Weisbach friction factor. For low shear Reynolds number ($R_* \leq 70$), which is consistent with the hydraulically smooth and transitional flow regimes under consideration, the friction factor λ_D can be obtained from the Colebrook–White formula (Colebrook and White 1937). The Colebrook–White formula is an implicit formula, but an explicit approximate version of that was proposed by Haaland (1983), which is

$$\frac{1}{\lambda_D^{0.5}} = -0.782 \ln \left[\left(\frac{k_s}{14.8\zeta} \right)^{1.1} + \frac{1.725\nu}{U\zeta} \right] \quad (8.145)$$

where k_s is Nikuradse's equivalent sand roughness ($k_s \approx 2d$).

Using q_b from Meyer-Peter and Müller (1948) and Eqs. (8.144) and (8.145), Eq. (8.143) for a sand-bed yields the dynamical differential equation for ζ . It is as follows:

$$\begin{aligned} (1 - \rho_0) \frac{\partial \zeta}{\partial t} - 12d(\Delta g d)^{0.5} \left(\frac{\lambda_D U^2}{8\Delta g d} + \mu_d \frac{\partial \zeta}{\partial x} - 0.035 \right)^{0.5} \\ \times \left[\frac{U}{8\Delta g d} \left(2\lambda_D \frac{\partial U}{\partial x} + U \frac{\partial \lambda_D}{\partial x} \right) + \mu_d \frac{\partial^2 \zeta}{\partial x^2} \right] = 0 \end{aligned} \quad (8.146)$$

Ripple formation on the sand-bed can be viewed as an instability phenomenon governed by the two dynamical equations [Eqs. (8.142) and (8.146)], when flow takes place with a mean velocity U_m forming a near-bed flow layer of thickness D in which the flow is influenced by the roughness due to ripples. For the stability or instability analysis of a system, the solution of the two equations is taken in the sinusoidal forms over the mean values as follows:

$$U = U_m + \tilde{U} \exp(-\hat{\lambda}t) \exp(ik_w x), \quad \zeta = D + \tilde{Z} \exp(-\hat{\lambda}t) \exp(ik_w x) \quad (8.147)$$

In the above, $\hat{\lambda}$ is a complex number. Its imaginary part $\text{Im}(\hat{\lambda})$ and real part $\text{Re}(\hat{\lambda})$ correspond to the circular frequency and the exponential decay rate, respectively, and \tilde{U} and \tilde{Z} are the complex constants. The length λ_r of such a ripple, simulated by a sinusoidal wave, is half of the wavelength of the wave (note that Fig. 8.25 shows that the ripple length is simulated best by a half sinusoidal wavelength), that is, $\lambda_r = \pi/k_w$. For an unstable ripple, $\text{Re}(\hat{\lambda}) < 0$ implies an exponential growth with time t that is actually inhibited by the nonlinear nature of parent equations [Eqs. (8.142) and (8.146)] to be lost in linearization. Substituting Eq. (8.147) into Eqs. (8.142) and (8.146) and then performing the linearization, the last term of Eq. (8.142) reduces to a constant having no role in the instability analysis. Thus, the homogeneous linear system of equations is obtained as follows:

$$\left[- \left(1 + \frac{7}{22} k_w^2 D^2 \right) \hat{\lambda} + i k_w U_m \right] \tilde{U} + k_w^2 D U_m \left(\frac{4 i k_w}{23} U_m - \frac{21}{22} \hat{\lambda} \right) \tilde{Z} = 0 \quad (8.148a)$$

$$\frac{i k_w U_m}{8 \Delta g d} \left(2 \lambda_{Dm} - \frac{2.698 v \lambda_{Dm}^{1.5}}{U_m D C_m} \right) \tilde{U} + \left[\frac{(1 - \rho_0) \hat{\lambda}}{12 d (g D)^{0.5} A_m} - \frac{0.195 i k_w B_m \lambda_{Dm}^{1.5} U_m^2}{\Delta g d D} - \mu_d k_w^2 \right] \tilde{Z} = 0 \quad (8.148b)$$

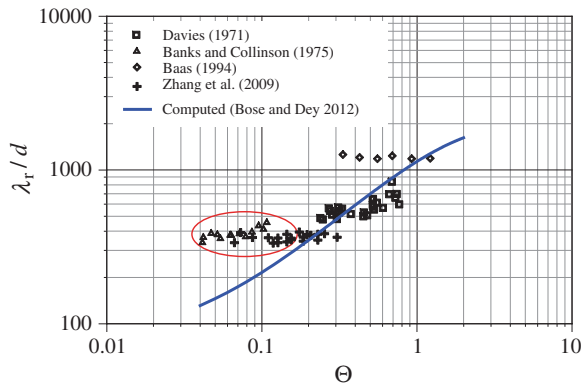
where λ_{Dm} is the λ_D given by Eq. (8.145) for $U = U_m$ and $\zeta = D$, $A_m = [\lambda_{Dm} U_m^2 (8 g D)^{-1} - 0.035 \Delta g d D^{-1}]^{0.5}$, $B_m = C_m^{-1} [0.122 (d/D)^{1.1} + G_m]$, $C_m = [0.111 (d/D)^{1.1} + G_m]$, and $G_m = 1.725 v [Fr_D D (g D)^{0.5}]^{-1}$. The above two equations can be normalized by introducing $X = \hat{\lambda} (D/g)^{0.5}$, $\hat{k}_w = k_w D$ and $U_m = Fr_D (g D)^{0.5}$. Eliminating \tilde{U} and $(g/D)^{0.5} \tilde{Z}$ from the resulting two equations, a quadratic equation of X is obtained as

$$\begin{aligned} & \frac{(1 - \rho_0)}{12 A_m} \left(1 + \frac{7}{22} \hat{k}_w^2 \right) X^2 - \left[\frac{(1 - \rho_0)}{12 A_m} i Fr_D \hat{k}_w + \left(1 + \frac{7}{22} \hat{k}_w^2 \right) \right. \\ & \times \left(\frac{0.195 i B_m Fr_D^2 \lambda_{Dm}^{1.5} \hat{k}_w}{\Delta} + \mu_d \frac{d}{D} \hat{k}_w^2 \right) + \frac{21}{176} \cdot \frac{i \lambda_{Dm} Fr_D^2 \hat{k}_w^3 E_m}{\Delta} \Big] X \\ & \left. - \frac{0.195 B_m Fr_D^3 \lambda_{Dm}^{1.5} \hat{k}_w}{\Delta} + i \mu_d \frac{d}{D} Fr_D \hat{k}_w^3 - \frac{1}{46} \cdot \frac{\lambda_{Dm} Fr_D^3 \hat{k}_w^4 E_m}{\Delta} = 0 \right. \end{aligned} \quad (8.149)$$

where $E_m = 2 - \{2.698 v \lambda_{Dm}^{0.5} [Fr_D D (g D)^{0.5} C_m]^{-1}\}$. Equation (8.149) has two complex roots for X . For the instability of bed due to formation of ripples, at least one of them must have a negative real part, as X is proportional to $\hat{\lambda}$. When a root simultaneously possesses a positive real part, then it represents a quickly decaying mode without changing overall instability.

To perform a numerical exercise, the values of $s = 2.65$, $\rho_0 = 0.4$, $v = 1.004 \times 10^{-6} \text{ m}^2 \text{ s}^{-1}$, and $g = 9.81 \text{ m s}^{-2}$ are taken. For a given value of d , $\text{Re}(X)$ is computed from Eq. (8.149). It is found that $\text{Re}(X)$ of one root is always positive, but for the other root, it is positive for small values of $\hat{k}_w = k_w D$ and very slowly changing to a negative value with an increase in \hat{k}_w . The length of the corresponding sinusoidal ripple is determined from $\lambda_r = \pi D / \hat{k}_w$ with \hat{k}_w to be the approximate transitional value. The theoretical curve for the nondimensional ripple length λ_r/d versus Shields parameter Θ is shown in Fig. 8.26. The layer of influence D is estimated from its maximum value being approximately 3.5 times the ripple height η_r , that is $D/\eta_r \approx 3.5$, as already mentioned. On the other hand, λ_r can be approximated by the horizontal projection of the sloping line at an angle of repose of 30° . Hence, $\eta_r/\lambda_r \approx \tan 30^\circ = 0.58$ and $D/\lambda_r (= D/\eta_r \times \eta_r/\lambda_r) \approx 2$. So, the change in sign of the positive root of Eq. (8.149) is so selected that $\lambda_r = D/2$ has values lying in the range of 0.1–0.25 m and that of D lying in the range of 0.2–0.5 m.

Fig. 8.26 Nondimensional ripple length λ_r/d as a function of Shields parameter Θ obtained theoretically by Bose and Dey (2012) and the plots of experimental data (Davies 1971; Banks and Collinson 1975; Baas 1994; Zhang et al. 2009)



In Fig. 8.26, the theoretical curve shows that λ_r/d increases with an increase in Θ . For the purpose of comparison, the experimental data plots are overlapped. The distribution of data plots somewhat confirms that the theory is capable of predicting the ripple lengths close to their observed values for the data of Davies (1971) and Zhang et al. (2009). Due to the shallowness of flow depths (~ 0.15 m) in the experiments by Banks and Collinson (1975), the flow layer D influenced by the ripples could have a possibility to extend close to the experimental flow depths, resulting in a departure of data plots (encircled) from the theoretical curve.

8.6 Bed Features in Gravel-Bed Streams

In the preceding sections, the characteristic features of the bedforms and the mathematical theories on their stability in sand-bed streams are discussed. In contrast, the bed features in gravel-bed streams are even more complex in nature. A sand-bed is usually composed of approximately narrow range of particle sizes, while a gravel-bed contains a wide range of particle sizes, such as fine sand to large cobbles or boulders. Thus, for a given flow condition, differential sediment transport rate prevails for different particle sizes; even the larger size fraction may remain immobile. As a consequence, an armoring of bed may occur, leading to an asymptotic reduction in sediment transport rate with time, unless another flow with higher flow velocity that may occur at a later period is capable to break the armor layer transporting all sizes indiscriminately. Thus, the complexities in gravel-bed features arise from selective transports. The gravel bedforms can be broadly divided into four categories: (a) Cluster, (b) riffle–pool sequence, (c) step–pool sequence, and (d) rapids and cascades.

A single stone protruding above the bed surrounded by the neighboring smaller particles forms a small-scale bedform, termed *cluster* (Brayshaw et al. 1983; Billi 1988). On the surface of gravel-beds, larger cobbles or boulders may act as anchor stones that support the formation of clusters where various sizes of small cobbles

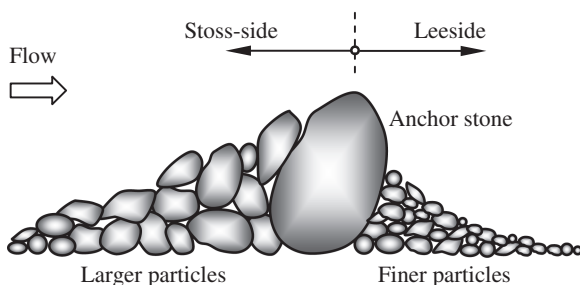


Fig. 8.27 Sketch of a cluster

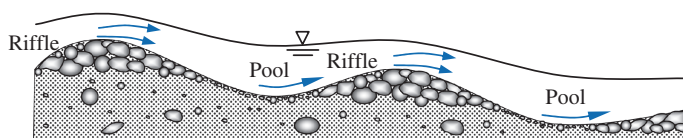


Fig. 8.28 Sketch of a riffle-pool sequence in a straight stream

and coarse gravels support each other (Fig. 8.27). Once a cluster is formed, it is then degenerated in the process of erosion at the periphery of the cluster, and subsequently, a new cluster is reformed and so on. In fully developed stage, a cluster consists of a stoss-side accumulation of larger particles and a leeside deposition of finer particles. The particles in the course of transport are prevented by the anchor stone which creates an accumulation of particles on the stoss side of the stone, while the leeside accumulation of particles is due to sheltering.

In gravel-bed streams, a *riffle-pool sequence* is formed as a stream flow structure alternating from the zones of relatively shallow to deeper flow over an undulating streambed (Fig. 8.28), but do not tend to form in sand-bed streams (Knighton 1998). A prominent feature of riffle-pool sequence is the bed particle sorting and distribution associated with the changes in bed elevations. Riffles that correspond to elevated zones in the bed topography are formed in shallow zones containing gravel deposits over which the flow takes place with a faster velocity. In contrast, pools that correspond to the deeper zones where sediment transport takes place as a bed load of fine sand or silt. The stream flow is characterized by a rapid flow over coarse sediment in the relatively steep riffle zones and a slower flow through the deeper pools. The sequence of spacing (pool to pool or riffle to riffle) within a streambed commonly occurs at intervals ranging from 5 to 7 stream width (Keller and Melhorn 1978). Riffle-pool sequences are found in straight, meandering, and braided reaches (Richards 1976). Pools are most easily developed with relatively coarse bed load in a meandering stream where the outer edge of each meander loop is deep and undercut, while riffles are formed in the shallow water crossovers between one meander to the next on the opposite margin of the stream (Fig. 8.29). The pools are the zones of active erosion, and the sediment

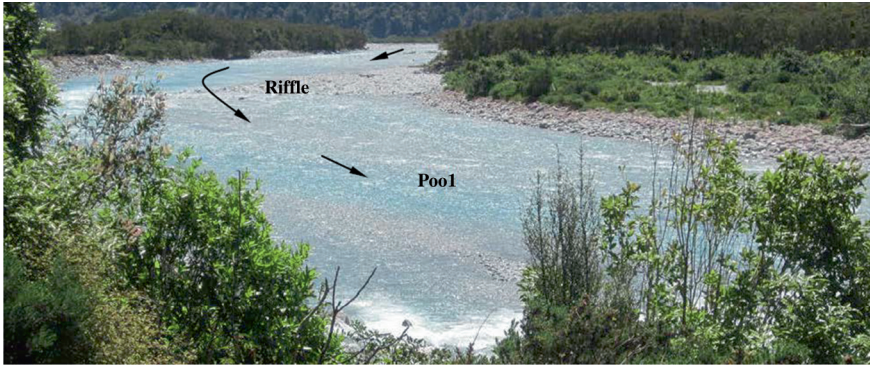


Fig. 8.29 Photograph of a riffle–pool sequence in a meandering stream. Photograph by the author

eroded tends to be deposited in the riffle zone between. Riffle–pool sequences are present in nearly all perennial streams where the sediment size is larger than coarse sand, and they are relatively stable in their position along the stream.

Step–pool sequence is often observed in steep (in the order of exceeding 2 % slope), upland, or mountain streams formed by cobbles and boulders. The steps are formed as a framework of larger cobbles or boulders that are tightly packed with finer particles featuring vertical drops over which the flow plunges into the deeper and relatively tranquil flow in the pool immediately downstream (Fig. 8.30). Steps are relatively a permanent structure. The spacing of steps and pools is, on an average, two to three times the stream width. The spacing of pools tends to become closer with an increase in slope. The height of steps tends to increase with the size of particle transport (Chin 1999). Step–pool sequences are most apparent during low stages, as they tend to be submerged at higher stages. It is also during low stages that step–pool sequence provides the most flow resistance. There is also significant energy dissipation, as the flow cascades over each step and goes into the relatively tranquil pools (Bathurst 1993).

Rapids whose morphological features can have a series of regularly spaced cobble or boulder ridges are associated with steep gradient and shallower stream flows. They are characterized by transverse, riblike arrangements of coarse particles that are oriented across the channel (that is, transverse to the flow) (Fig. 8.31) (McDonald and Banerjee 1971; Robert 1990). Rapids appear to persist in streams with wider range of bed slopes. On the other hand, *cascades* have a more disorganized, random structure (Fig. 8.32). Rapids and cascades are stable during most flows because except very high flows, the usual flows are incompetent in moving the coarser cobbles and boulders that form the main structure (Fig. 8.33).

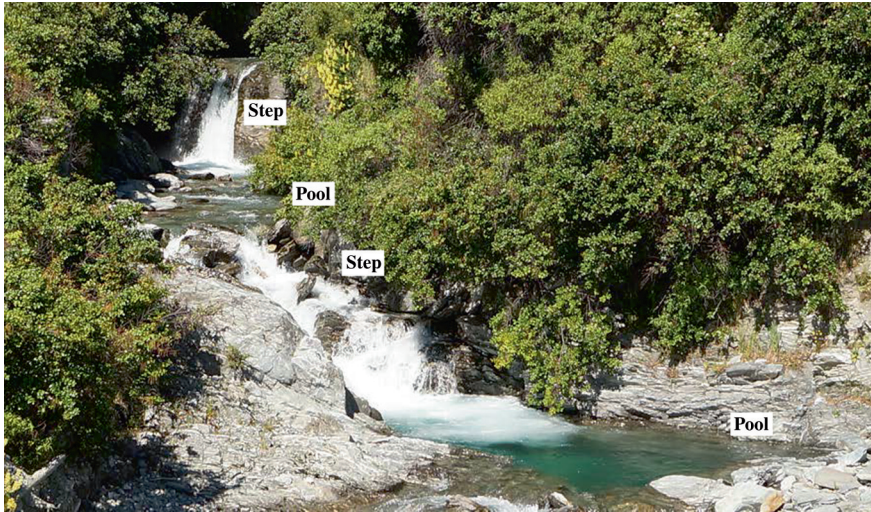


Fig. 8.30 Photograph of a step–pool sequence. Photograph by the author



Fig. 8.31 Photograph of rapids. Photograph by the author

8.7 Resistance to Flow Due to Bedforms

In this section, the resistance to flow from the sediment beds and bedforms is discussed. In case of ripples and dunes (that is, in the lower flow regime), the separated flow on the leeside of these bedforms is the primary cause of significant resistance to flow. It involves a generation of large-scale turbulence dissipating considerable amount of kinetic energy. In this regime, the rate of sediment transport is relatively low as the transport mechanism is the bed-load transport only. On the other hand, in case of plane bed and antidunes (that is, in the upper flow regime), the resistance to flow is less due to predominance of roughness due to particles. However, the kinetic energy is dissipated by standing waves and the



Fig. 8.32 Photograph of submerged cascades. Photograph by the author



Fig. 8.33 Photograph of rapids and cascades. Photograph by the author

formation of breaking antidunes causes to enhance the resistance to flow. The total (or effective) resistance to flow is decomposed into (1) resistance accounting for forces acting on individual particles, termed *resistance due to particles* or *skin friction*, and (2) resistance due to bedform configurations, termed *form resistance* or *form drag*. It is important to understand that the net pressure distribution over an entire bedform and the resulting flow separation due to adverse pressure gradient give rise to substantial form drag, while a portion of drag, in terms of skin friction drag, governs the bed particle transport.

Following the aforementioned resistance phenomenon and accordingly constructing a definition sketch (Fig. 8.34), the total (or effective) bed shear stress τ_0 acting over bedforms can be decomposed as follows:

$$\tau_0 = \tau'_0 + \tau''_0 \quad (8.150)$$

where τ'_0 is the bed shear stress due to particle roughness and τ''_0 is the bed shear stress due to form drag.

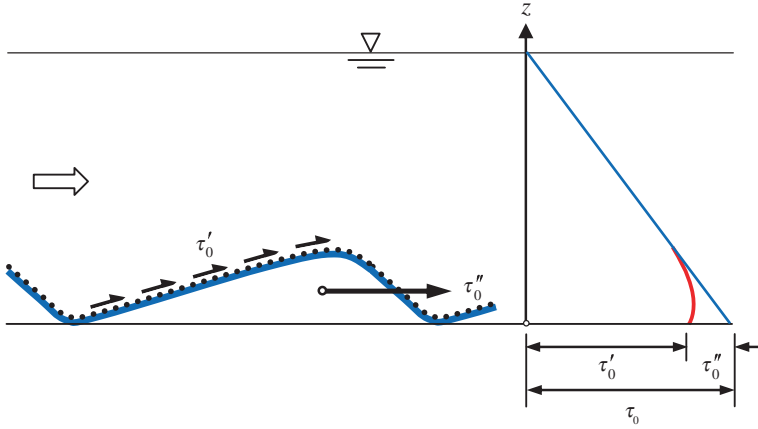


Fig. 8.34 Shear stress distribution over a dune and total bed shear stress decomposition

Equation (8.150) can be expressed in terms of the decomposition of total energy slope S_f and total hydraulic radius R_b as

$$\tau_0 = \rho g R_b S_f, \quad \tau'_0 = \rho g R_b S'_f, \quad \tau''_0 = \rho g R_b S''_f \Rightarrow S_f = S'_f + S''_f \quad (8.151a)$$

$$\tau_0 = \rho g R_b S_f, \quad \tau'_0 = \rho g R'_b S_f, \quad \tau''_0 = \rho g R''_b S_f \Rightarrow R_b = R'_b + R''_b \quad (8.151b)$$

where S'_f and R'_b are the energy slope and the hydraulic radius due to particle roughness, respectively, and S''_f and R''_b are the energy slope and the hydraulic radius due to form drag, respectively. In two-dimensional case, $R'_b = h'$ and $R''_b = h''$, where h' and h'' are the depths due to particle roughness and form drag, respectively.

Again, Eq. (8.150) can be expressed in terms of the decomposition of total shear velocity u_* and total friction factor λ_D as

$$\tau_0 = \rho u_*^2, \quad \tau'_0 = \rho u_*'^2, \quad \tau''_0 = \rho u_*''^2 \Rightarrow u_*^2 = u_*'^2 + u_*''^2 \quad (8.152a)$$

$$\tau_0 = \frac{\lambda_D}{8} \rho U^2, \quad \tau'_0 = \frac{\lambda'_D}{8} \rho U^2, \quad \tau''_0 = \frac{\lambda''_D}{8} \rho U^2 \Rightarrow \lambda_D = \lambda'_D + \lambda''_D \quad (8.152b)$$

where u'_* and λ'_D are the shear velocity and the friction factor due to particle roughness, respectively, and u''_* and λ''_D are the shear velocity and the friction factor due to form drag, respectively.

Further, Eq. (8.150) can be expressed in terms of Shields parameters as given by

$$\frac{\tau_0}{\Delta \rho g d} = \frac{\tau'_0}{\Delta \rho g d} + \frac{\tau''_0}{\Delta \rho g d} \Rightarrow \Theta = \Theta' + \Theta'' \quad (8.153)$$

where Θ'' is the Shields parameter due to form drag.

It is interesting to note that the Manning equation produces two different relationships for Manning roughness coefficients n , n' , and n'' . Using Eqs. (8.150) and (8.151a), and Eqs. (8.150) and (8.151b), the Manning equation yields

$$U = \frac{1}{n} R_b^{2/3} S_f^{0.5}, \quad U = \frac{1}{n'} R_b^{2/3} S_f^{0.5}, \quad U = \frac{1}{n''} R_b^{2/3} S_f^{0.5} \Rightarrow n^2 = n'^2 + n''^2 \quad (8.154a)$$

$$U = \frac{1}{n} R_b^{2/3} S_f^{0.5}, \quad U = \frac{1}{n'} R_b^{2/3} S_f^{0.5}, \quad U = \frac{1}{n''} R_b^{2/3} S_f^{0.5} \Rightarrow n^{1.5} = n'^{1.5} + n''^{1.5} \quad (8.154b)$$

In the above, the Manning roughness coefficients possess two different exponents (2 and 1.5), which can cause an inconsistency in analyses. However, an application of Chézy equation in the similar way can produce a consistent result. It is as follows:

$$\frac{1}{C_R^2} = \frac{1}{C_R'^2} + \frac{1}{C_R''^2} \quad (8.155)$$

where C_R is the total Chézy coefficient, and C_R' and C_R'' are the Chézy coefficients due to particle roughness and form drag, respectively. Making use of Eq. (8.155) and the relationship between Chézy and Manning coefficients, a consistent relationship for the Manning roughness coefficients can be obtained as

$$C_R = \frac{1}{n} R_b^{1/6}, \quad C_R' = \frac{1}{n'} R_b^{1/6}, \quad C_R'' = \frac{1}{n''} R_b^{1/6} \Rightarrow \frac{n^2}{R_b^{1/3}} = \frac{n'^2}{R_b^{1/3}} + \frac{n''^2}{R_b^{1/3}} \quad (8.156)$$

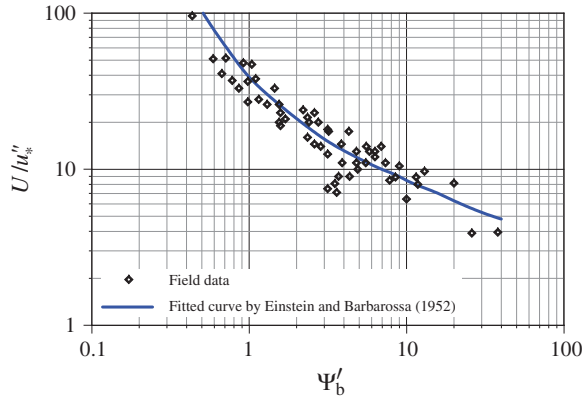
8.7.1 Einstein and Barbarossa's Method

Einstein and Barbarossa (1952) were the first to introduce the decomposition of total resistance into skin friction and form drag. Under a fully hydraulic rough regime, R_b' can be determined from the Manning–Strickler formula as

$$\frac{U}{u_*'} = 7.66 \left(\frac{R_b'}{k_s'} \right)^{1/6} \quad \wedge \quad u_*' = (g R_b' S_f)^{0.5} \quad (8.157)$$

In Eq. (8.157), the particle roughness height k_s' is considered as d_{65} . In case of particle roughness which does not produce fully hydraulic rough regime, R_b' can be determined from the logarithmic law of depth-averaged velocity. It is as follows:

Fig. 8.35 Flow resistance relationship by Einstein and Barbarossa (1952)



$$\frac{U}{u_*''} = \frac{1}{\kappa} \ln \left(12.27 \frac{R_b'}{k_s'} x_k \right) \quad (8.158)$$

where x_k is the correction factor [see Eq. (5.63) and Fig. 5.7]. Einstein and Barbarossa related the form drag with the sediment transport rate in lower flow regime.

$$\frac{U}{u_*''} = f(\Psi_b') \quad (8.159)$$

where Ψ_b' is the flow intensity parameter due to particle roughness, which is reciprocal of Θ' . It means that Ψ_b' is inversely proportional to τ_0' . Further, note that $U/u_*'' = (8/\lambda_D'')^{0.5}$. The flow intensity parameter is given by

$$\Psi_b' = \frac{\Delta d_{35}}{R_b' S_f} \quad (8.160)$$

Based on the field data, the functional relationship given by Eq. (8.159) was represented in graphical form as shown in Fig. 8.35 (Einstein and Barbarossa 1952). The U/u_*'' decreases with an increase in Ψ_b' in lower flow regime, for which the applicability of the diagram is limited.

The computation of total hydraulic radius R_b from a given discharge Q by Einstein and Barbarossa's method is illustrated in Example 7.2 (see Table 7.4).

8.7.2 Engelund's Method

Engelund (1966) used the energy slope decomposition [see Eq. (8.151a)] to determine the resistance to flow. The head loss due to form drag of a dune h_f'' , which is an expansion loss, can be estimated from the *Carnot equation* as

$$h_f'' = K_L \frac{(U_1 - U_2)^2}{2g} \quad (8.161)$$

where U_1 and U_2 are the average velocities on the crest and the trough, respectively, and K_L is the loss coefficient. The average velocities U_1 and U_2 are obtained as

$$U_1 = \frac{q}{h - 0.5\eta_d}, \quad U_2 = \frac{q}{h + 0.5\eta_d} \quad (8.162)$$

where q is the discharge per unit width ($= Uh$), h is the average flow depth, and η_d is the dune height. Therefore, Using Eq. (8.162), Eq. (8.161) becomes

$$h_f'' = \frac{K_L}{2g} \left(\frac{q}{h - 0.5\eta_d} - \frac{q}{h + 0.5\eta_d} \right)^2 \approx \frac{K_L}{2} \cdot \frac{\eta_d^2}{h} Fr^2 \quad (8.163)$$

The decomposition of total energy slope, Eq. (8.151a), can be given by

$$S_f = S_f' + S_f'' \quad \wedge \quad S_f'' \approx \frac{h_f''}{\lambda_d} = \frac{K_L}{2} \cdot \frac{\eta_d^2}{\lambda_d h} Fr^2 \quad (8.164)$$

The decomposition of Shields parameter, Eq. (8.153), can be expressed as

$$\Theta = \Theta' + \Theta'' \quad \wedge \quad \underbrace{\frac{\tau_0}{\Delta \rho g d}}_{\Theta} = \underbrace{\frac{h S_f'}{\Delta d}}_{\Theta'} + \underbrace{\frac{K_L}{2} \cdot \frac{\eta_d^2}{\Delta \lambda_d d} Fr^2}_{\Theta''} \quad (8.165)$$

A boundary layer where the velocity distribution is nonuniform is developed in the flow over a bedform, while the velocity distribution outside this layer is uniform. Engelund and Hansen (1967) assumed that the outer flow and the boundary layer flow are independent of each other, as there is no significant amount of energy exchanged between them. Hence, the energy slope of the boundary layer flow is equal to that of the outer layer and that of the total flow. Thus, it is given by

$$\tau_0' = \rho g h' S_f = \lambda_D' \frac{\rho U^2}{8} \Rightarrow \frac{8}{\lambda_D'} = \frac{U^2}{g h' S_f} \quad (8.166)$$

where λ_D' is the skin friction coefficient. Here, the boundary layer thickness δ is assumed to be equal to h' , that is the flow depth due to particle roughness. The expression of S_f is

$$S_f = \lambda_D \frac{U^2}{8 g h} \quad (8.167)$$

Therefore, Eqs. (8.166) and (8.167) produce

$$\frac{\lambda'_D}{h'} = \frac{\lambda_D}{h} \quad (8.168)$$

The friction factor λ'_D for the boundary layer is determined from the equation of Nikuradse for hydraulically rough regime as

$$\left(\frac{8}{\lambda'_D}\right)^{0.5} = \frac{1}{\kappa} \ln\left(12.2 \frac{h'}{k_s}\right) \Rightarrow \frac{U}{(gh'S_f)^{0.5}} = \frac{1}{\kappa} \ln\left(12.2 \frac{h'}{k_s}\right) \quad (8.169)$$

Using the experimental data of Guy et al. (1966), Engelund and Hansen (1967) proposed the following relationships:

$$\Theta'(\Theta' < 0.55) = 0.06 + 0.4\Theta'^2 \quad (8.170a)$$

$$\Theta'(0.55 < \Theta' < 1) = \Theta \quad (8.170b)$$

Equation (8.170b) refers to the plane bed and standing waves, where no expansion loss takes place. Later, Brownlie (1983) suggested a relationship for $\Theta' > 1$ as

$$\Theta'(\Theta' > 1) = \left(0.298 + \frac{0.702}{\Theta'^{1.8}}\right)^{-0.56} \quad (8.171)$$

Figure 8.36 shows the variation of Θ with Θ' obtained from Eqs. (8.170a) and (8.171). The curves compare well with the experimental results.

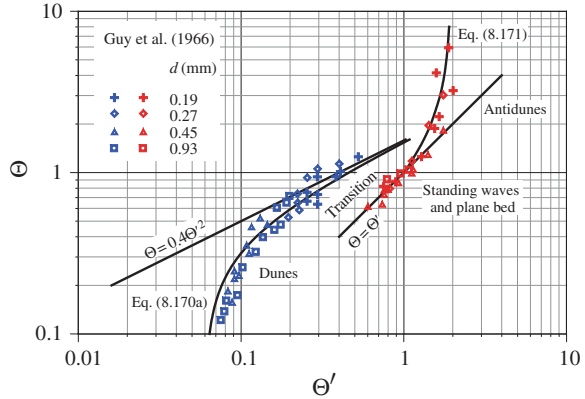
For the given values of discharge q , bed slope S_0 , and sediment size d , the flow depth can be predicted by Engelund's method as follows:

- Step 1: Assume a value of depth due to particle roughness h' .
- Step 2: Calculate $\Theta' [= h'S_0/(\Delta d)]$.
- Step 3: Obtain Θ from Fig. 8.36.
- Step 4: Calculate $h [= \Theta(\Delta d)/S_0]$.
- Step 5: Calculate U from Eq. (8.169) by using $k_s = 2.5d_{50}$.
- Step 6: Calculate $q = Uh$.
- Step 7: Compare the calculated value of q with the given value of q .
- Step 8: Repeat iteration (Step 1 to Step 6) until these two values of q converge.

8.7.3 Karim and Kennedy's Method

Karim and Kennedy (1981) derived the flow resistance in terms of the ratio of friction factor λ_{Dm} over a mobile bed to friction factor λ_{Di} over an immobile bed as

Fig. 8.36 Shields parameter Θ as a function of Shields parameter due to particle roughness Θ'



$$\frac{\lambda_{Dm}}{\lambda_{Di}} = 1.2 + 8.92 \frac{\eta_d}{h} \quad \wedge \quad \lambda_{Di} = 8 \left[\frac{1}{\kappa} \ln \left(12 \frac{h}{k_s} \right) \right]^{-2} \quad \vee \quad k_s = 2.5 d_{50} \quad (8.172)$$

Note that the notation for the median size of sediment d_{50} is used as d so far. Henceforth, both the notations d_{50} and d are used to refer to median size of sediment.

Karim and Kennedy used the expression for dune height η_d for $\Theta < 1.5$ given by Allen (1978) (Table 8.1) and $\eta_d(\Theta > 1.5) = 0$. They adopted the regression analysis to obtain an expression for depth-averaged flow velocity as

$$\frac{U}{(g R_b S_f)^{0.5}} = 6.683 \left(\frac{h}{d_{50}} \right)^{0.626} S_0^{0.503} \left(\frac{\lambda_{Dm}}{\lambda_{Di}} \right)^{-0.465} \quad (8.173)$$

For a given flow depth h , the average flow velocity can be determined from Eq. (8.174). The bedforms can be predicted as $\Theta \leq 1.2$ for lower flow regime, $1.2 < \Theta < 1.5$ for transition, and $\Theta \geq 1.5$ for upper flow regime.

8.7.4 van Rijn's Method

To calculate dune height η_d , van Rijn (1984b) gave an empirical equation [see Eq. (8.10)]. He suggested that the shear velocity due to particle roughness u'_* can be determined from

$$\frac{U}{u'_*} = \left(\frac{8}{\lambda'_D} \right)^{0.5} = \frac{1}{\kappa} \ln \left(12.2 \frac{h}{k'_s} \right) \quad (8.174)$$

By setting the bedform length $\lambda_d = 7.3h$, the particle roughness $k'_s = 3d_{90}$ and the bedform roughness (roughness contributes to form drag) $k''_s = 1.1\eta_d[1 - \exp(-25\eta_d/\lambda_d)]$, the total (or effective) bed roughness $k_s (= k'_s + k''_s)$ is obtained as

$$k_s = 3d_{90} + 1.1\eta_d \left[1 - \exp\left(-25 \frac{\eta_d}{\lambda_d}\right) \right] \quad (8.175)$$

The total Chézy coefficient C_R can be computed as $C_R = 18\log(12R_b/k_s)$. Then, using the Manning–Strickler equation with $k'_s = 3d_{90} = 6.8d_{50}$ yields

$$\frac{U}{u'_*} = \left(\frac{8}{\lambda'_D}\right)^{0.5} \approx 5 \left(\frac{h}{d_{50}}\right)^{1/6} \Rightarrow \lambda'_D \approx 0.32 \left(\frac{d_{50}}{h}\right)^{1/3} \quad (8.176)$$

Using Eqs. (8.167) and (8.174) for λ_D and λ'_D , respectively, the friction factor λ''_D due to form drag can be determined from Eq. (8.152b). Note that the approximate value of $\lambda''_D \approx \eta_d/\lambda_d$.

8.7.5 Nelson and Smith's Method

To derive the bed shear stress τ''_0 due to form drag, Nelson and Smith (1989) adopted the following procedure:

$$F_{Dx} = C_D \frac{\rho}{2} U_r^2 B \eta_d \Rightarrow \tau''_0 = \frac{F_{Dx}}{B \lambda_d} = C_D \frac{\rho}{2} U_r^2 \frac{\eta_d}{\lambda_d} \quad (8.177)$$

where F_{Dx} is the hydrodynamic drag force in streamwise direction (x -direction), C_D is the drag coefficient (assumed as 0.21), U_r is the reference streamwise flow velocity, and B is the channel width.

The reference flow velocity, which is the average velocity from trough to crest level of the bedform, can be determined from the logarithmic law, and then, from Eq. (8.177), τ''_0/τ'_0 is deduced as

$$U_r = \frac{1}{\kappa} \left(\frac{\tau'_0}{\rho}\right)^{0.5} \left[\ln\left(30 \frac{\eta_d}{k_s}\right) - 1 \right] \Rightarrow \frac{\tau''_0}{\tau'_0} = C_D \frac{1}{2} \cdot \frac{\eta_d}{\lambda_d \kappa^2} \left[\ln\left(30 \frac{\eta_d}{k_s}\right) - 1 \right]^2 \quad (8.178)$$

Nelson and Smith assumed the logarithmic law of time-averaged velocity $\bar{u}(z)$ for the ranges $k_s < z < \eta_d$ and $\eta_d < z < h$. They are

$$\bar{u}(k_s < z < \eta_d) = \frac{1}{\kappa} \left(\frac{\tau'_0}{\rho}\right)^{0.5} \ln\left(30 \frac{z}{k_s}\right), \quad \bar{u}(\eta_d < z < h) = \frac{1}{\kappa} \left(\frac{\tau'_0}{\rho}\right)^{0.5} \ln\left(30 \frac{z}{k_{sc}}\right) \quad (8.179)$$

where k_{sc} is the composite roughness height. Equating $\bar{u}(z = \eta_d)$ at the crest of the bedform and rearranging yield

$$\frac{\tau_0}{\tau'_0} = \left[\ln \left(30 \frac{\eta_d}{k_s} \right) \right]^2 \left[\ln \left(30 \frac{\eta_d}{k_{sc}} \right) \right]^{-2} \Rightarrow \frac{\tau''_0}{\tau'_0} = \left[\ln \left(30 \frac{\eta_d}{k_s} \right) \right]^2 \left[\ln \left(30 \frac{\eta_d}{k_{sc}} \right) \right]^{-2} - 1 \quad (8.180)$$

Using Eqs. (8.178) and (8.180) produces

$$C_D \frac{1}{2} \cdot \frac{\eta_d}{\lambda_d \kappa^2} \left[\ln \left(30 \frac{\eta_d}{k_s} \right) - 1 \right]^2 = \left[\ln \left(30 \frac{\eta_d}{k_s} \right) \right]^2 \left[\ln \left(30 \frac{\eta_d}{k_{sc}} \right) \right]^{-2} - 1 \quad (8.181)$$

For the given values of k_s , η_d , and λ_d , the composite roughness height k_{sc} can be solved from Eq. (8.181). Then, $\tau_0 (= \tau'_0 + \tau''_0)$, τ'_0 , and τ''_0 can be obtained from Eqs. (8.178) (second equation) and (8.180).

García (2008) argued that the composite roughness height k_{sc} can be determined from Keulegan's depth-averaged velocity formula. The expression for k_{sc} is

$$k_{sc} = 11h \exp \left(-\frac{\kappa U}{u_*} \right) \quad \wedge \quad u_* = \left(\frac{\tau''_0 + \tau'_0}{\rho} \right)^{0.5} \quad (8.182)$$

Later, García and Parker (1993) extended the Nelson and Smith's method for the hydraulically smooth flow. The modification of Eq. (8.178) for the case of hydraulically smooth flow is given by

$$\frac{\tau''_0}{\tau'_0} = C_D \frac{1}{2} \cdot \frac{\eta_d}{\lambda_d \kappa^2} \left[\ln \left(9 \frac{u'_* \eta_d}{v} \right) - 1 \right]^2 \quad (8.183)$$

8.7.6 Wright and Parker's Method

Wright and Parker (2004), who identified that Engelund's method could be well applicable to laboratory scale but did not perform satisfactorily for large-scale field applications, proposed a modified method that provides good results for both small- and large-scale applications. They defined Shields parameter due to particle roughness as

$$\Theta' = 0.05 + 0.7(\Theta Fr^{0.7})^{0.8} \quad (8.184)$$

They used the stratification adjusted form of the equation given by Brownlie. It is as follows:

$$\frac{U}{u'_*} = \frac{8.32}{\alpha} \left(\frac{h'}{k_s} \right)^{1/6} \quad \wedge \quad u'_* = (gh'S_0)^{0.5} \quad (8.185)$$

where α is the stratification adjustment constant. They considered $k_s = 3d_{90}$. The α is given by

$$\alpha \left(\frac{C_{0.05}}{S_0} \leq 10 \right) = 1 - 0.06 \left(\frac{C_{0.05}}{S_0} \right)^{0.77} \quad (8.186a)$$

$$\alpha \left(\frac{C_{0.05}}{S_0} > 10 \right) = 0.67 - 0.0025 \frac{C_{0.05}}{S_0} \quad (8.186b)$$

where $C_{0.05}$ is the reference concentration at reference level $a = 0.05h$.

The relationship between the depth and the discharge appropriate for the lower flow regime is developed by first assuming that the velocity distribution over a bed with dunes has roughly the same shape as that over a plane bed. Thus, k_s in Eq. (8.185) is to be replaced by a composite roughness k_{sc} and u'_* by u_* . Then, it is obtained as

$$\frac{U}{u_*} = \frac{8.32}{\alpha} \left(\frac{h}{k_{sc}} \right)^{1/6} \quad \wedge \quad u_* = (ghS_0)^{0.5} \quad (8.187)$$

Using continuity equation $q = Uh$, Eq. (8.187) can be expressed as

$$\frac{h}{d_{50}} = \left[\frac{\alpha}{8.32} \cdot \frac{\hat{q}}{S_0^{0.5}} \left(\frac{k_{sc}}{d_{50}} \right)^{1/6} \right]^{0.6} \quad \wedge \quad \hat{q} = \frac{q}{d_{50}(gd_{50})^{0.5}} \quad (8.188)$$

The relationship between the composite roughness and the particle roughness can then be obtained from Eqs. (8.185) and (8.187) as

$$k_{sc} = k_s \left(\frac{h}{h'} \right)^4 = \left(\frac{\Theta}{\Theta'} \right)^4 \quad (8.189)$$

The reference concentration $C_{0.05}$ can be calculated as follows:

$$\begin{aligned} E_{si} &= \frac{7.8 \times 10^{-7} (\zeta_\sigma \chi_i)^5}{1 + 2.6 \times 10^{-6} (\zeta_\sigma \chi_i)^5} \quad \wedge \quad \zeta_\sigma = 1 - 0.28\sigma_\phi \quad \vee \quad \chi_i = R_{pi}^{0.6} S_0^{0.08} \frac{u'_*}{w_{si}} \left(\frac{d_i}{d_{50}} \right)^{0.2} \\ &\wedge \quad R_{pi} = \frac{d_i (\Delta g d_i)^{0.5}}{v}, \quad \therefore \quad C_{0.05} = \sum \frac{E_{si}}{F_{bi}} \end{aligned} \quad (8.190)$$

where σ_ϕ is the standard deviation of bed sediment's particle size distribution based on Φ scale, d_i is the fractional particle size, and F_{bi} is the fraction of particle size d_i in bed sediment.

For the given discharge q , bed slope S_0 and particle size distribution (d_i and F_{bi}), Wright and Parker's method can be applied as follows:

- Step 1: Assume a flow depth h .
- Step 2: Calculate Θ and Fr .
- Step 3: Calculate Θ' from Eq. (8.184) and k_{sc} from Eq. (8.189).
- Step 4: Calculate $C_{0.05}$ from Eq. (8.190).
- Step 5: Calculate α from Eq. (8.186).
- Step 6: Calculate h from Eq. (8.188) and then compare the calculated value of h with the assumed value of h .
- Step 7: Repeat next iteration (Step 1 to Step 6) with calculated value of h (as the next assumed value of h) until the assumed and the calculated values converge.

8.8 Examples

Example 8.1 The depth-averaged flow velocity in a wide river is 1.2 m s^{-1} , flow depth 3.2 m, and energy slope 1.6×10^{-4} . The flow is fairly uniform within the measuring reach. The characteristics of bed sediment are the median size $d_{50} = 0.4 \text{ mm}$, $d_{65} = 0.55 \text{ mm}$, and $d_{90} = 0.9 \text{ mm}$ having a relative density of 2.65. Assume coefficient of kinematic viscosity of water $\nu = 10^{-6} \text{ m}^2 \text{ s}^{-1}$ and mass density of water $\rho = 10^3 \text{ kg m}^{-3}$.

- (a) Predict the type of bedform formation.
- (b) Compute the dimensions of the bedforms.

Solution

Given data are as follows:

Flow velocity, $U = 1.2 \text{ m s}^{-1}$; flow depth, $h = 3.2 \text{ m}$; energy slope, $S_f = 1.6 \times 10^{-4}$; sediment size, $d_{50} = 0.4 \text{ mm}$, $d_{65} = 0.55 \text{ mm}$, and $d_{90} = 0.9 \text{ mm}$; relative density, $s = 2.65$; kinematic viscosity of water, $\nu = 10^{-6} \text{ m}^2 \text{ s}^{-1}$; and mass density of water, $\rho = 10^3 \text{ kg m}^{-3}$.

For uniform flow, the energy slope equals the streamwise bed slopes. So, $S_f = S_0 = 1.6 \times 10^{-4}$.

Applied bed shear stress, $\tau_0 = \rho g h S_0 = 10^3 \times 9.81 \times 3.2 \times 1.6 \times 10^{-4} = 5.023 \text{ Pa}$.

Shear velocity, $u_* = (\tau_0/\rho)^{0.5} = (5.023/10^3)^{0.5} = 0.071 \text{ m s}^{-1}$.

Shields parameter, $\Theta = \tau_0/(\Delta \rho g d_{50}) = 5.023/(1.65 \times 10^3 \times 9.81 \times 0.4 \times 10^{-3}) = 0.776$.

Shear Reynolds number, $R_* = u_* k_s/\nu = 0.071 \times 0.55 \times 10^{-3}/10^{-6} = 39.05$ (Note: $k_s = d_{65}$ is assumed).

Flow Froude number, $Fr = U/(gh)^{0.5} = 1.2/(9.81 \times 3.2)^{0.5} = 0.21$.

Densimetric Froude number, $F_d = U/(\Delta g d_{50})^{0.5} = 1.2/(1.65 \times 9.81 \times 0.4 \times 10^{-3})^{0.5} = 14.91$.

Terminal fall velocity, $w_s = 0.06 \text{ m s}^{-1}$ [obtained from Cheng's (1997) formula (see Table 1.3) with nominal diameter $d_n = d_{50}/0.9$].

Use van Rijn's empirical formula for the determination of threshold bed shear stress and threshold shear velocity (see Table 4.1):

Particle parameter, $D_* = d_{50}(\Delta g/b^2)^{1/3} = 0.4 \times 10^{-3}[1.65 \times 9.81/(10^{-6})^2]^{1/3} = 10.118$.

Threshold Shields parameter, $\Theta_c (4 < D_* \leq 20) = 0.04 D_*^{-0.1} = 0.04 \times 10.118^{-0.1} = 0.0317$

Threshold bed shear stress, $\tau_{0c} = \Theta_c \Delta \rho g d_{50} = 0.0317 \times 1.65 \times 10^3 \times 9.81 \times 0.4 \times 10^{-3} = 0.205 \text{ Pa}$.

Threshold shear velocity, $u_{*c} = (\tau_{0c}/\rho)^{0.5} = (0.205/10^3)^{0.5} = 0.014 \text{ m s}^{-1}$

(a) Prediction of bedform type:

Simons et al.'s method:

On the basis of $Fr (= 0.21)$, which is less than unity, it indicates a lower flow regime with a possibility of formation of ripples, ripples on dunes, and dunes.

Simons and Richardson's method:

$$U\tau_0 = 1.2 \times 5.023 = 6.028 \text{ N m}^{-1} \text{ s}^{-1}$$

$$d_t = 0.4 \text{ mm (Note: Fall diameter } d_t \text{ is assumed to be equaling } d_{50})$$

From Fig. 8.9 ($U\tau_0$ versus d_t), bedforms are predicted to be dunes.

Liu's method:

$$\frac{u_*}{w_s} = \frac{0.071}{0.06} = 1.18, \quad R_* = 39.05$$

From Fig. 8.10 (u_*/w_s versus R_*), bedforms are predicted to be ripples.

Chabert and Chauvin's method:

From Fig. 8.11 (Θ versus R_*), bedforms are predicted to be dunes for $\Theta = 0.776$ and $R_* = 39.05$.

Athaullah method:

$$\frac{R_b}{d} = \frac{h}{d_{50}} = \frac{3.2}{0.4 \times 10^{-3}} = 8,000 \text{ (Note: it is assumed that } R_b = h), Fr = 0.21$$

From Fig. 8.12 (Fr versus R_b/d), it indicates a lower flow regime. Hence, the possible bedforms are dunes.

Southard and Boguchwal method:

From Fig. 8.13 (U versus d), bedforms are predicted to be dunes for $U = 1.2 \text{ m s}^{-1}$ and $d_{50} = 0.4 \text{ mm}$.

van Rijn method:

$$T_* = \frac{\tau_0 - \tau_{0c}}{\tau_{0c}} = \frac{5.023 - 0.205}{0.205} = 23.5$$

From Table 8.2 with $15 < T_* < 25$ and $D_* > 10$, it indicates washed-out dunes and sand waves (asymmetrical).

Bonnefille–Pernecker method:

From Fig. 8.14 (D_* versus R_*), bedforms are predicted to be plane bed for $D_* = 10.118$ and $R_* = 39.05$.

van der Berg and van Gelder method:

$$C'_R = 18 \log \left(\frac{4h}{d_{90}} \right) = 18 \log \left(\frac{4 \times 3.2}{0.9 \times 10^{-3}} \right) = 74.75$$

$$\Theta' = \frac{U^2}{\Delta g d C_R'^2} = \frac{1.2^2}{1.65 \times 9.81 \times 0.4 \times 10^{-3} \times 74.75^2} = 0.04$$

From Fig. 8.15 (Θ' versus D_*), bedforms are predicted to be ripples.

Karim method:

$$F_T = 2.716 \left(\frac{d_{50}}{h} \right)^{0.25} = 2.716 \left(\frac{0.4 \times 10^{-3}}{3.2} \right)^{0.25} = 0.287 > Fr (= 0.21)$$

$$F_U = 4.785 \left(\frac{d_{50}}{h} \right)^{0.27} = 4.785 \left(\frac{0.4 \times 10^{-3}}{3.2} \right)^{0.27} = 0.423$$

The condition $Fr < F_T$ corresponds to the lower flow regime (ripples and dunes).

Julien and Raslan method:

For the given data, $D_* = 10.118$ and $R_* = 39.05$. They correspond to the following conditions:

$$3 < D_* < 70 \text{ and } 11.6 < R_* < 70$$

Again,

$$\frac{1}{D_*} \cdot \frac{1}{\kappa} \ln\left(\frac{h}{20d_{50}}\right) = \frac{1}{10.118} \cdot \frac{1}{0.4} \ln\left(\frac{3.2}{20 \times 0.4 \times 10^{-3}}\right) = 1.48 > \Theta (= 0.776)$$

The above conditions correspond to the formation of dunes.

(b) Dimensions of bedforms:

The majority of different methods used for the prediction are in favor of the formation of dunes. Therefore, dimensions of bedforms as dunes are calculated here.

van Rijn formula:

$$\begin{aligned} \eta_d &= 0.11h \left(\frac{d}{h}\right)^{0.3} \left[1 - \exp\left(-0.5 \frac{\tau'_0 - \tau_{0c}}{\tau_{0c}}\right)\right] \left(25 - \frac{\tau'_0 - \tau_{0c}}{\tau_{0c}}\right) \\ &= 0.11 \times 3.2 \left(\frac{0.4 \times 10^{-3}}{3.2}\right)^{0.3} \left[1 - \exp\left(-0.5 \times \frac{5.023 - 0.205}{0.205}\right)\right] \\ &\quad \times \left(25 - \frac{5.023 - 0.205}{0.205}\right) = 0.036 \text{ m} \\ \lambda_d &= 7.3h = 7.3 \times 3.2 = 23.36 \text{ m} \Leftarrow \text{Eq. (8.10)} \end{aligned}$$

Julien and Klaassen formula:

$$\begin{aligned} \bar{\eta}_d &\approx 2.5h^{0.7}d^{0.3} = 2.5 \times 3.2^{0.7}(0.4 \times 10^{-3})^{0.3} = 0.54 \text{ m} \\ \bar{\lambda}_d &= 6.5h = 6.5 \times 3.2 = 20.8 \text{ m} \Leftarrow \text{Eq. (8.11)} \end{aligned}$$

Dimensions of dunes calculated from some other formulas, as given in Table 8.1, are furnished in Table 8.5.

Example 8.2 Water flows at a rate of $3 \text{ m}^2 \text{ s}^{-1}$ (discharge per unit width) in a wide channel. If the streamwise bed slope is 2.5×10^{-4} and the median size of sediment 0.5 mm with a relative density of 2.65, determine the flow depth by Engelund's method. Assume mass density of water is 10^3 kg m^{-3} .

Solution

Given data are as follows:

Flow discharge per unit width, $q = 3 \text{ m}^2 \text{ s}^{-1}$; bed slope, $S_0 = 2.5 \times 10^{-4}$; sediment size, $d_{50} = 0.5 \text{ mm}$; relative density, $s = 2.65$; and mass density of water, $\rho = 10^3 \text{ kg m}^{-3}$

Step 1: Assume a value of hydraulic radius due to particle roughness ($R'_b \approx h'$). Let the first trial value of h' be 1.5 m

Table 8.5 Results of dimensions of dunes

References	Height η_d (m)	Length λ_d (m)	Remark
Allen (1968)	0.343	2.01	
Gill (1971)	0.445	–	Assumed $n = 5.5$ and $\alpha = 0.6$
Orgis (1974)	2.867	–	Maximum dune height
Yalin (1977)	0.512	20.16	
Allen (1978)	0.892	–	
Watannabe (1989)	0.491	–	

Step 2: Calculate Θ' :

$$\Theta' = \frac{h'S_0}{\Delta d_{50}} = \frac{1.5 \times 2.5 \times 10^{-4}}{1.65 \times 0.5 \times 10^{-3}} = 0.455$$

Step 3: Obtain Θ from Fig. 8.36 or from Eq. (8.170a). It is $\Theta = 0.994$

Step 4: Calculate h :

$$h = \frac{\Theta \Delta d_{50}}{S_0} = \frac{0.994 \times 1.65 \times 0.5 \times 10^{-3}}{2.5 \times 10^{-4}} = 3.28 \text{ m}$$

Step 5: Calculate U from Eq. (8.169) by using $k_s = 2.5d_{50}$ and assuming $S_f = S_0$:

$$\begin{aligned}
 U &= \frac{(gh'S_0)^{0.5}}{\kappa} \ln \left(12.2 \frac{h'}{k_s} \right) \\
 &= \frac{(9.81 \times 1.5 \times 2.5 \times 10^{-4})^{0.5}}{0.4} \ln \left(12.2 \frac{1.5}{2.5 \times 0.5 \times 10^{-3}} \right) = 1.454 \text{ m s}^{-1}
 \end{aligned}$$

Step 6: Calculate q :

$$q = Uh = 1.454 \times 3.28 = 4.769 \text{ m}^2 \text{ s}^{-1}$$

Step 7: Calculated q is not equal to the given value of $q (= 3 \text{ m}^2 \text{ s}^{-1})$

Step 8: Repeat iteration (Step 1 to Step 6) until these two values of q converge.

The final results that match with the given value of $q (= 3 \text{ m}^2 \text{ s}^{-1})$ are as follows:

$$h' = 1.021 \text{ m (final trial value)}$$

$$\Theta' = 0.309$$

$$\Theta = 0.79$$

$$h = 2.607 \text{ m}$$

$$U = 1.152 \text{ m s}^{-1} \Rightarrow q = Uh = 1.152 \times 2.607 = 3 \text{ m}^2 \text{ s}^{-1}.$$

Example 8.3 A wide river has a streamwise bed slope of 3.5×10^{-4} . The flow is fairly uniform within the measuring reach. The characteristics of bed sediment are median size $d_{50} = 0.6$ mm and relative density $s = 2.65$. Assume coefficient of kinematic viscosity of water $\nu = 10^{-6} \text{ m}^2 \text{ s}^{-1}$ and mass density of water $\rho = 10^3 \text{ kg m}^{-3}$. Determine the type and dimensions of bedform, and estimate the flow discharge per unit width, if the flow depth is 2.5 m.

Solution

Given data are as follows:

Flow depth, $h = 2.5$ m; bed slope, $S_0 = 3.5 \times 10^{-4}$; sediment size, $d_{50} = 0.6$ mm; relative density, $s = 2.65$; kinematic viscosity of water, $\nu = 10^{-6} \text{ m}^2 \text{ s}^{-1}$; and mass density of water, $\rho = 10^3 \text{ kg m}^{-3}$

Applied bed shear stress, $\tau_0 = \rho g h S_0 = 10^3 \times 9.81 \times 2.5 \times 3.5 \times 10^{-4} = 8.584 \text{ Pa}$

Shear velocity, $u_* = (\tau_0/\rho)^{0.5} = (8.584/10^3)^{0.5} = 0.093 \text{ m s}^{-1}$

Shields parameter, $\Theta = \tau_0/(\Delta \rho g d_{50}) = 8.584/(1.65 \times 10^3 \times 9.81 \times 0.6 \times 10^{-3}) = 0.884$

Shear Reynolds number, $R_* = u_* k_s/\nu = 0.093(2 \times 0.6 \times 10^{-3})/10^{-6} = 111.6$
(Note: $k_s = 2d_{50}$ is assumed)

Particle parameter, $D_* = d_{50}(\Delta g/\nu^2)^{1/3} = 0.6 \times 10^{-3} [1.65 \times 9.81/(10^{-6})^2]^{1/3} = 15.178$

From Figs. 8.11 (Θ versus R_*) and 8.14 (D_* versus R_*), bedforms are predicted to be dunes.

By using Julien and Klaassen's formula (Eq. 8.11), the average dimensions of dunes are as follows:

$$\bar{\eta}_d \approx 2.5h^{0.7}d^{0.3} = 2.5 \times 2.5^{0.7}(0.6 \times 10^{-3})^{0.3} = 0.513 \text{ m}, \bar{\lambda}_d = 6.5h = 6.5 \times 2.5 = 16.25 \text{ m}$$

Total friction factor is calculated by van Rijn's method:

$$\lambda_D = \lambda'_D + \lambda''_D \approx 0.32 \left(\frac{d_{50}}{h} \right)^{1/3} + \frac{\bar{\eta}_d}{\bar{\lambda}_d} = 0.32 \left(\frac{0.6 \times 10^{-3}}{2.5} \right)^{1/3} + \frac{0.513}{16.25} = 0.051$$

The depth-averaged velocity is

$$U = u_* \left(\frac{8}{\lambda_D} \right)^{0.5} = 0.093 \left(\frac{8}{0.051} \right)^{0.5} = 1.16 \text{ m s}^{-1}$$

The flow discharge per unit width is

$$q = Uh = 1.16 \times 2.5 = 2.9 \text{ m}^2 \text{ s}^{-1}.$$

References

- Allen JRL (1968) Current ripples: their relation to patterns of water and sediment motion. North-Holland Publishing Company, Amsterdam
- Allen JRL (1978) Computational methods for dune time-lag: calculations using Stein's rule for dune height. *Sediment Geol* 20(3):165–216
- Ashley GM (1990) Classification of large scale subaqueous bed forms: a new look at an old problem. *J Sediment Petrol* 60(1):160–172
- Athallah M (1968) Prediction of bed forms in erodible channels. PhD thesis, Department of Civil Engineering, Colorado State University, Fort Collins, Colorado
- Baas JH (1993) Dimensional analysis of current ripples in recent and ancient depositional environments. Geological Ultralectura 106, Department of Geology, University of Utrecht, Utrecht
- Baas JH (1994) A flume study on the development and equilibrium morphology of current ripples in very fine sand. *Sedimentology* 41(2):185–209
- Baas JH (1999) An empirical model for the development and the equilibrium morphology of current ripples in fine sand. *Sedimentology* 46(1):123–138
- Baas JH, de Koning H (1995) Washed-out ripples: their equilibrium dimensions, migration rate, and relation to suspended-sediment concentration in very fine sand. *J Sediment Res A* 65(2):431–435
- Bagnold RA (1946) Motion of waves in shallow water. Interaction between waves and sand bottoms. *Proc R Soc London A* 187(1008):1–18
- Bagnold RA (1956) The flow of cohesionless grains in fluids. *Philos Trans R Soc London A* 249(964):315–319
- Banks NL, Collinson JD (1975) The size and shape of small-scale current ripples: an experimental study using medium sand. *Sedimentology* 22(4):583–599
- Barton JR, Lin PN (1955) A study of sediment transport in alluvial channels. Report number 55JRB2, Department of Civil Engineering, Colorado A and M College, Fort Collins, Colorado
- Bathurst JC (1993) Flow resistance through the channel network. In: Beven K, Kirkby MJ (eds) *Channel network hydrology*. Wiley, Chichester, pp 43–68
- Bechteler W, Vogel G, Vollmers HJ (1991) Model investigations on the sediment transport of a lower alpine river. In: Armanini A, di Silvio G (eds) *Fluvial hydraulics of mountain regions*. Lecture note in earth sciences. Springer, Berlin, pp 769–857
- Billi P (1988) A note on cluster bedform behaviour in a gravel-bed river. *Catena* 15(5):473–481
- Bose SK, Dey S (2009) Reynolds averaged theory of turbulent shear flow over undulating beds and formation of sand waves. *Phys Rev E* 80:036304
- Bose SK, Dey S (2012) Instability theory of sand-ripples formed by turbulent shear flows. *J Hydraul Eng* 138(8):752–756
- Brayshaw AC, Frostick LE, Reid I (1983) The hydrodynamics of particle clusters and sediment entrainment in coarse alluvial channels. *Sedimentology* 30(1):137–143
- Brooks NH (1954) Laboratory studies of the mechanics of streams flowing over a movable bed of fine sand. Doctoral thesis, California Institute of Technology, Pasadena
- Brownlie WR (1983) Flow depth in sand-bed channels. *J Hydraul Eng* 109(7):959–990
- Chabert J, Chauvin JL (1963) Formation de dunes et des rides dans les modèles fluviaux. *Bulletin du Centre de Recherches et d'essais de Chatou* 4:31–51
- Cheng N-S (1997) Simplified settling velocity formula for sediment particle. *J Hydraul Eng* 123(2):149–152
- Chin A (1999) The morphologic structure of step-pools in mountain streams. *Geomorphology* 27(3–4):191–204
- Colebrook CF, White CM (1937) Experiments with fluid friction in roughened pipes. *Proc R Soc London A* 161(906):367–381
- Davies TR (1971) Summary of experimental data for flume tests over fine sand. Report CE/3/71, Department of Civil Engineering, University of Southampton, Southampton

- Einstein HA, Barbarossa NL (1952) River channel roughness. *Trans Am Soc Civ Eng* 117:1121–1132
- Engelund F (1966) Hydraulic resistance of alluvial streams. *J Hydraul Div* 92(2):315–326
- Engelund F (1970) Instability of erodible beds. *J Fluid Mech* 42:225–244
- Engelund F, Fredsøe J (1982) Sediment ripples and dunes. *Ann Rev Fluid Mech* 14:13–37
- Engelund F, Hansen E (1967) A monograph on sediment transport in alluvial streams. Technical Press (Teknisk Forlag), Copenhagen
- Exner FM (1925) Über die wechselwirkung zwischen wasser und geschiebe in flüssen. *Sitzungsberichte der Akademie der Wissenschaften* 134(2a):165–203
- Fredsøe J (1974) On the development of dunes in erodible channels. *J Fluid Mech* 64:1–16
- Fredsøe J (1975) The friction factor and height-length relations in flow over a dune-covered bed. Progress report number 37, Institute of Hydrodynamic and Hydraulic Engineering (ISVA), Technical University of Denmark, Kongens Lyngby
- Fredsøe J, Deigaard R (1992) *Mechanics of coastal sediment transport*. World Scientific, Singapore
- Fuchs RA (1951) On the theory of short-crested oscillatory waves. Technical report series HE-116, Volume 326, Institute of Engineering Research, Fluid Mechanics Laboratory, University of California, Berkeley
- García MH (2008) Sediment transport and morphodynamics. In: García MH (ed) *Sedimentation engineering: processes, measurements, modeling, and practice*. Manuals and reports on engineering practice number 110, American Society of Civil Engineers, Reston, VA, pp 21–163
- García MH, Parker G (1993) Experiments on the entrainment of sediment into suspension by a dense bottom current. *J Geophys Res* 98(C3):4793–4807
- Gill MA (1971) Height of sand dunes in open channel flows. *J Hydraul Div* 97(12):2067–2074
- Guy HP, Simons DB, Richardson EV (1966) Summary of alluvial channel data from flume experiments, 1956–1961. United States geological survey watersupply paper number, 462-1, Washington, DC
- Haaland SE (1983) Simple and explicit formulas for the friction factor in turbulent flow. *J Fluids Eng* 105(5):89–90
- Hayashi T (1970) Formation of dunes and antidunes in open channels. *J Hydraul Div* 96(3):357–366
- Jaeggi MNR (1984) Formation and effects of alternate bars. *J Hydraul Eng* 110(2):142–156
- Julien PY (2010) *Erosion and sedimentation*, 2nd edn. Cambridge University Press, Cambridge
- Julien PY, Klaassen GJ (1995) Sand-dune geometry of large rivers during floods. *J Hydraul Eng* 121(9):657–663
- Julien PY, Raslan Y (1998) Upper-regime plane bed. *J Hydraul Eng* 124(11):1086–1096
- Karim F (1995) Bed configuration and hydraulic resistance in alluvial-channel flows. *J Hydraul Eng* 121(1):15–25
- Karim F (1999) Bed-form geometry in sand-bed flows. *J Hydraul Eng* 125(12):1253–1261
- Karim MF, Kennedy JF (1981) Computer-based predictors for sediment discharge and friction factor of alluvial streams. Report 242, Iowa Institute of Hydraulic Research, University of Iowa, Iowa
- Keller EA, Melhorn N (1978) Rhythmic spacing and origin of pools and riffles. *Geol Soc Am Bull* 89(5):723–730
- Kennedy JF (1961a) Stationary waves and antidunes in alluvial channels. Report number KH-R-2, WM Keck Laboratory of Hydraulics and Water Resources, California Institute of Technology, Pasadena
- Kennedy JF (1961b) Further laboratory studies of the roughness and suspended load on alluvial streams. Report number KH-R-3, WM Keck Laboratory of Hydraulics and Water Resources, California Institute of Technology, Pasadena
- Kennedy JF (1963) The mechanics of dunes and antidunes in erodible bed channels. *J Fluid Mech* 16(4):521–544
- Knighton DA (1998) *Fluvial forms and processes: a new perspective*. Arnold, London

- Lane EW, Kalinske AA (1941) Engineering calculations of suspended sediment. *Trans Am Geophys Union* 20(3):603–607
- Laursen EM (1958) The total sediment load of streams. *J Hydraul Div* 84(1):1–36
- Liu HK (1957) Mechanics of sediment-ripple formation. *J Hydraul Div* 83(2):1–23
- McDonald BC, Banerjee I (1971) Sediments and bed forms on a braided outwash plain. *Can J Earth Sci* 8(10):1282–1301
- Meyer-Peter E, Müller R (1948) Formulas for bed-load transport. In: *Proceedings of the second meeting of International Association for Hydraulic Research*, Stockholm, vol 3, pp 39–64
- Milne-Thompson LM (1960) *Theoretical hydrodynamics*. Macmillan, New York
- Nelson J, Smith CR (1989) Flow in meandering channels with natural topography. In: Ikeda S, Parker G (eds) *River meandering*. Water resources monograph number 12. American Geophysical Union, Washington, DC, pp 69–102
- Núñez-González F (2012) Bedload transport of sand-gravel mixtures with antidunes. Flume experiments. PhD thesis, Civil Engineering Faculty, Technical University of Catalonia, Barcelona Tech, Barcelona
- Núñez-González F, Martín-Vide JP (2011) Analysis of antidune migration direction. *J Geophys Res* 116(F02004). doi:10.1029/2010JF001761
- Orgis H (1974) Geschiebebetrieb und bettbildung. *Österreichische Ingenieur-Zeitschrift* 17(9):285–292
- Plate EJO (1957) Laboratory studies on the beginning of sediment ripple formation in an alluvial channel. Master thesis, Colorado State University, Fort Collins, Colorado
- Ranga Raju KG, Soni JP (1976) Geometry of ripples and dunes in alluvial channels. *J Hydraul Res* 14(3):241–249
- Raudkivi AJ (1963) Study of sediment ripple formation. *J Hydraul Div* 89(6):15–33
- Raudkivi AJ (1966) Bed forms in alluvial channels. *J Fluid Mech* 26:507–514
- Raudkivi AJ (1990) *Loose boundary hydraulics*. Pergamon, New York
- Raudkivi AJ (1997) Ripples on streambed. *J Hydraul Eng* 123(1):58–64
- Raupach MR, Antonia RA, Rajagopalan S (1991) Rough-wall turbulent boundary layers. *Appl Mech Rev* 44(1):1–25
- Richards KJ (1980) The formation of ripples and dunes on erodible bed. *J Fluid Mech* 99:597–618
- Richards KS (1976) The morphology of riffle-pool sequences. *Earth Surf Proc Land* 1(1):71–88
- Robert A (1990) Boundary roughness in coarse-grained channels. *Prog Phys Geogr* 14(1):42–70
- Simons DB, Richardson EV (1961) Forms of bed roughness in alluvial channels. *J Hydraul Div* 87(3):87–105
- Simons DB, Richardson EV (1966) Resistance to flow in alluvial channels. Professional paper 4-J22, United States Geological Survey, Washington, DC
- Simons DB, Richardson EV, Albertson ML (1961) Flume studies using medium sand (0.45 mm). United States geological survey water supply paper number 1498-A, United States Government Printing Office, Washington, DC
- Song CCS (1983) Modified kinematic model: application to bed forms. *J Hydraul Eng* 109(8):1133–1151
- Southard JB, Boguchwal LA (1990) Bed configurations in steady unidirectional water flows. Part 2. Synthesis of flume data. *J Sediment Petrol* 60(5):658–679
- Sukegawa N (1973) Condition for the formation of alternate bars in straight alluvial channels. In: *Proceedings of the international symposium of river mechanics*, Bangkok, A58:1–11
- Thackston EL, Krenkel PA (1967) Longitudinal mixing in natural streams. *J Sanitary Eng Div* 93(5):67–90
- Tison LH (1949) Origine des ondes de sable et des bancs de sable sous l'action des courants. *Transactions of the International Association for Hydraulic Structures Research*, Third Meeting, Report II-13, Grenoble
- Tjerry S, Fredsøe J (2005) Calculation of dune morphology. *J Geophys Res* 110(F04013). doi:10.1029/2004JF000171

- Tsubaki T, Kawasumi T, Yasutomi T (1953) On the influence of sand ripples upon the sediment transport in open channels. Report, Research Institute for Applied Mechanics, Kyushu University, Japan 2:241–256
- Valance A (2005) Formation of ripples over a sand bed submitted to a turbulent shear flow. *Eur Phys J B* 45(3):433–442
- van den Berg JH, van Gelder A (1993) A new bedform stability diagram, with emphasis on the transition of ripples to plane bed in flows over fine sand and silt. *Alluvial Sedimentation*, Special publication, International Association of Sedimentologists 17:11–21
- van Rijn LC (1984a) Sediment transport, part I: bed load transport. *J Hydraul Eng* 110(10):1431–1456
- van Rijn LC (1984b) Sediment transport, part III: bed forms and alluvial roughness. *J Hydraul Eng* 110(12):1733–1754
- van Rijn LC (1993) Principles of sediment transport in rivers, estuaries and coastal seas. Aqua Publications, The Netherlands
- Watannabe K (1989) A study of bed configurations in alluvial streams. PhD thesis, Kyushu University, Japan
- Williams PB, Kemp PH (1971) Initiation of ripples on flat sediment beds. *J Hydraul Div* 97(4):505–522
- Wright S, Parker G (2004) Flow resistance and suspended load in sand-bed rivers: simplified stratification model. *J Hydraul Eng* 130(8):796–805
- Yalin MS (1964) Geometrical properties of sand waves. *J Hydraul Div* 90(5):105–119
- Yalin MS (1977) *Mechanics of sediment transport*. Pergamon, Oxford
- Yalin MS (1985) On the determination of ripple geometry. *J Hydraul Eng* 111(8):1148–1155
- Zhang X-D, Tang L-M, Xu T-Y (2009) Experimental study of flow intensity influence on 2-D sand ripple geometry characteristics. *Water Sci Eng* 2(4):52–59

Chapter 9

Fluvial Processes: Meandering and Braiding

9.1 General

In general, *fluvial processes* that belong to the geomorphologic category cover the complete chronological processes of formation and evolution of a river system from where it originates to end up in an estuary. However, in a specific sense, fluvial processes that belong to the category of fluvial hydrodynamics focus on river morphological changes occurring due to natural processes and/or engineering activities, such as river regulation and training works. The fluvial processes of rivers are the result of the interaction of stream flow, sediment, and riverbed. The riverbed controls the flow and sediment transport, which in turn enhance changes in the riverbed. Thus, they are interdependent, but complement each other. The characteristics of rivers are related to the gradient of the terrain from extremely steep mountainous torrents to steep rivers at the foot-hills and rivers in the plains. Thus, a river could be regarded as it consisting of upper, middle, and lower reaches which correspond to erosion, regime, and aggradations states, respectively. In upper reach, the sediment transport capacity by the stream flow is generally greater than the prevailing sediment transport rate, leading to an erosion of the streambed. In middle reach, the sediment transport rate is less than the transport capacity by the stream due to gradual streambed armoring followed by a long-term bed-sorting process. This river reach is in a state of quiescent erosion or so-called regime. In lower reach, aggradations occur due to substantial reduction in transport capacity with decrease in valley slope.

According to the static and dynamic characteristics, alluvial river patterns are in general categorized as (1) straight, (2) meandering, and (3) braided rivers (Leopold and Wolman 1957):

1. *Straight rivers* have minimal *sinuosity*¹ (< 1.1) at the bankfull conditions. Usually, rivers, as simple straight open channels, exist only over short reaches

¹ The ratio of the curvilinear length to the linear distance (straight line) between the end points of the curve is known as *sinuosity* or *sinuosity index*. In case of a river, it is the ratio of the actual river length to the down-valley length. Its minimum value is unity for a perfectly straight river.

(Fig. 9.1); while long, straight rivers seldom occur in nature. At low flow stages, alluvial bars exist on either side of the stream. The thalweg² may wind in a sinuous route along the bars, even though the channel is straight. The thalweg may move with alternate bars as they migrate downstream.

2. *Meandering rivers* (sinuosity > 1.5) consist of a series of turns with alternate curvatures connected at the points of inflection or by short straight crossings, as shown in Figs. 9.2 and 9.3. They have a relatively low gradient. The natural meandering rivers are quite unstable due to predominant bank erosion downstream of concave banks. Deeper flows are prevalent in the bends and higher velocities along the outer concave banks. The flow depth at crossings is relatively shallow compared to that at bends. Meandering rivers migrate gradually and hence sinuosity tends to increase. Eventually, the channel forms almost a closed loop and the meander gets often cutoff during a flood. Meandering is therefore the result of streambed instability; in particular, when instability acts on the banks.

Here, it is pertinent to discuss that the rivers with a sinuosity of less than 1.1 is described as straight, those between 1.1 and 1.5 are *sinuous*, and meandering rivers have a sinuosity of greater than 1.5. Therefore, sinuous rivers are the transition between straight and meandering rivers. Although these descriptions are commonly used, they are somewhat arbitrary, since they are not based on any physical differences. Further, there is a tendency for the thalweg to swing from side to side along the rivers. This is observed even in straight rivers and is often associated with the development of riffles, pools, and alternate bars.

3. *Braided rivers* are wide and shallow and divided to branches by a number of semistable or unstable bars or islands (Figs. 9.4 and 9.5). More specifically, braided river can be defined as one that flows in two or more channels around alluvial bars or islands. They have a braided look at the low flow stages with exposed bars, but all or some of the bars are submerged during the high flow stages. However, in most of the occasions, the branching is such that one is the main stream and the others are subsidiary channels. The main stream is relatively stable, but it can change its route under some flow and sediment transport conditions, while the subsidiary channels are quite unstable and often change during floods.

In changing the planform geometry, that is the transition from meandering to braiding and vice versa, although it is best viewed as gradual, empirical equations were put forward to set up some potential relations for the threshold of meandering or braiding (Carson 1984). Leopold and Wolman (1957) gave a relationship to define the transition from meandering to braiding involving riverbed slope S_0 and bankfull discharge Q_{bf} ($\text{m}^3 \text{s}^{-1}$)

² The locus of lowest bed elevation or maximum flow depth within a watercourse is known as *thalweg*.



Fig. 9.1 Photograph of a straight river. Photograph by the author



Fig. 9.2 Aerial photograph of a meandering river (courtesy of O. Link, Universidad de Concepción, Chile)

$$S_0 = 0.012Q_{bf}^{-0.44} \quad (9.1)$$

The above equation, which is the simplest one, indicates that the threshold bed slope above which a river could exhibit a braided form increases with a decrease in bankfull discharge. In addition, Lane (1957) proposed slightly different criterion for the thresholds of meandering from a straight river and braiding from a meandering river by using mean annual discharge Q as

$$\begin{aligned} S_0 &= 7 \times 10^{-4} Q^{-0.25} \text{ (meandering threshold),} \\ S_0 &= 0.004 Q^{-0.25} \text{ (braiding threshold)} \end{aligned} \quad (9.2)$$



Fig. 9.3 Photograph of a meandering river. Photograph by the author



Fig. 9.4 Photograph of a braided river downstream of a valley glacier (courtesy of O. Link, Universidad de Concepción, Chile)



Fig. 9.5 Photograph of a braided river with gravel bars. Photograph by the author

The above equations are in metric units being applicable for sand-bed streams. Note that the bed slopes for these two thresholds (meandering and braiding) differ by a factor of approximately 6.

Equations (9.1) and (9.2) are too general. Henderson (1963) and Ferguson (1987) identified the importance of participation of sediment size d_{50} along with mean annual discharge Q in defining the threshold of braiding from meandering. Henderson and Ferguson suggested the following equations, respectively:

$$S_0 = 2 \times 10^{-4} d_{50}^{1.15} Q^{-0.44} \quad \text{and} \quad S_0 = 4.9 \times 10^{-3} d_{50}^{0.52} Q^{-0.21} \quad (9.3)$$

where d_{50} is in mm and Q is in $\text{m}^3 \text{s}^{-1}$.

Parker (1976) related planform geometry to a form parameter E as

$$E = \frac{S_e B}{\pi F r h} \quad \wedge \quad F r = \frac{U}{\sqrt{g h_d}} \quad (9.4)$$

where S_e is the energy slope, Fr is the flow Froude number, h is the flow depth, B is the average river width, U is the area-averaged flow velocity, g is the acceleration due to gravity, and h_d is the hydraulic depth. In the above equation, the parameters B , h , U , and h_d correspond to the bankfull conditions. The meandering corresponds to $E < 1$ and braiding to $E > 1$.

On the other hand, Millar (2000) argued that the bank vegetation affects planform geometry of a river. He showed that the resistance to bank erosion is to increase the threshold bed slope for braiding from meandering. He introduced a bank sediment friction angle ϕ_b in degrees in his equation. The ϕ_b takes into account the effects of binding of bank sediment by the roots of bank vegetation, sediment packing, etc. He suggested

$$S_0 = 2 \times 10^{-4} \phi_b^{1.75} d_{50}^{0.61} Q_{bf}^{-0.25} \quad (9.5)$$

where d_{50} is in m and Q_{bf} is in $\text{m}^3 \text{s}^{-1}$. The value of ϕ_b is approximately 40° for sparsely vegetated gravel banks, but it can be as high as 80° for heavily vegetated banks because of the grip made by the roots.

Hayashi and Ozaki (1978) proposed the criteria for the prediction of different planforms in terms of flow Froude number Fr and a nondimensional parameter $\tilde{B} = (BS_0/h_d)$ by using the stability analysis as follows:

$$\left. \begin{aligned} Fr &\geq 3.16\tilde{B}^{0.5} \text{ (straight)} \\ 3.16\tilde{B}^{0.5} &\geq Fr \geq 2\tilde{B}^{0.5} \text{ (transition from straight to meandering)} \\ 2\tilde{B}^{0.5} &\geq Fr \geq \tilde{B}^{0.5} \text{ (coexistence of meandering and braiding)} \\ \tilde{B}^{0.5} &\geq Fr \text{ (braiding)} \end{aligned} \right\} \quad (9.6)$$

9.2 Meandering Rivers

In alluvial plains of lower reaches, the rivers normally develop a single-twisting course, termed *meander*, as already discussed in preceding section. The degree of meandering of a river is defined by the *sinuosity*, which is the ratio of centerline length to wavelength of meander. Note that the thalweg length is also considered instead of centerline length by some authors. The sinuosity is a function of valley slope or stream power. For a meandering river, sinuosity that is always greater than unity increases with valley slope, but it reverts close to unity when braiding forms.

Figure 9.6 illustrates an idealized planform of a meandering river. In reality, unlike the idealized illustration, alternating bends of a meandering river are rather quasi-regular. The down-valley axis x in a rectilinear coordinate system represents the centerline of the meandering planform downstream of the valley slope, while the sinuous axis n in a curvilinear coordinate system defines the centerline of the meandering path. Points of inflection for changing the curvatures (also called crossovers) are denoted by I_{-1} , I_0 , I_1 , and I_2 . The deflection angle θ is the angle that creates the meandering path at any location n with the down-valley axis. It changes continuously along the sinuous axis n . Note that $\theta(n=0) = \theta_0$ is the maximum value of θ . It is pertinent to mention that the radius of curvature of meandering path denoted by r_c is not constant for a given meandering bend, so a single value of r_c is somewhat subjective to define for the meandering bend. For instance, the r_c is minimum at the apex of the bend and maximum at the crossings. Besides, the meandering wavelength is denoted by λ_m , the meandering arc length (that is the length along the meandering path between two repeating points of inflection) by L , the meandering belt width by B_m , the meandering amplitude (or meander width) by a_m , and the average flow width by B .

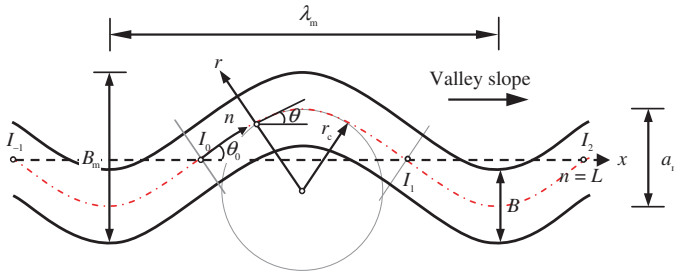


Fig. 9.6 Definition sketch of an idealized planform of a meandering river

The idea of the *sine*-generated curve was used by von Schelling (1951) to outline the most probable path between fixed points. For a given number of steps, he considered the Gaussian distribution for the changing over the direction at the terminus of each step. He showed that a criterion for the most probable path of a continuous curve is obtained if the variance or overall curvature becomes a minimum. Following the minimum variance concept, Langbein and Leopold (1966) argued that a meandering river to achieve the minimum variance is more stable than a straight river and gave the equation of a regular meandering path as

$$\theta = \theta_0 \cos \frac{2\pi x}{L} \quad (9.7)$$

The above equation thus produces a *sine*-generated curve that can fit well the meandering path of a river, provided appropriate values of θ_0 and L are chosen.

In a meandering bend, the centrifugal acceleration influences the flow, which is characterized by a helical motion with a super-elevated free surface. Flow near the free surface is deflected toward the outer bank and near the bed is inclined toward the inner bank. This phenomenon is already discussed in Sect. 2.7. As a stream actively curves to flow, obvious erosion takes place at the outer bank (looking convex from the ground alongside the stream) of the bend. The sediment eroded from the outer bank is transported inward and deposited on the inner edge of the next bend downstream, where the flow velocity is slower, building up an inner point bar (Figs. 9.7 and 9.8). Remembering that the zone of high velocity in a meandering bend shifts from inner (at the inflection zone) to outer side (at the apex zone) with the distance, the zone of maximum bed shear stress shifts similar way. This effect actively shifts the river very slowly toward the eroded banks. The cross-section at the meandering bend apex is normally asymmetrical having deep portion of the stream located along the outer bank and a broad, shallow portion extending from the inner bank toward the center of the stream (Fig. 9.7). The thalweg wanders from deep pool at the outer side of a bend over a shallow crossover to next deep pool at the outer side of the next bend, and so on (Fig. 9.7). As most of the natural river sediments are nonuniform, the asymmetry in cross-section in meandering bends is associated with a spanwise sediment sorting feature. By the influence of the helicoidal flow, finer particles tend to move inward.

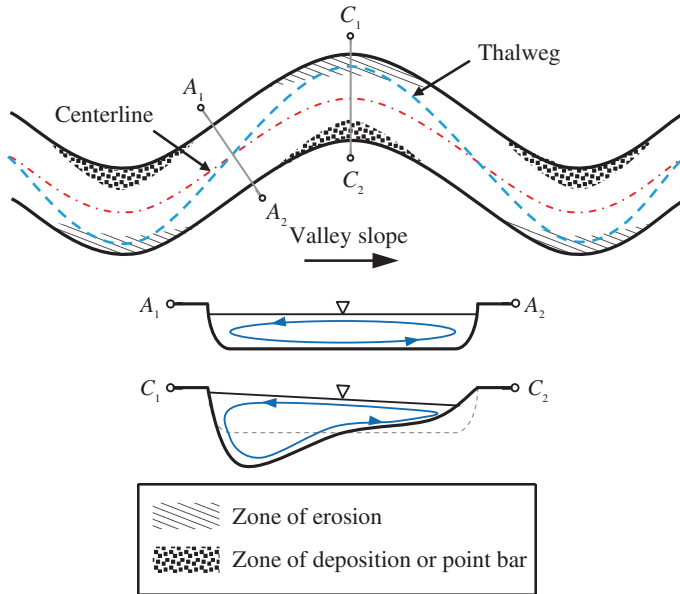


Fig. 9.7 Sketch showing zones of erosion and deposition in a meandering river

In this way, the coarser particles tend to accumulate near the outer banks with a gradual fining toward the inner banks. Dietrich and Smith (1984) argued that the maximum flow depth is inversely proportional to the ratio of radius of curvature of the bend to stream width, that is, $h_{\max} \sim (r_c/B)^{-1}$. Note that the river that has a tendency to braiding does not have an exclusively localized erosion and deposition at the bends only. Evidently, the braiding occurs only when the stream power exceeds a higher threshold. Thus, the sequence of straight, meandering, and braided rivers corresponds to an increase in valley slope or stream power magnitude.

The meander loops are, in general, inherently asymmetrical due to local differences in bank erodibility producing irregularities in bend forms, although Langbein and Leopold (1966) tried to define them by a so-called *sine*-generated curve [see Eq. (9.7)]. In reality, the nature of this asymmetry in meander loops is not random, but they are well defined and somewhat consistent. Such an asymmetry to exist in meander loops does not appear to be the result of probability, but seems to reflect certain inherent flow features through bends. The most important feature in the asymmetrical meander loops is the location of the inflection points that alter on opposite sides of the valley axis, producing a *delayed inflection* from one meandering turn to the next one downstream (Carson and Lapointe 1983; Parker et al. 1983). Consequently, the most meandering bends are facing down-valley. Thus, from a geometric viewpoint, restraint of the meander amplitude could be at the expense of that part of the traverse downstream of the inflection point. In this process, it produces an aborted form that is dominantly convex



Fig. 9.8 Photograph of a meandering river showing the erosion at outer banks and the formation of point bar in the inner bank (courtesy of L. Solari, University of Florence, Italy)



Fig. 9.9 Photograph of the meandering loops of a river showing the potentiality of cutoff by the broken line (courtesy of Z. Wang, Tsinghua University, China)

down-valley. Delayed inflection is attributed to a delayed thalweg crossover leading to spatial variations of bank erosion rates being in turn translated into a delayed inflection in the meander loops. Note that the delayed inflection appears to be prevalent for the meandering rivers that carry considerable suspended load (Carson and Griffiths 1987).

Meander *cutoff* is a fundamental process in the evolution of meandering rivers. As the planform of a meandering river progressively migrates in the downstream direction and expands in the transverse direction, the meander loops shift at a differential rate due to nonuniform erosion rates at the banks. The resulting shape in a developed state appears to form a bulb with inflection zones of a loop to come closer forming a neck (two closest portions of river). Eventually, the banks at the neck breach by a chute channel, called *cutoff*, that connects the neck of the loop (Gagliano and Howard 1984; Hooke 1995). Figure 9.9 displays the potentiality of cutoff at the necks of meandering loops of a river. Besides bank-breaching, cutoff may also occur when floods incise a floodplain channel or chute that evolves into the dominant conveyor of river flow (Hooke 1995; Gay et al. 1998). The cutoff causes the flow to abandon the meander and to continue straight downslope. After formation of a cutoff, a new meandering bend may slowly grow again. Cutoffs are a natural part of the evolution of a meandering river. The abandoned meander forms an *oxbow lake* that may persist over a long time period before getting it filled. The oxbow lake formation process through a meandering neck cutoff is schematically illustrated in Fig. 9.10.

Ripley (1927) studied the meandering rivers and gave the criterion for a meander loop to have a tendency to form a cutoff as $r_c < 40A^{0.5}$, where A is the flow cross-sectional area. However, he also suggested the criterion for a stable meandering bend as $40A^{0.5} < r_c < 110A^{0.5}$.

The aforementioned description is related to sand-bed meandering rivers, which are regarded as low-energy rivers. Carson and Griffiths (1987) reported that the characteristics of gravel-bed meandering rivers, regarded as high-energy rivers, are considerably different from sand-bed rivers in terms of meandering outline. The gravel-bed rivers exhibit a *premature inflection* instead of a delayed inflection that is observed for a low-energy river. Premature inflection in high-energy rivers results in up-valley migration of meandering course and is associated with over-widening of meandering bends (Carson 1986). In low flow stages, high-energy meandering rivers sometimes have a tendency to cut across the point bars. This along with over-widening of meandering bends in low flow stages may initiate to develop the braiding. Carson and Griffiths (1987) designated this type of rivers' configuration, which is in fact a transition between meandering and braiding, as *pseudo-meandering streams*.

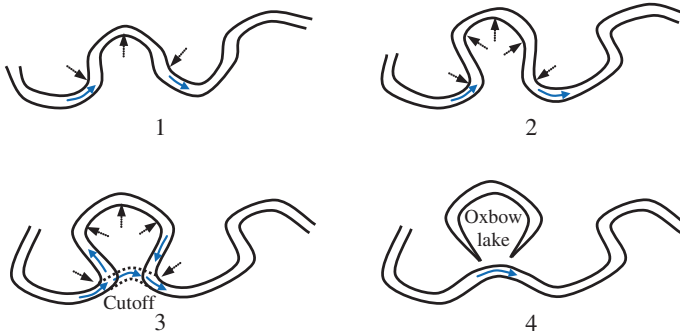


Fig. 9.10 Oxbow lake formation process following a meandering loop cutoff shown in the sequence of 1–4 line diagrams

9.2.1 Meander Planform Characteristics

Field and laboratory observations on the dimensions of meandering geometry have been used to develop empirical relationships between certain planform characteristics that are somewhat consistent for a wide range of river sizes. Various investigators, importantly Inglis (1947), Leopold and Wolman (1957), and Zeller (1967), recognized that the meandering wavelength λ_m is directly proportional to flow width B . The relationship that was obtained by Garde and Ranga Raju (2000) from the data plots is

$$\lambda_m \approx 6B \quad (9.8)$$

Further, Leopold and Wolman (1960) proposed the following relationships between different planform characteristics of meandering rivers:

$$\lambda_m = 4.6r_c^{0.98}, L = 11B^{1.01}, a_m = 6B^{1.1} \quad (9.9)$$

The units of the quantities in Eq. (9.9) are in m.

On the other hand, Chang (1988) suggested $r_c \approx 3B$.

9.2.2 Concepts of Meandering

Attempts have been made to identify the cause of meandering and to understand the background mechanism of its development. Some of the important concepts are discussed below:

Earth's Revolution Concept: The *Coriolis effect*³ is caused by the revolution of the earth, and the inertia of the mass of an object is to experience the effect. On the earth, an object that moves along a north–south path, or longitudinal line, undergoes apparent deflection to the right in the northern hemisphere and to the left in the southern hemisphere. Rather than rivers flowing directly as they would be in a nonrevolving system, the flow tends to the right in north of the equator and to the left in south of it. In the nineteenth century, naturalist Karl Ernst von Baer observed that the rivers in the northern hemisphere do most of their erosion on the side to the right of the direction of flow; and on the left in the southern hemisphere. The reason is attributed to the Coriolis effect. Albert Einstein (1926) simply observed that as the stream flow curves on the earth surface, the Coriolis effect induces rotational motion to the flow. The flow moves helicoidally downstream, as if a corkscrew moves. Einstein's discussion on the cause of meander was rather casual, but characteristically insightful, as his attribution of secondary currents to the Coriolis force might have been among the earliest. Besides, Gilbert (1884), Eakin (1910), and Lacey (1923) before Einstein's observation and Chatley (1938), Quraishy (1943), and Neu (1967) after Einstein's observation argued that the earth's revolution could be the cause of river meandering.

Instability Concept: Any irregularities or perturbations in the upstream flow cause a modification in the flow structure in the downstream direction leading to meandering. In fact, irregularities introduce instability to the flow and the bed to form meanders. The initial irregularities could be due to any obstacle or sediment deposition on the bed (Griggs 1906; Werner 1951), random velocity fluctuations due to turbulence (Hjulström 1957), oblique entry of flow in a channel (Friedkin 1945), or some other reasons. Agarwal (1983) observed alternate bars in an experimental flume by introducing a two-dimensional periodic disturbance on the bed.

Helicoidal Flow Concept: A group of investigators believed that the helicoidal flow due to secondary current of Prandtl's first kind (see Sect. 3.10) is potentially responsible for the occurrence of meandering. Since secondary current is present in all the stream flows, the asymmetry in secondary circulation due to asymmetrical cross-section and/or bed resistance of natural rivers is the cause to initiate meandering (Prus-Chacinski 1954; Leliavsky 1966; Onishi et al. 1976; Shen 1983). Once the meandering is initiated, secondary current of Prandtl's first kind is the governing mechanism.

Excess Flow Energy Concept: This concept is based on the energy content in the stream flow on which the meandering process is related. Flow in a meandering river is to reduce the excess energy (and in turn, to reduce the excess slope) of the flow by increasing its traveling length (Schoklitsch 1937; Inglis 1947). According to Bagnold, the energy loss in a bend is least if the ratio of bend radius to river width lies between 2 and 3. Based on Bagnold's concept of minimum bend loss,

³ The *Coriolis effect* is an apparent deflection of the path of an object in motion due to an induced transverse force normal to its path, when it is set in a rotating reference frame. In a reference frame with clockwise rotation, the deflection is to the left of the motion of the object, while with counter-clockwise rotation, the deflection is to the right.

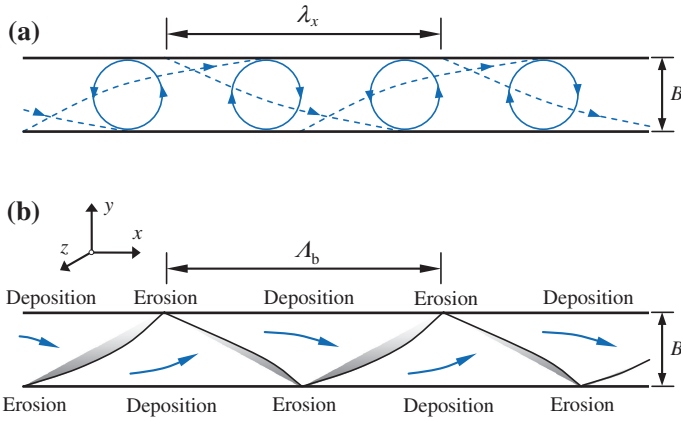


Fig. 9.11 Conceptual illustration of large-scale eddy concept after Yalin and da Silva (2001): **a** top view of large eddies appearing at a relatively regular interval and **b** top view of alternate bars appearing at a relatively regular interval

Leopold and Wolman (1960) and Ramette (1980) argued that the minimization of energy is associated with the formation of meandering in rivers. However, Yang (1971) expressed dissatisfaction about the legitimacy of the hypothesis that a river meanders in order to dissipate excess flow energy. Thus, he introduced a concept of minimum time rate of energy expenditure. According to his concept, during the evolution of a meandering river toward its equilibrium state, a river finds its course of flow in such a way so that the minimum time rate of potential energy expenditure per unit mass of water prevails along its course.

Large-Scale Eddy Concept: Yalin and da Silva (2001) argued that the meandering is caused by the large-scale eddies. They identified that the horizontal length scale (streamwise spacing) λ_x of large eddies in a straight rectangular open channel approximately equals the horizontal length λ_b of alternate bars (Figs. 9.11a, b); and both the length scales are six times of the flow width B . The formation of alternate bars at a relatively regular interval is analogous to the formation of dunes caused by the large-scale eddies that also appear at a relatively regular interval resulting in decrease and increase in bed shear stress (see Fig. 8.4). Thus, taking into account the relationship given by Eq. (9.8), one can relate

$$\lambda_x = \lambda_b = \lambda_m \approx 6B \quad (9.10)$$

Equation (9.10) therefore suggests that both alternate bars and meanders initiate because of the same mechanism, that is, the large-scale eddies or large-scale turbulence structure. Alternate bars are caused by the action of large-scale turbulence structure collapse on the erodible bed, and the threshold of meandering is caused by the action of turbulence structure collapse on the erodible banks (Fig. 9.11b).

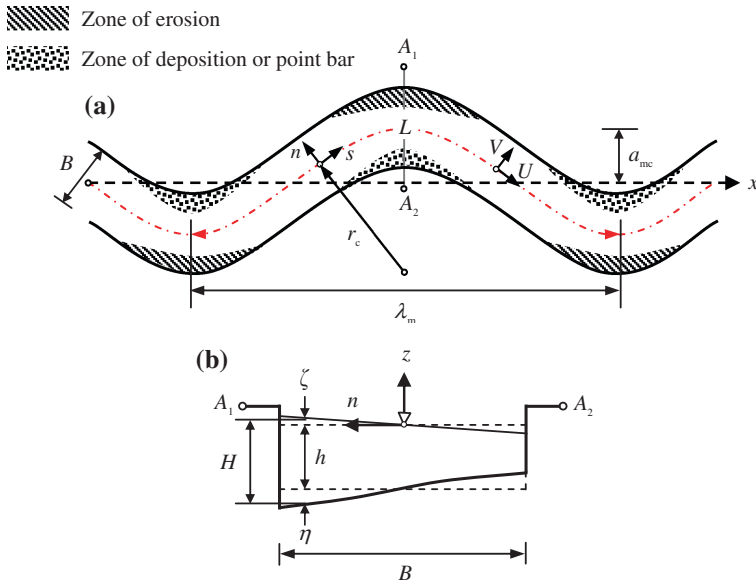


Fig. 9.12 Definition sketch: **a** meandering river with coordinate system and **b** cross-section of river at A_1 - A_2

9.3 Mathematical Modeling of Meandering Rivers

In this section, the flow and bed topography models developed by Ikeda and Nishimura (1986) and Odgaard (1989) are presented in details.

9.3.1 Ikeda and Nishimura's Model

9.3.1.1 Flow Field

Ikeda and Nishimura (1986) considered orthogonal curvilinear coordinates (s, n) to represent depth-averaged velocity components (U, V) (Fig. 9.12a). The U and V are decomposed as

$$U = \bar{U} + U', \quad V = V' \quad (9.11)$$

where \bar{U} is the reach-averaged velocity in s -direction, and U' and V' are the perturbed velocity components.

Referring to Fig. 9.12b, the average flow depth H is decomposed as

$$H = h + \zeta + \eta \quad (9.12)$$

where h is the reach-averaged flow depth, ζ is the super-elevation of the free surface due to curvilinear flow induced by centrifugal inertia, and η is the change of bed elevation with respect to mean bed level due to erosion or deposition.

According to Kikkawa et al. (1976), the η is

$$\frac{\eta}{h} = \left(\frac{r}{r_c}\right)^{\vartheta} - 1 \quad \wedge \quad \vartheta = \left[\frac{3}{4} \cdot \frac{\mu C_D}{1 + \eta_R \mu}\right]^{0.5} \frac{\xi_s}{\kappa} \cdot \frac{\bar{u}_*}{(\Delta g d_{50})^{0.5}} \left(\frac{4.167}{\lambda_f^{0.5}} - 6.6\right) \quad (9.13)$$

where $r = r_c + n$, ϑ is an exponent defining erosion factor, μ is the coefficient of dynamic viscosity, C_D and C_L are the drag and lift coefficients, respectively, ξ_s is the sheltering coefficient, η_R is C_L/C_D , κ is the von Kármán constant, \bar{u}_* is the shear velocity at the centerline $[= (ghS_0)^{0.5}]$, Δ is the submerged relative density, λ_f is the friction parameter $(= ghS_0/\bar{U}^2 = gh^3S_0/q^2)$, and q is the discharge per unit width.

Using Eq. (9.13) and approximation of r_c by a *sine*-generated curve $[r_c^{-1} = r_{c0}^{-1} \cos(k_{wb}s)]$, perturbed streamwise velocity U' can be obtained as follows (Ikeda et al. 1981):

$$\frac{U'}{\bar{U}} = \frac{n}{r_{c0}} [a \sin(k_{wb}s) + b \cos(k_{wb}s)] \quad (9.14)$$

where r_{c0} is the minimum radius of curvature at the bend apex, k_{wb} is the wave number of centerline of meandering, and a and b are as follows:

$$a = \frac{\lambda_f k_{wb} h (\vartheta + Fr^2 + 2)}{4\lambda_f^2 + (k_{wb}h)^2}, \quad b = \frac{2(\vartheta + Fr^2)\lambda_f^2 - (k_{wb}h)^2}{4\lambda_f^2 + (k_{wb}h)^2} \quad \wedge \quad Fr = \frac{\bar{U}}{(gh)^{0.5}} \quad (9.15)$$

The wave number in meandering rivers, according to Ikeda et al. (1981), is expressed as $k_{wb} = 1.5\lambda_f/h$.

The perturbed transverse velocity V' is given by

$$\frac{V'}{\bar{U}} = \frac{k_{wb}r_{c0}}{2} \cdot \frac{r_c}{r} \cdot \frac{h}{H} [a \cos(k_{wb}s) - (b + \vartheta + Fr^2) \sin(k_{wb}s)] \left[\left(\frac{B}{2r_{c0}}\right)^2 - \left(\frac{n}{r_{c0}}\right)^2 \right] \quad (9.16)$$

Assuming that the velocity defect law is preserved in streamwise velocity distributions in meandering rivers, the time-averaged streamwise velocity $\bar{u}(z)$ at any elevation z was obtained by Ikeda and Nishimura. It is

$$\frac{\bar{u}}{\bar{u}_*} = \varphi \frac{U}{\bar{U}} \left[\frac{\bar{U}}{\bar{u}_*} + \frac{1}{\kappa} (1 + \ln \hat{\eta}) \right] = \varphi \frac{U}{\bar{U}} \left[\frac{1}{\lambda_f^{0.5}} + \frac{1}{\kappa} G(\hat{\eta}) \right] \quad \wedge \quad \hat{\eta} = 1 + \frac{z}{H} \quad (9.17)$$

where φ is a function of $\hat{\eta}$ being unity in main flow zone and zero at the banks, $G(\hat{\eta}) = 1 + \ln \hat{\eta}$, and z is the vertical distance (Fig. 9.12b).

Then, centrifugally induced time-averaged transverse velocity component $v''(z)$ of the secondary current is given by

$$\frac{v''}{U} = \varphi^2 \left(\frac{U}{\bar{U}} \right)^2 \frac{H}{\kappa r} \chi \varphi_0 \frac{r_c}{r_{c0}} \cos(k_{wb}s - \sigma_L) \quad (9.18)$$

where χ is the factor for secondary current, $\varphi_0 = \varphi_1(\hat{\eta}) - \lambda_f^{0.5} \kappa^{-1} \varphi_2(\hat{\eta})$, $\varphi_1(\hat{\eta}) = -15(\hat{\eta}^2 \ln \hat{\eta} - 0.5\hat{\eta}^2 + 0.278)$, $\varphi_2(\hat{\eta}) = 7.5(\hat{\eta}^2 \ln^2 \hat{\eta} - \hat{\eta}^2 \ln \hat{\eta} + 0.5\hat{\eta}^2 - 0.352)$, and σ_L is the phase lag of the secondary current relative to meandering planform.

The vorticity equation for secondary current in a sinuous river is expressed as

$$\bar{u} \frac{\partial \Omega_s}{\partial s} - \frac{2}{r} \bar{u} \frac{\partial \bar{u}}{\partial z} = \varepsilon_t \frac{\partial^2 \Omega_s}{\partial z^2} \quad \wedge \quad \Omega_s \approx \frac{\partial v''}{\partial z} \quad (9.19)$$

where Ω_s is the vorticity of secondary current, which is approximated as above due to negligible time-averaged vertical velocity component, and ε_t is the turbulent diffusivity. At the centerline ($r = r_c$) of the meandering rivers, $\varphi = 1$, $U = \bar{U}$, and $H = h$. Using $r_c^{-1} = r_{c0}^{-1} \cos(k_{wb}s)$, Eq. (9.19) at the centerline becomes

$$\bar{U} \frac{\partial \Omega_s}{\partial s} - \frac{2 \cos(k_{wb}s)}{r_{c0}} \bar{U} \frac{\partial \bar{U}}{\partial z} = \varepsilon_t \frac{\partial^2 \Omega_s}{\partial z^2} \quad (9.20)$$

Substituting Eqs. (9.17) and (9.18) into Eq. (9.20) and then equating the coefficients of $\sin(k_{wb}s)$ and $\cos(k_{wb}s)$ to obtain two equations, the χ and σ_L are solved as

$$\chi = 2 \frac{dG}{d\hat{\eta}} \left(k_{wb} h \frac{\bar{U}}{\bar{u}_*} \cdot \frac{d\varphi_0}{d\hat{\eta}} \sin \sigma_L - \frac{\varepsilon_t}{\bar{u}_* h} \cdot \frac{d^3 \varphi_0}{d\hat{\eta}^3} \cos \sigma_L \right)^{-1} \quad (9.21a)$$

$$\sigma_L = \arctan \left[k_{wb} h \frac{d\varphi_0}{d\hat{\eta}} \left(\frac{\varepsilon_t}{\bar{u}_* h} \cdot \frac{\bar{u}_*}{\bar{U}} \cdot \frac{d^3 \varphi_0}{d\hat{\eta}^3} \right)^{-1} \right] \quad (9.21b)$$

Ikeda et al. (1985) proposed $\varepsilon_t/(\bar{u}_* h) = 0.1$ for the flow in sinuous rivers. Then, χ and σ_L take the forms

$$\chi = \left[k_{wb} h \left(\frac{1.11}{\lambda_f^{0.5}} - 1.42 \right) \sin \sigma_L + \cos \sigma_L \right]^{-1} \quad (9.22a)$$

$$\sigma_L = \arctan \left[k_{wb} h \left(\frac{1.11}{\lambda_f^{0.5}} - 1.42 \right) \right] \quad (9.22b)$$

Note that $k_{wb}h = 1.5\lambda_f$, as already stated.

The estimation of $\bar{u}(z)$ is possible from Eq. (9.17) using Eqs. (9.11), (9.14) and (9.15); and the time-averaged transverse velocity component $\bar{v}(z)$ can be calculated from the decomposition relationship $\bar{v} = V' + v''$, where V' is given by Eq. (9.16) and v'' can be obtained from Eq. (9.18) using Eqs. (9.22a, b).

9.3.1.2 Bed Deformation

In equilibrium state, the continuity equation of sediment transport resulting in a change of bed level is given and then its integral form is obtained as

$$\begin{aligned} \frac{r_c}{r} \cdot \frac{\partial q_{ts}}{\partial s} + \frac{1}{r} \cdot \frac{\partial (rq_{tn})}{\partial n} = 0 \quad \wedge \quad q_{ts} = q_{bs} + q_{ss} \quad \vee \quad q_{tn} = q_{bn} + q_{sn} \\ \Rightarrow q_{tn} = -\frac{r_c}{r} \int \frac{\partial q_{ts}}{\partial s} dn \end{aligned} \quad (9.23)$$

where q_{ts} and q_{tn} are the volumetric total-load transport rate in s - and r -direction, respectively, q_{bs} and q_{bn} are the volumetric bed-load transport rate in s - and r -direction, respectively, and q_{ss} and q_{sn} are the volumetric suspended-load transport rate in s - and r -direction, respectively.

Ikeda and Nishimura used Parker's (1979) formula, (Eq. 5.24), to estimate q_{bs} . Equation (5.24) is rearranged as

$$q_{bs} = 11.2(\Delta g d_{50}^3)^{0.5} \frac{(\Theta - 0.03)^{4.5}}{\Theta^3} \quad (9.24)$$

where Θ is the Shields parameter, which is $u_*^2/(\Delta g d_{50})$ for a horizontal bed of a straight river. Here, u_* is the local shear velocity. Due to helicoidally curvilinear flow in meandering rivers, Θ is corrected as

$$\Theta = \varphi^2 \left(\frac{U}{\bar{U}} \right)^2 \frac{\bar{u}_*^2}{\Delta g d_{50}} \quad (9.25)$$

Parker (1984) gave

$$\frac{q_{bn}}{q_{bs}} = \tan \beta + \frac{1 + \eta_R \mu}{\xi_s \mu} \left(\frac{\Theta_c}{\Theta} \right)^{0.5} \tan \alpha \quad \wedge \quad \alpha = \arctan \frac{\partial \eta}{\partial n}$$

where β is the angle made by the near-bed limiting streamline with s -direction, that is, $\arctan(\bar{v}_d/\bar{u}_d)$, \bar{v}_d is the near-bed time-averaged transverse velocity, \bar{u}_d is the near-bed time-averaged streamwise velocity, Θ_c is the threshold Shields parameter, and α is the angle made by the transverse bed slope with horizontal. For sand-beds, Kikkawa et al. (1976) approximated μ , η_R , and ξ_s as 0.43, 0.85 and 0.59, respectively; and the above equation becomes

$$\frac{q_{bn}}{q_{bs}} = \tan \beta + 5.38 \left(\frac{\Theta_c}{\Theta} \right)^{0.5} \frac{\partial \eta}{\partial n} \quad (9.26)$$

Ikeda and Nishimura obtained \bar{u}_d from the logarithmic law of velocity distribution for hydraulically rough flow applied to the roughness height level k_s as

$$\bar{u}_d = u_* \left(8.5 + \frac{1}{\kappa} \ln \frac{z+H}{k_s} \right)_{|z=-H+k_s} = 8.5u_* \quad \wedge \quad u_* = \varphi \frac{U}{\bar{U}} \bar{u}_* \quad (9.27)$$

$$\Rightarrow \bar{u}_d = 8.5\varphi \frac{U}{\bar{U}} \bar{u}_*$$

They obtained \bar{v}_d from the relationship $\bar{v} = V' + v''$, where $v''(\hat{\eta} = 0)$ at the bed is obtained from Eq. (9.18). Then, $\tan \beta$ is given by

$$\tan \beta = \left[\frac{V'}{\bar{U}} + \varphi^2 \left(\frac{U}{\bar{U}} \right)^2 \frac{H}{\kappa r} \chi \varphi_0(0) \frac{r_c}{r_{c0}} \cos(k_{wb}s - \sigma_L) \right] \left[8.5\varphi \left(\frac{U}{\bar{U}} \right) \lambda_f^{0.5} \right]^{-1} \quad (9.28)$$

where $\varphi_0(0) = -4.167 + 2.64 \lambda_f^{0.5} \kappa^{-1}$.

The suspended-load transport rate q_{ss} in s -direction and time-averaged concentration distribution $C(z)$ are given by

$$q_{ss} = \int_{-H}^0 C \bar{u} dz \quad (9.29a)$$

$$C = C_a \exp \left[-\frac{w_s}{\varepsilon_s} (z + H) \right] \quad (9.29b)$$

where C_a is the near-bed concentration, w_s is the terminal fall velocity of sediment, and ε_s is the sediment diffusivity. Above equations are the modified forms of Eqs. (6.1a) and (6.20) due to change of position of the origin of z -axis. The sediment diffusivity ε_s can be assumed as follows (Vanoni 1975):

$$\varepsilon_s = 0.077u_*H \quad (9.30)$$

Further, Ikeda and Nishimura (1985) gave C_a in empirical form as

$$C_a(u_* \leq 88.3w_s) = 2.31 \times 10^{-4} \left(\frac{u_*}{w_s} \right)^{1.6}, \quad C_a(u_* > 88.3w_s) = 0.3 \quad (9.31)$$

Inserting Eqs. (9.17) and (9.29b) into Eq. (9.29a) yields

$$\frac{q_{ss}}{UH} = \varphi \frac{U}{U} \Phi_{ss} \quad (9.32)$$

where

$$\begin{aligned} \Phi_{ss} = & C_a \{ [\psi_1 - \psi_2 \exp(\varpi^{-1})] \varpi + [\psi_3 - \psi_4 \exp(\varpi^{-1})] \varpi^2 \\ & + [\psi_5 - \psi_6 \exp(-\varpi^{-1})] \varpi^3 + \psi_7 [1 - \exp(-\varpi^{-1})] \varpi^4 \}, \\ \varpi = & \varepsilon_s / (w_s H) = 0.077u_* / w_s = 0.077\varphi U \bar{u}_* / (\bar{U} w_s), \quad \psi_1 = 1 - 5.798\lambda_f^{0.5}, \\ \psi_2 = & 1 + 2.678\lambda_f^{0.5}, \quad \psi_3 = 26.6\lambda_f^{0.5}, \quad \psi_4 = 6.95\lambda_f^{0.5}, \quad \psi_5 = -69.45\lambda_f^{0.5}, \\ \psi_6 = & 30.15\lambda_f^{0.5}, \text{ and } \psi_7 = 99.6\lambda_f^{0.5}. \end{aligned}$$

The suspended-load transport rate q_{sn} in n -direction is given by

$$q_{sn} = \int_{-H}^0 C \bar{v} dz \quad (9.33)$$

Inserting expressions for $\bar{v} (= V' + v'')$ and Eq. (9.29b) into Eq. (9.33) yields

$$\frac{q_{sn}}{UH} = \frac{V'}{U} \Phi_{sn1} - \varphi^2 \left(\frac{U}{U} \right)^2 \frac{H}{\kappa r} \chi \frac{r_c}{r_{c0}} \cos(k_{wb}s - \sigma_L) \Phi_{sn2} \quad (9.34)$$

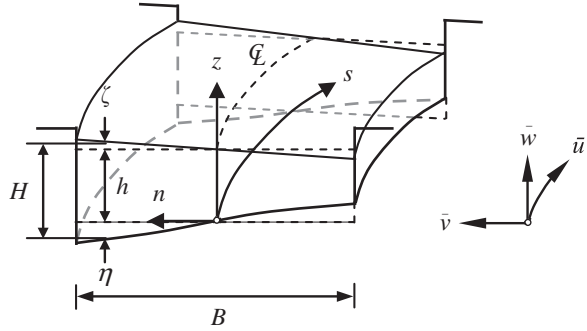
where $\Phi_{sn1} = C_a [1 - \exp(-\varpi^{-1})] \varpi$, $\Phi_{sn2} = C_a \{ [\xi_1 \exp(-\varpi^{-1}) - \xi_2] \varpi + [\xi_3 \exp(-\varpi^{-1}) - \xi_4] \varpi^2 + [\xi_5 \exp(-\varpi^{-1}) - \xi_6] \varpi^3 - 72.34 [\exp(-\varpi^{-1}) - 1] \varpi^4 \}$, $\xi_1 = 3.26 - 2.58\lambda_f^{0.5}$, $\xi_2 = -4.29 + 7.005\lambda_f^{0.5}$, $\xi_3 = -1.57 + 3.69\lambda_f^{0.5}$, $\xi_4 = 4.61 - 22.86\lambda_f^{0.5}$, $\xi_5 = -42.36 + 26.55\lambda_f^{0.5}$, and $\xi_6 = 15 + 13.28\lambda_f^{0.5}$.

Equation of bed-level variation can be obtained by substituting Eq. (9.26) into Eq. (9.23) as

$$\frac{\partial \eta}{\partial n} = -0.186 \left(\frac{\Theta}{\Theta_c} \right)^{0.5} \frac{1}{q_{bs}} \left[\frac{r_c}{r} \int \frac{\partial}{\partial s} (q_{bs} + q_{ss}) dn + q_{sn} + q_{bs} \tan \beta \right] \quad (9.35)$$

The bed- and suspended-load transport rates, q_{bs} , q_{bn} , q_{ss} , and q_{sn} , are obtained from Eqs. (9.24), (9.26), (9.32) and (9.34), respectively. The partial derivative

Fig. 9.13 Definition sketch showing cross-section of a sinusoidal river



$\partial q_{bs}/\partial s$ can be obtained from Eq. (9.24) by using Eqs. (9.11), (9.14) and (9.25). Further, $\partial q_{ss}/\partial s$ can be obtained from Eq. (9.32) in terms of H and u_* . Using the relationship given by Ikeda et al. (1981), that is, $\zeta = Fr^2 hn/r_c$, and Eq. (9.13), H is expressed as

$$H = h \left[Fr^2 \frac{n}{r_c} + \left(\frac{r}{r_c} \right)^{\vartheta} \right] \quad (9.36)$$

Thus, the term $\partial(q_{bs} + q_{ss})/\partial s$ in Eq. (9.35) can take the form

$$\begin{aligned} & \frac{1}{\bar{U}h} \cdot \frac{1}{k_{wb}} \cdot \frac{\partial}{\partial s} (q_{bs} + q_{ss}) \\ &= \varphi \frac{n}{r_{c0}} \left\{ \Psi_{bs} + \left[Fr^2 \frac{n}{r_c} + \left(\frac{r}{r_c} \right)^{\vartheta} \right] (\Phi_{ss} + \Psi_{ss}) \right\} \\ & \times [a \cos(k_{wb}s) - b \sin(k_{wb}s)] - \varphi \frac{U}{\bar{U}} \cdot \frac{n}{r_{c0}} \left[Fr^2 + \vartheta \left(\frac{r}{r_c} \right)^{\vartheta-1} \right] \Phi_{ss} \sin(k_{wb}s) \end{aligned} \quad (9.37)$$

where

$$\Psi_{bs} = 33.6 \frac{(\Delta g d_{50}^3)^{0.5}}{\bar{U}h} \varphi \frac{U}{\bar{U}} \cdot \frac{\bar{u}_*^2}{\Delta g d_{50}} \cdot \frac{(\Theta + 0.06)(\Theta - 0.03)^{3.5}}{\Theta^4},$$

$\Psi_{ss} = C_a \{ -\gamma_1 \exp(-\varpi^{-1}) + [\gamma_2 - \gamma_3 \exp(-\varpi^{-1})] \varpi + [\gamma_4 - \gamma_5 \exp(-\varpi^{-1})] \varpi^2 + [\gamma_6 - \gamma_7 \exp(-\varpi^{-1})] \varpi^3 + \gamma_8 [1 - \exp(-\varpi^{-1})] \varpi^4 \}$, $\gamma_1 = 26.6 \lambda_f^{0.5}$, $\gamma_2 = 2.6 - 15.07 \lambda_f^{0.5}$, $\gamma_3 = 2.6 + 13.91 \lambda_f^{0.5}$, $\gamma_4 = 95.76 \lambda_f^{0.5}$, $\gamma_5 = 55.17 \lambda_f^{0.5}$, $\gamma_6 = -319.5 \lambda_f^{0.5}$, $\gamma_7 = 238.3 \lambda_f^{0.5}$, and $\gamma_8 = 557.8 \lambda_f^{0.5}$. Then, the integration in Eq. (9.35) can be performed with the determination of integral constant from the condition that the average variation of bed level across the cross-section is zero, that is

$$\int_{-0.5B}^{0.5B} \eta dn = 0$$

9.3.2 Odgaard's Model

9.3.2.1 Flow Field and Bed Topography

Odgaard (1989) considered orthogonal curvilinear coordinates (s, n, z) to represent time-averaged velocity components $(\bar{u}, \bar{v}, \bar{w})$ and bed variations, as shown in Fig. 9.13. The plan view of a sinusoidal river is same as shown in Fig. 9.12a. In meandering rivers, the prevailing conditions are the flow depth to be smaller than the flow width ($H \ll B$) and the radius of curvature to be generally larger than the width ($r_c > B$). Under these conditions, all the terms containing \bar{w} can be dropped out in momentum and continuity equations as $\bar{w} \rightarrow 0$. This approximation makes the problem a two-dimensional. According to Rozovskii (1957), the two-dimensional momentum equations of flow can be written as

$$\bar{u} \frac{\partial \bar{u}}{\partial s} + \bar{v} \frac{\partial \bar{u}}{\partial n} + \frac{\bar{u}\bar{v}}{r} = \frac{1}{\rho} \left(-\frac{\partial \bar{p}}{\partial s} + \frac{\partial \tau_s}{\partial z} \right) \quad (9.38a)$$

$$\bar{u} \frac{\partial \bar{v}}{\partial s} + \bar{v} \frac{\partial \bar{v}}{\partial n} - \frac{\bar{u}^2}{r} = \frac{1}{\rho} \left(-\frac{\partial \bar{p}}{\partial n} + \frac{\partial \tau_n}{\partial z} \right) \quad (9.38b)$$

where r is the local radius of curvature, \bar{p} is the time-averaged hydrostatic pressure, and τ_s and τ_n are the shear stresses in s - and n -direction, respectively. The continuity equations of flow and sediment transport are

$$\frac{\partial \bar{u}}{\partial s} + \frac{1}{r} \cdot \frac{\partial (\bar{v}r)}{\partial n} = 0 \quad (9.39a)$$

$$\frac{\partial q_{bs}}{\partial s} + \frac{1}{r} \cdot \frac{\partial (q_{bn}r)}{\partial n} = 0 \quad (9.39b)$$

where q_{bs} and q_{bn} are the bed-load transport in s - and n -direction, respectively.

The integration (with respect to depth) of the pressure containing terms in Eqs. (9.38a, b) can be expressed in terms of the free-surface slopes (S_s and S_n) as $-gS_s$ in s -direction and $-gS_n$ in n -direction. Here, g is the acceleration due to gravity. Thus, the depth-averaged momentum and continuity equations become

$$U \frac{\partial U}{\partial s} + V \frac{\partial U}{\partial n} + \frac{UV}{r} = gS_s - \frac{\tau_{0s}}{\rho H} \quad (9.40a)$$

$$U \frac{\partial V}{\partial s} + V \frac{\partial V}{\partial n} - \frac{U^2}{r} = gS_n - \frac{\tau_{0n}}{\rho H} \quad (9.40b)$$

and

$$\frac{\partial(UH)}{\partial s} + \frac{1}{r} \cdot \frac{\partial(VHr)}{\partial n} = 0 \quad (9.41)$$

where U and V are the depth-averaged velocities in s - and n -direction, respectively, and τ_{0s} and τ_{0n} are the bed shear stresses in s - and n -direction, respectively. In the above, the approximate relationships are used as $\bar{u}\bar{v} \approx UV$ and $\bar{u}\bar{u} \approx U^2$, which are based on the field and laboratory experimental data (Dietrich and Smith 1983; Bergs 1989).

The \bar{u} distribution is represented by a power law as

$$\frac{\bar{u}}{U} = \frac{1+m}{m} \left(\frac{z}{H} \right)^{1/m} \quad \wedge \quad m = \kappa \frac{U}{u_*} = \kappa \left(\frac{8}{\lambda_D} \right)^{0.5} = \kappa \frac{C_R}{g^{0.5}} \quad \vee \quad u_* = \left(\frac{\tau_{0s}}{\rho} \right)^{0.5} \quad (9.42)$$

where m is an exponent indicating resistance to flow, λ_D is the Darcy–Weisbach friction factor, and C_R is the Chézy coefficient. Above relationship for m was given by Zimmermann and Kennedy (1978). In bankfull conditions, the m is $3 \leq m \leq 5$.

On the other hand, the \bar{v} distribution is represented as an addition of V and centrifugally induced transverse velocity component $v''(z)$ of the secondary current, which is approximated by a linear law as $2v_0''[(z/H)-0.5]$, where $v_0'' = v''(z = h + \zeta)$ (Rozovskii 1957; Kikkawa et al. 1976). Thus,

$$\bar{v} = V + v'' = V + 2v_0'' \left(\frac{z}{H} - \frac{1}{2} \right) \quad (9.43)$$

Subtracting Eq. (9.40b) from Eq. (9.38b) at $z = h + \zeta$ yields

$$\bar{u}_0 \frac{\partial \bar{v}_0}{\partial s} - U \frac{\partial V}{\partial s} + \bar{v}_0 \frac{\partial \bar{v}_0}{\partial n} - V \frac{\partial V}{\partial n} = \frac{\bar{u}_0^2 - U^2}{r} + \frac{\tau_{0n}}{\rho H} + \frac{1}{\rho} \cdot \frac{\partial \tau_n}{\partial z} \Big|_{z=h+\zeta} \quad (9.44)$$

where $\bar{u}_0 = \bar{u}(z = h + \zeta)$ and $\bar{v}_0 = \bar{v}(z = h + \zeta)$. The partial derivative in the last term of the right-hand side of Eq. (9.44) can be determined as

$$\frac{\partial \tau_n}{\partial z} = \frac{\partial}{\partial z} \left(\varepsilon_t \frac{\partial \bar{v}}{\partial z} \right)$$

Then, by solving ε_t from the power law and $\tau_s = \tau_{0s}[1 - (z/H)]$ and assuming an isotropic ε_t with \bar{v} given by Eq. (9.43), the above partial derivative at free surface is obtained as

$$\left. \frac{\partial \tau_n}{\partial z} \right|_{z=h+\zeta} = -\frac{m}{1+m} \cdot \frac{2\rho\kappa v_0'' u_*}{H} \quad (9.45)$$

The ratio of τ_{0n} to τ_{0s} is obtained from the deflection of the near-bed limiting streamline from s -axis, that is, $\tan\beta = \bar{v}_d/\bar{u}_d$. Then,

$$\frac{\tau_{0n}}{\tau_{0s}} = \frac{\bar{v}_d}{\bar{u}_d} = \frac{V - v_0''}{U} \quad (9.46)$$

Note that the expression for m in Eq. (9.42) leads to

$$\tau_{0s} = \rho\kappa^2 \frac{1}{m^2} U^2 \quad (9.47)$$

Substituting Eqs. (9.42), (9.43) and (9.47) into Eq. (9.40a) yields

$$\frac{1}{2} \cdot \frac{\partial U^2}{\partial s} + \frac{\kappa^2}{m^2 H} U^2 = gS_s - V \left(\frac{\partial U}{\partial n} + \frac{U}{r} \right) \quad (9.48)$$

Substituting Eqs. (9.42), (9.43), (9.45) and (9.46) into Eq. (9.44) yields

$$\begin{aligned} \frac{\partial V}{\partial s} + (1+m) \frac{\partial v_0''}{\partial s} + \frac{m}{U} \cdot \frac{\partial(v_0'' V)}{\partial n} + \frac{m}{2U} \cdot \frac{\partial(v_0'' v_0'')}{\partial n} \\ = \frac{1+2m}{m} \cdot \frac{U}{r} + \frac{\kappa^2}{mH} V - \frac{\kappa^2}{mH} \left(1 + \frac{2m^2}{1+m} \right) v_0'' \end{aligned} \quad (9.49)$$

Thus, the above mathematical analysis produces Eqs. (9.39a, b), (9.48) and (9.49) as governing equations for solving V , H , U , and v_0'' , respectively.

From field and laboratory results, Odgaard argued that the variables \bar{u} and H are essentially constant along the centerline, but vary somewhat linearly in transverse direction. Hence, they are linearized with respect to their centerline values:

$$\frac{U}{U_c} = 1 + \frac{n}{h} \tilde{U}_{cn} \quad \wedge \quad \tilde{U}_{cn} = \left[h \frac{\partial}{\partial n} \left(\frac{U}{U_c} \right) \right]_c \quad (9.50a)$$

$$\frac{H}{h} = 1 + \frac{n}{h} S_{cn} \quad \wedge \quad S_{cn} = \left. \frac{\partial H}{\partial n} \right|_c \quad (9.50b)$$

where U_c and h are the depth-averaged velocity and flow depth at the centerline, respectively, \tilde{U}_{cn} is the nondimensional transverse velocity gradient at the centerline, and S_{cn} is the transverse gradient of the bed at the centerline. In the above,

subscript “c” refers to the centerline value. From Eq. (9.41), V_c is obtained as an integral equation and then solved using Eqs. (9.50a, b) and $r = r_c + n$. Thus,

$$V_c = \frac{1}{hr_c} \cdot \frac{d}{ds} \int_0^{0.5B} rUHdn \Rightarrow V_c = \frac{\alpha_n}{8} U_c \frac{B^2}{h} \cdot \frac{d}{ds} (S_{cn} + \tilde{U}_{cn}) \quad (9.51)$$

where α_n is the transverse flux correction factor having an average value of 0.4.

Odgaard assumed $q_{bs} = [q_{bs}]_c (U/U_c)^M$, where $[q_{bs}]_c$ is the bed-load transport rate in s -direction at the centerline and M is an exponent varying from 2 to 4 (Simons and Sentürk 1977). Then, integration of Eq. (9.39b) yields

$$[q_{bn}]_c = \frac{1}{r_c} \cdot \frac{d}{ds} \int_0^{0.5B} q_{bs} r dn \Rightarrow [q_{bn}]_c = [q_{bs}]_c \frac{\beta_n}{8} \cdot \frac{B^2}{h} M \frac{d\tilde{U}_{cn}}{ds} \quad (9.52)$$

where $[q_{bn}]_c$ is the bed-load transport rate in n -direction at the centerline and β_n is the transverse sediment flux correction factor have an order of magnitude same as that of α_n .

Using Eqs. (9.26), (9.46) and (9.47), Eq. (9.52) yields

$$\frac{5.38}{\kappa} m (\Delta g d_{50})^{0.5} \Theta^{0.5} S_{cn} = \frac{\alpha_n}{8} \cdot \frac{B^2}{h} U_c M \frac{d\tilde{U}_{cn}}{ds} + [v_0'']_c - V_c \quad (9.53)$$

Substituting Eqs. (9.50a, b), (9.51) and (9.53) into Eqs. (9.48) and (9.49) and neglecting higher order terms, the resulting linear equations are

$$\frac{d\tilde{U}_{cn}}{d\hat{s}} + a_1 \tilde{U}_{cn} = \frac{1}{2} a_1 S_{cn} \quad \wedge \quad \hat{s} = \frac{s}{B} \quad (9.54a)$$

$$\frac{d^2 S_{cn}}{d\hat{s}^2} + a_2 \frac{d^2 \tilde{U}_{cn}}{d\hat{s}^2} + a_3 \frac{dS_{cn}}{d\hat{s}} + a_4 \frac{d\tilde{U}_{cn}}{d\hat{s}} + a_5 S_{cn} = a_6 \quad (9.54b)$$

where

$$\begin{aligned} a_1 &= \frac{2\kappa^2}{m^2} \cdot \frac{B}{h}, \quad a_2 = 1 - \frac{1+m}{2+m} M, \quad a_3 = 43 \frac{\Theta^{0.5}}{\alpha_n \kappa F_d} \cdot \frac{m(1+m)}{2+m} \cdot \frac{h}{B} \\ &+ \frac{2\kappa^2 m}{(1+m)(2+m)} \cdot \frac{B}{h}, \quad a_4 = \frac{2\kappa^2 m}{(1+m)(2+m)} \left[1 - M \left(1 + \frac{1}{2m} + \frac{1}{2m^2} \right) \right] \frac{B}{h}, \\ a_5 &= 43 \frac{\kappa \Theta^{0.5}}{\alpha_n (2+m) F_d} \left(1 + \frac{2m^2}{1+m} \right), \quad a_6 = \frac{8}{\alpha_n} \cdot \frac{1+2m}{m(2+m)} \cdot \frac{h}{r_c} \end{aligned}$$

where F_d is the densimetric Froude number $[= U_c / (\Delta g d_{50})^{0.5}]$. Further, using Eq. (9.54a), Eq. (9.54b) is rearranged as

$$\frac{d^3 \tilde{U}_{cn}}{d\hat{s}^3} + b_1 \frac{d^2 \tilde{U}_{cn}}{d\hat{s}^2} + b_2 \frac{d\tilde{U}_{cn}}{d\hat{s}} + b_3 \tilde{U}_{cn} = b_4 \quad (9.55)$$

where $b_1 = a_1 + 0.5a_1a_2 + a_3$, $b_2 = a_1a_3 + 0.5a_1a_4 + a_5$, $b_3 = a_1a_5$, and $b_4 = 0.5a_1a_6$. Equation (9.55) can be solved for \tilde{U}_{cn} for the given boundary conditions, and then, S_{cn} can be determined from Eq. (9.54a).

Note that in fully developed flow in a channel bend, the terms $d(\cdot)/d\hat{s} = 0$, and Eqs. (9.54a, b) reduce to

$$\frac{U}{U_c} = \left(\frac{H}{h}\right)^{0.5}, \quad S_{cn0} = \frac{GF_{dc}h}{r_c} \quad \wedge \quad G = \frac{(1+m)(1+2m)}{5.38\kappa\Theta^{0.5}m(1+m+2m^2)}$$

where S_{cn0} is the fully developed value of S_{cn} and F_{dc} is the F_d at the centerline.

An approximate solution of Eqs. (9.54a, b) can be obtained assuming $d^2\tilde{U}_{cn}/d^2\hat{s}$ to be negligible. Then, Eqs. (9.54a, b) produce

$$\frac{d^2 S_{cn}}{d\hat{s}^2} + \left(a_3 + \frac{a_4}{2}\right) \frac{dS_{cn}}{d\hat{s}} + a_5 S_{cn} = a_6 \quad (9.56)$$

At the starting section of the bend (that is $\hat{s} = 0$), both S_{cn} and $dS_{cn}/d\hat{s}$ vanish; and the solution of Eq. (9.56) is

$$S_{cn} = S_{cn0} \left\{ 1 - \left[1 + \left(\frac{a_0}{2\phi_0} \right)^2 \right]^{0.5} \cos(\phi_0\hat{s} - \psi_0) \exp\left(-\frac{a_0\hat{s}}{2}\right) \right\} \quad (9.57)$$

where $\phi_0 = 0.5(4a_5 - a_0^2)^{0.5}$, $a_0 = a_3 + 0.5a_4$, and $\psi_0 = \arctan(0.5a_0/\phi_0)$.

9.3.2.2 Stability of Meandering Rivers

In stability analysis, Odgaard (1989) introduced a small perturbation in the form of a traveling sinusoidal wave to the system of governing equations of a river flow coupled with the sediment transport. Then, their effect on river planform is determined by evaluating the growth rate of perturbation. The perturbation due to a traveling sinusoidal wave is introduced as river displacement $\xi(x, t)$ given by

$$\xi(x, t) = a_{mc}(t) \sin[k_{wb}(x - ct)] \quad (9.58)$$

where x is the coordinate distance along the unperturbed river axis or the valley slope (Fig. 9.12a), k_{wb} is the wave number ($= 2\pi/\lambda_m$), a_{mc} is the amplitude, λ_m is the meandering wavelength, c is the celerity of sinusoidal wave, and t is the time.

Approximating local radius of curvature as $r_c^{-1} = -d^2\xi/dx^2$ and using Eq. (9.58), Eq. (9.55) is solved for \tilde{U}_{cn} as

$$\tilde{U}_{cn} = \frac{Bk_{wb}^2 a_{mc}}{(e_1^2 + e_2^2)^{0.5}} N \sin[k_{wb}(x - ct) - \gamma_0] \quad \wedge \quad \gamma_0 = \arctan\left(\frac{e_2}{e_1}\right) \quad (9.59)$$

where $e_1 = b_3 - 2b_1 B^2 k_{wb}^2$, $e_2 = b_2 B k_{wb} - k_{wb}^3 B^3$, and

$$N = \frac{8\kappa^2}{\alpha_n} \cdot \frac{1 + 2m}{m^3(2 + m)}.$$

Substituting Eq. (9.59) into Eq. (9.54a) yields

$$S_{cn} = \frac{2Bk_{wb}^2 a_{mc}}{(e_1^2 + e_2^2)^{0.5}} N \left[1 + \left(\frac{Bk_{wb}}{a_1} \right)^2 \right]^{0.5} \sin[k_{wb}(x - ct) - \beta_0] \quad (9.60)$$

where $\beta_0 = \gamma_0 - \arctan(Bk_{wb}/a_1)$.

Odgaard assumed that the rate of bank retreat ξ_b is linearly proportional to the change of bed level at the bank:

$$\xi_b = EU_c \left(\frac{H_{bank}}{h} - 1 \right) \quad (9.61)$$

where E is the erosion parameter and H_{bank} is the near-bank value of H . Due to small curvature of the river, $\xi_b \approx \partial \xi / \partial t$. The closure of the analysis is achieved by substituting Eq. (9.58) into left-hand side of Eq. (9.61) and Eqs. (9.59) and (9.60) into right-hand side of Eq. (9.61). Performing required simplifications, the equations of growth rate of amplitude $\partial a_{mc} / \partial t$ and celerity c are obtained as follows:

$$\frac{1}{a_{mc}} \cdot \frac{\partial a_{mc}}{\partial t} = \frac{2EU_c}{B} KBk_{wb} \left[1 + \left(\frac{Bk_{wb}}{a_1} \right)^2 \right]^{0.5} \cos \beta_0 \quad \wedge \quad K = \frac{NB}{2h} \cdot \frac{Bk_{wb}}{(e_1^2 + e_2^2)^{0.5}} \quad (9.62a)$$

$$c = 2EU_c K \left[1 + \left(\frac{Bk_{wb}}{a_1} \right)^2 \right]^{0.5} \sin \beta_0 \quad (9.62b)$$

Note that the wave number k_{wb} corresponding to maximum amplitude growth, called *dominant wave number*, can be determined from the following condition:

$$\frac{\partial^2 a_{mc}}{\partial t \partial k_{wb}} = 0$$

9.4 Braided Rivers

Braided rivers are quite dynamic with strong fluvial activities (interactions between streambed morphology, flow, and sediment transport) to follow rapidly change in subdivided stream forms. The bars and islands characterize braiding by dividing streams by their sides. While bars are relatively unstable having complex features, islands are rather stable with well-defined shapes. Bars are modified by the processes of erosion and deposition and evolve over a short period of time. During high flow stages, major changes take place due to rapid rates of stream migration facilitated by high stream power and unstable banks. There can also be extensive changes in stream position as subdivided streams are abandoned or earlier abandoned streams are reactivated. However, even in a braided reach, a single dominant stream, in some cases, can be distinguishable. Planform of braided rivers can change radically with the change in discharge. For instance, Bristow and Best (1993) argued that the discharge fluctuations are a prerequisite for braiding especially in sand-bed rivers. Rivers may act as a single stream during bankfull conditions and exhibit characteristic braided pattern at lower stages. Therefore, the number of bars to be emerged may vary with flow stages; as such, complex sequence of erosion and deposition may occur with the variation of flow stages. Nevertheless, at both low and high stages, some of the rivers show braided pattern where some of the islands are in general permanent. Southard et al. (1984) reported that the process of bar growth and streambed erosion occurs almost simultaneously, and the majority of the emerged bars are the result of complex events of erosion and deposition. Robert (2003) gave a good overview on braided rivers.

Lane (1957) studied planforms of many braided rivers and their history. He came out with a conclusion that the braiding can be caused by (1) overloading and (2) steep slopes. *Overloading* refers to when the sediment discharge (inflow transport rate) exceeds the sediment capacity (outflow transport rate) of a river depositing sediment load (aggradations) throughout the reach. As a consequence, the river carrying most of the sediment load gradually changes its morphology as the excess sediment load settles progressively in the downstream direction. Besides, the fining of bed sediment size takes place in the downstream direction and is usually accompanied by a downstream reduction in bed slope. The deposition of sediment in an aggrading river makes it out of bankfull conditions. The river tends to widen and becomes shallow with an appearance of bars subjected to changes in morphology. At low stages, a series of small streams divide and rejoin through the exposed bars in more or less regular and repeatable processes. These streams are braided as the bed slope enhances with aggradations. On the other hand, *steep slope* that induces greater stream power for the given discharge results in a wide shallow river in which bars and islands are readily developed. Stream subdivision is continued until there is inadequate stream power to erode the banks (Leopold and Wolman 1957). A distinction is often made between bars and islands, although they have the same origin and may share similar morphological characteristics. While bars are only developed at low stages being unvegetated, but

often submerged in bankfull conditions, islands are more stable and may be vegetated, but emerge even in bankfull conditions.

Carson and Griffiths (1987) recognized three types of braided rivers: unstable multiple stream, stable multiple stream, and multi-thalweg. In *unstable multiple-stream pattern*, streams are separated by the bars and can be rapidly diverted from one stream to another depending on sediment deposition. *Stable multiple-stream pattern* consists of relatively stable streams even during high flow stages with subdivided streams separated by stable vegetated islands. On the other hand, *multi-thalweg* pattern is characterized by braids being separated by submerged bars during high flow stages.

9.4.1 Mechanism of Braid Formation

Complex mechanisms are involved in inception and development of braided planforms, depending on the stream flow characteristics and both erosional and depositional processes. Ashmore (1991) identified four types of mechanisms of braid formation: middle bar accretion, transverse bar conversion, chute cutoff, and multiple bar dissection. A summary of various mechanisms put forward by different investigators is presented below:

Leopold and Wolman (1957) were the first to study the mechanism of inception and development of braided planforms through laboratory experiments. They identified that the development of braided planforms by *middle bar accretion* takes place through a sequence of events that comprise of deposition in mid-river and erosion of banks. The characteristic shape of middle bars (also called *linguoid bars*) is rhombic or lobate in plan view and elongated in streamwise direction. In an unbraided river reach, localized flow converges to a high velocity at the upstream end of the narrower flanking river reach leading to an excessive erosion. It forms a sheet of bed-load sediment (that includes coarser to finer size fractions) that is transported along the riverbed. In transporting the bed load, a small submerged gravel bar where the flow becomes locally incompetent to transport the coarsest particles, called *lag deposits*, is formed. The upstream of the bar margin is made up by the coarse fraction of bed-load sediment that is transported along the middle portion of the river. Finer particles are in general transported over the bar, while a fraction of finer particles are deposited on the bar and/or trapped behind the coarser particles, leading to the enlargement of the emerging bar in all dimensions (vertical, streamwise, and transverse directions). Once the bar becomes sufficiently large, it starts affecting the divided streams along its sides by increase in the flow velocity or in turn, the stream power, which begins to attack the banks and widens the river by bank erosion. The bar gradually gets stabilized due to more deposition on and around it. The feedback process then recurs in another place along the river, eventually leading to the formation of braided planforms. Ashmore (1991) observed that the mechanism of middle bar formation is restricted to the near-threshold flow conditions (that is, the Shields parameter Θ is in the order of 0.06).



Fig. 9.14 Photograph of a middle bar in a river (courtesy of A. Radecki-Pawlik, Polish Academy of Sciences, Poland)

The mechanism therefore involves the deposition of coarser particles carried as a bed load by the stream flow, where a small change of local flow depth can be adequate to reduce the local bed shear stress below the threshold bed shear stress, being incompetent to transport the coarser particles. Figure 9.14 displays a photograph of a middle bar in a river.

In an experimental study, Ashmore (1991) observed that another kind of bar formation process, called the *transverse bar conversion*, is prevalent. The main morphological feature of a transverse bar is that it has downstream avalanche faces being developed under high stream power conditions. Initially, a contracted chute (narrow channel) with steep sides is formed due to bed erosion by the flow convergence, which possesses an enhanced stream power. Consequently, a substantial amount of sediment is removed due to the chute erosion and transported downstream. As a part of this process, as the flow diverges out of the contracted chute with a declining flow competency to carry sediment, a massive sediment load is then deposited forming an incipient bar. As the time progresses, the bed load continues to deposit in succession in the form of layers as it passes over and across the bar. This process contributes to the vertical accretion of the bar form by building up its surface. In the process of deposition of sediment, a steep slant face is formed where the deposited sediment starts to avalanche over the downstream edges of the bar. As the elevation of the bar grows, the emerging bar starts to



Fig. 9.15 Photograph of a transverse bar in a river (courtesy of A. Radecki-Pawlik, Polish Academy of Sciences, Poland)



Fig. 9.16 Photograph of the chute cutoff of a point bar in a river (courtesy of A. Radecki-Pawlik, Polish Academy of Sciences, Poland)

obstruct the flow that is then deflected off the edges of the bar. The mechanism of middle bar formation is thus different from that of transverse bar, where the bar accretions are initiated by the erosion and extensive deposition of large amount of bed load, rather than the deposition of only the coarser sediment particles which are locally incompetent to transport by the flow. In contrast to middle bars, when the bed shear stress is considerably greater than its threshold value, it is possible for the large amount of sediment required for the transverse bar mechanism to be eroded and deposited (Ashmore 1991). Figure 9.15 shows a photograph of a transverse bar in a river.



Fig. 9.17 Photograph of a dissected bar in a river (courtesy of A. Radecki-Pawlik, Polish Academy of Sciences, Poland)

According to Ashmore (1991), other two mechanisms involved in the formation of a braid can be described as erosional processes. They are *chute cutoff* and *multiple bar dissection*. In *chute cutoff*, the development of a chute due to bed erosion across a point bar is prevalent during the inception of braiding. Eventually, the point bar is separated off from the bank (Fig. 9.16). Chute, in this case, represents a relatively narrow stream that occurs due to flow concentration to run through a point bar surface. Chute cutoff may occur on single point bars in existing braided rivers or across alternate point bars in moderately straight rivers. In a developed state, the size of chute may become almost similar to that of main stream on the other side of the separated point bar. Further, middle bars can also be cutoff by a single stream or multiple streams exhibiting *multiple bar dissection* (Rundle 1985a, b). Flow concentration is responsible to the formation of cutoff into the bar surface. The dissection of bars usually occurs during high flow stages when the flow crosses over the submerged bar surface. In low flow stages, the dissected bars are exposed as two or more in numbers of smaller bars, as shown in Fig. 9.17.

There are additional situations associated with the braid formations that need to be discussed. *Avulsion* is defined as a relatively abrupt switching of the stream flow from one branch to another (Ferguson 1993). This situation prevails when chute cutoffs form. Also it may occur when the stream flows switch over to previously abandoned branches of stream. Another mechanism includes the blocking of a stream flow by a bar deposition and thus leading to the formation of an upstream pool and a downstream overfall.

References

- Agarwal VC (1983) Studies on the characteristics of meandering streams. PhD thesis, University of Roorkee, Roorkee
- Ashmore PE (1991) How do gravel-bed rivers braid? *Can J Earth Sci* 28(3):326–341
- Bergs MA (1989) Flow processes in a curved alluvial channel. PhD thesis, University of Iowa, Iowa City
- Bristow CS, Best JL (1993) Braided rivers: perspectives and problems. In: Best JL, Bristow CS (eds) *Braided rivers*. Geological Society of London, London pp 1–11 (Special publication number 75)
- Carson MA (1984) The meandering-braided river threshold: a reappraisal. *J Hydrol* 73(3–4):315–334
- Carson MA (1986) Characteristics of high-energy ‘meandering’ rivers: the Canterbury Plains, New Zealand: part one. *NZ Geogr* 40:12–17
- Carson MA, Griffiths GA (1987) Bedload transport in gravel channels. *New Zealand J Hydrol* 26(1):1–115
- Carson MA, Lapointe MF (1983) The inherent asymmetry of river meander planform. *J Geol* 91(1):41–55
- Chang HH (1988) *Fluvial processes in river engineering*. Wiley, New York
- Chatley H (1938) Hydraulics of large rivers. *J Junior Inst Eng* 48:401–416
- Dietrich WE, Smith JD (1983) Influence of the point bar on flow through curved channels. *Water Resour Res* 19(5):1173–1192
- Dietrich WE, Smith JD (1984) Bedload transport in a river meander. *Water Resour Res* 20(10):1355–1380
- Eakin HM (1910) The influence of the earth’s rotation upon the lateral erosion of streams. *J Geol* 18(5):435–447
- Einstein A (1926) The cause of the formation of meanders in the courses of rivers and of the so-called Baer’s law. *Die Naturwissenschaften* 14:1–3
- Ferguson RI (1987) Hydraulic and sedimentary controls of channel pattern. In: Richards KS (ed) *River channels: environment and process*. Basil Blackwell, Oxford, pp 129–158
- Ferguson RI (1993) Understanding braiding processes in gravel-bed rivers: progress and unsolved problems. In: Best JL, Bristow CS (eds) *Braided rivers*, Geological Society of London, London, pp 73–87 (Special publication number 75)
- Friedkin JF (1945) Laboratory study of the meandering of alluvial rivers. United States Waterways Experiment Station, Vicksburg
- Gagliano SM, Howard PG (1984) The neck cutoff oxbow lake cycle along the lower Mississippi river. In: Elliot CM (ed) *River meandering*. American Society of Civil Engineers, New York, pp 147–158
- Garde RJ, Ranga Raju KG (2000) *Mechanics of sediment transportation and alluvial stream* probable. New Age International Publishers, New Delhi
- Gay GR, Gay HH, Gay WH, Martinson HA, Meade RH, Moody JA (1998) Evolution of cutoffs across meander necks in Powder River, Montana, United States of America. *Earth Surf Proc Land* 23(7):651–662
- Gilbert GK (1884) The sufficiency of terrestrial rotation for the deflection of streams. *Am J Sci* 162:427–432 (Memories of the National Academy of Sciences, Series 3, Part 1)
- Griggs RF (1906) The Buffalo River: an interesting meandering stream. *Bull Geol Soc Am* 38(3):168–177
- Hayashi T, Ozaki S (1978) Alluvial bed form analysis I, formation of alternating bars and braids. In: *Proceedings of the United States-Japan bi-national seminar on erosion and sedimentation*, Hawaii, pp 7.1–7.39
- Henderson FM (1963) Stability of alluvial channels. *Trans Am Soc Civ Eng* 128:657–686
- Hjulström F (1957) A study of the meander problem. Bulletin 51, Institute of Hydraulics, Royal Institute of Technology, Stockholm

- Hooke JM (1995) River channel adjustment to meander cutoffs on the River Bollin and River Dane, northwest England. *Geomorphology* 14(3):235–253
- Ikeda S, Nishimura T (1985) Bed topography in bends of sand-silt rivers. *J Hydraul Eng* 111(11):1397–1411
- Ikeda S, Nishimura T (1986) Flow and bend profile in meandering sand-silt rivers. *J Hydraul Eng* 112(7):562–579
- Ikeda S, Parker G, Sawai K (1981) Bend theory of river meanders, part 1. Linear development. *J Fluid Mech* 112:363–377
- Ikeda S, Tanaka M, Chiyoda M (1985) Turbulent flow in a sinuous air duct. In: *Proceedings of the international symposium on refined flow modelling and turbulence measurements*. International Association for Hydraulic Research, The University of Iowa, Iowa City, pp 124.1–124.10
- Inglis CC (1947) Meanders and their bearing on river training. *Maritime and Waterways Engineering Division, The Institution of Civil Engineers, London*, pp 1–54
- Kikkawa H, Ikeda S, Kitagawa A (1976) Flow and bed topography in curved open channels. *J Hydraul Div* 102(9):1327–1342
- Lacey JM (1923) Some problems connected with rivers and canals in southern India. *Minutes Proc Inst Civ Eng (London)* 216(2):150–160
- Lane EW (1957) A study of the shape of channels formed by natural streams flowing in erodible material. *United States Army Engineer Division, Missouri River Division, Corps of Engineers, Omaha, Nebraska*
- Langbein WB, Leopold LB (1966) River meanders—theory of minimum variance. *Professional paper 422-H, United States Geological Survey, Washington, DC*, pp H1–H15
- Leliavsky S (1966) *An introduction to fluvial hydraulics*. Dover, New York
- Leopold LB, Wolman MG (1957) River channel patterns: braided, meandering and straight. *Professional paper 282-B, United States Geological Survey, Washington, DC*
- Leopold LB, Wolman MG (1960) River meanders. *Bull Geol Soc Am* 71:769–794
- Millar RG (2000) Influence of bank vegetation on alluvial channel patterns. *Water Resour Res* 36(4):1109–1118
- Neu HA (1967) Transverse flow in a river due to earth's rotation. *J Hydraul Div* 93(5):149–165
- Odgaard AJ (1989) River-meander model. I: development. *J Hydraul Eng* 115(11):1433–1450
- Onishi Y, Jain SC, Kennedy JF (1976) Effects of meandering in alluvial streams. *J Hydraul Div* 112(7):899–917
- Parker G (1976) On the causes and characteristic scales of meandering and braiding in rivers. *J Fluid Mech* 76:457–480
- Parker G (1979) Hydraulic geometry of active gravel rivers. *J Hydraul Div* 105(9):1185–1201
- Parker G (1984) Discussion of 'lateral bed load transport on side slopes'. *J Hydraul Eng* 110(2):197–203
- Parker G, Diplas P, Akiyama J (1983) Meander bends of high amplitude. *J Hydraul Eng* 109(10):1323–1337
- Prus-Chacinski TM (1954) Patterns of motion in open-channel bends. *Int Assoc Sci Hydrol* 383:311–318
- Quraishy MS (1943) River meandering and the earth's rotation. *Current Sci* 12:278
- Ramette M (1980) A theoretical approach on fluvial processes. In: *First international symposium on river sedimentation, Beijing*, pp C16.1–C16.18
- Ripley HC (1927) Relation of depth to curvature of channels. *Trans Am Soc Civ Eng* 90:207–238
- Robert A (2003) *River processes: an introduction to fluvial dynamics*. Arnold, London
- Rozovskii IL (1957) Flow of water in bends in open channels. *Academy of Sciences of the Ukrainian Soviet Socialist Republic, Kiev*
- Rundle A (1985a) The mechanism of braiding. *Z Geomorphol* 55(Supplement-Band):1–13
- Rundle A (1985b) Braid morphology and the formation of multiple channels. *Z Geomorphol* 55(Supplement-Band):15–37
- Schoklitsch A (1937) *Hydraulic structures, vol 1*. American Society of Mechanical Engineers, New York

- Shen HW (1983) Examination of present knowledge of river meandering. In: Elliot CM (ed) River meandering. In: Proceedings of the conference Rivers-83, American Society of Civil Engineers, New York, pp 1008–1012
- Simons DB, Sentürk F (1977) Sediment transport technology. Water Resources Publication, Fort Collins
- Southard JB, Smith ND, Kuhnle RA (1984) Chutes and lobes: newly identified elements of braiding in shallow gravelly streams. In: Koster EH, Steel RJ (eds) Sedimentology of gravels and conglomerates. Canadian Society of Petroleum Geologists, Calgary, pp 51–59 (Memoir 10)
- Vanoni VA (1975) Sedimentation engineering. ASCE manual number 54, American Society of Civil Engineers, New York
- von Schelling H (1951) Most frequent particle paths in a plane. *Trans Am Geophys Union* 32(2):222–226
- Werner PW (1951) On the origin of river meanders. *Trans Am Geophys Union* 32(6):898–902
- Yalin MS, da Silva AMF (2001) Fluvial processes. IAHR Monograph, International Association for Hydraulic Research, Delft
- Yang CT (1971) On river meanders. *J Hydrol* 13(3):231–253
- Zeller J (1967) Meandering channels in Switzerland. In: Proceedings of the symposium on river morphology, International Association of Scientific Hydrology, vol 75. Bern, pp 174–186
- Zimmermann C, Kennedy JF (1978) Transverse bed slopes in curved alluvial streams. *J Hydraul Div* 104(1):33–48

Chapter 10

Scour

10.1 General

Scour is a natural phenomenon of lowering the riverbed level due to removal of sediment by the erosive action of flowing stream. The magnitude of reduction in the riverbed level below an assumed natural level (or initial level) is termed *scour depth*. Scour is broadly classified as *general scour*, *contraction scour*, and *local scour*.

General scour in the river occurs as a result of the change in characteristics of the river. Based on the duration of scour development, general scour can be categorized as short-term scour and long-term scour. *Short-term scour* occurs during a single flood or several floods of shorter durations to appear in quick succession, while *long-term scour* takes a considerably long time, usually of the order of a number of years, and results in a progressive bed degradation and bank erosion. Short-term scour may also occur due to flow convergence, a shift in the meandering stream thalweg or braids within the stream and bedform migration. On the other hand, the long-term scour may be caused by the natural changes in the catchments, for example, channel straightening, volcanic activities, climate change, or by the human activities, for example, channel alterations, streambed mining, dam/reservoir construction, and land-use changes.

Contraction scour is the scour of streambed arising from accelerated flow through contraction of waterways, where flows over flood plains are converged by bridge causeways and channeled through the bridge waterways.

In contrast, *local scour* (also termed *localized scour*) is developed near the structures due to modification of the flow field as a result of obstruction to the flow by the structures. Scour within the contracted portion of rivers, scour downstream of structures, scour at bed sills, scour below horizontal pipelines, scour at bridge piers and abutments, and scour at other river training works are the examples of local scour.

Local scour is classified as clear-water scour and live-bed scour. *Clear-water scour* occurs when the sediment is removed from the scour hole but not supplied by the approaching flow. The equilibrium of scour is reached when the flow induced

force can no longer dislodge the sediment particles from the scour hole. On the other hand, *live-bed scour* occurs when the scour hole is continuously fed with the sediment by the approaching flow. The equilibrium of scour is attained over a period of time, when the rate of removal of sediment out of the scour hole equals the rate of supply of sediment into the scour hole. Usually, the magnitude of scour depth in live bed is to some extent less than that in clear-water, if the flow condition is such that the approaching flow velocity U equals or is slightly less the threshold flow velocity U_{cr} for the bed sediment motion.

This chapter summarizes the contraction scour and local scour at different structures including various aspects, such as mechanism of scour and design formulas for the prediction of scour depth. It is however pertinent to mention that despite large number of investigations, hydraulics of local scour is as yet not well established, because most of the studies came from the laboratory and only a few from the fields. As such, the scour prediction formulas can only provide a general guideline for the designers or engineers.

10.2 Scour Within Channel Contractions

A reduction in width of a watercourse by constructing parallel sidewalls is termed *channel contraction*. Contractions of river width to construct bridges, barrages, weirs, and cross-drainage works are common examples of channel contractions. The flow velocity in the contracted zone of the channel increases due to the reduction in flow area, and hence, the bed shear stress induced by the flow increases considerably. Consequently, the sediment bed within the channel contraction is scoured. Such localized scour in the contracted zone of the channel is called *contraction scour*.

Depending on the ratio of the length of the contraction L to the approaching channel width B_1 , channel contractions are designated as long or short. According to Komura (1966) and Dey and Raikar (2005), a contraction becomes long when $L/B_1 > 1$, whereas Webby (1984) considered it as $L/B_1 > 2$. Figures 10.1 and 10.2 show schematic of scour in a channel contraction and a photograph of the scoured bed, respectively. Smith (1967) proposed the angles of upstream and downstream transitions as 12.5° for a smooth transition to the contracted zone.

Local scour in a channel contraction is usually studied considering a configuration of long rectangular contraction, as shown schematically in Fig. 10.1. Because of the simple geometrical configuration of the problem, various analytical investigations to predict the equilibrium scour depth in long contractions were attempted. Straub (1934) was the pioneer to present a simplified one-dimensional theory of the equilibrium scour in long contractions. His work was later extended and modified by Laursen (1963), Komura (1966), Gill (1981), Lim (1993), and Lim and Cheng (1998). Further, Dey and Raikar (2005, 2006) studied the scour in long contractions in gravel-beds and proposed analytical models for the estimation of scour depth under both clear-water and live-bed scour conditions.

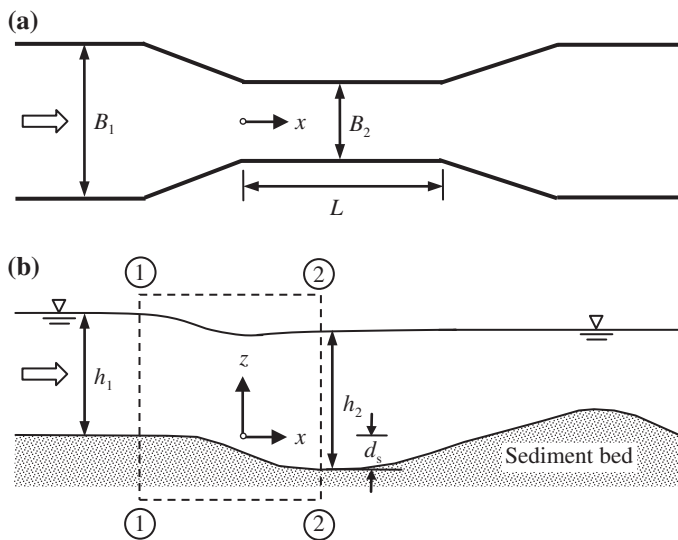


Fig. 10.1 Schematic of a rectangular channel contraction at equilibrium scour condition: **a** *plan view* and **b** *elevation view*

Fig. 10.2 Photograph showing an equilibrium scoured bed within a channel contraction



10.2.1 Laursen's Model

Laursen (1963) considered a channel contraction as shown in Fig. 10.1. The discharge in the channel is obtained from the continuity equation as

$$Q = U_1 h_1 B_1 = U_2 h_2 B_2 \quad (10.1)$$

where U_1 is the approaching flow velocity, h_1 is the approaching flow depth, U_2 is the flow velocity in contracted zone, h_2 is the flow depth in contracted zone, and B_2 is the contracted width of the channel.

Using the energy equation between sections 1 and 2, the scour depth d_s is obtained as

$$h_1 + \frac{U_1^2}{2g} = h_2 + \frac{U_2^2}{2g} - d_s + h_f \quad \wedge \quad h_f = K_L \left(\frac{U_2^2}{2g} - \frac{U_1^2}{2g} \right) \quad (10.2a)$$

$$\Rightarrow \frac{d_s}{h_1} = \frac{h_2}{h_1} - 1 + \left(\frac{1 + K_L}{2} \right) Fr_1^2 \left[\left(\frac{B_1}{B_2} \right)^2 \left(\frac{h_1}{h_2} \right)^2 - 1 \right] \quad (10.2b)$$

where h_f is the head loss due to flow in transition, Fr_1 is the approaching flow Froude number $[= U_1/(gh_1)^{0.5}]$, and K_L is the head loss coefficient.

When the scour in the contracted zone reaches an equilibrium, the bed shear stress becomes equal to its threshold value, that is, $\tau_{0c} = 0.628d_{50}$ (in Pa), where d_{50} is the median sediment size (in mm). The bed shear stress τ_{01} in the uncontracted zone (section 1) can be estimated using the Manning equation and the Strickler's relationship for Manning roughness coefficient n as

$$\tau_{01} = \frac{U_1^2 d_{50}^{0.33}}{30 h_1^{0.33}} \quad (10.3)$$

Taking the ratio of bed shear stress in the uncontracted zone to that in the contracted zone yields

$$\frac{\tau_{01}}{\tau_{0c}} = \frac{U_1^2}{120 d_{50}^{2/3} h_1^{1/3}} \quad (10.4)$$

Similar expression can also be written for the bed shear stress in the contracted zone. Hence, the flow depth ratio h_2/h_1 can be obtained from

$$\frac{\tau_{01}}{\tau_{02}} = \left(\frac{U_1}{U_2} \right)^2 \left(\frac{h_2}{h_1} \right)^{1/3} = \frac{\tau_{01}}{\tau_{0c}} \quad (10.5)$$

where τ_{02} is the bed shear stress in the contracted zone (section 2).

Using Eqs. (10.1) and (10.5), one can write

$$\frac{h_2}{h_1} = \left(\frac{\tau_{01}}{\tau_{0c}} \right)^{3/7} \left(\frac{B_1}{B_2} \right)^{6/7} \quad (10.6)$$

Substituting Eq. (10.6) into Eq. (10.2b) results

$$\frac{d_s}{h_1} = \left(\frac{\tau_{01}}{\tau_{0c}} \right)^{3/7} \left(\frac{B_1}{B_2} \right)^{6/7} - 1 + 1.87(1 + K_L) \left(\frac{d_{s0}}{h_1} \right)^{2/3} \left[\frac{(B_1/B_2)^{2/7}}{(\tau_{01}/\tau_{0c})^{6/7}} - 1 \right] \left(\frac{\tau_{01}}{\tau_{0c}} \right) \quad (10.7)$$

Neglecting the difference in the velocity heads and the loss through the transition, Eq. (10.7) reduces to

$$\frac{d_s}{h_1} = \left(\frac{\tau_{01}}{\tau_{0c}} \right)^{3/7} \left(\frac{B_1}{B_2} \right)^{6/7} - 1 \quad (10.8)$$

10.2.2 Dey and Raikar's Model

Dey and Raikar (2005, 2006) developed analytical models for clear-water and live-bed scour cases.

10.2.2.1 Clear-Water Scour Model

Dey and Raikar (2005) analytically computed the equilibrium clear-water scour depth in two ways: Considering sidewall correction and without considering sidewall correction.

Determination of scour depth considering sidewall correction: In clear-water scour, the equilibrium scour depth d_s reaches in a long contraction, when the flow velocity U_2 in the contracted zone becomes equal to threshold velocity U_{cr} for the sediment motion. The flow velocity $U_2|_{U_2=U_{cr}}$ in the contracted zone can be obtained from the well-known equation of bed shear stress as a function of dynamic pressure (Eq. 3.54). It is

$$\tau_{0c}(= \rho u_{*c}^2) = \frac{\lambda_D}{8} \rho U_2^2|_{U_2=U_{cr}} \Rightarrow U_2|_{U_2=U_{cr}} = u_{*c} \left(\frac{8}{\lambda_D} \right)^{0.5} \quad (10.9)$$

where ρ is the mass density of water, u_{*c} is the threshold shear velocity for sediment, and λ_D is the Darcy–Weisbach friction factor, which can be determined from Colebrook–White equation (Eq. 3.55).

In the contracted zone, the bed is rough consisting of sediment particles and the sidewalls are smooth. Hence, the friction factor $\lambda_{D|w}$ associated with the wall is considerably different from the friction factor $\lambda_{D|b}$ associated with the bed. Therefore, Vanoni's (1975) method of sidewall correction can be applied for the contracted zone of the channel, as given in Sect. 3.9, where the solution for $\lambda_{D|b}$ was obtained from the solution of Eqs. (3.63) and (3.64), which are here expressed as

$$\lambda_D|_b = 0.316 Re|_b \left(\frac{4U_2|_{U_2=U_{cr}} A}{vP|_w} - \frac{Re|_b P|_b}{P|_w} \right)^{-1.25} \quad (10.10a)$$

$$\frac{1}{\lambda_D|_b^{0.5}} = -0.86 \ln \left(\frac{k_s U_2|_{U_2=U_{cr}}}{3.7v Re|_b} + \frac{2.51}{Re|_b \lambda_D|_b^{0.5}} \right) \quad (10.10b)$$

where k_s is equivalent roughness height ($=2d_{50}$), $Re|_b$ is the flow Reynolds number associated with the bed, that is, $4U_2|_{U_2=U_{cr}} A|_b / (vP|_b)$, $A|_b$ is the flow area associated with the bed, $P|_b$ is the wetted perimeter associated with the bed ($=B_2$), A is the total flow area of contracted zone ($=h_2 B_2$), $P|_w$ is the wetted perimeter associated with the wall ($=2h_2$), and v is the kinematic viscosity of water.

In clear-water scour, at equilibrium scour condition, Eq. (10.1) becomes

$$U_1 h_1 B_1 = U_2|_{U_2=U_{cr}} h_2 B_2 \quad (10.11)$$

For the given U_1 , h_1 , B_1 , B_2 , and d_{50} , the unknowns $U_2|_{U_2=U_{cr}}$, h_2 , $Re|_b$, and $\lambda_D|_b$ can be determined numerically solving Eqs. (10.9), (10.10a, b) and (10.11). Then, neglecting the head loss in transition, energy equation [see the energy equation, Eq. (10.2a)] is used to determine equilibrium scour depth d_s as

$$d_s = h_2 + \frac{U_2|_{U_2=U_{cr}}^2}{2g} - h_1 - \frac{U_1^2}{2g} \quad (10.12)$$

Determination of scour depth without considering sidewall correction: In this simplified approach, the depth-averaged flow velocity $U_2|_{U_2=U_{cr}}$ in the contracted zone for equilibrium scour is determined assuming the logarithmic equation of the depth-averaged velocity as

$$\frac{U_2|_{U_2=U_{cr}}}{u_{*c}} = 5.75 \log \frac{h_2}{2d_{50}} + 6 \quad (10.13)$$

For the given U_1 , h_1 , B_1 , B_2 , and d_{50} , the unknowns $U_2|_{U_2=U_{cr}}$ and h_2 can be obtained numerically solving Eqs. (10.11) and (10.13). Then, equilibrium scour depth d_s can be determined from Eq. (10.12).

10.2.2.2 Live-Bed Scour Model

Dey and Raikar (2006) proposed a live-bed scour model for the estimation of scour depth within channel contractions. In live-bed scour, the equilibrium scour depth is reached, when the sediment supplied by the approaching flow into the contracted zone is balanced by the sediment transported out of the contracted zone. Thus, at the equilibrium, the sediment continuity equation between sections 1 and 2 of Fig. 10.1 is

$$q_b|_{u_* = u_{*1}} B_1 = q_b|_{u_* = u_{*2}} B_2 \quad (10.14)$$

where q_b is the bed-load transport rate of sediment. The bed-load transport rate q_b can be estimated by the formula of Fredsøe and Deigaard (1992) as

$$q_b = 1.55 \pi d_{50} u_* \left(1 - 0.7 \frac{u_{*c}}{u_*} \right) p \quad \wedge \quad p = \left[1 + \left(\frac{0.085 \pi \Delta g d_{50}}{u_*^2 - u_{*c}^2} \right)^4 \right]^{-0.25} \quad (10.15)$$

Assuming the logarithmic equation of average velocity for approaching flow, the shear velocity u_{*1} at section 1 is obtained as

$$u_{*1} = U_1 \left(5.75 \log \frac{h_1}{2d_{50}} + 6 \right)^{-1} \quad (10.16)$$

In the contracted zone, incorporating the logarithmic equation of average velocity in Eq. (10.1) yields

$$\frac{B_1}{B_2} \cdot \frac{h_1}{h_2} = \frac{u_{*2}}{U_1} \left(5.75 \log \frac{h_2}{2d_{50}} + 6 \right) \quad (10.17)$$

where u_{*2} is the shear velocity in the contracted zone.

For the given U_1 , h_1 , B_1 , B_2 , and d_{50} , the unknowns U_2 and h_2 can be determined numerically solving Eqs. (10.14), (10.15) and (10.17). Then, the energy equation [see the energy equation, Eq. (10.2a)] is used to determine equilibrium scour depth d_s as

$$d_s = h_2 - h_1 + \frac{U_2^2}{2g} - \frac{U_1^2}{2g} \quad (10.18)$$

10.2.3 Maximum Scour Depth Prediction

The parameters that influence the scour within channel contractions are as follows (Dey and Raikar 2005):

1. *Parameters relating to the channel contraction:* Channel opening ratio and channel shape.
2. *Parameters relating to the bed sediment:* Median particle size, particle size distribution, angle of repose, and cohesiveness.
3. *Parameters relating to the approaching flow condition:* Approaching flow velocity, approaching flow depth, shear velocity, and roughness.

4. *Parameters relating to the fluid:* Mass density, viscosity, gravitational acceleration, and temperature. Note that the temperature may not be important in scour problems, unless free surface is frozen.

The functional relationship showing the influence of above parameters on the equilibrium scour depth d_s in a long rectangular contraction can be given as

$$d_s = d_s(U_1, h_1, \rho, \rho_s, g, \nu, d_{50}, B_1, B_2, \sigma_g) \quad (10.19)$$

where ρ_s is the mass density of sediment, g is the gravitational acceleration, and σ_g is the geometric standard deviation of the particle size distribution.

Dey and Raikar (2005) argued that the scour in a long contraction starts when the excess approaching flow velocity $U_{1e}(= U_1 - U_1|_{U_2=U_{cr}}^{d_s=0})$ is greater than zero. For no-scour condition, U_{1e} is less than or equal to zero. Here, $U_1|_{U_2=U_{cr}}^{d_s=0}$ refers to the approaching flow velocity U_1 that initiates scour in a contraction. Therefore, $U_1|_{U_2=U_{cr}}^{d_s=0}$ corresponds to U_1 for which U_2 becomes U_{cr} for the undisturbed bed condition ($d_s = 0$) in the contracted zone. The $U_1|_{U_2=U_{cr}}^{d_s=0}$ can be determined as follows:

Considering negligible head loss ($h_f = 0$) and applying the energy equation between sections 1 and 2 for the bed sediments within contracted zone under threshold condition, that is $U_2 = U_{cr}$, before initiation of scour ($d_s = 0$), the following equation is obtained (Fig. 10.1) (Dey and Raikar 2005):

$$h_1 + \frac{1}{2g} \left(U_1|_{U_2=U_{cr}}^{d_s=0} \right)^2 = h_2 + \frac{1}{2g} \left(U_2|_{U_2=U_{cr}}^{d_s=0} \right)^2 \quad (10.20)$$

The continuity equation between sections 1 and 2 is

$$U_1|_{U_2=U_{cr}}^{d_s=0} h_1 B_1 = U_2|_{U_2=U_{cr}}^{d_s=0} h_2 B_2 \quad (10.21)$$

The threshold flow velocity at section 2 can be determined using the logarithmic equation of average velocity as

$$\frac{U_2|_{U_2=U_{cr}}^{d_s=0}}{u_{*c}} = 5.75 \log \frac{h_2}{2d_{50}} + 6 \quad (10.22)$$

Therefore, for the given h_1 , B_1 , B_2 , d_{50} , and u_{*c} (determined from the Shields diagram), the approaching flow velocity $U_1|_{U_2=U_{cr}}^{d_s=0}$ required to initiate the sediment motion within the contracted zone can be estimated solving Eqs. (10.20)–(10.22) numerically.

In the context of scour, it is appropriate that U_1 , in Eq. (10.19), is to be replaced by U_{1e} . In sediment–water interaction, the parameters g , ρ , and ρ_s are combined into a parameter Δg , where $\Delta = s - 1$ and s is the relative density of sediment ($= \rho_s/\rho$). Also, it is reasonable to use the channel opening ratio B_2/B_1 to account

for the combined effect of B_1 and B_2 . In addition, the influence of kinematic viscosity ν of water is insignificant for a turbulent flow over rough sediment beds (Yalin 1977). Therefore, applying these considerations, the Buckingham Π theorem (see Sect. 11.2.3) is used with U_{1e} and h_1 as repeating variables to obtain the following nondimensional equation:

$$\frac{d_s}{h_1} = f\left(F_{1e}, \frac{d_{50}}{h_1}, \frac{B_2}{B_1}\right) \quad (10.23)$$

where F_{1e} is the excess approaching flow Froude number $[= U_{1e}/(\Delta gh_1)^{0.5}]$. The condition $U_1 \rightarrow U_{cr}$ (that is the limiting condition for a clear-water scour, as $U_1 > U_{cr}$ corresponds to a live-bed scour) is recognized to be the most idealized condition for maximum equilibrium scour depth $[d_s]_{\max}(= d_s|_{U_1=U_{cr}})$ in long contractions under a clear-water scour condition (Gill 1981). Therefore, to determine the equation of maximum equilibrium scour depth $[d_s]_{\max}$ in long contractions, Eq. (10.23) is written for $U_1 \rightarrow U_{cr}$. Using the experimental data for clear-water scour, Dey and Raikar (2005) obtained the empirical equation of maximum equilibrium scour depth as follows:

$$\frac{[d_s]_{\max}}{h_1} = 0.368 F_{1ec}^{0.55} \left(\frac{B_2}{B_1}\right)^{-1.26} \left(\frac{d_{50}}{h_1}\right)^{-0.19} \quad (10.24)$$

where $F_{1ec} = U_{1ec}/(\Delta gh_1)^{0.5}$ and $U_{1ec} = U_{cr} - U_1|_{\frac{d_s=0}{U_2=U_{cr}}}$. Equation (10.24) is written for uniform sediments, as it does not include σ_g .

The equilibrium scour depth $d_s(\sigma_g)$ in nonuniform sediments can be estimated in terms of geometric standard deviation σ_g of sediments using the following relationship:

$$d_s(\sigma_g) = K_\sigma d_s \quad (10.25)$$

where K_σ is the coefficient due to sediment gradation. The coefficient K_σ is defined as the ratio of equilibrium scour depth in nonuniform sediment ($\sigma_g > 1.4$) to that in uniform sediment. The variation of K_σ with σ_g is shown in Fig. 10.3 (Dey and Raikar 2005).

10.2.4 Other Scour Depth Predictors

Phenomena involving scour in long contractions have been studied extensively in laboratories, from which a number of semianalytical and empirical equations have been developed to estimate the equilibrium scour depth under both clear-water and live-bed scour conditions. In general, they are based on a limited range of data. Table 10.1 furnishes the empirical equations of equilibrium scour depth proposed by different investigators.

Fig. 10.3 Variation of K_σ as a function of σ_g (Dey and Raikar 2005)

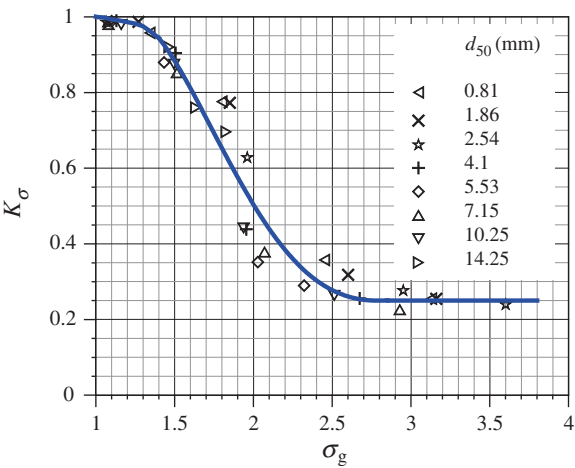


Table 10.1 Equations of equilibrium scour depth within channel contractions proposed by different investigators

References	Formula	Regime
Straub (1934)	$\frac{d_s}{h_1} = \left(\frac{B_2}{B_1}\right)^{-6/7} \left\{ \left[\left(\frac{\tau_{0c}}{2\tau_{01}}\right)^2 + \left(\frac{B_2}{B_1}\right)^{-1} \times \left(1 - \frac{\tau_{0c}}{\tau_{01}}\right) \right]^{0.5} + \frac{\tau_{0c}}{2\tau_{01}} \right\}^{-3/7} - 1$	Clear-water
Komura (1966)	$\frac{d_s}{h_1} = 1.6Fr_1^{0.2} \left(\frac{B_2}{B_1}\right)^{-0.67} \sigma_g^{-0.5} - 1$	Clear-water
	$\frac{d_s}{h_1} = 1.45Fr_1^{0.2} \left(\frac{B_2}{B_1}\right)^{-0.67} \sigma_g^{-0.2} - 1$	Live bed
Gill (1981)	$\frac{d_s}{h_1} = \left(\frac{B_2}{B_1}\right)^{-6/7} \left(\frac{\tau_{0c}}{\tau_{01}}\right)^{-3/7} - 1$	Clear-water
	$\frac{d_s}{h_1} = \left(\frac{B_2}{B_1}\right)^{-6/7} \left[\left(\frac{B_2}{B_1}\right)^{-1/m} \left(1 - \frac{\tau_{0c}}{\tau_{01}}\right) + \frac{\tau_{0c}}{\tau_{01}} \right]^{-3/7} - 1$ <p>where m is an exponent varying from 1.5 to 3</p>	Live bed
Lim (1993)	$\frac{d_s}{h_1} = 1.854F_{1d}^{0.75} \left(\frac{B_2}{B_1}\right)^{-0.75} \left(\frac{d_{50}}{h_1}\right)^{0.25} - 1$ <p>where $F_{1d} = U_1/(\Delta g d_{50})^{0.5}$</p>	Clear-water/live bed
Lim and Cheng (1998)	$\frac{d_s}{h_1} = \left(\frac{B_2}{B_1}\right)^{-0.75} - 1$	Clear-water/live bed

Note In order to obtain maximum equilibrium scour depth $[d_s]_{\max}$, equations of d_s are to be expressed for the threshold condition $U_1/U_{cr} \rightarrow 1$ or $\tau_{01}/\tau_{01c} \rightarrow 1$. For uniform sediments ($\sigma_g < 1.4$), the geometric standard deviation σ_g is considered to be unity

10.3 Scour Downstream of Structures

10.3.1 Scour Below Drop Structures

Drops are provided in rivers for lowering the bed level when the slope of the river is smaller than the natural ground slope. These structures therefore artificially increase the slope of the rivers. The stream flow running over the drops is called an *overfall*. In addition, the scour is developed downstream of the bed protection provided to control the slope or elevation of the riverbed to create a drop. The water released from the drop structures impinges on the free surface of the tailwater as a jet, which is called *plunging jet*. This freely falling jet may have considerable potential to scour the bed downstream of the structures, and such scour is known as *jet scour*. Scour due to jets occurs very rapidly, which causes danger to the stability of the channel bed, in addition to the devastating effects on the hydraulic structures. Considerable portion of the energy of the flowing stream is dissipated through turbulent mixing in the pool due to plunging jet. Figures 10.4a, b show schematic of scour below weir type and free overfall type drop structures.

The pioneering study on scour below a drop structure was due to Schoklitsch (1932). He proposed the following empirical relationship for the equilibrium scour depth for the flow over structures:

$$d_s = K_0 \frac{q^{0.57} H^{0.2}}{d_{90}^{0.32}} - h_t \quad \wedge \quad \begin{cases} d_{90} \text{ in mm, } K_0 = 4.75 \text{ (in s}^{0.6} \text{ m}^{0.3}) \\ d_{90} \text{ in m, } K_0 = 0.52 \text{ (in s}^{0.6} \text{ m}^{0.3}) \end{cases} \quad (10.26)$$

where q is discharge per unit width, H is the height between upstream and downstream water levels, d_{90} is the 90 % finer sediment size, and h_t is the tailwater depth.

Based on the dimensional analysis and using the experimental data, Kotoulas (1967) developed a relationship for the equilibrium scour depth downstream of a structure. It is

$$d_s = \frac{1.9}{g^{0.35}} \cdot \frac{q^{0.7} H^{0.35}}{d_{95}^{0.4}} - h_t \quad (10.27)$$

where d_{95} is the 95 % finer sediment size.

For free overfall type drop structures, Dey and Raikar (2007b) proposed a procedure to calculate the jet velocity U_0 and the jet thickness l_0 at the entry of jet into the tailwater.¹

¹ Dey and Raikar (2007b) considered section 0 at the upstream of the drop where the critical depth h_c occurs and section 0 at the entry of jet into the tailwater (Fig. 10.4b). The continuity equation applied between sections 1 and 0 is

Fahlbusch (1994) proposed an empirical equation of equilibrium scour depth for weir type drop structures. He expressed scour depth d_s as a function of q and jet velocity U_0 entering the tailwater depth h_t at an angle θ_j with the horizontal at the water level as

$$d_s = K_p \left(\frac{qU_0}{g} \sin \theta_j \right)^{0.5} - h_t \quad (10.28)$$

The coefficient K_p is dependent on sediment size. For gravel, $3 < K_p < 5$; for sand, $5 < K_p < 20$; and for silt, $K_p \approx 20$.

Later, a more generalized relationship of equilibrium scour depth for weir type drop structures was recommended (Graf 1998). It is

$$d_s = \frac{3.6}{\Delta^{4/9} g^{0.3}} \cdot \frac{q^{0.6} H^{0.5}}{d_{90}^{0.4}} - h_t \quad (10.29)$$

Also, D'Agostino and Ferro (2004) suggested a simplified equation of equilibrium scour depth for weir type drop structures as

$$\frac{d_s}{Z} = 0.975 \left(\frac{h}{Z} \right)^{0.863} \quad (10.30)$$

(Footnote 1 continued)

$$U_c h_c = U_0 l_0$$

where U_c is the critical velocity of the flow upstream of the drop. According to Bakhmeteff (1932), the jet velocity U_0 is given by

$$U_0 = C_0 [2g(h_0 + 1.5h_c)]^{0.5}$$

where C_0 is the velocity coefficient and h_0 is the height of drop above the tailwater level.

Using the value of end-depth-ratio ($= h_c/h_e$, where h_e is the end depth) for rectangular channels equaling 0.715 as given by Rouse (1936), the above equation becomes

$$U_0 = C_0 [2g(h_0 + 2.1h_e)]^{0.5}$$

Inserting into the continuity equation, the expression for jet thickness l_0 can be written as

$$l_0 = \frac{1.17h_e^{1.5}}{C_0(h_0 + 2.1h_e)^{0.5}}$$

Using the experimental data, the value of C_0 was estimated as 0.672.

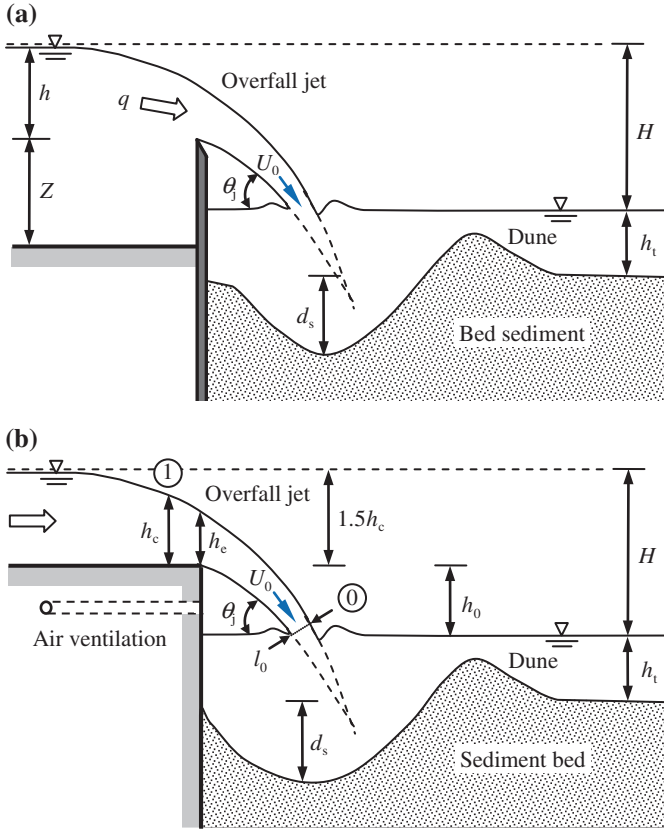


Fig. 10.4 Schematic of scour below drop structures: **a** weir type and **b** free overfall type

where Z is the crest height of the weir and h is the flow depth over a weir (Fig. 10.4a). Note that Eq. (10.30) does not take into account the effects of sediment size and tailwater depth.

Stein et al. (1993) developed an analytical equation to predict the equilibrium scour depth downstream of a headcut type drop structure for the condition of shallow tailwater depth ($d_s \gg h_t$) (Fig. 10.5). Neglecting the effects of tailwater depth, they proposed

$$d_s = \frac{C_d^2 \lambda_f \rho U_0^2 l_0}{\tau_{0c}} \sin \theta_j \quad \wedge \quad \lambda_f = 0.0275 \left(\frac{v}{q} \right)^{0.25} \quad (10.31)$$

where C_d is the jet diffusion coefficient ($= 2.6$).

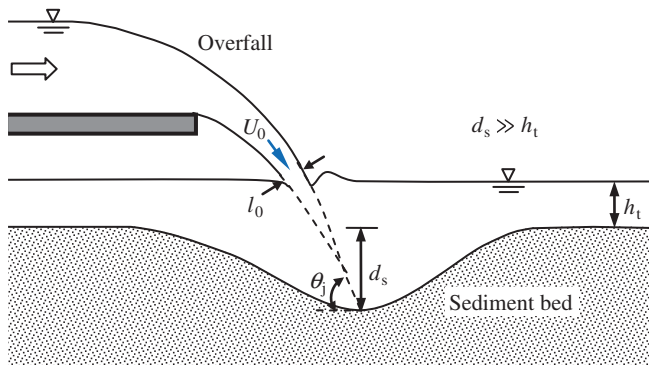


Fig. 10.5 Schematic of scour below a headcut

10.3.2 Scour Downstream of Grade-Control Structures

Grade-control structures are employed to prevent excessive riverbed degradation (Fig. 10.6). Bormann and Julien (1991) investigated the scour downstream of grade-control structures based on two-dimensional jet diffusion and particle stability. They put forward the following expression for the equilibrium scour depth:

$$d_s = \left\{ 1.8 \left[\frac{\sin \phi}{\sin(\phi + \theta_j)} \right]^{0.8} \frac{q^{0.6} U_1 \sin \theta_j}{(\Delta g)^{0.8} d_{90}^{0.4}} \right\} - Z_p \quad (10.32)$$

where U_1 is the approaching velocity, Z_p is the drop height of grade-control structure, θ_j is the jet angle near the original bed level, and ϕ is the angle of repose of bed sediment.

10.3.3 Scour Downstream of Bed Sills

Mountain streams are frequently subjected to channel incision. One of the methods to stabilize them is to employ a series of transverse structures called *bed sills*. Bed sills are generally preferred when the height of the riverbed is to be somewhat raised in order to reduce instability of the valley slope. The overfall plunging jet issued from a sill crest diffuses its energy in mixing process through rollers inside the downstream pool below. Further downstream, a uniform flow can be established if the riverbed has an equilibrium slope for a significant length. This condition is satisfied when the intermediate distance between two bed sills is adequately long. Flow over immediate upstream of a sill crest is characterized by a critical flow condition. At the edge of the sill, the flow becomes supercritical, being accelerated by that gravity as an overfall jet that has significant power to

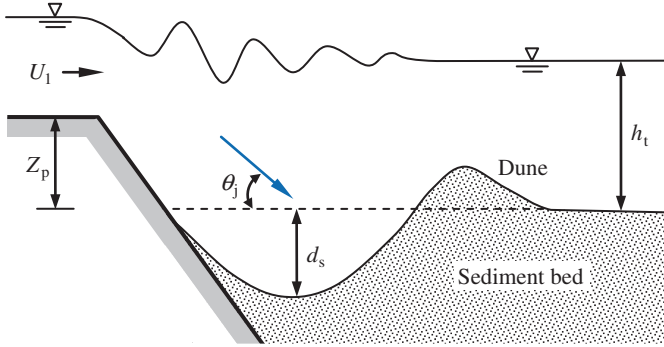


Fig. 10.6 Schematic of scour downstream of a grade-control structure

remove sediment from the bed downstream of a bed sill. Practically, scour downstream of a bed sill endangers its stability leading to the failure if the maximum scour depth is deep enough to expose the foundation (Fig. 10.7).

According to Gaudio et al. (2000), the maximum clear-water scour depth d_s at a bed sill can be given as a functional form. It is

$$d_s = d_s(g, v, \rho, \Delta\rho, q, h_1, d_{50}, a_1) \quad (10.33)$$

where h_1 is the uniform flow depth and a_1 is the morphological drop which is defined by

$$a_1 = (S_0 - S_{eq})L \quad (10.34)$$

where S_0 is the initial streamwise bed slope, S_{eq} is the equilibrium bed slope, and L is the distance between two neighboring sills. The equilibrium slope in clear-water condition can be expressed by the threshold Shields parameter Θ_c for the initiation of bed particle motion under fully developed turbulence flow condition. It is

$$\Theta_c = \frac{h_1 S_{eq}}{\Delta d_{50}} = \text{constant} \quad (10.35)$$

From the Manning equation, one can write

$$q = \frac{h_1^{5/3} S_{eq}^{0.5}}{n} \quad (10.36)$$

where n is the Manning roughness coefficient. Using Eqs. (10.35) and (10.36), the uniform flow depth and the equilibrium bed slope can be obtained as

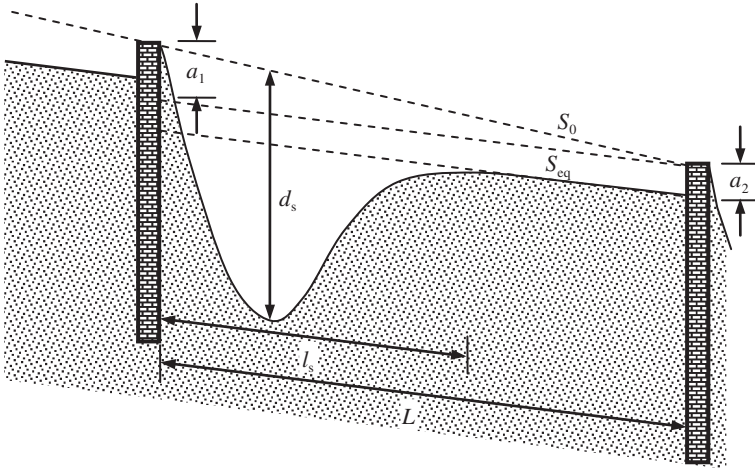


Fig. 10.7 Definition sketch of scour at a bed sill (Gaudio et al. 2000; Lenzi et al. 2002)

$$h_1 = \frac{(nq)^{6/7}}{(\Theta_c \Delta d_{50})^{3/7}} \quad (10.37a)$$

$$S_{eq} = \frac{(\Theta_c \Delta d_{50})^{10/7}}{(nq)^{6/7}} \quad (10.37b)$$

Equation (10.37a) provides the dependency of the uniform flow depth on other flow and sediment parameters. This allows h_1 to be dropped from Eq. (10.33).

The specific energy E_s on the sill is given by

$$E_s = 1.5 \left(\frac{q^2}{g} \right)^{1/3} \quad (10.38)$$

Applying Buckingham Π theorem (see Sect. 11.2.3) to Eq. (10.33) devoid of h_1 , one can write

$$\frac{d_s}{E_s} = f \left(\frac{q}{v}, \Delta, \frac{a_1}{\Delta d_{50}}, \frac{a_1}{E_s} \right) \quad (10.39)$$

For fully developed turbulent flow, kinematic viscosity v can be neglected. Further, Δ is assumed to be a constant. Equation (10.39) thus reduces to

$$\frac{d_s}{E_s} = f \left(\frac{a_1}{\Delta d_{50}}, \frac{a_1}{E_s} \right) \quad (10.40)$$

Experiments by Gaudio and Marion (2003) revealed that only the first nondimensional parameter of the right-hand side of Eq. (10.40) influences the scour depth. The empirical equation of scour depth given by Gaudio and Marion is

$$\frac{d_s}{E_s} = 0.18 \frac{a_1}{\Delta d_{50}} + 0.369 \quad (10.41)$$

The above equation is applicable for $1.3 \leq a_1/(\Delta d_{50}) \leq 9.1$. The length of the scour hole is as follows (Gaudio et al. 2000):

$$\frac{l_s}{E_s} = 1.87 \frac{a_1}{\Delta d_{50}} + 4.02 \quad (10.42)$$

Later, Lenzi et al. (2002) recognized that both the nondimensional parameters of the right-hand side of Eq. (10.40) affect the scour depth. They put forward expressions for the scour depth and the length of the scour hole as

$$\frac{d_s}{E_s} = 0.436 + 1.453 \left(\frac{a_1}{E_s} \right)^{0.863} + 0.06 \left(\frac{a_1}{\Delta d_{95}} \right)^{1.491} \quad (10.43a)$$

$$\frac{l_s}{E_s} = 4.479 + 0.023 \left(\frac{a_1}{E_s} \right)^{-1.81} + 2.524 \left(\frac{a_1}{\Delta d_{95}} \right)^{1.13} \quad (10.43b)$$

10.3.4 Scour Due to Horizontal Jets Issuing from a Gate Opening

The scour phenomenon downstream of a sluice gate opening is complex in nature owing to the abrupt change of the flow characteristics on the sediment bed (Dey and Sarkar 2006a) (Fig. 10.8). Scour initiates at the downstream edge of the apron when the bed shear stress exerted by the submerged jet exceeds the threshold bed shear stress for the bed sediment. In the initial stage, the evolution of the vertical dimension of scour hole is faster than the longitudinal one, and the suspended load is the only mode of sediment transport. However, with the development of the vertical dimension of the scour hole, the mode of sediment transport changes to a combination of suspended load and bed load. As the flow separation takes place at the edge of the apron having a reattachment of flow at the deepest point of the scour hole, the movement of the sediment particles is divided into two parts. Some amount of sediments move along the downstream slope of the scour hole and ultimately go out of the scour hole. The other part moves back toward the upstream along the upstream slope of the scour hole by the reversed flow. The upstream portion of the scour hole achieves a steep slope.

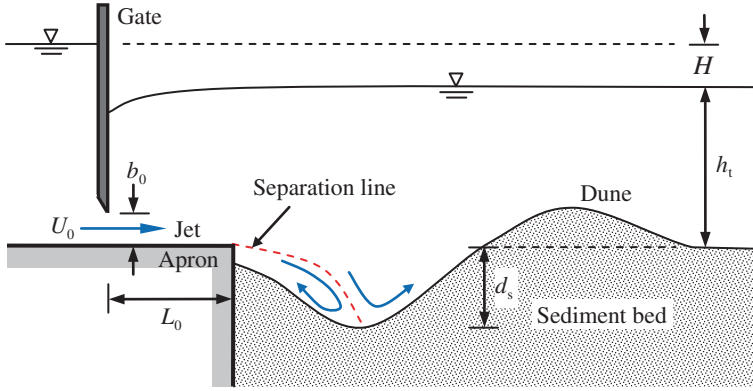


Fig. 10.8 Schematic of scour due to horizontal jet issuing from a sluice gate opening

The theory of submerged plane wall jet was developed by Dey et al. (2010). They derived the velocity and Reynolds stress distributions in submerged wall jets (see Sect. 10.8.1). The theory would help the future researchers to model scour downstream of an apron due to submerged wall jets. However, Dey and Sarkar (2006b) gave a semiempirical model of the same. The application of the theory of submerged wall jet to compute scour is discussed in Sect. 10.8.2.

Qayoum (1960) studied the scour downstream of a vertical gate without apron ($L_0 = 0$). Using the dimensional analysis, he proposed an empirical equation

$$d_s = \frac{2.78}{g^{0.2}} \cdot \frac{q^{0.4} H^{0.22} h_t^{0.4}}{d_{90}^{0.22}} - h_t \quad (10.44)$$

Altinbilek and Basmaci (1973) proposed an equation of scour depth due to submerged jets issuing from a sluice opening as

$$d_s = b_0 \left(\frac{b_0}{d_{50}} \tan \phi \right)^{0.5} \left[\frac{U_0}{(\Delta g b_0)^{0.5}} \right]^{1.5} \quad (10.45)$$

where b_0 is the thickness of sluice opening and U_0 is the issuing velocity of jet.

Breusers and Raudkivi (1991) gave

$$d_s = 8 \times 10^{-3} b_0 \left(\frac{U_0}{u_{*c}} \right)^2 \quad (10.46)$$

Hoffmans (1998) [also Hoffmans and Verheij (1997)] derived equilibrium scour depth due to submerged jets (with $L_0 = 0$) by applying the momentum principle between the vertical section at the sluice opening and the section passing through the dune crest as

$$d_s = b_0 \frac{50}{\lambda_s} \left(1 - \frac{U_{\text{crest}}}{U_0} \right) \quad (10.47)$$

where λ_s is the scour factor dependent on d_{90} , and U_{crest} is the average velocity over the downstream dune crest. The values of λ_s are $\lambda_s(d_{90} = 0.1 \text{ mm}) = 1.4$, $\lambda_s(d_{90} = 0.3 \text{ mm}) = 2$, $\lambda_s(d_{90} = 0.5 \text{ mm}) = 2.3$, $\lambda_s(d_{90} = 1 \text{ mm}) = 2.95$, $\lambda_s(d_{90} = 3 \text{ mm}) = 4.3$, $\lambda_s(d_{90} = 5 \text{ mm}) = 5.1$, $\lambda_s(d_{90} = 10 \text{ mm}) = 6.3$, and $\lambda_s(d_{90} \geq 12 \text{ mm}) = 6.8$.

Shalash (1959) and Dey and Sarkar (2006a) conducted experiments and proposed empirical equations of equilibrium scour depth downstream of an apron due to submerged jets issuing from a sluice opening. According to Shalash (1959),

$$d_s = 0.61 \frac{q^{0.6} (H + h_t)^{0.5}}{d_{90}^{0.4}} \left(1.5 \frac{H}{L_0} \right)^{0.6} - h_t \quad (10.48)$$

and according to Dey and Sarkar (2006a),

$$d_s = 2.59 b_0 \left[\frac{U_0}{(\Delta g d_{50})^{0.5}} \right]^{0.94} \left(\frac{b_0}{L_0} \right)^{0.37} \left(\frac{h_t}{b_0} \right)^{0.16} \left(\frac{d_{50}}{b_0} \right)^{0.25} \quad (10.49)$$

Eggenberger and Müller (1944) investigated scour downstream of hydraulic structures due to a combined overfall and submerged jet (Fig. 10.9). They gave a general relationship for equilibrium scour depth as

$$d_s = \frac{c_0}{15.849} \cdot \frac{q^{0.6} H^{0.5}}{d_{90}^{0.4}} - h_t \quad \wedge \quad c_0 = 22.88 - 10^3 (4.9 \hat{q}^3 - 6.3 \hat{q}^2 + 29 \hat{q} + 64)^{-1} \quad (10.50)$$

where $\hat{q} = q_1/q_0$, q_1 is the overfall discharge per unit width, and q_0 is the submerged jet discharge per unit width through a sluice opening. By definition of continuity, total discharge per unit width is $q = q_1 + q_0$. For overfall only, c_0 ($\hat{q} \gg 1$) = $22.88 \text{ s}^{0.6} \text{ m}^{-0.3}$; and for submerged jets only, c_0 ($\hat{q} \ll 1$) = $10.35 \text{ s}^{0.6} \text{ m}^{-0.3}$.

10.4 Scour Below Horizontal Pipelines

Local scour below pipelines, laid on and across the riverbeds to convey water, oil, gas, or any fluid, commonly occurs by the erosive action of flowing stream. Scour may leave a pipeline unsupported over a considerable distance resulting in fatigue failure due to flow-induced oscillation by wake vortex shedding. Therefore, one of

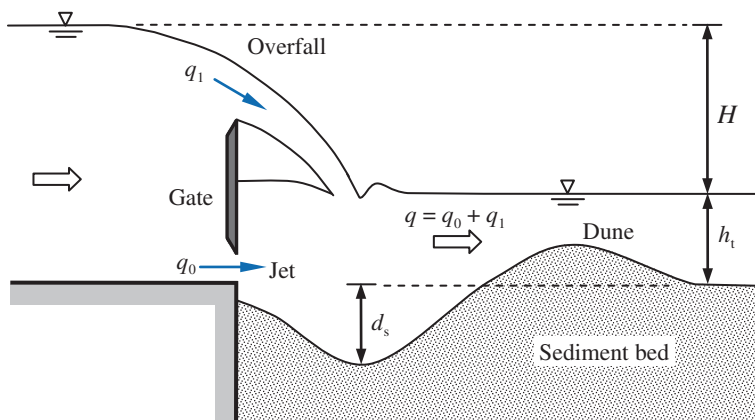


Fig. 10.9 Schematic of scour due to a combined action of overfall and submerged jet allowed by a sluice gate

the imperative aspects of pipeline design is to predict the magnitude of scour below pipelines.

When a pipeline is laid on an erodible bed with a little embedment e (Fig. 10.10), it is subjected to a hydrodynamic force, and a pressure gradient is set up between the two sides of the pipeline. At the same time, the pressure gradient between upstream and downstream contact points (A and B) is also set up in the sediment bed immediately below the pipeline. Due to this pressure gradient, the subsurface seepage flow is driven below the pipeline. As the flow velocity increases, the pressure gradient is simultaneously enhanced, because the pressure intensity is proportional to the quadratic of the flow velocity. With an increase in pressure gradient dp/dx (where p is the pressure intensity and x is the distance along the pipe perimeter), a condition is reached when the sediment below the pipeline starts to dislodge and is called *scour threshold*. The mechanism of scour below a pipeline under a steady flow is described as follows (Sumer and Fredsøe 2002):

Once a threshold point is reached, the seepage flux increases rapidly than the order of the pressure gradient by which the seepage is driven. At the same time, the surface of the sediment bed in the immediate downstream of the pipeline bulges. Eventually, the sediment–water mixture breaks through the space underneath the pipeline, which is called *piping* (Fig. 10.11). Sumer and Fredsøe (2002) derived the threshold condition of piping through a simple calculation by balancing the upward seepage pressure force and the submerged weight of sediment at the exit point B (see Fig. 10.10). It is

$$\frac{1}{\rho g} \cdot \frac{dp}{dx} \geq \Delta(1 - \rho_0)$$

Fig. 10.10 Schematic of seepage flow induced below a pipeline

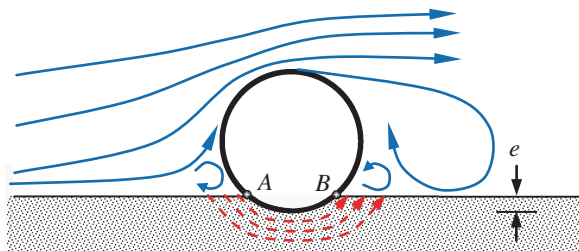
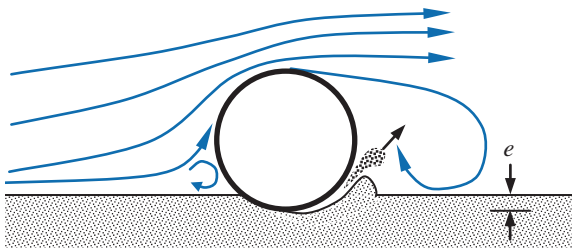


Fig. 10.11 Piping



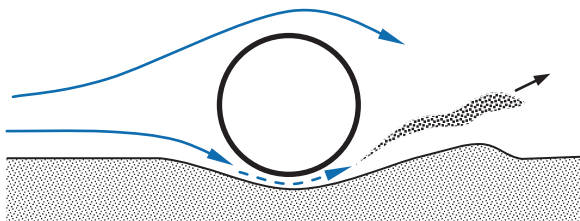
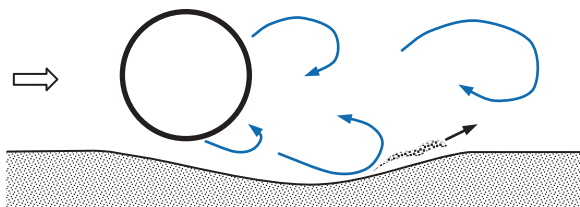
where ρ_0 is the porosity of the sediment. Further, Sumer et al. (2001) determined the threshold condition empirically in terms of velocity considering a small embedment e of the pipeline having an external diameter D . Using the above relationship and the laboratory experimental data, they proposed

$$\frac{U_{\text{gr}}^2}{\Delta g(1 - \rho_0)D} = 0.025 \exp\left(81 \frac{e}{D}\right)^{0.5} \quad (10.51)$$

where U_{gr} is the threshold velocity of scour below a pipeline. Note that the scour does not initiate all along the length of the pipeline simultaneously, but occurs locally.

After the piping process, a small gap is developed between the pipeline and the bed. A considerable magnitude of flow is diverted to the gap leading to a flow concentration in the gap. It enhances the shear stress acting on the bed immediately below the pipeline. The enhanced bed shear stress is of the order of magnitude of three times the bed shear stress of the approaching flow (Jensen et al. 1990). As a result, a large amount of sediment is scoured underneath the pipeline. The sediment–water mixture is spouted from the enlarged gap. Such scour process is known as *tunnel erosion* (Fig. 10.12). With an increase in gap size, the gap velocity decreases and the tunnel erosion gradually ceases. This stage is followed by *lee-wake erosion*.

As a result of tunnel erosion, a dune is formed on the downstream end of the pipeline and it gradually migrates further downstream. Finally, the dune disappears as the scour progresses. At this stage, the scour is governed by the *lee-wake*

Fig. 10.12 Tunnel erosion**Fig. 10.13** Lee-wake erosion

erosion, which occurs due to the vortex shedding on the downstream end of the pipeline (Fig. 10.13). At the end of the tunnel erosion, when the gap between the pipeline and the bed enlarges to a certain magnitude, the vortex shedding begins. The vortices that shed from the pipe wall sweep the sediment as they get convected downstream. During this period, the bed shear stress increases by about four times having a greater scour potential at the lee end of the pipe. However, the bed shear stress gradually reduces with the enlargement of the scour hole size. The equilibrium is reached when the bed shear stress underneath the pipeline reaches the value being equal to the threshold bed shear stress for sediment motion in clear-water case or equal to the approaching bed shear stress in live-bed case. Figure 10.14 shows the photograph of an equilibrium scour below a pipe in a flume.

10.4.1 Estimation of Gap Discharge

In studying scour below a pipeline, estimation of gap discharge is an important aspect. It can be determined analytically as described here. The schematic of a scour hole below a pipeline and the coordinate system are shown in Fig. 10.15, where the origin of the coordinate system lies at the contact point of the circular pipe with the initial bed level. According to Chao and Hennessy (1972), the *image method* of potential flow theory is applicable assuming a steady flow around the pipeline and neglecting the curvature effect of the scour hole. The potential function ϕ and the stream function ψ governing the flow are

Fig. 10.14 Photograph of an equilibrium scour below a pipe in an experimental flume. Flow took place from the right to left

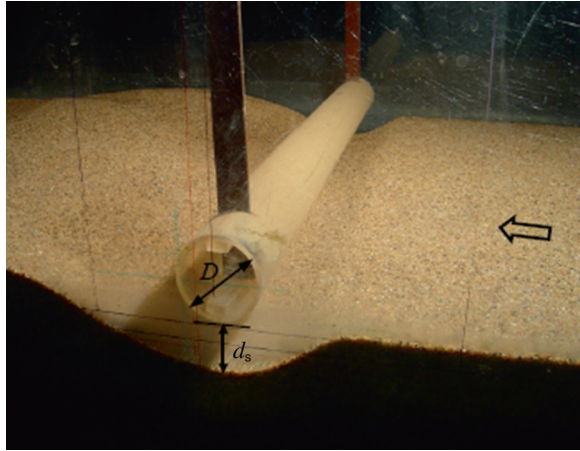
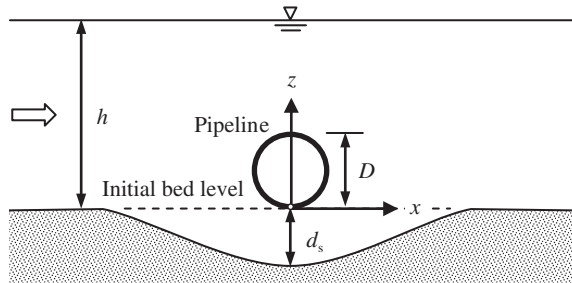


Fig. 10.15 Schematic of a scour hole below a pipeline and the coordinate system



$$\phi = U_0 x \left\{ 1 + \frac{D^2}{4[x^2 + (z - 0.5D)^2]} + \frac{D^2}{4[x^2 + (z + 2d_s + 0.5D)^2]} \right\} \quad (10.52a)$$

$$\psi = U_0(z + d_s) \left\{ 1 - \frac{D^2}{4[x^2 + (z - 0.5D)^2]} - \frac{D^2}{4[x^2 + (z + 2d_s + 0.5D)^2]} \right\} \quad (10.52b)$$

where U_0 is the depth-averaged velocity up to the elevation of the horizontal diameter of the pipeline, that is, $z = 0.5D$. It can be estimated assuming a logarithmic law of approaching velocity as $U_0 = 5.75u_* \log(2.765D/d_{50})$, where u_* is the approaching shear velocity. Here, it is intuitive that the flow through the gap is

contributed by the approaching flow velocity up to the elevation of the horizontal diameter of the pipeline from the bed level. Hence, the horizontal velocity component \bar{u} within the scour hole is given by

$$\bar{u} = \frac{\partial \phi}{\partial x} = U_0 \left\{ 1 + \frac{D^2}{4[x^2 + (z - 0.5D)^2]} - \frac{x^2 D^2}{2[x^2 + (z - 0.5D)^2]^2} + \frac{D^2}{4[x^2 + (z + 2d_s + 0.5D)^2]} - \frac{x^2 D^2}{2[x^2 + (z + 2d_s + 0.5D)^2]^2} \right\} \quad (10.53)$$

Integrating \bar{u} within limits $z = -d_s$ and $z = 0$, the gap discharge q_g is obtained as

$$q_g = \int_{-d_s}^0 \bar{u} dz = U_0 \left[d_s + 0.5D - \frac{D^2}{4(2d_s + 0.5D)} \right] \quad (10.54)$$

Alternatively, one can also estimate the gap discharge q_g from the graphical solution given by Chiew (1991) as h/D is a function of q_g/q , where h is the flow depth and q is the free stream discharge per unit width in the channel. However, it would be convenient to use his graphical solution if it is expressed as follows (Dey and Singh 2007):

$$q_g = 0.781q \left(\frac{D}{h} \right)^{0.787} \quad (10.55)$$

10.4.2 Scour Depth Estimation

Phenomena involved in local scour below underwater pipelines have been studied most extensively in the laboratory experiments, from which a number of empirical equations and the methodologies have been developed to estimate the equilibrium scour depth below pipelines. The important predictors of scour depth are summarized below:

Kjeldsen et al. (1973) were the pioneer to give an empirical relationship for equilibrium scour depth below pipelines. It is

$$d_s = 0.972 \left(\frac{U^2}{2g} \right)^{0.2} D^{0.8} \quad (10.56)$$

The Dutch research group (Bijker and Leeuwestein 1984) put forward the following empirical equation of scour depth below an underwater pipeline:

$$d_s = 0.929 \left(\frac{U^2}{2g} \right)^{0.26} \frac{D^{0.78}}{d_{50}^{0.04}} \quad (10.57)$$

The empirical equations proposed by Ibrahim and Nalluri (1986) for the estimation of scour depth below pipelines in clear-water and live-bed conditions are

$$\text{Clear-water scour: } \frac{d_s}{D} = 4.706 \left(\frac{U}{U_{cr}} \right)^{0.89} Fr^{1.43} + 0.06 \quad (10.58a)$$

$$\text{Live-bed scour: } \frac{d_s}{D} = 0.084 \left(\frac{U}{U_{cr}} \right)^{-0.3} Fr^{-0.16} + 1.33 \quad (10.58b)$$

where Fr is the Froude number $[= U/(gh)^{0.5}]$ and U_{cr} is the threshold velocity for sediment motion.

Chiew (1991) proposed the following iterative method to predict equilibrium scour depth below pipelines:

1. For a given value of h/D , determine the gap discharge q_g .
2. Assume a scour depth d_s and estimate the average gap velocity U_g below the pipeline by $U_g = q_g/d_s$.
3. Compute the shear stress τ_0 on the scoured bed using $\tau_0 = \lambda_D \rho U_g^2 / 8$, where the friction factor λ_D can be estimated from the Moody diagram for a relative roughness $(= d_{s0}/d_s)$ and a Reynolds number $(= U_g d_s / \nu)$.
4. Compare τ_0 with the threshold bed shear stress τ_{0c} obtained from the Shields diagram. Continue the iteration for different values of d_s until $\tau_{0c} = \tau_0$.

Moncada-M and Aguirre-Pe (1999) suggested the following empirical equation of equilibrium scour depth below an underwater pipeline:

$$\frac{d_s}{D} = 0.9 \tanh \left[1.4 \frac{U}{(gh)^{0.5}} \right] + 0.55 \quad (10.59)$$

With consideration of an initial gap e between the original bed level and the pipe bottom above the bed level, Moncada-M and Aguirre-Pe (1999) proposed

$$\frac{d_s}{D} = 2Fr \operatorname{sech} \left(1.7 \frac{e}{D} \right) \quad (10.60)$$

Based on wall correction method (Sect. 3.9), Dey and Singh (2007) put forward a simplified iterative method for the computation of equilibrium scour depth. Dey and Singh (2008) conducted an extensive experimental study to explore the

Fig. 10.16 Influence of pipe Froude number F_D on scour depth d_s (Dey and Singh 2008)

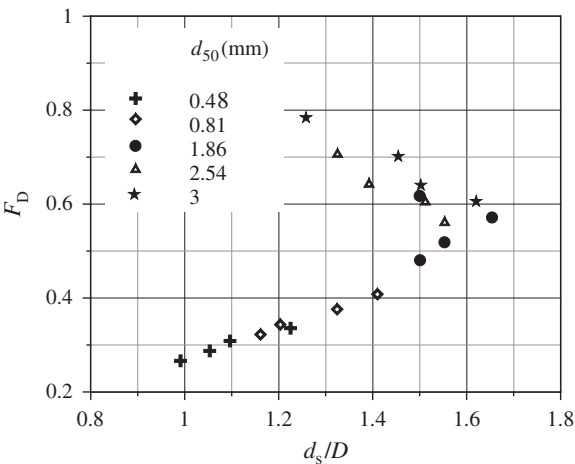
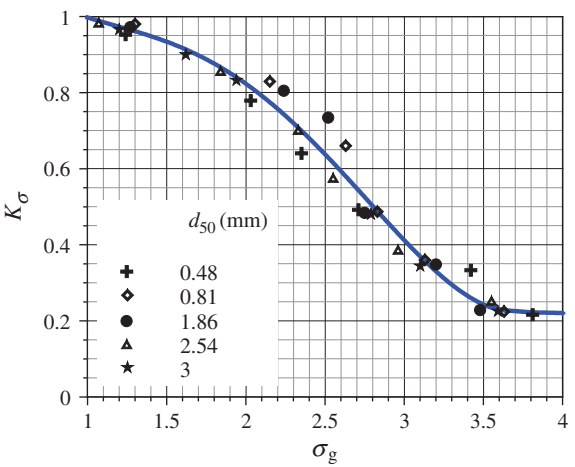


Fig. 10.17 Variation of K_σ as a function of σ_g (Dey and Singh 2008)



influence of various parameters on equilibrium scour depth in clear-water condition ($U/U_{cr} \approx 0.9$). The equilibrium scour depth d_s increases with an increase in approach flow depth h for shallow flow depths, becoming independent of higher flow depths when $h/D > 5$. The curve of scour depth versus pipe Froude number F_D [$= U/(\Delta g D)^{0.5}$] has a maximum value of $d_s/D = 1.65$ at $F_D = 0.58$ (Fig. 10.16).

Dey and Singh (2008) also studied the influence of sediment gradation on scour depth. The influence of sediment gradation was found to be prominent for non-uniform sediments, which reduce scour depth to a large extent due to the formation of armor layer within the scour hole. The variation of K_σ with σ_g is shown in Fig. 10.17. Further, the influence of different shaped cross sections of pipes on the

scour depth was investigated, where the *shape factors*² for circular, 45° (diagonal facing), and 90° (side facing) square pipes were obtained as 1, 1.29, and 1.91, respectively.

10.5 Scour at Bridge Piers

At bridge sites, localized scour in the vicinity of piers, over which the bridge superstructure rests, poses a challenging problem to the hydraulic engineers. Figure 10.18 shows the photograph of bridge piers, where the scour takes place even in the summer season at a lean flow discharge condition. Failure of bridges due to scour at pier foundations is a common occurrence, if the magnitude of scour is too large to uncover the pier foundations. The obstruction to the approaching flowing stream by a bridge pier causes a three-dimensional separation of flow forming a vortex flow and a periodical vortex shedding downstream of the pier. The complexity in flow structure increases with the development of the scour hole. To be more explicit, the flow separates at the upstream face of the pier as it travels by the side of the pier, creating a vortex trail, termed *horseshoe vortex*. The vortex moves downstream and as a result of which local scour takes place around the pier due to the removal of bed sediment. The scour at bridge piers has been studied extensively by various researchers. Reviews of the important experiments and field studies were given by Breusers et al. (1977), Dey (1997a, b), Melville and Coleman (2000), and Richardson and Davis (2001). Figure 10.19 shows the photograph of an equilibrium scour hole at a circular pier in an experimental flume. It gives an idea about the shape of the scour hole that occurs at a pier.

According to Raudkivi (1986), the approaching flow, which is stationary at the upstream face of the pier, is maximum at the free surface and decreases to zero at the bed in the free flow (unobstructed by the pier) reach. The stagnation pressure at the upstream face of the pier decreases in the downward direction causing the flow to be driven down along the face of the pier, producing a *downflow*. The downflow along the vertical plane of symmetry of the pier has a velocity profile with zero at the pier wall and again at some distance upstream of it. The maximum magnitude of downflow, at any elevation in the upstream, measured by Ettema (1980) occurs at $0.02\text{--}0.05b$ from the pier face being closer to the pier lower down. Here, b is the pier width across the flow (or pier diameter in case of a circular pier). The *horseshoe vortex* developed due to the flow separation at the upstream edge of the scour hole rolls to form a helical flow, which is similar to the ground roller downstream (leeside) of a dune crest (see Sect. 8.2.2). It migrates downstream by the side of the pier for a few pier diameters before losing its existence becoming a

² *Shape factor* is the ratio of the equilibrium scour depth for a given non-circular pipe to that for a circular shaped pipe having a same diameter to the vertical cross-sectional length of the non-circular pipe.



Fig. 10.18 Scour taking place at bridge piers in a field condition. Photograph by the author

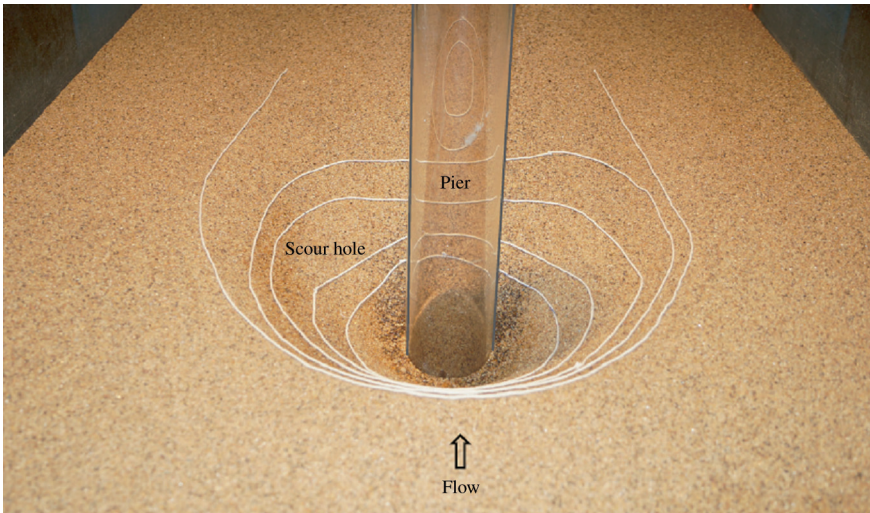


Fig. 10.19 Photograph of an equilibrium scour at a circular pier in an experimental flume

part of the general turbulence. The horseshoe vortex is a consequence of scour, not the cause of scouring. It also pushes the downflow inside the scour hole closer to the pier. The *bow wave*, formed at the free surface adjacent to the pier face rotating in a direction opposite to that of the horseshoe vortex, becomes pertinent in relatively shallow flows where it can interfere with the approaching flow causing a reduction in downflow velocity. The stagnation pressure also accelerates the flow by the side of the pier, resulting in a flow separation at the side and creating a *wake* with the cast-off vortices at the interfaces to the main flow. The cast-off vortices travel downstream with the flow and interact with the horseshoe vortex at the bed

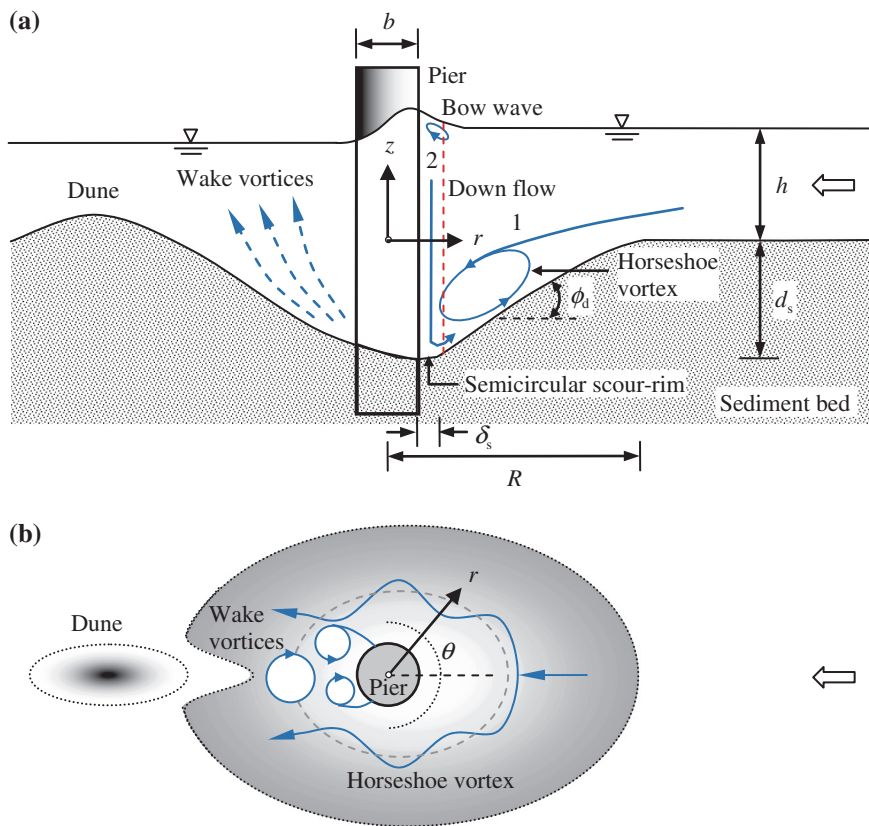


Fig. 10.20 Typical geometry of a scour hole and the components of flow field at a circular pier: **a** elevation view and **b** plan view

causing it to oscillate. Figures 10.20a, b show the typical geometry of a scour hole and the components of the flow field at a pier.

Conducting an experimental study, Dey (1991) described the clear-water scouring process at a circular pier. According to him, the horseshoe vortex is formed due to the diving mode of approaching flow into the scour hole. In the upstream of a pier, the sediment particles are mainly dislodged by the action of the downflow and subsequently pulled up along the upstream slope of the scour hole by the upward velocity of the horseshoe vortex. The scour hole is also fed by the sediment due to the collapse of the slant bed of scour hole, and finally, the sediment particles are drifted downstream by the arms of the horseshoe vortex along the circumference of the pier. The process of digging by the downflow along with the slant bed erosion continues until a quasi-equilibrium state is reached (Dey 1995). In this state, the scour hole is continually fed by a small amount of sediment particles due to slant bed erosion without a noticeable change in scour depth. The equilibrium, when the erosion ceases, is reached after a long period of time.

In quasi-equilibrium state, the average upstream slope of the scour hole, termed *dynamic angle of repose* ϕ_d , is about 10–20 % greater than the angle of repose ϕ of sediment in still water. A flat semicircular rim is formed around the upstream pier base (Fig. 10.20a). On downstream, the scour initiates at the pier base due to wake vortices (which act like a tornado) in the form of a spontaneous lifting of sediment particles by the action of suction from the each core of wake vortices. In the further downstream, a dune is progressively formed by the substantial deposition of sediment and side scouring. The dune, thus formed, slowly migrates downstream with the development of the scour hole. The erosion continues on both sides of the dune to form a shallow channel on either side having an adverse longitudinal slope that is flatter than the upstream slope.

Melville (1975), Dey et al. (1995), Dey (1995), Graf and Istiarto (2002) and Dey and Raikar (2007a) and Raikar and Dey (2008) measured the flow field in a scour hole at a pier. The flow measurement was done by hot-wire anemometry (Melville 1975), five-hole pitot sphere (Dey et al. 1995), and acoustic Doppler velocity profiler (Graf and Istiarto 2002). On the other hand, Dey and Raikar (2007a) and Raikar and Dey (2008) measured the flow by an acoustic Doppler velocimeter (ADV) and studied the characteristics of turbulent horseshoe vortex flow within the developing scour hole at cylindrical piers. Figure 10.21 shows the time-averaged velocity vectors at the upstream axis of symmetry of a pier in an equilibrium scour hole. The horseshoe vortex flow is well evident within the scour hole.

10.5.1 Kinematic Model of Horseshoe Vortex

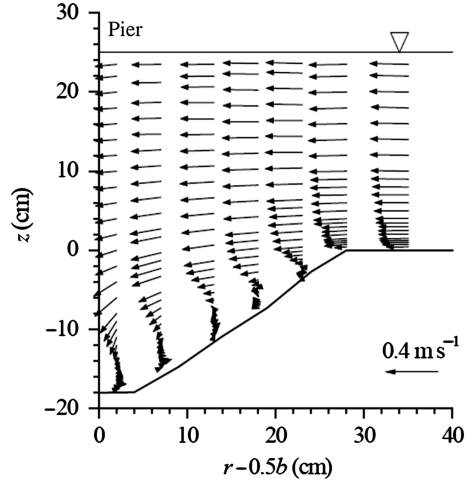
Dey et al. (1995) developed a kinematic model for the horseshoe vortex flow in a scour hole at a pier.

In the upstream, the azimuthal section of a quasi-equilibrium scour hole, as shown in Fig. 10.20a, is divided into zone 1, that is the zone vertically above the sloping bed, and zone 2, that is the zone vertically above the flat bed (semicircular rim) of the scour hole adjacent to the pier. The upstream edge of the scour hole can be approximately represented by a circular arc up to the azimuthal angle $\theta = \pm 75^\circ$. The width δ_s of zone 2 is expressed as $\varepsilon_w(R - 0.5b)$, where ε_w is a factor (≈ 0.1), R is the radius of the scour hole, that is, $[d_s \cot \phi_d / (1 - \varepsilon_w)] + 0.5b$, and d_s is the scour depth. In cylindrical polar coordinates, the velocity components (u_r , u_θ , u_z) are in r , θ , and z -direction, respectively.

The tangential velocity u_θ is represented by a power law preserving the no-slip condition at the bed

$$\frac{u_\theta}{U} = k_1 \sin \theta G^m \left(J + \frac{z}{d_s} \right)^{1/n} \quad (10.61)$$

Fig. 10.21 Velocity vectors at the upstream axis of symmetry of a pier in an equilibrium scour hole (Dey and Raikar 2007a)



where

$$\left. \begin{aligned} G(r) &= 1 \\ J(r) &= \frac{R - r}{(R - 0.5b)(1 - \varepsilon_w)} \end{aligned} \right\} \text{for zone 1, that is } 0.5b + \varepsilon_w(R - 0.5b) \leq r \leq R$$

$$\left. \begin{aligned} G(r) &= \frac{R - r}{(R - 0.5b)(1 - \varepsilon_w)} \\ J(r) &= 1 \end{aligned} \right\} \text{for zone 2, that is } 0.5b < r \leq 0.5b + \varepsilon_w(R - 0.5b)$$

where $k_1 = k_1(U, h, b, d_s)$, U is the depth-averaged approaching flow velocity, h is the approaching flow depth, and m and n are the exponents. The values of m and n were obtained as 2.1 and 3.9, respectively.

The radial velocity u_r changes direction in the scour hole. The u_r -distribution along z varies linearly in the scour hole ($z \leq 0$) and follows a power law above it ($z > 0$). On the other hand, the u_r -distribution along r is parabolic. Thus, the expression for u_r is

$$\frac{u_r}{U} = -k_2 \cos \theta (J + \zeta_1) \left(2 \frac{r}{b} - 1 \right) \quad (10.62)$$

where

$$\zeta_1(z) = 2 \frac{z}{d_s} \quad \text{for zone 1, that is } -\frac{(R - r)d_s}{(R - 0.5b)(1 - \varepsilon_w)} \leq z \leq 0$$

$$\zeta_1(z) = k_3 \left(\frac{z}{h} \right)^{1/\alpha} \quad \text{for zone 2, that is } 0 \leq z \leq h$$

where k_2 and k_3 are the coefficients similar to k_1 , $\alpha = \kappa U/u_*$, κ is the von Kármán constant, and u_* is the shear velocity. Note that Eqs. (10.61) and (10.62) violate the no-slip condition at the pier wall and the bed, respectively, and cannot be applicable to the immediate vicinity of them.

The expression for vertical velocity u_z , obtained by integrating the continuity equation (Eq. 2.164), is

$$\begin{aligned} \frac{u_z}{U} = & -k_1 \cos \theta \frac{d_s}{r} \cdot \frac{n}{1+n} G^m \left(J + \frac{z}{d_s} \right)^{(1+n)/n} + k_2 \cos \theta \frac{z}{r} \left\{ \left(4 \frac{r}{b} - 1 \right) (G + \zeta_2) \right. \\ & \left. - \operatorname{sgn}(r) \frac{r}{(R - 0.5b)(1 - \varepsilon_w)} \left(2 \frac{r}{b} - 1 \right) \right\} \end{aligned} \quad (10.63)$$

where

$$\begin{aligned} \zeta_2(z) &= \frac{z}{d_s} \quad \text{for zone 1, that is } -\frac{(R-r)d_s}{(R-0.5b)(1-\varepsilon_w)} \leq z \leq 0 \\ \zeta_2(z) &= k_3 \frac{\alpha}{1+\alpha} \left(\frac{z}{h} \right)^{1/\alpha} \quad \text{for zone 2, that is } 0 \leq z \leq h \\ \operatorname{sgn}(r) &= 1 \quad \text{for zone 1, that is } 0.5b + \varepsilon_w(R - 0.5b) \leq r \leq R \\ \operatorname{sgn}(r) &= 0 \quad \text{for zone 2, that is } 0.5b < r \leq 0.5b + \varepsilon_w(R - 0.5b) \end{aligned}$$

Equation (10.63) produces a strong downflow along the upstream face of the pier and a flow reversal in the scour hole. It however violates the no-slip condition at the pier wall and the bed. Dey et al. gave the expressions for the coefficients as

$$\begin{aligned} k_1 &= 1.9 Fr^{0.83} \left(\frac{h}{b} \right)^{0.69} \left(\frac{b}{d_s} \right)^2 \quad \wedge \quad Fr = \frac{U}{(gh)^{0.5}} \\ k_2 &= 2 Fr^{0.92} \left(\frac{h}{b} \right)^{0.57} \left(\frac{b}{d_s} \right)^2 \\ k_3 &= \frac{0.8}{k_2} \cdot \frac{1+\alpha}{\alpha} \left(2 \frac{R}{b} - 1 \right)^{-1} \end{aligned}$$

Dey and Bose (1994) used the expressions for u_r , u_θ , and u_z to compute the bed shear stress in the scour hole by applying the turbulent boundary-layer approach.

10.5.2 Scour Depth Prediction

Scour at piers is influenced by various parameters (Breusers et al. 1977), which are grouped as follows:

1. *Parameters related to the pier*: Size, shape, spacing, number, and orientation with respect to the approaching flow direction.
2. *Parameters related to the bed sediment*: Median particle size, particle size distribution, angle of repose, and cohesiveness.
3. *Parameters related to the approaching flow condition*: Approaching flow velocity, approaching flow depth, shear velocity, and roughness.
4. *Parameters related to the fluid*: Mass density, viscosity, gravitational acceleration, and temperature. Note that the temperature may not be important in scour problems, unless free surface is frozen.
5. *Parameters related to the time*: Time of scour for an evolving scour case.

A large number of empirical equations were proposed by various investigators to estimate the maximum scour depth at piers based on the data from the laboratory experiments and the field measurements. In general, these equations were derived from a limited range of data and are applicable to the conditions similar to those for which they are valid. Though the number of proposed equations for the estimation of maximum scour depth is overwhelming (Dey 1997a; Melville and Coleman 2000), it is however difficult to confirm their adequacy for the design purposes due to limited field measurements. Nevertheless, the design equations proposed by Melville and Coleman (2000), HEC18 (Richardson and Davis 2001), and Sheppard et al. (2014) seem to provide satisfactory estimations.

Melville and Coleman (2000) recommended a design equation for the estimation of maximum scour depth at piers based on empirical factors, called K -factors, which account for the effects of pier, flow, and sediment characteristics. The K -factors were determined by fitting the curves that overlap the data plots. Thus, the proposed K -factors potentially remain adequate from the viewpoint of a safe pier foundation design. The maximum scour depth d_s at a bridge pier formulated as a product of various K -factors is given as

$$d_s = K_h K_I K_d K_s K_z K_t \quad (10.64)$$

where K_h is the flow depth–pier size factor, K_I is the flow intensity factor, K_d is the sediment size factor, K_s is the pier shape factor, K_z is the pier alignment factor, and K_t is the time factor. The relationships for the K -factors are as follows:

The *flow depth–pier size factor* K_h is the scour depth d_s at a pier of width b for a given value of flow depth h . It is given by

$$\left. \begin{aligned} K_h(b/h < 0.7) &= 2.4b \\ K_h(0.7 \leq b/h < 5) &= 2(hb)^{0.5} \\ K_h(b/h \geq 5) &= 4.5h \end{aligned} \right\} \quad (10.65)$$

The *flow intensity factor* K_I is the ratio of the scour depth d_s for a given flow velocity U to that for the threshold flow velocity U_{cr} for the bed sediment motion. Thus, the flow intensity factor K_I represents the effects of flow intensity on scour

depth. It also accounts for the nonuniformity of sediment in terms of average approaching velocity U_a at armor peak. It is given by

$$\left. \begin{aligned} K_I &= \frac{U - (U_a - U_{cr})}{U_{cr}}, \quad \text{for } \frac{U - (U_a - U_{cr})}{U_{cr}} < 1 \\ K_I &= 1, \quad \text{for } \frac{U - (U_a - U_{cr})}{U_{cr}} \geq 1 \end{aligned} \right\} \quad (10.66)$$

where $U_a = 0.8U_{cra}$ and U_{cra} is the maximum average velocity for the bed to armor. Note that for uniform sediment, $U_a(\sigma_g < 1.3) = U_{cr}$. Under varied stream flow velocities over a bed of nonuniform sediment, a process of armoring prevails resulting in an exposure of coarser particles due to washing out of the finer fraction. The armoring effect is to reduce the scour depth. The U_{cr} and U_{cra} can be obtained from

$$\frac{U_{cr}}{u_{*c}} = 5.75 \log \left(5.53 \frac{h}{d_{50}} \right), \quad \frac{U_{cra}}{u_{*ca}} = 5.75 \log \left(5.53 \frac{h}{d_{50a}} \right) \quad (10.67)$$

where u_{*ca} is the threshold shear velocity for median size d_{50a} of armor particles, $d_{50a} = d_{max}/1.8$ and d_{max} is the maximum bed sediment size. Melville and Coleman suggested that the u_{*c} can be empirically calculated as $u_{*c}(0.1 \text{ mm} \leq d_{50} < 1 \text{ mm}) = 0.0115 + 0.0125d_{50}^{1.4}$ and $u_{*c}(1 \text{ mm} \leq d_{50} < 100 \text{ mm}) = 0.0305d_{50}^{0.5} - 6.5 \times 10^{-3}d_{50}^{-1}$.

Here, u_{*c} is in m s^{-1} and d_{50} in mm. For u_{*ca} , same expressions can be used replacing u_{*c} by u_{*ca} and d_{50} by d_{50a} .

The *sediment size factor* K_d is the ratio of the scour depth d_s for a given value of b/d_{50} to that for b/d_{50} for which d_s becomes maximum and beyond which, there is no effect of b/d_{50} on d_s . For nonuniform sediment, d_{50} is to be replaced by d_{50a} . It is

$$\left. \begin{aligned} K_d(b/d_{50} \leq 25) &= 0.57 \log \left(2.24 \frac{b}{d_{50}} \right) \\ K_d(b/d_{50} > 25) &= 1 \end{aligned} \right\} \quad (10.68)$$

However, for the piers embedded in gravel-beds, Raikar and Dey (2005b) proposed an additional set of sediment size factor. It is

$$\left. \begin{aligned} K_d(b/d_{50} \leq 9) &= 0.6 \log \left(3.88 \frac{b}{d_{50}} \right) \\ K_d(9 < b/d_{50} \leq 25) &= 0.184 \log \left(14070 \frac{b}{d_{50}} \right) \\ K_d(b/d_{50} > 25) &= 1 \end{aligned} \right\} \quad (10.69)$$

Table 10.2 Shape factors K_s for pier scour





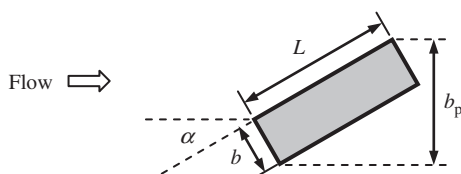
Shape	Name	K_s
	Circular	1
	Round nosed	1
	Square nosed	1.1
	Sharp nosed	0.9

Fig. 10.22 Oblique alignment of a rectangular pier with respect to approaching flow direction

The *shape factor* K_s is defined as the ratio of the scour depth d_s for a particular pier shape to that for the circular pier having a diameter same as the pier width. The shape factors K_s for different piers are furnished in Table 10.2.

The *alignment factor* K_α is the ratio of the scour depth d_s at an oblique pier to that at an aligned pier. In case of noncircular piers, the scour depth increases with an increase in the effective projected width of the piers. The K_α is given by

$$K_\alpha = \left(\frac{b_p}{b} \right)^{0.65} \quad (10.70)$$

where b_p is the projected width of a rectangular pier normal to the approaching flow ($= L \sin \alpha + b \cos \alpha$), α is the pier orientation with respect to the approaching flow or skewness, and L is the pier length (Fig. 10.22). For circular piers, $K_\alpha = 1$.

The *time factor* K_t is the ratio of the scour depth d_s for a given time t to the equilibrium scour depth. It depends on the scour condition, such as clear-water scour and live-bed scour. For live-bed scour, K_t can be approximated as unity, as equilibrium is attained rather rapidly, while for clear-water scour, K_t is given by

$$K_t = \exp \left[-0.03 \left| \frac{U_{cr}}{U} \ln \left(\frac{t}{t_e} \right) \right|^{1.6} \right] \quad (10.71)$$

where t_e is the time to reach equilibrium scour depth. It can be calculated from

Table 10.3 Bed condition factors K_{bed} for pier scour

Bed condition	Dune height, η_d (m)	K_{bed}
Clear-water	–	1.1
Plane bed and antidunes	–	1.1
Small dunes	$0.6 \leq \eta_d < 3$	1.1
Medium dunes	$3 \leq \eta_d < 9$	1.1–1.2
Large dunes	$\eta_d \geq 9$	1.3

Table 10.4 Alignment factors K_z for pier scour

α (degree)	$L/b = 4$	$L/b = 8$	$L/b = 12$
0	1	1	1
15	1.5	2	2.5
30	2	2.75	3.5
45	2.3	3.3	4.3
90	2.5	3.9	5

$$\left. \begin{aligned} t_e(\text{days}) &= 48.26 \frac{b}{U} \left(\frac{U}{U_{\text{cr}}} - 0.4 \right), \quad \text{for } \frac{h}{b} > 6 \text{ and } \frac{U}{U_{\text{cr}}} > 0.4 \\ t_e(\text{days}) &= 30.89 \frac{b}{U} \left(\frac{U}{U_{\text{cr}}} - 0.4 \right) \left(\frac{h}{b} \right)^{0.25}, \quad \text{for } \frac{h}{b} \leq 6 \text{ and } \frac{U}{U_{\text{cr}}} > 0.4 \end{aligned} \right\} \quad (10.72)$$

At threshold condition ($U = U_{\text{cr}}$), t_e being maximum, when $h > 6b$, is given as

$$t_e(\text{days}) = 28.96 \frac{b}{U} \quad (10.73)$$

where b is in m and U in m s^{-1} .

According to HEC18 (Richardson and Davis 2001), the scour depth at a pier in both clear-water and live-bed scour conditions is given by

$$\frac{d_s}{b} = 2K_s K_z K_{\text{bed}} K_a \left(\frac{h}{b} \right)^{0.35} Fr^{0.43} \quad (10.74)$$

where K_{bed} is the factor for bed condition (Table 10.3) and K_a is the factor for armoring of bed sediment. Further, for a maximum value of d_s at a round-nosed pier with aligned flow, if $Fr \leq 0.8$, then $d_s/b \leq 2.4$ and if $Fr > 0.8$, then $d_s/b \leq 3$ (Table 10.4).

The K_a that takes into account of armoring of bed sediment can be given as

$$K_a = 1, \quad \text{for } d_{50} < 2 \text{ mm or } d_{95} < 20 \text{ mm} \quad (10.75a)$$

$$K_a = 0.4U_r^{0.15}, \quad \text{for } d_{50} \geq 2 \text{ mm and } d_{95} \geq 20 \text{ mm} \quad \wedge \quad U_r = \frac{U - U_{\text{crs}}|_{d_{50}}}{U_{\text{cr}}|_{d_{50}} - U_{\text{crs}}|_{d_{95}}} \quad (10.75b)$$

where $U_{\text{crs}}|_{d_i}$ is the approaching flow velocity required for threshold of scour at a pier with sediment size d_i , $U_{\text{cr}}|_{d_i}$ is the threshold flow velocity for bed sediment of size d_i , and d_i is the i -percent finer sediment size. Note that in Eq. (10.75b), U_r should be positive ($U_r > 0$). The $U_{\text{crs}}|_{d_i}$ is estimated as

$$U_{\text{crs}}|_{d_i} = 0.645 \left(\frac{d_i}{b} \right)^{0.053} U_{\text{cr}}|_{d_i} \quad \wedge \quad U_{\text{cr}}|_{d_i} = 6.19h^{1/6}d_i^{1/3} \quad (10.76)$$

Further, Sheppard et al. (2014) proposed a method of scour depth prediction as

$$\frac{d_s}{b_e} = 2.5f_1f_2f_3, \quad \text{for } 0.4U_{\text{cr}} \leq U < U_{\text{cr}} \quad (10.77a)$$

$$\frac{d_s}{b_e} = f_1 \left[2.2 \left(\frac{U - U_{\text{cr}}}{U_{\text{peak}} - U_{\text{cr}}} \right) + 2.5f_3 \left(\frac{U_{\text{peak}} - U}{U_{\text{peak}} - U_{\text{cr}}} \right) \right], \quad \text{for } U_{\text{cr}} \leq U \leq U_{\text{peak}} \quad (10.77b)$$

$$\frac{d_s}{b_e} = 2.2f_1, \quad \text{for } U > U_{\text{peak}} \quad (10.77c)$$

where b_e is the effective pier diameter and U_{peak} is the live-bed peak flow velocity,

$$f_1 = \tanh \left[\left(\frac{h}{b_e} \right)^{0.4} \right], \quad f_2 = 1 - 1.2 \left[\ln \left(\frac{U}{U_{\text{cr}}} \right) \right]^2, \quad f_3 = \frac{\frac{b_e}{d_{50}}}{0.4 \left(\frac{b_e}{d_{50}} \right)^{1.2} + 10.6 \left(\frac{b_e}{d_{50}} \right)^{-0.13}},$$

$$\left. \begin{aligned} U_{\text{peak}} &= 5U_{\text{cr}}, \quad \text{if } 5U_{\text{cr}} \geq 0.6(gh)^{0.5} \\ U_{\text{peak}} &= 0.6(gh)^{0.5}, \quad \text{if } 5U_{\text{cr}} < 0.6(gh)^{0.5} \end{aligned} \right\}, \quad b_e = K_s b_p, \quad K_s = 0.86 + 0.97 \left| \alpha - \frac{\pi}{4} \right|^4$$

In the above, α is in radians and $K_s = 1$ for circular piers.

They suggested the empirical relationship for the computation of U_{cr} as

$$U_{\text{cr}}(5 \leq \Re \leq 70) = 2.5u_{*c} \ln \left\{ \frac{73.5h}{d_{50}} \left[\Re(2.85 + 0.002\Re - 0.58 \ln \Re) + \frac{111}{\Re} - 6 \right]^{-1} \right\} \quad (10.78a)$$

Table 10.5 Equations of equilibrium scour depth at piers proposed by different investigators

References	Formula	Regime	Note
Laursen and Toch (1956)	$\frac{d_s}{b} = 1.35 \left(\frac{h}{b} \right)^{0.3}$	Clear-water	Laursen and Toch's design curves were expressed by Neill (1964)
Shen et al. (1969)	$d_s = 2.23 \times 10^{-4} \left(\frac{Ub}{v} \right)^{0.619}$	Clear-water	
Hancu (1971)	$\frac{d_s}{b} = 2.42 \left(2 \frac{U}{U_{cr}} - 1 \right) \times \left(\frac{U_{cr}^2}{gb} \right)^{1/3}$	Clear-water/ live bed	For live bed, $2 \frac{U}{U_{cr}} - 1 = 1$
Breusers et al. (1977)	$\frac{d_s}{b} = 2 \tanh \left(\frac{h}{b} \right) K_I K_s K_z$	Clear-water/ live bed	$K_I = 0$, for $\frac{U}{U_{cr}} \leq 0.5$ $K_I = 2 \frac{U}{U_{cr}} - 1$, for $0.5 < \frac{U}{U_{cr}} < 1$ $K_I = 1$, for $\frac{U}{U_{cr}} \geq 1$
Jain and Fischer (1980)	$\frac{d_s}{b} = 1.86 \left(\frac{h}{b} \right)^{0.5} \times (Fr - Fr_c)^{0.25}$	Live bed	$Fr_c = \frac{U_{cr}}{(gh)^{0.5}}$
Jain (1981)	$\frac{d_s}{b} = 1.84 \left(\frac{h}{b} \right)^{0.3} Fr_c^{0.25}$	Sediment threshold	
Dey (1999)	$\frac{d_s}{b} = 1.77 \left(\frac{h}{b} \right)^{0.15}$	Sediment threshold	

$$U_{cr}(\Re > 70) = 2.5u_{*c} \ln \left(2.21 \frac{h}{d_{50}} \right) \quad (10.78b)$$

where

$$\Re = \frac{u_{*c} d_{50}}{2.32 \times 10^{-7}}, \text{ and}$$

$$u_{*c} = \left\{ 16.2 d_{50} \left[\frac{9.09 \times 10^{-6}}{d_{50}} - d_{50} (38.76 + 9.6 \ln d_{50}) - 0.005 \right] \right\}^{0.5}$$

Besides the aforementioned scour predictors that can produce potentially safe results for the scour depth, Table 10.5 furnishes some empirical equations of equilibrium scour depth proposed by different investigators.

Regarding the maximum limit of scour depth at circular piers, Melville and Coleman (2000) [also Melville and Sutherland (1988)] reported $d_s \leq 2.4b$ for flow Froude number $Fr < 1$. On the other hand, $d_s \leq 3b$ was recommended by HEC18 (Richardson and Davis 2001) and Jain and Fischer (1979). In the experiments conducted by Jain and Fischer (1979), the Fr was as high as 1.5 for the bed conditions of antidunes. However, for noncircular piers, these maximum limits increase and are to be corrected for pier shape and skewness, if any.



Fig. 10.23 Photograph of a wing-wall abutment. Photograph by the author



Fig. 10.24 Photograph of an equilibrium scour hole at a wing-wall abutment in a flume

10.6 Scour at Bridge Abutments

Abutments, located at either end of a bridge span, are the substructures over which the bridge superstructure rests (Fig. 10.23). Akin to bridge piers, they also help to transmit the weight of the bridge including traffic to the foundation bed. Piers are located within the bridge span (Sect. 10.5). Scour at bridge abutments is also equally or even more responsible for failure of bridges as compared to scour at piers. Similar to bridge piers, the flow separates at the upstream of the abutment as it travels by the side of the abutment, creating a vortex trail to move downstream. The result is that the sediment bed in the vicinity of the abutment is scoured, exposing the abutment foundation that may lead to the failure of the bridge.

A study of the US Federal Highway Administration in 1973 concluded that of 383 bridge failures, 25 % involved pier damage and 72 % involved abutment damage (Richardson et al. 1993). In a report submitted to the National Roads Board of New Zealand, Sutherland (1986) pointed out that of the 108 bridge failure records, 29 were attributed to abutment scour during 1960–1984. According to Kandasamy and Melville (1998), 6 out of 10 bridge failures that occurred in New Zealand during Cyclone Bola were related to the abutment scour. In another report of the Department of Scientific and Industrial Research of New Zealand, Macky (1990) mentioned that about 50 % of total expenditure was made toward the bridge damage repairing and maintenance, out of which 70 % was spent toward the abutment scour. Therefore, abutment scour, due to its practical importance, was studied extensively by various researchers [see the review by Barbhuiya and Dey (2004)]. Figure 10.24 shows the photograph of an equilibrium scour hole at a wing-wall abutment in an experimental flume. It gives an idea about the shape of the scour hole that occurs at an abutment.

The flow field at an abutment is complex in detail, and the complexity increases with the development of scour hole involving flow separation to develop three-dimensional vortex flow. Kwan and Melville (1994) [also in Kwan (1988)] used a hydrogen bubble technique to measure the three-dimensional flow field in a scour hole at a wing-wall abutment. They identified a *primary vortex*, which is quite similar to the horseshoe vortex at a pier, along with the *downflow* being the principal mechanism of scour at an abutment. On the upstream face of an abutment, a vertical pressure gradient is developed due to the stagnation of approaching flow by the abutment. The pressure gradient drives the fluid downward to roll up. Thus, primary vortex is developed and it enlarges its size with the development of the scour hole. They also reported that the primary vortex and the downflow are confined mainly in the scour hole beneath the line of the original bed level. The primary vortex is elliptical in shape with an inner core region as that of a forced vortex and an outer core region as that of a free vortex. The maximum velocity and downflow component in the vicinity of the abutment were measured as 1.35 and 0.75 times the approaching flow velocity, respectively. They also

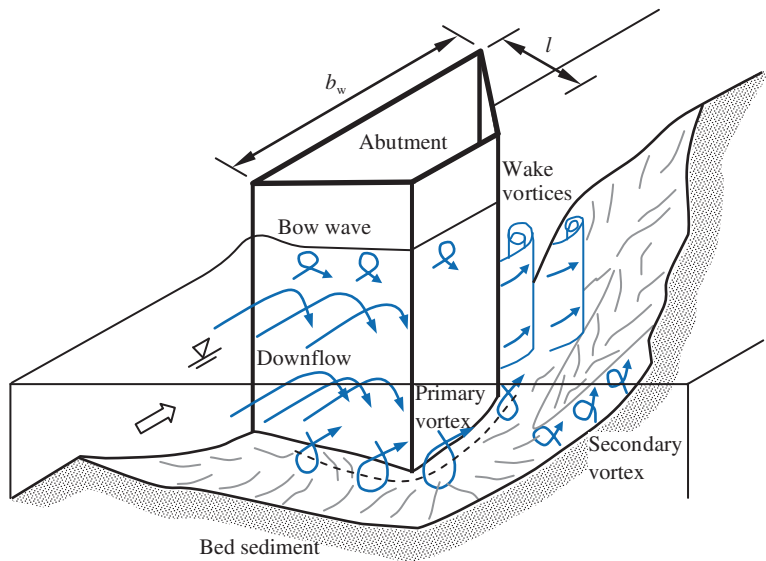


Fig. 10.25 Schematic of flow field at an abutment (Kwan 1988)

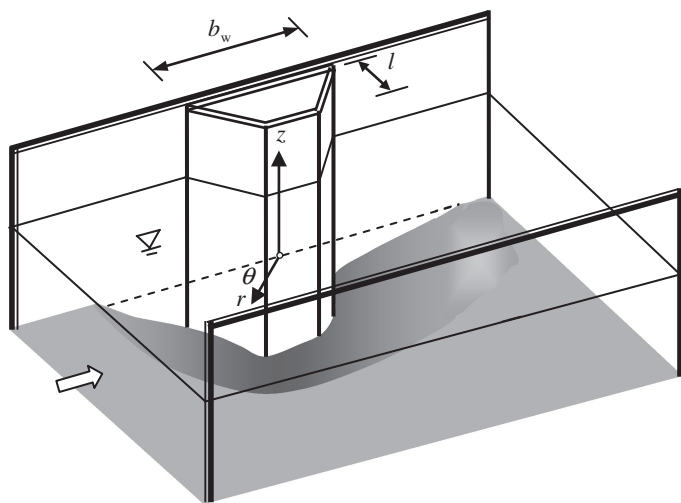


Fig. 10.26 Coordinate system for representation of flow and schematic of a scour hole at a 45° wing-wall abutment

identified a *secondary vortex* with counter rotational direction to that of the primary vortex occurring next to the primary vortex. The secondary vortex is believed to have the effect of restricting the scouring capacity of the primary vortex. In the downstream of abutment, *wake vortices* are created due to the

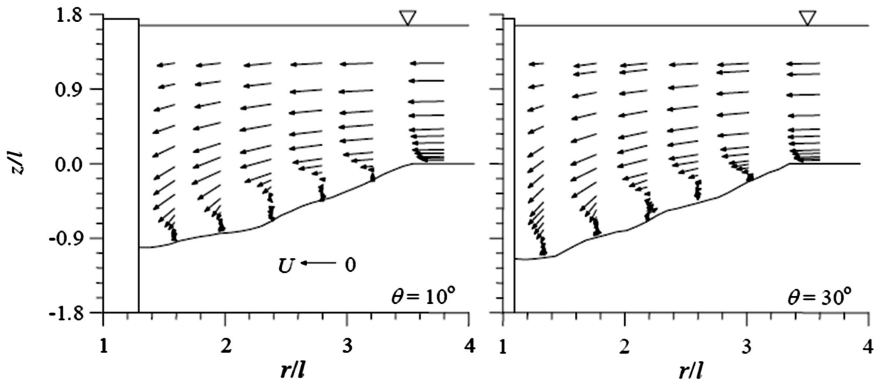


Fig. 10.27 Normalized velocity vectors at azimuthal sections ($\theta = 10^\circ$ and 30°) of a 45° wing-wall abutment after Dey and Barbhuiya (2006)

separation of flow at the upstream and downstream of the abutment corners. The unstable shear layers created due to the flow separation roll up to form eddy structures, termed *wake vortices*. The wake vortices drifted downstream by the mean flow act like small tornadoes lifting up sediment particles from the bed. The wake vortices are rather weak as compared to the primary vortex. Bow wave having a rotational motion opposite to that of primary vortex appears on the upstream face of the abutment near the free surface. The major flow components at a wing-wall abutment identified by Kwan (1988) are shown schematically in Fig. 10.25.

Dey and Barbhuiya (2005a, b, 2006) investigated the three-dimensional turbulent flow fields at semicircular, vertical-wall and 45° wing-wall abutments, embedded in a stabilized equilibrium scoured bed by using an ADV [also in Barbhuiya (2003)]. A cylindrical polar coordinate system, as shown in Fig. 10.26, was used by Dey and Barbhuiya (2006) to represent the normalized velocity vectors at azimuthal sections of a 45° wing-wall abutment with a scour hole. Figure 10.27 shows velocity vectors at $\theta = 10^\circ$ and 30° (Dey and Barbhuiya 2006). Here, z is the vertical distance, r is the radial distance, and l is the abutment length transverse to the flow. The characteristics of vortex flow inside the scour hole (that is, in the flow zone $z \leq 0$) together with the strong downflow along the upstream face of the abutment are evident. Note that as the length scales of the axes (ordinate and abscissa) are different in Fig. 10.27, the vortices are apparently stretched horizontally, but they are actually not so. The circulation is strong at the upstream of the abutment and decreases with an increase in θ . Above the scour hole (that is, in the flow zone $z > 0$), the flow is horizontal for $r > 3l$, and then, it gradually curves down toward the abutment.

10.6.1 Scour Depth Prediction

Parameters involved in scour phenomenon at abutments can be grouped in the similar way as those of pier scour (Sect. 10.5.2), except the following two parameters:

1. *Parameters related to the abutment*: Size, shape, and orientation with respect to the approaching flow direction.
2. *Parameters related to the geometry of channel*: Width, cross-sectional shape, and slope.

Most of the scour predictors were preliminarily obtained, as functional relationships, using the dimensional analysis based on the aforementioned parameters. Then, experimental and field data were used to give them a final shape as empirical equations. Proposed empirical equations for the estimation of maximum scour depth at abutments are overwhelming (Barbhuiya and Dey 2004), but their application is limited to the conditions similar to those for which they were validated. The design approaches proposed by Melville and Coleman (2000) and Froehlich (1989), which was recommended by HEC18 (Richardson and Davis 2001), for the estimation of maximum scour depth at abutments based on K -factors seem to be adequate from the viewpoint of the safety of abutment foundation.

According to Melville and Coleman (2000), the maximum equilibrium scour depth d_s at an abutment for both clear-water and live-bed conditions is given by

$$d_s = K_h K_I K_d K_s K_z K_G K_t \quad (10.79)$$

where K_G is the channel geometry factor and other K -factors are designated similar to that in Eq. (10.64). The relationships for K -factors, in case of abutment scour, are given as follows:

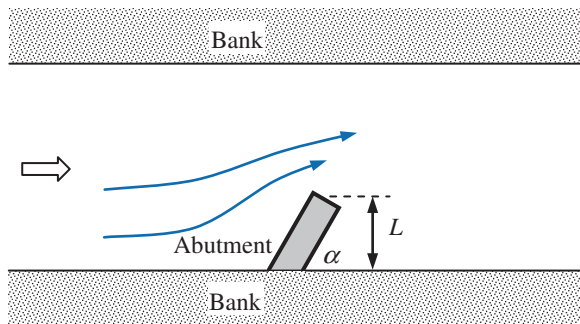
The *flow depth–pier size factor* K_h for abutment scour is

$$\left. \begin{aligned} K_h(l/h \leq 1) &= 2l \\ K_h(1 < l/h < 25) &= 2(hl)^{0.5} \\ K_h(l/h \geq 25) &= 10h \end{aligned} \right\} \quad (10.80)$$

The above K_h -factor is based on Melville (1992) who distinguished short and long abutments. For short abutments ($l/h \leq 1$), the scour depth d_s is independent of flow depth h and dependent on abutment length l . For long abutments ($l/h \geq 25$), the d_s is dependent on h and independent of l . For $1 < l/h < 25$, the d_s is dependent on both l and h . Note that l is projected length for skewed abutments (Fig. 10.28).

The *flow intensity factor* K_I given by Eq. (10.66) for the case of pier scour is also applicable for the abutment scour.

Fig. 10.28 Oblique alignment of an abutment (plan view)



The *sediment size factor* K_d for abutment scour is

$$\left. \begin{aligned} K_d(l/d_{50} \leq 25) &= 0.57 \log \left(2.24 \frac{l}{d_{50}} \right) \\ K_d(l/d_{50} > 25) &= 1 \end{aligned} \right\} \quad (10.81)$$

However, for the abutments embedded in gravel-beds, Raikar and Dey (2005a) proposed new sediment size factors as

$$\left. \begin{aligned} K_d(l/d_{50} \leq 10) &= 1.184 \log \left(0.588 \frac{l}{d_{50}} \right) \\ K_d(10 < l/d_{50} \leq 25) &= 0.226 \log \left(1052.8 \frac{l}{d_{50}} \right) \\ K_d(l/d_{50} > 25) &= 1 \end{aligned} \right\} \quad (10.82)$$

The *shape factor* K_s is defined as the ratio of the scour depth d_s for a given abutment shape to that for the vertical-wall abutment having a same length. The shape factors K_s for different abutments are given in Table 10.6.

For abutments, the values of *alignment factor* K_α for abutment scour are

$$\left. \begin{aligned} K_\alpha(l/h \geq 3) &= K_\alpha^* \\ K_\alpha(1 < l/h < 3) &= K_\alpha^* + (1 - K_\alpha^*) \left(1.5 - 0.5 \frac{b}{h} \right) \\ K_\alpha(l/h \leq 1) &= 1 \end{aligned} \right\} \quad (10.83)$$

The values of K_α^* in the above equation are obtained from Table 10.7.

The *channel geometry factor* K_G is defined as the ratio of the scour depth d_s at an abutment to that at the same abutment in the equivalent rectangular channel. In case of rectangular channels, $K_G = 1$. However, for abutments in compound channels, K_G depends on the abutment position in the compound channel. The K_G is

Table 10.6 Shape factors K_s for abutment scour

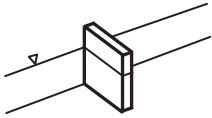
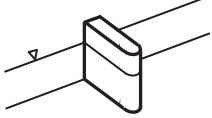
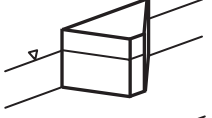
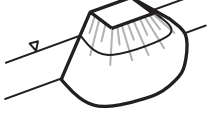
Shape	Name	K_s
	Vertical-wall	1
	Semicircular ended	0.75
	45° wing-wall	0.75
	Spill-through (Horizontal:Vertical)	
	0.5:1	0.6
	1:1	0.5
	1.5:1	0.45

Table 10.7 Factors K_α^* for abutment scour

α (degree)	30	45	60	90	120	135	150
K_α^*	0.9	0.95	0.98	1	1.05	1.07	1.08

$$K_G = \left\{ 1 - \left(\frac{l^*}{l} \right) \left[1 - \left(\frac{h^*}{h} \right)^{5/3} \left(\frac{n}{n^*} \right) \right] \right\}^{0.5} \tag{10.84}$$

where l^* is the abutment length spanning the flood channel, h^* is the flow depth in the flood channel, and n and n^* are the Manning roughness coefficients in the main and flood channels, respectively. In case of an inclined abutment, l and l^* are the projected abutment length and that spanning the flood channel, respectively.

For live-bed scour, the *time factor* K_t is unity; while for clear-water scour, K_t for abutment scour is given by

$$K_t = 0.1 \frac{U_{cr}}{U} \ln \left(\frac{t}{t_e} \right) + 1 \tag{10.85}$$

Table 10.8 Shape factors K_s for abutment scour

Abutment shape	K_s
Vertical-wall	1
Vertical-wall abutment with wing walls	0.82
Spill-through	0.55

The time t_e to reach equilibrium scour depth is given by

$$\left. \begin{aligned} t_e(\text{days})(l/h \geq 1.2) &= 25 \frac{h}{U} \\ t_e(\text{days})(l/h < 1.2) &= 20.83 \frac{h}{U} \end{aligned} \right\} \quad (10.86)$$

HEC18 (Richardson and Davis 2001) recommended Froehlich's (1989) equation of live-bed scour at abutments. The estimation of maximum scour depth is

$$\frac{d_s}{l} = 2.27 K_s K_\alpha \left(\frac{h}{l} \right)^{0.57} Fr^{0.61} + 1 \quad (10.87)$$

where $Fr = U_0/(gh)^{0.5}$, $U_0 = Q_0/A_0$, Q_0 is the flow rate obstructed by the abutment and approach embankment, and A_0 is the flow area of the approach cross section obstructed by the embankment. The values of *shape factors* K_s are furnished in Table 10.8.

The *alignment factor* K_α is given by

$$K_\alpha = \left(\frac{\alpha}{90} \right)^{0.13} \quad (10.88)$$

where α is the downstream angle of inclination of abutment with bank (Fig. 10.28), such that $\alpha < 90^\circ$ is for the abutment pointing downstream and $\alpha > 90^\circ$ for pointing upstream.

Table 10.9 furnishes some additional empirical scour depth predictors at abutments proposed by various investigators.

10.7 Scour Countermeasures

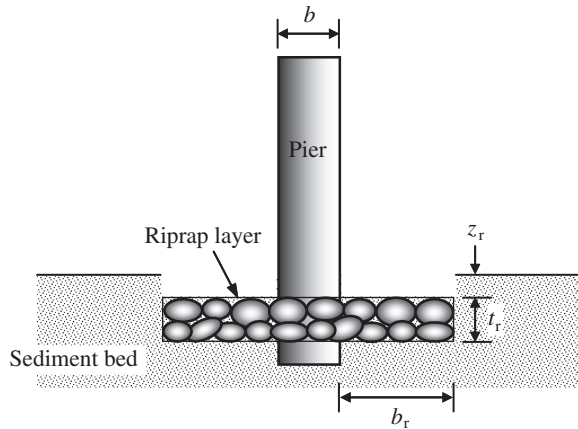
Engineering devices for countermeasure of scour at bridge piers are generally classified into two categories: *Flow-altering* and *bed-armoring countermeasures*. The working principle of flow-altering countermeasures is to diminish the strength of the downflow and the horseshoe vortex, which are the primary cause of pier scour. Of various types of flow-altering countermeasures, slot in a pier (Grimaldi et al. 2009), spirally wrapped cables on a pier (Dey et al. 2006), collars and horizontal plates attached to a pier (Kim et al. 2005; Parker et al. 1998),

Table 10.9 Equations of equilibrium scour depth at abutments proposed by various investigators

References	Formula	Regime	Note
Laursen (1963)	$\frac{d_s}{l} = 1.89 \left(\frac{h}{l}\right)^{0.5}$	Sediment threshold	
Liu et al. (1961)	$\frac{d_s}{l} = 1.1 \left(\frac{h}{l}\right)^{0.6} Fr^{0.33}$	Live bed	Spill-through abutments
	$\frac{d_s}{l} = 2.15 \left(\frac{h}{l}\right)^{0.6} Fr^{0.33}$	Live bed	Wing- and vertical-wall abutments
	$\frac{d_s}{l} = 12.5 \cdot \frac{h}{l} \cdot \frac{B_1}{B_2} \cdot Fr$	Clear-water	Vertical-wall abutments
Gill (1970, 1972)	$\frac{d_s}{l} = 8.375 \left(\frac{h}{l}\right)^{0.75} \left(\frac{d_{50}}{l}\right)^{0.25} \left(\frac{B}{B-l}\right)^{6/7} \frac{h}{-l}$	Sediment threshold	B is the approach stream width
Sturm and Janjua (1994)	$\frac{d_s}{l} = 7.7 \frac{h}{l} \left(\frac{1}{M} \cdot \frac{U}{U_{cr}} - 0.35\right)$	Clear-water and live bed	M is the discharge contraction ratio*
Lim (1997)	$\frac{d_s}{l} = K_s \frac{h}{l} \left\{ \Theta_c^{0.75} \left(\frac{d}{h}\right)^{0.25} \left[0.9 \left(\frac{l}{h}\right)^{0.5} + 1 \right] - 2 \right\}$	Clear-water	$F_d = \frac{U}{(\Delta g d_{50})^{0.5}}$
Kandasamy and Melville (1998)	$\frac{d_s}{l} = K_s K_h \left(\frac{h}{l}\right)^m$	Clear-water and live bed	$K_h = 5$ and $m = 1$ for $h/l \leq 0.04$, $K_h = 1$ and $m = 0.5$ for $0.04 < h/l < 1$, and $K_h = 1$ and $m = 0$ for $h/l > 1$
Dey and Barbhuiya (2004)	$\frac{d_s}{l} = 5.857 \left(\frac{U_{cr}}{\Delta g l}\right)^{0.314} \left(\frac{h}{l}\right)^{0.128} \left(\frac{d_{50}}{l}\right)^{0.167}$	Clear-water	Vertical-wall abutments
	$\frac{d_s}{l} = 6.483 \left(\frac{U_{cr}}{\Delta g l}\right)^{0.312} \left(\frac{h}{l}\right)^{0.101} \left(\frac{d_{50}}{l}\right)^{0.231}$	Clear-water	45° wing-wall abutments
	$\frac{d_s}{l} = 7.287 \left(\frac{U_{cr}}{\Delta g l}\right)^{0.192} \left(\frac{h}{l}\right)^{0.103} \left(\frac{d_{50}}{l}\right)^{0.296}$	Clear-water	Semicircular abutments

* M that is termed *discharge contraction ratio* is defined as the ratio of the discharge at approach section through the opening width to the total discharge

Fig. 10.29 Typical placement of a riprap layer at a pier



arrangement of sacrificial piles (Melville and Hadfield 1999; Chiew and Lim 2003; Haque et al. 2007), and flow deflection by upstream vanes or plates (Odgaard and Wang 1991; Lauchlan 1999) are pertinent. Tafarojnoruz et al. (2010) compiled a review of literature on flow-altering countermeasures at piers. On the other hand, bed-armoring countermeasures provide a physical barrier against scour. In practice, these barriers often consist of large and heavy units, which cannot be easily removed by the flow at piers (Melville and Coleman 2000; Lagasse et al. 2007; Melville et al. 2008). The most commonly employed protection of bridge piers (and also abutments) is the use of a riprap layer around the piers. In this section, riprap protection at piers is mainly discussed.

Figure 10.29 shows a schematic of the placement of a riprap layer at a pier of width b , considering the flow to be the normal to the plane of the drawing. Parameters involved in riprap protection design at piers are as follows:

1. Thickness t_r of riprap layer.
2. Coverage b_r of riprap layer at sides, upstream, and downstream of a pier.
3. Placement z_r of riprap layer with respect to the original bed level.
4. Median size d_{50r} of riprap stones and their gradation.

The thickness of the riprap layer is recommended typically in the range $t_r = 2-3d_{50r}$. Thicker layer can resist higher flow intensity (Chiew 1995). The general recommendation for riprap coverage is to place riprap around a pier extending up to $b_r = 3b$ from the pier wall in all directions (Parola 1995; Croad 1997; Parker et al. 1998; Lauchlan 1999). Parker et al. (1998) suggested b_r for rectangular piers is $b_r = 1.5b/\cos\alpha$. Regarding the placement of a riprap layer z_r , the surface of the riprap layer to be placed at the original streambed level is the common recommendation (Richardson and Davis 2001). Another recommendation is to place the riprap layer below the possible general scour depth level (Neill 1973; Breusers et al. 1977). Further, to improve the performance of a riprap protection, the use of a filter layer beneath the riprap layer is generally proposed. Filters that can be granular filters or synthetic filters prevent the passage of finer

bed sediment through the highly porous riprap layers, but also have sufficient permeability to prevent building up water pressure within the underlying bed sediment. Regarding riprap stones, it is important that they should be well graded, such that the maximum stone size should not exceed twice the median size of riprap stones, that is, $d_{\max} \leq 2d_{50r}$ (Richardson and Davis 2001), and the median size should not exceed twice the 15 % finer stone size, that is, $d_{50r} \leq 2d_{15r}$ (Croad 1997). To determine the riprap stone size d_{50r} , HEC-18 (Richardson and Davis 2001) and HEC-23 (Lagasse et al. 2001) recommended using the reorganized form of Isbash (1936) equation. It is

$$d_{50r} = 0.346 \frac{(KU)^2}{\Delta g} \quad (10.89)$$

where K is the pier shape coefficient. The values of K are that for round-nosed piers, $K = 1.5$ and for rectangular piers, $K = 1.7$.

Further, Lauchlan (1999) suggested an equation of riprap stone size taking into account the placement depth z_r below the original bed level. It is

$$d_{50r} = 0.3f_{SF}h \left(1 - \frac{z_r}{h}\right)^{2.75} Fr^{1.2} \quad (10.90)$$

where f_{SF} is a safety factor that has a minimum recommended value of 1.1.

In case of riprap protection at abutments, the coverage b_r of riprap layer around an abutment, called *launching apron*, is extended up to $b_r = 1.5d_s$ from the abutment wall in all directions. It should have a minimum thickness of $t_r = 2d_{50r}$. The spill-through abutments are additionally protected by stone-pitching on the slant face of the abutment. The median stone size d_{50r} of the riprap layer can be obtained from the equation given by Austroads (1994) as

$$d_{50r} = 1.026 \frac{hFr^2}{\Delta} \quad (10.91)$$

According to Atayee et al. (1993) and Richardson and Davis (2001), the median stone size can be obtained as

$$d_{50r}(Fr_2 \leq 0.8) = K_s \frac{h_2 Fr_2^2}{\Delta} \quad (10.92a)$$

$$d_{50r}(Fr_2 > 0.8) = K_s \frac{h_2 Fr_2^{0.14}}{\Delta} \quad (10.92b)$$

where h_2 is the flow depth in the contracted section of the bridge, Fr_2 is the flow Froude number in the contracted section $[= U_2/(gh_2)^{0.5}]$, and U_2 is the average flow velocity in the contracted section. The values of the shape factor K_s are 0.89 ($Fr \leq 0.8$) and 0.61 ($Fr > 0.8$) for spill-through abutments and 1.02 ($Fr \leq 0.8$) and 0.69 ($Fr > 0.8$) for vertical-wall abutments.

10.8 Appendix

10.8.1 Submerged Wall Jets (Dey et al. 2010)

Submerged plane wall jet is described as a fluid jet that impinges tangentially (or at an angle) on a solid boundary surrounded by the same fluid (still or moving) progressing along the solid boundary (Fig. 10.30a). By virtue of the initially abounding momentum, the streamwise velocity \bar{u} in the shear flow of jet exceeds that in external stream over a downstream reach (Launder and Rodi 1981). In a submerged wall jet, the flow zone of principal importance is the fully developed zone existing after the developing zone of jet (Fig. 10.30b). The jet is confined to a solid boundary on one side, and the other side is fluid bounded. The jet layer is overlain by a circulatory flow having an enormous mixing of fluid with a flow reversal. Since the boundary conditions for a submerged wall jet are such that the velocities at the solid boundary and on the separation line are zero ($\bar{u} = 0$), the velocity distribution has a peak within the jet layer. Below the peak velocity level (in the inner layer), the flow is characterized by a boundary-layer flow, and the upper flow zone is structurally similar to a free jet. Therefore, a submerged wall jet, characterized by a shear flow influenced by the solid boundary and an overlying circulatory flow layer, is of self-similar type of flow (Dey et al. 2010).

A typical \bar{u} -distribution in the fully developed zone describing various layers of flow is shown in Fig. 10.30a. The inner layer and outer layer of jet refer to the zones below and above the point of occurrence of peak velocity u_0 , called the *jet velocity*. Precisely, the jet layer ($0 \leq z \leq \delta$) that comprises of inner layer and outer layer extends up to the inflection point (that is, the point of change of sign of slope, $d\bar{u}^2/dz^2 = 0$) of a \bar{u} -distribution. Above the jet layer, there exists a circulatory flow layer that is divided by the separation line $\bar{u} = 0$ into inner layer and outer layer of the circulatory flow. The flow in the outer layer of the circulatory flow is directed toward upstream. Momentum exchange takes place through the separation line within the circulatory flow layer of the jet. The jet layer thickness δ is important from the viewpoint of scaling the vertical distance z (Dey et al. 2010).

A two-dimensional submerged plane wall jet issuing from a sluice opening is considered as the jet emerges in the form of a bunch of diverging streamlines. Another bunch of streamlines constitutes a circulatory flow above the jet in the circulatory flow layer. The limiting streamline on the solid boundary has a velocity $\bar{u} = 0$ due to no-slip. Let the equation of the jet layer be $z = \delta(x_1)$, where $x_1 = x + x_0$, extending up to the inflection point of \bar{u} -distribution. The jet layer is assumed as a boundary layer. Due to finite size of issuing jet, the point of emergence (that is the origin) of the jet is located upstream of the sluice opening at a certain distance x_0 . Applying the boundary-layer approximation to the two-dimensional Reynolds-averaged Navier–Stokes (RANS) equations of steady flow and eliminating pressure term, the following equation is obtained (Rajaratnam 1976):

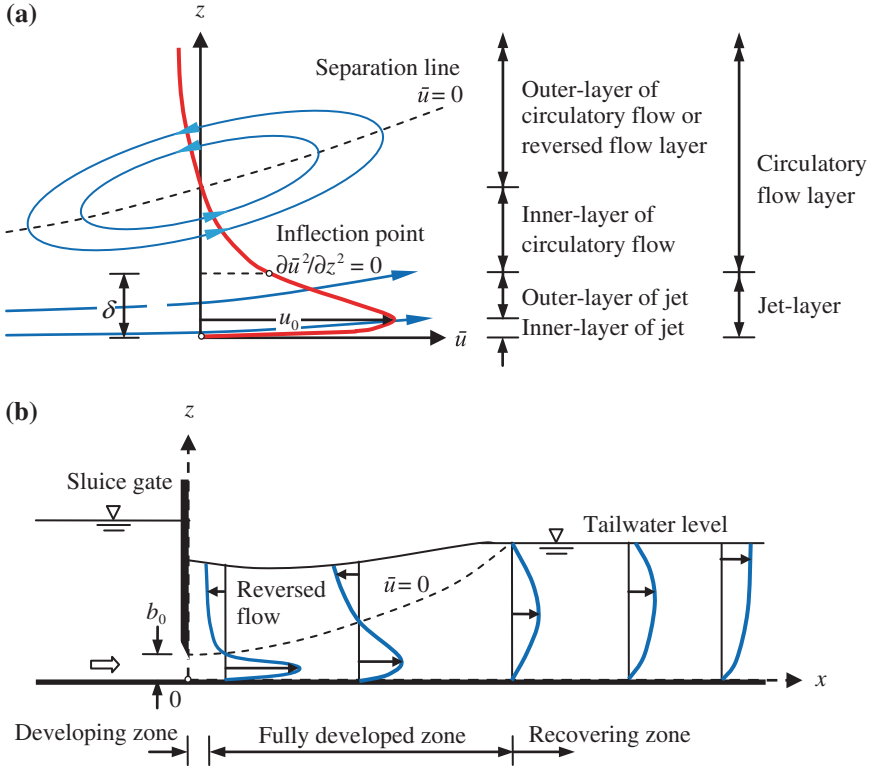


Fig. 10.30 **a** Typical sketch of \bar{u} -distribution superimposed on the flow field in the fully developed flow zone and **b** flow zones in a submerged wall jet (Dey et al. 2010)

$$\bar{u} \frac{\partial \bar{u}}{\partial x} + \bar{w} \frac{\partial \bar{u}}{\partial z} + \frac{\partial \overline{u'w'}}{\partial z} + \frac{\partial}{\partial x} (\overline{u'u'} - \overline{w'w'}) = \nu \frac{\partial^2 \bar{u}}{\partial z^2} \quad (10.93)$$

The continuity equation is

$$\frac{\partial \bar{u}}{\partial x} + \frac{\partial \bar{w}}{\partial z} = 0 \quad (10.94)$$

The flow in submerged plane wall jets is characterized by the self-similar class. To obtain the similarity solutions of Eqs. (10.93) and (10.94) by the transformation $\eta = z/\delta(x_1)$, where the horizontal length scale x_1 is dimensional for the theory, the solutions are of the form

$$\bar{u} = u_0 \varphi(\eta), \quad \overline{u'w'} = -u_0^2 \psi(\eta), \quad \overline{u'u'} - \overline{w'w'} = u_0^2 \sigma(\eta) \quad (10.95)$$

where $u_0 = u_0(x_1)$. It is pertinent to mention that a wall jet boundary layer is not amenable to similarity analysis, unless different scaling laws are assumed for the inner layer and the outer layer of the jet (Barenblatt et al. 2005). Inserting the above expressions into Eq. (10.93) and using Eq. (10.94), one obtains

$$\frac{\delta}{u_0} \cdot \frac{du_0}{dx} \varphi^2 - \left(\frac{d\delta}{dx} + \frac{\delta}{u_0} \cdot \frac{du_0}{dx} \right) \varphi' \int_0^\eta \varphi d\eta - \psi' = \frac{1}{R_\delta} \varphi'' - \frac{2\delta}{u_0} \cdot \frac{du_0}{dx} \sigma + \frac{d\delta}{dx} \sigma' \approx 0 \quad (10.96)$$

where $R_\delta = u_0 \delta / \nu$. The right-hand side of Eq. (10.96) vanishes, as the terms containing the difference of streamwise and vertical Reynolds normal stresses represented by σ are negligible and R_δ is too large. For a similarity solution, Eq. (10.96) must be independent of x or x_1 (Schwarz and Cosart 1961), that is

$$\frac{d\delta}{dx_1} = \beta, \quad \frac{\delta}{u_0} \cdot \frac{du_0}{dx_1} = -\beta\alpha \quad (10.97)$$

where β and α are constants. Hence, by integration, one can write

$$\delta = \beta x_1, \quad u_0 = \beta_0 x_1^{-\alpha} \quad (10.98)$$

where β_0 is a constant. Noticeably, the δ increases linearly with x_1 , and u_0 varies as $x_1^{-\alpha}$. For a free jet, α is 0.5 (Schlichting 1979).

The velocity distribution obtained using Eqs. (10.96) and (10.98) is given by

$$\alpha \varphi^2 + (1 - \alpha) \varphi' \int_0^\eta \varphi d\eta + \frac{1}{\beta} \psi' = 0 \quad (10.99)$$

Setting $\varphi(\eta) = f'(\eta)$, Eq. (10.99) becomes

$$\alpha f'^2 + (1 - \alpha) f f'' + \frac{1}{\beta} \psi' = 0 \quad (10.100)$$

By definition of the turbulence diffusivity ε_t , one can write

$$\overline{u'w'} = -\varepsilon_t \frac{\partial \bar{u}}{\partial z} = -u_0^2 \psi \quad (10.101)$$

Using Eq. (10.95), Eq. (10.101) yields

$$\psi = \frac{\varepsilon_t}{u_0^2} \cdot \frac{\partial}{\partial z} (u_0 \varphi) = \frac{\varepsilon_t}{u_0 \delta} \varphi' = \frac{\varepsilon_t}{\beta_0 \beta} \cdot \frac{\varphi'}{x_1^{1-\alpha}} = \frac{\bar{\varepsilon}_t}{\beta_0 \beta} f'' \quad (10.102)$$

In Eq. (10.102), the left-hand side being independent of x_1 implies that ε_t is proportional to $x_1^{1-\alpha}$, and hence, $\varepsilon_t = \bar{\varepsilon}_t x_1^{1-\alpha}$. In the narrow turbulent jet layer, $\bar{\varepsilon}_t$ may be assumed to be an averaged value of ε_t over η . Thus, one obtains

$$\alpha f'^2 + (1 - \alpha)ff'' + \frac{\bar{\varepsilon}_t}{\beta_0 \beta^2} f''' = 0 \quad (10.103)$$

The velocity distribution contains an arbitrary constant β_0 . Replacing β_0 by $4\bar{\varepsilon}_t/\beta^2$ in Eq. (10.103), one gets the following equation for f :

$$\alpha f'^2 + (1 - \alpha)ff'' + \frac{1}{4}f''' = 0 \quad (10.104)$$

The boundary conditions applicable for the solution of Eq. (10.104) are that at the peak velocity of the jet $f'(\eta = \eta_0) = \varphi(\eta = \eta_0) = 1$, $f(\eta = \eta_0) = 0$ (that is $\bar{w} = 0$), and $f'(\eta \rightarrow \infty) = 0$ (that is $\bar{u} = 0$). For a free jet, $\eta_0 = 0$ and $\alpha = 0.5$ (Schlichting 1979), and the solution of Eq. (10.104) is $f = \tanh \eta$. It is anticipated that due to the submergence, α is modified as

$$\alpha = 0.5 + \alpha_1 \quad (10.105)$$

where α_1 is an additional term mainly due to submergence. The solution of Eq. (10.104) can be given by

$$f(\eta) = \tanh(\eta - \eta_0) + \alpha_1 G(\eta) \quad (10.106)$$

Substituting Eq. (10.106) into Eq. (10.104) and equating the coefficients of α_1 , the differential equation for G is given by

$$G''' + 2 \tanh(\eta - \eta_0)G'' + 4 \operatorname{sech}^2(\eta - \eta_0)[G' - \tanh(\eta - \eta_0)G + \tanh^2(\eta - \eta_0) + 1] = 0 \quad (10.107)$$

with boundary conditions $G(\eta = \eta_0) = 0$, $G'(\eta = \eta_0) = 0$, and $G'(\eta \rightarrow \infty) = 0$. Equation (10.107) that has highly nonlinear coefficients is a linear differential equation. Galerkin's method is applied to obtain an approximate analytical solution. For this purpose, it is recognized that a function of the pattern of the leading term of Eq. (10.106) that satisfies the boundary condition is

$$G(\eta) = a_0 \tanh^2(\eta - \eta_0) \quad (10.108)$$

Substituting Eq. (10.108) into Eq. (10.107) and taking the weighted average with the weight appearing in the equation yield

$$a_0 \int_0^{\infty} \operatorname{sech}^2 \eta \tanh^3 \eta (5 - 9 \tanh^2 \eta) d\eta \approx - \int_0^{\infty} \operatorname{sech}^2 \eta \tanh^2 \eta (1 + \tanh^2 \eta) d\eta \quad (10.109)$$

Numerically evaluating the integrals in Eq. (10.109), one obtains $a_0 \approx 32/15$. Differentiating Eq. (10.106) with the value of a_0 in Eq. (10.108), one gets

$$\varphi(\eta) = \operatorname{sech}^2(\eta - \eta_0) \left[1 + \frac{64}{15} \alpha_1 \tanh(\eta - \eta_0) \right] \quad (10.110)$$

Giving the velocity distribution of a submerged wall jet by Eqs. (10.95) and (10.98), the profile holds for $\eta \geq \eta_0$, because below the point of η_0 (that is, within the inner layer of the jet), boundary effects come into account.

In the near-boundary zone (that is, within the inner layer of the jet) $0 \leq \eta \leq \eta_0$, the $1/m$ -th power law for $\varphi(\eta)$ can be assumed as in case of a flow over a solid plate. Noting that as $\varphi(\eta = \eta_0) = 1$, $\varphi'(\eta = \eta_0) = 0$, such a law is

$$\varphi(\eta) = \frac{1}{m} \left(\frac{\eta}{\eta_0} \right)^{1/m} \left(1 + m - \frac{\eta}{\eta_0} \right) \quad (10.111)$$

The Reynolds shear stress τ_{xz} is given by using Eqs. (10.101) and (10.102). It is

$$-\overline{u'w'} = \frac{\beta_0 \bar{e}_t}{\beta} x_1^{-2\alpha} \varphi'(\eta) \quad (10.112a)$$

$$\Rightarrow \tau_{xz} = -\rho \overline{u'w'} = \rho U_0^2 \xi (\hat{x} + \hat{x}_0)^{-2\alpha} \varphi'(\eta) \quad (10.112b)$$

where $\xi = \beta_0 \bar{e}_t / (\beta U_0^2 b_0^{2\alpha})$, $\hat{x} = x/b_0$, and $\hat{x}_0 = x_0/b_0$.

From Eqs. (10.110) and (10.111), the following expressions for φ' are obtained:

$$\varphi'(\eta \geq \eta_0) = -\operatorname{sech}^2(\eta - \eta_0) \left\{ 2 \tanh(\eta - \eta_0) + \frac{64}{15} \alpha_1 [2 \tanh^2(\eta - \eta_0) - 1] \right\} \quad (10.113a)$$

$$\varphi'(0 < \eta \leq \eta_0) = \frac{1}{m \eta_0} \left(1 + \frac{1}{m} \right) \left(\frac{\eta}{\eta_0} \right)^{(1-m)/m} \left(1 - \frac{\eta}{\eta_0} \right) \quad (10.113b)$$

The Reynolds shear stress vanishes at the solid boundary. Equation (10.113b) cannot be applicable to the very thin viscous sublayer in the vicinity of the boundary, where viscous shear stress prevails. Using the experimental data, Dey et al. (2010) estimated the values of coefficients and exponents as $\hat{x}_0 = 11.34$, $\beta = 0.078$, $\beta_1 = 3.17$, $\alpha = 0.455$, $\alpha_1 = -0.045$, $\eta_0 = 0.3$, $m = 6$, and $\xi = 79.87$.

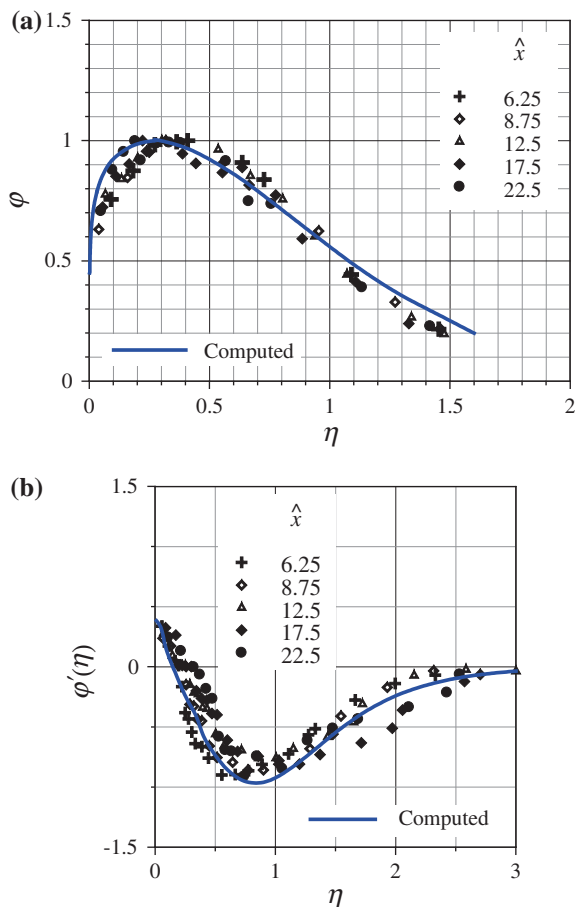


Fig. 10.31 **a** ϕ as a function of η and **b** ϕ' as a function of η for $U = 0.639 \text{ m s}^{-1}$ and $b_0 = 40 \text{ mm}$ in submerged plane wall jet (Dey et al. 2010)

Figures 10.31a, b show $\phi(\eta)$ and $\phi'(\eta)$ curves for $U = 0.639 \text{ m s}^{-1}$ and $b_0 = 40 \text{ mm}$ and the comparisons with the experimental data.

10.8.2 Computation of Scour Due to Submerged Wall Jets

The bed shear stress can be determined from Eq. (10.113b) by applying it to the near-bed level. In case of an erodible sediment bed, the bed is initially horizontal (before scour), and the fluid jet flows in the direction parallel to the horizontal bed surface of sediment. The jet erodes the bed forming a scour hole as shown in Fig. 10.32. The scour profile can be calculated by considering the bed shear stress distribution along the surface of the bed. To determine the bed shear stress τ_0 in the

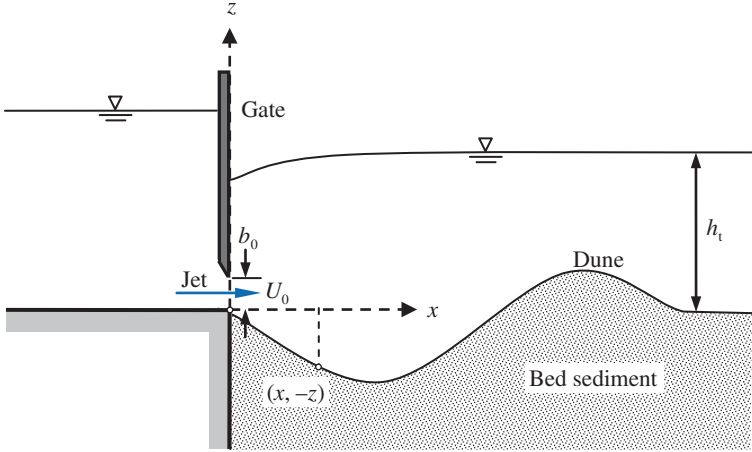


Fig. 10.32 Definition sketch of scour due to a submerged wall jet

scour hole, Eq. (10.113b) along with Eq. (10.112b) is thus applied to the particle level with an introduction to a shape function due to scour. With modification, the equation of bed shear stress τ_0 can then be given by

$$\tau_0(\hat{x}) = \rho U_0^2 \xi (\hat{x} + \hat{x}_0)^{-2\alpha} \frac{1}{m\eta_0} \left(1 + \frac{1}{m}\right) \left(\frac{\eta_b}{\eta_0}\right)^{(1-m)/m} \left(1 - \frac{\eta_b}{\eta_0}\right) G(\eta, \hat{x}) \quad (10.114)$$

where $\eta_b = k_s/\delta$ and $G(\eta, \hat{x})$ is a shape function to account for the bed shear stress variation when the bed is no longer horizontal. Here, k_s can be assumed as d_{50} . Note that the value of $\alpha = 0.5 + \alpha_1$ depends on submergence ratio $S [= (h_t - h_j)/h_j]$, where h_j is the conjugate tailwater depth of free jump $\{= 0.5b_0[(1 + 8F_0^2)^{0.5} - 1]\}$ and F_0 is the jet Froude number $[= U_0/(gb_0)^{0.5}]$.

Initially, the bed is horizontal ($\eta = 0$) and so $G(0, \hat{x}) = 1$. A Gaussian-like stress distribution with vertical distance can be assumed (Hogg et al. 1997):

$$G(\eta \geq 0, \hat{x}) = 1, \quad G(\eta < 0, \hat{x}) = \exp[(C_0\eta)^2] \quad (10.115)$$

where C_0 is the coefficient to be determined from the experimental data.

For equilibrium scour, Eq. (4.115) is reorganized as

$$\tau_0(\hat{x}) = \tau_{0c} \cos \theta \left(1 - \frac{\tan \theta}{\tan \phi}\right) \quad \wedge \quad \theta = \arctan\left(\frac{dz}{dx}\right) = \arctan\left(\hat{\delta} \frac{d\eta}{d\hat{x}}\right) \quad (10.116)$$

where $\hat{\delta} = \delta/b_0$. Using Eqs. (10.114) and (10.115), Eq. (10.116) which is a differential equation can be solved by Runge–Kutta method to determine the

variation of scour depth $\hat{z}(=\eta\hat{\delta})$ with \hat{x} , that is the nondimensional profile of equilibrium scour hole.

10.9 Examples

Example 10.1 Estimate the maximum equilibrium scour depth within a long contraction using the empirical equation given by Dey and Raikar for the following data:

Approaching flow depth, $h_1 = 5$ m

Approaching channel width, $B_1 = 70$ m

Channel width at contracted zone, $B_2 = 40$ m

Median size of sediment, $d_{50} = 2.6$ mm

Geometric standard deviation of sediment, $\sigma_g = 2.2$

Consider coefficient of kinematic viscosity of water $\nu = 10^{-6} \text{ m}^2 \text{ s}^{-1}$ and relative density of sediment $s = 2.65$

Solution

Use van Rijn's empirical formula for the determination of threshold shear velocity (see Table 4.1):

Particle parameter, $D_* = d_{50}(\Delta g/\nu^2)^{1/3} = 2.6 \times 10^{-3} [1.65 \times 9.81/(10^{-6})^2]^{1/3} = 65.77$

Threshold Shields parameter, $\Theta_c(20 < D_* \leq 150) = 0.013 D_*^{0.29} = 0.013 \times 65.77^{0.29} = 0.044$

Threshold bed shear stress, $\tau_{0c} = \Theta_c \Delta \rho g d_{50} = 0.044 \times 1.65 \times 10^3 \times 9.81 \times 2.6 \times 10^{-3} = 1.852 \text{ Pa}$

Threshold shear velocity, $u_{*c} = (\tau_{0c}/\rho)^{0.5} = (1.852/10^3)^{0.5} = 0.043 \text{ m s}^{-1}$

The approaching flow velocity $U_1|_{U_2=U_{cr}}^{d_s=0}$ that corresponds to the threshold of sediment motion within contraction is estimated from the solution of Eqs. (10.20)–(10.22) as follows:

$$\text{Eq. (10.20)} \Rightarrow 5 + \frac{1}{2 \times 9.81} \left(U_1|_{U_2=U_{cr}}^{d_s=0} \right)^2 = h_2 + \frac{1}{2 \times 9.81} \left(U_2|_{U_2=U_{cr}}^{d_s=0} \right)^2$$

$$\text{Eq. (10.21)} \Rightarrow U_1|_{U_2=U_{cr}}^{d_s=0} \times 5 \times 70 = U_2|_{U_2=U_{cr}}^{d_s=0} h_2 \times 40$$

$$\text{Eq. (10.22)} \Rightarrow \frac{U_2|_{U_2=U_{cr}}^{d_s=0}}{0.043} = 5.75 \log \frac{h_2}{2 \times 2.6 \times 10^{-3}} + 6$$

Numerically solving above three equations, $U_1|_{U_2=U_{cr}}^{d_s=0} = 0.565 \text{ m s}^{-1}$

The threshold velocity of approaching flow is determined as follows:

$$U_{cr} = 0.043 \left(5.75 \log \frac{5}{2 \times 2.6 \times 10^{-3}} + 6 \right) = 1 \text{ m s}^{-1}$$

Then, for $U_{lec} = U_{cr} - U_1|_{U_2=U_{cr}}^{d_s=0} = 1 - 0.565 = 0.435 \text{ m s}^{-1}$,

$$F_{lec} = \frac{U_{lec}}{(\Delta g h_1)^{0.5}} = \frac{0.435}{(1.65 \times 9.81 \times 5)^{0.5}} = 0.048$$

Using $B_2/B_1 = 40/70 = 0.571$ and $d_{50}/h_1 = 2.6 \times 10^{-3}/5 = 5.2 \times 10^{-4}$ in Dey and Raikar's equation (Eq. 10.24), the $[d_s]_{max}$ is estimated as

$$\frac{[d_s]_{max}}{h_1} = 0.368 \times 0.048^{0.55} \times 0.571^{-1.26} \times (5.2 \times 10^{-4})^{-0.19} = 0.59$$

\Leftarrow Eq. (10.24)

The maximum scour depth in uniform sediment is $[d_s]_{max} = 0.59h_1 = 0.59 \times 5 = 2.95 \text{ m}$

For nonuniform sediment with $\sigma_g = 2.2$ for which $K_\sigma = 0.38$ (Fig. 10.3), the maximum equilibrium scour depth in nonuniform sediment is $[d_s]_{max} = 0.38 \times 2.95 = 1.121 \text{ m}$.

Example 10.2 Calculate the equilibrium scour depth below a drop structure using the equations of various investigators for the following data:

Height between upstream and downstream water levels, $H = 1.5 \text{ m}$

Tailwater depth, $h_t = 0.9 \text{ m}$

Discharge per unit width, $q = 1.4 \text{ m}^2 \text{ s}^{-1}$

Angle of jet entering the tailwater, $\theta_j = 60^\circ$

Thickness of jet at the tailwater level, $l_0 = 0.1 \text{ m}$

Sediment size, $d_{90} = 32 \text{ mm}$ and $d_{95} = 38 \text{ mm}$

Relative density of sediment, $s = 2.65$

Solution

Schoklitsch's equation

$$d_s = 0.52 \frac{1.4^{0.57} \times 1.5^{0.2}}{(32 \times 10^{-3})^{0.32}} - 0.9 = 1.155 \text{ m} \Leftarrow \text{Eq. (10.26)}$$

Kotoulas' equation

$$d_s = \frac{1.9}{9.81^{0.35}} \cdot \frac{1.4^{0.7} \times 1.5^{0.35}}{(38 \times 10^{-3})^{0.4}} - 0.9 = 3.71 \text{ m} \Leftarrow \text{Eq. (10.27)}$$

Fahlbusch's equation

Velocity of jet entering the tailwater, $U_0 = q/l_0 = 1.4/0.1 = 14 \text{ m s}^{-1}$

Assume $K_p = 3.5$ (for gravels)

$$d_s = 3.5 \left(\frac{1.4 \times 14}{9.81} \sin 60^\circ \right)^{0.5} - 0.9 = 3.7 \text{ m} \Leftarrow \text{Eq. (10.28)}$$

Graf's equation

$$d_s = \frac{3.6}{1.65^{4/9} \times 9.81^{0.3}} \cdot \frac{1.4^{0.6} \times 1.5^{0.5}}{(32 \times 10^{-3})^{0.4}} - 0.9 = 7.726 \text{ m} \Leftarrow \text{Eq. (10.29)}$$

Eggenberger and Müller's equation

$$d_s = \frac{22.88}{15.849} \cdot \frac{1.4^{0.6} \times 1.5^{0.5}}{(32 \times 10^{-3})^{0.4}} - 0.9 = 7.673 \text{ m} \Leftarrow \text{Eq. (10.50)}$$

Example 10.3 Calculate the equilibrium scour depth downstream of a grade-control structure for the following data:

Approaching flow depth, $h = 1.2 \text{ m}$

Drop height, $Z_p = 0.5 \text{ m}$

Discharge per unit width, $q = 1.55 \text{ m}^2 \text{ s}^{-1}$

Angle of jet near the original bed level, $\theta_j = 55^\circ$

90 % finer size of sediment, $d_{90} = 4 \text{ mm}$

Angle of repose of sediment, $\phi = 40^\circ$

Relative density of sediment, $s = 2.65$

Solution

Bormann and Julien's equation is used to calculate equilibrium scour depth downstream of a grade-control structure.

Approaching flow velocity, $U_1 = q/h = 1.55/1.2 = 1.292 \text{ m s}^{-1}$

$$d_s = \left\{ 1.8 \left[\frac{\sin 40^\circ}{\sin(40^\circ + 55^\circ)} \right]^{0.8} \frac{1.55^{0.6} \times 1.292 \times \sin 55^\circ}{(1.65 \times 9.81)^{0.8} (4 \times 10^{-3})^{0.4}} \right\} - 0.5 = 1.213 \text{ m}$$

$\Leftarrow \text{Eq. (10.32)}$

Example 10.4 Calculate the equilibrium scour depth due to a horizontal jet issuing from a sluice gate opening using the equations of various investigators for the following data:

Height between upstream and downstream water levels, $H = 0.5$ m

Tailwater depth, $h_t = 2$ m

Discharge per unit width, $q = 1.6 \text{ m}^2 \text{ s}^{-1}$

Sluice gate opening, $b_0 = 0.5$ m

Sediment size, $d_{50} = 10$ mm and $d_{90} = 18$ mm

Angle of repose of sediment, $\phi = 42^\circ$

Relative density of sediment, $s = 2.65$

Dune height, $\eta_d = 0.1h_t$

Solution

Use van Rijn's empirical formula for the determination of threshold shear velocity (see Table 4.1):

Particle parameter, $D_* = d_{50}(\Delta g/v^2)^{1/3} = 10 \times 10^{-3}[1.65 \times 9.81/(10^{-6})^2]^{1/3} = 252.95$

Threshold Shields parameter, $\Theta_c(D_* > 150) = 0.055$

Threshold bed shear stress, $\tau_{0c} = \Theta_c \Delta \rho g d_{50} = 0.055 \times 1.65 \times 10^3 \times 9.81 \times 10 \times 10^{-3} = 8.903 \text{ Pa}$

Threshold shear velocity, $u_{*c} = (\tau_{0c}/\rho)^{0.5} = (8.903/10^3)^{0.5} = 0.094 \text{ m s}^{-1}$

Qayoum's equation

$$d_s = \frac{2.78}{9.81^{0.2}} \cdot \frac{1.6^{0.4} \times 0.5^{0.22} \times 2^{0.4}}{(18 \times 10^{-3})^{0.22}} - 2 = 3.826 \text{ m} \Leftarrow \text{Eq. (10.44)}$$

Altinbilek and Basmaci's equation

Jet velocity, $U_0 = q/b_0 = 1.6/0.5 = 3.2 \text{ m s}^{-1}$

$$d_s = 0.5 \left(\frac{0.5}{10 \times 10^{-3}} \tan 42^\circ \right)^{0.5} \left[\frac{3.2}{(1.65 \times 9.81 \times 0.5)^{0.5}} \right]^{1.5} = 4 \text{ m} \Leftarrow \text{Eq. (10.45)}$$

Breusers and Raudkivi's equation

$$d_s = 8 \times 10^{-3} \times 0.5 \left(\frac{3.2}{0.094} \right)^2 = 4.636 \text{ m} \Leftarrow \text{Eq. (10.46)}$$

Haffmans' equation

Averaged velocity over dune, $U_{\text{crest}} = q/(h_t - 0.1h_t) = q/(0.9h_t) = 1.6/(0.9 \times 2) = 0.889 \text{ m s}^{-1}$

Scour factor, $\lambda_s = 6.8$ for $d_{90} = 18 \text{ mm}$

$$d_s = 0.5 \frac{50}{6.8} \left(1 - \frac{0.889}{3.2} \right) = 2.655 \text{ m} \Leftarrow \text{Eq. (10.47)}$$

Eggenberger and Müller's equation

$$d_s = \frac{10.35}{15.849} \cdot \frac{1.6^{0.6} \times 0.5^{0.5}}{(18 \times 10^{-3})^{0.4}} - 2 = 1.053 \text{ m} \Leftarrow \text{Eq. (10.50)}$$

Example 10.5 Determine the equilibrium scour depth downstream of an apron of length $L_0 = 3 \text{ m}$ due to a horizontal jet issuing from a sluice gate opening for the data given in Example 10.4.

Solution*Shalash's equation*

$$d_s = 0.61 \frac{1.6^{0.6}(0.5 + 2)^{0.5}}{(18 \times 10^{-3})^{0.4}} \left(1.5 \frac{0.5}{3} \right)^{0.6} - 2 = 0.776 \text{ m} \Leftarrow \text{Eq. (10.48)}$$

Dey and Sarkar's equation

$$\begin{aligned} d_s &= 2.59 \times 0.5 \left[\frac{3.2}{(1.65 \times 9.81 \times 10 \times 10^{-3})^{0.5}} \right]^{0.94} \left(\frac{0.5}{3} \right)^{0.37} \left(\frac{2}{0.5} \right)^{0.16} \left(\frac{10 \times 10^{-3}}{0.5} \right)^{0.25} \\ &= 2.2 \text{ m} \Leftarrow \text{Eq. (10.49)} \end{aligned}$$

Example 10.6 Calculate the equilibrium scour depth downstream of a hydraulic structure due to a combined overfall and submerged jet for the following data:

Height between upstream and downstream water levels, $H = 1.2 \text{ m}$

Tailwater depth, $h_t = 1.5 \text{ m}$

Total discharge per unit width, $q = 1.6 \text{ m}^2 \text{ s}^{-1}$

Discharge through sluice opening, $q_0 = 0.6q$

Sediment size, $d_{90} = 12 \text{ mm}$

Solution*Eggenberger and Müller's equation*

Submerged jet discharge through sluice opening, $q_0 = 0.6q = 0.6 \times 1.6 = 0.96 \text{ m}^2 \text{ s}^{-1}$

Overfall discharge, $q_1 = q - q_0 = 1.6 - 0.96 = 0.64 \text{ m}^2 \text{ s}^{-1}$

Discharge ratio, $\hat{q} = q_1/q_0 = 0.64/0.96 = 0.67$

$$\begin{aligned} c_0 &= 22.88 - \frac{10^3}{4.9\hat{q}^3 - 6.3\hat{q}^2 + 29\hat{q} + 64} \\ &= 22.88 - \frac{10^3}{4.9 \times 0.67^3 - 6.3 \times 0.67^2 + 29 \times 0.67 + 64} = 10.7 \\ d_s &= \frac{10.7}{15.849} \cdot \frac{1.6^{0.6} \times 1.2^{0.5}}{(12 \times 10^{-3})^{0.4}} - 1.5 = 4.251 \text{ m} \Leftarrow \text{Eq. (10.50)} \end{aligned}$$

Example 10.7 Given pipe diameter, $D = 1.2 \text{ m}$; embedment, $e = 0.1 \text{ m}$; porosity of sediment, $\rho_0 = 0.4$; and relative density of sediment, $s = 2.65$, what is the threshold velocity of scour underneath the submarine pipeline?

Solution

From Eq. (10.51)

$$\begin{aligned} U_{\text{gr}}^2 &= 0.025 \Delta g (1 - \rho_0) D \exp\left(81 \frac{e}{D}\right)^{0.5} \\ &= 0.025 \times 1.65 \times 9.81 (1 - 0.4) 1.2 \times \exp\left(81 \frac{0.1}{1.2}\right)^{0.5} = 3.915 \end{aligned}$$

Therefore, $U_{\text{gr}} = 1.979 \text{ m s}^{-1}$

Example 10.8 Compute the equilibrium scour depth below a 0.1 m diameter underwater pipeline, laid on a sediment bed of $d_{50} = 0.6 \text{ mm}$ in a laboratory flume, subjected to a steady flow velocity of 0.35 m s^{-1} having a flow depth of 0.4 m. Take coefficient of kinematic viscosity of water $\nu = 10^{-6} \text{ m}^2 \text{ s}^{-1}$ and mass density of water $\rho = 10^3 \text{ kg m}^{-3}$.

Solution

Given data are as follows:

Pipe diameter, $D = 0.1 \text{ m}$; flow velocity, $U = 0.35 \text{ m s}^{-1}$; flow depth, $h = 0.4 \text{ m}$; sediment size, $d_{50} = 0.6 \text{ mm}$; kinematic viscosity of water, $\nu = 10^{-6} \text{ m}^2 \text{ s}^{-1}$; and mass density of water, $\rho = 10^3 \text{ kg m}^{-3}$

Use van Rijn's empirical formula for the determination of threshold bed shear stress (see Table 4.1):

Particle parameter, $D_* = d_{50}(\Delta g/\nu^2)^{1/3} = 0.6 \times 10^{-3}[1.65 \times 9.81/(10^{-6})^2]^{1/3} = 15.18$

Threshold Shields parameter, $\Theta_c(10 < D_* \leq 20) = 0.04 D_*^{-0.1} = 0.04 \times 15.18^{-0.1} = 0.03$

Threshold bed shear stress, $\tau_{0c} = \Theta_c \Delta \rho g d_{50} = 0.03 \times 1.65 \times 10^3 \times 9.81 \times 0.6 \times 10^{-3} = 0.291 \text{ Pa}$

Estimation of scour depth by Chiew's method

Discharge per unit width, $q = Uh = 0.35 \times 0.4 = 0.14 \text{ m}^2 \text{ s}^{-1}$. Then, q_g is

$$q_g = 0.781 \times 0.14 \left(\frac{0.1}{0.4} \right)^{0.787} = 0.0367 \text{ m}^2 \text{ s}^{-1} \Leftarrow \text{Eq. (10.55)}$$

Chiew proposed to determine friction factor λ_D from the Moody diagram. It can however also be determined from the Colebrook–White equation (Eq. 3.55). Remembering that the Colebrook–White equation is an implicit equation, it is therefore preferred here to use Haaland's (1983) explicit equation that gives an approximate solution for the Colebrook–White equation and can be used as a substitute. The original Haaland's equation is given for a pipe flow case having an average flow velocity U with an internal pipe diameter D_i as

$$\frac{1}{\lambda_D^{0.5}} = -0.782 \ln \left[\left(\frac{k_s}{3.7 D_i} \right)^{1.1} + \frac{6}{Re} \right] \quad \wedge \quad Re = \frac{U D_i}{\nu}$$

In this case, for the pressurized flow beneath the pipeline, the scour depth d_s and the average gap velocity U_g are analogous to D_i and U , respectively. The roughness height k_s can be assumed as d_{50} ($= 0.6 \text{ mm}$)

For the first trial, assume $d_s = 0.12 \text{ m}$ and then calculate the average gap velocity $U_g = q_g/d_s = 0.0367/0.12 = 0.306 \text{ m s}^{-1}$ and the Reynolds number $Re = U_g d_s/\nu = 0.306 \times 0.12/10^{-6} = 36,720$. The friction factor is determined from Haaland's equation as

$$\frac{1}{\lambda_D^{0.5}} = -0.782 \ln \left[\left(\frac{0.6 \times 10^{-3}}{3.7 \times 0.12} \right)^{1.1} + \frac{6}{36720} \right] \Rightarrow \lambda_D = 0.033$$

Thus, the bed shear stress in the scour hole beneath the pipeline is

$$\tau_0 = \frac{\lambda_D}{8} \rho U_g^2 = \frac{0.033}{8} \times 10^3 \times 0.306^2 \Rightarrow \tau_0 = 0.386 \text{ Pa} \quad \therefore \quad \tau_0 \neq \tau_{0c}$$

Following a trial-and-error method, the value of d_s that satisfies the condition $\tau_0 = \tau_{0c}$ ($= 0.291 \text{ Pa}$) is 0.136 m . Therefore, the equilibrium scour depth d_s is 0.136 m .

Example 10.9 Calculate the maximum scour depth at a rectangular pier for the following data:

Pier width, $b = 2$ m

Pier length, $L = 8$ m

Approaching flow depth, $h = 8$ m

Discharge per unit width, $q = 12 \text{ m}^2 \text{ s}^{-1}$

Flow skewness, $\alpha = 15^\circ$

Median size of sediment, $d_{50} = 0.9$ mm (uniform sediment)

Use (1) Melville and Coleman's method (2) HEC18 method and (3) Sheppard et al.'s method.

Also, determine the size of riprap stone for the scour countermeasure at the pier. Assume the riprap to be placed at the original bed level.

Solution

Approaching flow velocity, $U = q/h = 12/8 = 1.5 \text{ m s}^{-1}$

(1) *Calculation of scour depth by Melville and Coleman's method*

The threshold shear velocity and threshold approaching flow velocity are as follows:

$$u_{*c}(0.1 \text{ mm} \leq d_{50} < 1 \text{ mm}) = 0.0115 + 0.0125d_{50}^{1.4} = 0.0115 + 0.0125 \times 0.9^{1.4} \\ = 0.022 \text{ m s}^{-1}$$

$$U_{cr} = u_{*c} 5.75 \log \left(5.53 \frac{h}{d_{50}} \right) = 0.022 \times 5.75 \log \left(5.53 \frac{8}{0.9 \times 10^{-3}} \right) \\ = 0.593 \text{ m s}^{-1} \Leftarrow \text{Eq. (10.67)}$$

For uniform sediment, $U_a = U_{cr}$

Computation of K -factors is as follows:

1. For $b/h = 2/8 = 0.25 < 0.7$, $K_h = 2.4b = 2.4 \times 2 = 4.8 \text{ m} \Leftarrow \text{Eq. (10.65)}$
2. For $\frac{U - (U_a - U_{cr})}{U_{cr}} = \frac{1.5}{0.593} = 2.53 > 1$, $K_1 = 1 \Leftarrow \text{Eq. (10.66)}$
3. For $b/d_{50} = 2/(0.9 \times 10^{-3}) = 2222.2 > 25$, $K_d = 1 \Leftarrow \text{Eq. (10.68)}$
4. For a rectangular pier (square nosed), $K_s = 1.1$ (Table 10.2)
5. For $b_p = L \sin \alpha + b \cos \alpha = 8 \times \sin 15^\circ + 2 \times \cos 15^\circ = 4 \text{ m}$, $K_\alpha = (b_p/b)^{0.65} \\ = (4/2)^{0.65} = 1.569 \Leftarrow \text{Eq. (10.70)}$
6. For an equilibrium scour ($t = t_c$), $K_t = 1 \Leftarrow \text{Eq. (10.71)}$

Then, the scour depth is

$$d_s = K_h K_l K_d K_s K_z K_t = 4.8 \times 1 \times 1 \times 1.1 \times 1.569 \times 1 = 8.284 \text{ m} \Leftarrow \text{Eq. (10.64)}$$

(2) *Calculation of scour depth by HEC18 method*

Computation of K -factors is as follows:

1. For a rectangular pier, $K_s = 1.1$ (Table 10.2)
2. For $L/b = 8/2 = 4$ and $\alpha = 15^\circ$, $K_z = 1.5$ (Table 10.4)
3. For $Fr = 1.5/(9.81 \times 8)^{0.5} = 0.169$ and $U (= 1.5 \text{ m s}^{-1}) > U_{cr}$ ($= 0.593 \text{ m s}^{-1}$), the possible bedforms are small dunes (assumed). Thus, $K_{bed} = 1.1$ (Table 10.3)
4. For $d_{50} = 0.9 \text{ mm} < 2 \text{ mm}$, $K_a = 1 \Leftarrow \text{Eq. (10.75a)}$

Then, the scour depth is

$$\begin{aligned} \frac{d_s}{b} &= 2K_s K_z K_{bed} K_a \left(\frac{h}{b}\right)^{0.35} Fr^{0.43} = 2 \times 1.1 \times 1.5 \times 1.1 \times 1 \left(\frac{8}{2}\right)^{0.35} 0.169^{0.43} \\ &= 2.745 \Leftarrow \text{Eq. (10.74)} \\ d_s &= 2 \times 2.745 = 5.49 \text{ m} \end{aligned}$$

(3) *Calculation of scour depth by Sheppard et al.'s method*

The threshold shear velocity and threshold approaching flow velocity are calculated as follows:

$$\begin{aligned} u_{*c} &= \left\{ 16.2d_{50} \left[\frac{9.09 \times 10^{-6}}{d_{50}} - d_{50}(38.76 + 9.6 \ln d_{50}) - 0.005 \right] \right\}^{0.5} \\ &= \sqrt{16.2 \times 0.9 \times 10^{-3} \left\{ \frac{9.09 \times 10^{-6}}{0.9 \times 10^{-3}} - 0.9 \times 10^{-3} [38.76 + 9.6 \ln(0.9 \times 10^{-3})] - 0.005 \right\}} \\ &= 0.021 \text{ m s}^{-1} \\ \Re &= \frac{u_{*c} d_{50}}{2.32 \times 10^{-7}} = \frac{0.021 \times 0.9 \times 10^{-3}}{2.32 \times 10^{-7}} = 81.47 \quad (\Re > 70) \\ U_{cr} &= u_{*c} 2.5 \ln \left(2.21 \frac{h}{d_{50}} \right) = 0.021 \times 2.5 \ln \left(2.21 \frac{8}{0.9 \times 10^{-3}} \right) = 0.519 \text{ m s}^{-1} \Leftarrow \text{Eq. (10.78b)} \end{aligned}$$

The effective pier diameter is calculated as follows:

$$\begin{aligned} K_s &= 0.86 + 0.97 \left| \alpha - \frac{\pi}{4} \right|^4 = 0.86 + 0.97 \left| 15^\circ - \frac{\pi}{4} \right|^4 = 0.933 \\ b_e &= K_s b_p = 0.933 \times 4 = 3.732 \text{ m} \end{aligned}$$

The functions are calculated as follows:

$$f_1 = \tanh \left[\left(\frac{h}{b_e} \right)^{0.4} \right] = \tanh \left[\left(\frac{8}{3.732} \right)^{0.4} \right] = 0.876$$

$$f_3 = \frac{\frac{b_e}{d_{50}}}{0.4 \left(\frac{b_e}{d_{50}} \right)^{1.2} + 10.6 \left(\frac{b_e}{d_{50}} \right)^{-0.13}} = \frac{\frac{3.732}{0.9 \times 10^{-3}}}{0.4 \left(\frac{3.732}{0.9 \times 10^{-3}} \right)^{1.2} + 10.6 \left(\frac{3.732}{0.9 \times 10^{-3}} \right)^{-0.13}}$$

$$= 0.472$$

Then, the scour depth is calculated as follows:

For $5U_{cr} < 0.6(gh)^{0.5}$, $U_{peak} = 0.6(gh)^{0.5} = 0.6(9.81 \times 8)^{0.5} = 5.315 \text{ m s}^{-1}$.

$\therefore U_{cr} \leq U \leq U_{peak}$

$$\begin{aligned} \frac{d_s}{b_e} &= f_1 \left[2.2 \left(\frac{U - U_{cr}}{U_{peak} - U_{cr}} \right) + 2.5 f_3 \left(\frac{U_{peak} - U}{U_{peak} - U_{cr}} \right) \right] \\ &= 0.876 \left[2.2 \left(\frac{1.5 - 0.519}{5.315 - 0.519} \right) + 2.5 \times 0.472 \left(\frac{5.315 - 1.5}{5.315 - 0.519} \right) \right] \\ &= 1.216 \Leftarrow \text{Eq. (10.77b)} \\ d_s &= b_e \times 1.216 = 3.732 \times 1.216 = 4.538 \text{ m} \end{aligned}$$

Calculation of riprap stone size

By HEC-23 formula:

$$d_{50r} = 0.346 \frac{(KU)^2}{\Delta g} = 0.346 \frac{(1.7 \times 1.5)^2}{1.65 \times 9.81} = 0.139 \text{ m} \Leftarrow \text{Eq. (10.89)}$$

Note: For a rectangular pier, $K = 1.7$

By Lauchlan's equation:

Placement depth, $z_r = 0$

$$d_{50r} = 0.3 f_{SF} h \left(1 - \frac{z_r}{h} \right)^{2.75} Fr^{1.2} = 0.3 \times 1.1 \times 8 \left(1 - \frac{0}{8} \right)^{2.75} 0.169^{1.2} = 0.313 \text{ m}$$

$$\Leftarrow \text{Eq. (10.90)}$$

Note: $f_{SF} = 1.1$ is considered in the above calculation.

Example 10.10 Determine scour depth in the end of the second day for $q = 4 \text{ m}^2 \text{ s}^{-1}$ and other data same as in Example 10.9.

Solution

Approaching flow velocity, $U = q/h = 4/8 = 0.5 \text{ m s}^{-1} < U_{cr} (= 0.519 \text{ m s}^{-1})$

For $U/U_{cr} = 0.5/0.519 = 0.963 < 1$ (clear-water scour), $K_1 = 0.963 \Leftarrow \text{Eq. (10.66)}$

For $h/b = 8/2 = 4 < 6$ and $U/U_{cr} = 0.963 > 0.4$, the time t_e to reach equilibrium is

$$t_e = 30.89 \frac{b}{U} \left(\frac{U}{U_{cr}} - 0.4 \right) \left(\frac{h}{b} \right)^{0.25} = 30.89 \frac{2}{0.5} \left(\frac{0.5}{0.519} - 0.4 \right) \left(\frac{8}{2} \right)^{0.25} = 98.4 \text{ days}$$

$\Leftarrow \text{Eq. (10.72)}$

For $t = 2$ days, K_t is

$$K_t = \exp \left[-0.03 \left| \frac{U_{cr}}{U} \ln \left(\frac{t}{t_e} \right) \right|^{1.6} \right] = \exp \left[-0.03 \left| \frac{0.519}{0.5} \ln \left(\frac{2}{98.4} \right) \right|^{1.6} \right] = 0.755$$

$\Leftarrow \text{Eq. (10.71)}$

Then, the scour depth is

$$d_s = K_h K_l K_d K_s K_z K_t = 4.8 \times 0.962 \times 1 \times 1.1 \times 1.569 \times 0.755 = 6.017 \text{ m}$$

$\Leftarrow \text{Eq. (10.64)}$

Example 10.11 Calculate the maximum scour depth at a circular pier for the following data:

Pier diameter, $b = 2.5 \text{ m}$

Approaching flow depth, $h = 3.4 \text{ m}$

Discharge per unit width, $q = 11.9 \text{ m}^2 \text{ s}^{-1}$

Sediment size, $d_{50} = 20 \text{ mm}$, $d_{95} = 85 \text{ mm}$ and $d_{\max} = 99 \text{ mm}$

Use (1) Melville and Coleman's method and (2) HEC18 method.

Also, determine the size of riprap stone for the scour countermeasure at the pier. Assume the riprap to be placed 0.5 m below the original bed level.

Solution

Approaching flow velocity, $U = q/h = 11.9/3.4 = 3.5 \text{ m s}^{-1}$

(1) *Calculation of scour depth by Melville and Coleman's method*

The threshold shear velocity u_{*c} and threshold approaching flow velocities, U_{cr} , U_{cra} , and U_a are calculated as follows:

$$\begin{aligned}
u_{*c}(1 \text{ mm} \leq d_{50} < 100 \text{ mm}) &= 0.0305d_{50}^{0.5} - 6.5 \times 10^{-3}d_{50}^{-1} \\
&= 0.0305 \times 20^{0.5} - 6.5 \times 10^{-3} \times 20^{-1} = 0.136 \text{ m s}^{-1} \\
d_{50a} &= d_{\max}/1.8 = 99/1.8 = 55 \text{ mm} \\
u_{*ca}(1 \text{ mm} \leq d_{50} < 100 \text{ mm}) &= 0.0305d_{50a}^{0.5} - 6.5 \times 10^{-3}d_{50a}^{-1} \\
&= 0.0305 \times 55^{0.5} - 6.5 \times 10^{-3} \times 55^{-1} = 0.226 \text{ m s}^{-1} \\
U_{cr} &= u_{*c}5.75 \log \left(5.53 \frac{h}{d_{50}} \right) = 0.136 \\
&\quad \times 5.75 \log \left(5.53 \frac{3.4}{20 \times 10^{-3}} \right) \\
&= 2.325 \text{ m s}^{-1} \Leftarrow \text{Eq. (10.67)} \\
U_{cra} &= u_{*ca}5.75 \log \left(5.53 \frac{h}{d_{50a}} \right) = 0.226 \\
&\quad \times 5.75 \log \left(5.53 \frac{3.4}{55 \times 10^{-3}} \right) \\
&= 3.293 \text{ m s}^{-1} \Leftarrow \text{Eq. (10.67)} \\
U_a &= 0.8U_{cra} = 0.8 \times 3.293 = 2.634 \text{ m s}^{-1}
\end{aligned}$$

Computation of K -factors is as follows:

1. For $b/h = 2.5/3.4 = 0.735$ ($0.7 \leq b/h \leq 5$), $K_h = 2(hb)^{0.5} = 2(3.4 \times 2.5)^{0.5} = 5.831 \text{ m} \Leftarrow \text{Eq. (10.65)}$
2. For $\frac{U - (U_a - U_{cr})}{U_{cr}} = \frac{3.5 - (2.634 - 2.325)}{2.325} = 1.372 > 1$, $K_I = 1 \Leftarrow \text{Eq. (10.66)}$
3. For $b/d_{50a} = 2/(55 \times 10^{-3}) = 36.36 > 25$, $K_d = 1 \Leftarrow \text{Eq. (10.68)}$
4. For a circular pier, $K_s = 1$ (Table 10.2)
5. For a circular pier, $K_z = 1 \Leftarrow \text{Eq. (10.70)}$
6. For an equilibrium scour ($t = t_e$), $K_t = 1 \Leftarrow \text{Eq. (10.71)}$

Then, the scour depth is

$$d_s = K_h K_I K_d K_s K_z K_t = 5.831 \times 1 \times 1 \times 1 \times 1 \times 1 = 5.831 \text{ m} \Leftarrow \text{Eq. (10.64)}$$

(2) Calculation of scour depth by HEC18 method

$$U_{cr}|_{d_{50}} = 6.19h^{1/6}d_{50}^{1/3} = 6.19 \times 3.4^{1/6}(20 \times 10^{-3})^{1/3} \\ = 2.06 \text{ m s}^{-1} \Leftarrow \text{Eq. (10.76)}$$

$$U_{cr}|_{d_{95}} = 6.19h^{1/6}d_{95}^{1/3} = 6.19 \times 3.4^{1/6}(85 \times 10^{-3})^{1/3} \\ = 3.337 \text{ m s}^{-1} \Leftarrow \text{Eq. (10.76)}$$

$$U_{crs}|_{d_{50}} = 0.645 \left(\frac{d_{50}}{b} \right)^{0.053} U_{cr}|_{d_{50}} = 0.645 \left(\frac{20 \times 10^{-3}}{2} \right)^{0.053} 2.06 \\ = 1.041 \text{ m s}^{-1} \Leftarrow \text{Eq. (10.76)}$$

$$U_{crs}|_{d_{95}} = 0.645 \left(\frac{d_{95}}{b} \right)^{0.053} U_{cr}|_{d_{95}} = 0.645 \left(\frac{85 \times 10^{-3}}{2} \right)^{0.053} 3.337 \\ = 1.821 \text{ m s}^{-1} \Leftarrow \text{Eq. (10.76)}$$

$$U_r = \frac{U - U_{crs}|_{d_{50}}}{U_{cr}|_{d_{50}} - U_{crs}|_{d_{95}}} = \frac{3.5 - 1.041}{2.06 - 1.821} = 10.289 \Leftarrow \text{Eq. (10.75b)}$$

Computation of K -factors is as follows:

1. For a circular pier, $K_s = 1$ (Table 10.2)
2. For a circular pier, $K_\alpha = 1$
3. For $Fr = 3.5/(9.81 \times 3.4)^{0.5} = 0.6$ and $U (= 3.5 \text{ m s}^{-1}) > U_{cr}$ ($= 2.06 \text{ m s}^{-1}$), the possible bedforms are large dunes (assumed). Thus, $K_{bed} = 1.3$ (Table 10.3)
4. For $d_{50} = 20 \text{ mm} > 2 \text{ mm}$ and $d_{95} = 85 \text{ mm} > 20 \text{ mm}$, $K_a = 0.4U_r^{0.15} = 0.4 \times 10.289^{0.15} = 0.567 \Leftarrow \text{Eq. (10.75b)}$

Then, the scour depth is

$$\frac{d_s}{b} = 2K_sK_\alpha K_{bed}K_a \left(\frac{h}{b} \right)^{0.35} Fr^{0.43} = 2 \times 1 \times 1 \times 1.3 \times 0.567 \left(\frac{3.4}{2.5} \right)^{0.35} 0.6^{0.43} \\ = 1.318 \Leftarrow \text{Eq. (10.74)} \\ d_s = 2.5 \times 1.318 = 3.295 \text{ m}$$

Calculation of riprap stone size

By HEC-23 formula:

$$d_{50r} = 0.346 \frac{(KU)^2}{\Delta g} = 0.346 \frac{(1.5 \times 3.5)^2}{1.65 \times 9.81} = 0.589 \text{ m} \Leftarrow \text{Eq. (10.89)}$$

Note: For a circular pier, $K = 1.5$

By Lauchlan's equation:

Placement depth, $z_r = 0.5 \text{ m}$

$$d_{50r} = 0.3f_{SF}h\left(1 - \frac{z_r}{h}\right)^{2.75} Fr^{1.2} = 0.3 \times 1.5 \times 3.4 \left(1 - \frac{0.5}{3.4}\right)^{2.75} 0.6^{1.2} = 0.535 \text{ m}$$

\Leftarrow Eq. (10.90)

Note: $f_{SF} = 1.5$ is considered in the above calculation.

Example 10.12 Calculate the maximum scour depth at a spill-through abutment for the following data:

Abutment length = 10 m

Abutment length spanning to flood channel = 95 % of abutment length

Abutment slope, $S_a = 0.5$ (horizontal) : 1 (vertical)

Abutment alignment, $\alpha = 80^\circ$

Flow depth in main channel, $h_m = 8$ m

Flow depth in flood channel, $h^* = 2$ m

Discharge per unit width in main channel, $q = 20 \text{ m}^2 \text{ s}^{-1}$

Discharge per unit width in flood channel, $q^* = 5 \text{ m}^2 \text{ s}^{-1}$

Manning coefficient in main channel, $n = 0.022$ SI units

Manning coefficient in flood channel, $n^* = 0.03$ SI units

Sediment size, $d_{50} = 20$ mm, $d_{95} = 85$ mm, and $d_{\max} = 99$ mm

Assume the flow depth reduction to be 2 % in the contracted portion.

Use (1) Melville and Coleman's method and (2) HEC18 method.

Also, determine the size of riprap stone for scour countermeasure at the abutment.

Solution

Calculation is based on the flow in the flood channel, where 95 % of abutment length exists.

Approaching flow velocity in flood channel, $U = q^*/h^* = 5/2 = 2.5 \text{ m s}^{-1}$

Projected abutment length, $l = 10 \sin \alpha = 10 \sin 80^\circ = 9.848$ m

Projected abutment length in flood channel, $l^* = 10 \times 0.95 \sin \alpha = 10 \times 0.95 \sin 80^\circ = 9.356$ m

The threshold approaching flow velocities, U_{cr} , U_{cra} , and U_a , are as follows:

$$u_{*c} = 0.136 \text{ m s}^{-1}; u_{*ca} = 0.226 \text{ m s}^{-1}; d_{50a} = 55 \text{ mm (see Example 10.11)}$$

$$\begin{aligned} U_{cr} &= u_{*c} 5.75 \log \left(5.53 \frac{h^*}{d_{50}} \right) = 0.136 \times 5.75 \log \left(5.53 \frac{2}{20 \times 10^{-3}} \right) \\ &= 2.145 \text{ m s}^{-1} \Leftarrow \text{Eq. (10.67)} \end{aligned}$$

$$\begin{aligned} U_{cra} &= u_{*ca} 5.75 \log \left(5.53 \frac{h^*}{d_{50a}} \right) = 0.226 \times 5.75 \log \left(5.53 \frac{2}{55 \times 10^{-3}} \right) \\ &= 2.993 \text{ m s}^{-1} \Leftarrow \text{Eq. (10.67)} \end{aligned}$$

$$U_a = 0.8 U_{cra} = 0.8 \times 2.993 = 2.394 \text{ m s}^{-1}$$

Calculation of scour depth by Melville and Coleman's method

Computation of K -factors is as follows:

1. For $l/h^* = 9.848/2 = 4.924$ ($1 \leq l/h^* \leq 25$), $K_h = 2(h^*l)^{0.5} = 2(2 \times 9.848)^{0.5} = 8.876 \text{ m} \Leftarrow \text{Eq. (10.80)}$

Note: As the flow depth in flood channel is applicable, h is replaced by h^* in Eq. (10.80)

2. For $\frac{U - (U_a - U_{cr})}{U_{cr}} = \frac{2.5 - (2.394 - 2.145)}{2.145} = 1.049 > 1$, $K_I = 1 \Leftarrow \text{Eq. (10.66)}$
3. For $l/d_{50a} = 9.848/(55 \times 10^{-3}) = 179.05 > 25$, $K_d = 1 \Leftarrow \text{Eq. (10.81)}$
4. For a spill-through abutment with slope $S_a = 0.5:1$, $K_s = 0.6$ (Table 10.6)
5. For $\alpha = 80^\circ$, $K_\alpha^* = 0.993$ is obtained from Table 10.7. Then, for $l/h^* = 4.924 > 3$, $K_\alpha = 0.993 \Leftarrow \text{Eq. (10.83)}$
6. K_G is calculated, considering $h = h_m$, that is, the flow depth in main channel, as

$$K_G = \left\{ 1 - \left(\frac{l^*}{l} \right) \left[1 - \left(\frac{h^*}{h} \right)^{5/3} \left(\frac{n}{n^*} \right) \right] \right\}^{0.5}$$

$$= \left\{ 1 - \left(\frac{9.356}{9.848} \right) \left[1 - \left(\frac{2}{8} \right)^{5/3} \left(\frac{0.022}{0.03} \right) \right] \right\}^{0.5} = 0.345 \Leftarrow \text{Eq. (10.84)}$$

7. For an equilibrium scour ($t = t_e$), $K_t = 1 \Leftarrow \text{Eq. (10.85)}$

Then, the scour depth is

$$d_s = K_h K_I K_d K_s K_\alpha K_G K_t = 8.876 \times 1 \times 1 \times 0.6 \times 0.993 \times 0.345 \times 1 = 1.824 \text{ m} \Leftarrow \text{Eq. (10.79)}$$

Calculation of riprap stone size

By Austroads formula:

$$Fr = U/(gh^*)^{0.5} = 2.5/(9.81 \times 2)^{0.5} = 0.564$$

$$d_{50r} = 1.026 \frac{h^* Fr^2}{\Delta} = 1.026 \frac{2 \times 0.564^2}{1.65} = 0.396 \text{ m} \Leftarrow \text{Eq. (10.91)}$$

By Lauchlan's equation:

Shape factor, $K_s = 0.89$

Flow depth in contracted portion, $h_2 = 8 - 0.02 \times 8 = 7.84 \text{ m}$

Flow velocity in contracted portion, $U_2 = q/h_2 = 20/7.84 = 2.551 \text{ m s}^{-1}$

Froude number in contracted portion, $Fr_2 = U_2/(gh_2)^{0.5} = 2.551/(9.81 \times 7.84)^{0.5} = 0.291 < 0.8$

$$d_{50r} = K_s \frac{h_2 Fr_2^2}{\Delta} = 0.89 \frac{7.84 \times 0.291^2}{1.65} = 0.358 \text{ m} \Leftarrow \text{Eq. (10.92a)}$$

Example 10.13 Determine scour depth in the end of the second day for the discharge per unit width in flood channel $q = 4 \text{ m}^2 \text{ s}^{-1}$ and other data same as in Example 10.12.

Solution

Approaching flow velocity in flood channel, $U = q^*/h^* = 4/2 = 2 \text{ m s}^{-1}$

For $\frac{U - (U_a - U_{cr})}{U_{cr}} = \frac{2 - (2.394 - 2.145)}{2.145} = 0.816 < 1$, $K_1 = 0.816 \Leftarrow \text{Eq. (10.66)}$

For $l/h^* = 9.848/2 = 4.924 > 1.2$, the time t_e to reach equilibrium is

$$t_e = 25 \frac{h}{U} = 25 \frac{2}{2} = 25 \text{ days} \Leftarrow \text{Eq. (10.86)}$$

For $t = 2$ days, K_t is

$$K_t = 0.1 \frac{U_{cr}}{U} \ln\left(\frac{t}{t_e}\right) + 1 = 0.1 \frac{2.145}{2} \ln\left(\frac{2}{25}\right) + 1 = 0.729 \Leftarrow \text{Eq. (10.85)}$$

Then, the scour depth is

$$d_s = K_h K_1 K_d K_s K_z K_G K_t = 8.876 \times 0.816 \times 1 \times 0.6 \times 0.993 \times 0.345 \times 0.729 = 1.085 \text{ m} \Leftarrow \text{Eq. (10.79)}$$

Example 10.14 Calculate the maximum scour depth at a vertical-wall abutment for the following data:

Abutment length, $l = 12 \text{ m}$

Abutment alignment, $\alpha = 90^\circ$

Flow depth, $h = 8 \text{ m}$

Discharge per unit width, $q = 24 \text{ m}^2 \text{ s}^{-1}$

Median size of sediment, $d_{50} = 0.9 \text{ mm}$ (uniform sediment)

Solution

Approaching flow velocity, $U = q/h = 24/8 = 3 \text{ m s}^{-1}$

Threshold approaching flow velocity, $U_{cr} = 0.593 \text{ m s}^{-1}$ (see Example 10.9)

It is a live-bed flow condition ($U > U_{cr}$). Hence, Froehlich's (HEC 18) method is applicable

Calculation of scour depth by HEC18 method:

Computation of K -factors is as follows:

Flow Froude number, $Fr = U/(gh)^{0.5} = 3/(9.81 \times 8)^{0.5} = 0.339$

1. For a vertical-wall abutment, $K_s = 1$ (Table 10.8)
2. For $\alpha = 90^\circ$, $K_\alpha = 1 \Leftarrow \text{Eq. (10.88)}$

Then, the scour depth is

$$\begin{aligned}\frac{d_s}{l} &= 2.27 K_s K_\alpha \left(\frac{h}{l}\right)^{0.57} Fr^{0.61} + 1 = 2.27 \times 1 \times 1 \left(\frac{8}{12}\right)^{0.57} 0.339^{0.61} + 1 \\ &= 1.931 \Leftarrow \text{Eq. (10.87)} \\ d_s &= 12 \times 1.931 = 23.172 \text{ m}\end{aligned}$$

References

- Altinbilek HD, Basmaci Y (1973) Localized scour at the downstream of outlet structures. In: Proceedings of the eleventh congress on Large Dam, Madrid, pp 105–121
- Atayee AT, Pagan-Ortiz JE, Jones JS, Kilgore RT (1993) A study of riprap as a scour protection for spill-through abutments. American Society of Civil Engineers (ASCE) hydraulic engineering conference, San Francisco, California
- Austrroads (1994) Waterway design—a guide to the hydraulic design of bridges, culverts and floodways. Austrroads, Sydney
- Bakhmeteff BA (1932) Hydraulics of open channels. McGraw-Hill, New York
- Barbhuiya AK (2003) Clear water scour at abutments. PhD thesis, Department of Civil Engineering, Indian Institute of Technology, Kharagpur
- Barbhuiya AK, Dey S (2004) Velocity and turbulence at a wing-wall abutment. Proc Indian Acad Sci Sadhana 29(Feb):35–56
- Barenblatt GI, Chorin AJ, Prostokishin VM (2005) The turbulent wall jet: a triple-layered structure and incomplete similarity. Proc Natl Acad Sci 102(25):8850–8853
- Bijker EW, Leeuwestein W (1984) Interaction between pipeline and the seabed under the influence of waves and current. In: Proceedings of the symposium of International Union of Theoretical and Applied Mechanics/International Union of Geology and Geophysics, seabed mechanics, pp 235–242
- Bormann NE, Julien PY (1991) Scour downstream of grade-control structures. J Hydraul Eng 117(5):579–594
- Breusers HNC, Nicollet G, Shen HW (1977) Local scour around cylindrical piers. J Hydraul Res 15(3):211–252
- Breusers HNC, Raudkivi AJ (1991) Scouring. Balkema, Rotterdam
- Chao JL, Hennessy PV (1972) Local scour under ocean outfall pipe-lines. J Water Pollut Control Fed 44(7):1443–1447
- Chiew YM (1991) Prediction of maximum scour depth at submarine pipelines. J Hydraul Eng 117(4):452–466
- Chiew YM (1995) Mechanics of riprap failure at bridge piers. J Hydraul Eng 121(9):635–643
- Chiew YM, Lim SY (2003) Protection of bridge piers using a sacrificial sill. Water Marit Eng Proc Inst Civ Eng (London) 156(1):53–62
- Croad RN (1997) Protection from scour of bridge piers using riprap. Transit New Zealand research report number PR3-0071, Works Consultancy Services Limited, Central Laboratories, Lower Hutt, Wellington
- D'Agostino V, Ferro V (2004) Scour on alluvial bed downstream of grade-control structures. J Hydraul Eng 130(1):24–37
- Dey S (1991) Clear water scour around circular bridge piers: a model. PhD thesis, Department of Civil Engineering, Indian Institute of Technology, Kharagpur
- Dey S (1995) Three-dimensional vortex flow field around a circular cylinder in a quasi-equilibrium scour hole. Proc Indian Acad Sci Sadhana 20(Dec):871–885

- Dey S (1997a) Local scour at piers, part 1: a review of development of research. *Int J Sediment Res* 12(2):23–44
- Dey S (1997b) Local scour at piers, part 2: bibliography. *Int J Sediment Res* 12(2):45–57
- Dey S (1999) Time-variation of scour in the vicinity of circular piers. *Water Marit Energ Proc Inst Civ Eng (London)* 136(2):67–75
- Dey S, Barbhuiya AK (2004) Clear water scour at abutments. *Water Management Proc Inst Civ Eng (London)* 157(WM2):77–97
- Dey S, Barbhuiya AK (2005a) Turbulent flow field in a scour hole at a semicircular abutment. *Can J Civ Eng* 32(1):213–232
- Dey S, Barbhuiya AK (2005b) Flow field at a vertical-wall abutment. *J Hydraul Eng* 131(12):1126–1135
- Dey S, Barbhuiya AK (2006) 3D flow field in a scour hole at a wing-wall abutment. *J Hydraul Res* 44(1):33–50
- Dey S, Bose SK (1994) Bed shear in equilibrium scour around a circular cylinder embedded in loose bed. *Appl Math Model* 18(5):265–273
- Dey S, Bose SK, Sastry GLN (1995) Clear water scour at circular piers: a model. *J Hydraul Eng* 121(12):869–876
- Dey S, Nath TK, Bose SK (2010) Submerged wall jets subjected to injection and suction from the wall. *J Fluid Mech* 653:57–97
- Dey S, Raikar RV (2005) Scour in long contractions. *J Hydraul Eng* 131(12):1036–1049
- Dey S, Raikar RV (2006) Live-bed scour in long contractions. *Int J Sediment Res* 21(2):166–170
- Dey S, Raikar RV (2007a) Characteristics of horseshoe vortex in developing scour holes at piers. *J Hydraul Eng* 133(4):399–413
- Dey S, Raikar RV (2007b) Scour below a high vertical drop. *J Hydraul Eng* 133(5):564–568
- Dey S, Sarkar A (2006a) Scour downstream of an apron due to submerged horizontal jets. *J Hydraul Eng* 132(3):246–257
- Dey S, Sarkar A (2006b) Response of velocity and turbulence in submerged wall jets to abrupt changes from smooth to rough beds and its application to scour downstream of an apron. *J Fluid Mech* 556:387–419
- Dey S, Singh NP (2007) Clear-water scour depth below underwater pipelines. *J Hydro-Environ Res* 1(2):157–162
- Dey S, Singh NP (2008) Clear-water scour below underwater pipelines under steady flow. *J Hydraul Eng* 134(5):588–600
- Dey S, Sumer BM, Fredsøe J (2006) Control of scour at vertical circular piles under waves and current. *J Hydraul Eng* 132(3):270–279
- Engenberger W, Müller R (1944) Experimentelle und theoretische untersuchungen über das kolkproblem. Number 5, Mitteilungen der Versuchsanstalt für Wasserbau, ETH Zurich, Zurich
- Ettema R (1980) Scour at bridge piers. Report number 216, School of Engineering, University of Auckland, Auckland
- Fahlbusch FE (1994) Scour in rock riverbeds downstream of large dams. *Int J Hydropower Dams* 1(4):30–32
- Fredsøe J, Deigaard R (1992) *Mechanics of coastal sediment transport*. World Scientific, Singapore
- Fröhlich DC (1989) Local scour at bridge abutments. In: *Proceedings of the national conference on hydraulic engineering*, American Society of Civil Engineers, New Orleans, LA, pp 13–18
- Gaudio R, Marion A (2003) Time evolution of scouring downstream of bed sills. *J Hydraul Res* 41(3):271–284
- Gaudio R, Marion A, Bovolin V (2000) Morphological effects of bed sills in degrading rivers. *J Hydraul Res* 38(2):89–96
- Gill MA (1970) Bed erosion around obstructions in rivers. PhD thesis, University of London, London
- Gill MA (1972) Erosion of sand beds around spur-dikes. *J Hydraul Div* 98(9):1587–1602
- Gill MA (1981) Bed erosion in rectangular long constriction. *J Hydraul Div* 107(3):273–284

- Graf WH (1998) *Fluvial hydraulics: flow and transport processes in channels of simple geometry*. Wiley, Chichester
- Graf WH, Istiarto I (2002) Flow pattern in the scour hole around a cylinder. *J Hydraul Res* 40(1):13–20
- Grimaldi C, Gaudio R, Calomino F, Cardoso AH (2009) Countermeasures against local scouring at bridge piers: slot and combined system of slot and bed sill. *J Hydraul Eng* 135(5):425–431
- Haaland SE (1983) Simple and explicit formulas for the friction factor in turbulent flow. *J Fluids Eng* 105(5):89–90
- Hancu S (1971) Sur le calcul des affouillements locaux dans la zone des piles du pont. In: *Proceedings of the fourteenth congress of International Association for Hydraulic Research*, Paris, pp 299–305
- Haque MA, Rahman MM, Islam GMT, Hussain MA (2007) Scour mitigation at bridge piers using sacrificial piles. *Int J Sediment Res* 22(1):49–59
- Hoffmans GJCM (1998) Jet scour in equilibrium phase. *J Hydraul Eng* 124(4):430–437
- Hoffmans GJCM, Verheij HC (1997) *Scour manual*. Balkema, Rotterdam
- Hogg AJ, Huppert HE, Dade WB (1997) Erosion by planar turbulent wall jets. *J Fluid Mech* 338:317–340
- Ibrahim A, Nalluri C (1986) Scour prediction around marine pipelines. In: *Proceedings of the fifth international symposium on offshore mechanics and arctic engineering*, Tokyo, pp 679–684
- Isbash SV (1936) Construction of dams by depositing rock in running water. In: *Transactions of the second congress on Large Dams*, vol 5. Washington DC, pp 126–136
- Jain SC (1981) Maximum clear-water scour around circular piers. *J Hydraul Div* 107(5):611–626
- Jain SC, Fischer EE (1979) Scour around bridge piers at high Froude numbers. Report number FHWA-RD-79-104, Federal Highway Administration, US Department of Transportation, Washington DC
- Jain SC, Fischer EE (1980) Scour around bridge piers at high flow velocities. *J Hydraul Div* 106(11):1827–1841
- Jensen BL, Sumer BM, Jensen R, Fredsøe J (1990) Flow around and forces on a pipeline near scoured bed in steady current. *J Offshore Mech Arct Eng* 112(3):206–213
- Kandasamy JK, Melville BW (1998) Maximum local scour depth at bridge piers and abutments. *J Hydraul Res* 36(2):183–198
- Kim UY, Kim JS, Ahn SJ, Hahm CH (2005) Scour countermeasure using additional facility in front of bridge pier. In: *Proceedings of the thirty-first congress of International Association for Hydraulic Research*, Seoul, pp 5823–5829
- Kjeldsen SP, Gjørsvik O, Bringaker KG, Jacobsen J (1973) Local scour near offshore pipelines. In: *Proceedings of the second international conference on port and ocean engineering under arctic conditions*, University of Iceland, Iceland, pp 308–331
- Komura S (1966) Equilibrium depth of scour in long constrictions. *J Hydraul Div* 92(5):17–37
- Kotoulas D (1967) *Das kolkproblem unter besonderer berücksichtigung der faktoren zeit und geschiebemischung im rahmen der wildbachverbauung*. Dissertation, Technischen Hochschule Zürich, Zürich
- Kwan TF (1988) A study of abutment scour. Report number 451, School of Engineering, University of Auckland, Auckland
- Kwan TF, Melville BW (1994) Local scour and flow measurements at bridge abutments. *J Hydraul Res* 32(5):661–673
- Lagasse PF, Clopper PE, Zevenbergen LW, Girard LG (2007) Countermeasures to protect bridge piers from scour. NCHRP report 593, Transportation Research Board, Washington DC
- Lagasse PF, Zevenbergen LW, Schall JD, Clopper PE (2001) Bridge scour and stream instability countermeasures. Hydraulic engineering circular number 23 (HEC 23), Publication number NHI 01-003, Federal Highway Administration, Washington DC
- Lauchlan CS (1999) Pier scour countermeasures. PhD thesis, University of Auckland, Auckland
- Launder BE, Rodi W (1981) The turbulent wall jet. *Prog Aerosp Sci* 19(2–4):81–128
- Laursen EM (1963) An analysis of relief bridge scour. *J Hydraul Div* 89(3):93–118

- Laursen EM, Toch A (1956) Scour around bridge piers and abutments. Bulletin number 4, Iowa Highways Research Board, Ames, Iowa
- Lenzi MA, Marion A, Comiti F, Gaudio R (2002) Local scouring in low and high gradient streams at bed sills. *J Hydraul Res* 40(6):731–739
- Lim S-Y (1993) Clear water scour in long contractions. *Water Marit Eng Proc Inst Civ Eng (London)* 101(2):93–98
- Lim S-Y (1997) Equilibrium clear-water scour around an abutment. *J Hydraul Eng* 123(3):237–243
- Lim S-Y, Cheng N-S (1998) Scouring in long contractions. *J Irrig Drainage Eng* 124(5):258–261
- Liu HK, Chang FM, Skinner M (1961) Effect of bridge construction on scour and backwater. CER 60 HKL 22, Colorado State University, Civil Engineering Section, Fort Collins, Colorado
- Mackay GH (1990) Survey of roading expenditure due to scour. Report 90.09, Department of Scientific and Industrial Research, Hydrology Centre, Christchurch
- Melville BW (1975) Local scour at bridge sites. Report number 117, School of Engineering, University of Auckland, Auckland
- Melville BW (1992) Local scour at bridge abutments. *J Hydraul Eng* 118(4):615–631
- Melville BW, Coleman SE (2000) Bridge scour. Water Resources Publications, Fort Collins
- Melville BW, Hadfield AC (1999) Use of sacrificial piles as pier scour countermeasures. *J Hydraul Eng* 125(11):1221–1224
- Melville BW, Parola AC, Coleman SE (2008) Bridge-scour prevention and countermeasures. In: García MH (ed) *Sedimentation engineering: processes, measurements, modeling, and practice*, ASCE manuals and reports on engineering practice number 110, American Society of Civil Engineers, Reston, VA, pp 543–577
- Melville BW, Sutherland AJ (1988) Design method for local scour at bridge piers. *J Hydraul Eng* 114(10):1210–1226
- Moncada-M A, Aguirre-Pe J (1999) Scour below pipeline in river crossings. *J Hydraul Eng* 125(9):953–958
- Neill CR (1964) River bed scour, a review for bridge engineers. Contract number 281, Research Council of Alberta, Calgary, Alberta
- Neill CR (1973) Guide to bridge hydraulics. University of Toronto Press, Toronto (Roads and Transportation Association of Canada)
- Odgaard AJ, Wang Y (1991) Sediment management with submerged vanes 1: theory. *J Hydraul Eng* 117(3):267–283
- Parker G, Toro-Escobar C, Voigt RL (1998) Countermeasures to protect bridge piers from scour. Final report NCHRP project 24-7, Transportation Research Board, Washington DC
- Parola AC (1995) Boundary stress and stability of riprap at bridge piers. In: Thorne CR, Abt SR, Barends FBJ, Maynard ST, Pilarczyk KW (eds) *River, coastal and shoreline protection: erosion control using riprap and armor stone*. Wiley, Chichester, pp 149–158
- Qayoum A (1960) Die gesetzmäßigkeit der kolkbildung hinter unterströmter wehren unter spezieller berücksichtigung der gestaltung eines beweglichen sturzbettes. Dissertation, Technischen Hochschule Carolo-Wilhelmina, Braunschweig
- Raika RV, Dey S (2005a) Scour of gravel beds at bridge piers and abutments. *Water Management Proc Inst Civ Eng (London)* 158(Jun):157–162
- Raika RV, Dey S (2005b) Clear-water scour at bridge piers in fine and medium gravel beds. *Can J Civ Eng* 32(4):775–781
- Raika RV, Dey S (2008) Kinematics of horseshoe vortex development in an evolving scour hole at a square cylinder. *J Hydraul Res* 46(2):247–264
- Rajaratnam N (1976) *Turbulent jets*. Elsevier Science, Amsterdam
- Raudkivi AJ (1986) Functional trends of scour bridge piers. *J Hydraul Eng* 112(1):1–13
- Richardson EV, Davis SR (2001) Evaluating scour at bridges. Hydraulic engineering circular number 18 (HEC 18). Publication number NHI 01-001, Federal Highway Administration, US Department of Transportation, Washington DC

- Richardson EV, Harrison LJ, Richardson JR, Davis SR (1993) Evaluating scour at bridges. Publication number FHWA-IP-90-017, Federal Highway Administration, US Department of Transportation, Washington DC
- Rouse H (1936) Discharge characteristics of the free overfall. *Civ Eng* 6(4):125–134
- Schlichting H (1979) Boundary layer theory. McGraw-Hill Book Company, New York
- Schoklitsch A (1932) Kolkbildung unter überfallstrahlen. *Wasserwirtschaft* 24:341–343
- Schwarz WH, Cosart WP (1961) The two-dimensional turbulent wall jet. *J Fluid Mech* 10:481–495
- Shalash MSE (1959) Die kolkbildung beim ausfluss unter schützen. Dissertation, Technischen Hochschule München, Munich
- Shen HW, Schneider VR, Karaki S (1969) Local scour around bridge piers. *J Hydraul Div* 95(6):1919–1940
- Sheppard DM, Melville B, Demir H (2014) Evaluation of existing equations for local scour at bridge piers. *J Hydraul Eng* 140(1):14–23
- Smith CD (1967) Simplified design for flume inlets. *J Hydraul Div* 93(6):25–34
- Stein OR, Julien PY, Alonso CV (1993) Mechanics of jet scour downstream of a headcut. *J Hydraul Res* 31(6):723–738
- Straub LG (1934) Effect of channel contraction works upon regimen of movable bed streams. *Trans Am Geophys Union* 15(2):454–463
- Sturm TW, Janjua NS (1994) Clear water scour around abutments in floodplains. *J Hydraul Eng* 120(8):956–972
- Sumer BM, Fredsøe J (2002) The mechanism of scour in the marine environment. World Scientific, Singapore
- Sumer BM, Truelsen C, Sichmann T, Fredsøe J (2001) Onset of scour below pipelines and selfburial. *Coast Eng* 42(4):213–235
- Sutherland AJ (1986) Reports on bridge failure. RRU occasional paper, National Roads Board, Wellington
- Tafarojnoruz A, Gaudio R, Dey S (2010) Flow-altering countermeasures against scour at bridge piers: a review. *J Hydraul Res* 48(4):441–452
- Vanoni VA (1975) Sedimentation engineering. ASCE manual number 54, American Society of Civil Engineers, New York
- Webby MG (1984) General scour at contraction. RRU bulletin 73, National Roads Board, Bridge Design and Research Seminar, New Zealand, pp 109–118
- Yalin MS (1977) Mechanics of sediment transport. Pergamon, Oxford

Chapter 11

Dimensional Analysis and Similitude

11.1 General

Almost all problems on fluvial hydrodynamics involve complex mechanics of fluid–particle interactions and cannot be solved by only using the analytical methods, as described in the preceding chapters. These problems however rely heavily on the experimental or field data for their solutions. In reality, it is probably fair to say that the solutions of very few problems related to fluvial hydrodynamics can be obtained by analytical method alone. Hence, the solutions of most of the problems are achieved by using semianalytical approach extensively calibrated by the experimental and/or field data or purely empirical approach based on the experimental and/or field data. Thus, researchers and engineers working on the problems of fluvial hydrodynamics should be conversant with the procedures of experiments and/or field measurements to these problems in order to plan and conduct the necessary experiments or to interpret and make use of the data available in the literature. In this chapter, some techniques and ideas are discussed that are important in understanding and correlating the experimental data. It is needless to mention that an obvious goal of any experiment is to make the results as widely applicable as far as possible in the field conditions.

Dimensional analysis is therefore a powerful tool in synthesizing (ordering and grouping together) different parameters of experimental data and also analyzing the individual data groups. If a group of quantities has a dimensional representation simplest of unity when multiplied or divided together, it is called *non-dimensional group*. The great majority of experiment requires methods of measurements using numerical scales whose both units and dimensions are defined. In this chapter, laboratory and field measurements are used as a basis of analysis of parameters involved in fluvial hydrodynamics and hence of dimensional analysis. Therefore, the accuracy in measurements is of immense importance in obtaining reliable data for quantification of various parameters through a dimensional

analysis. In the context of measurement, it is pertinent to mention that in an address to the Institution of Civil Engineers in 1883, Kelvin spoke on the importance of measurement [available in Thomson (1889)]:

In physical science a first essential step in the direction of learning any subject, is to find principles of numerical reckoning, and methods for practicably measuring, some quality connected with it. I often say that when you can measure what you are speaking about, and express it in numbers, you know something about it; but when you cannot measure it, when you cannot express it in numbers, your knowledge is of a meagre and unsatisfactory kind: it may be the beginning of knowledge, but you have scarcely, in your thought, advanced to the stage of science, whatever the matter may be.

The prerequisite in the present logic requires consideration of a basic feature of measurement. There are two aspects of measurement. One is that of the dimensions used and the other of the units used. Dimensional analysis is based on the fact that a physical law must be independent of the units used to measure the physical variables. As a consequence, any valid equation must have the same dimensions in both the sides. Therefore, a dimensional analysis can be used not only to check the feasibility of a derived equation but also to develop a reasonable hypothesis about a complex physical situation (such as sediment dynamics) that can be tested by experiments or by more developed analytical theories of the phenomena. An equation that is dimensionally examined is, therefore, acceptable only if it includes all the possible variables, as it would be in an analytical derivation. Thus, in the application of dimensional analysis, the primary aspect is the right choice of the variables that might influence the phenomenon under observation.

An understandable objective of an experimental campaign is to make the outcomes applicable to the practical field situations as far as possible. To achieve this end, the concept of *similitude* is commonly used so that the measurements made in a laboratory model study can be used to describe the characteristics of similar systems in the practical field situations. A *model* is the representation of a physical system that can be used to predict the characteristics of the system in some desired respect. The physical system for which the predictions are to be made is termed the *prototype*. Thus, the similitude approach enables us to make experiments with a conveniently controlled condition in the laboratory and then to apply the results to a less convenient field condition. It is neither necessary the same fluid being used for the model and its prototype nor the model necessarily being smaller than its prototype. From these experimental model studies, empirical expressions can be formulated, or specific predictions of one or more parameters of some other similar system can be achieved with a reasonable degree of accuracy. Doing this, it is essential to establish the relationships between the laboratory models and the prototypical systems. This chapter provides an elaborate discussion: how can this be accomplished in a methodical approach?

11.2 Dimensional Analysis

11.2.1 Synthesis of Experimental Data

To illustrate a typical problem on fluid–particle interaction where experimental determination is required, consider a particle in the form of a small sphere that is set in a steady–uniform flow of an incompressible Newtonian fluid. An important aspect of this system, which could be of interest to a hydraulician exploring the motion of a particle in a fluid, is the drag force that acts on the sphere in the flow direction as a result of differential hydrodynamic pressure on either side (front and rear) of the sphere (in conjunction with the skin friction, which is relatively negligible on a smooth surface of a sphere). Note that it is always of the same kind of problem whether the sphere is at rest in a flowing fluid or the former is in motion in a static fluid medium. Although apparently the problem would be a relatively simple, it could not be generally solved by an analytical approach alone without taking the help of laboratory experimental results.

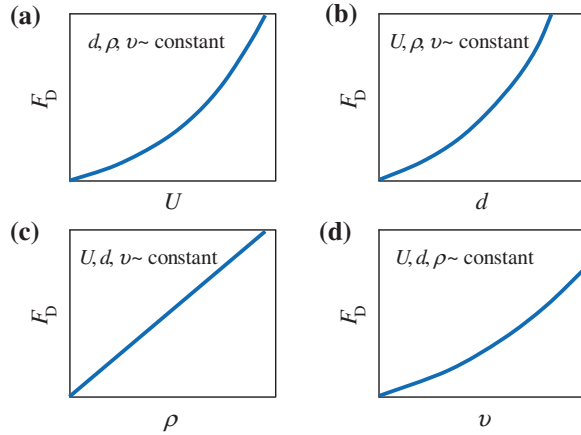
In planning an experimental program to study the problem, one has to decide first of all the parameters or the variables that influence the drag force F_D . One can thus prepare the list including the mean flow velocity U , the sphere diameter d , the mass density of fluid ρ , and the coefficient of kinematic viscosity of fluid ν . Thus, it yields a functional relationship as

$$F_D = f(U, d, \rho, \nu) \quad (11.1)$$

The above equation simply provides theoretical information that the drag force is expected to be a function of the variables contained within the parentheses. At this juncture, the character of the function is rather indefinite. Therefore, the primary objective of the experiments that are to be performed is to determine the functional relationship explicitly.

In most of the experiments, all parameters are independently varied, with the exception of one, which becomes the dependent variable. In Eq. (11.1), the dependent and the independent variables are the parameters in the left- and the right-hand side of the equation. In conducting the experiments in a significantly methodical way, the experimental program should be such that one of the independent variables, say the velocity, is allowed to vary, keeping others constant, measuring the corresponding drag force as a dependent variable. Importantly, the direct measurement of drag force is possible experimentally by a force sensor (Dwivedi et al. 2010). This test series yields the data set that could be graphically plotted to represent a curve as illustrated in Fig. 11.1a. Note that this curve, which certainly does not convey the generalized characteristics of the system (that is a general formulation) that is looked for, would only be suitable for the specific sphere diameter and fluid used in the experiments. In the similar way, the tests could therefore be repeated by varying each of the other variables in turn, keeping the rest as constant. These test series yield data sets to plot representative curves as

Fig. 11.1 Illustrative graphical representation of how drag force F_D is influenced by **a** U , **b** d , **c** ρ , and **d** v



illustrated in Figs. 11.1b–d. This approach to obtain the separate relationships for the drag force as a function of the individual influencing parameters, although conceptually logical, is in fact a difficult proposition. Last two experimental sets, as illustrated in Figs. 11.1c, d, would even be not feasible, because it would be necessary to vary fluid mass density keeping viscosity a constant and vice versa. Finally, it leaves an open question that how could one combine the data or results in Figs. 11.1a–d to formulate a general functional relationship that would be applicable for varied sphere diameters and different types of fluids?

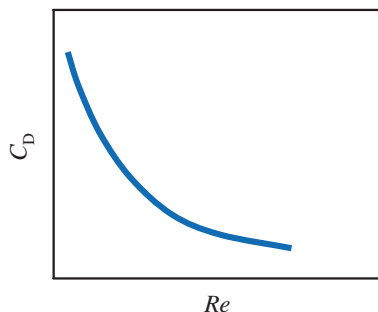
To eliminate the difficulties described above, in the following sections, it is shown that rather than handling with the original list of variables, for instance, as in Eq. (11.1), they can be arranged in non-dimensional groups of variables, so that

$$\frac{F_D}{\rho U^2 \pi d^2 / 8} = f_1 \left(\frac{Ud}{v} \right) \Rightarrow C_D = f_1(Re) \quad (11.2)$$

Thus, five dimensional variables could be reduced to only two non-dimensional variables. Note that a suitable or standard non-dimensional variable can be expressed by multiplying or dividing a non-dimensional group by a number and/or a constant, as is done in the left-hand side of Eq. (11.2) to express drag coefficient C_D . It suggests that the experiment would simply be planned varying the non-dimensional parameter Re (called sphere Reynolds number) and determining the corresponding value of C_D . A single universal curve could then represent the results of the experiment, as illustrated in Fig. 11.2. The curve would be applicable for any combination of sphere sizes and incompressible Newtonian fluids. To obtain this curve, one could plan the experiment choosing a sphere of convenient size and a fluid that is convenient to work with. The experiments thus would be simpler, as even different sizes of sphere or different fluids need not be used.

A great deal of the fallacies in application of dimensional analysis is associated with the erroneous selection of participating variables. To be quite safe, a common tendency is to include as many variables as possible. Note that inclusion of more

Fig. 11.2 Illustrative graphical representation of drag force using non-dimensional parameters as C_D a function of Re



than one dependent variables or exclusion of some of the participating independent variables in the functional relationship is a serious fault. However, the parameters that have no influence or exist as constants may be eliminated by themselves in the processes of analysis. Nevertheless, having an excessive number of variables than the required is as wrong as having less than required. In general, selection of a redundant variable could be due to overlooking the specific role of that variable being not relevant to the phenomenon and not become aware of that some seemingly insignificant variables are in reality not insignificant. As a guideline in making a correct choice of the variables, one can theoretically analyze the phenomenon under consideration *a priori* and accordingly assess which independent variables should be considered. To be explicit, one should have a good understanding about the role of a particular variable influencing the phenomenon.

The main limitation of the dimensional analysis lies on the fact that it might sometimes yield incomplete solutions, spurious correlations, and obvious results. Besides, the dimensional analysis cannot provide an insight into the actual mechanism of the physical processes, although it is extensively applied in fluvial hydrodynamics. Therefore, its applicability cannot be considered as a substitute for, if not more than a primary support to, the analytical method. An appropriate application of dimensional analysis always depends on experience and previous decisive examination of the investigated phenomenon.

11.2.2 Dimensional System

It has been already discussed in Chap. 1 that a qualitative description of a physical quantity can be presented in terms of basic dimensions: mass M , length L , and time T . Then again, the basic dimensions in hydrodynamics are force F , M , L , and T , since Newton's second law of motion in fluid and solid phases are

$$\mathbf{F} = \dot{m}\mathbf{U} \text{ (in fluid phase)} \quad \text{and} \quad \mathbf{F} = m\mathbf{a} \text{ (in solid phase)} \quad (11.3)$$

where \mathbf{F} is the force vector, \dot{m} is the mass rate of flow, \mathbf{U} is the velocity vector, m is the mass, and \mathbf{a} is the acceleration vector. Newton's second law of motion is therefore given in dimensional form as

$$F = MLT^{-2} \quad (11.4)$$

The above dimensional equation shows that the three dimensions in the right-hand side are independent. Therefore, the common system used in dimensional analysis is MLT system. Table 11.1 furnishes some quantities that are commonly used in fluvial hydrodynamics.

A quick examination of the dimensions of the two groups that appear in Eq. (11.2) shows that they are in fact non-dimensional products, as both the right- and left-hand sides yield $M^0L^0T^0 (=1)$. Thus, the advantage of a dimensional analysis is not only to reduce the numbers of variables from five to two, but also to appropriately arrange the variables in non-dimensional groups. It implies that the results illustrated in Fig. 11.2 are independent of the system of units and hence widely applicable. The foundation for the application of dimensional analysis to a variety of problems is found in the *Buckingham Π theorem*.

11.2.3 Buckingham Π Theorem

In *Buckingham Π theorem* (1915), the number of independent non-dimensional groups that can be arranged in describing a law governing a physical phenomenon involving number of n variables and m basic dimensions equals to $n - m$. The basis of the application of Buckingham Π theorem (henceforth Π theorem) belongs to the transformation of the relationship describing a physical phenomenon in terms of a set of variables involved, say $a_1, a_2, a_3, \dots, a_n$. Hence, there exists a functional relationship as

$$f(a_1, a_2, a_3, \dots, a_n) = 0 \quad (11.5)$$

If a set of non-dimensional groups $\Pi_1, \Pi_2, \Pi_3, \dots$ involves variables a_1, a_2, a_3, \dots and m dimensions, the relationship can exist for a reduced $n - m$ number of independent non-dimensional groups. Therefore, the non-dimensional functional relationship to exist is

$$\phi(\Pi_1, \Pi_2, \Pi_3, \dots, \Pi_{n-m}) = 0 \quad (11.6)$$

The number of non-dimensional Π parameters is therefore fewer than the number of original variables by m . The m is the minimum number of dimensions required to describe the original list of variables. As discussed, the dimensions required to describe the variables have the basic dimensions M , L , and T . However, in some cases, for instance, to describe a kinematic variable, only two dimensions, such as L and T , are required, or perhaps even one, such as L . To determine the Π

Table 11.1 Dimensions of physical quantities used in fluvial hydrodynamics

Quantity	Dimensions
Mass	M
Length	L
Time	T
Area	L^2
Volume	L^3
Force	MLT^{-2}
Velocity	LT^{-1}
Acceleration	LT^{-2}
Gravitational acceleration	LT^{-2}
Mass density	ML^{-3}
Specific weight	$ML^{-2}T^{-2}$
Pressure	$ML^{-1}T^{-2}$
Bed shear stress	$ML^{-1}T^{-2}$
Fluid flow discharge	L^3T^{-1}
Sediment transport rate (in volume)	L^2T^{-1}
Sediment transport rate (in weight)	MT^{-3}
Dynamic viscosity	$ML^{-1}T^{-1}$
Kinematic viscosity	L^2T^{-1}

parameters, one has to select m number of a variables that consist m dimensions among them, termed *repeating variables*. The repeating variables should not be a non-dimensional quantity. For instance, if the repeating variables a_1, a_2, a_3 contain M, L , and T , not necessarily in each individual one but in a group, then the non-dimensional Π parameters appropriate for the physical phenomenon are the product of the participating variables raised to various exponents as

$$\left. \begin{aligned} \Pi_1 &= a_1^{p_1} a_2^{q_1} a_3^{r_1} a_4 \\ \Pi_2 &= a_1^{p_2} a_2^{q_2} a_3^{r_2} a_5 \\ \Pi_3 &= a_1^{p_3} a_2^{q_3} a_3^{r_3} a_6 \\ &\dots \\ \Pi_{n-m} &= a_1^{p_{n-m}} a_2^{q_{n-m}} a_3^{r_{n-m}} a_n \end{aligned} \right\} \quad (11.7)$$

where p, q , and r are unknown exponents. In all the above Π parameters, there exist $m + 1$ number of variables having various values of exponents (including zero). In general (for $m = 3$), the Eq. (11.7) could be compiled in such a way that the three repeating variables, for example, characteristic length, velocity, and mass density, appear in every Π parameter differing the fourth variable with an exponent (\pm) unity. This arrangement confirms that all participating n variables are functional. Note that if only two dimensions are involved (that is $m = 2$), then two of the variables are selected as repeating variables and two unknown exponents are obtained for each Π parameter. To determine Π parameters, the exponents in the set of equations (Eq. 11.7) are to be evaluated. The dimensions of the a variables are substituted. The sum of exponents of each of M, L , and T of the right-hand side

of Eq. (11.7) is determined and equated to zero, respectively, because on the left-hand side of Eq. (11.7), the non-dimensional Π parameters yield $M^0 L^0 T^0 (=1)$. These produce three equations containing three unknowns (p , q , and r) for each Π parameter, so that the equations are solved simultaneously to determine the unknowns, and then, Π parameters are determined. Importantly, in number of cases, the list of variables is such that the non-dimensional parameters are evident by inspection or some of the listed variables are initially combined to achieve a desirable parameter. Next, the steps to be followed in the analysis by Π theorem are detailed, as an instruction to students and researchers.

11.2.4 Steps Involved in Analysis by Π Theorem

Step 1: Prepare a list of all the participating variables involved in a physical phenomenon to be studied. Here, one should be sure that all participating variables are included. The variables are any pertinent parameters that include dimensional and non-dimensional variables and constants as well (such as acceleration due to gravity g being a constant) participating in the physical phenomenon to be studied. Selection of the variables may not be easy in some complex fluvial systems. Experience from the previous experiments or field investigations or even the physical laws that govern the phenomenon would help to identify the variables. Indeed, the general classes of variables are of wide categories, and hence, each problem requires to be analyzed with care. For a firsthand identification of the variables in a sediment transport or a scour problem, the group of variables can be typically categorized that are related to *channel and/or structure geometry* (such as channel width, pier diameter, etc.), *sediment properties* (such as sediment size, mass density, etc.), *fluid properties* (such as mass density, viscosity, etc.), and most importantly *flow characteristics* (such as gravity, slope, flow depth, velocity, etc.). In case of time-dependent processes (such as unsteady flow, temporal scour, etc.), *time* of an event should be a variable.

To keep minimum number of variables facilitating to minimize the number of experiments or non-dimensional groups, the variables should be independent of each other. For instance, in a problem, the shear velocity u_* , flow depth h , slope S_0 , and g are the relevant variables; all of them cannot be listed as they are not independent [$u_* = (ghS_0)^{0.5}$]. Therefore, u_* can replace g and S_0 , but h should be retained as a variable. Another important point is that in fluvial phenomena (two-phase flow problems), the water mass density ρ , sediment mass density ρ_s , and g should not be retained separately. They should be replaced by a single variable as Δg or two variables as Δg and ρ . Here, $\Delta = s - 1$ and s is the relative density of sediment. All these logical selections are based on the laws to govern the physical phenomenon under investigation.

Step 2: Write each of the variables in terms of basic M , L , and T dimensions. The basic dimensions for typical variables that involve in problems of fluvial hydrodynamics are furnished in Table 11.1.

Step 3: Write the functional relationship. One can prepare a functional relationship as in Eq. (11.5).

Step 4: Select the repeating variables. The number of repeating variables required equals the number of reference dimensions m in the list of variables. One must avoid making dependent variable a repeating variable. Essentially, all of the required reference dimensions should be taken into the group of repeating variables. The repeating variables must be dimensionally independent of each other, such that a non-dimensional product cannot be formed by combining themselves. Often, one variable is selected that specifies the characteristic length, and others the kinematic and dynamic quantities, depending on the type of the problem if that involves only kinematic phenomenon or participation of force/mass as well.

Step 5: Write Π parameters as a product of the repeating variables that have unknown exponents and one of the non-repeating variables with an exponent unity. The unknown exponents are to be determined so that the Π parameters are non-dimensional.

Step 6: Determine each of the Π parameters as a product of the repeating and non-repeating variables in a non-dimensional form. For each of the Π expressions [see Eq. (11.7)], at first, one has to substitute the dimensions. The equations of the exponents can be written so that the sum of the exponents of each dimension is zero. The equations can then be solved simultaneously for evaluating exponents. Thus, the non-dimensional Π parameters can be obtained once the numerical values of the exponents are substituted back into the Π expressions. In this way, a functional relationship of the type of Eq. (11.6) can be established.

Step 7: Express the final form as one of the Π parameters as a function of others. Typically, one can write as

$$\Pi_1 = \phi(\Pi_2, \Pi_3, \dots, \Pi_{n-m}) \quad (11.8)$$

where Π_1 should contain a dependent variable preferably in the numerator. In the context of an explicit expression for Π_1 describing a physical problem, it is important to mention that the actual functional relationship among the Π parameters must be determined from the knowledge of the laboratory experimental or field data. However, one can recombine, if desired, to adjust the forms of the Π parameters without changing the number of independent parameters. Also, a Π parameter can be discarded, if its involvement is found to be trivial for the problem under investigation. For instance, the involvement of shear Reynolds number in rough-turbulent flow is insignificant. In studying problems of fluvial hydrodynamics, it is necessary to examine the values of the exponents for the dimensional variables obtained from the Π theorem forming the non-dimensional groups. If the non-dimensional groups are such that they do not specify standard non-dimensional numbers (such as Froude number, Reynolds number, etc.) used in fluvial hydrodynamics, then the role of the non-dimensional groups has little use in studying the problems. In this situation, it is advisable to redo the dimensional analysis changing the repeating variables from the original list. The procedure can be best illustrated by some examples.

Let a simple problem be considered on the hydrodynamic drag force acting on a sphere that has already been introduced in Sect. 11.2.1. It is recognized that the drag force F_D is influenced by the mean flow velocity U , the sphere diameter d , the fluid mass density ρ , and the fluid kinematic viscosity ν . The functional relationship thus exists as

$$f(F_D, U, d, \rho, \nu) = 0 \quad (11.9)$$

Equation (11.9) contains three dimensions, M , L , and T . The repeating variables are considered as U , d , and ρ . Hence, there are two Π parameters as

$$\Pi_1 = U^{p_1} d^{q_1} \rho^{r_1} F_D = (LT^{-1})^{p_1} L^{q_1} (ML^{-3})^{r_1} MLT^{-2} = M^0 L^0 T^0 \quad (11.10a)$$

$$\Pi_2 = U^{p_2} d^{q_2} \rho^{r_2} \nu = (LT^{-1})^{p_2} L^{q_2} (ML^{-3})^{r_2} L^2 T^{-1} = M^0 L^0 T^0 \quad (11.10b)$$

Equating exponents of M , L , and T in Eq. (11.10a), one gets $p_1 + q_1 - 3r_1 + 1 = 0$, $r_1 + 1 = 0$, and $-p_1 - 2 = 0$. Therefore, solving them simultaneously yields $p_1 = -2$, $q_1 = -2$, $r_1 = -1$ and then $\Pi_1 = F_D/(U^2 d^2 \rho)$. Similarly, one can obtain $\Pi_2 = \nu/(Ud)$ solving by Eq. (11.10b). By definition of dynamic pressure force on a sphere, the Π_1 parameter can be expressed in a standard form multiplying the denominator by a constant factor $\pi/8$. So, one can rearrange and rewrite $\Pi_1 = F_D/(\rho U^2 \pi d^2/8) = C_D$ and by taking reciprocal $\Pi_2 = Ud/\nu = Re$. The following relationship for the drag coefficient C_D is therefore obtained:

$$C_D = \phi(Re) \quad (11.11)$$

Next, another problem is discussed considering the formation of ripples which is common in fluvial systems. The length λ of ripples formed by a steady-uniform stream flow is considered to be determined by the shear velocity u_* , the median sediment size d , the kinematic viscosity ν , the mass density of water ρ , the mass density of sediment ρ_s , and the acceleration due to gravity g . With all variables together, the following functional relationship exists:

$$f(\lambda, u_*, d, \nu, \rho, \rho_s, g) = 0 \quad (11.12)$$

In fluid-sediment interaction (two-phase flow), the ρ , ρ_s , and g should be replaced by $\Delta g [= (s - 1)g]$. Therefore, Eq. (11.12) becomes

$$f_1(\lambda, u_*, d, \nu, \Delta g) = 0 \quad (11.13)$$

The above equation contains only two dimensions, which are L and T . It is therefore convenient to consider repeating variables as u_* and d . Then, there are three Π parameters as

$$\Pi_1 = u_*^{p_1} d^{q_1} \lambda = (LT^{-1})^{p_1} L^{q_1} L = L^0 T^0 \quad (11.14a)$$

$$\Pi_2 = u_*^{p_2} d^{q_2} v = (LT^{-1})^{p_2} L^{q_2} L^2 T^{-1} = L^0 T^0 \quad (11.14b)$$

$$\Pi_3 = u_*^{p_3} d^{q_3} \Delta g = (LT^{-1})^{p_3} L^{q_3} L T^{-2} = L^0 T^0 \quad (11.14c)$$

Equating exponents of L and T in Eq. (11.14a), one gets $p_1 + q_1 + 1 = 0$ and $-p_1 = 0$. Therefore, solving them simultaneously yields $p_1 = 0$, $q_1 = -1$, and then $\Pi_1 = \lambda/d$. Similarly, one can obtain $\Pi_2 = v/(u_* d)$ and $\Pi_3 = \Delta g d/u_*^2$ by solving Eqs. (11.14b) and (11.14c), respectively. Expressing in standard forms, the Π_2 parameter can be expressed as shear Reynolds number $R_* [= (u_* d)/v]$ and Π_3 parameter as Shields parameter $\Theta [= u_*^2/(\Delta g d)]$ by taking reciprocal of both the expressions. Hence, the following relationship for the non-dimensional ripple length can be obtained:

$$\frac{\lambda}{d} = \phi(R_*, \Theta) \quad (11.15)$$

To achieve explicit empirical or graphical relationships for Eqs. (11.11) and (11.15), experimental results are to be used.

11.3 Similitude

11.3.1 Concept of Dynamic Similitude for Model Studies

Similitude is in general sense defined as a known relationship between two phenomena. In fluvial hydrodynamics, this is usually a relationship between a full-scale physical system and its smaller version having similar or partially similar boundaries. The full-scale physical system is termed *prototype* and its smaller scale *model*. Physical model studies of a proposed fluvial system are frequently undertaken in the laboratory as an aid to the design engineers. If accurate quantitative results are to be obtained from a laboratory model study, there should be a thorough dynamic similitude between the model and the prototype. It is well known that most of the practical problems on fluvial system are highly intricate in nature so that a desirable solution of the hydrodynamic equations is rather hoping against hope. Even in many occasions, the equations are not at all applicable. The obvious benefit of using a laboratory model, if it is carefully fabricated representing a simulated miniature prototype, could lead to a much accurate prediction being applicable to the field.

To achieve a desired similitude between the model and the prototype, scaling laws or criteria of similitude must be fulfilled. *Geometric similarity* of the model and the prototype represents whether a model and its prototype are identical in shape but differ only in size. All dimensions are replicated at the same scale, keeping the corresponding angles same. The important deliberation toward a

geometric similar model is that the flow feature is to be geometrically similar. The linear dimensions L_p of the prototype to the corresponding dimensions L_m of the model are transformed by a length scale L_r , such that $L_p = L_r L_m$. Here, subscripts p, m, and r denote the prototype, model, and ratio of prototype to model conditions, respectively. The area and volume scales are L_r^2 and L_r^3 , respectively. Complete geometric similarity in many problems on sediment transport is a difficult proposition. For instance, the sediment particles of a small model could not be reduced in proportion, maintaining a length scale. For such situations, the term most frequently used is *geometric distortion* in which a model has a departure from a scaling law by not satisfying one or more of the geometric similarities. Model distortion in three dimensions thus implies a different horizontal L_{xr} , lateral L_{yr} , and/or vertical L_{zr} length scales, according to a Cartesian coordinate system. Here, x, y, and z are streamwise (that is, horizontal or longitudinal), spanwise (that is, transverse), and vertical coordinates, respectively. Therefore, the area scales for horizontal and vertical surfaces are $L_{xr}L_{yr}$ and $L_{zr}L_{yr}$ or $L_{zr}L_{xr}$ respectively, and the volume scale $L_{xr}L_{yr}L_{zr}$.

Kinematic similarity between the model and the prototype exists if in addition to geometric similarity, the velocities at all corresponding points in the flow field have similarity. It is therefore the similitude of the parameters involving space and time. It implies that the velocity scale U_r is

$$U_r = \frac{U_p}{U_m} \quad (11.16)$$

Therefore, the time scale T_r for kinematic similarity is

$$T_r \left(= \frac{T_p}{T_m} \right) = \frac{L_r}{U_r} \quad (11.17)$$

and the acceleration scale a_r is

$$a_r \left(= \frac{a_p}{a_m} \right) = \frac{L_r}{T_r^2} = \frac{U_r^2}{L_r} \quad (11.18)$$

In case of three-dimensional geometric distortion, the length scales in a Cartesian coordinate system are $L_{xr} = L_{xp}/L_{xm}$; $L_{yr} = L_{yp}/L_{ym}$, and $L_{zr} = L_{zp}/L_{zm}$. Thus, the velocity and acceleration scales are

$$\left. \begin{aligned} U_{xr} \left(= \frac{U_{xp}}{U_{xm}} \right) &= \frac{L_{xr}}{T_r}, \quad U_{yr} = \frac{L_{yr}}{T_r}, \quad U_{zr} = \frac{L_{zr}}{T_r} \\ a_{xr} \left(= \frac{a_{xp}}{a_{xm}} \right) &= \frac{L_{xr}}{T_r^2} = \frac{U_{xr}^2}{L_{xr}}, \quad a_{yr} = \frac{L_{yr}}{T_r^2} = \frac{U_{yr}^2}{L_{yr}}, \quad a_{zr} = \frac{L_{zr}}{T_r^2} = \frac{U_{zr}^2}{L_{zr}} \end{aligned} \right\} \quad (11.19)$$

Thus, kinematic similarity for a geometrically distorted model is obtained by keeping U_{xr} , U_{yr} , U_{zr} and a_{xr} , a_{yr} , a_{zr} as constants. Note that for an exact geometric similarity, length scales should be identical ($L_r = L_{xr} = L_{yr} = L_{zr}$), and for an exact kinematic similarity, velocity scales should be identical ($U_r = U_{xr} = U_{yr} = U_{zr}$).

Finally, *dynamic similarity* between the model and the prototype exists if the individual forces at all corresponding points in the flow field have similarity. It implies that the ratios of the individual forces in prototype to those in model are same at all corresponding points. Importantly, the forces in both the systems must be parallel and act in the same direction in order to preserve the dynamic behavior of fluids similar. The types of individual forces that could influence the fluid flow in a channel are inertia I , pressure force P , gravity G , and viscous V . For dynamic similarity of a geometric similar system, the inertia I_r , pressure force P_r , gravity G_r , and viscous V_r scales are

$$\left. \begin{aligned} I_r &= \rho_r L_r^3 \left(\frac{U_r^2}{L_r} \right) = \rho_r U_r^2 L_r^2 \\ P_r &= \Delta p_r L_r^2 \\ G_r &= \rho_r L_r^3 g_r \\ V_r &= \nu_r \rho_r \left(\frac{\Delta U_r}{\Delta L_r} \right) L_r^2 = \nu_r \rho_r U_r L_r \end{aligned} \right\} \quad (11.20)$$

where Δp , ΔU , and ΔL are the pressure, velocity, and length differences, respectively. Thus, for dynamic similarity, the following equation can be formed:

$$I_r = P_r = G_r = V_r = \text{constant} \quad (11.21)$$

It leads to the following set of relationships:

$$\frac{I_m}{P_m} = \frac{I_p}{P_p}, \frac{I_m}{G_m} = \frac{I_p}{G_p}, \frac{I_m}{V_m} = \frac{I_p}{V_p} \quad (11.22)$$

From the knowledge of Eq. (11.20), Eq. (11.22) can be expressed as

$$\frac{U_p^2}{\Delta p_p / \rho_p} = \frac{U_m^2}{\Delta p_m / \rho_m}, \frac{U_p^2}{g_p L_p} = \frac{U_m^2}{g_m L_m}, \frac{U_p L_p}{\nu_p} = \frac{U_m L_m}{\nu_m} \quad (11.23)$$

The non-dimensional quantity obtained from the first expression in Eq. (11.23) that is related to the ratio of the inertia force to the pressure force is known as the *Euler number*. It is expressed as

$$Eu = \frac{U}{(2\Delta p / \rho)^{0.5}} \quad (11.24)$$

The non-dimensional quantity obtained from the second expression in Eq. (11.23) that is related to the ratio of the inertia force to the gravity force is known as the *Froude number*. It is expressed as

$$Fr = \frac{U}{(gL)^{0.5}} \quad (11.25)$$

The non-dimensional quantity obtained from the third expression in Eq. (11.23) that is related to the ratio of the inertia force to the viscous force is known as the *Reynolds number*. It is expressed as

$$Re = \frac{UL}{\nu} \quad (11.26)$$

For a dynamic similarity, the Euler, Froude, and Reynolds scales are unity, that is,

$$Eu_r = Fr_r = Re_r = 1 \quad \Rightarrow \quad Eu_p = Eu_m, Fr_p = Fr_m, Re_p = Re_m \quad (11.27)$$

Strictly, the dynamic similarity is preserved only if all the scaling laws (criteria of similitude) are unity [as in Eq. (11.27)] in addition to the fulfillment of geometric and kinematic similarities. In reality, it becomes a difficult proposition, if not impossible, to satisfy all the conditions due to limitation of types of fluids, spatial dimensions, and others. Nevertheless, it is not always necessary to fulfill all the scaling laws, because one or other forces, in most of the problems, may remain insignificant. For instance, in case of a falling sphere in a static fluid medium, only the Reynolds similitude criterion can ensure dynamic similarity, while the Euler and the Froude similitude criteria affect little. On the other hand, in case of flow over a spillway model, only the Froude similitude criterion can ensure similarity. Note that this approach is reasonable as long as one similitude criterion governs the physical phenomenon and others can be neglected.

Scale effect could result in if all pertinent non-dimensional scaling laws (Eq. 11.27) or conditions of similitude are not the same in the model and the prototype. The scale effect is thus a consequence of dynamic non-similarity between the model and the prototype working with a similitude criterion (say, Froude number) and neglecting others. The minimization of errors arising due to the scale effect could be done by adjusting the model reduction against the limits of the similarity.

For the computation of Fr or Re , the length L must be a specific characteristic length that is significant in the flow field. For an open channel flow, the gravity force is the determining law. Hence, the Froude number Fr is the relevant non-dimensional number or the similitude criterion (scaling law) being extensively used in model studies. Using a Froude similitude criterion, the velocity scale can be obtained from Eq. (11.27) as

$$U_r(g_r = 1) = L_r^{0.5} \quad (11.28)$$

In the above equation, g_r is considered to be unity, if the model and the prototype location have not much elevation difference. Similarly, the time, the acceleration, the discharge, and the force scales can be obtained as

$$\left. \begin{aligned} T_r &= L_r^{0.5} \\ a_r &= U_r/T_r = 1 \\ Q_r &= U_r L_r^2 = L_r^{2.5} \\ F_r &= \rho_r L_r^3 \end{aligned} \right\} \quad (11.29)$$

where Q and F are the discharge and force, respectively. If the viscosity is the determining law, then the Reynolds number Re is the relevant similitude criterion. The Reynolds similitude criterion yields the velocity, the time, the acceleration, the discharge, and the force scales as

$$\left. \begin{aligned} U_r &= v_r/L_r \\ T_r &= L_r^2/v_r \\ a_r &= v_r^2/L_r^3 \\ Q_r &= L_r v_r \\ F_r &= \rho_r v_r^2 \end{aligned} \right\} \quad (11.30)$$

Importantly, a coupled Froude and Reynolds similitude criterion would be almost infeasible unless it is a distorted model. Let it be checked here. If U_r in Eq. (11.28) is eliminated by the equation of U_r from Eq. (11.30), then one gets $v_r = L_r^{1.5}$. It means that for a chosen length scale L_r , it is almost impossible to satisfy the kinematic viscosity scale v_r with the water or any other common fluids.

For three-dimensional geometric distortion, the inertia, the pressure, the gravity, and the viscosity scales are

$$\left. \begin{aligned} I_{xr} &= (\rho_r U_{xr}^2 L_{xr}^2) = \rho_r \frac{L_{xr}^4}{T_r^2}, \quad I_{yr} = \rho_r \frac{L_{yr}^4}{T_r^2}, \quad I_{zr} = \rho_r \frac{L_{zr}^4}{T_r^2} \\ P_{xr} &= \Delta p_r L_{xr}^2, \quad P_{yr} = \Delta p_r L_{yr}^2, \quad P_{zr} = \Delta p_r L_{zr}^2 \\ G_{xr} &= \rho_r L_{xr}^3 g_r, \quad G_{yr} = \rho_r L_{yr}^3 g_r, \quad G_{zr} = \rho_r L_{zr}^3 g_r \\ V_{xr} &= v_r \rho_r U_{xr} L_{xr}, \quad V_{yr} = v_r \rho_r U_{yr} L_{yr}, \quad V_{zr} = v_r \rho_r U_{zr} L_{zr} \end{aligned} \right\} \quad (11.31)$$

Therefore, for a two-dimensional geometric distortion ($x_r \neq z_r$ and $y_r = z_r$), the Froude similitude criterion yields the velocity, the time, the acceleration, the discharge, and the force scales as

$$\left. \begin{aligned} U_r &= L_{zr}^{0.5} \\ T_r &= L_{xr}/L_{zr}^{0.5} \\ a_r &= L_{zr}/L_{xr} \\ Q_r &= L_{yr} L_{zr}^{1.5} = L_{zr}^{2.5} \\ F_r &= \rho_r L_{xr} L_{zr}^2 \end{aligned} \right\} \quad (11.32)$$

Note that a two-dimensional distorted model with $x_r \neq z_r$ is termed *tilted model* and with $y_r \neq z_r$ *distorted model*. The tilted and distorted models rely on ignoring the transverse and vertical convective accelerations as compared to the acceleration due to gravity.

11.3.2 Immobile Bed Model Studies

An immobile bed implies that the bed is either rigid or loose with no sediment transport, that is, the Shields parameter of flow is less than its threshold value for the sediment motion. For immobile bed models, well-known Manning equation is commonly used to represent the bed resistance to the turbulent flow through an open channel, although it is not an easy task to ensure a turbulent flow in the model satisfying the dynamic similarity. This is discussed in the end of this section. There are two similitude criteria for the immobile bed models: (1) resistance (Manning equation) and (2) Froude similitude criteria. The similitude criterion corresponding to Manning equation is given by

$$\frac{L_r^{2/3} S_{0r}^{0.5}}{U_r n_r} = 1 \quad (11.33)$$

where S_0 is the bed slope and n is the roughness coefficient. In Eq. (11.33), the hydraulic radius is replaced by the length scale. For an undistorted model, $S_{0r} = 1$. Using the Froude similitude criterion ($U_r = L_r^{0.5}$), one obtains

$$\frac{L_r^{1/6}}{n_r} = 1 \quad \Rightarrow \quad L_r = n_r^6 \quad (11.34)$$

The above equation suggests that it is desirable to ascertain the length scale L_r on the basis of the values of n in the model and the prototype. As it is essential to maintain a turbulent flow in the model for the applicability of Manning equation, one should check the Reynolds similitude criterion together with the Froude similitude criterion. For the same fluid in model and prototype, the Reynolds similitude criterion is expressed as

$$Re_r (v_r = 1) = U_r L_r (U_r = L_r^{0.5}) = L_r^{1.5} \quad (11.35)$$

The L_r should therefore be chosen in such a way so that Re_m corresponds to the turbulent flow. According to Allen (1947), the flow is turbulent, if $Re_m \geq 1.4 \times 10^3$, where L_m is the hydraulic depth (ratio of flow area to flow top width). Therefore, it is usually difficult to work with a natural river model. (1) On the one hand, L_r is to be determined from n_r , and on the other hand, Re_m should correspond to the turbulent flow for that value of L_r . (2) Further, n is related to Nikuradse's equivalent sand roughness k_s , as $n \sim k_s^{1/6}$ (Strickler 1923). Note that

Strickler's empirical formula $n = k_s^{1/6} / (6.7g^{0.5})$ introduces a parameter that describes the bed roughness. The roughness length scale k_{sr} should maintain the same resistance parameter corresponding to a hydraulically rough flow regime [shear Reynolds number $R_* (= u_* k_s / \nu) > 70$, where u_* is the shear velocity] in both model and prototype. Although the roughness length scale can be maintained for a macro-rough bed (boulder- or large gravel-bed) in prototype, the near-bed flow condition could change the flow regime to a smooth or a transitional one for using fine sediments, as the viscous sublayer thickness δ' in a model can easily submerge the roughness in the model. One can examine it as $\delta' = 11.6\nu/u_*$, $\delta'_r(v_r = 1) = u_{*r}^{-1} = L_r^{-0.5}$ for the same fluid used in model and prototype, suggesting a large sublayer thickness and potentially prevailing a smooth flow in the model.

It would therefore be a difficult proposition to maintain all these conditional combinations. Thus, one can try to overcome this problem by using a distorted model, where the vertical scale L_{zr} is smaller than the horizontal one L_{xr} for a tilted model. Then, the Froude similitude criterion for a tilted model is

$$U_r = L_{zr}^{0.5} \quad (11.36)$$

It is pertinent to mention the hydraulic depth in the expression of the Froude number is characterized by the vertical scale. However, the slope scale is

$$S_{0r} = \frac{L_{zr}}{L_{xr}} \quad (11.37)$$

The Manning similitude criterion is thus given by

$$\frac{L_{zr}^{2/3} S_{0r}^{0.5}}{U_r n_r} = \frac{L_{zr}^{2/3} (L_{zr}/L_{xr})^{0.5}}{L_{zr}^{0.5} n_r} = 1 \quad \Rightarrow \quad n_r = \frac{L_{zr}^{2/3}}{L_{xr}^{0.5}} \quad (11.38)$$

Considering Strickler's relationship, one obtains $n_r \sim k_{sr}^{1/6}$. Hence, Eq. (11.38) yields $k_{sr} = L_{zr}^4 / L_{xr}^3$. It is obvious that the bed roughness in model is governed by the ratio L_{zr}^4 / L_{xr}^3 . For example, to keep the same bed roughness in model and prototype ($k_{sr} = 1$), the condition $L_{zr} = L_{xr}^{0.75}$ must be satisfied. Therefore, one has an option to select one scaling parameter (one degree of freedom) out of three (L_{zr} or S_{0r} or k_{sr}). It implies that the geometric distortion for a tilted model is possible within some limits in order to seek a desirable bed roughness in a model. In an earlier study, Stevens et al. (1942) reported that for models of rivers, the ranges of horizontal and vertical scales should be $2000 > L_{xr} > 100$ and $150 > L_{zr} > 50$, respectively. Nevertheless, a distorted model has always some disadvantages. For instance, velocities and flow fields may not be truly reproduced (USBR 1953).

It is therefore inevitable that the rough flow over a rigid bed should be simulated by a tilted model. In such problems, the flow depth is scaled as that of exact similitude, while the roughness size is to have a different scale. This helps to have a matching roughness size in prototype by increasing (changing) the flow depth

and the roughness size in the model as long as the roughness in the model is comparable with that in prototype. Note that all these exercises are done by sacrificing the kinematic similarity due to a model distortion.

11.3.3 Mobile Bed Model Studies

Study of similitude in mobile bed involves scour, erosion, aggradations, degradations, bedform migration, etc. Due to complex fluid–sediment interaction, an appropriate model study is always challenging. There are four similitude criteria for a mobile bed study to be fulfilled: (1) resistance (Manning equation), (2) Froude, (3) Shields, and (4) particle or shear Reynolds similitude criteria. A tilted model is inevitable due to a slope scale $S_{0r} = L_{zr}/L_{xr}$, preserving the transverse length scale $L_{yr} = L_{zr}$.

Studying a problem of sediment threshold, criteria (1) and (2) applied to a tilted model given by Eq. (11.38) yield $d_r = L_{zr}^4/L_{xr}^3$. Here, the sediment particle size d is assumed to be equal to the roughness height k_s . The Shields similitude criterion $\Theta_r = 1$ produces the following relationship:

$$\Theta_r = \frac{\tau_{0cr}}{\Delta_r \rho_r g_r d_r} (\rho_r = g_r = 1) = 1 \quad \Rightarrow \quad d_r = \frac{L_{zr} S_{0r}}{\Delta_r} \quad (11.39)$$

where τ_{0c} is the threshold bed shear stress ($= \rho g L_z S_0$). In this context, it is worth mentioning that the particle parameter $D_* [= d(\Delta g/v^2)^{1/3}]$, the shear Reynolds number $R_* [= (u_* d)/\nu]$, and the Shields parameter are interchangeable as $D_* = R_*^{2/3}/\Theta^{1/3}$. Therefore, one may choose either $D_{*r} = 1$ or $R_{*r} = 1$. The expressions for D_{*r} and R_{*r} are as follows:

$$\left. \begin{aligned} D_{*r} &= \frac{d_r (\Delta_r g_r)^{1/3}}{v_r^{2/3}} (g_r = v_r = 1) = 1 \quad \Rightarrow \quad d_r = \frac{1}{\Delta_r^{1/3}} \\ R_{*r} &= \frac{(g_r L_{zr} S_{0r})^{0.5} d_r}{v_r} (g_r = v_r = 1) = 1 \quad \Rightarrow \quad d_r = \frac{1}{(L_{zr} S_{0r})^{0.5}} \end{aligned} \right\} \quad (11.40)$$

Eliminating Δ_r using first relation of Eq. (11.40) and inserting $S_{0r} = L_{zr}/L_{xr}$ in Eq. (11.39), one gets $d_r = L_{xr}^{0.5}/L_{zr}$. By using $d_r = L_{zr}^4/L_{xr}^3$ (Manning–Strickler similitude criterion), the vertical length scale becomes $L_{zr} = L_{xr}^{7/10}$, the particle length scale $d_r = L_{xr}^{-0.2} = L_{zr}^{-2/7}$, and slope scale $S_{0r} = (L_{zr} d_r^2)^{-1} = (d_r/L_{zr})^{1/3} = L_{xr}^{-0.3}$. Hence, from Eq. (11.40), one obtains $\Delta_r = d_r^{-3} = (L_{zr}/d_r)^{2/3} = L_{xr}^{0.6}$. Note that from the second relation of Eq. (11.40), one can also obtain a condition, which is however redundant, as it is $d_r = L_{xr}^{0.5}/L_{zr}$. It suggests that there remain four independent variables (L_{xr} , L_{zr} , d_r , and Δ_r) against three equations $\left[d_r = L_{zr}^4/L_{xr}^3 = L_{zr} S_{0r}/\Delta_r = \Delta_r^{-1/3} \text{ (or } L_{zr}^{-0.5} S_{0r}^{-0.5}) \right]$. The problem can be solved

completely if one of the variables can be selected arbitrarily and other variables are solved from the equations. It means the designer has one degree of freedom. Interestingly, if the same size of the sediment is used in the model and the prototype ($d_r = 1$), then a reduction in relative density of sediment Δ_m in model is required.

In case of bed-load transport, the similitude criterion of bed-load transport intensity function Φ_b yields

$$\Phi_{br} = \frac{q_{br}}{(\Delta_r g_r d_r^3)^{0.5}} (g_r = 1) = 1 \quad \Rightarrow \quad q_{br} = \Delta_r^{0.5} d_r^{1.5} \quad (11.41)$$

where q_b is the bed-load transport rate. Using $\Delta_r = (L_{xr}/d_r)^{2/3}$, one can express bed-load scale as $q_{br} = L_{xr}^{1/3} d_r^{7/6}$. It is interesting to note that $q_{br} = 1$ for $\Theta_r = 1$. Therefore, the similitude criterion of bed-load transport is equivalent to that of sediment threshold, as there are four unknowns against three equations. Again, the problem can be solved completely if one of the variables is selected.

In case of suspended-load transport rate, the similarity criterion of suspended sediment concentration can be obtained from the Rouse equation (Eq. 6.27). The similitude criterion of Rouse number is therefore

$$\zeta_r = \frac{w_{sr}}{\kappa_r (\tau_r / \rho_r)^{0.5}} (\rho_r = g_r = 1) = 1 \quad \Rightarrow \quad w_{sr} = (L_{xr} S_{0r})^{0.5} \quad (11.42)$$

where ζ = Rouse number or exponent of Rouse equation of sediment concentration, w_s is the terminal fall velocity of sediment particle, and κ is the von Kármán constant. With $S_{0r} = L_{xr}/L_{xr}$, Eq. (11.42) becomes $w_{sr} = L_{xr}/L_{xr}^{0.5} = d_r^{-1}$. Alternatively, using Eq. (1.40), the terminal fall velocity scale can also be determined as $w_{sr} = d_r^{-1}$ provided $D_{*r} = 1$. The similitude criterion of sediment suspension that is defined as the ratio of sediment terminal fall velocity to shear velocity of flow is identical to that of sediment threshold criterion, that is, $w_{sr}/u_{*r} = 1$ and $d_r = L_{xr}^{0.5}/L_{xr}$. Therefore, the complete solution of the problem is possible.

In case of scour of a sediment bed, the time scale t to change the bed elevation can be determined from the sediment continuity equation given by Exner (1925) (Eq. 8.36). It is

$$\frac{\partial q_{br}}{\partial L_{xr}} = -(1 - \rho_0)_r \frac{\partial L_{xr}}{\partial t_r} [(1 - \rho_0)_r = 1] \quad \Rightarrow \quad t_r = \frac{L_{xr} L_{xr}}{q_{br}} \quad (11.43)$$

where ρ_0 is the porosity of sediment. It is assumed that the scale of the porosity related term $(1 - \rho_0)_r$ is unity. Using $L_{xr} = L_{xr}^{4/3}/d_r^{1/3}$ (Manning–Strickler similitude criterion) and $q_{br} = L_{xr}^{1/3} d_r^{7/6}$, one can express time scale as $t_r = L_{xr}^2/d_r^{1.5}$. This time scale is also useful for bedform migration and aggradations/degradations of beds. However, the exchange time t_e (or time for a particle to be removed) during the bed-load transport can be scaled from the concept of Einstein's (1950) bed-load transport model. It is $t_{er} = d_r/w_{sr} = d_r^2 = L_{xr}/L_{xr}^2$.

In some mobile bed model studies, the complete similitude is not feasible under certain circumstances. In such cases, one criterion of similitude can usually be given up in place of having an advantage of two degrees of freedom, although it risks yielding erroneous results. This type of similitude is called *incomplete similitude*. However, there are two ways to preserve the criteria of similitude in both model and prototype. They are (1) Froude ($Fr_r \neq 1$) and (2) particle ($D_{*r} \neq 1$) quasi-similitude criteria. Using Manning and Strickler relationships, the Froude quasi-similitude criterion is given by

$$Fr_r = \frac{U_r}{L_{xr}^{0.5}} = \left(\frac{L_{zr}}{L_{xr}} \right)^{0.5} \left(\frac{L_{zr}}{d_r} \right)^{1/3} \quad (11.44)$$

It means the Froude similitude criterion is supplemented by the Froude quasi-similitude criterion with an additional degree of freedom, such as L_{xr} , L_{zr} , and d_r . The Froude quasi-similitude model thus allows to consider different Froude numbers in model and prototype provided similar flow condition (subcritical flow) to prevail in both the systems. A gradually varied flow that has a near-constant Froude number (an average value) over a certain reach of prototypical channel is quasi-simulated by a flow with different Froude number in the laboratory model having similar flow condition (subcritical flow) as that in prototype. For instance, a low Fr_p can be simulated with same bed sediment at higher Fr_m as long as the flow is subcritical. In the Froude quasi-similitude criterion, Eqs. (11.39), (11.40) and (11.44) (or $\Theta_r = 1$, $D_{*r} = 1$, and $Fr_r \neq 1$) are to be simultaneously satisfied. The Shields ($\Theta_r = 1$) and particle ($D_{*r} = 1$) similitude criteria yield the relationship $d_r = L_{xr}^{0.5}/L_{zr}$, and thus, Froude quasi-similitude criterion using Eq. (11.44) gives $Fr_r = L_{zr}^{-1/3}$. To be explicit, the relation $Fr_p(Fr_p < 1) = L_{zr}^{-1/3} Fr_m(Fr_m < 1)$ implies a slightly different Froude number in model and prototype. It is apparent that the Froude quasi-similitude is restricted to a gradually varied subcritical flow. Therefore, although this type of model can reasonably simulate the bed-load and suspended-load transports, it is unable to simulate the flow kinematics and dynamics to a desired degree of accuracy. Similitude in cross section without distortion can be obtained with $y_r = z_r$ and planer bed geometry with $x_r = y_r$.

On the other hand, the particle quasi-similitude criterion is

$$D_{*r} = \frac{d_r(\Delta_r g_r)^{1/3}}{v_r^{2/3}} \quad (g_r = v_r = 1) = d_r \Delta_r^{1/3} \quad (11.45)$$

The particle quasi-similitude model can be used for bed-load dominant sediment transport cases. For instance, the bed-load transport of coarse sediment in prototype can be simulated with a smaller value of particle parameter ($D_{*m} < D_{*p}$) in the model provided the flow being hydraulically rough ($R_* > 70$). This type of model has a limitation that there remains always an uncertainty in prediction of suspended-load transport or bedform migration due to the scale effects, as Shields similitude criterion is preserved ($\Theta_r = 1$), but particle similitude criterion is not

preserved ($D_{*r} \neq 1$). As $D_* = R_*^{2/3}/\Theta^{1/3}$, the non-preservation of particle similitude criterion ($D_{*r} \neq 1$) implies non-preservation of shear Reynolds similitude criterion ($R_{*r} \neq 1$) as well. Therefore, using Eq. (11.39), $S_{0r} = L_{zr}/L_{xr}$, and $L_{xr} = L_{zr}^{4/3}/d_r^{1/3}$ (Manning–Strickler similitude criterion), one can obtain $D_{*r} = d_r^{7/9} L_{zr}^{2/9}$ and $R_{*r} = (L_{zr} S_{0r})^{0.5} d_r = L_{zr}^{1/3} d_r^{7/6}$.

11.4 Examples

Example 11.1 Consider a velocity distribution in the wall shear layer of a fluid flowing over an immobile sediment bed. The time-averaged velocity u at a distance z from the virtual bed level depends on the median sediment size d , the flow depth h , the coefficient of kinematic viscosity of fluid ν , the mass density of fluid ρ , and the bed shear stress τ_0 . Use the dimensional analysis to obtain a set of Π parameters and a possible functional relationship for u .

Solution

The functional relationship to exist is

$$f(u, z, d, h, \nu, \rho, \tau_0) = 0$$

The above equation contains three dimensions, that is, M , L , and T . The repeating variables are considered as τ_0 , d , and ρ . Hence, there are four non-dimensional Π parameters as

$$\Pi_1 = \tau_0^{p_1} d^{q_1} \rho^{r_1} u = (ML^{-1}T^{-2})^{p_1} L^{q_1} (ML^{-3})^{r_1} LT^{-1} = M^0 L^0 T^0$$

$$\Pi_2 = \tau_0^{p_2} d^{q_2} \rho^{r_2} z = (ML^{-1}T^{-2})^{p_2} L^{q_2} (ML^{-3})^{r_2} L = M^0 L^0 T^0$$

$$\Pi_3 = \tau_0^{p_3} d^{q_3} \rho^{r_3} h = (ML^{-1}T^{-2})^{p_3} L^{q_3} (ML^{-3})^{r_3} L = M^0 L^0 T^0$$

$$\Pi_4 = \tau_0^{p_4} d^{q_4} \rho^{r_4} \nu = (ML^{-1}T^{-2})^{p_4} L^{q_4} (ML^{-3})^{r_4} L^2 T^{-1} = M^0 L^0 T^0$$

By equating the exponents of M , L , and T of Π_1 parameter, the following equations are obtained:

$$M \Rightarrow p_1 + r_1 = 0$$

$$L \Rightarrow -p_1 + q_1 - 3r_1 + 1 = 0$$

$$T \Rightarrow -2p_1 - 1 = 0$$

By solving the three equations simultaneously, one obtains $p_1 = -0.5$, $q_1 = 0$, and $r_1 = 0.5$, and therefore, $\Pi_1 = u/(\tau_0/\rho)^{0.5}$.

By equating the exponents of M , L , and T of Π_2 parameter, the following equations are obtained:

$$\begin{aligned}
M &\Rightarrow p_2 + r_2 = 0 \\
L &\Rightarrow -p_2 + q_2 - 3r_2 + 1 = 0 \\
T &\Rightarrow -2p_2 = 0
\end{aligned}$$

By solving the three equations simultaneously, one obtains $p_2 = 0$, $q_2 = -1$, and $r_2 = 0$, and therefore, $\Pi_2 = z/d$. Similarly, one can also obtain $\Pi_3 = h/d$. By equating the exponents of M , L , and T of Π_4 parameter, the following equations are obtained:

$$\begin{aligned}
M &\Rightarrow p_4 + r_4 = 0 \\
L &\Rightarrow -p_4 + q_4 - 3r_4 + 2 = 0 \\
T &\Rightarrow -2p_4 - 1 = 0
\end{aligned}$$

By solving the three equations simultaneously, one obtains $p_4 = -0.5$, $q_4 = -1$, and $r_4 = 0.5$, and therefore, $\Pi_4 = v/[d(\tau_0/\rho)^{0.5}]$. Hence, the set of Π parameters forms the following relationship:

$$\phi\left(\frac{u}{(\tau_0/\rho)^{0.5}}, \frac{z}{d}, \frac{h}{d}, \frac{v}{d(\tau_0/\rho)^{0.5}}\right) = 0$$

Inserting $u_* = (\tau_0/\rho)^{0.5}$ and $R_* = u_*d/v$, and then rearranging, the functional relationship for u is obtained as

$$u = u_* \phi_1\left(\frac{z}{d}, \frac{h}{d}, R_*\right)$$

Example 11.2 Consider a bed-load transport by the flowing fluid over a mobile sediment bed. The bed-load transport rate q_b (volume per unit time and width) depends on the median sediment size d , the coefficient of kinematic viscosity of fluid ν , the mass density of fluid ρ , the mass density of sediment ρ_s , the acceleration due to gravity g , the bed shear stress of flow τ_0 , and the threshold bed shear stress τ_{0c} for the sediment motion. Use the dimensional analysis to determine a set of Π parameters and a possible functional relationship for the bed-load transport intensity function.

Solution

The original functional relationship to exist is

$$f(q_b, d, \nu, \rho, \rho_s, g, \tau_0, \tau_{0c}) = 0$$

In fluid–sediment interaction (two-phase flow), ρ , ρ_s , and g should be combined and replaced by $\Delta g [= (s-1)g]$ and ρ . Thus, the modified functional relationship becomes

$$f(q_b, d, v, \rho, \Delta g, \tau_0, \tau_{0c}) = 0$$

The above equation contains three dimensions, that is, M , L , and T . The repeating variables are considered as τ_0 , d , and Δg . Hence, there are four Π parameters as

$$\begin{aligned}\Pi_1 &= \tau_0^{p_1} d^{q_1} (\Delta g)^{r_1} q_b = (ML^{-1}T^{-2})^{p_1} L^{q_1} (LT^{-2})^{r_1} L^2 T^{-1} = M^0 L^0 T^0 \\ \Pi_2 &= \tau_0^{p_2} d^{q_2} (\Delta g)^{r_2} v = (ML^{-1}T^{-2})^{p_2} L^{q_2} (LT^{-2})^{r_2} L^2 T^{-1} = M^0 L^0 T^0 \\ \Pi_3 &= \tau_0^{p_3} d^{q_3} (\Delta g)^{r_3} \rho = (ML^{-1}T^{-2})^{p_3} L^{q_3} (LT^{-2})^{r_3} ML^{-3} = M^0 L^0 T^0 \\ \Pi_4 &= \tau_0^{p_4} d^{q_4} (\Delta g)^{r_4} \tau_{0c} = (ML^{-1}T^{-2})^{p_4} L^{q_4} (LT^{-2})^{r_4} ML^{-1} T^{-2} = M^0 L^0 T^0\end{aligned}$$

By equating the exponents of M , L , and T of Π_1 parameter, the following equations are obtained:

$$\begin{aligned}M &\Rightarrow p_1 = 0 \\ L &\Rightarrow -p_1 + q_1 + r_1 + 2 = 0 \\ T &\Rightarrow -2p_1 - 2r_1 - 1 = 0\end{aligned}$$

By solving the three equations simultaneously, one obtains $p_1 = 0$, $q_1 = -1.5$, and $r_1 = -0.5$, and therefore, $\Pi_1 = q_b/[d^{1.5}(\Delta g)^{0.5}]$

By equating the exponents of M , L , and T of Π_2 parameter, the following equations are obtained:

$$\begin{aligned}M &\Rightarrow p_2 = 0 \\ L &\Rightarrow -p_2 + q_2 + r_2 + 2 = 0 \\ T &\Rightarrow -2p_2 - 2r_2 - 1 = 0\end{aligned}$$

By solving the three equations simultaneously, one obtains $p_2 = 0$, $q_2 = -1.5$, and $r_2 = -0.5$, and therefore, $\Pi_2 = v/[d^{1.5}(\Delta g)^{0.5}]$.

By equating the exponents of M , L , and T of Π_3 parameter, the following equations are obtained:

$$\begin{aligned}M &\Rightarrow p_3 + 1 = 0 \\ L &\Rightarrow -p_3 + q_3 + r_3 - 3 = 0 \\ T &\Rightarrow -2p_3 - 2r_3 = 0\end{aligned}$$

By solving the three equations simultaneously, one obtains $p_3 = -1$, $q_3 = 1$, and $r_3 = 1$, and therefore, $\Pi_3 = \rho \Delta g d / \tau_0$.

By equating the exponents of M , L , and T of Π_4 parameter, the following equations are obtained:

$$M \Rightarrow p_4 + 1 = 0$$

$$L \Rightarrow -p_4 + q_4 + r_4 - 1 = 0$$

$$T \Rightarrow -2p_4 - 2r_4 + 2 = 0$$

By solving the three equations simultaneously, one obtains $p_4 = -1$, $q_4 = 0$, and $r_4 = 0$, and therefore, $\Pi_4 = \tau_{0c}/\tau_0$

Hence, the set of Π parameters forms the following relationship:

$$\phi \left(\frac{q_b}{d^{1.5}(\Delta g)^{0.5}}, \frac{v}{d^{1.5}(\Delta g)^{0.5}}, \frac{\rho \Delta g d}{\tau_0}, \frac{\tau_{0c}}{\tau_0} \right) = 0$$

For bed-load transport formulation, it is desirable to express the ratio τ_{0c}/τ_0 as a difference of τ_0 and τ_{0c} in non-dimension. Hence, τ_{0c}/τ_0 is replaced by $(\tau_0 - \tau_{0c})/\tau_{0c}$, known as transport stage parameter T_* . Inserting $\Phi_b = q_b/(\Delta g d^3)^{0.5}$, $D_* = d(\Delta g/v^2)^{1/3}$, $\Theta = \tau_0/(\rho \Delta g d)$, and $T_* = (\tau_0 - \tau_{0c})/\tau_{0c}$, and then rearranging, the functional relationship for bed-load transport function Φ_b is

$$\Phi_b = \phi_1(D_*, \Theta, T_*)$$

Example 11.3 A 3,750 m long gravel-bed river has a width of 100 m and carries a discharge of $120 \text{ m}^3 \text{ s}^{-1}$ with a flow depth of 3 m. If the median size of gravel is 6 mm, simulate a model in a laboratory space having a maximum length of 25 m. Take the relative density of gravel as 2.65.

Solution

For the prototype, flow depth $h_p = 3 \text{ m}$, width $b_p = 100 \text{ m}$, and discharge $Q_p = 120 \text{ m}^3 \text{ s}^{-1}$ and the prototype flow velocity is $U_p = Q_p/(h_p b_p) = 120/(3 \times 100) = 0.4 \text{ m s}^{-1}$. The prototype Manning roughness coefficient is $n_p = d_p^{1/6}/(6.7 g^{0.5}) = (6 \times 10^{-3})^{1/6}/(6.7 \times 9.81^{0.5}) = 0.02 \text{ m}^{-1/3} \text{ s}$.

The length scale is $L_r = L_p/L_m = 3750/25 = 150$. From the Froude similitude criterion, the velocity scale is $U_r = L_r^{0.5} = 150^{0.5} = 12.25$. Therefore, the model flow depth is $h_m = h_p/L_r = 3/150 = 0.025 \text{ m}$, the bed material size $d_m = d_p/L_r = 6 \times 10^{-3}/150 = 4 \times 10^{-5} \text{ m}$ (or 0.04 mm), and the flow velocity $U_m = U_p/U_r = 0.4/12.25 = 0.0327 \text{ m s}^{-1}$.

The prototype Froude number is $Fr_p = U_p/(gh_p)^{0.5} = 0.4/(9.81 \times 3)^{0.5} = 0.0737 < 1$ (subcritical flow). The prototype streamwise slope obtained from the Manning equation is $S_{0p} = (n_p U_p)^2/h_p^{4/3} = (0.02 \times 0.4)^2/3^{4/3} = 1.48 \times 10^{-5}$. Note that $S_{0p} = S_{0m}$. The prototype shear velocity is $u_{*p} = (gh_p S_{0p})^{0.5} = (9.81 \times 3 \times 1.48 \times 10^{-5})^{0.5} = 0.021 \text{ m s}^{-1}$. The prototype Shields parameter is $\Theta_p = u_{*p}^2/(\Delta g d_p) = 0.021^2/(1.65 \times 9.81 \times 6 \times 10^{-3}) = 0.0045 < \Theta_{cp} (= 0.056)$, obtained from the Shields diagram, implying the gravel-bed to be immobile.

The prototype Reynolds number is $Re_p = U_p h_p / \nu = 0.4 \times 3 / 10^{-6} = 1.2 \times 10^6 > 1400$ (turbulent flow) (Allen 1947), and the prototype shear Reynolds number $R_{*p} = u_{*p} d_p / \nu = 0.021 \times 6 \times 10^{-3} / 10^{-6} = 126 > 70$ (hydraulically rough flow). Thus, the flow is rough-turbulent in the prototype. The model shear velocity is $u_{*m} = (gh_m S_{0m})^{0.5} = (9.81 \times 0.025 \times 1.48 \times 10^{-5})^{0.5} = 1.905 \times 10^{-3} \text{ m s}^{-1}$. On the other hand, the model Reynolds number is $Re_m = U_m h_m / \nu = 0.0327 \times 0.025 / 10^{-6} = 817.5 < 1400$ (laminar flow), and the model shear Reynolds number $R_{*m} = u_{*m} d_m / \nu = 1.905 \times 10^{-3} \times 4 \times 10^{-5} / 10^{-6} = 0.076 < 70$. Thus, the flow is smooth-laminar in the model.

To preserve the rough-turbulent flow in model, adopt a tilted model by selecting one of the scaling parameters (one degree of freedom) out of three (L_{xr} , S_{0r} , and $k_{sr} \approx d_r$) (see Sect. 11.3.2). Let us set a roughness scale be $d_r = 0.4$. Note that this scale depends on the larger size of gravels that can be used in the laboratory model study. In this case, it is $d_m = d_p / d_r = 6 \times 10^{-3} / 0.4 = 0.015 \text{ m}$ or 15 mm. Thus, the vertical length scale determined from the relationship $d_r = L_{xr}^4 / L_{xr}^3$ is $L_{xr}(L_r = L_{xr}) = L_{xr}^{0.75} d_r^{0.25} = 150^{0.75} \times 0.4^{0.25} = 34.1$, and from the Froude similitude, the velocity scale $U_r = L_{xr}^{0.5} = 34.1^{0.5} = 5.84$. The discharge scale is $Q_r = L_{yr} L_{xr}^{1.5} = 150 \times 34.1^{1.5} = 29,869$ (consider non-distorted tilted model, $L_r = L_{xr} = L_{yr}$) [see Eq. (11.32)], and then, $Q_m = Q_p / Q_r = 120 / 29869 = 4.018 \times 10^{-3} \text{ m}^3 \text{ s}^{-1}$. The model flow velocity is $U_m = U_p / U_r = 0.4 / 5.84 = 0.0685 \text{ m s}^{-1}$, and the Reynolds number $Re_m (Re_r = L_{xr}^{1.5}) = Re_p / Re_r = U_p h_p / (\nu L_{xr}^{1.5}) = 0.4 \times 3 / (10^{-6} \times 34.1^{1.5}) = 6,026.3 > 1,400$ (turbulent flow). Thus, the model flow depth is $h_m = h_p / L_{xr} = 3 / 34.1 = 0.088 \text{ m}$. The model slope scale is $S_{0m} = S_{0p} / (L_{xr} / L_{xr}) = 1.48 \times 10^{-5} / (34.1 / 150) = 6.51 \times 10^{-5}$, and the shear velocity $u_{*m} = (gh_m S_{0m})^{0.5} = (9.81 \times 0.088 \times 6.51 \times 10^{-5})^{0.5} = 7.497 \times 10^{-3} \text{ m s}^{-1}$. The model shear Reynolds number is $R_{*m} = u_{*m} d_m / \nu = 7.497 \times 10^{-3} \times 0.015 / 10^{-6} = 112.46 > 70$ (hydraulically rough flow). It confirms that the flow in model is rough-turbulent that complies with the prototype flow condition.

Example 11.4 A sand-bed river has a streamwise slope of 5×10^{-5} and carries a discharge of $3 \times 10^4 \text{ m}^3 \text{ s}^{-1}$ with a flow depth of 6 m and a velocity of 2.5 m s^{-1} . If the median size of sediment is 1 mm, find the scales to completely simulate a laboratory model with polystyrene made artificial bed sediment. Take the relative density of sand as 2.65 and polystyrene as 1.05.

Solution

For the prototype, slope is $S_{0p} = 5 \times 10^{-5}$, flow depth $h_p = 6 \text{ m}$, and sand size $d_p = 1 \times 10^{-3} \text{ m}$. The prototype shear velocity is $u_{*p} = (gh_p S_{0p})^{0.5} = (9.81 \times 6 \times 5 \times 10^{-5})^{0.5} = 0.054 \text{ m s}^{-1}$, and the Shields parameter $\Theta_p = u_{*p}^2 / (\Delta g d_p) = 0.054^2 / (1.65 \times 9.81 \times 1 \times 10^{-3}) = 0.18$. The threshold Shields parameter obtained from van Rijn's relationship (Table 4.1) is $\Theta_{cp} = 0.033$. Therefore, the condition $\Theta_p > \Theta_{cp}$ implies the prototype sediment bed to be mobile.

The submerged relative density scale is $\Delta_r = \Delta_p/\Delta_m = (2.65 - 1)/(1.05 - 1) = 33$. The particle scale obtained from Eq. (11.40) is $d_r = \Delta_r^{-1/3} = 33^{-1/3} = 0.312$, and thus, the model sediment size $d_m = d_p/d_r = 1 \times 10^{-3}/0.312 = 3.21 \times 10^{-3}$ m or 3.21 mm. Note that the polystyrene-made sediment particles having size of 3.21 mm should simulate a Nikuradse's equivalent sand roughness k_s of 3.21 mm. It, of course, depends on the texture of the polystyrene-made sediment particles, not the size only. The streamwise length scale obtained from the relation $\Delta_r = L_{xr}^{0.6}$ is $L_{xr} = \Delta_r^{1.67} = 33^{1.67} = 343.5$, and thus, the vertical scale $L_{zr} = L_{xr}^{7/10} = 343.5^{7/10} = 59.6$. The model flow depth is $h_m = h_p/L_{zr} = 6/59.6 = 0.101$ m. The slope scale is $S_{0r} = L_{xr}^{-0.3} = 343.5^{-0.3} = 0.173$, and the model slope $S_{0m} = S_{0p}/S_{0r} = 5 \times 10^{-5}/0.173 = 2.89 \times 10^{-4}$. The velocity scale is $U_r = L_{zr}^{0.5} = 59.6^{0.5} = 7.72$, and the model velocity $U_m = U_p/U_r = 2.5/7.72 = 0.324$ m s⁻¹. The discharge scale obtained from Eq. (11.32) is $Q_r = L_{zr}^{2.5} = 59.6^{2.5} = 2.742 \times 10^4$, and the model discharge $Q_m = Q_p/Q_r = 3 \times 10^4/(2.742 \times 10^4) = 1.094$ m³ s⁻¹.

Example 11.5 A 5,000 m long gravel-bed river has an average streamwise slope of 5×10^{-3} and carries a discharge with a flow depth of 5 m. If the median size of gravel is 25 mm, find the scales to simulate a laboratory model within a space of maximum length of 25 m. Take the relative density of gravel as 2.65.

Solution

For the prototype, slope is $S_{0p} = 5 \times 10^{-3}$, flow depth $h_p = 5$ m, and sand size $d_p = 0.025$ m. The prototype shear velocity is $u_{*p} = (gh_p S_{0p})^{0.5} = (9.81 \times 5 \times 5 \times 10^{-3})^{0.5} = 0.495$ m s⁻¹, the shear Reynolds number $R_{*p} = u_{*p} d_p / \nu = 0.495 \times 0.025 / 10^{-6} = 12,375 > 70$, and the Shields parameter $\Theta_p = u_{*p}^2 / (\Delta g d_p) = 0.495^2 / (1.65 \times 9.81 \times 0.025) = 0.606 > \Theta_{cp}$ ($= 0.056$, obtained from the Shields diagram), implying the flow to be hydraulically rough and the gravel-bed to be mobile. The prototype bed-load transport rate calculated from Meyer-Peter and Müller (1948) formula is $q_{bp} = 8(\Delta g d_p)(\Theta_p - \Theta_{cp})^{1.5} = 8(1.65 \times 9.81 \times 0.025)(0.606 - 0.056)^{1.5} = 1.32$ m² s⁻¹. The streamwise length scale is $L_{xr} = 5000/25 = 200$. For an undistorted model, the sediment size scale is $d_r = L_{zr}^{-2/7} (L_{xr} = L_{zr}) = 200^{-2/7} = 0.22$ and the model sediment size $d_m = d_p/d_r = 0.025/0.22 = 0.114$ m or 114 mm, which is impracticable.

Consider an incomplete similitude with particle quasi-similitude criterion ($D_{*r} \neq 1$), which would be appropriate as finer gravel to be used in the model. It would still preserve hydraulically rough flow. It means that the particle similitude criterion is supplemented by the particle quasi-similitude criterion with two degrees of freedom, such as L_{xr} or L_{zr} and d_r . Select the arbitrarily vertical length scale as $L_{zr} = 150$ and the particle size scale $d_r = 20$. The transverse length scale can be as the original one; that is $y_r = 200$. Therefore, the streamwise length scale is

$L_{xr} = L_{xr}^{4/3} / d_r^{1/3} = 150^{4/3} / 20^{1/3} = 293.6$, the shear Reynolds scale $R_{*r} = L_{xr}^{1/3} d_r^{7/6} = 150^{1/3} \times 20^{7/6} = 175.1$, and the model shear Reynolds number $R_{*m} = R_{*p} / R_{*r} = 12375 / 175.1 = 70.7 > 70$ (hydraulically rough flow).

The discharge scale is $Q_r = L_{yr} L_{xr}^{1.5} = 200 \times 150^{1.5} = 3.674 \times 10^5$, and the velocity scale $U_r = L_{xr}^{0.5} = 150^{0.5} = 12.25$. The model sediment size is $d_m = d_p / d_r = 0.025 / 20 = 1.25 \times 10^{-3}$ m or 1.25 mm. The relative submerged density scale is $\Delta_r = (L_{xr} / d_r)^{2/3} = (150 / 20)^{2/3} = 3.83$, and the model relative submerged density $\Delta_m = \Delta_p / \Delta_r = 1.65 / 3.83 = 0.43$. Therefore, the relative density of sediment to be used in the model is $s_r = 1 + 0.43 = 1.43$. Artificial sediment made of polyoxymethylene that has relative density of approximately 1.43 can be used in model. The slope scale is $S_{or} = (d_r / L_{xr})^{1/3} = (20 / 150)^{1/3} = 0.511$, and the model slope $S_{om} = S_{op} / S_{or} = 5 \times 10^{-3} / 0.511 = 9.785 \times 10^{-3}$. The bed-load scale is $q_{br} = L_{xr}^{1/3} d_r^{7/6} = 150^{1/3} \times 20^{7/6} = 175.1$, and the model bed-load transport rate $q_{bm} = q_{bp} / q_{br} = 1.32 / 175.1 = 7.539 \times 10^{-3} \text{ m}^2 \text{ s}^{-1}$. The time scale of bed degradations is $t_r = L_{xr}^2 / d_r^{1.5} = 150^2 / 20^{1.5} = 251.6$. It means that the bed degradation in prototype for an hour corresponds to that in model for $60 \times 60 / 251.6 = 14.3$ s.

References

- Allen J (1947) Scale models in hydraulic engineering. Longmans and Green, London
- Buckingham E (1915) Model experiments and the form of empirical equations. Trans Am Soc Mech Eng 37:263–295
- Dwivedi A, Melville B, Shamseldin AY (2010) Hydrodynamic forces generated on a spherical sediment particle during entrainment. J Hydraul Eng 136(10):756–769
- Einstein HA (1950) The bed-load function for sediment transportation in open channel flows. Technical bulletin number 1026, United States Department of Agriculture, Soil Conservation Service, Washington, DC
- Exner FM (1925) Über die wechselwirkung zwischen wasser und gesschiebe in flüssen. Sitzungsberichte der Akademie der Wissenschaften 134(2a):165–203
- Meyer-Peter E, Müller R (1948) Formulas for bed-load transport. In: Proceedings of the second meeting of International Association for Hydraulic Research, Stockholm, vol 3, pp 39–64
- Stevens JC, Bardsley CE, Lane EW, Straub LG (1942) Hydraulic models. Manuals on engineering practice number 25, American Society of Civil Engineers, New York
- Strickler A (1923) Beiträge zur frage der geschwindigkeitsformel und der rauhkeitszahlen für ströme kanäle und geschlossene leitungen. Mitteilungen des Eidgenoessischer Amtes für Wasserwirtschaft, Number 16, Bern
- Thomson W (1889) Lord Kelvin: Electrical units of measurement. Popular lectures and addresses. vol 1. Macmillan, London, pp 73–74
- USBR (1953) Hydraulic laboratory practice. Engineering monograph number 18, United States Bureau of Reclamation, Denver, Colorado

About the Author



Subhasish Dey is a Professor and Head in the Department of Civil Engineering at Indian Institute of Technology Kharagpur. He also holds an Adjunct Professor position in the Physics and Applied Mathematics Unit at Indian Statistical Institute Kolkata. Besides he has held numerous visiting professorships, including those at Universität Stuttgart, Technische Universität Darmstadt, University of Iowa, Technical University of Denmark, Adelaide University, University of Bradford, Tsinghua University, University of Hong Kong, Università di Pisa, Università della Calabria, Politecnico di Milano, University of Florence, University of Oulu, Instituto Superior Tecnico Lisbon, National Taiwan University, National Chung Hsing University, National Cheng Kung University, Nanyang Technological University, and Laboratoire Central des Ponts et Chaussées. He is an Associate Editor of *Journal of Hydraulic Engineering*, *Journal of Hydraulic Research*, *Sedimentology*, *Acta Geophysica*, *Journal of Hydro-Environment Research*, *International Journal of Sediment Research* and *Journal of Numerical Mathematics and Stochastics*.

He has published 135 articles in international referred journals. His research areas are applied hydrodynamics, turbulence and sediment transport, in which he has more than 30 years of experience. He is internationally known for his research and acclaimed for his contributions in developing theories and solution methodologies of various problems on hydraulics.

Author Index

A

Abbott, J. E., 294, 297–299, 320
 Aberle, J., 172, 173, 178
 Absi, R., 136
 Acaroglu, E. R., 429
 Ackers, P., 430–432, 435
 Agarwal, V. C., 540
 Aguirre-Pe, J., 587
 Ahmad, M. S. S., 436
 Ahn, S. J., 608
 Ahrens, J. P., 20
 Akiyama, J., 361, 536
 Aksoy, S., 197
 Albertson, M. L., 453, 486, 489, 499
 Alexander, A. J., 217, 296
 Alger, G. R., 9
 Allen, J. R. L., 226, 453, 461, 515, 523
 Allen, J., 656, 665
 Alonso, C. V., 117, 304, 575
 Altinbilek, H. D., 580
 Anderson, A. G., 337, 403
 Andreopoulos, J., 150
 Antonia, R. A., 150, 153, 162, 500
 Antsyferov, S. M., 350
 Apperley, L. W., 197
 ASCE Task Force, 111
 Ashida, K., 244, 267, 299, 300
 Ashley, G. M., 471
 Ashmore, P. E., 556–559
 Atayee, A. T., 611
 Athaullah, M., 469, 470
 Atkins, R., 399
 Atkinson, J. D., 162
 Austroads, 611
 Ayala, L., 298, 299, 320
 Azuma, R., 115, 116, 396, 398, 400

B

Baas, J. H., 455, 457, 465, 505
 Bagnold, R. A., 15, 197, 261, 262, 285, 286, 288, 377–380, 385, 386, 424, 430, 456, 500
 Baird, D. C., 423
 Bakhmeteff, B. A., 574
 Bala, M., 239
 Balakrishnan, M., 239
 Ball, J. E., 218, 219
 Ballio, F., 172
 Bandyopadhyay, P., 156
 Bandyopadhyay, P. R., 148
 Banerjee, I., 507
 Banks, N. L., 505
 Barbarossa, N. L., 511, 512
 Barbhuiya, A. K., 602, 604, 605, 609
 Bardsley, C. E., 657
 Barekyan, A. S., 272
 Barenblatt, G. I., 399, 614
 Barenblatt, G. N., 348
 Barton, J. R., 486, 489, 499
 Basmaci, Y., 580
 Bathurst, J. C., 507
 Bayram, A., 112
 Bechteler, W., 472
 Bélanger, J. B., 89
 Belleudy, P., 315
 Bennett, S., 312, 314, 315, 317
 Bennett, S. J., 316
 Bergs, M. A., 550
 Best, J., 312, 314, 315, 317
 Best, J. L., 555
 Bigillon, F., 400
 Bijker, E. W., 359, 372, 587
 Billi, P., 505
 Bishop, A. A., 426, 428

Blasius, H., 73
 Bogard, D. G., 316
 Boguchwal, L. A., 471
 Borah, D. K., 303, 304
 Bormann, N. E., 576
 Bose, S. K., 114, 123, 146, 162, 167, 169, 171,
 182, 241–243, 297, 307–309, 311–317,
 351, 356, 365, 382–386, 396, 491, 492,
 499–501, 505, 580, 592, 594, 612, 613,
 616, 617
 Bottaro, A., 133
 Bovolin, V., 577–579
 Bradshaw, P., 124
 Brayshaw, A. C., 197, 505
 Breugem, A., 401, 402
 Breusers, H. N. C., 580, 588, 594, 600, 610
 Bridge, J., 312, 314, 315, 317
 Bridge, J. S., 316
 Bringaker, K. G., 586
 Bristow, C. S., 555
 Brodkey, R. S., 155, 158
 Brooks, N. H., 369, 370, 395, 486, 489, 499
 Brown, C. B., 280
 Brown, G. L., 354
 Brownlie, W. R., 203, 432, 469, 514
 Brush, L. M., 332
 Buckingham, E., 646
 Buffington, J. M., 190, 191
 Byrne, R. J., 210

C

Calantoni, J., 230
 Calomino, F., 316, 317, 608
 Camenen, B., 19, 25, 112
 Campbell, L., 172, 173, 178
 Cao, Z., 222, 241, 252
 Cardoso, A. H., 119, 608
 Carson, M. A., 530, 536, 538, 556
 Carstens, M. R., 192, 332
 Casey, H. J., 216, 221, 223, 224
 Castro-Orgaz, O., 389, 390, 394, 396
 Celik, I., 361, 381, 385
 Cellino, M., 395, 398, 400
 Chabert, J., 469, 470
 Champagne, J. Y., 315
 Champagne, J. -Y., 400
 Chang, F. M., 267, 268, 369, 371, 425, 609
 Chang, H. H., 359, 539
 Chang, H. -K., 19
 Chang, S. Y., 301
 Chao, J. L., 584
 Charru, F., 269, 298, 320
 Chatley, H., 540

Chaudhry, M. H., 62
 Chauvin, J. L., 469, 470
 Chen, C., 117
 Chen, W. Y., 162
 Chen, X., 230
 Cheng, K. J., 357
 Cheng, N. -S., 18, 19, 25, 235, 271, 306, 307,
 309, 315, 381, 382, 384, 385, 438, 520,
 564, 572
 Chepil, W. S., 197, 229, 250
 Chew, Y. T., 148
 Chien, N., 267, 280, 283, 339, 342, 350, 388,
 395, 403, 418
 Chiew, Y. M., 226, 586, 587, 610
 Chiew, Y. -M., 235, 306, 307, 309, 381, 382,
 384, 385
 Chin, A., 507
 Chin, C. O., 305
 Chiyoda, M., 544
 Choi, K. S., 147
 Chorin, A. J., 614
 Chou, Y. J., 233, 234, 237, 238
 Chow, V. T., 43, 55, 62, 134, 227
 Christensen, B. A., 7
 Chua, L. H. C., 315
 Cioffi, F., 395
 Clauser, F. H., 120
 Clifford, N. J., 241
 Clopper, P. E., 610, 611
 Clunie, D., 172, 173, 178
 Colby, B. R., 419, 422–424
 Colebrook, C. F., 121, 503
 Coleman, N. L., 117, 211, 223, 335, 338, 344,
 394–398
 Coleman, S., 172, 173, 178
 Coleman, S. E., 589, 595, 600, 605, 610
 Coles, D., 116
 Collinson, J. D., 505
 Comiti, F., 578, 579
 Corino, E. R., 155
 Correia, L., 304
 Cosart, W. P., 614
 Cramer, H., 163
 Croad, R. N., 610, 611
 Crowe, C. T., 312, 314

D

D'Agostino, V., 574
 da Silva, A. M. F., 541
 Dade, W. B., 618
 Dai, M., 357, 358
 Damgaard, J. S., 269
 Dancey, C., 239

Dancey, C. L., 239
 Danxun, L., 281
 Das, R., 114, 123, 149–151, 154, 155, 160,
 172–179, 241, 242, 308, 309, 311–317,
 383
 Davies, T. R., 505
 Davies, T. R. H., 197, 221
 Davis, S. R., 589, 595, 598, 600, 602, 605,
 608, 610, 611
 de Koning, H., 465
 de Ruiter, J. C. C., 264, 293
 de Saint-Venant, B., 41, 53
 de Vries, M., 80
 Dean, R. B., 117
 Debnath, K., 217, 221, 226, 264, 294, 384
 Deigaard, R., 10, 19, 25, 112, 306, 307, 309,
 386, 387, 399, 463, 464, 569
 Demir, H., 595, 599
 Detert, M., 154
 Dey, S., 7, 11, 62, 114, 117, 119, 122, 123,
 125, 149–151, 154, 155, 160, 162, 167,
 169, 171–179, 182, 190, 196, 215–218,
 221, 226, 229, 230, 241–243, 248, 250,
 264, 294, 307–309, 311–317, 351, 356,
 382–386, 389, 390, 394, 396–398, 491,
 492, 499–501, 505, 564, 567–573,
 579–581, 586–589, 591–596, 600, 602,
 604–606, 608–610, 612, 613, 616, 617
 Dey Sarker, H. K., 217, 221, 226, 384
 Dietrich, W. E., 19, 20, 240, 536, 550
 Dinkelacker, A., 197
 Diplas, P., 239, 251, 403, 536
 Dittrich, A., 178
 Donat, J., 272
 Dong, Z., 117
 Doppler, D., 400
 Dou, G. R., 273
 Drake, T. G., 230, 240, 241, 308
 du Boys, M. P., 264, 371
 Duan, J. G., 230
 Duan, Z., 357, 358
 Durst, F., 150
 Dwivedi, A., 643
 Dyer, K. R., 123

E

Eagleson, P. S., 13, 218
 Eakin, H. M., 540
 Eckelman, L. D., 158
 Eggenberger, W., 581
 Egiazaroff, J. V., 222, 244, 302
 Einstein, A., 540

Einstein, H. A., 196, 197, 261, 264, 274,
 277–281, 283, 293, 299, 305, 307, 308,
 337, 342, 350, 359, 363–367, 372, 388,
 395, 403, 418–420, 427, 511, 512, 659
 Elata, C., 395, 398
 El-Samni, E. A., 197, 277
 Emmerling, R., 197
 Engelund, F., 270, 283, 299, 306, 320, 360,
 427, 435, 454, 491, 496, 497, 512–514
 Ettema, R., 589
 Evaggelopoulos, N., 239
 Exner, F. M., 273, 356, 461, 474, 659

F

Fahlbusch, F. E., 574
 Favre, H., 280, 283
 Ferguson, R. I., 533, 559
 Fernandez Luque, R., 226, 264, 268, 283, 284,
 293, 298, 299, 306, 307, 309, 320
 Ferro, V., 574
 Fischer, E. E., 600
 Florey, Q. L., 246
 Fotopoulos, S., 239
 Franca, M. J., 172
 Francis, J. R. D., 288, 294, 297–299, 320, 608
 Fredsøe, J., 10, 19, 25, 112, 283, 299, 306, 307,
 309, 315, 320, 360, 362, 386, 387, 454,
 460–464, 491, 495, 502, 569, 582, 583
 French, J. R., 241
 Frenkiel, F. N., 162
 Frey, P., 315
 Friedkin, J. F., 540
 Friedrichs, C. T., 123, 124
 Frijlink, H. C., 267, 270
 Froehlich, D. C., 303, 605, 608
 Frostick, L. E., 197, 505
 Fuchs, R. A., 485
 Fujita, M., 354, 355
 Fukushima, Y., 361

G

Gad-el-Hak, M., 148
 Gagliano, S. M., 538
 Gallagher, M., 316
 Gallerano, F., 395
 Galletti, B., 133
 Galperin, B., 123
 García, M., 298, 299, 320
 García, M. H., 114, 124, 133, 172, 269,
 352–354, 361, 387, 399, 461, 517
 Garde, R. J., 192, 271, 380, 539

Gaudio, R., 114, 123, 241, 242, 308, 309,
311–317, 383, 394, 397, 398, 577–579,
608, 610
Gay, G. R., 538
Gay, H. H., 538
Gay, W. H., 538
Gerritsen, F., 348, 389, 393
Gersten, K., 110
Gessler, J., 231, 296
Gessner, F. B., 133
Ghani, A. A., 436
Gilbert, G. K., 216, 221, 223, 224, 272, 280,
283, 540
Gill, M. A., 461, 523, 564, 571, 572, 609
Giráldez, J. V., 389, 390, 394, 396
Girard, L. G., 610
Gjørsvik, O., 586
Glover, R. E., 246
Goldstein, S., 17
Goncharov, V. N., 191
Gore, R. A., 312, 314
Goring, D., 117, 119, 172, 174, 316, 317
Goring, D. G., 316
Gradshteyn, I. S., 165, 168, 169
Graf, W. H., 114, 117, 119, 266, 269, 304, 306,
309, 395, 429, 574, 592
Grass, A. J., 96, 118, 150, 155, 216, 221, 223,
224, 232, 242, 346, 355, 382, 384, 399
Griffiths, G., 172, 174
Griffiths, G. A., 538, 556
Griggs, R. F., 540
Grimaldi, C., 608
Gross, T. F., 124
Guenec, B., 241
Guo, J., 19, 117, 368, 377, 396, 423
Gust, G., 119, 315, 317, 397
Guy, H. P., 306, 307, 309, 457, 460, 486, 489,
499, 514
Gyr, A., 197

H

Haaland, S. E., 121, 503, 625
Hadfield, A. C., 610
Hahm, C. H., 608
Hallermeier, R. J., 19
Hancu, S., 600
Hanes, D. M., 272
Hanratty, T. J., 158
Hansen, E., 270, 427, 435, 513, 514
Haque, M. A., 610
Hardisty, J., 226
Harrison, L. J., 602
Hassid, S., 123

Hayashi, T., 486, 489, 534
Head, M. R., 156
Heathershaw, A. D., 240
Hembree, C. H., 419, 422–424
Henderson, F. M., 533
Hennessy, P. V., 584
Hershey, H. C., 158
Hessel, M., 197
Hetsroni, G., 312, 314, 316
Heywood, H., 9
Hino, M., 395
Hinze, J. O., 142
Hjelmfelt, A., 357
Hjulström, F., 193, 540
Ho, H. W., 332
Hoffmans, G. J. C. M., 580
Hogg, A. J., 618
Holly, F. M., 299, 300
Hooke, J. M., 538
Howard, P. G., 538
Hoyer, K., 197
Hsu, I. -S., 298, 299, 320
Hsu, S. H., 301
Hsu, S. M., 299, 300
Hu, C. H., 282, 298, 299, 320
Huang, J. T., 13, 301
Hui, Y. J., 282, 298, 299, 320
Hunt, J. N., 341, 391
Huntley, D. A., 123
Huppert, H. E., 618
Hurther, D., 400
Hussain, M. A., 610

I

Ibrahim, A., 587
Ikeda, S., 79, 132, 133, 223, 226, 542–544,
546–548, 550
Inglis, C. C., 539, 540
Ippen, A. T., 13, 218, 395, 398
Irwin, H. P. A. H., 153
Isbash, S. V., 611
Ishigaki, T., 230
Islam, G. M. T., 610
Istiarto, I., 592
Itakura, T., 351, 360
Iversen, J. D., 226
Iwagaki, Y., 197, 205, 221, 223

J

Jacobsen, J., 586
Jaeger, C., 64
Jaeggi, M. N. R., 467

Jain, S. C., 540, 600
 Janjua, N. S., 609
 Jansen, P., 80
 Javonovic, J., 150
 Jeffreys, H., 196
 Jensen, B. L., 583
 Jensen, R., 583
 Jia, Y., 230, 244, 299, 302, 379
 Jiménez, J. A., 20
 Jiménez, J., 112
 Jinka, G. H., 154
 Jobson, J. E., 332
 Johnson, J. W., 337, 403
 Jones, J. S., 611
 Jonsson, G. I., 248
 Julien, P. Y., 7, 19, 25, 117, 230, 281, 368,
 396, 403, 423, 436, 457, 459, 460, 474,
 575, 576

K

Kalinske, A. A., 197, 270, 271, 340, 362, 364,
 496
 Kampé de Fériet, J., 162
 Kandasamy, J. K., 602, 609
 Kantha, L. H., 123
 Karahan, E., 189, 190, 216, 221–224, 252,
 309, 384, 385
 Karaki, S., 600
 Karim, F., 434, 457, 473
 Karim, M. F., 433, 434, 514
 Kawasumi, T., 486, 489, 499
 Keller, E. A., 506
 Keller, J. B., 84, 212, 218, 297
 Kemp, P. H., 456
 Kennedy, J. F., 189, 433, 434, 460, 466, 481,
 484–486, 489, 491, 499, 514, 540, 550
 Keshavarzy, A., 218, 219
 Keulegan, G. H., 134, 363, 420
 Khullar, N. K., 404
 Kikkawa, H., 79, 298, 299, 320, 543, 546, 550
 Kilgore, R. T., 611
 Kilingeman, P. C., 244, 292, 299, 300
 Kim, J. S., 608
 Kim, S. -C., 123, 124
 Kim, U. Y., 608
 Kirkgöz, M. S., 117
 Kironoto, B. A., 114, 117, 119, 306, 309
 Kishi, T., 351, 360
 Kitagawa, A., 79, 543, 546, 550
 Kjeldsen, S. P., 586
 Klaassen, G. J., 460
 Klebanoff, P. S., 162
 Kline, S. J., 155, 158, 190

Knighton, D. A., 506
 Koll, K., 172, 173, 178
 Kolmogorov, A. N., 139
 Komar, P. D., 13, 14, 189, 190
 Komura, S., 12, 564, 572
 Kos'yan, R. D., 350
 Kothyari, U. C., 404
 Kotoulas, D., 573
 Kovacs, A., 230
 Kozakiewicz, A., 112
 Kramer, H., 11, 191, 199, 216, 221, 223, 224
 Krenkel, P. A., 496
 Krey, H., 199
 Krogstad, P. Å., 150, 153
 Krumbein, W. C., 8, 9
 Kuhnle, R. A., 555
 Kurihara, M., 222
 Kwan, T. F., 602–604

L

Lacey, J. M., 540
 Lagasse, P. F., 610, 611
 Lajeunesse, E., 269, 298, 320
 Lambert, M. F., 125
 Lane, E. W., 8, 197, 227, 245, 304, 362, 364,
 403, 496, 531, 555, 657
 Langbein, W. B., 535, 536
 Lapointe, M. F., 536
 Larson, M., 112
 Lauchlan, C. S., 610, 611
 Launder, B. E., 612
 Laursen, E. M., 348, 425, 427, 486, 489, 499,
 564, 565, 600, 609
 Laushey, L. M., 193
 Lavelle, J. W., 349
 Lavy, E. E., 192
 Le Guennec, B., 241
 Lee, D. I., 16
 Lee, H. Y., 298, 299, 301, 320
 Lee, J., 7
 Lee, M. K., 158
 Leeder, M., 312, 314, 315, 317
 Leeuwestein, W., 587
 Leliavsky, S., 199, 540
 Lelouvetel, J., 400
 Lemmin, U., 114, 117, 172, 398, 400
 Lenau, C., 357
 Lenzi, M. A., 578, 579
 Leopold, L. B., 240, 529, 530, 535, 536, 539,
 541, 555, 556
 Lester, C. M., 134
 Lewis, G. L., 226
 Li, D., 136, 396

Li, Z., 13, 14
 Liggett, J. A., 391
 Lim, S. -Y., 134–136, 435, 564, 572, 609
 Lim, S. Y., 610
 Lin, P. N., 20, 486, 489, 499
 Lin, Y. -C., 234, 235, 307, 308
 Ling, C. H., 196, 211, 216, 237
 Liou, J. -C., 19
 Liu, H. K., 456, 469, 609
 López, F., 124, 399
 Lu, S. S., 159
 Luchik, T. S., 316
 Lumley, J. L., 142–148
 Lundgren, H., 248
 Lyn, D. A., 393, 395, 397, 398

M

Ma, J., 230
 Maa, J. P. -Y., 123, 124
 Macky, G. H., 602
 Madsen, O. S., 20, 269
 Majumdar, H., 332
 Malverti, L., 269, 298, 320
 Manes, C., 178
 Mansour-Tehrani, M., 96, 399
 Mantz, P. A., 189, 202, 216, 221–224
 Mao, Y., 399, 400, 401
 Marion, A., 577–579
 Martinson, H. A., 538
 Martín-Vide, J. P., 477, 478, 480
 Mateos, L., 389, 390, 394, 396
 Mavis, F. T., 193
 McCave, I. N., 189, 190
 McClatchey, J., 241
 McDonald, B. C., 507
 McEwan, I., 172–174, 178, 316
 McLean, D. G., 244, 292, 299, 300
 McLean, S., 172, 173, 178
 McLean, S. R., 174, 241, 308, 352, 353, 360, 392, 399
 McNown, J. S., 20
 McTigue, D. F., 351
 Meade, R. H., 538
 Mehta, A. J., 7
 Mei, C. C., 357
 Meier, G. E. A., 197
 Melhorn, N., 506
 Melville, B., 595, 599, 643
 Melville, B. W., 305, 589, 592, 595, 600, 602, 605, 609, 610
 Meng, J., 222, 252
 Meroney, R. N., 117
 Metzler, S. P., 155, 158

Meyer-Peter, E., 216, 221, 223, 224, 266, 280, 283, 302, 495, 502, 503, 666
 Michiue, M., 244, 267, 299, 300
 Middleton, G. V., 95
 Miglio, A., 309, 315–317, 394, 397, 398
 Millar, R. G., 533
 Miller, M. C., 189, 190
 Miller, R. L., 210
 Milne-Thompson, L. M., 482, 489
 Mingmin, H., 238
 Misri, R. L., 271
 Mizuyama, T., 354, 355
 Molinas, A., 431, 432, 435, 436
 Moncada-M, A., 587
 Monin, A. S., 312
 Montes, J. S., 391–394
 Montgomery, D. R., 190, 191
 Moody, J. A., 538
 Morsi, S. A., 217, 296
 Mosyak, A., 316
 Moto, Y., 230
 Müller, R., 216, 221, 223, 224, 266, 302, 495, 502, 503, 581, 666
 Muste, M., 395

N

Nakagawa, H., 107, 116, 117, 131, 132, 144, 145, 153, 154, 158, 159, 162, 169, 172, 230, 264, 293, 312, 399
 Nakato, T., 365, 368
 Nalluri, C., 587
 Nath, T. K., 580, 612, 613, 616, 617
 Naumann, A., 17, 214, 234
 Neill, C. R., 192, 216, 221, 223, 224, 600, 610
 Nelson, J., 241, 308, 516
 Neu, H. A., 540
 Newman, G. R., 146
 Nezu, I., 107, 115–117, 119, 131, 132, 136, 144–146, 153, 154, 158, 159, 162, 169, 172, 312, 381, 382, 396, 398–400
 Ni, J. R., 346, 347
 Nicollet, G., 589, 594, 600, 610
 Nielsen, P., 269, 354, 355
 Nikora, V., 117, 119, 172–174, 178, 316, 317
 Nikora, V. I., 316
 Nikuradse, J., 110
 Niño, Y., 269, 298, 299, 320, 399
 Nishimura, T., 542, 547
 Nomicos, G. N., 395
 Noh, M., 395, 396
 Nowell, A. R. M., 124

Núñez-González, F., 458, 466, 477, 478, 480
Nychas, S. G., 158

O

Odgaard, A. J., 80, 542, 549, 553, 610
Offen, G. R., 155, 158
Oguz, B., 399
Oliver, D. R., 20
Onishi, Y., 540
Orgis, H., 461, 523
Oseen, C., 17
Ozaki, S., 534

P

Pagan-Ortiz, J. E., 611
Paintal, A., 190, 191, 271
Papanicolaou, A. N., 239
Papanicolaou, A., 190, 239
Paphitis, D., 190, 203
Paquier, A., 315
Parker, G., 226, 230, 244, 249, 267, 268, 292,
299, 300, 354, 361, 397, 403, 517, 533,
536, 543, 545, 546, 548, 608, 610
Parola, A. C., 610
Partheniades, E., 403
Patel, P. L., 299, 301, 302
Pender, G., 222, 252
Perkins, H. J., 131, 133
Peterson, A. W., 117
Plate, E. J. O. F., 486, 489, 499
Pokrajac, D., 172, 173, 178
Pope, D., 19, 25
Pope, S. B., 124, 312
Poreh, M., 298
Posada, G. L., 435
Prandtl, L., 66, 103, 108, 131
Prasad, S. N., 304
Prostokishin, V. M., 614
Prus-Chacinski, T. M., 540

Q

Qayoum, A., 580
Qian, N., 396, 398
Qin, Y. Y., 244, 301
Qiwei, H., 238
Qu, Z., 281
Quraishy, M. S., 540

R

Rahman, M. M., 610

Raikaar, R. V., 114, 117, 119, 309, 316, 317,
564, 567–573, 592, 593, 596, 606
Rajagopalan, S., 500
Rajaratnam, N., 117, 612
Ramette, M., 541
Ranga Raju, K. G., 271, 299, 301, 302, 380,
404, 461, 539
Rao, M. V. P., 197, 221
Raslan, Y., 474
Rasmussen, K. R., 226
Raudkivi, A. J., 19, 25, 305, 454–457, 580,
589
Raupach, M. R., 148, 500
Recking, A., 315
Reichardt, H., 210, 215, 221
Reid, I., 197, 505
Reitz, W., 197
Reynolds, A. J., 114
Reynolds, O., 95, 97
Reynolds, W. C., 155, 190
Richards, K. J., 457
Richards, K. S., 506
Richardson, E. V., 267, 268, 306, 307, 309,
369, 371, 403, 425, 426, 428, 453–455,
457, 460, 468, 469, 486, 489, 499, 514,
589, 595, 598, 600, 602, 605, 608, 610,
611
Richardson, J. F., 20, 344
Richardson, J. R., 602
Richardson, L. F., 137
Rickenmann, D., 272
Ripley, H. C., 538
Robert, A., 507, 555
Robinson, S. K., 96
Rodi, W., 117, 119, 136, 361, 381, 385, 612
Rodríguez, J. F., 133, 172
Rosati, A., 123
Rouse, H., 17, 337, 348, 574
Rozovskii, I. L., 78–80, 549, 550
Rubey, W., 18, 19, 25, 281
Rubinow, S. I., 84, 212, 218, 297
Rundle, A., 559
Runstadler, P. W., 155, 190
Ryzhik, I. M., 165, 168, 169

S

Saffman, P. G., 85, 212, 217, 296
Sagiv, A., 298
Salkield, A. P., 399
Samad, M. F. A., 197, 221
Samaga, B. R., 380
Sarkar, A., 11, 579–581
Sarkar, S., 147, 172, 218, 241, 309

Sastry, G. L. N., 592
 Sawai, K., 543, 548
 Sayre, W. W., 332
 Schall, J. D., 611
 Schewe, G., 197
 Schiller, L., 17, 214, 234
 Schlichting, H., 110, 117, 210, 614, 615
 Schmid, A., 240, 242
 Schmidt, W., 334
 Schneider, V. R., 600
 Schoklitsch, A., 198, 266, 272, 540, 573
 Schultz, J. C., 296
 Schwarz, W. H., 614
 Sechet, P., 241
 Seginer, J., 298
 Sekine, M., 298, 299, 320
 Seminara, G., 230
 Sentürk, F., 419, 552
 Sha, Y. Q., 20
 Shah-Fairbank, S. C., 423
 Shalash, M. S. E., 581
 Shamseldin, A. Y., 643
 She, K., 19, 25
 Shen, H. W., 403, 540, 589, 594, 600, 610
 Sheppard, D. M., 595, 599
 Shields, A. F., 189, 190, 193, 199, 201, 216,
 221, 223, 224, 266
 Shivaprasad, B. G., 148
 Shreve, R. L., 240, 241, 308
 Sichmann, T., 583
 Simões, F. J. M., 432
 Simons, D. B., 9, 226, 267, 268, 306, 307, 309,
 369, 371, 419, 425, 426, 428, 453–455,
 457, 460, 468, 469, 486, 489, 499, 514,
 552
 Simpson, R. L., 148
 Singamsetti, S. R., 332
 Singh, N. P., 586–588
 Sinnakaudan, S. K., 436
 Skinner, M., 609
 Sloss, L. L., 8
 Smart, G. M., 268
 Smith, C. D., 564
 Smith, C. R., 96, 155, 158, 516
 Smith, J. D., 174, 209, 210, 352, 353, 360, 392,
 399, 536, 550
 Smith, N. D., 555
 Solari, L., 218, 230, 241, 309
 Song, C. C. S., 476, 489, 491
 Song, T., 114, 117, 129, 130
 Soni, J. P., 461
 Soulsby, R. L., 19, 21, 25, 123, 203, 269, 399
 Southard, J. B., 95, 315, 317, 471, 555

Spalding, D. B., 113
 Stapleton, K. R., 123
 Stebbings, J., 249
 Steffler, P. M., 117
 Stein, O. R., 575
 Stevens, J. C., 657
 Stevens, M. A., 226
 Stokes, G. G., 16, 84
 Straub, F. A., 155, 190
 Straub, L. G., 266, 564, 572, 657
 Streeter, V. L., 47
 Strickler, A., 656
 Stuart, R. J., 96, 399
 Sturm, T. W., 609
 Sugimoto, S., 348
 Sukegawa, N., 467
 Sumer, B. M., 112, 315, 381, 385, 399, 582,
 583, 608
 Suszka, L., 269
 Sutherland, A. J., 240, 600, 602

T

Tafarojnoruz, A., 610
 Tan, S. K., 134–136
 Tanaka, M., 544
 Tanaka, S., 348
 Tang, L. -M., 505
 Task Committee, 197
 Taylor, G. I., 142
 Thacker, W. C., 349
 Thackston, E. L., 496
 Thomson, W., 642
 Thorne, P. D., 240
 Tiederman, W. G., 316
 Tison, L. H., 486, 489, 499
 Tjerry, S., 461, 462, 464
 Toch, A., 600
 Toro-Escobar, C., 608, 610
 Townsend, A. A., 133
 Tracy, H. J., 134
 Trim, L., 19, 25
 Trowbridge, J. H., 124
 Truelsen, C., 583
 Tsubaki, T., 486, 489, 499
 Tsujimoto, T., 132, 264, 293

U

Umeyama, M., 348, 389, 393
 US Interagency Committee, 7
 USBR, 247, 423, 657
 USWES, 190, 199, 216, 221, 223, 224, 436

V

- Valance, A., 455
 Valiani, A., 397
 van Atta, C. W., 162
 van Beek, R., 226, 268, 283, 284, 298, 299, 320
 van Bendegom, L., 80
 van den Berg, J., 80
 van den Berg, J. H., 473
 van Driest, E. R., 105, 115, 119
 van Gelder, A., 473
 van Ingen, C., 398
 van Rijn, L. C., 112, 114, 203, 213, 219, 229, 264, 268, 294, 295, 297–299, 302, 310, 335, 338, 340, 344, 345, 357, 359, 361, 372, 373, 380, 385, 391, 460, 472, 473, 502, 515
 Vanoni, V. A., 9, 121, 191, 193, 216, 221, 223, 224, 339, 340, 342, 395, 546, 567
 Velikanov, M. A., 196, 373, 375
 Verheij, H. C., 580
 Vigilar, G., 251
 Vinkovic, I., 400
 Vogel, G., 472
 Voigt, R. L., 608, 610
 Vollmers, H. J., 472
 von Kármán, T., 106, 108
 von Schelling, H., 535
 Voulgaris, B., 124

W

- Wadell, H., 9
 Walters, R., 172, 173
 Wan, Z., 280, 283, 418
 Wang, G. Q., 346, 347
 Wang, J., 117
 Wang, M. F., 13, 301
 Wang, S. S. Y., 12, 18, 19, 21, 25, 203, 230, 244, 299, 302, 379
 Wang, X., 136, 281, 396, 398
 Wang, Y., 610
 Wang, Z. Y., 136, 396
 Watannabe, K., 461, 523
 Watters, G. Z., 197, 221
 Webby, M. G., 564
 Weitbrecht, V., 154
 Werner, P. W., 540
 White, B. R., 296
 White, C. M., 121, 197, 202, 216, 221–224, 503
 White, F. M., 393
 White, S. J., 216, 221, 223, 224
 White, W. R., 430, 431, 435

- Whitehouse, R. J. S., 203, 226, 269
 Whiting, P. J., 240
 Wiberg, P. L., 209, 210
 WIHEE, 377, 378
 Williams, J. J., 240
 Williams, P. B., 456
 Williams, P. G., 298
 Willis, J. C., 350
 Willmarth, W. W., 159
 Wilson, K. C., 112, 267, 386
 Wolman, M. G., 529, 530, 539, 541, 555, 556
 Wong, M., 267
 Woo, H. S., 403
 Wood, W. L., 368
 Wright, L. D., 123, 124
 Wright, S., 354, 517
 Wu, B., 432, 435, 436
 Wu, F. -C., 233–235, 237, 238, 307, 308
 Wu, W., 12, 18, 19, 21, 25, 203, 244, 299, 302, 379

X

- Xia, Z., 117
 Xie, J. H., 13, 301, 377, 380, 385
 Xu, T. -Y., 505

Y

- Yaglom, A. M., 312
 Yalin, M. S., 112, 138, 189, 190, 196, 216, 221–224, 252, 264, 289, 293, 309, 384, 385, 454, 457, 459–461, 523, 541, 571
 Yang, C. T., 194, 196, 419, 431–433, 435, 437, 438, 541
 Yang, S. -Q., 134–136, 435
 Yasutomi, T., 486, 489, 499
 Yen, C. L., 301
 Yu, M., 136, 396
 Yue, J., 357, 358

Z

- Zagustin, K., 343
 Zakaria, N. A., 436
 Zaki, W. N., 20, 344
 Zakin, J. L., 316
 Zanen, A., 80
 Zanke, U. C. E., 193, 223, 224
 Zanke, U., 19, 25
 Zaric, Z., 150
 Zeller, J., 539
 Zevenbergen, L. W., 610, 611
 Zhang, H., 230

- | | |
|---|---------------------|
| Zhang, Q., 357, 358 | Zheng, J., 281 |
| Zhang, R. J., 13, 19, 25, 301, 377, 380 | Zhou, Y., 145 |
| Zhang, X. -D., 505 | Zimmermann, C., 550 |
| Zhang, Z., 357, 358 | Zyserman, J., 362 |

Subject Index

A

Acceleration, 30, 31
 advective acceleration, 31
 convective acceleration, 31
 local acceleration, 31
 temporal acceleration, 31
Added fluid mass, 296, 391
Advection–diffusion equation, 329, 332, 333, 357, 496
Angle of repose, 13, 210, 218
Anisotropy, 146
 anisotropic invariant function, 147, 148
 anisotropic invariant map (AIM), 147
 anisotropic turbulence, 131
 Reynolds stress anisotropy tensor, 146
Antidune mobility number, 479, 480
Autocorrelation, 101

B

Bars, 467
 alternate bars, 467, 541
 linguoid bars, 556
 middle bars, 467, 556, 559
 point bars, 467
 tributary bars, 467
Bedform model
 Bose–Dey instability theory, 491
 Exner’s model, 474
 kinematic model, 476
 potential flow model
 Hayashi’s model, 486
 Kennedy’s model, 481
 Song’s model, 476, 489
Bedforms, 453
 antidunes, 465
 breaking waves, 465
 standing waves, 465
 chutes and pools, 466
 dunes, 458
 plane bed, 465
 ripples, 454
 transition, 465
Bed layer, 359, 361, 365, 380, 403
Bed-load transport, 261
 bed-load transport intensity, 263, 277
 bed-load transport rate, 263, 264
 definition, 261, 263
Bed-load transport concepts
 bedform concept, 273
 bed shear stress concept, 264
 du Boys type equations, 266
 du Boys’ approach, 264
 empirical relationships, 270
 deterministic concept, 285
 Bagnold’s approach, 285
 Yalin’s Approach, 289
 discharge concept, 272
 equal mobility concept, 292
 pavement, 292
 subpavement size, 292
 probabilistic concept, 274
 Einstein’s approach, 274
 empirical refinement of Einstein formula, 280
 Engelund and Fredsøe’s approach, 283
 modified Einstein’s approach, 281
 velocity concept, 272
Bed-material load, 417, 418
Bedform resistance
 form resistance (or form drag), 509
 resistance due to particles (or skin friction), 509
Bedform resistance calculation
 Einstein and Barbarossa’s method, 511
 Engelund’s method, 512
 Karim and Kennedy’s method, 514
 Nelson and Smith’s method, 516
 van Rijn’s method, 515
 Wright and Parker’s method, 517

Bélangier equation, 89
 Boundary layer, 65
 boundary layer separation, 68
 boundary layer thickness, 66, 67, 74
 displacement thickness, 67
 laminar boundary layer, 66, 72
 momentum thickness, 67
 separated boundary layer, 68
 shape factor, 68
 turbulent boundary layer, 66, 67, 73
 velocity defect, 67, 108
 von Kármán momentum integral equation, 69, 71
 Boussinesq hypothesis, 105, 135, 337
 Braided rivers, 530, 555
 Braid formation, 556
 avulsion, 559
 chute cutoff, 559
 linguoid bars, 556
 middle bar accretion, 556
 multiple bar dissection, 559
 multi-thalweg, 556
 stable multiple-stream pattern, 556
 transverse bar conversion, 557
 unstable multiple-stream pattern, 556
 Burst, 155, 156
 bursting period, 158
 ejection events, 401
 ejections, 159–161, 240–242
 inward interactions, 159, 160
 outward interactions, 159
 sweep events, 240, 242, 402
 sweeps, 159–161, 240–242
 turbulent burst, 155, 240, 241

C

Carnot equation, 512
 Cauchy–Riemann equations, 481
 Chézy coefficient, 54, 266, 362, 511, 516
 Chézy equation, 54
 Clauser method, 120
 Coherent structures, 96, 156
 hairpin vortices, 156, 242, 401
 Coles' wake parameter, 116
 Conservation of energy, 54
 Bernoulli's equation, 55, 56, 71
 Coriolis coefficient, 55
 energy coefficient, 55
 energy equation for gradually varied flow, 57
 energy equation for open-channel flow, 56
 Conservation of mass, 35

continuity equation, 36, 37–39, 85, 86, 98, 126, 480, 492, 549, 565, 613
 continuity equation for an unsteady flow, 41
 continuity equation for open-channel flow, 39
 continuity equation in three dimensions, 37
 Conservation of momentum, 41
 Boussinesq coefficient, 42
 equations of motion for inviscid flow, 43
 equations of motion for viscous flow, 44
 Euler equations, 43
 momentum coefficient, 42
 momentum equation for gradually varied steady flow, 48
 momentum equation for gradually varied unsteady flow, 51
 momentum equation for open-channel flow, 48
 momentum equation for steady uniform flow, 53
 momentum equation in three dimensions, 43
 Navier–Stokes equations, 44
 Convection, 327
 advection, 327, 329, 333
 diffusion, 327, 329, 332, 333
 Coriolis effect, 540
 Creeping flow, 82
 Critical condition, 51, 59
 Critical depth, 50, 51, 58
 Critical flow, 51, 58, 59
 Critical flow condition, 50, 51, 59
 Curvilinear flow, 62, 63, 491

D

de Saint-Venant equation, 53, 127, 182, 495
 Definition of sediment threshold, 190
 general transport, 191
 medium transport, 191
 no transport, 191
 weak transport, 191
 Dey–Lambert's approach, 125
 Dimensional analysis, 643
 Buckingham Π theorem, 646
 repeating variables, 647, 650
 Dip phenomenon, 133
 modified logarithmic law, 134, 136
 modified log-wake law, 117, 136, 137
 Distribution of sediment concentration, 333, 336, 354, 356
 diffusion concept, 328

- Hunt equation, 341
 - Lane and Kalinske equation, 340
 - Ni and Wang equation, 346
 - Rouse equation, 336
 - Umeyama equation, 348
 - van Rijn equation, 344
 - Zagustin equation, 343
 - energy concept, 373
 - Velikanov's approach (also gravitational theory), 373
 - Double-averaging concept, 172
 - double-averaging methodology, 172
 - form-induced shear stress, 177–179
 - space-time-averaging, 172
 - time-space-averaging, 172
 - Dynamic angle of repose, 592
 - Dynamic equation for gradually varied unsteady flow, 53
- E**
- Eddy viscosity, 6, 78, 100, 105, 132, 332
 - Effects of bed load
 - on length scales of turbulence, 312
 - on velocity distribution, 309
 - on von Kármán constant κ , 315
 - Effects of suspended load
 - on bed-load transport, 386
 - on turbulence characteristics, 397
 - on velocity distribution, 387
 - on von Kármán constant κ , 394
 - Castro-Orgaz et al.'s contribution, 389
 - Einstein and Chien's contribution, 388
 - Umeyama and Gerritsen's contribution, 389
 - Einstein's integrals, 364
 - Ejection cushion, 401
 - Energy containing range, 107, 141, 145
 - Energy deficiency region, 153
 - Energy equilibrium region, 153
 - Energy excess region, 153
 - Eulerian approach, 31, 32
 - Excess bed shear stress, 261, 297, 426, 454, 458
- F**
- Flow in curved channels, 74
 - bed shear stress distribution in curved channels, 80
 - superelevation in curved channels, 77
 - velocity distributions in curved channels, 77
 - Flow intensity parameter, 278, 420, 426, 512
 - Flow layers, 106, 107
 - buffer layer, 106, 107, 113, 115
 - free surface layer, 107, 108
 - inner layer, 107, 108, 113, 120
 - intermediate layer, 107–109
 - logarithmic layer, 107
 - transition, 106, 110, 111
 - turbulent outer layer, 107, 116
 - turbulent wall shear layer, 107, 109
 - viscous sublayer, 66, 67, 103, 106, 107, 109–113
 - wall shear layer, 107–109
 - Flow regimes, 110, 111
 - hydraulically rough flow, 110, 111, 202
 - hydraulically smooth flow, 110, 202
 - hydraulically transitional flow, 110, 111, 202
 - Fluid and suspended sediment mixture, 14
 - fluid–sediment mixture, 14
 - kinematic viscosity of fluid–sediment mixture, 15
 - mass density of fluid–sediment mixture, 15, 389
 - sediment concentration, 14, 15
 - specific weight of fluid–sediment mixture, 15
 - Fluid flow, 29
 - irrotational, 32, 34
 - limiting streamline, 29, 65, 69, 612
 - pathline, 29, 30
 - streakline, 29
 - streamline, 29, 30, 39, 489
 - Fluvial processes, 529
 - Fick's law, 328
 - first law, 328
 - second law, 328
 - Fractional bed-load transport, 299–302
 - hiding–exposure correction factor, 301
- G**
- Gradually varied flow, 57, 59
 - adverse slope, 62
 - backwater curve, 60
 - critical slope, 61
 - drawdown curve, 60
 - horizontal slope, 61
 - mild slope, 61
 - steep slope, 61
 - Gravel-bed streams, 505
 - cluster, 505, 506
 - rapids and cascades, 505, 507, 509
 - riffle–pool sequence, 505–507
 - step–pool sequence, 505, 507, 508

H

- Hiding factor, 278, 279
- Higher-order correlations, 148
 - coefficient of kurtosis, 150
 - excess kurtosis, 150
 - skewness, 148, 149
 - third-order correlations, 148, 149
- Hydrodynamic drag and lift, 81
 - drag, 81
 - form drag (or pressure drag), 81, 509–512, 516
 - lift due to Magnus effect, 84, 85, 196, 218
 - lift due to shear effect, 217
 - lift, 81, 84
 - shear lift, 85, 294
 - skin friction drag, 81, 509

I

- Inertial subrange, 107, 138, 141, 143, 145
- Isotropic turbulence theory, 137
 - dissipation range, 107, 141, 145
 - energy cascade process, 137
 - integral scale, 137
 - Kolmogorov micro-scales, 140
 - length scale, 137–143, 145
 - macro-turbulence, 137
 - macro-turbulent eddies, 138
 - Taylor micro-scale, 142
 - time scale, 137–141, 143
 - turbulence Reynolds number, 138, 142, 143
 - universal equilibrium range, 139, 141, 143, 145
 - velocity scale, 137, 138

K

- Kelvin–Helmholtz instability, 456
- Kolmogorov hypotheses, 139
 - Kolmogorov first similarity hypothesis, 139
 - Kolmogorov hypothesis of energy spectrum function, 145
 - Kolmogorov hypothesis of local isotropy, 139
 - Kolmogorov second similarity hypothesis, 140
 - Kolmogorov's $-5/3$ -th power law, 145
- Kronecker delta, 100, 146

L

- Lagrangian approach, 30–32

- Laminar flow, 6, 95, 96, 106
- Laplace equation, 480, 487
- Lift correction factor, 278, 279
- Lift force concept, 196

M

- Manning equation, 54, 511, 577
- Meandering concepts
 - earth's revolution concept, 540
 - excess flow energy concept, 540
 - helicoidal flow concept, 540
 - instability concept, 540
 - large-scale eddy concept, 541
- Meandering models
 - Ikeda and Nishimura's model, 542
 - Odgaard's model, 549
- Meandering rivers
 - cutoff, 530, 537–539
 - meandering, 530–542
 - oxbow lake, 538, 539
 - premature inflection, 538
 - pseudo-meandering streams, 538
 - sinuosity, 529, 530, 534
 - thalweg, 530, 534–536
- Mixing length, 78, 103–106, 109, 129, 130, 138, 312, 313, 331, 346, 389, 392
- Mobility number, 430
- Modified mixing length model of van Driest, 105, 115
- Multi-ejection, 400, 401

N

- Nikuradse's equivalent sand roughness, 110
- Nonequilibrium sediment concentration, 354
- Nonuniform streamwise variation of concentration, 356
- Normal flow depth, 54
- No-slip, 6, 29, 69, 109, 612

P

- Physical properties of fluid and sediment, 4
 - mass densities of fluid and sediment, 4
 - relative densities of fluid and sediment, 5
 - specific weights of fluid and sediment, 5
 - submerged density, 5
 - submerged relative density, 5
 - submerged specific weight, 5
- Pickup rate, 264, 292
 - sediment pickup function, 264, 292
- Potential flow, 480
 - Cauchy–Riemann equations, 481

- circulation, 34
 - Laplace equation, 480
 - normal strain rate, 35, 38, 47
 - shear strain rate, 35, 142
 - Stokes stream function, 82
 - stream function, 38, 39, 480
 - velocity potential function, 480
 - vorticity, 34, 131, 132, 544
- Prediction of bedforms, 468
- Pressure distribution in curvilinear flow, 62
 - Boussinesq approximation, 64, 493
 - flow with small free surface curvature, 64
- Probabilistic concept of entrainment, 230
 - Gessler's approach, 231
 - Grass's approach, 232
 - Wu and Chou's approach, 233
- Probability distributions of turbulence, 162
 - Bose–Dey universal probability theory, 162
 - conditional distributions, 169
 - exponential based Gram–Charlier, 308
 - Gaussian based Gram–Charlier, 162
- Q**
- Quadrant analysis, 158
 - conditional statistics, 158, 159
 - detection function, 159
 - hole size, 159
- R**
- RANS equations, 100, 101, 174, 492
- Reference concentration, 336, 359
- Reference level, 336, 359
- Reynolds-averaged Navier–Stokes equations, 100
- Reynolds conditions, 98
- Reynolds decomposition, 97, 173, 206, 331, 492
- Reynolds equations, 99
- Reynolds stresses, 98, 100
 - Reynolds normal stresses, 100
 - Reynolds shear stresses, 100
 - Reynolds stress anisotropy tensor, 146
- Reynolds stress tensor, 100
- Roughness
 - d*-type, 112
 - equivalent roughness, 110–112, 125
 - equivalent sand roughness, 110, 111
 - k*-type, 111
 - Nikuradse's equivalent sand roughness, 110
 - sand roughness, 111
- Roughness sublayer, 172
 - form-induced sublayer, 172, 173
 - interfacial sublayer, 172, 173
 - roughness geometry function, 174
- Rouse number, 337, 363, 384
- Rousean formulation, 337
- S**
- Saltation, 261, 294, 295
 - characteristic parameters, 295
 - characteristics of saltation, 294
 - particle trajectory, 295
- Scour, 563
 - contraction scour, 563, 564
 - general scour, 563
 - local scour, 563
 - mode of scour
 - clear-water scour, 563
 - live-bed scour, 563, 564
- Scour countermeasures, 608
- Scour types
 - bridge abutments, 602
 - bridge piers, 589
 - channel contractions, 664
 - Dey and Raikar's model, 567
 - Laursen's model, 565
 - downstream of structures, 573
 - bed sills, 576
 - drop structures, 573
 - grade control structures, 576
 - horizontal jets, 579
 - submerged wall jets, 580, 617
 - horizontal pipelines, 581
- Secondary currents, 131
 - Prandtl's first kind, 131, 132, 540
 - Prandtl's second kind, 132
- Sediment
 - angle of repose, 13, 210, 218
 - critical angle of repose, 13
 - cumulative frequency curve, 10
 - dry mass density, 12
 - dry specific weight, 12
 - frequency curve, 10
 - frequency histogram, 10, 11
 - geometric mean size, 11, 301
 - geometric standard deviation, 11
 - gradation coefficient, 11
 - particle size distribution curve, 10, 11
 - phi (Φ) units, 8
 - porosity, 12

- Sediment (*cont.*)
 - size distribution, 10
 - void ratio, 12
 - Sediment entrainment probability, 305
 - entrainment probability function, 306
 - Sediment transport mode
 - bed load, 261
 - contact load, 261, 262
 - suspended load, 261, 262, 327
 - total load, 417
 - wash load, 262, 263, 402
 - Shape of a sediment particle
 - Corey shape factor, 9
 - roundness, 9
 - shape parameter, 9
 - sphericity, 9
 - surface coefficient, 10
 - volume coefficient, 9
 - Shields diagram, 201, 202
 - Shields parameter, 201, 202
 - Sidewall correction, 121
 - Similitude, 651
 - dynamic similarity, 653
 - geometric similarity, 651
 - distorted model, 656
 - geometric distortion, 652, 655
 - scale effect, 654
 - tilted model, 656
 - incomplete similitude, 660
 - kinematic similarity, 652, 653
 - Size of a sediment particle
 - area diameter, 7
 - fall diameter, 7
 - nominal diameter, 7, 18
 - sedimentation diameter, 7
 - sieve diameter, 7
 - Slip-spinning mode, 218
 - Solid diffusivity, 332
 - Sorting and armoring
 - active layer, 303, 304
 - armoring, 303–305, 505, 596
 - armor layer, 303–305
 - sediment sorting, 303, 535
 - threshold armoring condition, 304
 - Specific energy, 57
 - alternate depths, 58
 - specific energy diagram, 57, 58
 - subcritical, 58
 - supercritical, 58
 - Specific force, 50
 - sequent depths, 50
 - specific force diagram, 50
 - Spectral function
 - energy spectrum function, 144, 145
 - spectral density function, 124, 144, 145
 - Stable channel design, 245
 - straight trapezoidal channels, 245
 - threshold channel, 246
 - Stokes hypothesis, 47
 - Stokes' law, 82
 - Straight rivers, 529–531
 - Stratification effects on concentration distribution, 352
 - heavy-fluid zone, 352
 - light-fluid zone, 352
 - Stream power, 288, 378, 379, 424, 425, 465, 468
 - Streamtube, 30
 - Surface creep, 295
 - Suspended load by diffusion approach, 362
 - Bijker's approach, 372
 - Brooks' approach, 369
 - Chang et al.'s approach, 369
 - Einstein's approach, 363
 - Lane and Kalinske's approach, 362
 - van Rijn's approach, 372
 - Suspended load by energy concept, 373
 - Bagnold's approach, 377
 - Velikanov's approach, 373
 - Wu et al.'s approach, 379
 - Suspended-load transport, 262, 327
 - definition, 262, 327, 328
 - Suspended-load transport capacity, 376, 377
 - Suspended-load transport intensity, 328
 - Suspension number, 337
- T**
- Terminal fall velocity, 16
 - drag coefficient, 16, 17
 - hindered settling effect, 20
 - settling velocity, 16
 - Threshold bed shear stress concept, 198
 - Dey's approach, 215
 - Iwagaki's approach, 205
 - Ling's approach, 211
 - Shields' approach, 199
 - White's approach, 202
 - Wiberg and Smith's approach, 209
 - Threshold bed shear stress on sloping beds, 224
 - on an arbitrary bed slope, 228
 - on a side slope, 226
 - on a streamwise sloping bed, 225
 - Threshold condition, 189
 - Threshold condition for sediment suspension, 380
 - Bose and Dey's probabilistic approach, 382

- Cheng and Chiew's probabilistic approach, 381
 - Threshold mode
 - lifting threshold, 211
 - rolling threshold, 211
 - Threshold of nonuniform sediment motion, 243
 - Threshold shields parameter, 198, 201
 - Threshold velocity concept, 191
 - critical velocity, 191
 - threshold velocity, 191
 - Yang's threshold velocity model, 194
 - Total-load transport computation
 - direct approach, 418, 425
 - Ackers and White's approach, 430
 - Bishop et al.'s approach, 426
 - Brownlie's approach, 432
 - Engelund and Hansen's approach, 427
 - Graf and Acaroglu's approach, 429
 - Karim and Kennedy's approach, 433
 - Laursen's approach, 425
 - Molinas and Wu's approach, 435
 - Sinnakaudan et al.'s approach, 436
 - Yang and Lim's approach, 435
 - Yang's approach, 431
 - indirect approach, 417, 418
 - Bagnold's approach, 424
 - Chang et al.'s approach, 425
 - Einstein's approach, 418
 - modified Einstein procedure, 419
 - Total-load transport intensity, 418
 - Total-load transport of nonuniform sediments, 436
 - Transport parameter, 419
 - Transport stage parameter, 472
 - Turbulence factor, 203, 222
 - Turbulence induced entrainment concept, 239
 - Turbulence intensity, 100, 118, 137
 - Turbulence properties, 96
 - diffusivity, 96
 - fluctuations, 96
 - mixing process, 96
 - randomness, 96
 - self-perpetuating motion, 96
 - Turbulence theories, 103
 - Prandtl's mixing length theory, 103
 - similarity hypothesis of von Kármán, 106
 - Turbulent diffusivity, 6, 78, 95, 105, 332, 338, 343
 - Turbulent flow, 95
 - Turbulent kinetic energy, 123, 146, 150
 - TKE dissipation rate, 124, 137, 139–142, 152, 153
 - TKE flux, 150
 - Turbulent kinetic energy budget, 151
 - advection, 152
 - diffusion, 152
 - dissipation, 152
 - production, 152
 - Turbulent stresses, 98, 100
- U**
- Uniformity parameter, 11
 - Kramer's uniformity parameter, 11
 - Unit stream power, 431, 432
- V**
- Velocity distribution, 72, 73, 108
 - law in buffer layer, 115
 - law of the wall, 107
 - linear law in viscous sublayer, 109
 - logarithmic law, 109, 114, 125, 176
 - log-wake law, 116, 117, 120
 - modified logarithmic law, 136
 - modified log-wake law, 117, 136, 137
 - velocity defect law, 116, 117, 351
 - Velocity potential function, 480, 482, 487
 - Virtual bed level, 113, 114, 173, 176, 177, 219, 233, 297
 - Virtual reference level, 113
 - Viscosity of fluid, 6
 - coefficient of dynamic viscosity, 6
 - coefficient of eddy viscosity, 6, 105
 - coefficient of kinematic viscosity, 6
 - Newton's law of viscosity, 6
 - Viscous dissipation range, 107
 - von Kármán constant, 105, 241, 243, 309, 311, 312, 394, 396
 - vorticity, 34, 131, 132, 544
- W**
- Wake function, 116
 - Wash load, 262, 263, 402
 - definition, 403
 - suspended wash-load transport intensity, 404
 - Wave number, 143–145, 457, 553
- Z**
- Zero-plane displacement, 114, 177

